BIOTROPHIC PLANT-MICROBE INTERACTIONS

EDITED BY: Pietro D. Spanu and Ralph Panstruga
PUBLISHED IN: Frontiers in Plant Science and Frontiers in Microbiology

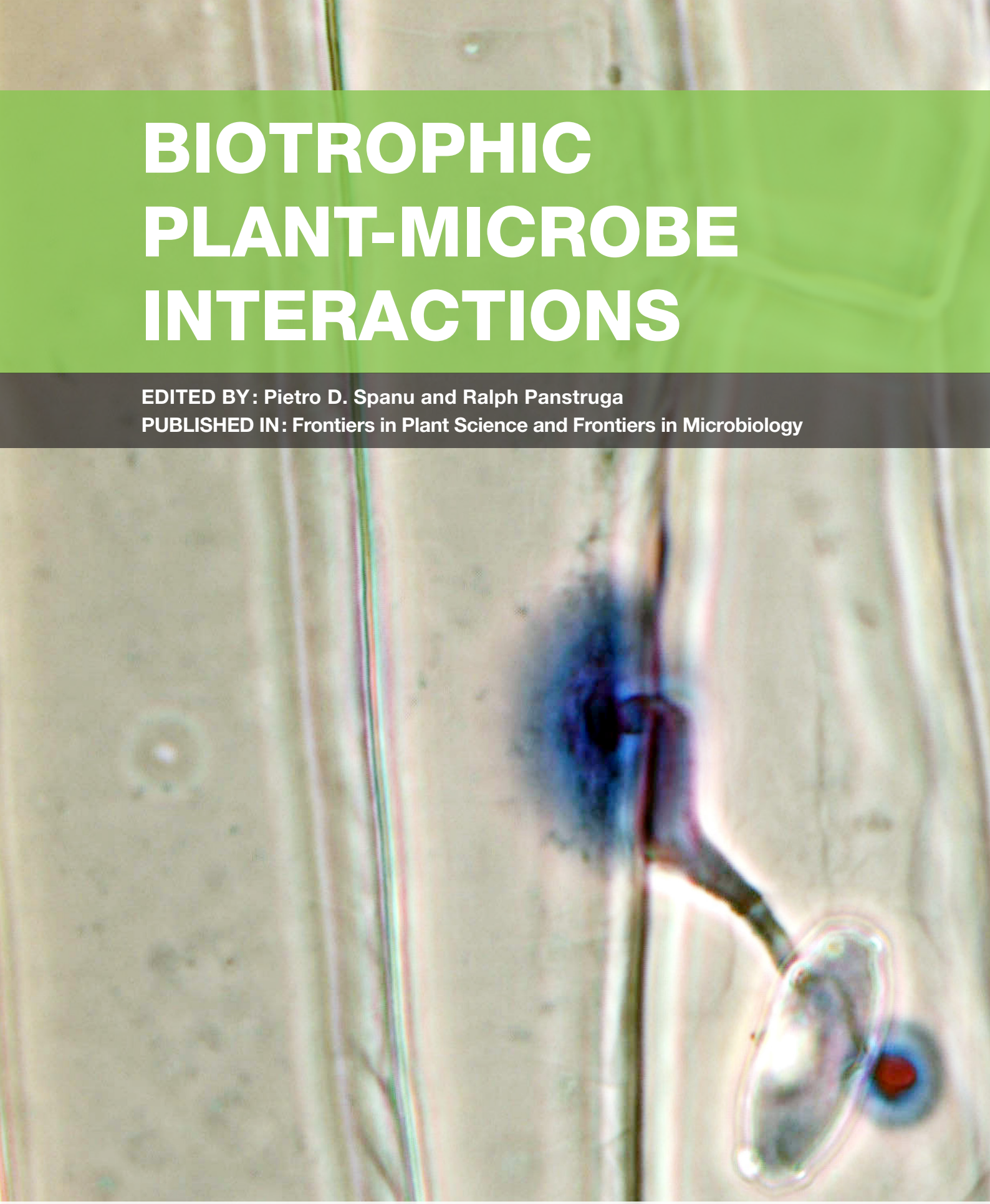

frontiers Research Topics

frontiers

ISSN 1664-8714
ISBN 978-2-88945-138-8
DOI 10.3389/978-2-88945-138-8

About Frontiers

Frontiers is more than just an open-access publisher of scholarly articles: it is a pioneering approach to the world of academia, radically improving the way scholarly research is managed. The grand vision of Frontiers is a world where all people have an equal opportunity to seek, share and generate knowledge. Frontiers provides immediate and permanent online open access to all its publications, but this alone is not enough to realize our grand goals.

Frontiers Journal Series

The Frontiers Journal Series is a multi-tier and interdisciplinary set of open-access, online journals, promising a paradigm shift from the current review, selection and dissemination processes in academic publishing. All Frontiers journals are driven by researchers for researchers; therefore, they constitute a service to the scholarly community. At the same time, the Frontiers Journal Series operates on a revolutionary invention, the tiered publishing system, initially addressing specific communities of scholars, and gradually climbing up to broader public understanding, thus serving the interests of the lay society, too.

Dedication to Quality

Each Frontiers article is a landmark of the highest quality, thanks to genuinely collaborative interactions between authors and review editors, who include some of the world's best academicians. Research must be certified by peers before entering a stream of knowledge that may eventually reach the public - and shape society; therefore, Frontiers only applies the most rigorous and unbiased reviews.
Frontiers revolutionizes research publishing by freely delivering the most outstanding research, evaluated with no bias from both the academic and social point of view.
By applying the most advanced information technologies, Frontiers is catapulting scholarly publishing into a new generation.

What are Frontiers Research Topics?

Frontiers Research Topics are very popular trademarks of the Frontiers Journals Series: they are collections of at least ten articles, all centered on a particular subject. With their unique mix of varied contributions from Original Research to Review Articles, Frontiers Research Topics unify the most influential researchers, the latest key findings and historical advances in a hot research area! Find out more on how to host your own Frontiers Research Topic or contribute to one as an author by contacting the Frontiers Editorial Office: **researchtopics@frontiersin.org**

BIOTROPHIC PLANT-MICROBE INTERACTIONS

Topic Editors:
Pietro D. Spanu, Imperial College London, UK
Ralph Panstruga, RWTH Aachen University, Germany

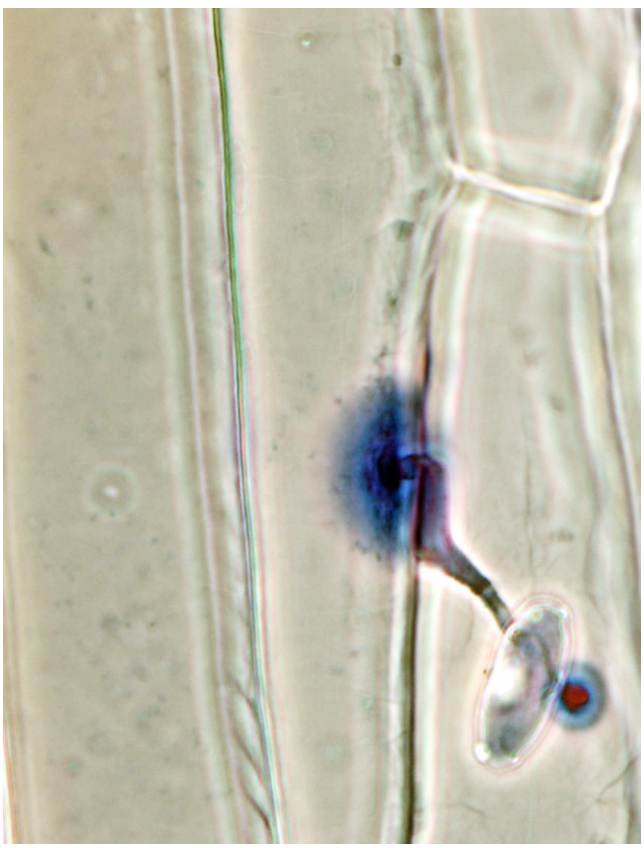

Conidium (asexual spore) of *Blumeria graminis* f.sp. *hordei*, the obligate biotrophic fungus that causes barley powdery mildew disease, 24h hours after landing on a barley leaf. The conidium first produces a primary germ tube (bottom right of the spore) aimed at sensing the surface; it then develops a secondary germ tube that differentiates a swollen, hooked appressorium (top left of the spore) from which a penetrating peg is formed. The host cell perceives the attack and responds by synthesising "papillae": cell wall fortifications in correspondence of the two hyphae, visible as blue- and purple-stained deposits below the fungal structures.
Image by Pietro D. Spanu

Throughout their life, plants interact with all sorts of microbes. Some of these are detrimental and cause disease; some interactions are mutually beneficial for both partners. It is clear that most, if not all, of the interactions are regulated by highly complex checks and balances sustained by signalling and exchange of messengers and nutrients. The interactions where both partners are alive for a significant part of their time together are called biotrophic. In this e-book we bring together 33 articles representing the current state-of-the-art in research about diverse biotrophic plant-microbe associations aimed at describing and understanding how these complex and ubiquitous partnerships work and ultimately support much of the land-based biosphere.

Citation: Spanu, P. D., Panstruga, R., eds. (2017). Biotrophic Plant-Microbe Interactions. Lausanne: Frontiers Media. doi: 10.3389/978-2-88945-138-8

Table of Contents

Resistance and defence against biotrophic pathogens

Chapter 3: Signalling within and between partners

frontiers in Plant Science

EDITORIAL
published: 13 February 2017
doi: 10.3389/fpls.2017.00192

Editorial: Biotrophic Plant-Microbe Interactions

Pietro D. Spanu[1] *and Ralph Panstruga*[2]*

[1] *Department of Life Sciences, Imperial College London, London, UK,* [2] *Unit of Plant Molecular Cell Biology, Institute for Biology I, RWTH Aachen University, Aachen, Germany*

Keywords: obligate biotrophs, hemibiotrophs, necrotrophs, endophytes, symbionts, haustorium, saprotrophs, mycorrhiza

Editorial on the Research Topic

Biotrophic Plant-Microbe Interactions

BIOTROPHS AND OTHER PARTNERS

Organisms inhabit the biosphere not as isolated entities: they interact with others. These may be individuals of the same species. In fact, the most common interactions are likely to be with very different beings. The interactions may be fleeting, or life-long, they may be simply sharing the same space, or may be complex behavioral and developmental processes (Buxa et al.; Genre and Russo) from which one or both partners derive an advantage and improve their reproductive success.

OPEN ACCESS

Edited by:
Brigitte Mauch-Mani, University of Neuchâtel, Switzerland

Reviewed by:
Hans Thordal-Christensen, University of Copenhagen, Denmark

****Correspondence:***
Ralph Panstruga
panstruga@bio1.rwth-aachen.de

Specialty section:
This article was submitted to Plant Microbe Interactions, a section of the journal Frontiers in Plant Science

Received: *16 January 2017*
Accepted: *30 January 2017*
Published: *13 February 2017*

Citation:
Spanu PD and Panstruga R (2017) Editorial: Biotrophic Plant-Microbe Interactions. Front. Plant Sci. 8:192. doi: 10.3389/fpls.2017.00192

INTERACTIONS DEFINED BY EXCHANGE OF FOOD

Plants are no exception to this universal rule: they share their personal space with myriads of microbes (Souza et al.). In the case of living plants, this may result in seemingly neutral (Shaw et al.; Voisey et al.), mutually beneficial (Banhara et al.; Calabrese et al.; Manck-Gotzenberger and Requena) or detrimental (Bindschedler et al.; Langenbach et al.) interactions; the respective microbes are commonly called endophytes, symbionts and pathogens, respectively. The best studied interactions are those which result in transfer of resources, such as nutrients, from one partner to the other. These "trophic" relations are frequently used to categorize interactions between plants and microbes. In simple terms, when the plants remain alive during the nutrient exchanges, we talk of "biotrophic interactions" and refer to the microbes as "biotrophs" (Spanu and Kämper, 2010). This is typically the case in symbiotic relationships, but also in some instances of parasitism. Biotrophy is thus contrasted to "necrotrophy," that is when the microbes kill plant cells and tissues, to feed off the remains, which is characteristic for several phytopathogens (Shaw et al.). In practice, we recognize many intermediate states characterized by temporal and/or spatial transitions between biotrophy and necrotrophy, and refer to these relations as hemibiotrophic (Vleeshouwers and Oliver, 2014). When microbes are simply able to feed off dead plant remains whilst playing no part in the killing, we call them saprotrophs (Lewis, 1973).

The consensus is that saprotrophy is the ancestral status for plant-associated microbes (Martin et al., 2016). Requirements needed to access nutrients from dead plants include the ability to degrade biopolymers, actively explore solid matter, and deal with potentially toxic compounds left by the dead plant. Interacting with a live plant partner requires much more complex and sophisticated mechanisms, first and foremost the capacity to deal with and take control of plant immunity (Ruhe et al.), which evolved to protect plants from unwanted, harmful encroachment.

The ability to manipulate host metabolism and to redirect nutrients for their own benefit are further essential skills for these types of microbes (Calabrese et al.; Manck-Gotzenberger and Requena). To realize these necessities, many microbial species evolved secreted effector proteins that exert various activities in the plant host (Kunjeti et al.; Petre et al.; Pitino et al.; Xiang et al.).

IS KILLING SIMPLER THAN SHARING?

For many years, biotrophy has been regarded as the most complex form of trophic relation between organisms. This has led many to consider biotrophy to be more "advanced" (Lewis, 1973)—perhaps a controversial and not particularly useful term. In recent years, there has been a revision of this: true necrotroph lifestyles are supported by highly sophisticated/evolved killing mechanisms (Oliver and Solomon, 2010). They are not simple blunderers that happen to have developed from saprotrophic organisms (Delaye et al., 2013).

It has been widely accepted that the distinction between biotrophic and necrotrophic interactions may also be evident in distinct pathways that host plants use to signal responses to the invading microbe. Thus, salicylic acid-mediated responses are regarded as typical of reactions to biotrophic attack, while jasmonic acid- and ethylene-mediated ones are believed to be associated with necrotrophy (Glazebrook, 2005). This distinction is now brought into question, with data revealing roles for jasmonic acid signaling in the unquestionably biotrophic interaction of grapevine with downy mildew (Guerreiro et al.).

THE COMPULSION TO FEED OFF LIFE: OBLIGATE BIOTROPHS

This revision notwithstanding, biotrophic microbes have developed exquisitely complex mechanisms to access plant resources. The rich niche represented by a plant host is characterized by having fewer microbial competitors than, say, soil or water. So, unlocking access confers a significant advantage: abundant resources available with "predictable" frequency throughout time and space. Once this space was occupied, some microbes appear to have lost the original capacity to grow on non-live material: these are recognized as the "obligate biotrophs." The most extreme of the obligate biotrophs have become so dependent of a live host that we are unable to recreate a suitable environment in axenic cultures under laboratory conditions. Examples of these are the very ancient mutualistic symbiont arbuscular mycorrhizal fungi (Buxa et al.; Genre and Russo) that are near ubiquitous colonizers of plant roots, the common powdery mildew (Gafni et al.; Xu et al.; Bindschedler et al.; Bourras et al.; Orton and Brown; Rajaraman et al.; Zheng et al.) and rust (Tang et al.; Langenbach et al.; Liu et al.; Liu et al.; Petre et al.) fungi (from taxonomically very distant groups, namely ascomycetes and basidiomycetes), as well as some of the oomycetes such as downy mildews (Guerreiro et al.; Kulkarni et al.; Raaymakers and van den Ackerveken) and white rusts (Ruhe et al.).

It is important to remember that some organisms are likely to be actually obligate biotrophs in nature, even if they are still culturable in axenic conditions in the laboratory. The fungi that cause smuts on several plant hosts, the Ustilaginaceae, are thus naturally obligate biotrophs, in the sense that there is no record of growth and reproduction in non-plant or soil environments, in the wild (Brefort et al., 2009).

ONE HAUSTORIUM DOES NOT MAKE A BIOTROPH (PACE ARISTOTLE)

In addition to complex molecular mechanisms aimed at tuning plant immunity, many biotrophic microbial eukaryotes produce complicated morphological structures exquisitely adapted at abstracting nutrient from plant cells: these are termed haustoria. They are terminal branch extensions of the microbial cells and hyphae that penetrate through the cell walls. The most elaborate of these are observed in the arbuscular mycorrhizae, which produce the eponymous "arbuscules" resembling small trees or bushes (hence the name; Calabrese et al.; Manck-Gotzenberger and Requena). Similar structures are made by some of the powdery mildews, in a marvelous example of the evolutionary convergence principle (Parniske, 2000). At the other end of the complexity spectrum, we find the simple bulbous haustoria made by rust fungi and oomycetes. A common feature of all true haustoria/arbuscules is that they are formed by hyphae that penetrate the host cell wall, but do not perforate the plant cell membrane. Rather, the plasma membrane invaginates and gives rise to a new structure, the perihaustorial/periarbuscular membrane, with very special properties that are distinct from the contiguous plasma membrane (Koh et al., 2005). In the organisms that make them, most of the crucial nutrient and signaling exchanges are thought to happen here (Voegele and Mendgen, 2003).

However, biotrophs are not restricted to haustoria-forming fungi. There are plenty of purely apoplastic biotrophs, i.e. biotrophs that do not establish any highly specialized haustoria. Examples of this comprise the fungal tomato pathogen *Cladosporium fulvum* (Joosten and de Wit, 1999) and the corn smut pathogen *U. maydis* (Brefort et al., 2009). Self-evidently, exchanges between plant host and the microbial "guest" must take place in the apoplast in these instances. It should be noted, though, that apoplastic signaling can also be relevant in interactions where haustoria are formed (Raaymakers and van den Ackerveken). A most extreme form of apoplastic biotrophy is evident in the so-called "endophytic" microbes (Voisey et al.). These are microorganisms that colonize plant hosts, *prima facie* asymptomatically. In recent years, the importance and potential of these interactions has been recognized and led to concerted efforts at exploiting the advantages conferred on the host in terms of enhanced resistance to pathogen infection, for example (Johnson et al., 2013). Conversely, there are also pathogens such as many of the *Phytophthora* species that are traditionally regarded as necrotrophs (at least for the most agronomically significant part of their infection cycle) that make *bona fide* haustoria (Whisson et al., 2016).

HEMIBIOTROPHS: INTERACTIONS THAT STRADDLE THE DIVIDE

Typical hemibiotrophic microbes start off with an asymptomatic phase (Di et al.), which then switches to a killing spree—the necrotrophic phase when host cell death is commonly associated with extensive microbial colonization and sporulation. An intriguing question is whether the asymptomatic phase can be equated with true biotrophy. The crucial point is whether at this time the microbe is active, growing and taking up nutrients from the host (in which case we have true biotrophy), or whether they are simply surviving on endogenous stored reserves (in which case they are not really biotrophs). A further possibility is that the microbial partner is actually dormant and hence it might be truly justified to call this a latent phase. Of course, a last option is that the microbe is simply undetectable, relative to the clearly visible biomass at later stages, when exponential growth accompanies the necrotrophic phase, and sporulation. Defining which of these is true is challenging because there is very little microbial biomass per plant tissue at this time. Molecular biology-based methodologies or advanced transcriptome analysis are now sensitive enough (O'Connell et al., 2012; Bindschedler et al.; Kulkarni et al.; Kunjeti et al.; Shu et al.), but biochemical and physiological analysis may be difficult, or impossible, with current methodologies.

If the first phase of infection in hemibiotrophs is truly biotrophic, we may then ask ourselves what the position of archetypal necrotrophs really is. In *Botrytis*, that phase is usually described as latent. But is it? It is becoming apparent that there are intriguing instances of truly endophytic *Botrytis* species (Shaw et al.). These are normally concealed due to their intrinsically asymptomatic nature. Then there are pathogens that do not know what they are: take *Leptosphaeria maculans*, the fungus that causes black-leg on brassicas (Sonah et al.). These start off with a short a symptomatic/biotrophic infection on leaves, which switch to necrotrophy visible as dead leaf lesions. The disease then turns to an asymptomatic/biotrophic and endophytic stage in which the fungus grows intercellularly, reaching the crown of the mature plant where necrotrophic cankers are formed. *L. maculans* is clearly a fungus with many tricks up its sleeve.

THE TECHNICAL CHALLENGES OF STUDYING BIOTROPHY

A significant number of microbes that grow on plants causing disease, or even those with a mutualistic steady state, cannot be grown in axenic ("pure") culture. This big drawback severely limits experimentation, as it is difficult to collect enough biological material for biochemical and physiological experimentation. All manipulations are to be done in presence of a host, complicating biochemical and other types of analyses. Additionally, with few exceptions, genetic manipulations of these microorganisms are either extremely laborious or impossible at present. This hampers tremendously cell biological and functional analysis of the respective plant-microbe interactions (Bindschedler et al.). Novel techniques and methodologies, e.g., for the visualization of encounters between plants and biotrophs (Ghareeb et al.) are thus highly desired to further expand the tool-box to study these organisms.

RESISTANCE AGAINST BIOTROPHIC PATHOGENS

The plant immune system evolved to cope also with biotrophic pathogens. A key initial event of immunity is the perception of pathogen-derived molecules ("patterns") by membrane-resident receptors (often dubbed pattern recognition receptors; Raaymakers and van den Ackerveken; Rajaraman et al.). A second layer of plant defense rests on the direct or indirect recognition of secreted pathogen effectors ("avirulence proteins"; Bourras et al.) by typically cytoplasmic immune sensors ("resistance proteins"; also termed nucleotide binding-oligomerisation domain (NOD)-like receptors) that usually confer isolate-specific resistance (Williams et al.). Execution of the actual defense response often involves re-organization of the host cytoskeleton (Tang et al.) and secretory activity (Xu et al.; Liu et al.). In addition, phytohormone signaling (Di et al.; Guerreiro et al.) and other plant components may contribute to resistance (Liu et al.), or immunity might be conditioned by the absence of essential host factors (Zheng et al.).

MUTUAL INFLUENCE OF BIOTROPHS AND OTHER MICROBES

A largely neglected aspect of the biology of interactions between plants and biotrophic microbes is their modulation by any third partner(s). In fact, the rhizosphere and phyllosphere of plants is colonized by various epi-/endophytes, and multiple pathogens and/or symbionts may occur at the same time on a given plant. Thus, biotrophic microbes may need to compete with other microorganisms for their ecological niche (Ruhe et al.). This might cause altered infection phenotypes of biotrophic pathogens in the presence of other pathogens (Orton and Brown) or epi-/endophytes (Gafni et al.) and also could result in modulation of symbiotic interactions by phytopathogens (Souza et al.).

CONCLUDING REMARKS

Despite significant progress in various areas, the analysis of interactions between plants and biotrophic microbes remains a challenging business. In the short term, we expect that expanding research efforts in those areas such as gen- and other –omics is likely to yield dividends even for the more intractable associations (Bindschedler et al.). Moreover, we predict that a mechanistic understanding of how the plethora of effectors, which appear to be encoded by all microbes interacting with plants, will undoubtedly progress

our knowledge of the complexities of interkingdom signaling. It remains to be seen how all of this may eventually be translated into a capacity to intervene to mitigate the action of harmful pathogens and further the activity of desirable ones.

AUTHOR CONTRIBUTIONS

RP and PS jointly wrote and edited the text.

FUNDING

PS was supported by the BBSRC grant BB/M000710/1. Research in the lab of RP is currently supported by the following grants of the Deutsche Forschungsgemeinschaft (DFG): ERA-CAPS "DURESTrit" (PA861/13-1), priority program SPP1819 "Rapid evolutionary adaptation: potential and constraints; PA861/14-1) and the ANR-DFG cooperation "X-KINGDOM-MIF" (PA861/15-1).

REFERENCES

Brefort, T., Doehlemann, G., Mendoza-Mendoza, A., Reissmann, S., Djamei, A., Kahmann, R., et al. (2009). *Ustilago maydis* as a pathogen. *Annu. Rev. Phytopathol.* 47, 423–445. doi: 10.1146/annurev-phyto-080508-081923

Delaye, L., García-Guzmán, G., and Heil, M. (2013). Endophytes versus biotrophic and necrotrophic pathogens—are fungal lifestyles evolutionarily stable traits? *Fungal Divers.* 60, 125–135. doi: 10.1007/s13225-013-0240-y

Glazebrook, J. (2005). Contrasting mechanisms of defense against biotrophic and necrotrophic pathogens. *Annu. Rev. Phytopathol.* 43, 205–227. doi: 10.1146/annurev.phyto.43.040204.135923

Johnson, L. J., Bonth, A. C. M., de Briggs, L. R., Caradus, J. R., Finch, S. C., Fleetwood, D. J., et al. (2013). The exploitation of epichloae endophytes for agricultural benefit. *Fungal Divers.* 60, 171–188. doi: 10.1007/s13225-013-0239-4

Joosten, M., and de Wit, P. (1999). THE TOMATO-*CLADOSPORIUM FULVUM* INTERACTION: a versatile experimental system to study plant-pathogen interactions. *Annu. Rev. Phytopathol.* 37, 335–367. doi: 10.1146/annurev.phyto.37.1.335

Koh, S., André, A., Edwards, H., Ehrhardt, D., and Somerville, S. (2005). *Arabidopsis thaliana* subcellular responses to compatible *Erysiphe cichoracearum* infections. *Plant J.* 44, 516–529. doi: 10.1111/j.1365-313X.2005.02545.x

Lewis, D. H. (1973). Concepts in fungal nutrition and the origin of biotrophy. *Biol. Rev.* 48, 261–277. doi: 10.1111/j.1469-185X.1973.tb00982.x

Martin, F., Kohler, A., Murat, C., Veneault-Fourrey, C., and Hibbett, D. S. (2016). Unearthing the roots of ectomycorrhizal symbioses. *Nat. Rev. Microbiol.* 14, 760–773. doi: 10.1038/nrmicro.2016.149

O'Connell, R. J., Thon, M. R., Hacquard, S., Amyotte, S. G., Kleemann, J., Torres, M. F., et al. (2012). Lifestyle transitions in plant pathogenic *Colletotrichum* fungi deciphered by genome and transcriptome analyses. *Nat. Genet.* 44, 1060–1065. doi: 10.1038/ng.2372

Oliver, R. P., and Solomon, P. S. (2010). New developments in pathogenicity and virulence of necrotrophs. *Curr. Opin. Plant Biol.* 13, 415–419. doi: 10.1016/j.pbi.2010.05.003

Parniske, M. (2000). Intracellular accommodation of microbes by plants. A common developmental program for symbiosis and disease? *Curr. Opin. Plant Biol.* 3, 320–328. doi: 10.1016/S1369-5266(00)00088-1

Spanu, P., and Kämper, J. (2010). Genomics of biotrophy in fungi and oomycetes - emerging patterns. *Curr. Opin. Plant Biol.* 13, 409–414. doi: 10.1016/j.pbi.2010.03.004

Vleeshouwers, V. G. A. A., and Oliver, R. P. (2014). Effectors as tools in disease resistance breeding against biotrophic, hemibiotrophic, and necrotrophic plant pathogens. *Mol. Plant-Microbe Interact.* 27, 196–206. doi: 10.1094/MPMI-10-13-0313-IA

Voegele, R. T., and Mendgen, K. (2003). Rust haustoria. Nutrient uptake and beyond. *New Phytol.* 159, 93–100. doi: 10.1046/j.1469-8137.2003.00761.x

Whisson, S. C., Boevink, P. C., Wang, S., and Birch, P. R. (2016). The cell biology of late blight disease. *Curr. Opin. Microbiol.* 34, 127–135. doi: 10.1016/j.mib.2016.09.002

Conflict of Interest Statement: The authors declare that the research was conducted in the absence of any commercial or financial relationships that could be construed as a potential conflict of interest.

frontiers in Plant Science

OPINION
published: 21 January 2016
doi: 10.3389/fpls.2016.00015

Plant Pathogens Affecting the Establishment of Plant-Symbiont Interaction

Eduardo M. de Souza[1], *Camille E. Granada*[1,2] *and Raul A. Sperotto*[1,3]*

[1] *Programa de Pós-Graduação em Biotecnologia, Centro Universitário UNIVATES, Lajeado, Brazil,* [2] *Centro de Gestão Organizacional, Centro Universitário UNIVATES, Lajeado, Brazil,* [3] *Setor de Genética e Biologia Molecular do Museu de Ciências Naturais, Centro de Ciências Biológicas e da Saúde, Centro Universitário UNIVATES, Lajeado, Brazil*

Keywords: mycorrhiza, rhizobium, signal transduction, pathogen, symbiont, plant interaction

Hundreds of different microorganisms are attached to the surface of roots. Therefore, it is not surprising that plants have the ability to distinguish threatening intruders from beneficial microbiota (Tóth and Stacey, 2015). Pathogens can be discriminated by plant cells through a myriad of plasma membrane and intracellular receptors that recognize molecules released by microbes, in a process called innate immune system. In spite of the immune ability of plants to prevent pathogen infection, symbiotic signaling molecules are perceived by the host plant, triggering signaling cascades that lead to symbiont infection and accommodation (Tóth and Stacey, 2015). However, some symbiotic signaling molecules can induce responses that are normally associated with plant innate immunity (Pauly et al., 2006), and several observations that are consistent with a rapid, defense-like response occurring in legumes when infected by rhizobia have been obtained, mainly involving programmed cell death, cell wall thickening, reactive oxygen species (ROS) generation, defense phytohormones and salicylic acid (SA) production (Jones and Dangl, 2006; Stacey et al., 2006; Dodds and Rathjen, 2010; Montiel et al., 2012). Similar to bacterial pathogens, symbionts alone also have the ability to actively suppress innate immune response, as previously shown (Liang et al., 2013).

Plant-symbiont-pathogen interaction is an emerging topic, and several questions in this field have been elucidated in the recent years. However, the main focus of these studies is commonly limited to the effects of symbiont microorganisms on the activation of plant defense responses and elicitation of induced systemic resistance to pathogens (Pieterse et al., 2001; de Vleeschauwer and Höfte, 2009), which usually does not come with the normal costs of reduced growth rates and reproductive outcomes in resistance-expressing plants (Spaepen et al., 2009). Studies considering plant pathogens as limiting factors to the symbiosis establishment are still scarce (Faessel et al., 2010; de Román et al., 2011; van Dam and Heil, 2011; Ballhorn et al., 2014). However, such studies are highly relevant for the use of symbiotic inoculum in particular in monocultures of pathogen-susceptible crops. In this opinion article, we focus on rhizobial and mycorrhizal symbiosis inhibition mediated by plant pathogens. We present the current state-of-the-art through the compilation and comparison of available information that can help to elucidate intriguing questions, as the sensing and signaling of plant-symbiont-pathogen interaction.

DIRECT ANTAGONISM BETWEEN PLANT PATHOGENS AND SYMBIONT MICROORGANISMS

From the moment that plant pathogens and symbionts make plant tissues their major source of space, C, N, and other nutrients, both start to compete frequently. One of the main mechanisms employed in this contest is direct antagonism, which is well studied from the "symbiont against

OPEN ACCESS

Edited by:
Ralph Panstruga,
RWTH Aachen University, Germany

Reviewed by:
Sebastian Schornack,
University of Cambridge, UK
Hannah Kuhn,
RWTH Aachen University, Germany

***Correspondence:**
Raul A. Sperotto
rasperotto@univates.br

Specialty section:
This article was submitted to Plant Biotic Interactions, a section of the journal Frontiers in Plant Science

Received: *24 November 2015*
Accepted: *07 January 2016*
Published: *21 January 2016*

Citation:
de Souza EM, Granada CE and Sperotto RA (2016) Plant Pathogens Affecting the Establishment of Plant-Symbiont Interaction. Front. Plant Sci. 7:15. doi: 10.3389/fpls.2016.00015

pathogen" perspective (Kumar et al., 2011). This antagonism is based on the production of several antimicrobial products, which act mostly on the rhizosphere (Mucha et al., 2006, 2009; Zou et al., 2007). However, both involved players can attack, defend and counterattack (Raaijmakers et al., 2009). Pathogens are able to respond by inactivating symbiont genes responsible for antimicrobial production, along with changing their own metabolism in order to tolerate the attacks, or even synthesizing substances able to inactivate the antimicrobial product (Duffy et al., 2003; Schouten et al., 2004). Such defense mechanisms against antimicrobial activities initiated by symbionts allow the resistance of soil-borne (on the rhizosphere) and above ground pathogens (on the shoots).

Plant pathogens are also able to attack their opponents using similar molecular weapons (Duffy et al., 2003), which include hydrogen cyanide (Benizri et al., 2005), alkaloids (Antunes et al., 2008), and bacteriocins (Holtsmark et al., 2008). Most of the secondary metabolites produced by plant pathogens are probably unknown, due to the fact that in multi-species communities (as the rhizosphere environment), the myriad of produced compounds tends to be different from that produced in laboratory conditions, using isolated cultures (Netzker et al., 2015). Using such weapons, plant pathogens can modify the structure and abundance of soil microbial populations, including plant symbionts (Mrabet et al., 2006; Liu et al., 2010; Chihaoui et al., 2012), causing deleterious impacts for both plant and microorganism. Even though some studies report a reduction on the symbiosis process in plants inoculated with plant pathogens or even an inhibition on the symbiont development of *in vitro* dual culture, most of them do not investigate the sequential events which lead to symbiosis or symbiont development failure (Muthomi et al., 2007; Lahlali and Hijri, 2010). Such sequential molecular events should be better investigated preferably mimicking natural conditions, in order to be applied to increase the success of agricultural inoculation and plant symbiont interaction.

In a recent report, Sillo et al. (2015) used morphological and gene expression analyses to show an inhibition of the ectomycorrhizal growth caused by phytopathogenic fungus in dual culture conditions. The expression analysis of genes related to cell wall hydrolytic enzymes and hydrophobins, putatively involved in the fungus-fungus interaction, allowed the identification of significantly up- and down-regulated genes in both symbiont and pathogens. Apparently, the inhibition process involves chitinolytic enzymes. As the mRNA levels can be different from the protein levels or activities, the study of both fungal secretomes and metabolomes could be effective for a better understanding of this process.

MYCORRHIZAL AND RHIZOBIAL SYMBIOSIS INDIRECTLY INHIBITED BY PLANT PATHOGENS

Plants present several mechanisms to control infections by deleterious organisms. One of the most rapid defense reactions to pathogen attack is the so-called oxidative burst, which includes ROS production (Apel and Hirt, 2004; Gechev et al., 2006; Nanda et al., 2010), along with synthesis of the endogenous signaling molecule salicylic acid (SA—de Román et al., 2011). ROS cause directly strengthening of cell walls via cross-linking of glycoproteins (Delaney et al., 1994; Torres et al., 2006) and SA activates synthesis of chitinase and β-1,3-glucanase, which contribute to a broad-spectrum resistance against diverse bacteria, fungi and viruses (de Román et al., 2011).

Some of the resistance mechanisms, however, may exert ecological costs when they have a negative effect on beneficial plant-microbe interactions. Even though there is increasing evidence that ROS are needed to fully establish the symbiosis, Lohar et al. (2007), Cárdenas et al. (2008) and Munoz et al. (2012) related that ROS elevation might provoke a rhizobial infection abortion in *Medicago truncatula*, *Phaseolus vulgaris,* and *Glycine max* plants, respectively. Since ROS can act as secondary messengers impacting many processes during plant defense, the elucidation of the mechanisms that control ROS signaling during symbiosis could contribute in defining a powerful strategy to enhance the efficiency of the symbiotic interaction. Also, Blilou et al. (1999) and Stacey et al. (2006) showed that reduced levels of SA results in increased rhizobial infection in *Lotus japonicus*, *M. truncatula,* and *Pisum sativum*. Exogenous SA application in alfalfa plants results in inhibition of nodule primordia formation and reduction in emerging nodules number (Martínez-Abarca et al., 1998). Interestingly, exogenous SA application completely blocks nodulation of *Vicia sativa* (vetch, an indeterminate-type nodulating plant) by *Rhizobium leguminosarum*. In contrast, addition of SA to *Lotus japonicus* (a determinate-type nodulating plant) does not inhibit nodulation by *Mesorhizobium loti* (van Spronsen et al., 2003). Further efforts should be made to find molecular mechanisms that regulate the different signal transduction pathways of indeterminate- and determinate-type nodulating plants in response to SA.

Mycorrhizal infection is also probably being influenced by SA-dependent defense mechanisms, since enhanced SA levels are detected in mycorrhiza-resistant mutant (*myc*$^{-}$) of *Pisum sativum* in comparison to wild type plants (Blilou et al., 1999), and exogenous SA applied to rice roots reduces mycorrhization at the early stage of plant infection (Blilou et al., 2000). Also, SA reduction leads to elevation of mycorrhizal colonization, infection units, and arbuscules. On the contrary, in tobacco plants that constitutively produce elevated levels of SA, lower colonization levels are observed (Herrera Medina et al., 2003). During rhizobial colonization, SA seems to suppress infection thread formation, but for mycorrhizal colonization the exact stage of inhibition has not been described, although prepenetration apparatus formation seems to be a good target candidate (Gutjahr and Paszkowski, 2009).

Such negative effects may even cross the border between a plant's aerial parts and its roots (de Román et al., 2011; van Dam and Heil, 2011). Induction of SA-dependent resistance to pathogens in foliar tissues of soybean plants, transiently inhibit the mycorrhization of soybean roots (Faessel et al., 2010; de Román et al., 2011), confirming a negative impact of the elicitation of foliar defenses on root-mycorrhizal interactions. According to de Román et al. (2011), the negative effect is likely

linked to changes in the defense status of the plant rather than to changes in resource allocation patterns, since no allocation or fitness costs associated with the induction of resistance are detected. Recently, Ballhorn et al. (2014) showed that an aboveground hemibiotrophic plant pathogen induces a defense response that inhibits the belowground mycorrhizal colonization, and that systemically induced polyphenol oxidase activity is functionally involved in this aboveground-belowground interaction.

Induced plant resistance against pathogen causes no significant effect on the frequency of mycorrhizal colonization in soybean roots, but reduces the intensity of colonization and the proportion of arbuscules, along with the number of *Bradyrhizobium* nodules (Faessel et al., 2010). A similar pattern was shown in pea *myc*$^{-2}$ mutants (Gianinazzi-Pearson et al., 1991), in which the fungus is able to form appressoria and penetrate into roots, but fails to form arbuscules. Also, the mutant *myc*$^{-2}$ was characterized by an enhanced expression of the *Psam4* (*Pisum sativum arbuscular mycorrhiza-regulated*) gene, which encodes a proline-rich protein, generally associated with cell wall strengthening in plant-pathogen interaction (Marsh and Schultze, 2001). In *Medicago truncatula* hairy roots, PR-10 (pathogenesis-related-10) protein is upregulated in root cells close to the hyphopodium and subsequently repressed during formation and fungal passage of the prepenetration apparatus (Siciliano et al., 2007). Only local, weak, and transient defense responses are activated during early steps of beneficial plant microbe interactions, and low amounts of ROS and SA are necessary in the earlier steps of both rhizobial and mycorrhyzal symbiosis (Faessel et al., 2010), facilitating the access of these microorganisms inside the plant tissue. Local defense responses, such as chitinase and β-1,3-glucanase activities are enhanced during early steps of compatible mycorrhizal interactions (Pozo and Azcón-Aguilar, 2007), but these enzymatic activities are repressed at a later stage of mycorrhiza formation. Rhizobia produce cyclic β-glucans suppressing the induction of plant defense (Mithöfer et al., 1996), starting cortical cells division which lead to a nodule primordium (Tóth and Stacey, 2015). It would be interesting to test whether the spatio-temporal expression pattern of PR-10 protein correlates with SA activity, as well as combining SA application with high-resolution imaging in order to check the effect of SA in early infection structures.

It is important to highlight that some studies use acibenzolar S-methyl (ASM) as a synthetic inducer of the SA pathway. ASM induces successful disease resistance in many plant-pathogen combinations, but there are also reports where it did not significantly induce resistance (Heil, 2007). Therefore, effects of ASM have to be evaluated for each plant-pathogen combination. Unexpectedly, the P content of soybean increases when ASM is applied to leaves (Faessel et al., 2010). One plausible explanation is that ASM interacts with root exudation of organic acids, which in turn mobilize insoluble P. Another explanation would be that ASM regulates still unknown functions of plant development which compensate mycorrhization inhibition, probably caused by enhanced P nutrition. Field studies are required to confirm these side-effects and their possible consequences on crop yield. This is an example why experiments should preferably be carried out at densities and scenarios as realistic as possible, since we can expect plants to be adapted only to events that are common over evolutionary time spans. Future studies aiming toward the identification of the mechanisms in this co-operative effort should involve studying the interaction under different nutrient conditions and densities of rhizobial/mycorrhizal colonization and monitoring physiological and transcriptomic changes in both plant roots and symbiont microorganism during the various phases of the interaction.

FUTURE PERSPECTIVES

We must admit that there is a gap on the evaluation of plant pathogen effects over the symbiosis capacity of rhizobia and mycorrhiza. This type of analysis should be more and more stimulated, since the evaluation of putative interferences from plant pathogens in plant-symbiont interactions is mandatory to enhance the effectiveness of the application of agricultural inoculants in natural environments. It is already known that pathogens and symbionts might utilize identical or overlapping molecular mechanisms for their colonization (Wang et al., 2012; Rey et al., 2015), further complicating the study of plant-symbiont-pathogen interaction. In order to better understand this triple interaction, *omic* analyses in controlled systems, containing the host plant and micro-symbionts, could provide valuable information to complement knowledge acquired through studies on the competition of pathogen and symbiont. Such studies can identify molecular players which act in different levels (RNAs, proteins, enzymatic activities, metabolites, inhibitors, and enhancers), and some of them are probably putative targets for enhanced efficiency of plant-symbiont interaction.

AUTHOR CONTRIBUTIONS

ED, CG, and RS wrote the paper.

ACKNOWLEDGMENTS

The authors are supported by FAPERGS and Centro Universitário UNIVATES.

REFERENCES

Antunes, P. M., Miller, J., Carvalho, L. M., Klironomos, J. N., and Newman, J. A. (2008). Even after death the endophytic fungus of *Schedonorus phoenix* reduces the arbuscular mycorrhizas of other plants. *Funct. Ecol.* 22, 912–918. doi: 10.1111/j.1365-2435.2008.01432.x

Apel, K., and Hirt, H. (2004). Reactive oxygen species: metabolism, oxidative stress and signal transduction. *Annu. Rev. Plant*

Biol. 55, 373–379. doi: 10.1146/annurev.arplant.55.031903.141701

Ballhorn, D. J., Younginger, B. S., and Kautz, S. (2014). An aboveground pathogen inhibits belowground rhizobia and arbuscular mycorrhizal fungi in *Phaseolus vulgaris*. *BMC Plant Biol.* 14:321. doi: 10.1186/s12870-014-0321-4

Benizri, E., Piutti, S., Verger, S., Pagès, L., Vercambre, G., Poessel, J. L., et al. (2005). Replant diseases: bacterial community structure and diversity in peach rhizosphere as determined by metabolic and genetic fingerprinting. *Soil Biol. Biochem.* 37, 1738–1746. doi: 10.1016/j.soilbio.2005.02.009

Blilou, I., Ocampo, J. A., and Garcia-Garrido, J. M. (1999). Resistance of pea roots to endomycorrhizal fungus or *Rhizobium* correlates with enhanced levels of endogenous salicylic acid. *J. Exp. Bot.* 50, 1663–1668. doi: 10.1093/jxb/50.340.1663

Blilou, I., Ocampo, J. A., and García-Garrido, J. M. (2000). Induction of Ltp (lipid transfer protein) and Pal (phenylalanine ammonia lyase) gene expression in rice roots colonized by the arbuscular mycorrhizal fungus *Glomus mosseae*. *J. Exp. Bot.* 51, 1969–1977. doi: 10.1093/jexbot/51.353.1969

Cárdenas, L., Martínez, A., Sánchez, F., and Quinto, C. (2008). Fast, transient and specific intracellular ROS changes in living root hair cells responding to Nod factors (NFs). *Plant J.* 56, 802–813. doi: 10.1111/j.1365-313X.2008.03644.x

Chihaoui, S. A., Mhadhbi, H., and Mhamdi, R. (2012). The antibiosis of nodule-endophytic agrobacteria and its potential effect on nodule functioning of *Phaseolus vulgaris*. *Arch. Microbiol.* 194, 1013–1021. doi: 10.1007/s00203-012-0837-7

Delaney, T. P., Uknes, S., Vernooij, B., Friedrich, L., Weymann, K., Negrotto, D., et al. (1994). A central role of salicylic Acid in plant disease resistance. *Science* 266, 1247–1250. doi: 10.1126/science.266.5188.1247

de Román, M., Fernández, I., Wyatt, T., Sahrawy, M., Heil, M., and Pozo, M. J. (2011). Elicitation of foliar resistance mechanisms transiently impairs root association with arbuscular mycorrhizal fungi. *J. Ecol.* 99, 7–15. doi: 10.1111/j.1365-2745.2010.01752.x

de Vleeschauwer, D., and Höfte, M. (2009). "Rhizobacteria-induced systemic resistance," in *Plant Innate Immunity,* ed L. C. van Loon (London: Elsevier), 224–283.

Dodds, P. N., and Rathjen, J. P. (2010). Plant immunity: towards an integrated view of plant–pathogen interactions. *Nat. Rev. Genet.* 11, 539–548. doi: 10.1038/nrg2812

Duffy, B., Schouten, A., and Raaijmakers, J. M. (2003). Pathogen self-defense: mechanisms to counteract microbial antagonism. *Annu. Rev. Phytopathol.* 41, 501–538. doi: 10.1146/annurev.phyto.41.052002.095606

Faessel, L., Nassr, N., Lebeau, T., and Walter, B. (2010). Chemically-induced resistance on soybean inhibits nodulation and mycorrhization. *Plant Soil* 329, 259–268. doi: 10.1007/s11104-009-0150-7

Gechev, T. S., Van Breusegem, F., Stone, J. M., Denev, I., and Laloi, C. (2006). Reactive oxygen species as signals that modulate plant stress responses and programmed cell death. *Bioessays* 28, 1091–1101. doi: 10.1002/bies.20493

Gianinazzi-Pearson, V., Gianinazzi, S., Guillemin, J. P., Trouvelot, A., and Duc, G. (1991). "Genetic and cellular analysis of resistance to vesicular arbuscular (VA) mycorrhizal fungi in pea mutants," in *Advances in Molecular Genetics of Plant-Microbe Interactions*, eds H. Hennecke and D. P. S. Verma (Dordrecht: Springer), 336–342.

Gutjahr, C., and Paszkowski, U. (2009). Weights in the balance: Jasmonic Acid and Salicylic Acid signaling in root-biotroph interactions. *Mol. Plant Microbe Interact.* 22, 763–772. doi: 10.1094/MPMI-22-7-0763

Heil, M. (2007). "Trade-offs associated with induced resistance," in *Induced Resistance for Plant Defence: A Sustainable Approach to Crop Protection*, eds D. Walters, C. A. Newton, and G. D. Lyon (Oxford: Blackwell), 157–177.

Herrera Medina, M. J., Gagnon, H., Piché, Y., Ocampo, J. A., García Garrido, J. M., and Vierheilig, H. (2003). Root colonization by arbuscular mycorrhizal fungi is affected by the salicylic acid content of the plant. *Plant Sci.* 164, 993–998. doi: 10.1016/S0168-9452(03)00083-9

Holtsmark, I., Eijsink, V. G., and Brurberg, M. B. (2008). Bacteriocins from plant pathogenic bacteria. *FEMS Microbiol. Lett.* 280, 1–7. doi: 10.1111/j.1574-6968.2007.01010.x

Jones, J. D., and Dangl, J. L. (2006). The plant immune system. *Nature* 444, 323–329. doi: 10.1038/nature05286

Kumar, H., Dubey, R. C., and Maheshwari, D. K. (2011). Effect of plant growth promoting rhizobia on seed germination, growth promotion and suppression of Fusarium wilt of fenugreek (*Trigonella foenum-graecum* L.). *Crop Prot.* 30, 1396–1403. doi: 10.1016/j.cropro.2011.05.001

Lahlali, R., and Hijri, M. (2010). Screening, identification and evaluation of potential biocontrol fungal endophytes against *Rhizoctonia solani* AG3 on potato plants. *FEMS Microbiol. Lett.* 311, 152–159. doi: 10.1111/j.1574-6968.2010.02084.x

Liang, Y., Cao, Y., Tanaka, K., Thibivilliers, S., Wan, J., Choi, J., et al. (2013). Non legumes respond to rhizobial Nod factors by suppressing the innate immune response. *Science* 341, 1384–1387. doi: 10.1126/science.1242736

Liu, J., Wang, E. T., Ren, D. W., and Chen, W. X. (2010). Mixture of endophytic *Agrobacterium* and *Sinorhizobium meliloti* strains could induce nonspecific nodulation on some woody legumes. *Arch. Microbiol.* 192, 229–234. doi: 10.1007/s00203-010-0543-2

Lohar, D. P., Haridas, S., Gantt, J. S., and VandenBosch, A. (2007). A transient decrease in reactive oxygen species in roots leads to root hair deformation in the legume-rhizobia symbiosis. *New Phytol.* 173, 39–49. doi: 10.1111/j.1469-8137.2006.01901.x

Marsh, J. F., and Schultze, M. (2001). Analysis of arbuscular mycorrhiza using symbiosis-defective plant mutants. *New Phytol.* 150, 525–532. doi: 10.1046/j.1469-8137.2001.00140.x

Martínez-Abarca, F., Herrera-Cervera, J. A., Bueno, P., Sanjuan, J., Bisseling, T., and Olivares, J. (1998). Involvement of salicylic acid in the establishment of the *Rhizobium meliloti* – Alfalfa symbiosis. *Molec. Plant-Microbe Interac.* 11, 153–155. doi: 10.1094/MPMI.1998.11.2.153

Mithöfer, A., Bhagwat, A. A., Feger, M., and Ebel, J. (1996). Suppression of fungal β-glucan-induced plant defense in soybean (*Glycine max*) by cyclic 1,3-1,6-β-glucans from the symbiont *Bradyrhizobium japonicum*. *Planta* 199, 270–275. doi: 10.1007/BF00196568

Montiel, J., Nava, N., Cárdenas, L., Sánchez-López, R., Arthikala, M. K., Santana, O., et al. (2012). A *Phaseolus vulgaris* NADPH oxidase gene is required for root infection by Rhizobia. *Plant Cell Physiol.* 53, 1751–1767. doi: 10.1093/pcp/pcs120

Mrabet, M., Mnasri, B., Romdhane, S. B., Laguerre, G., Aouani, M. E., and Mhamdi, R. (2006). Agrobacterium strains isolated from root nodules of common bean specifically reduce nodulation by *Rhizobium gallicum*. *FEMS Microbiol. Ecol.* 56, 304–309. doi: 10.1111/j.1574-6941.2006.00069.x

Mucha, J., Dahm, H., Strzelczyk, E., and Werner, A. (2006). Synthesis of enzymes connected with mycoparasitism by ectomycorrhizal fungi. *Arch. Microbiol.* 185, 69–77. doi: 10.1007/s00203-005-0068-2

Mucha, J., Zadworny, M., and Werner, A. (2009). Cytoskeleton and mitochondrial morphology of saprotrophs and the pathogen *Heterobasidion annosum* in the presence of *Suillus bovinus* metabolites. *Mycol. Res.* 113, 981–990. doi: 10.1016/j.mycres.2009.06.002

Munoz, N., Robert, G., Melchiorre, M., Racca, R., and Lascano, R. (2012). Saline and osmotic stress differentially affects apoplastic and intracellular reactive oxygen species production, curling and death of root hair during *Glycine max* L.–*Bradyrhizobium japonicum* interaction. *Environm. Experim. Botany* 78, 76–83. doi: 10.1016/j.envexpbot.2011.12.008

Muthomi, J. W., Otieno, P. E., Cheminingwa, G. N., Nderitu, J. H., and Wagacha, J. M. (2007). Effect of legume root rot pathogens and fungicide seed treatment on nodulation and biomass accumulation. *J. Biol. Sci.* 7, 1163–1170. doi: 10.3923/jbs.2007.1163.1170

Nanda, A. K., Andrio, E., Marino, D., Pauly, N., and Dunand, C. (2010). Reactive oxygen species during plant-microorganism early interactions. *J. Integrat. Plant Biol.* 52, 195–204. doi: 10.1111/j.1744-7909.2010.00933.x

Netzker, T., Fischer, J., Weber, J., Mattern, D. J., König, C. C., Valiante, V., et al. (2015). Microbial communication leading to the activation of silent fungal secondary metabolite gene clusters. *Front. Microbiol.* 6:299. doi: 10.3389/fmicb.2015.00299

Pauly, N., Pucciariello, C., Mandon, K., Innocenti, G., Jamet, A., Baudouin, E., et al. (2006). Reactive oxygen and nitrogen species and glutathione: key players in the legume-Rhizobium symbiosis. *J. Exp. Bot.* 57, 1769–1776. doi: 10.1093/jxb/erj184

Pieterse, C. M. J., van Pelt, J. A., van Wees, S. C. M., Ton, J., Léon-Kloosterziel, K., Keurentjes, J. J. B., et al. (2001). Rhizobacteria-mediated induced systemic resistance: triggering, signalling and expression. *Eur. J. Plant Pathol.* 107, 51–61. doi: 10.1023/A:1008747926678

Pozo, M. J., and Azcón-Aguilar, C. (2007). Unraveling mycorrhiza-induced resistance. *Curr. Opin. Plant Biol.* 10, 393–398. doi: 10.1016/j.pbi.2007.05.004

Raaijmakers, J. M., Paulitz, T. C., Steinberg, C., Alabouvette, C., and Moënne-Loccoz, Y. (2009). The rhizosphere: a playground and battlefield for soilborne pathogens and beneficial microorganisms. *Plant Soil* 321, 341–361. doi: 10.1007/s11104-008-9568-6

Rey, T., Chatterjee, A., Buttay, M., Toulotte, J., and Schornack, S. (2015). *Medicago truncatula* symbiosis mutants affected in the interaction with a biotrophic root pathogen. *New Phytol.* 206, 497–500. doi: 10.1111/nph.13233

Schouten, A., van den Berg, G., Edel-Hermann, V., Steinberg, C., Gautheron, N., Alabouvette, C., et al. (2004). Defense responses of *Fusarium oxysporum* to 2, 4-diacetylphloroglucinol, a broad-spectrum antibiotic produced by *Pseudomonas fluorescens*. *Mol. Plant-Microbe Interact.* 17, 1201–1211. doi: 10.1094/MPMI.2004.17.11.1201

Siciliano, V., Genre, A., Balestrini, R., Cappellazzo, G., de Wit, P. J. G. M., and Bonfante, P. (2007). Transcriptome analysis of arbuscular mycorrhizal roots during development of the prepenetration apparatus. *Plant Physiol.* 144, 1455–1466. doi: 10.1104/pp.107.097980

Sillo, F., Zampieri, E., Giordano, L., Lione, G., Colpaert, J. V., Balestrini, R., et al. (2015). Identification of genes differentially expressed during the interaction between the plant symbiont *Suillus luteus* and two plant pathogenic allopatric *Heterobasidion* species. *Mycol. Progress* 14, 1–13. doi: 10.1007/s11557-015-1130-3

Spaepen, S., Vanderleyden, J., and Okon, Y. (2009). "Plant growth-promoting actions of rhizobacteria," in *Plant Innate Immunity,* ed L. C. Van Loon (London: Elsevier), 284–321.

Stacey, G., McAlvin, C. B., Kim, S. Y., Olivares, J., and Soto, M. J. (2006). Effects of endogenous salicylic acid on nodulation in the model legumes *Lotus japonicus* and *Medicago truncatula*. *Plant Physiol.* 141, 1473–1481. doi: 10.1104/pp.106.080986

Torres, M. A., Jones, J. D. G., and Dangl, J. L. (2006). Reactive Oxygen Species signaling in response to pathogens. *Plant Physiol.* 141, 373–378. doi: 10.1104/pp.106.079467

Tóth, K., and Stacey, G. (2015). Does plant immunity play a critical role during initiation of the legume-rhizobium symbiosis? *Front. Plant Sci.* 6:401. doi: 10.3389/fpls.2015.00401

van Dam, N. M., and Heil, M. (2011). Multitrophic interactions below and above ground: en route to the next level. *J. Ecol.* 99, 77–88. doi: 10.1111/j.1365-2745.2010.01761.x

van Spronsen, P. C., Tak, T., Rood, A. M., van Brussel, A. A., Kijne, J. W., and Boot, K. J. (2003). Salicylic acid inhibits indeterminate-type nodulation but not determinate-type nodulation. *Mol. Plant Microbe Interact.* 16, 83–91. doi: 10.1094/MPMI.2003.16.1.83

Wang, E., Schornack, S., Marsh, J. F., Gobbato, E., Schwessinger, B., Eastmond, P., et al. (2012). A common signaling process that promotes mycorrhizal and oomycete colonization of plants. *Curr. Biol.* 22, 2242–2246. doi: 10.1016/j.cub.2012.09.043

Zou, C. S., Mo, M. H., Gu, Y. Q., Zhou, J. P., and Zhang, K. Q. (2007). Possible contributions of volatile-producing bacteria to soil fungistasis. *Soil Biol. Biochem.* 39, 2371–2379. doi: 10.1016/j.soilbio.2007.04.009

Conflict of Interest Statement: The authors declare that the research was conducted in the absence of any commercial or financial relationships that could be construed as a potential conflict of interest.

The Guest Associate Editor Ralph Panstruga and Reviewer Hannah Kuhn declared their shared affiliation, and the Editor states that the process nevertheless met the standards of a fair and objective review.

frontiers in Plant Science

ORIGINAL RESEARCH
published: 10 May 2016
doi: 10.3389/fpls.2016.00625

Analysis of Cryptic, Systemic *Botrytis* Infections in Symptomless Hosts

Michael W. Shaw[1], Christy J. Emmanuel[1†], Deni Emilda[2†], Razak B. Terhem[2†], Aminath Shafia[1†], Dimitra Tsamaidi[1†], Mark Emblow[1†] and Jan A. L. van Kan[2]*

[1] School of Agriculture, Policy and Development, University of Reading, Whiteknights, Reading, UK, [2] Laboratory of Phytopathology, Wageningen University, Wageningen, Netherlands

Botrytis species are generally considered to be aggressive, necrotrophic plant pathogens. By contrast to this general perception, however, *Botrytis* species could frequently be isolated from the interior of multiple tissues in apparently healthy hosts of many species. Infection frequencies reached 50% of samples or more, but were commonly less, and cryptic infections were rare or absent in some plant species. Prevalence varied substantially from year to year and from tissue to tissue, but some host species routinely had high prevalence. The same genotype was found to occur throughout a host, representing mycelial spread. *Botrytis cinerea* and *Botrytis pseudocinerea* are the species that most commonly occur as cryptic infections, but phylogenetically distant isolates of *Botrytis* were also detected, one of which does not correspond to previously described species. Sporulation and visible damage occurred only when infected tissues were stressed, or became mature or senescent. There was no evidence of cryptic infection having a deleterious effect on growth of the host, and prevalence was probably greater in plants grown in high light conditions. Isolates from cryptic infections were often capable of causing disease (to varying extents) when spore suspensions were inoculated onto their own host as well as on distinct host species, arguing against co-adaptation between cryptic isolates and their hosts. These data collectively suggest that several *Botrytis* species, including the most notorious pathogenic species, exist frequently in cryptic form to an extent that has thus far largely been neglected, and do not need to cause disease on healthy hosts in order to complete their life-cycles.

Keywords: gray mold, systemic infection, wild vegetation, *Botrytis*

OPEN ACCESS

Edited by:
Pietro Daniele Spanu, Imperial College London, UK

Reviewed by:
Katherine Denby, University of Warwick, UK
Linda Joy Johnson, AgResearch, New Zealand

***Correspondence:**
Jan A. L. van Kan
jan.vankan@wur.nl

†Present Address:
Christy J. Emmanuel, Department of Botany, University of Jaffna, Jaffna, Sri Lanka;
Deni Emilda, Indonesian Agency for Agricultural Research and Development, Indonesian Tropical Fruits Research Institute, Solok, Indonesia;
Razak B. Terhem, Faculty of Forestry, Universiti Putra Malaysia, Serdang, Malaysia;
Aminath Shafia, Ministry of Fisheries and Agriculture, Male, Maldives;
Dimitra Tsamaidi, Faculty of Crop Science, Agricultural University of Athens, Athens, Greece;
Mark Emblow, School of Biological Sciences, University of Bristol, Bristol, UK

Specialty section:
This article was submitted to Plant Biotic Interactions, a section of the journal Frontiers in Plant Science

Received: *19 February 2016*
Accepted: *24 April 2016*
Published: *10 May 2016*

Citation:
Shaw MW, Emmanuel CJ, Emilda D, Terhem RB, Shafia A, Tsamaidi D, Emblow M and van Kan JAL (2016) Analysis of Cryptic, Systemic Botrytis Infections in Symptomless Hosts. Front. Plant Sci. 7:625. doi: 10.3389/fpls.2016.00625

INTRODUCTION

Botrytis is an ascomycete fungal genus of plant pathogens. Most members of the genus are specialized species infecting a narrow range of monocotyledonous host plants. Typically, they are aggressive, necrotrophic pathogens (Staats et al., 2005). Some have an extended quiescent phase following infection (*Botrytis allii*). An exception to the rule of narrow host range is the clade including the species *Botrytis cinerea sensu lato*. This clade is by far the most economically damaging group within the genus; *B. cinerea s.l.* has a recorded host range including over 1400 (mostly dicotyledonous) hosts (Elad et al., 2015). The typical symptoms leading to economic loss are the occurrence of spreading, fast-growing necrotic lesions bearing abundant pigmented, hydrophobic, conidia.

Botrytis conidia are dispersed in windy conditions. Rainfall aids dispersal through the sharp motions of infected tissues resulting from raindrop impact. Conidia require high humidity to infect; infection tests in laboratory are typically performed with high concentrations of spore suspensions (10^6/ml). The likelihood that conidia will produce a lesion is greatly increased if a nutrient source is available due to host cell damage, insect honeydew or exogenously supplied sugars (van den Heuvel, 1981; Dik, 1992).

Typically *B. cinerea* causes loss in crops by damage to the harvestable part of the crop, flowers, fruits, or leaves, or by girdling stems. The tools to manage *B. cinerea* in crops include (partial) host resistance, avoidance of damage allowing saprophytic infections to occur and then spread, environmental modification to reduce the probability of conditions suitable for spore germination and dispersal, and the use of fungicide. The latter can be effective, but typically there are no consistent critical periods. Although in a single experiment, one or a few fungicide application times may stand out as effective, these application times may not be reproducible in repeat experiments or easy to relate to environmental conditions (e.g., McQuilken and Thomson, 2008). Spores are present in low concentrations in the air over most of the year (Hausbeck and Moorman, 1996; Kerssies et al., 1997; Boff et al., 2001; Boulard et al., 2008). A common strategy for application of fungicides is to maintain continuous cover. This is undesirable on environmental and economic grounds and leads to rapid development of resistance to new fungicides.

A number of publications have suggested that a range of plant species may harbor infections by *B. cinerea s.l.* and other species, including *Botrytis deweyae*, which cause no visible symptoms on the plant at the initial time of infection, are long-lived, can be isolated from newly grown host tissues, but cause necrotic lesions as the plant moves into a reproductive phase. Cultivated hosts in which this form of infection has been studied include *Hemerocallis* (Grant-Downton et al., 2014), hybrid commercial *Primula* (Barnes and Shaw, 2002, 2003), and lettuce (Sowley et al., 2010). In wild-growing plants, Rajaguru and Shaw (2010) found widespread infection in leaves of *Taraxacum* and, to a lesser extent, wild *Primula vulgaris*. A sampling for endophytes in *Centaurea stoebe* revealed the frequent occurrence of *Botrytis* spp., including isolates not derived from known species (Shipunov et al., 2008).

It is becoming increasingly clear that this situation is quite common. A simple distinction between pathogens and non-pathogens may not be possible for many fungal species, as several pathogens have extended cryptic phases (Stergiopoulos and Gordon, 2014). The most obvious examples, and most similar to the *Botrytis* case, are seedborne smut fungi (Schafer et al., 2010), with a cryptic phase from seed until flower maturation. In a more complex example, isolates of *Fusarium oxysporum* can cause devastating disease, with individual fungal genotypes often displaying a very narrow host range or be a benign root endophyte (Gordon and Martyn, 1997; Demers et al., 2015), wherein both endophytic and pathogenic behavior appear to be polyphyletic (Gordon and Martyn, 1997).

The discovery of distributed, symptomless infection by *Botrytis* sp. in a range of hosts suggests that a proportion of inoculum might arise from these sources, and that the fungus may exist for an important part as an endophyte or intimate phyllosphere inhabitant, with conidia only being produced when the host approaches the end of its life-cycle. Understanding this cryptic infection is important for controlling the disease in hosts in which it happens, and for managing disease in other hosts where the cryptic form may serve as an unexpected source of inoculum. In this paper we draw together data on plant species that act as hosts to symptomless distributed infections of *Botrytis*; how the infection varies over time and location; whether particular fungal clonal lineages are adapted to particular hosts; the fungal species involved; the effect of the infection on the host. The aim of experiments collated here was to explore an unexpected mode of infection by a fungus often considered to be a "model necrotroph."

MATERIALS AND METHODS

Surface Sterilization

Samples of plant tissues were disinfected with 70% ethanol for 1 min followed by 50% solution of bleach (Domestos, Unilever: 5% NaOCl in alkaline solution with surfactants) for 1 min and rinsed three times in sterile distilled water. In early work, sampled tissues were dipped in paraquat before plating to kill the host tissue and encourage pathogen outgrowth. Seed sterilization was carried out by soaking 0.5 g of seed in 100 ml of 0.10 g/l of the systemic fungicide "Shirlan" (active ingredient 500 g/l Fluazinam, Syngenta Crop Protection UK Ltd.) for 2 h and dried overnight before sowing. This was chosen as the most effective and least phytotoxic of a range of fungicides tested.

Isolation and Culturing, UK

Sampled tissues were placed on plates of *Botrytis* selective medium (Edwards and Seddon, 2001). Samples which turned the medium brown were observed under a dissecting microscope after 12 d exposure to 12 h/day daylight + near UV illumination at 18°C. Fungal colonies growing from the samples and showing the characteristic erect, thick, black conidiophores with *Botrytis*-like conidia were sub-cultured onto malt extract agar.

Isolation and Culturing, Netherlands

Botrytis-selective medium was prepared as described by Kritzman and Netzer (1978) with some modifications. The specific composition was (g/l): $NaNO_3$, 1.0; K_2HPO_4, 1.2; $MgSO_4.7H_2O$, 0.2; KCl, 0.15; glucose, 20.0; agar, 15.0. pH was adjusted to 4.5 and the medium sterilized for 20 min at 120°C. After being cooled to 65°C the following ingredients were added (g/l): tetracycline, 0.02; $CuSO_4$, 2.2; p-chloronitrobenzene (PCNB), 0.015; chloramphenicol, 0.05; tannic acid, 5.

Statistical Test of Clustering

If the frequency of a tissue sample in plant i being infected is p_i, the proportion of infected samples on that plant, then a statistic indicating the degree of clustering in a dataset of n plants was

calculated as

$$\sum_{i}^{n} p_i \ln (p_i)$$

This weights multiple occurrences strongly. The probability of the degree of clustering observed if infected samples occurred independently was judged by repeatedly randomly allocating the total number of positives seen among the total number of samples, grouping the samples into sets representing the individual plants, and recalculating the statistic above. The observed value was compared with an ordered list of the test statistic calculated on the randomizations.

Sampling Sites, Host Species, and Collected Plant Material

England

The Reading University campus, about 130 ha, includes a substantial area of grassland mown annually for hay, mown amenity lawn, formal gardens, woodland, and a lake. Soils are sandy loam overlying river alluvium. Samples of *Taraxacum officinale* and *Bellis perennis* were collected across the campus from mown grassland; *Arabidopsis thaliana* was collected from cultivated beds across the campus and surrounding urban areas; *Tussilago farfara* was collected from lake margins. *Rubus fruticosa agg* and cultivated strawberry were collected from farms near Reading, Brighton and Bath. Further samples of *T. officinale* and *P. vulgaris* were collected from meadow areas near Brighton and Bath.

Netherlands

T. officinale plants were sampled in four different sites in Wageningen, representing different ecosystems with distinct soil composition. Sampling sites were located around the Wageningen University campus (surrounded by conventional experimental fields and an organic farm with fruit orchards), Binnenveld along the "Grift" canal (boulder clay, grassland with intensive agricultural activities), the floodplain of the Rhine (river clay, grassland grazed by sheep and occasional mowing) and the "Wageningse Eng" (terminal moraine adjacent to the Rhine, loam and sandy soil, recreational use). From each site 25 symptomless, apparently healthy dandelion plants were collected and stored overnight in a cold room until plating, which was done the next day. Plants were cut into three different parts; two leaves, the stem and the flower head. Each tissue sample was surface sterilized by dipping for 30 s successively in 5% bleach, 50% ethanol, and clean water. The leaves, stem and flower head were cut with clean scissors into pieces of 1 cm, of which 3–5 pieces were placed on *Botrytis*-selective medium as described above. Cultures were incubated at room temperature for 6 days. Cultures with the morphological characteristics of *Botrytis* and typical dark-brown color were transferred. A subset of colonies was transferred to fresh medium with lower concentration of $CuSO_4$ (2 mg/L), and again incubated at room temperature for 2 days. A *Botrytis*-specific immunoassay (Envirologix, Portland, Maine, USA) (Dewey et al., 2008, 2013) was used to verify that cultures represent a *Botrytis* species.

Genotyping, Gene Sequencing, and Phylogenetic Analyses

Nine microsatellite primers (Bc1–Bc7, Bc9, Bc10) for *B. cinerea* developed by Fournier et al. (2002) were used to genotype isolates randomly sampled from treatments. All isolates were genotyped with all nine primer pairs. The PCR reaction contained 2 µl of water, 5 µl PCR master-mix (Abgene, UK), 1 µl of each forward and reverse primers, and 1 µl of template DNA. The program cycles were: denaturing at 94°C for 3 min, 30 cycles of 94°C for 30 s, annealing temperatures 50°C, (Bc1, Bc3, Bc6, and Bc9), 53°C (Bc2 and Bc5), or 59°C (Bc4, Bc7, and Bc10), and 72°C for 30 s.

DNA isolation and the amplification of fragments of three house-keeping genes (Heat Shock Protein 60, HSP60; Glyceraldehyde 3-Phosphate Dehydrogenase, G3PDH; DNA-dependent RNA Polymerase subunit II, RPB2) were performed as described by Staats et al. (2005). Amplification of three additional genes (G3890, FG1020, MRR1) was performed based on sequences reported by Leroch et al. (2013). Gene fragments were sequenced by Macrogen (Amsterdam, Netherlands), and subsequent phylogenetic analysis was performed as described by Staats et al. (2005).

All primers used for the amplification of microsatellite markers or genes for sequencing are listed in **Table S1**.

Specific Experimental Designs

Experiment 1: Cryptic Systemic Infection in *Arabidopsis thaliana*

A. thaliana plants were grown in a filtered air flow supplied to individually covered pots in a CE room, with a 16 h light and 8 h dark period. Inside the covers, day-time temperature was 26.5°C and night 18.5°C; relative humidity in day and night ranged between 80 and 85%. Light intensity was 200–250 µmol/m^2/s. The plants were watered from below so as to keep the compost just moist: every day up to 2 weeks from sowing then at two-day intervals. Spores were collected from plates of *B. cinerea* B05.10 using a cyclone collector and serially diluted in talc powder through five stages, each by a factor of 10. Five milligrams of diluted spore dust was dusted on plants 21 days after sowing using a porthole in the top of the plant cover, otherwise kept covered with sticky tape. Controls were dusted with talc powder only. Ten replicates were maintained for each treatment and control. Sampling of plant tissues was done on BSM plates 10 days after inoculation. From each plant, two stem segments (∼2 cm), three rosette leaves, two stem leaves, a piece of root (∼2 cm long), and two inflorescences were separately sampled as surface disinfected and non-surface disinfected.

Experiment 2: Pathogenicity and Host Specialization

(A) Isolates ES13 (from lettuce), Gsel G07 (from *Senecio vulgaris*), Arab A07 (from wild *A. thaliana*), and Dan D07 (from *T. officinale*) were inoculated onto detached leaves of *A. thaliana, T. officinale, S. vulgaris, T. farfara,* and lettuce by placing a 5-mm agar plug of the fungal culture grown on PDA on the adaxial side of a surface sterilized leaf of the host to be tested. The leaf was placed on damp filter paper in 20 × 10 cm plastic boxes with the lid covered. A plug of PDA was used as a control. Ten replicates

were made; a single box contained only one type of leaf. Sizes of the necrotic lesion on the leaves were measured after 5 days, as the maximum dimension on asymmetric leaves. Data were analyzed by analysis of variance allowing for the split-plot design. (B) Conidia were harvested from 8 to 10 day old cultures grown on PDA and suspended in sterile water with 0.01% Tween-20 solution, separated by vortex-mixing and adjusted to 1000/µl. Droplets of 5 µl were inoculated on 1 cm^2 leaf pieces cut from leaves of lettuce, *S. vulgaris, T. farfara,* and *T. officinale*. Infected leaf pieces were counted after 5 days. Results were analyzed using a generalized linear model with Bernouilli error and a logistic transform.

Experiment 3: Pathogenicity and Host Specialization

Detached leaves of tomato (cv. Moneymaker) or leaves of whole plants of *Nicotiana benthamiana* and *T. officinale* (grown from surface-sterilized seeds) were inoculated with 2 µl droplets of conidial suspensions of different *Botrytis* isolates (10^6/ml in Potato Dextrose Broth, 12 g/l). Inoculated plant material was incubated in a plastic tray with transparent lid at 20°C in high humidity. Disease development was recorded on consecutive days from 3 to 7 days post inoculation. The proportion of inoculation droplets clearly expanding beyond the site of inoculation was taken as a measure for disease incidence (in %), the diameter of an expanding lesion (in mm) was taken as a measure for disease severity.

Experiment 4: Sporulation and Transmission in Lettuce

Fungicide seed sterilization was carried out by soaking 0.5 g of seeds in 100 ml of (0.10 g/l) systemic fungicide "Shirlan" (Syngenta) for 2 h and drying overnight before sowing. Seedlings were transplanted to 1 L pots when three true leaves were emerged; in half the pots ten 1 cm plugs of a *Trichoderma harzianum* T39 culture were placed in the compost at transplanting. A suspension of *Botrytis* ES13 (10^5 spores/ml) was sprayed onto half the plants 4 weeks after transplanting. Plants were covered with polythene bags for 24 h to retain high humidity following inoculation. Seed treated and untreated plants were arranged in randomized blocks each containing a replicate of the experiment (±seed sterilization × ±*Botrytis* inoculation × ±*Trichoderma* inoculation). At 14 weeks, plants were harvested and samples plated on BSM. Five 1-cm diameter leaf disks from five different leaves, five samples scraped from inside the stem, and five 1-cm long pieces of tap and secondary root system were randomly selected from each test plant. All samples were from healthy tissue with no visual sign or symptoms of damage. Samples were washed under running tap water, then surface sterilized, and placed on BSM to detect *Botrytis*, as described above.

Experiment 5: Transmission in Dandelion

Forty non-sterilized and 40 surface-sterilized seeds of *T. officinale* (sampled on the river banks of the Rhine) were grown on BSM for 3 days to test whether they were infected by *Botrytis*. Seeds were then transferred to wet filter paper for a week and 20 selected germinated seedlings were transferred into an autoclaved sand-soil (1:1) mixture. The plants were grown in separate plastic pots for 2 months until they were of sufficient size for infection assays. Symptomless *Botrytis* infection in *T. officinale* leaves was monitored before the infection assay was performed. One leaf of each plant was selected, surface sterilized and cultured on a BSM plate. *Botrytis* outgrowth was evaluated by checking the color change in the medium and subsequent sporulation.

Experiment 6: Effects on Host and Environmental Interactions

Commercially produced lettuce seed cv. "All the Year Round" was germinated in large seed trays. Two weeks later, seedlings were transplanted to 1 L pots of John Innes 2 compost. Thirty seedlings were tested for infection by *Botrytis* as before; no infection was found. Pots were grouped in sets of four, inoculated or not. A 2^6 factorial design with treatments inoculation × temperature × shading × nitrogen form was then laid out with six randomized blocks of inoculation × shading × nitrogen form in each glasshouse (192 plants in total). Groups of four pots were shaded using green mesh approximately 30 cm above the pots, draped down the sides. Pots were fertilized twice weekly with either 4 mM KNO_3 or 4 mM $(NH_4)_2SO_4$ +2 mM K_2SO_4. Thirty-six days after sowing, the pots to be inoculated were moved to a separate glasshouse. They were arranged in trays of 16 and inoculated with dry spores by tapping a plate above the tray, followed by enclosure in black plastic for 30 min to allow spores to settle. At 1, 2, and 3 months after sowing one plant was removed from each set of four and dissected to give 12 tissue samples: edge and central samples from an old leaf, a mature leaf, and a young leaf, three stem and three root samples. These were plated on BSM as before and the presence of *Botrytis* noted. At the third harvest, both remaining plants were cut at the base and oven-dried before weighing. The weight of the tissues that were removed to test for the presence of *Botrytis* was negligible. Temperature effects are confounded with glasshouse block effects in this design, but this was unavoidable; differences in nitrogen form are also confounded with sulfate supply, also this was unavoidable. The two compartments had the same aspect, shape and shading patterns, so the largest single difference was temperature.

RESULTS

Host Range and Prevalence

Botrytis species were frequently isolated from the interior of multiple tissues in apparently healthy hosts of many species (**Table 1**). Prevalence reached 50% of samples or more (as in *T. officinale*), but was usually less, and cryptic infections other than in flowers were rare or absent in *T. farfara*, *B. perennis,* or *P. vulgaris*. Prevalence varied substantially from tissue to tissue. Species in which fruit infection is frequently reported did not necessarily harbor latent infection in other tissues of the plant: in *R. fruticosa* agg. and cultivated strawberries *Fragaria* ×*ananassae*, leaf infection was not found. There was no clear association with particular plant families in the small sample represented here, nor with perenniality. Repeated surveys are

TABLE 1 | Percentage of samples showing cryptic infection with *Botrytis* in various host plant species.

Family	Host species	Growth form	Growing situation[a]	Location[a]	Sample size	Flower sample size[b]	Organ isolated from				Randomly associated?
							Fruit or petals	Leaf	Stem	Root	
Asteraceae	*Tussilago farfara*	Perennial cryptophyte	Lake edge	RU	45	10	0[c]	0	0	2	n/a[d]
	Bellis perennis	Perennial herb	Lawn	RU	55	21	0	0	3	0	n/a
	Gerbera x hybrida	Perennial herb	Indoor crop	RU	96	96	0	0	0	0	n/a
	Taraxacum officinale complex	Perennial herb	Open grassland, lawn	RU	107	75	27	29	21	16	$P < 0.001$
				WU	100	100	72	87	72	–[c]	n.t.[e]
	Cirsium vulgare	Perennial herb	Open grassland	RU	24	18	2	4	1	0[c]	$P > 0.5$
	Senecio vulgaris	Ruderal	Cultivated ground	RU	82	62	31	37	26	9	$P = 0.002$
	Centaurea scabiosa	Perennial cryptophyte	Wild	RU	35	23	22	49	23	21	$P = 0.6$
	Achillea millefolium	Perennial herb	Open grassland	RU	44	35	56	32	16	11	$P = 0.002$
Brassicacae	*Arabidopsis thaliana*	Short-lived annual herb	Wild	RU	66	41	30	48	41	5	$P < 0.001$
Primulacae	*Primula vulgaris*	Perennial herb	Wild	SE	382	–	–	8	–	–	n/a
Rosaceae	*Potentilla fruticosa*	Perennial shrub	Landscape planting	RU	100[f]	–	–	8	7	–	$P < 0.001$
	Rubus fruticosa agg.	Perennial climber	Hedges	SE	219	219	101	0	0	0	n/a
	Fragaria × ananassae	Perennial herb	Crop	SE	203	203	77	0	0	0	n/a

[a] *RU: grounds of Reading University, UK; SE: several locations across southern England; WU, four locations around Wageningen, NL.*
[b] *Fruiting structures were not necessarily present in all plants sampled.*
[c] *0: no infection found; – not sampled.*
[d] *Test not applicable: infestation found in only one organ per plant.*
[e] *Not tested.*
[f] *Three bushes, samples 40, 40, 20. All infections came from the bush with sample size 20.*

available for the perennial herb *T. officinale* and the short-lived annual *A. thaliana*. Prevalence varied substantially from year to year, from place to place and from tissue to tissue (**Table 2**).

Evidence for Spread in and Over a Single Host: Experiment 1

Published evidence about the spread of *Botrytis* in a single host is available for cultivated hybrid *Primula* (Barnes and Shaw, 2003) and lettuce (Sowley et al., 2010). In the majority of host species in which isolations could be made from distinct tissues, multiple isolations from a single plant were more common than expected (**Tables 1, 2**). *A. thaliana* that were grown in a sterile air-stream and inoculated as seedlings with dry conidia at low density developed normally and did not show any disease symptoms or evidence of stress. *Botrytis* could be isolated from multiple tissues, many of which only developed after the time of inoculation (Experiment 1). Isolations were strongly clustered in individual plants, consistent with systemic spread in the plant (**Figure 1**; randomization test $P < 0.001$).

In *Cyclamen persicum*, inoculation of four plants with a spore suspension followed by enclosure in a plastic bag led to serious necrosis development with abundant sporulation. The plants recovered upon removal of the bags and produced new flushes of leaves and eventually flowered, without further signs of *Botrytis*. Of 14 seed capsules examined (381 seeds) one capsule yielded two *Botrytis* infected seeds (out of 47) and a second capsule yielded 56 *Botrytis* infected seeds (out of 57). The seeds from the other 12 capsules were completely free of *Botrytis*. Isolations were attempted from leaves, roots, exterior and interior samples from the corms. *B. cinerea s.l.* was isolated from roots of two plants and the exterior and interior of the corm of two others (**Table 3**).

TABLE 2 | Percentage of tissue samples of wild-growing *Taraxacum officinale* complex and *Arabidopsis thaliana* from which *Botrytis* could be isolated after surface sterilization, at different locations and years.

Species	Year	Location	Source	Root %	Leaf %	Stem %	Flower %	Sample size
T. officinale	2005–6[a]	Reading	Cooray	5	6	–[b]	–	100
	2005–6[a]	Bath	Cooray	13	5	–[b]	–	110
	2005–6[a]	Brighton	Cooray	0	4	–[b]	–	132
	2007–8[a]	Reading	Shafia	18	29	–[b]	27	108
	2008	Reading	Thriepland	17	31	–[b]	–	(182)[c]
	2014	Reading	Emblow	0	1	–[b]	6	24
	2014	Wageningen	Onland and Hoevenaars	–[b]	87	72	72	100
A. thaliana	2007–8[a]	Reading	Shafia	5	50	41	29	66
	2010	Reading	Shaw	10	20	0	0	20
	2013	Reading	Emmanuel	4	2	3	3	76
	2014	Reading	Emmanuel	0	0	0	5	22
	2014	Reading	Emblow	0	0	0	0	31

[a]*Data were sampled separately in autumn, spring and summer; proportions of samples infested were homogenous (χ^2 $P > 0.2$).*
[b]*–, not sampled.*
[c]*From nine seedling families. There were no significant differences between families (χ^2-test, $P = 0.2$).*

FIGURE 1 | Clustering of recovery of *B. cinerea* B05.10 from surface sterilized tissues of *Arabidopsis thaliana* grown in a sterile airflow and inoculated with dry spores at the two leaf stage. Each drawing of a plant represents the samples into which it was dissected. *B. cinerea* was recovered from samples colored red; note the strong clustering of infected samples in individual plants ($P < 0.001$).

TABLE 3 | Recovery of *Botrytis* from different tissues of four *Cyclamen persica* plants cv. Midori earlier inoculated and diseased, but recovered and symptomless at the time of sampling.

Plant	Root	Flower pedicel	Petal	Leaf	Outer corm	Inner corm
Midori White (plant #1)	1	1	1	0	0	0
Midori White (plant #2)	0	1	0	0	1	0
Midori Scarlet (plant #1)	1	1	0	0	0	0
Midori Scarlet (plant #2)	0	1	0	0	0	1

Phylogeny and Species Variation of Internal Infections in Dandelion

We aimed to test whether strains of *Botrytis* developing cryptic asymptomatic infection form a separate phylogenetic group, distinct from strains that cause necrotic infections. A preliminary phylogenetic clustering of 47 *Botrytis* isolates sampled from asymptomatic dandelion in Netherlands was performed based on HSP60 and G3PDH gene sequences (not shown). Thirty-five out of forty-seven isolates grouped with the *B. cinerea* species complex and 10 grouped with *Botrytis pseudocinerea,* all members of clade 1 in the genus *Botrytis* (Staats et al., 2005). Two other isolates grouped into clade 2, i.e., isolates DAN5 and DAN39. Based on this result, eight isolates grouping with *B. cinerea* and three isolates grouping with *B. pseudocinerea,* together with the unknown isolates DAN5 and DAN39, were selected for additional analysis of the RPB2 gene sequence. Using as backbone the multiple sequence alignment of 29 known species of the genus *Botrytis* (Hyde et al., 2014), the concatenated sequences of three genes (HSP60, G3PDH, and RPB2) from the 13 isolates sampled from asymptomatic dandelion were included for phylogenetic tree construction (**Figure 2**). Eight isolates were related, but not identical, to *B. cinerea* type isolate MUCL7. Three isolates were related but not identical to *B. pseudocinerea* isolate VD110. Isolate DAN5 clustered with, but is not identical to, *Botrytis caroliniana* and *Botrytis fabiopsis,* while DAN39 clustered very tightly with two *Botrytis mali* isolates and is probably a member of this species. There was good agreement between phylogenetic trees for individual gene sequences HSP60, G3PDH, and RPB2 (**Figures S1**–**S3**). In order to provide a better phylogenetic resolution of isolates that were most closely related to *B. cinerea,* 16 isolates were analyzed in more detail for the sequences of three additional genes (G3890, FG1020, MRR1; **Figures S4**–**S6**). The combined phylogeny for these three genes (not shown) revealed that nine of the 16 isolates were closely

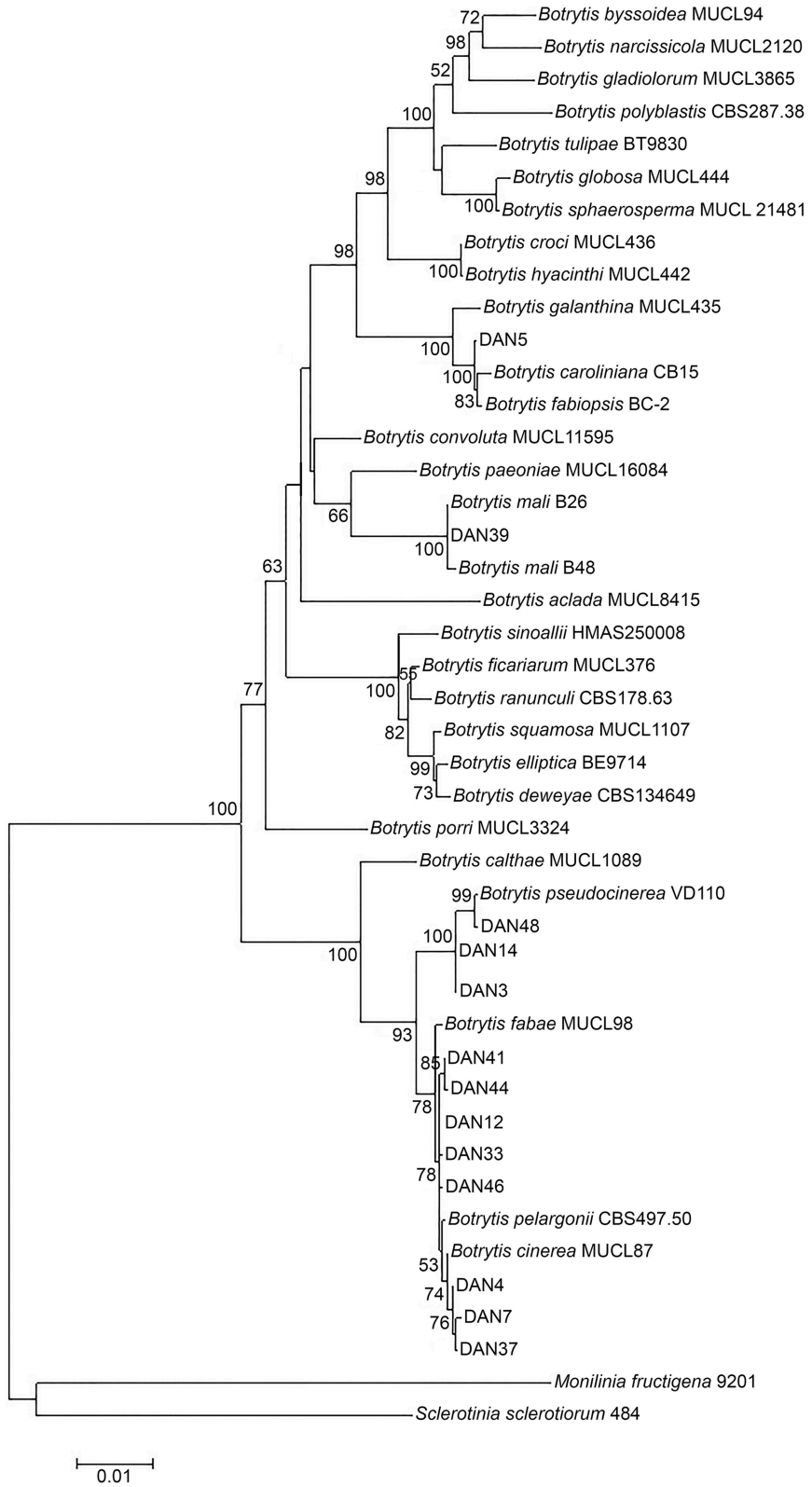

FIGURE 2 | Phylogenetic position of 13 *Botrytis* isolates from asymptomatic dandelion (labeled by DAN and a number) in the genus based on concatenated HSP60, G3PDH, and RPB2 sequences. Recognized *Botrytis* species are taken from Hyde et al. (2014). Phylogenetic tree construction used a maximum likelihood method with 1000 bootstraps. Only bootstrap values higher than 50% are displayed at the nodes.

related to *Botrytis* type S, a subgroup of isolates within the *B. cinerea* complex that was initially predominantly sampled from strawberry and is typified by a characteristic insertion of 21 nucleotides in the MRR1 gene (Leroch et al., 2013). The other seven isolates were closely related to *B. cinerea* but distinct from both *B. cinerea* groups N and S (not shown).

Mating Type Analysis

To investigate the mating type of the 47 isolates sampled from asymptomatic dandelion in Netherlands, PCR reactions were carried out that amplify a gene in the MAT locus (Amselem et al., 2011). Both mating type alleles (MAT1-1 and MAT1-2) were found in similar proportions in the isolates from the *B. cinerea* species complex and from *B. pseudocinerea*. In both cases the mating types were present in close to a 1:1 ratio. This observation does not necessarily imply that the isolates are progeny from sexual reproduction but at least they have the possibility of finding compatible mating partners within the same host species. Isolate DAN5 has mating type MAT1-1 and isolate DAN39 has mating type MAT1-2 (**Table 4**).

Pathogenicity and Host Specialization

If isolates from asymptomatic plants are distinct from pathogenic strains and unable to cause disease, they would not pose a threat to neighboring plants and especially crops. If such isolates, however, have the capacity to cause necrotic symptoms (given the right circumstances), they could at some point in time strongly increase the risk of disease development, either in the symptomless host, or in neighboring (crop) plants. In the next two experiments we therefore aimed to test the capacity of *Botrytis* isolates from symptomless plants to cause necrotic symptoms on host species from which they were recovered, as well as on other plant species. Artificial inoculation under laboratory conditions requires a suitable spore density, availability of nutrients, and proper environmental conditions to accomplish necrotic infection. We therefore used standard methods with either mycelium on agar plugs or spore suspensions as inoculum.

Experiment 2

Isolates sampled from five different host species (*A. thaliana*, *T. officinale*, *S. vulgaris*, *T. farfara,* and lettuce; one isolate per host origin) were inoculated on newly grown, asymptomatic plants of four host species (the same as above with the exception of *T. farfara*) in all possible combinations. Inoculations were performed with cultures grown on an agar plug and lesion sizes were monitored (**Figure 3**). In this test there were differences in virulence ($P < 0.001$) and in host susceptibility ($P < 0.001$) and a significant ($P = 0.001$) but minor interaction between host susceptibility and pathogen virulence in both cases. There was no tendency for isolates to be more pathogenic or less pathogenic on their host of origin. Results were similar when inoculation was performed with spore suspensions.

TABLE 4 | Distribution of mating types in 47 *Botrytis* isolates from dandelion, as determined by diagnostic PCR.

Species	Mating type MAT1-1	Mating type MAT1-2
B. cinerea	19	16
B. pseudocinerea	5	5
DAN5, related to *B. caroliniana* and *B. fabiopsis*	1	–
DAN39, putative *B. mali*	–	1

Experiment 3

Eight *Botrytis* isolates sampled from asymptomatic dandelion in Netherlands were selected for artificial infection assays on leaves of tomato, *N. benthamiana* and *T. officinale* plants. Three isolates were selected from the *B. cinerea* species complex, three were from *B. pseudocinerea* and the remaining two were isolates DAN5 (related to *B. caroliniana* and *B. fabiopsis*) and DAN39 (putative *B. mali*). As a reference, the commonly aggressive *B. cinerea* strain B05.10 was always inoculated on the opposite leaf half. Results of these infection experiments are shown in **Figure 4**. The *B. cinerea* and *B. pseudocinerea* isolates all produced expanding lesions on leaves of tomato and *N. benthamiana*, disease incidence was 100%. On *T. officinale* leaves, disease incidence for all isolates from asymptomatic dandelion was below 40%, while for *B. cinerea* strain B05.10 it ranged from 60 to 90%. Isolate DAN5 was entirely unable to cause disease on the three hosts tested. At most it caused small black dots at the inoculation sites, which never developed into expanding lesions at later time points. Isolate DAN39 was able to cause expanding lesions on tomato and *N. benthamiana*, but not on *T. officinale* leaves. The lesion diameters differed between isolates and hosts. In general, the diameters of lesions caused by *B. cinerea* and *B. pseudocinerea* isolates on tomato leaves were similar to those of strain B05.10, while on *N. benthamiana* leaves, the lesions were smaller than those of B05.10 (**Figure 4**). Symptoms on *T. officinale* leaves were generally few and mild. *B. pseudocinerea* isolates sampled from symptomless dandelion differed in disease severity on dandelion, the most virulent isolate (DAN40) caused lesions of similar size as those caused by *B. cinerea* B05.10 whereas the two others (isolates DAN14 and DAN28) caused lesions quite smaller than those of B05.10 (**Figure 4**). The experiments above show that *Botrytis* isolates sampled from asymptomatic plant species have the capacity to cause necrotic lesions on the hosts from which they were sampled, as well as on distinct, unrelated plant species.

Sporulation, Vertical Transmission, and Closure of the Life-Cycle

The following experiments were designed to examine whether cryptic infections can be long-lived within a plant and can pass from seeds to mature plants.

Experiment 4, Lettuce

This experiment was intended to test the hypothesis that cryptic infection would reduce host growth, and that competing endophytes would reduce this effect. A batch of lettuce seed was used from plants grown outdoors and displaying a 98% frequency of seed infection with *B. cinerea*. A randomized block full factorial experiment was done with treatments combining seed disinfection with fluazinam, spray inoculation with *B. cinerea*

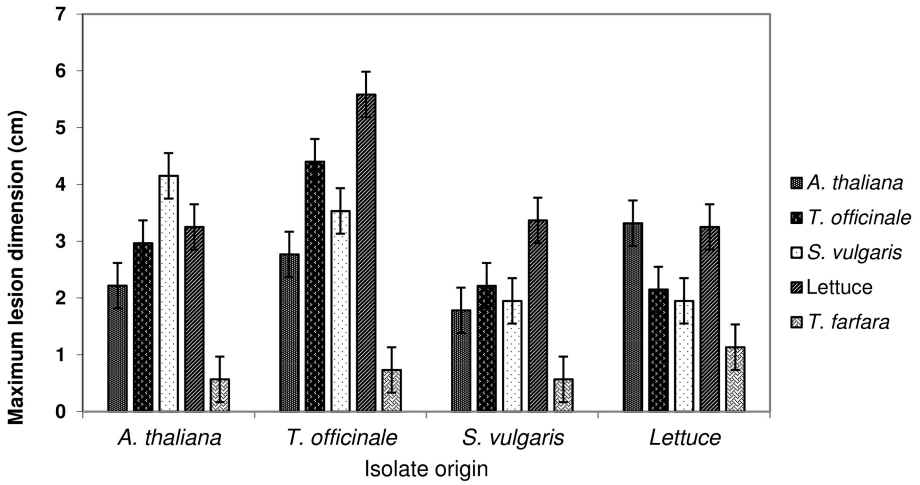

FIGURE 3 | Lesion diameters 5 days after agar plug inoculations of isolates of *Botrytis* sampled from four hosts onto entire detached leaves of *Arabidopsis thaliana, Taraxacum officinale, Senecio vulgare,* cultivated lettuce, and *Tussilago farfara*. Error bars represent 1 *SED*; non-overlapping bars are different at $P = 0.05$ (uncorrected for multiple comparisons).

spore suspension 4 weeks after transplanting (approximately at 10 leaf stage) and compost inoculation with a *T. harzianum* T39 isolate thought to be a possible biocontrol agent for the internal *Botrytis*. There were no significant differences in the proportion of plant samples from which *Botrytis* was recovered (28 ± 3%), so the hypothesis could not be assessed. Only two of the 17 plants from which isolated *Botrytis* cultures were further characterized displayed symptoms of *Botrytis* infection. Treatment with *T. harzianum* neither had a detectable impact on the colonization of the lettuce plants by *Botrytis* nor on the genotypes recovered from plants exposed to *T. harzianum.*

To further investigate the results, microsatellite haplotypes were determined from 15 isolates from different tissues of fungicide treated plants and from 13 isolates from untreated plants (**Table 5**). All the isolates from fungicide *untreated* plants were identical to each other (haplotype B), but distinct from the isolate used for inoculation (haplotype C). The fungicide *treated* plants contained six different haplotypes including three recoveries of the inoculated isolate (haplotype C) and a single representative of haplotype B, characterizing the fungicide *untreated* plants (**Table 5**; randomization test $P < 0.001$ against the null hypothesis of random recovery).

This observation suggests that a pre-existing cryptic infection originating from a seed-borne isolate of *Botrytis* excluded further infection until an advanced phase of plant growth, and that the level of internal infection sustained was similar regardless of the source of inoculum.

Experiment 5, *Taraxacum officinale*

Two batches of dandelion plants were grown, one from non-sterilized seeds and the other from surface-sterilized seeds. Placing untreated seeds directly on selective medium established that *Botrytis* cultures grew out from 100% of the seeds. Both batches of dandelion plants were symptomless throughout their growth. There was no significant difference in the number of leaves or leaf lengths between plants grown from surface-sterilized seeds and the plants grown from untreated seeds (not shown). *Botrytis* infection in leaves was investigated after 2 months of growth, when plants reached maturity. *Botrytis* infection was observed in four out of 20 leaves from dandelion plants derived from non-sterilized seeds in the first trial, and 1 out 17 leaves in the second trial. All the plants derived from surface-sterilized seeds were free of *Botrytis.* The difference is significant at $P = 0.02$. Therefore, in dandelion, seed infection can survive and grow throughout a proportion of plants until flowering produces the next generation of seed.

Effects on the Host and Environmental Interactions: Experiment 6

Cryptic infection might impose a defensive load on a host plant. This experiment was designed to test whether factors tending to improve host growth, and thereby reducing resources available for defense, would reduce infection. To measure the effect of cryptic *Botrytis* infection on growth, commercial seed with a low level of *Botrytis* contamination was used and half of the plants deliberately dusted with *Botrytis* spores. Temperature, fertilization and light were varied to produce different growing conditions.

Inoculation of lettuce with *Botrytis* spores not leading to necrotic infection did not result in changes in the frequency with which *Botrytis* could be isolated from the plants (factorial anova $P = 0.8$). Infection frequencies were approximately doubled in unshaded plants compared to plants grown in shaded conditions, and approximately doubled in plants grown at 20°C compared to plants grown at 14°C (**Figure 5**). Ammonium and sulfate fertilization gave about a 10% relative increase in infection over nitrate fertilization ($P = 0.07$).

At final harvest, the *Botrytis*-inoculated plants were 19% lighter in weight than the uninoculated plants (anova $P =$

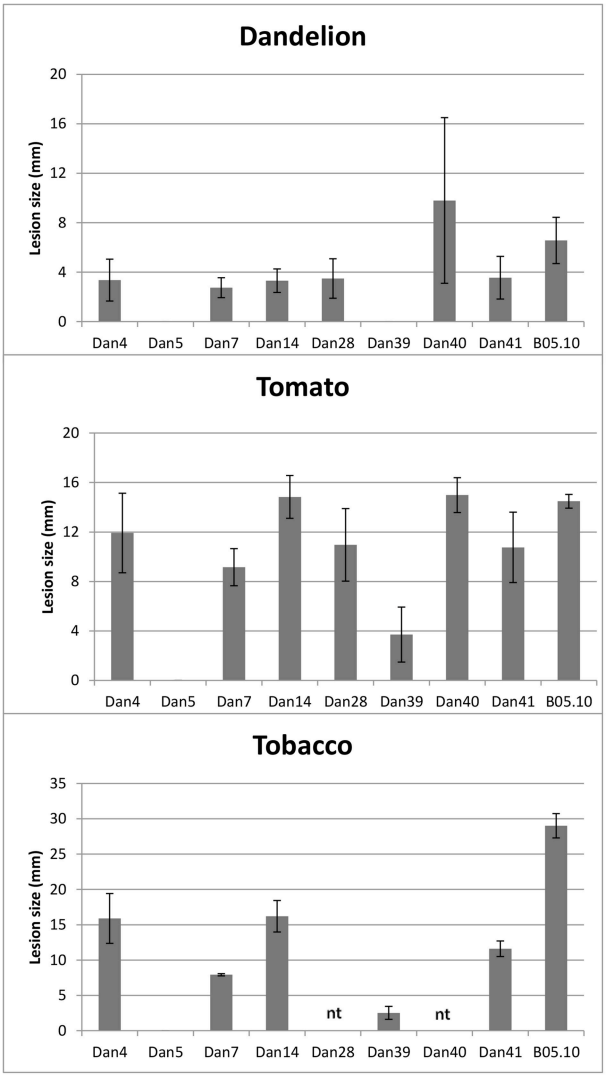

FIGURE 4 | Lesion diameter on leaves of *Taraxacum officinale* at 5 days after inoculation ($N = 6$), tomato at 3 days after inoculation ($N = 8$) and *N. benthamiana* at 3 days after inoculation ($N = 3$), following inoculation with *Botrytis* isolates or *B. cinerea* strain B05.10. Data presented are means with standard deviations indicated with the error bars.

0.02) in unshaded conditions and 23% lighter in weight (anova $P = 0.05$) in shaded conditions. This result was quantitatively reproducible. The relation between the weight of a lettuce plant and the proportion of *Botrytis*-infected surface sterilized samples from the same plant depended on whether plants were shaded or unshaded (**Figure 6**). In unshaded plants there was a weak *positive* relation between cryptic infection and weight (+ 0.3 percentage points per 1 percentage point increase in infection, $P = 0.01$). In shaded plants there was a weak and non-significant negative relation (−0.3 percentage points per 1 percentage point increase in infection, $P = 0.2$).

This experiment establishes that cryptic infection was not limited by inoculum supply (confirming experiment 4), that conditions favoring host growth, especially light, also favored cryptic infection, and that *Botrytis* inoculation, despite not altering the final levels of infection, was strongly detrimental to growth.

TABLE 5 | SSR genotypes, based on eight loci, of *Botrytis* isolates recovered from a randomized block factorial experiment on lettuce with treatments of fungicide seed treatment, spray inoculation with isolate ES13 (haplotype C) at the 4-leaf stage and soil inoculation with *T. harzianum T39.*

Fluazinam	*B. cinerea* inoculation	*T. harzianum* T39 inoculation[a]	Plant ID	Root	Stem	Leaf
+	+	−	6			C, C
			7		E	
			17		E[b]	D,D[b]
	−	+	8	F		
			13			B
			16		A	
		−	3			C,F
			4	A		
			5		A	
−	+	+	2			B,B,B,B
			9		B,B	
		−	1			B,B,B,B
			14		B	
	−	+	11		B	
			15			B
		−	10			B
			12		B	

Letters A–H represent distinct haplotypes found in the Botrytis strains isolated from the host tissue samples.
[a]No samples from the fungicide + T. harzianum + Botrytis inoculation were genotyped.
[b]Symptomatic at time of sampling.

DISCUSSION

Specialist *Botrytis* species such as *B. aclada* and *B. allii* have been understood to have a life-cycle involving extended periods of symptomless growth (Maude and Presly, 1977; du Toit et al., 2004). Seed infection by species in the *B. cinerea* complex leading to seedling infection has been well-known for some time in species such as linseed (Harold et al., 1997) because of its contribution to seedling death. It has been less appreciated that long-lived cryptic infection with generalist *Botrytis* is possible. This has previously been shown in cultivated primula (Barnes and Shaw, 2003) and in lettuce (Sowley et al., 2010). Quiescent infections of a few host cells which give rise to spreading necrosis at fruit maturity are characteristic of many fruit diseases (e.g., Prusky and Lichter, 2007; Puhl and Treutter, 2008). The mode of growth discussed here is different, as it is a form of infection in which the fungus is able to grow with the host and spread to new plant parts. The results above show that many host species growing in natural settings and showing no disease symptoms frequently have disseminated infections of *Botrytis* species.

This is of both scientific and practical interest. We become increasingly aware that plants harbor many endophytic species (e.g., Shipunov et al., 2008) and that these may have profound

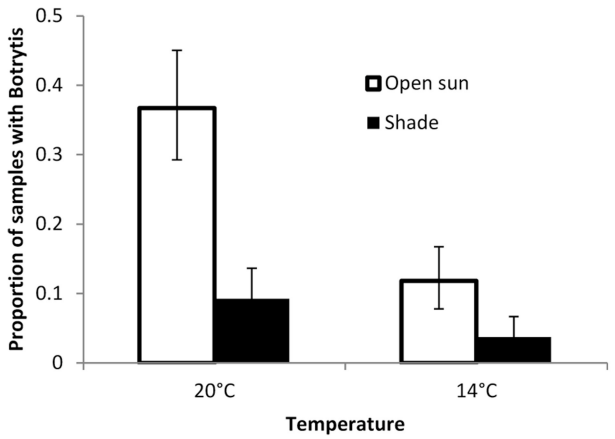

FIGURE 5 | Proportion of samples of lettuce plant tissue from which *Botrytis* isolates could be recovered after surface sterilization when grown in shaded or open positions in glasshouse conditions. Back-transformed data from anova on square root transformed data. Error bars are 1 *SED*.

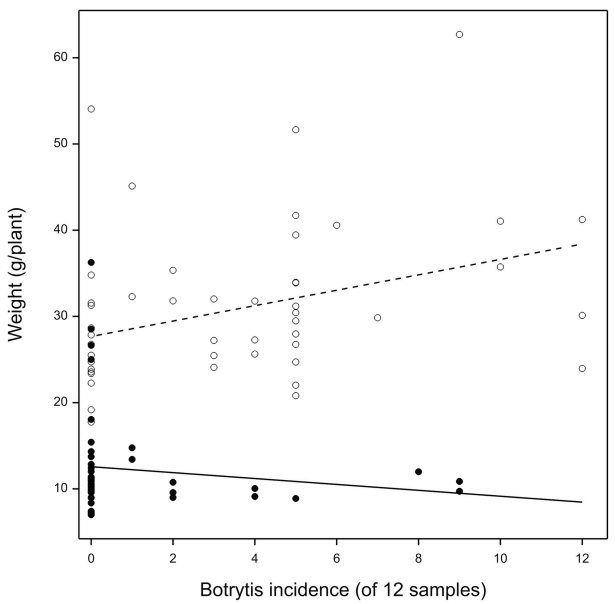

FIGURE 6 | Dry weight at harvest (g) of lettuce plants grown in shaded (closed circles) or unshaded (open circles) glasshouse conditions in relation to the number of tissue samples (of 12) from each plant in the experiment ($n = 96$) from which *Botrytis* isolates could be recovered after surface sterilization.

effects on their susceptibility to stress and to pathogens (Rodriguez et al., 2009). Understanding that a pathogen like *Botrytis*, which is investigated mostly in the context of rapidly spreading necrotic infections may also exist as a widespread symptomless infection with minimal effects on the host should seriously alter our understanding of pathogenesis. There are quantitative differences between isolates in their pathogenicity on different species, but we did not obtain any evidence for isolates taken from a particular host to be particularly adapted to that host. Furthermore, both *B. cinerea*, *B. pseudocinerea,* and other lineages or cryptic species of *Botrytis* appeared to occur in this asymptomatic form. From a practical point of view, management of *Botrytis* in species where cryptic infection is common needs to focus on environmental conditions; it may be ineffective to try to prevent low levels of infection, since permanent cover by systemic fungicide would be needed. In particular, results in lettuce suggest a balanced system in which host defenses are activated sufficiently to prevent infection increasing above a certain density, because plants grown from "clean" seed acquired the same level of infection as plants grown from the infection-carrying seed infection. The question whether cryptic infection is harmful or beneficial to a plant is difficult to address because of the difficulty of growing plants free from *Botrytis* infection but also in a natural setting.

Because the findings reported may be deemed somewhat surprising, it is important to consider possible artifacts. The most obvious is that these isolations could represent independent, spatially restricted early stages or quiescent infections from environmental conidia. There are several arguments against an important contribution of these artifacts to the observations summarized here. (1) Barnes and Shaw (2003) showed that the sterilization procedure was highly effective in killing adherent spores on seed and other tests with inoculated material have shown the procedure to be effective on leaf tissue. (2) *T. officinale* and *B. perennis* grow in the same habitat and often in close proximity but have very different prevalence rates, showing that we are dealing with at least an established association between fungus and host. (3) In greenhouse work, Barnes and Shaw (2003) showed that the same isolate was repeatedly recovered from single hosts, but that adjacent plants rarely hosted identical isolates. This is weak evidence by itself, but supports the hypothesis that this type of infection is at least partially systemic, because it predicts that recovery of isolates or genotypes will be clustered on particular plants. However, clustering can also be ascribed to variation in susceptibility among plants.

Phylogenetic analysis of a subset of isolates sampled from dandelion in Netherlands showed that *B. cinerea* and *B. pseudocinerea* were the predominant species. The latter is a recently described species which is morphologically very similar but phylogenetically distinct from *B. cinerea* (Walker et al., 2011). Based on the morphology of the isolates sampled from a spectrum of plants in the UK, it may be assumed that these also mostly represent *B. cinerea* and *B. pseudocinerea*, although this would need extensive sequence analysis to be confirmed. The phylogenetic analysis also identified two isolates of distinct *Botrytis* species belonging to clade 2 (Staats et al., 2005), one of which (DAN39) is presumably from *B. mali,* a postharvest pathogen of apple with an as yet poorly explored distribution (O'Gorman et al., 2008). It is perhaps relevant to note that this isolate was sampled from a dandelion plant growing in a grass patch adjacent to an apple and pear orchard of an organic farm. The second isolate from *Botrytis* clade 2, DAN5, was related but not identical to *B. caroliniana* and *B. fabiopsis,* and might represent a novel *Botrytis* species. An earlier study by

Shipunov et al. (2008) on endophytic fungi in *Centaurea stoebe* identified, besides *B. cinerea*, six distinct phylogenetic groups of *Botrytis* isolates. Four of these groups were closely related to *B. cinerea* and one of them might represent *B. pseudocinerea* (which had not yet been described at the time of the study by Shipunov et al., 2008). The isolates bot079 and bot378 reported in Shipunov et al. (2008), however, were very distant from the clade containing *B. cinerea* and grouped with *B. paeoniae*, alike the *B. mali* isolate DAN39. Unfortunately the isolates from *C. stoebe* are no longer available for further phylogenetic comparison (A. Shipunov, personal communication). The above results and those of Shipunov et al. (2008) demonstrate that several new *Botrytis* species can be retrieved as endophytes from a single host in a limited sampling. A more extensive phylogenetic analysis of *Botrytis* isolates from multiple hosts and locations would likely reveal many more novel species. If more extensive sampling and further phylogenetic analysis would indeed confirm a greater diversity of *Botrytis* species than previously appreciated (Staats et al., 2005; Hyde et al., 2014), it raises the question as to how many times the cryptic life-style has arisen.

As with all endophytic organisms, the question arises as to how the host defense system and the pathogen are interacting (Schulz and Boyle, 2005; Newton et al., 2010). There are a number of possibilities. First, the fungus may evade the host defense system by not producing signals which activate defenses strongly enough to destroy the fungus. This is consistent with the increased infection frequency in unshaded lettuce plants in experiment 6: rapidly photosynthesizing plants are likely to have more nutrients in the apoplast, and thus allow more pronounced growth if they do not also have better defense. It is likely that *Botrytis* produces little or no phytotoxic metabolites and proteins, or plant cell wall degrading enzymes, while it displays symptomless internal infection behavior. If it did produce such compounds, as *Botrytis* "normally" does (reviewed by van Kan, 2006), this would result in irreversible damage to plant cells and culminate in disease symptoms. It remains elusive why *Botrytis* does not produce such damaging compounds during cryptic infection. Is it by lack of a (plant-derived) signal to activate the expression of the genes, or is the plant actively suppressing the expression of virulence genes?

An alternative view of the interaction is that host defense continually destroys *Botrytis* locally, but establishment in new areas is frequent enough to maintain the fungus associated with the plant. In experiment 6, spray inoculation with *B. cinerea* spores incurred a 20% reduction in growth, without altering infection density. This reduction in growth might reflect the cost of effective defense against a forceful attack; this defense evidently does not alter the balance between systemic infection and host defense. The similarity in frequency of cryptic infection in plants which did and did not have seed-borne infection removed by fungicide in experiment 5 again points to a balanced system in which too much local growth can be eliminated by the host. The hypothesis of a balanced growth/elimination system implies that previously infested plant tissues might become uninfested, as well as the reverse. We have no data on this. Experiments to address this question would be complex because of the destructive nature of current methods to detect infection.

The spore density at the point of first encounter is likely a crucial determinant in whether the interaction becomes asymptomatic or necrotic. At high spore density, and in the presence of nutrients, the fungus can rapidly and efficiently germinate (van den Heuvel, 1981) and produce a spectrum of phytotoxic metabolites and proteins at sufficient concentrations to cause death of multiple plant cells (van Kan, 2006) and set necrotic development in motion. Causing host cell death is in essence a physiologically irreversible decision, although there are cases where primary necrotic lesions fail to develop into an expanding lesion, possibly due to an effective restriction of the fungus by the host (Benito et al., 1998; Coertze and Holz, 2002). In order to achieve symptomless *Botrytis* infection in plants in our experiments, it was important to start the infection with a low inoculum dosage. The low number of spores and concomitant low density of germlings on the plant surface might not release sufficient phytotoxic metabolites and proteins to activate the plant cell death machinery, and thereby fail to kill cells that would act as an entry point for the fungus. Failure to induce cell death would force the fungus to enter the plant through natural openings and grow in the plant interior where it can retrieve nutrients. The growth of the fungus inside the plant would need to remain restricted and be synchronized with that of the host, possibly by mechanisms similar to those reported for *Epichloë* endophytes(Tanaka et al., 2012).

A final possible view of the interaction in this system is that the infection is in some circumstances beneficial to the host plant, so that specific signals from *Botrytis* lead to over-riding of normal defense signals. A hint that this might be so is given by the positive relation between lettuce growth and the frequency with which *Botrytis* could be recovered from the plants in experiment 7, presumably representing the density of infection. The nature of such signaling processes can only be conjectured at present. Recent studies by Weiberg et al. (2013) described how small RNAs of *Botrytis cinerea* can actively silence host genes that are involved in immunity, and thereby promote virulence of the pathogen. Conversely, it is conceivable that small RNAs from a host plant could silence *Botrytis* genes that are required for the activation of virulence mechanisms, and so prevent the production of damaging fungal proteins and metabolites. In the fungal grass endophyte *Epichloë*, the symbiotic interaction depends on an intact reactive oxygen signaling and MAP kinase signaling. The disruption of components of either of these signaling processes results in breakdown of symbiosis and switch to disease development (Tanaka et al., 2012).

The economic importance of this form of infection could be considerable in a susceptible crop such as lettuce, cyclamen or *Primula* × *polyantha* in which persistent infections last for the lifetime of the crop, causing disease and loss at maturity or after harvest. The importance of the demonstration of a large reservoir of infested vegetation in the wider environment depends mainly on how much inoculum it supplies. If this is sufficiently low, there could be no economic implications. On the other hand, given the number of plant species shown to harbor infection, infections

in natural vegetation could be an important source of conidia into otherwise clean protected environments. It is less clear what could be done about it, but it suggests that effective integrated management of *Botrytis* should assume that inoculum is present not only in the air but probably latent in the crops. The best management strategies will focus on the physiological state of the plant and the intrinsic resistance or tolerance of the host to necrotic disease development.

If we can understand the mechanism that determines whether the interaction becomes symptomless or necrotic, it might be possible to steer the interaction in one or other direction, by modifying the environmental conditions, or by applying chemicals that trigger a switch in lifestyle. This might result in active suppression of necrotic development of *Botrytis*, or in the forced interruption of the symptomless infection.

AUTHOR CONTRIBUTIONS

MS and JvK coordinated the sampling, designed and supervised the experiments, and wrote the manuscript. CE, DE, RT, AS, DT, and ME performed the experiments. CE prepared **Figure 1**, RT prepared **Figure 2**, DE prepared **Figure 4**.

ACKNOWLEDGMENTS

A substantial contribution to this work was made by Anuja Rajaguru, who sadly died before the preparation of this paper. The authors acknowledge funding from the Commonwealth Studentships Commission, the Gatsby Foundation, the UK Department of Food and Rural Affairs, the Ministry of Education of Malaysia, the Universiti Putra Malaysia, and the Indonesian Ministry of Agriculture. The authors are grateful to Alice Vanden Bon for expert technical assistance. The authors are grateful to Wageningen University students Violeta Onland, Koen Hoevenaars, and Elisabeth Yánez Navarrete for sampling and preliminary characterization of isolates from dandelion, as well as to prof. Matthias Hahn (Univ, Kaiserslautern, Germany) for fruitful discussion about the phylogenetic analysis. The authors are grateful to Dr. D. O'Gorman, Dr. G. Bakkeren, and Dr. J. R. Úrbez Torres from Agriculture and Agri-Food Canada, Summerland, British Columbia, Canada, for providing the DNA samples of *Botrytis mali*.

SUPPLEMENTARY MATERIAL

The Supplementary Material for this article can be found online at: http://journal.frontiersin.org/article/10.3389/fpls.2016.00625

Figure S1 | Phylogenetic position of 47 *Botrytis* isolates from asymptomatic dandelion (labeled by DAN and a number) in the genus based on HSP60 sequences. Sequences of recognized *Botrytis* species are taken from Hyde et al. (2014), sequences from *B. mali* were determined by O'Gorman et al. (2008), the sequence of isolate BOT079 was determined by Shipunov et al. (2008). Phylogenetic tree construction used a maximum likelihood method with 1000 bootstraps. Only bootstrap values higher than 50% are displayed at the nodes.

Figure S2 | Phylogenetic position of 47 *Botrytis* isolates from asymptomatic dandelion (labeled by DAN and a number) in the genus based on G3PDH sequences. Sequences of recognized *Botrytis* species are taken from Hyde et al. (2014), sequences from *B. mali* were determined by O'Gorman et al. (2008). Phylogenetic tree construction used a maximum likelihood method with 1000 bootstraps. Only bootstrap values higher than 50% are displayed at the nodes.

Figure S3 | Phylogenetic position of 13 *Botrytis* isolates from asymptomatic dandelion (labeled by DAN and a number) in the genus based on RPB2 sequences. Sequences of recognized *Botrytis* species are taken from Hyde et al. (2014), sequences from *B. mali* were determined by O'Gorman et al. (2008). Phylogenetic tree construction used a maximum likelihood method with 1000 bootstraps. Only bootstrap values higher than 50% are displayed at the nodes.

Figure S4 | Phylogenetic position of 16 *Botrytis cinerea* isolates from asymptomatic dandelion (labeled by DAN and a number) in the genus based on G3890 sequences. *B. cinerea* strain B05.10 serves as the reference and *B. calthae* strain MUCL2830 was used as an outgroup. Phylogenetic tree construction used a maximum likelihood method with 1000 bootstraps. Only bootstrap values higher than 50% are displayed at the nodes.

Figure S5 | Phylogenetic position of 16 *Botrytis cinerea* isolates from asymptomatic dandelion (labeled by DAN and a number) in the genus based on FG1020 sequences. Sequences from *B. cinerea* strain B05.10 and *B. pseudocinerea* strain VD110 (determined by Leroch et al., 2013) serve as the reference while *B. calthae* strain MUCL2830 was used as an outgroup. Phylogenetic tree construction used a maximum likelihood method with 1000 bootstraps. Only bootstrap values higher than 50% are displayed at the nodes.

Figure S6 | Phylogenetic position of 14 *Botrytis* isolates from asymptomatic dandelion (labeled by DAN and a number) in the genus based on MRR1 sequences. Sequences from *B. cinerea* strain B05.10, *Botrytis* N11SE08 and *B. pseudocinerea* strain VD256 (determined by Leroch et al., 2013) serve as the references. Phylogenetic tree construction used a maximum likelihood method with 1000 bootstraps. Only bootstrap values higher than 50% are displayed at the nodes.

Table S1 | Sequences of primers used in this study.

REFERENCES

Amselem, J., Cuomo, C. A., van Kan, J. A. L., Viaud, M., Benito, E. P., Couloux, A., et al. (2011). Genomic analysis of the necrotrophic fungal pathogens *Sclerotinia sclerotiorum* and *Botrytis cinerea*. *PLoS Genet.* 7:e1002230. doi: 10.1371/journal.pgen.1002230

Barnes, S. E., and Shaw, M. W. (2002). Factors affecting symptom production by latent *Botrytis cinerea* in *Primula x polyantha*. *Plant Pathol.* 51, 746–754. doi: 10.1046/j.1365-3059.2002.00761.x

Barnes, S. E., and Shaw, M. W. (2003). Infection of commercial hybrid primula seeds by *Botrytis cinerea* and latent disease spread through the plants. *Phytopathology* 93, 573–578. doi: 10.1094/PHYTO.2003.93.5.573

Benito, E. P., ten Have, A., van 't Klooster, J. W., and van Kan, J. A. L. (1998). Fungal and plant gene expression during synchronized infection of tomato leaves by *Botrytis cinerea*. *Eur. J. Plant Pathol.* 104, 207–220.

Boff, P., Kastelein, P., de Kraker, J., Gerlagh, M., and Köhl, J. (2001). Epidemiology of grey mould in annual waiting-bed production of strawberry. *Eur. J. Plant Pathol.* 107, 615–624. doi: 10.1023/A:1017932927503

Boulard, T., Chave, M., Fatnass, H., Poncet, C., and Roy, J. C. (2008). *Botrytis cinerea* spore balance of a greenhouse rose crop. *Agric. For. Meteorol.* 148, 504–511. doi: 10.1016/j.agrformet.2007.11.014

Coertze, S., and Holz, G. (2002). Epidemiology of *Botrytis cinerea* on grape: wound infection by dry, airborne conidia. *South Afr. J. Enol. Vitic.* 23, 72–77.

Demers, J. E., Gugino, B. K., and Jimenez-Gasco, M. D. (2015). Highly diverse endophytic and soil *Fusarium oxysporum* populations associated with field-grown tomato plants. *Appl. Environ. Microbiol.* 81, 81–90. doi: 10.1128/AEM.02590-14

Dewey, F. M., Hill, M., and DeScenzo, R. (2008). Quantification of *Botrytis* and laccase in winegrapes. *Am. J. Enol. Vitic.* 59, 47–54.

Dewey, F. M., Steel, C. C., and Gurr, S. J. (2013). Lateral-flow devices to rapidly determine levels of stable *Botrytis* antigens in table and dessert wines. *Am. J. Enol. Vitic.* 64, 291–295. doi: 10.5344/ajev.2012.12103

Dik, A. J. (1992). "Interactions among fungicides, pathogens, yeasts, and nutrients in the phyllosphere," in *Microbial Ecology of Leaves*, eds J. H. Andrews and S. S. Hirano (New York, NY: Springer-Verlag), 412–429.

du Toit, L. J., Derie, M. L., and Pelter, G. Q. (2004). Prevalence of *Botrytis* spp. in onion seed crops in the Columbia basin of Washington. *Plant Dis.* 88, 1061–1068. doi: 10.1094/PDIS.2004.88.10.1061

Edwards, S. G., and Seddon, B. (2001). Selective media for the specific isolation and enumeration of *Botrytis cinerea* conidia. *Lett. Appl. Microbiol.* 32, 63–66. doi: 10.1046/j.1472-765x.2001.00857.x

Elad, Y., Pertot, I., Cotes Prado, A. M., and Stewart, A. (2015). "Plant hosts of *Botrytis* spp.," in *Botrytis – The Fungus, The Pathogen and Its Management in Agricultural Systems,* eds S. Fillinger and Y. Elad (Cham: Springer International Publishing Switzerland), 413–486.

Fournier, E., Giraud, T., Loiseau, A., Vautrin, D., Estoup, A., Solignac, M., et al. (2002). Characterization of nine polymorphic microsatellite loci in the fungus *Botrytis cinerea* (Ascomycota). *Mol. Ecol. Notes* 2, 253–255. doi: 10.1046/j.1471-8286.2002.00207.x

Gordon, T. R., and Martyn, R. D. (1997). The evolutionary biology of *Fusarium oxysporum*. *Ann. Rev. Phytopathol.* 35, 111–128.

Grant-Downton, R. T., Terhem, R. B., Kapralov, M. V., Mehdi, S., Rodriguez-Enriquez, M. J., Gurr, S. J., et al. (2014). A novel *Botrytis* species is associated with a newly emergent foliar disease in cultivated *Hemerocallis PLoS ONE* 9:e89272. doi: 10.1371/journal.pone.0089272

Harold, J. F. S., Fitt, B. D. L., and Landau, S. (1997). Temperature and effects of seed-borne *Botrytis cinerea* or *Alternaria linicola* on emergence of linseed (*Linum usitatissimum*) seedlings. *J. Phytopathol.* 145, 89–97. doi: 10.1111/j.1439-0434.1997.tb00369.x

Hausbeck, M. K., and Moorman, G. W. (1996). Managing *Botrytis* in greenhouse-grown flower crops. *Plant Dis.* 80, 1212–1219.

Hyde, K. D., Nilsson, R. H., Alias, S. A., Ariyawansa, H. A., Blair, J. E., Cai, L., et al. (2014). One stop shop: backbones trees for important phytopathogenic genera: I. *Fungal Divers.* 67, 21–125. doi: 10.1007/s13225-014-0298-1

Kerssies, A., Bosker-van Zessen, A. I., Wagemakers, C. A. M., and van Kan, J. A. L. (1997). Variation in pathogenicity and DNA polymorphism among *Botrytis cinerea* isolates sampled inside and outside a glasshouse. *Plant Dis.* 81, 781–786.

Kritzman, G., and Netzer, D. (1978). Selective medium for isolation and identification of *Botrytis* spp. from soil and onion seed. *Phytoparasitica* 6, 3–7. doi: 10.1007/BF02981180

Leroch, M., Plesken, C., Weber, R. W. S., Kauff, F., Scalliet, G., and Hahn, M. (2013). Gray mold populations in German strawberry fields are resistant to multiple fungicides and dominated by a novel clade closely related to *Botrytis cinerea*. *Appl. Environ. Microbiol.* 79, 159–167. doi: 10.1128/AEM.02655-12

Maude, R. B., and Presly, A. H. (1977). Neck rot (*Botrytis allii*) of bulb onions. *Ann. Appl. Biol.* 86, 163–180. doi: 10.1111/j.1744-7348.1977.tb01829.x

McQuilken, M. P., and Thomson, J. (2008). Evaluation of anilinopyrimidine and other fungicides for control of grey mould (*Botrytis cinerea*) in container-grown *Calluna vulgaris*. *Pest Man. Sci.* 64, 748–754. doi: 10.1002/ps.1552

Newton, A. C., Fitt, B. D. L., Atkins, S. D., Walters, D. R., and Daniell, T. J. (2010). Pathogenesis, parasitism and mutualism in the trophic space of microbe–plant interactions. *Trends Microbiol.* 18, 365–373. doi: 10.1016/j.tim.2010.06.002

O'Gorman, D. T., Sholberg, P. L., Stokes, S. C., and Ginns, J. (2008). DNA sequence analysis of herbarium specimens facilitates the revival of *Botrytis mali*, a postharvest pathogen of apple. *Mycologia* 100, 227–235. doi: 10.3852/mycologia.100.2.227

Prusky, D., and Lichter, A. (2007). Activation of quiescent infections by postharvest pathogens during transition from the biotrophic to the necrotrophic stage. *FEMS Microbiol. Lett.* 268, 1–8. doi: 10.1111/j.1574-6968.2006.00603.x

Puhl, I., and Treutter, D. (2008). Ontogenetic variation of catechin biosynthesis as basis for infection and quiescence of *Botrytis cinerea* in developing strawberry fruits *J. Plant Dis.Protect.* 115, 247–251. doi: 10.1007/BF03356272

Rajaguru, B. A. P., and Shaw, M. W. (2010). Genetic differentiation between hosts and locations in populations of latent *Botrytis cinerea* in Southern England. *Plant Pathol.* 59, 1081–1090. doi: 10.1111/j.1365-3059.2010.02346.x

Rodriguez, R. J., White, J. F. Jr., Arnold, A. E., and Redman, R. S. (2009). Fungal endophytes: diversity and functional roles. *New Phytol.* 182, 314–330. doi: 10.1111/j.1469-8137.2009.02773.x

Schafer, A. M., Kemler, M., Bauer, R., and Begerow, D. (2010). The illustrated life cycle of *Microbotryum* on the host plant *Silene latifolia*. *Botany* 88, 875–885. doi: 10.1139/B10-061

Schulz, B., and Boyle, C. (2005). The endophytic continuum. *Mycol. Res.* 109, 661–686. doi: 10.1017/S095375620500273X

Shipunov, A., Newcombe, G., Raghavendra, A. K. H., and Anderson, C. L. (2008). Hidden diversity of endophytic fungi in an invasive plant. *Am. J. Bot.* 95, 1096–1108. doi: 10.3732/ajb.0800024

Sowley, E. N. K., Dewey, F. M., and Shaw, M. W. (2010). Persistent, symptomless, systemic, and seedborne infection of lettuce by *Botrytis cinerea*. *Eur. J. Plant Pathol.* 126, 61–71. doi: 10.1007/s10658-009-9524-1

Staats, M., van Baarlen, P., and van Kan, J. A. L. (2005). Molecular phylogeny of the plant pathogenic genus *Botrytis* and the evolution of host specificity. *Mol. Biol. Evol.* 22, 333–346. doi: 10.1093/molbev/msi020

Stergiopoulos, I., and Gordon, T. R. (2014). Cryptic fungal infections: the hidden agenda of plant pathogens. *Front. Plant Sci.* 5:506. doi: 10.3389/fpls.2014.00506

Tanaka, A., Takemoto, D., Chujo, T., and Scott, B. (2012). Fungal endophytes of grasses. *Curr. Opin. Plant Biol.* 15, 462–468. doi: 10.1016/j.pbi.2012.03.007

van den Heuvel, J. (1981). Effect of inoculum composition on infection of French bean leaves by conidia of *Botrytis cinerea*. *Neth. J. Plant Pathol.* 87, 55–64. doi: 10.1007/BF01976657

van Kan, J. A. L. (2006). Licensed to kill: the lifestyle of a necrotrophic plant pathogen. *Trends Plant Sci.* 11, 247–253. doi: 10.1016/j.tplants.2006.03.005

Walker, A. S., Gautier, A., Confais, J., Martinho, D., Viaud, M., Le Pecheur, P., et al. (2011). *Botrytis pseudocinerea*, a new cryptic species causing gray mold in French vineyards in sympatry with *Botrytis cinerea*. *Phytopathology* 11, 1433–1445. doi: 10.1094/PHYTO-04-11-0104

Weiberg, A., Wang, M., Lin, F. M., Zhao, H. W., Zhang, Z. H., Kaloshian, I., et al. (2013). Fungal small RNAs suppress plant immunity by hijacking host RNA interference pathways. *Science* 342, 118–123. doi: 10.1126/science.1239705

Conflict of Interest Statement: The authors declare that the research was conducted in the absence of any commercial or financial relationships that could be construed as a potential conflict of interest.

frontiers in Plant Science

ORIGINAL RESEARCH
published: 25 May 2016
doi: 10.3389/fpls.2016.00679

GintAMT3 – a Low-Affinity Ammonium Transporter of the Arbuscular Mycorrhizal *Rhizophagus irregularis*

*Silvia Calabrese[1†], Jacob Pérez-Tienda[2†], Matthias Ellerbeck[3†], Christine Arnould[4], Odile Chatagnier[4], Thomas Boller[1], Arthur Schüßler[3], Andreas Brachmann[3], Daniel Wipf[4], Nuria Ferrol[2] and Pierre-Emmanuel Courty[1]**

[1] Department of Environmental Sciences, Botany, Zurich-Basel Plant Science Center, University of Basel, Basel, Switzerland, [2] Departamento de Microbiología del Suelo y Sistemas Simbióticos, Estación Experimental del Zaidín, Consejo Superior de Investigaciones Científicas, Granada, Spain, [3] Faculty of Biology, Genetics, Ludwig-Maximilians-University Munich, Planegg-Martinsried, Germany, [4] Agroécologie, AgroSup Dijon, Centre National de la Recherche Scientifique, Institut National de la Recherche Agronomique, Université Bourgogne Franche-Comté, Dijon, France

OPEN ACCESS

Edited by:
Ralph Panstruga, RWTH Aachen University, Germany

Reviewed by:
Paola Bonfante, University of Torino, Italy
Natalia Requena, Karlsruhe Institute of Technology, Germany

***Correspondence:**
Pierre-Emmanuel Courty
pierre-emmanuel.courty@unifr.ch

† These authors have contributed equally to this work.

Specialty section:
This article was submitted to Plant Biotic Interactions, a section of the journal Frontiers in Plant Science

Received: *15 December 2015*
Accepted: *02 May 2016*
Published: *25 May 2016*

Citation:
Calabrese S, Pérez-Tienda J, Ellerbeck M, Arnould C, Chatagnier O, Boller T, Schüßler A, Brachmann A, Wipf D, Ferrol N and Courty P-E (2016) GintAMT3 – a Low-Affinity Ammonium Transporter of the Arbuscular Mycorrhizal Rhizophagus irregularis. Front. Plant Sci. 7:679. doi: 10.3389/fpls.2016.00679

Nutrient acquisition and transfer are essential steps in the arbuscular mycorrhizal (AM) symbiosis, which is formed by the majority of land plants. Mineral nutrients are taken up by AM fungi from the soil and transferred to the plant partner. Within the cortical plant root cells the fungal hyphae form tree-like structures (arbuscules) where the nutrients are released to the plant-fungal interface, i.e., to the periarbuscular space, before being taken up by the plant. In exchange, the AM fungi receive carbohydrates from the plant host. Besides the well-studied uptake of phosphorus (P), the uptake and transfer of nitrogen (N) plays a crucial role in this mutualistic interaction. In the AM fungus *Rhizophagus irregularis* (formerly called *Glomus intraradices*), two ammonium transporters (AMT) were previously described, namely GintAMT1 and GintAMT2. Here, we report the identification and characterization of a newly identified *R. irregularis* AMT, GintAMT3. Phylogenetic analyses revealed high sequence similarity to previously identified AM fungal AMTs and a clear separation from other fungal AMTs. Topological analysis indicated GintAMT3 to be a membrane bound pore forming protein, and GFP tagging showed it to be highly expressed in the intraradical mycelium of a fully established AM symbiosis. Expression of GintAMT3 in yeast successfully complemented the yeast AMT triple deletion mutant (*MAT*a *ura3 mep1*Δ *mep2*Δ::*LEU2 mep3*Δ::*KanMX2*). GintAMT3 is characterized as a low affinity transport system with an apparent K_m of 1.8 mM and a V_{max} of 240 $nmol^{-1}$ min^{-1} 10^8 $cells^{-1}$, which is regulated by substrate concentration and carbon supply.

Keywords: arbuscular mycorrhizal fungi, ammonium transporter, low affinity transporter, extraradical mycelium, intraradical mycelium

Abbreviations: AM, arbuscular mycorrhiza; AMF, arbuscular mycorrhizal fungi; AMT, ammonium transporter; ERM, extraradical mycelium; HATS, high affinity transport system(s); IRM, intraradical mycelium; LATS, low affinity transport system(s); N, nitrogen; GS/GOGAT, glutamine synthetase/glutamate oxoglutarate aminotransferase.

INTRODUCTION

Nitrogen is an essential, often limiting, macronutrient for plants. Since the availability of nitrogen (N) in form of ammonium (NH_4^+) or nitrate (NO_3^-) in the environment is quite low, plants have evolved different strategies to overcome this problem. Under natural conditions 70–90% of land plant species are associated with nearly ubiquitous AM fungi, which can increase nutrient and water supply of their host. This goes along with improved plant fitness, growth, and disease resistance. In exchange, the fungal partners receive up to 20% of the photosynthates from the plant (Pearson and Jakobsen, 1993; Graham, 2000; Smith and Read, 2008). Previously it has been assumed that AMF play only a minor role in N nutrition of their host plant. However, several studies testing the contribution of AM fungi to plant N supply revealed that N uptake of the host plant via mycorrhizal uptake pathway can reach 42% (Mäder et al., 2000).

Several studies showed that inorganic NO_3^- and NH_4^+ (Bago et al., 1996; Govindarajulu et al., 2005; Jin et al., 2005) or small peptides and amino acids (organic form) (Hawkins et al., 2000) can be absorbed from the soil by extraradical mycelium (ERM) of AMF. There is also some weak evidence that AMF can absorb N from complex organic matter (Leigh et al., 2009; Hodge et al., 2010) and that they take up amino acids from the environment by the expression of amino acid permeases in the ERM (Cappellazzo et al., 2008). Although fungi and plants use many different resources to obtain N, it has been demonstrated that NH_4^+ often is the primary N source (Villegas et al., 1996; Hawkins et al., 2000; Toussaint et al., 2004). Assimilation of NH_4^+ through the GS/GOGAT pathway is energetically less costly compared to the reduction and assimilation of NO_3^- (Johansen et al., 1996; Marzluf, 1996; Bago et al., 2001; Breuninger et al., 2004; Govindarajulu et al., 2005; Jin et al., 2005).

Once absorbed, most of the inorganic N taken up by the AMF is assimilated and incorporated into arginine, constituting more than 90% of total free amino acids in the ERM. The arginine is translocated to the intraradical mycelium (IRM) (Govindarajulu et al., 2005; Cruz et al., 2007), where it is perhaps bound to the negatively charged polyphosphate in the fungal vacuole, forming a link between nitrogen and phosphorus transport (Martin, 1985; Govindarajulu et al., 2005). In the arbuscule, arginine is metabolized by arginase and urease in the urea cycle, and the free NH_4^+ is released into the periarbuscular space where it is taken up by the plant host (Bago et al., 2001; Govindarajulu et al., 2005; Tian et al., 2010).

For a long time it was not clear whether specialized transporters function in the AM symbiotic N exchange. Since the discovery of the first AMTs in *Saccharomyces cerevisiae* (Marini et al., 1994) and *Arabidopsis thaliana* (Ninnemann et al., 1994) several such transporters were characterized in plants (Gazzarrini et al., 1999; Sohlenkamp et al., 2000; Couturier et al., 2007; Guether et al., 2009a), fungi (Javelle et al., 1999, 2003a,b; López-Pedrosa et al., 2006; Lucic et al., 2008; Pérez-Tienda et al., 2011; Ellerbeck et al., 2013) and other organisms (Van Dommelen et al., 1998; Mayer et al., 2006). The so-called high-affinity transporter systems (HATSs) operate in the micromolar range, exhibit saturation kinetics, and the uptake of ammonia leads to depolarization of the transmembrane electrical potential (Ullrich et al., 1984; Wang et al., 1994). In contrast, low-affinity transporter systems (LATSs) are highly active in the millimolar range (Fried et al., 1965; Vale et al., 1988; Wang et al., 1993; Shelden et al., 2001).

Physiological studies in plant roots and the AMF *Rhizophagus irregularis* have revealed that uptake systems for ammonium and nitrate follow biphasic kinetics with respect to external substrate concentrations (Pérez-Tienda et al., 2011). The first AMF AMT, characterized from *R. irregularis* (syn. *Glomus irregularis*, formerly named *Glomus intraradices*), GintAMT1, is a high affinity transporter (López-Pedrosa et al., 2006; Pérez-Tienda et al., 2011). Using immunolocalization and expression analysis of microdissected cells, it was shown that GintAMT1 and a second AMT, GintAMT2 (Pérez-Tienda et al., 2012), were both expressed in the ERM and IRM, participating in the uptake of NH_4^+ from the soil solution and possibly in retrieval of NH_4^+ leaking out during fungal metabolism at the symbiotic interface. Since then, three related AMTs (GpyrAMT1, GpyrAMT2, GpyrAMT3) were characterized from the glomeromycotan fungus *Geosiphon pyriformis*, which forms a symbiosis with the cyanobacterium *Nostoc* (Ellerbeck et al., 2013).

On the plant side, the expression of several mycorrhiza inducible AMTs could be specifically assigned to arbuscule-colonized cortical cells. Such transporters were identified in *Lotus japonicus* (LjAMT2;2) (Guether et al., 2009b), *Medicago truncatula* (predicted AMT: IMGAG| 1723.m00046) (Gomez et al., 2009), *Glycine max* (GmAMT1;4, GmAMT3;1, GmAMT4;1, and GmAMT4;4) (Kobae et al., 2010), and S*orghum bicolor* (SbAMT3;1, SbAMT4) (Koegel et al., 2013a). The discovery of specialized transporters at the symbiotic interface was an important step to gain more insight into the symbiotic N transfer.

Here we report the discovery, biochemical characterization and localization of GintAMT3, a new AMF AMT from *R. irregularis,* which is expressed primarily in the IRM and represents a low affinity AMT.

MATERIALS AND METHODS

Plant Growth Conditions for Expression Analysis

Experiments were performed with sorghum (*Sorghum bicolor* (L.) Moench), cv Pant-5. This cultivar is closely related to BTx623, the sorghum cultivar used for genome sequencing (Paterson et al., 2009). Seeds of cv Pant-5 were kindly provided by sorghum breeders of I.G.F.R.I. (CCS Agriculture University of Hissar, Haryana, India) and G. B. Pant University of Agriculture and Technology (Pantanagar, Uttaranchal, India). Seeds were surface-sterilized (10 min in 2.5% KClO) and then rinsed with sterile deionized water several times for 1 d and soaked in sterile deionized water overnight. Seeds were pre-germinated on autoclaved sand at 25°C for 24 h and then grown in the dark

at room temperature for 72 h. The fungal isolate *Rhizophagus irregularis* BEG-75 (Botanical Institute, Basel, Switzerland) was propagated by trap cultures as previously described (Oehl et al., 2004). To establish AM symbiosis, pregerminated seeds were individually inoculated in compartmented microcosms (Koegel et al., 2013b), where one plant and one hyphal compartment are connected, but separated by two 21 μm nylon meshes and an air gap in between. The air gap was created by placing two 5 mm plastic meshes between the two 21 μm nylon meshes. The two compartments were filled with sterile (120°C, 20 min) growth substrate consisting of a mixture of zeolithe (Symbion, Czech Republic) and sand (1: 1 v/v). About 100 spores were added to the mixture. For the controls (non-mycorrhizal plants), the same amount of autoclaved inoculum was added to the mixture. To correct for possible differences in microbial communities, each pot received 1 ml of filtered washing of AMF inoculum. Plants were grown in a glasshouse with day : night temperatures of c. 28°C : 15°C. Plants were watered twice a week during experiments. From the first week on, 8 ml of modified Hoagland solution was applied weekly. Three different Hoagland solutions, modified after Gamborg and Wetter (1975), were prepared to obtain different N sources or N concentrations : −N, 1x NO_3^- and 1x NH_4^+ (Koegel et al., 2013a).

Populus trichocarpa (derived from cuttings, clone 10174, Orléans, France) grew together with *S. bicolor,* in a tripartite compartment system, in a zeolithe:sand substrate (1:1; w:w). Thereby, single compartments were separated by 21 μm and 3 mm meshes to allow AMF hyphae but no plant root growth in between the compartments. Plants were inoculated with 1 ml liquid inocula of *R. irregularis,* isolate BEG75 (InoculumPlus, Dijon, France), in 0.01 M citrate buffer (pH 6) containing about 110 spores/ml. Plants were fertilized once a week with 10 ml of Hoagland solution without phosphorus. From the 22nd week on, when all plants showed Pi depletion as indicated by anthocyan accumulation, 10 ml Hoagland solution containing either low Pi ([Pi] = 28 μM) or high Pi ([Pi] = 560 μM) concentration was applied in the compartment for the ERM for 9 weeks. As a control both plant species were grown separately in a single compartment, receiving the fertilizer directly to their root systems.

Rhizophagus irregularis Monoxenic Cultures under Different N Treatments

Rhizophagus irregularis monoxenic cultures were established in bi-compartmental Petri dishes to allow separating the root compartment from the hyphal compartment (St-Arnaud et al., 1996; Fortin et al., 2002). Cultures were started on M medium (Chabot et al., 1992) by placing an explant of *Agrobacterium rhizogenes* transformed-carrot (*Daucus carota*) roots colonized with the AMF in the root compartment. Petri dishes were incubated in the dark at 24°C until the hyphal compartment, which contained M medium without sucrose (M–C medium), was profusely colonized by the fungus (∼6 weeks). The content of the hyphal compartment was then removed and replaced by liquid M–C medium (15 ml) containing either 3.2 mM NO_3^- (high N) or in a modified M media containing 0.8 mM NO_3^- (low N). The mycelium then colonized this medium over the subsequent 2 weeks. At this point, the medium was removed and replaced by fresh liquid M–C medium without NO_3^-. The time of medium exchange was referred as time 0 for the N starvation treatment, and mycelia were harvested 2 and 7 days later. For the N re-supply experiments, mycelia grown in low N media and N-starved for 48 h were supplemented with different N sources and concentrations (3 mM or 30 μM nitrate or ammonium, or 5 mM glutamine) or water (control plates). The ERM was harvested 24 h later. For treatments with acetate or the inhibitor of GS, MSX, the N-starved mycelia (grown in the low N media for 2 weeks and for 2 days in a N-free media) were supplied with 4 mM acetate or 2.5 mM MSX, respectively, together with 3 mM ammonium sulfate. In all experiments, mycelia were collected with forceps, rinsed with sterilized water, dried with sterilized filter paper, immediately frozen in liquid N and stored at −80°C until used. All treatments were independently repeated four times.

Root Colonization Measurements

A subsample of fresh roots was immersed in 10% KOH and stored in the fridge at 4°C overnight. At the next day the roots were rinsed under the tap and immersed in 2% HCl for 1 h at room temperature. Afterward the roots were rinsed under the tap, immersed in 0.05% trypan blue and stored in the fridge at 4°C overnight. The next day the trypan blue was removed, roots were rinsed with tap water and immersed in lactic-acid glycerol water for destaining. Total root colonization was measured using the grid line intersection method as described by Brundrett et al. (1984). Differences between means of variables were assessed by *t*-test ($p \leq 0.5$), using Microsoft Excel 2010.

In Silico Analysis

The sequencing, assembly, and annotation of the *R. irregularis* genome was described in (Tisserant et al., 2012). All *R. irregularis* sequences are available at the Phytozome website[1] and at GenBank/European Molecular Biology Laboratory (EMBL)/DNA Data Bank of Japan (DDBJ). Using BLAST search and the INTER-PRO domains (IPR018047 and IPR001905) at the JGI website, we identified gene models coding for putative AMTs in the draft genome. Gene prediction at the JGI was performed using gene predictors (FGENESH, and GENEWISE), and gene models were selected by the JGI annotation pipeline (Tisserant et al., 2012). Selection of the AMT models was based on expressed sequence tag (EST) support, completeness, and homology to a curated set of proteins. The putative homologs detected were characterized based on conserved domains, identities, and *e*-values in comparison with fungal AMT sequences available at the NCBI GenBank[2] and UNIPROT[3] (**Figure 1**).

[1]https://phytozome.jgi.doe.gov/pz/portal.html

[2]http://www.ncbi.nlm.nih.gov/

[3]http://expasy.org/

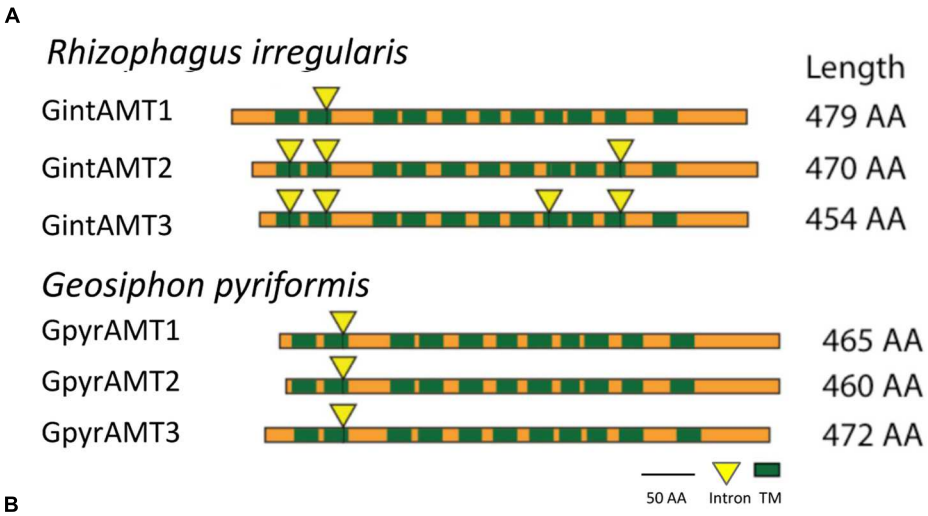

B

Amino acid identity (similarity)

	GpyrAMT3	GpyrAMT2	GpyrAMT1	GintAMT3	GintAMT2
GintAMT1	65% (81%)	61% (77%)	57% (74%)	60% (75%)	63% (79%)
GintAMT2	65% (81%)	58% (74%)	61% (74%)	65% (80%)	
GintAMT3	60% (77%)	56% (71%)	59% (73%)		
GpyrAMT1	59% (76%)	60% (74%)			
GpyrAMT2	63% (78%)				

FIGURE 1 | Topologies of glomeromycotan AMTs and their genetic relationship. (A) Transmembrane domain (TMD) topology and intron localization of the six glomeromycotan AMTs. Green boxes indicate TMD positions, yellow triangles mark intron positions. Both are highly conserved, while N and C termini differ in length and are less conserved. **(B)** Reciprocal BLAST (Altschul et al., 1997) analysis (Blosum62 matrix) revealed a high conservation at the sequence level between the six transporters. They share at least 56% AA identity and 71% AA similarity. Intra-species comparisons are marked in dark gray.

Signal peptides were predicted with SignalP 3.0[4] and subcellular location with TargetP 1.1[5]. Conserved protein domains were analyzed using prosite[6] and InterProScan[7].

Full-length amino acid sequences of fungal AMTs were retrieved using BLAST[8] and the JGI[9] webpage. Sequence alignments were performed with the ClustalW2 package. For phylogenetic analyses, the alignments were imported into the Molecular Evolutionary Genetics Analyses software (MEGA), version 5.05 (Tamura et al., 2011). Neighbour-joining (NJ) method was applied with the Poisson correction model, the pairwise deletion option and bootstrap test with 1,000 replicates.

A two-dimensional model was generated with Protter – visualize proteoforms (Omasits et al., 2013) and a 3D model was calculated via SWISS-MODEL[10] , based on 2b2hA, an AMT from *Archaeoglobus fulgidus*, AMT-1 (**Supplementary Figure S1**).

Sampling, RNA Isolation and Quantitative Reverse Transcription-PCR

RNA extraction and cDNA synthesis were performed as described previously (Courty et al., 2009). Primers used as controls or for analysis had an efficiency ranging between 90 and 110%. Plant parts were harvested separately and the ERM was extracted from the substrate by immersing the substrate in water and harvesting the floating mycelium with a 32 μm sieve. Mycelium was snap frozen in liquid nitrogen and stored at −80°C. Plant roots were carefully washed under tap water to remove all soil adhering to the roots. Three subsamples of 100 mg of fresh roots were snap-frozen and stored at −80°C for further gene expression analysis by qRT-PCR.

cDNAs were obtained using the iScript^{TM}cDNA Synthesis Kit (BIO RAD Laboratories, Paolo Alto, CA, US). For quantification a two-step quantitative RT-PCR (qRT-PCR) approach was used. Gene specific primers were designed in Primer 3[11] and amplify 3.1[12]. Target gene expression was normalized to the expression of the transcription elongation factor TEF1α in *R. irregularis*. qRT-PCRs were run in a 7500 real-time PCR systems (Applied

[4]http://www.cbs.dtu.dk/services/SignalP/
[5]http://www.cbs.dtu.dk/services/TargetP/
[6]http://us.expasy.org/prosite
[7]https://www.ebi.ac.uk/interpro/interproscan.html
[8]http://blast.ncbi.nlm.nih.gov
[9]http://jgi.doe.gov/
[10]http://swissmodel.expasy.org/
[11]http://bioinfo.ut.ee/primer3-0.4.0/
[12]http://engels.genetics.wisc.edu/amplify

Biosystems) using the following settings: 95°C for 3 min and then 40 cycles of 95°C for 30 s, 60°C for 1 min and 72°C for 30 s. For each transporter three biological and three technical replicates ($n = 9$) per treatment were conducted.

Isolation of GintAMT3 and Functional Expression in Yeast

Full-length doubled-stranded cDNA was synthesized from RNA of the ERM using the SMARTer^{TM} cDNA Synthesis Kit (Clontech, US, Canada). GintAMT3 (JGI Protein ID: 218175; JGI Transcript ID: 218287; NCBI accession number: KU933909) was then amplified using the primer pair GintAMT3_fl_Fwd/GintAMT3_fl_Rev (**Supplementary Table S1**). Full-length GintAMT3 was cloned into pDR196 using the Gateway technology (Invitrogen), as described previously (Wipf et al., 2003), resulting in the pDR196-GintAMT3 plasmid construct. pDR196-GintAMT3 and as a control the empty vector were transformed into the *Saccharomyces cerevisae* strain 31019b (*MAT*a *ura3 mep1*Δ *mep2*Δ::*LEU2 mep3*Δ::*KanMX2*) (Marini et al., 1997) as described by Dohmen et al. (1991). Transformants were selected on SD media lacking uracil and further transferred on yeast nitrogen base (YNB-N) glucose media without ammonium and amino acids supplemented with NH_4Cl as the sole nitrogen source (1 and 3 mM). Sequence identities and integrities were verified by sequencing.

[^{14}C]Methylamine Uptake Assay

Initial [^{14}C]methylamine uptake rates (American Radiolabeled Chemicals, Inc., St. Louis, MO, USA) for amino acids were measured as described previously (Marini et al., 1997). Single colonies were grown in liquid YNB-N supplemented with 6% glucose and 500 μg/mL L-proline to logarithmic phase and were centrifuged at an OD_{600} of 0.5 to 0.8. Cells were washed twice in sterile water and resuspended in 50 mM KH_2PO_4 buffer pH 5, to a final OD_{600} of 5. Before the uptake measurements an aliquot of yeast cells was supplemented with 20 mM glucose, incubated at 30°C for 5 min at 1,000 rpm. To start the reaction an equal amount of pre-warmed KH_2PO_4 buffer containing 15 kBq of [^{14}C]methylamine and unlabelled methylamine (0–15 mM) was added. Cells were incubated at 30°C, 1,000 rpm, and 45 μl subsamples were taken after 1, 2, 3, and 4 min, diluted in 5 ml KH_2PO_4/sorbitol buffer, separated from the incubation buffer on glass fibre filters (Whatman), and washed twice with the same buffer. Radioactivity retained on the filter was assayed by liquid scintillation spectrometry (Packard).

Expression Analysis at the Cellular Level by Laser Capture Microdissection

Sorghum roots were washed with tap water to remove the substrate. Pieces of 10–15 mm were cut with a razor blade from differentiated regions of the mycorrhizal and non-mycorrhizal roots. The root segments were embedded in OCT (EMS, Delta Microscopies Aygues-Vives, France) and then frozen at −23°C. 40 μm thin sections were cut with a Cryocut (Cryocut 1800 Leica), and the cuts were placed on Fisher Probe-On slides (Fisher Scientific, Ilkirch, France). The sections were washed and fixed as follows: 3 min 70% EtOH, 30 min DEPC H_2O, 2 min 100% EtOH. The slides were then dried for 20 min at 37°C on a warming plate and kept at −80°C before use.

An Arcturus XT microdissection system (Applied Biosystems, Foster City, CA, USA) was used to collect the cells from the mycorrhizal and non-mycorrhizal root sections. Eight replicates of two different cell types were collected: arbuscule-containing cells (ARBs), and cortical cells from non-mycorrhizal roots (Cs). A total of 5,000–15,000 cells were cut out for each sample. RNA from collected cells was extracted using the Arcturus Pico Pure RNA isolation Kit (Excilone, Applied Biosystems, Foster City, CA, USA), with an in-column DNase treatment following manufacturer's instructions. Quantity and quality of the extracted RNAs were verified using a bioanalyzer with RNA pico chips (Agilent, Santa Clara, CA, USA). Synthesis of cDNA and quantitative reverse transcriptase polymerase chain reaction (qRT-PCR) analysis was done as previously described using the iScript cDNA Synthesis kit (Bio-Rad, Hercules, CA, USA), starting with 100 pg RNA.

RESULTS

In Silico Analysis of GintAMT3

Based on the high conservation of amino acid sequences, a consensus signature for AMTs has been defined corresponding to Prosite PDOC00937, InterPro IPR001905, and Pfam 00909. The *ab initio* annotation and subsequent automated BLAST and INTERPRO searches of the *R. irregularis* draft genome sequence (Tisserant et al., 2012) identified three gene models containing these conserved AMT domains, from which two were already characterized, namely *GintAMT1* (López-Pedrosa et al., 2006) and *GintAMT2* (Pérez-Tienda et al. (2012). The length of the nucleotide sequence of *GintAMT3* is 1,798 bp. The coding exon sequence (1,365 bp) was confirmed by EST alignment and cDNA sequencing, and it is interrupted by four short introns of 92 bp, 130 bp, 125 bp, and 86 bp length, typical of *R. irregularis* (Tisserant et al., 2012).

Comparisons between cDNA and genomic sequences of the *R. irregularis* AMT genes revealed 1, 3, and 4 introns for *GintAMT1*, *GintAMT2,* and *GintAMT3*, respectively. Their positions are conserved between the genes, whenever present in more than one gene (**Figure 1A**). Location of intron 2 is even conserved in all six AMT genes of *R. irregularis* and *G. pyriformis*, indicating its presence in a common ancestral gene before these glomeromycotan species split. This is remarkable as the two AMF are distantly related and probably have separated more than 400 million years ago (Schüßler et al., 2001). A comparison with an AMT gene of the basidiomycete *Ustilago maydis*, *UmUMP2*, revealed an intron in a different position, 60 base pairs further downstream between codons for two other highly conserved residues, a glycine and an asparagine residue. Thus, the position of intron number 2 is conserved among glomeromycotan AMT genes but, based on present data, also appears to be specific for

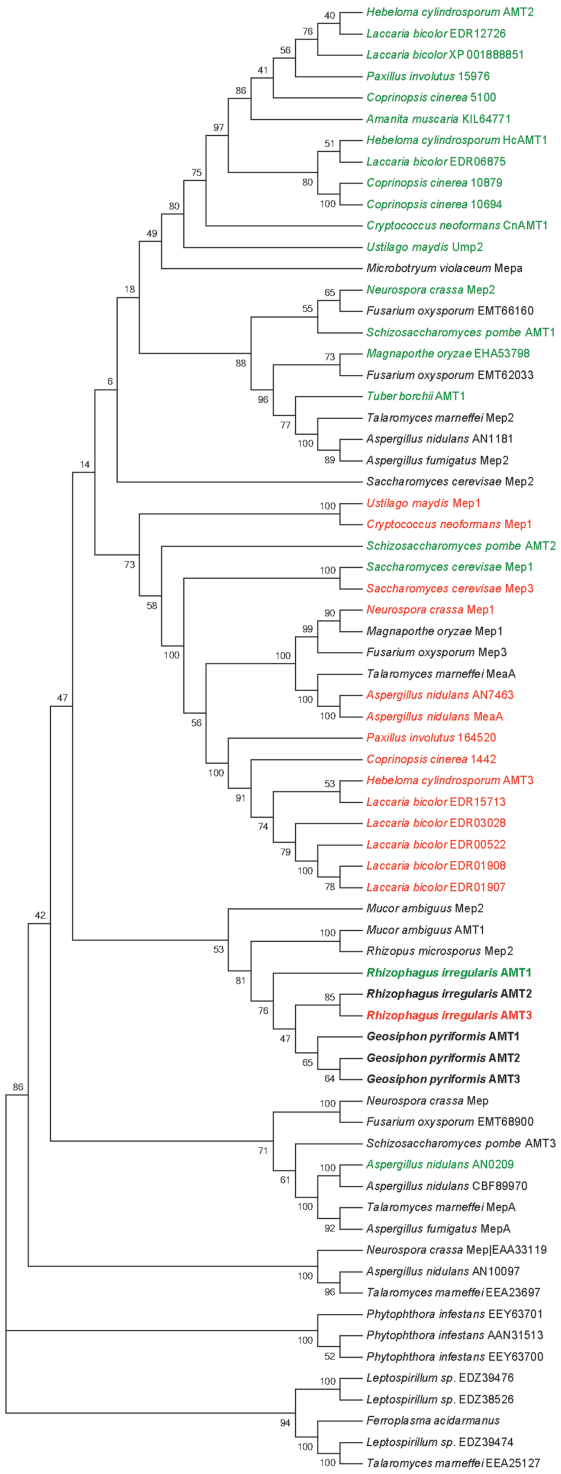

FIGURE 2 | Phylogenetic tree ("NJ Bootstrap Consensus Tree") of fungal Mep/AMT proteins. Transporter names or accession numbers are indicated. Bootstrap values are derived from 1000 replications. HATSs are highlighted in green and low affinity transporter are highlighted in red. Glomeromycotan AMTs are highlighted in bold. Phylogenetic tree was constructed using MEGA6.06 package (Tamura et al., 2013). Gene names, protein IDs and bootstapping values are indicated. Sequences obtained from (*Continued*)

FIGURE 2 | Continued

the JGI databank: *Aspergillus nidulans* AMT (AN7463), AMT (AN0209), AMT (AN10097), AMT (AN1181); *Coprinopsis cinerea* AMT (1442), AMT (5100), AMT (10879), AMT (10694); *Rhizophagus irregularis* AMT1 (337025), AMT2 (314209), AMT3 (21817); *Paxillus involutus* AMT (164520), AMT (15976), AMT (KIJ11108). Sequences obtained from the *NCBI* databank*: Aspergillus fumigatus* Mep2 (EAL90420), MepA (EAL91508); *Amanita muscaria* (KIL64771); *Cryptococcus neoformans* Mep1 (XP_566614), AMT1 (XP_567361); *Ferroplasma acidarmanus* (WP_019841313); *Fusarium oxysporum* AMT (EMT62033), AMT (EMT68900), AMT (EMT66160), Mep3 (EMT61925); *Geosiphon pyriformis* AMT1 (AGO45860), AMT2 (AGO45861), AMT3 (AGO45862); *Hebeloma cylindrosporum* AMT1 (AAM21926), AMT2 (AAK82416), AMT (AAK82417); *Laccaria bicolor* AMT (EDR12726), AMT (EDR06875), AMT (EDR03028), AMT (EDR01908), AMT (EDR01907), AMT (EDR00522), AMT (EDR15713), AMT (XP_001888851); *Leptospirillum sp.* AMT (EDZ39474), AMT (EDZ39476), AMT (EDZ38526); *Magnaporthe oryzae* AMT (EHA53798), Mep1 (EHA48931); *Microbotryum violaceum Mepa* (AAD40955); *Neurospora crassa* Mep1 (EAA35174), Mep2 (EAA32441), Mep (KHE86570), Mep (EAA33119); *Mucor ambiguous* AMT1 (GAN10886), Mep2 (GAN10300); *Phytophthora infestans* AMT (AAN31513), AMT (EEY53846), AMT (EEY63701), AMT (EEY63700); *Rhizopus microspores putative* Mep2 (CEJ04454); *Saccharomyces cerevisae* Mep1 (P40260), Mep2 (P41948), Mep3 (P53390); *Schizosacchromyces pombe* AMT1 (NP_588424), AMT2 (CAB65815), AMT3 (P53390); *Talaromyces marneffei* MepA (EEA28528), MeaA (EEA28073), Mep2 (EEA20421), putative AMT (EEA25127), putative AMT (EEA23697); *Tuber borchii* AMT1 (AAL11032); *Ustilago maydis* Mep1 (KIS67424), UMP2 (KIS66151).

this phylum. The 6 encoded proteins show high levels of amino acid identity and similarity (**Figure 1B**).

The introns 1 and 4 are conserved between *GintAMT2* and *GintAMT3*, suggesting recent gene duplication. Intron 3 only exists in *GintAMT3*. Also the positions of predicted transmembrane domains (TMDs, green rectangles in **Figure 1A**) are highly conserved between the AMF AMTs.

A phylogenetic analysis was performed to compare the protein sequences of the glomeromycotan AMTs with the ones from other fungi. This analysis revealed a close relationship of the six glomeromycotan AMTs, and a clear homology with one AMT family of the Ascomycetes, represented by SpAMT1 (**Figure 2**). For the non-glomeromycotan AMTs, we observed a clear separation of the AMTs according to their affinities, with the exception of the *S. cerevisiae* high-affinity transporter ScMEP2, which is more closely related to the low affinity *S. cerevisiae* AMTs than to its orthologs in other fungi (**Figure 2**).

Root Colonization Depending on N and P Conditions

After 30 weeks of growth, symbioses between *R. irregularis* and the two host plants, poplar and sorghum, were well established (**Supplementary Table S2**). Root hyphal colonization rates ranged between 79 and 93% and were not significantly different ($n = 7$). In sorghum, three times more arbuscules were found in the low Pi treatment as compared to the high Pi treatment, while no significant differences were found in poplar. In the 3 months old sorghum plants, set under three different N conditions, hyphal colonization ranged between 94 and 99% ($n = 4$) (**Supplementary Table S2**).

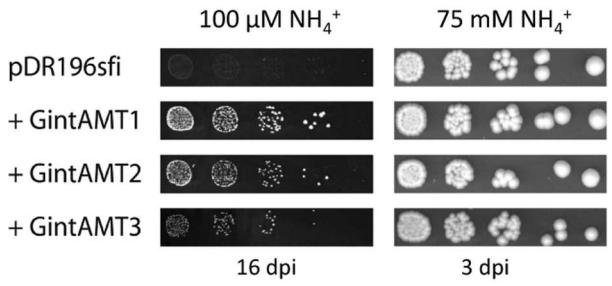

FIGURE 3 | Complementation of ammonium uptake deficiency in a yeast triple mutant by glomeromycotan AMTs. Ammonium uptake-deficient yeast cells (*mep1–3*Δ) were transformed with an expression vector containing various AMT genes under control of the strong *PMA1* promoter. Fivefold dilution series of the transformants were incubated either on minimal medium containing 50 µM $(NH_4)_2SO_4$ (=100 µM NH_4^+) as sole nitrogen source for 16 days **(left)** or on synthetic complete medium [containing roughly 37.5 mM $(NH_4)_2SO_4$] for 3 days **(right)**. *Rhizophagus irregularis* AMTs are able to partly complement the growth deficiency of the Δ*mep1–3* yeast mutant on low NH_4^+ concentrations (100 µM, **left**).

Yeast Complementation, GFP Localization, and Ammonium Uptake

The putative transporter gene *GintAMT3* was tested for complementation of the yeast *mep1-3*Δ mutant (strain MLY131a/α, Lorenz and Heitman, 1998) in comparison with the already known AMT genes. Cells were transformed with variants of the plasmid pDR196*sfi* containing the different AMT genes or a stuffer gene (a part of a human aldolase gene without ORF) cloned into the *SfiI* sites. The genes were constitutively expressed under the *PMA1* promoter. All three transporter genes of *R. irregularis* at least partly restored the ammonium uptake capability in yeast, as proven by their capability to restore growth of the *mep1-3*Δ mutant on medium containing 50 µM $(NH_4)_2SO_4$ as sole nitrogen source (**Figure 3**). *GintAMT1* complemented more efficiently the mutant phenotype than GintAMT2 and GintAMT3, demonstrated by larger colonies in a successive 5x dilution series on medium containing 50 µM $(NH_4)_2SO_4$ as sole nitrogen source (**Figure 3**).

To test if the different complementation efficiencies observed by the different AMTs could be due to an incorrect protein localization in the heterologous system, we cloned *GintAMT1*, *GintAMT2,* and *GintAMT3* to the 5′ end of a green fluorescent protein (GFP) coding gene into the expression vector pDR196*sfi* and transformed the yeast *mep1–3*Δ mutant with these constructs, resulting in the expression of C-terminal GFP-tagged AMT fusion proteins in yeast cells. The localization of these fusion proteins was performed with a Leica SP5 confocal laser-scanning microscope (CLSM, **Figure 4**). All tagged proteins were localized to the plasma membrane (PM) in *S. cerevisiae* (**Figure 4**). Additionally, we observed vacuolar or perinuclear membrane localization for some of them indicative of an endoplasmic reticulum localization, most probably as an overexpression artifact (**Figure 4**). All tagged transporters behaved like the untagged versions (not shown), either complementing the growth defect of the yeast mutant

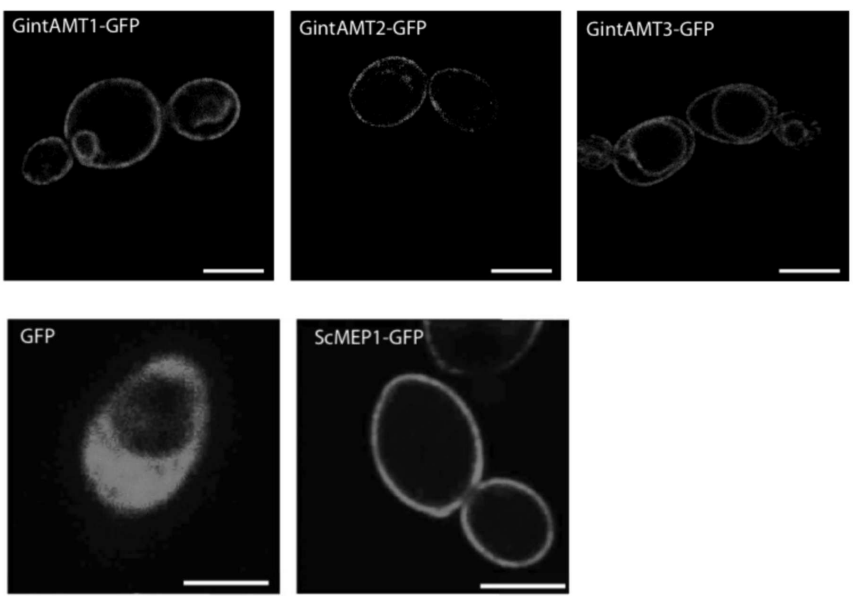

FIGURE 4 | Localization of GFP-tagged glomeromycotan AMTs in *S. cerevisiae*. C-terminally GFP-tagged versions of ScMEP1, GintAMT1, GintAMT2, and GintAMT3 as well as soluble GFP were cloned into pDR196sfi and expressed in *S. cerevisiae* under control of the *PMA1* promoter. The cells were grown to logarithmic growth phase and the localization of the fusion proteins was assessed by confocal microscopy. All three *R. irregularis* AMTs tagged with GFP were localized at the plasma membrane (PM), like ScMEP1-GFP (**lower center**), the positive control. Soluble GFP was localized to the cytoplasm of *S. cerevisiae* (**lower left**). Additional vacuolar membrane localization was visible for GintAMT3-GFP (**upper right**). GintAMT1-GFP (**upper left**) displayed an additional nuclear membrane localization. Bars are 2.5 µm.

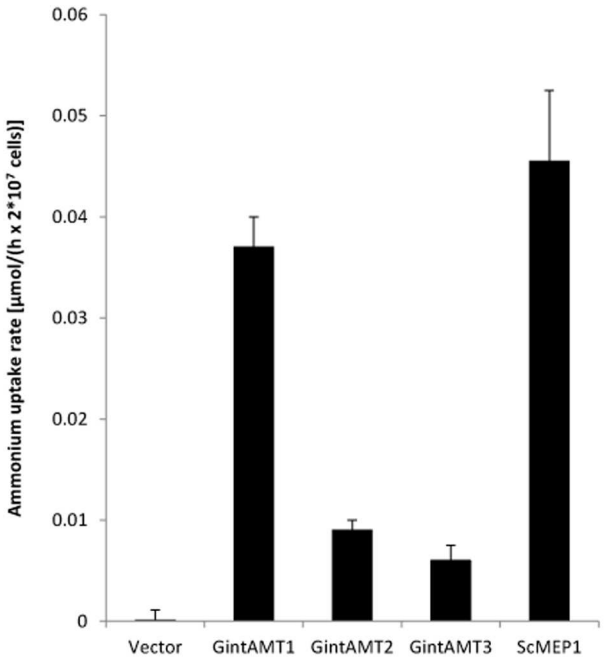

FIGURE 5 | Quantification of ammonium uptake in yeast cells expressing glomeromycotan AMTs. Yeast cells expressing the stated genes from the plasmid pDR196sfi were grown over night in synthetic complete medium lacking uracil (HC-U), washed and cultured in liquid medium containing a starting concentration of 2 mM ammonium. Samples were taken after 10, 30, 60, 120, 180, 240, and 300 min, and residual ammonium was determined. Yeast cells expressing *ScMEP1* and *GintAMT1* took up ammonium quite rapidly. *GintAMT2* and *GintAMT3* expressing cells imported ammonium at a slower rate, but clearly above background level ("Vector"). Bars show average of 3–4 experiments and standard deviation.

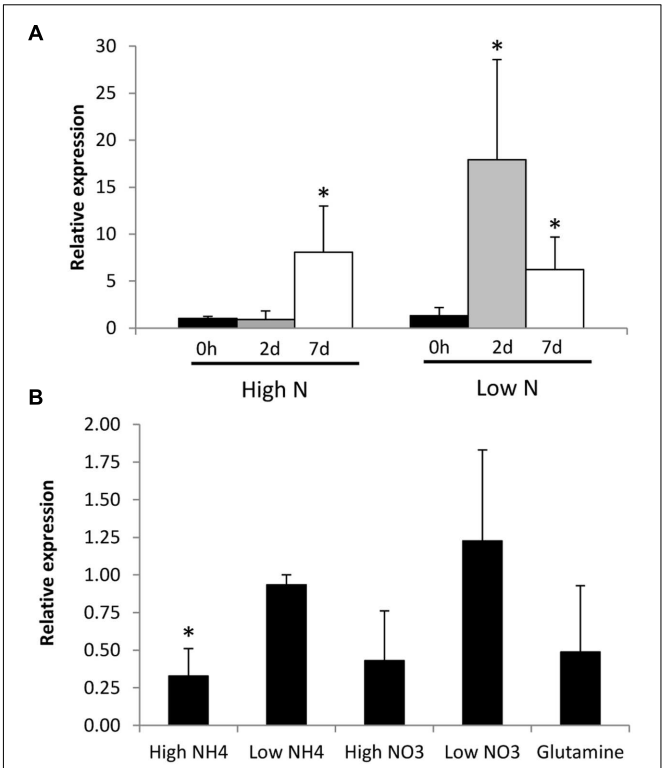

FIGURE 6 | Effect of N availability on *Gint*AMT3 gene expression. **(A)** Real-time RT-PCR analysis of *GintAMT3* mRNA levels in the ERM of *R. irregularis* developed in liquid M-C medium in the presence of either 3.2 mM (High N) or 0.8 mM nitrate (Low N) and exposed for different periods of time to a N-free medium. **(B)** Effect of N addition to the N-starved mycelium on *GintAMT3* expression. Gene expression was analyzed by real-time RT-PCR in ERM grown in 25% N media, maintained for 48 h in a N-free media (Control) and exposed for 24 h to 3 mM (High) or 30 µM (Low) of NH_4^+ or NO_3^-, or 5 mM glutamine. Control plates were supplemented with H_2O. Data were calibrated by the expression values obtained for the gene encoding the EF1α. Error bars represent SE of the mean of three independent experiments. *: statistically significant ($p < 0.05$) in comparison to the respective control value.

(GintAMT1-GFP, GintAMT2-GFP, GintAMT3-GFP) or not (soluble GFP).

Ammonium Removal Assay

To measure the different ammonium transport capacities of the transporters, ammonium removal assays according to Ellerbeck et al. (2013) were performed. In this experimental setup, dense yeast cultures ($OD_{600} = 2$) were incubated in relatively high ammonium concentrations (1 mM) for several hours and the remaining ammonium in the medium was measured at distinct time points (after 10, 30, 60, 120, 180, 240, and 300 min). Therefore, no kinetics but overall ammonium uptake can be measured. The results of the removal assays confirmed the yeast complementation assays. The 3 AMTs of *R. irregularis* transported ammonium to a varying but always lower extent than ScMEP1 (**Figure 5**). GintAMT2 and GintAMT3 showed lower ammonium removal activity in these experiments (**Figure 5**) than GintAMT1, supporting the results from the complementation assays on plate (**Figure 3**).

GintAMT Expression Levels

Regulation of *GintAMT3* gene expression by N starvation was assessed in the ERM of *R. irregularis* developed in monoxenic cultures in M–C medium (standard or high N) or in a modified medium containing reduced N (low N), and then incubated for different periods of time in a N-free M medium. *GintAMT3* transcript levels increased when the fungus was exposed to the N-free medium. When the fungus was grown in the low-N media, *GintAMT3* up-regulation was observed 2 days after N deprivation, while in the ERM grown in the high N medium *GintAMT3* up-regulation was observed 5 days later (**Figure 6A**).

To further investigate the effect of N on *GintAMT3* transcript levels, we also determined whether the addition of different N sources to the N-deprived mycelia had an effect on its expression (**Figure 6B**). Relative to the N-deprived ERM, *GintAMT3* transcript levels significantly decreased 24 h after the addition of 3 mM NH_4^+. Feeding the mycelium with nitrate, glutamine, or 30 µM NH_4^+ did not significantly change *GintAMT3* gene expression, although a slight decrease was observed after the addition of 3 mM nitrate or glutamine.

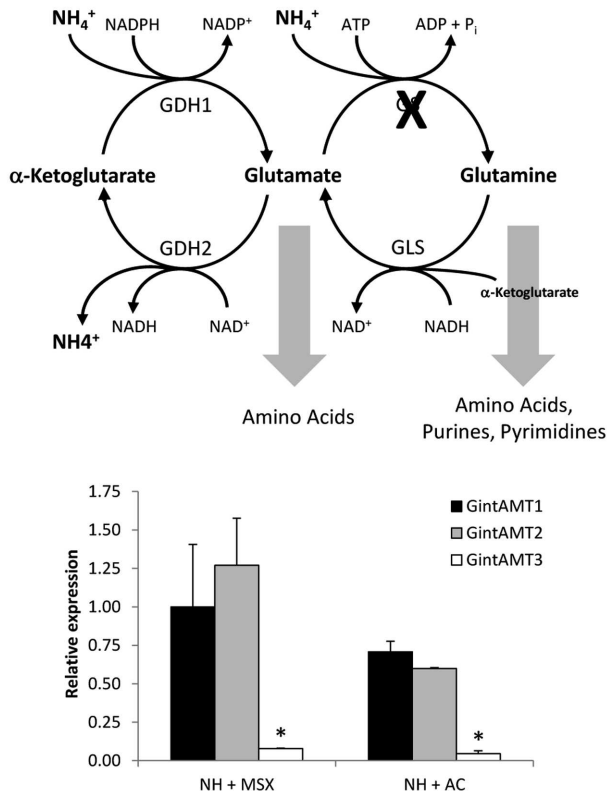

FIGURE 7 | Effect of MSX and acetate on *GintAMTs* gene expression. Gene expression was analyzed by real time RT-PCR in the N-deprived mycelia (NH) and supplied for 24 h to 3 mM NH_4^+ plus 2.5 mM MSX (NH + MSX), or 3 mM NH_4^+ plus 4 mM acetate (NH + AC). Data were calibrated by the expression values obtained for the gene encoding the EF1α. Error bars represent SE of the mean of three independent experiments. *: statistically significant ($p < 0.05$) in comparison to the respective control value.

The effect of the GS inhibitor MSX on the expression levels of the three *R. irregularis* AMT genes was also tested. For this purpose, the N-deprived ERM was incubated for 24 h in the presence of 2.5 mM MSX in the NH_4^+ re-supplementation media. Under these conditions, NH_4^+ should be accumulated and glutamine should be depleted. MSX caused a down-regulation of *GintAMT3* gene expression, but did not have any effect on *GintAMT1* and *GintAMT2* transcript levels (**Figure 7**). To determine if transcription of the *R. irregularis* AMT genes were affected by carbon supply, *GintAMT*s gene expression was assessed in the N-deprived ERM supplemented with NH_4^+ and acetate, a carbon source taken up and assimilated by the ERM (Pfeffer et al., 1999). Relative to the N-deprived mycelium, supplying the ERM with ammonium and acetate induced down-regulation of the three *GintAMT*s, with the strongest and statistically significant effect for *GintAMT3* (**Figure 7**).

Expression of all three *R. irregularis* AMT was assessed in ERM and IRM when the fungus was associated with poplar and sorghum. In this experimental set-up the fungus had either access to a low Pi source or a high Pi source. The expression level for the high affinity transporter GintAMT1 was low and similar in the ERM and in the IRM, independently of the Pi availability. GintAMT2 was strongly expressed in the ERM and IRM, independently of Pi availability (**Supplementary Figure S2**). Expression level of *GintAMT3* was far higher in the IRM than in the ERM. *GintAMT3* was significantly more strongly expressed under high Pi conditions compared to low-Pi in the IRM (**Figure 8A**). Expression patterns of all three transporters were the same in both plant species. When we measured gene expression of *GintAMT3* in laser-microdissected arbusculated cells we did not observe significant differences between high Pi and low Pi condition (**Figure 8B**). Moreover, *GintAMT3* expression was at least twice as high in the IRM as compared to the ERM, independent of the N source (**Figure 9**).

[^{14}C]Methylamine Uptake Assay

Functional expression of *GintAMT3* in the yeast triple mutant revealed it to be a low affinity transporter with an apparent K_m of 1.8 mM and a V_{max} of 240 nmol^{-1} min $^{-1}$ 10^8 cells^{-1}. We observed a steep increase in methylamine uptake until reaching a plateau at about 6 mM. However, increasing the amount of supplied methylamine showed that GintAMT3 is still able to take up methylamine at a steady pace (**Figure 10**).

DISCUSSION

In the AM symbiosis, the main role of the AM fungal partners is the acquisition of mineral nutrients from the soil, in the ERM, and the transfer of these nutrients to the IRM and from there, by way of the periarbuscular space, to the plant. Though P is the most-often named mineral nutrient in this context, N can be a limiting factor for plant growth as well, and the N delivered by AMFs may play an important role for plant growth and health. According to current knowledge, AMF take up N in the ERM, preferentially in form of ammonium, metabolize it to arginine in the GS/GOGAT pathway and in the urea cycle, and transport it to the IRM in the form of arginine (Casieri et al., 2013). At the plant fungal interface (in the arbuscule), ammonia is thought to be released from arginine through the action of arginase and urease and then transported to the plant. For the plant partner, it has been shown already that the expression of certain AMTs is specifically upregulated in arbuscule-containing cells, and that that these plant AMTs reside in the periarbuscular membrane. However, not much is known yet about the localization and regulation of the fungal AMTs involved in this process. In our study, we describe a new functional AMT, GintAMT3, of *R. irregularis*, and we try to characterize its role in the symbiotic N transfer.

AMF Ammonium Transporters: A Separated Phylogenetic Group

Sequence homology analysis revealed high intraspecific and interspecific sequence conservation of GintAMT3 to the two already known AMTs of *R. irregularis* (López-Pedrosa et al., 2006; Pérez-Tienda et al., 2011) and the three AMTs previously identified in *Geosiphon pyriformis* (Ellerbeck et al., 2013) (**Figure 1**). All six glomeromycotan AMTs shared high sequence

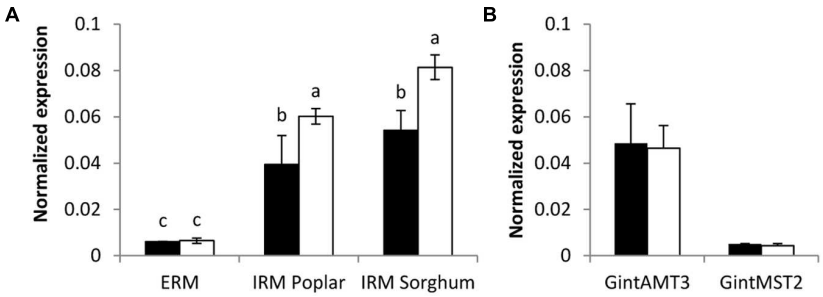

FIGURE 8 | Quantification of *GintAMT3* under phosphate stress. Gene expression was measured by quantitative polymerase chain reaction in the ERM and IRM of **(A)** inoculated *P. trichocarpa* and *S. bicolor* and in **(B)** microdissected arbusculated cells in *S. bicolor*. **(A)** The sorghum and poplar plants grew in a tripartite compartment system where only the fungus had access to the high phosphorous source (open bars) or low phosphorous source (closed bars). Differences between ERM and IRM were tested with a one-way ANOVA. Data were calibrated by the expression values obtained for the gene encoding the transcription elongation factor TEF1α. Values are means of nine replicates, error bars represent SD. Difference between treatments were tested with a one-way ANOVA. Lower case letters indicate significant difference (Tukey's *t*-test; $p < 0.05$). **(B)** Inoculated *S. bicolor* grew in a two-partite compartment system where only the fungus had access to the high phosphorous (open bars) or low phosphorous (closed bars) source. Arbusculated cells were laser microdissected and transcript abundances of *GintAMT3* and *GintMST2* (monosaccharide transporter essential for functional symbiosis, Helber et al. (2011)) as a positive control were measured by qPCR. Data were calibrated by the expression values obtained for the gene encoding the transcription elongation factor TEF1α. Values are means of six replicates, error bars represent SD. Difference between treatments was tested with Tukey's *t*-test ($p < 0.05$).

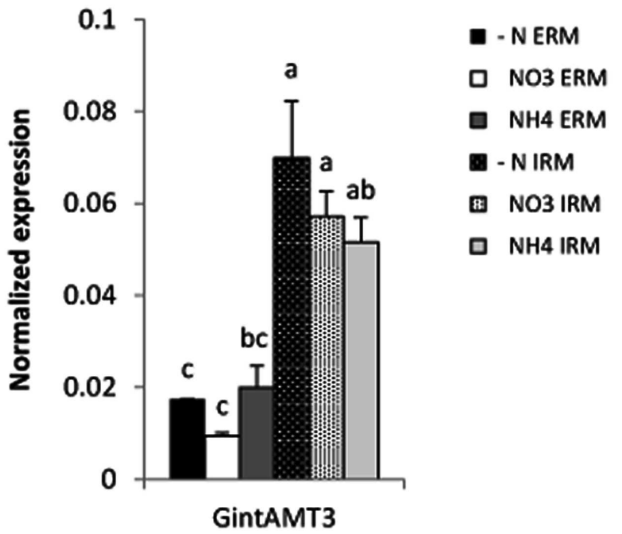

FIGURE 9 | Quantification of *GintAMT3* expression in *R. irregularis* by qPCR. Inoculated *S. bicolor* grew in a two-partite compartment system where only the fungus had access to the second compartment. In this system only the fungus had access to the applied nutrients. Hyphal compartments received either Hoagland solution containing no nitrogen source (–N), or nitrate (NO_3) or ammonium (NH_4) as the sole nitrogen source. Gene expression of *GintAMT3* was measured in the ERM and IRM. Data were calibrated by the expression values obtained for the gene encoding the transcription elongation factor TEF1α. Values are means of nine replicates, error bars represent SD. Difference between treatments were tested with a one-way ANOVA. Lower case letters indicate significant difference (Tukey's *t*-test; $p < 0.05$).

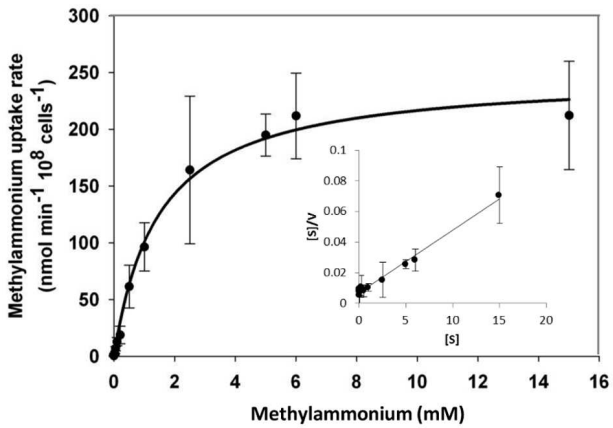

FIGURE 10 | Biochemical characterization of GintAMT3. Heterologous expression of pDR196-GintAMT3 in yeast strain 31019b (*MAT*a *ura3 mep1*Δ *mep2*Δ::*LEU2 mep3*Δ::*KanMX2*) (Marini et al., 1997). [^{14}C]methylamine uptake rates were measured at pH 5 at different substrate concentrations. Inset: Hanes–Woolf plot.

similarity and the 11 TM helices of AMTs. Positioning of the intron sequences showed further, that the glomeromycotan AMT genes are highly conserved. The closest homolog to GintAMT3 is GintAMT2, which shared 80% of sequence similarity. The additional intron sequences in the GintAMT2 and GintAMT3 genes suggested a recent gene duplication event.

Phylogenetic analysis of AMTs from Ascomycota, Basidiomycota, Zygomycota and Glomeromycota revealed that the six AMTs from Glomeromycota species (three from *R. irregularis*) clustered separately from the HATS and LATS of Ascomycota and Basidiomycota (**Figure 2**), indicating a distinct AMT evolution in these fungal phyla. Note that some of the AMTs of Ascomycota and Basidiomycota have been identified in species forming ectomycorrhizas, such as *Tuber borchii* (Montanini et al., 2002), *Hebeloma cylindrosporum* (Javelle et al., 2001, 2003a,b), *Amanita muscaria* (Willmann et al., 2007), and *Laccaria bicolor* (Lucic et al., 2008).

GintAMT3 Is a Low Affinity Transporter System

Both a LATS and a HATS have already been described in *R. irregularis* (Pérez-Tienda et al., 2012). GintAMT1 has been characterized as a HATS with an apparent K_m of 26 μM (López-Pedrosa et al., 2006). The kinetics of the second AMT, GintAMT2, could not be determined by methylammonium uptake assay (Pérez-Tienda et al., 2011), but qRT-PCR measurements revealed that GintAMT2 is constitutively expressed under N-limiting conditions, suggesting a role in ammonium retention rather than in ammonium uptake (Pérez-Tienda et al., 2011). We characterized GintAMT3 as a LATS with an apparent K_m of 1.8 mM and a V_{max} of 240 $nmol^{-1}$ min^{-1} 10^8 $cells^{-1}$. In our experiments, expression of GintAMT3 is dependent on the N nutritional status of the AM fungus but independent from the provided N source under N limiting conditions. Severe N stress induced expression of GintAMT3 independently of the supplied N source and abundance of GintAMT3 transcript decreased within a few days. These results indicate the existence of unknown regulatory mechanisms involved in transcriptional or post-transcriptional regulation of AMTs in AMF. Further, we could show that GintAMT3 expression is not only dependent on N nutrition status but also on fungal carbon status, indicating a tight connection to symbiotic interactions. A similar observation was reported in *Hebeloma cylindrosporum*, a Basidiomycota fungus forming ectomycorrhizal symbiosis (Javelle et al., 2003b).

Using a compartmented system, we analyzed fungal nutrient transporterts in the ERM and IRM when associated with *Sorghum bicolor*. Independently of the N source, the expression level of GintAMT3 in the IRM was significantly more than twofold induced compared to the ERM. As P is also a major nutrient transferred by the AM fungus to the plant, we assessed the effect of P availability on GintAMT3 expression in the ERM and IRM when *R. irregularis* was associated with *S. bicolor* or with poplar, and found an induction of GintAMT3 in the IRM by P. The high expression of GintAMT3 in the IRM indicates that it might be located in the arbuscules.

Microdissection of *S. bicolor* roos revealed indeed that GintAMT3 is expressed in the symbiotic root tissue, and specifically in arbuscule-containing cells. Heterologous expression of GFP tagged GintAMT3 in yeast revealed localization of the AMT in the PM and vacuolar membrane. Given that current experimental evidence supports a role for AMT proteins in ammonium uptake (Khademi et al., 2004; Lamoureux et al., 2010) and that ammonium is the N form taken up by the plant at the arbuscular interface (Govindarajulu et al., 2005; Tian et al., 2010), expression of AMT genes in the arbuscules indicates that there might exist a competition between the plant and the fungus for N that is present in the interfacial apoplast (Guether et al., 2009a). As it was proposed for the high-affinity transporters GintAMT1 and GintAMT2, the high expression of GintAMT3 in the arbuscules also suggests a role for this transporter in ammonium retrieval from the periarbuscular space, but in situations where the ammonium concentrations are high. Additionally to its incorporation in metabolism, the vacuolar localization of GintAMT3 indicated that ammonium could be stored in vacuoles to maintain low cytoplasmic ammonium concentrations as shown in yeast (Soupene et al., 2001) or plants (von Wirén et al., 2000; Loqué et al., 2005), or in intracellular vesicles (Chalot et al., 2006). Studies on ammonium/methylammonium transporters (AMT/MEP) of enteric bacteria have shown that these transporters function as ammonia channels. Ammonium is deprotonated at the channel entrance and ammonia is transported through it. The transport through the channel is energy-independent and bidirectional (Soupene et al., 1998, 2002; Khademi et al., 2004). Therefore, it might also be possible that GintAMT3 function as a bidirectional transporter for import and export of ammonium from the vacuole. Furthermore, it is also possible that GintAMT3 functions as an export carrier for ammonium from the arbuscules to the periarbuscular space. However, to assess possible bidirectional transport properties of GintAMT3, patch clamp measurements are necessary. Knockdown of GintAMT3 by host induced gene silencing and virus induced genes silencing could illustrate the importance of this transporter for a functional symbiosis (Helber et al., 2011).

CONCLUSION

Here, we demonstrate that GintAMT3 encodes a functional low affinity transporter. We show that it is localized in the fungal membrane, and that it is expressed in the ERM and IRM of colonized poplar and sorghum plants. Increased expression in the IRM under high-P conditions indicates further that more ammonium is transferred when the AM fungus has increased access to a P source.

AUTHOR CONTRIBUTIONS

SC, JP, and ME made the *in silico* analysis. ME, SC, and OC made the yeast complementation. SC and OC performed the methylamine uptake assay. SC and CA performed laser capture microdissection. CA and ME made the GFP localization. SC and JP made root colonization and expression analysis. JP performed MSX and acetate assays. All co-authors participate in writing.

ACKNOWLEDGMENTS

This project was supported by the Swiss National Science Foundation (grant no. PZ00P3_136651 to P-EC., grant No. 127563 to TB) the Conseil Régional de Bourgogne PARI AGREE grant to DW and the Spanish Ministry of Economy and Competitivity (Projects AGL2012-35611 and AGL2015-67098-R).

SUPPLEMENTARY MATERIAL

The Supplementary Material for this article can be found online at: http://journal.frontiersin.org/article/10.3389/fpls.2016.00679

FIGURE S1 | Predicted 2D (A) and 3D topology (B,C) of GintAMT3. Models were constructed using Protter – visualize proteoforms (Omasits et al., 2013) and SWISS-MODEL (Benkert et al., 2011). 3D model shows potential tertiary structure of GintAMT3 when incorporated into the membrane **(B)** and from the top from the extracellular side to the intracellular side **(C)**.

FIGURE S2 | Quantification of *GintAMT1* (A) and *GintAMT2* (B) transcripts under phosphate stress. Gene expression was measured by quantitative polymerase chain reaction in the ERM and ORM of inoculated *P. trichocarpa* and *S. bicolor*. The sorghum and poplar plants grew in a tripartite compartment system where only the fungus had access to the high phosphorus source (open bars) or low phosphorus source (closed bars). Differences between ERM and IRM were tested with a one-way ANOVA. Data were calibrated by the expression values obtained for the gene encoding the transcription elongation factor TEF1α. Values are means of nine replicates, error bars represent SD. Differences between treatments were tested with a one-way ANOVA. Lower case letters indicate significant difference (Tuckey HSD; $p < 0.05$).

TABLE S1 | Primer list.

TABLE S2 | Mycorrhizal colonization. Hyphal and arbuscular colonization rates in different treatments were compared by one-way ANOVA. Lowercase letters indicate significant differences between treatments ($p < 0.05$).

REFERENCES

Altschul, S. F., Madden, T. L., Schäffer, A. A., Zhang, J., Zhang, Z., Miller, W., et al. (1997). Gapped BLAST and PSI-BLAST: a new generation of protein database search programs. *Nucleic Acids Res.* 25, 3389–3402. doi: 10.1093/nar/25.17.3389

Bago, B., Pfeffer, P., and Shachar-Hill, Y. (2001). Could the urea cycle be translocating nitrogen in the arbuscular mycorrhizal symbiosis? *New Phytol.* 149, 4–8. doi: 10.1046/j.1469-8137.2001.00016.x

Bago, B., Vierheilig, H., Piché, Y., and Azcón-Aguilar, C. (1996). Nitrate depletion and pH changes induced by the extraradical mycelium of the arbuscular mycorrhizal fungus *Glomus intraradices* grown in monoxenic culture. *New Phytol.* 133, 273–280. doi: 10.1111/j.1469-8137.1996.tb01894.x

Benkert, P., Biasini, M., and Schwede, T. (2011). Toward the estimation of the absolute quality of individual protein structure models. *Bioinformatics* 27, 343–350. doi: 10.1093/bioinformatics/btq662

Breuninger, M., Trujillo, C. G., Serrano, E., Fischer, R., and Requena, N. (2004). Different nitrogen sources modulate activity but not expression of glutamine synthetase in arbuscular mycorrhizal fungi. *Fungal Genet. Biol.* 41, 542–552. doi: 10.1016/j.fgb.2004.01.003

Brundrett, M. C., Piché, Y., and Peterson, R. L. (1984). A new method for observing the morphology of vesicular–arbuscular mycorrhizae. *Can. J. Bot.* 62, 2128–2134. doi: 10.1139/b84-290

Cappellazzo, G., Lanfranco, L., Fitz, M., Wipf, D., and Bonfante, P. (2008). Characterization of an amino acid permease from the endomycorrhizal fungus *Glomus mosseae*. *Plant Physiol.* 147, 429–437. doi: 10.1104/pp.108.117820

Casieri, L., Ait Lahmidi, N., Doidy, J., Fourrey, C., Migeon, A., Bonneau, L., et al. (2013). Biotrophic transportome in mutualistic plant-fungal interactions. *Mycorrhiza* 23, 597–625. doi: 10.1007/s00572-013-0496-9

Chabot, S., Bel-Rhlid, R., Chenevert, R., and Piché, Y. (1992). Hyphal growth promotion in vitro of the VA mycorrhizal fungus, *Gigaspora margarita* Becker and Hall, by the activity of structurally specific flavonoid compounds under CO_2-enriched conditions. *New Phytol.* 122, 461–467. doi: 10.1111/j.1469-8137.1992.tb00074.x

Chalot, M., Blaudez, D., and Brun, A. (2006). Ammonia: a candidate for nitrogen transfer at the mycorrhizal interface. *Trends Plant Sci.* 11, 263–266. doi: 10.1016/j.tplants.2006.04.005

Courty, P.-E., Hoegger, P., Kilaru, S., Kohler, A., Buée, M., Garbaye, J., et al. (2009). Phylogenetic analysis, genomic organization, and expression analysis of multi-copper oxidases in the ectomycorrhizal basidiomycete Laccaria bicolor. *New Phytol.* 182, 736–750. doi: 10.1111/j.1469-8137.2009.02774.x

Couturier, J., Montanini, B., Martin, F., Brun, A., Blaudez, D., and Chalot, M. (2007). The expanded family of ammonium transporters in the perennial poplar plant. *New Phytol.* 174, 137–150. doi: 10.1111/j.1469-8137.2007.01992.x

Cruz, C., Egsgaard, H., Trujillo, C., Ambus, P., Requena, N., Martins-Loução, M. A., et al. (2007). Enzymatic evidence for the key role of arginine in nitrogen translocation by arbuscular mycorrhizal fungi. *Plant Physiol.* 144, 782–792. doi: 10.1104/pp.106.090522

Dohmen, R. J., Strasser, A. W. M., Höner, C. B., and Hollenberg, C. P. (1991). An efficient transformation procedure enabling long-term storage of competent cells of various yeast genera. *Yeast* 7, 691–692. doi: 10.1002/yea.320070704

Ellerbeck, M., Schüßler, A., Brucker, D., Dafinger, C., Loos, F., and Brachmann, A. (2013). Characterization of three ammonium transporters of the Glomeromycotan fungus *Geosiphon pyriformis*. *Eukaryot. Cell* 12, 1554–1562. doi: 10.1128/EC.00139-13

Fortin, J. A., Bécard, G., Declerck, S., Dalpé, Y., St-Arnaud, M., Coughlan, A. P., et al. (2002). Arbuscular mycorrhiza on root-organ cultures. *Can. J. Bot.* 80, 1–20. doi: 10.1139/b01-139

Fried, M., Zsoldos, F., Vose, P. B., and Shatokhin, I. L. (1965). Characterizing the NO3 and NH4 uptake process of rice roots by use of 15N labelled NH4NO3. *Physiol. Plant* 18, 313–320. doi: 10.1111/j.1399-3054.1965.tb06894.x

Gamborg, O. L., and Wetter, L. (1975). *Plant Tissue Culture Methods. National research council of Canada*. Saskatoon: Prairie Regional Lab.

Gazzarrini, S., Lejay, L., Gojon, A., Ninnemann, O., Frommer, W. B., and von Wirén, N. (1999). Three functional transporters for constitutive, diurnally regulated, and starvation-induced uptake of ammonium into *Arabidopsis* roots. *Plant Cell* 11, 937–947. doi: 10.1105/tpc.11.5.937

Gomez, S. K., Javot, H., Deewatthanawong, P., Torres-Jerez, I., Tang, Y., Blancaflor, E., et al. (2009). *Medicago truncatula* and *Glomus intraradices* gene expression in cortical cells harboring arbuscules in the arbuscular mycorrhizal symbiosis. *BMC Plant Biol.* 9:10. doi: 10.1186/1471-2229-9-10

Govindarajulu, M., Pfeffer, P. E., Jin, H., Abubaker, J., Douds, D. D., Allen, J. W., et al. (2005). Nitrogen transfer in the arbuscular mycorrhizal symbiosis. *Nature* 435, 819–823. doi: 10.1038/nature03610

Graham, J. (2000). Assessing costs of arbuscular mycorrhizal symbiosis in agroecosystems. *Curr. Adv. Mycorrhizae Res.* 4, 111–126.

Guether, M., Balestrini, R., Hannah, M., He, J., Udvardi, M. K., and Bonfante, P. (2009a). Genome-wide reprogramming of regulatory networks, transport, cell wall and membrane biogenesis during arbuscular mycorrhizal symbiosis in Lotus japonicus. *New Phytol.* 182, 200–212. doi: 10.1111/j.1469-8137.2008.02725.x

Guether, M., Neuhäuser, B., Balestrini, R., Dynowski, M., Ludewig, U., and Bonfante, P. (2009b). A mycorrhizal-specific ammonium transporter from *Lotus japonicus* acquires nitrogen released by arbuscular mycorrhizal fungi. *Plant Physiol.* 150, 73–83. doi: 10.1104/pp.109.136390

Hawkins, H.-J., Johansen, A., and George, E. (2000). Uptake and transport of organic and inorganic nitrogen by arbuscular mycorrhizal fungi. *Plant Soil* 226, 275–285. doi: 10.1023/a:1026500810385

Helber, N., Wippel, K., Sauer, N., Schaarschmidt, S., Hause, B., and Requena, N. (2011). A versatile monosaccharide transporter that operates in the arbuscular mycorrhizal fungus Glomus sp is crucial for the symbiotic relationship with plants. *Plant Cell* 23, 3812–3823. doi: 10.1105/tpc.111.089813

Hodge, A., Helgason, T., and Fitter, A. H. (2010). Nutritional ecology of arbuscular mycorrhizal fungi. *Fungal Ecol.* 3, 267–273. doi: 10.1016/j.funeco.2010.02.002

Javelle, A., André, B., Marini, A.-M., and Chalot, M. (2003a). High-affinity ammonium transporters and nitrogen sensing in mycorrhizas. *Trends Microbiol.* 11, 53–55. doi: 10.1016/S0966-842X(02)00012-4

Javelle, A., Morel, M., Rodríguez-Pastrana, B.-R., Botton, B., André, B., Marini, A.-M., et al. (2003b). Molecular characterization, function and regulation of ammonium transporters (Amt) and ammonium-metabolizing enzymes (GS, NADP-GDH) in the ectomycorrhizal fungus *Hebeloma cylindrosporum*. *Mol. Microbiol.* 47, 411–430. doi: 10.1046/j.1365-2958.2003.03303.x

Javelle, A., Chalot, M., Söderström, B., and Botton, B. (1999). Ammonium and methylamine transport by the ectomycorrhizal fungus *Paxillus involutus* and ectomycorrhizas. *FEMS Microbiol. Ecol.* 30, 355–366. doi: 10.1111/j.1574-6941.1999.tb00663.x

Javelle, A., Rodrıguez-Pastrana, B.-R., Jacob, C., Botton, B., Brun, A., André, B., et al. (2001). Molecular characterization of two ammonium transporters from the ectomycorrhizal fungus Hebeloma cylindrosporum. *FEBS Lett.* 505, 393–398. doi: 10.1016/S0014-5793(01)02802-2

Jin, H., Pfeffer, P. E., Douds, D. D., Piotrowski, E., Lammers, P. J., and Shachar-Hill, Y. (2005). The uptake, metabolism, transport and transfer of nitrogen in an arbuscular mycorrhizal symbiosis. *New Phytol.* 168, 687–696. doi: 10.1111/j.1469-8137.2005.01536.x

Johansen, A., Finlay, R. D., and Olsson, P. A. (1996). Nitrogen metabolism of external hyphae of the arbuscular mycorrhizal fungus *Glomus intraradices*. *New Phytol.* 133, 705–712. doi: 10.1111/j.1469-8137.1996.tb01939.x

Khademi, S., O'Connell, J., Remis, J., Robles-Colmenares, Y., Miercke, L. J. W., and Stroud, R. M. (2004). Mechanism of ammonia transport by Amt/MEP/Rh: structure of AmtB at 1.35 Å. *Science* 305, 1587–1594. doi: 10.1126/science.1101952

Kobae, Y., Tamura, Y., Takai, S., Banba, M., and Hata, S. (2010). Localized expression of arbuscular mycorrhiza-inducible ammonium transporters in soybean. *Plant Cell Physiol.* 51, 1411–1415. doi: 10.1093/pcp/pcq099

Koegel, S., Ait Lahmidi, N., Arnould, C., Chatagnier, O., Walder, F., Ineichen, K., et al. (2013a). The family of ammonium transporters (AMT) in Sorghum bicolor: two AMT members are induced locally, but not systemically in roots colonized by arbuscular mycorrhizal fungi. *New Phytol.* 198, 853–865. doi: 10.1111/nph.12199

Koegel, S., Boller, T., Lehmann, M. F., Wiemken, A., and Courty, P.-E. (2013b). Rapid nitrogen transfer in the Sorghum bicolor-Glomus mosseae arbuscular mycorrhizal symbiosis. *Plant Signal. Behav.* 8:e25229. doi: 10.4161/psb.25229

Lamoureux, G., Javelle, A., Baday, S., Wang, S., and Berneche, S. (2010). Transport mechanisms in the ammonium transporter family. *Transfusion Clin. Biol.* 17, 168–175. doi: 10.1016/j.tracli.2010.06.004

Leigh, J., Hodge, A., and Fitter, A. H. (2009). Arbuscular mycorrhizal fungi can transfer substantial amounts of nitrogen to their host plant from organic material. *New Phytol.* 181, 199–207. doi: 10.1111/j.1469-8137.2008.02630.x

López-Pedrosa, A., González-Guerrero, M., Valderas, A., Azcón-Aguilar, C., and Ferrol, N. (2006). GintAMT1 encodes a functional high-affinity ammonium transporter that is expressed in the extraradical mycelium of *Glomus intraradices*. *Fungal Genet. Biol.* 43, 102–110. doi: 10.1016/j.fgb.2005.10.005

Loqué, D., Ludewig, U., Yuan, L., and von Wirén, N. (2005). Tonoplast intrinsic proteins AtTIP2; 1 and AtTIP2; 3 facilitate NH3 transport into the vacuole. *Plant Physiol.* 137, 671–680. doi: 10.1104/pp.104.051268

Lorenz, M. C., and Heitman, J. (1998). The MEP2 ammonium permease regulates pseudohyphal differentiation in *Saccharomyces cerevisiae*. *EMBO J.* 17, 1236–1247. doi: 10.1093/emboj/17.5.1236

Lucic, E., Fourrey, C., Kohler, A., Martin, F., Chalot, M., and Brun-Jacob, A. (2008). A gene repertoire for nitrogen transporters in *Laccaria bicolor*. *New Phytol.* 180, 343–364. doi: 10.1111/j.1469-8137.2008.02580.x

Mäder, P., Vierheilig, H., Streitwolf-Engel, R., Boller, T., Frey, B., Christie, P., et al. (2000). Transport of 15N from a soil compartment separated by a polytetrafluoroethylene membrane to plant roots via the hyphae of arbuscular mycorrhizal fungi. *New Phytol.* 146, 155–161. doi: 10.1046/j.1469-8137.2000.00615.x

Marini, A. M., Soussi-Boudekou, S., Vissers, S., and Andre, B. (1997). A family of ammonium transporters in *Saccharomyces cerevisiae*. *Mol. Cell. Biol.* 17, 4282–4293. doi: 10.1128/MCB.17.8.4282

Marini, A. M., Vissers, S., Urrestarazu, A., and Andre, B. (1994). Cloning and expression of the MEP1 gene encoding an ammonium transporter in *Saccharomyces cerevisiae*. *EMBO J.* 13, 3456–3463.

Martin, F. (1985). 15N-NMR studies of nitrogen assimilation and amino acid biosynthesis in the ectomycorrhizal fungus Cenococcum graniforme. *FEBS Lett.* 182, 350–354. doi: 10.1016/0014-5793(85)80331-8

Marzluf, G. A. (1996). Regulation of nitrogen metabolism in mycelial fungi. *Biochem. Mol. Biol.* 3, 357–368. doi: 10.1007/978-3-662-10367-8_16

Mayer, M., Schaaf, G., Mouro, I., Lopez, C., Colin, Y., Neumann, P., et al. (2006). Different transport mechanisms in plant and human AMT/Rh-type ammonium transporters (vol 127, pg 133, 2006). *J. Gen. Physiol.* 127, 353–353. doi: 10.1085/jgp.20050936920060216c

Montanini, B., Moretto, N., Soragni, E., Percudani, R., and Ottonello, S. (2002). A high-affinity ammonium transporter from the mycorrhizal ascomycete Tuber borchii. *Fungal Genet. Biol.* 36, 22–34. doi: 10.1016/S1087-1845(02)00001-4

Ninnemann, O., Jauniaux, J. C., and Frommer, W. B. (1994). Identification of a high-affinity NH4+ transporter from plants. *Embo J.* 13, 3464–3471.

Oehl, F., Sieverding, E., Mäder, P., Dubois, D., Ineichen, K., Boller, T., et al. (2004). Impact of long-term conventional and organic farming on the diversity of arbuscular mycorrhizal fungi. *Oecologia* 138, 574–583. doi: 10.1007/s00442-003-1458-2

Omasits, U., Ahrens, C. H., Müller, S., and Wollscheid, B. (2013). Protter: interactive protein feature visualization and integration with experimental proteomic data. *Bioinformatics* 30, 884–886. doi: 10.1093/bioinformatics/btt607

Paterson, A. H., Bowers, J. E., Bruggmann, R., Dubchak, I., Grimwood, J., Gundlach, H., et al. (2009). The Sorghum bicolor genome and the diversification of grasses. *Nature* 457, 551–556. doi: 10.1038/nature07723

Pearson, J., and Jakobsen, I. (1993). Symbiotic exchange of carbon and phosphorus between cucumber and three arbuscular mycorrhizal fungi. *New Phytol.* 124, 481–488. doi: 10.1111/j.1469-8137.1993.tb03839.x

Pérez-Tienda, J., Testillano, P. S., Balestrini, R., Fiorilli, V., Azcón-Aguilar, C., and Ferrol, N. (2011). GintAMT2, a new member of the ammonium transporter family in the arbuscular mycorrhizal fungus *Glomus intraradices*. *Fungal Genet. Biol.* 48, 1044–1055. doi: 10.1016/j.fgb.2011.08.003

Pérez-Tienda, J., Valderas, A., Camañes, G., García-Agustín, P., and Ferrol, N. (2012). Kinetics of NH4+ uptake by the arbuscular mycorrhizal fungus *Rhizophagus irregularis*. *Mycorrhiza* 22, 485–491. doi: 10.1007/s00572-012-0452-0

Pfeffer, P. E., Douds, D. D., Bécard, G., and Shachar-Hill, Y. (1999). Carbon uptake and the metabolism and transport of lipids in an arbuscular mycorrhiza. *Plant Physiol.* 120, 587–598. doi: 10.1104/pp.120.2.587

Schüßler, A., Schwarzott, D., and Walker, C. (2001). A new fungal phylum, the *Glomeromycota*: phylogeny and evolution. *Mycol. Res.* 105, 1413–1421. doi: 10.1017/S0953756201005196

Shelden, M., Dong, B., de Bruxelles, G., Trevaskis, B., Whelan, J., Ryan, P., et al. (2001). *Arabidopsis* ammonium transporters, AtAMT1;1 and AtAMT1;2, have different biochemical properties and functional roles. *Plant Soil* 231, 151–160. doi: 10.1023/a:1010303813181

Smith, S. E., and Read, D. J. (2008). *Mycorrhizal Symbiosis*. London: Academic Press.

Sohlenkamp, C., Shelden, M., Howitt, S., and Udvardi, M. (2000). Characterization of *Arabidopsis* AtAMT2, a novel ammonium transporter in plants. *FEBS Lett.* 467, 273–278. doi: 10.1016/S0014-5793(00)01153-4

Soupene, E., He, L., Yan, D., and Kustu, S. (1998). Ammonia acquisition in enteric bacteria: physiological role of the ammonium/methylammonium transport B (AmtB) protein. *Proc. Natl. Acad. Sci. U.S.A.* 95, 7030–7034. doi: 10.1073/pnas.95.12.7030

Soupene, E., Lee, H., and Kustu, S. (2002). Ammonium/methylammonium transport (Amt) proteins facilitate diffusion of NH3 bidirectionally. *Proc. Natl. Acad. Sci. U.S.A.* 99, 3926–3931. doi: 10.1073/pnas.062043799

Soupene, E., Ramirez, R. M., and Kustu, S. (2001). Evidence that fungal MEP proteins mediate diffusion of the uncharged species NH3 across the cytoplasmic membrane. *Mol. Cell. Biol.* 21, 5733–5741. doi: 10.1128/mcb.21.17.5733-5741.2001

St-Arnaud, M., Hamel, C., Vimard, B., Caron, M., and Fortin, J. (1996). Enhanced hyphal growth and spore production of the arbuscular mycorrhizal fungus *Glomus intraradices* in an in vitro system in the absence of host roots. *Mycol. Res.* 100, 328–332. doi: 10.1016/S0953-7562(96)80164-X

Tamura, K., Peterson, D., Peterson, N., Stecher, G., Nei, M., and Kumar, S. (2011). MEGA5: Molecular evolutionary genetics analysis using maximum likelihood, evolutionary distance, and maximum parsimony methods. *Mol. Biol. Evol.* 28, 2731–2739. doi: 10.1093/molbev/msr121

Tamura, K., Stecher, G., Peterson, D., Filipski, A., and Kumar, S. (2013). MEGA6: molecular evolutionary genetics analysis version 6.0. *Mol. Biol. Evol.* 30, 2725–2729. doi: 10.1093/molbev/mst197

Tian, C., Kasiborski, B., Koul, R., Lammers, P. J., Bücking, H., and Shachar-Hill, Y. (2010). Regulation of the nitrogen transfer pathway in the arbuscular mycorrhizal symbiosis: gene characterization and the coordination of expression with nitrogen flux. *Plant Physiol.* 153, 1175–1187. doi: 10.1104/pp.110.156430

Tisserant, E., Kohler, A., Dozolme-Seddas, P., Balestrini, R., Benabdellah, K., Colard, A., et al. (2012). The transcriptome of the arbuscular mycorrhizal fungus *Glomus intraradices* (DAOM 197198) reveals functional tradeoffs in an obligate symbiont. *New Phytol.* 193, 755–769. doi: 10.1111/j.1469-8137.2011.03948.x

Toussaint, J.-P., St-Arnaud, M., and Charest, C. (2004). Nitrogen transfer and assimilation between the arbuscular mycorrhizal fungus *Glomus intraradices* Schenck & Smith and Ri T-DNA roots of Daucus carota L. in an in vitro compartmented system. *Can. J. Microbiol.* 50, 251–260. doi: 10.1139/w04-009

Ullrich, W. R., Larsson, M., Larsson, C.-M., Lesch, S., and Novacky, A. (1984). Ammonium uptake in Lemna gibba G1, related membrane potential changes, and inhibition of anion uptake. *Physiol. Plant.* 61, 369–376. doi: 10.1111/j.1399-3054.1984.tb06342.x

Vale, F., Volk, R., and Jackson, W. (1988). Simultaneous influx of ammonium and potassium into maize roots: kinetics and interactions. *Planta* 173, 424–431. doi: 10.1007/bf00401031

Van Dommelen, A., Keijers, V., Vanderleyden, J., and de Zamaroczy, M. (1998). (Methyl)ammonium transport in the nitrogen-fixing bacterium *Azospirillum brasilense*. *J. Bacteriol.* 180, 2652–2659.

Villegas, J., Williams, R. D., Nantais, L., Archambault, J., and Fortin, J. A. (1996). Effects of N source on pH and nutrient exchange of extramatrical mycelium in a mycorrhizal Ri T-DNA transformed root system. *Mycorrhiza* 6, 247–251. doi: 10.1007/s005720050132

von Wirén, N., Gazzarrini, S., Gojon, A., and Frommer, W. B. (2000). The molecular physiology of ammonium uptake and retrieval. *Curr. Opin. Plant Biol.* 3, 254–261. doi: 10.1016/S1369-5266(00)80074-6

Wang, M. Y., Glass, A., Shaff, J. E., and Kochian, L. V. (1994). Ammonium uptake by rice roots (III. Electrophysiology). *Plant Physiol.* 104, 899–906. doi: 10.1104/pp.104.3.899

Wang, M. Y., Siddiqi, M. Y., Ruth, T. J., and Glass, A. (1993). Ammonium uptake by rice roots (II. Kinetics of 13NH4+ Influx across the Plasmalemma). *Plant Physiol.* 103, 1259–1267. doi: 10.1104/pp.103.4.1259

Willmann, A., Weiß, M., and Nehls, U. (2007). Ectomycorrhiza-mediated repression of the high-affinity ammonium importer gene AmAMT2 in *Amanita muscaria*. *Curr. Genet.* 51, 71–78. doi: 10.1007/s00294-006-0106-x

Wipf, D., Benjdia, M., Rikirsch, E., Zimmermann, S., Tegeder, M., and Frommer, W. B. (2003). An expression cDNA library for suppression cloning in yeast mutants, complementation of a yeast his4 mutant, and EST analysis from the symbiotic basidiomycete *Hebeloma cylindrosporum*. *Genome* 46, 177–181. doi: 10.1139/g02-121

Conflict of Interest Statement: The authors declare that the research was conducted in the absence of any commercial or financial relationships that could be construed as a potential conflict of interest.

frontiers in Plant Science

ORIGINAL RESEARCH
published: 14 April 2016
doi: 10.3389/fpls.2016.00487

Arbuscular mycorrhiza Symbiosis Induces a Major Transcriptional Reprogramming of the Potato *SWEET* Sugar Transporter Family

*Jasmin Manck-Götzenberger and Natalia Requena **

Molecular Phytopathology, Botanical Institute, Karlsruhe Institute of Technology, Karlsruhe, Germany

Biotrophic microbes feeding on plants must obtain carbon from their hosts without killing the cells. The symbiotic *Arbuscular mycorrhizal* (AM) fungi colonizing plant roots do so by inducing major transcriptional changes in the host that ultimately also reprogram the whole carbon partitioning of the plant. AM fungi obtain carbohydrates from the root cortex apoplast, in particular from the periarbuscular space that surrounds arbuscules. However, the mechanisms by which cortical cells export sugars into the apoplast for fungal nutrition are unknown. Recently a novel type of sugar transporter, the SWEET, able to perform not only uptake but also efflux from cells was identified. Plant SWEETs have been shown to be involved in the feeding of pathogenic microbes and are, therefore, good candidates to play a similar role in symbiotic associations. Here we have carried out the first phylogenetic and expression analyses of the potato SWEET family and investigated its role during mycorrhiza symbiosis. The potato genome contains 35 SWEETs that cluster into the same four clades defined in *Arabidopsis*. Colonization of potato roots by the AM fungus *Rhizophagus irregularis* imposes major transcriptional rewiring of the SWEET family involving, only in roots, changes in 22 of the 35 members. None of the SWEETs showed mycorrhiza-exclusive induction and most of the 12 induced genes belong to the putative hexose transporters of clade I and II, while only two are putative sucrose transporters from clade III. In contrast, most of the repressed transcripts (10) corresponded to clade III SWEETs. Promoter-reporter assays for three of the induced genes, each from one cluster, showed re-localization of expression to arbuscule-containing cells, supporting a role for SWEETs in the supply of sugars at biotrophic interfaces. The complex transcriptional regulation of SWEETs in roots in response to AM fungal colonization supports a model in which symplastic sucrose in cortical cells could be cleaved in the cytoplasm by sucrose synthases or cytoplasmic invertases and effluxed as glucose, but also directly exported as sucrose and then converted into glucose and fructose by cell wall-bound invertases. Precise biochemical, physiological and molecular analyses are now required to profile the role of each potato SWEET in the arbuscular mycorrhizal symbiosis.

Keywords: SWEET transporters, potato, *Arbuscular mycorrhiza,* root, sugar transport, plants, symbiosis

OPEN ACCESS

Edited by:
Ralph Panstruga, Rheinisch-Westfälische Technische Hochschule (RWTH) Aachen, Germany

Reviewed by:
Pierre-Marc Delaux, Centre National de la Recherche Scientifique, France
Andrea Genre, University of Turin, Italy
Pere Mestre, Institut National de la Recherche Agronomique, France

****Correspondence:***
Natalia Requena
natalia.requena@kit.edu

Specialty section:
This article was submitted to Plant Biotic Interactions, a section of the journal Frontiers in Plant Science

Received: *12 February 2016*
Accepted: *25 March 2016*
Published: *14 April 2016*

Citation:
Manck-Götzenberger J and Requena N (2016) Arbuscular mycorrhiza Symbiosis Induces a Major Transcriptional Reprogramming of the Potato SWEET Sugar Transporter Family. Front. Plant Sci. 7:487. doi: 10.3389/fpls.2016.00487

INTRODUCTION

Plants are the major factories of reduced carbon on the earth and therefore most of the other living organisms are absolutely dependent on them. This statement is particularly true for obligate biotrophic microorganisms that feed on living plants and are, thus, committed to modify the plant cell program toward the release of sugars into the extracellular space. It is not long ago that the molecular mechanisms of how plants release sugars to the extracellular space were unknown, and thus, the identification of SWEET transporters as key players in this process represented a landmark (Chen et al., 2010).

SWEET transporters are integral membrane proteins with seven transmembrane domains that cannot only catalyze the efflux of carbohydrates but also their uptake (Chen et al., 2010; Chen, 2014). SWEETs were discovered in a screening using FRET glucose or sucrose sensors to identify pH independent sugar transporters in *Arabidopsis* (Chen et al., 2010, 2012; Lin et al., 2014). They are though very conserved throughout the plant kingdom, and Angiosperms contain a large number of *SWEET* genes, in average 20 according to Eom et al. (2015), but up to 52 in soybean (Patil et al., 2015). Phylogenetic analyses in several plants have shown that SWEETs can be grouped in 4 clades that were first defined in *Arabidopsis* (Chen et al., 2010; Chong et al., 2014; Wei et al., 2014; Feng et al., 2015; Patil et al., 2015). Assignment to one clade seems to correlate with the substrate transported rather than with the physiological function exerted by the SWEETs (Eom et al., 2015). Thus, from the functional analyses mainly carried out in *A. thaliana* and rice, it appears that SWEETs in clades I and II preferentially transport hexoses, while the characterized SWEETs from clade III are sucrose transporters (Chen et al., 2010, 2012; Lin et al., 2014). Clade IV contains less SWEET genes than the other clades and they have been shown to be vacuolar transporters controlling the flux of fructose across the tonoplast (Chen et al., 2010; Chardon et al., 2013; Guo et al., 2014).

SWEETs serve many different functions in plants, including the export from the phloem parenchyma cells in source tissues previous to phloem loading by SUT/SUC importers, pollen nutrition by the tapetum, embryo development or nectar secretion (Ge et al., 2000; Chen et al., 2010, 2012, 2015b; Lin et al., 2014). Therefore, it is not surprising that if the efflux of sugars from cells requires the participation of SWEET transporters, microbes feeding on living plant cells manipulate their expression to increase sugar release. And indeed, several rice SWEET promoters have been shown to be the target of several TAL (transcriptional activator-like) effectors from the pathogenic bacteria *Xanthomonas oryzae* pv. *oryzae* (Chu et al., 2006; Yang et al., 2006; Antony et al., 2010; Chen et al., 2010; Streubel et al., 2013). The responsible TAL effectors delivered into the plant cytoplasm by means of the type III secretion system reach the nucleus to induce the expression of specific SWEETs, guaranteeing sucrose delivery into the apoplast of colonized cells. Although, so far no other examples of the mechanisms of ectopic SWEET induction by microbes have been elucidated, it is known that many microorganisms including symbiotic bacteria, fungi and oomycetes induce SWEET expression during plant colonization (Gamas et al., 1996; Yu et al., 2010; Chong et al., 2014; Chen et al., 2015a). Thus, it is tempting to speculate that convergent evolution might have made the promoter of SWEETs a very attractive target for biotrophic organisms. This is supported by the findings of Streubel et al. (2013) who proved that the promoter of the rice OsSWEET14 contains binding sites for at least four different TAL effectors. But also by the results of Cohn et al. (2014) showing that not only in rice, but also in the dicot cassava, SWEET promoters are the target of TAL effectors from *X. axonopodis* pv. *manihotis*.

The symbiotic AM fungi are well known for their beneficial effects on plants (Smith and Smith, 2011). These soil fungi from the phylum Glomeromycota colonize the cortex of plant roots and establish a mycelial network in the soil that allows plants to access scarce mineral nutrients such as phosphorous. In turn, mycorrhizal plants provide AM fungi with carbon, as they are obligate biotrophs and can only complete their life cycle in symbiosis (Smith and Smith, 2012). Soil phosphate is transported along the mycelial network into the inner cortex of the root, where it is delivered at specialized fungal structures called arbuscules that also serve for the sugar uptake from the plant. Arbuscules are tree-like structures formed by profuse dichotomous hyphal branching in the lumen of cortical cells surrounded by a plant derived plasma membrane called the periarbuscular membrane (PAM). The PAM is very special as it has a different protein composition from the rest of the plasma membrane, hosting the transporters that will be key in the nutrient exchange with the fungal partner (Pumplin and Harrison, 2009; Zhang et al., 2015). Plants forming AM symbiosis have a dramatically different physiology, as they are not only better provided with mineral nutrients but also have an increased sink strength toward the root that imposes a carbon partitioning reallocation (Wright et al., 1998; Graham, 2000; Boldt et al., 2011). The form in which carbon is provided from the host plant to the AM fungus is still under debate, although most of the experimental evidence suggests that glucose is the main form taken up by the fungus (Shachar-Hill et al., 1995; Solaiman and Saito, 1997; Pfeffer et al., 1999). However, the finding that AM fungi lack the enzyme for *de novo* fatty acid biosynthesis, the type I FAS, (Tisserant et al., 2013; Salvioli et al., 2016; Tang et al., 2016) led to the hypothesis that, in addition to sugars, plants might be providing lipids as a source of carbon to their symbionts (Wewer et al., 2014). Currently, however, there is no experimental evidence on the mechanisms of how fatty acids could be released into the periarbuscular space or taken up into the fungus. In contrast, molecular support for sugar import into the fungus from the apoplastic space was obtained with the identification of the high affinity monosaccharide transporter MST2 from the AM fungus *Rhizophagus irregularis,* only expressed in symbiosis at arbuscule containing cells and intercellular hyphae (Helber et al., 2011). MST2 can transport several monosaccharides, including some pentoses, but it has the greatest affinity for glucose. Its inactivation by HIGS (host induced gene silencing) severely impaired arbuscule formation suggesting that this transporter is critical for the symbiosis (Helber et al., 2011).

The key questions are, however, how does glucose reach the apoplastic space in colonized cells? And, how does the plant

regulate the release of sugars into the apoplast? Enzymatic and promoter-reporter assays have clearly shown that mycorrhizal roots have a significant increase in cell wall-bound (CW) invertase activity (Wright et al., 1998; Schaarschmidt et al., 2006). Furthermore, CW invertase activity is located in the apoplast surrounding arbuscule-containing cells and intercellular hyphae, suggesting that apoplastic sucrose is cleaved prior uptake by the fungus (Schaarschmidt et al., 2006). Sucrose is the main form in which sugars are transported toward sink tissues including the root. However, after leaving the vascular tissue at the root, sucrose has to go through the endodermis to reach the cortical cells. Because sucrose is then expected to move symplastically to overcome the casparian strip (Kaiser et al., 2014), the involvement of SWEET exporters in cortical cells containing arbuscules is anticipated. In order to test this hypothesis, we decided to characterize the SWEET family of transporters in the mycorrhizal plant *Solanum tuberosum* (hereafter potato).

Here we show that potato contains a large SWEET family with 35 members, and that mycorrhiza colonization imposes a major transcriptional regulation of SWEETs in roots. The promoter activity of three up-regulated SWEETs during mycorrhiza colonization was analyzed using the GUS reporter gene and showed highest induction in arbuscule-containing cells. Altogether, our results point toward an important role for SWEET transporters during the mycorrhiza symbiosis.

MATERIALS AND METHODS

Plant Material and Growth Conditions

Solanum tuberosum cv. Desiree was propagated as cuttings axenically in plastic containers with Murashige and Skoog medium with vitamins and 25 g/l sucrose (Murashige and Skoog, 1962) solidified with 1 g/l Phytagel (P8169, Sigma-Aldrich, Germany; http://www.sigmaaldrich.com/germany.html) at 21°C and 16/8 h day/night rhythm.

For the tissue analysis, 2 week old cuttings were transferred to 9 cm/500 ml pots with a sand:gravel (1:4) mixture. The plants were fertilized once a week with 50 ml half strength Long Ashton nutrient solution with high phosphate content (665 μM; Hewitt, 1966). After 3 weeks at 23°C and 16/8 h day/night rhythm, roots, stems and leaves were harvested separately for RNA extraction. Five plants from independent pots were pooled to form one biological replicate, three biological replicates were used. For the harvest of tubers, plants were grown until tuberisation.

For mycorrhiza colonization, potato cuttings were transferred to pots as described above and adapted for 1 week to those conditions (23°C). After that, they were inoculated by mixing the substrate with 2 months old *Daucus carota* hairy root cultures grown monoxenically in association with *Rhizophagus irregularis* DAOM 197,198 (Schenck and Smith, 1982; Krüger et al., 2012) on M-medium with sucrose at 27°C in darkness (Bécard and Fortin, 1988). One Petri dish of carrot roots was used to inoculate a 500 ml pot. Plants were fertilized with half strength Long Ashton nutrient solution with 5 μM phosphate. Non-mycorrhizal controls were treated the same. Roots were harvested 4, 6, and 8 wpi (weeks post inoculation) for RNA extraction. Three plants from independent pots were pooled to form one biological replicate. Three biological replicates per treatment were used.

Medicago truncatula Jemalong A17 was transformed as described using *Agrobacterium rhizogenes* ARquaI (Kuhn et al., 2010). Five weeks after transformation, wild type roots were cut and the plants were propagated one additional week on medium supplied with 400 mg/l Augmentin (AmoxiClav, Hikma Farmaceutical, Portugal; http://www.hikma.com/). After that, the composite plants were transferred to 50 ml growth tubes (Stuewe & Sons, Inc., USA; https://www.stuewe.com/) with the same substrate described above which was directly inoculated with mycorrhizal carrot roots (1/4 Petri dish per 50 ml tube). They were fertilized with 5 ml half strength Long Ashton nutrient solution (low phosphate, 20 μM) once a week and harvested at 5 wpi.

Identification of *SWEET* Genes, Phylogeny, and Synteny Analysis

SWEET genes were identified via BLASTP search in the National Center for Biotechnology Information (NCBI; http://www.ncbi.nlm.nih.gov/) and the Solanaceae Genomics Network database (SGN; Bombarely et al., 2011; http://solgenomics.net/). The 35 SWEET genes identified were named *S. tuberosum SWEET1* to *SWEET*17. Numbers were given according to their closest homolog of *Arabidopsis thaliana* (Chen et al., 2010). For numbers that were present more than once small letters from a to g were assigned according to their positions in the genome (**Supplementary Table 1**).

Phylogenetic analyses were conducted using Clustal Omega (Sievers et al., 2011, https://www.ebi.ac.uk/Tools/msa/clustalo/) for protein sequence alignment and Mega 6 (Tamura et al., 2013, http://www.megasoftware.net/) for the phylogenetic tree construction. The Neighbor-joining method with the p-distance substitution model was applied, performing Bootstrapping with 1000 replicates and missing data was deleted pairwise. The clades were classified according to Chen et al. (2010). The accession numbers of the sequences used can be found in **Supplementary Table 1** and were obtained from NCBI, the *Arabidopsis* Information Resource (TAIR; Lamesch et al., 2012; https://www.*Arabidopsis*.org) or from the SGN. For synteny analysis, the genome positions of the potato *SWEETs* (**Supplementary Table 1**) and the positions of the corresponding tomato homologs were used (Feng et al., 2015).

Topology Prediction and Manual Annotation

The transmembrane helices of all SWEETs were predicted by TMHMM Server v.2.0 (http://www.cbs.dtu.dk/services/TMHMM/). For those not showing the typical seven transmembrane domain structure, a manual annotation was carried out using BLASTX in NCBI as well as by using cDNA analyses. The number of transmembrane helices of the final predicted proteins can be found in **Supplementary Table 1**. All the potato sequences used in this paper were sent to NCBI and are available

with GenBank accession numbers KU686963 to KU686997 (**Supplementary Table 1**).

Expression Data and Quantitative Real-Time Expression Analyses

Expression data of RNA-seq experiments from the Potato Genome Sequencing Consortium was shown as fragments per kilobase of transcript per million mapped reads (FPKM). Values were obtained from the Spud DB Solanaceae Genomics resource (Hirsch et al., 2014; http://solanaceae.plantbiology.msu.edu/) for those SWEETs having a potato genome annotation. Nine of the 35 potato *SWEET* genes are currently not annotated in the potato genome and therefore, their expression was analyzed by RT-PCR with 40 cycles (see primer list **Supplementary Table 2**). Total RNA was extracted using the innuPREP RNA Kit (Analytik Jena AG, http://www.analytik-jena.de/), quantified by the NanoDrop ND-100 spectrophotometer (http://www.nanodrop.com/). cDNA was synthesized as described elsewhere (Kuhn et al., 2010) with the reverse transcriptase SuperScript II (Invitrogen, USA; https://www.lifetechnologies.com/de/de/home.html).

Real time expression analyses were carried out using an iCycler MyIQ (Bio-Rad, USA; http://www.bio-rad.com/) and MESA Green 231qPCR Master Mix Plus (Eurogentec, Germany; http://www.eurogentec.com/eu-home.html) with three technical replicates per reaction and three independent biological replicates. Expression of the translation elongation factor 1-alpha (*Stef1*; AJ536671) was used for normalization. *StPT4* (AY793559), *StInvCD141* (Z22645), *RiTEF* (DQ282611), and *RiMST2* (HM143864) served as indicators of symbiosis status. Primers used can be found in **Supplementary Table 2**.

Promoter Analysis

Promoter elements were searched in the 2 kb region upstream of the ATG for each SWEET gene from potato and from tomato (see **Supplementary Table 3** for sequence details). For *StSWEET7d*, *StSWEET12c*, *StSWEET12e*, *SlSWEET3,* and *SlSWEET12a*, only smaller fragments could be obtained from the databases (1491, 1207, 1900, 1235, and 863 bp, respectively).

For promoter-reporter assays, 2 kb fragments of the *SWEET2c*, *SWEET7a,* and *SWEET12a* promoters were cloned into the Gateway binary vector pPGFPGUS-RR, containing the reporter genes GFP (green fluorescent protein) and GUS (β-Glucuronidase) as well as a red root cassette (RR, constitutively expressed DsRed) for root transformation control (Kuhn et al., 2010). *A. rhizogenes*-mediated transformation of *M. truncatula* and mycorrhizal inoculation with *R. irregularis* was carried out as described above. GUS staining was performed as described elsewhere (Kuhn et al., 2010) with the following modifications: the staining was fixed with 50% EtOH for 2 h. After that, the roots were cleared in 10% KOH for 30–45 min at 95°C and fungal cell walls were stained with WGA-FITC (wheat germ agglutinine-fluorescein isothiocyanate, Sigma Aldrich) according to Rech et al. (2013). For each construct, at least 10 independently transformed roots were analyzed.

Microscopy and Image Processing

Roots expressing GUS were microscoped using a Leica TCS SP5 (DM5000) equipped with the digital color camera DFC295. Objectives used were HC PL FLUOTAR 10.0 × 0.03 DRY, HCX PL APO CS 20.0 × 0.70 DRY UV, and HCX APO lambda blue 63.0 × 1.20 WATER UV CORR (Leica, Wetzlar, Germany; http://www.leica-microsystems.com/de/) at 21°C. Differential interference contrast (DIC) pictures were obtained using appropriate DIC prisms for the three objectives and FITC fluorescence was recorded using filter cube L5. Images were collected using LASAF v2.6 and ImageJ 1.48p (http://fiji.sc/Fiji).

Statistical Analyses

Expression analysis data were statistically tested for differences between non-mycorrhizal and mycorrhizal roots (three biological replicates, respectively) using the Student's *t*-Test with a two-tailed distribution and homoscedasticity. Differences were considered as significant with a value of $p < 0.05$ (marked with $*$) and $p < 0.01$ (marked with $**$).

RESULTS AND DISCUSSION

Identification and Phylogenetic Analysis of the SWEET Family in Potato

In order to get insights into the mechanisms of sugar homeostasis in roots during mycorrhiza formation and in particular into the role of SWEETs, we first carried out *in silico* sequence analyses in the genome of potato (*S. tuberosum* group Phureja). Following the comprehensive phylogenetic analysis that was carried out in the model plant *Arabidopsis thaliana* (Chen et al., 2010), we identified 35 gene sequences coding for putative SWEETs using BLASTP searches in NCBI as well as in the SGN (Sol Genomics Network) databases (**Figure 1**). This number is much higher than the average number of SWEETs for angiosperms (*ca*. 20) (Eom et al., 2015) perhaps reflecting the genome triplications and gene tandem duplications observed in the *Solanum* lineage (Xu et al, 2011; Sato et al., 2012). We named the potato SWEETs following the *A. thaliana* nomenclature (Chen et al., 2010). Protein alignment of the 35 potato SWEETs with 29 sequences from tomato, 17 from *A. thaliana,* and 21 from rice allowed the construction of a phylogenetic tree. All 35 potato SWEETs cluster into the four clades defined by Chen et al. (2010). Most of the SWEETs from potato belong to clade III (15), followed by SWEETs from clades I and II (11 and 6, respectively). In addition, potato has also three SWEETs in the clade IV, whose members have been shown to transport fructose across the tonoplast (Chen et al., 2010; Chardon et al., 2013; Guo et al., 2014).

Interestingly, in tomato only 29 SWEET transporters have been identified (Feng et al., 2015). This reduction is homogenously distributed among the clades. The overall identity of all potato SWEETs is *ca*. 41%, while the overall identity of all SWEETs depicted in the phylogenetic tree of **Figure 1** is 39%, indicating a high degree of conservation among SWEET proteins. Pairwise comparison of potato and tomato SWEETs revealed that some members are up to 97% identical, being the overall

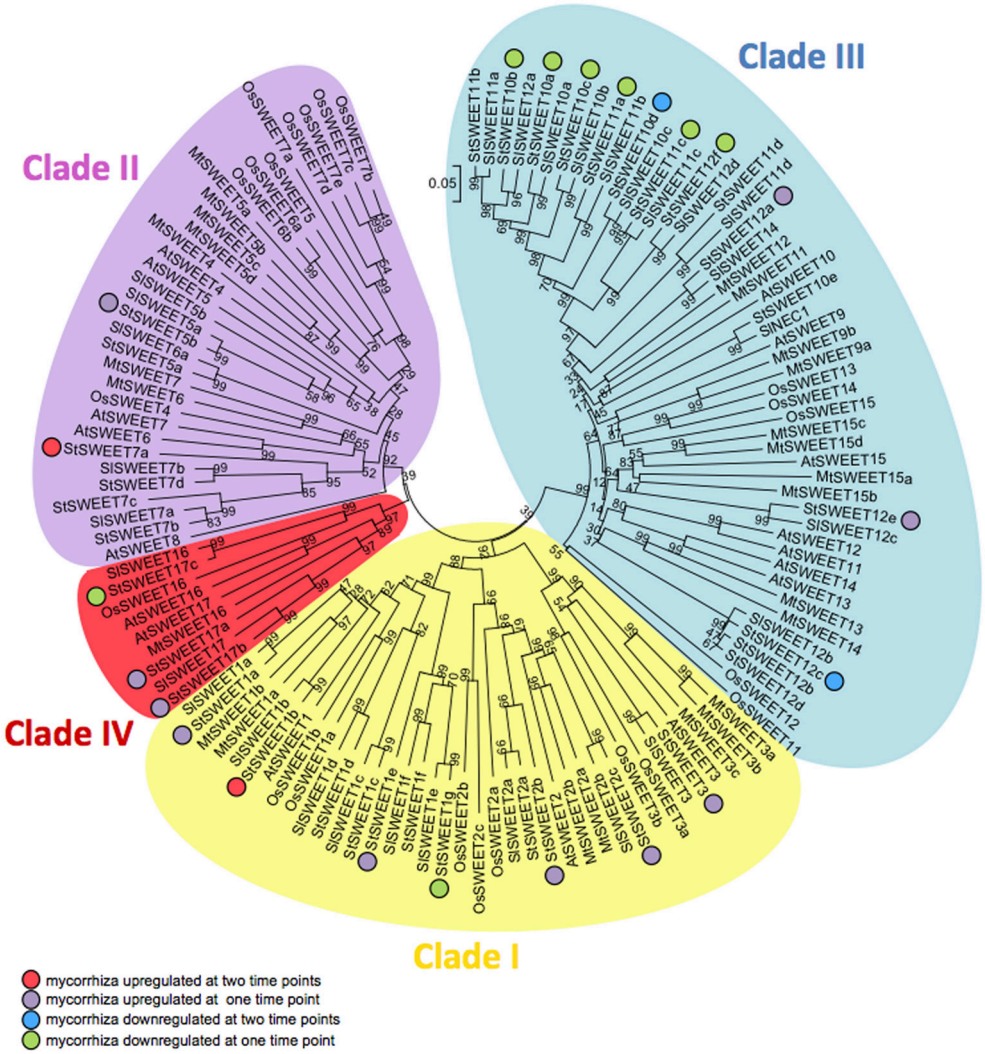

FIGURE 1 | Phylogenetic tree of potato, tomato, rice, *M. truncatula,* and *A. thaliana* SWEETs. The unrooted tree was generated based on an amino acid alignment using Clustal Omega. The phylogenetic tree was constructed using the neighbor-joining method and the p-distance model using MEGA 6. Scale bar represents evolutionary distance in number of amino acid differences per site. Bootstrapping was performed with 1000 replicates and values are displayed on branches in %. Colored circles represent regulation by mycorrhization in the same color code as in **Figure 5**. Gene names and accession numbers can be found in **Supplementary Table 1**.

identity between tomato and potato of ca. 42%, mirroring the overall similarity between the two genomes (Sato et al., 2012; **Supplementary Table 4**).

The organization of genes encoding SWEETs in the potato genome showed that they are widely distributed among 11 from the 12 chromosomes (**Figure 2**). Chromosome 3 encodes the highest number of SWEETs (13 members), while chromosome 10 contains no *SWEET* genes. The expansion of SWEETs in chromosome 3 seems to be Solanaceae specific as they are absent in *Arabidopsis*, rice and *Medicago*. In support of a specific function in Solanaceae, expression data in tomato have shown a common regulation for six of those genes (Feng et al., 2015). One partial *SWEET* gene (XM_006368013) was not ascribed to any chromosome, however it is likely located on chromosome 5 because manual annotation and expression analyses showed that together with the partial *SWEET* gene XM_006359017 located on chromosome 5, both comprise one single gene (see topology predictions below). Our synteny analysis shows that all potato *SWEET* genes having an ortholog in tomato are located in the same chromosome in both species (**Figure 2**), consistent with the global synteny observed between the two genomes (Sato et al., 2012). Seven potato *SWEET* genes do not have orthologs in tomato, while only one tomato gene misses an ortholog in potato. The synteny analysis showed that most potato *SWEET* genes are located in the same arrangement as in the tomato chromosomes, with only two inversions observed in chromosome 6 (**Figure 2**). All *SWEET* genes encoding transporters from clade IV are located in chromosome 1 in tandem, whereas members of the

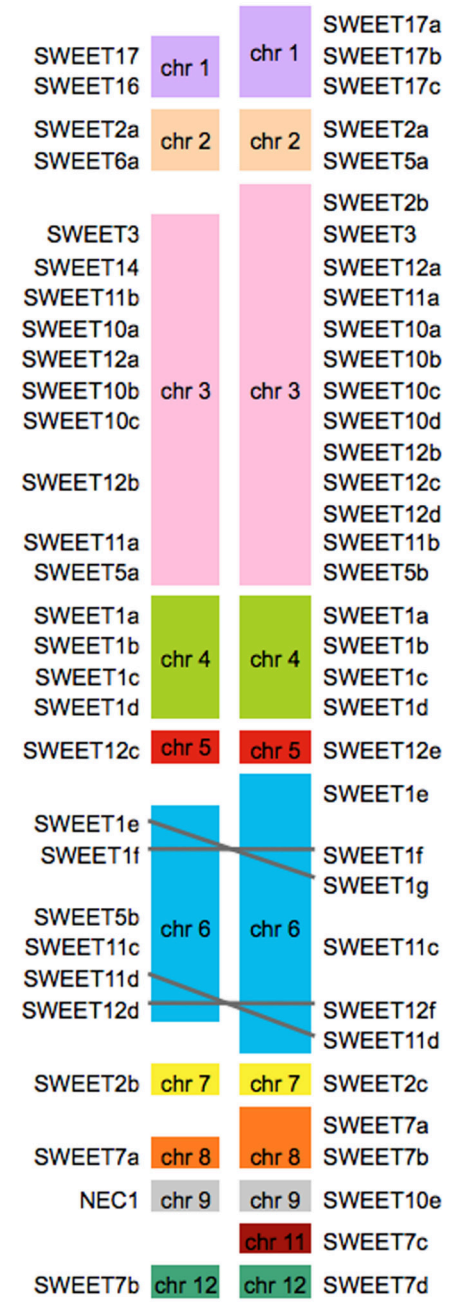

FIGURE 2 | Synteny analyses of *SWEET* genes in potato and tomato. *SWEET* genes are present in almost all chromosomes with the exception of chromosome 10 in potato and 10 and 11 in tomato. The distribution of the genes in both genomes is almost identical, with only two inversions in chromosome 6, mirroring the general high degree of synteny between both genomes.

other clades are not specifically associated to any particular chromosome.

The discovery of SWEETs as sugar transporters was seminal because thus far only proteins with 12 transmembrane domains (TMs) or 14 TMs had been shown to be able to transport monosaccharides and disaccharides across membranes (Chen et al., 2010). In contrast, plant SWEETs were shown to contain only seven TMs and to form a structure with two tandem triple helix bundles (TM1-3) and (TM5-7) separated by a linker region including a less conserved TM (TM4). This structure allows the formation of two pseudosymmetrical halves that permits sugar passage through the membrane (Tao et al., 2015). Interestingly, bacterial SemiSWEETs contain only three TMs and are thought to achieve sugar transport by oligomerizing with other SemiSWEETs and are, therefore, considered ancestor proteins of eukaryotic SWEETs (Xuan et al., 2013; Wang et al., 2014; Xu et al., 2014; Tao et al., 2015). Surprisingly topology predictions for the potato SWEETs using TMHMM revealed that although most of them belong to the seven TM groups, several exceptions existed and 12 potato SWEETs did not conform to this pattern according to the annotations from NCBI and SGN (**Supplementary Figure 1**). However, a closer look to their sequences and expression analyses (data not shown) revealed that in most cases those genes and their proteins were wrongly annotated. Only one protein seems not to conform to the seven TMs pattern (SWEET7c), that only contains the first four TM domains. However *SWEET7c* seems to be a pseudogene because downstream of the domain coding for the fourth TMs another gene is located coding for an F-box protein (XM_006356285.2, F-box protein At2g32560-like). A putative correct annotation for all potato *SWEET* genes has been submitted to the NCBI database (Accessions KU686963 to KU686997).

Tissue Expression Analyses of Potato SWEETs

We next analyzed *in silico* the transcriptional profile of potato *SWEET* genes using the Spud DB, comparing several tissues (Xu et al, 2011; Hirsch et al., 2014), mainly focusing on the expression profiles in roots. Nine from the 35 *SWEET* genes are not present in the SGN database and are therefore missing from the Spud DB. We analyzed those using RT-PCR in leaf, stem, root and tuber tissues from the potato cultivar Desiree. Results from the RNA-seq data in Spud DB showed that some of the *SWEET* genes were almost not detectable in most of the tissues analyzed such as *SWEET1f*, a few others were only expressed in one or two tissues. Thus, *SWEET7a* and *7d* are almost exclusively expressed in fruit, *SWEET1e and 5b* mainly in flower, and *SWEET12a* and *5a* in fruit and flower (**Figure 3A**, **Supplementary Table 5**). The only *SWEET* gene expressed almost exclusively in root is, according to Spud DB, *SWEET12d*. However, FPKM values are in general relatively low, and thus care must be taken when interpreting their meaning. From the 8 *SWEET* genes analyzed by RT-PCR, only *SWEET10a* and *12c* appeared as root specific, whereas *SWEET7c* and *11d* showed stem-specific expression (**Figure 3B**). However, we did not analyze tissues such as flower or stolons and therefore, more in depth expression analysis should be required. In general, the highest expression levels were found in leaf tissue, while mature tuber showed very low levels of expression for all *SWEET* genes, with the exception of *SWEET1b*. The two most

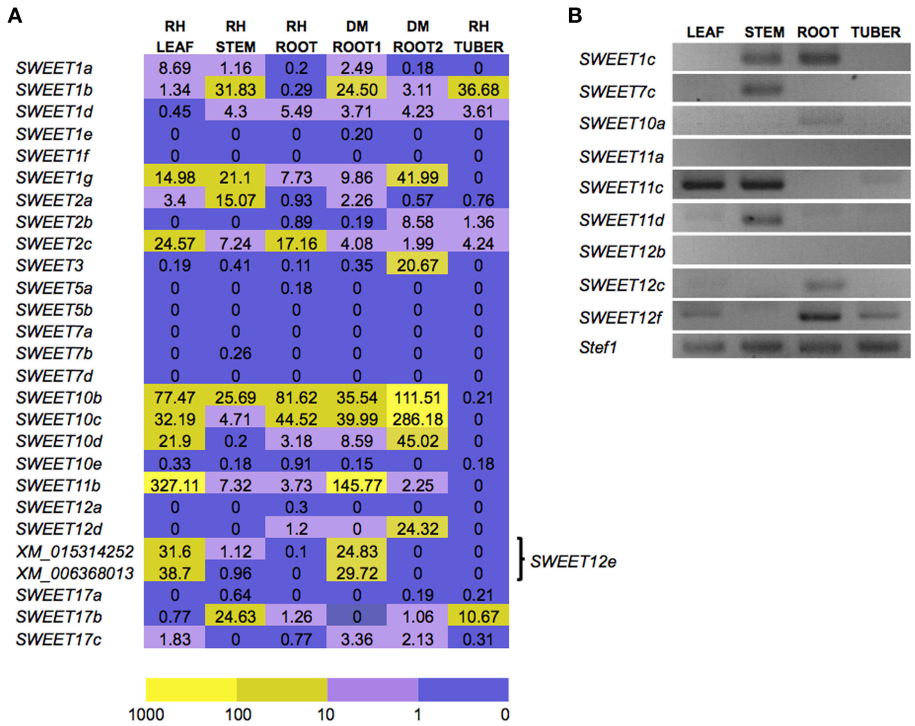

FIGURE 3 | Expression analyses of potato *SWEET* genes. (A) *In silico* expression analysis of 26 of the 35 potato *SWEET* genes in several tissues, including flower, leaf, stem, root, stolon, and tuber from either RH89-039-16 (RH) or DM3-1 (DM), according to the RNA-seq data from the Spud DB expressed as FPKM values (fragments per kilobase of transcript per million mapped reads). Two independent root expression data sets are available for DM root (DM ROOT1, DM ROOT2). Since *SWEET12e* was not correctly annotated prior to this work, two transcripts can be found corresponding to this gene. The color code indicates level of expression in logarithmic scale from dark purple to bright yellow. **(B)** RT-PCR expression analyses in leaf, stem, root, and tuber for the nine potato *SWEET* genes not annotated in the SGN database. The house keeping gene elongation factor 1α (*Stef1*) was used as control. Forty cycles were used for the PCR.

expressed genes are *SWEET11b* in leaf and *SWEET1b* in petals, followed by *SWEET10b* in one of the root samples. These results show that although some SWEETs have been shown to have a specific function in some tissues, the high level of conservation in sequence and in expression anticipates a large degree of functional redundancy in potato.

Transcriptional Regulation of Potato *SWEET* Genes during Mycorrhiza Symbiosis

To investigate the possibility that SWEETs are involved in sugar downloading processes during AM symbiosis, transcriptional changes in the expression of all potato SWEETs were analyzed in colonized roots. Potato plants were inoculated with the fungus *R. irregularis* and harvested at three time-points (4, 6, and 8 weeks post inoculation, wpi). To assess the development of the symbiosis, we first measured the expression of *StPT4* (an arbuscule-specific plant phosphate transporter) and of *RiTEF* (*R. irregularis* Translation elongation factor 1a). The level of *RiTEF* indicates the level of fungal colonization within the roots, while the plant phosphate transporter *StPT4* is only located in functional arbuscular branches and therefore it is a good indicator of active symbiosis (Harrison et al., 2002). Furthermore, we also analyzed the expression of the *InvCD141* gene, encoding a CW invertase whose ortholog in tomato is induced during AM symbiosis around arbuscules and intercellular hyphae (Schaarschmidt et al., 2006). In addition, we analyzed the expression of the fungal monosaccharide transporter *MST2* from *R. irregularis* (*RiMST2*) induced during symbiosis (Helber et al., 2011). While *StPT4, RiTEF,* and *RiMST2* were almost exclusively expressed in mycorrhizal samples as expected, the CW invertase showed also expression in non-colonized roots, although fungal colonization significantly raised its expression levels (**Figure 4A**). This result suggests that root colonization by *R. irregularis* caused an increase in apoplastic sucrose, contributing to increase the sink strength of mycorrhizal roots. The expression of all genes was highest at 6 wpi indicating that this was likely the time-point at which the symbionts were more active at nutrient exchange (**Figure 4A**).

We then analyzed the expression of all *SWEET* genes at 6 and 8 wpi. No transcript, or only barely measurable expression, was observed for three of the genes analyzed (*SWEETs 1f, 7d,* and *12b*), in general in accordance with the data from Spud DB (**Figure 4B**, **Supplementary Table 5**). In contrast, we could measure expression for 4 *SWEET* genes that had not been previously detected or only at very low levels in the Spud DB. Thus, *SWEET1e*, *5b,* and *17a* showed expression, albeit low, in control roots and were induced in response to fungal colonization, mainly at 6 wpi, coinciding with the

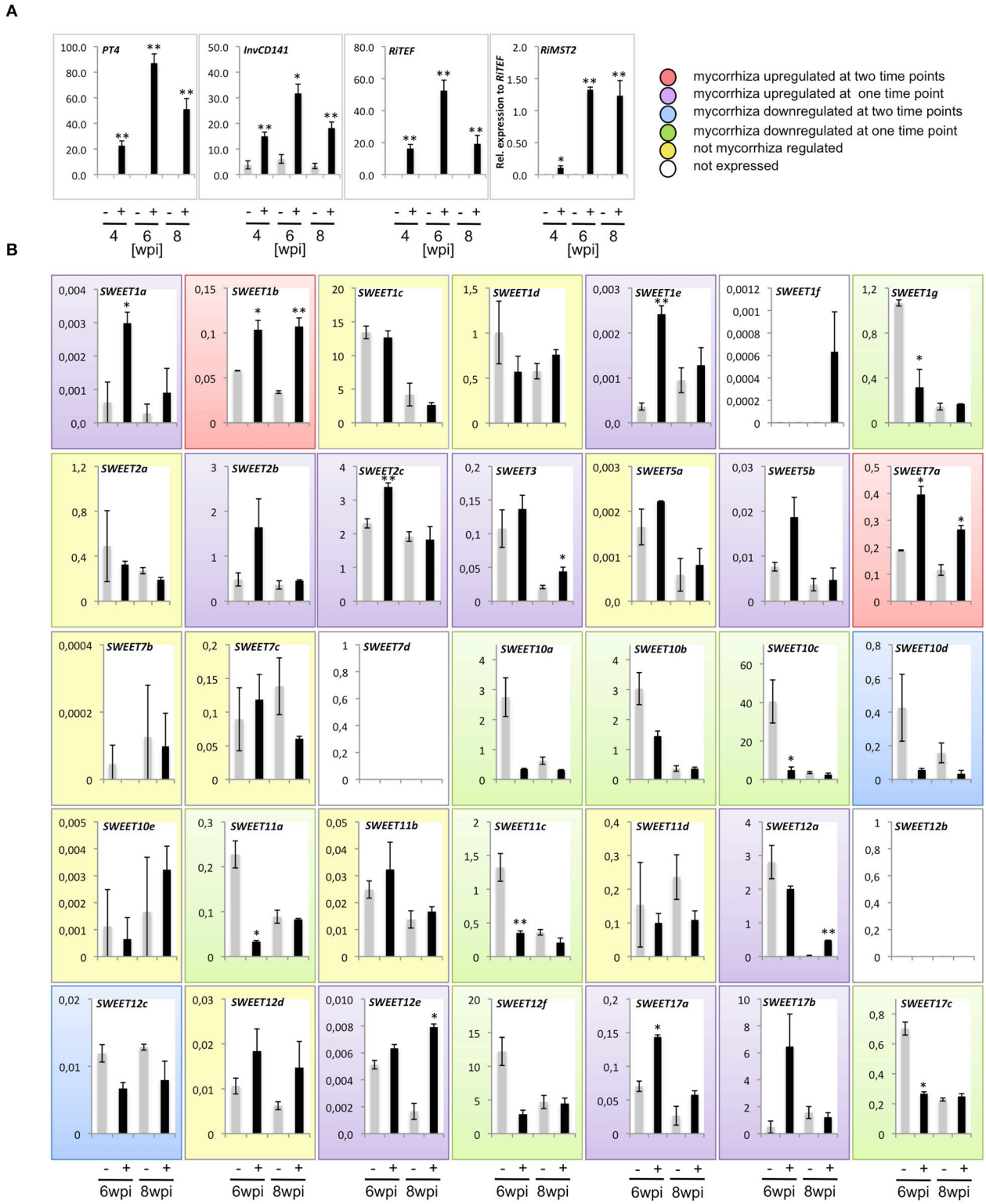

FIGURE 4 | Expression analysis of all potato *SWEETs* in roots in response to colonization by the *Arbuscular mycorrhizal* fungus *R. irregularis*. (A) The expression of the phosphate transporter *PT4* and the cell wall-bound invertase *InvCD141* from potato, as well as the fungal translation elongation factor 1a *RiTEF* and the monosaccharide transporter gene *RiMST2* were analyzed at 4, 6, and 8 weeks post inoculation (wpi). **(B)** Expression of potato *SWEETs* was measured at 6 and 8wpi. Expression is shown as relative expression to potato elongation factor 1α (*Stef1*) or to *RiTEF* for *RiMST2*. Error bars represent standard error of the mean. Non colonized samples are indicated by minus (–) and colonized samples by plus (+), per treatment the average expression of three biological replicates is shown. Student's *t*-test was used to calculate significance of mycorrhized compared to non mycorrhized samples in the same time point (**$p < 0.01$, *$p < 0.05$).

highest symbiotic activity (**Figures 4A,B**). Similarly, *SWEET7a* was also expressed in control roots, and induced even further by *R. irregularis* at both time-points (**Figure 4B**).

Remarkably, from all 35 potato *SWEET* genes, none of them showed a mycorrhiza-restricted induction, although two of them were clearly induced during symbiosis at 6 and 8 wpi (*SWEETs 1b* and *7a*), and 10 were induced at least in one time point (*SWEETs 1a, 1e, 2b, 2c, 3, 5b, 12a, 12e, 17a,* and *17b*). Interestingly analysis of expression data in the MtGEA (http://mtgea.noble.org/v3/) showed that several *SWEETs* were also induced during mycorrhiza symbiosis in *Medicago truncatula*. Thus, *MtSWEET1b*, *MtSWEET6,* and *MtSWEET9b* showed highest expression in arbuscule-containing cells, coincident with their putative potato relatives (*StSWEET1a*, *1b*, *7a,* and *12a*). In rice, analyses of expression in mycorrhizal roots only showed a clear induction for *OsSWEET3b* (Fiorilli et al., 2015), that also matches with the mycorrhizal induction of *StSWEET3*. These results suggest that several SWEETs might have been recruited for mycorrhiza symbiosis early in plant evolution.

Arbuscular mycorrhizal colonization also led to downregulation of some of the transporters. Thus, the expression of two of them (*SWEETs 10d* and *12c*) was repressed at both time-points, while 7 of them (*SWEETs 1g, 10a, 10b, 10c, 11a, 12f,* and *17c*) showed repression at 6 wpi (**Figure 4B**). Data from the MtGEA only showed a clear downregulation in arbuscule-containing cells for MtSWEET16 that cluster within the clade IV of tonoplast transporters. In contrast, RNA-seq data from rice only showed downregulation of *SWEET16* when comparing large lateral roots, which become colonized by mycorrhiza, vs. fine lateral roots that are not (Fiorilli et al., 2015).

Remarkably, 7 of the 10 repressed potato SWEETs belong to what appears to be a Solanum-specific subclade within clade III. Interestingly, the orthologs of five from them in tomato were shown to be repressed in roots in response to different stresses including sugars, temperature and salt, while at the same time induced by the same stresses in leaves (Feng et al., 2015). These results suggest that such group of genes plays a role in the carbon allocation between roots and shoots in tomato in response to external stimuli. In analogy, AM fungal colonization appears to be perceived as a stress for the roots of potato and could be then affecting the sugar partitioning between root and shoot. More biochemical and physiological data would be required to ascertain how the downregulation of such genes affects the sugar allocation to roots.

Eight of the 12 mycorrhiza-induced *SWEET* genes encode proteins from clade I or II that likely transport hexoses (**Figures 1**, **4B**), while most of the repressed genes encode for proteins of clade III, presumed sucrose transporters (**Figures 1**, **4B**). This could be interpreted as an increase in hexoses vs. sucrose being transported across root plant membranes in response to colonization that could serve for fungal nutrition. However, given that SWEETs are bi-directional transporters and that the precise root tissue and subcellular location of each SWEET is not determinable on its sequence basis, more experimental evidence is required. In this sense it is interesting that all five SWEET transporters induced by *Xanthomonas* TAL effectors in rice belong to the clade III (Streubel et al., 2013) and thus presumed sucrose transporters. Eom et al. (2015) suggest that this might be explained by the fact that, in contrast to sucrose, the hexose pools in the cytoplasm are limited and thus, they might be not sufficient to maintain pathogenic growth.

Although, transcriptional inductions and repressions were modest in most cases, it should be taken into account that they were measured in whole root systems, and thus if only happening in colonized areas, a large dilution effect is expected. In general, the extensive transcriptional reprogramming observed involving 22 of the 35 transporters highlights a complex carbohydrate reorganization that roots undergo during mycorrhizal symbiosis. And it also suggests that a large degree of functional redundancy might exist.

Promoter Analysis of Potato SWEET Transporters

A putative role for the carboxy terminal domain of SWEETs in the posttranslational regulation of their activity has been postulated (Niittylae et al., 2007). However, several lines of evidence have shown that transcriptional regulation might be sufficient to control SWEET activity. Thus, for instance, TAL-mediated SWEET expression induction by pathogens, or overexpression of specific SWEETs is enough to produce significant phenotypic differences (reviewed in Eom et al., 2015). Therefore, and assuming that SWEET genes could be targets for mycorrhiza induction, we next analyzed the promoter of potato *SWEETs* for mycorrhiza-specific motifs (**Supplementary Table 3**). In particular we searched for the CTTC motif, that has been previously shown to be sufficient for expression in cells containing arbuscules and that is often associated to the phosphate starvation motif P1BS, GnATATnC (Rubio et al., 2001), both in close vicinity to the ATG (Karandashov et al., 2004; Chen et al., 2011; Lota et al., 2013). The core motif of the CTTC element is TCTTGTTC, however, shorter versions lacking the 3′C (TCTTGTT), versions where G is exchanged to C, and a version with both modifications have also been found in mycorrhiza inducible promoters (Lota et al., 2013). Therefore, we also searched for such modifications in the promoter of all potato *SWEET* genes.

The complete CTTC consensus sequence was only found in the promoters of *SWEET7c*, *10a,* and *17a,* although only *SWEET17a* was induced by *R. irregularis* at 6 wpi, and in none of the three promoters the P1BS motif was present. Modified versions of the CTTC consensus sequence could be identified in promoters of 28 of the 35 *SWEET* genes, with the exception of *SWEET1c*, *1d*, *1f*, *1g*, *2a, 2b,* and *12f*. The P1BS motif was present in 12 *SWEET* promoters, however it was never in the 30 bp region upstream of the CTTC motif as described (Chen et al., 2011; Lota et al., 2013). We could not identify a clear correlation between the presence of the CTTC motif and a mycorrhiza-induced expression (**Supplementary Table 3**) and therefore, future deletion experiments will be necessary to

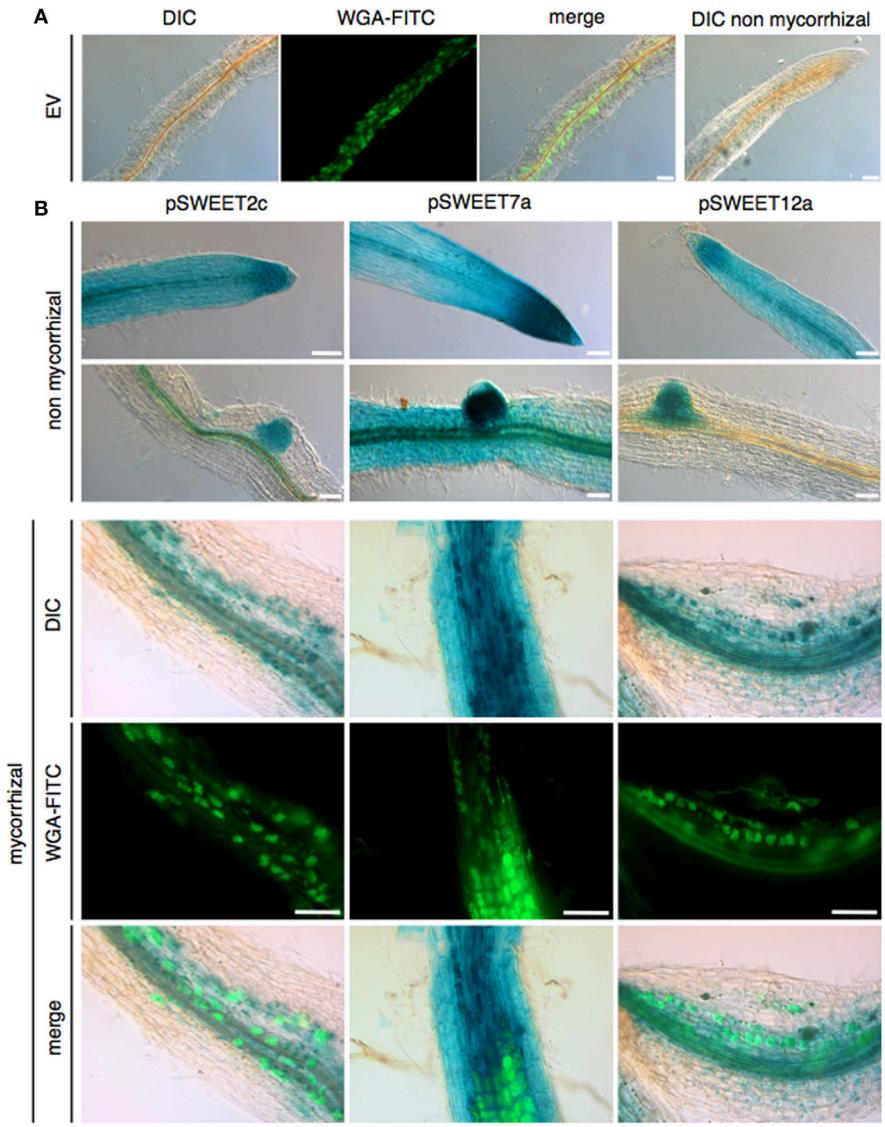

FIGURE 5 | Promoter-reporter assays of three *SWEET* promoters during AM symbiosis. 2kb fragments upstream of the ATG of potato *SWEETs 2c, 7a,* and *12a* were cloned in front of the GUS reporter gene and transformed in *M. truncatula*. Composite plants were inoculated with *R. irregularis* and harvested 5 wpi (weeks post inoculation). β-Glucuronidase staining and WGA-FITC (wheat germ agglutinin-fluorescein isothiocyanate) counterstaining of fungal cell walls was carried out in mycorrhizal and non-mycorrhizal control roots. **(A)** Empty vector control roots. **(B)** Non-mycorrhizal and mycorrhizal promoter-reporter roots. Scale bars represent 100 μm. DIC: differential interference contrast, WGA-FITC signal is shown in green.

determine its importance or not for the mycorrhiza induction of SWEET genes.

In order to gather information on the spatial expression pattern of mycorrhiza-induced *SWEETs* in roots, promoter-reporter assays using the *GUS* gene were carried out in a heterologous system, in *M. truncatula* transformed with *Agrobacterium rhizogenes*. To that end, three mycorrhiza-induced genes, one from each clade, were selected. The promoter of *SWEET2c* (clade I) showed activity in non-colonized roots mainly at the root tip, as well as faint expression in the cortex. Upon fungal colonization, expression level was increased and re-localized mainly to arbuscule-containing cells (**Figure 5**). This is in agreement with the presence of several CTTC motifs, two short and one short with a G to C exchange (**Supplementary Table 3**). Recently, the putative ortholog of SWEET2c from *Arabidopsis*, one of the three highest expressed *SWEETs* in *Arabidopsis* roots, has been functionally characterized (Chen et al., 2015a). Surprisingly, although it belongs to the clade I, AtSWEET2 localizes at the tonoplast and most likely performs as glucose importer. Because AtSWEET2 is mainly localized in root tips, its function has been associated to prevent losses of carbon into the rhizosphere, and consistently, its deletion not only increases glucose efflux but also the plant susceptibility to the pathogenic oomycete *Pythium irregulare* (Chen et al., 2015a).

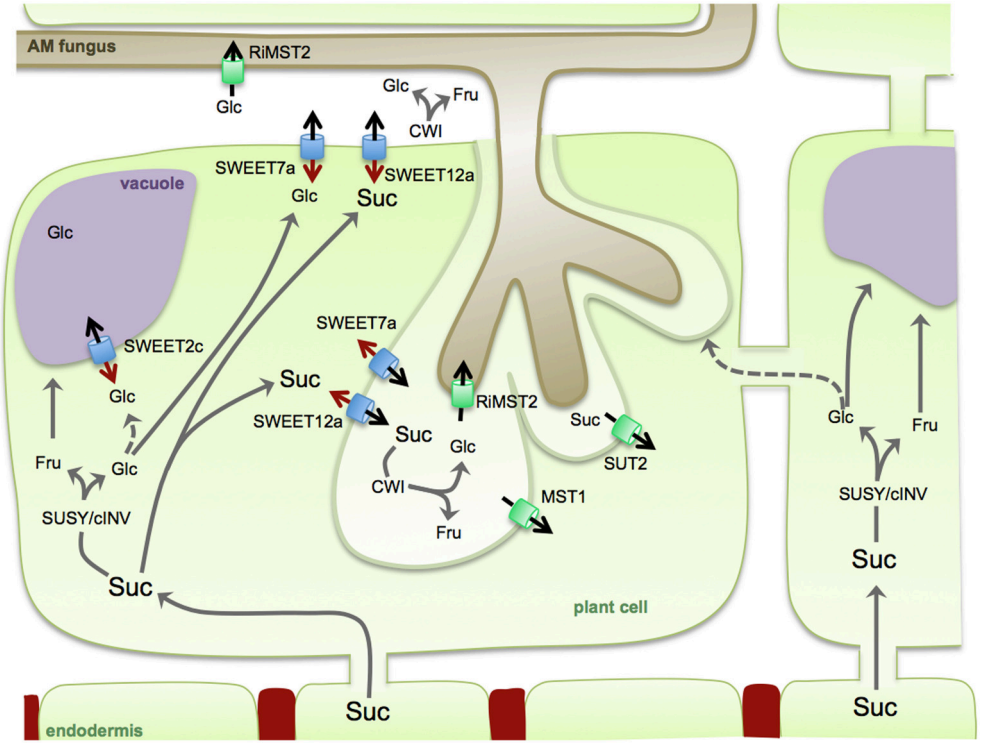

FIGURE 6 | Model of sugar partitioning during arbuscular mycorrhiza symbiosis. Sucrose (Suc) is delivered to arbuscule containing cells symplastically from the endodermis to overcome the casparian strip (in red). In the cytoplasm, Suc can be cleaved by sucrose synthase (SUSY) or cytoplasmic invertase (cINV) to glucose (Glc) and fructose (Fru). To maintain the favorable concentration gradient, hexoses could be translocated into the vacuole via tonoplast located SWEETs or other transporters. Alternatively, hexoses could be exported into the apoplast with the help of SWEET7a. Direct export of sucrose into the apoplast or the periarbuscular space could be achieved by sucrose efflux transporters from clade III such as SWEET12a. In the apoplast and periarbuscular space sucrose is cleaved by cell wall-bound invertase (CWI). The sugars in the apoplast are either taken up by the fungus via monosaccharide transporters such as RiMST2 or by the plant cell via monosaccharide transporters such as MST1 (shown in *M. truncatula*) and via sucrose transporters such as SUT2 (shown for *S. lycopersicum*). Neighbor cells might also contribute to the nutrition of the arbuscule containing cell by providing sugars symplastically. Black arrows on SWEETs: sugar transport direction as described above. Red arrows on SWEETs: alternative sugar transport direction.

The *Vitis vinifera* putative ortholog, *VvSWEET2a*, is also induced in leaves upon inoculation with *Plasmopara viticola* or with *Botrytis cinerea* (Chong et al., 2014), suggesting that this *SWEET* gene might be a common target of different microorganisms. However, in order to infer if the mycorrhizal induction and re-localization of potato SWEET2c to arbuscule-containing cells would also serve as a mechanism to control sugar efflux toward the AM fungus preventing a parasitic behavior, localization and inactivation studies should be carried out. An alternative hypothesis is that SWEET2c could contribute to maintain the concentration gradient of sucrose in cortical cells by sequestering glucose derived from the activity of cytoplasmic invertases or sucrose synthases. In support of this second scenario, Baier et al. (2010) demonstrated that sucrose synthase was induced in arbuscule containing cells and that its inactivation severely impaired arbuscule development.

Promoter-reporter activity for *SWEET7a*, from clade II, confirmed that although this gene is ubiquitously and highly expressed in the root under non-mycorrhizal conditions (**Figure 5**), symbiosis induces its expression and this is largely occurring in arbuscule-containing cells that show a much stronger GUS activity than non-colonized cortical cells. This is consistent with the presence of several modified CTTC motifs (**Supplementary Table 3**). Potato *SWEET7a* does not have an ortholog in tomato, indicating that if it plays a mycorrhiza important role, this function might be redundant with another potato *SWEET*. This is likely, given that most of the up-regulated *SWEETs* during mycorrhiza symbiosis, such as *SWEET7a,* belong to the clades I and II that presumably transport hexoses.

In contrast, only two genes from clade III were induced during AM symbiosis (**Figures 1**, **4**). One of them is *SWEET12a*, whose transcript was induced at 8 wpi, although it was also highly expressed at 6 wpi. GUS activity showed that while in control roots promoter activity was restricted to the root tip, in mycorrhizal roots *SWEET12a* had a strong promoter activity in the cortex, particularly in arbuscule-containing cells (**Figure 5**). This result is consistent with the presence of two CTTC short motifs in the promoter (**Supplementary Table 3**). Experiments in progress to delete these motifs will show whether they are required or not for the expression of potato *SWEET12a* in arbuscule-containing cells.

The fact that all three of these promoter-reporter constructs from *SWEETs* induced during mycorrhiza colonization in potato also showed this pattern in the heterologous plant *M. truncatula* supports the idea that the promoter elements and transcription factors driving mycorrhiza and/or arbuscule expression of *SWEETs* must be conserved in both plants. More detailed analyses are now required to identify whether these would be promoter elements only specific to SWEET genes or conserved in other mycorrhiza-induced genes. The results of the promoter-reporter analyses also showed that the induction of *SWEETs* expression was not widely distributed but focused in arbuscule-enriched areas, indicating a redirection of the carbon sink toward colonized cortical cells.

In conclusion, our work here offers the first overview of the SWEET family in potato, and particularly suggests a putative involvement for some SWEETs during mycorrrhiza symbiosis. The results show that the transport of hexoses across the plant plasma membrane, assuming this is the main role for SWEETs in clade I and II, is highly induced during mycorrhiza formation (eight induced genes), while most repressed genes belong to the clade III (eight genes) and only two induced. If an export activity for SWEET hexose transporters such as SWEET7a would be assumed, these findings would be consistent with the fact that *R. irregularis* induces its monosaccharide transporter MST2 with highest affinity for glucose (Helber et al., 2011). However, the fact that the CW invertase is always expressed in cells containing arbuscules and in cells in contact with intercellular hyphae, suggests that sucrose export into the apoplast is also enhanced during colonization (Schaarschmidt et al., 2006 and our results here). Although, increases in invertase activity in the root do not result in changes in colonization, inhibition of root invertase activity does, suggesting that hexose concentration in the apoplast is not the limiting factor for the symbiosis but that sucrose cleavage in the apoplast is key for the symbiosis (Schaarschmidt et al., 2007a). Altogether, this would be in support for a role of the two induced *SWEETs* from clade III, putative sucrose exporters, during AM symbiosis. Because the cellular localization of all three SWEETs analyzed in mycorrhizal roots points toward an induction in arbuscules, we think that the supply of carbohydrates to the fungus is a complex process involving many different transport processes. As depicted in our model (**Figure 6**), sucrose reaches the cortex symplastically and it could be directly exported to the periarbuscular space (PAS) and to the apoplast of cells in contact with the fungus with the help of SWEET transporters from clade III, such as SWEET12a, induced by the fungus in arbuscule containing cells. Sucrose in the PAS could then be cleaved with help of the CW invertase, and glucose would be taken up into the fungal cell by the fungal monosaccharide transporter MST2. But which function would then have the induced SWEETs from clade I and II? One possibility is that sucrose could be cleaved in the cytoplasm by sucrose synthase and/or cytoplasmic invertase. Both activities have been shown in arbuscule containing cells and they could help to maintain the concentration gradient. Glucose could then be further exported in the PAS by some of the induced SWEETs from clade I and II. Vacuolar SWEETs such as the induced SWEET2c could also contribute to maintain the favorable sucrose gradient in arbuscule containing cells by sequestering glucose and/or fructose in the vacuole.

Alternatively, mycorrhiza induced SWEETs from clade I and II might be functioning not as exporters but rather as importers, competing with the fungus at the apoplast for the re-import of the sugar into the plant cytoplasm to support the high metabolic activity of the colonized cells or to avoid defense responses elicited by high amount of hexoses (Schaarschmidt et al., 2007b). In support of that, other transporters have been identified featuring in arbuscule containing cells to re-import sugar from the apoplast, including a monosaccharide transporter in *M. truncatula* and a sucrose transporter in tomato (Harrison, 1996; Bitterlich et al., 2014). More studies, in particular regarding the biochemistry, subcellular localization, and physiology of the potato SWEETs regulated during symbiosis are required to be able to draw a more precise model of their role in sugar partitioning during mycorrhizal symbiosis.

AUTHOR CONTRIBUTIONS

NR, JM planned the experiments and wrote the manuscript, JM carried out the experiments.

ACKNOWLEDGMENTS

We thank Dr. Stahl and Dr. Temme from KWS SAAT AG for their gift of potato axenic cultures. We thank Carolin Heck for comments on the manuscript. JM holds a fellowship from the Baden-Württemberg Landesgraduiertenförderung.

SUPPLEMENTARY MATERIAL

The Supplementary Material for this article can be found online at: http://journal.frontiersin.org/article/10.3389/fpls.2016.00487

Supplementary Figure 1 | Topology analysis of potato SWEETs. The upper panel shows the predicted domain structure of potato SWEETs in the NCBI database that were predicted to have more or less than 7 TM domains. Manual annotation and expression data (here not shown) revealed that almost all of them were wrongly annotated. Only *SWEET7c* that is possibly a pseudogene contains only 4 TM domains.

Supplementary Table 1 | Accession numbers of sequences used in this study and genome positions and transmembrane domain prediction for potato SWEETs.

Supplementary Table 2 | Primers used in this study.

Supplementary Table 3 | Promoter element analysis of potato and tomato SWEETs.

Supplementary Table 4 | Identity matrices among potato and between potato and tomato SWEETs.

Supplementary Table 5 | RNA-seq data for annotated potato SWEETs from the Spud DB.

REFERENCES

Antony, G., Zhou, J., Huang, S., Li, T., Liu, B., White, F., et al. (2010). Rice *xa13* recessive resistance to bacterial blight is defeated by induction of the disease susceptibility gene Os-11N3. *Plant Cell* 22, 3864–3876. doi: 10.1105/tpc.110.078964

Baier, M. C., Keck, M., Gödde, V., Niehaus, K., Küster, H., and Hohnjec, N. (2010). Knockdown of the symbiotic sucrose synthase MtSucS1 affects arbuscule maturation and maintenance in mycorrhizal roots of *Medicago truncatula*. *Plant Physiol.* 152, 1000–1014. doi: 10.1104/pp.109.149898

Bécard, G., and Fortin, J. A. (1988). Early events of vesicular–arbuscular mycorrhiza formation on Ri T-DNA transformed roots. *New Phytol.* 108, 211–218. doi: 10.1111/j.1469-8137.1988.tb03698.x

Bitterlich, M., Krügel, U., Boldt-Burisch, K., Franken, P., and Kühn, C. (2014). The sucrose transporter SlSUT2 from tomato interacts with brassinosteroid functioning and affects *Arbuscular mycorrhiza* formation. *Plant J.* 78, 877–889. doi: 10.1111/tpj.12515

Boldt, K., Pörs, Y., Haupt, B., Bitterlich, M., Kühn, C., Grimm, B., et al. (2011). Photochemical processes, carbon assimilation and RNA accumulation of sucrose transporter genes in tomato *Arbuscular mycorrhiza*. *J. Plant Physiol.* 168, 1256–1263. doi: 10.1016/j.jplph.2011.01.026

Bombarely, A., Menda, N., Tecle, I. Y., Buels, R. M., Strickler, S., Fischer-York, T., et al. (2011). The Sol Genomics Network (solgenomics.net): growing tomatoes using Perl. *Nucleic Acids Res.* 39, D1149–D1155. doi: 10.1093/nar/gkq866

Chardon, F., Bedu, M., Calenge, F., Klemens, P. A., Spinner, L., Clement, G., et al. (2013). Leaf fructose content is controlled by the vacuolar transporter SWEET17 in *Arabidopsis*. *Curr. Biol.* 23, 697–702. doi: 10.1016/j.cub.2013.03.021

Chen, A., Gu, M., Sun, S., Zhu, L., Hong, S., and Xu, G. (2011). Identification of two conserved *cis*- acting elements, MYCS and P1BS, involved in the regulation of mycorrhiza-activated phosphate transporters in eudicot species. *New Phytol.* 189, 1157–1169. doi: 10.1111/j.1469-8137.2010.03556.x

Chen, H. Y., Huh, J. H., Yu, Y. C., Ho, L. H., Chen, L. Q., Tholl, D., et al. (2015a). The *Arabidopsis* vacuolar sugar transporter SWEET2 limits carbon sequestration from roots and restricts *Pythium* infection. *Plant J.* 83, 1046–1058. doi: 10.1111/tpj.12948

Chen, L. Q. (2014). SWEET sugar transporters for phloem transport and pathogen nutrition. *New Phytol.* 201, 1150–1155. doi: 10.1111/nph.12445

Chen, L. Q., Hou, B. H., Lalonde, S., Takanaga, H., Hartung, M. L., Qu, X. Q., et al. (2010). Sugar transporters for intercellular exchange and nutrition of pathogens. *Nature* 468, 527–532. doi: 10.1038/nature09606

Chen, L. Q., Lin, I. W., Qu, X. Q., Sosso, D., McFarlane, H. E., Londoño, A., et al. (2015b). A cascade of sequentially expressed sucrose transporters in the seed coat and endosperm provides nutrition for the *Arabidopsis* embryo. *Plant Cell* 27, 607–619. doi: 10.1105/tpc.114.134585

Chen, L. Q., Qu, X. Q., Hou, B. H., Sosso, D., Osorio, S., Fernie, A. R., et al. (2012). Sucrose efflux mediated by SWEET proteins as a key step for phloem transport. *Science* 335, 207–211. doi: 10.1126/science.1213351

Chong, J., Piron, M. C., Meyer, S., Merdinoglu, D., Bertsch, C., and Mestre, P. (2014). The SWEET family of sugar transporters in grapevine: VvSWEET4 is involved in the interaction with *Botrytis cinerea*. *J. Exp. Bot.* 65, 6589–6601. doi: 10.1093/jxb/eru375

Chu, Z., Fu, B., Yang, H., Xu, C., Li, Z., Sanchez, A., et al. (2006). Targeting *xa13*, a recessive gene for bacterial blight resistance in rice. *Theor. Appl. Genet.* 112, 455–461. doi: 10.1007/s00122-005-0145-6

Cohn, M., Bart, R. S., Shybut, M., Dahlbeck, D., Gomez, M., Morbitzer, R., et al. (2014). *Xanthomonas axonopodis* virulence is promoted by a transcription activator-like effector-mediated induction of a SWEET sugar transporter in cassava. *Mol. Plant Microbe Interact.* 27, 1186–1198. doi: 10.1094/MPMI-06-14-0161-R

Eom, J. S., Chen, L. Q., Sosso, D., Julius, B. T., Lin, I. W., Qu, X. Q., et al. (2015). SWEETs, transporters for intracellular and intercellular sugar translocation. *Curr. Opin. Plant Biol.* 25, 53–62. doi: 10.1016/j.pbi.2015.04.005

Feng, C. Y., Han, J. X., Han, X. X., and Jiang, J. (2015). Genome-wide identification, phylogeny, and expression analysis of the SWEET gene family in tomato. *Gene* 573, 261–272. doi: 10.1016/j.gene.2015.07.055

Fiorilli, V., Vallino, M., Biselli, C., Faccio, A., Bagnaresi, P., and Bonfante, P. (2015). Host and non-host roots in rice: cellular and molecular approaches reveal differential responses to arbuscular mycorrhizal fungi. *Front. Plant Sci.* 6:636. doi: 10.3389/fpls.2015.00636

Gamas, P., Niebel Fde C., Lescure, N., and Cullimore, J. (1996). Use of a subtractive hybridization approach to identify new *Medicago truncatula* genes induced during root nodule development. *Mol. Plant Microbe Interact.* 9, 233–242. doi: 10.1094/MPMI-9-0233

Ge, Y. X., Angenent, G. C., Wittich, P. E., Peters, J., Franken, J., Busscher, M., et al. (2000). NEC1, a novel gene, highly expressed in nectary tissue of *Petunia hybrida*. *Plant J.* 24, 725–734. doi: 10.1046/j.1365-313x.2000.00926.x

Graham, J. H. (2000) "Assessing costs of arbuscular mycorrhizal symbiosis agroecosystems fungi," in *Current Advances in Mycorrhizae Research*, eds G. K. Podila and D. D. Jr. Douds (St. Paul, MN: APS Press), 127–140.

Guo, W. J., Nagy, R., Chen, H. Y., Pfrunder, S., Yu, Y. C., Santelia, D., et al. (2014). SWEET17, a facilitative transporter, mediates fructose transport across the tonoplast of *Arabidopsis* roots and leaves. *Plant Physiol.* 164, 777–789. doi: 10.1104/pp.113.232751

Harrison, M. J. (1996). A sugar transporter from *Medicago truncatula*: altered expression pattern in roots during vesicular-arbuscular (VA) mycorrhizal associations. *Plant J.* 9, 491–503. doi: 10.1046/j.1365-313X.1996.09040491.x

Harrison, M. J., Dewbre, G. R., and Liu, J. (2002). A phosphate transporter from *Medicago truncatula* involved in the acquisition of phosphate released by arbuscular mycorrhizal fungi. *Plant Cell* 14, 2413–2429. doi: 10.1105/tpc.004861

Helber, N., Wippel, K., Sauer, N., Schaarschmidt, S., Hause, B., and Requena, N. (2011). A versatile monosaccharide transporter that operates in the arbuscular mycorrhizal fungus *Glomus* sp. is crucial for the symbiotic relationship with plants. *Plant Cell* 23, 3812–3823. doi: 10.1105/tpc.111.089813

Hewitt, E. J. (1966). *Sand and Water Culture Methods Used in the Study of Plant Nutrition.* Technical Communication No. 22. Commonwealth Bureau, London.

Hirsch, C. D., Hamilton, J. P., Childs, K. L., Cepela, J., Crisovan, E., Vaillancourt, B., et al. (2014). Spud DB: a resource for mining sequences, genotypes, and phenotypes to accelerate potato breeding. *Plant Genome* 7, 1–12. doi: 10.3835/plantgenome2013.12.0042

Kaiser, C., Kilburn, M. R., Clode, P. L., Fuchslueger, L., Koranda, M., Cliff, J. B., et al. (2014). Exploring the transfer of recent plant photosynthates to soil microbes: mycorrhizal pathway vs direct root exudation. *New Phytol.* 205, 1537–1551. doi: 10.1111/nph.13138

Karandashov, V., Nagy, R., Wegmüller, S., Amrhein, N., and Bucher, M. (2004). Evolutionary conservation of phosphate transport in the *Arbuscular mycorrhizal* symbiosis. *Proc. Natl Acad. Sci. U.S.A.* 101, 6285–6290. doi: 10.1073/pnas.0306074101

Krüger, M., Krüger, C., Walker, C., Stockinger, H., and Schüssler, A. (2012). Phylogenetic reference data for systematics and phylotaxonomy of arbuscular mycorrhizal fungi from phylum to species level. *New Phytol.* 193, 970–984. doi: 10.1111/j.1469-8137.2011.03962.x

Kuhn, H., Küster, H., and Requena, N. (2010). Membrane steroid-binding protein 1 induced by a diffusible fungal signal is critical for mycorrhization in *Medicago truncatula*. *New Phytol.* 185, 716–733. doi: 10.1111/j.1469-8137.2009.03116.x

Lamesch, P., Berardini, T. Z., Li, D., Swarbreck, D., Wilks, C., Sasidharan, R., et al. (2012). The *Arabidopsis* Information Resource (TAIR): improved gene annotation and new tools. *Nucleic Acids Res.* 40, D1202–D1210. doi: 10.1093/nar/gkr1090

Lin, I. W., Sosso, D., Chen, L. Q., Gase, K., Kim, S. G., Kessler, D., et al. (2014). Nectar secretion requires sucrose phosphate synthases and the sugar transporter SWEET9. *Nature* 508, 546–549. doi: 10.1038/nature13082

Lota, F., Wegmüller, S., Buer, B., Sato, S., Bräutigam, A., Hanf, B., et al. (2013). The cis- acting CTTC-P1BS module is indicative for gene function of *LjVTI12*, a Qb-SNARE protein gene that is required for arbuscule formation in *Lotus japonicus*. *Plant J.* 74, 280–293. doi: 10.1111/tpj.12120

Murashige, T., and Skoog, F. (1962). A revised medium for rapid growth and bio-assays with tobacco tissue cultures. *Physiol. Plant* 15, 473–497. doi: 10.1111/j.1399-3054.1962.tb08052.x

Niittylae, T., Fuglsang, A. T., Palmgren, M. G., Frommer, W. B., and Schulze, W. X. (2007). Temporal analysis of sucrose-induced phosphorylation changes in plasma membrane proteins of Arabidopsis. *Mol. Cell Proteomics* 6, 1711–1726. doi: 10.1074/mcp.M700164-MCP200

Patil, G., Valliyodan, B., Deshmukh, R., Prince, S., Nicander, B., Zhao, M., et al. (2015). Soybean (*Glycine max*) SWEET gene family: insights through comparative genomics, transcriptome profiling and whole genome re-sequence analysis. *BMC Genomics* 16:520. doi: 10.1186/s12864-015-1730-y

Pfeffer, P. E., Douds, D. D., Bécard, G., and Shachar-Hill, Y. (1999). Carbon uptake and the metabolism and transport of lipids in an arbuscular mycorrhiza. *Plant Physiol.* 120, 587–598. doi: 10.1104/pp.120.2.587

Pumplin, N., and Harrison, M. J. (2009). Live-cell imaging reveals periarbuscular membrane domains and organelle location in *Medicago truncatula* roots during arbuscular mycorrhizal symbiosis. *Plant Physiol.* 151, 809–819. doi: 10.1104/pp.109.141879

Rech, S. S., Heidt, S., and Requena, N. (2013). A tandem Kunitz protease inhibitor (KPI106)–serine carboxypeptidase (SCP1) controls mycorrhiza establishment and arbuscule development in *Medicago truncatula*. *Plant J.* 75, 711–725. doi: 10.1111/tpj.12242

Rubio, V., Linhares, F., Solano, R., Martín, A. C., Iglesias, J., Leyva, A., et al. (2001). A conserved MYB transcription factor involved in phosphate starvation signaling both in vascular plants and in unicellular algae. *Genes Dev.* 15, 2122–2133. doi: 10.1101/gad.204401

Salvioli, A., Ghignone, S., Novero, M., Navazio, L., Bagnaresi, P., and Bonfante, P. (2016). Symbiosis with an endobacterium increases the fitness of a mycorrhizal fungus, raising its bioenergetic potential. *ISME J.* 10, 130–144. doi: 10.1038/ismej.2015.91

Sato, S. Tabata, S., Hirakawa, H., Asamizu, E., Shirasawa, K., Isobe, S. (The Tomato Genome Consortium) (2012). The tomato genome sequence provides insights into fleshy fruit evolution. *Nature* 485, 635–641. doi: 10.1038/nature11119

Schaarschmidt, S., Gonzalez, M. C., Roitsch, T., Strack, D., Sonnewald, U., and Hause, B. (2007a). Regulation of arbuscular mycorrhization by carbon. The symbiotic interaction cannot be improved by increased carbon availability accomplished by root-specifically enhanced invertase activity. *Plant Physiol.* 143, 1827–1840. doi: 10.1104/pp.107.096446

Schaarschmidt, S., Kopka, J., Ludwig-Müller, J., and Hause, B. (2007b). Regulation of arbuscular mycorrhization by apoplastic invertases: enhanced invertase activity in the leaf apoplast affects the symbiotic interaction. *Plant J.* 51, 390–405. doi: 10.1111/j.1365-313X.2007.03150.x

Schaarschmidt, S., Roitsch, T., and Hause, B. (2006). Arbuscular mycorrhiza induces gene expression of the apoplastic invertase LIN6 in tomato (*Lycopersicon esculentum*) roots. *J. Exp. Bot.* 57, 4015–4023. doi: 10.1093/jxb/erl172

Schenck, N. C., and Smith, G. S. (1982). Additional new and unreported species of mycorrhizal fungi (Endogonaceae) from Florida. *Mycologia* 74, 77–92. doi: 10.2307/3792631

Shachar-Hill, Y., Pfeffer, P. E., Douds, D., Osman, S. F., Doner, L. W., and Ratcliffe, R. G. (1995). Partitioning of intermediary carbon metabolism in vesicular-arbuscular mycorrhizal leek. *Plant Physiol.* 108, 7–15.

Sievers, F., Wilm, A., Dineen, D., Gibson, T. J., Karplus, K., Li, W., et al. (2011). Fast, scalable generation of high-quality protein multiple sequence alignments using Clustal Omega. *Mol. Syst. Biol.* 7:539. doi: 10.1038/msb.2011.75

Smith, S. E., and Smith, F. A. (2011). Roles of arbuscular mycorrhizas in plant nutrition and growth: new paradigms from cellular to ecosystem scales. *Annu. Rev. Plant Biol.* 62, 227–250. doi: 10.1146/annurev-arplant-042110-103846

Smith, S. E., and Smith, F. A. (2012). Fresh perspectives on the roles of arbuscular mycorrhizal fungi in plant nutrition and growth. *Mycologia* 104, 1–13. doi: 10.3852/11-229

Solaiman, M. D. Z., and Saito, M. (1997). Use of sugars by intraradical hyphae of arbuscular mycorrhizal fungi revealed by radiorespirometry. *New Phytol.* 136, 533–538. doi: 10.1046/j.1469-8137.1997.00757.x

Streubel, J., Pesce, C., Hutin, M., Koebnik, R., Boch, J., and Szurek, B. (2013). Five phylogenetically close rice SWEET genes confer TAL effector-mediated susceptibility to *Xanthomonas oryzae* pv. *oryzae*. *New Phytol.* 200, 808–819. doi: 10.1111/nph.12411

Tamura, K., Stecher, G., Peterson, D., Filipski, A., and Kumar, S. (2013). MEGA6: Molecular Evolutionary Genetics Analysis version 6.0. *Mol. Biol. Evol.* 30, 2725–2729. doi: 10.1093/molbev/mst197

Tang, N., San Clemente, H., Roy, S., Bécard, G., Zhao, B., and Roux, C. (2016). A survey of the gene repertoire of Gigaspora rosea unravels conserved features among Glomeromycota for obligate biotrophy. *Front. Microbiol.* 7:233. doi: 10.3389/fmicb.2016.00233

Tao, Y., Cheung, L. S., Li, S., Eom, J. S., Chen, L. Q., Xu, Y., et al. (2015). Structure of a eukaryotic SWEET transporter in a homotrimeric complex. *Nature* 527, 259–263. doi: 10.1038/nature15391

Tisserant, E., Malbreil, M., Kuo, A., Kohler, A., Symeonidi, A., Balestrini, R., et al. (2013). Genome of an arbuscular mycorrhizal fungus provides insight into the oldest plant symbiosis. *Proc. Natl Acad. Sci. U.S.A.* 110, 20117–20122. doi: 10.1073/pnas.1313452110

Wang, J., Yan, C., Li, Y., Hirata, K., Yamamoto, M., Yan, N., et al. (2014). Crystal structure of a bacterial homologue of SWEET transporters. *Cell Res.* 24, 1486. doi: 10.1038/cr.2014.144

Wei, X., Liu, F., Chen, C., Ma, F., and Li, M. (2014). The Malus domestica sugar transporter gene family: identifications based on genome and expression profiling related to the accumulation of fruit sugars. *Front. Plant Sci.* 5:569. doi: 10.3389/fpls.2014.00569

Wewer, V., Brands, M., and Dörmann, P. (2014). Fatty acid synthesis and lipid metabolism in the obligate biotrophic fungus *Rhizophagus irregularis* during mycorrhization of *Lotus japonicus*. *Plant J.* 79, 398–412. doi: 10.1111/tpj.12566

Wright, D. P., Read, D. J., and Scholes, J. D. (1998). Mycorrhizal sink strength influences whole plant carbon balance of *Trifolium repens* L. *Plant Cell Environ.* 21, 881–891. doi: 10.1046/j.1365-3040.1998.00351.x

Xu, Y., Tao, Y., Cheung, L. S., Fan, C., Chen, L. Q., Xu, S., et al. (2014). Structures of bacterial homologues of SWEET transporters in two distinct conformations. *Nature* 515, 448–452. doi: 10.1038/nature13670

Xu, X., Pan, S., Cheng, S., Zhang, B., Mu, D., Ni, P. (The Potato Genome Sequencing Consortium) (2011). Genome sequence and analysis of the tuber crop potato. *Nature* 475, 189-195. doi: 10.1038/nature10158

Xuan, Y. H., Hu, Y. B., Chen, L. Q., Sosso, D., Ducat, D. C., Hou, B. H., et al. (2013). Functional role of oligomerization for bacterial and plant SWEET sugar transporter family. *Proc. Natl Acad. Sci. U.S.A.* 110, E3685–E3694. doi: 10.1073/pnas.1311244110

Yang, B., Sugio, A., and White, F. F. (2006). Os8N3 is a host disease-susceptibility gene for bacterial blight of rice. *Proc. Natl Acad. Sci. U.S.A.* 103, 10503–10508. doi: 10.1073/pnas.0604088103

Yu, X., Wang, X., Wang, C., Chen, X., Qu, Z., Yu, X., et al. (2010). Wheat defense genes in fungal (*Puccinia striiformis*) infection. *Funct. Integr. Genomics* 10, 227–239. doi: 10.1007/s10142-010-0161-8

Zhang, X., Pumplin, N., Ivanov, S., and Harrison, M. J. (2015). EXO70I is required for development of a sub-domain of the periarbuscular membrane during arbuscular mycorrhizal symbiosis. *Curr. Biol.* 25, 2189–2195. doi: 10.1016/j.cub.2015.06.075

Conflict of Interest Statement: The authors declare that the research was conducted in the absence of any commercial or financial relationships that could be construed as a potential conflict of interest.

frontiers in Plant Science

ORIGINAL RESEARCH
published: 17 September 2015
doi: 10.3389/fpls.2015.00667

Colonization of root cells and plant growth promotion by *Piriformospora indica* occurs independently of plant common symbiosis genes

Aline Banhara[1], *Yi Ding*[2†], *Regina Kühner*[1], *Alga Zuccaro*[2,3] *and Martin Parniske*[1*]

[1] Faculty of Biology, Institute of Genetics, University of Munich, Martinsried, Germany, [2] Department of Organismic Interactions, Max Planck Institute for Terrestrial Microbiology, Marburg, Germany, [3] Cluster of Excellence on Plant Sciences, Botanical Institute, University of Cologne, Cologne, Germany

OPEN ACCESS

Edited by:
Ralph Panstruga,
RWTH Aachen University, Germany

Reviewed by:
Andrea Genre,
University of Turin, Italy
Patrick Schäfer,
University of Warwick, UK
Sébastien Duplessis,
Institut National de la Recherche Agronomique, France

***Correspondence:**
Martin Parniske,
Genetics, Faculty of Biology, University of Munich (LMU), Großhaderner Strasse 4, 82152 Martinsried, Germany
parniske@lmu.de

†Present Address:
Yi Ding,
Boyce Thompson Institute for Plant Research, Ithaca, NY, USA

Specialty section:
This article was submitted to Plant Biotic Interactions, a section of the journal Frontiers in Plant Science

Received: 13 January 2015
Accepted: 13 August 2015
Published: 17 September 2015

Citation:
Banhara A, Ding Y, Kühner R, Zuccaro A and Parniske M (2015) Colonization of root cells and plant growth promotion by Piriformospora indica occurs independently of plant common symbiosis genes. Front. Plant Sci. 6:667. doi: 10.3389/fpls.2015.00667

Arbuscular mycorrhiza (AM) fungi (Glomeromycota) form symbiosis with and deliver nutrients via the roots of most angiosperms. AM fungal hyphae are taken up by living root epidermal cells, a program which relies on a set of plant common symbiosis genes (CSGs). Plant root epidermal cells are also infected by the plant growth-promoting fungus *Piriformospora indica* (Basidiomycota), raising the question whether this interaction relies on the AM-related CSGs. Here we show that intracellular colonization of root cells and intracellular sporulation by *P. indica* occurred in CSG mutants of the legume *Lotus japonicus* and in *Arabidopsis thaliana*, which belongs to the Brassicaceae, a family that has lost the ability to form AM as well as a core set of CSGs. *A. thaliana* mutants of homologs of CSGs (HCSGs) interacted with *P. indica* similar to the wild-type. Moreover, increased biomass of *A. thaliana* evoked by *P. indica* was unaltered in HCSG mutants. We conclude that colonization and growth promotion by *P. indica* are independent of the CSGs and that AM fungi and *P. indica* exploit different host pathways for infection.

Keywords: ***Piriformospora indica*, *Lotus japonicus*, *Arabidopsis thaliana*, biotrophy, common symbiosis genes, intracellular colonization, growth promotion**

Introduction

Plants form mutualistic interactions with fungi from different taxonomic groups. Arbuscular mycorrhiza (AM) is a widespread symbiosis between plants and fungi of the phylum Glomeromycota (Parniske, 2008; Smith and Read, 2008) and is considered a key factor that allowed plants to colonize land more than 400 million years ago (Schüßler and Walker, 2011). The ancestral nature of this interaction raises the question to what extent other and potentially younger interactions between plant roots and fungi evolved by co-opting the genetic framework for AM formation. Candidates for such interactions include endomycorrhizal interactions formed with fungi of the order Sebacinales of the phylum Basidiomycota (Selosse et al., 2009).

An experimental model for this group of fungi is *Piriformospora indica*, which infects various taxonomically unrelated hosts and can increase plant growth and biomass (Peškan-Berghöfer et al., 2004; Waller et al., 2005; Shahollari et al., 2007; Sherameti et al., 2008; Camehl et al., 2010, 2011; Hilbert et al., 2012; Nongbri et al., 2012; Lahrmann et al., 2013; Venus and Oelmüller, 2013).

Phythormones like ethylene, jasmonic acid and gibberellins seem to positively influence root colonization by *P. indica*, while salicylic acid has an inhibitory effect

(Jacobs et al., 2011; Khatabi et al., 2012). Genes involved in the synthesis of indole-3-acetaldoxime-derived compounds restrict the growth of *P. indica* within *Arabidopsis thaliana* roots (Nongbri et al., 2012). Indole-3-acetaldoxime is also an intermediate in the biosynthesis of the phytohormone indole-3-acetic acid (IAA) (Mikkelsen et al., 2009; Burow et al., 2010), which has been implicated in the *P. indica*-induced host growth promotion, together with cytokinin (Vadassery et al., 2008).

In the initial stages of plant root colonization, *P. indica* invades living plant cells (Jacobs et al., 2011; Zuccaro et al., 2011; Lahrmann and Zuccaro, 2012; Lahrmann et al., 2013). This initial stage is followed by the death of colonized cells even though the plant host displays no macroscopic signs of disease (Deshmukh et al., 2006; Jacobs et al., 2011; Zuccaro et al., 2011; Lahrmann and Zuccaro, 2012; Qiang et al., 2012). In *A. thaliana* roots, *P. indica* continuously infects cells *de novo* and colonized living cells are found beside dying and dead colonized cells 3 days after infection (Qiang et al., 2012).

During the early stage of the interaction, a plant-derived membrane has been observed which surrounds and separates *P. indica* hyphae from the plant cytoplasm (Jacobs et al., 2011; Lahrmann and Zuccaro, 2012; Lahrmann et al., 2013). The structural arrangement of this interaction is similar to that of transcellular and arbuscular hyphae of AM fungi, which are equally surrounded by a peri-fungal membrane (Bonfante and Genre, 2010).

We explored whether these structural similarities are reflected by a shared genetic basis between both symbioses. The successful invasion of the outer cell layers by AM fungi requires an ancestral plant genetic program that is conserved among angiosperms and encompasses the common symbiosis genes (CSGs). In legumes, the CSGs are required for both AM and the root nodule symbiosis with nitrogen-fixing bacteria (Kistner et al., 2005; Gutjahr, 2014; Svistoonoff et al., 2014), and encode the symbiosis receptor-like kinase SYMRK (Antolín-Llovera et al., 2014; Ried et al., 2014), the nucleoporins of the NUP107–160/NUP84 subcomplex (Alber et al., 2007) NUP85, NUP133, and the SEC13 HOMOLOG1 (SEH1) NENA (Kanamori et al., 2006; Saito et al., 2007; Groth et al., 2010), CASTOR and POLLUX, cation channels localized at the nuclear envelope (Charpentier et al., 2008; Venkateshwaran et al., 2012), as well as the nucleoplasmatic complex formed by a calcium and calmodulin-dependent protein kinase (CCaMK) and CYCLOPS responsible for calcium signal decoding (Singh and Parniske, 2012; Singh et al., 2014). The signal transduction pathway involving the products of the CSGs leads from the perception of microbial signals at the plasma membrane to the transcriptional activation of genes in the nucleus (Gutjahr and Parniske, 2013). In the legume *Lotus japonicus* CSG mutants are all impaired in the intracellular accommodation of both rhizobia and AM fungi (Kistner et al., 2005).

A. thaliana is a member of the Brassicaceae, a family which lost the ability to establish AM symbiosis (Delaux et al., 2014). This loss is correlated with the absence of a specific set of CSGs, including *CCaMK* and *CYCLOPS* (Delaux et al., 2014). Despite this loss, *A. thaliana* retained homologs of common symbiosis genes (HCSGs). Based on phylogenetic and/or synteny analyses, orthologs or candidate orthologs of legume CSGs in *A. thaliana* have been identified for *POLLUX* (Ané et al., 2004; Delaux et al., 2013) and genes coding for members of the NUP107–160 subcomplex, including *NUP133* and *SEC13* (Wiermer et al., 2012; Binder and Parniske, 2013). Importantly, an *AtPOLLUX* version was able to restore nodulation in the non-nodulating mutant *dmi1–4* of *M. truncatula* (Venkateshwaran et al., 2012), indicating relative conservation of its symbiotic activity in *A. thaliana*. *SYMRK* encodes a malectin-like domain leucine-rich repeat receptor-like kinase, a gene family that has expanded to 50 members in *A. thaliana* (Hok et al., 2011). However, based on synteny analysis (Kevei et al., 2005) and the lack of SYMRK-specific amino-acid sequence patterns in the kinase domain (Markmann et al., 2008), a SYMRK ortholog appears to be absent from the *A. thaliana* genome. ShRK1 (SYMRK-homologous Receptor-like Kinase 1) and ShRK2 are the closest SYMRK homologs in *A. thaliana*. The domain organization of ShRK1 and 2 is identical to that of *L. japonicus* SYMRK (Markmann et al., 2008).

To explore the role of *L. japonicus* CSGs and *A. thaliana* HCSGs in the interaction with *P. indica*, we investigated whether the fungus was able to penetrate root cells, complete its life cycle and promote host plant growth in the respective mutant backgrounds.

Materials and Methods

Fungal Strains and Growth Conditions

P. indica (Verma et al., 1998, DSM11827, Leibniz Institute DSMZ—German Collection of Microorganisms and Cell Cultures, Braunschweig, Germany) and *Piriformospora williamsii* (Basiewicz et al., 2012) were grown at 28°C in the dark on plates with solid (1.5% agar) complete medium (CM) (Pham et al., 2004). For studies with plants grown in soil, fungal mycelium was propagated in liquid CM medium, in the dark, at RT and 120 rpm shaking. Mycelium was washed three times with sterile distilled water directly prior to mixing with soil substrate.

For experiments on plates, fungal chlamydospores were obtained from 4 to 6-week-old cultures, as follows: Tween water (0.002% Tween 20) was added to plates containing mycelium, which was rubbed off from the agar surface, and the resulting spore suspension was collected and centrifuged three times at 3000 *g* for washing. Chlamydospore concentration was estimated using a Fuchs–Rosenthal counting chamber and adjusted to the desired 5×10^5 ml^{-1} with Tween water.

Plant Genotypes and Growth Conditions

For co-cultivation with *P. indica, L. japonicus* seeds (Supplementary Table 1) were surface sterilized in a 2% sodium hypochlorite solution for 7 min, washed three times with sterile water for 5 min each, and imbibed in water overnight. Seeds were then put on plates with solid modified Hoagland's medium [HO, 5 mM KNO_3; 5 mM $Ca(NO_3)_2$; 2 mM $MgSO_4$; 4 mM KH_2PO_4; 0.03 g l^{-1} Sprint 138 iron chelate; 0.1% micronutrients solution containing 2.86 g l^{-1} H_3BO_3; 1.81 g l^{-1} $MnCl_2.4H_2O$; 0.08 g l^{-1} $CuSO_4.5H_2O$; 0.02 g l^{-1} 85% $MoO_3.H_2O$; based on Hoagland and Arnon (1950)] and kept for 4 days at 24°C in the dark for germination.

A. thaliana seeds were obtained from "The Nottingham *A. thaliana* Stock Centre"—NASC (Scholl et al., 2000)

(Supplementary Table 2). For co-cultivation with *P. indica* or *P. williamsii* and tests for plant growth promotion, *A. thaliana* seeds were sterilized by incubation for 5 min in 70% ethanol, 0.05% Tween 20 followed by 2 min in 100% ethanol, left to dry and stratified for 48 h at 4°C in the dark. Plants were then grown under long day conditions (16 h:8 h, light:dark, at 23°C, 85 μmol.m^{-2} s^{-1}), on half-strength (½) Murashige and Skoog medium (MS, Murashige and Skoog, 1962) with or without sucrose (0.05%) or on modified HO solidified with gelrite 4 g l^{-1}, and four times more phosphate than in the original recipe.

Seven to ten-day-old *A. thaliana* or four-day-old *L. japonicus* plants were mock-inoculated with 1 ml Tween water (control) or either *P. indica* or *P. williamsii* chlamydospore suspensions. Non-germinated seeds and retarded seedlings were removed from the plates before inoculation. Co-cultures or mock-inoculated plants were grown at 24°C under long day conditions (16 h:8 h, light:dark). Biomass of seedlings was determined using a digital microbalance 7 days post inoculation (dpi).

For analysis of growth promotion under different nutrient regimes, plants were grown on the following media: modified HO with no KNO_3 or $Ca(NO_3)_2$, supplemented with 0.05 mM KNO_3, 0.5 mM KNO_3, or 5 mM KNO_3 (standard concentration), modified HO depleted of phosphate or with 4 mM KH_2PO_4(standard concentration); and modified HO depleted of ammonium or with 10 or 20 mM NH_4Cl. Where necessary, potassium and calcium concentrations were compensated with KCl and $CaCl_2$, respectively.

For growth promotion experiments in soil, plants were grown on either low-nutrient soil (50–100 mg l^{-1} N, 50–100 mg l^{-1} P, 100–150 mg l^{-1} K) or high-nutrient soil (500 mg l^{-1} N, 500 mg l^{-1} P, 500 mg l^{-1} K) mixed with 1 g fresh or autoclaved mycelium per 100 g sterile substrate for inoculation and mock-inoculation, respectively. Plant height was determined 7, 11, 16, and 21 dpi.

Sequence Alignments

Complete protein sequences were obtained from The Arabidopsis Information Resource (TAIR—www.arabidopsis.org) for *A. thaliana*, and from the GenBank for *L. japonicus*. Alignments (Supplementary Figures 7–9) were performed with MAFFT 6.822 (Katoh et al., 2002) or ClustalW2 (Larkin et al., 2007; Goujon et al., 2010) with the default settings. Searches for conserved domains in the protein sequences were performed using ScanProsite (de Castro et al., 2006) and/or InterProScan (Jones et al., 2014), and based on data available from Kanamori et al. (2006), Markmann et al. (2008), and Groth et al. (2010).

Determination of Fungal Colonization by Microscopy

To observe *P. indica* intracellular sporulation in *A. thaliana* and *L. japonicus* roots, colonized roots at 14 dpi were incubated at 96°C for 1 (*A. thaliana*) or 10 min (*L. japonicus*) in 10% (w/v) KOH and double-stained in the dark at room temperature for 20 min with 10 μg ml^{-1} WGA-AF488 (Wheat Germ Agglutinin-Alexa Fluor 488) (Molecular Probes, Karlsruhe, Germany) to visualize fungal structures, and 10 μg ml^{-1} propidium iodide (PI) to visualize plant cell walls. Samples were analyzed with a Leica DMI6000B microscope using differential interference contrast or epifluorescence (GFP filter set for WGA-AF488: excitation 450–490 nm, emission 500–550 nm; TX2 filter settings for PI: 540–580 nm excitation, 608–683 nm emission).

Root colonization and plant cell viability were analyzed by confocal laser scanning microscopy (CLSM). Fungal cell walls within colonized roots at 4 (*A. thaliana*), and 3 dpi (*L. japonicus*) were affinity-labeled for 10 min with 10 μg ml^{-1} WGA-AF488 (Molecular Probes, Karlsruhe, Germany). Membranes were stained with 3 μM FM4-64 (Molecular Probes, Karlsruhe, Germany) for 4 min (at 260 mm Hg). Root samples were imaged with TCS-SP5 or TCS-SP8 confocal microscopes (Leica, Bensheim, Germany) with excitation at 488 nm for WGA-AF488 and detection at 500–540 nm. FM4-64 was excited at 633 nm and detected at 650–690 nm. Propidium iodide was excited at 540 nm and detected at 600–630 nm.

Quantification of Fungal Colonization by qPCR

Roots of *A. thaliana* and *L. japonicus* colonized with *P. indica* (14 dpi) were thoroughly washed to remove fungal hyphae from the root surface. Two hundred micrograms of root material were then used for DNA extraction according to the protocol of Doyle and Doyle (1987). Real-time qPCR analyses were performed from 10 ng DNA mixed with the appropriate primers: *P. indica Transcription Elongation Factor* (Butehorn et al., 2000); *A. thaliana Ubiquitin* (Khatabi et al., 2012); or *L. japonicus Ubiquitin* (Takeda et al., 2009) in 10 μl SYBRgreen Supermix (BIORAD) using the following amplification protocol: 2′–95°C; 40 × (30″–95°C; 30″–59°C; 30″–72°C); melting curve 95°C–60°C–95°C. Fungal colonisation was quantified by the $2^{-\Delta Ct}$ method (Livak and Schmittgen, 2001) by subtracting the raw threshold cycle (Ct) values of *P. indica* TEF from those of plant UBI to obtain ΔCt.

β-Glucuronidase (GUS) Staining Assays

GUS staining assays were performed with the *L. japonicus* symbiosis-reporter line T90 (Webb et al., 2000). Colonized roots at 3, 7, and 14 dpi with *P. indica* chlamydospores or Tween water were vacuum infiltrated with X-Gluc staining solution (100 mM sodium phosphate buffer pH 7.0; 10 mM EDTA; 0.1% Triton-X 100; 0.5 mg ml^{-1} X-Gluc; 1 mM $K_3[Fe(CN)_6]$; 1 mM $K_4[Fe(CN)_6].3H_2O$) three times for 10 min, followed by incubation at 37°C for 18 h in the dark. Root systems were inspected for GUS staining with a Leica MZFLIII stereomicroscope.

The *Mesorhizobium loti* MAFF303099 strain constitutively expressing *Ds*RED (Maekawa et al., 2009) was used to inoculate roots of the *L. japonicus* T90 line as a suspension in Fahraeus medium (Fahraeus, 1957) adjusted to an OD_{600} of 0.05.

Statistical Analyses

Statistical analyses were performed with R version 3.0.2 (2013-09-25) "Frisbee Sailing" (R Core Team, 2013) using the package "agricolae" (De Mendiburu, 2010). Pairwise or multiple comparisons of the different subsets of data were performed with the Kruskal–Wallis test followed by a Bonferroni–Holm correction using the mock-inoculated samples as control group. Two-sided, unpaired *t*-tests with equal variance were used to analyze relative amount of fungal DNA within plant roots.

Results and Discussion

Intracellular Infection and Sporulation by *P. indica* Occurs Independently of *L. japonicus* and *A. thaliana* Common Symbiosis Genes

We investigated whether the classical CSGs are involved in the interaction between roots of the legume *L. japonicus* and *P. indica*. In root epidermal cells of *L. japonicus* wild-type (ecotype "Gifu"), and in CSG mutants intracellular hyphae were detected at 7 dpi (**Figure 1**) and sporulation at 14 dpi (Supplementary Figure 1), evidencing that *P. indica* entered host cells and successfully completed its life cycle in all genotypes tested. These observations indicate that the CSGs are not required for the successful infection of host cells by *P. indica*.

The *L. japonicus* symbiosis-reporter line T90 carries a promoter:*GUS* fusion and is activated in response to

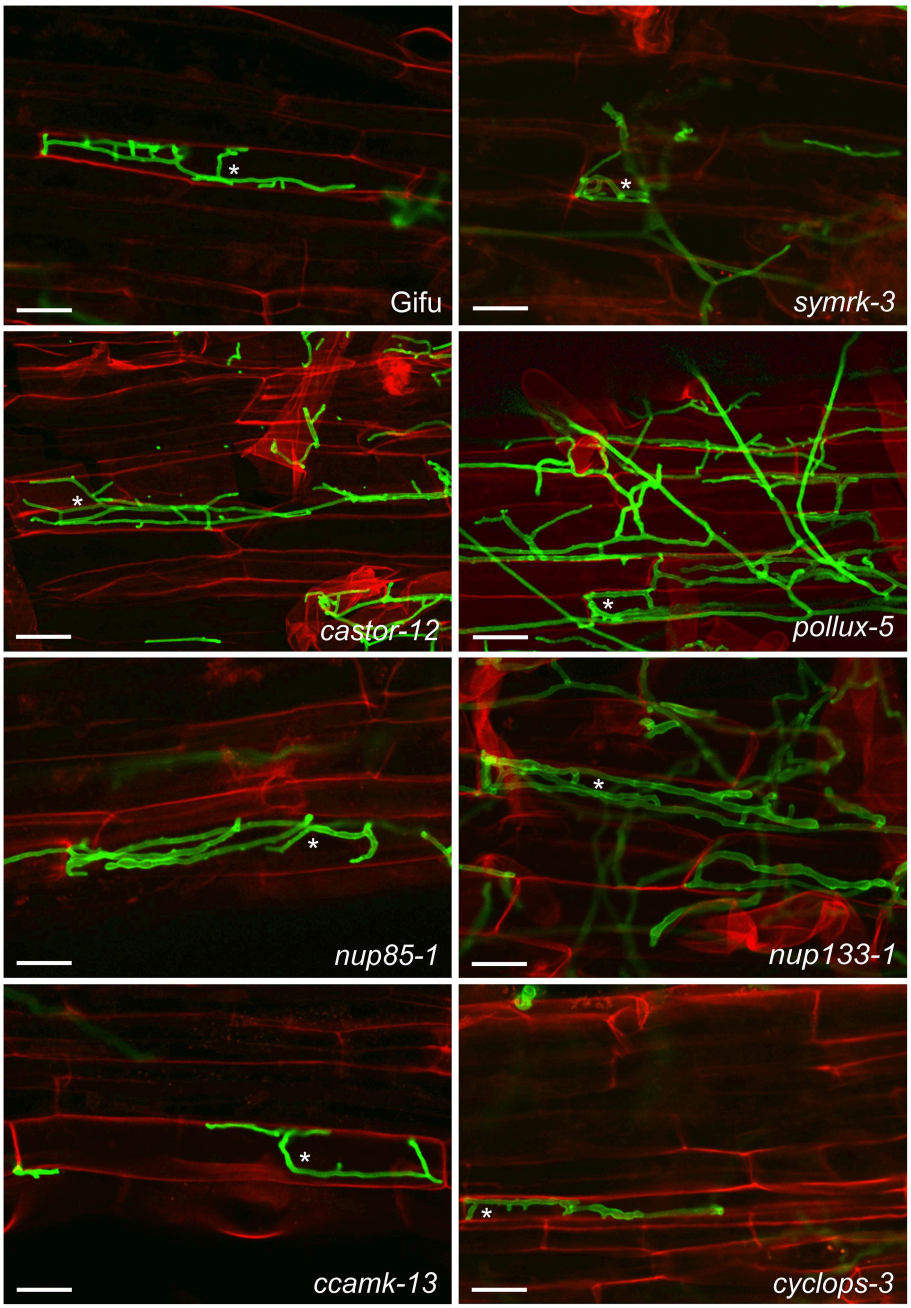

FIGURE 1 | Colonization of *L. japonicus* root cells by *P. indica*. Wild-type (Gifu) and the indicated common symbiosis mutants were analyzed 7 dpi with *P. indica* chlamydospores. Intracellular hyphae were present in all genotypes (examples are indicated by asterisks). Roots were cleared and double stained with propidium iodide (red), for cell wall visualization, and WGA-AF488 (green), for fungal structures. Scale bar: 25 μm.

Mesorhizobium loti or nodulation factors, and AM fungi (Webb et al., 2000; Radutoiu et al., 2003; Kistner et al., 2005). T90 reporter activation requires *L. japonicus* CSGs (Kistner et al., 2005; Gossmann et al., 2012) and dominant active alleles of *SYMRK* and *CCaMK* are sufficient for T90 induction (Ried et al., 2014 and unpublished data). However, we did not detect GUS activity (blue staining) in *P. indica* or mock-inoculated roots, while blue staining was observed in *M. loti Ds*Red inoculated roots (Supplementary Figure 2). These data indicate that the promoter:GUS fusion of the T90 line and the signal transduction pathway upstream are not activated during the interaction of *L. japonicus* with *P. indica*.

Moreover, we observed that *A. thaliana* wild-type (Col-0), which lacks some of the key CSGs (Delaux et al., 2014), supported intracellular root colonization and sporulation by *P. indica* (**Figure 2** and Supplementary Figure 3). In addition, intracellular infection and sporulation also occurred in the roots of the *A. thaliana* HCSG mutants *pollux*, *nup133*, *sec13*, and the double mutants *sec13* × *nup133* and *shrk1* × *shrk2* (**Figure 2** and Supplementary Figure 3), indicating that the fungus could successfully infect these mutants and complete its life cycle. These observations strongly support the conclusion that neither the CSGs which *A. thaliana* lost during its evolution nor the experimentally mutated HCSGs are required for the interaction with *P. indica*.

Growth of *P. indica* within *L. japonicus* and *A. thaliana* Root Cells

Fungal structures were detectable within the boundaries of root epidermal cells in both *L. japonicus* (**Figure 1** and Supplementary Figure 1) and *A. thaliana* (Supplementary Figure 3). We investigated whether these hyphae would penetrate into living plant cells. To determine the vitality status of the root cells, we used the lipophilic stain FM4-64 in combination with time-lapse imaging. After FM4-64 staining, *P. indica* hyphae were observed within cells containing mobile structures including possible vesicles in *A. thaliana* (**Figure 2**). In this host, we could detect three states of colonized root cells that differed in the mobility or presence of intracellular content. In the first state, vesicle-like structures moved at a speed similar to that observed within neighboring non-infected cells (Supplementary Movie 1) or cells of non-colonized roots (Supplementary Movie 3). In exceptional cases, some of these cells contained small, intact vacuoles. In the second state, the FM4-64-stained material showed very little or no movement (Supplementary Movie 2), and occasionally collapsed vacuoles were observed. We also observed invaded cells with no cytoplasmic content, probably representing a third state of cellular infection, during which the fungus grows within likely dead cells (Supplementary Figure 4, Supplementary Movie 2). This observation supports a three-stage model of cellular infection, in which *P. indica* first colonizes individual roots cells that show vesicular movement. In stage 2, vesicular movement has undergone at least partial arrest. In stage 3 the cellular content has disappeared, possibly through autophagocytosis or consumption by the fungus (Supplementary Figure 4). Immobilized, irregular fluorescent structures are also present within probably dying cells of non-colonized roots (Supplementary Movie 3, white arrowhead). Such dying cells have been attributed to a developmental program implicated in developmental events such as the removal of root cap cells (Fendrych et al., 2014).

Movement of FM4-64-labeled material in *P. indica*-infected cells could also be documented in the *A. thaliana* HSCG mutant *pollux* (Supplementary Movie 4), and the double mutants *sec13* × *nup133* and *shrk1* × *shrk2*, indicating that similar stages of cell activity occur independently of HCSGs. Because of the technically demanding process of obtaining such movies, a quantitative comparison of colonization stages between the wild-type and the HCSG mutants was not performed.

Increased Relative Fungal Biomass within Roots of *L. japonicus* Common Symbiosis Mutants

In order to quantify the relative fungal biomass within host roots, we determined the ratio between fungal DNA and plant DNA. Interestingly, in *L. japonicus*, we detected a tendency for an increased relative amount of fungal DNA in most of the tested common symbiosis mutants, with a significant difference to the wild-type in *nup85-1*, *ccamk-13*, and *cyclops-3* (**Figure 3**). This higher ratio of fungal to plant DNA may be the result of increased fungal proliferation, reduced root growth, and/or plant cell death in the mutants. Curiously, this effect was only observed on *L. japonicus* but not on *A. thaliana* mutants (**Figure 3**). Our results reveal that CSG-mediated pathways affect the relative *P. indica* colonization level in *L. japonicus*, and that this regulation is not operational in *A. thaliana*. Interestingly, CSGs potentially have a cell protecting effect (Esseling et al., 2004; Genre et al., 2009; Evangelisti et al., 2014). Apart from its signaling role in symbiosis (Antolín-Llovera et al., 2014; Ried et al., 2014), *SYMRK* has been implicated in desensitization of root hair cells against mechanic stress (Esseling et al., 2004), and *CCaMK* increased tolerance against the cell killing effect of *Colletotrichum* (Genre et al., 2009). In a *ccamk* mutant of *M. truncatula* infected by the hemi-biotrophic fungal pathogen *Colletotrichum trifolii,* the switch from biotrophy to necrotrophy occurred earlier (Genre et al., 2009).

In barley, a dense colonization by *P. indica* is associated with root cell death (Deshmukh et al., 2006; Camehl et al., 2010; Nongbri et al., 2012). There is evidence that excessive *P. indica* proliferation is associated with cell death and/or with detrimental effects on the growth of the plant host (Deshmukh et al., 2006; Camehl et al., 2010; Nongbri et al., 2012). It is therefore possible that *L. japonicus ccamk* mutants suffer from an earlier onset of the necrotrophic phase of *P. indica* colonization, and that CSGs contribute to the maintenance of plant cellular integrity after fungal invasion. On the other hand, the CSGs are critical for lipochitooligo-saccharide (LCO)-induced lateral root emergence (Oláh et al., 2005; Maillet et al., 2011). While it is unclear whether *P. indica* stimulates lateral root emergence and, if so, whether it does it via the common symbiosis pathway, the altered fungal to plant biomass ratio of the CSG mutants could be due to a reduction in host root proliferation.

Plant Growth Promotion by *P. indica* is influenced by Nutrient Availability

In order to obtain an experimental system for the genetic dissection of the *P. indica*-mediated growth promotion

(Peškan-Berghöfer et al., 2004; Shahollari et al., 2007; Sherameti et al., 2008; Camehl et al., 2010, 2011; Nongbri et al., 2012; Lahrmann et al., 2013; Venus and Oelmüller, 2013), we explored the influence of the substrate and nutrient availability. We evaluated the effect of *P. indica* on *L. japonicus* and *A. thaliana* grown in soil with two different nutrient concentrations. In both plant species, co-cultivation with *P. indica* in soil with high nutrient concentrations had little or no effect on the mean stem height. However, in soil with lower nutrient contents, *P. indica* inoculation roughly doubled the mean stem height of *A. thaliana* plants at 21 dpi, whereas there was only a small but significant effect on *L. japonicus* (**Figure 4**).

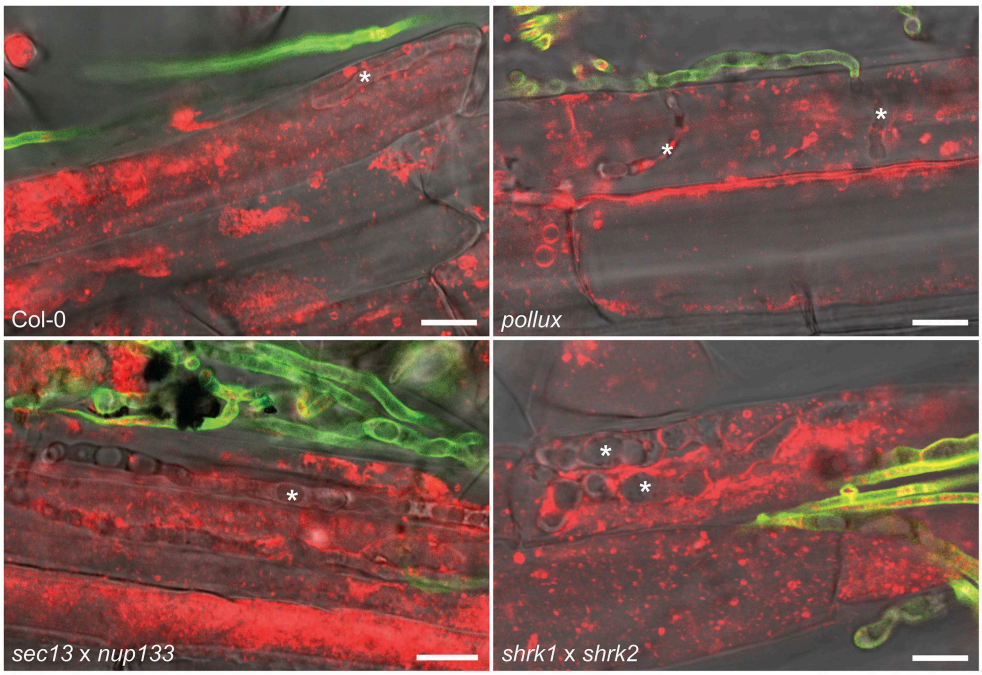

FIGURE 2 | Colonization of *A. thaliana* root cells by *P. indica*. Hyphae (indicated by asterisks) were detected 4 dpi with *P. indica* chlamydospores within root cells of wild-type (Col-0) and the indicated HCSG mutants. Extracellular hyphae were stained with WGA-AF488 (green) but intracellular hyphae were not or weakly fluorescent, probably due to limited access of WGA-AF488 to the fungal cell wall within root cells. FM4-64-stained plant material (red) within invaded host cells is indicative of stage 1 or 2 of the infection process. Scale bar 10 μm.

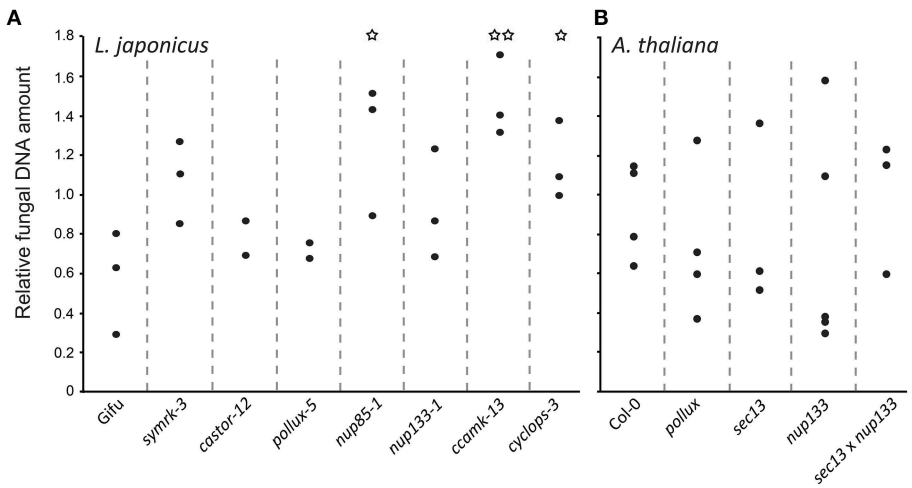

FIGURE 3 | Quantification of *P. indica* in *L. japonicus* (A) and *A. thaliana* (B) wild-type and mutant roots. Real-time qPCR was used to quantify DNA from surface-washed *P. indica*-colonized roots at 14 dpi grown on modified HO medium using primers for the fungal gene *Transcription Elongation Factor* (*TEF*) and for *A. thaliana* and *L. japonicus Ubiquitin* (*UBI*) genes. Differences between the wild-type and mutants were investigated with a two-sided, unpaired *t*-test. $^{*}P < 0.05$, $^{**}P < 0.01$.

When *A. thaliana* plants were grown on agar plates with ½MS medium and no sugar, and inoculated with chlamydospores of *P. indica*, a growth promoting effect was observed. In contrast, when 0.05% sucrose was added to the medium, the plants were generally bigger and no increase was observed in the mean fresh weight of *P. indica*-inoculated plants compared to mock-treated plants (Supplementary Figure 5).

Since *A. thaliana* plants grown in the presence of *P. indica* exhibit increased uptake of nitrogen and phosphate (Shahollari et al., 2007; Kumar et al., 2011; Das et al., 2014), we investigated whether the concentration of nitrate [supplied as $Ca(NO_3)_2$ and/or KNO_3], phosphate (KH_2PO_4), or ammonium (NH_4Cl) on modified HO medium influenced the growth promotion of *A. thaliana* plants by *P. indica*. Co-cultivation with the fungus had a positive effect on the mean fresh weight of the plants under all nutrient conditions tested, except on a medium that limited plant growth due to the lack of a nitrogen source (Supplementary Figure 6). For the subsequent experiments, including those already reported in Lahrmann et al. (2013), we used modified HO medium, which consistently supported the growth-promoting effect by *P. indica*.

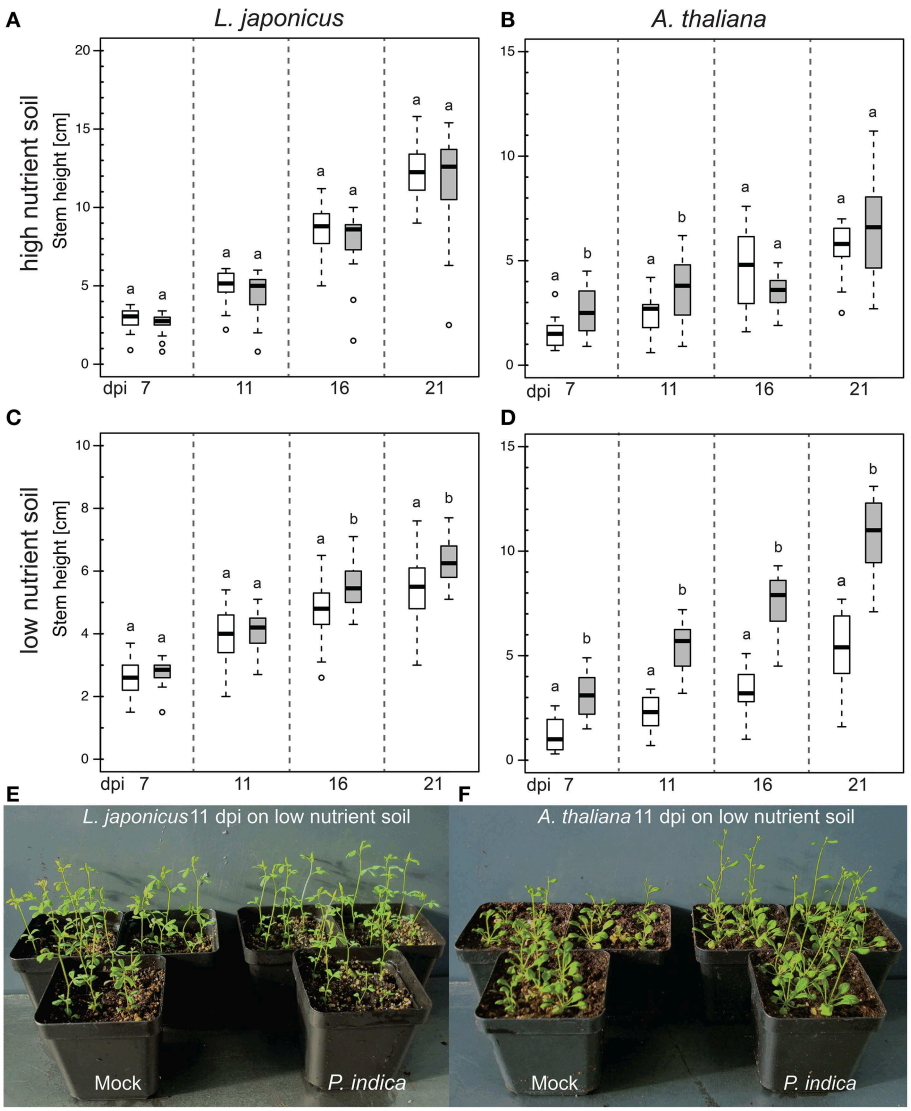

FIGURE 4 | Effect of *P. indica* on the stem height of *L. japonicus* and *A. thaliana* grown in high or low nutrient soil. Box-plots represent the stem height of ca. 20 plants per treatment at the indicated dpi. **(A,B)** In high-nutrient soil (500 mg l^{-1} N, 500 mg l^{-1} P, 500 mg l^{-1} K), inoculation with *P. indica* did not change plant stem height at 21 dpi ($p > 0.05$). **(C,D)** On low-nutrient soil (50–100 mg l^{-1} N, 50–100 mg l^{-1} P, 100–150 mg l^{-1} K), *P. indica* inoculation led to an increase in the mean stem height at 21 dpi ($p < 0.05$). Statistical analyses were performed with a Kruskal–Wallis test followed by a Bonferroni–Holm correction using the mock-inoculated plants as control group. For each mock/*P. indica*-inoculated pair, box-plots sharing the same letter do not significantly differ (at the 5% significance level). White boxes: mock; gray boxes: *P. indica*-inoculated; open circles: outliers. (**E,F**) Exemplary pictures of *P. indica*- and mock-inoculated plants grown in low nutrient soil. Experiments were performed three times with similar results.

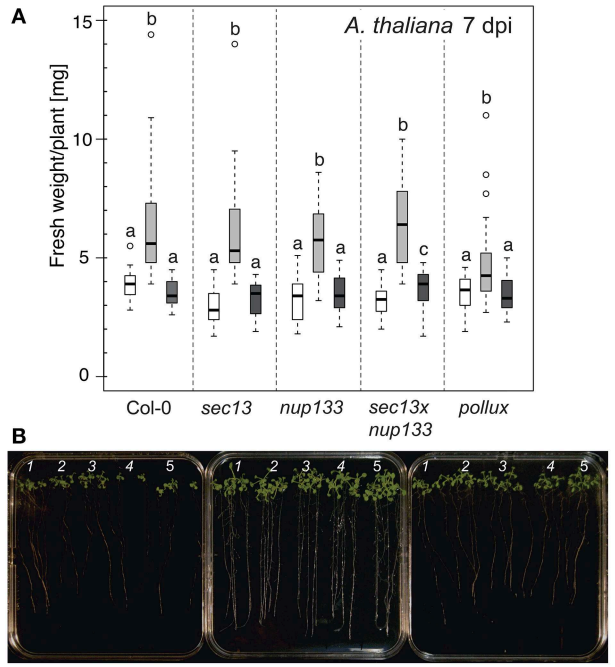

FIGURE 5 | Effect of *P. indica* or *P. williamsii* on the biomass of *A. thaliana*. (A) Box-plots show the fresh weight of the indicated *A. thaliana* genotypes (ca. 15 plants/genotype) grown in the presence or absence of *P. indica* or *P. williamsii*. All plant genotypes accumulated more biomass upon co-cultivation with *P. indica* but not with *P. williamsii*. White box: mock; light gray box: *P. indica*; dark gray box: *P. williamsii*. Open circles: outliers. Statistical analyses were performed using a Kruskal–Wallis test followed by a Bonferroni–Holm correction using the mock-inoculated samples as control group. Groups that do not share the same letter are significantly different (at the 5% significance level). Comparisons between the three treatments were made for each genotype separately. Plant biomass was determined 7 dpi. **(B)** Representative plates showing sets of 14-day-old plants grown on modified HO medium are shown 7 days after mock-treatment with Tween water (left) or inoculation with either *P. indica* (center) or *P. williamsii* (right) chlamydospores. 1: *pollux*; 2: *sec13* × *nup133*; 3: *nup133*; 4: *sec13*; 5: Col-0.

A. thaliana homologs of Common Symbiosis Genes are not required for *P. indica*-induced Growth Promotion

We investigated the influence of *A. thaliana* HCSGs on the host growth-promoting effect of *P. indica*. As a control, we included the closely related sebacinoid fungus *P. williamsii* (Basiewicz et al., 2012; Lahrmann et al., 2013), which did not induce or induced very little growth promotion of *A. thaliana* Col-0 (Lahrmann et al., 2013). Wild-type and mutant plants inoculated with *P. indica* had a significant higher mean fresh weight than control or *P. williamsii*-inoculated plants (**Figure 5**). Importantly, wild-type and mutant roots did not differ in their biomass upon *P. indica* inoculation. We conclude that the HCSGs *POLLUX*, *NUP133*, and *SEC13* are not required for the growth promotion of *A. thaliana* by *P. indica*, confirming previous observations with *atpollux* mutants (Shahollari et al., 2007).

Conclusions

Despite the similarities between colonization of plant roots by AM fungi and *P. indica*, our data indicate that CSGs which are essential for AM development (Gutjahr and Parniske, 2013) are not required for root colonization by *P. indica*. In the AM symbiosis, signal transduction for the initiation of the intracellular accommodation program is mediated by the products of CSGs (Takeda et al., 2012). Since *P. indica* intracellular colonization was observed in the absence of individual CSGs or existing homologs in *A. thaliana*, we conclude that alternative pathways must exist that support intracellular accommodation of *P. indica*. Conceptually this could be achieved through the manipulation of general programs such as polarized secretion, endocytosis, plant immunity, and/or phytohormone signaling (Schäfer et al., 2009; Dörmann et al., 2014; Evangelisti et al., 2014). Identification of such compatibility programs is of prime interest because they might offer entry ports not only for beneficial fungi like *P. indica* but also to hyphal pathogens with similar infection strategies. This is in agreement with the recent observation that CSG mutants of *M. truncatula* show unaltered infection and haustorial development by the phytopathogenic oomycete *Phytophthora palmivora* (Rey et al., 2014). However, little is known about plant factors that are directly involved in the intracellular accommodation of *P. indica*. Tubby-like proteins, implicated in vesicle trafficking in mammals (Mukhopadhyay and Jackson, 2011), are required for normal colonization of *A. thaliana* roots by *P. indica*, and have been pinpointed as possible compatibility factors during the early stages of plant–fungus interaction (Reitz et al., 2012, 2013).

Acknowledgments

We thank Andreas Binder for taking part in double blind experiments related to the plant growth responses. Part of this work was supported by a grant from the German Research Foundation (DFG) to MP (PA 493/8-3) in the frame of the Research unit FOR 964 "Calcium signaling via protein phosphorylation in plant model cell types during environmental stress adaption." AZ and YD acknowledge support from the Max-Planck-Gesellschaft and AZ acknowledges support from the Cluster of Excellence on Plant Science (CEPLAS, EXC 1028).

Supplementary Material

The Supplementary Material for this article can be found online at: http://journal.frontiersin.org/article/10.3389/fpls.2015.00667

References

Alber, F., Dokudovskaya, S., Veenhoff, L. M., Zhang, W., Kipper, J., Devos, D., et al. (2007). The molecular architecture of the nuclear pore complex. *Nature* 450, 695–701. doi: 10.1038/nature06405

Ané, J. M., Kiss, G. B., Riely, B. K., Penmetsa, R. V., Oldroyd, G. E., Ayax, C., et al. (2004). *Medicago truncatula* DMI1 required for bacterial and fungal symbioses in legumes. *Science* 303, 1364–1367. doi: 10.1126/science.1092986

Antolín-Llovera, M., Ried, M. K., and Parniske, M. (2014). Cleavage of the SYMBIOSIS RECEPTOR-LIKE KINASE ectodomain promotes complex formation with Nod factor receptor 5. *Curr. Biol.* 24, 422–427. doi: 10.1016/j.cub.2013.12.053

Basiewicz, M., Weiss, M., Kogel, K. H., Langen, G., Zorn, H., and Zuccaro, A. (2012). Molecular and phenotypic characterization of *Sebacina vermifera* strains associated with orchids, and the description of *Piriformospora williamsii* sp. nov. *Fungal Biol.* 116, 204–213. doi: 10.1016/j.funbio.2011.11.003

Binder, A., and Parniske, M. (2013). Analysis of the *Lotus japonicus* nuclear pore NUP107-160 subcomplex reveals pronounced structural plasticity and functional redundancy. *Front. Plant Sci.* 4:552. doi: 10.3389/fpls.2013.00552

Bonfante, P., and Genre, A. (2010). Mechanisms underlying beneficial plant-fungus interactions in mycorrhizal symbiosis. *Nat. Commun.* 1, 48. doi: 10.1038/ncomms1046

Burow, M., Halkier, B. A., and Kliebenstein, D. J. (2010). Regulatory networks of glucosinolates shape *Arabidopsis thaliana* fitness. *Curr. Opin. Plant Biol.* 13, 348–353. doi: 10.1016/j.pbi.2010.02.002

Butehorn, B., Rhody, D., and Franken, P. (2000). Isolation and characterisation of *Pitef1* encoding the translation elongation factor EF-1 alpha of the root endophyte *Piriformospora indica*. *Plant Biol.* 2, 687–692. doi: 10.1055/s-2000-16647

Camehl, I., Drzewiecki, C., Vadassery, J., Shahollari, B., Sherameti, I., Forzani, C., et al. (2011). The OXI1 kinase pathway mediates *Piriformospora indica*-induced growth promotion in Arabidopsis. *PLoS Pathog.* 7:e1002051. doi: 10.1371/journal.ppat.1002051

Camehl, I., Sherameti, I., Venus, Y., Bethke, G., Varma, A., Lee, J., et al. (2010). Ethylene signalling and ethylene-targeted transcription factors are required to balance beneficial and nonbeneficial traits in the symbiosis between the endophytic fungus *Piriformospora indica* and *Arabidopsis thaliana*. *New Phytol.* 185, 1062–1073. doi: 10.1111/j.1469-8137.2009.03149.x

Charpentier, M., Bredemeier, R., Wanner, G., Takeda, N., Schleiff, E., and Parniske, M. (2008). *Lotus japonicus* CASTOR and POLLUX are ion channels essential for perinuclear calcium spiking in legume root endosymbiosis. *Plant Cell* 20, 3467–3479. doi: 10.1105/tpc.108.063255

Das, J., Ramesh, K. V., Maithri, U., Mutangana, D., and Suresh, C. K. (2014). Response of aerobic rice to *Piriformospora indica*. *Indian J. Exp. Biol.* 52, 237–251.

de Castro, E., Sigrist, C. J., Gattiker, A., Bulliard, V., Langendijk-Genevaux, P. S., Gasteiger, E., et al. (2006). ScanProsite: detection of PROSITE signature matches and ProRule-associated functional and structural residues in proteins. *Nucleic Acids Res.* 34, W362–W365. doi: 10.1093/nar/gkl124

Delaux, P. M., Séjalon-Delmas, N., Bécard, G., and Ané, J. M. (2013). Evolution of the plant-microbe symbiotic 'toolkit'. *Trends Plant Sci.* 18, 298–304. doi: 10.1016/j.tplants.2013.01.008

Delaux, P. M., Varala, K., Edger, P. P., Coruzzi, G. M., Pires, J. C., and Ané, J. M. (2014). Comparative phylogenomics uncovers the impact of symbiotic associations on host genome evolution. *PLoS Genet.* 10:e1004487. doi: 10.1371/journal.pgen.1004487

De Mendiburu, F. (2010). *Agricolae*: *Statistical Procedures for Agricultural Research*. Thesis, National Engineering University (UNI), Lima-Peru.

Deshmukh, S., Hückelhoven, R., Schäfer, P., Imani, J., Sharma, M., Weiss, M., et al. (2006). The root endophytic fungus *Piriformospora indica* requires host cell death for proliferation during mutualistic symbiosis with barley. *Proc. Natl. Acad. Sci. U.S.A.* 103, 18450–18457. doi: 10.1073/pnas.0605697103

Dörmann, P., Kim, H., Ott, T., Schulze-Lefert, P., Trujillo, M., Wewer, V., et al. (2014). Cell-autonomous defense, re-organization and trafficking of membranes in plant-microbe interactions. *New Phytol.* 204, 815–822. doi: 10.1111/nph.12978

Doyle, J. J., and Doyle, J. L. (1987). A rapid DNA isolation procedure for small quantities of fresh leaf tissue. *Phytochem Bull.* 19, 11–15.

Esseling, J. J., Lhuissier, F. G., and Emons, A. M. (2004). A nonsymbiotic root hair tip growth phenotype in NORK-mutated legumes: implications for nodulation factor-induced signaling and formation of a multifaceted root hair pocket for bacteria. *Plant Cell* 16, 933–944. doi: 10.1105/tpc.019653

Evangelisti, E., Rey, T., and Schornack, S. (2014). Cross-interference of plant development and plant-microbe interactions. *Curr. Opin. Plant Biol.* 20C, 118–126. doi: 10.1016/j.pbi.2014.05.014

Fahraeus, G. (1957). The infection of clover root hairs by nodule bacteria studied by a simple glass slide technique. *J. Gen. Microbiol.* 16, 374–381. doi: 10.1099/00221287-16-2-374

Fendrych, M., van Hautegem, T., van Durme, M., Olvera-Carrillo, Y., Huysmans, M., Karimi, M., et al. (2014). Programmed cell death controlled by ANAC033/SOMBRERO determines root cap organ size in Arabidopsis. *Curr. Biol.* 24, 931–940. doi: 10.1016/j.cub.2014.03.025

Genre, A., Ortu, G., Bertoldo, C., Martino, E., and Bonfante, P. (2009). Biotic and abiotic stimulation of root epidermal cells reveals common and specific responses to arbuscular mycorrhizal fungi. *Plant Physiol.* 149, 1424–1434. doi: 10.1104/pp.108.132225

Gossmann, J. A., Markmann, K., Brachmann, A., Rose, L. E., and Parniske, M. (2012). Polymorphic infection and organogenesis patterns induced by a *Rhizobium leguminosarum* isolate from Lotus root nodules are determined by the host genotype. *New Phytol.* 196, 561–573. doi: 10.1111/j.1469-8137.2012.04281.x

Goujon, M., McWilliam, H., Li, W., Valentin, F., Squizzato, S., Paern, J., et al. (2010). A new bioinformatics analysis tools framework at EMBL-EBI. *Nucleic Acids Res.* 38, W695–W699. doi: 10.1093/nar/gkq313

Groth, M., Takeda, N., Perry, J., Uchida, H., Dräxl, S., Brachmann, A., et al. (2010). *NENA*, a *Lotus japonicus* homolog of *Sec13*, is required for rhizodermal infection by arbuscular mycorrhiza fungi and rhizobia but dispensable for cortical endosymbiotic development. *Plant Cell* 22, 2509–2526. doi: 10.1105/tpc.109.069807

Gutjahr, C. (2014). Phytohormone signaling in arbuscular mycorhiza development. *Curr. Opin. Plant Biol.* 20C, 26–34. doi: 10.1016/j.pbi.2014.04.003

Gutjahr, C., and Parniske, M. (2013). Cell and developmental biology of arbuscular mycorrhiza symbiosis. *Annu. Rev. Cell Dev. Biol.* 29, 593–617. doi: 10.1146/annurev-cellbio-101512-122413

Hilbert, M., Voll, L. M., Ding, Y., Hofmann, J., Sharma, M., and Zuccaro, A. (2012). Indole derivative production by the root endophyte *Piriformospora indica* is not required for growth promotion but for biotrophic colonization of barley roots. *New Phytol.* 196, 520–534. doi: 10.1111/j.1469-8137.2012.04275.x

Hoagland, D. R., and Arnon, D. I. (1950). *The Water-culture Method for Growing Plants without Soil*. Berkeley, CA: University of California.

Hok, S., Danchin, E. G., Allasia, V., Panabières, F., Attard, A., and Keller, H. (2011). An *Arabidopsis* (malectin-like) leucine-rich repeat receptor-like kinase contributes to downy mildew disease. *Plant Cell Environ.* 34, 1944–1957. doi: 10.1111/j.1365-3040.2011.02390.x

Jacobs, S., Zechmann, B., Molitor, A., Trujillo, M., Petutschnig, E., Lipka, V., et al. (2011). Broad-spectrum suppression of innate immunity is required for colonization of *Arabidopsis* roots by the fungus *Piriformospora indica*. *Plant Physiol.* 156, 726–740. doi: 10.1104/pp.111.176446

Jones, P., Binns, D., Chang, H. Y., Fraser, M., Li, W., McAnulla, C., et al. (2014). InterProScan 5: genome-scale protein function classification. *Bioinformatics* 30, 1236–1240. doi: 10.1093/bioinformatics/btu031

Kanamori, N., Madsen, L. H., Radutoiu, S., Frantescu, M., Quistgaard, E. M., Miwa, H., et al. (2006). A nucleoporin is required for induction of Ca^{2+} spiking in legume nodule development and essential for rhizobial and fungal symbiosis. *Proc. Natl. Acad. Sci. U.S.A.* 103, 359–364. doi: 10.1073/pnas.0508883103

Katoh, K., Misawa, K., Kuma, K., and Miyata, T. (2002). MAFFT: a novel method for rapid multiple sequence alignment based on fast Fourier transform. *Nucleic Acids Res.* 30, 3059–3066. doi: 10.1093/nar/gkf436

Kevei, Z., Seres, A., Kereszt, A., Kalò, P., Kiss, P., Tóth, G., et al. (2005). Significant microsynteny with new evolutionary highlights is detected between *Arabidopsis* and legume model plants despite the lack of macrosynteny. *Mol. Genet. Genomics* 274, 644–657. doi: 10.1007/s00438-005-0057-9

Khatabi, B., Molitor, A., Lindermayr, C., Pfiffi, S., Durner, J., von Wettstein, D., et al. (2012). Ethylene supports colonization of plant roots by the mutualistic fungus *Piriformospora indica*. *PLoS ONE* 7:e35502. doi: 10.1371/journal.pone.0035502

Kistner, C., Winzer, T., Pitzschke, A., Mulder, L., Sato, S., Kaneko, T., et al. (2005). Seven *Lotus japonicus* genes required for transcriptional reprogramming of the root during fungal and bacterial symbiosis. *Plant Cell* 17, 2217–2229. doi: 10.1105/tpc.105.032714

Kumar, M., Yadav, V., Kumar, H., Sharma, R., Singh, A., Tuteja, N., et al. (2011). *Piriformospora indica* enhances plant growth by transferring phosphate. *Plant Signal. Behav.* 6, 723–725. doi: 10.4161/psb.6.5.15106

Lahrmann, U., Ding, Y., Banhara, A., Rath, M., Hajirezaei, M. R., Döhlemann, S., et al. (2013). Host-related metabolic cues affect colonization strategies of a root endophyte. *Proc. Natl. Acad. Sci. U.S.A.* 110, 13965–13970. doi: 10.1073/pnas.1301653110

Lahrmann, U., and Zuccaro, A. (2012). *Opprimo ergo sum*–evasion and suppression in the root endophytic fungus *Piriformospora indica*. *Mol. Plant Microbe Interact.* 25, 727–737. doi: 10.1094/MPMI-11-11-0291

Larkin, M. A., Blackshields, G., Brown, N. P., Chenna, R., McGettigan, P. A., McWilliam, H., et al. (2007). Clustal W and Clustal X version 2.0. *Bioinformatics* 23, 2947–2948. doi: 10.1093/bioinformatics/btm404

Livak, K. J., and Schmittgen, T. D. (2001). Analysis of relative gene expression data using real-time quantitative PCR and the 2(-Delta Delta C(T)) Method. *Methods* 25, 402–408. doi: 10.1006/meth.2001.1262

Maekawa, T., Maekawa-Yoshikawa, M., Takeda, N., Imaizumi-Anraku, H., Murooka, Y., and Hayashi, M. (2009). Gibberellin controls the nodulation signaling pathway in *Lotus japonicus*. *Plant J.* 58, 183–194. doi: 10.1111/j.1365-313X.2008.03774.x

Maillet, F., Poinsot, V., André, O., Puech-Pagès, V., Haouy, A., Gueunier, M., et al. (2011). Fungal lipochitooligosaccharide symbiotic signals in arbuscular mycorrhiza. *Nature* 469, 58–63. doi: 10.1038/nature09622

Markmann, K., Giczey, G., and Parniske, M. (2008). Functional adaptation of a plant receptor-kinase paved the way for the evolution of intracellular root symbioses with bacteria. *PLoS Biol.* 6:e68. doi: 10.1371/journal.pbio.0060068

Mikkelsen, M. D., Fuller, V. L., Hansen, B. G., Nafisi, M., Olsen, C. E., Nielsen, H. B., et al. (2009). Controlled indole-3-acetaldoxime production through ethanol-induced expression of CYP79B2. *Planta* 229, 1209–1217. doi: 10.1007/s00425-009-0907-5

Mukhopadhyay, S., and Jackson, P. K. (2011). The tubby family proteins. *Genome Biol.* 12:225. doi: 10.1186/gb-2011-12-6-225

Murashige, T., and Skoog, F. (1962). A revised medium for rapid growth and bio assays with tobacco tissue cultures. *Physiol. Plant.* 15, 473–497. doi: 10.1111/j.1399-3054.1962.tb08052.x

Nongbri, P. L., Johnson, J. M., Sherameti, I., Glawischnig, E., Halkier, B. A., and Oelmüller, R. (2012). Indole-3-acetaldoxime-derived compounds restrict root colonization in the beneficial interaction between *Arabidopsis* roots and the endophyte *Piriformospora indica*. *Mol. Plant Microbe Interact.* 25, 1186–1197. doi: 10.1094/MPMI-03-12-0071-R

Oláh, B., Brière, C., Bécard, G., Dénarié, J., and Gough, C. (2005). Nod factors and a diffusible factor from arbuscular mycorrhizal fungi stimulate lateral root formation in Medicago truncatula via the DMI1/DMI2 signalling pathway. *Plant J.* 44, 195–207. doi: 10.1111/j.1365-313X.2005.02522.x

Parniske, M. (2008). Arbuscular mycorrhiza: the mother of plant root endosymbioses. *Nat. Rev. Microbiol.* 6, 763–775. doi: 10.1038/nrmicro1987

Peškan-Berghöfer, T., Shahollari, B., Giong, P. H., Hehl, S., Markert, C., Blanke, V., et al. (2004). Association of *Piriformospora indica* with *Arabidopsis thaliana* roots represents a novel system to study beneficial plant–microbe interactions and involves early plant protein modifications in the endoplasmic reticulum and at the plasma membrane. *Physiol. Plant.* 122, 465–477. doi: 10.1111/j.1399-3054.2004.00424.x

Pham, G., Kumari, R., Singh, A., Malla, R., Prasad, R., Sachdev, M., et al. (2004). "Axenic culture of symbiotic fungus *Piriformospora indica*," in *Plant Surface Microbiology,* eds A. Varma, L. Abbott, D. Werner and R. Hampp (Berlin Heidelberg: Springer), 593–613.

Qiang, X., Zechmann, B., Reitz, M. U., Kogel, K. H., and Schäfer, P. (2012). The mutualistic fungus *Piriformospora indica* colonizes *Arabidopsis* roots by inducing an endoplasmic reticulum stress-triggered caspase-dependent cell death. *Plant Cell* 24, 794–809. doi: 10.1105/tpc.111.093260

Radutoiu, S., Madsen, L. H., Madsen, E. B., Felle, H. H., Umehara, Y., Grønlund, M., et al. (2003). Plant recognition of symbiotic bacteria requires two LysM receptor-like kinases. *Nature* 425, 585–592. doi: 10.1038/nature02039

R Core Team. (2013). *R: A Language and Environment for Statistical Computing*. Vienna: R Foundation for Statistical Computing.

Reitz, M. U., Bissue, J. K., Zocher, K., Attard, A., Hückelhoven, R., Becker, K., et al. (2012). The subcellular localization of Tubby-like proteins and participation in stress signaling and root colonization by the mutualist *Piriformospora indica*. *Plant Physiol.* 160, 349–364. doi: 10.1104/pp.112.201319

Reitz, M. U., Pai, S., Imani, J., and Schäfer, P. (2013). New insights into the subcellular localization of Tubby-like proteins and their participation in the *Arabidopsis-Piriformospora indica* interaction. *Plant Signal Behav.* 8:e25198. doi: 10.4161/psb.25198

Rey, T., Chatterjee, A., Buttay, M., Toulotte, J., and Schornack, S. (2014). *Medicago truncatula* symbiosis mutants affected in the interaction with a biotrophic root pathogen. *New Phytol.* 206, 497–500. doi: 10.1111/nph.13233

Ried, M. K., Antolin-Llovera, M., and Parniske, M. (2014). Spontaneous symbiotic reprogramming of plant roots triggered by receptor-like kinases. *Elife* 3:e03891. doi: 10.7554/elife.03891

Saito, K., Yoshikawa, M., Yano, K., Miwa, H., Uchida, H., Asamizu, E., et al. (2007). NUCLEOPORIN85 is required for calcium spiking, fungal and bacterial symbioses, and seed production in *Lotus japonicus*. *Plant Cell* 19, 610–624. doi: 10.1105/tpc.106.046938

Schäfer, P., Pfiffi, S., Voll, L. M., Zajic, D., Chandler, P. M., Waller, F., et al. (2009). Phytohormones in plant root-*Piriformospora indica* mutualism. *Plant Signal. Behav.* 4, 669–671. doi: 10.4161/psb.4.7.9038

Scholl, R. L., May, S. T., and Ware, D. H. (2000). Seed and molecular resources for *Arabidopsis*. *Plant Physiol.* 124, 1477–1480. doi: 10.1104/pp.124.4.1477

Schüßler, A., and Walker, C. (2011). "Evolution of the 'plant-symbiotic' fungal phylum, Glomeromycota," in *Evolution of fungi and fungal-like organisms,* eds. S. Pöggeler and J. Wöstemeyer (Berlin Heidelberg: Springer), 163–185.

Selosse, M. A., Dubois, M. P., and Alvarez, N. (2009). Do Sebacinales commonly associate with plant roots as endophytes? *Mycol. Res.* 113, 1062–1069. doi: 10.1016/j.mycres.2009.07.004

Shahollari, B., Vadassery, J., Varma, A., and Oelmüller, R. (2007). A leucine-rich repeat protein is required for growth promotion and enhanced seed production mediated by the endophytic fungus *Piriformospora indica* in *Arabidopsis thaliana*. *Plant J.* 50, 1–13. doi: 10.1111/j.1365-313X.2007.03028.x

Sherameti, I., Tripathi, S., Varma, A., and Oelmüller, R. (2008). The root-colonizing endophyte *Pirifomospora indica* confers drought tolerance in *Arabidopsis* by stimulating the expression of drought stress-related genes in leaves. *Mol. Plant Microbe Interact.* 21, 799–807. doi: 10.1094/MPMI-21-6-0799

Singh, S., Katzer, K., Lambert, J., Cerri, M., and Parniske, M. (2014). CYCLOPS, a DNA-binding transcriptional activator, orchestrates symbiotic root nodule development. *Cell Host Microbe* 15, 139–152. doi: 10.1016/j.chom.2014.01.011

Singh, S., and Parniske, M. (2012). Activation of calcium- and calmodulin-dependent protein kinase (CCaMK), the central regulator of plant root endosymbiosis. *Curr. Opin. Plant Biol.* 15, 444–453. doi: 10.1016/j.pbi.2012.04.002

Smith, S. E., and Read, D. J. (2008). *Mycorrhizal Symbiosis*. Amsterdam: Academic.

Svistoonoff, S., Hocher, V., and Gherbi, H. (2014). Actinorhizal root nodule symbioses: what is signalling telling on the origins of nodulation? *Curr. Opin. Plant Biol.* 20, 11–18. doi: 10.1016/j.pbi.2014.03.001

Takeda, N., Maekawa, T., and Hayashi, M. (2012). Nuclear-localized and deregulated calcium- and calmodulin-dependent protein kinase activates rhizobial and mycorrhizal responses in *Lotus japonicus*. *Plant Cell* 24, 810–822. doi: 10.1105/tpc.111.091827

Takeda, N., Sato, S., Asamizu, E., Tabata, S., and Parniske, M. (2009). Apoplastic plant subtilases support arbuscular mycorrhiza development in *Lotus japonicus*. *Plant J.* 58, 766–777. doi: 10.1111/j.1365-313X.2009.03824.x

Vadassery, J., Ritter, C., Venus, Y., Camehl, I., Varma, A., Shahollari, B., et al. (2008). The role of auxins and cytokinins in the mutualistic interaction between *Arabidopsis* and *Piriformospora indica*. *Mol. Plant Microbe Interact.* 21, 1371–1383. doi: 10.1094/MPMI-21-10-1371

Venkateshwaran, M., Cosme, A., Han, L., Banba, M., Satyshur, K. A., Schleiff, E., et al. (2012). The recent evolution of a symbiotic ion channel in the legume family altered ion conductance and improved functionality in calcium signaling. *Plant Cell* 24, 2528–2545. doi: 10.1105/tpc.112.098475

Venus, Y., and Oelmüller, R. (2013). Arabidopsis ROP1 and ROP6 influence germination time, root morphology, the formation of F-actin bundles, and symbiotic fungal interactions. *Mol. Plant* 6, 872–886. doi: 10.1093/mp/sss101

Verma, S., Varma, A., Rexer, K.-H., Hassel, A., Kost, G., Sarbhoy, A., et al. (1998). *Piriformospora indica*, gen. et sp. nov., a new root-colonizing fungus. *Mycologia* 90, 896–903. doi: 10.2307/3761331

Waller, F., Achatz, B., Baltruschat, H., Fodor, J., Becker, K., Fischer, M., et al. (2005). The endophytic fungus *Piriformospora indica* reprograms barley to salt-stress tolerance, disease resistance, and higher yield. *Proc. Natl. Acad. Sci. U.S.A.* 102, 13386–13391. doi: 10.1073/pnas.0504423102

Webb, K. J., Skøt, L., Nicholson, M. N., Jørgensen, B., and Mizen, S. (2000). *Mesorhizobium loti* increases root-specific expression of a calcium-binding protein homologue identified by promoter tagging in *Lotus japonicus*. *Mol. Plant Microbe Interact.* 13, 606–616. doi: 10.1094/MPMI.2000.13.6.606

Wiermer, M., Cheng, Y. T., Imkampe, J., Li, M., Wang, D., Lipka, V., et al. (2012). Putative members of the *Arabidopsis* Nup107-160 nuclear pore sub-complex contribute to pathogen defense. *Plant J.* 70, 796–808. doi: 10.1111/j.1365-313X.2012.04928.x

Zuccaro, A., Lahrmann, U., Güldener, U., Langen, G., Pfiffi, S., Biedenkopf, D., et al. (2011). Endophytic life strategies decoded by genome and transcriptome analyses of the mutualistic root symbiont *Piriformospora indica*. *PLoS Pathog.* 7:e1002290. doi: 10.1371/journal.ppat.1002290

Conflict of Interest Statement: The authors declare that the research was conducted in the absence of any commercial or financial relationships that could be construed as a potential conflict of interest.

frontiers in Plant Science

REVIEW
published: 07 June 2016
doi: 10.3389/fpls.2016.00797

Fighting Asian Soybean Rust

Caspar Langenbach[1], Ruth Campe[2], Sebastian F. Beyer[1], André N. Mueller[1] and Uwe Conrath[1]*

[1] Department of Plant Physiology, RWTH Aachen University, Aachen, Germany, [2] BASF Plant Science Company GmbH, Limburgerhof, Germany

Phakopsora pachyrhizi is a biotrophic fungus provoking SBR disease. SBR poses a major threat to global soybean production. Though several *R* genes provided soybean immunity to certain *P. pachyrhizi* races, the pathogen swiftly overcame this resistance. Therefore, fungicides are the only current means to control SBR. However, insensitivity to fungicides is soaring in *P. pachyrhizi* and, therefore, alternative measures are needed for SBR control. In this article, we discuss the different approaches for fighting SBR and their potential, disadvantages, and advantages over other measures. These encompass conventional breeding for SBR resistance, transgenic approaches, exploitation of transcription factors, secondary metabolites, and antimicrobial peptides, RNAi/HIGS, and biocontrol strategies. It seems that an integrating approach exploiting different measures is likely to provide the best possible means for the effective control of SBR.

Keywords: Asian soybean rust, *Phakopsora pachyrhizi*, fungicide insensitivity, host resistance, non-host resistance, plant breeding, plant biotechnology

Edited by:
Pietro Daniele Spanu, Imperial College London, UK

Reviewed by:
Brigitte Mauch-Mani, Université de Neuchâtel, Switzerland
Francismar Corrêa Marcelino-Guimarães, Embrapa Soybean, Brazil

****Correspondence:***
Caspar Langenbach
langenbach@bio3.rwth-aachen.de

Specialty section:
This article was submitted to Plant Biotic Interactions, a section of the journal Frontiers in Plant Science

Received: *23 December 2015*
Accepted: *22 May 2016*
Published: *07 June 2016*

Citation:
Langenbach C, Campe R, Beyer SF, Mueller AN and Conrath U (2016) Fighting Asian Soybean Rust. Front. Plant Sci. 7:797. doi: 10.3389/fpls.2016.00797

INTRODUCTION

SBR is currently the most severe soybean (*Glycine max*) disease. SBR is caused by *Phakopsora pachyrhizi*. The biotrophic basidiomycete threatens soybean production all over the globe, but the threat is most severe in the major soybean growing areas in South America. In Brazil SBR has caused crop losses of more than US$ 10 billion since its first endemic outbreak in 2001 (Yorinori et al., 2005; da Silva et al., 2014). Currently, three major strategies serve to manage SBR (**Figure 1**). First, applying chemical fungicides. Second, breeding or engineering of SBR-resistant soybean cultivars, and third, employing specific cultivation practices, such as planting early ripening varieties, monitoring fields, eliminating secondary hosts, and introducing soybean-free growth periods (60–90 days) in the threatened areas (Hartman et al., 2005; Godoy, 2011; Kendrick et al., 2011). Here, we elaborate on these strategies, and we also discuss the potential of AMPs, RNAi/HIGS, and biocontrol measures for controlling SBR. A detailed description of the life cycle, host range and distribution of *P. pachyrhizi* has been provided earlier (Goellner et al., 2010).

Abbreviations: AMP, Antimicrobial peptide; CRISPR, Clustered regularly interspersed short palindromic repeats; DMI, Demethylation inhibitor; dsRNA, Double stranded RNA; ETI, Effector-triggered immunity; FRAC, Fungicide Resistance Action Committee; HESP, Haustoria-expressed secreted protein; HIGS, Host-induced gene silencing; IAP, Intragenic antimicrobial peptide; JA, Jasmonic acid; MDR, Muldidrug resistance; NB-LRR, Nucleotide-binding leucine-rich repeat; NHR, non-host resistance; PDR, Partial disease resistance; QoI, Quinone outside inhibitor; *R* gene, Resistance gene; RNAi, RNA interference; *Rpp*, Resistance to *P. pachyrhizi*; *S* gene, Susceptibility gene; SA, Salicylic acid; SAR, Systemic acquired resistance; SBR, Asian soybean rust; SDHI, Succinate dehydrogenase inhibitor; siRNA, Small interfering RNA; TF, Transcription factor; TILLING, Targeting induced local lesions in genomes; VIGS, Virus-induced gene silencing.

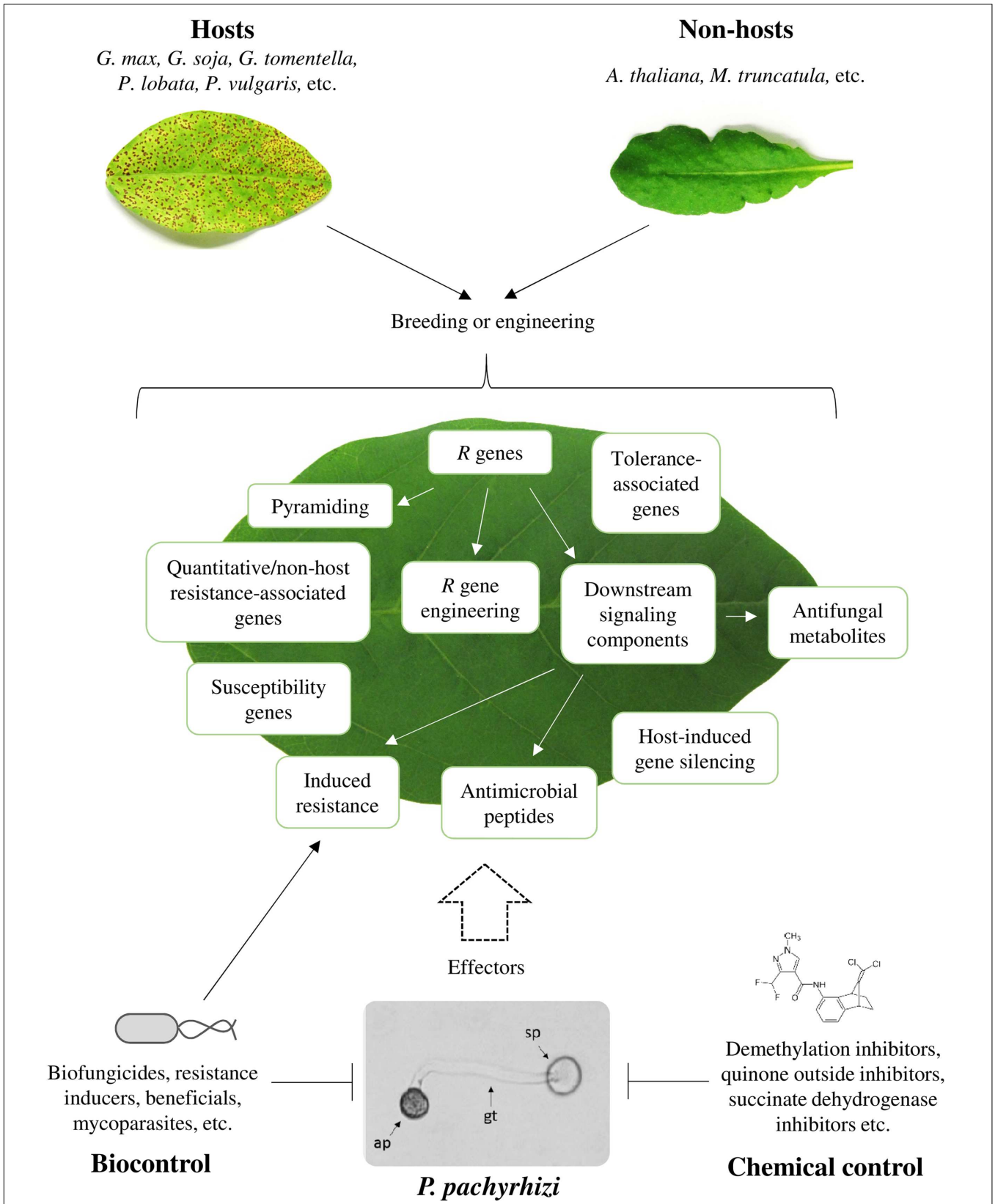

FIGURE 1 | Strategies for controlling SBR. Exploitation of different genetic resources (host and non-host plants), biocontrol agents, and chemical fungicides to combat *Phakopsora pachyrhizi*. ap, appressorium; gt, germ tube; sp, uredospore.

Chemical Control of SBR

Fungicide use is the most effective means for controlling SBR these days. In Brazil, at least three fungicide applications are needed per season thus raising costs of ∼US$2 billion for soybean disease control annually (Godoy et al., 2015). In contrast to multisite fungicides (e.g., mancozeb) with comparatively low performance, the DMI and the QoI classes of fungicide are prime chemicals for fighting *P. pachyrhizi*. Since 2013, fungicides of the highly active SDHI class are available for SBR control (Guicherit et al., 2014). Because this new fungicide class performs extraordinarily well, the number of available SDHI fungicides and the intensity of their use is likely to steadily increase over the next couple of years (Godoy et al., 2015). However, the excessive use of fungicides increases the chance of fungal strains with evolved insensitivity to the fungicides in use. In the recent past, this was true for the azole-class fungicides to which *P. pachyrhizi* and other fungal pathogens have become insensitive (Godoy, 2012). The FRAC assigned rust fungi, including *P. pachyrhizi*, to the low-risk group of fungi (Brent and Holloman, 2007). However, *P. pachyrhizi* and other causes of polycyclic plant diseases are highly likely to evolve fungicide insensitivity because of the high number of spores they produce (Bradley, 2007).

The mechanism of fungal insensitivity to DMIs is highly complex and variable. After several years of fungicide use, a significant reduction in DMI efficacy to *P. pachyrhizi* was detected in Brazil (Scherm et al., 2009; Barbosa et al., 2013; Reis et al., 2015). The insensitivity is caused either by point mutations in the fungal *cyp51* gene or by *cyp51* overexpression (Schmitz et al., 2014). The major mechanism of QoI and SDHI insensitivity is by point mutations in the *cyt b* and *sdh b/c/d* genes, respectively. These mutations were reported for many plant-pathogenic fungi (Kim et al., 2003; Grasso et al., 2006a; Sierotzki et al., 2007; Sierotzki and Scalliet, 2013). The most common mutation for QoI insensitivity [substitution of glycine to alanine at position 143 of Cyt b] was not yet detected in rusts probably because of presence of a type-I intron after codon 143 (Grasso et al., 2006a,b,c; Oliver, 2014; Klosowski et al., 2015). Nucleotide substitutions in this codon would prevent intron splicing thus leading to a defective Cyt b protein (Grasso et al., 2006a). However, another *cyt b* mutation (F129L) was reported to confer QoI insensitivity in various fungi including *P. pachyrhizi* (Leiminger et al., 2014; Klosowski et al., 2015). For *P. pachyrhizi* SDHI insensitivity was not reported yet. However, the increased use of SDHIs is likely to further enhance the selection pressure for SDHI insensitivity in *P. pachyrhizi* (Godoy et al., 2015). MDR, as reported for *Botrytis cinerea* and other fungi (Kretschmer et al., 2009) also was not observed in *P. pachyrhizi* so far. To assess the risk and impact of fungicide-insensitive isolates, we recommend generating insensitive fungal mutants in the laboratory. Investigating such mutants is likely to disclose mechanisms underlying fungicide insensitivity, enable recommendations for avoiding selection of insensitive fungal populations, and developing novel mode-of-action fungicides. Applying fungicides preventively or as early as possible in the diseases cycle before or shortly after *P. pachyrhizi* infection is crucial for effective SBR control (Mueller et al., 2009; Godoy, 2012). Therefore, early SBR detection and precise forecasts are required for efficient SBR disease management.

Probably the best and most sustainable control of SBR is by providing soybean genotypes resisting *P. pachyrhizi* (see below). Growth of SBR resistant genotypes is likely to be associated with reduced fungicide use. This then might decrease soybean production costs, improve the CO_2 footprint of soybean products, and minimize the potential risk of ecological and sanitary actions resulting from extensive use of fungicides (Maltby et al., 2009; Verweij et al., 2009; Wightwick et al., 2010).

Resources of SBR Resistance in Soybean

R Genes, *R* Gene Pyramids, and Engineered *R* Genes

Analysis of soybean genotypes disclosed six dominant *R* genes conferring immunity (no visible symptoms) or resistance (reddish brown lesions and reduced sporulation) to specific *P. pachyrhizi* isolates. Those loci were referred to as *Rpp* 1–6 genes (Bromfield and Hartwig, 1980; McLean and Byth, 1980; Bromfield and Melching, 1982; Hartwig and Bromfield, 1983; Hartwig, 1986; Garcia et al., 2008; Li et al., 2012). However, *Rpp* genes provide resistance exclusively to individual *P. pachyrhizi* isolates (race-specific disease resistance). Therefore, no currently available soybean genotype would ward off all *P. pachyrhizi* isolates (Monteros et al., 2007). In addition, *Rpp* gene-mediated resistance was swiftly overcome in the field (Yorinori et al., 2005; Garcia et al., 2008). Employing recessive *R* genes might represent another approach for providing stable SBR resistance (Calvo et al., 2008). In fact, three recessive *R* genes to *P. pachyrhizi* have been identified in the soybean genotypes PI 200456, PI 224270, and BR01-18437 (Calvo et al., 2008; Pierozzi et al., 2008). These genes are now awaiting exploitation in breeding and genetic engineering for SBR resistance.

Developing elite lines and varieties requires breeders to combine traits from multiple parents, a process called gene pyramiding or stacking (Francis et al., 2012). Pyramiding *R* genes into a single genetic background is another proposed strategy for conferring soybean resistance to multiple *P. pachyrhizi* isolates (Hartman et al., 2005; Garcia et al., 2008; Lemos et al., 2011; Maphosa et al., 2012; Yamanaka et al., 2013, 2015; Bhor et al., 2014). The SBR resistant Japanese soybean cultivar Hyuuga represents a natural example of *R* gene pyramiding (Kendrick et al., 2011). In line with this finding, soybean genotypes harboring two pyramided *Rpp* genes exhibited higher SBR resistance than their ancestors containing only single *R* genes (Maphosa et al., 2012; Bhor et al., 2015). Synergistic effects were also observed when three *R* genes were bred into a single soybean genotype (Lemos et al., 2011; Yamanaka et al., 2013, 2015). Remarkably, a combination of multiple *R* genes conferred resistance to different *P. pachyrhizi* isolates from various origin (including two highly virulent strains from Brazil; Yamanaka et al., 2015). Although molecular markers facilitate breeding approaches, traditional breeding is still time consuming, and introducing unwanted traits (Salomon and Sessa, 2012). Furthermore, SBR resistance based on static *R* gene pyramids will likely be overcome upon longer use in the field (McDonald,

2014) as has been reported for other crops like wheat or barley (McDonald and Linde, 2002). Therefore, transforming expression cassettes with alternative *R* gene combinations into elite soybean lines and dynamic turnover of such lines in the field might represent a promising strategy for providing sustainable and effective SBR resistance (McDonald and Linde, 2002). However, for cloning and utilization of such multi *R* gene expression cassettes the identity of *Rpp* genes needs to be revealed. Although SBR resistance loci have been mapped to different linkage groups on various chromosomes (reviewed by Bhor et al., 2014), the identity of *Rpp* genes has remained largely unknown. One exception is represented by the NB-LRR encoding gene *Rpp4C4* that is likely responsible for *Rpp4*-mediated SBR resistance (Meyer et al., 2009).

Another possibility to enhance the resistance of soybean to SBR is to identify and exploit *R* genes conferring resistance to multiple pathogens. Several examples of such broadly active *R* genes exist in nature (Nombela et al., 2003; Narusaka et al., 2009; Atamian et al., 2012; Lozano-Torres et al., 2012). A complementary approach for broadened pathogen effector recognition uses random mutagenesis or rational design of synthetic NB-LRR immune receptors. Editing the potato NB-LRR receptor R3a at a single amino acid significantly expanded its response to *Phytophthora infestans*-derived effectors (Segretin et al., 2014). Effectively mutating the R3a orthologue I2 in tomato enhanced the response to the *P. infestans* AVR3a effector, conferred partial immunity to potato blight, and expanded the response spectrum to *Fusarium oxysporum* f. sp. *lycopersici* effectors compared to tomato plants expressing the wild-type I2 gene (Giannakopoulou et al., 2015). *R* gene engineering might also succeed in exploiting multiple *Rpp* genes for conferring an expanded response to multiple *P. pachyrhizi* isolates. *Rpp4C4* (Meyer et al., 2009) may serve for engineering such *R* gene variants by untargeted protein evolution. Furthermore, genome editing may be used for the targeted evolution of NB-LRRs. In fact, genome-wide sequence analysis predicted nearly all soybean NB-LRR-encoding genes an be targeted specifically by CRISPR/Cas9 (Xie et al., 2014).

Signaling Components of *R* Gene-Mediated SBR Resistance

Several studies reported differential defense responses to SBR attack in susceptible and resistant soybean genotypes. The studies included analysis of transcriptional dynamics, proteome changes, or metabolic alterations to identify loci, genes, proteins, and metabolites associated with ETI to *P. pachyrhizi* in soybean.

Signaling network hubs and phytohormones

Transcriptome analysis disclosed different components of *Rpp2*-mediated resistance to SBR in soybean (van de Mortel et al., 2007; Pandey et al., 2011). Of 140 candidates tested by VIGS, eleven genes clearly contributed to *Rpp2*-mediated SBR resistance. The genes encompassed *GmEDS1*, *GmPAD4*, and *GmNPR1*.

NPR1 is a master regulator of SAR in *Arabidopsis thaliana* and some other plants (reviewed by Fu and Dong, 2013). When overexpressed in *Arabidopsis*, rice, tobacco, or apple, NPR1 enhances resistance to infectious oomycetes, bacteria, and fungi (including obligate biotrophic fungi such as powdery mildew; Cao et al., 1998; Chern et al., 2005; Chen et al., 2012). Because of possible side effects of *NPR1* overexpression (Chern et al., 2005), such as yield reduction, the potential of this gene for generating SBR-resistant soybean varieties awaits assessment.

EDS1 and PAD4 are key regulators of several types of plant disease resistance (basal, *R* gene-mediated, and NHR). The two proteins are required for accumulation of SA, and they control various SA-dependent defense pathways (Falk et al., 1999; Jirage et al., 1999; Nawrath et al., 2002; Lipka et al., 2005; Wiermer et al., 2005; Langenbach et al., 2013; Wang et al., 2014). Because silencing of *GmEDS1* or *GmPAD4* lead to susceptibility of otherwise resistant soybean lines carrying *Rpp2*, EDS1 and PAD4 seem to control also *Rpp2*-mediated SBR resistance in soybean (Pandey et al., 2011). SA accumulation is thus likely to limit the growth and reproduction of *P. pachyrhizi* in soybean. Because *PAD4* is also required for *Arabidopsis* postinvasion NHR to *P. pachyrhizi* (Langenbach et al., 2013), SA-associated defense responses seem to be highly effective in antagonizing SBR disease. However, overexpression of SA biosynthesis genes is likely not to provide a realistic agronomical solution for SBR control because constitutive SA accumulation often causes dwarfism (Bowling et al., 1994; Li et al., 2001).

In *Arabidopsis* and soybean, *P. pachyrhizi* activates expression of JA-responsive genes at early stages of infection (Loehrer et al., 2008; Alves et al., 2015) and before actual penetration [likely by secreted *P. pachyrhizi* effectors (Campe et al., 2014)]. Since JA is considered eliciting immune responses against necrotrophic pathogens (Pieterse et al., 2012) *P. pachyrhizi* pretends being a necrotroph at initial stages of colonization. By doing so, it may circumvent effective SA-dependent defense signaling which is known to be crucial to ward off biotrophic pathogens. Thus, engineering soybean plants for the fast and robust accumulation of SA, or exploiting SA-activated downstream signaling components for resistance might be a suited strategy for providing soybean varieties resisting SBR at low risks for energetic tradeoffs.

Transcription factors

The importance of TFs in conferring SBR resistance became obvious when van de Mortel et al. (2007) and Schneider et al. (2011) found that TF genes are being overrepresented among genes whose expression is activated in the biphasic transcriptional response in SBR-resistant soybean genotypes harboring *Rpp2* or *Rpp3*. Amongst others, genes encoding WRKY, bHLH, and MYB TFs were activated in incompatible, but not compatible, soybean-*P. pachyrhizi* interactions. When *GmWRKY36*, *GmWRKY40*, *GmWRKY45*, and *GmMYB84* were individually silenced using VIGS, *Rpp2*-mediated SBR resistance was gone (Pandey et al., 2011). Several other studies also revealed differential expression of TFs in incompatible or compatible soybean-*P. pachyrhizi* interactions (Panthee et al., 2009; Morales et al., 2013; Aoyagi et al., 2014). In fact, there seems to be considerable overlap of TF activity in *Rpp2*, *Rpp3*, and *Rpp4*-mediated soybean disease resistance (Morales et al., 2013). Therefore, these TFs seem to be excellent candidates for engineering SBR resistance. However, manipulation of TF

balance may affect agronomic traits because TFs regulate a diverse array of loci.

In another approach, Cooper et al. (2011) compared nuclear proteome changes in a resistant vs. susceptible genotype at 24 h after inoculation with *P. pachyrhizi*. Their analysis disclosed more than 200 proteins that specifically accumulated in the nucleus of SBR-resistant soybean plants harboring *Rpp1* (Cooper et al., 2011). Silencing two predicted soybean TFs (Glyma14g11400, PHD superfamily and Glyma12g30600, zinc finger TF) via VIGS partially compromised *Rpp1*-conferred SBR resistance (Cooper et al., 2013). Similarly, Bencke-Malato et al. (2014) demonstrated that accumulation of mRNA transcripts for several WRKY TFs was faster and more robust in a resistant than susceptible soybean accession. Consistently, the simultaneous silencing of four identified *WRKY* genes rendered soybean plants more susceptible to SBR disease. Because the authors did not succeed in producing *WRKY*-overexpressing soybean lines (Bencke-Malato et al., 2014), the potential of *WRKY* overexpression for providing SBR resistance to susceptible soybean genotypes remained unclear.

Secondary metabolism

Plants can halt or slow down infection by constitutive or inducible accumulation of antimicrobial and/or cell wall-fortifying secondary metabolites (Chiang and Norris, 1983; Hahlbrock and Scheel, 1989; Chang et al., 1995; Dixon et al., 2002; Boerjan et al., 2003; La Camera et al., 2004; Vogt, 2010). Secondary metabolites also contribute to the outcome of the soybean–*P. pachyrhizi* interaction. Daidzein, genistein, and glyceollin are isoflavonoids that accumulate in both resistant and susceptible soybean genotypes upon *P. pachyrhizi* infection (Lygin et al., 2009). Glyceollin efficiently reduces *P. pachyrhizi* uredospore germination *in vitro* (Lygin et al., 2009). Further evidence for a role of phytoalexins in SBR resistance was provided by Bilgin et al. (2009). The authors disclosed that SBR resistance in a *Glycine tomentella* accession correlated with the presence of a flavonoid that also inhibited *P. pachyrhizi* spore germination (Chung and Singh, 2008). The high potential of phytoalexins in defeating SBR is further supported by medicarpin accumulating in *P. pachyrhizi*-infected *Medicago truncatula*, a non-host of *P. pachyrhizi*. Consistently, medicarpin inhibits *P. pachyrhizi* spore germination (Ishiga et al., 2015). Providing such comparative large-scale metabolic profiles from resistant vs. susceptible soybean varieties, or other SBR-resistant species would likely identify more secondary metabolites inhibiting SBR. Genes in their biosynthesis pathways could be used to engineer SBR resistance in transgenic soybean. Alternatively, the compound(s) themselves could serve as natural fungicides in spray application, especially if they can be produced at low costs and in sufficient quantities for use in agriculture. In a variety of studies, genes in the phenylpropanoid and flavonoid metabolism were overrepresented when analyzing the transcriptional response of infected soybean genotypes with SBR resistance (van de Mortel et al., 2007; Choi et al., 2008; Panthee et al., 2009; Schneider et al., 2011). Overall, activation of these genes was faster and stronger in SBR-resistant accessions than in susceptible ones (van de Mortel et al., 2007; Schneider et al., 2011). Functional evidence for the importance of phenylpropanoid pathway genes in soybean's SBR resistance was provided by Pandey et al. (2011). The authors demonstrated that silencing of soybean phenylalanine ammonia-lyase (*GmPAL*) or *O*-methyl transferase1 (*GmOMT1*) compromised *Rpp2*-mediated SBR resistance. *OMT1* silencing also partially impaired *Rpp1*-mediated SBR resistance (Cooper et al., 2013) and significantly decreased lignin content (Pandey et al., 2011). The latter result points to an important role of lignification in rejecting SBR.

Susceptibility Genes and Effector Targets

Different from dominant *R* genes conferring effective, but exclusively race-specific and non-durable resistance (Yorinori et al., 2005; Garcia et al., 2008), the loss of functional *S* genes can eventually provide durable disease resistance (Pavan et al., 2010; Gawehns et al., 2013). For example, in barley absence of the *S* gene *Mlo* results in an incompatible interaction with *Blumeria graminis* f. sp. *hordei* that resembles NHR (Humphry et al., 2006). *S* genes function either as susceptibility factors or suppressors of plant defense. Thus they are potential targets of fungal effectors. Consistent with this assumption knocking out *S* genes leads to recessive resistance with effectivity to multiple races of a given pathogen (Pavan et al., 2010). This type of resistance is very stable. The resistance of plants harboring recessive alleles of *Mlo* (barley) or *eIF4E* (pepper) has not been overcome in the field for 30–50 years (Lyngkjær et al., 2000; Kang et al., 2005). Breeding for *S* gene variants insensitive to manipulation by pathogen effectors therefore has huge potential for durable, broad-spectrum disease resistance; although loss-of-function mutations in *S* genes may be associated with pleiotropic detrimental effects (Büschges et al., 1997).

Soybean *S* genes to SBR have not been identified so far. However, several approaches might identify potential *S* gene alleles for SBR resistance in soybean. Because most *S* genes of agricultural value were identified in screens for recessive resistance in wild species of plant (Bai et al., 2005), searching for such a resistance in wild *Glycine* might similarly provide genetic resources for breeding or engineering SBR resistance in *G. max*.

Another option for identifying soybean *S* genes to SBR is via sequence homology search to known *S* genes. Functional analysis can be done using, for example, soybean insertion mutants (Mathieu et al., 2009), performing VIGS (Zhang and Ghabrial, 2006; Zhang et al., 2010, 2013; Pandey et al., 2011), TILLING (Cooper et al., 2008), or applying targeted genome editing techniques such as CRISPR/Cas9 (Jacobs et al., 2015). However, currently only one gene [the Cys(2)His(2) zinc finger TF palmate-like pentafoliata1, *PALM1*] that would classify as an SBR *S* gene is known from *M. truncatula* (Uppalapati et al., 2012). Alternatively, fungal effectors might serve as guides to identify novel *S* genes in soybean and other plants since several effectors of bacteria, fungi, or oomycetes were shown to target plant *S* genes (reviewed by Gawehns et al., 2013). Although various analyses identified stage-specific rust proteins that might have bona-fide effector function (Loehrer and Schaffrath, 2011; Stone et al., 2012; Link et al., 2014), their role as virulence factors awaits functional confirmation. Identification of effector proteins and corresponding *S* gene targets was likely hampered by

missing *P. pachyrhizi* genome information (Loehrer et al., 2014). Transformation protocols enabling generation of *P. pachyrhizi* knockout mutants are also missing.

Another approach for identifying *S* gene alleles conferring SBR resistance is via screening of mutagenized soybean populations for loss-of-susceptibility mutants. The tetraploid nature of the soybean crop and the potential existence of multiple *S* gene copies might hamper this approach. Because 12 duplicated copies of a given DNA region might be present in the soybean genome (Cannon and Shoemaker, 2012), mutagenesis-induced phenotypic variation might be buffered by gene redundancy (Bolon et al., 2014). However, fast neuron irradiation recently provided more than 27,000 unique soybean mutants with significant phenotypic variation (Bolon et al., 2011, 2014). The mutants may facilitate genetic screens for loss of SBR susceptibility mutants with interesting resistance phenotypes similar to the *M. truncatula irg1* mutant (Ishiga et al., 2015). Identified *S* gene alleles for SBR resistance in soybean might be engineered in elite soybean lines via genome editing (Jacobs et al., 2015).

Genes Providing Quantitative SBR Resistance or Tolerance

Forward genetic screens using activation-tagged soybean plants (Mathieu et al., 2009) could identify genes and loci that quantitatively contribute to SBR resistance. Genes and loci for SBR resistance can potentially also be found exploiting fungal effectors targeting proteins with a role in apoplastic immunity [e.g., the *Ustilago maydis* effector Pit2 targets maize apoplastic cysteine proteases (Mueller et al., 2013)].

PDR to SBR is found in 'slow rusting' soybean accessions such as SRE-Z-11A, SRE-Z-11B, and SRE-Z-15A (Tukamuhabwa and Maphosa, 2010). These genotypes can potentially provide useful genes and loci for quantitative SBR resistance. PDR is characterized by low infection frequency, long-lasting latency, small lesions, and reduced spore production per uredinium. Thus, PDR reduces SBR epidemics (Tukamuhabwa and Maphosa, 2010). Since PDR is polygenic and effective to multiple pathogen races (Long et al., 2006), identification, and transfer of genes from partially resistant to susceptible soybean varieties might provide only partial but durable resistance to diverse *P. pachyrhizi* isolates. Because of PDR's polygenic nature and the time-consuming process for selecting partially resistant progeny, such soybean varieties have not attracted much attention as sources for SBR resistance in the past (Hartman et al., 2005).

Besides soybean genotypes with partial resistance, SBR-tolerant accessions also have not been a subject of molecular research. Although susceptible to SBR, these genotypes do better tolerate the presence of *P. pachyrhizi* and produce reasonably high yield even when severely infected. Yield may increase by 30–60% using SBR-tolerant varieties in the presence of *P. pachyrhizi* (Tukamuhabwa and Maphosa, 2010). Furthermore, planting tolerant varieties does not pose selection pressure on *P. pachyrhizi*, thus minimizing the risk of selecting adapted pathogen races (Arias et al., 2008). However, SBR disease tolerance of a given soybean accession is assessed with respect to its yield capacity. This requires multi-site field trials and hinders evaluation of a genotype's tolerance and commercial value at small scale laboratory conditions (Tukamuhabwa and Maphosa, 2010). Nonetheless, identification of genes for SBR tolerance using, e.g., comparative transcriptome or proteome analysis, may enable provision of soybean varieties with capacity for enhanced yield at high SBR pressure.

Antimicrobial Peptides

AMPs can provide disease resistance to plants (Rahnamaeian, 2011). However, AMPs did not serve to fight SBR so far. Brand et al. (2012) introduced a method for the identification and employment of putative AMPs encrypted in soybean protein sequences. This approach was meant to provide an alternative to transgenic approaches that expressed AMPs from other organisms. Using *in situ* assays, Brand et al. (2012) found that IAPs conferred SBR resistance in a manner similar to AMPs from *Phyllomedusa* ssp. (dermaseptin SI) or *Drosophila melanogaster* (penetratin) when co-incubated with fungal uredospores on susceptible soybean leaves. In addition, soybean plants expressing a putative antimicrobial fragment of the *G. max* D-myo-inositol 3-phosphate synthase [IAP gb|ABM17058.1| (213–231)] showed enhanced resistance to *P. pachyrhizi* (Brand et al., 2012). These findings illustrate the feasibility of trans- or cisgenic AMP expression for SBR resistance.

Alternative Sources of SBR Resistance

Wild *Glycine* Species and Other Alternative Hosts

Wild perennial *Glycine* species might serve as valuable resources of germplasm for SBR resistance. This is because *Glycine clandestina, Glycine canescens, Glycine tabacina, Glycine tomentella*, and *Glycine argyrea* all display pathotype-specific resistance to *P. pachyrhizi* (Burdon and Speer, 1984; Burdon, 1987, 1988; Jarosz and Burdon, 1990). In *G. clandestina, G. canescens*, and *G. argyrea* differential SBR resistance phenotypes are linked to presence or absence of single or multiple (pyramided) *R* genes (Burdon and Speer, 1984; Burdon, 1987, 1988; Jarosz and Burdon, 1990). The resistance of *G. tomentella* accession PI 441001 to *P. pachyrhizi*, however, was associated with accumulation of an antifungal flavonoid inhibiting *P. pachyrhizi* spore germination (Chung and Singh, 2008). Because Singh and Nelson (2015) obtained fertile SBR-resistant plants from crosses of *G. max* and *G. tomentella*, transfer of *R* genes from wild perennial species to commercial soybean varieties via intersubgenic hybridization seems to be a powerful strategy for SBR resistance. The novel hybrid plant is still to be analyzed for its yield and resistance to multiple *P. pachyrhizi* isolates which will disclose the commercial value of the hybrid.

Other SBR resistance traits are present in *G. soja*. The species is closer related to *G. max* than its above mentioned wild perennial relatives (Bromfield, 1984). However, because of presence of undesired traits, generating hybrids for commercialization using *G. soja* or the wild, perennial *Glycine* species will likely require elaborate backcrossing and selection. Identifying the genetic basis of SBR resistance in wild species followed by engineered transfer of genes and/or traits to elite varieties might represent an alternative, more promising strategy for SBR

resistance. The approach circumvents the drawbacks associated with hybridization strategies. However, only few attempts (e.g., Soria-Guerra et al., 2010) identified gene candidates to condition SBR resistance in wild *Glycine* species.

Kudzu (*Pueraria lobata*) is a leguminous weed that hosts *P. pachyrhizi* and could provide traits for SBR resistance. Genetic variation is high among different kudzu populations but low within a same population (Sun et al., 2005). As a consequence, individual kudzu plants are resistant/immune or susceptible to diverse *P. pachyrhizi* isolates (Bonde et al., 2009). In a kudzu genotype with immunity to SBR the early abrogation of *P. pachyrhizi* infection correlated with cell wall appositions and cell death in the leaf epidermis (Jordan et al., 2010). This finding suggests presence of early, effective defense responses in immune kudzu genotypes. Big differences in the response to *P. pachyrhizi* infection were also seen in several other legume species (Slaminko et al., 2008). *Vigna adenantha* PI 312898, for instance, is immune to SBR as are individual bean (*Phaseolus vulgaris*) cultivars (Miles et al., 2007; Souza et al., 2014). However, lack of genomic information and low genetic accessibility of alternative *P. pachyrhizi* hosts impede candidate gene identification and gene transfer.

Non-host Plants

Over the past decade, employing non-host plants has become a promising approach for identifying resistance traits. Due to the pervasive nature of NHR, the strategy explores a vast genetic resource. NHR is a multi-layered, complex type of plant disease resistance that shares signaling and defense mechanisms with host resistance (Schulze-Lefert and Panstruga, 2011). Classification of a given plant species as a host or non-host can be difficult because there seems to be a gradual continuum from host to non-host with many intermediate resistances (Bettgenhaeuser et al., 2014). Exploring the molecular basis of this variety of resistances and pyramiding underlying genes and loci in the soybean crop may represent a powerful approach for SBR resistance and provide an alternative to chemical fungicides and traditional breeding.

Arabidopsis and *M. truncatula* are the best described plants in terms of NHR to *P. pachyrhizi*. Since *P. pachyrhizi* does not produce macroscopic symptoms on any of 28 wild-type accessions tested, *Arabidopsis* can be considered a true non-host for *P. pachyrhizi* (Loehrer et al., 2008). Although initial stages of *P. pachyrhizi* development are identical on *Arabidopsis* and soybean, proliferation of *P. pachyrhizi* hyphae into the leaf mesophyll is rare in *Arabidopsis* (Loehrer et al., 2008). To determine the molecular basis of the preinvasion resistance to *P. pachyrhizi* in this plant, Loehrer et al. (2008) used *Arabidopsis* mutants with known compromised resistance to other non-adapted fungal pathogens. Colonization of the mesophyll occurred in *Arabidopsis penetration* mutant *pen1*, *pen2*, and *pen3*. However, despite hyphal growth and rarely observed haustoria in the mesophyll of *pen* mutants, the fungus failed to successfully colonize the plant. It also did not complete its life cycle, indicative of functional postinvasion resistance to *P. pachyrhizi* in these mutants. The postinvasion resistance was compromised in the *Arabidopsis* triple mutant *pen2 pad4 sag101* in which *P. pachyrhizi* frequently developed haustoria (Langenbach et al., 2013). However, extensive mesophyll colonization and sporulation did not occur in any *Arabidopsis* mutants tested.

To identify components of *Arabidopsis* postinvasion resistance to *P. pachyrhizi*, Langenbach et al. (2013, 2016) performed comparative transcriptional profiling of genes specifically activated upon *P. pachyrhizi* infection in *pen2* (a mutant with intact postinvasion resistance) but not *pen2 pad4 sag101* (with compromised postinvasion resistance). The screen identified BRIGHT TRICHOMES 1 (BRT1), an UDP-glycosyltransferase in the phenylpropanoid metabolism. Postinvasion resistance to *P. pachyrhizi* was impaired in the *pen2 brt1* double mutant. In this genotype the fungus developed more haustoria than in *pen2*. Since *brt1* mutants were not affected in preinvasion SBR resistance (Langenbach et al., 2013), BRT1 seems to specifically contribute to postinvasion NHR to the disease.

To identify more genes that function in *Arabidopsis* NHR to SBR, Langenbach et al. (2016) searched for genes co-regulated with *BRT1*. Upon confirming the genes' importance in *Arabidopsis* postinvasion resistance, the authors expressed these genes in soybean. Four so-called postinvasion-induced NHR genes (*PINGs*) indeed reduced SBR disease severity. The supposed function of individual PING proteins is quite diverse and includes an EARLI4-like phospholipase (PING4), a group I receptor-like kinase (PING5), a GDSL-like lipase (PING7), and a germin-like protein (PING9). The exact mode of action of PINGs in conferring resistance to *P. pachyrhizi* has remained elusive (Langenbach et al., 2016). However, the study discloses that interspecies gene transfer is a promising strategy for conferring SBR resistance to soybean. Gene donor and receiver plant obviously do not need to be closely related, although it is likely that the successful transfer of a protein's function from one species to another implies conservation or convergence of its physiological environment (e.g., signaling networks). Thus, employing phylogenetically related non-hosts might further enhance the success of interspecies NHR gene transfer as a means for SBR resistance. Because *P. pachyrhizi* infects many plants, non-hosts to the fungus are rare, especially in the legume family of plants. *M. truncatula* is the only reported leguminous non-host as sporulation of *P. pachyrhizi* has not been observed on this plant (Uppalapati et al., 2012; Ishiga et al., 2015). The former authors did a forward genetic screen to identify *M. truncatula* mutants with altered resistance to *P. pachyrhizi*. Because of its diploid genome, *M. truncatula* is better suited for forward genetic screening than the allopolyploid soybean crop (Gill et al., 2009). Furthermore, there is highly conserved microsynteny between soybean and *M. truncatula* (Yan et al., 2003). The screen by Uppalapati et al. (2012) identified an *inhibitor of rust germ tube differentiation* (*irg*)*1* mutant on which *P. pachyrhizi* failed to promote preinfection structures. It turned out that the loss of abaxial epicuticular wax crystals and the reduced surface hydrophobicity inhibited fungal development on *irg1* (Uppalapati et al., 2012). The mutation was mapped to *PALM1* encoding a Cys(2)His(2) zinc finger TF controlling the expression of genes involved in long-chain fatty acid biosynthesis and transport (Uppalapati et al., 2012).

To further investigate the role of surface hydrophobicity or epicuticular waxes on *P. pachyrhizi* development, Ishiga et al. (2013) recorded the fungal transcriptome during germination on a hydrophobic surface (glass slides coated with epicuticular wax from wild-type plants and *irg1/palm1* mutants) and on the leaf surface of *M. truncatula* wild-type plants and the *irg1/palm1* mutant. They found expression of kinase family genes was activated on the hydrophobic surface and on the *M. truncatula* wild type but not on *irg1/palm1*. This result suggested that leaf hydrophobicity or epicuticular waxes may trigger expression of *P. pachyrhizi* genes involved in pre-penetration structure formation (Ishiga et al., 2013). Importance of cutin or cuticular waxes to both, germination and appressoria formation has also been reported for other fungal pathogens of plants (Mendoza-Mendoza et al., 2009; Hansjakob et al., 2011; Weidenbach et al., 2014). Further characterization of the *irg1/palm1* mutant may help better understand asymmetric epicuticular wax loading on leaf surfaces and its importance to plant-pathogen interactions. Additionally, identifying *IRG1/PALM1* orthologues and/or modifying epicuticular wax composition in soybean might be useful to conferring resistance to *P. pachyrhizi*.

Transcriptome analysis of the *M. truncatula–P. pachyrhizi* interaction revealed induction of many genes in the phenylpropanoid, flavonoid, and isoflavonoid pathways (Ishiga et al., 2015). Accompanying metabolome studies disclosed accumulation of the isoflavonoid derivative medicarpin and its intermediates in *P. pachyrhizi*-inoculated plants. Because medicarpin inhibited the germination and differentiation of *P. pachyrhizi* uredospores *in vitro* (Ishiga et al., 2015), the phytoalexin might contribute to NHR to *P. pachyrhizi* in *M. truncatula*. Various studies with *P. pachyrhizi* hosts also pointed to a role of phytoalexins in the interaction of plants with the fungus (Chung and Singh, 2008; Lygin et al., 2009). As the expression of genes in the secondary metabolism is strongly affected upon *P. pachyrhizi* infection in soybean (van de Mortel et al., 2007; Choi et al., 2008; Panthee et al., 2009; Schneider et al., 2011), secondary metabolites seem to be crucial to both host resistance and NHR to SBR.

RNA Interference and Host-Induced Gene Silencing

Another option for controlling SBR is by using RNAi to specifically silence essential *P. pachyrhizi* genes. HIGS, a specific RNAi technique, provided protection from sucking insects, nematodes, fungi, oomycetes, bacteria, and viruses (Koch and Kogel, 2014). To our knowledge there is not a single report on the application of HIGS in soybean for fighting SBR or other fungal diseases. However, knockdown of nematode genes by siRNAs expressed in soybean was demonstrated (Steeves et al., 2006; Li et al., 2010; Niu et al., 2012; Youssef et al., 2013). Moreover, the successful silencing of fungal genes, including those of the rust fungi *Puccinia striiformis*, *P. triticina*, and *P. graminis* in other crops (Yin et al., 2010; Panwar et al., 2013) is testament to the huge potential of this approach for fighting SBR. Various stage-specifically expressed fungal genes that may represent potential HIGS targets (e.g., genes encoding putative effectors like HESPs, kinase family proteins, cell wall degrading enzymes, metabolism-linked genes, succinate dehydrogenase, etc.) have already been identified in *P. pachyrhizi* (Posada-Buitrago and Frederick, 2005; Stone et al., 2012; Tremblay et al., 2012, 2013; Ishiga et al., 2013; Link et al., 2014). Since external application of dsRNAs has proven effective for the control of insect pests (Hunter et al., 2012), this approach might present a non-transgenic alternative to HIGS-mediated SBR control.

Biocontrol

In vitro studies and greenhouse and field trials reported protection by beneficial microbes with antagonistic properties to *P. pachyrhizi*. The fungus *Simplicillium lanosoniveum* preferentially colonizes *P. pachyrhizi* uredinia on infected soybean leaves and thereby significantly reduces SBR development in the field (Ward et al., 2012). Similarly, Kumar and Jha (2002) observed hypertrophy and shrinkage of *P. pachyrhizi* uredospores when colonized with *Trichothecium rosae*. Moreover, several strains of *Bacillus* spp. reduce SBR severity (Dorighello et al., 2015). One *Bacillus* strain that is the active ingredient in the organically approved commercial fungicide Ballad® provides SBR control. Besides antagonistic organisms, plant volatiles, such as farnesyl-acetate, can be used for biocontrol of SBR (Mendgen et al., 2006). Same is true for coffee oil and essential oils from *Hyptis marrubioides*, *Aloysia gratissima,* and *Cordia verbenacea* which suppressed spore germination *in vitro* and reduced SBR severity under greenhouse and/or field conditions (da Silva et al., 2014; Dorighello et al., 2015). Moreover, acibenzolar-*S*-methyl treatment or soil application of silicon reduced SBR severity on soybean leaves (da Cruz et al., 2013). Silicon most likely acts in two ways. First, it establishes a physical penetration barrier when deposited in the subcuticular layer and second, it primes plants for enhanced defense (Ma and Yamaji, 2006; da Cruz et al., 2013). Furthermore, soil application of saccharin and shale water were reported to induce SBR resistance in soybean (Srivastava et al., 2011; Mehta et al., 2015). These examples illustrate the potential of SBR biocontrol. However, the cost-benefit ratio and feasibility of field scale biocontrol needs to be determined to estimate the actual agronomic value of such approaches.

CONCLUSION

Phakopsora pachyrhizi is the causal agent of SBR and thus a major threat to global soybean production. Novel compounds in the SDHI class of fungicides hold promise for successful SBR control in the upcoming years, but *P. pachyrhizi* is likely to become increasingly insensitive to SDHI action as it has been observed for DMI and QoI fungicides. Similarly, the SBR resistance conferred by individual *R* genes was swiftly overcome in the field, but the pyramiding (stacking) of known and yet to be identified *R* genes might overcome traditional *R* gene inefficacy. Exploiting pathway

components for the major plant defense hormones, SA and JA, seems not to be a realistic option for SBR control because component overexpression often impairs plant growth and yield. By contrast, transcription coactivator utilization could have huge potential but their efficacy for effective SBR control is still awaiting assessment in both the lab and field. Synthetic biology approaches to engineer *R* genes and phytoalexin biosynthesis pathways are promising, especially because several phytoalexins antagonize *P. pachyrhizi* both *in vitro* and *in situ*. Loss or elimination of *S* genes also is promising for SBR control but this approach has rarely been followed up. Same is true for the exploitation of soybean accessions with tolerance or PDR to SBR. Though promising, their potential for SBR control is currently unclear. Wild *Glycine* species, alternative *P. pachyrhizi* hosts, and especially non-host plants are promising sources of germplasm for SBR resistance while AMPs, RNAi/HIGS, and biocontrol approaches hold promise for sustainable soybean production in the future. It seems that an integrated approach exploiting different measures is likely to provide the best possible means for the effective control of SBR.

AUTHOR CONTRIBUTIONS

CL, RC, SB, and AM contributed various chapters to the article. CL composed the review. CL, AM, and UC thoroughly reviewed the consecutive manuscript drafts.

FUNDING

Work on *Phakopsora pachyrhizi*-plant interactions in the Conrath lab is supported by BASF Plant Science Company GmbH, German Research Foundation (DFG, CO186/10-1), and the Bioeconomy Science Center (BioSC).

ACKNOWLEDGMENTS

We thank Holger Schultheiss for valuable comments on the manuscript. We also appreciate provision of information by Cláudia Vierira Godoy and Francismar Corrêa Marcelino-Guimarães.

REFERENCES

Alves, M. S., Soares, Z. G., Vidigal, P. M. P., Barros, E. G., Poddanosqui, A. M. P., Aoyagi, L. N., et al. (2015). Differential expression of four soybean bZIP genes during *Phakopsora pachyrhizi* infection. *Funct. Integr. Genomics* 15, 685–696. doi: 10.1007/s10142-015-0445-0

Aoyagi, L. N., Lopes-Caitar, V. S., de Carvalho, M. C. C. G., Darben, L. M., Polizel-Podanosqui, A., Kuwahara, M. K., et al. (2014). Genomic and transcriptomic characterization of the transcription factor family R2R3-MYB in soybean and its involvement in the resistance responses to *Phakopsora pachyrhizi*. *Plant Sci.* 229, 32–42. doi: 10.1016/j.plantsci.2014.08.005

Arias, C. A. A., Toledo, J. F. F., Almeida, L. A., Pipolo, G. E. S., Carneiro, R. V., Abdelnoor, R. V., et al. (2008). "Asian rust in Brazil: varietal resistance," in *Facing the Challenge of Soybean Rust in South America*, eds H. Kudo, K. Suenaga, R. M. S. Soares, and A. Toledo (Tsukuba: JIRCAS), 29–30.

Atamian, H. S., Eulgem, T., and Kaloshian, I. (2012). SlWRKY70 is required for Mi-1-mediated resistance to aphids and nematodes in tomato. *Planta* 235, 299–309. doi: 10.1007/s00425-011-1509-6

Bai, Y., van der Hulst, R., Bonnema, G., Marcel, T. C., Meijer-Dekens, F., Niks, R. E., et al. (2005). Tomato defense to *Oidium neolycopersici*: dominant Ol genes confer isolate-dependent resistance via a different mechanism than recessive ol-2. *Mol. Plant Microbe Interact.* 18, 354–362. doi: 10.1094/MPMI-18-0354

Barbosa, G. F., da Cruz Centurion, M. A. P., Marin, B. T., and Barbosa, G. F. (2013). Effect of reduced fungicide doses on control of soybean Asian rust and bean yield. *Interciencia* 38, 347–352.

Bencke-Malato, M., Cabreira, C., Wiebke-Strohm, B., Bücker-Neto, L., Mancini, E., Osorio, M. B., et al. (2014). Genome-wide annotation of the soybean WRKY family and functional characterization of genes involved in response to *Phakopsora pachyrhizi* infection. *BMC Plant Biol.* 14:236. doi: 10.1186/s12870-014-0236-0

Bettgenhaeuser, J., Gilbert, B., Ayliffe, M., and Moscou, M. J. (2014). Nonhost resistance to rust pathogens – a continuation of continua. *Front. Plant Sci.* 5:664. doi: 10.3389/fpls.2014.00664

Bhor, T. J., Chimote, V. P., and Deshmukh, M. P. (2014). Inheritance of rust (*Phakopsora pachyrhizi*) resistance in soybean. *J. Food Legum* 27, 177–185. doi: 10.4238/2014.July.25.18

Bhor, T. J., Chimote, V. P., and Deshmukh, M. P. (2015). Molecular tagging of Asiatic soybean rust resistance in exotic genotype EC 241780 reveals complementation of two genes. *Plant Breed.* 134, 70–77. doi: 10.1111/pbr.12240

Bilgin, D., de Lucia, E. H., Zangerl, A. R., and Singh, R. J. (2009). *Plant-Derived Biofungicide Against Soybean Rust Disease.* U.S. Provisional Patent Application No 12/370,373. Washington, DC: U.S. Patent and Trademark Office.

Boerjan, W., Ralph, J., and Baucher, M. (2003). Lignin biosynthesis. *Annu. Rev. Plant Biol.* 54, 519–546. doi: 10.1146/annurev.arplant.54.031902.134938

Bolon, Y., Stec, A. O., Michno, J., Roessler, J., Bhaskar, P. B., Ries, L., et al. (2014). Genome resilience and prevalence of segmental duplications following fast neutron irradiation of soybean. *Genetics* 198, 967–981. doi: 10.1534/genetics.114.170340

Bolon, Y.-T., Haun, W. J., Xu, W. W., Grant, D., Stacey, M. G., Nelson, R. T., et al. (2011). Phenotypic and genomic analyses of a fast neutron mutant population resource in soybean. *Plant Physiol.* 156, 240–253. doi: 10.1104/pp.110.170811

Bonde, M. R., Nester, S. E., Moore, W. F., and Allen, T. W. (2009). Comparative susceptibility of kudzu accessions from the southeastern United States to infection by *Phakopsora pachyrhizi*. *Plant Dis.* 93, 593–598. doi: 10.1094/PDIS-93-6-0593

Bowling, S. A., Guo, A., Cao, H., Gordon, A. S., Klessig, D. F., and Dong, X. (1994). A mutation in *Arabidopsis* that leads to constitutive expression of systemic acquired resistance. *Plant Cell* 6, 1845–1857. doi: 10.1105/tpc.6.12.1845

Bradley, C. A. (2007). "Fungicide resistance management in soybean," in *Using Foliar Fungicides to Manage Soybean Rust*, eds A. E. Dorrance, M. A. Draper, and D. E. Hershman (Columbus, OH: Land-Grant Universities Cooperating NCERA-208 and OMAF), 57–60.

Brand, G. D., Magalhães, M. T. Q., Tinoco, M. L. P., Aragão, F. J. L., Nicoli, J., Kelly, S. M., et al. (2012). Probing protein sequences as sources for encrypted antimicrobial peptides. *PLoS ONE* 7:e45848. doi: 10.1371/journal.pone.0045848

Brent, K. J., and Holloman, D. W. (2007). *Fungicide Resistance in Crop Pathogens: How Can It Be Managed?* Brussels: CropLife International.

Bromfield, K. R. (1984). *Soybean Rust*. St. Paul, MN: American Phytopathological Society.

Bromfield, K. R., and Hartwig, E. E. (1980). Resistance to soybean rust (*Phakopsora pachyrhizi*) and mode of inheritance. *Crop Sci.* 20, 254–255. doi: 10.1071/AR9800951

Bromfield, K. R., and Melching, J. S. (1982). Sources of specific resistance to soybean rust. *Phytopathology* 72:706.

Burdon, J. J. (1987). Phenotypic and genetic patterns of resistance to the pathogen *Phakopsora pachyrhizi* in populations of *Glycine canescens*. *Oecologia* 73, 257–267. doi: 10.1007/BF00377516

Burdon, J. J. (1988). Major gene resistance to *Phakopsora pachyrhizi* in *Glycine canescens*, a wild relative of soybean. *Theor. Appl. Genet.* 75, 923–928. doi: 10.1007/BF00258055

Burdon, J. J., and Speer, S. S. (1984). A set of differential *Glycine* hosts for the identification of races of *Phakopsora pachyrhizi* Syd. *Euphytica* 33, 891–896. doi: 10.1007/BF00021917

Büschges, R., Hollricher, K., Panstruga, R., Simons, G., Wolter, M., Frijters, A., et al. (1997). The barley Mlo gene: a novel control element of plant pathogen resistance. *Cell* 88, 695–705. doi: 10.1016/S0092-8674(00)81912-1

Calvo, ÉS., Kiihl, R. A. S., Garcia, A., Harada, A., and Hiromoto, D. M. (2008). Two major recessive soybean genes conferring soybean rust resistance. *Crop Sci.* 48, 1350–1354. doi: 10.2135/cropsci2007.10.0589

Campe, R., Loehrer, M., Conrath, U., and Goellner, K. (2014). *Phakopsora pachyrhizi* induces defense marker genes to necrotrophs in *Arabidopsis thaliana*. *Physiol. Mol. Plant Pathol.* 87, 1–8. doi: 10.1016/j.pmpp.2014.04.005

Cannon, S. B., and Shoemaker, R. C. (2012). Evolutionary and comparative analyses of the soybean genome. *Breed. Sci.* 61, 437–444. doi: 10.1270/jsbbs.61.437

Cao, H., Li, X., and Dong, X. (1998). Generation of broad-spectrum disease resistance by overexpression of an essential regulatory gene in systemic acquired resistance. *Proc. Natl. Acad. Sci. U.S.A.* 95, 6531–6536. doi: 10.1073/pnas.95.11.6531

Chang, Y. C., Nair, M. G., and Nitiss, J. L. (1995). Metabolites of daidzein and genistein and their biological activities. *J. Nat. Prod.* 58, 1901–1905. doi: 10.1021/np50126a016

Chen, X.-K., Zhang, J.-Y., Zhang, Z., Du, X.-L., Du, B.-B., and Qu, S.-C. (2012). Overexpressing MhNPR1 in transgenic Fuji apples enhances resistance to apple powdery mildew. *Mol. Biol. Rep.* 39, 8083–8089. doi: 10.1007/s11033-012-1655-3

Chern, M., Fitzgerald, H. A., Canlas, P. E., Navarre, D. A., and Ronald, P. C. (2005). Overexpression of a rice NPR1 homolog leads to constitutive activation of defense response and hypersensitivity to light. *Mol. Plant Microbe. Interact.* 18, 511–520. doi: 10.1094/MPMI-18-0511

Chiang, H. S., and Norris, D. M. (1983). Phenolic and tannin contents as related to anatomical parameters of soybean resistance to agromyzid bean flies. *J. Agric. Food Chem.* 31, 726–730. doi: 10.1021/jf00118a012

Choi, J. J., Alkharouf, N. W., Schneider, K. T., Matthews, B. F., and Frederick, R. D. (2008). Expression patterns in soybean resistant to *Phakopsora pachyrhizi* reveal the importance of peroxidases and lipoxygenases. *Funct. Integr. Genomics* 8, 341–359. doi: 10.1007/s10142-008-0080-0

Chung, G., and Singh, R. J. (2008). Broadening the genetic base of soybean: a multidisciplinary approach. *Crit. Rev. Plant Sci.* 27, 295–341. doi: 10.1080/07352680802333904

Cooper, B., Campbell, K. B., Feng, J., Garrett, W. M., and Frederick, R. (2011). Nuclear proteomic changes linked to soybean rust resistance. *Mol. Biosyst.* 7, 773–783. doi: 10.1039/C0MB00171F

Cooper, B., Campbell, K. B., McMahon, M. B., and Luster, D. G. (2013). Disruption of Rpp1-mediated soybean rust immunity by virus-induced gene silencing. *Plant Signal. Behav.* 8:e27543. doi: 10.4161/psb.27543

Cooper, J. L., Till, B. J., Laport, R. G., Darlow, M. C., Kleffner, J. M., Jamai, A., et al. (2008). TILLING to detect induced mutations in soybean. *BMC Plant Biol.* 8:9. doi: 10.1186/1471-2229-8-9

da Cruz, M. F. A., Rodrigues, F. Á, Polanco, L. R., da Silva Curvêlo, C. R., Nascimento, K. J. T., Moreira, M. A., et al. (2013). Inducers of resistance and silicon on the activity of defense enzymes in the soybean-*Phakopsora pachyrhizi* interaction. *Bragantia* 72, 162–172. doi: 10.1590/S0006-87052013005000025

da Silva, A. C., de Souza, P. E., Amaral, D. C., Zeviani, W. M., and Pinto, J. E. B. P. (2014). Essential oils from *Hyptis* marrubioides, *Aloysia gratissima* and *Cordia verbenacea* reduce the progress of Asian soybean rust. *Acta Sci. Agron.* 36, 159–166. doi: 10.4025/actasciagron.v36i2.17441

Dixon, R. A., Achnine, L., Kota, P., Liu, C.-J., Reddy, M. S. S., and Wang, L. (2002). The phenylpropanoid pathway and plant defence-a genomics perspective. *Mol. Plant Pathol.* 3, 371–390. doi: 10.1046/j.1364-3703.2002.00131.x

Dorighello, D. V., Bettiol, W., Maia, N. B., and de Campos Leite, R. M. V. B. (2015). Controlling Asian soybean rust (*Phakopsora pachyrhizi*) with *Bacillus* spp. and coffee oil. *Crop Prot.* 67, 59–65. doi: 10.1016/j.cropro.2014.09.017

Falk, A., Feys, B. J., Frost, L. N., Jones, J. D. G., Daniels, M. J., and Parker, J. E. (1999). EDS1, an essential component of *R* gene-mediated disease resistance in *Arabidopsis* has homology to eukaryotic lipases. *Proc. Natl. Acad. Sci. U.S.A.* 96, 3292–3297. doi: 10.1073/pnas.96.6.3292

Francis, D. M., Merk, H. L., and Namuth-Covert, D. (2012). Gene pyramiding using molecular markers. *Plant Breed. Genomics*. Available at: http://articles.extension.org/pages/32465/gene-pyramiding-using-molecular-markers

Fu, Z. Q., and Dong, X. (2013). Systemic acquired resistance: turning local infection into global defense. *Annu. Rev. Plant Biol.* 64, 839–863. doi: 10.1146/annurev-arplant-042811-105606

Garcia, A., Calvo, E. S., de Souza Kiihl, R. A., Harada, A., Hiromoto, D. M., and Vieira, L. G. (2008). Molecular mapping of soybean rust (*Phakopsora pachyrhizi*) resistance genes: discovery of a novel locus and alleles. *Theor. Appl. Genet.* 117, 545–553. doi: 10.1007/s00122-008-0798-z

Gawehns, F., Cornelissen, B. J. C., and Takken, F. L. W. (2013). The potential of effector-target genes in breeding for plant innate immunity. *Microb. Biotechnol.* 6, 223–229. doi: 10.1111/1751-7915.12023

Giannakopoulou, A., Steele, J. F. C., Segretin, M. E., Bozkurt, T., Zhou, J., Robatzek, S., et al. (2015). Tomato I2 immune receptor can be engineered to confer partial resistance to the oomycete *Phytophthora infestans* in addition to the fungus *Fusarium oxysporum*. *Mol. Plant Microbe Interact.* 27, 624–637. doi: 10.1094/MPMI-07-15-0147-R

Gill, N., Findley, S., Walling, J. G., Hans, C., Ma, J., Doyle, J., et al. (2009). Molecular and chromosomal evidence for allopolyploidy in soybean. *Plant Physiol.* 151, 1167–1174. doi: 10.1104/pp.109.137935

Godoy, C. V. (2011). "*Phakopsora pachyrhizi*: the performance of soybean rust fungicides over years and regions in Brazil," in *Modern Fungicides and Antifungal Compounds VI*, eds H. W. Dehne, H. B. Deising, U. Gisi, K. H. Kuck, P. E. Russell, and H. Lyr (Braunschweig: Deutsche Phytomedizinische Gesellschaft e.V. Selbstverlag), 203–209.

Godoy, C. V. (2012). "Risk and management of fungicide resistance in the Asian soybean rust fungus *Phakopsora pachyrhizi*," in *Fungicide Resistance in Crop Protection: Risk and Management*, ed. T. S. Thind (Wallingford: CABI), 87–95. doi: 10.1079/9781845939052.0000

Godoy, C. V., Bueno, A. F., and Gazziero, D. L. P. (2015). Brazilian soybean pest management and threats to its sustainability. *Outlooks Pest Manag.* 26, 113–117. doi: 10.1564/v26_jun_06

Goellner, K., Loehrer, M., Langenbach, C., Conrath, U., Koch, E., and Schaffrath, U. (2010). *Phakopsora pachyrhizi*, the causal agent of Asian soybean rust. *Mol. Plant Pathol.* 11, 169–177. doi: 10.1111/j.1364-3703.2009.00589.x

Grasso, V., Palermo, S., Sierotzki, H., Garibaldi, A., and Gisi, U. (2006a). Cytochrome b gene structure and consequences for resistance to Qo inhibitor fungicides in plant pathogens. *Pest Manag. Sci.* 62, 465–472. doi: 10.1002/ps.1236

Grasso, V., Sierotzki, H., Garibaldi, A., and Gisi, U. (2006b). Characterization of the cytochrome b gene fragment of *Puccinia* species responsible for the binding site of QoI fungicides. *Pestic. Biochem. Physiol.* 84, 72–82. doi: 10.1016/j.pestbp.2005.05.005

Grasso, V., Sierotzki, H., Garibaldi, A., and Gisi, U. (2006c). Relatedness among agronomically important rusts based on mitochondrial cytochrome b gene and ribosomal ITS sequences. *J. Phytopathol.* 154, 110–118. doi: 10.1111/j.1439-0434.2006.01070.x

Guicherit, E., Bartlett, D., Dale, S. M., Haas, H. U., Scalliet, G., Walter, H., et al. (2014). "Solatenol-the second generation benzonorbornene SDHI carboxamide with outstanding performance against key crop diseases," in *Modern Fungicides and Antifungal Compounds VII*, eds H. W. Dehne, H. B. Deising, B. Fraaije, U. Gisi, D. Hermann, A. Mehl, et al. (Braunschweig: Deutsche Phytomedizinische Gesellschaft e.V. Selbstverlag), 67–72.

Hahlbrock, K., and Scheel, D. (1989). Physiology and molecular biology of phenylpropanoid metabolism. *Annu. Rev. Plant Physiol. Plant Mol. Biol.* 40, 347–369. doi: 10.1146/annurev.pp.40.060189.002023

Hansjakob, A., Riederer, M., and Hildebrandt, U. (2011). Wax matters: absence of very-long-chain aldehydes from the leaf cuticular wax of the glossy11 mutant of maize compromises the prepenetration processes of *Blumeria graminis*. *Plant Pathol.* 60, 1151–1161. doi: 10.1111/j.1365-3059.2011.02467.x

Hartman, G. L., Frederick, R. D., and Miles, M. R. (2005). Breeding for resistance to soybean rust. *Plant Dis.* 89, 664–666. doi: 10.1094/PD-89-0664

Hartwig, E., and Bromfield, K. (1983). Relationships among three genes conferring specific resistance to rust in soybeans. *Crop Sci.* 23, 237–239. doi: 10.2135/cropsci1983.0011183X002300020012x

Hartwig, E. E. (1986). Identification of a fourth major gene conferring resistance to soybean rust. *Crop Sci.* 26, 1135–1136. doi: 10.2135/cropsci1986.0011183X002600060010x

Humphry, M., Consonni, C., and Panstruga, R. (2006). mlo-based powdery mildew immunity: silver bullet or simply non-host resistance? *Mol. Plant Pathol.* 7, 605–610. doi: 10.1111/j.1364-3703.2006.00362.x

Hunter, W. B., Glick, E., Paldi, N., and Bextine, B. R. (2012). Advances in RNA interference: dsRNA treatment in trees and grapevines for insect pest suppression. *Southwest. Entomol.* 37, 85–87. doi: 10.3958/059.037.0110

Ishiga, Y., Rao Uppalapati, S., Gill, U. S., Huhman, D., Tang, Y., and Mysore, K. S. (2015). Transcriptomic and metabolomic analyses identify a role for chlorophyll catabolism and phytoalexin during Medicago nonhost resistance against Asian soybean rust. *Sci. Rep.* 5:13061. doi: 10.1038/srep13061

Ishiga, Y., Uppalapati, S. R., and Mysore, K. S. (2013). Expression analysis reveals a role for hydrophobic or epicuticular wax signals in pre-penetration structure formation of *Phakopsora pachyrhizi*. *Plant Signal. Behav.* 8:e26959. doi: 10.4161/psb.26959

Jacobs, T. B., LaFayette, P. R., Schmitz, R. J., and Parrott, W. A. (2015). Targeted genome modifications in soybean with CRISPR/Cas9. *BMC Biotechnol.* 15:16. doi: 10.1186/s12896-015-0131-2

Jarosz, A. M., and Burdon, J. J. (1990). Predominance of a single major gene for resistance to *Phakopsora pachyrhizi* in a population of *Glycine argyrea*. *Heredity* 64, 347–353. doi: 10.1038/hdy.1990.43

Jirage, D., Tootle, T. L., Reuber, T. L., Frost, L. N., Feys, B. J., Parker, J. E., et al. (1999). *Arabidopsis thaliana* PAD4 encodes a lipase-like gene that is important for salicylic acid signaling. *Proc. Natl. Acad. Sci. U.S.A.* 96, 13583–13588. doi: 10.1073/pnas.96.23.13583

Jordan, S. A., Mailhot, D. J., Gevens, A. J., Marois, J. J., Wright, D. L., Harmon, C. L., et al. (2010). Characterization of kudzu (*Pueraria* spp.) resistance to Phakopsora pachyrhizi, the causal agent of soybean rust. *Phytopathology* 100, 941–948. doi: 10.1094/PHYTO-100-9-0941

Kang, B.-C., Yeam, I., Frantz, J. D., Murphy, J. F., and Jahn, M. M. (2005). The pvr1 locus in *Capsicum* encodes a translation initiation factor eIF4E that interacts with Tobacco etch virus VPg. *Plant J.* 42, 392–405. doi: 10.1111/j.1365-313X.2005.02381.x

Kendrick, M. D., Harris, D. K., Ha, B.-K., Hyten, D. L., Cregan, P. B., Frederick, R. D., et al. (2011). Identification of a second Asian soybean rust resistance gene in Hyuuga soybean. *Phytopathology* 101, 535–543. doi: 10.1094/PHYTO-09-10-0257

Kim, Y.-S., Dixon, E. W., Vincelli, P., and Farman, M. L. (2003). Field resistance to strobilurin (QoI) fungicides in *Pyricularia grisea* caused by mutations in the mitochondrial cytochrome b gene. *Phytopathology* 93, 891–900. doi: 10.1094/PHYTO.2003.93.7.891

Klosowski, A. C., May De Mio, L. L., Miessner, S., Rodrigues, R., and Stammler, G. (2015). Detection of the F129L mutation in the cytochrome b gene in *Phakopsora pachyrhizi*. *Pest Manag. Sci.* 72, 1211–1215. doi: 10.1002/ps.4099

Koch, A., and Kogel, K. (2014). New wind in the sails: improving the agronomic value of crop plants through RNAi-mediated gene silencing. *Plant Biotechnol. J.* 12, 821–831. doi: 10.1111/pbi.12226

Kretschmer, M., Leroch, M., Mosbach, A., Walker, A.-S., Fillinger, S., Mernke, D., et al. (2009). Fungicide-driven evolution and molecular basis of multidrug resistance in field populations of the grey mould fungus *Botrytis cinerea*. *PLoS Pathog.* 5:e1000696. doi: 10.1371/journal.ppat.1000696

Kumar, S., and Jha, D. K. (2002). *Trichothecium roseum*: a potential agent for the biological control of soybean rust. *Indian Phytopathol.* 55, 232–234.

La Camera, S., Gouzerh, G., Dhondt, S., Hoffmann, L., Fritig, B., Legrand, M., et al. (2004). Metabolic reprogramming in plant innate immunity: the contributions of phenylpropanoid and oxylipin pathways. *Immunol. Rev.* 198, 267–284. doi: 10.1111/j.0105-2896.2004.0129.x

Langenbach, C., Campe, R., Schaffrath, U., Goellner, K., and Conrath, U. (2013). UDP-glucosyltransferase UGT84A2/BRT1 is required for *Arabidopsis* nonhost resistance to the Asian soybean rust pathogen *Phakopsora pachyrhizi*. *New Phytol.* 198, 536–545. doi: 10.1111/nph.12155

Langenbach, C., Schultheiss, H., Rosendahl, M., Tresch, N., Conrath, U., and Goellner, K. (2016). Interspecies gene transfer provides soybean resistance to a fungal pathogen. *Plant Biotechnol. J.* 14, 699–708. doi: 10.1111/pbi.12418

Leiminger, J. H., Adolf, B., and Hausladen, H. (2014). Occurrence of the F129L mutation in *Alternaria solani* populations in Germany in response to QoI application, and its effect on sensitivity. *Plant Pathol.* 63, 640–650. doi: 10.1111/ppa.12120

Lemos, N. G., de Lucca e Braccini, A., Abdelnoor, R. V., de Oliveira, M. C. N., Suenaga, K., and Yamanaka, N. (2011). Characterization of genes Rpp2, Rpp4, and Rpp5 for resistance to soybean rust. *Euphytica* 182, 53–64. doi: 10.1007/s10681-011-0465-3

Li, J., Todd, T. C., Oakley, T. R., Lee, J., and Trick, H. N. (2010). Host-derived suppression of nematode reproductive and fitness genes decreases fecundity of *Heterodera glycines* Ichinohe. *Planta* 232, 775–785. doi: 10.1007/s00425-010-1209-7

Li, S., Smith, J. R., Ray, J. D., and Frederick, R. D. (2012). Identification of a new soybean rust resistance gene in PI 567102B. *Theor. Appl. Genet.* 125, 133–142. doi: 10.1007/s00122-012-1821-y

Li, X., Clarke, J. D., Zhang, Y., and Dong, X. (2001). Activation of an EDS1-mediated R -gene pathway in the snc1 mutant leads to constitutive, NPR1-independent pathogen resistance. *Mol. Plant Microbe Interact.* 14, 1131–1139. doi: 10.1094/MPMI.2001.14.10.1131

Link, T. I., Lang, P., Scheffler, B. E., Duke, M. V., Graham, M. A., Cooper, B., et al. (2014). The haustorial transcriptomes of *Uromyces appendiculatus* and *Phakopsora pachyrhizi* and their candidate effector families. *Mol. Plant. Pathol.* 15, 379–393. doi: 10.1111/mpp.12099

Lipka, V., Dittgen, J., Bednarek, P., Bhat, R., Wiermer, M., Stein, M., et al. (2005). Pre- and postinvasion defenses both contribute to nonhost resistance in *Arabidopsis*. *Science* 310, 1180–1183. doi: 10.1126/science.1119409

Loehrer, M., Langenbach, C., Goellner, K., Conrath, U., and Schaffrath, U. (2008). Characterization of nonhost resistance of *Arabidopsis* to the Asian soybean rust. *Mol. Plant Microbe Interact.* 21, 1421–1430. doi: 10.1094/MPMI-21-11-1421

Loehrer, M., and Schaffrath, U. (2011). "Asian soybean rust – meet a prominent challenge in soybean cultivation," in *Soybean - Biochemistry, Chemistry and Physiology*, ed. T. -B. Ng (Rijeka: InTech), 83–100. doi: 10.5772/15651

Loehrer, M., Vogel, A., Huettel, B., Reinhardt, R., Benes, V., Duplessis, S., et al. (2014). On the current status of *Phakopsora pachyrhizi* genome sequencing. *Front. Plant Sci.* 5:377. doi: 10.3389/fpls.2014.00377

Long, J., Holland, J. B., Munkvold, G. P., and Jannink, J.-L. (2006). Responses to selection for partial resistance to crown rust in oat. *Crop Sci.* 46, 1260–1265. doi: 10.2135/cropsci2005.06-0169

Lozano-Torres, J. L., Wilbers, R. H. P., Gawronski, P., Boshoven, J. C., Finkers-Tomczak, A., Cordewener, J. H. G., et al. (2012). Dual disease resistance mediated by the immune receptor Cf-2 in tomato requires a common virulence target of a fungus and a nematode. *Proc. Natl. Acad. Sci. U.S.A.* 109, 10119–10124. doi: 10.1073/pnas.1202867109

Lygin, A. V., Li, S., Vittal, R., Widholm, J. M., Hartman, G. L., and Lozovaya, V. V. (2009). The importance of phenolic metabolism to limit the growth of *Phakopsora pachyrhizi*. *Phytopathology* 99, 1412–1420. doi: 10.1094/PHYTO-99-12-1412

Lyngkjær, M. F., Newton, A. C., Atzema, J. L., and Baker, S. J. (2000). The barley mlo-gene: an important powdery mildew resistance source. *Agronomy* 20, 745–756. doi: 10.1051/agro:2000173

Ma, J. F., and Yamaji, N. (2006). Silicon uptake and accumulation in higher plants. *Trends Plant Sci.* 11, 392–397. doi: 10.1016/j.tplants.2006.06.007

Maltby, L., Brock, T. C. M., and van den Brink, P. J. (2009). Fungicide risk assessment for aquatic ecosystems: importance of interspecific variation, toxic mode of action, and exposure regime. *Environ. Sci. Technol.* 43, 7556–7563. doi: 10.1021/es901461c

Maphosa, M., Talwana, H., and Tukamuhabwa, P. (2012). Enhancing soybean rust resistance through Rpp2, Rpp3 and Rpp4 pair wise gene pyramiding. *African J. Agric. Res.* 7, 4271–4277. doi: 10.5897/AJAR12.1123

Mathieu, M., Winters, E. K., Kong, F., Wan, J., Wang, S., Eckert, H., et al. (2009). Establishment of a soybean (*Glycine max* Merr. L) transposon-based mutagenesis repository. *Planta* 229, 279–289. doi: 10.1007/s00425-008-0827-9

McDonald, B. A. (2014). Using dynamic diversity to achieve durable disease resistance in agricultural ecosystems. *Trop. Plant Pathol.* 39, 191–196. doi: 10.1590/S1982-56762014000300001

McDonald, B. A., and Linde, C. (2002). Pathogen population genetics, evolutionary potential, and durable resistance. *Annu. Rev. Phytopathol.* 40, 349–379. doi: 10.1146/annurev.phyto.40.120501.101443

McLean, R. J., and Byth, D. E. (1980). Inheritance of resistance to rust (*Phakopsora pachyrhizi*) in soybeans. *Aust. J. Agric. Res.* 31, 951–956. doi: 10.1071/AR9800951

Mehta, Y. R., Marangoni, M. S., Matos, J. N., Mandarino, J. M. G., and Galbieri, R. (2015). Systemic acquired resistance of soybean to soybean rust induced by shale water. *Am. J. Plant Sci.* 6, 2249–2256. doi: 10.4236/ajps.2015.614227

Mendgen, K., Wirsel, S. G. R., Jux, A., Hoffmann, J., and Boland, W. (2006). Volatiles modulate the development of plant pathogenic rust fungi. *Planta* 224, 1353–1361. doi: 10.1007/s00425-006-0320-2

Mendoza-Mendoza, A., Berndt, P., Djamei, A., Weise, C., Linne, U., Marahiel, M., et al. (2009). Physical-chemical plant-derived signals induce differentiation in *Ustilago maydis*. *Mol. Microbiol.* 71, 895–911. doi: 10.1111/j.1365-2958.2008.06567.x

Meyer, J. D. F., Silva, D. C. G., Yang, C., Pedley, K. F., Zhang, C., van de Mortel, M., et al. (2009). Identification and analyses of candidate genes for Rpp4-mediated resistance to Asian soybean rust in soybean. *Plant Physiol.* 150, 295–307. doi: 10.1104/pp.108.134551

Miles, M. R., Pastor-Corrales, M. A., Hartman, G. L., and Frederick, R. D. (2007). Differential response of common bean cultivars to *Phakopsora pachyrhizi*. *Plant Dis.* 91, 698–704. doi: 10.1094/PDIS-91-6-0698

Monteros, M. J., Missaoui, A. M., Phillips, D. V., Walker, D. R., and Boerma, H. R. (2007). Mapping and confirmation of the "Hyuuga" red-brown lesion resistance gene for Asian soybean rust. *Crop Sci.* 47, 829–834. doi: 10.2135/cropsci06.07.0462

Morales, A. M. A. P., O'Rourke, J. A., van de Mortel, M., Scheider, K. T., Bancroft, T. J., Borém, A., et al. (2013). Transcriptome analyses and virus induced gene silencing identify genes in the Rpp4-mediated Asian soybean rust resistance pathway. *Funct. Plant Biol.* 40, 1029–1047. doi: 10.1071/FP12296

Mueller, A. N., Ziemann, S., Treitschke, S., Aßmann, D., and Doehlemann, G. (2013). Compatibility in the *Ustilago maydis*–maize interaction requires inhibition of host cysteine proteases by the fungal effector Pit2. *PLoS Pathog.* 9:e1003177. doi: 10.1371/journal.ppat.1003177

Mueller, T. A., Miles, M. R., Morel, W., Marois, J. J., Wright, D. L., Kemerait, R. C., et al. (2009). Effect of fungicide and timing of application on soybean rust severity and yield. *Plant Dis.* 93, 243–248. doi: 10.1094/PDIS-93-3-0243

Narusaka, M., Shirasu, K., Noutoshi, Y., Kubo, Y., Shiraishi, T., Iwabuchi, M., et al. (2009). RRS1 and RPS4 provide a dual resistance-gene system against fungal and bacterial pathogens. *Plant J.* 60, 218–226. doi: 10.1111/j.1365-313X.2009.03949.x

Nawrath, C., Heck, S., Parinthawong, N., and Metraux, J. P. (2002). EDS5, an essential component of salicylic acid-dependent signaling for disease resistance in *Arabidopsis*, is a member of the MATE transporter family. *Plant Cell* 14, 275–286. doi: 10.1105/tpc.010376

Niu, J., Jian, H., Xu, J., Chen, C., Guo, Q., Liu, Q., et al. (2012). RNAi silencing of the Meloidogyne incognita Rpn7 gene reduces nematode parasitic success. *Eur. J. Plant Pathol.* 134, 131–144. doi: 10.10007/s10658-012-9971-y

Nombela, G., Williamson, V. M., and Muñiz, M. (2003). The root-knot nematode resistance gene Mi-1.2 of tomato is responsible for resistance against the whitefly *Bemisia tabaci*. *Mol. Plant Microbe Interact.* 16, 645–649. doi: 10.1094/MPMI.2003.16.7.645

Oliver, R. P. (2014). A reassessment of the risk of rust fungi developing resistance to fungicides. *Pest Manag. Sci.* 70, 1641–1645. doi: 10.1002/ps.3767

Pandey, A. K., Yang, C., Zhang, C., Graham, M. A., Horstman, H. D., Lee, Y., et al. (2011). Functional analysis of the Asian soybean rust resistance pathway mediated by Rpp2. *Mol. Plant Microbe Interact.* 24, 194–206. doi: 10.1094/MPMI-08-10-0187

Panthee, D. R., Marois, J. J., Wright, D. L., Narváez, D., Yuan, J. S., and Stewart, C. N. (2009). Differential expression of genes in soybean in response to the causal agent of Asian soybean rust (*Phakopsora pachyrhizi* Sydow) is soybean growth stage-specific. *Theor. Appl. Genet.* 118, 359–370. doi: 10.1007/s00122-008-0905-1

Panwar, V., McCallum, B., and Bakkeren, G. (2013). Endogenous silencing of *Puccinia triticina* pathogenicity genes through in planta-expressed sequences leads to the suppression of rust diseases on wheat. *Plant J.* 73, 521–532. doi: 10.1111/tpj.12047

Pavan, S., Jacobsen, E., Visser, R. G. F., and Bai, Y. (2010). Loss of susceptibility as a novel breeding strategy for durable and broad-spectrum resistance. *Mol. Breed.* 25, 1–12. doi: 10.1007/s11032-009-9323-6

Pierozzi, P. H. B., Ribeiro, A. S., Moreira, J. U. V., Laperuta, L. D. C., Rachid, B. F., Lima, W. F., et al. (2008). New soybean (*Glycine max* Fabales, Fabaceae) sources of qualitative genetic resistance to Asian soybean rust caused by *Phakopsora pachyrhizi* (Uredinales, Phakopsoraceae). *Genet. Mol. Biol.* 31, 505–511. doi: 10.1590/S1415-47572008000300018

Pieterse, C. M. J., van der Does, D., Zamioudis, C., Leon-Reyes, A., and van Wees, S. C. M. (2012). Hormonal modulation of plant immunity. *Annu. Rev. Cell Dev. Biol.* 28, 489–521. doi: 10.1146/annurev-cellbio-092910-154055

Posada-Buitrago, M. L., and Frederick, R. D. (2005). Expressed sequence tag analysis of the soybean rust pathogen *Phakopsora pachyrhizi*. *Fungal Genet. Biol.* 42, 949–962. doi: 10.1016/j.fgb.2005.06.004

Rahnamaeian, M. (2011). Antimicrobial peptides: modes of mechanism, modulation of defense responses. *Plant Signal. Behav.* 6, 1325–1332. doi: 10.4161/psb.6.9.16319

Reis, E. M., Deuner, E., Zanatta, M., Reis, E. M., Deuner, E., and Zanatta, M. (2015). In vivo sensitivity of *Phakopsora pachyrhizi* to DMI and QoI fungicides. *Summa Phytopathol.* 41, 21–24. doi: 10.1590/0100-5405/1975

Salomon, D., and Sessa, G. (2012). "Biotechnological strategies for engineering plants with durable resistance to fungal and bacterial pathogens," in *Plant Biotechnology and Agriculture -Prospects for the 21st Century-*, eds A. Altman and P. M. Hasegawa (Cambridge, MS: Academic Press), 329–342. doi: 10.1016/B978-0-12-381466-1.00021-3

Scherm, H., Christiano, R. S. C., Esker, P. D., Del Ponte, E. M., and Godoy, C. V. (2009). Quantitative review of fungicide efficacy trials for managing soybean rust in Brazil. *Crop Prot.* 28, 774–782. doi: 10.1016/j.cropro.2009.05.006

Schmitz, H. K., Medeiros, C.-A., Craig, I. R., and Stammler, G. (2014). Sensitivity of *Phakopsora pachyrhizi* towards quinone-outside-inhibitors and demethylation-inhibitors, and corresponding resistance mechanisms. *Pest Manag. Sci.* 70, 378–388. doi: 10.1002/ps.3562

Schneider, K. T., van de Mortel, M., Bancroft, T. J., Braun, E., Nettleton, D., Nelson, R. T., et al. (2011). Biphasic gene expression changes elicited by *Phakopsora pachyrhizi* in soybean correlates with fungal penetration and haustoria formation. *Plant Physiol.* 157, 355–371. doi: 10.1104/pp.111.181149

Schulze-Lefert, P., and Panstruga, R. (2011). A molecular evolutionary concept connecting nonhost resistance, pathogen host range, and pathogen speciation. *Trends Plant Sci.* 16, 117–125. doi: 10.1016/j.tplants.2011.01.001

Segretin, M. E., Pais, M., Franceschetti, M., Chaparro-garcia, A., Bos, J. I. B., Banfield, M. J., et al. (2014). Single amino acid mutations in the potato immune receptor R3a expand response to *Phytophthora* effectors. *Mol. Plant Microbe Interact.* 27, 624–637. doi: 10.1094/MPMI-02-14-0040-R

Sierotzki, H., Frey, R., Wullschleger, J., Palermo, S., Karlin, S., Godwin, J., et al. (2007). Cytochrome b gene sequence and structure of *Pyrenophora teres* and *P. tritici-repentis* and implications for QoI resistance. *Pest Manag. Sci.* 63, 225–233. doi: 10.1002/ps.1330

Sierotzki, H., and Scalliet, G. (2013). A review of current knowledge of resistance aspects for the next-generation succinate dehydrogenase inhibitor fungicides. *Phytopathology* 103, 880–887. doi: 10.1094/PHYTO-01-13-0009-RVW

Singh, R. J., and Nelson, R. L. (2015). Intersubgeneric hybridization between *Glycine max* and *G. tomentella*: production of F1, amphidiploid, BC1, BC2, BC3, and fertile soybean plants. *Theor. Appl. Genet.* 128, 1117–1136. doi: 10.1007/s00122-015-2494-0

Slaminko, T. L., Miles, M. R., Frederick, R. D., Bonde, M. R., and Hartman, G. L. (2008). New legume hosts of *Phakopsora pachyrhizi* based on greenhouse evaluations. *Plant Dis.* 92, 767–771. doi: 10.1094/PDIS-92-5-0767

Soria-Guerra, R. E., Rosales-Mendoza, S., Chang, S., Haudenshield, J. S., Padmanaban, A., Rodriguez-Zas, S., et al. (2010). Transcriptome analysis of resistant and susceptible genotypes of *Glycine tomentella* during *Phakopsora pachyrhizi* infection reveals novel rust resistance genes. *Theor. Appl. Genet.* 120, 1315–1333. doi: 10.1007/s00122-009-1258-0

Souza, T. L. P. O., Dessaune, S. N., Moreira, M. A., and Barros, E. G. (2014). Soybean rust resistance sources and inheritance in the common bean (*Phaseolus vulgaris* L.). *Genet. Mol. Res.* 13, 5626–5636. doi: 10.4238/2014.July.25.18

Srivastava, P., George, S., Marois, J. J., Wright, D. L., and Walker, D. R. (2011). Saccharin-induced systemic acquired resistance against rust (*Phakopsora pachyrhizi*) infection in soybean: effects on growth and development. *Crop Prot.* 30, 726–732. doi: 10.1016/j.cropro.2011.02.023

Steeves, R. M., Todd, T. C., Essig, J. S., and Trick, H. N. (2006). Transgenic soybeans expressing siRNAs specific to a major sperm protein gene suppress *Heterodera glycines* reproduction. *Funct. Plant Biol.* 33, 991–999. doi: 10.1071/FP06130

Stone, C. L., McMahon, M. B., Fortis, L. L., Nuñez, A., Smythers, G. W., Luster, D. G., et al. (2012). Gene expression and proteomic analysis of the formation of *Phakopsora pachyrhizi* appressoria. *BMC Genomics* 13:269. doi: 10.1186/1471-2164-13-269

Sun, J. H., Li, Z., Jewett, D. K., Britton, K. O., Ye, W. H., and Ge, X. (2005). Genetic diversity of *Pueraria lobata* (kudzu) and closely related taxa as revealed by inter-simple sequence repeat analysis. *Weed Res.* 45, 255–260. doi: 10.1111/j.1365-3180.2005.00462.x

Tremblay, A., Hosseini, P., Li, S., Alkharouf, N. W., and Matthews, B. F. (2012). Identification of genes expressed by *Phakopsora pachyrhizi*, the pathogen causing soybean rust, at a late stage of infection of susceptible soybean leaves. *Plant Pathol.* 61, 773–786. doi: 10.1111/j.1365-3059.2011.02550.x

Tremblay, A., Hosseini, P., Li, S., Alkharouf, N. W., and Matthews, B. F. (2013). Analysis of *Phakopsora pachyrhizi* transcript abundance in critical pathways at four time-points during infection of a susceptible soybean cultivar using deep sequencing. *BMC Genomics* 14:614. doi: 10.1186/1471-2164-14-614

Tukamuhabwa, P., and Maphosa, M. (2010). *State of Knowledge on Breeding for Durable Resistance to Soybean Rust Disease in the Developing World*. Rome: FAO.

Uppalapati, S. R., Ishiga, Y., Doraiswamy, V., Bedair, M., Mittal, S., Chen, J., et al. (2012). Loss of abaxial leaf epicuticular wax in *Medicago truncatula* irg1/palm1 mutants results in reduced spore differentiation of anthracnose and nonhost rust pathogens. *Plant Cell* 24, 353–370. doi: 10.1105/tpc.111.093104

van de Mortel, M., Recknor, J. C., Graham, M. A., Nettleton, D., Dittman, J. D., Nelson, R. T., et al. (2007). Distinct biphasic mRNA changes in response to Asian soybean rust infection. *Mol. Plant Microbe Interact.* 20, 887–899. doi: 10.1094/MPMI-20-8-0887

Verweij, P. E., Snelders, E., Kema, G. H. J., Mellado, E., and Melchers, W. J. G. (2009). Azole resistance in *Aspergillus fumigatus*: a side-effect of environmental fungicide use? *Lancet. Infect. Dis.* 9, 789–795. doi: 10.1016/S1473-3099(09)70265-8

Vogt, T. (2010). Phenylpropanoid biosynthesis. *Mol. Plant* 3, 2–20. doi: 10.1093/mp/ssp106

Wang, J., Shine, M. B., Gao, Q. M., Navarre, D., Jiang, W., Liu, C., et al. (2014). Enhanced disease susceptibility1 mediates pathogen resistance and virulence function of a bacterial effector in soybean. *Plant Physiol.* 165, 1269–1284. doi: 10.1104/pp.114.242495

Ward, N. A., Robertson, C. L., Chanda, A. K., and Schneider, R. W. (2012). Effects of Simplicillium lanosoniveum on *Phakopsora pachyrhizi*, the soybean rust pathogen, and its use as a biological control agent. *Phytopathology* 102, 749–760. doi: 10.1094/PHYTO-01-11-0031

Weidenbach, D., Jansen, M., Franke, R. B., Hensel, G., Weissgerber, W., Ulferts, S., et al. (2014). Evolutionary conserved function of barley and *Arabidopsis* 3-KETOACYL-CoA SYNTHASES in providing wax signals for germination of powdery mildew fungi. *Plant Physiol.* 166, 1621–1633. doi: 10.1104/pp.114.246348

Wiermer, M., Feys, B. J., and Parker, J. E. (2005). Plant immunity: the EDS1 regulatory node. *Curr. Opin. Plant Biol.* 8, 383–389. doi: 10.1016/j.pbi.2005.05.010

Wightwick, A., Walters, R., Allinson, G., Reichman, S., and Menzies, N. (2010). "Environmental risks of fungicides used in horticultural production systems," in *Fungicides*, ed. O. Carisse (Rijeka: InTech), 273–304.

Xie, K., Zhang, J., and Yang, Y. (2014). Genome-wide prediction of highly specific guide RNA spacers for CRISPR-Cas9-mediated genome editing in model plants and major crops. *Mol. Plant* 7, 923–926. doi: 10.1093/mp/ssu009

Yamanaka, N., Lemos, N. G., Uno, M., Akamatsu, H., Yamaoka, Y., Abdelnoor, R. V., et al. (2013). Resistance to Asian soybean rust in soybean lines with the pyramided three *Rpp* genes. *Crop Breed. Appl. Biotechnol.* 13, 75–82. doi: 10.1590/S1984-70332013000100009

Yamanaka, N., Morishita, M., Mori, T., Lemos, N. G., Hossain, M. M., Akamatsu, H., et al. (2015). Multiple *Rpp*-gene pyramiding confers resistance to Asian soybean rust isolates that are virulent on each of the pyramided genes. *Trop. Plant Pathol.* 40, 283–290. doi: 10.1007/s40858-015-0038-4

Yan, H. H., Mudge, J., Kim, D.-J., Larsen, D., Shoemaker, R. C., Cook, D. R., et al. (2003). Estimates of conserved microsynteny among the genomes of *Glycine max*, *Medicago truncatula* and *Arabidopsis thaliana*. *Theor. Appl. Genet.* 106, 1256–1265. doi: 10.1007/s00122-002-1183-y

Yin, C., Jurgenson, J. E., and Hulbert, S. H. (2010). Development of a host-induced RNAi system in the wheat stripe rust fungus *Puccinia striiformis* f. *sp. tritici*. *Mol. Plant Microbe Interact.* 24, 554–561. doi: 10.1094/MPMI-10-10-0229

Yorinori, J. T., Paiva, W. M., Frederick, R. D., Costamilan, L. M., Bertagnolli, P. F., and Hartman, G. E. (2005). Epidemics of soybean rust (*Phakopsora pachyrhizi*) in Brazil and Paraguay from 2001 to 2003. *Plant Dis.* 89, 675–677. doi: 10.1094/PD-89-0675

Youssef, R. M., Kim, K. H., Haroon, S. A., and Matthews, B. F. (2013). Post-transcriptional gene silencing of the gene encoding aldolase from soybean cyst nematode by transformed soybean roots. *Exp. Parasitol.* 134, 266–274. doi: 10.1016/j.exppara.2013.03.009

Zhang, C., Bradshaw, J. D., Whitham, S. A., and Hill, J. H. (2010). The development of an efficient multipurpose Bean pod mottle virus viral vector set for foreign gene expression and RNA silencing. *Plant Physiol.* 153, 52–65. doi: 10.1104/pp.109.151639

Zhang, C., and Ghabrial, S. A. (2006). Development of Bean pod mottle virus-based vectors for stable protein expression and sequence-specific virus-induced gene silencing in soybean. *Virology* 344, 401–411. doi: 10.1016/j.virol.2005.08.046

Zhang, C., Whitham, S. A., and Hill, J. H. (2013). Virus-induced gene silencing in soybean and common bean. *Methods Mol. Biol.* 975, 149–156. doi: 10.1007/978-1-62703-278-0_11

Conflict of Interest Statement: Author RC is an employee of BASF Plant Science Company GmbH.

frontiers in Plant Science

ORIGINAL RESEARCH
published: 20 June 2016
doi: 10.3389/fpls.2016.00820

Obligate Biotroph Pathogens of the Genus *Albugo* Are Better Adapted to Active Host Defense Compared to Niche Competitors

*Jonas Ruhe[1], Matthew T. Agler[1], Aleksandra Placzek[1], Katharina Kramer[1], Iris Finkemeier[1,2] and Eric M. Kemen[1]**

[1] Max Planck Institute for Plant Breeding Research, Cologne, Germany, [2] Institute of Plant Biology and Biotechnology, University of Muenster, Münster, Germany

Recent research suggested that plants behave differently under combined versus single abiotic and biotic stress conditions in controlled environments. While this work has provided a glimpse into how plants might behave under complex natural conditions, it also highlights the need for field experiments using established model systems. In nature, diverse microbes colonize the phyllosphere of *Arabidopsis thaliana*, including the obligate biotroph oomycete genus *Albugo*, causal agent of the common disease white rust. Biotrophic, as well as hemibiotrophic plant pathogens are characterized by efficient suppression of host defense responses. Lab experiments have even shown that *Albugo* sp. can suppress non-host resistance, thereby enabling otherwise avirulent pathogen growth. We asked how a pathogen that is vitally dependent on a living host can compete in nature for limited niche space while paradoxically enabling colonization of its host plant for competitors? To address this question, we used a proteomics approach to identify differences and similarities between lab and field samples of *Albugo* sp.-infected and -uninfected *A. thaliana* plants. We could identify highly similar apoplastic proteomic profiles in both infected and uninfected plants. In wild plants, however, a broad range of defense-related proteins were detected in the apoplast regardless of infection status, while no or low levels of defense-related proteins were detected in lab samples. These results indicate that *Albugo* sp. do not strongly affect immune responses and leave distinct branches of the immune signaling network intact. To validate our findings and to get mechanistic insights, we tested a panel of *A. thaliana* mutant plants with induced or compromised immunity for susceptibility to different biotrophic pathogens. Our findings suggest that the biotroph pathogen *Albugo* selectively interferes with host defense under different environmental and competitive pressures to maintain its ecological niche dominance. Adaptation to host immune responses while maintaining a partially active host immunity seems advantageous against competitors. We suggest a model for future research that considers not only host–microbe but in addition microbe–microbe and microbe–host environment factors.

Keywords: biotrophy, *Albugo*, apoplast, proteomics, field studies, microbe–microbe interactions, systemic acquired resistance, immunity

OPEN ACCESS

Edited by:
Ralph Panstruga, RWTH Aachen University, Germany

Reviewed by:
Andrea Polle, Georg-August-Universität Göttingen, Germany
Sylvain Cordelier, Université de Reims Champagne-Ardenne, France

****Correspondence:***
Eric M. Kemen
kemen@mpipz.mpg.de

Specialty section:
This article was submitted to Plant Biotic Interactions, a section of the journal Frontiers in Plant Science

Received: *6 January 2016*
Accepted: *25 May 2016*
Published: *20 June 2016*

Citation:
Ruhe J, Agler MT, Placzek A, Kramer K, Finkemeier I and Kemen EM (2016) Obligate Biotroph Pathogens of the Genus Albugo Are Better Adapted to Active Host Defense Compared to Niche Competitors. Front. Plant Sci. 7:820. doi: 10.3389/fpls.2016.00820

INTRODUCTION

In the wild, plants are exposed simultaneously to a variety of environmental stresses. Plant responses to biotic stress caused by microbes or abiotic stress like heat, starvation, or drought are largely distinct, but partly overlapping (Richards et al., 2012). In the laboratory, specific conditions are usually tested in isolation to study how plants react to stress on a molecular level. Ultimately, researchers would like to apply this knowledge to crop plants under field conditions and for this it is important to elucidate how laboratory-based knowledge transfers into nature.

Arabidopsis thaliana is the best-studied species of flowering plant (Koornneef and Meinke, 2010), but knowledge about how it behaves in the wild on a molecular level is still limited. This is because abiotic and biotic stimuli constantly fluctuate during wild plant growth, limiting replicability of field experiments. Under controlled conditions several studies examined how plants behave in response to single factors like salt and osmotic stress (Kreps et al., 2002), temperature change (Fowler and Thomashow, 2002; Kreps et al., 2002; Rizhsky et al., 2004) and drought (Rabello et al., 2008), starvation (Palenchar et al., 2004; Lian et al., 2006), or biotic stresses (Schenk et al., 2000; De Vos et al., 2005; Amrine et al., 2015; Lewis et al., 2015). Responses apparently interact, however, since gene expression analysis demonstrated that single stress responses cannot sufficiently predict changes after combined stresses (Mittler, 2006; Rasmussen et al., 2013). Therefore, to understand, for example, biotic stress responses, lab experiments with single stresses in isolation should be compared to the same stress under natural conditions.

The first studies on plant behavior under natural conditions showed that the transcriptome is mostly affected by circadian rhythm, environmental stimuli, and plant age (Nagano et al., 2012; Richards et al., 2012). Many gene clusters co-expressed under natural conditions are enriched in loci responsive to (a-)biotic stimuli, which suggests that stress-responsive genes are deployed during the whole life cycle of *A. thaliana* (Richards et al., 2012). It is not clear yet how these transcription results translate into protein abundances in the field.

In the field, white blister rust, caused by the obligate biotroph oomycete genus *Albugo*, is one of the most widespread diseases of Brassicaceae (Ploch and Thines, 2011). *Albugo* sp. enter via stomata, form intercellular hyphae, penetrate the plant cell wall and invaginate the plant plasma membrane with haustoria in order to take up plant nutrients and release effector proteins into host cells (Kemen et al., 2005; Rafiqi et al., 2010; Spanu and Kämper, 2010; Kemen and Jones, 2012). To complete their whole lifecycle on the living host plant, obligate biotroph pathogens must be highly adapted to the host. Research on the effector complement of hemibiotroph and biotroph pathogens has already provided insights into how efficiently these pathogens interact with their respective host (De Wit et al., 2009; Caillaud et al., 2013; Asai et al., 2014; Irieda et al., 2014). For example, the biotrophic downy mildew pathogen *Hyaloperonospora arabidopsidis* (*Hpa*), which has an overlapping host range with *Albugo* sp., and suppresses host responsiveness to salicylic acid (SA) in infected cells (Asai et al., 2014). It is known that hemi-biotrophic and necrotrophic pathogens trigger host secretion to the apoplast of defense-related proteins including pathogenesis-related (PR) proteins (Floerl et al., 2008, 2012; Ali et al., 2014; Kim et al., 2014). However, the influence of obligate biotroph pathogens on the *A. thaliana* apoplastic secretome is still unknown.

Host plant colonization by obligate biotrophs of the genus *Albugo* is associated with suppression of non-host resistance (NHR; Cooper et al., 2008). Specifically, *Albugo* sp. suppressed the "runaway cell death" phenotype, allowing a formerly avirulent downy mildew species to infect (Cooper et al., 2008). Assuming this phenomenon would extend to other non-host pathogens, *Albugo* sp. could thereby influence the microbial community composition of the host. We previously used network modeling of microbial community structures in the phyllosphere to show that the community composition is not only affected by abiotic factors and host genotype, but also by microbial hubs, including *Albugo* (Agler et al., 2016). Microbial hubs are taxa that are highly interconnected in a microbial community network and have significant effects on the community structure (Agler et al., 2016). It is still unclear whether hubs affect microbial colonization via direct microbe–microbe interactions or if they depend on host-mediated defense responses like suppression of NHR and effector-triggered immunity (ETI).

We investigated how *Albugo*, which is vitally dependent on a living host, can paradoxically compete in nature for a limited niche while in effect breaking host resistance to colonization. This was done by performing shotgun proteomics on leaf apoplastic fluid samples of *Albugo* sp.-infected and -uninfected *A. thaliana*. We examined plant samples from two different wild sites and a common garden experiment to compare the results with experiments performed under controlled laboratory conditions. Our results conclusively show that both wild-grown and lab-grown *A. thaliana* supports extensive *Albugo* sp. colonization, but the secretomes between wild and lab plants were significantly different. Regardless of *Albugo* sp. infection status, wild plants showed a broad spectrum of defense-related proteins at high abundances and lab-grown plants did not. We hypothesized that the activated immune system in wild plants leads to high hormone levels of, e.g., SA or abscisic acid (ABA). We used *A. thaliana* hormone mutants to mimic variable hormone levels in the field and found that *Albugo laibachii* strains are less affected in their infection rate than the natural competitor *Hpa*. Thus, our findings reveal how the biotroph pathogen *Albugo* only selectively interferes with host defense under different environmental conditions to maintain its ecological niche. Adaptation to host immune responses while maintaining partially active immunity seems advantageous against competitors.

MATERIALS AND METHODS

Plant Growth Conditions

Arabidopsis thaliana seeds were stratified on moist soil for 7 days at 4°C in darkness, before transfer into growth chambers with short day conditions (10 h light, 14 h darkness, 23/20°C, constant

60% humidity). Plants were grown for 6 weeks prior to infection, except ABA mutants which were grown for 4 weeks. For apoplastic fluid proteomics experiments in the lab (see Extraction of Apoplastic Fluid from *A. thaliana* Leaves), *A. thaliana* Ws-0 was used. Since all mutants used for qPCR experiments (see DNA Extraction and Oomycete Growth Quantification via qPCR) were in Col-0 background, wild type Col-0 was used as a control for infections in these experiments.

Arabidopsis thaliana Infections with Oomycete Pathogen Isolates

Spore solutions were prepared by washing spores from *Albugo candida* Nc2 or *A. laibachii* Nc14 or MPI1 infected leaf material with tap water and held on ice for 1 h. One milliliter spore solution was sprayed per plant (16×10^4 spores/ml) on 6-week-old *A. thaliana* using airbrush guns (Conrad Electronics GmbH). Plants were kept overnight in a dark cold room to promote spore germination, then were further grown in cabinets (Sanyo Inc.) with a dark–light cycle of 10 h light at 22°C and 14 h darkness at 16°C.

Infections with *Hpa* Noco2 were done similarly by washing infected leaves to make a conidiospore solution (4×10^4 spores/ml), then spraying on *A. thaliana* plants (Stuttmann et al., 2011).

Sampling of Wild *A. thaliana* Plants

Wild *A. thaliana* plants were sampled in Pulheim (Pul, 50°59′08.5″N 6°49′35.4″E) and Geyen (Gey, 50°58′43.9″N 6°47′35.8″E). Leaf material was pooled from several plants with white rust infection symptoms or asymptomatic plants at each site to reach appropriate amounts (≥2 g) for apoplastic fluid extractions. While sampling asymptomatic plants, care was taken to use only leaves where the whole plant did not show any white rust sporulation. Sampling was done in spring and fall 2013 (only fall at Gey) and in spring 2014. A third (fourth) replicate was also taken from Gey (Pul) in spring 2015, but liquid chromatography tandem mass spectrometry (LC-MS/MS) analysis (see below) was performed with an updated workflow combining in-solution digestion and analysis on a Q Exactive Plus. This increased sensitivity, coverage and resolution; the absolute values are therefore not comparable with samples analyzed on the LTQ Velos after in-gel digestion.

Growth of plants in the common garden experiment at the Max-Planck-Institute, Cologne, Germany, was described in Agler et al. (2016). *A. thaliana* Ws-0 and Sf-2, which is an *A. thaliana* ecotype resistant to *Albugo* infections, were planted and sampling was performed exactly as described for the wild sites.

Extraction of Apoplastic Fluid from *A. thaliana* Leaves

For laboratory experiments, ∼7 g of leaves were harvested from uninfected mock (H_2O sprayed) or *Albugo* sp.-infected (10 dpi) plants and immersed in 180 mM 2-(*N*-morpholino)ethanesulfonic acid (MES) (Duchefa Biochemie; pH 5.5) infiltration buffer. Leaves sampled from natural sites or the common garden experiment (2–9 g) were washed twice with ddH_2O to reduce dirt that was sticking to the leaves prior to immersion in infiltration buffer. A vacuum was applied with three cycles of 2:30 min followed by slow release over the course of 10 min to infiltrate the leaves homogenously. The leaves were blot-dried with tissue and placed in a 50 ml falcon tube with holes in the bottom in a centrifugation bottle. Apoplastic fluid was collected via centrifugation (Thermo Scientific) at 4°C and 900 × *g* for 10 min and was then sterile filtered (0.22 μm syringe filter, Spectrum Labs). Proteins were precipitated via chloroform/methanol precipitation (Wessel and Flügge, 1984). Pellets were dissolved in Laemmli sample buffer (Laemmli, 1970) for in-gel digestion and stored at −20°C until LC-MS/MS analysis.

LC–MS/MS Analysis

For samples analyzed with the LTQ Velos machine (lab and wild samples replicates 1–3), about 20 μg of apoplast protein extract per sample was separated at 125 V on a linear 12% Tris-Glycine sodium dodecyl sulfate-polyacrylamide gel electrophoresis (SDS-PAGE) for approximately 2 h. Gels were stained with PageBlue protein staining solution (Fermentas). Each gel lane was dissected into 30–32 slices. Gel slices were destained, reduced, alkylated, and trypsinated by a Proteineer dp robot (Bruker Daltonics). Peptides were separated on a Thermo/Proxeon Easy nLC II in a two-column configuration (precolumn 3 cm × 100 μm, 5 μm C18AQ medium, analytical column 10 cm × 75 μm, 3 μm C18AQ) coupled to a LTQ-Velos ion trap (Thermo Scientific). Peptides were eluted over a segmented linear 130 min gradient running from 5 to 95% acetonitrile (ACN)/H_2O with 0.5% formic acid (FA) at a flow-rate of 300 nl/min. Survey full-scan mass spectra were acquired in a mass range from 400 to 1600 *m/z*. MS/MS spectra were acquired with collision-induced dissociation (CID) at 35 eV on multiply charged precursor ions using a Top10 method with active exclusion for 60 s in a window from 0.2 Da below to 1.5 Da above the precursor mass. The ion selection threshold was set to 500 counts for MS2, the activation Q was set to 0.25 and the activation time to 10 ms. The resulting RAW files were converted to MGF format using Proteome discoverer 1.4.0288 (Thermo Scientific).

For samples analyzed on the Q Exactive Plus machine (lab samples, wild sample replicate 4 and common garden experiment samples), 5–20 μg apoplast protein extract per sample were digested in solution. The protein pellet was dissolved in 8 M urea, 0.1 M Tris–HCl pH 8.0, 1 mM $CaCl_2$. Cysteins were reduced by adding dithiothreitol (DTT) to a final concentration of 5 mM and incubation for 30 min. Subsequently, alkylation was performed by adding chloroacetamide to a final concentration of 14 mM and incubation for 30 min. The reaction was quenched by addition of DTT. Urea concentration was adjusted to 2 M by dilution with 0.1 M Tris–HCl pH 8.0, 1 mM $CaCl_2$. Trypsin digestion (1:100 enzyme-to-protein ratio) was performed over night at 37°C and stopped by addition of 1% FA. Peptides were desalted with StageTips (Empore C18, 3 M) as described in Rappsilber et al. (2007). Dried peptides were redissolved in 2% ACN, 0.1% trifluoroacetic acid for analysis and adjusted to a final concentration of 0.18 μg/μl. Samples were analyzed using an EASY-nLC 1000 (Thermo Fisher) coupled to a Q Exactive Plus

mass spectrometer (Thermo Fisher). Peptides were separated on 16 cm frit-less silica emitters (New Objective, 0.75 μm inner diameter), packed in-house with reversed-phase ReproSil-Pur C18 AQ 3 μm resin (Dr. Maisch). Peptides (1 μg) were loaded on the column and eluted for 120 min using a segmented linear gradient of 0–95% solvent B (solvent A 5% ACN, 0.5% FA; solvent B 100% ACN, 0.5% FA) at a flow-rate of 250 nl/min. Mass spectra were acquired in data-dependent acquisition mode with a Top15 method. MS spectra were acquired in the Orbitrap analyzer with a mass range of 300–1750 *m/z* at a resolution of 70,000 FWHM (full width at half maximum) and a target value of 3×10^6 ions. Precursors were selected with an isolation window of 1.3 *m/z*. High-energy collisional dissociation fragmentation was performed at a normalized collision energy of 25. MS/MS spectra were acquired with a target value of 10^5 ions at a resolution of 17,500 FWHM and a fixed first mass of *m/z* 100. Peptides with a charge of +1, greater than 6, or with unassigned charge state were excluded from fragmentation for MS2, dynamic exclusion for 30 s prevented repeated selection of precursors.

MS Data Processing

MS/MS spectra were searched against the *A. thaliana* proteome (TAIR10) and against the *A. laibachii* Nc14/*A. candida* Nc2 (Kemen et al., 2011; McMullan et al., 2015) proteomes. A database containing 248 common contaminants and reverse "decoy" sequences were included. Trypsin specificity was required and a maximum of two missed cleavages allowed. Carbamidomethylation of cysteine residues was set as fixed modification and oxidation of methionine as variable modification. LTQ Velos data was searched using X! Tandem (version 2013.02.01.1; Craig and Beavis, 2004). A fragment monoisotopic mass error of 0.4 Da was permitted with a parent monoisotopic mass error of ±0.3 Da. Protein identifications were validated via the trans-proteomic-pipeline (TPP version 4.6.2; Deutsch et al., 2010), using default settings. For refinement and quantification of protein identifications APEX spectral counting (version 1.1.0) was used (Braisted et al., 2008). The APEX abundances of observed proteins were calculated using the results from PeptideProphet and ProteinProphet analyses (part of TPP) and a false discovery rate (FDR) of 1%. For further analyses proteins were filtered for secreted proteins, based on TargetP 1.1 predictions (Emanuelsson et al., 2000) (Supplementary Material: Tables S3–S7).

Q Exactive data were processed using MaxQuant software (version 1.5.2.8[1]; Cox and Mann, 2008) with label-free quantification (LFQ) and iBAQ enabled (Cox et al., 2014). Minimal peptide length was set to seven amino acids. Peptide-spectrum-matches and proteins were retained if they were below a FDR of 1%. Subsequent quantitative statistical analyses were performed in Perseus (version 1.5.2.6[1]; Cox and Mann, 2012). LFQ intensities were log2 transformed. iBAQ values were used to filter for the 100 most abundant proteins, which were further analyzed based on their LFQ values (Supplementary Material: Table S8).

[1]http://www.maxquant.org

Due to different mass spectrometers and sample preparations a direct comparison based on protein abundances is not possible for samples analyzed with different setups.

Statistical Analyses of Proteomics Samples

To evaluate how the composition of proteomic samples varied between different treatments and sampling sites, we used redundancy analyses (RDA) in the R-package Vegan 2.2-1 (Oksanen et al., 2015). We first built an unconstrained model with the command RDA of all proteins in the sample with their respective APEX or LFQ abundance value. This model was then constrained by the factors location, infection status, or sample type (treatment). For visualization, we plotted the first constrained axes (if the factor was only two levels, only one constrained and one unconstrained axis are generated) and calculated the total variation of protein composition that was correlated to the constraining variables. To test if the constraining was significant ($p < 0.05$), we used the ANOVA function built into Vegan, which uses random permutations of factor classes followed by Tukey honestly significant difference (HSD) in R 3.0.2 (R Core Team, 2013). Ellipses of confidence intervals were plotted to help visualizing significant correlations. The built-in ordiellipse function was used to calculate the 95% confidence limits based on standard error.

RDA with all of the Q Exactive Plus-measured samples, constrained for the factor "treatments," indicated that five samples strongly diverged from their respective replicates (Supplementary Figure S1A). Due to technical reasons, these samples had abnormal MS/MS identification rates and showed low correlation to all other samples (Supplementary Figure S1B). For further analyses, these samples were excluded.

To determine if asymptomatic wild-grown *A. thaliana* plants were free of *Albugo* growth, the identified MS/MS spectra of these samples were searched against the *A. laibachii* Nc14 proteome and *A. thaliana* proteome and the ratio of *Albugo* proteins/*A. thaliana* proteins was compared with the ratios in *Albugo*-infected samples (Supplemenatry Tables S1 and S2).

DNA Extraction and Oomycete Growth Quantification via qPCR

Plants from the mutant infection assay were harvested at 10 dpi (*A. laibachii*/*A. candida* infections or mock) or at 5 dpi (*Hpa* Noco2 infections or mock) and were immediately frozen in tubes in liquid nitrogen. Three adult plants (or five seedlings) were pooled and ground to powder using a liquid nitrogen-cooled mortar and pestle and DNA was extracted following a phenol/chloroform-extraction protocol (McKinney et al., 1995). In short, ground powder was taken, added to extraction buffer (50 mM Tris pH 8.0, 200 mM NaCl, 0.2 mM ethylenediaminetetraacetic acid (EDTA), 0.5% SDS, 0.1 mg/ml proteinase K (Sigma–Aldrich) and incubated at 37°C for 30 min. One volume phenol was added, centrifuged and the top aqueous layer recovered and was mixed with 1 volume chloroform/isoamyl alcohol (24:1; Sigma-Aldrich).

After centrifugation, the top aqueous layer was recovered and mixed with 3 M sodium acetate and two volumes pure ethanol to precipitate the nucleic acids. DNA was pelleted by centrifugation and washed twice with 70% ethanol. It was resuspended in 50 µl nuclease free water (NFW) and used for qPCR. DNA concentrations were determined via NanoDrop (Thermo Scientific) and diluted to 1 ng/µl. One qPCR reaction contained 7.5 µl SsoAdvanced universal SYBR Green supermix (Bio-Rad), 0.3 µl of each primer (10 mM), 1.9 µl NFW and 5 µl DNA. Samples were measured in triplicates in a CFX Connect real-time PCR detection system (Bio-Rad) using the following program: (1) 95°C, 2 min; (2) (95°C, 20 s, then 56°C, 20 s, then 72°C, 30 s) ×40, 72°C, 5 min followed by a temperature gradient from 65 to 95°C. To quantify the amount of oomycete DNA per plant sample two standard genes were used (*A. thaliana* EF1-α: 5′-AAGGAG GCTGCTGAGATGAA-3′, 5′-TGGTGGTCTCGAACTTCCAG-3′; Oomycete internal transcribed spacer (ITS) 5.8s: 5′-ACTTT CAGCAGTGGATGTCTA-3′, 5′-GATGACTCACTGAATTCTG CA-3′). The amount of oomycete DNA was normalized to the respective plant DNA content and infected plant mutants were normalized to infected Col-0 wild type plants via calculating the $\Delta\Delta C$q.

Amplicon Sequencing of Microbial Communities

DNA extraction, amplicon library preparation, and sequencing were performed as previously described (Agler et al., 2016). In short, DNA was extracted with bead beating and SDS/lysozyme lysis with a phenol/chloroform cleanup. Amplification was performed for four amplicon regions (bacterial 16S rRNA gene regions V3/V4 and V5/V6/V7, Fungal ITS1 and ITS2) in two steps: The first step employed universal amplification primers and oligonucleotide clamps to block host amplification. The second step employed primers consisting of a concatenation of the Illumina adapter P5 (forward) or P7 (reverse), an index sequence (reverse only), a linker region, and the base primer for the region being amplified. Amplicon libraries were quantified fluorescently and products were combined in equimolar concentrations and were sequenced on an Illumina MiSeq lane using a mixture of custom sequencing primers complementary to the linker/primer region of the concatenated primers.

To process the reads, we used the custom pipeline described in Agler et al. (2016). For downstream analyses, operational taxonomic unit (OTU) tables were rarefied to an even depth of reads per sample and summarized to the genus level. A bar chart was plotted including all genera with >5% abundance in any one sample (Supplementary Figures S2 and S3). Beta diversity plots were generated using principal coordinates analyses based on Bray–Curtis similarities between rarefied samples (**Figure 5**; Supplementary Figure S4). Alpha diversity (number of observed taxa) was calculated based on the average of 10 rarefactions of the data (**Figure 5**; Supplementary Figure S4). The raw sequencing data is available on Qiita[2].

[2]https://qiita.ucsd.edu/; study 10369

Albugo Strain Determination with Microsatellite Markers

Microsatellite markers were used to analyze genetic diversity between wild *A. laibachii* strains as in Agler et al. (2016). Three primer sets (AlSSR2[F/R], AlSSR6 [F/R], and AlSSR10 [F/R]) were employed which produce amplicons with which *A. laibachii* strains are easily distinguished. PCRs were performed as previously described (Agler et al., 2016) with equal amounts of extracted DNA from endophytic compartment samples as template. Products were visualized on a 3% high-resolution agarose gel (Bio-Budget) with a 100 bp ladder. In some gels weak bands appeared in the background at lengths unexpected for the used markers. These were considered as non-target amplification and only bright bands of similar intensity were analyzed. If the length of amplified bands for all three markers were indistinguishable, we considered strains to be the same.

RESULTS

The Secretome of Wild-Grown *A. thaliana* Differs Significantly from Lab-Grown Plants

To get insights into the physiology of wild versus lab-grown plants we used a shotgun proteomics approach to elucidate plant secretomes on plants from two different wild sampling sites and from plants grown in a common garden experiment. We chose two sites nearby Cologne, Germany (Pul and Gey), due to their stable *A. thaliana* population structure and repeated observations of naturally occurring white rust symptoms caused by *Albugo* sp. These sampling sites are located within 2.5 km of one another and at similar elevations such that weather-caused environmental conditions are essentially similar. We sampled leaf material, pooled leaves from several plants at a site, during the early vegetative growth phase of *A. thaliana* in fall before its resting stage over winter and in spring, before it goes into its reproductive stage. All analyses are based on three biological replicates (two spring and one winter) from Pul, and two biological replicates (one spring and one winter) from Gey. We compared wild plants with or without visible white rust infection to lab-grown infected and uninfected mock plants. We focused our analyses on the plant apoplastic space, as it has been shown in previous work that upon biotic and abiotic stress perception there is a massive increase in secretion of defense- or stress-associated proteins into this compartment (Doehlemann and Hemetsberger, 2013; Delaunois et al., 2014). The apoplast is therefore a good analytical readout for plant responses.

Analyses revealed between 370 and 585 unique secreted *Arabidopsis* proteins per sample, with abundance values spanning four orders magnitude (Supplementary Material: Tables S3–S7). We used constrained RDA of the 100 most abundant proteins across all uninfected samples to unravel the factors determining the variation of secretome compositions. Seventy-six percent of the total protein variation (ANOVA based on 999 random class permutations for significance of the

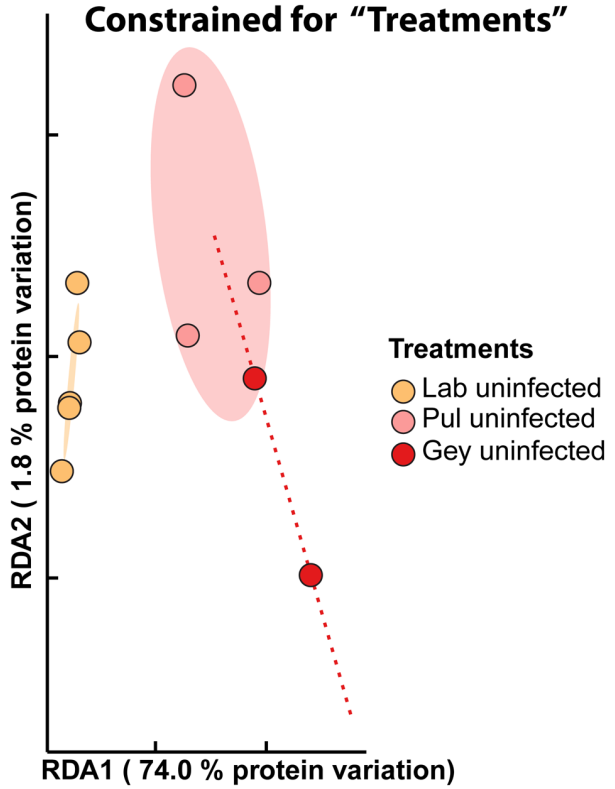

FIGURE 1 | The secretome of uninfected wild *A. thaliana* differs significantly from *A. thaliana* grown in controlled environment. The apoplastic fluid proteome (100 most abundant secreted proteins) of asymptomatic wild *A. thaliana* from Pul and Gey clusters significantly different to uninfected lab plants. Seventy-six percent of the variation in protein composition of these samples can be explained by constraining for these different "treatments" [lab uninfected (yellow, $n = 5$), Pul uninfected (pink, $n = 3$), Gey uninfected (red, $n = 2$)] (ANOVA, p-value: 0.004). Confidence ellipses (lines) (0.95) based on the standard error show an overlap of Pul and Gey samples indicating their strong similarity.

treatment constraint, p-value: 0.004) was constrained by the factor "treatments," distinguishing lab, Pul, and Gey samples (**Figure 1**). Here, uninfected lab samples cluster together and are significantly different from wild samples (0.95 confidence interval; **Figure 1**). Samples from different wild sites, however, show significant overlaps of their confidence intervals (**Figure 1**). This demonstrates that wild plants differ significantly from plants grown under controlled conditions even in an uninfected stage and that samples from two different wild sites are more similar to each other than to lab-grown plants.

To check if the phenotypically uninfected wild plants were free of *Albugo* sp. growth, we annotated the protein spectra against the *A. laibachii* Nc14 genome and compared this with laboratory uninfected samples (Supplementary Table S1). Two of the five asymptomatic natural samples (Pul uninfected first and third replicate) exhibited augmented amounts of *Albugo* proteins (11.57% respectively 14.37%), while the other samples were comparable to background levels in non-inoculated control laboratory experiments (maximum 3.07%). The higher levels in the two asymptomatic *Arabidopsis* samples could result from asymptomatic endophytic *Albugo* sp. growth (not visible during sampling) or contamination from *Albugo* spores attached to the leaves. However, they do not cluster closely together with corresponding samples showing white rust symptoms (Supplementary Figure S5C), suggesting that they do not behave like infected samples.

To demonstrate reproducibility of our experimental setup, we performed constrained ordination analyses with the factor "replicates" (three biological replicates) for all lab samples (uninfected and infected). Variation between replicates was not significantly more than random variation (ANOVA, p-value: 0.509), indicating the reproducibility of the results under controlled conditions (Supplementary Figure S6). On the other hand, "replicates" was a highly significant factor explaining most of the total variation (58%) in wild samples (for both infected and uninfected samples; ANOVA, p-value: 0.004; Supplementary Figure S5C). Not surprisingly, the reproducibility of wild samples is low in comparison to the lab likely because the samples from different sampling dates and seasons (spring/fall) were exposed to different environmental stresses.

Considering the overall difference in secretome composition of uninfected wild and lab plants we had a closer look at the 100 most abundant proteins. Forty-two proteins had significantly different abundances between lab plants and wild Pul or Gey plants (Student's t-test, p-value ≤ 0.05; **Figure 2**). For uninfected plants, the four overall most abundant proteins in the apoplastic fluid samples (annotated as: PR5 AT1G75040.1, PR1 AT2G14610.1, BG3 AT3G57240.1, PR2 AT3G57260.1) were significantly more abundant in the wild samples and are associated with responses to abiotic or biotic stimulus gene ontology (GO biological process, Berardini et al., 2004; **Figure 2**). In total, twelve proteins that had significantly higher abundance in the wild samples are associated with response to [a]biotic stimulus or to stress (GO biological process). This indicates that phenotypically healthy wild plants have an activated immune system which distinguishes them from plants grown in a controlled lab environment.

The Oomycete Pathogen *A. laibachii* Does Not Suppress the Activated Immune System of Wild *A. thaliana*

To determine to which extent the oomycete pathogen *Albugo* manipulates its host under controlled conditions and in the wild, we infected *A. thaliana* with two *A. laibachii* strains (isolates Nc14 and MPI1) and an *A. candida* strain (isolate Nc2). The strains Nc14 and Nc2 have been isolated from *A. thaliana* field plantings in Norwich, UK, while the MPI1 strain was the most frequently occurring *Albugo* sp. strain in our common garden experiments in Cologne, Germany (Kemen et al., 2011; McMullan et al., 2015; Agler et al., 2016). Microsatellite markers (van Treuren et al., 1997) demonstrated that in Pul and Gey *A. thaliana* plants were infected with various strains of *A. laibachii* whereas we did not detect *A. candida* with specific primers in any wild or common garden experiment (Supplementary Figure S7 and Agler et al., 2016, for the common garden experiment).

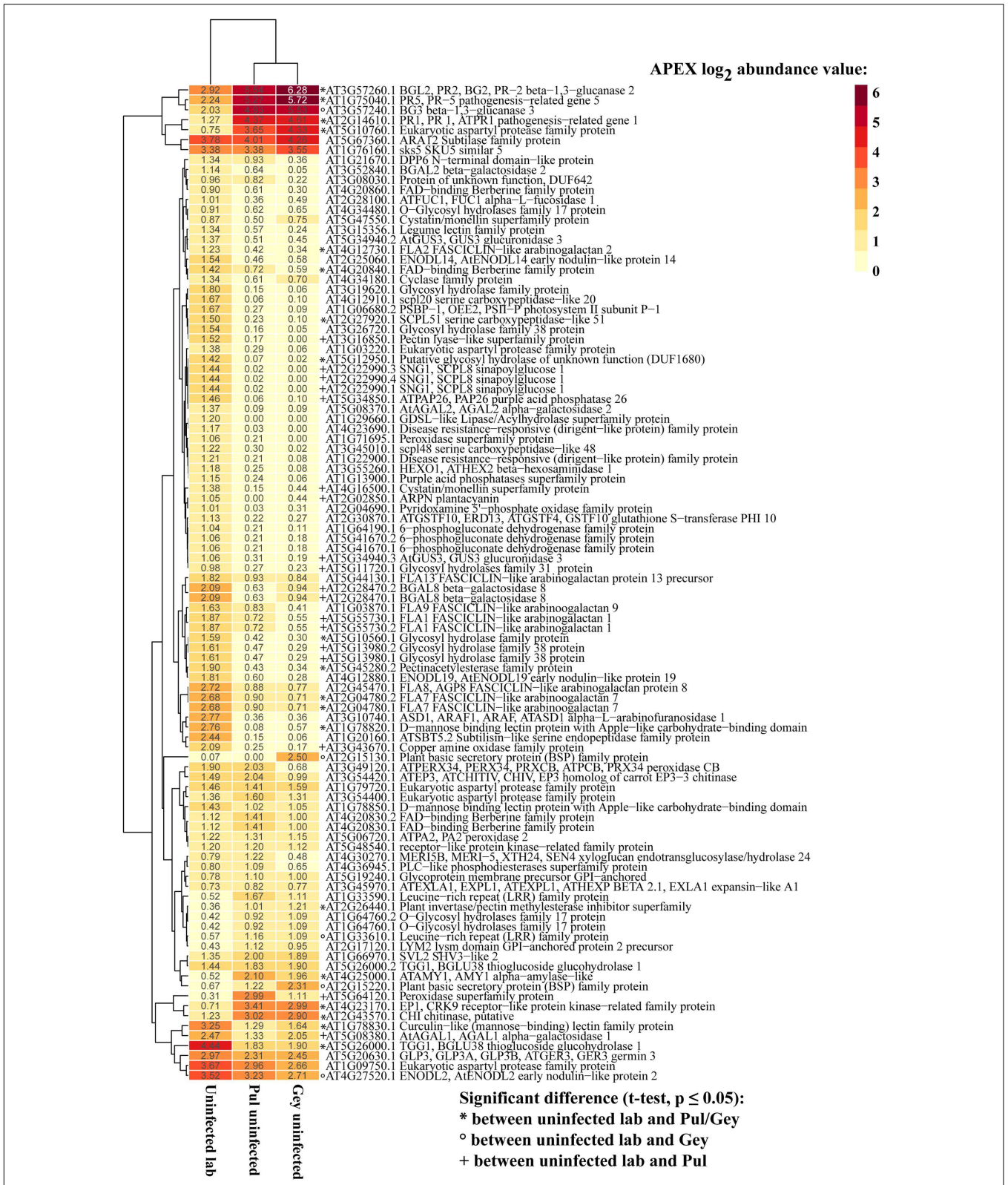

FIGURE 2 | Phenotypically uninfected wild *A. thaliana* plants have high abundances of defense-related proteins. Heatmap of the 100 most abundant secreted *A. thaliana* proteins detected in uninfected lab and wild apoplastic fluid samples. The four most abundant proteins were significantly more abundant in wild plants and pathogenesis related. APEX abundance values were averaged across replicates and $\log_2$ transformed. Significant differences between samples are indicated by symbols.

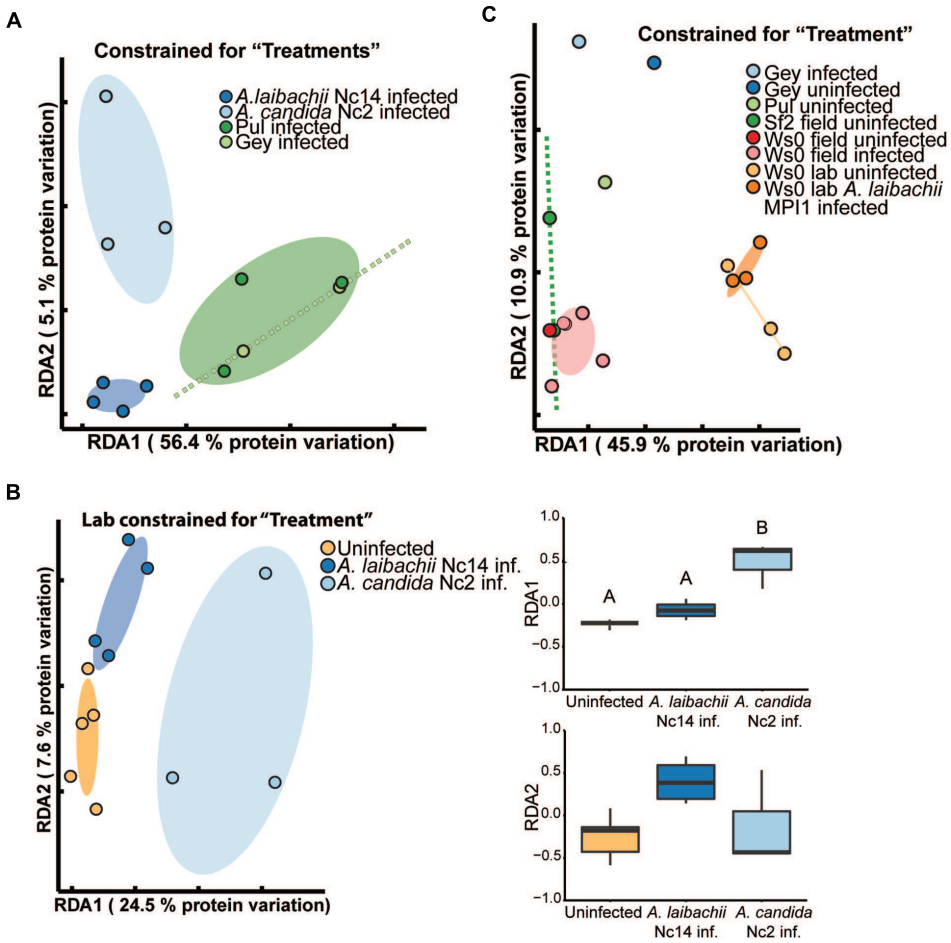

FIGURE 3 | Wild white rust *Albugo* sp. infections differ from lab infections, but *Albugo laibachii* does not change the *A. thaliana* secretome significantly. (A) RDA constrained for factor "treatments" with all infected samples. Wild samples from Pul (dark green, $n = 3$) and Gey (light green, $n = 2$) cluster significantly different to laboratory infections of *A. laibachii* Nc14 (dark blue, $n = 4$) and *A. candida* Nc2 (light blue, $n = 3$). Confidence ellipses are based on standard error. **(B)** RDA constrained for factor "treatments" with all laboratory samples. Uninfected (yellow, $n = 5$) and *A. laibachii* Nc14 (dark blue, $n = 4$) infected samples cluster closely together apart from *A. candida* Nc2 (light blue, $n = 3$) infected samples. The spread of the protein samples on both axes plotted in boxplots indicates a significant difference between *A. candida* Nc2 and *A. laibachii* Nc14/uninfected samples along RDA1-axis with 24.5% of the total variation (Tukey honestly significant difference (HSD), p-value < 0.05). (C) *Arabidopsis thaliana* Ws-0 grown in a common garden experiment under wild conditions (red, asymptomatic plants; pink, *Albugo*-infected plants) has significantly different secretome compositions compared to *A. thaliana* Ws-0 grown under laboratory conditions (yellow, uninfected; orange, *Albugo*-infected). Confidence ellipses (0.95) are based on standard error. All samples presented in **(C)** were analyzed with a Q Exactive Plus following in-solution digestion (see liquid chromatography tandem mass spectrometry (LC-MS/MS) Analysis).

Constrained analyses revealed clear differences in protein composition of the infected samples: 63% of the total protein variation was constrained by distinguishing the samples from Pul, Gey, and the two *Albugo* lab infections (factor "treatment"; ANOVA, p-value: 0.015; **Figure 3A**). Pul and Gey infections clustered closely together with significant separation from both *A. laibachii* Nc14 and *A. candida* Nc2 infected samples in the laboratory (**Figure 3A**). Even though the wild samples were from spatially separated sampling sites and infected with different *A. laibachii* strains, there were no significant differences in their secretome composition. Comparable to the apoplastic secretome of uninfected and asymptomatic *A. thaliana* plants (see The Secretome of Wild-Grown *A. thaliana* Differs Significantly From Lab-Grown Plants), wild plants showing a white rust phenotype differ significantly from plants showing white rust symptoms following infections under controlled lab conditions.

To unravel to which extent *Albugo* sp. can change the *A. thaliana* protein secretion following successful colonization, we compared for each environmental condition (laboratory/wild) the secretome of plants showing successful infection of *Albugo* with uninfected plants. Under laboratory conditions, 32% of the total variation were constrained by separating uninfected, *A. candida* Nc2 infected and *A. laibachii* Nc14 infected samples (ANOVA, p-value: 0.013; **Figure 3B**). All uninfected/symptomless samples clustered closely together with *A. laibachii* Nc14 infected leaf samples, apart and with no significant overlap with *A. candida* Nc2 infected samples.

Considering the spread of the plotted samples along RDA1 (*x*-axis; explains 24% of the protein variation) there is a significant difference between the *A. candida* Nc2 and uninfected/*A. laibachii* Nc14 infected samples (Tukey HSD, *p*-value: 0.001; **Figure 3B**). The uninfected and *A. laibachii* Nc14 infected samples cluster closely together without significant differences along this axis and with only weak differences along the *y*-axis. Therefore, under controlled conditions *A. laibachii* Nc14 infections had non-significant effects on the abundance of secreted *A. thaliana* proteins.

In order to better unravel the environmental influences on *Arabidopsis* secretomes and to check whether differences between lab and field were due to differences between Ws-0 used in the lab and wild plants, we planted *A. thaliana* Ws-0 (*Albugo* susceptible) and Sf-2 (*Albugo* resistant) plants, in a common garden experiment (described in Agler et al., 2016). Nearly all wild-grown *A. thaliana* Ws-0 plants were infected in spring (mostly by *A. laibachii* strain MPI1) and we compared these to laboratory experiments with an isolate of this *Albugo* strain. The high infection rates of Ws-0 impeded sampling of asymptomatic plants. RDA constrained for "treatments" (ANOVA, *p*-value: 0.001) showed a significant difference between the secretomes of field- and lab-grown *A. thaliana* Ws-0. Under laboratory conditions, *A. thaliana* Ws-0 plants infected with *A. laibachii* MPI1 did not significantly differ from uninfected plants. This was comparable to field-grown *A. thaliana*, which showed dense clustering of samples irrespective of infection status (**Figure 3C**). *Albugo*-resistant *A. thaliana* Sf-2 samples clustered closely with *A. thaliana* Ws-0. The single replicate from Pul and Gey that was analyzed with the same method clustered away from the plants of the common garden experiment but were more variable. Therefore, these results confirmed differences that were observed between lab-grown plants ((un-)infected) and wild *Arabidopsis* samples from Pul and Gey (**Figures 1** and **3A**).

Constraining for differences between infected and uninfected samples by site (i.e., within each of Pul and Gey) explained 24% of the variation in secretome composition, but this was not significant (ANOVA, *p*-value: 0.744; Supplementary Figure S5A). Similarly, constraining for infection status across both natural sites, which only distinguishes all plants with white rust symptoms from symptomless plants, explained 6% of the total protein variation and was not significant (ANOVA, *p*-value: 0.686; Supplementary Figure S5B). This indicates that similar to results in the lab, the protein composition in *A. thaliana* apoplastic fluid is highly similar in *A. laibachii*-infected and -uninfected wild plants (overlapping confidence ellipses based on standard error; Supplementary Figure S5A). Similar to uninfected wild plants (**Figure 2**), *A. laibachii*-infected wild plants exhibited high levels of PR proteins like beta-1, 3-glucanases (PR2 AT3G57260.1, AT3G57240.1), PR1 (AT2G14610.1) and PR5 (AT1G75040.1; APEX $\log_2$ abundance > 5.0; **Figure 4**). Since there was no significant difference (paired *t*-test, *p*-value ≥ 0.05) in abundance of these proteins in uninfected wild plants compared to wild plants showing white rust symptoms, *A. laibachii* infection does not significantly affect *A. thaliana* defense protein secretion. Furthermore, *A. laibachii* infections do not reduce the secretion of defense proteins that were already present in plants prior to infection. These results suggest that the obligate biotroph *A. laibachii* is adapted to *A. thaliana* triggered immune responses in the wild and can complete its infection cycle without severe suppression of the apoplastic protein based defense machinery.

Bacterial Alpha Diversity Changes with *Albugo* sp. Infection While Fungal Community Compositions Are More Stable

To unravel which biotic factors might have triggered the observed elevated levels of PR proteins under field conditions regardless of *Albugo* infection status, we characterized the endophytic microbial communities of *Albugo* sp. infected versus uninfected *A. thaliana* plants in Pul and Gey via amplicon sequencing (bacterial 16S rRNA, fungal ITS).

The sampling was done at the same time points as for proteomics and the processing was described in Agler et al. (2016) (see Amplicon Sequencing of Microbial Communities). Unconstrained ordination of the infected and uninfected wild samples indicated that the bacterial communities were fairly variable and clustered by the sampling time point (**Figure 5**; Supplementary Figure S4). Similar to fungi, bacterial communities grouped by plant generations (the samples that were harvested in December 2013 and March 2014 are one plant generation since *A. thaliana* germinates in fall, is vegetative over winter and dies in late spring following reproduction; **Figure 5**; Supplementary Figure S4). Contrary to the bacterial communities, only the fungal community in Gey clusters separately from Pul samples, supporting previous results suggesting that fungi are more location-specific than bacteria (Agler et al., 2016; Coleman-Derr et al., 2016). Endophytic fungi, detected at Pul or Gey, belonged largely to the order Pleosporales or the class of Leotiomycetes, which are, often necrotrophic, ascomycotal fungi (Supplementary Figure S3). Calculating the alpha diversity within the bacterial and fungal communities in the infected and uninfected samples revealed a decrease of the diversity in infected plants (**Figure 5**; Supplementary Figure S4).

Taken together the results indicate that *Albugo* sp. infections have a stronger influence on the colonization of bacteria where sample clustering is more variable and *Albugo*-infection status correlates to diversity (Agler et al., 2016). We therefore propose that fungi trigger the observed host immune responses, since these communities are similar in infected and uninfected samples and therefore seem to be less under the control of *Albugo*.

Albugo laibachii Infections Are Less Affected by Altered Host Hormone Levels than *Hpa*

Arabidopsis thaliana immune responses to biotic stresses often result in alteration of plant hormone levels including SA-mediated defense against (hemi-)biotrophs or jasmonic acid

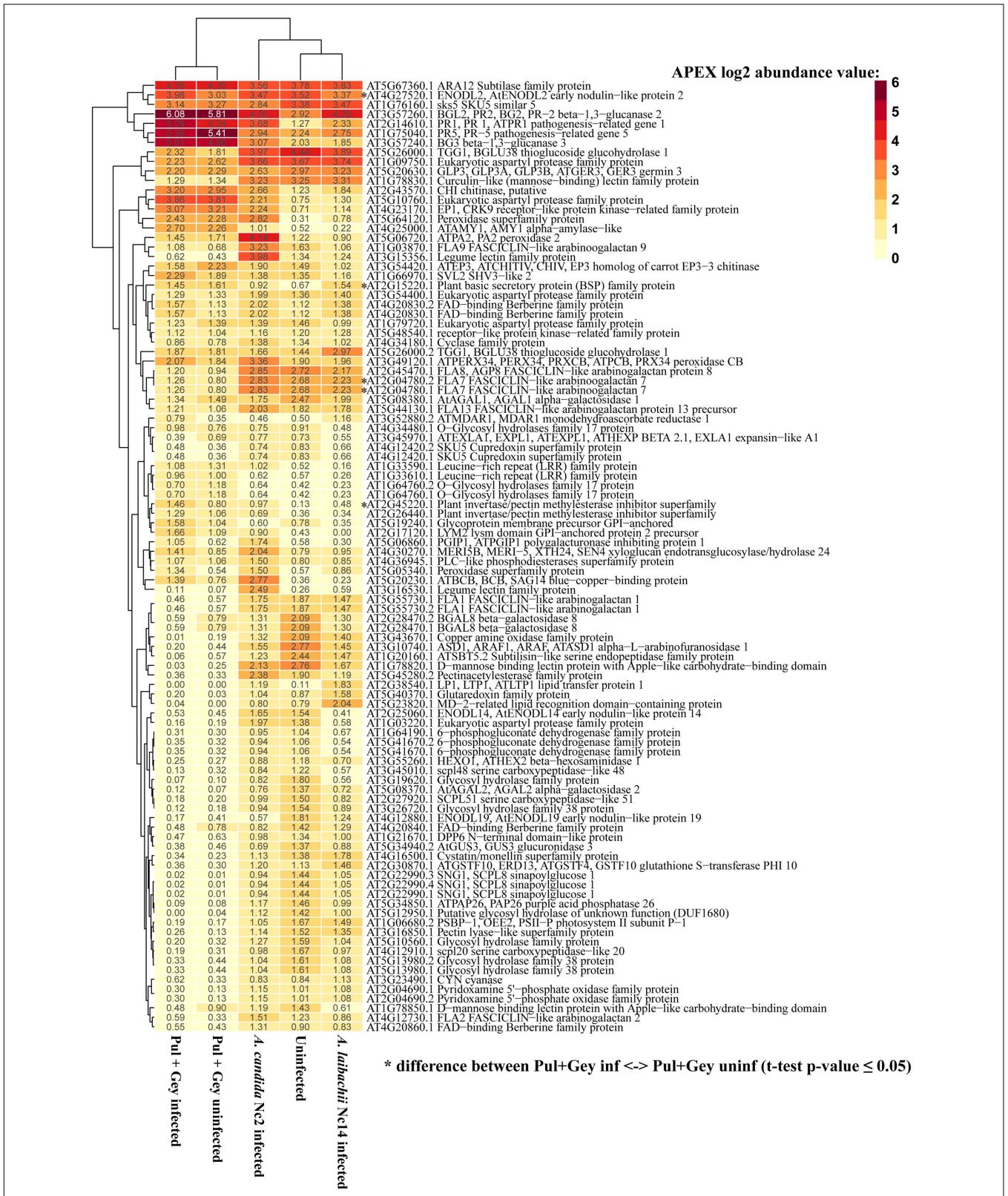

FIGURE 4 | Asymptomatic, uninfected wild *A. thaliana* plants show an activated immune system, which is not changed by *Albugo* sp. infections. The most abundant *A. thaliana* proteins in wild *Albugo* sp.-infected and -uninfected plants are related to defense responses. APEX abundance values were averaged across replicates and $\log_2$ transformed. Significant differences between wild samples are indicated by symbols.

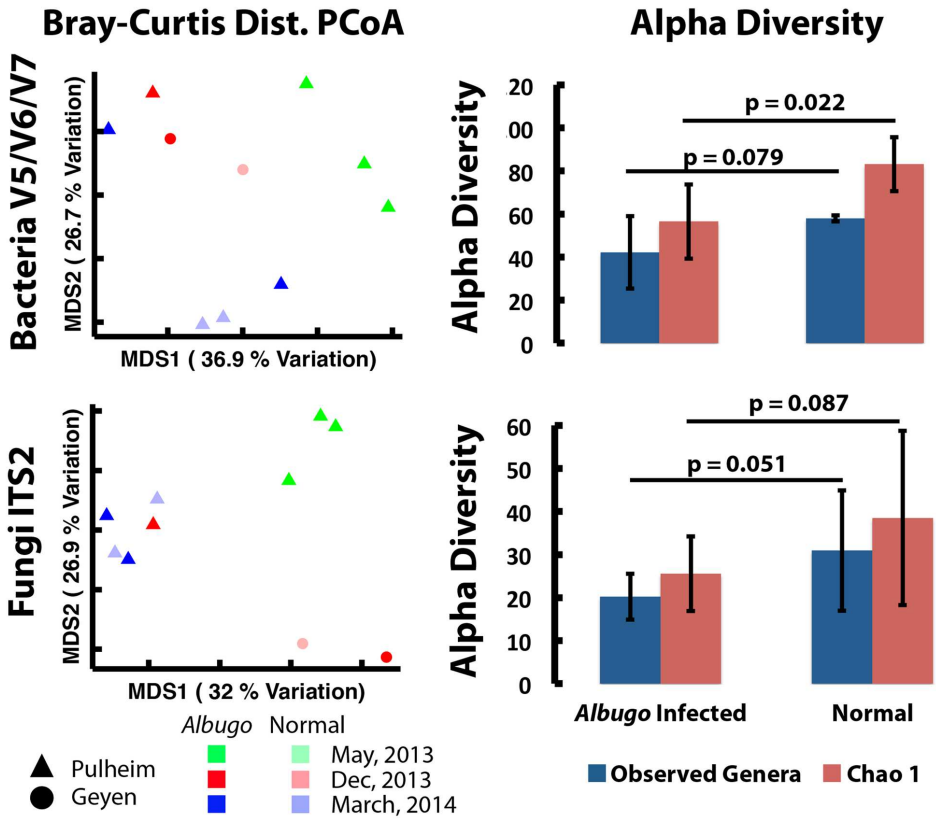

FIGURE 5 | Unconstrained ordination of bacterial and fungal communities and their respective alpha diversity. Principle component analyses of microbial communities from Pul and Gey, based on amplicon sequencing (bacterial 16S rRNA V5/V6/V7 region, fungal ITS2 region). The alpha diversity within bacterial and fungal communities decreases in infected plants.

(JA)/ethylene-mediated defense against necrotrophs (Thomma et al., 1998; Glazebrook, 2005). Especially PR1, PR2, and PR5 proteins were shown to be SA responsive (Uknes et al., 1992), and we showed that they were highly abundant in all wild *A. thaliana* samples. *Hpa* has an overlapping host range and is a natural competitor of *Albugo* sp. on *A. thaliana*, because as obligate biotrophic oomycetes they occupy a similar niche.

During our experimentation, we phenotypically observed far more *A. laibachii* infection in the wild than other biotrophic pathogens of *A. thaliana* like *Hpa*. Therefore, we wanted to know if *A. laibachii* is better adapted to the primed immune system (i.e., constantly high PR protein levels) than *Hpa*. We compared both pathogens in growth assays on *A. thaliana* hormone mutants for their infection efficiency (**Figure 6**). Oomycete growth quantification via qPCR showed that *Hpa* Noco2 is especially affected in ABA biosynthesis-deficient mutants (*aba3-1*, *aba2-12*, negative effect), an SA-induction deficient mutant (*sid2-2*, positive effect) and a mutant with constitutive expression of PR-genes (*cpr5*, positive effect) compared to *A. laibachii*. Furthermore, *Hpa* Noco2 growth is significantly lowered in the *ein2-1* mutant (ethylene insensitive), which has elevated JA levels after pathogen treatment and constitutive *PR1* expression (Penninckx et al., 1998; Chen et al., 2009). Two different *A. laibachii* strains (MPI1 and Nc14) were tested. Contrary to *Hpa*, *A. laibachii* Nc14 and MPI1 colonization was very resilient, since its growth was only affected (relative to mock control) in the *cpr5* (Nc14/MPI1) and the *aba2-12* (MPI1) mutant backgrounds. In total, *Hpa* Noco2 growth varied more in the different mutant backgrounds (significant difference to mock control in five of eight mutants), than *A. laibachii* (significant difference in one of eight mutants for Nc14 and two of eight mutants for MPI1). This suggests that *A. laibachii* strains show a high plasticity to adapt to a broad range of host pre-existing defense fluctuations. This plasticity might give an advantage in competing for limited growth space in nature.

DISCUSSION

Arabidopsis thaliana is the best-studied flowering plant under controlled lab conditions (Koornneef and Meinke, 2010). How *A. thaliana* physiology changes and what happens on a molecular level under natural conditions compared to lab conditions is largely unknown. We have addressed this knowledge gap by comparing the apoplastic secretome of *A. thaliana* plants grown under standard experimental conditions in the lab with wild plants in stable, well-established, populations or with wild-grown

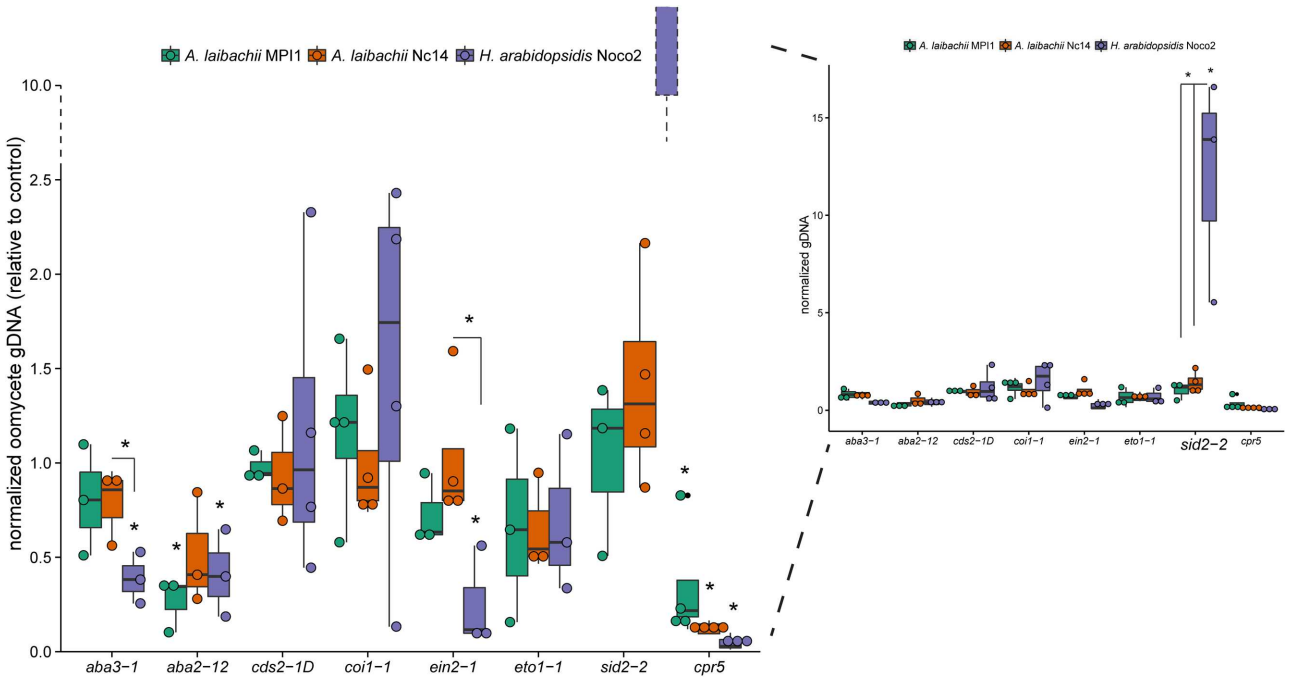

FIGURE 6 | Oomycete growth quantification via qPCR in different *A. thaliana* hormone mutants. Oomycete growth (*A. laibachii* MPI1/Nc14, *H. arabidopsidis* Noco2) was quantified via qPCR at 10 dpi (*A. laibachii*) or 5 dpi (*H. arabidopsidis*) in different *A. thaliana* hormone mutants (Col-0 as control). *A. laibachii* Nc14 growth (orange) was only significantly different to the control in *cpr5* mutants. *H. arabidopsidis* Noco2 growth (purple) was affected in *aba3-1*, *aba2-12*, *ein2-1*, *sid2-2*, and *cpr5* mutants. Asterisks indicate significant differences to Col-0 control infections and differences of infections within a mutant group (*t*-test, $p < 0.05$, $n = 3$ or 4).

plants in a common garden experiment. Our data demonstrates that morphologically healthy, wild- or field-grown *A. thaliana* plants are significantly different in physiology from plants grown under controlled lab conditions. The main difference is that naturally grown plants have significantly higher abundances of defense- and stress-related proteins in the apoplastic space (**Figure 2**).

Asymptomatic Wild *A. thaliana* Has an Induced Immune System

The apoplastic space is important for plant defense and pathogen virulence, as it is one of the main contact points of the host to invading pathogens (e.g., Kaffarnik et al., 2009; Floerl et al., 2012; Ali et al., 2014; Kim et al., 2014) and beneficial endophytes (e.g., Dong et al., 1994; Chi et al., 2005). Colonizing pathogens are generally recognized by plant cells in the apoplast where they are directly attacked by plant defenses. Upon microbe recognition, plants try to limit their growth by, e.g., reacting with a burst of reactive oxygen species (ROS; Daudi et al., 2012) or producing antimicrobial proteins from the PR-family (PR proteins; Loon et al., 2006). In apoplastic fluids extracted from wild, asymptomatic *A. thaliana* plants we found the most abundant proteins were PR2 (pathogenesis-related 2), PR5, BG3 (beta-1,3-glucanase 3), PR1 and eukaryotic aspartyl protease, which indicates triggered immune responses. Especially PR1, PR2, and PR5 are known marker proteins for SA-dependent systemic acquired resistance (SAR; Uknes et al., 1992, 1993), which is a long-lasting form of broad-spectrum disease resistance against avirulent pathogens in the whole plant (Maleck et al., 2000). High abundance of PR1 and SAR often goes along with redox regulation and accumulation of ROS, which are generated by nicotinamide adenine dinucleotide phosphate (NADPH) oxidases or apoplastic peroxidases (Mammarella et al., 2015). *A. thaliana* encodes several peroxidases, of which the apoplastic peroxidase 34 (PRX34, AT3G49120.1) is specifically activated under plant defense conditions, as well as peroxidase 33 (PRX33, AT3G49110.1; Daudi et al., 2012; Mammarella et al., 2015). However, PRX34 and PRX33 peroxidases were not significantly different in abundance in lab or wild plants and PRX33 was generally only very low abundant (not among top 100 proteins, **Figure 4**). A further 16 extracellular class III peroxidases that were shown to be expressed in leaves (Welinder et al., 2002), were either not detected or only at very low abundances with no difference between symptomless wild and lab samples. This could suggest that no ROS-burst or hypersensitive response was triggered in asymptomatic wild plants. In lab-grown unchallenged plants, only low levels of PR-proteins were detectable, consistent with the basal level that has been described for *A. thaliana* in previous studies (Floerl et al., 2012; Trentin et al., 2015).

The most abundant protein in untreated lab grown samples is a thioglucoside glucohydrolase (known as myrosinase; AT5G26000.1), which is significantly more abundant compared

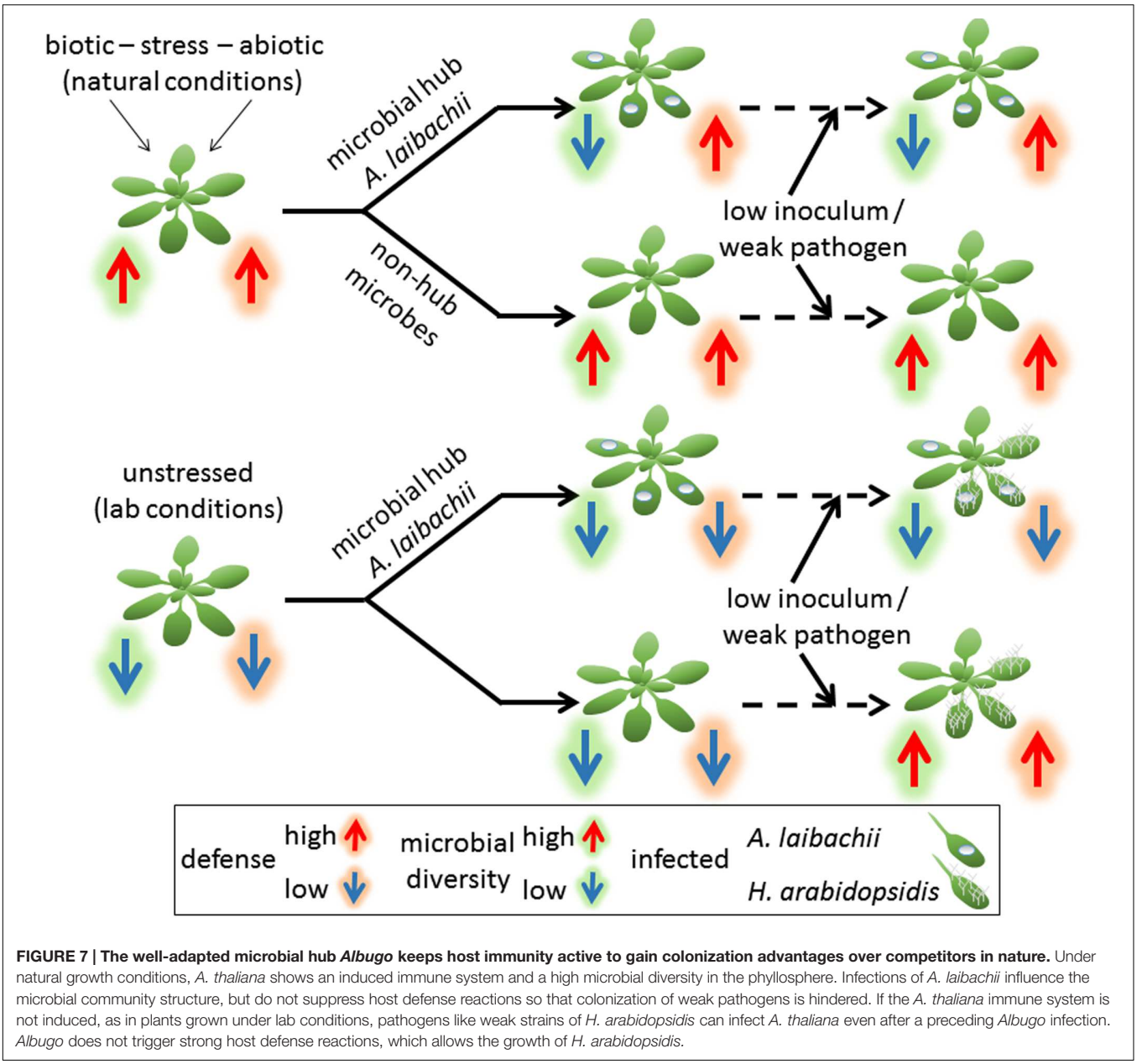

FIGURE 7 | The well-adapted microbial hub *Albugo* keeps host immunity active to gain colonization advantages over competitors in nature. Under natural growth conditions, *A. thaliana* shows an induced immune system and a high microbial diversity in the phyllosphere. Infections of *A. laibachii* influence the microbial community structure, but do not suppress host defense reactions so that colonization of weak pathogens is hindered. If the *A. thaliana* immune system is not induced, as in plants grown under lab conditions, pathogens like weak strains of *H. arabidopsidis* can infect *A. thaliana* even after a preceding *Albugo* infection. *Albugo* does not trigger strong host defense reactions, which allows the growth of *H. arabidopsidis*.

to asymptomatic field samples (**Figure 2**). Glucosinolates are secondary metabolites that can be cleaved by the enzyme thioglucoside glucohydrolase resulting in toxic products against fungi and insects (Barth and Jander, 2006; Halkier and Gershenzon, 2006; Bednarek et al., 2009). As such it can deter generalist herbivores, but might attract crucifer specialists (Barth and Jander, 2006). Taking lab-uninfected *A. thaliana* protein abundances as a measure for protein levels under unstressed conditions, we hypothesize that microbes colonizing healthy, uninfected wild plants lead to suppression of myrosinases and glucosinolates in nature. Thus, defense against eukaryotic microbes might be lowered, facilitating the colonization of fungi and oomycetes in nature and ultimately leading to the induced immune system.

Restructuring the Leaf Microbial Community by the Microbial Hub *A. laibachii* Is Not Mediated via Host Protein Secretion

Naturally grown *A. thaliana* plants accommodate a broad range of microbes (Vorholt, 2012; Agler et al., 2016), which are probably responsible for the observed activated defense and myrosinase suppression. Thus, our goal was to dissect the endophytic microbial community to identify responsible key organisms. Our community profiling revealed that bacteria did not differ markedly between the two wild populations of Pul and Gey, whereas fungal communities showed a significant location specificity. This indicates a rather homogenous spread

of bacterial inoculum, while fungal dispersal/growth is more unequal and site specific. This agrees with previous reports that bacterial communities vary in their relative abundance of species between sites, while fungal communities differ by presence/absence between different sites (Agler et al., 2016; Coleman-Derr et al., 2016). Bacterial and fungal communities were fairly stable over one plant generation (December 2013, March 2014) even though challenged by natural biotic and abiotic fluctuations, but differed significantly from one to the next plant generation (May 2013).

Endophytic fungi belonged largely to the order Pleosporales, which has many members that are necrotrophic plant pathogens like the detected *Alternaria* sp., *Ascochyta* sp. or *Boeremia* sp. Even though these fungi were detected as endophytes via sequencing, the plants did not show any signs of necrosis and were otherwise healthy during sampling. Possibly, these fungi initially colonized plants and triggered the observed immune responses and the primed host immune system restricted their growth. Although *Alternaria brassicicola* was shown to trigger SA-marker gene expression, growth restriction, and resistance against *A. brassicicola* relies on callose-deposition (Ton and Mauch-Mani, 2004). Even though we did not observe the callose synthase enzymes (e.g., AtGSL5), we cannot exclude their activation, since they are cellular and not detectable in the apoplast.

Besides fungi, the most abundant eukaryotic microbes observed in wild *A. thaliana* populations were the causal agents of white rust symptoms, *Albugo* sp. Endophytic bacterial communities of wild *A. thaliana* plants changed after infection by *Albugo* sp. showing significantly reduced alpha diversity and Gammaproteobacteria (mostly *Pseudomonas* sp.) dominating bacterial communities. Again, this is consistent with Agler et al. (2016), which highlighted an *A. laibachii*-mediated reduction of the bacterial alpha diversity of endo- and epiphytes and a stabilization of the community structure. Identifying *A. laibachii* as a hub organism structuring the *A. thaliana* microbial community left one main question: Does the hub reduce bacterial diversity via triggering plant defense or is there a direct interaction between hub and microbes? With this work, we can now show that the increase of relative abundance of major bacterial taxa and limiting the bacterial diversity is not mediated via the host protein secretion, as the hub microbe *A. laibachii* does not influence the *A. thaliana* protein secretion significantly. This suggests that direct microbe–microbe interactions might take place in the apoplastic space that result in observed decreased diversity of bacteria. Investigating the secretome of *Albugo* sp. during apoplastic space colonization could better resolve such microbe–microbe interactions.

Albugo laibachii Tolerates Apoplastic Broad-Spectrum Immune Responses Instead of Suppressing Them

Even though *A. laibachii* was shown to suppress resistance-gene-mediated broad-spectrum resistance (non-systemic; Cooper et al., 2008), we showed that this does not translate into broad effects on suppressing apoplastic defense. Thus, *Albugo* sp. are still able to go through their whole infection cycle without suppressing already activated host immune responses in the apoplast. In controlled lab conditions, where replicability was significantly higher, revealed that *A. laibachii* Nc14-infections lowered the protein abundance of only four *A. thaliana* proteins (serine carboxypeptidase-like protein, pectinacetylesterase family protein, mannose binding lectin protein and alpha-galactosidase; Supplementary Figure S8). Two of these proteins, pectinacetylesterase and alpha-galactosidase, could be involved in cell wall organization processes and could therefore be *A. laibachii* target proteins for haustoria formation in the host cells. The other two proteins, serine carboxypeptidase and mannose binding lectin protein, might contribute to plant defense reactions as carboxypeptidases are involved in protein degradation and many lectins bind foreign polysaccharides and can play a role in pathogen recognition (Lehfeldt et al., 2000; Sharon and Lis, 2004). Nevertheless, *A. laibachii* has suppressive effects on the abundance of only 4% of the host secreted proteins, none of which are classics of defense, like PR proteins or peroxidases (Supplementary Figure S8). Therefore, one might speculate that instead of broad-spectrum suppression, *Albugo* must have developed some mechanisms to protect its hyphae from immune responses. Similar mechanisms have been observed for fungal pathogens that use α-1-3-glucan to protect chitin in the cell wall from degradation by plant chitinases (Oliveira-Garcia and Valent, 2015).

Being adapted to the naturally occurring immune responses in wild host plants and not triggering further defense reactions seems to be advantageous in competing for limited growth space. *A. laibachii* appears to not only tolerate host-mediated broad-spectrum immune responses but also its growth is very resilient in host plants with altered hormone levels. On the other hand, the potential competitor *Hpa* – a common obligate biotroph pathogen on *A. thaliana* in the wild (Holub et al., 1994) is strongly affected (positively and negatively) by hormonal changes. The *cpr5* mutant secretome might be most similar to wild *A. thaliana* plants as it has high protein concentrations of PR1, PR2, PR5 and the defensin protein PDF1.2 (Bowling et al., 1997). The *cpr5* mutant also harbors high levels of SA compared to Col-0 wild type plants and was shown to be fully resistant against *Hpa* Noco2 (Bowling et al., 1997; Clarke et al., 2000). Infection screens were formerly based on conidiophores or spore counts at 7 dpi (Bowling et al., 1997; Clarke et al., 2000). We also did not observe sporulation after *Hpa* Noco2 infections at 5 dpi, but the more sensitive qPCR quantification revealed low levels of *Hpa* growth (**Figure 6**). *A. laibachii* infections were routinely harvested at 10 dpi and showed weak white rust sporulation in *cpr5* mutants, as well as stronger quantified growth than *Hpa*, highlighting the capability of *A. laibachii* to grow even under induced plant defense. Furthermore, *Hpa* infections were affected in *aba2-12*, *aba3-1*, *ein2-1*, and *sid2-2* mutant background while *A. laibachii* was not. The *sid2-2* mutant, defective in ISOCHORISMATE SYNTHASE 1, does not accumulate pathogen-inducible SA and is impaired in its SAR activation (Nawrath and Métraux, 1999; Bernsdorff et al., 2015). Thus the *sid2-2* mutant is hyper susceptible to *Hpa* infections, whereas *A. laibachii* grew only

slightly better on these plants (**Figure 6**; Nawrath and Métraux, 1999). The mutants that are impaired in ABA biosynthesis (*aba3-1*, *aba2-12*) did not affect *A. laibachii* Nc14 growth (*A. laibachii* MPI1 was affected in *aba2-12*), but *Hpa* Noco2 grew significantly less in all of these (**Figure 6**; Léon-Kloosterziel et al., 1996; Adie et al., 2007). The impairment of ABA synthesis results in decreased levels of JA and increased levels of SA-induced genes after pathogen infection, compared to wild type (Adie et al., 2007). Together, our results imply different strategies of the two pathogens: *Hpa* can quickly take advantage of suppressed defense where it probably would outcompete *A. laibachii*, but it is also more susceptible to plant defenses than the highly plastic and robust *Albugo*. Probably the latter situation is more common in many plant populations, explaining our observation of less *Hpa* in the wild.

In summary, our work gives significant new experimental insight into how plants behave under natural conditions on a molecular level and dissects clear, significant differences to experiments under controlled lab conditions (**Figure 7**). It further indicates that oomycete pathogens of the genus *Albugo*, which are important microbial hubs regulating the *A. thaliana* microbial community in the wild, are extremely fine-tuned to neither trigger strong host defense reactions, nor to act on broad-spectrum defense suppression in the apoplast. Therefore, we hypothesize that *Albugo* is well adapted to an active host immune system, which gives them an advantage over competitors in fighting for limited growth space in the same niche.

AUTHOR CONTRIBUTIONS

Experiments were conceived and designed by JR, MA, IF, and EK. The experiments were performed by JR, MA, AP, KK, and IF. Data analysis was conducted by JR and MA. The manuscript was written by JR and EK. All authors corrected the manuscript and discussed the data.

FUNDING

We acknowledge funding by the Max Planck Society and the Cluster of Excellence on Plant Science (CEPLAS).

ACKNOWLEDGMENT

The authors would like to thank Jaqueline Bautor for help with *Hpa* infections, and Thomas Colby and Anne Harzen for their excellent technical support in proteomics experiments.

SUPPLEMENTARY MATERIAL

The Supplementary Material for this article can be found online at: http://journal.frontiersin.org/article/10.3389/fpls.2016.00820

REFERENCES

Adie, B. A. T., Pérez-Pérez, J., Pérez-Pérez, M. M., Godoy, M., Sánchez-Serrano, J.-J., Schmelz, E. A., et al. (2007). ABA is an essential signal for plant resistance to pathogens affecting JA biosynthesis and the activation of defenses in *Arabidopsis*. *Plant Cell* 19, 1665–1681. doi: 10.1105/tpc.106.048041

Agler, M. T., Ruhe, J., Kroll, S., Morhenn, C., Kim, S.-T., Weigel, D., et al. (2016). Microbial hub taxa link host and abiotic factors to plant microbiome variation. *PLoS Biol.* 14:e1002352. doi: 10.1371/journal.pbio.1002352

Ali, A., Alexandersson, E., Sandin, M., Resjö, S., Lenman, M., Hedley, P., et al. (2014). Quantitative proteomics and transcriptomics of potato in response to *Phytophthora infestans* in compatible and incompatible interactions. *BMC Genomics* 15:497. doi: 10.1186/1471-2164-15-497

Amrine, K. C. H., Blanco-Ulate, B., and Cantu, D. (2015). Discovery of core biotic stress responsive genes in *Arabidopsis* by weighted gene co-expression network analysis. *PLoS ONE* 10:e0118731. doi: 10.1371/journal.pone.0118731

Asai, S., Rallapalli, G., Piquerez, S. J. M., Caillaud, M.-C., Furzer, O. J., Ishaque, N., et al. (2014). Expression profiling during *Arabidopsis*/downy mildew interaction reveals a highly-expressed effector that attenuates responses to salicylic acid. *PLoS Pathog.* 10:e1004443. doi: 10.1371/journal.ppat.1004443

Barth, C., and Jander, G. (2006). *Arabidopsis myrosinases* TGG1 and TGG2 have redundant function in glucosinolate breakdown and insect defense. *Plant J.* 46, 549–562. doi: 10.1111/j.1365-313X.2006.02716.x

Bednarek, P., Piślewska-Bednarek, M., Svatoš, A., Schneider, B., Doubský, J., Mansurova, M., et al. (2009). A glucosinolate metabolism pathway in living plant cells mediates broad-spectrum antifungal defense. *Science* 323, 101–106. doi: 10.1126/science.1163732

Berardini, T. Z., Mundodi, S., Reiser, L., Huala, E., Garcia-Hernandez, M., Zhang, P., et al. (2004). Functional annotation of the *Arabidopsis* genome using controlled vocabularies. *Plant Physiol.* 135, 745–755. doi: 10.1104/pp.104.040071

Bernsdorff, F., Döering, A.-C., Gruner, K., Schuck, S., Bräutigam, A., and Zeier, J. (2015). Pipecolic acid orchestrates plant systemic acquired resistance and defense priming via salicylic acid-dependent and -independent pathways. *Plant Cell* 28, 102–129. doi: 10.1105/tpc.15.00496

Bowling, S. A., Clarke, J. D., Liu, Y., Klessig, D. F., and Dong, X. (1997). The cpr5 mutant of *Arabidopsis* expresses both NPR1-dependent and NPR1-independent resistance. *Plant Cell* 9, 1573–1584. doi: 10.1105/tpc.9.9.1573

Braisted, J., Kuntumalla, S., Vogel, C., Marcotte, E., Rodrigues, A., Wang, R., et al. (2008). The APEX quantitative proteomics tool: generating protein quantitation estimates from LC-MS/MS proteomics results. *BMC Bioinformat.* 9:529. doi: 10.1186/1471-2105-9-529

Caillaud, M. C., Asai, S., Rallapalli, G., Piquerez, S., Fabro, G., and Jones, J. D. (2013). A downy mildew effector attenuates salicylic acid-triggered immunity in *Arabidopsis* by interacting with the host mediator complex. *PLoS Biol.* 11:e1001732. doi: 10.1371/journal.pbio.1001732

Chen, H., Xue, L., Chintamanani, S., Germain, H., Lin, H., Cui, H., et al. (2009). ETHYLENE INSENSITIVE3 and ETHYLENE INSENSITIVE3-LIKE1 Repress SALICYLIC ACID INDUCTION DEFICIENT2 expression to negatively regulate plant innate immunity in *Arabidopsis*. *Plant Cell* 21, 2527–2540. doi: 10.1105/tpc.108.065193

Chi, F., Shen, S.-H., Cheng, H.-P., Jing, Y.-X., Yanni, Y. G., and Dazzo, F. B. (2005). Ascending migration of endophytic rhizobia, from roots to leaves, inside rice plants and assessment of benefits to rice growth physiology. *Appl. Environ. Microbiol.* 71, 7271–7278. doi: 10.1128/AEM.71.11.7271-7278.2005

Clarke, J. D., Volko, S. M., Ledford, H., Ausubel, F. M., and Dong, X. (2000). Roles of Salicylic acid, jasmonic acid, and ethylene in cpr-induced resistance in *Arabidopsis*. *Plant Cell* 12, 2175–2190. doi: 10.2307/3871113

Coleman-Derr, D., Desgarennes, D., Fonseca-Garcia, C., Gross, S., Clingenpeel, S., Woyke, T., et al. (2016). Plant compartment and biogeography affect microbiome composition in cultivated and native Agave species. *New Phytol.* 209, 798–811. doi: 10.1111/nph.13697

Cooper, A. J., Latunde-Dada, A. O., Woods-Tör, A., Lynn, J., Lucas, J. A., Crute, I. R., et al. (2008). Basic Compatibility of *Albugo candida* in *Arabidopsis thaliana* and *Brassica juncea* causes broad-spectrum suppression of innate immunity. *Mol. Plant Microbe Interact.* 21, 745–756. doi: 10.1094/MPMI-21-6-0745

Cox, J., Hein, M. Y., Luber, C. A., Paron, I., Nagaraj, N., and Mann, M. (2014). Accurate proteome-wide label-free quantification by delayed normalization and maximal peptide ratio extraction, termed MaxLFQ. *Mol. Cell. Proteomics* 13, 2513–2526. doi: 10.1074/mcp.M113.031591

Cox, J., and Mann, M. (2008). MaxQuant enables high peptide identification rates, individualized p.p.b.-range mass accuracies and proteome-wide protein quantification. *Nat. Biotechnol.* 26, 1367–1372. doi: 10.1038/nbt.1511

Cox, J., and Mann, M. (2012). 1D and 2D annotation enrichment: a statistical method integrating quantitative proteomics with complementary high-throughput data. *BMC Bioinforma.* 13(Suppl. 16):S12. doi: 10.1186/1471-2105-13-S16-S12

Craig, R., and Beavis, R. C. (2004). TANDEM: matching proteins with tandem mass spectra. *Bioinformatics* 20, 1466–1467. doi: 10.1093/bioinformatics/bth092

Daudi, A., Cheng, Z., O'brien, J. A., Mammarella, N., Khan, S., Ausubel, F. M., et al. (2012). The apoplastic oxidative burst peroxidase in *Arabidopsis* is a major component of pattern-triggered immunity. *Plant Cell* 24, 275–287. doi: 10.1105/tpc.111.093039

De Vos, M., Van Oosten, V. R., Van Poecke, R. M. P., Van Pelt, J. A., Pozo, M. J., Mueller, M. J., et al. (2005). Signal signature and transcriptome changes of arabidopsis during pathogen and insect attack. *Mol. Plant Microbe Interact.* 18, 923–937. doi: 10.1094/MPMI-18-0923

De Wit, P. J. G. M., Mehrabi, R., Van Den Burg, H. A., and Stergiopoulos, I. (2009). Fungal effector proteins: past, present and future. *Mol. Plant Pathol.* 10, 735–747. doi: 10.1111/j.1364-3703.2009.00591.x

Delaunois, B., Jeandet, P., Clément, C., Baillieul, F., Dorey, S., and Cordelier, S. (2014). Uncovering plant-pathogen crosstalk through apoplastic proteomic studies. *Front. Plant Sci.* 5:249. doi: 10.3389/fpls.2014.00249

Deutsch, E. W., Mendoza, L., Shteynberg, D., Farrah, T., Lam, H., Tasman, N., et al. (2010). A guided tour of the trans-proteomic pipeline. *Proteomics* 10, 1150–1159. doi: 10.1002/pmic.200900375

Doehlemann, G., and Hemetsberger, C. (2013). Apoplastic immunity and its suppression by filamentous plant pathogens. *New Phytol.* 198, 1001–1016. doi: 10.1111/nph.12277

Dong, Z., Canny, M. J., Mccully, M. E., Roboredo, M. R., Cabadilla, C. F., Ortega, E., et al. (1994). A nitrogen-fixing endophyte of sugarcane stems (A New Role for the Apoplast). *Plant Physiol.* 105, 1139–1147.

Emanuelsson, O., Nielsen, H., Brunak, S., and Von Heijne, G. (2000). Predicting subcellular localization of proteins based on their N-terminal amino acid sequence. *J. Mol. Biol.* 300, 1005–1016. doi: 10.1006/jmbi.2000.3903

Floerl, S., Druebert, C., Majcherczyk, A., Karlovsky, P., Kües, U., and Polle, A. (2008). Defence reactions in the apoplastic proteome of oilseed rape (*Brassica napus* var. napus) attenuate *Verticillium longisporum* growth but not disease symptoms. *BMC Plant Biol.* 8:129. doi: 10.1186/1471-2229-8-129

Floerl, S., Majcherczyk, A., Possienke, M., Feussner, K., Tappe, H., Gatz, C., et al. (2012). *Verticillium longisporum* infection affects the leaf apoplastic proteome, metabolome, and cell wall properties in *Arabidopsis thaliana*. *PLoS ONE* 7:e31435. doi: 10.1371/journal.pone.0031435

Fowler, S., and Thomashow, M. F. (2002). *Arabidopsis* transcriptome profiling indicates that multiple regulatory pathways are activated during cold acclimation in addition to the cbf cold response pathway. *Plant Cell* 14, 1675–1690. doi: 10.1105/tpc.003483

Glazebrook, J. (2005). Contrasting mechanisms of defense against biotrophic and necrotrophic pathogens. *Annu. Rev. Phytopathol.* 43, 205–227. doi: 10.1146/annurev.phyto.43.040204.135923

Halkier, B. A., and Gershenzon, J. (2006). Biology and biochemistry of glucosinolates. *Annu. Rev. Plant Biol.* 57, 303–333. doi: 10.1146/annurev.arplant.57.032905.105228

Holub, E., Beynon, J., and Crute, I. (1994). Phenotypic and genotypic characterization of interactions between isolates of *Peronospora parasitica* and accessions of *Arabidopsis thaliana*. *Mol. Plant Microbe Interact.* 7, 223–239. doi: 10.1094/MPMI-7-0223

Irieda, H., Maeda, H., Akiyama, K., Hagiwara, A., Saitoh, H., Uemura, A., et al. (2014). *Colletotrichum orbiculare* secretes virulence effectors to a biotrophic interface at the primary hyphal neck via exocytosis coupled with SEC22-mediated traffic. *Plant Cell* 26, 2265–2281.

Kaffarnik, F. A. R., Jones, A. M. E., Rathjen, J. P., and Peck, S. C. (2009). Effector Proteins of the bacterial pathogen *Pseudomonas syringae* alter the extracellular proteome of the host plant, *Arabidopsis thaliana*. *Mol. Cell. Proteomics* 8, 145–156. doi: 10.1074/mcp.M800043-MCP200

Kemen, E., Gardiner, A., Schultz-Larsen, T., Kemen, A. C., Balmuth, A. L., Robert-Seilaniantz, A., et al. (2011). Gene gain and loss during evolution of obligate parasitism in the white rust pathogen of *Arabidopsis thaliana*. *PLoS Biol.* 9:e1001094. doi: 10.1371/journal.pbio.1001094

Kemen, E., and Jones, J. D. G. (2012). Obligate biotroph parasitism: can we link genomes to lifestyles? *Trends Plant Sci.* 17, 448–457. doi: 10.1016/j.tplants.2012.04.005

Kemen, E., Kemen, A. C., Rafiqi, M., Hempel, U., Mendgen, K., Hahn, M., et al. (2005). Identification of a protein from rust fungi transferred from haustoria into infected plant cells. *Mol. Plant Microbe Interact.* 18, 1130–1139. doi: 10.1094/MPMI-18-1130

Kim, J. Y., Wu, J., Kwon, S. J., Oh, H., Lee, S. E., Kim, S. G., et al. (2014). Proteomics of rice and *Cochliobolus miyabeanus* fungal interaction: insight into proteins at intracellular and extracellular spaces. *Proteomics* 14, 2307–2318. doi: 10.1002/pmic.201400066

Koornneef, M., and Meinke, D. (2010). The development of *Arabidopsis* as a model plant. *Plant J.* 61, 909–921. doi: 10.1111/j.1365-313X.2009.04086.x

Kreps, J. A., Wu, Y., Chang, H.-S., Zhu, T., Wang, X., and Harper, J. F. (2002). Transcriptome changes for *Arabidopsis* in response to salt, osmotic, and cold stress. *Plant Physiol.* 130, 2129–2141. doi: 10.1104/pp.008532

Laemmli, U. K. (1970). Cleavage of structural proteins during the assembly of the head of bacteriophage T4. *Nature* 227, 680–685. doi: 10.1038/227680a0

Lehfeldt, C., Shirley, A. M., Meyer, K., Ruegger, M. O., Cusumano, J. C., Viitanen, P. V., et al. (2000). Cloning of the SNG1 gene of *Arabidopsis* reveals a role for a serine carboxypeptidase-like protein as an acyltransferase in secondary metabolism. *Plant Cell* 12, 1295–1306. doi: 10.2307/3871130

Léon-Kloosterziel, K. M., Gil, M. A., Ruijs, G. J., Jacobsen, S. E., Olszewski, N. E., Schwartz, S. H., et al. (1996). Isolation and characterization of abscisic acid-deficient *Arabidopsis mutants* at two new loci. *Plant J.* 10, 655–661. doi: 10.1046/j.1365-313X.1996.10040655.x

Lewis, L. A., Polanski, K., De Torres-Zabala, M., Jayaraman, S., Bowden, L., Moore, J., et al. (2015). Transcriptional dynamics driving MAMP-triggered immunity and pathogen effector-mediated immunosuppression in *Arabidopsis* leaves following infection with *Pseudomonas syringae* pv tomato DC3000. *Plant Cell* 27, 3038–3064. doi: 10.1105/tpc.15.00471

Lian, X., Wang, S., Zhang, J., Feng, Q., Zhang, L., Fan, D., et al. (2006). Expression Profiles of 10,422 Genes at Early Stage of Low Nitrogen Stress in Rice Assayed using a cDNA Microarray. *Plant Mol. Biol.* 60, 617–631. doi: 10.1007/s11103-005-5441-7

Loon, L. C. V., Rep, M., and Pieterse, C. M. J. (2006). Significance of inducible defense-related proteins in infected plants. *Annu. Rev. Phytopathol.* 44, 135–162. doi: 10.1146/annurev.phyto.44.070505.143425

Maleck, K., Levine, A., Eulgem, T., Morgan, A., Schmid, J., Lawton, K. A., et al. (2000). The transcriptome of *Arabidopsis thaliana* during systemic acquired resistance. *Nat. Genet.* 26, 403–410. doi: 10.1038/82521

Mammarella, N. D., Cheng, Z., Fu, Z. Q., Daudi, A., Bolwell, G. P., Dong, X., et al. (2015). Apoplastic peroxidases are required for salicylic acid-mediated defense against *Pseudomonas syringae*. *Phytochemistry* 112, 110–121. doi: 10.1016/j.phytochem.2014.07.010

McKinney, E. C., Ali, N., Traut, A., Feldmann, K. A., Belostotsky, D. A., Mcdowell, J. M., et al. (1995). Sequence-based identification of T-DNA insertion mutations in *Arabidopsis*: actin mutants act2-1 and act4-1. *Plant J.* 8, 613–622. doi: 10.1046/j.1365-313X.1995.8040613.x

McMullan, M., Gardiner, A., Bailey, K., Kemen, E., Ward, B. J., Cevik, V., et al. (2015). Evidence for suppression of immunity as a driver for genomic introgressions and host range expansion in races of *Albugo candida*, a generalist parasite. *eLife* 4:e04550. doi: 10.7554/eLife.04550

Mittler, R. (2006). Abiotic stress, the field environment and stress combination. *Trends Plant Sci.* 11, 15–19. doi: 10.1016/j.tplants.2005.11.002

Nagano, A. J., Sato, Y., Mihara, M., Antonio, B. A., Motoyama, R., Itoh, H., et al. (2012). Deciphering and prediction of transcriptome dynamics under fluctuating field conditions. *Cell* 151, 1358–1369. doi: 10.1016/j.cell.2012.10.048

Nawrath, C., and Métraux, J. P. (1999). Salicylic acid induction-deficient mutants of *Arabidopsis* express PR-2 and PR-5 and accumulate high levels of camalexin after pathogen inoculation. *Plant Cell* 11, 1393–1404. doi: 10.2307/3870970

Oksanen, J., Blanchet, F. G., Kindt, R., Legendre, P., Minchin, P. R., O'Hara, R. B., et al. (2015). *vegan: Community Ecology Package. R Package Version 2.2-1*. Available at: http://CRAN.R-project.org/package = vegan

Oliveira-Garcia, E., and Valent, B. (2015). How eukaryotic filamentous pathogens evade plant recognition. *Curr. Opin. Microbiol.* 26, 92–101. doi: 10.1016/j.mib.2015.06.012

Palenchar, P., Kouranov, A., Lejay, L., and Coruzzi, G. (2004). Genome-wide patterns of carbon and nitrogen regulation of gene expression validate the combined carbon and nitrogen (CN)-signaling hypothesis in plants. *Genome Biol.* 5, 1–15. doi: 10.1186/gb-2004-5-11-r91

Penninckx, I. A. M. A., Thomma, B. P. H. J., Buchala, A., Métraux, J.-P., and Broekaert, W. F. (1998). Concomitant activation of jasmonate and ethylene response pathways is required for induction of a plant defensin gene in *Arabidopsis*. *Plant Cell* 10, 2103–2113. doi: 10.1105/tpc.10.12.2103

Ploch, S., and Thines, M. (2011). Obligate biotrophic pathogens of the genus Albugo are widespread as asymptomatic endophytes in natural populations of *Brassicaceae*. *Mol. Ecol.* 20, 3692–3699. doi: 10.1111/j.1365-294X.2011.05188.x

R Core Team (2013). *R: A Language and Environment for Statistical Computing*. Vienna: R Foundation for Statistical Computing. Available at: http://www.R-project.org/

Rabello, A., Guimarães, C., Rangel, P., Da Silva, F., Seixas, D., De Souza, E., et al. (2008). Identification of drought-responsive genes in roots of upland rice (*Oryza sativa* L). *BMC Genomics* 9:485. doi: 10.1186/1471-2164-9-485

Rafiqi, M., Gan, P. H. P., Ravensdale, M., Lawrence, G. J., Ellis, J. G., Jones, D. A., et al. (2010). Internalization of flax rust avirulence proteins into flax and tobacco cells can occur in the absence of the pathogen. *Plant Cell* 22, 2017–2032. doi: 10.1105/tpc.109.072983

Rappsilber, J., Mann, M., and Ishihama, Y. (2007). Protocol for micro-purification, enrichment, pre-fractionation and storage of peptides for proteomics using StageTips. *Nat. Protoc.* 2, 1896–1906. doi: 10.1038/nprot.2007.261

Rasmussen, S., Barah, P., Suarez-Rodriguez, M. C., Bressendorff, S., Friis, P., Costantino, P., et al. (2013). Transcriptome responses to combinations of stresses in *Arabidopsis*. *Plant Physiol.* 161, 1783–1794. doi: 10.1104/pp.112.210773

Richards, C. L., Rosas, U., Banta, J., Bhambhra, N., and Purugganan, M. D. (2012). Genome-wide patterns of *Arabidopsis* gene expression in nature. *PLoS Genet.* 8:e1002662. doi: 10.1371/journal.pgen.1002662

Rizhsky, L., Liang, H., Shuman, J., Shulaev, V., Davletova, S., and Mittler, R. (2004). When defense pathways collide. the response of *Arabidopsis* to a combination of drought and heat stress. *Plant Physiol.* 134, 1683–1696. doi: 10.1104/pp.103.033431

Schenk, P. M., Kazan, K., Wilson, I., Anderson, J. P., Richmond, T., Somerville, S. C., et al. (2000). Coordinated plant defense responses in *Arabidopsis* revealed by microarray analysis. *Proc. Natl. Acad. Sci. U.S.A.* 97, 11655–11660. doi: 10.1073/pnas.97.21.11655

Sharon, N., and Lis, H. (2004). History of lectins: from hemagglutinins to biological recognition molecules. *Glycobiology* 14, 53R–62R. doi: 10.1093/glycob/cwh122

Spanu, P., and Kämper, J. (2010). Genomics of biotrophy in fungi and oomycetes — emerging patterns. *Curr. Opin. Plant Biol.* 13, 409–414. doi: 10.1016/j.pbi.2010.03.004

Stuttmann, J., Hubberten, H.-M., Rietz, S., Kaur, J., Muskett, P., Guerois, R., et al. (2011). Perturbation of *Arabidopsis* amino acid metabolism causes incompatibility with the adapted biotrophic pathogen *Hyaloperonospora arabidopsidis*. *Plant Cell* 23, 2788–2803. doi: 10.1105/tpc.111.087684

Thomma, B. P. H. J., Eggermont, K., Penninckx, I. A. M. A., Mauch-Mani, B., Vogelsang, R., Cammue, B. P. A., et al. (1998). Separate jasmonate-dependent and salicylate-dependent defense-response pathways in *Arabidopsis* are essential for resistance to distinct microbial pathogens. *Proc. Natl. Acad. Sci. U.S.A.* 95, 15107–15111. doi: 10.1073/pnas.95.25.15107

Ton, J., and Mauch-Mani, B. (2004). β-amino-butyric acid-induced resistance against necrotrophic pathogens is based on ABA-dependent priming for callose. *Plant J.* 38, 119–130. doi: 10.1111/j.1365-313X.2004.02028.x

Trentin, A. R., Pivato, M., Mehdi, S. M. M., Barnabas, L. E., Giaretta, S., Fabrega-Prats, M., et al. (2015). Proteome readjustments in the apoplastic space of *Arabidopsis thaliana* ggt1 mutant leaves exposed to UV-B radiation. *Front. Plant Sci.* 6:128. doi: 10.3389/fpls.2015.00128

Uknes, S., Mauch-Mani, B., Moyer, M., Potter, S., Williams, S., Dincher, S., et al. (1992). Acquired resistance in *Arabidopsis*. *Plant Cell* 4, 645–656. doi: 10.1105/tpc.4.6.645

Uknes, S., Winter, A. M., Delaney, T., Vernooij, B., Morse, A., Friedrich, L., et al. (1993). Biological induction of systemic acquired resistance in *Arabidopsis*. *MPMI-Mol. Plant Microbe Interact.* 6, 692–698. doi: 10.1094/MPMI-6-692

van Treuren, R., Kuittinen, H., Kärkkäinen, K., Baena-Gonzalez, E., and Savolainen, O. (1997). Evolution of microsatellites in *Arabis petraea* and *Arabis lyrata*, outcrossing relatives of *Arabidopsis thaliana*. *Mol. Biol. Evol.* 14, 220–229. doi: 10.1093/oxfordjournals.molbev.a025758

Vorholt, J. A. (2012). Microbial life in the phyllosphere. *Nat. Rev. Microbiol.* 10, 828–840. doi: 10.1038/nrmicro2910

Welinder, K. G., Justesen, A. F., Kjærsgård, I. V. H., Jensen, R. B., Rasmussen, S. K., Jespersen, H. M., et al. (2002). Structural diversity and transcription of class III peroxidases from *Arabidopsis thaliana*. *Eur. J. Biochem.* 269, 6063–6081. doi: 10.1046/j.1432-1033.2002.03311.x

Wessel, D., and Flügge, U. I. (1984). A method for the quantitative recovery of protein in dilute solution in the presence of detergents and lipids. *Anal. Biochem.* 138, 141–143. doi: 10.1016/0003-2697(84)90782-6

Conflict of Interest Statement: The authors declare that the research was conducted in the absence of any commercial or financial relationships that could be construed as a potential conflict of interest.

frontiers in Plant Science

ORIGINAL RESEARCH
published: 08 March 2016
doi: 10.3389/fpls.2016.00269

Identification of *Phakopsora pachyrhizi* Candidate Effectors with Virulence Activity in a Distantly Related Pathosystem

*Sridhara G. Kunjeti †‡, Geeta Iyer‡, Ebony Johnson, Eric Li, Karen E. Broglie, Gilda Rauscher and Gregory J. Rairdan **

DuPont Experimental Station, Wilmington, DE, USA

OPEN ACCESS

Edited by:
Pietro Daniele Spanu, Imperial College London, UK

Reviewed by:
Bret Cooper, United States Department of Agriculture, USA
Joe Win, The Sainsbury Laboratory, UK

***Correspondence:**
Gregory J. Rairdan
grairdan@gmail.com

†Present Address:
Sridhara G. Kunjeti, Department of Plant Pathology, University of California, Salinas, CA, USA

‡*These authors have contributed equally to this work.*

Specialty section:
This article was submitted to Plant Biotic Interactions, a section of the journal Frontiers in Plant Science

Received: *06 January 2016*
Accepted: *21 February 2016*
Published: *08 March 2016*

Citation:
Kunjeti SG, Iyer G, Johnson E, Li E, Broglie KE, Rauscher G and Rairdan GJ (2016) Identification of Phakopsora pachyrhizi Candidate Effectors with Virulence Activity in a Distantly Related Pathosystem. Front. Plant Sci. 7:269. doi: 10.3389/fpls.2016.00269

Phakopsora pachyrhizi is the causal agent of Asian Soybean Rust, a disease that causes enormous economic losses, most markedly in South America. *P. pachyrhizi* is a biotrophic pathogen that utilizes specialized feeding structures called haustoria to colonize its hosts. In rusts and other filamentous plant pathogens, haustoria have been shown to secrete effector proteins into their hosts to permit successful completion of their life cycle. We have constructed a cDNA library from *P. pachyrhizi* haustoria using paramagnetic bead-based methodology and have identified 35 *P. pachyrhizi* candidate effector (CE) genes from this library which are described here. In addition, we quantified the transcript expression pattern of six of these genes and show that two of these CEs are able to greatly increase the susceptibility of *Nicotiana benthamiana* to *Phytophthora infestans*. This strongly suggests that these genes play an important role in *P. pachyrhizi* virulence on its hosts.

Keywords: Asian soybean rust, soybean, effectors, virulence

INTRODUCTION

Soybean rust is a devastating disease that threatens soybean crops worldwide. Its effect is most pronounced in Brazil, where crop losses and extra fungicide expenses have been calculated to be in the billions of dollars (Yorinori et al., 2005). While extensive effort has been made to discover effective genetic resistance to this disease in soybean there are currently no known resistant commercial cultivars and extensive germplasm screening has not identified soy varieties that are resistant to all known rust isolates (Walker et al., 2014). These observations, plus the fact that *Phakopsora pachyrhizi* has an unusually broad host range for an obligate biotroph (Keogh, 1976; Slaminko et al., 2008), suggest that this pathogen is very adept at evading host defenses.

Many filamentous pathogens, including rusts, exert their virulence through effector proteins that are transferred into plant cells from haustoria (Garnica et al., 2014); specialized feeding structures that become embedded in host cells without breaching the plasma membrane. Fungal effectors translocate from haustoria into plant cells through a poorly-understood mechanism and then act to modulate the physiology of their host (Petre et al., 2014). Effectors were first identified as avirulence genes that triggered strong host defense responses known as ETI (effector-triggered immunity), but many effectors have since been shown to play an important virulence function for the pathogen expressing them (Kamoun, 2007). While some effectors are thought to play a role in nutrient uptake, most characterized effectors that have a

demonstrated virulence activity act by suppressing host defenses (Göhre and Robatzek, 2008). There are many examples of effectors from filamentous pathogens that have been shown to suppress plant defenses. In oomycetes, Avr3a and Avrblb2 from *Phytophthora infestans* were shown to suppress plant defense responses (Bos et al., 2010; Bozkurt et al., 2011) as were a large number of predicted effectors from *Hyaloperonospora arabidopsidis* (Fabro et al., 2011). In fungi, the rice blast (*Magnaporthe oryzae*) effector AvrPiz-t suppresses immunity in rice by targeting a RING E3 ubiquitin ligase (Park et al., 2012), while corn smut (*Ustilago maydis*) Pep1 can subdue corn defense responses via the suppression of peroxidase activity (Hemetsberger et al., 2012).

Like other filamentous pathogens, rust proteins have been identified that trigger ETI in plant cells (Dodds et al., 2004; Catanzariti et al., 2006), and a number of intriguing studies have demonstrated biochemical activities attributable to secreted rust proteins (Kemen et al., 2013; Pretsch et al., 2013; Petre et al., 2015a,b) but to date no rust effectors have been clearly shown to block plant defenses or enhance pathogen virulence. In this study, we have developed an improved method to generate a cDNA library from *P. pachyrhizi* haustoria and have bioinformatically identified 35 candidate effectors. Gene expression analysis of six of these CEs showed expression patterns consistent with these genes having a role in virulence. Additionally, we were able to show that when expressed *in planta*, two of these candidate effectors were able to dramatically enhance *P. infestans* virulence on *Nicotiana benthamiana*, suggesting that these effectors are important for *P. pachyrhizi* virulence on hosts.

MATERIALS AND METHODS

Plant Growth and Infection Conditions

Glycine max was grown in a growth chamber at 22°C with a 16 h photoperiod until the primary (unifoliate) leaves had fully expanded. All experiments with *P. pachyrhizi* were performed in an USDA/APHIS-approved biocontainment facility. All inoculation experiments were conducted with a GA-05, an internal *P. pachyrhizi* field isolate collected from a soybean field in Georgia in 2005.

Before inoculation, spores were suspended in an aqueous solution of 0.01% Tween 20, heat-shocked at 40°C for 5 min and mixed thoroughly; the spore concentration was then adjusted to 1×10^5 with a hemocytometer. Plants were spray-inoculated with the urediniospore suspension, incubated at 100% relative humidity in the dark for 24–36 h and then transferred to a growth chamber set at 22°C, 70% RH, 16 h photoperiod.

P. pachyrhizi cDNA Library Construction

Fifty-four infected leaves were detached 8 days following inoculation, briefly rinsed with H_2O and transferred to a chilled blender, where they were homogenized in 100 ml of homogenization buffer (0.3 M Sorbitol, 20 mM MOPS, 0.2% PVP, 1 mM DTT, 0.1% BSA, pH 7.2) with 0.2% RNA protect solution (Qiagen). The homogenate was filtered first through Nytex 100 mesh and then through Nytex 25. The filtrate was then concentrated by centrifugation and resuspended in suspension buffer: 0.3 M Sorbitol, 10 mM MOPS, 0.2% BSA, 1 mM $CaCl_2$, 1 mM $MnCl_2$, and kept on ice. The resuspension was divided into six aliquots of 1 ml each and mixed with Con-A-biotin paramagnetic beads which were prepared by mixing 150 µl of 1 mg/ml Con-A-biothin, 150 µl of streptavidin paramagnetic beads and suspension buffer in a total volume of 900 µl. Con-A-streptavidin bead complex (200 µl) was added to each 1 ml aliquot of the resuspended homogenate and mixed at 4°C for 30 min. The mixture was then washed by placing tubes in magnetic stands and exchanging suspension buffer three times after beads have aggregated proximal to the stand. After the last wash was removed, the beads were suspended in 250 µl of Trizol and transferred to a glass dounce, where the collected tissue was homogenized. Trizol solution was transferred to a microfuge tube with 200 µl of chloroform, mixed and centrifuged. The aqueous phase was then transferred to a new tube and the RNA was precipitated with NaCl and isopropanol. Precipitated RNA was pelleted and resuspended in 20 µl H_2O. This total RNA was used to make a cDNA library using the Clontech SMART directional cDNA kit according to the manufacturer's recommendations.

Gene Expression Profiling

Soybean (*Glycine max*, var. Jack) plants were grown to the VC stage and then spray-inoculated with a suspension of *P. pachyrhizi* spores (GA05-1; 100 k spores/ml 0.01% Tween 20). Unifoliate leaves were collected from three replicate plants and flash frozen in liquid nitrogen at 0, 12, 24, 36, 48, 72, 96, and 168 h post-infection (hpi). Total RNA was prepared from either uninfected or infected leaf tissue using Trizol Reagent (Life Technologies #15596-026). Isolated total RNA was DNAse-treated and cDNA synthesized using the QuantiTect Reverse Transcription Kit (Qiagen #205311). Absolute quantification of transcript levels was determined by TaqMan qPCR (TaqMan Gene Expression Master Mix; Applied Biosystems #4309849). Each sample was run in triplicate on a QuantStudio™ 6 Flex Real-Time PCR System (Applied Biosystems) using cDNA generated from 200 ng of total RNA and the primers (200 nM each) and probes (100 nM) indicated in **Supplementary Table 1**. QuantStudio 6 and 7 Flex Software was employed for analysis. Effector transcript levels in infected plants are expressed relative to those of a *P. pachyrhizi* α-tubulin gene DN739993.1, (van de Mortel et al., 2007) that was used as an internal control for expression studies.

Effector Virulence Assays

N. benthamiana plants were grown in a controlled environment green house at 22°C with 55% humidity at 16 h light. Agrobacteria were incubated in induction buffer (1 l MMA: 5 g MS salts, 1.95 g MES, 20 g sucrose, 200 µM acetosyringone, pH 5.6) for at least 1 h prior to infiltration into leaves as described (Bos et al., 2006).

P. infestans (wild-type isolated from an infested tomato field in New Castle County, Delaware) was grown on pea agar at 18°C in the dark. Two leaves of 4- to 5-week old *N. benthamiana* plants were agro-infiltrated at an OD_{600} of 0.3 with the binary vector pMAXY226 (tagged with 3x FLAG toward the C-terminus) on one half of the mid-vein and an effector cloned into pMAXY226 (tagged with 3x FLAG toward the C-terminus) into the other half of the same leaf. *P. infestans* sporangia were harvested and

diluted to ∼100,000 spores/ml (Kamoun et al., 1998; Schornack et al., 2010). Droplets (10 μl) of zoospores were applied onto the abaxial side of detached leaves 24 h post agro-infiltration and incubated for several days on wet paper towels in 100% relative humidity (King et al., 2014). To determine lesion size, leaves were placed on a light box and photographed. On the resulting image, the border of the lesion that was visible (dark brown region) was marked manually on digital images of standardized size. An example of a marked image is shown in **Supplementary Figure 1**. Lesion area within this border was then calculated with Image-Pro Analyzer (v7.0) software from these images.

Effectors CSEP-07, CSEP-08, CSEP-09, and CSEP-35 were synthesized (Genscript, Piscataway, NJ) without signal peptide and cloned into an expression vector fused with 3x FLAG tag at the 3′ end of the gene. Mature effector PexRD2 was amplified from the genomic DNA of *P. infestans* using KOD DNA high fidelity polymerase (Novagen) and was also sub-cloned into the expression vector with a 3x FLAG tag. The sequence of PexRD2 was confirmed by sequencing. All three cloned vectors were sequence-verified and transformed into *Agrobacterium tumefaciens* (AGL1 competent cells).

Agro-infiltrated *N. benthamiana* leaves were harvested at 5 days post-infiltration (dpi). Total protein extracts were prepared by grinding five leaf discs (6.0 mm each) in 1 ml radioimmunoprecipitation assay (RIPA) lysis and extraction buffer (Pierce® RIPA buffer product no. 89900; Thermo Scientific, Rockford, IL, USA) in the presence of 0.1 mM protease inhibitor HALT Protease and Phosphatase inhibitor cocktail (Thermo Scientific, no. 78442).

Accession Numbers

Sequence data from this article can be found in the GenBank data library under accession numbers KU695151–KU695185.

RESULTS

In order to understand *P. pachyrhizi* virulence, we sought to identify genes that encode effector proteins. Rust effectors are synthesized in and translocated into host cells from specialized structures called haustoria, so we generated and screened a cDNA library from isolated haustoria, an approach that has been successful in identifying effectors from other rust fungi (Hahn and Mendgen, 1992; Catanzariti et al., 2006).

We developed a new method for isolating haustorial RNA as we were initially unsuccessful in isolating RNA from haustoria using concanavalin A-conjugated beads, the method that has been successfully used to generate cDNA libraries from other rust species (Hahn and Mendgen, 1997; Catanzariti et al., 2006). Link et al. (2014) also noted difficulty in identifying high-quality RNA from *P. pachyrhizi* haustoria using Con-A sepharose beads, but were ultimately successful in generating a haustorial transcriptome using next-generation sequencing. We homogenized soybean leaves infected with *P. pachyrhizi* field isolate GA-05 8 days prior and filtered the extract through Nytex membranes. Instead of a Sepharose A column, we used streptavidin-conjugated paramagnetic beads that were then coated with biotin-concanavalin A (**Figure 1A**). These concanavalin A beads were then added to filtered extract of leaves that had been inoculated with *P. pachyrhizi* 8 days prior. The bound fraction of the extract was washed twice, greatly reducing chloroplast abundance (**Figures 1B–D**), and then RNA was extracted. We extracted 2.7 μg of high quality RNA from 54 infected leaves, and this RNA was used to construct a directional cDNA library (**Figure 1E**). We obtained quality sequence from 6481 clones using Sanger sequencing, which provided us with 500–900 bp of 5′ sequence for each clone. This collection of sequences was then assembled into 1944 contigs, 1633 of which were singletons. We identified 995 ORFs predicted to encode proteins of fifty amino acids or more in these 1944 contigs and these ORFs. A BLAST search identified 187 of these sequences that had a closest homolog from the plant kingdom and these were disregarded. The remaining 808 sequences were then analyzed with the SignalP algorithm to identify sequences with predicted secretory signal peptides (Emanuelsson et al., 2007). If the sequence did not encode any signal peptides, or if an ORF encoding a signal peptide was not the longest ORF for that sequence, the clone was disregarded. In addition the sequence was discarded if there was not a stop codon seen 5′ to the start codon of the largest ORF, which eliminates partial transcripts with incomplete ORFs. This left us with a collection of clones with sequences of predicted haustorially-expressed secreted proteins (HESPs). Within this collection of HESPs we found homologs of a number of previously characterized HESPs, such as hexose transporter 1, AAT1, and RTP1 (Hahn and Mendgen, 1997; Mendgen et al., 2000; Voegele et al., 2001).

While only six rust effectors have been validated to date (Petre et al., 2014), the most striking similarity of these effectors is that they do not have homology to any proteins from species outside of Pucciniales (Saunders et al., 2012; Petre et al., 2014). We thus used this as the primary criterion to identify the strongest effector candidates from *P. pachyrhizi*. We searched the HESP collection against Genbank and fully sequenced a representative clone from each contig that did not have clear homologs from any non-Pucciniales species. The predicted proteins from fully-sequenced clones were again searched against the Genbank protein database to rule out non-rust orthologs and the remaining sequences comprise our collection of *P. pachyrhizi* candidate effectors. These coding sequences are predicted to encode *P. pachyrhizi* candidate secreted effector proteins and they were thus named Pp-CSEP-01 to Pp-CSEP-35 (**Supplementary Files 1, 2**).

Within our collection of CEs, twenty-four are unique to *P. pachyrhizi*, while twelve have orthologs in at least one other rust species (**Table 1**). We also found that 31/35 of our CEs were identified in the *P. pachyrhizi* Thai1 transcriptome described by Link et al. (2014), although only fifteen of these were identified as secreted proteins in that study (**Table 1**). Nine of the CEs identified here were not annotated as secreted proteins in Link et al. (2014) because the assembled transcript was not full length and presumably would not have been identified as an ORF. While effectors from filamentous pathogens have been shown to evolve rapidly (Allen et al., 2004; Dodds et al., 2006; Win et al., 2007), we found that most of the *P. pachyrhizi* Thai1 homologs were highly conserved with the CEs we identified from GA-05. Only CSEP-01, CSEP-14, and CSEP-22 have clear

Thai1 homologs with <90% amino acid identity. Interestingly, CEs that have homologs in other rust species are only relatively distantly related to these proteins, with no orthologs having more than 50% amino acid identity. A public EST collection generated from germinating urediniospores (Posada-Buitrago and Frederick, 2005) was searched for these sequences and only six CEs were found (**Table 1**). This EST collection contains over 34,000 sequences while our haustorial collection consists of <6500 clones, suggesting that the transcripts of 29/35 of these CEs are more abundant in haustoria than urediniospores. While true effectors are often strongly induced while the pathogen is in planta, it is not always the case (Dodds et al., 2004; Catanzariti et al., 2006), so we cannot exclude the transcripts that are expressed in urediniospores from our CE collection.

We wished to determine if the expression of these CEs were induced in planta. To determine the expression patterns of these CEs we analyzed the transcript levels of a random subset of six effectors during an infection time course using qRT-PCR (**Figure 2**). We measured CE transcript abundance as a fraction of the abundance of *P. pachyrhizi* α-tubulin, a gene shown to be constitutively expressed in rust species (Hacquard et al., 2011). We found that in 5/6 cases the CEs were strongly induced in planta, with two primary expression patterns observed: CSEP-03 and CSEP-07 transcript levels were undetectable in early infection and induced after day 3; in contrast, CSEP-06, CSEP-08, and CSEP-09 are maximally induced by 24 h and then continue to express throughout infection. CSEP-32 is the only CE strongly expressed at 12 h post-inoculation and is maximally induced at 24 h after which expression decreases. This also is consistent with the library data, as CSEP-32 is the only of these six CEs that could be found in the Posada-Buitrago EST collection (Posada-Buitrago and Frederick, 2005).

True effectors facilitate pathogen infection and we used a *N. benthamiana*/*P. infestans* pathosystem to detect virulence phenotypes of our CEs. This pathosystem was previously used to demonstrate the increased pathogen growth in *N. benthamia* transiently expressing *P. infestans* effector PexRD2 (King et al., 2014). We chose this system to assay *P. pachyrhizi* effectors because, like *P. pachyrhizi*, *P. infestans* is a hyphal pathogen and may be susceptible to the same plant defense responses. In addition, *N. benthamiana* is well-known for its high level of foreign protein expression (Goodin et al., 2008) and *P. infestans* only grows modestly on this host which allows for increased virulence to be more readily measured than a better-adapted plant-pathogen interaction.

We expressed *P. pachyrhizi* CEs via agrobacterium-mediated transient expression. CEs were cloned into a T-DNA vector that expresses the mature (signal peptide-truncated), epitope-tagged effector under the regulation of the strong double-Mirabilis Mosaic Virus promoter (Dey and Maiti, 1999). Each leaf was infiltrated with an effector and empty-vector control side-by-side. Twenty-four hours after infiltration *N. benthamiana* leaves were detached and both halves of the leaf were drop-inoculated with *P. infestans* zoospores and then incubated at room temperature as described by King et al. (2014). Four CEs, CSEP-07, CSEP-08, CSEP-09, and CSEP-35, were chosen to test. Expression of two of these CEs, CSEP-07, and CSEP-09 showed a dramatic

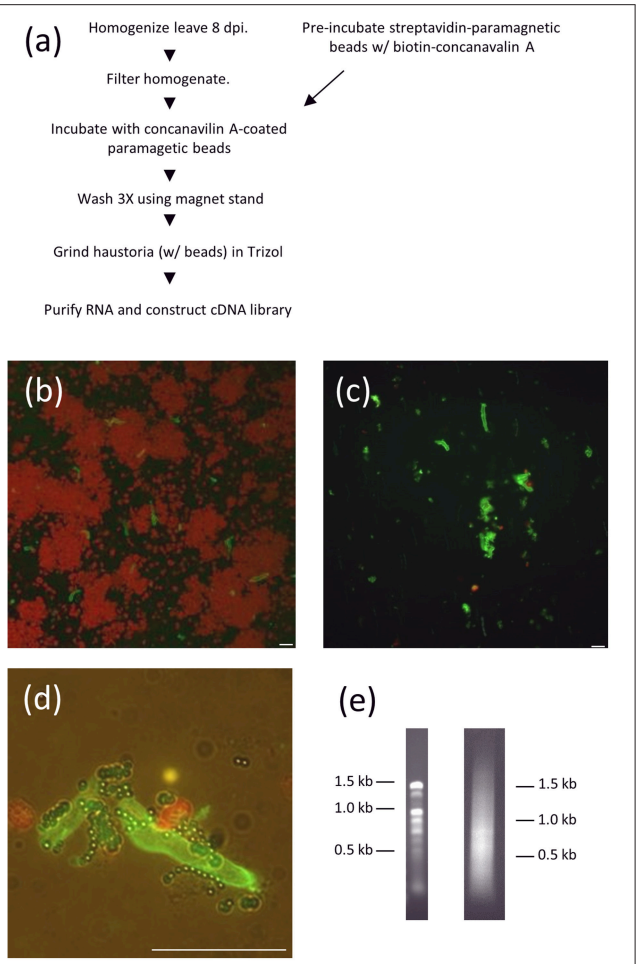

FIGURE 1 | RNA purification from isolated *P. pachyrhizi* haustoria. (A) Schematic of haustorial RNA purification. **(B)** Micrograph of ConA-FITC-stained haustoria after homogenization and filtration through Nytex membrane. Red objects are chloroplasts. Bar = 10 μm **(C)** ConA-FITC stained haustoria after paramagnetic bead purification. Bar = 10 μm **(D)** Close up of ConA-FITC stained haustoria after purification showing association with paramagnetic beads. Bar = 10 μm **(E)** 1% Agarose gel separation of 1 μg haustorial RNA (left) and 0.5 μg cDNA prep (right).

increase of *P. infestans* growth at s7 days post-inoculation, and these two effectors were chosen to study in greater detail. In further experiments, *P. infestans* growth was quantified 7 days after inoculation by photographing leaves and analyzing them with ImagePro Analyzer v7.0. **Figure 3A** shows representative infected leaves expressing CSEP-07, CSEP-09, and *P. infestans* PexRD2 as a positive control. The area infected in each lesion was calculated and plotted in **Figure 3B**. A clearly statistically significant increase in *P. infestans* growth was seen in tissue expressing these three effectors compared to controls; a paired student's *t*-test calculated the *p*-value to be <0.001 in each case. To confirm that the effectors being tested were expressed in the plant tissue, protein was extracted from plants infiltrated at the same time and immunoblotted using the α-FLAG antibody (**Figure 3C**). No macroscopic cell death phenotype was seen at the time of protein harvest (5-dpi).

TABLE 1 | Candidate *Phakopsora pachyrhizi* effectors.

Pp CSEP	Public EST[a]	Orf size (AA)	Cysteines	Unique to *Pp*[b]	Ortholog accession number (Organism)[c]	Link et al. contig[d]
Pp-CSEP-01	N	76	2	x		**5608**
Pp-CSEP-02	N	55	5	x		4757
Pp-CSEP-03	N	208	8	49	XP_003322944 (*Pgt*)	
Pp-CSEP-04	N	204	2	x		**5072**
Pp-CSEP-05	N	291	1	x		**3430**
Pp-CSEP-06	N	218	3	35	XP_003324954 (*Pgt*)	**4760**
Pp-CSEP-07	N	105	5	x		6714
Pp-CSEP-08	N	198	12	34	XP_007408015 (*Mlp*)	**3139**
Pp-CSEP-09	N	182	12	37	XP_007408015 (*Mlp*)	**8880**
Pp-CSEP-10	N	103	3	x		**5608**
Pp-CSEP-11	N	147	1	x		**7075**
Pp-CSEP-12	N	192	3	28	XP_007404648 (*Mlp*)	**3185**
Pp-CSEP-13	N	142	4	x		**1885**
Pp-CSEP-14	N	126	2	x		7139
Pp-CSEP-15	N	311	4	x		1327†
Pp-CSEP-16	N	270	2	46	KNF03382 (*Pst*)	**3900**
Pp-CSEP-17	N	240	4	x		2907†
Pp-CSEP-18	N	195	6	x		864†
Pp-CSEP-19	N	183	2	x		324
Pp-CSEP-20	N	327	5	x		3176†
Pp-CSEP-21	N	131	0	x		3969
Pp-CSEP-22	N	294	1	x		1454†
Pp-CSEP-23	N	134	0	x		**6204**
Pp-CSEP-24	N	312	2	x		2715†
Pp-CSEP-25	N	357	4	x		1326†
Pp-CSEP-26	N	196	7	32	XP_003332659 (*Pgt*)	
Pp-CSEP-27	Y	348	11	30	XP_003328542 (*Pgt*)	8815†
Pp-CSEP-28	N	321	3	x		7972†
Pp-CSEP-29	N	301	4	30	KNF03382 (Pst)	1256
Pp-CSEP-30	N	119	0	x		
Pp-CSEP-31	Y	213	9	x		**1525**
Pp-CSEP-32	Y	142	0	42	XP_003326807 (*Pgt*)	**3471**
Pp-CSEP-33	Y	161	8	34	XP_007403891 (*Mlp*)	
Pp-CSEP-34	Y	200	1	x		1607
Pp-CSEP-35	Y	291	20	44	KNZ58433 (*Ps*)	**4224**

[a] *presence of CSEP in public urediospore EST collection.*

[b] *x represents a CE for which orthologs could not be identified. Numbers are the percent amino acid identity of closest ortholog; numbers in bold are annotated as secreted proteins in Link et al. (2014).*

[c] *accession number of closest identified ortholog, source organism in parenthesis. Pgt, Puccinia graminis f. sp tritici, Mlp, Melampsora larici-populina; Pst, Puccinia striiformis f. sp. Tritici; Ps, Puccinia sorghi.*

[d] *contigs in bold are annotated as secreted proteins in Link et al. (2014).*

† *assembled transcript in Link et al. (2014) is not full-length.*

DISCUSSION

A biotrophic pathogen's ability to infect and colonize a host is at least partially a function of the collection of the effectors that it expresses during its life cycle. Identifying and characterizing the effectors of *P. pachyrhizi* is an important step toward understanding how this pathogen infects important crops like soybean and causes devastating economic consequences. We identified 35 *P. pachyrhizi* coding sequences that meet our strict criteria for effector candidates; a secretory signal peptide and the absence of any clear homologs outside of Pucciniales. Over half of predicted effectors are smaller than 200 amino acids, and over 80% are <300. In addition, most transcripts encoding these CEs were not found in a germinating urediniospore EST collection, suggesting haustorial enrichment.

Three rust genomes have been sequenced to date, *Puccinia graminis* f. sp. *tritici*, *Puccinia stiiformis* f. sp. *tritici, Melampspora larici-populina* (Duplessis et al., 2011; Cantu et al., 2013), and each has been shown to have a large number of families of short, secreted proteins that are presumed to be effectors important for pathogenesis. In addition, there have been thorough transcriptomic analyses of coffee rust, bean rust, and

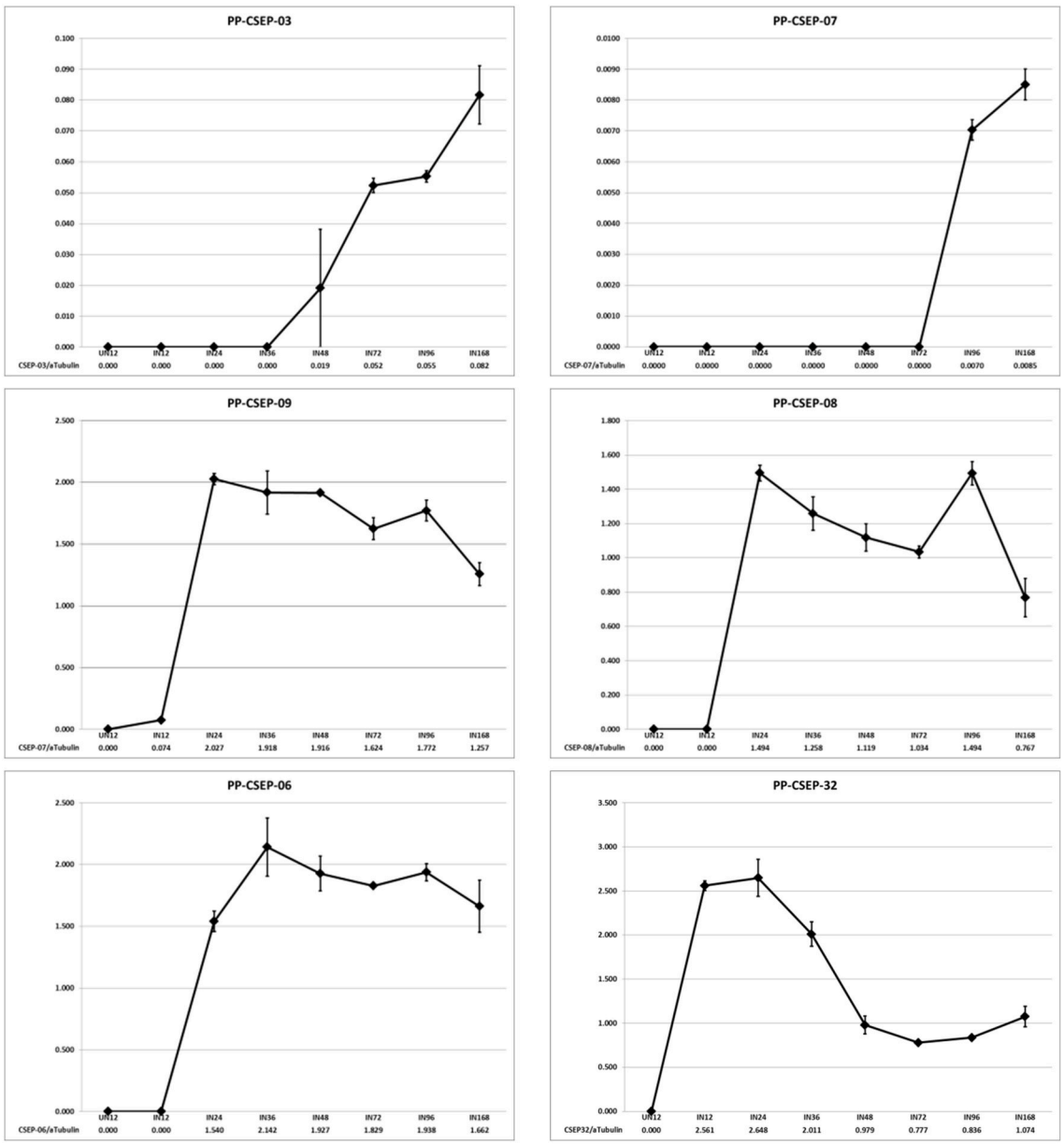

FIGURE 2 | Expression profiles of selected *P. pachyrhizi* candidate effectors. RNA was harvested from soybean leaves at 12, 24, 36, 48, 72, 96, and 168 h after spray inoculation and transcript levels were quantified using qRT-PCR. RNA was also harvested from uninoculated tissue as a negative control (UN12). Error bars are standard error of the mean of three biological repeats.

soybean rust haustoria (Fernandez et al., 2012; Link et al., 2014). Each of these studies has identified many more candidate effectors than we present here. This is partly because our criteria for what qualifies as a candidate effector (CE) is stricter than in these reports, and partly because the next-generation sequencing methods used in these studies provides a much deeper sampling of transcript diversity.

When we initially tried to purify haustoria from infected leaves using a column of concanavalin A-conjugated sepharose B we found that the resulting RNA was too degraded to make cDNA libraries of the desired quality. We consequently modified our haustorial purification methodology to utilize streptavidin-conjugated paramagnetic beads that were pre-bound to biotin-concanavalin A and then used to bind *P. pachyrhizi* haustoria. Paramagnetic bead capture resulted in a greatly shortened window of time between homogenization of the infected leaves and extraction of RNA because of very short washing steps and because it was not required to liberate the haustoria from the beads before they were used for RNA extraction.

Two of our effector candidates, Pp CSEP-07 and Pp CSEP-09, are able to increase the virulence of *P. infestans* on *N. benthamiana* expressing them. Since these two effectors have such dramatic phenotypes, counteracting their biochemical

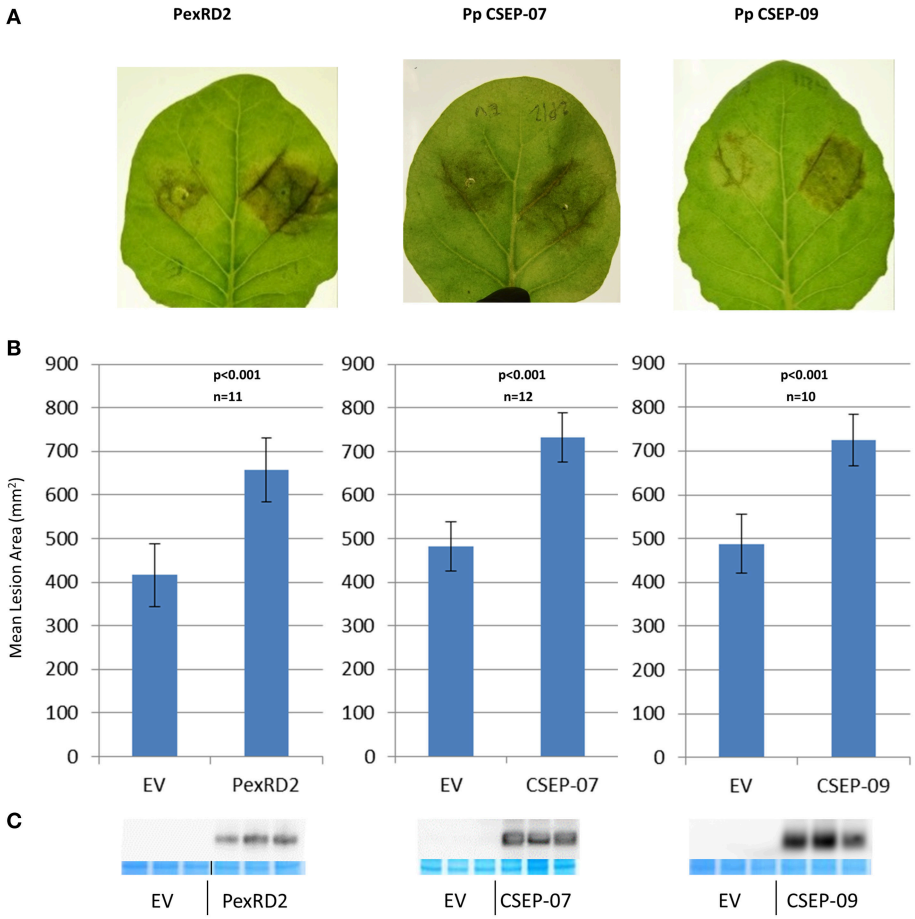

FIGURE 3 | Virulence phenotypes of *P. pachyrhizi* candidate effectors CSEP-07 and CSEP-09 (A) Representative leaves infiltrated agro-infiltrated with empty vector (left half of leaf) or indicated gene (right half of leaf), followed by inoculation with *P. infestans* zoospores. Images were taken at 7 days after zoospore inoculation. **(B)** Quantification of *P. infestans* lesion area 7 days after inoculation. *P*-value is from a two-tailed paired Student's *t*-test. Results are an average of at least 10 inoculated leaves. **(C)** Immunoblot showing expression of indicated proteins from three plants that were agro-infiltrated but not inoculated with *P. infestans*. For each CE, protein was extracted from three independently infiltrated plants and immunoblotted with α-FLAG antibody. Directly below, protein from the same extraction was also loaded on a second gel and stained to demonstrate equal loading. This experiment was repeated twice with similar results.

activity may significantly impair the virulence of *P. pachyrhizi* and doing so may provide a method for controlling the disease. The observation that a rust effector can enhance the virulence of *P. infestans* also suggests that at least some plant defenses to rust and *P. infestans* are shared, and it is likely that they are counteracted by both fungal and oomycete pathogens despite these pathogens being very distantly related to each other.

AUTHOR CONTRIBUTIONS

SK, GI, EJ, and EL performed the experiments KB, GR, and GJR conceived and supervised the experiments and analyzed results. SK and GJR wrote the manuscript.

ACKNOWLEDGMENTS

We would like to thank Michelle Hamilton for assistance in making the cDNA library, Carl Simmons for bioinformatics assistance, and Jim Sweigard for sharing biological material and for helpful advice.

SUPPLEMENTARY MATERIAL

The Supplementary Material for this article can be found online at: http://journal.frontiersin.org/article/10.3389/fpls.2016.00269

Supplementary Figure 1 | Examples of the region identified to mark lesion area. The border of the lesion was manually marked on a digital image of an infected leaf on a lightbox. The border is defined as the junction between the dark brown region of the leaf and the greener, unaffected region.

Supplementary Table 1 | Primers for qRT-PCR experiments.

Supplementary File 1 | CSEP nucleotide sequences.

Supplementary File 2 | CSEP amino acid sequences.

REFERENCES

Allen, R. L., Bittner-Eddy, P. D., Grenville-Briggs, L. J., Meitz, J. C., Rehmany, A. P., Rose, L. E., et al. (2004). Host-parasite coevolutionary conflict between Arabidopsis and downy mildew. *Science* 306, 1957–1960. doi: 10.1126/science.1104022

Bos, J. I., Armstrong, M. R., Gilroy, E. M., Boevink, P. C., Hein, I., Taylor, R. M., et al. (2010). *Phytophthora infestans* effector AVR3a is essential for virulence and manipulates plant immunity by stabilizing host E3 ligase CMPG1. *Proc. Natl. Acad. Sci. U.S.A.* 107, 9909–9914. doi: 10.1073/pnas.0914408107

Bos, J. I., Kanneganti, T. D., Young, C., Cakir, C., Huitema, E., Win, J., et al. (2006). The C-terminal half of *Phytophthora infestans* RXLR effector AVR3a is sufficient to trigger R3a-mediated hypersensitivity and suppress INF1-induced cell death in *Nicotiana benthamiana*. *Plant J.* 48, 165–176. doi: 10.1111/j.1365-313X.2006.02866.x

Bozkurt, T. O., Schornack, S., Win, J., Shindo, T., Ilyas, M., Oliva, R., et al. (2011). *Phytophthora infestans* effector AVRblb2 prevents secretion of a plant immune protease at the haustorial interface. *Proc. Natl. Acad. Sci. U.S.A.* 108, 20832–20837. doi: 10.1073/pnas.1112708109

Cantu, D., Segovia, V., MacLean, D., Bayles, R., Chen, X., Kamoun, S., et al. (2013). Genome analyses of the wheat yellow (stripe) rust pathogen *Puccinia striiformis* f. sp. tritici reveal polymorphic and haustorial expressed secreted proteins as candidate effectors. *BMC Genomics* 14:270. doi: 10.1186/1471-2164-14-270

Catanzariti, A. M., Dodds, P. N., Lawrence, G. J., Ayliffe, M. A., and Ellis, J. G. (2006). Haustorially expressed secreted proteins from flax rust are highly enriched for avirulence elicitors. *Plant Cell* 18, 243–256. doi: 10.1105/tpc.105.035980

Dey, N., and Maiti, I. B. (1999). Structure and promoter/leader deletion analysis of mirabilis mosaic virus (MMV) full-length transcript promoter in transgenic plants. *Plant Mol. Biol.* 40, 771–782. doi: 10.1023/A:1006285426523

Dodds, P. N., Lawrence, G. J., Catanzariti, A. M., Ayliffe, M. A., and Ellis, J. G. (2004). The Melampsora lini AvrL567 avirulence genes are expressed in haustoria and their products are recognized inside plant cells. *Plant Cell* 16, 755–768. doi: 10.1105/tpc.020040

Dodds, P. N., Lawrence, G. J., Catanzariti, A. M., Teh, T., Wang, C. I., Ayliffe, M. A., et al. (2006). Direct protein interaction underlies gene-for-gene specificity and coevolution of the flax resistance genes and flax rust avirulence genes. *Proc. Natl. Acad. Sci. U.S.A.* 103, 8888–8893. doi: 10.1073/pnas.0602577103

Duplessis, S., Cuomo, C. A., Lin, Y. C., Aerts, A., Tisserant, E., Veneault-Fourrey, C., et al. (2011). Obligate biotrophy features unraveled by the genomic analysis of rust fungi. *Proc. Natl. Acad. Sci. U.S.A.* 108, 9166–9171. doi: 10.1073/pnas.1019315108

Emanuelsson, O., Brunak, S., von Heijne, G., and Nielsen, H. (2007). Locating proteins in the cell using TargetP, SignalP and related tools. *Nat. Protoc.* 2, 953–971. doi: 10.1038/nprot.2007.131

Fabro, G., Steinbrenner, J., Coates, M., Ishaque, N., Baxter, L., Studholme, D. J., et al. (2011). Multiple candidate effectors from the oomycete pathogen *Hyaloperonospora arabidopsidis* suppress host plant immunity. *PLoS Pathog.* 7:e1002348. doi: 10.1371/journal.ppat.1002348

Fernandez, D., Tisserant, E., Talhinhas, P., Azinheira, H., Vieira, A., Petitot, A. S., et al. (2012). 454-pyrosequencing of Coffea arabica leaves infected by the rust fungus *Hemileia vastatrix* reveals in planta-expressed pathogen-secreted proteins and plant functions in a late compatible plant-rust interaction. *Mol. Plant Pathol.* 13, 17–37. doi: 10.1111/j.1364-3703.2011.00723.x

Garnica, D. P., Nemri, A., Upadhyaya, N. M., Rathjen, J. P., and Dodds, P. N. (2014). The ins and outs of rust haustoria. *PLoS Pathog.* 10:e1004329. doi: 10.1371/journal.ppat.1004329

Göhre, V., and Robatzek, S. (2008). Breaking the barriers: microbial effector molecules subvert plant immunity. *Annu. Rev. Phytopathol.* 46, 189–215. doi: 10.1146/annurev.phyto.46.120407.110050

Goodin, M. M., Zaitlin, D., Naidu, R. A., and Lommel, S. A. (2008). *Nicotiana benthamiana*: its history and future as a model for plant-pathogen interactions. *Mol. Plant Microbe Interact.* 21, 1015–1026. doi: 10.1094/MPMI-21-8-1015

Hacquard, S., Veneault-Fourrey, C., Delaruelle, C., Frey, P., Martin, F., and Duplessis, S. (2011). Validation of *Melampsora larici-populina* reference genes for in planta RT-quantitative PCR expression profiling during time-course infection of poplar leaves. *Physiol. Mol. Plant Pathol.* 75, 106–112. doi: 10.1016/j.pmpp.2010.10.003

Hahn, M., and Mendgen, K. (1992). Isolation by ConA binding of haustoria from different rust fungi and comparison of their surface qualities. *Protoplasma* 170, 95–103. doi: 10.1007/BF01378785

Hahn, M., and Mendgen, K. (1997). Characterization of in planta-induced rust genes isolated from a haustorium-specific cDNA library. *Mol. Plant Microbe Interact.* 10, 427–437. doi: 10.1094/MPMI.1997.10.4.427

Hemetsberger, C., Herrberger, C., Zechmann, B., Hillmer, M., and Doehlemann, G. (2012). The *Ustilago maydis* effector Pep1 suppresses plant immunity by inhibition of host peroxidase activity. *PLoS Pathog.* 8:e1002684. doi: 10.1371/journal.ppat.1002684

Kamoun, S. (2007). Groovy times: filamentous pathogen effectors revealed. *Curr. Opin. Plant Biol.* 10, 358–365. doi: 10.1016/j.pbi.2007.04.017

Kamoun, S., van West, P., Vleeshouwers, V. G., de Groot, K. E., and Govers, F. (1998). Resistance of *nicotiana benthamiana* to *phytophthora infestans* is mediated by the recognition of the elicitor protein INF1. *Plant Cell* 10, 1413–1426. doi: 10.1105/tpc.10.9.1413

Kemen, E., Kemen, A., Ehlers, A., Voegele, R., and Mendgen, K. (2013). A novel structural effector from rust fungi is capable of fibril formation. *Plant J.* 75, 767–780. doi: 10.1111/tpj.12237

Keogh, R. (1976). The host range and distribution of *Phakopsora pachyrhizi* in New South Wales. *Aust. Plant Pathol. Soc. Newslett.* 5, 51–52. doi: 10.1071/APP9760051

King, S. R., McLellan, H., Boevink, P. C., Armstrong, M. R., Bukharova, T., Sukarta, O., et al. (2014). *Phytophthora infestans* RXLR effector PexRD2 interacts with host MAPKKK epsilon to suppress plant immune signaling. *Plant Cell* 26, 1345–1359. doi: 10.1105/tpc.113.120055

Link, T. I., Lang, P., Scheffler, B. E., Duke, M. V., Graham, M. A., Cooper, B., et al. (2014). The haustorial transcriptomes of Uromyces appendiculatus and *Phakopsora pachyrhizi* and their candidate effector families. *Mol. Plant Pathol.* 15, 379–393. doi: 10.1111/mpp.12099

Mendgen, K., Struck, C., Voegele, R. T., and Hahn, M. (2000). Biotrophy and rust haustoria. *Physiol. Mol. Plant Pathol.* 56, 141–145. doi: 10.1006/pmpp.2000.0264

Park, C. H., Chen, S., Shirsekar, G., Zhou, B., Khang, C. H., Songkumarn, P., et al. (2012). The *Magnaporthe oryzae* effector AvrPiz-t targets the RING E3 ubiquitin ligase APIP6 to suppress pathogen-associated molecular pattern-triggered immunity in rice. *Plant Cell* 24, 4748–4762. doi: 10.1105/tpc.112.105429

Petre, B., Joly, D. L., and Duplessis, S. (2014). Effector proteins of rust fungi. *Front. Plant Sci.* 5:416. doi: 10.3389/fpls.2014.00416

Petre, B., Lorrain, C., Saunders, D. G., Win, J., Sklenar, J., Duplessis, S., et al. (2015a). Rust fungal effectors mimic host transit peptides to translocate into chloroplasts. *Cell. Microbiol.* doi: 10.1111/cmi.12530. [Epub ahead of print].

Petre, B., Saunders, D. G., Sklenar, J., Lorrain, C., Win, J., Duplessis, S., et al. (2015b). Candidate effector proteins of the rust pathogen *Melampsora larici-populina* target diverse plant cell compartments. *Mol. Plant Microbe Interact.* 28, 689–700. doi: 10.1094/MPMI-01-15-0003-R

Posada-Buitrago, M. L., and Frederick, R. D. (2005). Expressed sequence tag analysis of the soybean rust pathogen *Phakopsora pachyrhizi*. *Fungal Genet. Biol.* 42, 949–962. doi: 10.1016/j.fgb.2005.06.004

Pretsch, K., Kemen, A., Kemen, E., Geiger, M., Mendgen, K., and Voegele, R. (2013). The rust transferred proteins-a new family of effector proteins exhibiting protease inhibitor function. *Mol. Plant Pathol.* 14, 96–107. doi: 10.1111/j.1364-3703.2012.00832.x

Saunders, D. G., Win, J., Cano, L. M., Szabo, L. J., Kamoun, S., and Raffaele, S. (2012). Using hierarchical clustering of secreted protein families to classify and rank candidate effectors of rust fungi. *PLoS ONE* 7:e29847. doi: 10.1371/journal.pone.0029847

Schornack, S., van Damme, M., Bozkurt, T. O., Cano, L. M., Smoker, M., Thines, M., et al. (2010). Ancient class of translocated oomycete effectors targets the host nucleus. *Proc. Natl. Acad. Sci. U.S.A.* 107, 17421–17426. doi: 10.1073/pnas.1008491107

Slaminko, T. L., Miles, M. R., Frederick, R. D., Bonde, M. R., and Hartman, G. L. (2008). New legume hosts of *Phakopsora pachyrhizi* based on greenhouse evaluations. *Plant Dis.* 92, 767–771. doi: 10.1094/PDIS-92-5-0767

van de Mortel, M., Recknor, J. C., Graham, M. A., Nettleton, D., Dittman, J. D., Nelson, R. T., et al. (2007). Distinct biphasic mRNA changes in response to

Asian soybean rust infection. *Mol. Plant Microbe Interact.* 20, 887–899. doi: 10.1094/MPMI-20-8-0887

Voegele, R. T., Struck, C., Hahn, M., and Mendgen, K. (2001). The role of haustoria in sugar supply during infection of broad bean by the rust fungus *Uromyces fabae*. *Proc. Natl. Acad. Sci. U.S.A.* 98, 8133–8138. doi: 10.1073/pnas.131186798

Walker, D. R., Harris, D. K., King, Z. R., Li, Z., Boerma, H. R., Buckley, J. B., et al. (2014). Evaluation of soybean germplasm accessions for resistance to populations in the Southeastern United States, 2009–2012. *Crop Sci.* 54, 1673–1689. doi: 10.2135/cropsci2013.08.0513

Win, J., Morgan, W., Bos, J., Krasileva, K. V., Cano, L. M., Chaparro-Garcia, A., et al. (2007). Adaptive evolution has targeted the C-terminal domain of the RXLR effectors of plant pathogenic oomycetes. *Plant Cell* 19, 2349–2369. doi: 10.1105/tpc.107.051037

Yorinori, J. T., Paiva, W. M., Frederick, R. D., Costamilan, L. M., Bertagnolli, P. F., Hartman, G. E., et al. (2005). Epidemics of Soybean Rust (*Phakopsora pachyrhizi*) in Brazil and Paraguay from 2001 to 2003. *Plant Dis.* 89, 675–677. doi: 10.1094/PD-89-0675

Conflict of Interest Statement: The authors declare that the research was conducted in the absence of any commercial or financial relationships that could be construed as a potential conflict of interest. This research is protected by US patent US20140283207 A1.

frontiers in Microbiology

ORIGINAL RESEARCH
published: 18 May 2016
doi: 10.3389/fmicb.2016.00709

Studying the Mechanism of *Plasmopara viticola* RxLR Effectors on Suppressing Plant Immunity

Jiang Xiang[1†], *Xinlong Li*[1†], *Jiao Wu*[1], *Ling Yin*[2], *Yali Zhang*[1] *and Jiang Lu*[1*]

[1] *The Viticulture and Enology Program, College of Food Science and Nutritional Engineering, China Agricultural University, Beijing, China,* [2] *Guangxi Crop Genetic Improvement and Biotechnology Laboratory, Guangxi Academy of Agricultural Sciences, Nanning, China*

The RxLR effector family, produced by oomycete pathogens, may manipulate host physiological and biochemical events inside host cells. A group of putative RxLR effectors from *Plasmopara viticola* have been recently identified by RNA-Seq analysis in our lab. However, their roles in pathogenesis are poorly understood. In this study, we attempted to characterize 23 PvRxLR effector candidates identified from a *P. viticola* isolate "ZJ-1-1." During host infection stages, expression patterns of the effector genes were varied and could be categorized into four different groups. By using transient expression assays in *Nicotiana benthamiana*, we found that 17 of these effector candidates fully suppressed programmed cell death elicited by a range of cell death-inducing proteins, including BAX, INF1, PsCRN63, PsojNIP, PvRxLR16 and R3a/Avr3a. We also discovered that all these PvRxLRs could target the plant cell nucleus, except for PvRxLR55 that localized to the membrane. Furthermore, we identified a single effector, PvRxLR28, that showed the highest expression level at 6 hpi. Functional analysis revealed that PvRxLR28 could significantly enhance susceptibilities of grapevine and tobacco to pathogens. These results suggest that most *P. viticola* effectors tested in this study may act as broad suppressors of cell death to manipulate immunity in plant.

Keywords: ***Plasmopara viticola,*** **grapevine, RxLR effector, cell death, immunity**

OPEN ACCESS

Edited by:
Pietro Daniele Spanu, Imperial College London, UK

Reviewed by:
Takaki Maekawa, Max Planck Institute for Plant Breeding Research, Germany
Ben Petre, The Sainsbury Laboratory, UK
Liliana M. Cano, University of Florida, USA

***Correspondence:**
Jiang Lu
jiangluvitis@cau.edu.cn

[†] *These authors have contributed equally to this work.*

Specialty section:
This article was submitted to Plant Biotic Interactions, a section of the journal Frontiers in Microbiology

Received: *19 February 2016*
Accepted: *28 April 2016*
Published: *18 May 2016*

Citation:
Xiang J, Li X, Wu J, Yin L, Zhang Y and Lu J (2016) Studying the Mechanism of Plasmopara viticola RxLR Effectors on Suppressing Plant Immunity. Front. Microbiol. 7:709. doi: 10.3389/fmicb.2016.00709

INTRODUCTION

During co-evolution with microbial pathogens, plants have evolved multiple layers of innate immune surveillance that successful pathogens have evolved to evade or suppress. The first layer is comprised of pattern recognition receptors (PRRs) that recognize broadly conserved pathogen molecules (pathogen/microbe-associated molecular patterns, PAMP/MAMPs), and activate defense responses including the induction of defense genes, production of reactive oxygen species (ROS) and deposition of callose (Jones and Dangl, 2006). This recognition leads to the so-called PAMP (or pattern)- triggered immunity (PTI; Katagiri and Tsuda, 2010). However, successful pathogens can deliver effectors into plant cell to suppress or interfere with PTI, resulting in effector-triggered susceptibility. The second layer of defense is mediated by resistance (R) proteins that directly or indirectly recognize the presence of pathogen effectors, leading to effector-triggered immunity (ETI; Jones and Dangl, 2006). A hallmark of this recognition is the programmed cell death (PCD), termed hypersensitive response (HR) which

helps resist biotrophic pathogens (Dodds and Rathjen, 2010). However, this distinction between PAMPs and effectors, or between PTI and ETI, is blurred and has been challenged by recent studies (Thomma et al., 2011). Additionally, not all microbial defense activators conform to the common distinction between PAMPs and effectors, and downstream defense pathways in plants activated during PTI and ETI often overlap and operate against a broad spectrum of pathogens. These layers of immunity likely function together as a continuum (Thomma et al., 2011).

Many plant pathogens can secrete effector proteins to counteract immune response of plant. The role of effector proteins in pathogenesis has been characterized most extensively in bacteria. For example, it has been well known that bacterial species could secrete 20–40 effectors into the cytoplasm of plant cells via a type-III secretion system (TTSS; Grant et al., 2006). During infection, many of these bacterial effectors suppress defense responses, PTI and/or ETI, through a variety of mechanisms (Hann et al., 2010). In contrast, researches on effectors from fungi and oomycetes are relatively few.

Oomycete pathogens are a phylogenetically distinct eukaryotic lineage within the Stramenopiles and are evolutionary related to brown algae, which cause some of the most destructive plant diseases and result in huge economic losses in the world (Soanes et al., 2007; Stassen and Van den Ackerveken, 2011). Over the last few years, the genomes of several hemibiotrophic oomycete pathogens, including *Phytophthora ramorum* (the causal agents of sudden oak death), *Phytophthora sojae* (soybean root rot pathogen) and *Phytophthora infestans* (potato late blight pathogen), have been sequenced (Tyler et al., 2006; Haas et al., 2009). The genomes of two biotrophic oomycete pathogens, *Hyaloperonospora arabidopsidis*, a pathogen causes downy mildew in *Arabidopsis thaliana* (Baxter et al., 2010), and *Plasmopara halstedii*, which infects sunflower germlings and young plantlets (Sharma et al., 2015), have also been sequenced. Bioinformatic analysis of the sequenced genomes revealed that oomycete pathogens maintain an extraordinarily large superfamily of secreted proteins that could potentially act as effectors. The superfamily of effectors can broadly be divided into two groups: apoplastic effectors and host-translocated effectors. Host- translocated effectors were mainly identified as Crinklers and RxLR effectors (Stassen and Van den Ackerveken, 2011). The most extensively studied effectors are RxLR effectors, defined by a conserved N-terminal secretory signal peptide followed by an RxLR amino acid motif. However, many aspects of the mechanisms by which oomycete RxLR effectors target to the interior of plant cells remain unsolved (Petre and Kamoun, 2014).

With 134 putative *RxLR* effector genes in *H. arabidopsidis,* 260 RxLR-like proteins in *P. halstedii,* over 350 predicted RxLR effectors in *P. ramorum* and *P. sojae,* and more than 550 *RxLR* sequences in the genome of *P. infestans*, assessing functions of all RxLR effector candidates is a tremendous challenge (Tyler et al., 2006; Haas et al., 2009; Baxter et al., 2010; Sharma et al., 2015). Thus, the development of a medium/ high- throughput system to explore their function in plants is strongly desired. Recently, large-scale function surveys to identify avirulence or virulence role of predicted RxLR effectors from oomycetes have already been undertaken. Until now, only a small number of avirulence genes have been characterized from *Phytophthora* species and *H. arabidopsidis*, including *P. sojae Avr1a* (Qutob et al., 2009), *Avr1b* (Shan et al., 2004), *Avr3a* (Dong et al., 2011b), *Avr3b* (Dong et al., 2011a), *Avr3c* (Dong et al., 2009), *Avr4/6* (Dou et al., 2010), *Avr5* (Dong et al., 2011b), *P. infestans Avr2* (Gilroy et al., 2011), *Avr3a* (Armstrong et al., 2005), *Avrblb1* (Vleeshouwers et al., 2008), *Avrblb2* (Oh et al., 2009), *Avr4* (van Poppel et al., 2008), *H. arabidopsidis ATR13* and *ATR1* (Allen et al., 2004; Rehmany et al., 2005). However, there are more virulence effectors that suppress the immunity of their hosts. For example, most of the surveyed 169 RxLR effectors of *P. sojae* could suppress cell death triggered by multiple elicitors in soybean and tobacco (Wang et al., 2011). Forty-three of 64 tested RxLR effector candidates in *H. arabidopsidis* isolate Emoy2 were able to affect plant immunity by suppressing callose deposition and facilitating bacterial growth (Fabro et al., 2011). Whereafter, a study revealed that all but one of the thirteen *RxLR* genes from isolate Waco9 of *H. arabidopsidis* could impair plant immunity (Vinatzer et al., 2014). These studies conclude that suppression of immunity is a major function of the RxLR secretome.

The oomycete *Plasmopara viticola* ([Berk. et Curt.] Berl. et de Toni) is an obligate biotroph that causes devastating downy mildew disease of grapevine. *P. viticola* is considered a typical obligate biotroph that derives all of its nutrition from living cells of grapevines via globose haustoria to complete its life cycle (Gessler et al., 2011). During the infection process, *P. viticola* can secrete a set of putative effector proteins to subvert the defense mechanism of grapevine (Casagrande et al., 2011). Preliminary search for *P. viticola* effectors in an *in vitro* germinated spore library containing 1543 cDNA clones resulted in the identification of 2 putative RxLR effectors expressed upon infection (Mestre et al., 2012). But a follow-up study about these two effectors has never been reported. A transcriptome of a *P. viticola* isolate "ZJ-1-1" was recently sequenced in our lab. Bioinformatic surveys revealed that a set of 20 RxLR-containing proteins were predicted during the infection of a *V. amurensis* "Shuanghong" grapevine (Yin et al., 2015). Then additional 11 RxLR effectors were digged out by delving further into the RNA-seq data (unpublished). Multiple alignments of the amino acid sequences of these 31 effectors showed that only PvRxLR5 and PvRxLR16 share 57.03% similarity. BLASTP searches revealed that three PvRxLR effectors (PvRxLR10, 21 and 25) from "ZJ-1-1" isolate show homology to effectors from *Bremia lactucae*, *H. arabidopsidis* or *P. infestans*. It seems that the majority of PvRxLR effectors are specific for *P. viticola*.

As a first step toward elucidating the molecular basis for colonization of *P. viticola* in grapevines, the *P. viticola* repertoire of candidate RxLR effectors were cloned and functionally analyzed. Out of 31 predicted RxLR effector candidates, 23 were cloned successfully. Expression patterns, subcellular localizations and their abilities to suppress cell death triggered by various elicitors were explored. Furthermore, *in planta* functional analysis revealed that *PvRxLR28* enhances plant susceptibility. Collectively, the candidate effectors identified here provide valuable information for their roles in *P. viticola* virulence.

MATERIALS AND METHODS

Plant Material, Strains, and Growth Condition

The grapevine (*V. vinifera* cv. Thompson Seedless) and tobacco (*N. benthamiana*) used in this study were grown in the greenhouse at 25°C with a photoperiod of 18 h light/6 h darkness. *Escherichia coli* and *Agrobacterium tumefaciens* strains carrying the disarmed Ti plasmid were routinely grown on Luria-Bertani (LB) agar or broth at 37°C and 28°C, respectively. *Plasmopara viticola* isolate "ZJ-1-1" was subcultured on grapevine leaf discs every 10 days at 22°C in 16/8 h light/dark cycles.

Construction of Expression Plasmids

The oligonucleotides used for plasmid construction and the constructs used in this study are documented in the Supporting Information, **Table S1**. The *RxLR* genes were amplified using cDNA from *P. viticola* isolate "ZJ-1-1" based on the results of RNA-seq analysis (Yin et al., 2015). For the PVX assay, the open reading frames of *RxLR* genes without the predicted signal peptide were amplified using primers (**Table S1**). The amplified fragments were cut using appropriate restriction enzymes and ligated into the PVX vector pGR107 to generate pGR107-PvRxLR. To make the subcellular location construct pH7FWG2, 0-PvRxLR, we used the pGR107-PvRxLR as template to amplify the genes with the primers. The PCR fragments were inserted into entry vector pDONR222 and were subsequently transferred to the plant expression vector pH7FWG2, 0 with Gateway Technology (Invitrogen). To generate the stable expression recombinant vector, *PvRxLR28* PCR products were digested and ligated between *XhoI* and *BstBI* sites of a pER8 plasmid with an estrogen-inducible promoter (Zuo et al., 2000). All plasmids were validated by sequencing (Majorbio, Inc., Shanghai, China).

RNA Isolation, cDNA Synthesis and Quantitative RT-PCR

Grapevine leaf discs infected with spore drops of *P. viticola* "ZJ-1-1" were harvested at indicated time points and RNA was extracted using CTAB method as previously described (Iandolino et al., 2004). All cDNA Synthesis and quantitative RT-PCR reactions were conducted by using protocols established in our lab (Wu et al., 2010). The relative expression values were determined using the actin from *P. viticola* as reference gene (Schmidlin et al., 2008). Primers were designed using Beacon Designer 8.10 software with the default settings.

Agrobacterium-Mediated Transient Expression in Planta

Constructs were transformed into *A. tumefaciens* strain GV3101 by electroporation (Hellens et al., 2000). The pGR107-PvRxLR transformants were selected using tetracycline (12.5 μg/ml), kanamycin (50 μg/ml) and rifampicin (50 μg/ml), and the pH7FWG2,0 transformants were selected using spectinomycin (50 μg/ml) and rifampicin (50 μg/ml). To analyze the suppression of cell death triggered by different elicitors in *N. benthamiana*, *Agrobacteria* containing the corresponding constructs were cultured in LB medium containing 50 μg/ mL of kanamycin at 28°C with shaking at 200 rpm for 48 h. The culture was harvested and washed three times in 10 mM $MgCl_2$, then resuspended in 10 mM $MgCl_2$ to achieve a final OD_{600} of 0.4. For infiltration of pH7FWG2,0 into leaves, recombinant strains of *A. tumefaciens* were grown in LB medium with 50 μg/mL spectinomycin for 48 h, harvested, suspended in infiltration medium [10 mM $MgCl_2$, 5 mM MES (pH 5.7), and 150 μM acetosyringone] to an $OD_{600} = 0.4$ before infiltration. Then 100 μL of *A. tumefaciens* cell suspension was infiltrated into leaves using a syringe without a needle. Green fluorescence and symptom development were monitored 1–2 d and 4–8 d after infiltration, respectively. *Agrobacterium*-mediated vacuum infiltration was used for grapevine transient expression assay as described (Guan et al., 2011).

Generation of the *PvRxLR28*-Transgenic *N. benthamiana*

Transgenic tobacco plants were generated by leaf-disc transformation approach (Gallois and Marinho, 1995). Briefly, leaf discs were placed into *Agrobacterium* suspension carrying a plasmid of interest for 30 min and co-cultured with bacteria for 2 d. Then the infected leaf tissue was placed adaxial side down onto a fresh shoot induction medium containing 1mg/mL of 6-BA, 30 mg/mL of hygromycin and 300 mg/mL timentin. About 1 month later, 1–2 cm tall shoots were excised and transferred into a selective rooting medium which contains 0.2 mg/L of IAA, 30 mg/mL of hygromycin and 300 mg/mL timentin. Roots were generated within 2–3 weeks in culture and transferred to soil for seeds collected. All plants were kept in growth cabinet at 25°C with a 16 h light and 8 h dark regime. T2 transforments were treated with 17-β- estradiol (100μM) and Silwet L-77 (0.01%) 48 h prior to conducting further experiments.

Pathogen Infection Assays

For *P. viticola* infection, 2 days post-infiltration grapevine leaf discs were inoculated with 30 μL of spore suspensions with a concentration of 10^5 spores/ mL on the abaxial surface. Infected disc samples were kept in a growth cabinet at 22°C with a 16 h photoperiod. Phenotype was monitored within 4–5 d.

For *Phytophthora parasitica* infection, two approaches were used as described (Rajput et al., 2014). Briefly, *P. parasitica* was grown on 10% (v/v) V8 juice agar at 25°C in the dark and zoospores were prepared as reported previously (Zhang et al., 2012). For detached leaves, 20 μL of zoospore suspensions with a concentration of 100 zoospores/μL were applied onto the abaxial side of detached *N. benthamiana* leaves. The phenotype was monitored within 72 h, and photographs were taken at 36 h post-inoculation. For whole seedlings, the infection assays were performed by using the root-dip inoculation method. The whole transgenic plants were inoculated with zoospores. The GFP-transgenic lines were used as controls. The inoculated plants were maintained in a moist chamber, and disease progression was monitored within 10 days.

Protein Extraction and Western Blot

N. benthamiana leaf tissues were ground in liquid nitrogen and mixed with an equal volume of cold protein extraction buffer

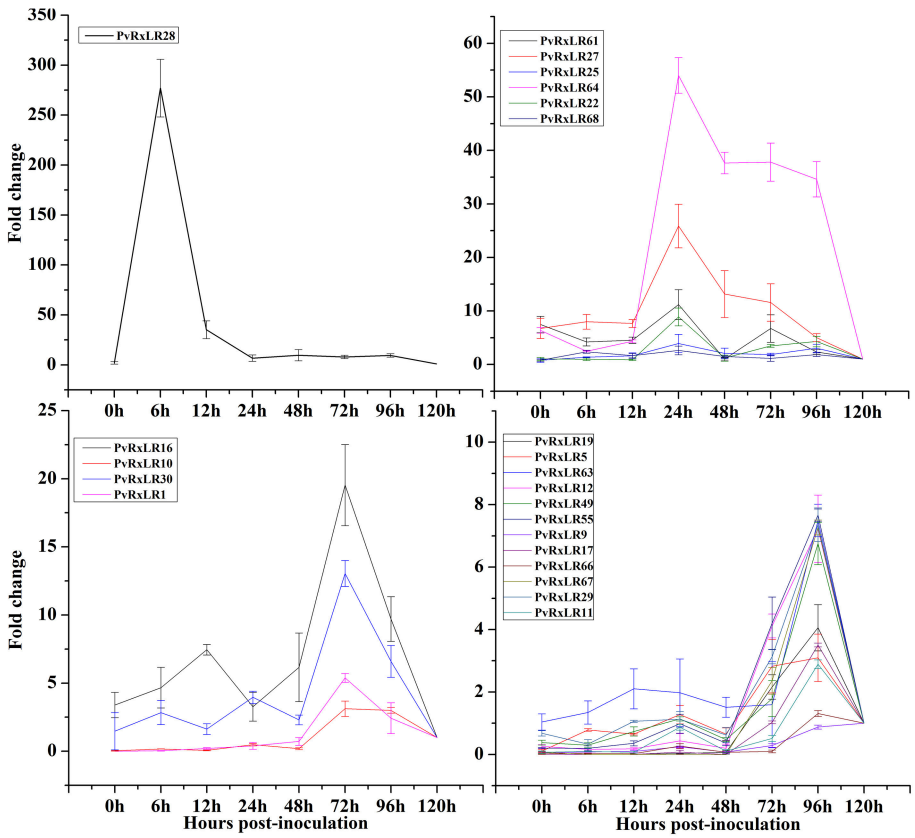

FIGURE 1 | Expression patterns of 23 *PvRxLR* effector genes from *P. viticola* isolate "ZJ-1-1" during the pathogen-grapevine infection. Relative *PvRxLRs* mRNA levels were quantified by quantitative RT-PCR in samples and grapevine leaves inoculated with *P. viticola* at different time-points post infiltration. *P. viticola* actin transcripts were used as a reference. Error bars represent standard errors (SEs) from three biological replicates.

[50 mM HEPS, 150 mM KCl, 1 mM EDTA (pH 8.0), 0.1% triton X-100, 1 mM DTT, 1 × Protease Inhibitor Cocktail (Sigma)]. Suspensions were mixed and centrifuged at 12,000 rpm for 15 min at 4°C. The supernatant was transferred to a new tube and boiled in 5 × SDS loading buffer. Proteins were separated by 12% SDS-PAGE and transferred to a nitrocellulose blotting membrane. The membrane was washed with PBST for 15 min and then blocked in 5% non-fat milk for 1 h. Mouse monoclonal anti-Flag antibody (Transgen Biotech) was added at a ratio of 1:2000 and incubated overnight at 4°C, followed by three washed with PBST. Then the membranes incubated with goat anti-mouse lgG (H&L)-HRP polyclonal antibody (Jiamay Biotech) for 1 h at a ratio of 1: 5000 at RT. After three washes with PBST, the membranes were visualized using HRP-ECL system.

Confocal Microscopy

To analyze the subcellular localizations of the PvRxLRs in *N. benthamiana*, patches cut from leaf samples were immersed into PBS buffer which contains 5 mg/L 4′, 6-diamidino-2-phenylindole (DAPI) for staining the nuclei for 10 min. Then the patches were mounted on microscope slides and observed with a Nikon C1 Si/TE2000E confocal laser scanning microscope. For co-localization, co-infiltrated leaves with *Agrobacterium* contain pH7FWG2,0-PvRxLR55-GFP and pBI121- Avh241-mCherry constructs were detected at 2 dpi. The excitation/emission wavelengths for GFP, DAPI and RFP were 488 nm/505–530 nm, 405 nm/420–480 nm and 543 nm/600–630 nm, respectively. EZ-C1 3.00 software was used for image processing.

Analysis of H_2O_2 Level

H_2O_2 was monitored *in situ* using 3, 3-diaminobenzi-dine (DAB) (Sigma) staining as described previously (Thordal-Christensen et al., 1997). Briefly, the infected leaves 12 h after inoculation were soaked in DAB solution at 1 mg/mL and maintained for 8 h at 25°C. Then the samples were transferred into 95% ethanol and boiled for 15 min until the chlorophyll was completely bleached. The bleached leaves were further soaked in 2.5 g/mL trichloracetic aldehyde solution to clear the background. The H_2O_2 level was quantified by Image J and Photoshop.

RESULTS

Expression Patterns of Candidate RxLR Effector Genes of *P. viticola*

When the compatible *P. viticola* strain "ZJ-1-1" was inoculated onto the"downy mildew-resistant" *V. amurensis* "Shuanghong"

grapevine, the disease progressed quickly on the infected leaves, and branched hyphae with many haustoria and sporangia were visible by 3 days post-inoculation (Li et al., 2015a). When the transcriptional levels of effector genes were measured at different time courses during the infection (0, 6, 12, 24, 48, 72, 96, and 120 hpi), all the 23 *PvRxLR* genes identified from the *P. viticola* strain "ZJ-1-1" were up-regulated at some time points. However, the expression patterns, which could be grouped into four different kinds, varied greatly among these effectors (**Figure 1**). In general, the *PvRxLR* genes of the first two groups were highly expressed at the earlier infection stages (6 and 24 hpi), while in the other two groups, increasing gene expressions occurred much latter (72 and 96 hpi). *PvRxLR28,* for example, increased more than 275-fold at 6 hpi, and then declined sharply at the subsequent interacting time points. A similar pattern of induction was described for RxLR effectors of *H. arabidopsidis* and *P. sojae* which has been termed "immediate-early, low" (Wang et al., 2011; Anderson et al., 2012).

Subcellular Localizations of PvRxLRs in *N. benthamiana*

The localizations of these pathogen effectors after entering a plant cell could well be an indication of their mode of action (Dowen et al., 2009; Schornack et al., 2010). To determine the subcellular localizations of PvRxLRs, we generated green fluorescent protein-tagged versions of the 23 effectors downstream of their signal peptide cleavage site. Fusion plasmids were expressed transiently in *N. benthamiana* using agroinfiltration. Results showed that 6 effector proteins strictly localized to the nucleus, while 16 of them localized to both nucleus and the cytoplasm (**Figure 2A**, **Figure S1**). The only exception is the effector PvRxLR55 that was only detected in the cell membrane. For further confirmation, co-localization of PvRxLR55-GFP has been done with a plasma membrane protein Avh241 (Yu et al., 2012). It was observed that the GFP signal of PvRxLR55-GFP overlapped with Avh241—mCherry fluorescence signal, suggesting the localization of PvRxLR55 to the plasma membrane (**Figure 2B**).

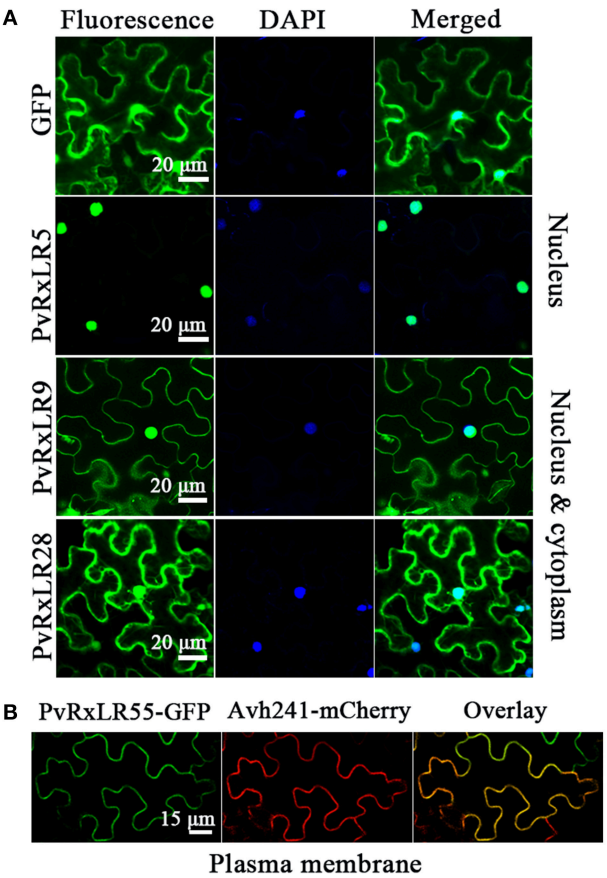

FIGURE 2 | Subcellular localizations of PvRxLR proteins. (A) *N. benthamiana* leaf tissues showing expression of the PvRxLRs-GFP fusion protein driven by the 35S promoter. Scale bar = 20 μm. **(B)** Co-localization of PvRxLR55 protein with plasma membrane marker Avh241. PvRxLR55-GFP showing GFP signal merges completely with Avh241-mCherry. GFP fusion to the PvRxLR55 protein is shown in green, Avh241-mCherry in red and overlay of the two proteins in dark field view. Scale bar = 15 μm.

PvRxLRS Suppress Different Elicitors-Induced Cell Death in *N. benthamiana*

Virulence of the effectors was assessed by testing their abilities of inhibiting programmed cell death in tobacco using transient over-expression. The elicitors used in the present study included the mouse BAX (Lacomme and Santa Cruz, 1999), the PAMP elicitor INF1 from *P. infestans* (Kamoun et al., 1998), the *P. sojae* effector CRN63 (Liu et al., 2011), the necrosis-inducing protein PsojNIP (Qutob et al., 2002) and the Avr3a/R3a (Armstrong et al., 2005). The PvRxLR16 of *P. viticola* was also used as an elicitor as it could induce cell death in *N. benthamiana*. *Agrobacterium* strains carrying each effector gene were infiltrated into *N. benthamiana* leaves 12 h prior to infiltration of the cell death-inducers. Of the 22 effectors tested, 17 effector proteins completely inhibited cell death induced by the above elicitors, while the remaining five (PvRxLR19, PvRxLR25, PvRxLR61, PvRxLR63, and PvRxLR67) partially suppressed the tobacco PCD (**Figure 3**, **Figure S2**). As expected, the negative control of GFP alone did not suppress the PCD. Notably, our results are consistent with previous findings that seven effectors (PvRxLR1, 5, 9, 10, 11, 19, 25) could repress BAX- and INF-induced cell death (Yin et al., 2015). These results suggest that each of the 17 effectors may act as a broad suppressor of cell death to interrupt plant immunity.

The C-Terminus and the Nuclear Localization Are Required for Mediating THE Suppression of PCD

To understand how the PvRxLRs work, effector PvRxLR28, the most dramatic up regulating one triggered by pathogen-host interaction was chosen for study in detail. Seven deletion mutants of PvRxLR28 were generated and tested for their abilities to inhibit BAX-induced PCD. **Figure 4A** demonstrated that positions from 150 to 200 of PvRxLR28 were required for suppressing the cell death. The result also indicated that the

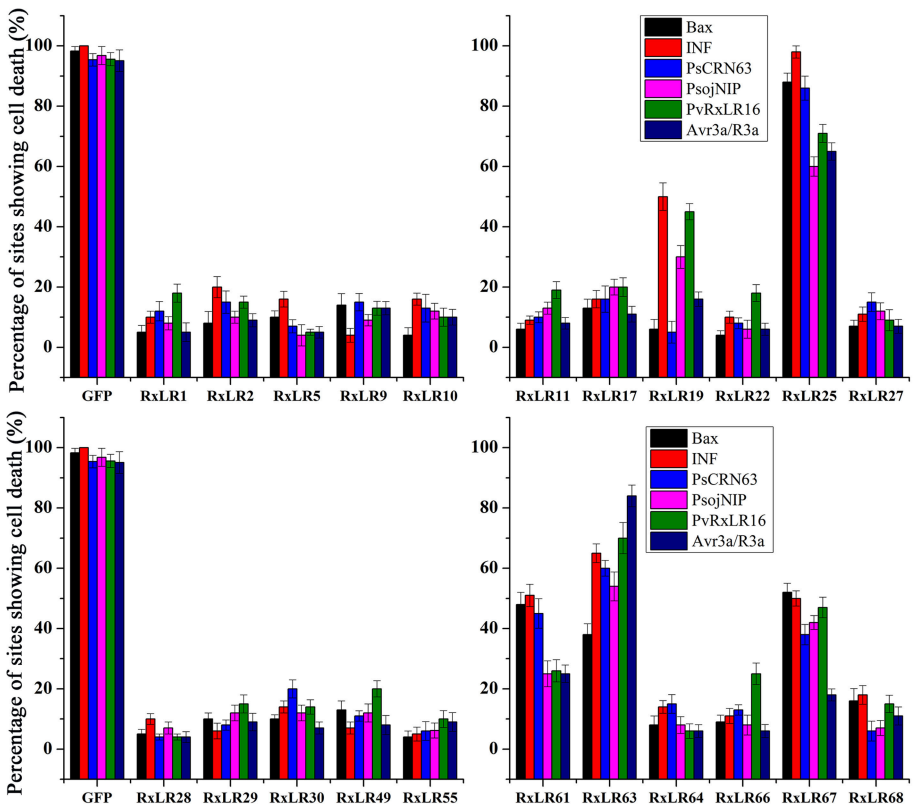

FIGURE 3 | Suppression of different elicitors-induced cell death in *N. benthamiana* by PvRxLR effectors. *Agroinfiltration* sites in each *N. benthamiana* leaf expressing *PvRxLRs* and *GFP* (negative control) were challenged after 12 h with *A. tumefaciens* carrying the indicated elicitors. Experiments were repeated three times with 8 sites for each elicitor or GFP and assessed with percentage of cell death sites 5 d after cell death inducer infiltration.

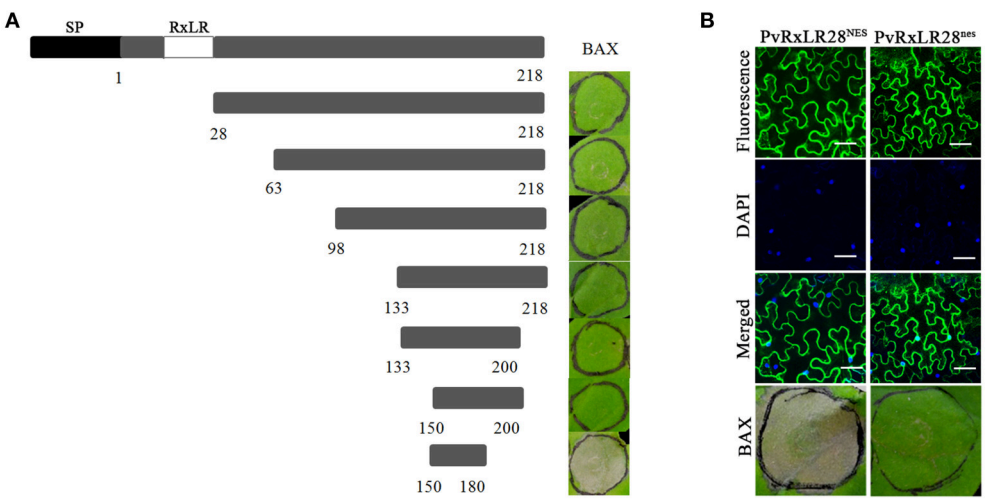

FIGURE 4 | The C-terminus and the nuclear localization are essential for the function of PvRxLR28 effector. (A) Deletion analysis of PvRxLR28. Deletion mutants were expressed by agroinfiltration in *N. benthamiana* to assay suppression of cell death induced by BAX. Typical symptoms were photographed 5 d after infiltration of the BAX. **(B)** Nuclear localization is required for mediating the suppression of PCD. NES impairs accumulation of GFP: PvRxLR28 in *N. benthamiana* nucleus. *N. benthamiana* leaves were agroinfiltrated with the indicated constructs 48 h before assessment of GFP confocal imaging. Scale bars, 50 μm. NES and nes represent the nuclear export signal and nonfunctional NES respectively. Scale bar = 30 μm.

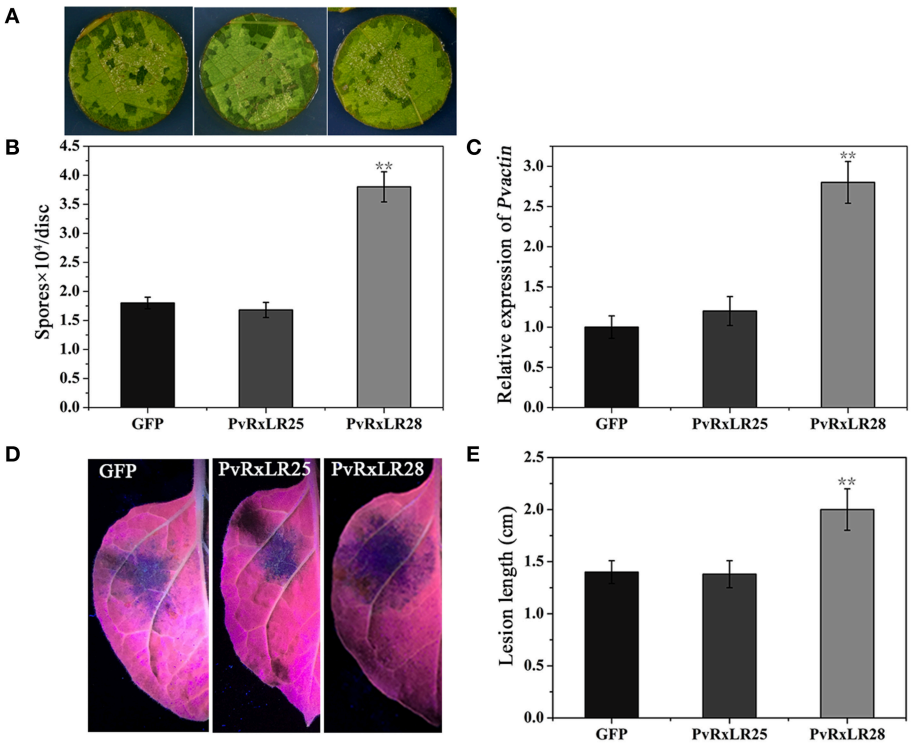

FIGURE 5 | Suppression of the plant resistance by transient expressing *PvRxLR28*. (A) Phenotypes of grapevine leaf discs expressing *GFP*, *PvRxLR25* or *PvRxLR28*. The representative pictures were taken at 5 d post infection of *P. viticola*. **(B)** Average zoospore numbers of *P. viticola* on a total of 50 infected discs. Error bars represent SD from three independent biological replicates (**$P < 0.01$, Dunnett's test). **(C)** The transcript accumulation of *P. viticola* actin. The development of pathogen was calculated by qRT-PCR assays of *P. viticola* actin at 5 dpi. Transcript level of grapevine actin gene was used as an internal reference (**$P < 0.01$, Dunnett's test). **(D)** Lesions of the *N. benthamiana* leaves expressing *GFP*, *PvRxLR25* or *PvRxLR28* at 36 hpi. **(E)** Lesion diameters of *N. benthamiana* leaves expressing the indicated genes inoculated with *P. parasitica*. Statistical analyses were performed using a Dunnett's test (**$P < 0.01$).

conserved N-terminal RxLR motif was not necessary for the PCD suppressions.

In order to determine whether the localization is crucial for PvRxLR28 to suppress PCD, a synthetic NES (nuclear exclusion signal) and a nes (nonfunctional NES) were added to the C terminus, respectively. Cell death symptoms were observed when the NES was attached to PvRxLR28, but not with the attachment of the nes (**Figure 4B**). It is clear that the ability of PvRxLR28 to repress cell death relies on the nuclear localization.

PvRxLR28 Expression Enhances Plant Susceptibility to Pathogens

As PCD is a hallmark of HR-based immunity in plants (Abramovitch et al., 2003), we dissected the effects of *PvRxLR28* expression on plant immunity. GFP and effector PvRxLR25, which could not suppress cell death induced by elicitors, were chosen as controls. *PvRxLR28* was transiently expressed in the leaves of grapevine and tobacco 2 days prior inoculation of *P. viticola* and *P. parasitica* zoospores, respectively. *P. viticola* development was evaluated by monitoring zoospore numbers and *PvActin* transcript accumulation in infected leaf discs. *P. parasitica* development was evaluated by lesion length on leaf areas. More zoospores of *P. viticola* were produced in *PvRxLR28* - expressing grapevine leaves, and higher expression of actin transcripts was also observed compared to controls (**Figures 5A–C**). Similarly, the lesion diameter was significantly larger in *PvRxLR28*- than *PvRxLR25*- or *GFP*-expressing tobacco (**Figures 5D,E**). These results show that transient expression of *PvRxLR28* could impair plant resistance to pathogens.

To verify the above observation, we generated a *PvRxLR28: Flag* fusion construct driven by an estrogen-inducible promoter, and introduced it into *N. benthamiana* leaf discs by *Agrobacterium*-mediated transformation. A total of 35 independent transgenic lines (T0) including 21 *PvRxLR28*-expressing plants and 14 GFP- expressing plants were obtained. T1 lines were generated by self-pollination. RT-PCR and Western-blot analysis confirmed that *PvRxLR28* and *GFP* were highly expressed in several T2 lines after induced by oestradiol (**Figure 6**). Similar to transient expression assay, stable *PvRxLR28*-transgenic plants also blocked cell death triggered by the six elicitors (**Figure 7**). When the transgenic plants were challenged with oomycete *P. parasitica*, detached leaf tissues of *PvRxLR28*-transgenic plants developed larger lesion than the ones of *GFP* lines (**Figures 8A,B**). When they were sprayed with *P. parasitica*, the *PvRxLR28*-transgenic plants also showed earlier and severer symptoms with higher death rate than control lines

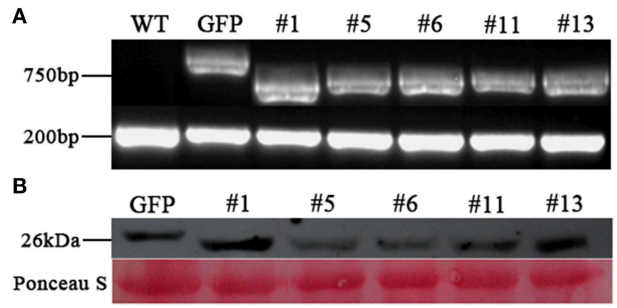

FIGURE 6 | Expression analysis of *PvRxLR28* in transgenic *N. benthamiana*. **(A)** RT-PCR analysis of *PvRxLR28* expression in transgenic lines of T2 generation, and *EF1-α* was used as a control. **(B)** Western blot analysis of total proteins from transgenic *N. benthamiana* lines using monoclonal antibody against flag. The leaves for RT-PCR and western blot were collected at 2d post spraying of 17-β- estradiol (100 μM) and Silwet L-77 (0.01%).

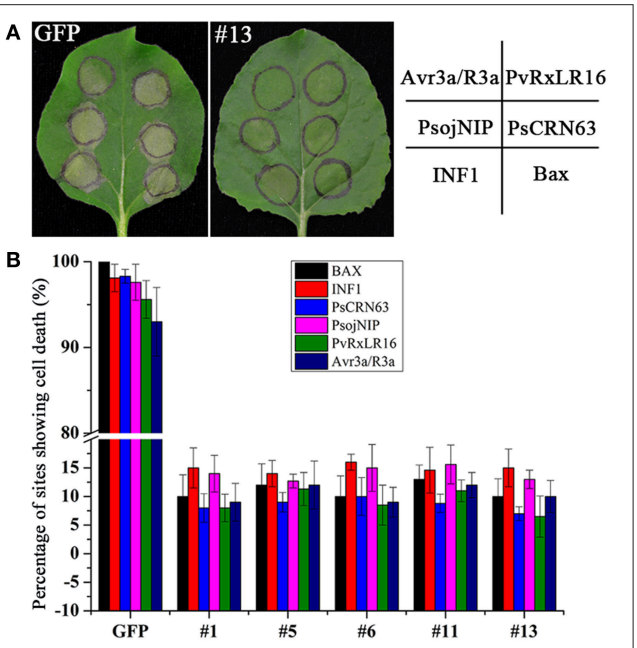

FIGURE 7 | Suppression of cell death in *PvRxLR28*- transgenic *N. benthamiana*. **(A)** Phenotypes of leaves challenged with cell death inducers 5 d after infiltration. **(B)** Showing percentages of cell death sites on the *PvRxLR28*- transgenic lines assessed from 16 infiltrated leaves of three independent experiments.

even though both *PvRxLR28*- and *GFP*-transgenic plants showed symptoms of wilting and stunting (**Figures 8C,D**). The above findings clearly indicated that effector PvRxLR28 enhanced plant susceptibility to oomycete pathogens.

PvRxLR28 Expression Reduces the Transcriptional Levels of the Defense-Related Genes and Impairs the H_2O_2 Accumulation in *N. benthamiana*

To preliminarily explore the role of PvRxLR28 in plant immune response, expressional levels of selected host defense-related genes were examined using qRT-PCR. Since salicylic acid (SA), jasmonic acid (JA) and ethylene (ET) are three main phytohormones essential for the immune response against pathogen (Vlot et al., 2009; Ballaré, 2011; Robert-Seilaniantz et al., 2011). Marker genes *PR1b* and *PR2b* (SA), *LOX* (JA) and *EFR1* (ET), in each of these phytohormone mediated signaling pathways, were analyzed. These genes all positively contribute to the resistance against pathogen. Expression levels of these four defense-related genes were significantly decreased in *PvRxLR28*-transgenic lines during *P. parasitica* infection (**Figure 9A**), suggesting that PvRxLR28 may enhance plant susceptibility by repressing the expression of the defense-related genes in plants.

To expand understanding of the mechanism that leads to host susceptibility to pathogen, we also analyzed the accumulation of H_2O_2 in *N. benthamiana* leaves which takes part in the defense responses (Thordal-Christensen et al., 1997). The H_2O_2 levels in the transgenic plants were measured at the early infective stages of *P. parasitica* using DAB staining method. As a result, the relative staining was significantly lower in the *PvRxLR28*-transgenic lines than that in the *GFP* lines (**Figure 9B**). In order to elucidate the possible mechanisms underlying the reduced H_2O_2 accumulation in *PvRxLR28*-transgenic plants, the expression levels of *RbohA* and *RbohB* genes that encode ROS-producing proteins were also measured (**Figure 9C**). Expression of these genes was significantly reduced in the stable *PvRxLR28*-transgenic plants and thus the H_2O_2 reduction might be caused by down-regulation of ROS-producing genes. In conclusion, PvRxLR28 effector enhancing plant susceptibility is likely by reducing the transcriptional levels of the defense-related genes and impairing the H_2O_2 accumulation.

DISCUSSION

Despite the worldwide economic impact of diseases caused by *P. viticola*, little is known about the molecular basis of the pathogenicity of this species. The study of the secrete proteins from the pathogen may greatly advance our understanding of pathogen virulence. In the secretome of *P. viticola* isolate "ZJ-1-1," a total of 31 putative RxLR effectors have been predicted. Here we used a virus *in planta* over-expression system to assess the potential of PvRxLRs to manipulate immune response in non-host plant. The utility of the screening approach has been validated in studies of effectors from *Phytophthora sojae* (Wang et al., 2011), *Globodera rostochiensis* (Ali et al., 2015) and *Valsa mali* (Li et al., 2015b). Of 23 *PvRxLR* effector genes cloned (**Table S2**), only *PvRxLR16* could directly trigger cell death, while 17 were able to completely and 5 partially suppress PCD induced by various elicitors. Findings from this study strongly suggest that *P. viticola* secreted RxLR effectors to suppress PTI, ETI and other types of host immune responses during the pathogen infection. Although the mechanism of broad PCD/defense suppression by *P. viticola* effectors is not clear, it is possible that they target a

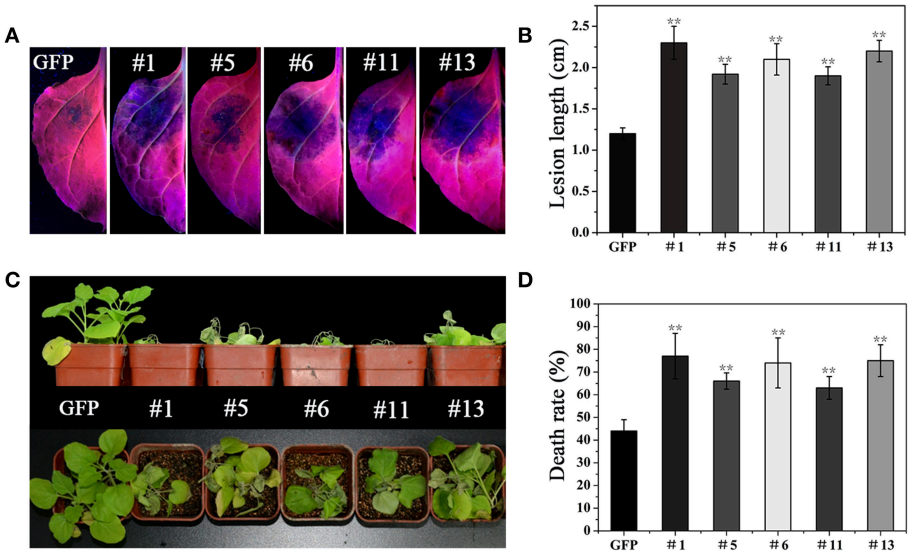

FIGURE 8 | Suppression of the resistance in *PvRxLR28*-transgenic *N. benthamiana*. **(A)** Detached leaves of *GFP*- and *PvRxLR28*-transgenic plants 36 h post inoculated with *P. parasitica* zoospores. **(B)** Average lesion diameters of the inoculated leaves at 36 hpi. Error bars represent standard deviation calculated from 12 independent biological replicates (**$P < 0.01$, Dunnett's test). **(C)** The transgenic lines inoculated with zoospores of *P. parasitica* using the root dip method at 4 dpi. **(D)** Death rates of transgenic plants inoculated with *P. parasitica*. The experiments were repeated four times with similar results. 20 plants for each line were used for each treatment in each experiment. Bars represent the standard errors. Asterisks indicate statistical significance (**$P < 0.01$, Dunnett's test).

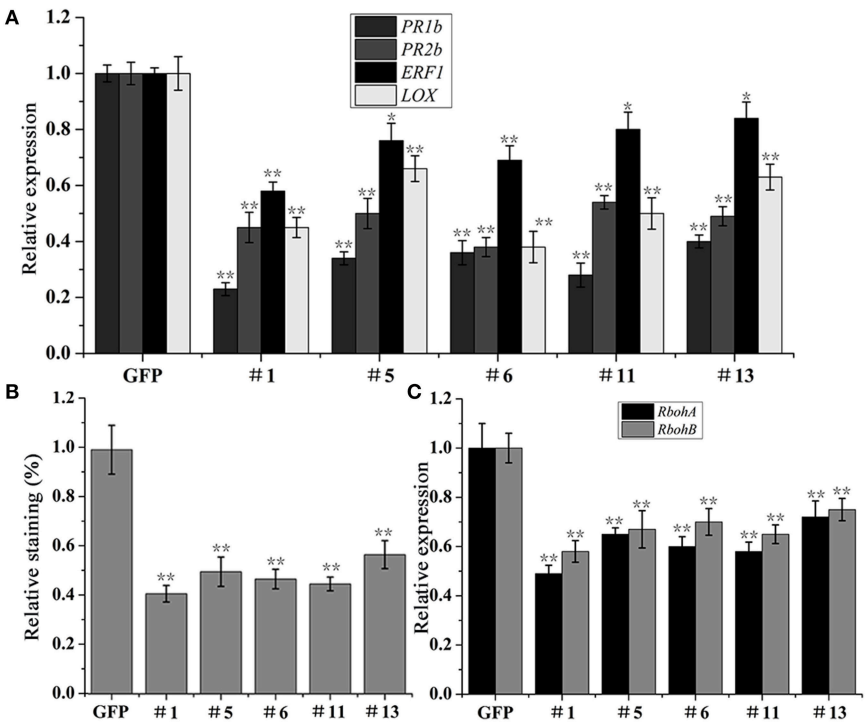

FIGURE 9 | Suppression of pathogenesis-related genes and H_2O_2 accumulation in *N. benthamiana* by PvRxLR28. **(A)** Relative expression levels of *PR1b*, *PR2b*, *ERF1*, *LOX* genes in the transgenic lines at 36 dpi with *P. parasitica* zoospores. The relative expression levels were normalized to the *EF1α* gene. Error bars represent standard errors (**$P < 0.01$, *$P < 0.05$, Dunnett's test). **(B)** Relative intensity of DAB staining in *P. parasitica*-infected *N. benthamiana*. Asterisks indicate significant differences (**$P < 0.01$, Dunnett's test). **(C)** Relative expression levels of ROS-producing genes *RbohA* and *RbohB*. Asterisks indicate significant differences (**$P < 0.01$, Dunnett's test).

central component downstream from the convergence node of resistance network, or multiple distinct pathways.

To confirm the roles of effectors in plant immunity, PvRxLR28 was chosen for further research. As *P. viticola* was recalcitrant to genetically manipulate because of its obligate lifestyle, the effector PvRxLR28 was expressed in plant cells by transiently and stably integrated transgenes. Overexpression of the *PvRxLR28* in tobacco and grapevine enhanced their susceptibility to *P. parasitica* and *P. viticola,* respectively, suggesting that this effector contributes to pathogen virulence. The H_2O_2accumulation and the defense marker genes in the transgenic plants were significantly lower than in the control lines, indicating PvRxLR28 can promote pathogen infection by reducing H_2O_2levels and suppressing SA and JA signaling pathways which usually act antagonistically in plant defense. Due to the difficulty of obtaining stable transgenic grapevines, the effector candidate PvRxLR28 was stably expressed in non-host *N. benthamiana* in the current study. Therefore, a more convincing conclusion about the enhancement of host susceptibility to the pathogen by PvRxLR effectors should come from a transgenic grapevine experiment.

It has been documented that N-terminal RxLR motif is involved in translocation mechanism, while the C-terminus is important for function (Whisson et al., 2007; Dou et al., 2008). A series of deletion mutants of PvRxLR28 indicated that the C-terminus of PvRxLR28 is essential for suppressing PCD, although our present data could not demonstrate that the RxLR is responsible for entering the plant cell. This unique characteristic of RxLR effectors seems conserved in different oomycete pathogens. Similar to previous reports (Boch and Bonas, 2010; Kelley et al., 2010; Caillaud et al., 2013; Zheng et al., 2014), all the tested PvRxLR effectors except PvRxLR55 could localized to the plant cell nucleus, implicating that most RxLR effectors of *P. viticola* tested in this study may function by manipulating the host nuclear processes to attenuate the plant defense and subsequently promote pathogen infection.

Interestingly, the percentage of putative effectors that can suppress elicitor-induced PCD varied a good deal among different species. For example, in a study of *V. mali* effectors, only 7 out of 70 randomly selected effectors exhibited the capacity to suppress BAX-induced PCD (Li et al., 2015b), while 107 of 169 RxLR effectors from *P. sojae* (Wang et al., 2011), and 43 of 64 RxLR effectors from *H. arabidopsidis* (Fabro et al., 2011) could suppress cell death induced by BAX or plant immunity. It seems likely that the pathogens whose lifestyle contains biotrophic phase may have a high percentage of effectors which can suppress PCD or immune response. Our study showed that 22 of 23 *P. viticola* effectors can completely or partially suppress PCD in *N.benthamiana*, which are consistent with the hypothesis. It also appears that there is a high degree of functional redundancy in effectors suppressing PCD in these pathogens. The molecular basis of this functional redundancy bears further investigation.

In conclusion, results from this study clearly indicate that majority of the tested PvRxLR effectors could suppress PCD in *N. benthamiana*, and thus they may make primary contribution to pathogen virulence. In addition, functional studies of PvRxLR secretome will ultimately help to elucidate the mechanisms underlying the pathogenicity of *P. viticola* to grapevine.

AUTHOR CONTRIBUTIONS

YZ and JL conceived the research. JL, JX, and XL designed the research. JX, XL, LY, and JW performed the experiments. JL, JX, and XL wrote the article.

ACKNOWLEDGMENTS

We are grateful to Professor Yuanchao Wang and Professor Daolong Dou (Nanjing Agricultural University) for providing pGR107 vector and elicitors. This research was supported by National Natural Science Foundation of China (grant no. 31471754), China Agriculture Research System (grant no. CARS-30-yz-2), and China Agricultural University Scientific Fund (grant no. 2012RC019).

SUPPLEMENTARY MATERIAL

The Supplementary Material for this article can be found online at: http://journal.frontiersin.org/article/10.3389/fmicb.2016.00709

Table S1 | Primers used in this study.

Table S2 | Genbank accession numbers and amino acid sequences of the PvRXLRs.

Figure S1 | Subcellular localizations of PvRxLRs in *N. benthamiana* leaf tissues.

Figure S2 | Suppression of different elicitors-triggered cell death in *N. benthamiana* by PvRxLR effectors.

REFERENCES

Abramovitch, R. B., Kim, Y. J., Chen, S., Dickman, M. B., and Martin, G. B. (2003). *Pseudomonas* type III effector AvrPtoB induces plant disease susceptibility by inhibition of host programmed cell death. *EMBO J.* 22, 60–69. doi: 10.1093/emboj/cdg006

Ali, S., Magne, M., Chen, S., Obradovic, N., Jamshaid, L., Wang, X., et al. (2015). Analysis of *Globodera rostochiensis* effectors reveals conserved functions of SPRYSEC proteins in suppressing and eliciting plant immune responses. *Front. Plant Sci.* 6:623. doi: 10.3389/fpls.2015.00623

Allen, R. L., Bittner-Eddy, P. D., Grenville-Briggs, L. J., Meitz, J. C., Rehmany, A. P., Rose, L. E., et al. (2004). Host-parasite coevolutionary conflict between Arabidopsis and downy mildew. *Science* 306, 1957–1960. doi: 10.1126/science.1104022

Anderson, R. G., Casady, M. S., Fee, R. A., Vaughan, M. M., Deb, D., Fedkenheuer, K., et al. (2012). Homologous RXLR effectors from *Hyaloperonospora arabidopsidis* and *Phytophthora sojae* suppress immunity in distantly related plants. *Plant J.* 72, 882–893. doi: 10.1111/j.1365-313X.2012.05079.x

Armstrong, M. R., Whisson, S. C., Pritchard, L., Bos, J. I., Venter, E., Avrova, A. O., et al. (2005). An ancestral oomycete locus contains late blight avirulence gene

Avr3a, encoding a protein that is recognized in the host cytoplasm. *Proc. Natl. Acad. Sci. U.S.A.* 102, 7766–7771. doi: 10.1073/pnas.0500113102

Ballaré, C. L. (2011). Jasmonate-induced defenses: a tale of intelligence, collaborators and rascals. *Trends Plant Sci.* 16, 249–257. doi: 10.1016/j.tplants.2010.12.001

Baxter, L., Tripathy, S., Ishaque, N., Boot, N., Cabral, A., Kemen, E., et al. (2010). Signatures of adaptation to obligate biotrophy in the *Hyaloperonospora arabidopsidis* genome. *Science* 330, 1549–1551. doi: 10.1126/science.1195203

Boch, J., and Bonas, U. (2010). *Xanthomonas* AvrBs3 family-type III effectors: discovery and function. *Annu. Rev. Phytopathol.* 48, 419–436. doi: 10.1146/annurev-phyto-080508-081936

Caillaud, M.-C., Asai, S., Rallapalli, G., Piquerez, S., Fabro, G., and Jones, J. D. (2013). A downy mildew effector attenuates salicylic acid–triggered immunity in Arabidopsis by interacting with the host mediator complex. *PLoS Biol.* 11:e1001732. doi: 10.1371/journal.pbio.1001732

Casagrande, K., Falginella, L., Castellarin, S. D., Testolin, R., and Di Gaspero, G. (2011). Defence responses in Rpv3-dependent resistance to grapevine downy mildew. *Planta* 234, 1097–1109. doi: 10.1007/s00425-011-1461-5

Dodds, P. N., and Rathjen, J. P. (2010). Plant immunity: towards an integrated view of plant–pathogen interactions. *Nat. Rev. Genet.* 11, 539–548. doi: 10.1038/nrg2812

Dong, S., Qutob, D., Tedman-Jones, J., Kuflu, K., Wang, Y., Tyler, B. M., et al. (2009). The *Phytophthora sojae* avirulence locus *Avr3c* encodes a multi-copy RXLR effector with sequence polymorphisms among pathogen strains. *PLoS ONE* 4:e5556. doi: 10.1371/journal.pone.0005556

Dong, S., Yin, W., Kong, G., Yang, X., Qutob, D., Chen, Q., et al. (2011a). *Phytophthora sojae* avirulence effector Avr3b is a secreted NADH and ADP-ribose pyrophosphorylase that modulates plant immunity. *PLoS Pathog.* 7:e1002353. doi: 10.1371/journal.ppat.1002353

Dong, S., Yu, D., Cui, L., Qutob, D., Tedman-Jones, J., Kale, S. D., et al. (2011b). Sequence variants of the *Phytophthora sojae* RXLR effector Avr3a/5 are differentially recognized by Rps3a and Rps5 in soybean. *PLoS ONE* 6:20172. doi: 10.1371/journal.pone.0020172

Dou, D., Kale, S. D., Liu, T., Tang, Q., Wang, X., Arredondo, F. D., et al. (2010). Different domains of *Phytophthora sojae* effector Avr4/6 are recognized by soybean resistance genes *Rps 4* and *Rps 6*. *Mol. Plant-Microbe Interact.* 23, 425–435. doi: 10.1094/MPMI-23-4-0425

Dou, D., Kale, S. D., Wang, X., Jiang, R. H., Bruce, N. A., Arredondo, F. D., et al. (2008). RXLR-mediated entry of *Phytophthora sojae* effector Avr1b into soybean cells does not require pathogen-encoded machinery. *Plant Cell* 20, 1930–1947. doi: 10.1105/tpc.107.056093

Dowen, R. H., Engel, J. L., Shao, F., Ecker, J. R., and Dixon, J. E. (2009). A family of bacterial cysteine protease type III effectors utilizes acylation-dependent and-independent strategies to localize to plasma membranes. *J. Biol. Chem.* 284, 15867–15879. doi: 10.1074/jbc.M900519200

Fabro, G., Steinbrenner, J., Coates, M., Ishaque, N., Baxter, L., Studholme, D. J., et al. (2011). Multiple candidate effectors from the oomycete pathogen *Hyaloperonospora arabidopsidis* suppress host plant immunity. *PLoS Pathog.* 7:e1002348. doi: 10.1371/journal.ppat.1002348

Gallois, P., and Marinho, P. (1995). "Leaf disk transformation using *Agrobacterium tumefaciens*-expression of heterologous genes in tobacco," in *Plant Gene Transfer and Expression Protocols,* ed H. Jones (New York, NY: Springer), 39–48. doi: 10.1385/0-89603-321-X:39

Gessler, C., Pertot, I., and Perazzolli, M. (2011). *Plasmopara viticola*: a review of knowledge on downy mildew of grapevine and effective disease management. *Phytopathol. Mediterr.* 50, 3–44. doi: 10.14601/Phytopathol_Mediterr-9360

Gilroy, E. M., Breen, S., Whisson, S. C., Squires, J., Hein, I., Kaczmarek, M., et al. (2011). Presence/absence, differential expression and sequence polymorphisms between *PiAVR2* and *PiAVR2*-like in *Phytophthora infestans* determine virulence on *R2* plants. *New Phytol.* 191, 763–776. doi: 10.1111/j.1469-8137.2011.03736.x

Grant, S. R., Fisher, E. J., Chang, J. H., Mole, B. M., and Dangl, J. L. (2006). Subterfuge and manipulation: type III effector proteins of phytopathogenic bacteria. *Annu. Rev. Microbiol.* 60, 425–449. doi: 10.1146/annurev.micro.60.080805.142251

Guan, X., Zhao, H., Xu, Y., and Wang, Y. (2011). Transient expression of glyoxal oxidase from the Chinese wild grape *Vitis pseudoreticulata* can suppress powdery mildew in a susceptible genotype. *Protoplasma* 248, 415–423. doi: 10.1007/s00709-010-0162-4

Haas, B. J., Kamoun, S., Zody, M. C., Jiang, R. H., Handsaker, R. E., Cano, L. M., et al. (2009). Genome sequence and analysis of the Irish potato famine pathogen *Phytophthora infestans*. *Nature* 461, 393–398. doi: 10.1038/nature08358

Hann, D. R., Gimenez-Ibanez, S., and Rathjen, J. P. (2010). Bacterial virulence effectors and their activities. *Curr. Opin. Plant Biol.* 13, 388–393. doi: 10.1016/j.pbi.2010.04.003

Hellens, R. P., Edwards, E. A., Leyland, N. R., Bean, S., and Mullineaux, P. M. (2000). pGreen: a versatile and flexible binary Ti vector for *Agrobacterium*-mediated plant transformation. *Plant Mol. Biol.* 42, 819–832. doi: 10.1023/A:1006496308160

Iandolino, A., da Silva, F. G., Lim, H., Choi, H., Williams, L., and Cook, D. (2004). High-quality RNA, cDNA, and derived EST libraries from grapevine (*Vitis vinifera* L.). *Plant Mol. Biol. Rep.* 22, 269–278. doi: 10.1007/BF02773137

Jones, J. D., and Dangl, J. L. (2006). The plant immune system. *Nature* 444, 323–329. doi: 10.1038/nature05286

Kamoun, S., van West, P., Vleeshouwers, V. G., de Groot, K. E., and Govers, F. (1998). Resistance of *Nicotiana benthamiana* to *Phytophthora infestans* is mediated by the recognition of the elicitor protein INF1. *Plant Cell* 10, 1413–1425. doi: 10.1105/tpc.10.9.1413

Katagiri, F., and Tsuda, K. (2010). Understanding the plant immune system. *Mol. Plant-Microbe Interact.* 23, 1531–1536. doi: 10.1094/MPMI-04-10-0099

Kelley, B. S., Lee, S. J., Damasceno, C., Chakravarthy, S., Kim, B. D., Martin, G. B., et al. (2010). A secreted effector protein (SNE1) from *Phytophthora infestans* is a broadly acting suppressor of programmed cell death. *Plant J.* 62, 357–366. doi: 10.1111/j.1365-313X.2010.04160.x

Lacomme, C., and Santa Cruz, S. (1999). Bax-induced cell death in tobacco is similar to the hypersensitive response. *Proc. Natl. Acad. Sci. U.S.A.* 96, 7956–7961. doi: 10.1073/pnas.96.14.7956

Li, X., Wu, J., Yin, L., Zhang, Y., Qu, J., and Lu, J. (2015a). Comparative transcriptome analysis reveals defense-related genes and pathways against downy mildew in *Vitis amurensis* grapevine. *Plant Physiol. Biochem.* 95, 1–14. doi: 10.1016/j.plaphy.2015.06.016

Li, Z., Yin, Z., Fan, Y., Xu, M., Kang, Z., and Huang, L. (2015b). Candidate effector proteins of the necrotrophic apple canker pathogen *Valsa mali* can suppress BAX-induced PCD. *Front. Plant Sci.* 6:579. doi: 10.3389/fpls.2015.00579

Liu, T., Ye, W., Ru, Y., Yang, X., Gu, B., Tao, K., et al. (2011). Two host cytoplasmic effectors are required for pathogenesis of *Phytophthora sojae* by suppression of host defenses. *Plant Physiol.* 155, 490–501. doi: 10.1104/pp.110.166470

Mestre, P., Piron, M.-C., and Merdinoglu, D. (2012). Identification of effector genes from the phytopathogenic oomycete *Plasmopara viticola* through the analysis of gene expression in germinated zoospores. *Fungal Biol.* 116, 825–835. doi: 10.1016/j.funbio.2012.04.016

Oh, S.-K., Young, C., Lee, M., Oliva, R., Bozkurt, T. O., Cano, L. M., et al. (2009). In planta expression screens of *Phytophthora infestans* RXLR effectors reveal diverse phenotypes, including activation of the *Solanum bulbocastanum* disease resistance protein Rpi-blb2. *Plant Cell* 21, 2928–2947. doi: 10.1105/tpc.109.068247

Petre, B., and Kamoun, S. (2014). How do filamentous pathogens deliver effector proteins into plant cells? *PLoS Biol.* 12:e1001801. doi: 10.1371/journal.pbio.1001801

Qutob, D., Kamoun, S., and Gijzen, M. (2002). Expression of a *Phytophthora sojae* necrosis-inducing protein occurs during transition from biotrophy to necrotrophy. *Plant J.* 32, 361–373. doi: 10.1046/j.1365-313X.2002.01439.x

Qutob, D., Tedman-Jones, J., Dong, S., Kuflu, K., Pham, H., Wang, Y., et al. (2009). Copy number variation and transcriptional polymorphisms of *Phytophthora sojae* RXLR effector genes *Avr1a* and *Avr3a*. *PLoS ONE* 4:e5066. doi: 10.1371/journal.pone.0005066

Rajput, N. A., Zhang, M., Ru, Y., Liu, T., Xu, J., Liu, L., et al. (2014). *Phytophthora sojae* effector PsCRN70 suppresses plant defenses in *Nicotiana benthamiana*. *PLoS ONE* 9:e98114. doi: 10.1371/journal.pone.0098114

Rehmany, A. P., Gordon, A., Rose, L. E., Allen, R. L., Armstrong, M. R., Whisson, S. C., et al. (2005). Differential recognition of highly divergent downy mildew avirulence gene alleles by *RPP1* resistance genes from two Arabidopsis lines. *Plant Cell* 17, 1839–1850. doi: 10.1105/tpc.105.031807

Robert-Seilaniantz, A., Grant, M., and Jones, J. D. (2011). Hormone crosstalk in plant disease and defense: more than just jasmonate-salicylate antagonism.

Annu. Rev. Phytopathol. 49, 317–343. doi: 10.1146/annurev-phyto-073009-114447

Schmidlin, L., Poutaraud, A., Claudel, P., Mestre, P., Prado, E., Santos-Rosa, M., et al. (2008). A stress-inducible resveratrol O-methyltransferase involved in the biosynthesis of pterostilbene in grapevine. *Plant Physiol.* 148, 1630–1639. doi: 10.1104/pp.108.126003

Schornack, S., van Damme, M., Bozkurt, T. O., Cano, L. M., Smoker, M., Thines, M., et al. (2010). Ancient class of translocated oomycete effectors targets the host nucleus. *Proc. Natl. Acad. Sci. U.S.A.* 107, 17421–17426. doi: 10.1073/pnas.1008491107

Shan, W., Cao, M., Leung, D., and Tyler, B. M. (2004). The *Avr1b* locus of *Phytophthora sojae* encodes an elicitor and a regulator required for avirulence on soybean plants carrying resistance gene *Rps 1b*. *Mol. Plant-Microbe Interact.* 17, 394–403. doi: 10.1094/MPMI.2004.17.4.394

Sharma, R., Xia, X., Cano, L. M., Evangelisti, E., Kemen, E., Judelson, H., et al. (2015). Genome analyses of the sunflower pathogen *Plasmopara halstedii* provide insights into effector evolution in downy mildews and *Phytophthora*. *BMC Genomics* 16:741. doi: 10.1186/s12864-015-1904-7

Soanes, D. M., Richards, T. A., and Talbot, N. J. (2007). Insights from sequencing fungal and oomycete genomes: what can we learn about plant disease and the evolution of pathogenicity? *Plant Cell* 19, 3318–3326. doi: 10.1105/tpc.107.056663

Stassen, J. H., and Van den Ackerveken, G. (2011). How do oomycete effectors interfere with plant life? *Curr. Opin. Plant Biol.* 14, 407–414. doi: 10.1016/j.pbi.2011.05.002

Thomma, B. P., Nürnberger, T., and Joosten, M. H. (2011). Of PAMPs and effectors: the blurred PTI-ETI dichotomy. *Plant Cell* 23, 4–15. doi: 10.1105/tpc.110.082602

Thordal-Christensen, H., Zhang, Z., Wei, Y., and Collinge, D. B. (1997). Subcellular localization of H_2O_2 in plants. H_2O_2 accumulation in papillae and hypersensitive response during the barley—powdery mildew interaction. *Plant J.* 11, 1187–1194. doi: 10.1046/j.1365-313X.1997.11061187.x

Tyler, B. M., Tripathy, S., Zhang, X., Dehal, P., Jiang, R. H., Aerts, A., et al. (2006). *Phytophthora* genome sequences uncover evolutionary origins and mechanisms of pathogenesis. *Science* 313, 1261–1266. doi: 10.1126/science.1128796

van Poppel, P. M., Guo, J., van de Vondervoort, P. J., Jung, M. W., Birch, P. R., Whisson, S. C., et al. (2008). The *Phytophthora infestans* avirulence gene *Avr4* encodes an RXLR-dEER effector. *Mol. Plant-Microbe Interact.* 21, 1460–1470. doi: 10.1094/MPMI-21-11-1460

Vinatzer, B. A., Pel, M. J. C., Wintermans, P. C. A., Cabral, A., Robroek, B. J. M., Seidl, M. F., et al. (2014). Functional Analysis of *Hyaloperonospora arabidopsidis* RXLR Effectors. *PLoS ONE* 9:e110624. doi: 10.1371/journal.pone.0110624

Vleeshouwers, V., Rietman, H., Krenek, P., Champouret, N., Young, C., Oh, S.-K., et al. (2008). Effector genomics accelerates discovery and functional profiling of potato disease resistance and *Phytophthora infestans* avirulence genes. *PLoS ONE* 3:e2875. doi: 10.1371/journal.pone.0002875

Vlot, A. C., Dempsey, D. M. A., and Klessig, D. F. (2009). Salicylic acid, a multifaceted hormone to combat disease. *Annu. Rev. Phytopathol.* 47, 177–206. doi: 10.1146/annurev.phyto.050908.135202

Wang, Q., Han, C., Ferreira, A. O., Yu, X., Ye, W., Tripathy, S., et al. (2011). Transcriptional Programming and Functional Interactions within the *Phytophthora sojae* RXLR Effector Repertoire. *Plant Cell* 23, 2064–2086. doi: 10.1105/tpc.111.086082

Whisson, S. C., Boevink, P. C., Moleleki, L., Avrova, A. O., Morales, J. G., Gilroy, E. M., et al. (2007). A translocation signal for delivery of oomycete effector proteins into host plant cells. *Nature* 450, 115–118. doi: 10.1038/nature06203

Wu, J., Zhang, Y., Zhang, H., Huang, H., Folta, K. M., and Lu, J. (2010). Whole genome wide expression profiles of *Vitis amurensis* grape responding to downy mildew by using Solexa sequencing technology. *BMC Plant Biol.* 10:234. doi: 10.1186/1471-2229-10-234

Yin, L., Li, X., Xiang, J., Qu, J., Zhang, Y., Dry, I. B., et al. (2015). Characterization of the secretome of *Plasmopara viticola* by *de novo* transcriptome analysis. *Physiol. Mol. Plant Pathol.* 91, 1–10. doi: 10.1016/j.pmpp.2015.05.002

Yu, X., Tang, J., Wang, Q., Ye, W., Tao, K., Duan, S., et al. (2012). The RxLR effector Avh241 from Phytophthora sojae requires plasma membrane localization to induce plant cell death. *New Phytol.* 196, 247–260. doi: 10.1111/j.1469-8137.2012.04241.x

Zhang, M., Meng, Y., Wang, Q., Liu, D., Quan, J., Hardham, A. R., et al. (2012). PnPMA1, an atypical plasma membrane H+-ATPase, is required for zoospore development in Phytophthora parasitica. *Fungal Biol.* 116, 1013–1023. doi: 10.1016/j.funbio.2012.07.006

Zheng, X., McLellan, H., Fraiture, M., Liu, X., Boevink, P. C., Gilroy, E. M., et al. (2014). Functionally redundant RXLR effectors from *Phytophthora infestans* act at different steps to suppress early flg22-triggered immunity. *PLoS Pathog.* 10:e1004057. doi: 10.1371/journal.ppat.1004057

Zuo, J., Niu, Q. W., and Chua, N. H. (2000). An estrogen receptor-based transactivator XVE mediates highly inducible gene expression in transgenic plants. *Plant J.* 24, 265–273. doi: 10.1046/j.1365-313x.2000.00868.x

Conflict of Interest Statement: The authors declare that the research was conducted in the absence of any commercial or financial relationships that could be construed as a potential conflict of interest.

frontiers in Plant Science

METHODS
published: 01 March 2016
doi: 10.3389/fpls.2016.00246

COLORFUL-Circuit: A Platform for Rapid Multigene Assembly, Delivery, and Expression in Plants

Hassan Ghareeb[1,2]*, *Sabine Laukamm*[1] and *Volker Lipka*[1]*

[1] Department of Plant Cell Biology, Albrecht-von-Haller Institute of Plant Sciences, Georg-August-University of Göttingen, Göttingen, Germany, [2] Department of Plant Biotechnology, National Research Centre, Cairo, Egypt

Advancing basic and applied plant research requires the continuous innovative development of the available technology toolbox. Essential components of this toolbox are methods that simplify the assembly, delivery, and expression of multiple transgenes of interest. To allow simultaneous and directional multigene assembly on the same plant transformation vector, several strategies based on overlapping sequences or restriction enzymes have recently been developed. However, the assembly of homologous and repetitive DNA sequences can be inefficient and the frequent occurrence of target sequences recognized by commonly used restriction enzymes can be a limiting factor. Here, we noted that recognition sites for the restriction enzyme *SfiI* are rarely occurring in plant genomes. This fact was exploited to establish a multigene assembly system called "COLORFUL-Circuit." To this end, we developed a set of binary vectors which provide a flexible and cost efficient cloning platform. The gene expression cassettes in our system are flanked with unique *SfiI* sites, which allow simultaneous multi-gene cassette assembly in a hosting binary vector. We used COLORFUL-Circuit to transiently and stably express up to four fluorescent organelle markers in addition to a selectable marker and analyzed the impact of assembly design on coexpression efficiency. Finally, we demonstrate the utility of our optimized "COLORFUL-Circuit" system in an exemplary case study, in which we monitored simultaneously the subcellular behavior of multiple organelles in a biotrophic plant–microbe interaction by Confocal Laser Scanning Microscopy.

Keywords: multigene coexpression, circuit design, synthetic biology, binary vectors, gene stacking, plant biotechnology

OPEN ACCESS

Edited by:
Ralph Panstruga,
RWTH Aachen University, Germany

Reviewed by:
Joop E. M. Vermeer,
University of Zurich, Switzerland
Yvon Jaillais,
École normale supérieure de Lyon, France

***Correspondence:**
Hassan Ghareeb
hassan.ghareeb@biologie.uni-goettingen.de;
Volker Lipka
volker.lipka@biologie.uni-goettingen.de

Specialty section:
This article was submitted to Plant Biotic Interactions, a section of the journal Frontiers in Plant Science

Received: *31 December 2015*
Accepted: *14 February 2016*
Published: *01 March 2016*

Citation:
Ghareeb H, Laukamm S and Lipka V (2016) COLORFUL-Circuit: A Platform for Rapid Multigene Assembly, Delivery, and Expression in Plants. Front. Plant Sci. 7:246. doi: 10.3389/fpls.2016.00246

INTRODUCTION

The coordinated expression of foreign genes in plant cells by genetic engineering is one of the most important technologies in basic and applied plant research (Brophy and Voigt, 2014; Farré et al., 2015). The most common method used for genetic engineering of plants is *Agrobacterium tumefaciens*-mediated transformation. An essential step toward genetic manipulation via *A. tumefaciens* is the construction of binary vectors containing gene expression cassettes. The basic structure of a gene cassette is a promoter, the gene of interest and a transcriptional terminator. For overexpression in plants two promoter elements, the cauliflower mosaic virus CaMV 35S promoter (35S) and the polyubiquitin 10 (UBQ10) promoter of *Arabidopsis thaliana* are commonly used. Both provide constitutive and high levels of gene expression (Grefen et al., 2010). To stop the gene transcription process, the terminators of the cauliflower mosaic virus 35S (T35S), nopaline synthase

(Tnos), and octopine synthase (Tocs) of the *A. tumefaciens* have been frequently used (Mitsuhara et al., 1996; Martin et al., 2009). An enormous number of binary plasmids containing combinations of these regulatory elements were developed to enable foreign gene transfer and expression in plant cells (Lee and Gelvin, 2008). The use of these vectors for transgene delivery into plants contributed to our understanding of gene function and genetic networking, and supported the development of plant biotechnology (Dafny-Yelin and Tzfira, 2007). However, their application was mainly limited to expression of one single gene of interest in addition to the selectable marker. Thus, the available molecular toolbox for one-step transformation with more than one transgene is far from being satisfactory despite increasing demands (Atkinson and Urwin, 2012; Ainley et al., 2013; van Erp et al., 2014). Therefore, stable overexpression of multi-transgenes is still considered to be one of the bottlenecks that constrain the engineering of complex metabolic pathways or the improvement of quantitative traits (Bohmert et al., 2002; Naqvi et al., 2010; Giuliano, 2014).

To ease the construction of multigene assemblies, several approaches that make use of DNA overlapping sequences or restriction enzymes have recently been developed (Tzfira et al., 2005; Li and Elledge, 2007; Quan and Tian, 2009; Naqvi et al., 2010; Zeevi et al., 2012; Emami et al., 2013; Liu et al., 2013; Sarrion-Perdigones et al., 2013; Binder et al., 2014; Engler et al., 2014; Hecker et al., 2015). A powerful assembly technique that can be used for joining multiple DNA fragments simultaneously in a single tube is Gibson Assembly (Gibson et al., 2009). Gibson Assembly allows joining the DNA molecules *via* overlapping ends. By concerted action of a 5′ exonuclease, a DNA polymerase and a DNA ligase, single strands of overlapping sequences are generated, annealed, empty gaps filled, and then ligated. Application of Gibson assembly can be limited when homologous sequences and repetitive sequences have to be combined. The same holds true for other overlap-based assembly platforms such as overlap extension polymerase chain reaction, circular polymerase extension cloning, sequence and ligase independent cloning, InFusion® (Clontech) and Multisite Gateway® system (Thermo Fisher Scientific; reviewed in Liu et al., 2013). In addition, these techniques are expensive.

Alternatively, restriction enzyme-based assembly systems can be used for multigene construction. Pioneering work by Tzfira et al. (2005) and Zeevi et al. (2012) provided sets of binary vectors that allow multiple gene cassette assembly using a limited set of DNA-modifying enzymes. In these systems the gene cassettes are ligated together *via* compatible flanking overhangs which are produced by rare-cutting restriction enzymes, zinc-finger nucleases and homing endonucleases. Despite the unquestionable utility and elegance of these systems their applicability is limited due to their dependency on comparatively expensive enzymes. Another powerful approach for simultaneous DNA fragment assembly is provided by Golden Gate and Golden Gate-related systems (Engler et al., 2008; Emami et al., 2013; Sarrion-Perdigones et al., 2013). The latter cloning strategies are based on type II restriction enzymes, such as *BsaI*, *BsmBI,* and *SapI*, which cut DNA outside of the recognition sites and produce unique overhangs that allow combinatorial DNA assembly. However, we noticed that the restriction enzyme recognition sites used in Golden Gate cloning occur at relatively high frequencies in the genome sequences of plants (see below). Consequently, Golden Gate cloning often requires site-directed mutation of the naturally occurring restriction enzyme recognition sites in the cloned DNA fragment. Therefore this cloning system can be laborious or even of limited utility, in particular when codon optimization is not possible, e.g., in case of promoters or other noncoding DNA sequences. In summary, despite important recent improvements there is still a need to develop DNA assembly methods that can overcome the aforementioned limitations and facilitate multiple gene expression.

Moreover, it has to be kept in mind that the construct design of multigene assemblies may influence the expression efficiency of genetic circuits (Peremarti et al., 2010). For example, repetitive use of the same promoter in multigene constructs may negatively impact on transgene expression (Mette et al., 2000). To assess the performance of individual promoters in multigene assembly and to quantify the gene expression they control, adequate reporter genes are required. Fluorescent proteins (FPs) are instrumental reporters and provide an easy readout to monitor gene expression. Several FPs have been recently developed to cover wide ranges of emission spectra (Kremers et al., 2011). Simultaneous employment of spectrally distant FPs can thus be used to monitor gene expression derived from different gene cassettes (Zeevi et al., 2012; Binder et al., 2014; Hecker et al., 2015). The fluorescent proteins mTurquoise2, Venus, TagRFP-T and mKate2 are spectrally distant, and represent the brightest and most photostable in their spectral ranges (Nagai et al., 2002; Shaner et al., 2008; Shcherbo et al., 2009; Goedhart et al., 2012) making them convenient for multi-reporter purposes.

Besides their suitability to monitor promoter activities and transgene stability, FPs can also be used as markers in plant cell biology. For example, the coexpression of two FP fusions can provide evidence for protein co-localization using conventional fluorescence or confocal microscopy or protein–protein interaction using fluorescence resonance energy transfer (FRET) microscopy (Tzfira et al., 2005; Hecker et al., 2015). More complex live-cell imaging experiments, such as the co-localization of several proteins or studying the spatiotemporal dynamics of several cell organelles, require the use of three or more FPs. However, the FPs-encoding genes generally share a common origin and thus have a high DNA sequence homology (Kremers et al., 2011). This may be problematic as homology of the coding sequences can cause gene silencing (Cogoni and Macino, 1999). Since circuit dynamics can be influenced by the choice of the coding sequence and/or the deployment of the regulatory elements (Peremarti et al., 2010; Brophy and Voigt, 2014), an optimal design of multigene circuit constructs allowing efficient gene expression is necessary.

Here, we developed a set of binary vectors, which we named "COLORFUL-Circuit" that allow for cost-efficient and straightforward cloning of multiple foreign genes, variable FP tagging as well as easy and straightforward promoter exchange. A prominent characteristic of the vectors is that they allow simultaneous assembly of gene cassettes after digestion with one

restriction enzyme. We optimized the design of the COLORFUL-Circuit assemblies to increase the efficiency of gene expression of two to four homologous FPs in stable transgenic plants. We believe that the COLORFUL-Circuit platform represents a valuable asset to the genetic circuit design toolbox that provides a number of substantial advantages for scientists working on basic and applied aspects of plant biology.

MATERIALS AND METHODS

Plant Growth Conditions and Inoculation with *Golovinomyces orontii*

Seeds of *A. thaliana* (Col-0) or *Nicotiana benthamiana* were vernalized at 4°C for 2 days. Plants were grown in a climate chamber (Johnson Controls, USA) under long day conditions (16/8 h) with 130 $\mu mol \cdot m^{-2} \cdot s^{-1}$ at 22/18 and 25/22°C, respectively. For inoculation experiments with *G. orontii*, 4-week old plants were inoculated with the conidiospores of the fungus and then incubated in a growth chamber under short day conditions (8/16 h) with 130 $\mu mol \cdot m^{-2} \cdot s^{-1}$ at 22/18 and 25/22°C, respectively.

Frequency Determination of Restriction Enzymes Cleavage Sites in Plant Genomes

The chromosomal DNA sequences excluding the randomly assembled nucleotide sequences of *A. thaliana* (ecotype Col-0), rapeseed (*Brassica napus* cultivar Darmor-*bzh*), tomato (*Solanum lycopersicum* cultivar Heinz 1706), and rice (*Oryza sativa* cultivar Nipponbare; Initiative, 2000; Consortium, 2012; Kawahara et al., 2013; Chalhoub et al., 2014) were retrieved from the *Arabidopsis* Information Resource database (ftp://ftp.arabidopsis.org/home/tair/home/tair/Sequences/whole_chromosomes), Genoscope database (http://www.genoscope.cns.fr/brassicanapus/data), Sol genomics network database (ftp://ftp.sgn.cornell.edu/genomes/Solanum_lycopersicum/assembly/current_build), and Rice Genome Annotation Project database (ftp://ftp.plantbiology.msu.edu/pub/data/Eukaryotic_Projects/o_sativa/annotation_dbs/pseudomolecules/version_7.0/all.dir), respectively. Then, the cleavage sites of the restriction enzymes *SfiI*, *BsmBI*, *BsaI* and *SapI* in each chromosome were detected and counted using the software Geneious®8.1.7 (Biomatters Ltd). Finally, the number of cleavage sites per megabase (MB) in the entire genome for each restriction enzyme was calculated.

DNA Assembly and Plasmid Constructions

For PCR amplification of the DNA fragments that were used for cloning, the oligonucleotide primers listed in Supplementary Table S1 were used. The basic gene cassette (C1) modules were cloned in a pUC19 cloning vector (Clontech, Saint-Germain-en-Laye, France), which was modified to contain the *SfiI*-A and *RsrII*, *SfiI*-B recognition sites. The UBQ10 was cloned via *RsrII* cloning sites, and mKate2 was fused to UBQ10 using *BamHI* restriction sites, which were present in the reverse primer that was used to amplify the UBQ10 and the forward primer used for generation of the mKate2 fragment. Likewise, we sequentially fused LTI6b and T35S using the cloning sites *EcoRI*/*SpeI*, and *SpeI*/*SfiI*-B, respectively, to generate the C1 cassette. The C1.1, C1.2, and C1.3 cassettes were generated by PCR amplification of the C1 cassette using pairs of oligonucleotide primers that replace the *SfiI*-A and *SfiI*-B with *SfiI*-C and *SfiI*-D, *SfiI*-E and *SfiI*-F, and *SfiI*-G and *SfiI*-H, respectively as indicated in **Figure 1A**. Meanwhile, four binary vector backbones were PCR-amplified from the plasmid pXNS2pat-YFP (accession number KF499077; Dahncke and Witte, 2013) using four pairs of primers that add distinct *SfiI* cleavage sites in the flanks of the backbones to specifically allow ligation with the overhangs of either C1, C1.1, C1.2, or C1.3 gene cassette as indicated in Supplementary Figure S1. The gene cassettes C1, C1.1, C1.2, or C1.3 and their corresponding vector backbones were cleaved with *SfiI* (NEB, Germany), separated on agarose gel electrophoresis, and then cleaned up from the gel using innuPREP DOUBLEpure Kit (Analytik Jena, Germany). For the *SfiI* cleavage, 0.5–1 μg DNA, 2 μl CutSmart® buffer and 0.2–0.5 μl *SfiI* (20 unit/μl) were added in 20 μl total volume, and then incubated for 1–16 h at 50°C in a thermocycler (MyCycler™, Bio-Rad, USA). Note that *SfiI* functions more efficiently in excess of DNA containing multiple cleavage sites of the enzyme. The *SfiI*-cleaved vector backbone was then ligated with the corresponding gene cassette to produce pC1, pC1.1, pC1.2, and pC1.3. To generate binary vectors expressing the fluorescent organelle markers, the gene encoding TagRFP-T-SKL was PCR amplified and cloned into pC1.1 *via BamHI* and *SpeI* restriction sites to produce pC2. Venus and mTurquoise2 were cloned into pC1.2 and pC1.3, respectively, via *BamHI* and *EcoRI*. Then pC1.2 and pC1.3 were cleaved with *EcoRI* and *SpeI*, and then MAP4 and N7, which were PCR amplified using primers that add 20 bp overlapping to 3′-ends of Venus or mTurquoise2, and 5′-ends of T35S, were fused into the vectors via Gibson Assembly (NEB, Gibson et al., 2009) to generate pC3 and pC4, respectively. The UBQ10 promoters in pC2 and pC4 were replaced with the 35S promoters using the *RsrII* cloning sites. The Tocs terminator was PCR amplified and replaced the T35S of pC2 using the *SpeI* and *SfiI* cloning sites.

To construct multigene binary vectors, we amplified the backbone of pGreenII "hosting vectors" (Hellens et al., 2000) by PCR using primer pairs, which add *SfiI* recognition sites compatible with the free *SfiI* overhangs of the gene cassettes to be assembled. The vector backbones and the plasmids pC1, pC2, pC3, and pC4 were digested with *SfiI*, separated on agarose gel electrophoresis, and then the corresponding DNA fragments were cleaned up from the gel. The gene cassettes C2 and C3 were ligated with a hosting vector, which harbors compatible overhangs to the *SfiI*-C and *SfiI*-E sites, to produce the plasmid containing double-gene cassette pC2–C3. Likewise, we produced the plasmid containing triple-gene cassettes pC1–C3 and quadruple-gene cassettes pC1–C4 (version I). For assembling the multigene into a hosting binary vector, we ligated 50 ng vector backbone in 1:1 molar ratio with the *SfiI*-cleaved gene cassettes in a 20 μl total reaction that contained 2 μl buffer and 1 μl T4 DNA ligase (1 unit/μl; Thermo Fisher Scientific, Germany). The gene cassettes C2i and C3i were generated by PCR amplification from pC2 and pC3 using primer pairs, which contained swapped recognition sites of *SfiI*-C and *SfiI*-D and *SfiI*-E and *SfiI*-F, respectively. The C2i and C3i cassettes were *SfiI* cleaved and then ligated with the *SfiI*-cleaved vector backbones of

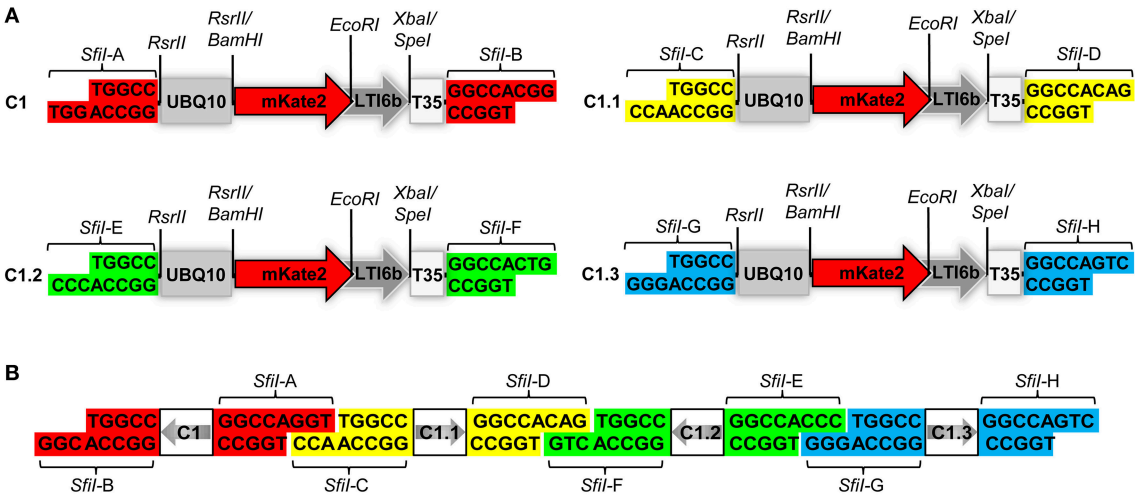

FIGURE 1 | Structural design of the COLORFUL-Circuit vectors and assembly. (A) Schematic view showing the modular design of the C1 gene expression cassette (1896 bp). The gene cassettes C1, C1.1, C1.2, and C1.3 only differ in the color coded unique *SfiI* overhangs (*SfiI*-A, *SfiI*-B, *SfiI*-C, *SfiI*-D, *SfiI*-E, *SfiI*-F, *SfiI*-G, and *SfiI*-H). UBQ10, polyubiquitin 10 promoter; mKate2, far-red fluorescent protein encoding gene; LTI6b, low temperature induced protein as a membrane marker; T35S, terminator of the cauliflower mosaic virus 35S; *SfiI*, *RsrII*, *EcoRI*, *XbaI/SpeI,* recognition sites of the corresponding restriction enzymes. **(B)** Diagram depicting the concept of COLORFUL-Circuit assembly of four tandemly arranged gene cassettes (C1–C1.1–C1.2–C1.3). The *SfiI* unique overhangs flanking each gene cassette allow combinatorial assembly, after *SfiI* cleavage and subsequent DNA ligation. The gray arrows indicate transcriptional orientations of the gene cassettes. *SfiI* overhangs with the same color flank one gene cassette. Note, that figure elements are not drawn to scale.

pC2 and pC3 to produce the plasmids pC2 and pC3i, respectively. The plasmid pC1–C4 (version II) was generated by ligating the *SfiI*-cleaved cassettes C1, C2i, C3i, and C4, and the quadruple-gene hosting vector backbone. Similarly, the pC1–C4 (version III) and pC1–C4 (version IV) were constructed except that the C3i was exchanged with C3 in the earlier and C2 was used instead of C2i in the later.

Transient Plant Transformation

A single colony of *A. tumefaciens* was used to inoculate 2 ml LB medium with the appropriate antibiotics and was grown for 1–2 days at 28°C. Subsequently, 0.5 ml of the grown culture were used to inoculate 4.5 ml of LB medium containing the appropriate antibiotics and 20 μM sterile acetosyringone. Cultures were grown overnight at 28°C with shaking and then were centrifuged for 10 min at 4500 × g. The pellet was resuspended in an infiltration solution containing 10 mM $MgCl_2$, 10 mM MES-K (pH 5.6) and 100 μM acetosyringone to obtain a final OD_{600} of 0.4. The cultures were incubated at room temperature for 2–4 h. Then, the abaxial side of *N. benthamiana* leaves was infiltrated with the bacterial suspension. After 2–3 days, the fluorescence signals were detected using Confocal Laser Scanning Microscopy (CLSM).

Stable Plant Transformation

A double floral dip protocol was combined from previously established protocols (Clough and Bent, 1998; Davis et al., 2009). First, six pots, 8 cm^2, each containing five plants were used for the transformation. As the first inflorescence shoots were emerged, they were excised and 1 week later the first floral dip was preceded. Three days before the transformation, *Agrobacterium* cultures were inoculated in 25 ml LB liquid medium containing 50 μg/ml Rifampicin, 30 μg/ml Gentamicin, 2.5 μg/ml Tetracycline, and 50 μg/ml Kanamycin. The cultures were incubated at 28°C with shaking (190 rpm). Two days later, the grown cultures were inoculated in 500 ml of LB liquid medium with the same antibiotic concentrations and incubated for 24 h at 28°C with shaking (190 rpm). The bacterial cultures were centrifuged at 4500 × g for 20 min at room temperature. The pellet was resuspended in 500 ml infiltration medium (0.5X MS with Gamborg B5 vitamins, 5% sucrose, and 150 μl/l Silwet L-77). The suspension was transferred into a 500-ml beaker, where the plants were dipped. Afterwards, the plants were placed into a transparent plastic bag and incubated on their side in the dark for 16–24 h. In the next day, the plants were returned back to normal growth conditions. A second floral dip was performed 5 days later using bacteria grown in YEBS medium with half concentrations of the antibiotics as the main culture. The bacteria were resuspended in infiltration medium with 300 μl/l Silwet L-77. We obtained a high transformation rates using this protocol. After 4 weeks, seeds were collected. Stably transformants were selected by on-soil Basta® selection. One-week-old seedlings were sprayed with 1:1000 Basta (containing 120 mg\ml phosphinothricin, Bayer CropScience, Germany). The treatment was conducted every 2 days and repeated three times. The stable transformation rate was determined as the percent of Basta-resistant T1 plants from the total treated plants. Survived plants, which were 2–3 weeks old, were used for CLSM.

Transgene Stability Assay

Transgenic plants that carry single T-DNA insertion for C1–C4 (III) or C1–C4(IV) were used to study the transgenerational

stability. For this purpose, seeds of the T2 generations from three independent lines for each construct were sterilized by adding 500 µl of 70% ethanol and mixing using a Rotator (20 rpm) for 5 min. The 70% ethanol was replaced by 500 µl of 99% ethanol for 1 min and then discarded. The seeds were air-dried, then sown onto ½MS/MES agar medium (MS 2.2 g/l, MES 0.5 g/l, plant agar 7 g/l, pH 5.8) supplemented with 10 mg/l PPT and kept at 4°C for 2 days. The seedlings were grown in a climate chamber (Johnson Controls, United Stated of America) under short day conditions (8 h light/16 h dark) with 150 $\mu mol \cdot m^{-2} \cdot s^{-1}$ at 22/18°C for 12 days. The Basta-resistant plants were screened for expression of the individual organelle markers using CLSM.

Confocal Laser Scanning Microscopy

Leaves from transiently transformed *N. benthamiana* or T1 or T2 of stably transformed *Arabidopsis* were used for CLSM. All images were captured using HyD and PMT detectors and 20x or 63x objectives of TSC-SP5 microscope (Leica, Bensheim, Germany). mTurquoise2 and Venus were excited using 458 and 514 nm lines of an argon laser, respectively, whereas TagRFP-T and mKate2 were excited with 561 and 594 nm lasers. Fluorescence emissions were detected at 462–485 nm for mTurquoise2, 520–540 nm for Venus, 565–580 nm for TagRFP-T, and 620–640 nm for mKate2. The images were sequentially scanned with a resolution of 512 × 512 pixels and 200 Hz scanning speed. A linear spectral unmixing was performed for the TagRFP-T and mKate2 channels. The maximum projection and image merging and linear spectral unmixing were performed using imageJ.

RESULTS AND DISCUSSION

Principle and Basic Vectors of the COLORFUL-Circuit Platform

Expression of foreign genes *in planta* via *Agrobacterium*-mediated transformation requires construction of binary vectors. We generated a set of binary vectors to allow single gene or multigene construction, delivery and expression in plants. For single gene expression, we started by generating a modular gene cassette (C1) that allows simple cloning steps and contains easily exchangeable modules: a UBQ10 promoter (Grefen et al., 2010), a gene encoding the far-red fluorescent reporter gene mKate2 (Shcherbo et al., 2009) fused to the plasma membrane protein low temperature induced protein 6b (LTI6b; Cutler et al., 2000), followed by a T35S terminator (Mitsuhara et al., 1996; **Figure 1A**). For generation of C1, we first introduced *RsrII* recognition sites at the left and right flanks of UBQ10 by PCR site-directed mutagenesis (**Figure 1A**). The restriction enzyme *RsrII* recognizes the sequence CG^GWCCG, allowing us to produce two distinct recognition sites by assigning two different nucleotides at position four of the recognition sites at the left (adenine) and right border (thymine). Consequently, upon *RsrII* cleavage two unique three-nucleotide overhangs are produced that allow a subsequent unidirectional exchange of promoter sequences. Next, we fused the mKate2 reporter gene to the 3′-end of the UBQ10 promoter using *BamHI* restriction sites present in the 3′-oligonucleotide primer used for generation of the UBQ10 module and the 5′-oligonucleotide primer used for PCR-amplification of the mKate2 module (Supplementary Table S1). Likewise, in subsequent steps we fused LTI6b via *EcoRI*/*SpeI* and finally, T35S via *SpeI*/*SfiI* which produced the full-length gene cassette C1 depicted in **Figure 1A**.

Notably, the 5′- and 3′-ends of the C1 cassette contain recognition sites for the restriction enzyme *SfiI*, namely *SfiI*-A and *SfiI*-B, which stem from the cloning vector (**Figure 1A**). *SfiI* is a type II restriction enzyme that recognizes the sequence GGCCNNNN^NGGCC. The nucleotides at position 6–8 of the *SfiI* recognition site typically define a sticky overhang. These overhang sequences can be freely modified to generate unique non-palindromic ends allowing unidirectional cloning. We exploited this fact to generate additional gene cassettes that can be later utilized for multigene assembly. To this end, we PCR-amplified the intact C1 cassette with oligonucleotide primers, which exchange the *SfiI*-A and *SfiI*-B sites with two other distinct *SfiI* cloning sites *SfiI*-C and *SfiI*-D, thus generating a derivative cassette called C1.1 (**Figure 1A**; Supplementary Table S1). Similarly, we generated two other gene cassettes C1.2 and C1.3, in which the unique *SfiI* recognition sites *SfiI*-E and *SfiI*-F, and *SfiI*-G and *SfiI*-H, respectively, replaced the *SfiI*-A and *SfiI*-B sites (**Figure 1A**). Each unique *SfiI* overhang was designed to complement with one other *SfiI* overhang in a manner that allows the assembly of four gene cassettes in alternate orientations (**Figure 1B**). We exploited these gene cassettes below for the establishment of a platform, which we named "COLORFUL-Circuit," for multigene assembly, delivery, and expression of up to four different genes of interest controlled by distinct promoters and terminators.

Establishment of Multicolor Fluorescent Organelle Markers for *Agrobacterium*-Mediated Transformation of Plants

To allow *Agrobacterium*-mediated transformation of the gene cassettes, we cloned the C1, C1.1, C1.2, and C1.3 cassettes separately into binary vectors. This was accomplished by PCR amplification of the vector backbone of pXNS2pat-YFP (Dahncke and Witte, 2013) using oligonucleotide primers that add terminal *SfiI* cloning sites, which permitted subsequent ligation with the *SfiI* overhangs (*SfiI*-A and *SfiI*-B) of the C1 cassette to produce the binary vector pC1 (**Figure 2A**, Supplementary Figure S1). Similarly, we generated the C1.1-, C1.2- and, C1.3-containing binary vectors pC1.1, pC1.2, and pC1.3, respectively (Supplementary Figure S1).

To allow monitoring of synchronous gene expression in later multigene assembly vectors, we first cloned into our basic vectors pC1.1, pC1.2, and pC1.3 different gene fusions encoding fluorescent organelle markers and regulatory elements. To this end, the peroxisomal targeting sequence SKL (Keller et al., 1991), the microtubule-binding domain of the mouse microtubule-associated protein 4 (MAP4; Aizawa et al., 1991; West et al., 1991), and the nuclear localization signal N7 (Cutler et al., 2000), were used to generate the fluorescent organelle markers TagRFP-T-SKL, Venus-MAP4 and mTurquoise2-N7 (**Figure 2A**). This

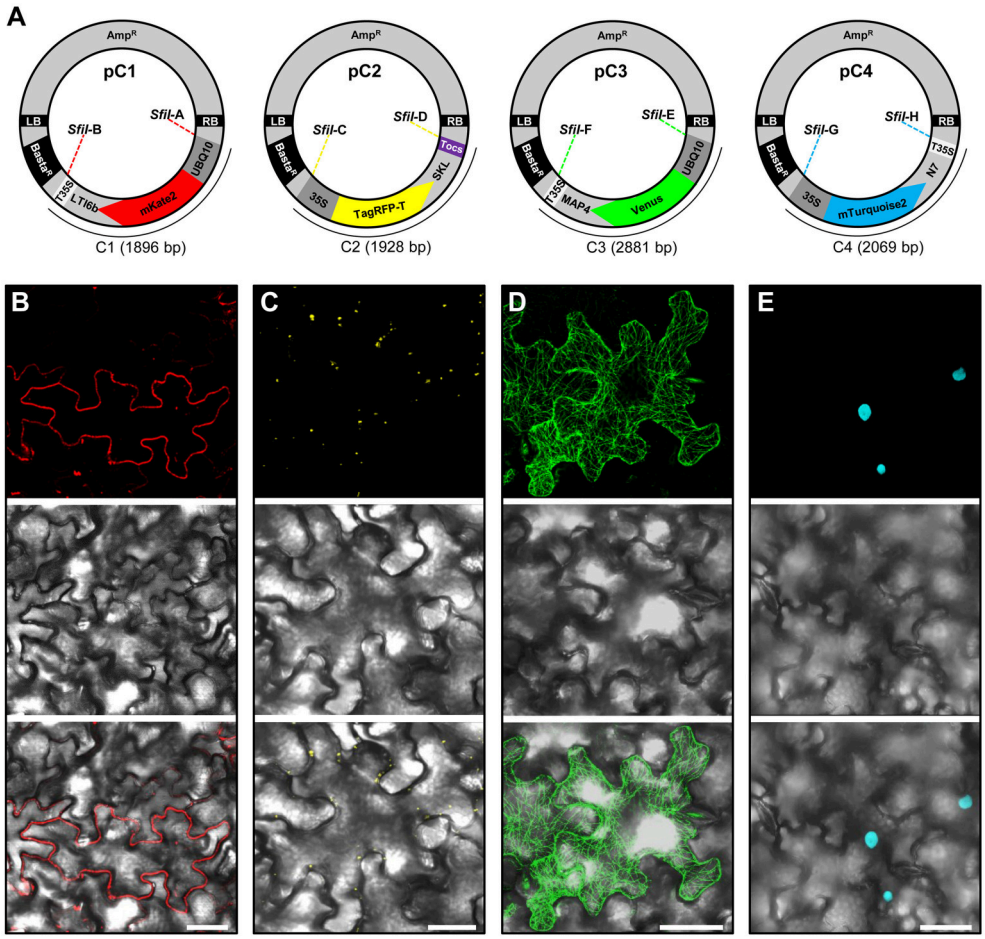

FIGURE 2 | Construction and transient expression of fluorescent organelle markers. (A) Schematic view of the modular pC1 (6178 bp), pC2 (6210 bp), pC3 (7163 bp), and pC4 (6351 bp) binary vectors expressing fluorescent organelle markers. The vector backbone (4282 bp) is represented outside of the *SfiI* recongintion sequences (*Sfi*A, *Sfi*B, *Sfi*C, *Sfi*D, *Sfi*E, *Sfi*F, *Sfi*G, and *Sfi*H) that flank the gene cassettes encoding the fluorescent organelle markers C1 (1896 bp), C2 (1928 bp), C3 (2881 bp), and C4 (2069 bp). The vector backbone was amplified from the plasmid pXNS2pat-YFP. UBQ10, polyubiquitin 10 promoter; 35S, cauliflower mosaic virus CaMV 35S promoter; T35, terminator of the cauliflower mosaic virus 35S; Tocs, terminator of octopine synthase; mKate2, TagRFP-T, Venus and mTurquoise2, fluorescent protein encoding genes; LTI6b, low temperature induced protein as a membrane marker; SKL, peroxisomal targeting sequence; MAP4, microtubule binding domain of the mouse microtubule-associated protein 4; N7, nuclear localization signal; Basta^R, selectable marker conferring Basta resistance in plants; Amp^R, selectable marker conferring ampicillin resistance in *E. coli* and *A. tumefaciens*; LB/RB, left/right borders of T-DNA. The figure is not drawn to scale. **(B–E)** *Agrobacterium*-mediated transient expression of the fluorescent organelle markers indicated in **(A)**. **(B)** Membrane localization of mKate2-LTI6b produced from pC1. **(C)** Peroxisomal localization of TagRFP-T-SKL produced from pC2. **(D)** Microtubule localization of Venus-MAP4 produced from pC3. **(E)** Nuclear localization of mTurquoise2-N7 produced from pC4. Top, middle and bottom panels in **(B–E)** represent fluorescence, bright field and overlay of confocal images. The images in **(C–E)** represent maximum projections of z-stacks obtained by confocal laser scanning microscopy. Scale bar = 50 μm.

was achieved by introducing the cloning sites *BamHI* and *SpeI* into TagRFP-T-SKL and subsequent replacement of mKate2-LTI6b in pC1.1 to produce the vector pC2 (**Figure 2A**). Similarly, mKate2 in pC1.2 and pC1.3 was replaced with Venus and mTurquoise2, respectively, using the *BamHI* and *EcoRI* cloning sites. Subsequently, pC1.2 and pC1.3 were cleaved with *EcoRI* and *SpeI*, and MAP4 and N7 were fused to 3′-ends of Venus and mTurquoise2, and 5′-ends of T35S using Gibson Assembly (see Materials and Methods, Gibson et al., 2009) to generate the binary vectors pC3 and pC4, respectively (**Figure 2A**). Finally, the promoters of the gene cassettes C2 and C4 were exchanged with the 35S promoter using *RsrII*, and the terminator of pC2 was exchanged with Tocs using *SpeI*/*SfiI* (**Figure 2A**).

To test the functionality of the individual organelle marker plasmids pC1, pC2, pC3, and pC4, we transiently expressed them separately in *N. benthamiana* leaves *via Agrobacterium*-mediated transformation and subsequently performed CLSM. These analyses showed that the four organelle markers were expressed and localized to the respective organelles as expected (**Figures 2B–E**).

COLORFUL-Circuit Simplifies Multigene Assembly

As outlined above, gene cassettes harbored by the vectors pC1–pC4 are characterized by unique overhangs that are produced by a single enzyme, *SfiI*, and allow simultaneous multigene assembly

(**Figure 1B**). Another notable feature of *SfiI* is that cleavage sites for this enzyme rarely occur in the genomes of *A. thaliana*, rapeseed, tomato and rice with only 3.1–40.8 sites per MB on average (**Table 1** and Supplementary Tables S2–S5). This provides a clear advantage of *SfiI* over the enzymes *BsaI, BsmBI,* and *SapI*, which are commonly used for Golden Gate and Golden Gate-related cloning systems (Emami et al., 2013; Sarrion-Perdigones et al., 2013; Binder et al., 2014; Engler et al., 2014), as recognition sequences for these enzymes occur at 216.7–267.2, 98–341.9, and 69.5–150.6 sites per MB, respectively (**Table 1** and Supplementary Tables S2–S5). Consequently, the *SfiI* cleavage sites in our vectors allow an easier and straightforward assembly of large genomic DNA fragments. In addition, *SfiI* is a relatively cheap restriction enzyme, offering a cost-efficient and simple alternative to other DNA assembly systems.

Next, we tested the practicability of our COLORFUL-Circuit multigene assembly system. For this purpose, we first digested pC1, pC2, pC3, and pC4 with *SfiI*, separated the gene cassettes from the plasmid backbones using agarose gel electrophoresis, and then extracted the corresponding gene cassettes C1 (1896 bp), C2 (1928 bp), C3 (2881 bp), and C4 (2069 bp) from the agarose gel. Subsequently, the three adjacent gene cassette pairs (C1 + C2, C2 + C3, and C3 + C4) were separately ligated and the ligation reactions were checked by agarose gel electrophoresis (**Figure 3A**). These experiments confirmed the ligation of the gene cassettes as the expected sizes of each ligated pair was evident (C1 + C2 = 3824 bp; C2 + C3 = 4809 bp; C3 + C4 = 4950 bp; **Figure 3A**). In a next step, we tested whether all four gene cassettes can be ligated in a single cloning step. Again, agarose gel electrophoresis confirmed the production of all possible assemblies as we were able to detect ligated DNA fragments corresponding to double (C1 + C2 = 3824 bp; C2 + C3 = 4809 bp; C3 + C4 = 4950 bp), triple (C1 + C2 + C3 = 6705 bp; C2 + C3 + C4 = 6878 bp), and quadruple (C1+ C2 + C3 + C4 = 8774 bp) gene cassette assemblies that were unidirectionally ligated (**Figure 3B**).

Finally, we generated binary vectors hosting the multigene assemblies for *Agrobacterium*-mediated plant transformation. To this end, we introduced *SfiI* restriction sites matching the 5′- and 3′-overhangs of our gene cassettes C1 to C4 into the vector backbone of pGreenII (Hellens et al., 2000). Then, we produced vectors containing double (pC2–C3; **Figure 3C**), triple (pC1–C3; **Figure 3D**) and quadruple [pC1–C4 (version I), **Figure 3E**] gene cassettes using *SfiI* restriction and subsequent ligation. It is important to notice that the multigene hosting vectors contain selectable markers that confer kanamycin resistance in *Escherichia coli* and *A. tumefaciens* (**Figures 3C–E**). Since the single-gene cassette-containing plasmids pC1, pC2, pC3, and pC4 confer bacterial resistance to ampicillin (**Figure 2A**), counter-selection for kanamycin avoids contamination with traces of the individual undigested plasmids and thereby maximizes the rate of correct recombinants. In support of this, we typically obtained vectors harboring the correct multigene assemblies at an average frequency of 87% (Supplementary Figure S2). Taken together, these experiments confirmed that our COLORFUL-Circuit system can be efficiently used to generate multigene assemblies.

TABLE 1 | Cleavage site frequency of the restriction enzymes *SfiI*, *BsmBI, BsaI,* and *SapI* occurring in the genomes of *A. thaliana*, rapeseed, tomato and rice.

Name of organism	Size (MB*)	Number of cleavage sites per MB*			
		SfiI	*BsaI*	*BsmBI*	*SapI*
A. thaliana	119.146348	3.1	265.9	275.8	150.6
Rapeseed	650.398471#	4.9	237.7	257.3	115.9
Tomato	703.594776	4.5	216.7	98	69.5
Rice	373.245519	40.8	267.2	341.9	134.2

*Megabase, #genome size without the randomly assembled nucleotide sequences.

COLORFUL-Circuit Assemblies Allow Robust Transient Coexpression of Up to Four Genes of Interest

Transient coexpression of multiple genes is conventionally achieved by co-transformation of single plasmids *via* agroinfiltration or gene bombardment. This strategy is laborious and time consuming. Moreover, uniform coexpression of transgenes in all transformed cells cannot be obtained. For example, co-transformation of vectors encoding two genes from separate T-DNAs was shown to yield 74–84% of cells that coexpressed both genes, whereas up to 100% of cells coexpressed both genes when encoded from a single plasmid (Hecker et al., 2015). To analyze coexpression efficiency in our double, triple and quadruple gene assemblies, we first transiently expressed the corresponding COLORFUL-Circuit constructs pC2–C3, pC1–C3, and pC1–C4 (version I) in *N. benthamiana* leaves *via* agroinfiltration and monitored the expression of fluorescent organelle markers by CLSM. These analyses showed that all organelle markers encoded by the respective constructs were efficiently coexpressed (Supplementary Figure S3A) and showed the expected subcellular localization (Supplementary Figure S3B). With a maximum number of up to four efficiently coexpressed transgenes our system provides an advantage over the recently published "Binary 2in1 vector"-system, which allows coexpression of up to two genes from the same T-DNA (Hecker et al., 2015).

Stable Transformation and Coexpression Rates Negatively Correlate with the Number of Genes within the Assembly

Next, we stably transformed *Arabidopsis* Col-0 plants with our COLORFUL-Circuit constructs, determined the transformation rates and analyzed the expression of the individual reporter genes encoded by the respective assemblies. With transformation rates of 2.6 and 2.5%, respectively, the single gene cassette C1 and the double-gene cassette C2–C3 were efficiently delivered and integrated into the plant genomes (**Figure 4**). In contrast, the transformation rates determined for the triple construct C1–C3 and the quadruple construct C1–C4, were 7.5- and 8-fold lower, respectively, compared to the transformation rate observed for C1 (**Figure 4**). Thus, our data support the previous observation

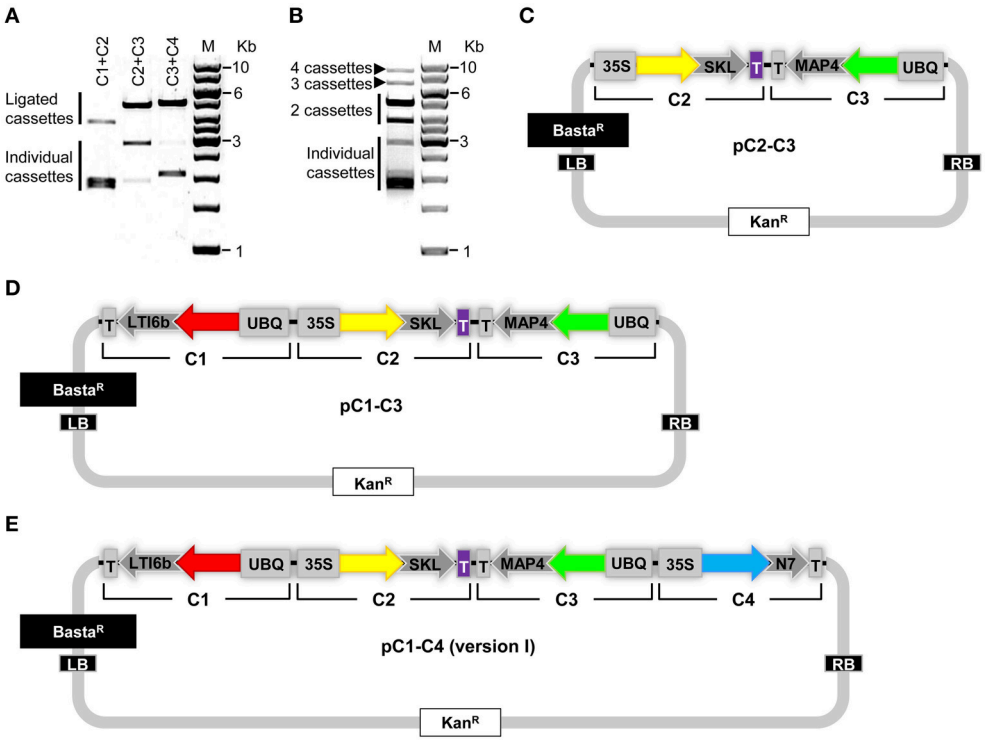

FIGURE 3 | Generation of COLORFUL-Circuit multigene assemblies. (A) Ligation of the *SfiI*-cleaved gene cassettes C1, C2, C3, and C4 followed by agarose gel electrophoresis verified the production of higher molecular weight DNA fragments corresponding to the assembled molecules. C1, 1896 bp, and C2, 1928 bp (ligated C1 + C2 = 3824 bp); C2 and C3, 2881 bp (ligated C2 + C3 = 4809 bp); and C3 and C4, 2069 bp (ligated C3 + C4 = 4950 bp). M: GeneRuler^{TM} 1-Kb DNA ladder. **(B)** DNA assembly of the four individual gene cassettes (C1, C2, C3, and C4) upon ligation. All possible unidirectionally ligated gene cassettes are produced; (C1 + C2 = 3824 bp; C2 + C3 = 4809 bp; C3 + C4 = 4950 bp), (C1 + C2 + C3 = 6705 bp; C2 + C3 + C4 = 6878 bp), and (C1+ C2 + C3 + C4 = 8774 bp). M: GeneRuler^{TM} 1-Kb DNA ladder. **(C–E)** Modules of the COLORFUL-Circuit multigene binary vectors that allow double-gene cassette assembly (pC2–C3), Triple-gene cassette assembly (pC1–C3) and quadruple-gene cassette assembly [pC1–C4 (version I)], respectively. C1, C2, C3, and C4: individual gene cassettes. The vector backbone was amplified from the plasmid pGreenII. UBQ: polyubiquitin 10 promoter; 35S: cauliflower mosaic virus CaMV 35S promoter; T: terminator of the cauliflower mosaic virus 35S (gray) and terminator of octopine synthase (purple); red, yellow, green and turquoise arrows: fluorescent protein encoding genes of mKate2, TagRFP-T, Venus and mTurquoise2, respectively; LTI6b, low temperature induced protein as a membrane marker; SKL, peroxisomes targeting sequence; MAP4, microtubule binding domain of the mouse microtubule-associated protein 4; N7, nuclear localization signal; Basta^R, selectable marker confers Basta resistance in plants; Kan^R, selectable marker confers kanamycin resistance in *E. coli* and *A. tumefaciens*; LB/RB, left/right borders of T-DNA. The figures are not drawn to scale.

that transformation rates of potato and tobacco plants negatively correlate with the size of the T-DNA that is to be delivered (Bohmert et al., 2002). However, with transformation rates between 0.32 and 2.6% we were still able to isolate a satisfactory number of transformants for all constructs, which were used for further analysis.

To analyze the expression of the individual reporter genes in the obtained transgenic *Arabidopsis*, we selected 50 stable cassette transformants per assembly and detected the fluorescent gene products by CLSM. We were able to identify individual transgenic plants expressing all two or three organelle markers encoded by the respective double and triple gene assemblies C2–C3 and C1–C3, respectively (**Figures 5A,B**). In order to obtain quantitative data, we determined both, the expression frequency of every individual organelle marker and, in addition, the coexpression rates of all reporter genes encoded by the respective multigene construct in each individual transgenic plant. These analyses showed that either organelle marker encoded from the double-gene assembly C2–C3 was detectable in 90% of the transformants (**Figure 5C**), and that both organelle markers were coexpressed in 88% of the plants (**Figure 5D**). Thus, compared to the 10% of all *Arabidopsis* transformants that coexpressed two genes using the Binary 2in1 vector system (Hecker et al., 2015), our COLORFUL-Circuit pC2–C3 provided higher rates of coexpression (**Figure 5D**). However, in plants carrying the triple reporter C1–C3 assembly, the expression frequency of the individual organelle markers was reduced to 54–72% (**Figure 5C**), with only 50% of the analyzed plants coexpressing all three organelle markers (**Figure 5D**). Finally, and in marked contrast to the fact that we were able to robustly detect all four fluorescent organelle markers in our transient expression experiments (Supplementary Figures S3A,B), none of the 50 selected transgenic plants transformed with the quadruple C1–C4 assembly coexpressed all four reporter genes (**Figures 5C,D**). Together, our data show that not only the transformation rates, but also the coexpression rates

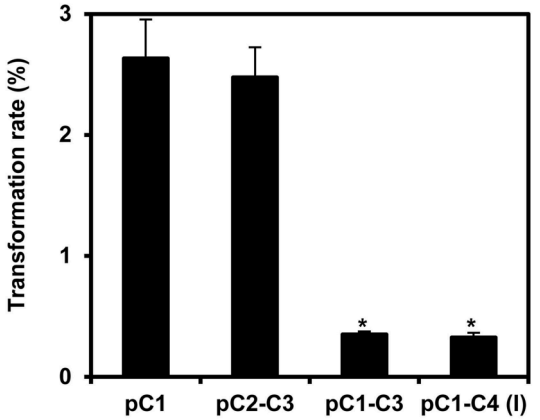

FIGURE 4 | Transformation rates of the COLORFUL-Circuit T-DNAs stably integrated in *Arabidopsis*. Transformation rate was calculated as percent of Basta-resistant T1 plants obtained from seeds that were harvested from plants transformed with *Agrobacterium* strains harboring binary vectors containing either single-(pC1), double-(pC2–C3), triple-(pC1–C3), or quadruple-gene cassettes [pC1–C4 (version I)] in addition to the Basta selectable marker. The data represent the means ± SEM of three experiments. Asterisks indicate significant differences in comparison to pC1 using student *t*-test, $p < 0.01$.

negatively correlate with the number of genes encoded within the assembly.

Assembly Design Impacts Efficiency of Multigene Coexpression

We reasoned that one potential explanation for the reduced coexpression efficiency observed with our triple and quadruple assemblies may be the high homology between the assembled genes, encoding Kate2 and TagRFP-T, as well as Venus and mTurquoise2, which share 96 and 97% sequence similarity, respectively. Moreover, these homologous genes were organized in inverted orientations within our original assemblies (**Figure 3E**). It is well known that inverted repeats may enhance DNA methylation and consequently trigger gene silencing (Stam et al., 1998). In addition, gene silencing may also be enhanced because of a possible transcriptional read-through from the oppositely oriented gene cassettes C2 and C3 (**Figure 3E**). Consequently, we reconsidered and changed our assembly design strategy. To this end, we reversed the direction of the C2 and C3 cassettes by PCR amplification using oligonucleotide primers that swap the original *SfiI*-C and *SfiI*-D, and *SfiI*-E and *SfiI*-F sites (**Figure 1A**), respectively, to produce the inverted gene cassettes C2i and C3i, respectively (**Figure 6A**). C2i and C3i were ligated into the progenitor vector backbones of pC2 and pC3 using the *SfiI* cloning sites to generate the binary vectors pC2i and pC3i, respectively. In addition, we replaced the sequences for Tocs with T35S using the cloning sites *SpeI* and *SfiI*-C in pC2i to test whether the identity of the transcriptional terminator influences coexpression efficiency (**Figure 6A**). We used combinations of the *SfiI*-cleaved gene cassettes C1, C2, C2i, C3, C3i, and C4, as previously described for constructing pC1–C4 (version I), to produce three different vectors harboring quadruple-gene assemblies, which we named pC1–C4 (version II), pC1–C4 (version III), and pC1–C4 (version IV; **Figure 6A**). Subsequently, we transiently expressed these newly developed quadruple-gene assemblies in *N. benthamiana*, and used CLSM to detect the encoded fluorescent organelle markers. For the pC1–C4 (version II), we only detected expression of either one or three organelle markers in two independent experiments (Supplementary Figures S4A,B). Therefore, pC1–C4 (II) was excluded from subsequent stable gene expression analysis, as it failed to coexpress the four gene fusions. For pC1–C4 (version III) and pC1–C4 (version IV) all four organelle markers were repeatedly detectable by CLSM (Supplementary Figure S4A) and fully coexpressed in all investigated cells (Supplementary Figure S4B).

Next, we analyzed the efficiency of stable transformation and multigene expression of pC1–C4 (version III) and pC1–C4 (version IV) designs in *Arabidopsis*. Again, plants transformed with either new quadruple-gene assembly showed lower transformation rates (0.32 and 0.31%, respectively) in comparison to those transformed with pC1 (2.32%), but had a comparable rate (0.36%) to the original pC1–C4 (version I; **Figure 6B**). As before, we selected 50 stable transformants per assembly and analyzed the expression of the respective fluorescent organelle markers by CLSM. With both remaining new quadruple assemblies, all four organelle markers could be observed in individual transformants (**Figure 6C**). To quantitatively evaluate the expression performance of each multigene assembly, we calculated the expression frequency of each individual organelle marker and their coexpression rates as previously described. These analyses revealed that each of the four organelle markers was expressed at similar frequency (68–74%) in plants carrying C1–C4 (version IV), whereas their expression frequency highly varied (26–72%) in plants carrying C1–C4 (version III; **Figure 6D**). These results show that the expression frequencies of the organelle markers encoded by C1–C4 (version III) and C1–C4 (version IV) were significantly enhanced compared to the original assembly C1–C4 (version I; **Figure 5C**), albeit with distinct robustness. Notably, improved multigene expression appears to be associated with avoidance of the opposing transcriptional orientation of the C2 and C3 cassettes in the C1–C4 (version III) and C1–C4 (version IV) assemblies (**Figure 6A**), supporting our early assumption that the design of the multigene affects the outcome of gene expression. We also observed that the increase in the expression frequency of the individual organelle markers (**Figure 6D**) positively correlated with their coexpression rates (**Figure 6E**). Interestingly, the coexpression rate of the four organelle markers observed in plants carrying C1–C4 (version IV) was more than two-fold higher (68%) if compared to plants transformed with C1–C4 (version III), which showed a coexpression rate of 26% (**Figure 6E**). Apparently, these differences result mainly from suppressed expression of the organelle markers encoded by C1 and C3 in C1–C4 (version III; **Figure 6D**). The assemblies C1–C4 (version III) and C1–C4 (version IV) have similar modular organization with one gene showing outward orientation followed by three consecutive

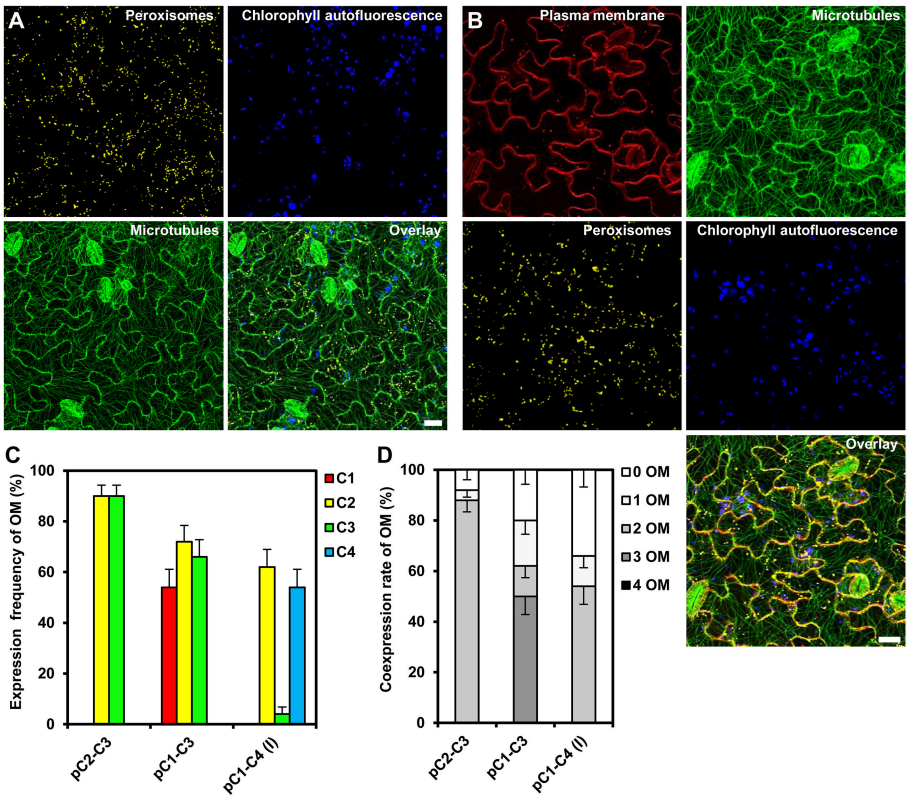

FIGURE 5 | Gene expression efficiency of the COLORFUL-Circuit assemblies in stable *Arabidopsis* transformants. (A) and **(B)** Leaf cells of transgenic *Arabidopsis* plants stably expressing double and triple organelle markers encoded by C2–C3 and C1–C3 T-DNAs, which are depicted in **Figures 3C,D**, respectively. Chlorophyll autofluorescence is provided as a control. The images are maximum projections of z-stacks obtained by CLSM. Scale bar = 20 μm. **(C)** Expression frequency of organelle markers (OM) calculated as percent of T1 transgenic plants expressing C1 (plasma membrane marker), C2 (peroxisomal marker), C3 (microtubule marker), or C4 (nuclear marker). Data represent percentages ± SEM ($n = 50$ plants). **(D)** Coexpression rate of organelle markers (OM) calculated as percent of T1 transgenic plants that coexpress the indicated number of organelle markers. $n = 50$ plants.

genes with the same directionality but opposite outward orientation (**Figure 6A**). However, the second gene cassette within the assemblies, C2i and C2 harbor different terminators T35S and Tocs, respectively (**Figure 6A**), suggesting that the outperformance of the multigene coexpression mediated by C1–C4 (version IV) is attributed to the Tocs terminator. Possible explanations may be that the Tocs sequence confers a stronger transcriptional termination or prevents transcriptional read-through. Alternatively, or additionally, the lower overall sequence homology within the multigene construct may also result in reduced gene silencing effects. Regardless of what the exact reason for the observed differences may be, our results corroborate the importance of assembly design for multigene expression. This conclusion is also supported by experiments in which we analyzed transgenerational stability of the organelle marker genes in the filial T2 generation. In these experiments we selected three independent transgenic lines of the T1 generation harboring the constructs C1–C4 (version III) and C1–C4 (version IV), which coexpressed all four organelle markers. Intriguingly, all T2 plants harboring the T-DNA of the C1–C4 (version III) expressed only one organelle marker, i.e., the peroxisomal marker encoded by C2i (**Figure 6F**; Supplementary Figure S5). In marked contrast, most (i.e., >70%) of the T2 offspring deriving from the C1–C4 (version IV) transgenic plants coexpressed all four organelle markers (**Figure 6F**; Supplementary Figure S5). Interestingly, only the UBQ10 promoter-driven organelle markers C1 and C3i showed reduced transgenerational stability, whereas 35S promoter-driven markers C2 and C4 could be detected in all T2 plants (Supplementary Figure S5). Together, these findings also highlight the importance of the 5′ regulatory sequences for transgenerational expression and thus, multigene assembly design. Accordingly, we recommend utilization of the C1–C4 (version IV) design as the optimal COLORFUL-Circuit assembly for coexpression of up to four genes.

COLORFUL-Circuit Allows Spatio-Temporal Visualization of Multiple Organelle Dynamics during Biotrophic Plant-Microbe Interactions

As an exemplary case study, we tested the utility of our multigene expressing line C1–C4 (version IV) by simultaneously monitoring the subcellular behavior of organelles that occur

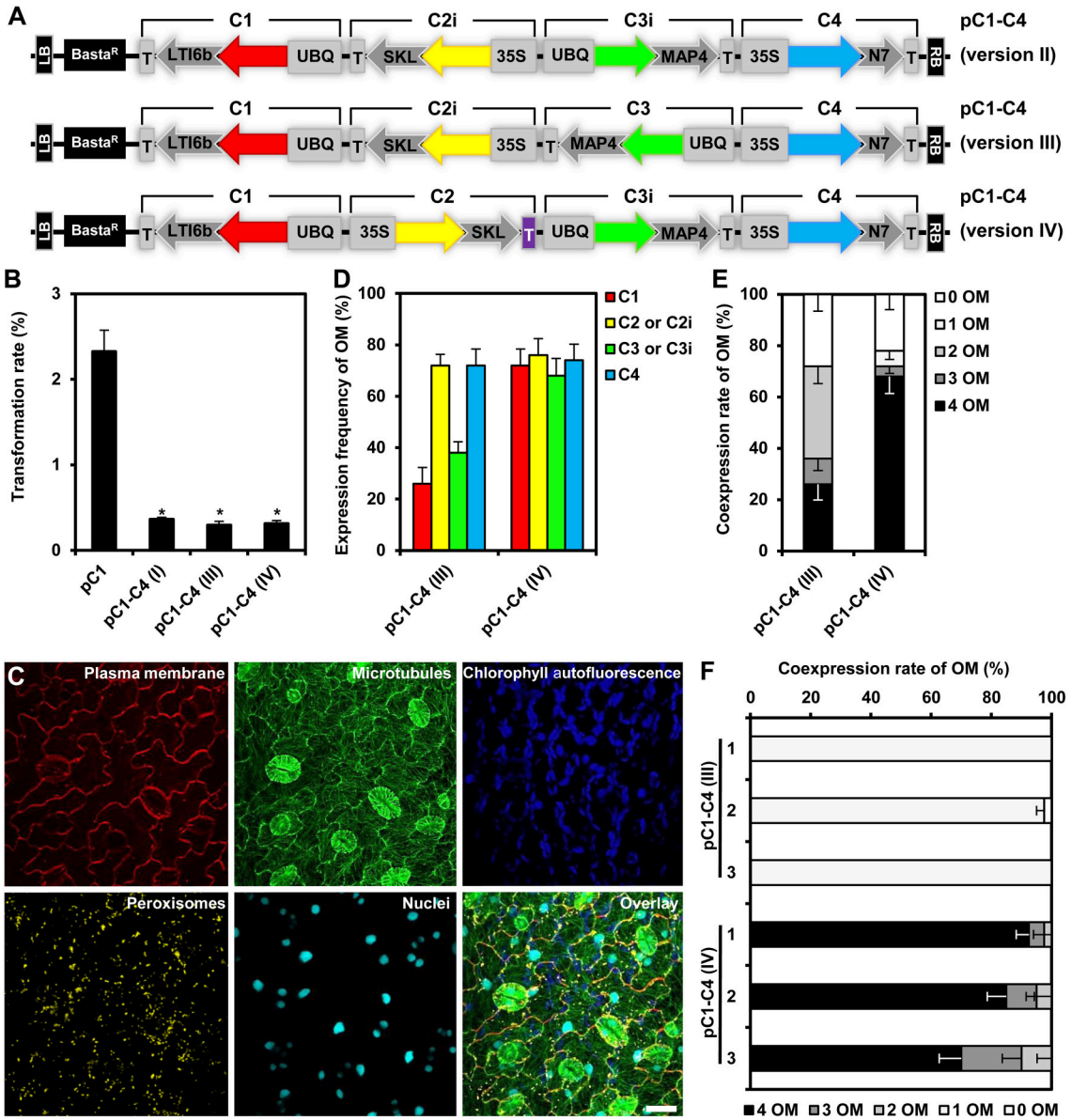

FIGURE 6 | Design, transformation rates and gene expression efficiency of the quadruple-gene assemblies in stable *Arabidopsis* transformants. **(A)** Structural organization of the T-DNAs of different quadruple-gene assemblies; pC1–C4 (version II; top), pC1–C4 (version III; middle) and pC1–C4 (version IV; bottom). C1, C2, C2i, C3, C3i, and C4 indicate the gene cassettes modules compositing the multigene assemblies. The vector backbone was amplified from the plasmid pGreenII. UBQ10: polyubiquitin 10 promoter; 35S, cauliflower mosaic virus CaMV 35S promoter; T, terminator of the cauliflower mosaic virus 35S (gray), and terminator of octopine synthase (purple); red, yellow, green, and turquoise arrows: fluorescent protein encoding genes of mKate2, TagRFP-T, Venus and mTurquoise2, respectively; LTI6b: low temperature induced protein as a membrane marker; SKL: peroxisomes targeting sequence; MAP4: microtubule binding domain of the mouse microtubule-associated protein 4; N7: nuclear localization signal; Basta^R: selectable marker confers Basta resistance in plants; Kan^R: selectable marker confers kanamycin resistance in *E. coli* and *A. tumefaciens*; LB/RB: left/right borders of T-DNA. The figures are not drawn to scale. **(B)** Stable transformation rates of the multigene T-DNAs indicated in **(A)** calculated as the percent of the Basta-resistant *Arabidopsis* plants from T1 seeds. The data represent the means ± SEM of three experiments. Asterisks indicate significant differences in comparison to pC1 using student *t*-test, $p < 0.01$. pC1 contains a single gene cassette (UBQ10-mKate2-LTI6b-T35S) in addition to the Basta selectable marker. **(C)** Leaf cells of *Arabidopsis* stably expressing quadruple fluorescent organelle markers encoded from pC1–C4 (version IV). Chlorophyll autofluorescence is provided as a control. The images represent the maximum projection of z-stacks obtained by confocal laser scanning microscopy. Scale bar = 20 μm. **(D)** Expression frequency of organelle markers (OM) for C1 (membrane marker), C2 or C2i (peroxisomes marker), C3 or C3i (microtubules marker), or C4 (nuclear marker). Data represent percentages ± SEM ($n = 50$ plants). **(E)** Coexpression rate of organelle markers (OM) in T1 generation of transgenic plants harboring the T-DNAs indicated in **(A)**. $n = 50$ plants. **(F)** Coexpression rate of OMs in the T2 generation of three independent transgenic lines harboring the T-DNAs C1–C4 (version III) or C1–C4 (version IV). Please, note that offspring of T1 plants which coexpressed all four OMs was used. $n = 40$ plants.

during the compatible interaction between Arabidopsis and the obligate biotrophic powdery mildew fungus *G. orontii*. In general, upon contact with the leaf surface of a potential host plant the conidiospores of powdery mildew fungi germinate and develop penetration organs called appressoria, which they use to invade through the host outer epidermal cuticle and cell wall. Subsequently, in compatible interactions, haustorial complexes are established within penetrated epidermal cells, and serve the uptake of plant nutrients and the transfer of fungal effector molecules (Koh et al., 2005; Micali et al., 2008, 2011). Typically, haustoria invaginate and modify the host plant plasma membrane to form a specialized exchange interface with the host cytoplasm called extrahaustorial membrane (EHM; Koh et al., 2005; Micali et al., 2011). Nutrient uptake results in development of secondary hyphae and radial ectoparasitic colonization of the host that is accompanied by secondary haustoria formation in neighboring epidermal cells (Micali et al., 2008). Finally, an epiphytic network of fungal hyphae covers the leaf surface and new conidiospores are produced, giving rise to the typical powdery mildew disease symptoms (Micali et al., 2008). Previous studies which focused on early compatible and incompatible Arabidopsis–powdery mildew interactions revealed that attempted invasion and successful host colonization impact dramatically on plant cell membrane integrity, cytoskeleton structure and organelle dynamics (Koh et al., 2005; Takemoto et al., 2006; Chandran et al., 2010; Micali et al., 2011; Hardham, 2013), thus reflecting either efficient cell-autonomous defense mechanisms or the establishment of compatibility. However, studies aiming at simultaneous observation of multiple FP-tagged membranes, structures and organelles during compatible and incompatible Arabidopsis–powdery mildew interactions have not yet been conducted. Here, we used the COLORFUL-Circuit line C1–C4 (version IV) which coexpresses FP-tagged reporter constructs for the plasma membrane, peroxisomes, microtubules and the nucleus to simultaneously analyze the subcellular behavior of these organelles at compatible Arabidopsis–*G. orontii* interaction sites with a focus on mature haustoria. To this end, we inoculated 4-week old transgenic Arabidopsis Col-0 plants harboring C1–C4 (version IV) with conidiospores of *G. orontii* and used CLSM to visualize the localization of the respective reporter constructs at sites of established haustoria at 4 days post inoculation. The representative images shown in **Figure 7** show two distinct mature haustoria in a side-view (**Figure 7A**) and a top-view perspective (**Figure 7B**), respectively. Both sites show that the plasma membrane marker LTI6b localizes to the EHM. This is interesting as former analyses performed with the same protein fused to GFP did not allow detection in the EHM of early haustoria induced by the compatible powdery mildew *Golovinomyces cichoracearum* (Koh et al., 2005). This may suggest that distinct powdery mildew species induce specific EHMs that differ in regard to protein composition.

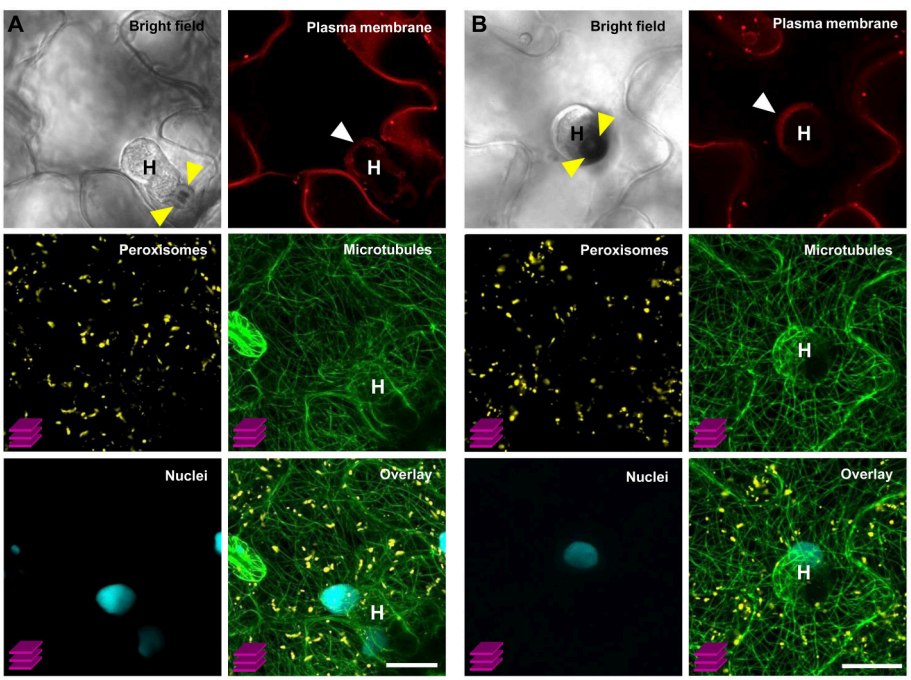

FIGURE 7 | Simultaneous visualization of multiple subcellular markers at mature haustorial complexes of *G. orontii* in *Arabidopsis*. Conidiospores of *G. orontii* were used to inoculate 4-week old *Arabidopsis* plants expressing the multiorganelle markers C1–C4 (version IV) from **Figure 6A**. Sites of fungal attack were analyzed at 4 days post inoculation by CLSM (z-stacks, except for the images of bright field and plasma membrane marker). **(A)** Side-view and **(B)** top-view of distinct mature haustoria (marked with a white H) within epidermal leaf cells. Callose encasement of the haustorial neck in **(A)** and the callose papilla in **(B)** are indicated with yellow arrowheads. Haustoria are surrounded by the extrahaustorial membrane (white arrowhead). Peroxisomes are homogenously distributed within the cell. Nuclei are located in close proximity to the haustorial complexes. Microtubules envelop the haustorial complexes. Scale bar = 20 μm.

An alternative explanation, which we consider more likely, is that the protein repertoires recruited into the EHM vary in a developmentally dependent manner. Similarly, Micali et al. (2011) observed that the Arabidopsis resistance protein RPW8.2 accumulated at the EHM of mature haustoria but not at EHM of young haustoria. Interestingly, peroxisomes were homogenously distributed and did not accumulate close to the haustorial complexes as observed before by Koh et al. (2005) for early interaction sites with *G. cichoracearum*. Again, this may indicate development-dependent alterations in the subcellular behavior and localization dynamics of the individual reporter proteins. Future analysis should address this question with time-course CLSM experiments. Consistent with the previous analysis by Koh et al. (2005) we found a tight spatial association of the nuclei of the invaded epidermal plant cells with the haustorial complexes. Moreover, we found that microtubules envelop the mature haustorial complexes, supporting earlier observations by Takemoto et al. (2006) and Hardham (2013) that microtubules are subject to pathogen-induced structural reorganization. It is important to mention that the COLORFUL-Circuit system allows the easy and straightforward exchange of individual modules. Thus, it will be possible to simultaneously visualize for example the interplay of the actin and microtubule cytoskeleton for organellar transport and localized arrest, by exchanging the plasma membrane marker with an actin-filament associated protein, for example the actin-binding domain 2 of Arabidopsis fimbrin 1 (Wang et al., 2008). Moreover, other organelle markers such as those described by Nelson et al. (2007) can be used to generate transgenic plants for the purpose of parallel subcellular localization studies of up to four distinct compartments. It is important to notice, however, that our system does not only allow cell biological studies, like those described so far. Also, our versatile system offers the possibility to manipulate metabolite fluxes or even to introduce entirely novel biosynthetic pathways by simultaneously or spatio-temporally regulating production of respective enzymatically active proteins under control of adequate tissue- or stimulus-specific promoter sequences.

Taken together, we established a new vector system called "COLORFUL-Circuit" that allows multigene assembly, delivery, and *in planta* coexpression. The vectors can be flexibly customized by exchanging any module of the existing gene cassettes. COLORFUL-Circuit is privileged by the utilization of a single and inexpensive rare-cutting restriction enzyme, *SfiI*, which simplifies the assembly of large genomic DNA fragments. The usage of COLORFUL-Circuit assembly saves time for transient and stable multigene coexpression, and consequently provides biotechnological advantages for simultaneous improvement of multiple plant treats and engineering of complex metabolic pathways. Moreover, our system can be exploited for basic research questions, e.g., by utilization of fluorescent protein-tagged reporters. The future of plant cell biology and biotechnology is COLORFUL.

AUTHOR CONTRIBUTIONS

HG and VL designed the experiments, HG and SL performed the experiments, HG, SL and VL analyzed and discussed the results and HG and VL wrote the paper.

ACKNOWLEDGMENTS

We thank Gabriele Schauermann and Anna Maria Köhler, Georg-August-Universität Göttingen, for technical assistance, Fernan Federici and Jim Hasseloff, University of Cambridge, for providing us with templates for TagRFP-T and mKate2, Dorus Gadella and Joachim Goedhart, University of Amsterdam, for the template of mTurquoise2.

SUPPLEMENTARY MATERIAL

The Supplementary Material for this article can be found online at: http://journal.frontiersin.org/article/10.3389/fpls.2016.00246

REFERENCES

Ainley, W. M., Sastry-Dent, L., Welter, M. E., Murray, M. G., Zeitler, B., Amora, R., et al. (2013). Trait stacking via targeted genome editing. *Plant Biotechnol. J.* 11, 1126–1134. doi: 10.1111/pbi.12107

Aizawa, H., Emori, Y., Mori, A., Murofushi, H., Sakai, H., and Suzuki, K. (1991). Functional analyses of the domain structure of microtubule-associated protein-4 (MAP-U). *J. Biol. Chem.* 266, 9841–9846.

Atkinson, N. J., and Urwin, P. E. (2012). The interaction of plant biotic and abiotic stresses: from genes to the field. *J. Exp. Bot.* 63, 3523–3543. doi: 10.1093/jxb/ers100

Binder, A., Lambert, J., Morbitzer, R., Popp, C., Ott, T., Lahaye, T., et al. (2014). A modular plasmid assembly kit for multigene expression, gene silencing and silencing rescue in plants. *PLoS ONE* 9:2. doi: 10.1371/journal.pone.0088218

Bohmert, K., Balbo, I., Steinbüchel, A., Tischendorf, G., and Willmitzer, L. (2002). Constitutive expression of the β-ketothiolase gene in transgenic plants. A major obstacle for obtaining polyhydroxybutyrate-producing plants. *Plant Physiol.* 128, 1282–1290. doi: 10.1104/pp.010615

Brophy, J. A., and Voigt, C. A. (2014). Principles of genetic circuit design. *Nat. Methods* 11, 508–520. doi: 10.1038/nmeth.2926

Chalhoub, B., Denoeud, F., Liu, S., Parkin, I. A., Tang, H., Wang, X., et al. (2014). Early allopolyploid evolution in the post-Neolithic *Brassica napus* oilseed genome. *Science* 345, 950–953. doi: 10.1126/science.1253435

Chandran, D., Inada, N., Hather, G., Kleindt, C. K., and Wildermuth, M. C. (2010). Laser microdissection of *Arabidopsis* cells at the powdery mildew infection site reveals site-specific processes and regulators. *Proc. Natl. Acad. Sci. U.S.A.* 107, 460–465. doi: 10.1073/pnas.0912492107

Clough, S. J., and Bent, A. F. (1998). Floral dip: a simplified method for *Agrobacterium*-mediated transformation of *Arabidopsis thaliana*. *Plant J.* 16, 735–743. doi: 10.1046/j.1365-313x.1998.00343.x

Cogoni, C., and Macino, G. (1999). Homology-dependent gene silencing in plants and fungi: a number of variations on the same theme. *Curr. Opin. Microbiol.* 2, 657–662. doi: 10.1016/s1369-5274(99)00041-7

Consortium, T. G. (2012). The tomato genome sequence provides insights into fleshy fruit evolution. *Nature* 485, 635–641. doi: 10.1038/nature 11119

Cutler, S. R., Ehrhardt, D. W., Griffitts, J. S., and Somerville, C. R. (2000). Random GFP::cDNA fusions enable visualization of subcellular structures in cells of *Arabidopsis* at a high frequency. *Proc. Natl. Acad. Sci. U.S.A.* 97, 3718–3723. doi: 10.1073/pnas.97.7.3718

Dafny-Yelin, M., and Tzfira, T. (2007). Delivery of multiple transgenes to plant cells. *Plant Physiol.* 145, 1118–1128. doi: 10.1104/pp.107.106104

Dahncke, K., and Witte, C.-P. (2013). Plant purine nucleoside catabolism employs a guanosine deaminase required for the generation of xanthosine in *Arabidopsis*. *Plant Cell* 25, 4101–4109. doi: 10.1105/tpc.113.117184

Davis, A. M., Hall, A., Millar, A. J., Darrah, C., and Davis, S. J. (2009). Protocol: streamlined sub-protocols for floral-dip transformation and selection of transformants in *Arabidopsis thaliana*. *Plant Methods* 5:3. doi: 10.1186/1746-4811-5-3

Emami, S., Yee, M.-C., and Dinneny, J. R. (2013). A robust family of Golden Gate *Agrobacterium* vectors for plant synthetic biology. *Front. Plant Sci.* 4:339. doi: 10.3389/fpls.2013.00339

Engler, C., Kandzia, R., and Marillonnet, S. (2008). A one pot, one step, precision cloning method with high throughput capability. *PLoS ONE* 3:11. doi: 10.1371/journal.pone.0003647

Engler, C., Youles, M., Gruetzner, R., Ehnert, T.-M., Werner, S., Jones, J. D., et al. (2014). A golden gate modular cloning toolbox for plants. *ACS Synth. Biol.* 3, 839–843. doi: 10.1021/sb4001504

Farré, G., Twyman, R. M., Christou, P., Capell, T., and Zhu, C. (2015). Knowledge-driven approaches for engineering complex metabolic pathways in plants. *Curr. Opin. Biotechnol.* 32, 54–60. doi: 10.1016/j.copbio.2014.11.004

Gibson, D. G., Young, L., Chuang, R.-Y., Venter, J. C., Hutchison, C. A. III, and Smith, H. O. (2009). Enzymatic assembly of DNA molecules up to several hundred kilobases. *Nat. Methods* 6, 343–345. doi: 10.1038/nmeth.1318

Giuliano, G. (2014). Plant carotenoids: genomics meets multi-gene engineering. *Curr. Opin. Plant Biol.* 19, 111–117. doi: 10.1016/j.pbi.2014.05.006

Goedhart, J., von Stetten, D., Noirclerc-Savoye, M., Lelimousin, M., Joosen, L., Hink, M. A., et al. (2012). Structure-guided evolution of cyan fluorescent proteins towards a quantum yield of 93%. *Nat. Commun.* 3:751. doi: 10.1038/ncomms1738

Grefen, C., Donald, N., Hashimoto, K., Kudla, J., Schumacher, K., and Blatt, M. R. (2010). A ubiquitin-10 promoter-based vector set for fluorescent protein tagging facilitates temporal stability and native protein distribution in transient and stable expression studies. *Plant J.* 64, 355–365. doi: 10.1111/j.1365-313X.2010.04322.x

Hardham, A. R. (2013). Microtubules and biotic interactions. *Plant J.* 75, 278–289. doi: 10.1111/tpj.12171

Hecker, A., Wallmeroth, N., Peter, S., Michael, R. B., Harter, K., and Grefen, C. (2015). Binary 2in1 vectors improve in planta (co-) localisation and dynamic protein interaction studies. *Plant Physiol.* 168, 776–787. doi: 10.1104/pp.15.00533

Hellens, R. P., Edwards, E. A., Leyland, N. R., Bean, S., and Mullineaux, P. M. (2000). pGreen: a versatile and flexible binary Ti vector for *Agrobacterium*-mediated plant transformation. *Plant Mol. Biol.* 42, 819–832. doi: 10.1023/A:1006496308160

Initiative, A. G. (2000). Analysis of the genome sequence of the flowering plant *Arabidopsis thaliana*. *Nature* 408, 796. doi: 10.1038/35048692

Kawahara, Y., de la Bastide, M., Hamilton, J. P., Kanamori, H., Mccombie, W. R., Ouyang, S., et al. (2013). Improvement of the *Oryza sativa* Nipponbare reference genome using next generation sequence and optical map data. *Rice* 6:4. doi: 10.1186/1939-8433-6-4

Keller, G.-A., Krisans, S., Gould, S. J., Sommer, J. M., Wang, C. C., Schliebs, W., et al. (1991). Evolutionary conservation of a microbody targeting signal that targets proteins to peroxisomes, glyoxysomes, and glycosomes. *J. Cell Biol.* 114, 893–904. doi: 10.1083/jcb.114.5.893

Koh, S., André, A., Edwards, H., Ehrhardt, D., and Somerville, S. (2005). *Arabidopsis thaliana* subcellular responses to compatible *Erysiphe cichoracearum* infections. *Plant J.* 44, 516–529. doi: 10.1111/j.1365-313X.2005.02545.x

Kremers, G.-J., Gilbert, S. G., Cranfill, P. J., Davidson, M. W., and Piston, D. W. (2011). Fluorescent proteins at a glance. *J. Cell Sci.* 124, 157–160. doi: 10.1242/jcs.072744

Lee, L.-Y., and Gelvin, S. B. (2008). T-DNA binary vectors and systems. *Plant Physiol.* 146, 325–332. doi: 10.1104/pp.107.113001

Li, M. Z., and Elledge, S. J. (2007). Harnessing homologous recombination *in vitro* to generate recombinant DNA via SLIC. *Nat. Methods* 4, 251–256. doi: 10.1038/nmeth1010

Liu, W., Yuan, J. S., and Stewart C. N. Jr. (2013). Advanced genetic tools for plant biotechnology. *Nat. Rev. Genet.* 14, 781–793. doi: 10.1038/nrg3583

Martin, K., Kopperud, K., Chakrabarty, R., Banerjee, R., Brooks, R., and Goodin, M. M. (2009). Transient expression in *Nicotiana benthamiana* fluorescent marker lines provides enhanced definition of protein localization, movement and interactions *in planta*. *Plant J.* 59, 150–162. doi: 10.1111/j.1365-313X.2009.03850.x

Mette, M. F., Aufsatz, W., Van Der Winden, J., Matzke, M., and Matzke, M. A. (2000). Transcriptional silencing and promoter methylation triggered by double−stranded RNA. *EMBO J.* 19, 5194–5201. doi: 10.1093/emboj/19.19.5194

Micali, C., Göllner, K., Humphry, M., Consonni, C., and Panstruga, R. (2008). The powdery mildew disease of *Arabidopsis*: a paradigm for the interaction between plants and biotrophic fungi. *Arabidopsis Book* 6:e0115. doi: 10.1199/tab.0115

Micali, C. O., Neumann, U., Grunewald, D., Panstruga, R., and O'connell, R. (2011). Biogenesis of a specialized plant–fungal interface during host cell internalization of *Golovinomyces orontii* haustoria. *Cell. Microbiol.* 13, 210–226. doi: 10.1111/j.1462-5822.2010.01530.x

Mitsuhara, I., Ugaki, M., Hirochika, H., Ohshima, M., Murakami, T., Gotoh, Y., et al. (1996). Efficient promoter cassettes for enhanced expression of foregin genes in Dicotyledonous and Monocotyledonous plants. *Plant Cell Physiol.* 37, 49–59. doi: 10.1093/oxfordjournals.pcp.a028913

Nagai, T., Ibata, K., Park, E. S., Kubota, M., Mikoshiba, K., and Miyawaki, A. (2002). A variant of yellow fluorescent protein with fast and efficient maturation for cell-biological applications. *Nat. Biotechnol.* 20, 87–90. doi: 10.1038/nbt0102-87

Naqvi, S., Farré, G., Sanahuja, G., Capell, T., Zhu, C., and Christou, P. (2010). When more is better: multigene engineering in plants. *Trends Plant Sci.* 15, 48–56. doi: 10.1016/j.tplants.2009.09.010

Nelson, B.K., Cai, X., and Nebenführ, A. (2007). A multicolored set of *in vivo* organelle markers for co-localization studies in Arabidopsis and other plants. *Plant J.* 51, 1126–1136. doi: 10.1111/j.1365-313X.2007.03212.x

Peremarti, A., Twyman, R. M., Gómez-Galera, S., Naqvi, S., Farré, G., Sabalza, M., et al. (2010). Promoter diversity in multigene transformation. *Plant Mol. Biol.* 73, 363–378. doi: 10.1007/s11103-010-9628-1

Quan, J., and Tian, J. (2009). Circular polymerase extension cloning of complex gene libraries and pathways. *PLoS ONE* 4:7. doi: 10.1371/journal.pone.0006441

Sarrion-Perdigones, A., Vazquez-Vilar, M., Palací, J., Castelijns, B., Forment, J., Ziarsolo, P., et al. (2013). GoldenBraid 2.0: a comprehensive DNA assembly framework for plant synthetic biology. *Plant Physiol.* 162, 1618–1631. doi: 10.1104/pp.113.217661

Shaner, N. C., Lin, M. Z., Mckeown, M. R., Steinbach, P. A., Hazelwood, K. L., Davidson, M. W., et al. (2008). Improving the photostability of bright monomeric orange and red fluorescent proteins. *Nat. Methods* 5, 545–551. doi: 10.1038/nmeth.1209

Shcherbo, D., Murphy, C. S., Ermakova, G. V., Solovieva, E. A., Chepurnykh, T. V., Shcheglov, A. S., et al. (2009). Far-red fluorescent tags for protein imaging in living tissues. *Biochem. J.* 418, 567–574. doi: 10.1042/BJ20081949

Stam, M., Viterbo, A., Mol, J. N., and Kooter, J. M. (1998). Position-dependent methylation and transcriptional silencing of transgenes in inverted T-DNA repeats: implications for posttranscriptional silencing of homologous host genes in plants. *Mol. Cell. Biol.* 18, 6165–6177. doi: 10.1128/mcb.18.11.6165

Takemoto, D., Jones, D. A., and Hardham, A. R. (2006). Re-organization of the cytoskeleton and endoplasmic reticulum in the Arabidopsis *pen1-1* mutant inoculated with the non-adapted powdery mildew pathogen, *Blumeria graminis* f. sp. hordei. *Mol. Plant Pathol.* 7, 553–563. doi: 10.1111/j.1364-3703.2006.00360.x

Tzfira, T., Tian, G.-W., Vyas, S., Li, J., Leitner-Dagan, Y., Krichevsky, A., et al. (2005). pSAT vectors: a modular series of plasmids for autofluorescent protein tagging and expression of multiple genes in plants. *Plant Mol. Biol.* 57, 503–516. doi: 10.1007/s11103-005-0340-5

van Erp, H., Kelly, A. A., Menard, G., and Eastmond, P. J. (2014). Multigene engineering of triacylglycerol metabolism boosts seed oil content in *Arabidopsis*. *Plant Physiol.* 165, 30–36. doi: 10.1104/pp.114.236430

Wang, Y. S., Yoo, C. M., and Blancaflor, E. B. (2008). Improved imaging of actin filaments in transgenic *Arabidopsis* plants expressing a green fluorescent protein fusion to the C- and N-termini of the fimbrin actin-binding domain 2. *New Phytol.* 177, 525–536. doi: 10.1111/j.1469-8137.2007.02261.x

West, R. R., Tenbarge, K. M., and Olmsted, J. (1991). A model for microtubule-associated protein 4 structure. Domains defined by comparisons of human, mouse, and bovine sequences. *J. Biol. Chem.* 266, 21886–21896.

Zeevi, V., Liang, Z., Arieli, U., and Tzfira, T. (2012). Zinc finger nuclease and homing endonuclease-mediated assembly of multigene plant transformation vectors. *Plant Physiol.* 158, 132–144. doi: 10.1104/pp.111.184374

Conflict of Interest Statement: The authors declare that the research was conducted in the absence of any commercial or financial relationships that could be construed as a potential conflict of interest.

frontiers in Plant Science

REVIEW
published: 15 February 2016
doi: 10.3389/fpls.2016.00123

Mildew-Omics: How Global Analyses Aid the Understanding of Life and Evolution of Powdery Mildews

Laurence V. Bindschedler[1], Ralph Panstruga[2] and Pietro D. Spanu[3]*

[1] School of Biological Sciences, Royal Holloway, University of London, Egham, UK, [2] Unit of Plant Molecular Cell Biology, Institute for Biology I, RWTH Aachen University, Aachen, Germany, [3] Department of Life Sciences, Imperial College London, London, UK

The common powdery mildew plant diseases are caused by ascomycete fungi of the order Erysiphales. Their characteristic life style as obligate biotrophs renders functional analyses in these species challenging, mainly because of experimental constraints to genetic manipulation. Global large-scale ("-omics") approaches are thus particularly valuable and insightful for the characterisation of the life and evolution of powdery mildews. Here we review the knowledge obtained so far from genomic, transcriptomic and proteomic studies in these fungi. We consider current limitations and challenges regarding these surveys and provide an outlook on desired future investigations on the basis of the various –omics technologies.

Keywords: *Blumeria graminis*, powdery mildews, genomics, transcriptomics, proteomics

OPEN ACCESS

Edited by:
Stéphane Hacquard, Max Planck Institute for Plant Breeding Research, Germany

Reviewed by:
Dario Cantu, University of California, Davis, USA
Mary C. Wildermuth, University of California, Berkeley, USA

****Correspondence:***
Ralph Panstruga
panstruga@bio1.rwth-aachen.de

Specialty section:
This article was submitted to Plant Biotic Interactions, a section of the journal Frontiers in Plant Science

Received: *18 November 2015*
Accepted: *22 January 2016*
Published: *15 February 2016*

Citation:
Bindschedler LV, Panstruga R and Spanu PD (2016) Mildew-Omics: How Global Analyses Aid the Understanding of Life and Evolution of Powdery Mildews. Front. Plant Sci. 7:123. doi: 10.3389/fpls.2016.00123

INTRODUCTION

Infections with fungi that cause powdery mildew disease result in a characteristic white fuzzy patina on the surface of aerial plant organs (primarily leaves and stems). Many plant species can be affected by these pathogenic fungi, displaying characteristic and easily recognizable disease symptoms (Glawe, 2008). All powdery mildews belong to the Erysiphales, an ascomycete order that represents an ancient monophyletic lineage that evolved over 100 million years ago (Takamatsu, 2004; Braun and Cook, 2012). Over this time, they diversified into more than 400 species that are able to colonize nearly 10,000 plant species (Takamatsu, 2004). They are all obligate biotrophic pathogens that establish highly integrated relationships with their hosts. In agriculture, they represent an ever-present threat with a significant impact on the quality and quantity of food plants, forage crops, and ornamentals (Dean et al., 2012).

Large-scale "-omics" techniques such as genomics, transcriptomics, proteomics and metabolomics are known to generate massive and complex data sets ("big data"). In combination, these approaches have the potential to comprehensively dissect a biological system and define how all its components interact dynamically ("systems biology"). Potential integrative insights include the reconstruction of metabolic networks (Droste et al., 2011) and complex signaling pathways (Tieri et al., 2011). Consequently, these methods have been used, individually or in combination, in numerous species and conditions, including different types of fungal phytopathogens (Tan et al., 2009). The handling, integration and interpretation of data from various –omics platforms remains nevertheless a challenging task (Gomez-Cabrero et al., 2014).

In this article, we review the contribution of large-scale –omics studies over the past 15 years to improve our understanding of the fundamental biology of powdery mildew fungi, their evolution,

and the relationship with their hosts. In particular, we survey the findings from the first sets of genomic, transcriptomic and proteomic studies and discuss the insights obtained, their significance and inter-relationships.

POWDERY MILDEW GENOMES

The genomes of several powdery mildew species, *formae speciales*, and isolates have been sequenced, partially assembled, annotated and analyzed (**Table 1**). The best studied to date are those of *Blumeria graminis* f.sp. *hordei*, *B. graminis* f.sp. *tritici* and *Erysiphe necator*, which cause mildews on barley (*Hordeum vulgare*), wheat (*Triticum aestivum*) and grapevine (*Vitis vinifera*), respectively (Spanu et al., 2010; Spanu and Panstruga, 2012; Hacquard et al., 2013; Wicker et al., 2013; Jones et al., 2014; Panstruga and Spanu, 2014). Some limited information on the pea powdery mildew (*E. pisi)* and one *Arabidopsis thaliana*-infecting powdery mildew (*Golovinomyces orontii*) is also available (Spanu et al., 2010). A new significant set of analyses is currently underway in the context of the JGI CSP Project "Comparative Genomics of Powdery Mildews and Associated Plants" (JGI[1]) to expand the taxonomic and pathogenic spectrum: this effort will include the fungi that cause powdery mildews on grapevine (*E. necator*), hops (*Podosphaera macularis*), brassicas (*E. cruciferarum, G. orontii*), tomato [*Pseudooidium* (*neo-*)*lycopersici*], lettuce (*G. cichoracearum*), pepper (*Leveillula taurica*), cucumber (*P. xanthii*) and strawberry (*P. aphanis*).

The initial sequencing efforts yielded some striking and unexpected results. The first surprise was that the genome sizes are much larger than expected. At the time, two sets of ideas influenced the expectation: the average size of genomes from filamentous ascomycetes that had been fully sequenced and assembled was around 40 Mb (e.g., *Neurospora crassa* and *Magnaporthe oryzae*; Galagan et al., 2003; Dean et al., 2005); moreover, the obligate parasitic life-style of the powdery mildew predicated a reduction in genome size and complexity, in line with the trend toward generalized simplification of body, development and genomes seen in many parasites (Poulin and Randhawa, 2015). This forecast turned out to be spectacularly wrong: the genomes of *B. graminis* and *E. necator* species are in fact ∼120–180 Mb, i.e., several times larger than closely related ascomycetes. Comparable findings were observed in some taxonomically unrelated fungi that have similar biotrophic lifestyles, such as the fungi causing rusts (Duplessis et al., 2011) and the mycorrhizal truffles (Martin et al., 2010).

[1]http://jgi.doe.gov/comparative-genomics-of-powdery-mildews/

TABLE 1 | Compilation of powdery mildew omics studies.

Type of –omics study	Powdery mildew species	Impact/key insights	Reference
Genomics			
	Blumeria graminis f.sp. *hordei*; *Golovinomyces oontii*, *Erysiphe pisi*	First powdery mildew genomes; genome size; gene number and content; effectors	Spanu et al., 2010
	Blumeria graminis f.sp. *tritici*	Evolution of grass powdery mildews	Wicker et al., 2013
	Blumeria graminis f.sp. *hordei*	Mosaic haplotype pattern of the barley powdery mildew genome	Hacquard et al., 2013
	Erysiphe necator	Copy number variation of *EnCYP51* and its impact on fungicide resistance	Jones et al., 2014
Transcriptomics			
	Blumeria graminis f.sp. *hordei*	First powdery mildew ESTs	Thomas et al., 2001
	Blumeria graminis f.sp. *hordei*	First time-resolved transcript analysis	Thomas et al., 2002
	Blumeria graminis f.sp. *hordei*	First microarray analysis	Both et al., 2005b
	Blumeria graminis f.sp. *hordei*	Expression of metabolic pathway genes	Both et al., 2005a
	Blumeria graminis f.sp. *hordei*	Haustorial transcriptome (epidermal peels); discovery of the N-terminal effector motif Y/F/WxC	Godfrey et al., 2010
	Erysiphe necator	Gene expression during conidiation	Wakefield et al., 2011
	Erysiphe necator	Development of microsatellite markers	Frenkel et al., 2012
	Golovinomyces orontii	Haustorial transcriptome (isolated haustoria)	Weßling et al., 2012
	Podosphaera plantaginis	Single nucleotide polymorphism (SNP) design for metapopulation studies	Tollenaere et al., 2012
	Blumeria graminis f.sp. *hordei*	Transcript profile of compatible versus incompatible interaction	Hacquard et al., 2013
	Erysiphe necator	Transcriptionally active transposable elements	Jones et al., 2014
Proteomics			
	Blumeria graminis f.sp. *hordei*	Asexual spore proteome	Noir et al., 2009
	Blumeria graminis f.sp. *hordei*	First comparative proteomic analysis (spores, epiphytic sporulating hyphae and haustoria)	Bindschedler et al., 2009
	Blumeria graminis f.sp. *hordei*	Haustorial proteome (isolated haustoria)	Godfrey et al., 2009
	Blumeria graminis f.sp. *hordei*	Large-scale proteogenomics; proteome of haustoria and sporulating hyphae	Bindschedler et al., 2011
	Blumeria graminis f.sp. *hordei*	Identification of EKA proteins	Amselem et al., 2015b

In all these cases, the extraordinary expansion in genome size is caused by a massive accumulation of repetitive DNA that is the result of retro-transposon activity throughout the evolution of these fungi (Spanu et al., 2010; Wicker et al., 2013; Jones et al., 2014; Amselem et al., 2015a). There is evidence that these retro-transposons are still active, because several transcripts and proteins encoded by these elements have been identified in powdery mildew transcriptomes and proteomes, respectively (Jones et al., 2014; Amselem et al., 2015b; see also below).

The increase in powdery mildew genome size is accompanied by a reduction in the number of protein-coding genes. Around 6,500 protein-coding genes have been identified in *B. graminis* and *E. necator* (Spanu et al., 2010; Wicker et al., 2013; Jones et al., 2014), a number that is considerably lower than in most other fungal phytopathogens (Schmidt and Panstruga, 2011). Overall, these opposing trends result in a marked decrease in gene density compared to taxonomically related fungi (**Figure 1**). This reduction is the result of smaller size of gene families, the near-absence of paralogs, and the elimination of some conserved ascomycete core genes, including the loss of a few metabolic pathways (Spanu et al., 2010; Wicker et al., 2013; Jones et al., 2014). However, genes for most canonical signaling pathways are still present and intact in the *B. graminis* f.sp. *hordei* genome (Kusch et al., 2014). The loss of genes that are otherwise conserved may be attributed to disruption of the loci caused by retro-transposition (Spanu et al., 2010). The absence of a similar set of metabolic pathways in very distantly related plant parasites such as powdery mildews, rust fungi and downy mildew oomycetes (Spanu et al., 2010) is likely to be an indicator of convergent evolution of these obligate

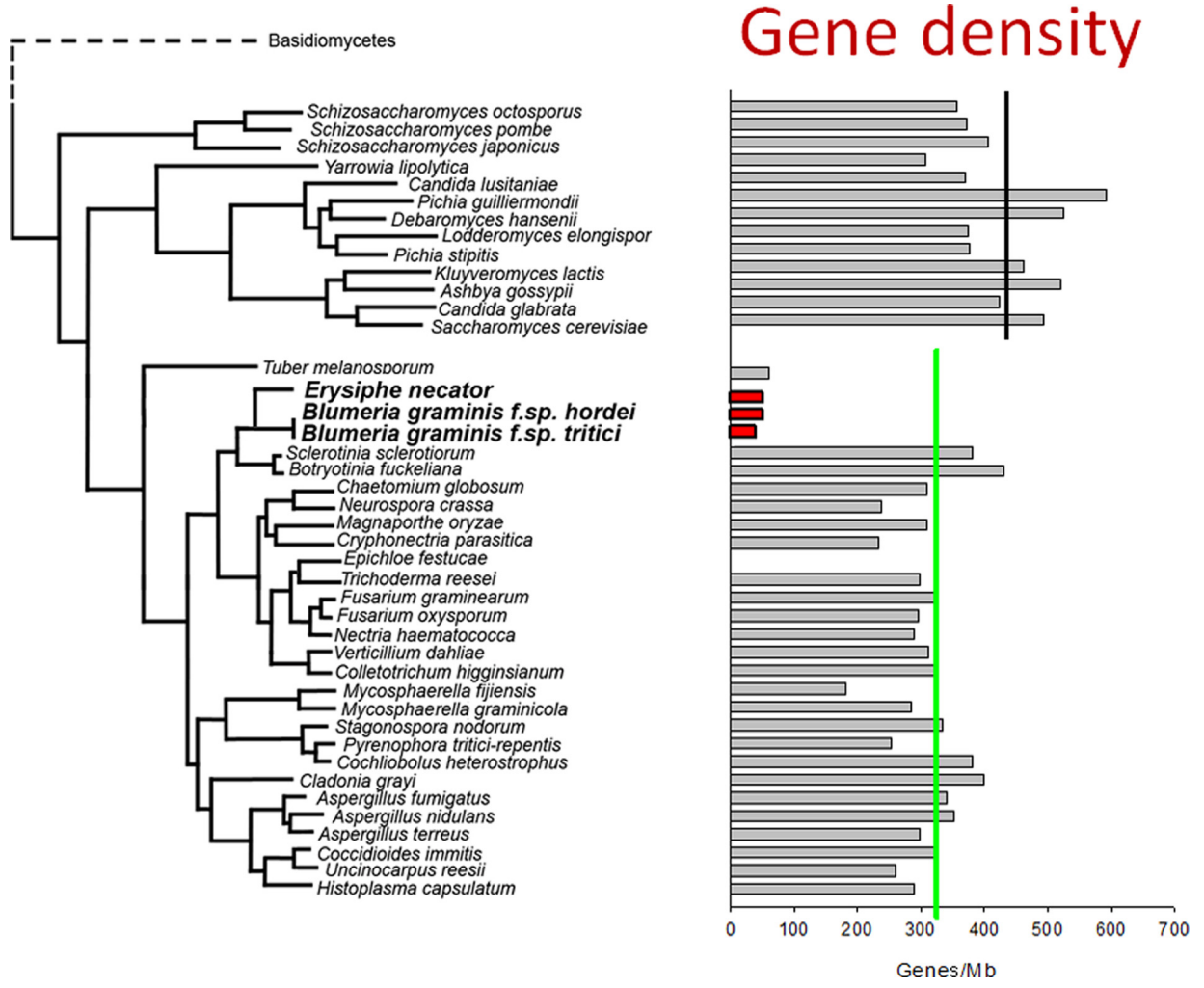

FIGURE 1 | Low gene density in the genomes of powdery mildew fungi. The protein-coding gene densities of hemiascomycete and ascomycete genomes were calculated based on published genome sizes and the gene counts of the annotated genomes. The values are plotted as a bar diagram that shows relative taxonomic positions (in a similar way as was used to display relative genome size in a previous study; Spanu et al., 2010). The average gene density of hemiascomycetes (black line) and ascomycetes (green line) are indicated. The gene density in the annotated *Blumeria graminis* genomes (red bars) and of the mycorrhizal truffle fungus (*Tuber melanosporum*) are remarkably lower than those of other ascomycetes. This is the result of both increased genome size and loss of some protein–coding genes, as discussed in the text.

pathogens to inhabit a common ecological niche – the live plant cell.

The first comparative analyses of different isolates of both the barley and the wheat powdery mildews demonstrated that extant genomes are essentially mosaics generated over tens of thousands of years by rare sexual recombination events that date back to prior to the domestication of the respective host cereals (Hacquard et al., 2013; Wicker et al., 2013). The maintenance of isolate diversity at the genomic level suggests that there is still much potential for adaptation.

The generation and maintenance of large genomes, full of repetitive DNA, is presumably costly in metabolic terms, and risky in genetic terms, because it can lead to gene disruption by mobile genetic elements. There is evidence that this "cost" is balanced by the advantages posed by active retro-transposition. But what are the terms of this trade-off? The key to explaining this is the existence of an extraordinarily expanded super-family of species- or mildew-specific Candidate Secreted Effector Proteins (CSEPs), on the one hand. Several hundred CSEPs have been identified in the barley and wheat powdery mildew genomes (Pedersen et al., 2012; Wicker et al., 2013; Kusch et al., 2014; **Figure 2**). On the other hand, genes encoding CSEPs are associated with DNA derived from retro-transposons (Pedersen et al., 2012), as are some of the atypical avirulence genes identified in *B. graminis*, which encode non-CSEP proteins (Ridout et al., 2006; Bourras et al., 2015; Amselem et al., 2015b). The concept

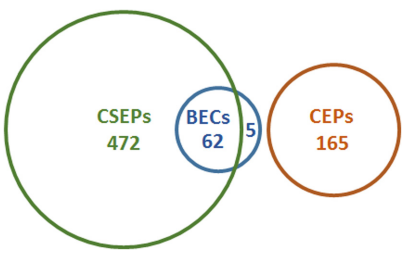

FIGURE 2 | Candidate effector genes in *B. graminis*. Several terms are used to name *B. graminis* candidate effectors in the published literature: candidate secreted effector proteins (CSEPs), candidate effector proteins (CEPs), and *Blumeria* effector candidates (BECs). Some of these sets overlap, as shown here for *B. graminis* f.sp. *hordei* in the Euler diagram. CSEPs were originally defined as proteins encoded by bioinformatically annotated genes whose products are predicted to be secreted and that do not have orthologs in non-powdery mildew fungi (found by BLAST searches; Spanu et al., 2010). BECs were defined as proteins identified by protein mass spectrometry that are specifically associated with haustoria and that are predicted to be secreted (Pliego et al., 2013). The five BECs that are not CSEPs include virulence proteins such as BEC1005 and BEC1019, which resemble an endoglycosidase and a metalloprotease, respectively (Pliego et al., 2013; Whigham et al., 2015). Note the high degree of overlap between CSEPs and BECs illustrated by the Euler diagram. Numbers given for these two categories are updated figures from Pedersen et al. (2012) and Bindschedler et al. (2011). CEPs refers to proteins encoded by genes in *B. graminis* f.sp. *tritici* that were identified on the basis of evidence of positive selection (Wicker et al., 2013). While the latter type of analysis has not been carried out for the barley pathogen, it can be assumed that similar numbers exist there because the majority of protein-coding genes has orthologs in both *formae speciales*. The size of the sets as shown in the diagram is proportional to the number of effector candidates identified.

that effector proteins in filamentous plant pathogens are located in particularly plastic regions of the genomes was first observed in the oomycetes (Raffaele et al., 2010). In the barley powdery mildew fungus, closely related *CSEP* paralogs are physically linked to similar repetitive DNA, suggesting that the increase in *CSEP* numbers in the genome may have been caused by recombination events leading to gene duplications (Pedersen et al., 2012). In fact, genome analysis of *E. necator* revealed that copy number variation is a frequent phenomenon in this powdery mildew species, with ca. 1–5% of the assemblies of five different isolates being subject to this structural genomic adaptation. A striking instance of copy number variation in the *E. necator* genome relates to the *EnCYP51* gene. This gene encodes a cytochrome P450 lanosterol C-14α-demethylase, which is a key enzyme involved in fungal sterol biosynthesis. The respective protein is the target of a class of fungicides termed DMIs (sterol demethylase inhibitors). A single amino acid exchange in CYP51 (Y136F) renders this protein insensitive to DMI fungicides. DNA sequence analysis of 89 *E. necator* isolates showed extensive copy number variation of *EnCYP51,* ranging from one to fourteen copies, which generally correlated with the occurrence of the Y136F mutation. Isolates collected from fungicide-treated vineyards typically were fungicide-resistant and had multiple *CYP51* copies encoding the Y136F variant (Jones et al., 2014). Taken together, the large and highly repetitive powdery mildew genomes may represent ideal substrates for extensive genome plasticity.

Many *B. graminis CSEPs* show significant evidence of positive evolutionary selection pressure, which caused sequence diversification of the encoded proteins (Pedersen et al., 2012; Wicker et al., 2013). Indeed, a novel set of genes encoding candidate effector proteins (CEPs) were identified because of unusually high ratios of non-synonymous to synonymous substitutions that result from positive selection pressure (**Figure 2**). Notably, the CEPs do not have evident canonical secretion signals (signal peptides) and are thus distinct from the CSEPs (Wicker et al., 2013). It remains to be seen whether and how these proteins are actually translocated into the hosts, as is expected of *bona fide* effectors. Poorly characterized non-conventional secretory pathways may need to be invoked here (Ding et al., 2012). Currently, few instances of such non-canonical secretion of phytopathogen-derived proteins have been reported (Ospina-Giraldo et al., 2010; Lowe et al., 2015). Interestingly, the genome of the grapevine powdery mildew pathogen *E. necator* seems to harbor considerably fewer CSEPs than the *B. graminis* genomes (approximately 150 vs. 430–550 CSEPs). Additionally, the 150 *E. necator* effector candidates lack any signs of positive evolutionary selection, which may indicate the current absence of an extensive evolutionary arm's race between *E. necator* and its plant host, *Vitis vinifera*. This is in accordance with the fact that most cultivated grapevine varieties lack effective powdery mildew resistance genes and are thus susceptible to the disease (Jones et al., 2014). The current challenges in powdery mildew genomics are: broadening the spectrum of species sequenced in this monophyletic group, a deeper analysis of genome variation (including copy number variation) in existing populations, an understanding of the

short-term micro-evolutionary potential of these fungi and the establishment of a fully assembled and "finished" reference genome. The first of these challenges (extending the coverage across the order of the Erysiphales) will be met in the next few years through the efforts of a broad international consortium led by Shauna Somerville, Mary Wildermuth and colleagues[2]; one hope is that this information may lead to discoveries and new hypotheses explaining the diversification and host adaptation of these ubiquitous plant pathogenic fungi over their long-term evolution.

Analysis of population genome diversity, particularly in the cereal mildews, could deliver invaluable information about how strains move, distribute across the agronomic spectrum, and change in response to deployment of hosts with new or new combinations of resistance genes. Such a field pathogenomic approach has been highly successful in revealing dynamic changes in wheat yellow rust population structure (Hubbard et al., 2015). Understanding the genetic and genomic responses to fungicide use and comprehending the evolution of resistance to essential pesticides has a great potential to increase our ability to mitigate risk to crop and food security. This challenge is at present unmet in the powdery mildews.

Related to the above, we have very little understanding of the potential for generation of variation through rapid, short-term genetic and/or epigenetic changes in the powdery mildews. A systematic analysis of genome changes in isolated, controlled environments, possibly under diverse selection pressures, will be needed to address this issue.

All these challenges would be greatly facilitated by the availability of fully assembled and finished reference sequences (Thomma et al., 2015). All the powdery mildew genome sequences published to date are highly fragmented. This is due, in large part, to the extremely repetitive character of the genomic DNA, which has made complete assembly impossible with the available technologies. The obligate nature of the organisms themselves also makes it difficult to obtain high amounts of large, intact and pure DNA uncontaminated by host or other associated microorganisms. The availability of new "third generation" sequencing technologies, in particular the direct long-read methodologies (Faino and Thomma, 2014), coupled with very deep "second generation" sequencing and advances in computing and software promise to improve the existing assemblies significantly. It remains to be seen if these enhancements will deliver the full assembly and the complete coverage achieved with other filamentous ascomycetes (Goodwin et al., 2011; Faino et al., 2015). This may be particularly critical because, although the existing genomes have high coverage, the current assemblies are especially poor in the repeat-rich areas. Perversely, these are precisely the areas which appear to harbor a large proportion of the highly interesting genes encoding candidate effectors (CSEPs and CEPs) and EKA family proteins (see below), which are of great relevance to understanding the establishment of the relationship with the host, in particular those modulating host recognition (Bourras et al., 2015). We can thus assume that the effector repertoire of the powdery mildews is even larger than currently known. True completion of finished sequences is therefore of high importance in this respect.

POWDERY MILDEW TRANSCRIPTOMES

A first attempt to study the transcriptome of a powdery mildew pathogen at a larger scale was performed in the pre-genomic era in *B. graminis* f.sp. *hordei* on the basis of expressed sequence tags (ESTs). Using RNA from either ungerminated conidia or conidia germinated on glass plates, two cDNA libraries were generated and used to sequence a random selection of 2,676 clones. This resulted in 4,908 ESTs that represent a total of 1,669 individual sequences. Proteins encoded by these cDNAs were predicted to cover a broad range of different functions (Thomas et al., 2001). Thereafter, serial analysis of gene expression (SAGE) was employed to obtain first insights into the dynamics of gene expression during fungal pathogenesis. SAGE is a method that categorizes cDNAs based on the presence of short oligonucleotide sequences. These sequence tags can then be used to quantify the number of transcripts in a given sample. Thomas et al. (2002) used SAGE to measure the abundance of *B. graminis* f.sp. *hordei* cDNAs in samples from ungerminated conidia, conidia with incipient germ tubes, and germinated conidia with a fully formed appressorium. The authors ended up with 6,336 different tags that were believed to represent unique transcripts. Of these, the 916 tags that occurred at least six times in one of the three samples were used for quantification of cDNA abundance, which revealed different patterns of cDNA accumulation during the early stages of *B. graminis* f.sp. *hordei* pathogenesis. Approximately 20% of the 6,336 tags could be mapped to one of the 1,669 EST-based unigenes previously identified by the same authors (Thomas et al., 2001; see also above), thereby tagging ca. 80% of these unigenes (Thomas et al., 2002).

The next phase in the analysis of powdery mildew transcriptomes was the deployment of cDNA microarrays. Both and co-workers developed a custom-made microarray that harbored 3,327 *B. graminis* f.sp. *hordei* cDNAs representing 2,077 unigenes (Both et al., 2005a,b). These corresponded to cDNAs from conidia, germinating conidia and hyphae (before the onset of conidiation) and included the previously reported EST set (Thomas et al., 2001). The authors utilized the microarray to analyze the transcript profile of *B. graminis* f.sp. *hordei* in the course of barley infection. Eight different RNA samples, derived from heavily inoculated barley plants, were used to synthesize labeled cDNA and probe the microarray. The experiment included four time points prior to host cell penetration (ungerminated conidia; 4, 8 and 15 hpi) and two time points after host cell penetration (3 and 5 dpi) as well as two samples (3 and 5 dpi) from the barley epidermal cell layer after the removal of epiphytic structures, essentially representing haustoria as the main fungal structure. Results of this analysis revealed a global switch in the gene expression pattern between fungal pre- and post-penetration stages, mainly caused by the accumulation of transcripts related to protein biosynthesis (e.g., encoding ribosomal proteins) at later stages of plant colonization. In addition, 51 genes were identified for which the expression

[2]http://jgi.doe.gov/comparative-genomics-of-powdery-mildews/

profile over time correlated well with the expression of *cap20*, a gene with a well-known virulence function in *Colletotrichum gloeosporioides* (Both et al., 2005b). The same experimental setup further uncovered the coordinated expression of genes that encode enzymes within the same pathways of primary metabolism. Striking examples of this include glycolysis (high transcript levels of the respective genes in mature appressoria and infected epidermis) and lipid metabolism (high transcript levels during fungal germination). These data provided first insights in the type and order of metabolic processes in the course of fungal development and infection (Both et al., 2005a).

To investigate the transcript profile of the grapevine powdery mildew pathogen *E. necator* during development, Wakefield et al. (2011) used the cDNA amplified fragment length polymorphism (cDNA-AFLP) technology, which is a method to fingerprint restriction fragments derived from cDNAs. In this study, the authors put emphasis on later stages of fungal pathogenesis [RNA samples for cDNA synthesis collected prior to conidiation (3 dpi), at conidiophore formation (5 dpi) and during full sporulation (8 dpi)] and also included a sample that represents the formation of sexual ascospores following mating of two opposing mating types (4 weeks post inoculation). The analysis identified 620 cDNA-AFLP fragments that showed differential expression between the four developmental phases under investigation (Wakefield et al., 2011).

A stage-specific transcriptome analysis was conducted on the basis of epidermal peels of heavily *B. graminis* f.sp. *hordei*-infected barley plants from which fungal surface structures were eliminated prior to removal of the epidermal cell layer, as described above. This sample material, which was highly enriched for mature fungal haustoria, was used for cDNA library synthesis and sequencing, which yielded 3,200 unigenes. Among these, 107 candidates for secreted effector protein were identified, which ultimately resulted in the identification of a conserved amino-terminal sequence motif (Y/F/W-x-C) present in the majority of these effector candidates (Godfrey et al., 2010). This sequence motif, whose functional relevance is currently unknown, was later found to be present in many *B. graminis* f.sp. *hordei* CSEPs identified by genome-wide analysis (307 of 491 predicted and analyzed effector proteins; Pedersen et al., 2012).

The advent of next generation sequencing technologies enabled entirely new possibilities for transcriptomic analyses of powdery mildew fungi. For example, the cDNA sequencing of enriched haustorial complexes from *G. orontii*-infected *A. thaliana* plants provided unprecedented insights into the haustorial transcriptome of this powdery mildew pathogen. Sequence analysis of *G. orontii* haustorial cDNAs on the basis of the 454 GS FLX pyrosequencing platform led to the assembly of 7,077 contigs with >5-fold average coverage. Highly represented transcripts encoded proteins involved in protein turnover, detoxification of reactive oxygen species and fungal pathogenesis, including secreted effector candidates. By contrast, transcripts coding for transporter proteins for nutrient uptake were less abundant than expected (Weßling et al., 2012). Transcriptome analysis on the basis of either SOLiD or Illumina short read platforms also assisted annotation of the *B. graminis* and *E. necator* genomes (Spanu et al., 2010; Wicker et al., 2013; Jones et al., 2014) and revealed a multitude of transcripts derived from transposable elements, indicating that these are transcriptionally active (Jones et al., 2014).

Further details of powdery mildew transcriptome dynamics were uncovered in a study that investigated the interaction between *Arabidopsis* and *B. graminis* f.sp. *hordei* by deep Illumina-based RNA-sequencing (Hacquard et al., 2013). Usually, *Arabidopsis* is not a host plant for *B. graminis* f.sp. *hordei*; however, the grass powdery mildew pathogen is able to complete its life cycle on the immuno-compromised *Arabidopsis pen2 pad4 sag101* triple mutant (Lipka et al., 2005). Transcript profiling of early pathogenesis of two *B. graminis* f.sp. *hordei* isolates (a virulent and an avirulent one) on this *Arabidopsis* mutant revealed DNA packaging, nucleosome organization and regulation of chromatin structure as potentially relevant processes around the time of conidium germination (at 6 hpi). During host cell entry (at 12 hpi), the abundance of transcripts related to pathogenesis increased. These also included transcripts coding for CSEPs. In fact, accumulation of *CSEP* transcripts occurred in two successive waves during plant colonization (at 12 and 18–24 hpi). Results of detailed qRT-PCR analyses of a subset of the differentially expressed genes in barley suggest that the *B. graminis* f.sp. *hordei* transcript pattern seen in the non-host plant *Arabidopsis* largely reflects the pattern in the native host, barley. Differences between the transcriptional program of the virulent and avirulent *B. graminis* f.sp. *hordei* isolate concentrated on the 24 h time-point and affected a surprisingly low number of genes (just 76 genes). The majority of these genes (43 of the 76) code for CSEPs, suggesting that the main difference in the fungal expression profile between a compatible and an incompatible interaction resides in the expression of genes encoding effectors (Hacquard et al., 2013).

Finally, next generation-based transcript profiling has been used as a tool to discover markers for population genetic studies. Frenkel et al. (2012) employed 454 GS FLX sequencing of RNA from conidia and mycelium of the grapevine powdery mildew pathogen *E. necator*. This yielded approximately 32,000 sequence contigs that were mined for the presence of microsatellite markers. Of 116 potential markers identified, 31 were tested and detailed, which resulted in 11 microsatellites polymorphic among *E. necator* isolates. Eight of these were then used to analyze the *E. necator* population structure in Europe and North America, which revealed that genetic diversity in eastern USA is much greater than in Europe (Frenkel et al., 2012). A similar approach was applied to study population structure of *P. plantaginis*, the powdery mildew pathogen of *Plantago lanceolata* (plantain), on the archipelago Åland in Finland. Sequencing of RNA extracted from mixed spore material (derived from 16 different isolates) yielded 45,245 sequence contigs which were then mined for single nucleotide polymorphisms (SNPs) for sample genotyping. In the end, a panel of 27 SNP loci was employed for genotyping, which revealed a mixed meta-population of *P. plantaginis*. Additionally, the study disclosed that infection with mixed genotypes on a single host leaf is a common phenomenon within this meta-population (Tollenaere et al., 2012).

Taken together, various attempts have been made in the past 15 years to examine the transcriptome of different powdery mildew fungi (**Table 1**). These comprised studies that either recorded transcript dynamics during fungal pathogenesis (Thomas et al., 2002; Both et al., 2005a,b; Wakefield et al., 2011; Hacquard et al., 2013; Jones et al., 2014) or that focused on a single (pooled) sample (Thomas et al., 2001; Frenkel et al., 2012; Tollenaere et al., 2012) or an enriched infection structure (i.e., haustoria; Godfrey et al., 2010; Weßling et al., 2012). Overall, the studies suffer from a lack of comparability since different host (barley, *Arabidopsis*, *P. lanceolata*, grapevine) and powdery mildew species (*B. graminis* f.sp. *hordei*, *G. orontii*, *P. plantaginis,* and *E. necator*), different experimental techniques (ESTs, SAGE, microarrays, cDNA-AFLP and various next generation sequencing platforms) and in the time-course studies different time-points were used. Moreover, the results have only been partially integrated with the genome (see above) and proteome (see below) data that are now available. Thus, there is still a need for a comprehensive time-resolved transcriptome analysis of a single plant-powdery mildew interaction by deep next generation sequencing that covers the full asexual life cycle from ungerminated conidia to conidiophore formation and sporulation. It would be particularly auspicious if these analyses could be carried out in the context of completely assembled and finished genome sequences. Integration of the data sets would be extremely beneficial in terms of full validation of the gene models in the genome annotation, whilst greatly facilitating the interpretation of global trends in gene expression. In this regard, the above-mentioned JGI CSP Project "Comparative Genomics of Powdery Mildews and Associated Plants" seems especially promising, as it will produce comparative transcriptome data using RNASeq for each sequenced powdery mildew species and its associated host plant at germination, penetration, and proliferation phases of infection.

POWDERY MILDEW PROTEOMES

Large-scale proteome studies of *B. graminis* f.sp. *hordei* were performed on conidia (Bindschedler et al., 2009; Noir et al., 2009), secondary hyphae (Bindschedler et al., 2009, 2011), isolated haustoria (Godfrey et al., 2009) and haustoria in barley epidermis (Bindschedler et al., 2009, 2011; **Table 1**). The resulting peptide information was used during annotation of the *B. graminis* f.sp. *hordei* genome to aid the identification and manual curation of open reading frames (ORFs) and gene models. Based on the ca. 1,500 proteins that had been identified by mass spectrometry (Bindschedler et al., 2011), more than 20% of the 6,500 predicted ORFs were experimentally validated as expressed proteins.

Two-dimensional gel electrophoresis of proteins extracted from ungerminated conidia of *B. graminis* f.sp. *hordei* (Noir et al., 2009) enabled the identification of 123 fungal polypeptides. The main group of proteins belonged to primary metabolism, such as carbohydrate, protein, amino acid, nucleic acid, and lipid/fatty acid metabolism, suggesting that the pathogen is armed for storing compounds, as well as for protein biosynthesis. These findings corroborate those obtained from the survey of transcriptomes based on microarrays (Both et al., 2005a). Additionally, several proteins involved in redox processes and detoxification were found.

The haustorial proteome of purified haustoria (Godfrey et al., 2009), or of infected epidermis following removal of epiphytic hyphae (see above; Bindschedler et al., 2009, 2011), was analyzed by liquid chromatography coupled with nano-electrospray mass spectrometry. In these samples there were many enzymes from primary metabolism. Enzymes associated with alcoholic fermentation, such as pyruvate decarboxylase, were not found, although these proteins are known to be abundant in other fungi (Godfrey et al., 2009). This finding is consistent with the absence of genes encoding these enzymes, as noted when the first *B. graminis* genome was annotated (Spanu et al., 2010). The haustorial proteome is characterized by an overrepresentation of proteins involved in monosaccharide metabolism and stress responses, including heat-shock proteins (Bindschedler et al., 2009, 2011; Godfrey et al., 2009).

Bioinformatic prediction of effectors from pathogenic fungi has been facilitated by the availability of the respective genomes (Schmidt and Panstruga, 2011). However, by definition, effector sequences are diverse and species-specific. Identification often relies on very broad criteria such as small size, predicted protein secretion (i.e., presence of a signal peptide), species-specificity and, possibly, a high cysteine content in the apoplastic effectors (Stergiopoulos and de Wit, 2009).

Large-scale proteomics has contributed to effector discovery through the identification of tissue- or cell-specific *B. graminis* f.sp. *hordei* proteins (Godfrey et al., 2009; Bindschedler et al., 2011). Comparison of the proteomes of haustoria and hyphae revealed that identified haustoria-specific proteins are on average smaller in size than proteins specific to hyphae. Overall, a quarter of the proteins identified only in the haustorial proteome within infected epidermis were not detected in the proteome of sporulating hyphae (Bindschedler et al., 2011). Of these seemingly haustoria-specific proteins, originally 61 and upon refined analysis 67 are predicted to be secreted, i.e. they have a canonical amino-terminal secretion signal and no transmembrane domain. Based on these features they were regarded as *B. graminis* f.sp. *hordei* effector candidates (BECs) expressed in haustoria (**Figure 2**). The large proportion of BECs in the haustorial proteome suggests that they are highly expressed, since proteins in higher abundance (on the basis of more peptides) are usually more easily identified in non-targeted proteome studies. Note that the vast majority of BECs are encoded by *CSEP* genes and are thus identical to matching CSEPs (Pedersen et al., 2012). However, this does not apply to all BECs, since the criterion of the exclusive presence of these proteins in powdery mildews, which was deployed for the classification of the CSEPs, was not used for the assignment of proteins to the BEC category. Two of the BECs that are not CSEPs, are virulence factors necessary for full pathogenic development (Pliego et al., 2013). CSEPs and BECs therefore represent two overlapping and thus in part redundant sets of *Blumeria* effector candidates. (**Figure 2**).

Mining the proteome of purified haustoria led to the identification of more than 200 *B. graminis* f.sp. *hordei* proteins

(Godfrey et al., 2009). However, in this study secreted proteins and putative effectors appear under-represented. Conversely, the proteome of infected epidermis allowed the identification of ca. 300 *Blumeria* proteins, including the 67 defined as BECs that are exclusively present in haustoria (Bindschedler et al., 2011). This may be explained by considering that effectors efficiently secreted from haustoria will not accumulate inside them, rendering their detection as intrinsic haustorium peptides a challenging task.

The function in pathogenic development of 50 of the 67 BECs was tested on the basis of host-induced gene silencing (Nowara et al., 2010). Results obtained in this study provided experimental evidence for a virulence role of eight of the effector candidates (Pliego et al., 2013). These included BEC1011 and BEC1054, two RNase-like proteins from CSEP family 21 (CSEP0264 and CSEP0064); BEC1005, a putative glucanase; and BEC1019, a metalloprotease-like protein (Whigham et al., 2015). Mass spectrometry-based proteomics data from a previous study (Bindschedler et al., 2011) were recently re-analyzed to search for the presence of translated products from the large family of retro-transposons associated with the Avrk1 and Avra10 phenotype (EKA family, Ridout et al., 2006), using a novel transposon sequence database that was not available at the time of genome assembly (Spanu et al., 2010). Based on this retrospective examination, several EKA proteins were identified experimentally. Notably, some of the proteins from the retro-transposons associated to Avra10 were found only in haustoria-containing samples (Amselem et al., 2015b).

Taken together, these studies reinforce the notion that "*in planta*" proteomics is an invaluable complement to genomic and transcriptomic studies for the discovery of functional effectors, in particular for biotrophic fungi such as powdery mildews. However, the low biomass of the pathogen in the early stages of infection remains a challenge for such proteomic investigations, which was only partly resolved by the isolation of infected epidermis from barley primary leaves.

An additional bottleneck for the experimental discovery of proteins by mass spectrometry-based proteomics is the dependence on a well-sequenced, well-assembled and ideally also well-annotated genome, since large scale *de novo* peptide sequencing still remains a major technical challenge, despite continuous improvements at the instrument and software level (Ma and Johnson, 2012). Consequently, the lack of ORFs in genome or transcriptome databases conditions that the matching proteins cannot be identified with database-dependent search engines and prediction software. This limitation reinforces the need for further improving genome coverage, assemblies and annotations of powdery mildew fungi.

MISSING AND EMERGING MILDEW-OMES

To our knowledge, there are currently no systematic studies of the powdery mildew metabolome. This could be in part due to the relatively less advanced status of this sub discipline and/or the challenges related to the technologies involved in detection of specific metabolomes of obligate parasites and pathogens growing inside a host. It may also be due to the fact that given the paucity of genes encoding secondary metabolism enzymes in the powdery mildew genomes (Spanu et al., 2010), there has been relatively little impetus to follow this line of investigation, so far. Similarly, systematic large scale approaches to unravel the interaction of powdery mildew proteins with their respective host proteins (interactomics; Collura and Boissy, 2007) are also missing. Up to now, studies mainly focused on individual protein–protein interactions of secreted powdery mildew effector candidates with their potential host targets (Zhang et al., 2012; Schmidt et al., 2014; Ahmed et al., 2015; Pennington et al., in press). A first attempt to investigate such interactions at larger scale resulted in the establishment of a protein–protein interaction network from *G. orontii* haustorial effectors and their respective *Arabidopsis* host proteins. This study revealed convergence of multiple effector proteins on a limited set of host targets ("hubs") that themselves are highly interconnected with further host proteins and likewise targeted by pathogen effectors from other kingdoms of life (oomycetes and bacteria; Weßling et al., 2014). This work also uncovered a set of host targets that are seemingly specific for *G. orontii* effectors. These plant interactors comprise different types of transcriptional regulators plus a number of proteins with diverse functions (Weßling et al., 2014).

OUTLOOK FOR MILDEW-OMICS

The past 15 years have seen the laying of effective foundations for the large scale survey of genes, transcripts and proteins in the powdery mildew fungi, in spite of the difficulties posed by their obligate biotrophic nature. Advances in methods, technology and analysis software are still required to fill the inevitable gaps that exist. However, as these techniques become more cost-effective, there is an expectation that the missing tesserae of the mosaic will be found and placed in the right order, so that a "big picture" will emerge with greater clarity. These building-blocks are essential for the next challenge: moving the field into a true "systems biology" approach, that is an integration of the information to create realistic modeling of the systems themselves to provide real heuristic value to our investigation. Moreover, because the life style of powdery mildew fungi is inherently intertwined with that of their host, the biggest prize of all will be unraveling the complexity and dynamics of the interactome, for which a start has been recently achieved (Weßling et al., 2014). The site-specific nature of the interaction with the haustoria being in direct contact with host cells poses particular challenges for transcriptomic, proteomic and metabolic studies of these infection structures. Laser microdissection-based enrichment of infection sites, as recently performed in the context of the *Arabidopsis*-powdery mildew interaction (Chandran et al., 2010), is a promising technique to temper this problem.

For all mentioned –omics approaches, the functional validation of identified components is essential. Despite some recent progress in transient transformation protocols (Vela-Corcía et al., 2015), the stable transformation of powdery mildew fungi and thus the targeted generation of knock-out

mutants remains elusive. An alternative method for functional assays exploits the phenomenon of host-induced gene silencing (Nowara et al., 2010), which has already been used successfully for the identification of some *Blumeria* effector candidates (Pliego et al., 2013; Whigham et al., 2015). If successful, the integration of insights from –omics studies with the results from functional investigations hold the promise to improve our ability to control these ubiquitous diseases, and mitigating their effect on our food and crop security.

AUTHOR CONTRIBUTIONS

LB, RP, and PS jointly worked out the review concept. Primary author of the genome section is PS, primary author of the transcriptome section is RP and primary author of the proteomics section is LB; all other sections were written together. The authors jointly edited the manuscript.

FUNDING

This work was supported by grants from the BBSRC to PS (BB/M000710/1) and the Deutsche Forschungsgemeinschaft (DFG) Priority Programme SPP 1819 to RP (PA 861/14-1).

ACKNOWLEDGMENT

We thank the two reviewers of our manuscript for their constructive criticism.

REFERENCES

Ahmed, A. A., Pedersen, C., Schultz-Larsen, T., Kwaaitaal, M., Jørgensen, H. J., and Thordal-Christensen, H. (2015). The barley powdery mildew candidate secreted effector protein CSEP0105 inhibits the chaperone activity of a small heat shock protein. *Plant Physiol.* 168, 321–333. doi: 10.1104/pp.15.00278

Amselem, J., Lebrun, M.-H., and Quesneville, H. (2015a). Whole genome comparative analysis of transposable elements provides new insight into mechanisms of their inactivation in fungal genomes. *BMC Genomics* 16:141. doi: 10.1186/s12864-015-1347–1341

Amselem, J., Vigouroux, M., Oberhaensli, S., Brown James, K M, Bindschedler, L. V., Skamnioti, P., et al. (2015b). Evolution of the EKA family of powdery mildew avirulence-effector genes from the ORF 1 of a LINE retrotransposon. *BMC Genomics* 16:917. doi: 10.1186/s12864-015-2185-x.

Bindschedler, L. V., Burgis, T. A., Mills, D. J. S., Ho, J. T. C., Cramer, R., and Spanu, P. D. (2009). *In planta* proteomics and proteogenomics of the biotrophic barley fungal pathogen *Blumeria graminis* f. sp *hordei*. *Mol. Cell. Proteomics* 8, 2368–2381. doi: 10.1074/mcp.M900188-MCP200

Bindschedler, L. V., McGuffin, L. J., Burgis, T. A., Spanu, P. D., and Cramer, R. (2011). Proteogenomics and *in silico* structural and functional annotation of the barley powdery mildew *Blumeria graminis* f. sp. *hordei*. *Methods* 54, 432–441. doi: 10.1016/j.ymeth.2011.03.006

Both, M., Csukai, M., Stumpf, M. P. H., and Spanu, P. D. (2005a). Gene expression profiles of *Blumeria graminis* indicate dynamic changes to primary metabolism during development of an obligate biotrophic pathogen. *Plant Cell* 17, 2107–2122. doi: 10.1105/tpc.105.032631

Both, M., Eckert, S. E., Csukai, M., Müller, E., Dimopoulos, G., and Spanu, P. D. (2005b). Transcript profiles of *Blumeria graminis* development during infection reveal a cluster of genes that are potential virulence determinants. *Mol. Plant Microbe Interact.* 18, 125–133. doi: 10.1094/MPMI-18-0125

Bourras, S., McNally, K. E., Ben-David, R., Parlange, F., Roffler, S., Praz, C. R., et al. (2015). Multiple avirulence loci and allele-specific effector recognition control the *Pm3* race-specific resistance of wheat to powdery mildew. *Plant Cell* 27, 2991–3012. doi: 10.1105/tpc.15.00171

Braun, U., and Cook, R. T. A. (2012). *Taxonomic Manual of the Erysiphales (Powdery Mildews)*. Utrecht: CBS-KNAW Fungal Biodiversity Centre.

Chandran, D., Inada, N., Hather, G., Kleindt, C. K., and Wildermuth, M. C. (2010). Laser microdissection of *Arabidopsis* cells at the powdery mildew infection site reveals site-specific processes and regulators. *Proc. Natl. Acad. Sci. U.S.A.* 107, 460–465. doi: 10.1073/pnas.0912492107

Collura, V., and Boissy, G. (2007). From protein-protein complexes to interactomics. *Subcell. Biochem.* 43, 135–183. doi: 10.1007/978-1-4020-5943-8_8

Dean, R., van Kan, J. A. L., Pretorius, Z. A., Hammond-Kosack, K. E., Di Pietro, A., Spanu, P. D., et al. (2012). The Top 10 fungal pathogens in molecular plant pathology. *Mol. Plant Pathol.* 13, 414–430. doi: 10.1111/j.1364-3703.2011.00783.x

Dean, R. A., Talbot, N. J., Ebbole, D. J., Farman, M. L., Mitchell, T. K., Orbach, M. J., et al. (2005). The genome sequence of the rice blast fungus *Magnaporthe grisea*. *Nature* 434, 980–986. doi: 10.1038/nature03449

Ding, Y., Wang, J., Wang, J., Stierhof, Y.-D., Robinson, D. G., and Jiang, L. (2012). Unconventional protein secretion. *Trends Plant Sci.* 17, 606–615. doi: 10.1016/j.tplants.2012.06.004

Droste, P., Miebach, S., Niedenführ, S., Wiechert, W., and Nöh, K. (2011). Visualizing multi-omics data in metabolic networks with the software Omix: a case study. *Biosystems* 105, 154–161. doi: 10.1016/j.biosystems.2011.04.003

Duplessis, S., Cuomo, C. A., Lin, Y.-C., Aerts, A., Tisserant, E., Veneault-Fourrey, C., et al. (2011). Obligate biotrophy features unraveled by the genomic analysis of rust fungi. *Proc. Natl. Acad. Sci. U.S.A.* 108, 9166–9171. doi: 10.1073/pnas.1019315108

Faino, L., Seidl, M. F., Datema, E., van den Berg, G. C. M., Janssen, A., Wittenberg, A. H. J., et al. (2015). Single-molecule real-time sequencing combined with optical mapping yields completely finished fungal genome. *MBio* 6, 4 e00936–e01015. doi: 10.1128/mBio.00936-915

Faino, L., and Thomma, B. P. H. J. (2014). Get your high-quality low-cost genome sequence. *Trends Plant Sci.* 19, 288–291. doi: 10.1016/j.tplants.2014.02.003

Frenkel, O., Portillo, I., Brewer, M. T., Péros, J. P., Cadle-Davidson, L., and Milgroom, M. G. (2012). Development of microsatellite markers from the transcriptome of *Erysiphe necator* for analysing population structure in North America and Europe. *Plant Pathol.* 61, 106–119. doi: 10.1111/j.1365-3059.2011.02502.x

Galagan, J. E., Calvo, S. E., Borkovich, K. A., Selker, E. U., Read, N. D., Jaffe, D., et al. (2003). The genome sequence of the filamentous fungus *Neurospora crassa*. *Nature* 422, 859–68. doi: 10.1038/nature01554

Glawe, D. A. (2008). The powdery mildews: a review of the world's most familiar (yet poorly known) plant pathogens. *Annu. Rev. Phytopathol.* 46, 27–51. doi: 10.1146/annurev.phyto.46.081407.104740

Godfrey, D., Böhlenius, H., Pedersen, C., Zhang, Z. G., Emmersen, J., and Thordal-Christensen, H. (2010). Powdery mildew fungal effector candidates share N-terminal Y/F/WxC-motif. *BMC Genomics* 11:317. doi: 10.1186/1471-2164-11-317

Godfrey, D., Zhang, Z. G., Saalbach, G., and Thordal-Christensen, H. (2009). A proteomics study of barley powdery mildew haustoria. *Proteomics* 9, 3222–3232. doi: 10.1002/pmic.200800645

Gomez-Cabrero, D., Abugessaisa, I., Maier, D., Teschendorff, A., Merkenschlager, M., Gisel, A., et al. (2014). Data integration in the era of omics: current and future challenges. *BMC Syst. Biol.* 8(Suppl. 2), I1. doi: 10.1186/1752-0509-8-S2-I1

Goodwin, S. B., M'barek, S. B., Dhillon, B., Wittenberg, A. H. J., Crane, C. F., Hane, J. K., et al. (2011). Finished genome of the fungal wheat pathogen *Mycosphaerella graminicola* reveals dispensome structure, chromosome plasticity, and stealth pathogenesis. *PLoS Genet.* 7:e1002070. doi: 10.1371/journal.pgen.1002070

Hacquard, S., Kracher, B., Maekawa, T., Vernaldi, S., Schulze-Lefert, P., and Ver Loren van Themaat, E. (2013). Mosaic genome structure of the barley powdery mildew pathogen and conservation of transcriptional programs in divergent hosts. *Proc. Natl. Acad. Sci. U.S.A.* 110, E2219–E2228. doi: 10.1073/pnas.1306807110

Hubbard, A., Lewis, C. M., Yoshida, K., Ramirez-Gonzalez, R. H., de Vallavieille-Pope, C., Thomas, J., et al. (2015). Field pathogenomics reveals the emergence of a diverse wheat yellow rust population. *Genome Biol.* 16:23. doi: 10.1186/s13059-015-0590-598

Jones, L., Riaz, S., Morales-Cruz, A., Amrine, K. C. H., McGuire, B., Gubler, W. D., et al. (2014). Adaptive genomic structural variation in the grape powdery mildew pathogen, *Erysiphe necator*. *BMC Genomics* 15:1081. doi: 10.1186/1471-2164-15–1081

Kusch, S., Ahmadinejad, N., Panstruga, R., and Kuhn, H. (2014). *In silico* analysis of the core signaling proteome from the barley powdery mildew pathogen (*Blumeria graminis* f.sp. *hordei*). *BMC Genomics* 15:843. doi: 10.1186/1471-2164-15-843

Lipka, V., Dittgen, J., Bednarek, P., Bhat, R., Wiermer, M., Stein, M., et al. (2005). Pre- and postinvasion defenses both contribute to nonhost resistance in *Arabidopsis*. *Science* 310, 1180–1183. doi: 10.1126/science.1119409

Lowe, R. G. T., McCorkelle, O., Bleackley, M., Collins, C., Faou, P., Mathivanan, S., et al. (2015). Extracellular peptidases of the cereal pathogen *Fusarium graminearum*. *Front. Plant Sci.* 6:962. doi: 10.3389/fpls.2015.00962

Ma, B., and Johnson, R. (2012). *De novo* sequencing and homology searching. *Mol. Cell. Proteomics* 11:O111.014902. doi: 10.1074/mcp.O111.014902

Martin, F., Kohler, A., Murat, C., Balestrini, R., Coutinho, P. M., Jaillon, O., et al. (2010). Perigord black truffle genome uncovers evolutionary origins and mechanisms of symbiosis. *Nature* 464, 1033–1038. doi: 10.1038/nature08867

Noir, S., Colby, T., Harzen, A., Schmidt, J., and Panstruga, R. (2009). A proteomic analysis of powdery mildew (*Blumeria graminis* f.sp. *hordei*) conidiospores. *Mol. Plant Pathol.* 10, 223–236. doi: 10.1111/j.1364-3703.2008.00524.x

Nowara, D., Gay, A., Lacomme, C., Shaw, J., Ridout, C., Douchkov, D., et al. (2010). HIGS: Host-Induced Gene Silencing in the obligate biotrophic fungal pathogen *Blumeria graminis*. *Plant Cell* 22, 3130–3141. doi: 10.1105/tpc.110.077040

Ospina-Giraldo, M. D., Griffith, J. G., Laird, E. W., and Mingora, C. (2010). The CAZyome of *Phytophthora* spp. a comprehensive analysis of the gene complement coding for carbohydrate-active enzymes in species of the genus *Phytophthora*. *BMC Genomics* 11:525. doi: 10.1186/1471-2164-11–525

Panstruga, R., and Spanu, P. D. (2014). Powdery mildew genomes reloaded. *New Phytol.* 202, 13–14. doi: 10.1111/nph.12635

Pedersen, C., Ver Loren van Themaat, E., McGuffin, L. J., Abbott, J. C., Burgis, T. A., Barton, G., et al. (2012). Structure and evolution of barley powdery mildew effector candidates. *BMC Genomics* 13:694. doi: 10.1186/1471-2164-13–694

Pennington, H. G., Gheorghe, D. M., Damerum, A., Pliego, C., Spanu, P. D., Cramer, R., et al. (in press). Interactions between the powdery mildew effector BEC1054 and barley proteins identify candidate host targets. *J. Proteome Res.* doi: 10.1021/acs.jproteome.5b00732 [Epub ahead of print].

Pliego, C., Nowara, D., Bonciani, G., Gheorghe, D. M., Xu, R., Surana, P., et al. (2013). Host-induced gene silencing in barley powdery mildew reveals a class of ribonuclease-like effectors. *Mol. Plant-Microbe Interact.* 26, 633–642. doi: 10.1094/MPMI-01-13-0005-R

Poulin, R., and Randhawa, H. S. (2015). Evolution of parasitism along convergent lines: from ecology to genomics. *Parasitology* 142(Suppl. 1), S6–S15. doi: 10.1017/S0031182013001674

Raffaele, S., Farrer, R. A., Cano, L. M., Studholme, D. J., MacLean, D., Thines, M., et al. (2010). Genome evolution following host jumps in the Irish potato famine pathogen lineage. *Science* 330, 1540–1543. doi: 10.1126/science.1193070

Ridout, C. J., Skamnioti, P., Porritt, O., Sacristan, S., Jones, J. D. G., and Brown, J. K. M. (2006). Multiple avirulence paralogues in cereal powdery mildew fungi may contribute to parasite fitness and defeat of plant resistance. *Plant Cell* 18, 2402–2414. doi: 10.1105/tpc.106.043307

Schmidt, S. M., Kuhn, H., Micali, C., Liller, C., Kwaaitaal, M., and Panstruga, R. (2014). Interaction of a *Blumeria graminis* f. sp. *hordei* effector candidate with a barley ARF-GAP suggests that host vesicle trafficking is a fungal pathogenicity target. *Mol. Plant Pathol.* 15, 535–549. doi: 10.1111/mpp.12110

Schmidt, S. M., and Panstruga, R. (2011). Pathogenomics of fungal plant parasites: what have we learnt about pathogenesis? *Curr. Opin. Plant Biol.* 14, 392–399. doi: 10.1016/j.pbi.2011.03.006

Spanu, P. D., Abbott, J. C., Amselem, J., Burgis, T. A., Soanes, D. M., Stüber, K., et al. (2010). Genome expansion and gene loss in powdery mildew fungi reveal tradeoffs in extreme parasitism. *Science* 330, 1543–1546. doi: 10.1126/science.1194573

Spanu, P. D., and Panstruga, R. (2012). Powdery mildew genomes in the crosshairs. *New Phytol.* 195, 20–22. doi: 10.1111/j.1469-8137.2012.04173.x

Stergiopoulos, I., and de Wit, P. (2009). Fungal effector proteins. *Annu. Rev. Phytopathol.* 47, 233–263. doi: 10.1146/annurev.phyto.112408.132637

Takamatsu, S. (2004). Phylogeny and evolution of the powdery mildew fungi (Erysiphales, Ascomycota) inferred from nuclear ribosomal DNA sequences. *Mycoscience* 45, 147–157. doi: 10.1007/S10267-003-0159-3

Tan, K.-C., Ipcho, S. V. S., Trengove, R. D., Oliver, R. P., and Solomon, P. S. (2009). Assessing the impact of transcriptomics, proteomics and metabolomics on fungal phytopathology. *Mol. Plant Pathol.* 10, 703–715. doi: 10.1111/j.1364-3703.2009.00565.x

Thomas, S. W., Glaring, M. A., Rasmussen, S. W., Kinane, J. T., and Oliver, R. P. (2002). Transcript profiling in the barley mildew pathogen *Blumeria graminis* by serial analysis of gene expression (SAGE). *Mol. Plant Microbe Interact.* 15, 847–856. doi: 10.1094/MPMI.2002.15.8.847

Thomas, S. W., Rasmussen, S. W., Glaring, M. A., Rouster, J. A., Christiansen, S. K., and Oliver, R. P. (2001). Gene identification in the obligate fungal pathogen *Blumeria graminis* by expressed sequence tag analysis. *Fungal Genet. Biol.* 33, 195–211. doi: 10.1006/fgbi.2001.1281

Thomma, B. P. H. J., Seidl, M. F., Shi-Kunne, X., Cook, D. E., Bolton, M. D., van Kan, J. A. L., et al. (2015). Mind the gap; seven reasons to close fragmented genome assemblies. *Fungal Genet. Biol.* doi: 10.1016/j.fgb.2015.08.010 [Epub ahead of print].

Tieri, P., de la Fuente, A., Termanini, A., and Franceschi, C. (2011). Integrating omics data for signaling pathways, interactome reconstruction, and functional analysis. *Methods Mol. Biol.* 719, 415–433. doi: 10.1007/978-1-61779-027-0_19

Tollenaere, C., Susi, H., Nokso-Koivisto, J., Koskinen, P., Tack, A., Auvinen, P., et al. (2012). SNP design from 454 sequencing of *Podosphaera plantaginis* transcriptome reveals a genetically diverse pathogen metapopulation with high levels of mixed-genotype infection. *PLoS ONE* 7:e52492. doi: 10.1371/journal.pone.0052492

Vela-Corcía, D., Romero, D., Torés, J., Vicente, A., De Vicente, A., and Pérez-García, A. (2015). Transient transformation of *Podosphaera xanthii* by electroporation of conidia. *BMC Microbiol.* 15:338. doi: 10.1186/s12866-014-0338–338

Wakefield, L., Gadoury, D. M., Seem, R. C., Milgroom, M. G., Sun, Q., and Cadle-Davidson, L. (2011). Differential gene expression during conidiation in the grape powdery mildew pathogen, *Erysiphe necator*. *Phytopathology* 101, 839–846. doi: 10.1094/PHYTO-11-10–0295

Weßling, R., Epple, P., Altmann, S., He, Y., Yang, L., Henz, S. R., et al. (2014). Convergent targeting of a common host protein-network by pathogen effectors from three kingdoms of life. *Cell Host Microbe* 16, 364–375. doi: 10.1016/j.chom.2014.08.004

Weßling, R., Schmidt, S. M., Micali, C. O., Knaust, F., Reinhardt, R., Neumann, U., et al. (2012). Transcriptome analysis of enriched *Golovinomyces orontii* haustoria by deep 454 pyrosequencing. *Fungal Genet. Biol.* 49, 470–482. doi: 10.1016/j.fgb.2012.04.001

Whigham, E., Qi, S., Mistry, D., Surana, P., Xu, R., Fuerst, G., et al. (2015). Broadly conserved fungal effector BEC1019 suppresses host cell death and enhances

pathogen virulence in powdery mildew of barley (*Hordeum vulgare* L.). *Mol. Plant Microbe Interact.* 28, 968–983. doi: 10.1094/MPMI-02-15-0027-FI

Wicker, T., Oberhaensli, S., Parlange, F., Buchmann, J. P., Shatalina, M., Roffler, S., et al. (2013). The wheat powdery mildew genome shows the unique evolution of an obligate biotroph. *Nat. Genet.* 45, 1092–1096. doi: 10.1038/ng.2704

Zhang, W.-J., Pedersen, C., Kwaaitaal, M., Gregersen, P. L., Mørch, S. M., Hanisch, S., et al. (2012). Interaction of barley powdery mildew effector candidate CSEP0055 with the defence protein PR17c. *Mol. Plant Pathol.* 13, 1110–1119. doi: 10.1111/j.1364-3703.2012.00820.x

Conflict of Interest Statement: The authors declare that the research was conducted in the absence of any commercial or financial relationships that could be construed as a potential conflict of interest.

frontiers in Plant Science

ORIGINAL RESEARCH
published: 01 December 2016
doi: 10.3389/fpls.2016.01784

Comparative Transcriptomic Analysis of Virulence Factors in *Leptosphaeria maculans* during Compatible and Incompatible Interactions with Canola

*Humira Sonah[1], Xuehua Zhang[2], Rupesh K. Deshmukh[1], M. Hossein Borhan[3], W. G. Dilantha Fernando[2] and Richard R. Bélanger[1]**

[1] *Département de Phytologie, Faculté des Sciences de l'Agriculture et de l'Alimentation, Université Laval, Québec QC, Canada,* [2] *Department of Plant Science, University of Manitoba Winnipeg, Winnipeg, MB, Canada,* [3] *Agriculture and Agri-Food Canada, Saskatoon, SK, Canada*

OPEN ACCESS

Edited by:
Pietro Daniele Spanu, Imperial College London, UK

Reviewed by:
William Underwood, Agricultural Research Service (USDA), USA
Rohan George Thomas Lowe, La Trobe University, Australia

***Correspondence:**
Richard R. Bélanger
richard.belanger@fsaa.ulaval.ca

Specialty section:
This article was submitted to Plant Biotic Interactions, a section of the journal Frontiers in Plant Science

Received: *30 April 2016*
Accepted: *11 November 2016*
Published: *01 December 2016*

Citation:
Sonah H, Zhang X, Deshmukh RK, Borhan MH, Fernando WGD and Bélanger RR (2016) Comparative Transcriptomic Analysis of Virulence Factors in Leptosphaeria maculans during Compatible and Incompatible Interactions with Canola. Front. Plant Sci. 7:1784. doi: 10.3389/fpls.2016.01784

Leptosphaeria maculans is a hemibiotrophic fungus that causes blackleg of canola (*Brassica napus*), one of the most devastating diseases of this crop. In the present study, transcriptome profiling of *L. maculans* was performed in an effort to understand and define the pathogenicity genes that govern both the biotrophic and the necrotrophic phase of the fungus, as well as those that separate a compatible from an incompatible interaction. For this purpose, comparative RNA-seq analyses were performed on *L. maculans* isolate D5 at four different time points following inoculation on susceptible cultivar Topas-DH16516 or resistant introgression line Topas-*Rlm2*. Analysis of 1.6 billion Illumina reads readily identified differentially expressed genes that were over represented by candidate secretory effector proteins, CAZymes, and other pathogenicity genes. Comparisons between the compatible and incompatible interactions led to the identification of 28 effector proteins whose chronology and level of expression suggested a role in the establishment and maintenance of biotrophy with the plant. These included all known *Avr* genes of isolate D5 along with eight newly characterized effectors. In addition, another 15 effector proteins were found to be exclusively expressed during the necrotrophic phase of the fungus, which supports the concept that *L. maculans* has a separate and distinct arsenal contributing to each phase. As for CAZymes, they were often highly expressed at 3 dpi but with no difference in expression between the compatible and incompatible interactions, indicating that other factors were necessary to determine the outcome of the interaction. However, their significantly higher expression at 11 dpi in the compatible interaction confirmed that they contributed to the necrotrophic phase of the fungus. A notable exception was *LysM* genes whose high expression was singularly observed on the susceptible host at 7 dpi. In the case of TFs, their higher expression at 7 and 11 dpi on susceptible Topas support an important role in regulating

the genes involved in the different pathogenic phases of *L. maculans*. In conclusion, comparison of the transcriptome of *L. maculans* during compatible and incompatible interactions has led to the identification of key pathogenicity genes that regulate not only the fate of the interaction but also lifestyle transitions of the fungus.

Keywords: *Avr* genes, CAZymes, compatible interactions, effectors, incompatible interactions, RNA-seq transcriptome profiling

INTRODUCTION

Blackleg disease (stem canker) caused by *Leptosphaeria maculans* (Desm.) Ces. & De Not. is one of the major constraints to canola (*Brassica napus* L.) production worldwide (Fitt et al., 2006). Infection by the fungus is known to cause more than 50% yield losses in canola (Kutcher et al., 2013). The major difficulty for combating the pathogen lies in the understanding of its complex lifestyle, which includes alternative biotrophic, and necrotrophic, phases, along with a symptomless endophytic phase (Howlett et al., 2001; Van de Wouw et al., 2016). Management of blackleg disease includes crop rotations, seed treatment and fungicide applications, and preferably, disease-resistant cultivars, arguably the most effective approach (Delourme et al., 2006).

Canola shows two types of resistance against *L. maculans*: qualitative and quantitative. Single or few major genes that are known to be involved in a gene for gene interaction govern qualitative resistance. Major genes provide resistance particularly at the seedling stage whereas quantitative resistance involves many small effect genes that are mostly expressed during the adult plant stage (Raman et al., 2012; Huang et al., 2014). To date, several resistance genes with major effect have been identified in *Brassica* species, but only two, *LepR3* and *Rlm2*, have been cloned and well characterized (Delourme et al., 2006; Long et al., 2011; Larkan et al., 2013, 2015; Van de Wouw et al., 2014). On the other hand, better progress has been achieved with *L. maculans* where 14 avirulence genes have been identified, and seven of them, namely *AvrLm1, AvrLm4-7, AvrLm6, AvrLm11, AvrLmJ1*, *AvrLm2,* and *AvrLm3* have been cloned (Gout et al., 2006; Fudal et al., 2007; Parlange et al., 2009; Balesdent et al., 2013; Van de Wouw et al., 2014, 2016; Ghanbarnia et al., 2015; Plissonneau et al., 2016). Interestingly, some of these avirulence genes have been found to be clustered, with clusters *AvrLm1*-2-6 and *AvrLm3*-4-7-9-*AvrLepR1* being the notable examples (Balesdent et al., 2002; Ghanbarnia et al., 2012). For the most part, avirulence genes, including *L. maculans Avrs*, are small-secreted proteins (SSPs) with several cysteine residues, and often referred to as effectors (Stukenbrock and McDonald, 2009; Rouxel et al., 2011).

Effectors are key elements in fungal virulence against plants and particularly important during the biotrophic phase of infection (Kloppholz et al., 2011). *L. maculans*, being a hemibiotroph, will initially rely on effectors to suppress plant defenses, and then will subsequently use effectors to kill plant cells. In *L. maculans*, most putative or candidate effectors are localized in transposon-rich repetitive DNA and are affected by a repeat-induced point mutation (Rouxel et al., 2011). The putative effector genes are mostly over-expressed during primary leaf infection (Soyer et al., 2014). Such information about the genomic localization, gene organization, and expression dynamics is helpful to understand the host-pathogen interaction and more particularly for the identification of *bona fide* effectors. Similarly, transcription factors (TFs), and carbohydrate active enzymes (CAZymes) are known to play a pivotal role in host-pathogen interactions, and are, along with effectors, prime targets for studying virulence factors in fungi (Guo et al., 2011; Lombard et al., 2014; Lowe et al., 2014; Malinovsky et al., 2014).

Transcription factors are essential players in the signal transduction pathways. In *L. maculans*, TF LmStuA is found to be required for normal growth, perithecium formation, pathogenicity on oilseed rape leaves, and expression of effectors (Soyer et al., 2015). The silencing of *LmStuA* triggers drastic effects on the morphogenesis and pathogenicity of *L. maculans*, indicating that it may affect a large number of genes and pathways (Soyer et al., 2015). Similarly, several CAZymes in *L. maculans* genome have been predicted to have a functional role in pathogenesis (Lowe et al., 2014). CAZymes are important to break down the polysaccharides of plant cell walls, to establish infection, and also, to facilitate access to nutrients during the necrotrophic and saprophytic growth phases. For instance, global transcriptomic analyses of the hemibiotroph *Colletotrichum higginsianum* revealed that genes encoding secreted proteins without a functional annotation are expressed predominantly during the initial biotrophic phase, whereas expression of secreted lytic enzymes (including CAZymes) was higher in the subsequent necrotrophic phase (O'Connell et al., 2012). A similar finding was observed in *Leptosphaeria biglobosa,* a necrotroph expressing more cell wall degrading genes than *L. maculans* (Lowe et al., 2014). However, *L. maculans* expressed many genes in the carbohydrate binding module (CBM) class of CAZymes, particularly CBM50 genes, during early infection, and cell wall degrading enzymes at later stages of growth (Lowe et al., 2014). This suggests that expression of secreted proteins without functional annotation is a general feature of biotrophy, whereas expression of cell wall degrading enzymes is generally associated with necrotrophy. Other important necrotrophy-related genes code for sirodesmin PL (Sir), a phytotoxin that belongs to the class of epipolythiodioxopiperazine (ETP). The production of sirodesmin by *L. maculans* is thought to be suppressed by brassinin, a phytoalexin of canola (Pedras et al., 1993). In *L. maculans*, a cluster of 23 genes including polyketide synthase (PKS), non-ribosomal peptide synthase (NRPs) genes, and 18 Sir genes have been identified (Gardiner et al., 2004).

The infection process is highly dependent on host recognition and molecular cross-talk between the host and the pathogen where pathogenicity-related genes play an important role.

However, any given host-pathogen interaction is a very complex phenomenon, which makes it difficult to understand the factors dictating compatibility or incompatibility. In Arabidopsis, Huibers et al. (2009) were able to discriminate genes induced during compatible from incompatible interactions with the downy mildew pathogen *Hyaloperonospora arabidopsidis* (downy mildew). Similarly, other studies have been conducted to compare gene expression profiling under compatible and incompatible interactions (Wang et al., 2010; Sestili et al., 2011; Li et al., 2015).

Expression profiling during the development of disease is an effective approach to better understand the pathogenesis process. Current improvements in sequencing technologies have provided new opportunities to evaluate gene expression under different conditions by sequencing the entire transcriptome (Wang et al., 2009). Compared to other hybridization based transcriptome profiling platforms like microarrays, RNA-seq provides access to simultaneous transcript discovery and abundance estimation, identification of differentially-expressed genes (DEGs) and associated molecular cellular pathways, and alternative splicing variants (Wang et al., 2009; Trapnell et al., 2012). However, RNA-seq analysis requires scalable, fast, and statistically relevant software tools that can handle complex and large sequence data. Fortunately, considerable efforts have been devoted to the development of specialized software tools to perform effective RNA-seq analysis (Garber et al., 2011; Trapnell et al., 2012; Seyednasrollah et al., 2015; Sonah et al., 2016).

The *L. maculans*-canola compatible interaction has been previously addressed using the RNA-seq approach (Lowe et al., 2014; Haddadi et al., 2016). These studies made significant efforts toward the understanding of susceptible reaction in canola after *L. maculans* infection and provides the first in-depth look into the transcriptomic profile of this interaction. In this study, our objective was to compare the pathogen responses against susceptible and resistant host genotypes in order to obtain a precise definition of the virulence factors expressed by *L. maculans* during its biotrophic and necrotrophic phase. For this purpose, we performed the RNA-seq transcriptome profiling of *L. maculans* inoculated on susceptible and resistant canola lines at four developmental stages over five biological replications. A particular emphasis was placed on the identification of DEGs including effectors, CAZymes, and other pathogenesis-related genes during blackleg disease development in canola.

MATERIALS AND METHODS

Plant Material and *L. maculans* Inoculation

Canola (*B. napus*) breeding lines, Topas DH16516 (Topas-wild), a double haploid line susceptible to *L. maculans* and Topas-*Rlm2*, an introgression line resistant to *L. maculans* isolates carrying *AvrLm2* (Larkan et al., 2016a,b) were used as plant material. Seven-day old seedlings of both resistant and susceptible canola lines grown under controlled environment were point inoculated with pycnidiospores suspension of *L. maculans* isolate D5. *L. maculans* isolate D5 contains known avirulence effectors *AvrLm1*, *AvrLm4-7*, *AvrLm2,* and *AvrLmJ1* but lacks *AvrLm6* (Raman et al., 2012). Five biological replicates each with leaves from eight plants per sample were collected at 3, 5, 7, and 11 days post inoculation (dpi). The *L. maculans* isolate D5 was cultured in V8® agar plates at 25°C. For RNA extraction, two fungal agar plugs were inoculated in V8® liquid media and incubated at 22°C. After 7 days, the mycelium was harvested for RNA extraction.

Sample Preparation and Illumina Sequencing

Total RNA for all samples was extracted using a combined Trizol/Qiagen RNeasy mini kit (Qiagen, Mississauga, ON, Canada). The RNA quality and quantity was accessed using NanoDrop ND-1000 spectrophotometer (NanoDrop technologies) and further verified by agarose gel electrophoresis. Four micrograms of total RNA from all samples were used to make individual barcoded cDNA library using TruSeq RNA library preparation kit v2 with some modifications. Individual library was assessed using the Agilent 2100 Bioanalyzer (Agilent Technologies). The products resulted in a smear with an average fragment size of approximately 260 bp. A total of six individual libraries were pooled using the uniform amount of each library and the quality of the final library pools was also assessed. Single end, 100 bp sequencing was performed using an Illumina HiSeq 2000 sequencer at the Génome Québec Innovation Centre (McGill University, Quebec, Canada).

RNA-seq Data Analysis

RNA-seq reads were quality-checked with fastqc, which performs various quality checks for the raw reads. Read processing was performed by using Trimmomatic software (Bolger et al., 2014). Reads were trimmed from both ends until the average of all 5 bp sliding windows reached a Phred score of 25 or higher and all the sequences shorter than 35 bases were discarded. Processed reads were aligned to the *L. maculans* genome and transcriptome with Tophat2 (Trapnell et al., 2009). Most of the parameters in Tophat was set as default. A mismatch of two bases were allowed for the alignment. The minimum and maximum intron length was set to 50 and 500,000 respectively. Reads aligned to multiple sites were removed prior to further analysis.

Novel transcripts that did not overlap with any annotated transcripts were identified using Cufflink tools. The gene expression level for each annotated as well as non-annotated novel transcripts were estimated as the number of Fragments (reads) per kilobase of transcript per million mapped reads (FPKM), considering only uniquely mapped reads in exonic region by using the Cufflink software. The differentially expressed genes (DEGs) were identified using four different tools including Cuffdiff (Trapnell et al., 2012), EdgeR (Robinson et al., 2010), DESeq2 (Love et al., 2014), and CLC Genomics Workbench. We used FDR < 0.0001 and the absolute value of $\log_2$ (Fold-change) >1.5 relative to axenic culture as the threshold for the identification of DEGs. We used quartile normalization that excludes the top 25% of expressed genes to improve detection of less abundant genes. With the Cufflink software, we used -M option to mask rRNA, -b, and -u option for bias correction and option to normalize for aligned tags instead of total tags. HTseq tool was used to count reads prior to

DEGs identification. The DESeq2 package was used to estimate sample quality (PCA) and the expression level of transcripts. The regularized rlog transformation and variance stabilizing transformation were used for data visualization. Time course analysis for all the four time points were carried out to find the genes that reacted in a time-specific manner using DESeq2 package.

Functional Annotation and Gene Ontology

Standard gene ontology (GO) was used to describe DE gene functionality, a hypergeometric test and the $p < 0.05$ of Pearson Chi-Square test between the gene numbers of the two input dataset were used to map the DT genes to GO terms based on the BGI WEGO (Web Gene Ontology Annotation Plot, http://wego.genomics.org.cn/cgi-bin/wego/index.pl). Single enrichment analysis (SEA), a function of AgriGO was used to examine GO term enrichment using *Magnaporthe grisea* as a background reference using Fisher statistical test and 0.05 significance level and other default parameters. Transcription factors were identified using Fungal Transcription Factor Database (FTFD) (Park et al., 2008). The FTFD pipeline sorts fungal TFs initially based on the relevant InterPro terms like DNA-binding motifs, and then the false-positive TFs are filtered with different criteria. CAZymes were identified using dbCAN server (Yin et al., 2012). The dbCAN hosted an analytical pipeline compiled with CDD (conserved domain database) search, family specific hidden Markov model and literature curation (Yin et al., 2012). For the classification of putative secreted peptidases, the sequences for the secreted proteins predicted by WoLF PSORT (cutoff score = 15) were submitted to MEROPS Batch Blast analysis (http://merops.sanger.ac.uk, Rawlings et al., 2014).

Identification of Candidate Secreted Effector Proteins (CSEPs)

Predicted protein sequences from the *L. maculans* genome were retrieved from the JGI MycoCosm (http://genome.jgi.doe.gov/Lepmu1/Lepmu1.home.html) (Rouxel et al., 2011; Grigoriev et al., 2014). SignalP (cutoff probability = 0.8), TargetP (cutoff probability = 0.8), Psort (cutoff score = 15), BlastP (cutoff $e = 1e^{-05}$), and TMHMM software tools along with Secretool pipeline were used to predict small-secretory proteins (Petersen et al., 2011; Cortázar et al., 2014). To prioritize candidate effector genes, the entire secretome was analyzed by EffectorP a machine learning method optimized for the prediction of fungal effectors (Sperschneider et al., 2015). Crinkler type effectors were also searched in the *L. maculans* genome with the FEMO software tool implemented in MEME suit by using conserved domain LFLAK (http://meme-suite.org/tools/fimo). Proteins with LFLAK-domain within the initial 100 AA were considered for further analysis. To verify the search parameters, Crinkler effector search was also performed in *Phytophthora sojae* genome and compared with earlier report by Haas et al. (2009). After an initial search with FIMO, candidate Crinkler effectors were analyzed with secretool pipeline and subsequently with effectorP software tool.

RESULTS

Disease Progress on Compatible and Incompatible Host

On plants of either the compatible host Topas-wild or the introgression line Topas-*Rlm2* carrying a major resistance gene, disease symptoms were not observed until 7 dpi. After this asymptomatic early growth stage, symptoms became visible exclusively on Topas-wild plants expanding into clear lesions and zones of chlorotic tissues at 11 dpi. In the case of Topas-*Rlm2* plants, there was no visible lesion beyond the site of inoculation (**Figure 1**). The disease progress on susceptible Topas-wild cotyledons caused by *L. maculans* was similar to that previously described on Westar (Lowe et al., 2014).

Transcriptome Sequencing with the Time Course of Disease Progress

A total of 1.6 billion single-end reads consisting of approximately an average of 33 million reads for each cDNA library were obtained. The entire data set was submitted to SRA NCBI database and can be accessed with accession number SRP078092. The raw reads obtained were uniform across the different libraries. After performing quality assessment and read processing, about 0.1% of the reads with poor quality and shorter length were discarded. Mapping of the processed reads to the *L. maculans* genome showed a very high percentage of mapping for the axenic samples (Supplementary Table 1). The percentage of reads from *in planta* samples mapped to the *L. maculans* reference genome increased over time from <0.5% at 3 dpi to about 12% at 11 dpi in compatible host Topas-wild (**Figure 2**, Supplementary Table 1). By contrast, mapped fungal reads remain stable in the incompatible interaction with Topas-*Rlm2* and were well below 1% even at 11 dpi (**Figure 2**, Supplementary Table 1), a result well in line with the phenotype observed in **Figure 1**. Comparing the percent of mapped reads in the early asymptomatic growth stage in Topas-wild plants, only a marginal increase was observed between 3 and 5 dpi. This percentage more than doubled between 5 and 7 dpi and registered a 10-fold increase from 7 to 11 dpi (Supplementary Table 1).

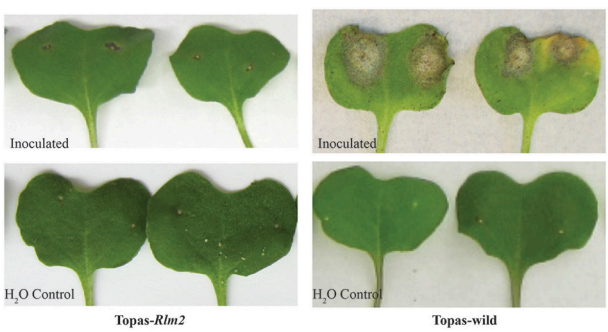

FIGURE 1 | Disease symptoms at 11 days post inoculation on leaves of compatible (Topas-wild) and incompatible (Topas-*Rlm2*) canola host inoculated with *Leptosphaeria maculans* D5 isolate or water.

The principal components (PCs) analysis highlighted a clear differential effect of the treatments along with the uniformity of the five biological replications within a treatment (**Figure 3**). The first principal component explained 58% of the expression variation supporting the large phenotypic differences between the conditions over the time period.

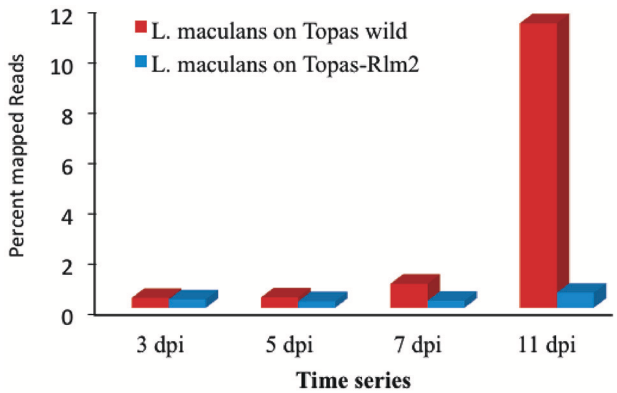

FIGURE 2 | Percentage of mapped reads to the *Leptosphaeria maculans* genome at 3, 5, 7, and 11 days post inoculation (dpi). RNA-seq was performed for *L. maculans* isolate D5 inoculated to Topas-wild (compatible) and Topas-*Rlm2* (incompatible) canola genotypes.

Comparison of Gene Expression Profiling during *In vitro* and *In planta* Growth of *L. maculans*

The number of DEGs in *L. maculans* between *in vitro* axenic samples and samples at different *in planta* growth stages showed an interesting pattern of gene expression turnover over time. The overall pattern of DEGs identified with different software tools was similar (Supplementary Figure 1). The highest number of DEGs for both the compatible (Topas-wild) and incompatible (Topas-*Rlm2*) interactions was recorded in the early events (3 dpi) and was similar in both cases (**Figure 4**). This number was reduced by around three-fold at 5 dpi in both interactions and remained fairly level over the next sampling times in Topas-*Rlm2* plants. On the other hand, it increased steadily in Topas-wild plants to exceed by roughly three times the number of DEGs found in Topas-*Rlm2* plants (**Figure 4**).

When looking at the top 20 upregulated DEGs at 3 dpi in the compatible interaction (Topas-wild), most of them were linked to uncharacterized proteins for which functional annotation was not available (**Table 1**). Since the uncharacterized proteins are unique to *L. maculans*, homology-based annotation failed to

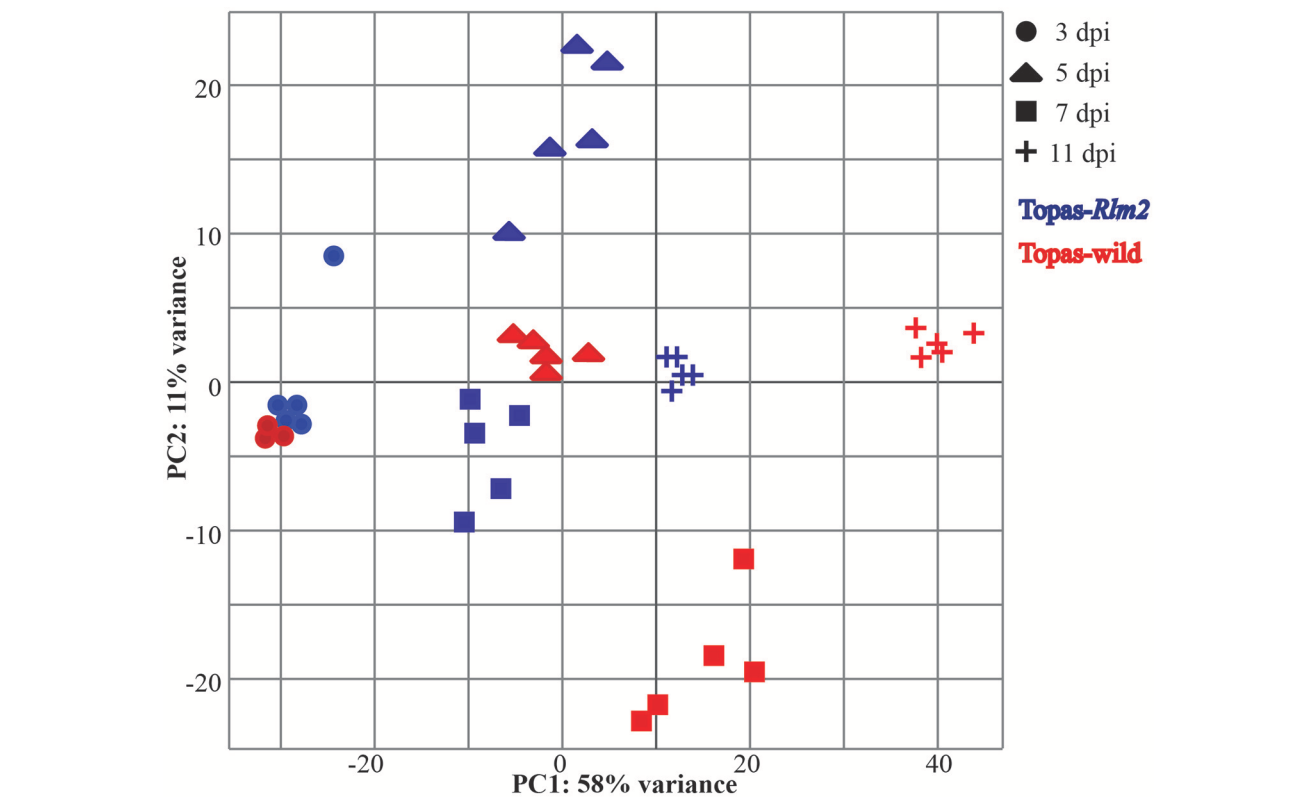

FIGURE 3 | Principal components (PCs) of RNA-seq expression profile obtained for *Leptosphaeria maculans in planta* samples during compatible and incompatible interactions. A total of five biological replications for 3, 5, 7, and 11 days post inoculation (dpi) were used for RNA-seq expression profiling of *L. maculans* inoculated to compatible host Topas-wild (blue) and incompatible host Topas-*Rlm2* (Red).

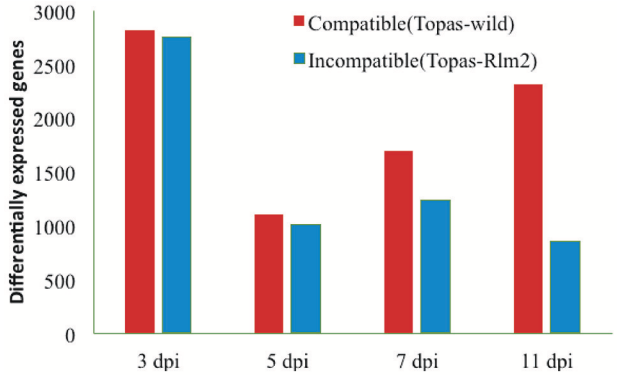

FIGURE 4 | Differentially expressed *Leptosphaeria maculans* genes identified at 3, 5, 7, and 11 dpi during compatible and incompatible interactions. Differentially expressed genes were identified by comparing *in planta* samples with axenic cultures. Analyses were performed with five biological replicates and a threshold value of FDR < 0.0001 and $\log_2$ fold-change > 1.5.

characterize them. Genes involved in chitin binding, fasciclin, and related adhesion glycoproteins known to play roles in early stages of infection were found to be highly upregulated (**Table 1**). Interestingly, of the top 20 upregulated genes of *L. maculans* identified during the compatible interaction with Topas-wild, 18 were also found associated with the incompatible interaction (Topas-*Rlm2*) (**Table 1**, Supplementary Table 2). However, the number of common genes gradually decreased over time to 11, 6, and 4 at 5, 7, and 11 dpi, respectively (**Table 1**, Supplementary Table 2). Time series analysis showed high expression of *Avr* genes during the biotrophic phase at 7 dpi while most of the highly expressed genes during the necrotrophic phase at 11 dpi were associated with molecular functions involved in catalase activity, hydrolases, CAZymes, peptidases, and transporters (**Table 1**, **Figure 5**).

Expression of CSEPs in *L. maculans* during Compatible and Incompatible Interactions

A total of 552 classically secreted proteins were identified using computational pipeline comprising SignalP and TMHMM software tools along with Secretool pipeline. Following further analyses, 134 genes were prioritized as high confidence CSEPs based on the results obtained with EffectorP software. In the case of the compatible interaction with Topas-wild, an important increase in upregulated CSEPs was observed at 7 and 11 dpi, while very limited differences over time were noted in the incompatible interaction (**Figure 6**).

Out of the 134 CSEPs, 35 genes were not expressed in either the compatible or incompatible host. However, a total of 28 genes showed the highest expression level at 7 dpi in the compatible interaction, which would link them to the biotrophic phase of the fungus (**Table 2**). This profile was similar to that of known *Avr* genes, which were mostly found to be highly expressed at 7 dpi in the compatible interaction, with the obvious exception of *AvrLm6* that remained unchanged throughout the sampling periods (**Figures 5**, **7**). The expression patterns of *AvrLm1*, *AvrLm2*, *AvrLm4-7*, *AvrLm11*, and *AvrLmJ1* were similar in the compatible interaction as their expression increased over time to reach a peak at 7 dpi, and subsided at 11 dpi. As for the incompatible interaction, limited expression was observed for all known *Avr* genes with no distinctive pattern (**Table 2**, **Figure 7**). Of additional significance, an expression pattern similar to *Avr* genes was found for 23 other effectors in the compatible interaction, including eight specific to *L. maculans* and not previously reported as effectors (**Table 2**). Of these, gene_6114 and gene_2728 are particularly interesting for their differentially higher expression at 7 dpi in Topas-wild. Finally, gene_9004 showed the highest expression at 7 dpi during the compatible interaction at a level of almost 24,000 FPKM.

In addition to the effectors listed in **Table 2**, 15 other genes identified as CSEPs showed higher levels of expression exclusively during the compatible interaction at 11 dpi when the fungus had entered its necrotrophic phase (**Table 3**). Furthermore, the crinkler effector search performed initially in *P. sojae* identified exactly the same set of proteins reported earlier by Haas et al. (2009) (Supplementary Table 3). This validated the method used here to identify crinkler effectors in *L. maculans* genome. The initial search identified 63 proteins with LFLAK-like domain present within the initial 100 AA (Supplementary Table 4). Further analysis with secretool revealed only five proteins and EffectorP confirmed only one candidate (Gene_2728, Lema_T080290.1) as a crinkler effector (Gene_2728, Lema_T080290.1). Gene_2728 showed the highest expression at 7 dpi during the compatible interaction (Supplementary Figure 2).

Transcription Factors Associated with Effector Expression

TFs regulate the expression of a number of genes simultaneously, and their upregulation during *in vivo* conditions was indicative of their importance in the outcome of the interaction. Both compatible and incompatible interactions were regulated by a large number of upregulated TFs in *L. maculans* in the early events (3 dpi) followed by a sharp decline at 5 dpi (**Figure 8**). As with the phenotypes, a clear distinction between compatible and incompatible interactions appeared at 7 dpi where nearly 100 TFs were upregulated in the former case compared to 40 in the latter, and these differences were even more manifest at 11 dpi (Supplementary Table 5). Among TFs, the LmStuA TF (gene_1191), a member of APSES domain containing proteins was found to be strongly upregulated at 7 dpi in the compatible interaction with Topas-wild, thus suggesting its importance in the infection process. Mostly Zn2Cys6 TFs were upregulated during the compatible interaction (Supplementary Table 5).

Expression of CAZymes in *L. maculans* during Compatible and Incompatible Interactions

Plant-fungal interactions involve a variety of CAZymes that are used by the fungal pathogen to infect its host. RNA-seq data for *L. maculans* infecting compatible host Topas-wild and incompatible host Topas-*Rlm2* showed a high number of

TABLE 1 | List of the top 20 upregulated *Leptosphaeria maculans* genes during the compatible interaction with canola cultivar Topas-wild at each of the four sampling points.

Gene name	Gene ID	Locus	FPKM	SE	*Log_2 (FC)	Padj	Functional annotations
3 dpi							
Gene_11912	Lema_T061640	lm_SuperContig_8_v2:1610355–1610701	12276	1400.46	13.04	0.00E+00	Hypothetical protein
Gene_4884	Lema_T109090	lm_SuperContig_18_v2:862571–862990	14727	2585.81	10.89	0.00E+00	Hypothetical protein
Gene_9702	Lema_T050310	lm_SuperContig_5_v2:114784–120578	1424	229.89	10.79	0.00E+00	Chitin binding/Carbohydrate-Binding Module Family 18
Gene_1799	Lema_T087550	lm_SuperContig_11_v2:702412–703074	8854	1176.77	10.36	0.00E+00	Hypothetical protein (CSEP)
Gene_8310	Lema_T032040	lm_SuperContig_2_v2:2602620–2603501	1040	261.13	10.24	7.00E-159	Hypothetical protein
Gene_11624	Lema_T058760	lm_SuperContig_8_v2:828284–829346	1890	257.48	10	0.00E+00	Hypothetical protein SSP(Effector)
Gene_6862	Lema_T118070	lm_SuperContig_21_v2:752639–754522	1097	214.03	9.74	0.00E+00	G-protein coupled receptor activity
Gene_2936	Lema_T094030	lm_SuperContig_14_v2:218210–219154	1330	153.58	9.56	0.00E+00	Hypothetical protein
Gene_9395	Lema_T042140	lm_SuperContig_4_v2:1136979–1138783	1911	277.28	9.48	0.00E+00	Alcohol dehydrogenase
Gene_6482	Lema_T114270	lm_SuperContig_20_v2:529112–533279 (-)	6078	667.23	8.52	0.00E+00	Hypothetical protein
Gene_8982	Lema_T038010	lm_SuperContig_3_v2:2203740–2205537	1054	150.79	8	0.00E+00	Transporter activity
Gene_11976	Lema_T062280	lm_SuperContig_8_v2:1760041–1760879	2812	828.34	7.86	0.00E+00	Fasciclin and related adhesion glycoproteins
Gene_7649	Lema_T025430	lm_SuperContig_2_v2:804099–805458	1215	335.02	7.7	0.00E+00	Predicted transporter
Gene_11804	Lema_T060560	lm_SuperContig_8_v2:1317923–1319474	1108	232.60	7.65		Hypothetical protein SSP(Effector)
Gene_5070	Lema_T110950	lm_SuperContig_19_v2:299282–300301	1331	384.38	7.19	9.90E-111	Hypothetical protein
Gene_3811	Lema_T093240	lm_SuperContig_15_v2:1293850–1295649	1757	427.33	7.14	0.00E+00	Transporter activity
Gene_5572	Lema_T015460	lm_SuperContig_1_v2:975571–976381	1529	191.58	6.44	0.00E+00	Hypothetical protein
Gene_6173	Lema_T021470	lm_SuperContig_1_v2:2566440–2566907	1504	256.68	6.41	5.90E-221	Hypothetical protein
Gene_2652	Lema_T079530	lm_SuperContig_13_v2:633177–634702	2616	398.51	6.26	0.00E+00	Hypothetical protein
Gene_1331	Lema_T073560	lm_SuperContig_10_v2:445682–445936	1122	371.94	6.22	0.00E+00	Hypothetical protein
5 dpi							
Gene_4884	Lema_T109090	lm_SuperContig_18_v2:862571–862990	33992	1715.82	13.06	0.00E+00	Hypothetical protein
Gene_10161	Lema_T054900	lm_SuperContig_5_v2:1424583–1425111	1399	427.40	12.98	2.50E-90	Hypothetical protein
Gene_2216	Lema_T084480	lm_SuperContig_12_v2:827863–828642	1931	368.22	11.52	3.90E-96	Predicted protein SSP(Effector)
Gene_10273	Lema_T056020	lm_SuperContig_5_v2:1712896–1714128	1282	381.49	11.44	0.00E+00	Transcription factor
Gene_8310	Lema_T032040	lm_SuperContig_2_v2:2602620–2603501	1143	435.53	11.34	2.20E-214	Oxidoreductase activity
Gene_9395	Lema_T042140	lm_SuperContig_4_v2:1136979–1138783	1072	263.45	9.61	0.00E+00	Alcohol dehydrogenase
Gene_11804	Lema_T060560	lm_SuperContig_8_v2:1317923–1319474	2104	547.85	9.55	0.00E+00	Hypothetical protein (CSEP)
Gene_6173	Lema_T021470	lm_SuperContig_1_v2:2566440–2566907	4527	730.72	8.97	0.00E+00	Hypothetical protein
Gene_6375	Lema_T113200	lm_SuperContig_20_v2:228262–228840	1117	482.45	8.47	1.60E-196	Hypothetical protein (CSEP)
Gene_1799	Lema_T087550	lm_SuperContig_11_v2:702412–703074	1209	279.42	8.46	1.70E-289	Hypothetical protein (CSEP)
Gene_11976	Lema_T062280	lm_SuperContig_8_v2:1760041–1760879	1441	225.72	7.87	0.00E+00	Fasciclin and related adhesion glycoproteins

(Continued)

TABLE 1 | Continued

Gene name	Gene ID	Locus	FPKM	SE	*Log_2 (FC)	Padj	Functional annotations
Gene_6483	Lema_T114280	lm_SuperContig_20_v2:534387–534664	1243	384.15	7.2	0.00E+00	Hypothetical protein
Gene_8491	Lema_T033100	lm_SuperContig_3_v2:491445–491728	1283	356.20	6.66	3.50E-20	Hypothetical protein
Gene_1613	Lema_T076380	lm_SuperContig_10_v2:1509441–1509941	2525	1043.94	6.4	7.30E-75	Hypothetical protein (CSEP)
Gene_616	Lema_T006160	lm_SuperContig_0_v2:2286680–2287371	1062	295.59	6.35	5.50E-208	Hypothetical protein
Gene_7940	Lema_T028340	lm_SuperContig_2_v2:1614035–1614898	4379	1327.86	6.33	0.00E+00	Transporter activity
Gene_415	Lema_T004150	lm_SuperContig_0_v2:1345345–1345518	1090	232.24	6.14	0.00E+00	Aminotransferase/Catalytic activity
Gene_6466	Lema_T114110	lm_SuperContig_20_v2:490947–492054	1030	361.07	5.94	1.90E-196	Ion channel activity
Gene_2652	Lema_T079530	lm_SuperContig_13_v2:633177–634702	1060	337.82	5.92	4.20E-292	Hypothetical protein
Gene_234	Lema_T002340	lm_SuperContig_0_v2:882882–883215	1670	221.35	5.58	1.00E-18	Hypothetical protein
7 dpi							
Gene_6534	Lema_T114790	lm_SuperContig_20_v2:655034–655196	18463	3470.09	18.02	1.30E-126	Predicted protein
Gene_10161	Lema_T054900	lm_SuperContig_5_v2:1424583–1425111	2763	185.07	13.08	1.30E-130	Hypothetical protein
Gene_2216	Lema_T084480	lm_SuperContig_12_v2:827863–828642	5389	739.19	12.12	3.80E-162	Predicted protein SSP(Effector)
Gene_1515	Lema_T075400	lm_SuperContig_10_v2:1026907–1027349	1157	262.25	11.46	2.50E-193	Hypothetical protein
Gene_8929	Lema_T037480	lm_SuperContig_3_v2:1850027–1850254	3062	510.96	11.38	6.90E-256	Hypothetical protein
Gene_11912	Lema_T061640	lm_SuperContig_8_v2:1610355–1610701	2410	453.43	10.77	1.20E-221	Hypothetical protein
Gene_2066	Lema_T082980	lm_SuperContig_12_v2:398032–399219	2890	507.44	10.73	7.10E-274	Hypothetical protein
Gene_8487	Lema_T033060	lm_SuperContig_3_v2:287922–288676	5468	1962.05	10.62	0.00E+00	Hypothetical protein (CSEP)
Gene_10780	Lema_T049660	lm_SuperContig_6_v2:1607018–1607681	3553	316.20	9.31	0.00E+00	Hypothetical protein (AvrLm1)
Gene_170	Lema_T001700	lm_SuperContig_0_v2:571327–571980	1695	466.93	9.31	0.00E+00	Hypothetical protein (CSEP)
Gene_6375	Lema_T113200	lm_SuperContig_20_v2:228262–228840	3556	1067.76	9.26	0.00E+00	Hypothetical protein (CSEP)
Gene_9004	Lema_T038230	lm_SuperContig_3_v2:2336899–2337410	23963	3704.18	9.06	0.00E+00	Hypothetical protein (CSEP)
Gene_616	Lema_T006160	lm_SuperContig_0_v2:2286680–2287371	9230	1311.26	8.58	0.00E+00	Hypothetical protein
Gene_4884	Lema_T109090	lm_SuperContig_18_v2:862571–862990	1940	697.48	8.04	4.40E-135	Hypothetical protein
Gene_2397	Lema_T086290	lm_SuperContig_12_v2:1374587–1375064	2131	209.12	8.04	0.00E+00	Hypothetical protein (AvrLm4-7)
Gene_1613	Lema_T076380	lm_SuperContig_10_v2:1509441–1509941	11945	2426.45	7.76	0.00E+00	Hypothetical protein (CSEP)
Gene_7362	Lema_T123070	lm_SuperContig_25_v2:296506–296973	1952	519.68	7.66	5.40E-226	Hypothetical protein (CSEP)
Gene_234	Lema_T002340	lm_SuperContig_0_v2:882882–883215	12153	4475.87	7.56	0.00E+00	Hypothetical protein
Gene_1799	Lema_T087550	lm_SuperContig_11_v2:702412–703074	1064	240.87	7.38	0.00E+00	Hypothetical protein (CSEP)
Gene_6961	Lema_T119060	lm_SuperContig_22_v2:294086–294450	6654	1114.42	6.32	0.00E+00	Hypothetical protein (AvrLm11)
Gene_11177	Lema_T070880	lm_SuperContig_7_v2:982889–983113	6770	895.39	5.79	0.00E+00	Hypothetical protein (AvrLmJ1)
11 dpi							
Gene_9481	Lema_T043000	lm_SuperContig_4_v2:1367322–1368521	2280	179.23	13.5	0.00E+00	Vacuolar protein sorting-associated protein
Gene_10161	Lema_T054900	lm_SuperContig_5_v2:1424583–1425111	1760	173.39	12.26	6.50E-123	Hypothetical protein

(Continued)

TABLE 1 | Continued

Gene name	Gene ID	Locus	FPKM	SE	*Log_2 (FC)	Padj	Functional annotations
Gene_7308	Lema_T122530	lm_SuperContig_25_v2:145516–147997	1128	265.94	10.79	0.00E+00	Glucose dehydrogenase
Gene_2216	Lema_T084480	lm_SuperContig_12_v2:827863–828642	1906	121.93	10.46	1.50E-131	Predicted protein SSP(Effector)
Gene_11875	Lema_T061270	lm_SuperContig_8_v2:1510198–1511697	1484	458.66	10.25	0.00E+00	Peptidase S26A, signal peptidase I/Proteolysis
Gene_2066	Lema_T082980	lm_SuperContig_12_v2:398032–399219	1316	182.72	9.44	1.20E-212	Hypothetical protein
Gene_11099	Lema_T070100	lm_SuperContig_7_v2:754032–755352	2233	136.92	9.05	0.00E+00	Peptidoglycan-binding LysM (Lm5LysM)
Gene_170	Lema_T001700	lm_SuperContig_0_v2:571327–571980	1377	101.99	8.84	0.00E+00	Hypothetical protein (CSEP)
Gene_12054	Lema_T063060	lm_SuperContig_9_v2:365423–366979	1857	106.76	8.42	0.00E+00	3-dehydroquinate synthase activity
Gene_10765	Lema_T049510	lm_SuperContig_6_v2:1209331–1209753	15579	1656.89	8.12	1.40E-127	Hypothetical protein
Gene_616	Lema_T006160	lm_SuperContig_0_v2:2286680–2287371	5059	356.09	7.55	0.00E+00	Hypothetical protein
Gene_10767	Lema_T049530	lm_SuperContig_6_v2:1211326–1212274	2212	253.35	7.23	0.00E+00	Glucose/ribitol dehydrogenase
Gene_1012	Lema_T010120	lm_SuperContig_0_v2:3437723–3438128	1319	310.89	7.13	2.50E-235	Hypothetical protein (CSEP)
Gene_9092	Lema_T039110	lm_SuperContig_4_v2:302019–302430	12896	2333.41	7.08	4.20E-155	Response to stress
Gene_304	Lema_T003040	lm_SuperContig_0_v2:1104438–1107822	1149	150.74	6.8	2.70E-294	Haloacid dehalogenase-like hydrolase
Gene_11976	Lema_T062280	lm_SuperContig_8_v2:1760041–1760879	1061	112.38	6.37	6.70E-263	Fasciclin and related adhesion glycoproteins
Gene_7609	Lema_T025030	lm_SuperContig_2_v2:575802–582958	3787	960.67	6.09	1.10E-83	Hypothetical protein
Gene_6173	Lema_T021470	lm_SuperContig_1_v2:2566440–2566907	1252	141.60	6.06	4.20E-177	Hypothetical protein
Gene_9004	Lema_T038230	lm_SuperContig_3_v2:2336899–2337410	2751	214.78	5.78	0.00E+00	Hypothetical protein (CSEP)
Gene_368	Lema_T003680	lm_SuperContig_0_v2:1246649–1246843	1027	216.39	5.24	4.00E-198	Hypothetical protein (CSEP)
Gene_1613	Lema_T076380	lm_SuperContig_10_v2:1509441–1509941	2195	113.31	5.15	6.30E-275	Hypothetical protein (CSEP)
Gene_3471	Lema_T089840	lm_SuperContig_15_v2:160448–161311	746	150.76	7.37	1.30E-257	Cutinase/catalytic activity

**The fold change was estimated by comparing in planta gene expression at 3, 5, 7, and 11 days post inoculation (dpi) with axenic cultures of L. maculans.*

Analyses were performed with five biological replicates. dpi, days post inoculation; FPKM, Fragments per kilobase of transcript per million mapped reads; FC, fold-change; SE, Standard error for FPKM.

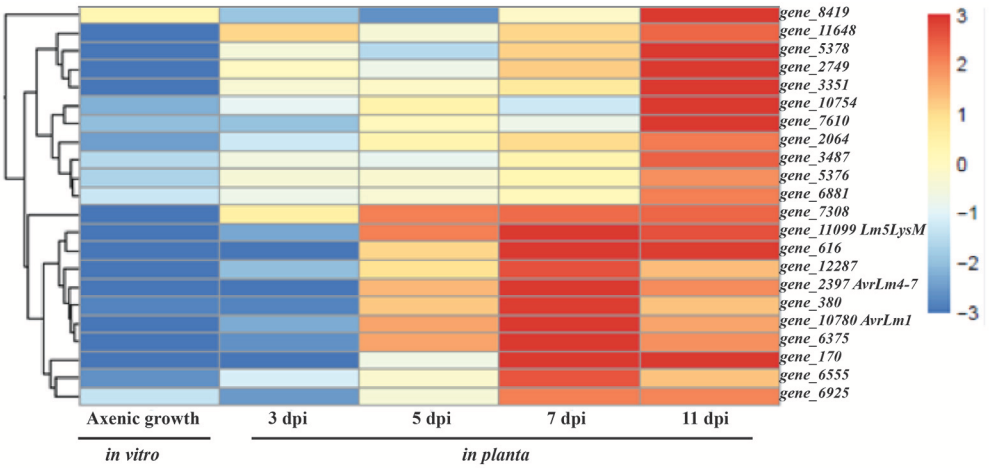

FIGURE 5 | Heat map of time series analysis showing expression pattern of the top 22 genes in *Leptosphaeria maculans* during compatible interaction with host Topas-wild. Gene_2397, gene_10780, and gene_11099 represents *AvrLm4-7*, *AvrLm1*, and *Lm5LysM*, respectively. Analyses were performed with five biological replicates.

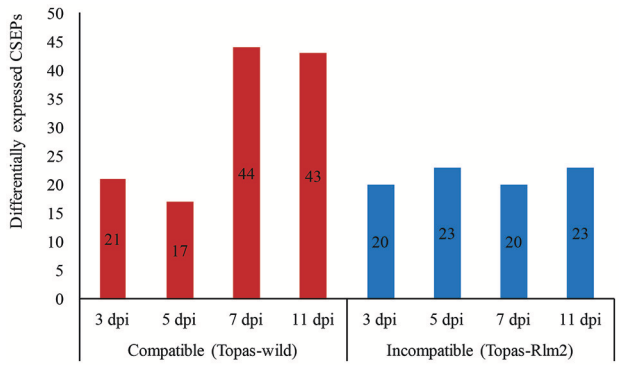

FIGURE 6 | Number of upregulated candidate small secretory effector proteins (CSEPs) identified by RNA-seq analyses performed in *Leptosphaeria maculans* at different stages of disease development during compatible and incompatible interactions. Upregulated genes were identified by comparing *in planta* samples at different growth stages with axenic cultures. dpi, days post inoculation. Analyses were performed with five biological replicates and a threshold value of FDR < 0.0001 and $\log_2$ fold-change > 1.5.

differentially expressed CAZymes at 3 dpi (**Figure 9**). At 5 dpi, this number dropped drastically. It remained fairly constant thereafter in the case of the incompatible interaction (**Figure 9**). By contrast, we observed a rapid increase in differentially expressed CAZymes from 5 to 7 dpi in the compatible interaction, and this number exceeded 200 at 11 dpi, supporting their role in the necrotrophic phase of the fungus.

Among the differentially expressed CAZymes, glycosyl hydrolase (GH), carbohydrate esterase (CE) domain containing genes were more prevalent followed by those belonging to auxiliary activities (AAs) class (Supplementary Table 6). During the early stages (3 dpi) of *L. maculans* infection, cellulose and pectin-degrading enzymes such as PL3, CE4, GH43, and GH3 were upregulated in both interactions compared to axenic growth. At the later stage (11 dpi), CE1, PL1, GT34, and GH28 were only upregulated in the compatible interaction. Carbohydrate binding molecules (CBM) were another prevalent group among DEGs. In *L. maculans*, enzymes with LysM motifs are a well-studied class of CAZymes. Among the LysM domain containing genes present in *L. maculans* genome, *Lm2LysM* (Gene_4592) and *Lm5LysM* (Gene_11099) genes showed a higher level of expression at 7 dpi during the compatible interaction (Supplementary Figure 3). However, *Lm4LysM* (Gene_7646) gene was not expressed during either the compatible or incompatible interaction. The expression pattern for some of the CAZymes at different growth stages of *L. maculans* during compatible and incompatible interaction is shown in Supplementary Figure 4.

Expression of Important Peptidases, Secondary Metabolites, and Necrosis-Inducing Proteins (NIPs)

At the early stages of infection, a similar number of differentially expressed peptidases were observed in both interactions. However, as the fungus transitioned from the biotrophic phase at 7 dpi to the necrotrophic phase at 11 dpi, the difference in the number of differentially expressed peptidases between the compatible and incompatible interaction steadily increases to a ratio of over 60 to 1 at 11 dpi (**Figure 10**, Supplementary Table 7). Among the different classes of peptidases, serine proteases and carboxypeptidases were highly upregulated during *L. maculans* compatible interaction (**Figure 11**, Supplementary Table 7).

In *L. maculans*, a cluster of 23 genes including PKS, NRPs genes and 18 Sir genes have been identified (Gardiner et al., 2004). Most of these genes showed a similar pattern of expression at all the stages of infection with a higher expression at 11 dpi compared to early growth stages of *L. maculans in planta* (Supplementary Figure 5A). By contrast,

TABLE 2 | Expression pattern of 28 effector proteins, including known *Avr* genes, during *Leptosphaeria maculans* compatible and incompatible interactions with canola.

Gene name	Gene ID	Expression value (FPKM*)								*Avr* genes	Previously reported
		Topas-wild (compatible)				Topas-*Rlm2* (incompatible)					
		3 dpi	5 dpi	7 dpi	11 dpi	3 dpi	5 dpi	7 dpi	11 dpi		
Gene_9004	Lema_T038230	0.0	122.3	23963.3	2751.1	0.0	106.3	257.6	38.1		1
Gene_1613	Lema_T076380	161.7	2525.2	11944.8	2194.9	79.6	1065.7	1667.9	435.4		1
Gene_1720	Lema_T086760	0.0	299.4	8458.8	2802.2	7.9	744.5	1618.6	1428.4		1
Gene_11177	Lema_T070880	77.5	928.2	6769.7	2786.3	10.6	106.3	487.2	375.2	*AvrLmJ1*	1.2
Gene_6961	Lema_T119060	51.0	1646.3	6653.6	1346.6	32.0	899.8	627.7	263.3	*AvrLm11*	2
Gene_8487	Lema_T033060	82.9	1626.7	5468.1	728.6	91.9	463.7	322.1	58.5		1
Gene_12203	Lema_T064550	361.8	939.2	4087.3	3933.3	350.5	1046.2	470.3	385.3		
Gene_2817	Lema_T081180	32.0	32.3	3930.2	1420.1	30.6	354.6	679.8	164.6		1
Gene_6375	Lema_T113200	67.4	1117.1	3555.8	959.4	23.7	437.1	627.4	188.6		1
Gene_10780	Lema_T049660	57.3	673.4	3553.0	875.5	29.0	108.0	205.8	134.1	*AvrLm1*	2
Gene_7223	Lema_T121680	61.1	448.7	2982.2	1139.6	71.0	323.9	211.3	291.7		1
Gene_6114	Lema_T020880	14.5	937.1	2479.8	722.8	14.4	145.6	8.9	71.3		1
Gene_2397	Lema_T086290	23.6	237.1	2130.8	859.7	18.8	64.8	134.7	116.7	*AvrLm4-7*	2
Gene_7362	Lema_T123070	0.0	87.8	1952.3	412.2	0.0	232.6	93.3	308.9		2
Gene_1698	Lema_T086540	15.8	411.8	1775.8	607.6	18.6	230.1	110.7	118.2		1
Gene_170	Lema_T001700	0.0	41.2	1695.1	1377.3	17.5	297.1	289.5	150.6		
Gene_6860	Lema_T118050	385.1	636.1	1551.7	918.3	325.5	351.1	233.1	192.1		1
Gene_2728	Lema_T080290	0.5	1.6	804.9	112.6	17.7	49.6	124.6	141.4		
Gene_5357	Lema_T013310	225.6	210.0	574.7	236.9	137.6	65.9	43.7	21.3		
Gene_10809	Lema_T049950	0.0	62.8	526.2	154.7	5.2	12.4	20.3	20.2	*AvrLm2*	1
Gene_8681	Lema_T035000	0.0	296.1	466	56.8	0.0	75.9	83.1	157.4		1
Gene_7202	Lema_T121470	19.3	116.8	453.4	211.5	7.3	45.3	22.4	49.2		
Gene_7203	Lema_T121480	0.0	85.6	435.3	97.3	0.0	18.0	59.7	0.0		1.2
Gene_3097	Lema_T095640	48.1	40.4	369.8	155.8	59.6	219.7	185.9	66.1		1
Gene_11572	Lema_T058240	0.0	0.0	300.2	3.7	0.0	17.5	225.4	0.0		
Gene_9602	Lema_T044210	0.0	56.1	136.2	54.6	0.0	19.9	3.3	1.1		1
Gene_11574	Lema_T058260	0.0	0.0	130.6	2.9	0.0	0.0	110.4	16.6		
Gene_11156	Lema_T070670	57.9	30.8	89.1	25.1	22.5	5.3	3.5	9.2		

RNA-seq analysis was performed for L. maculans isolate D5 inoculated to Topas-wild (compatible) and Topas-Rlm2 (incompatible) canola genotypes.
**Analyses were performed with five biological replicates. dpi, days post inoculation; FPKM, Fragments per kilo-base of transcript per million mapped reads; 1, (Haddadi et al., 2016); 2, (Lowe et al., 2014).*

Sir O (oxidoreductase) and Sir T (thioredoxin reductase) showed higher level of expression at both 3 dpi and 11 dpi (Supplementary Figure 5A). However, comparative analyses indicated that there was no difference in expression at 3 dpi between the interactions (Supplementary Figure 5B). Most of the NRPs showed high level of expression at 3 dpi and 11 dpi but NRP gene_904 showed high expression at 7 dpi (FPKM 876) that receded at 11 dpi (FPKM 112.2). For the two necrosis- and ethylene inducing proteins (Neps) in *L. maculans*, Nep1-like proteins (NPP1, gene_11090) showed higher expression during the pathogenic phases of the fungus (Supplementary Table 8).

Functional Categorization and Gene Ontology (GO) Enrichment of the DEGs

Differential molecular responses in *L. maculans* under compatible and incompatible interactions were observed based on the functional categorization of DEGs (**Figure 11**, Supplementary Figure 6). The DEGs were grouped into three main classes, molecular function, cellular component, and biological process, and several subclasses based on gene ontology terms assigned using WEGO tool. During early asymptomatic stage at 3 dpi, upregulated genes with similar functional categories were observed under both conditions (Supplementary Figure 6). However, the molecular responses of *L. maculans* between the compatible and incompatible hosts differed significantly over time, and were more prominent at 7 and 11 dpi (**Figure 11**; Supplementary Figure 6). The most striking differences were found in the number of genes expressed in each sub-category and in the prevalence of functional categories linked to a transition between the biotrophic and necrotrophic phases such as carboxypeptidases, ligase, peroxidases, cell-wall biogenesis, and stimuli (**Figure 11**).

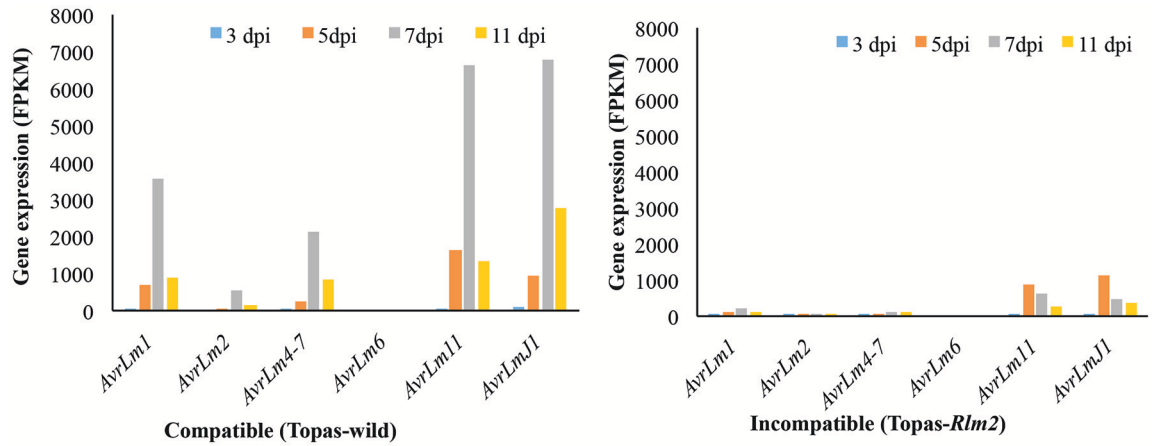

FIGURE 7 | Expression pattern of known *Avr* genes at different disease developmental stages in *Leptosphaeria maculans* during compatible and incompatible interactions. FPKM, Fragments per kilo-base of transcript per million mapped reads; dpi, days post inoculation. Analyses were performed with five biological replicates.

TABLE 3 | Expression pattern of 15 effector proteins highly expressed during the necrotrophic phase of a compatible interaction of *Leptosphaeria maculans* with canola.

Gene name	Gene ID	Expression value (FPKM*)							
		Topas-wild (compatible)				Topas-*Rlm2* (incompatible)			
		3 dpi	5 dpi	7 dpi	11 dpi	3 dpi	5 dpi	7 dpi	11 dpi
Gene_8419	Lema_T124480	62.8	21.6	230.5	4859.8	47.2	112.1	409.5	223.9
Gene_6367	Lema_T023410	0.0	130.8	611.8	2132.9	46.1	265.2	325.7	184.8
Gene_368	Lema_T003680	237.6	357.1	74.3	1026.7	215.5	243.9	0.0	318.7
Gene_3948	Lema_T103880	0.0	0.0	36.6	829.0	20.0	0.0	110.7	2.2
Gene_4618	Lema_T102900	1.0	0.0	197.2	338.5	1.2	0.0	0.0	89.5
Gene_8514	Lema_T033330	8.5	11.1	34.2	258.5	9.5	201.0	72.1	150.0
Gene_2889	Lema_T081900	0.0	11.6	16.7	224.8	0.0	50.0	0.0	4.4
Gene_11386	Lema_T056380	19.0	15.1	156.2	202.1	37.9	21.1	34.0	16.1
Gene_776	Lema_T007760	54.7	55.9	45.3	178.5	44.6	109.6	60.7	90.8
Gene_387	Lema_T003870	7.3	21.3	99.0	174.5	43.8	72.1	44.1	85.2
Gene_775	Lema_T007750	37.0	0.0	32.6	99.1	31.9	49.7	65.1	34.4
Gene_588	Lema_T005880	16.7	25.2	67.5	97.2	24.8	31.7	10.0	4.5
Gene_1689	Lema_T077140	16.6	6.2	26.3	56.8	25.2	34.7	8.6	13.7
Gene_8091	Lema_T029850	27.5	4.4	27.4	45.4	28.4	4.2	27.1	4.5
Gene_4923	Lema_T109480	13.0	4.7	57.3	61.9	9.9	6.3	32.3	3.1

**Analyses were performed with five biological replicates. dpi, days post inoculation; FPKM, Fragments per kilo-base of transcript per million mapped reads.*

Hierarchical clustering and GO enrichment of DEGs during the compatible interaction was also performed using AgriGO tool. Most of the DEGs were found to belong to binding and catalytic functions (Supplementary Figure 7). Localization (GO:0051179, 3.21e-62), cellular process (GO:0009987, 2.37e-258), signal transduction (GO:0007165, 3.48e-13), response to stress (GO:0006950, 8.44e-11), and transcription regulator activity (GO:0030528, 3.3e-15), were the most significantly enriched GO terms at 3 and 5 dpi. At 7 dpi, localization (GO:0051179, 2.35e-61), transport (GO:0006810, 1.68e-61), catabolic process (GO:0009056, 1.03e-11), metabolic process (GO:0008152, 0), gene expression (GO:0010467, 3.93e-38), binding (GO:0005488, 6.84e-319), and transferase activity (GO:0016741, 8.4e-09) were linked to the highest number of genes, and at 11 dpi, hydrolytic activity, mostly monooxygenase activity (GO:0051179, 5.86e-09), transcription regulator activity (GO:0030528, 2.49e-21), transcription factor activity (GO:0051179, 3.14e-14), and regulation of biological process (GO:0050789, 7.09e-26) were the most common enriched GO terms (Supplementary Figure 7).

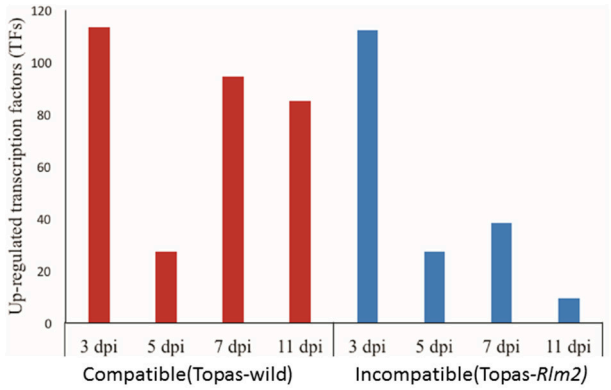

FIGURE 8 | Number of transcription factors (TFs) upregulated in *Leptosphaeria maculans* at 3, 5, 7, and 11 days post inoculation (dpi) on compatible host Topas-wild and incompatible host Topas-*Rlm2*. Upregulated genes were identified by comparing *in planta* samples at different growth stages with axenic cultures. Analyses were performed with five biological replicates and a threshold value of FDR < 0.0001 and $\log_2$ fold-change > 1.5.

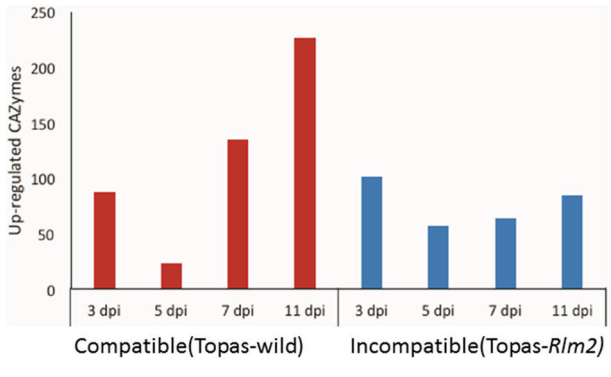

FIGURE 9 | Number of carbohydrate active enzymes (CAZymes) upregulated at 3, 5, 7, and 11 days post inoculation (dpi) of *Leptosphaeria maculans* inoculated to compatible host Topas-wild and in-compatible host Topas-*Rlm2*. Upregulated genes were identified by comparing *in planta* samples with axenic cultures. Analyses were performed with five biological replicates and a threshold value of FDR < 0.0001 and $\log_2$ fold-change > 1.5.

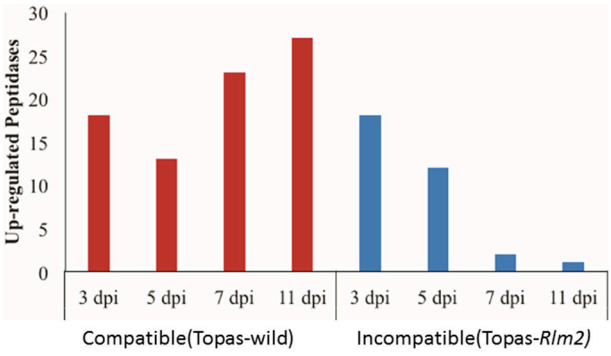

FIGURE 10 | Number of upregulated peptidases observed at 3, 5, 7, and 11 days post inoculation (dpi) of *Leptosphaeria maculans* inoculated to compatible host Topas-wild and in-compatible host Topas-*Rlm2*. Upregulated genes were identified by comparing *in planta* samples with axenic cultures. Analyses were performed with five biological replicates and a threshold value of FDR < 0.0001 and $\log_2$ fold-change > 1.5.

DISCUSSION

In the present study, we performed a comprehensive analysis of the *L. maculans* transcriptome profile during compatible and incompatible interactions with canola. Based on comparative analyses, key genes that dictate both the interaction between canola and *L. maculans* and the different pathogenic stages of the fungus were highlighted. Among the genes of particular significance, our results have identified candidate effectors, TFs, CAZymes, peptidases, and other pathogenesis-related genes that are specifically upregulated as *L. maculans* initiates a biotrophic interaction with the plant, and transitions to a necrotrophic phase. The differential expression of genes during compatible and incompatible interactions offers a precise insight into the mechanisms of pathogenesis in the *L. maculans*-canola interactions.

The effectiveness of transcriptome analyses in plant-pathogen interactions depends primarily on the approach of expression quantification, statistical methods avoiding possible errors and reliance on normalized comparisons, experimental design with sufficient replications and appropriate plant or pathogen material to address relevant biological questions (Williams et al., 2014). In this work, introgression lines Topas-wild and Topas-*Rlm2* were used to study *L. maculans* molecular responses during disease development. Topas-wild is a common cultivar from Canada well known and exploited for its susceptibility to *L. maculans* isolate D5 (Larkan et al., 2013). On the other hand, Topas-*Rlm2* is a recently developed cultivar that carries *Rlm2*, a major resistance gene that prevents infection from *L. maculans* isolate D5 (Larkan et al., 2015). As such, this cultivar provided a unique opportunity to investigate the subtle elements that distinguish the ability of *L. maculans* to infect or not its host. The importance of obtaining good reproducible phenotypes for transcriptomic analyses cannot be overstated as it remains the reference basis for all analyses. On the basis of visual observations, this condition was clearly met as Topas-wild plants exhibited clear symptoms of infection over the course of the experiment that culminated with the presence of extensive necrotic tissues at 11 dpi while the infection never extended beyond the point of inoculation in Topas-*Rlm2* plants. Other studies have reported similar symptom progression at varying time points (Lowe et al., 2014; Haddadi et al., 2016), thus suggesting that experimental conditions can influence the rapidity with which *L. maculans* can infect its host. For this reason, it is critical to ensure that sampling procedures include enough replications that will capture an accurate biological variability within a condition. In this work we have used five biological replications to enhance both the biological and statistical power to compare gene expression across stages and conditions. We have also collected the whole infected cotyledons for analysis to achieve a thorough

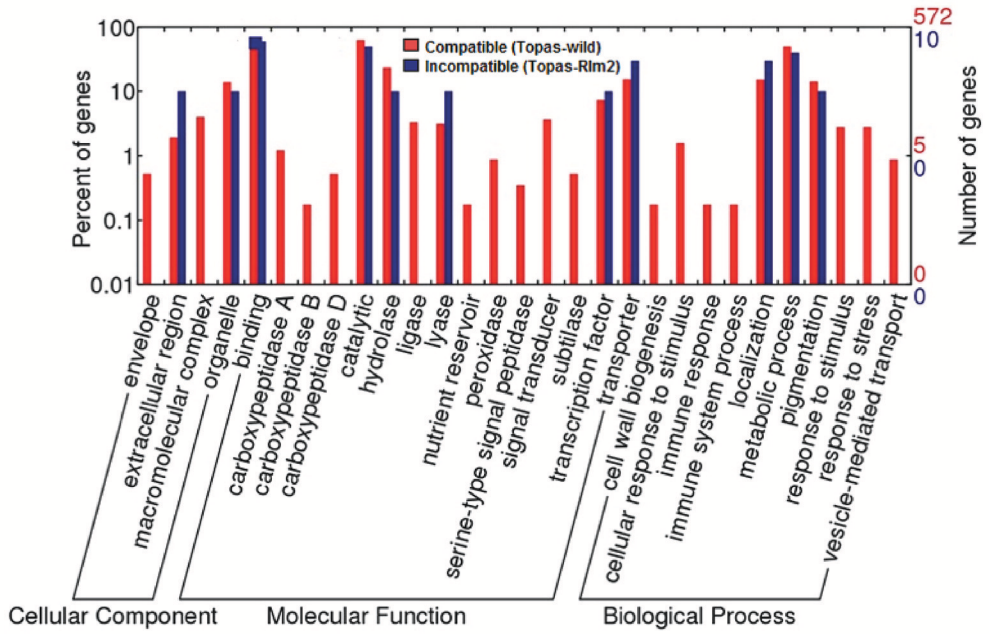

FIGURE 11 | Functional categorization of upregulated genes at 7 days post inoculation (dpi) during compatible and incompatible canola-*Leptosphaeria maculans* interactions. The right y-axis indicates the number of genes in a category. The left y-axis indicates the percentage of a specific category of genes in the main category. Upregulated genes were identified by comparing *in planta* samples with axenic cultures. Analyses were performed with five biological replicates and a threshold value of FDR < 0.0001 and $\log_2$ fold-change > 1.5.

understanding of pathogen transcriptome activities at cotyledon level during infection. This approach was validated by our PC analysis (see **Figure 3**) where the clustering of samples confirmed a uniformity within a given treatment and a variability among treatments thereby supporting that observed phenotypes were indeed associated with differential gene expression. This further supported subsequent statistical analyses of DEGs.

Expression of Known *Avrs* and CSEPs during Biotrophic and Necrotrophic Phases

Several *Avr* and *R* genes have been identified and/or proposed to play a role in the *L. maculans*-canola interaction (Balesdent et al., 2002; Ghanbarnia et al., 2012). Following our analyses, all known *Avr* genes observed by Lowe et al. (2014) were also found to be highly expressed at 7 dpi, and reduced in their expression at 11 dpi in the compatible interaction. Based on a comparison with Topas-*Rlm2*, it is apparent that the period 5–7 dpi harbors the biotrophic phase of *L. maculans* and 11 dpi is more consistent with the necrotrophic phase. As such the differential expression of *Avrs* at 7 dpi indicates that some of them are clearly involved primarily in the establishment of biotrophy, and possibly the transition to necrotrophy but are no longer relevant when *L. maculans* has entered its necrotrophic phase.

With the availability of full genome sequences and more advanced computational tools and pipelines, we were able to identify and characterize effectors in *L. maculans* and better address their potential role/functionality. From strict computational predictions, there are 552 classically secreted proteins in *L. maculans,* which represents an unrealistic number in terms of functional effectors (Sonah et al., 2016). Recently developed tools based on machine learning were used here to further prioritize 134 CSEPs that showed evidence of upregulation in RNA-seq data. At 3 dpi, which corresponded to an asymptomatic growth phase, a common set of effectors highly expressed in both the compatible and incompatible conditions was observed, which suggests they play a minimal role in the fate of the interaction. By contrast, the expression pattern of effectors varied drastically between the compatible and incompatible conditions at 7 dpi. This approach allowed to narrow down the list of possible functional effectors to 28 that were uniquely upregulated at 7 dpi only under compatible conditions and thus presumed to be important for the establishment and maintenance of the biotrophic phase. As a matter of fact, many of the identified effectors here were either known *Avr*, or genes for which a role in pathogenicity was suggested (Haddadi et al., 2016). In addition, eight new effectors are proposed on the basis of their features and expression, and should be interesting candidates in future functionality assays. The studies by Haddadi et al. (2016) and Lowe et al. (2014) used different strains of *L. maculans*, which explains the differences in the number of differentially expressed effectors. For instance, *AvrLm6* was not expressed in our study since the *L. maculans* strain D5 does not have *AvrLm6*. This suggests that it should be important to properly assess resistant germplasm with specific *L. maculans* strains present in a given region.

Compared to biotrophic effectors, very few effectors responsible for the necrotrophic phase are known (Lo Presti et al., 2015). In the present study, on the basis of comparative

expression in compatible and incompatible interactions, we have identified 15 effectors that were distinct from *Avr* genes (and associated effectors) in their chronology of expression. This suggests that these effectors are specific to the necrotrophic phase of the fungus and that *L. maculans*, as a hemibiotroph, has indeed evolved different mechanisms to support its biotrophic and necrotrophic phase. At the same time, high expression of a single crinkler-type effector at 7 dpi in *L. maculans* suggests its involvement in the transition from a biotrophic to a necrotrophic phase. However, the occurrence of a single crinkler in *L. maculans* compared to 74 in *P. sojae* suggests that *L. maculans* does not have the crinkler-mediated mechanism leading to the necrotrophic phase found in *P. sojae* and other oomycetes.

A biotrophic-necrotrophic effector system that has been well studied is that of *Phytophthora infestans* in its interaction with potato (Whisson et al., 2007). During the biotrophic phase, *P. infestans* secretes AVR3a from its haustoria to suppress cell-death; as the oomycete moves to a necrotrophic stage, *AVR3a* is downregulated (Whisson et al., 2007). Similarly, our results showed that all 28 genes, including known *Avr* genes, were highly expressed during the biotrophic phase at 7 dpi and their expression reduced during the necrotrophic phase at 11 dpi. The same genes showed limited or no expression in the incompatible interaction. This suggests that these genes produce functional effectors and are key factors responsible for cross-talk between *L. maculans* and its host. Another gene found here, *Lm5LysM*, is highly expressed at 7 dpi and shows homology with the *SLP1* gene of *M. grisea* that is expressed at the interface between the fungal cell wall and host cell plasma membrane during biotrophic invasion. The LysM-type effectors have been previously associated with biotrophy and shown to be involved in plant-fungus interactions (Gust et al., 2012; Kombrink and Thomma, 2013; Lowe et al., 2014).

Expression Pattern of NLPs Confirming the Necrotrophic Stage in *L. maculans*

In the present study, the highest level of expression for Lm-NLP (gene_11090) gene at 11 dpi, as *L. maculans* entered into its necrotrophic phase, is an observation consistent with the results of Haddadi et al. (2016). Indeed, these authors used the NLP gene expression profile as a means to distinguish genes related to the biotrophic or necrotrophic phase in *L. maculans*; the induction of necrosis by Lm-NLP was confirmed with a transient assay in tobacco (Haddadi et al., 2016). Our results do confirm that the highest expression of NLPs is synchronized with the necrotrophic phase, while that of known *Avrs* with the biotrophic phase. *Avrs* and *NLPs* can thus be considered as valid markers to characterize CSEPs as biotrophic or necrotrophic effectors. Similar findings were observed in *P. infestans* where INF1 and Nep1-like effectors are secreted at later stages of infection that correspond to *P. infestans* transitioning from a biotrophic to a necrotrophic stage (Kanneganti et al., 2006).

Expression Dynamics of CAZymes and TFs

The increasing number of upregulated CAZymes from 5 to 11 dpi in the compatible interaction can be related to the biphasic life style of *L. maculans* as previously suggested by Lowe et al. (2014). This is particularly relevant when compared to the incompatible interaction, where this number remained relatively unchanged over the course of infection. Our results showed that GH, CE, and AA were the most prevalent groups of CAZymes among upregulated genes. During the early stages (3 dpi) of *L. maculans* infection, mostly cellulose and pectin-*degrading* enzymes were the most prevalent groups of CAZymes among upregulated genes. On the other hand, GH, CE and AA families were predominantly upregulated during the necrotrophic stage. Pathogenic fungi face the plant cell wall as a first barrier to establish infection. Plant cell walls are mainly composed of carbohydrates and glycoproteins. To breakdown this barrier, plant pathogenic fungi need to secrete a diverse range of carbohydrate-active enzymes (CAZymes). However, our results clearly showed that the release of CAZymes in the early stages is not a key determinant of the interaction since their number and expression were similar in both interactions.

CAZymes are also involved in nutrient uptake and those prominently expressed at later stages of infection are thought to be involved in uptake of amino acid and sugars from the host. Our results bring stronger support to the concept suggested by Lowe et al. (2014) that CAZymes play an important role in *L. maculans*-canola interaction, notably during the establishment of necrotrophy.

Biphasic expression turnover similar to that of CAZymes was also observed with TFs. As the infection progressed in the compatible interaction, a much higher number of differentially expressed TFs was noted especially from 5 to 7 dpi. This period is critical in the fate of the interaction since it is clearly synchronized with the establishment of the infection in the compatible interaction. Of particular importance, the LmStuA TF, a member of APSES domain-containing proteins, showed its highest expression at 7 dpi in *L. maculans* interaction with Topas-wild. The expression profile of APSES domain-containing genes observed in this study is well aligned with an earlier report by Soyer et al. (2015). The StuA TF was found to be involved in morphogenesis, metabolites production and effector regulation (Baeza-Montañez et al., 2015; Soyer et al., 2015). Recently, StuA was suggested to play a key role in the *L. maculans*-canola interaction since its silencing led to a reduced expression of *AvrLm1*, *AvrLm6,* and *AvrLm4-7*, at 7dpi (Soyer et al., 2015). Moreover, the Zn2Cys6 TFs were upregulated in the compatible interaction supporting its role in regulating pathogenicity-related genes during the biotrophic phase. The Zn2Cys6 TFs have been reported to be involved in different regulatory functions. They are also unique to fungi and have been extensively studied in *Saccharomyces cerevisiae* and *Aspergillus nidulans* (Shimizu et al., 2003; Vienken et al., 2005).

Secondary Metabolites Involved in the Pathogenesis of *L. maculans*

Secondary metabolites like NRPs and phytotoxins such as sirodesmin were found to have a differential expression

pattern between the compatible and incompatible interactions. Differences in gene expression pattern between the compatible and incompatible interaction were observed for NRPs, known to be involved in the production of phytotoxins, siderophores, and pigments, mostly at 11 dpi. Another important phytotoxin involved in the establishment of necrosis is sirodesmin, which is regulated by Sir genes (Gardiner et al., 2004; Haddadi et al., 2016). Most Sir genes were found to be highly expressed at 11 dpi compared to *in planta L. maculans* early growth stages in this study. A notable exception was SirO and SirT, which were highly expressed at 3 dpi and are thought to be involved in the production of sirodesmin early in the infection process. Indeed, Gardiner et al. (2004) have also reported significant amount of sirodesmin production at 4 dpi with *L. maculans*. On the other hand, the fact that SirT was equally expressed in the compatible and incompatible interactions at 3 dpi in our work would suggest that additional factors must complement their activity for infection to occur.

Based on our WEGO functional annotation, the respective vigorous and restricted growth of *L. maculans* on the compatible and incompatible hosts correlated very well with enrichment of genes in functional categories. Toward the later stages of the experiment, very few classes of functional categories were represented in the incompatible interaction, an observation that clearly confirms the inability of *L. maculans* to infect Topas-*Rlm2*. However, it is not possible to conduct robust statistical analyses because of the disparity in the number of genes between the compatible (572) and incompatible interactions (10). Nevertheless, these analyses give a good qualitative visualization of the genes and functions, and their relative importance in the case of compatibility. Interestingly, these analyses also highlighted in the compatible interaction how specific functional classes were indicative of the biotrophic or necrotrophic stage, and the transition from one to the other.

Validation of DEGs identified with transcriptome profiling is always a concern to build a confidence about the significance of results. The validation of DEGs by qPCR is expected for the microarray studies or transcriptomic studies with no or limited biological replications (Deshmukh et al., 2010; Xie et al., 2016). For instance, microarray studies mostly relied on qPCR to validate the results since there is a limit for the number of probes hybridized to the target in microarrays. Therefore, the highest level of gene expression is never truly represented for highly expressed genes. This also leads to a bias of data normalization and reduced linear range. By contrast, RNA-seq provides digital expression for the entire transcripts without any minimum or maximum count limit. In our study, we have used five replications, in line with the robust standards accepted for RNA-seq experiments (Fang and Cui, 2011). This is further supported by the fact that all previously identified Avr genes (*AvrLm1*, *AvrLm4-7*, *AvrLm11*, *AvrLmJ1*, *AvrLm2*) had an expression pattern consistent with expectations and previous reports (Lowe et al., 2014; Haddadi et al., 2016).

CONCLUSIONS

Hemibiotrophic fungi such as *L. maculans* have a distinctive life style that involves complex molecular processes and the expression turnover of thousands of genes. The atlas of gene expression provided here will be helpful to understand the molecular crosstalk between canola and *L. maculans* as it relates to compatibility or incompatibility, and could be exploited toward the deployment of novel strategies to overcome blackleg disease. The comparison made between the compatible and incompatible interaction highlighted the role of specific CSEPs, CAZymes, TFs, and secondary metabolites involved in the infection process. The differential expression pattern observed for these classes of pathogenicity-related genes can serve as a valuable resource to differentiate compatible and incompatible interactions in the context of developing resistant canola germplasm. In addition, our time series analysis based on a comprehensive and comparative differential gene expression as *L. maculans* infects a susceptible or resistant host has brought to light elements that define the biotrophic and necrotrophic phases of the fungus, as well as some of the mechanisms involved in the transition between the two phases.

AUTHOR CONTRIBUTIONS

HS performed RNA extractions, library preparations, data analysis, and compilation; XZ and WF performed all bio-assays, maintained the fungal cultures, and performed RNA extractions, HB developed introgression line and provided seed material, RD and RB contributed to data analysis and overall conclusions, HS and RB wrote initial draft of the MS with final contributions from XZ, RD, HB, and WF. RB designed and directed the project.

FUNDING

This study is funded by the Agri-Innovation program Growing Forward 2, SaskCanola and Agriculture and Agri-Food Canada, and the Canada Research Chair in plant protection to RB.

ACKNOWLEDGMENTS

The authors would like to thank the Agri-Innovation Program Growing Forward 2, SaskCanola, Agriculture and Agri-Food Canada and the Canada Research Chair in Plant Protection to RRB for financial support. The authors also thank Brian Boyle from Institut de Biologie integrative et des Systemes at Laval University for his valuable suggestions regarding RNA-seq library preparations, Caroline Labbé for technical assistance in many aspects of this work, and Paula Parks for help with the greenhouse assays.

SUPPLEMENTARY MATERIAL

The Supplementary Material for this article can be found online at: http://journal.frontiersin.org/article/10.3389/fpls.2016.01784/full#supplementary-material

REFERENCES

Baeza-Montañez, L., Gold, S. E., Espeso, E. A., and García-Pedrajas, M. D. (2015). Conserved and distinct functions of the "stunted" (StuA)-homolog Ust1 during cell differentiation in the corn smut fungus *Ustilago maydis*. *Mol. Plant Microbe Interact.* 28, 86–102. doi: 10.1094/MPMI-07-14-0215-R

Balesdent, M. H., Attard, A., Kühn, M. L., and Rouxel, T. (2002). New avirulence genes in the phytopathogenic fungus *Leptosphaeria maculans*. *Phytopathology* 92, 1122–1133. doi: 10.1094/PHYTO.2002.92.10.1122

Balesdent, M. H., Fudal, I., Ollivier, B., Bally, P., Grandaubert, J., Eber, F., et al. (2013). The dispensable chromosome of *Leptosphaeria maculans* shelters an effector gene conferring avirulence towards *Brassica rapa*. *New Phytol.* 198, 887–898. doi: 10.1111/nph.12178

Bolger, A. M., Lohse, M., and Usadel, B. (2014). Trimmomatic: a flexible trimmer for Illumina sequence data. *Bioinformatics* 30, 2114–2120. doi: 10.1093/bioinformatics/btu170

Cortázar, A. R., Aransay, A. M., Alfaro, M., Oguiza, J. A., and Lavín, J. L. (2014). SECRETOOL: integrated secretome analysis tool for fungi. *Amino Acids* 46, 471–473. doi: 10.1007/s00726-013-1649-z

Delourme, R., Chevre, A., Brun, H., Rouxel, T., Balesdent, M., Dias, J., et al. (2006). Major gene and polygenic resistance to *Leptosphaeria maculans* in oilseed rape (*Brassica napus*). *Eur. J. Plant Pathol.* 114, 41–52. doi: 10.1007/s10658-005-2108-9

Deshmukh, R., Singh, A., Jain, N., Anand, S., Gacche, R., Singh, A., et al. (2010). Identification of candidate genes for grain number in rice (*Oryza sativa* L.). *Funct. Integr. Genomics* 10, 339–347. doi: 10.1007/s10142-010-0167-2

Fang, Z., and Cui, X. (2011). Design and validation issues in RNA-seq experiments. *Brief. Bioinform.* 12, 280–287. doi: 10.1093/bib/bbr004

Fitt, B. D. L., Brun, H., Barbetti, M. J., and Rimmer, S. R. (2006). "World-wide importance of phoma stem canker (*Leptosphaeria maculans* and *L. biglobosa*) on oilseed rape (*Brassica napus*)," in *Sustainable Strategies for Managing Brassica napus (Oilseed Rape) Resistance to Leptosphaeria maculans (Phoma Stem Canker)*, eds B. D. L. Fitt, N. Evans, B. J. Howlett, and B. M. Cooke (Springer), 3–15.

Fudal, I., Ross, S., Gout, L., Blaise, F., Kuhn, M. L., Eckert, M. R., et al. (2007). Heterochromatin-like regions as ecological niches for avirulence genes in the *Leptosphaeria maculans* genome: map-based cloning of AvrLm6. *Mol. Plant Microbe Interact.* 20, 459–470. doi: 10.1094/MPMI-20-4-0459

Garber, M., Grabherr, M. G., Guttman, M., and Trapnell, C. (2011). Computational methods for transcriptome annotation and quantification using RNA-seq. *Nat. Methods* 8, 469–477. doi: 10.1038/nmeth.1613

Gardiner, D. M., Cozijnsen, A. J., Wilson, L. M., Pedras, M. S. C., and Howlett, B. J. (2004). The sirodesmin biosynthetic gene cluster of the plant pathogenic fungus *Leptosphaeria maculans*. *Mol. Microbiol.* 53, 1307–1318. doi: 10.1111/j.1365-2958.2004.04215.x

Ghanbarnia, K., Fudal, I., Larkan, N. J., Links, M. G., Balesdent, M. H., Profotova, B., et al. (2015). Rapid identification of the *Leptosphaeria maculans* avirulence gene AvrLm2 using an intraspecific comparative genomics approach. *Mol. Plant Pathol.* 16, 699–709. doi: 10.1111/mpp.12228

Ghanbarnia, K., Lydiate, D. J., Rimmer, S. R., Li, G., Kutcher, H. R., Larkan, N. J., et al. (2012). Genetic mapping of the *Leptosphaeria maculans* avirulence gene corresponding to the LepR1 resistance gene of *Brassica napus*. *Theor. Appl. Genet.* 124, 505–513. doi: 10.1007/s00122-011-1724-3

Gout, L., Fudal, I., Kuhn, M. L., Blaise, F., Eckert, M., Cattolico, L., et al. (2006). Lost in the middle of nowhere: the AvrLm1 avirulence gene of the Dothideomycete *Leptosphaeria maculans*. *Mol. Microbiol.* 60, 67–80. doi: 10.1111/j.1365-2958.2006.05076.x

Grigoriev, I. V., Nikitin, R., Haridas, S., Kuo, A., Ohm, R., Otillar, R., et al. (2014). MycoCosm portal: gearing up for 1000 fungal genomes. *Nucleic Acids Res.* 42, D699–D704. doi: 10.1093/nar/gkt1183

Guo, M., Chen, Y., Du, Y., Dong, Y., Guo, W., Zhai, S., et al. (2011). The bZIP transcription factor MoAP1 mediates the oxidative stress response and is critical for pathogenicity of the rice blast fungus *Magnaporthe oryzae*. *PLoS Pathog.* 7:e1001302. doi: 10.1371/journal.ppat.1001302

Gust, A. A., Willmann, R., Desaki, Y., Grabherr, H. M., and Nürnberger, T. (2012). Plant LysM proteins: modules mediating symbiosis and immunity. *Trends Plant Sci.* 17, 495–502. doi: 10.1016/j.tplants.2012.04.003

Haas, B. J., Kamoun, S., Zody, M. C., Jiang, R. H., Handsaker, R. E., Cano, L. M., et al. (2009). Genome sequence and analysis of the Irish potato famine pathogen *Phytophthora infestans*. *Nature* 461, 393–398. doi: 10.1038/nature08358

Haddadi, P., Ma, L., Wang, H., and Borhan, M. H. (2016). Genome-wide transcriptomic analyses provide insights into the lifestyle transition and effector repertoire of *Leptosphaeria maculans* during the colonization of *Brassica napus* seedlings. *Mol. Plant Pathol.* 17, 1196–1210. doi: 10.1111/mpp.12356

Howlett, B. J., Idnurm, A., and Pedras, M. S. C. (2001). *Leptosphaeria maculans*, the causal agent of blackleg disease of Brassicas. *Fungal Genet. Biol.* 33, 1–14. doi: 10.1006/fgbi.2001.1274

Huang, Y.-J., Qi, A., King, G. J., and Fitt, B. D. (2014). Assessing quantitative resistance against *Leptosphaeria maculans* (phoma stem canker) in *Brassica napus* (oilseed rape) in young plants. *PLoS ONE* 9:e84924. doi: 10.1371/journal.pone.0084924

Huibers, R. P., De Jong, M., Dekter, R. W., and Van Den Ackerveken, G. (2009). Disease-specific expression of host genes during downy mildew infection of Arabidopsis. *Mol. Plant Microbe Interact.* 22, 1104–1115. doi: 10.1094/MPMI-22-9-1104

Kanneganti, T. D., Huitema, E., Cakir, C., and Kamoun, S. (2006). Synergistic interactions of the plant cell death pathways induced by *Phytophthora infestans* Nep1-like protein PiNPP1. 1 and INF1 elicitin. *Mol. Plant Microbe Interact.* 19, 854–863. doi: 10.1094/MPMI-19-0854

Kloppholz, S., Kuhn, H., and Requena, N. (2011). A secreted fungal effector of *Glomus intraradices* promotes symbiotic biotrophy. *Curr. Biol.* 21, 1204–1209. doi: 10.1016/j.cub.2011.06.044

Kombrink, A., and Thomma, B. P., (2013). LysM effectors: secreted proteins supporting fungal life. *PLoS Pathog.* 9:e1003769. doi: 10.1371/journal.ppat.1003769

Kutcher, H., Brandt, S., Smith, E., Ulrich, D., Malhi, S., and Johnston, A. (2013). Blackleg disease of canola mitigated by resistant cultivars and four-year crop rotations in western Canada. *Can. J. Plant Pathol.* 35, 209–221. doi: 10.1080/07060661.2013.775600

Larkan, N., Yu, F., Lydiate, D., Rimmer, S. R., and Borhan, M. H. (2016a). Single R gene introgression lines for accurate dissection of the Brassica - Leptosphaeria pathosystem. *Front. Plant Sci.* 7:1771. doi: 10.3389/fpls.2016.01771

Larkan, N. J., Lydiate, D. J., Parkin, I. A. P., Nelson, M. N., Epp, D. J., Cowling, W. A., et al. (2013). The *Brassica napus* blackleg resistance gene *LepR3* encodes a receptor-like protein triggered by the *Leptosphaeria maculans* effector AVRLM1. *New Phytol.* 197, 595–605. doi: 10.1111/nph.12043

Larkan, N. J., Ma, L., and Borhan, M. H. (2015). The *Brassica napus* receptor-like protein Rlm2 is encoded by a second allele of the LepR3/Rlm2 blackleg resistance locus. *Plant Biotechnol. J.* 13, 983–992. doi: 10.1111/pbi.12341

Larkan, N. J., Raman, H., Lydiate, D. J., Robinson, S. J., Yu, F., Barbulescu, D. M., et al. (2016b). Multi-environment QTL studies suggest a role for cysteine-rich protein kinase genes in quantitative resistance to blackleg disease in *Brassica napus*. *BMC Plant Biol.* 16:183. doi: 10.1186/s12870-016-0877-2

Li, X., Wu, J., Yin, L., Zhang, Y., Qu, J., and Lu, J. (2015). Comparative transcriptome analysis reveals defense-related genes and pathways against downy mildew in *Vitis amurensis* grapevine. *Plant Physiol. Biochem.* 95, 1–14. doi: 10.1016/j.plaphy.2015.06.016

Lo Presti, L., Lanver, D., Schweizer, G., Tanaka, S., Liang, L., Tollot, M., et al. (2015). Fungal effectors and plant susceptibility. *Annu. Rev. Plant Biol.* 66, 513–545. doi: 10.1146/annurev-arplant-043014-114623

Lombard, V., Golaconda Ramulu, H., Drula, E., Coutinho, P. M., and Henrissat, B. (2014). The carbohydrate-active enzymes database (CAZy) in 2013. *Nucleic Acids Res.* 42, D490–D495. doi: 10.1093/nar/gkt1178

Long, Y., Wang, Z., Sun, Z., Fernando, D. W., McVetty, P. B., and Li, G. (2011). Identification of two blackleg resistance genes and fine mapping of one of these two genes in a *Brassica napus* canola cultivar 'Surpass 400'. *Theor. Appl. Genet.* 122, 1223–1231. doi: 10.1007/s00122-010-1526-z

Love, M., Anders, S., and Huber, W. (2014). Differential analysis of count data–the DESeq2 package. *Genome Biol.* 15, p550. doi: 10.1186/s13059-014-0550-8

Lowe, R. G., Cassin, A., Grandaubert, J., Clark, B. L., Van De Wouw, A. P., Rouxel, T., et al. (2014). Genomes and transcriptomes of partners in plant-fungal-interactions between canola (*Brassica napus*) and two Leptosphaeria species. *PLoS ONE* 9:e103098. doi: 10.1371/journal.pone.0103098

Malinovsky, F. G., Batoux, M., Schwessinger, B., Youn, J. H., Stransfeld, L., Win, J., et al. (2014). Antagonistic regulation of growth and immunity by the Arabidopsis basic helix-loop-helix transcription factor homolog of brassinosteroid enhanced expression2 interacting with increased leaf inclination1 binding bHLH1. *Plant Physiol.* 164, 1443–1455. doi: 10.1104/pp.113.234625

O'Connell, R. J., Thon, M. R., Hacquard, S., Amyotte, S. G., Kleemann, J., Torres, M. F., et al. (2012). Lifestyle transitions in plant pathogenic Colletotrichum fungi deciphered by genome and transcriptome analyses. *Nat. Genet.* 44, 1060–1065. doi: 10.1038/ng.2372

Park, J., Park, J., Jang, S., Kim, S., Kong, S., Choi, J., et al. (2008). FTFD: an informatics pipeline supporting phylogenomic analysis of fungal transcription factors. *Bioinformatics* 24, 1024–1025. doi: 10.1093/bioinformatics/btn058

Parlange, F., Daverdin, G., Fudal, I., Kuhn, M. L., Balesdent, M. H., Blaise, F., et al. (2009). *Leptosphaeria maculans* avirulence gene *AvrLm4-7* confers a dual recognition specificity by the *Rlm4* and *Rlm7* resistance genes of oilseed rape, and circumvents *Rlm4*-mediated recognition through a single amino acid change. *Mol. Microbiol.* 71, 851–863. doi: 10.1111/j.1365-2958.2008.06547.x

Pedras, M. S. C., Taylor, J. L., and Nakashima, T. T. (1993). A novel chemical signal from the "blackleg" fungus: beyond phytotoxins and phytoalexins. *J. Org. Chem.* 58, 4778–4780. doi: 10.1021/jo00070a002

Petersen, T. N., Brunak, S., Von Heijne, G., and Nielsen, H. (2011). SignalP 4.0: discriminating signal peptides from transmembrane regions. *Nat. Methods* 8, 785–786. doi: 10.1038/nmeth.1701

Plissonneau, C., Daverdin, G., Ollivier, B., Blaise, F., Degrave, A., Fudal, I., et al. (2016). A game of hide and seek between avirulence genes AvrLm4-7 and AvrLm3 in *Leptosphaeria maculans*. *New Phytol.* 209, 1613–1624. doi: 10.1111/nph.13736

Raman, R., Taylor, B., Marcroft, S., Stiller, J., Eckermann, P., Coombes, N., et al. (2012). Molecular mapping of qualitative and quantitative loci for resistance to *Leptosphaeria maculans* causing blackleg disease in canola (*Brassica napus* L.). *Theor. Appl. Genet.* 125, 405–418. doi: 10.1007/s00122-012-1842-6

Rawlings, N. D., Waller, M., Barrett, A. J., and Bateman, A. (2014). *MEROPS*: the database of proteolytic enzymes, their substrates and inhibitors. *Nucleic Acids Res.* 42, D503–D509. doi: 10.1093/nar/gkt953

Robinson, M. D., McCarthy, D. J., and Smyth, G. K. (2010). edgeR: a Bioconductor package for differential expression analysis of digital gene expression data. *Bioinformatics* 26, 139–140. doi: 10.1093/bioinformatics/btp616

Rouxel, T., Grandaubert, J., Hane, J. K., Hoede, C., Van De Wouw, A. P., Couloux, A., et al. (2011). Effector diversification within compartments of the *Leptosphaeria maculans* genome affected by repeat-induced point mutations. *Nat. Commun.* 2, 202. doi: 10.1038/ncomms1189

Sestili, S., Polverari, A., Luongo, L., Ferrarini, A., Scotton, M., Hussain, J., et al. (2011). Distinct colonization patterns and cDNA-AFLP transcriptome profiles in compatible and incompatible interactions between melon and different races of *Fusarium oxysporum* f. sp. melonis. *BMC Genomics* 12:122. doi: 10.1186/1471-2164-12-122

Seyednasrollah, F., Laiho, A., and Elo, L. L. (2015). Comparison of software packages for detecting differential expression in RNA-seq studies. *Brief. Bioinform.* 16, 59–70. doi: 10.1093/bib/bbt086

Shimizu, K., Hicks, J. K., Huang, T. P., and Keller, N. P. (2003). Pka, Ras and RGS protein interactions regulate activity of AflR, a Zn (II) 2Cys6 transcription factor in *Aspergillus nidulans*. *Genetics* 165, 1095–1104.

Sonah, H., Deshmukh, R. K., and Bélanger, R. R. (2016). Computational prediction of effector proteins in fungi: opportunities and challenges. *Front. Plant Sci.* 7:126. doi: 10.3389/fpls.2016.00126

Soyer, J. L., El Ghalid, M., Glaser, N., Ollivier, B., Linglin, J., Grandaubert, J., et al. (2014). Epigenetic control of effector gene expression in the plant pathogenic fungus *Leptosphaeria maculans*. *PLoS Genet.* 10:e1004227. doi: 10.1371/journal.pgen.1004227

Soyer, J. L., Hamiot, A., Ollivier, B., Balesdent, M. H., Rouxel, T., and Fudal, I. (2015). The APSES transcription factor LmStuA is required for sporulation, pathogenic development and effector gene expression in *Leptosphaeria maculans*. *Mol. Plant Pathol.* 16, 1000–1005. doi: 10.1111/mpp.12249

Sperschneider, J., Gardiner, D. M., Dodds, P. N., Tini, F., Covarelli, L., Singh, K. B., et al. (2015). EffectorP: predicting fungal effector proteins from secretomes using machine learning. *New Phytol.* 210, 743–761. doi: 10.1111/nph.13794

Stukenbrock, E. H., and McDonald, B. A. (2009). Population genetics of fungal and oomycete effectors involved in gene-for-gene interactions. *Mol. Plant Microbe Interact.* 22, 371–380. doi: 10.1094/MPMI-22-4-0371

Trapnell, C., Pachter, L., and Salzberg, S. L. (2009). TopHat: discovering splice junctions with RNA-Seq. *Bioinformatics* 25, 1105–1111. doi: 10.1093/bioinformatics/btp120

Trapnell, C., Roberts, A., Goff, L., Pertea, G., Kim, D., Kelley, D. R., et al. (2012). Differential gene and transcript expression analysis of RNA-seq experiments with TopHat and Cufflinks. *Nat. Protoc.* 7, 562–578. doi: 10.1038/nprot.2012.016

Van de Wouw, A. P., Lowe, R. G. T., Elliott, C. E., Dubois, D. J., and Howlett, B. J. (2014). An avirulence gene, AvrLmJ1, from the blackleg fungus, *Leptosphaeria maculans*, confers avirulence to Brassica juncea varieties. *Mol. Plant Pathol.* 15, 523–530. doi: 10.1111/mpp.12105

Van de Wouw, A. P., Marcroft, S. J., and Howlett, B. J. (2016). Blackleg disease of canola in Australia. *Crop Pasture Sci.* 67, 273–283. doi: 10.1071/CP15221

Vienken, K., Scherer, M., and Fischer, R. (2005). The Zn(II)2Cys6 putative Aspergillus nidulans transcription factor repressor of sexual development inhibits sexual development under low-carbon conditions and in submersed culture. *Genetics* 169, 619–630 doi: 10.1534/genetics.104.030767

Wang, X., Liu, W., Chen, X., Tang, C., Dong, Y., Ma, J., et al. (2010). Differential gene expression in incompatible interaction between wheat and stripe rust fungus revealed by cDNA-AFLP and comparison to compatible interaction. *BMC Plant Biol.* 10:9. doi: 10.1186/1471-2229-10-9

Wang, Z., Gerstein, M., and Snyder, M. (2009). RNA-Seq: a revolutionary tool for transcriptomics. *Nat. Rev. Genet.* 10, 57–63. doi: 10.1038/nrg2484

Whisson, S. C., Boevink, P. C., Moleleki, L., Avrova, A. O., Morales, J. G., Gilroy, E. M., et al. (2007). A translocation signal for delivery of oomycete effector proteins into host plant cells. *Nature* 450, 115–118. doi: 10.1038/nature06203

Williams, A. G., Thomas, S., Wyman, S. K., and Holloway, A. K. (2014). RNA-seq Data: challenges in and recommendations for experimental design and analysis. *Curr. Protoc. Hum. Genet.* 83, 11.13.1–11.13.20. doi: 10.1002/0471142905.hg1113s83

Xie, J., Li, S., Mo, C., Xiao, X., Peng, D., Wang, G., et al. (2016). Genome and transcriptome sequences reveal the specific parasitism of the nematophagous *Purpureocillium lilacinum* 36-1. *Front. Microbiol.* 7:1084. doi: 10.3389/fmicb.2016.01084

Yin, Y., Mao, X., Yang, J., Chen, X., Mao, F., and Xu, Y. (2012). dbCAN: a web resource for automated carbohydrate-active enzyme annotation. *Nucleic Acids Res.* 40, W445–W451. doi: 10.1093/nar/gks479

Conflict of Interest Statement: The authors declare that the research was conducted in the absence of any commercial or financial relationships that could be construed as a potential conflict of interest.

frontiers in Plant Science

ORIGINAL RESEARCH
published: 22 June 2016
doi: 10.3389/fpls.2016.00847

De novo Transcriptome Sequencing to Dissect Candidate Genes Associated with Pearl Millet-Downy Mildew (*Sclerospora graminicola* Sacc.) Interaction

Kalyani S. Kulkarni[1,2†], Harshvardhan N. Zala[1†], Tejas C. Bosamia[3], Yogesh M. Shukla[4*], Sushil Kumar[1], Ranbir S. Fougat[1], Mruduka S. Patel[1], Subhash Narayanan[5] and Chaitanya G. Joshi[6]*

[1] Department of Agricultural Biotechnology, Anand Agricultural University, Anand, India, [2] Department of Biotechnology, ICAR-Indian Institute of Rice Research, Hyderabad, India, [3] Department of Biotechnology, Junagadh Agriculture University, Junagadh, India, [4] Department of Biochemistry, Anand Agricultural University, Anand, India, [5] Plant Tissue Culture Lab, Anand Agricultural University, Anand, India, [6] Department of Animal Biotechnology, Anand Agricultural University, Anand, India

OPEN ACCESS

Edited by:
Ralph Panstruga, RWTH Aachen University, Germany

Reviewed by:
Patrick Vincourt, Institut National de la Recherche Agronomique, France
Annalisa Polverari, University of Verona, Italy

***Correspondence:**
Kalyani S. Kulkarni
kalyaniaau@gmail.com;
kulkarni@icar.gov.in;
Yogesh M. Shukla
yshukla12000@yahoo.com

† These authors have contributed equally to this work.

Specialty section:
This article was submitted to Plant Biotic Interactions, a section of the journal Frontiers in Plant Science

Received: *02 March 2016*
Accepted: *30 May 2016*
Published: *22 June 2016*

Citation:
Kulkarni KS, Zala HN, Bosamia TC, Shukla YM, Kumar S, Fougat RS, Patel MS, Narayanan S and Joshi CG (2016) De novo Transcriptome Sequencing to Dissect Candidate Genes Associated with Pearl Millet-Downy Mildew (Sclerospora graminicola Sacc.) Interaction. Front. Plant Sci. 7:847. doi: 10.3389/fpls.2016.00847

Understanding the plant-pathogen interactions is of utmost importance to design strategies for minimizing the economic deficits caused by pathogens in crops. With an aim to identify genes underlying resistance to downy mildew, a major disease responsible for productivity loss in pearl millet, transcriptome analysis was performed in downy mildew resistant and susceptible genotypes upon infection and control on 454 Roche NGS platform. A total of ~685 Mb data was obtained with 1 575 290 raw reads. The raw reads were pre-processed into high-quality (HQ) reads making to ~82% with an average of 427 bases. The assembly was optimized using four assemblers *viz*. Newbler, MIRA, CLC and Trinity, out of which MIRA with a total of 14.10 Mb and 90118 transcripts proved to be the best for assembling reads. Differential expression analysis depicted 1396 and 936 and 1000 and 1591 transcripts up and down regulated in resistant inoculated/resistant control and susceptible inoculated/susceptible control respectively with a common of 3644 transcripts. The pathways for secondary metabolism, specifically the phenylpropanoid pathway was up-regulated in resistant genotype. Transcripts up-regulated as a part of defense response included classes of R genes, PR proteins, HR induced proteins and plant hormonal signaling transduction proteins. The transcripts for skp1 protein, purothionin, V type proton ATPase were found to have the highest expression in resistant genotype. Ten transcripts, selected on the basis of their involvement in defense mechanism were validated with qRT-PCR and showed positive co-relation with transcriptome data. Transcriptome analysis evoked potentials of hypersensitive response and systemic acquired resistance as possible mechanism operating in defense mechanism in pearl millet against downy mildew infection.

Keywords: pearl millet, downy mildew, transcriptome, pathogenesis related proteins, hypersensitive response, phenyl propanoid pathway
Sequences Accession numbers: SRX885597

INTRODUCTION

Pearl millet (*Pennisetum glaucum* (L.) R. Br.) is the sixth most important global cereal, primarily grown as a rainfed crop in the low rainfall zones of Sub-Saharan Africa and the Indian subcontinent where it contributes to the staple diet of people (Martel et al., 1997; Rajaram et al., 2013). India has seven million ha area under pearl millet with a production of 9.25 million tons (ICAR-AICPMIP Project co-ordinator review, 2015). It has wide adaptability and is looked at as one of the most significant crops in the scenario of food security and changing climate conditions. The crop productivity is severely constrained by several biotic stresses, major among them is downy mildew (DM) disease caused by the oomycete obligate pathogen, *Sclerospora graminicola* (Sacc.) Schroet. The oomycetes differ from fungi and includes economically important plant pathogens like downy mildews of poaceae, cucurbitaceae, vitaceae (Kamoun et al., 2015). The oomycetes, *S. graminicola* has been reported to hamper pearl millet yield loss up to 20–40% annually (Thakur et al., 2011). The development of downy mildew disease is favored by high relative humidity (85–90%), moderate temperature (20–30°C) and characterized by leafy inflorescence, leaf chlorosis, and failure to set seeds (Thakur et al., 2008).

The main concern regarding this oomycete is variability resulting from heterothallic nature and sexual cross compatibility among the isolates (Shetty, 1987). Besides this, the commercially released pearl millet hybrids have narrow genetic base and uniformity making it vulnerable for pathogen attack and development of new virulent strains (Thakur et al., 2011). Management strategies for the control of this disease include treatment with chemical fungicide, application of chemicals inducing resistance and resistance breeding. Of these, the most cost effective management lies in expending genetic resistance for breeding disease-resistant cultivars (Yadav et al., 2013). Moreover, genetic resistance remains a cost effective management for farmers considering the short-medium term. However, the emergence of new pathogen strains when R genes are deployed in cultivars, particularly in the case of plant-oomycete interactions (Solanum spp.-*Phytophthora* spp., Brassicaceae spp.-*Hyaloperonospora parasitica,* Poaceae *spp.-Sclerosporales*), there is a need to focus on reinforcing more sustainable resistance mechanisms (Kale, 2012; Fawke et al., 2015). Understanding such plant-oomycete interactions is vital for research interventions as it provides a way ahead to design strategies for minimizing the economic deficits caused by pathogen in crop (Dodds and Rathjen, 2010; Boyd et al., 2013). Although, the nature of pearl millet-downy mildew interaction has been studied at genetics as well as at biochemical level, there is a need to unravel the molecular basis of resistance to downy mildew infection (Thakur et al., 2011).

A comprehensive knowledge of genes is essential for undertaking genetic approaches for pearl millet improvement especially regarding disease resistance genes. The genome size of pearl millet is relatively large and current unavailability of reference genome further add to the need of identifying genes related to specific traits (Varshney et al., 2009; Varshney, 2014). In the light of this, unraveling the host-pathogen interaction and understanding the associated gene expression changes occurring at that particular time point is quintessential.

Transcriptome analysis through Next generation sequencing (NGS) technologies is a robust and efficient method for exploring the pattern of gene expression in host. Transcriptome sequencing or RNA-seq surpasses cloning and appends appreciation for the complexity of transcriptome by allowing RNA analysis through cDNA sequencing at massive scale (Margulies et al., 2005). It has been employed widely in exploiting physiological dynamics of model as well as non-model crop plants (Ozsolak and Milos, 2011). The quantification of gene expression deciphers the relative and differential expression patterns of a specific transcript or gene at a particular time point (Metzker, 2010). Transcriptome sequencing has been widely used for understanding the plant-oomycetes interaction in terms of compatibility/ incompatibility and elucidating the pathways involved in defense mechanism (Gao et al., 2013; Hayden et al., 2014; Meyer et al., 2016).

Several reports have also focussed on studying plant-pathogen interaction through transcriptome analysis (Liang et al., 2014; Reeksting et al., 2014; Weng et al., 2014; Li et al., 2015; Tan et al., 2015; Wang et al., 2015). Of more importance, the relative change in expression of host attacked by the pathogen can also be very well-tracked by RNA-seq of host (Westermann et al., 2012). In the present study, transcriptome sequencing was executed on downy mildew resistant and susceptible pearl millet genotypes upon inoculation with downy mildew pathogen and water as control in order to identify the genes and mechanism underlying downy mildew resistance.

MATERIALS AND METHODS

Pearl Millet Genotype and Sample Preparation

The seeds of downy mildew resistant genotype (P310-17) and susceptible genotype (7042S) used in the present study were obtained from the International Crop Research Institute for Semi-Arid Tropics (ICRISAT), Telangana, India. The genotypes were selected for transcriptome sequencing based on the level of downy mildew resistance and susceptibility against local Anand pathotype in the downy mildew virulence nursery (Thakur et al., 2007, 2008).

Downy mildew infected leaves of pearl millet showing whitish growth on the abaxial surface were collected in the evening from the susceptible genotype maintained in the polyhouse. The leaves were thoroughly washed with water and cleaned to remove old sporangia. Leaves were cut into small pieces, placed with abaxial surface upside in a tray lined with moistened filter paper and maintained in incubator chamber (Model I-36NL Percival Scientific Incubator, USA) at step down protocol of 20°C and 95% humidity for 8 h and at 0°C until inoculation. The sporangia were collected from the leaves showing downy mildew whitish growth using paint brush and collected in minimal required distilled water to keep the spore suspension concentrated. The inoculum was kept in dark for 15–20 min

and observed under microscope for release of zoospores. Using haemocytometer, the zoospores count was adjusted to 4×10^4/ml followed by inoculating the 2 days old seedlings of resistant and susceptible genotypes in three replications and water served as control (Safeeulla, 1976; Jones et al., 2001; Thakur et al., 2011). The seedlings were observed visually every 6 h for morphological changes on the surface. Seedlings harvested from three replications of each treatment were pooled after 36 h post inoculation for transcriptome sequencing. The resistant inoculated, resistant control, susceptible inoculated and susceptible control samples were represented as RI, RC, SI, and SC respectively. The methodology of experiment is represented in **Supplementary Figure 1**.

454 Sequencing

Total RNA was isolated from seedling tissues using NucleoSpin® RNA kit, Macherey-Nagel, USA following manufactures instruction. Total RNA was spectrophotometrically quantified on Infinite M200 Pro, Tecan and 1 μL of each sample was used for assessing RNA quality using RNA Nano chip on Agilent 2100 Bioanalyzer, USA. Samples having RNA Integrity Number (RIN) more than eight were processed further for mRNA isolation expending the mRNA isolation kit, Roche following manufacturer's instructions. The quality of mRNA was assessed by running each sample on RNA 6000 Pico Chip on the Agilent 2100 Bioanalyzer. The cDNA libraries were synthesized by using cDNA Rapid Library Preparation kit, Roche and assessed on an Agilent 2100 DNA High Sensitivity chip on Agilent 2100 Bioanalyzer. The cDNA libraries were clonally amplified, and sequenced on a full GS FLX Titanium Pico Titer Plate Kit 70 × 75 mm on Genome Sequencer FLX Instrument, Roche, USA available in house. Full processing was conducted, comprising both the Image Processing (i.e., "Raw wells" data files) and Signal Processing (Read flowgrams and basecalls) during the run time. The Post-Run data analysis was done after the completion of the run on a dedicated data processing computer (cluster) i.e., DataRig which is a Linux-based computer dedicated to running Genome Sequencer FLX System data processing and data analysis software, GS run processor. The sequenced raw reads were processed for removal of MID adaptor sequences by using the Perl script. Raw reads generated by 454 sequencing were deposited in the NCBI's SRA database with the accession number SRX885597.

Pre-Processing of Raw Reads

The raw reads emanating from sequencing of each sample were subjected to pre-processing by Prinseq-lite-0.20.4 (Schmieder and Edwards, 2011; http://prinseq.sourceforge.net/) for removal of low complexity sequences using the parameters- removal of reads with length of ≤100 bp, removal of low-quality Phred sequences of ≤20, removal of exact duplicate sequences and trimming of reads. The cleaned raw reads were further filtered for rRNA sequences using Ribopicker-0.4.3 (Schmieder et al., 2012; http://ribopicker.sourceforge.net/) with an optimized highly stringent criterion of least 90% identity and 95% coverage in BlastN search against ribosomal RNA database SILVA.

De novo Assembly Optimization

The pre-processed high-quality reads were merged and input into the data assembly softwares *viz*., GS Assembler, Newbler (Margulies et al., 2005), proprietary software of 454 Roche with 90% identity, 40 bp overlap, cDNA option; MIRA (chevreux.org/projects_mira.html) with 454, est option in manifest file; CLC genomics workbench (www.clcbio.com) with default parameters and Trinity (Haas et al., 2013) with default parameters for assembling into transcripts. The four assemblers were evaluated based on the statistics of total number of reads used in the assembly, N50 value, largest contig size, number of contigs generated and mean contig length. For further assembly optimization, BlastX of assembled contigs was done with the close relative of pearl millet, *Setaria italica* protein database with an e-value of 1E-6.

Functional Annotation of Transcripts

The assembled transcripts were BlastX with Nr database having e-value cut-off of 1E-6 on Blast2GO (Conesa et al., 2005) platform to obtain GO annotation. Blast was done against the pathogen host interaction database (PHI base) with e-value cut-off of 1E-10 (Winnenburg et al., 2006). The KEGG maps were deduced having EC numbers of the selected sequences. Graphs were plotted by WEGO, an online tool using GO numbers for functional classification (Ye et al., 2006).

Differential Gene Expression Analysis of Transcripts

The level of transcripts expression was analyzed on the basis of number of reads mapping to each transcript. Bowtie was used for aligning the reads of each sample onto the assembled transcripts (Langmead and Salzberg, 2012). The resulting files of aligned reads were input in DESeq, a tool for quantifying the abundances of a set of target sequences from sampled subsequences based on a model using the negative binomial distribution (Anders and Huber, 2010). The differentially expressed transcripts between the pair of the samples were graphically represented by Venn diagram by inputting the transcript identifiers in VennPlex for creating Venn diagram (Cai et al., 2013). Heat maps for particular classes of transcripts were prepared using Multi experiment Viewer (MeV) v4.9.0 (Saeed et al., 2003).

Pathway Mapping of Differentially Expressed Transcripts

The differentially expressed transcripts in resistant and susceptible genotypes were mapped to biological pathways using a web-based Kyoto Encyclopedia of Genes and Genomes (KEGG) automatic annotation server (KAAS) by executing BlastX against the manually curated KEGG GENES (Kyoto encyclopedia of genes and genomes) database. The result contains KO (KEGG Orthology) assignments and automatically generated KEGG pathways.

Validation of Prominent Defense Related Genes Through qRT-PCR

The differentially expressed transcripts involved in plant defense based on the functional annotation were selected for validation

through quantitative Real-Time PCR (qRT-PCR). The fasta sequences of transcripts were retrieved and input in batch primer3 online tool (You et al., 2008) by selecting the generic option and following criterion: Product size (bp) of 100–200, primer size of 18–22 nts, temperature melting 59–62°C, rest of the parameters were default. The primer sequences of transcripts are listed in **Supplementary Table 1**. The first strand cDNA was synthesized from an aliquot of total RNA for each sample using RevertAid First Strand cDNA Synthesis Kit (ThermoFisher Scientific, USA) and served as template for qRT-PCR. The qRT-PCR was performed using TakaraSYBR green mix (Japan) on CFX96™ Real-Time PCR detection system, BioRad, USA following standard qRT-PCR guidelines. The stability of endogenous reference genes upon downy mildew infection in pearl millet was analyzed using RefFinder (Xie et al., 2012). RefFinder compares and rank the tested candidate reference genes based on the rankings from given by each program. Tubulin (Tub_10) was used as endogenous reference gene for normalization. The Cq values for primers were examined using CFX Manager™ software 2.1, BioRad and qBASE+ v3.0 (https://www.biogazelle.com/) was used for gene expression data analysis following Livak's $-\Delta\Delta$ CT method.

RESULTS

The downy mildew infected leaves kept for sporulation displayed whitish growth on the abaxial surface indicating profuse sporulation of the pathogen. Inoculum prepared from sporulated leaves was observed under microscopic field for its morphology and release of zoospores which is mandatory for infection. Palm shaped sporangiophore bearing sporangia; peculiar structure of downy mildew pathogen was observed (**Figure 1**).

Trancriptome Sequencing, *De novo* Assembly, and Functional Annotation

The sequencing of four pearl millet libraries subjected to 454 GSFLX Titanium, Roche platform generated 684.97 Mb data. The total raw reads for the samples, RC, RI, SC, SI was 1 575 290. The pre-processing of these raw reads *viz*. low quality (0.15%), short (3.78%), duplicate (12.7%), and rRNA (0.85%) reads removal yielded a total of 1295196 high-quality (HQ) reads (∼82%) with an average of 427 bases. A large percentage of HQ reads (78%) was distributed between 400 and 550 bases (**Supplementary Figure 2**). The detailed summary of the sequenced data and pre-processing is presented in **Table 1**.

The HQ reads were utilized for assembling into contigs, aptly known as transcripts keeping in view of transcriptome sequencing. With the increasing number of softwares available for analyzing the sequencing data, it becomes imperative to optimize the assembly for acquiring meaningful annotation of the transcripts. The detailed description of the assemblers employed and the parameters used for optimization is briefed in **Table 2**.

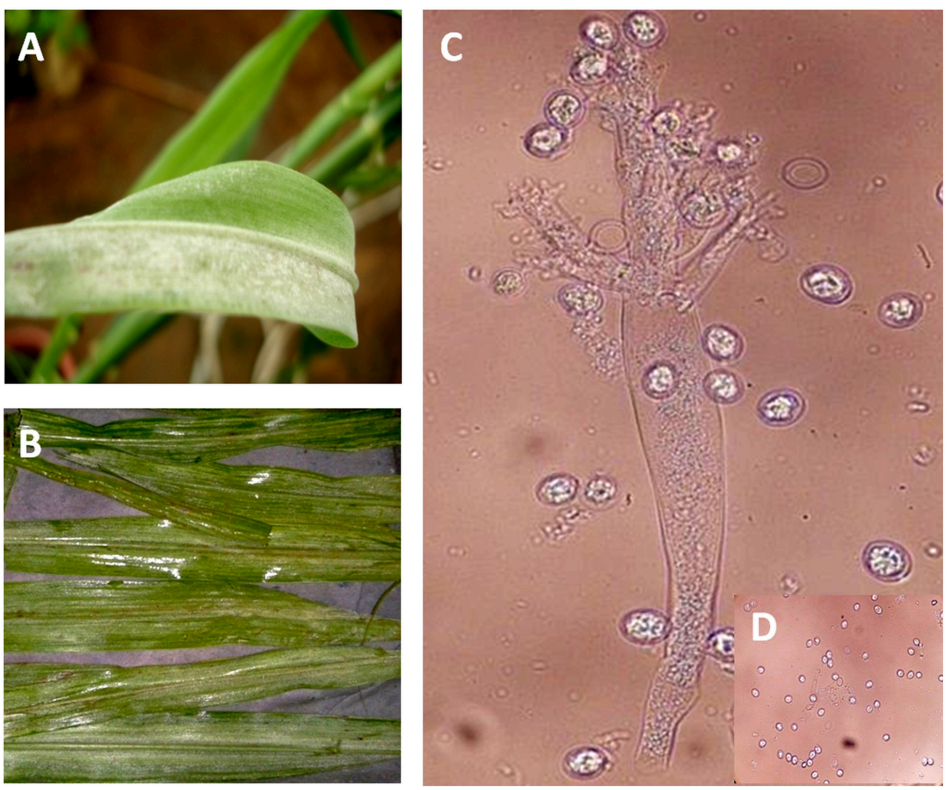

FIGURE 1 | Sporangiophore and zoospore of downy mildew pathogen. (A) Downy mildew growth on abaxial leaf surface. **(B)** Downy mildew infected leaves kept for sporulation. **(C)** Downy mildew sporangiophore. **(D)** Zoospore release.

TABLE 1 | Pre-processing of raw reads obtained by 454 sequencing of pearl millet genotypes (inoculated and control).

Sample	Total reads*	Low-quality reads#	Trashed reads§	Duplicate reads¶	rRNA reads†	High-quality reads**	Average length†† (bases)
RC	344,111	472	11,647	45,898	3048	283,046	432
RI	484,284	729	19,044	62,992	4055	397,464	431
SC	255,888	459	10,472	28,370	1961	214,626	424
SI	491,007	798	18,518	67,161	4470	400,060	424
Total	1,575,290	2458 (0.15%)	59,681 (3.86%)	204,421 (12.97%)	13,534 (0.85%)	1,295,196 (82.21%)	427

*Total number of reads for each sample.
#Number of low-quality reads (Phred quality score of <20) removed.
§Number of short reads (<100 bp) removed.
¶Number of exact duplicate reads removed.
†Number of reads identified as rRNA sequences removed.
**Number of high-quality reads.
††Average length of high-quality reads.

TABLE 2 | Summary statistics of *de novo* assembled transcripts from pearl millet genotypes (inoculated and control).

Parameters/Programs	Newbler	CLC	MIRA	Trinity
Transcripts (≥100 bases)	16658	30038	53318	26690
Total size (Mb)	13.69	24.68	42.59	25.86
Large transcripts (≥500 bases)	11005	20 299	41703	19 608
Maximum length (bases)	13594	15147	12556	17444
Average length (bases)	821	822	800	969
N50 (bases)	1099	970	838	1219
Reads mapped (%)	77.55	85.43	96.20	89.52
Number of singletons	106363	64733	36800	135425
Total size (Mb)	38.08	25.35	14.10	55.46
Transcripts with significant hits (%)[a]	12179 (73.11)	21688 (72.20)	30333 (56.89)	19986 (74.88)
Transcripts with ≥80% coverage[b]	11110	18443	25563	17356
Setaria italica proteins hits[c]	22213	27824	28567	27226
S. italica proteins with ≥80% coverage[d]	13213	18668	19679	18004

[a]Transcripts showing significant hits ($E \leq$ 1e-6) with S. italica proteins.
[b]Transcripts showing 80% or greater coverage of S. italica proteins.
[c]Unique S. italica proteins to which transcripts show significant hits ($E \leq$ 1e-6).
[d]Unique S. italica proteins to which transcripts show 80% or greater coverage.

Out of the four assemblers, the maximum number of transcripts (53318) was registered by MIRA with total assembly size of 42.59 Mb. The number of large transcripts (≥500 bp) was higher for MIRA assembly as compared to other three assemblers. The maximum length, average length and the highest N50 value were recorded for Trinity assembler. The reads other than those utilized for generating transcripts, also known as singletons were the maximum for Trinity followed by Newbler, CLC, and MIRA. Transcripts with >80% coverage with *S. italica* proteins were represented more in MIRA as compared to the other three assemblers (**Supplementary Table 2**). Additionally, the percentage of HQ reads utilized for assembling by each assembler was determined by back mapping reads on to each assembly generated by individual assembler for cognizing the overall alignment rates wherein the maximum alignment percentage was shown by MIRA (96.2%) followed by Trinity, CLC and Newbler. The total number of transcripts including singletons was 90118 for MIRA. Based on all the mentioned parameters, MIRA was considered for *de novo* assembly.

Out of the transcripts subjected to annotation in Blast2GO, 69% showed Blast hits and 38% of sequences were annotated against the Nr database (**Supplementary Table 3**). Out of the total transcripts, 7.01% were annotated as oomycetes sequences in the nr databases. The maximum number of transcripts was annotated against the UniProt Knowledgebase (UniProtKB) followed by GR_PROTEIN database and TAIR database. The annotated transcripts were subjected to KEGG pathway wherein the transcripts were linked to enzymes in a number of pathways available in KEGG. The maximum number of annotated transcripts was ascribed to hydrolases (9485) followed by transferases (4844) and oxidoreductases (2267) class of enzymes (**Table 3**). The data on species distribution of the transcripts conceded the highest blast hits with *S. italica* followed by *Sorghum bicolor*, *Medicago trunculata*, *Zea mays,* and *Oryza sativa* (**Figure 2**). Blast hits were also obtained with *Phytophthora parasitica* and *Phytophthora sojae,* two closely related oomycete species of *S. graminicola*. The pearl millet transcripts were categorized into the cellular components, molecular functions and biological processes gene ontologies (GO) and were assigned GO numbers. In cellular component ontology, the maximum number of transcripts was associated with cell (GO:0005623), intercellular organelle (GO:0043226) and membrane bound organelles (GO:0016020). In the molecular function ontology, the maximum number of transcripts were attributed to catalytic activity (GO: 0003824), binding (GO:0005488), and transporter activity (GO:0005215) while in the biological processes ontology, the maximum number of transcripts was represented by metabolic processes (GO:0008152), cellular processes (GO:0009987), and localization (GO: 0051179) (**Figure 3**).

Differential Expression of Transcripts during Pearl Millet-Downy Mildew Interaction

The 2 days old grown seedlings of resistant and susceptible genotypes inoculated with downy mildew inoculum *viz*, RI, and

SI respectively, displayed hypersensitive response in the form of brown streaks which was earlier in resistant inoculated seedlings than the susceptible inoculated seedlings.

The observation on number of differentially expressed transcripts reflected more number of transcripts up-regulated in RI than SI. Total of 1396 transcripts were up-regulated between RI/RC and 939 were down-regulated. In the SI/SC, 1000 transcripts were up-regulated and 1591 were down-regulated. The transcripts commonly up and down regulated between RI/RC and SI/SC were 1446 and 482, respectively. The contra regulated transcripts i.e., commonly expressed but with diverse regulation polarity values were 1716 (**Figure 4**).

TABLE 3 | Functional annotation statistics of transcripts assembled by MIRA.

Particular	# Number
Total numbers of transcript sequences	90118
Numbers of sequences with Blast Hits	61727 (68.5%)
Numbers of sequences with Mapping	39167 (43.46%)
Numbers of sequences with Annotation	34915 (38.74%)
Total number of GOs annotation	661484
UNIPROTKB	647831 (97.94%)
GR_PROTEIN	12939 (1.96%)
TAIR	556 (0.08%)
KEGG Annotation	18484
Hydrolases	9485 (51.31%)
Transferases	4844 (26.21%)
Oxidoreductases	2267 (12.26%)
Lyases	919 (4.97%)
Ligases	638 (3.45%)
Isomerases	331 (1.79%)

Transcripts expressed as part of defense mechanism upon pathogen attack includes several classes of genes in order to render resistance to that pathogen. The response starts from the cell wall and relays *via* hormonal signaling ultimately giving resistance to the pathogen. In the present study, we divided the transcripts into classes based on their function. Differential expression was noticed for cell wall related transcripts, signaling molecules, transcription factors, and genes involved in secondary metabolic pathways (**Figure 5**).

The transcripts for cell wall hydrolases were differentially up-regulated with different fold changes in the resistant as compared to the susceptible. The polygalacturonase-like proteins and hydroxyproline-rich glycoprotein family proteins were also up-regulated along with exclusive expression of 14 kda proline rich proteins in resistant genotype.

In the antioxidant enzymes, respiratory burst oxidase, superoxide dismutase, and glutathione reductase were expressed differentially. One of the respiratory burst oxidase transcripts was expressed two and a half fold higher in the resistant than the susceptible genotype.

Differentially expressed transcripts involved in signal transduction included calcium signaling pathway component calmodulin, cyclic nucleotide gated channel proteins (CNGC), v-type proton ATPase, various classes of protein kinases like receptor like protein kinase, cyclic dependent nucleotide kinases (CDPK), leucine-rich repeat receptor-like protein kinase family proteins, lrr receptor-like serine threonine-protein kinases rpk2, mitogen-activated protein kinase (MAPK), mpk14, MAPKK, MAPKKK, cysteine-rich receptor-like protein kinase, and serine threonine-protein kinase. The maximum number of transcripts was attributed to serine protein threonine kinases followed

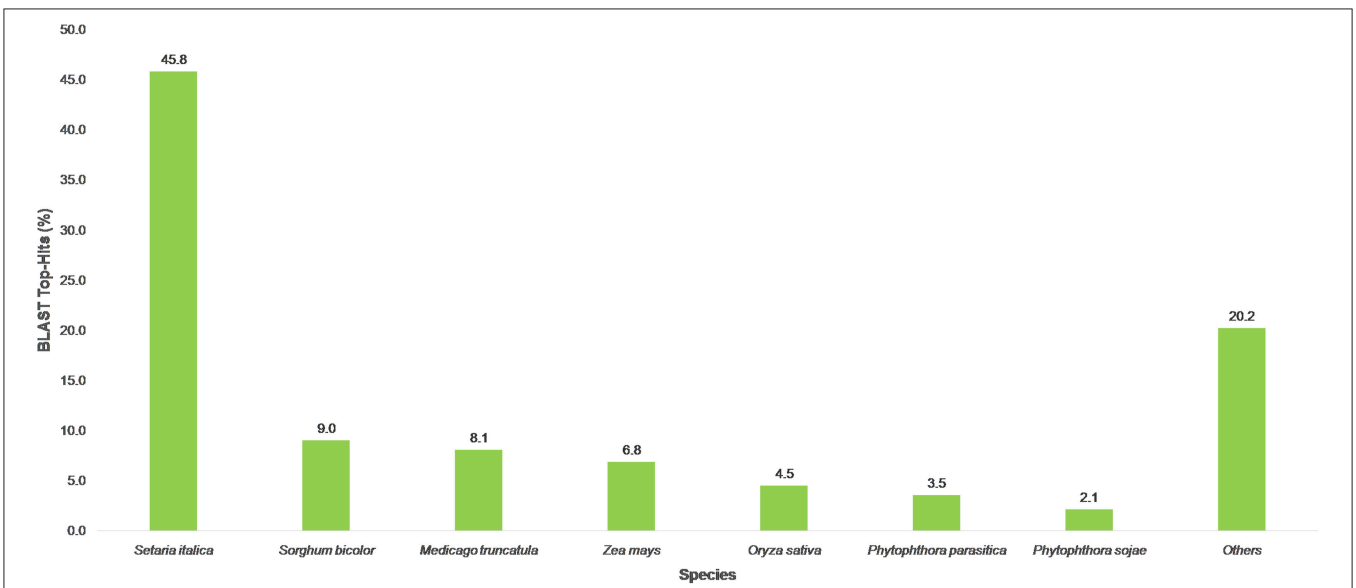

FIGURE 2 | Distribution of BLAST Top-hits species.

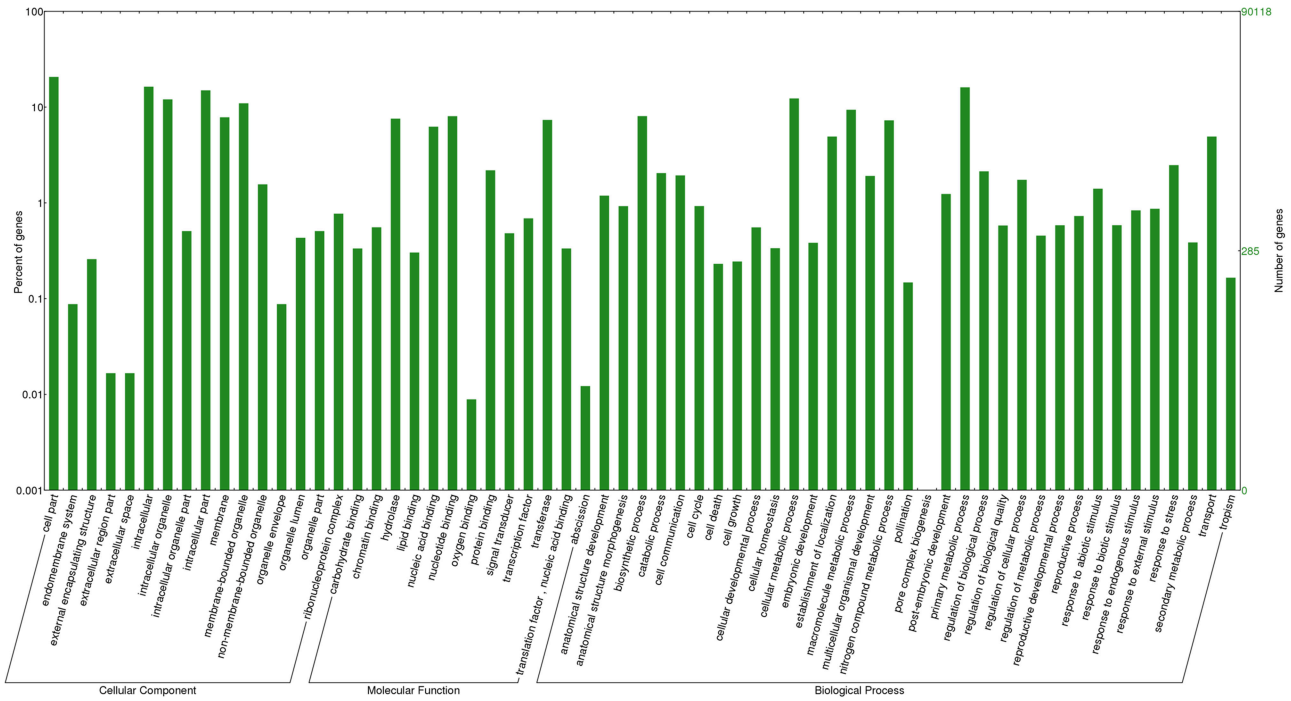

FIGURE 3 | Gene ontology distribution of pearl millet transcripts. Percentage of transcripts categorized in cellular component, molecular function and biological process are depicted.

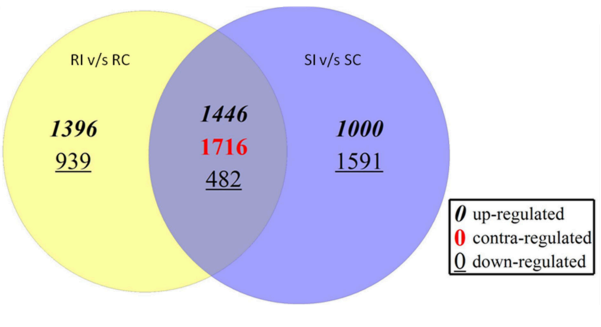

FIGURE 4 | Number of differentially expressed transcripts in resistant and susceptible pearl millet genotypes upon downy mildew inoculation.

by lrr receptor-like protein kinases. One transcript each for V type proton ATPase (pm_c1717), serine threonine-protein kinase (pm_c50377), ankyrin protein kinase and transcript for lrr receptor-like protein kinase (pm_c14579) were found to have relatively higher fold expression among the transcripts in resistant genotype.

The transcripts for WRKY, MYB, NAC, bZIP, bhlh transcription factor families were differentially expressed with the maximum number of transcripts for WRKY followed by NAC and MYB. Nevertheless, higher differential expression was noted for the MYB transcripts (INNBLQX02ID2QT, >3-fold change; pm_c25208, >2.5-fold change) followed by each transcript for NAC (INNBLQX01EOCCS), bhlh (pm_c9881) and bZIP (pm_c29637). One transcript each for heat stress transcription factor (INNBLQX02FJ30R) and ethylene-responsive transcription factor (pm_c6719) were also differentially expressed with higher fold change in resistant over susceptible.

Secondary metabolite pathway transcripts expressed differentially belonged to phenylpropanoid, terpenoid, and flavonoid biosynthesis pathways. The enzymes of phenylpropanoid biosynthesis pathway included phenylalanine ammonia lyase, tyrosine ammonia lyase, and chorismate mutase. Transcripts for isochorismate synthase, an enzyme for salicyclic acid precursor were highly expressed in resistant genotype. Phytoene synthase transcript was among the most highly expressed in resistant genotype. Although the expression of transcripts was noted in susceptible genotype, the level was expression was very low as compared to resistant genotype. Differentially expressed transcripts for flavonoid biosynthesis pathway enzymes included for cinnamyl alcohol dehydrogenase, flavonoid monooxygenase, coumaroyl shikimate 3-hydroxylase 2, monodehydroascorbate reductase-like, dihydroflavonol 4-reductase flavanone 4-reductase.

Total of nine classes of PR proteins were differentially represented in the resistant and susceptible genotype *viz.* pr 1, beta glucanase, chitinase, thaumatin, bowman-birk type trypsin inhibitor-like, purothionin, and oxalate oxidase. The highest expression of transcript was determined for purothionin (PR 13) in resistant genotype with four-fold higher expression. Transcripts for beta glucanase, oxalate

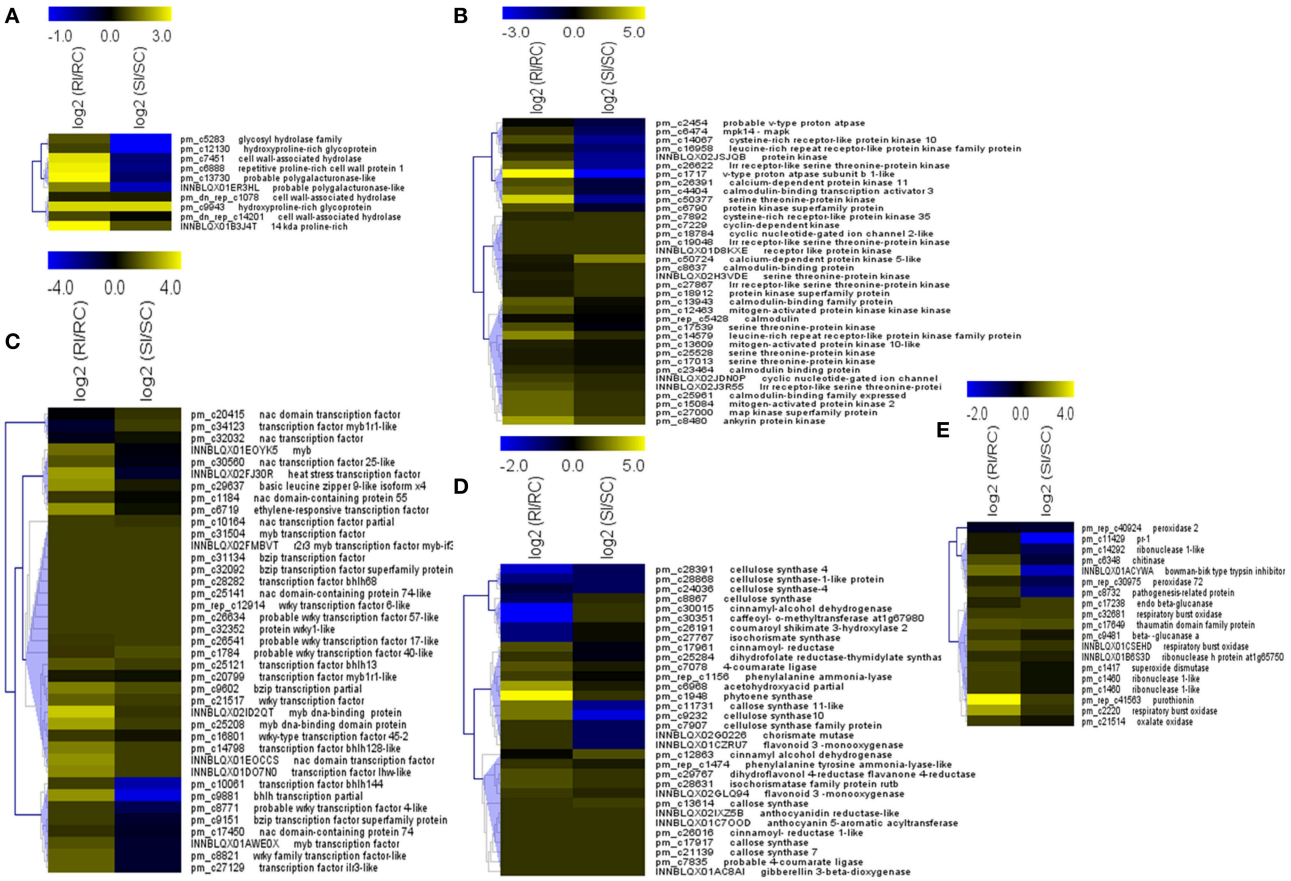

FIGURE 5 | Classes of differentially expressed transcripts in resistant and susceptible pearl millet genotypes upon downy mildew inoculation. Transcripts for **(A)** Cell wall associated proteins, **(B)** Signaling compounds, **(C)** Transcription factors, **(D)** Secondary metabolism pathway, **(E)** Pathogenesis related proteins and hypersensitive response are depicted. Relative expression levels of each transcript is shown as heat map (hierarchical clustering with Pearson Uncentered correlation and complete linkage method). Scale represents upregulation (Yellow) to downregulation (Blue).

oxidase, ribonuclease and thaumatin were also expressed in susceptible genotype but with low expression than the resistant genotype.

The differentially expressed R gene related transcripts were skp, sgt, nbs-lrr, rpp (resistance to *Peronospora parasitica*), rf45, f-box lrr, mlo, and nb-arc (**Table 4**). In pearl millet-downy mildew incompatible interaction, the transcripts having the highest and exclusive up-regulation were for skp protein followed by leucine-rich repeat-containing protein, disease-resistance protein sgt1nbs-lrr disease resistance protein homolog, and mlo-like protein 14. The maximum number of R gene transcripts belonged to nbs-lrr proteins, which is the largest R gene family proteins followed by rpp like proteins. Relatively low expression of R gene transcripts was noted in the susceptible genotype as compared to the resistant genotype. Transcripts for resistant gene analogs (RGA) were also up regulated in the resistant genotype. The role of RGA, belonging to non-TIR NBS LRR group has been indicated in pearl millet-downy mildew interaction (Veena et al., 2016).

In KEGG annotation, the maximum transcripts were ascribed to carbohydrate, energy metabolism followed by amino acid metabolism among the primary metabolic pathways (**Figure 6**). Secondary metabolite pathway transcripts were ascertained in higher number in RI/RC. Transcripts for signal transduction pathway were higher in the RI/RC than SI/SC. Up-regulated pathways in the RI/RC included oxidative phosphorylation (ko00190), phenylalanine metabolism (ko00360), phenylalanine tyrosine tryptophan metabolism (ko00400), phenylpropanoid (ko00940), ubiquitin mediated proteolysis (ko04120), MAPK signaling (ko04010), cAMP signaling (ko04024), plant hormone signal transduction (ko04075), and plant pathogen interaction (ko04626).

The 10 transcripts validated through qRT-PCR represented functional classes of transcripts involved in plant defense mechanism like pathogenesis related proteins (PR), transcription factors, signaling and secondary metabolite pathways. The tubulin transcript, Tub_10 was ranked first according to its stability and used for normalizing relative gene expression of transcripts (**Supplementary Table 4**). Differential expression of

TABLE 4 | Differential expression of defense related R gene transcripts.

Transcript ID	Transcript Name	Specifics	RI/RC	SI/SC
pm_c22034	Disease-resistance protein sgt1	Suppressor of G2 allele of SKP1. Development of HR during R gene-mediated disease resistance	2.32	0
pm_c11050	skp1-like protein 21-like isoform x1	Component of SCF(ASK-cullin-F-box) E3 ubiquitin ligase complexes, F-box domain	4.00	0
pm_rep_c15934	skp1 interacting partner	Component of SCF(ASK-cullin-F-box) E3 ubiquitin ligase complexes, F-box domain	1.00	0.26
pm_c28289	Disease resistance protein rpm1	Nucleotide-binding, LRR HR	1.00	0
pm_c28993	Disease resistance protein rpm1	Nucleotide-binding, LRR HR	1.00	0
pm_c32590	Disease resistance protein rpm1-like	Nucleotide-binding, LRR HR	0.00	0.26
INNBLQX01AUN3U	Disease resistance protein rpm1	Nucleotide-binding, LRR HR	1.00	0
pm_c41149	Disease resistance protein rpm1	Nucleotide-binding, LRR HR	0.00	−0.74
pm_c28390	Disease resistance rpp13-like protein 1-like	Coiled coil, Leucine rich repeats, NB-ARC	1.00	0
INNBLQX01AHM5E	Disease resistance rpp13-like protein 2-like	Coiled coil, Leucine rich repeats, NB-ARC	0.42	0
INNBLQX01B7G0R	Disease resistance rpp13-like protein 3-like	Coiled coil, Leucine rich repeats, NB-ARC	0.58	0
pm_c28132	Disease resistance rpp13-like protein 3-like	Coiled coil, Leucine rich repeats, NB-ARC	−1.00	0
INNBLQX01AHDT3	Disease resistance rpp13-like protein 1	Coiled coil, Leucine rich repeats, NB-ARC	−1.00	0
INNBLQX01ENYQL	Disease resistance rpp13-like protein 2-like	Coiled coil, Leucine rich repeats, NB-ARC	1.26	0.40
INNBLQX02ITIJ1	Disease resistance rpp13-like protein 1-like isoform x2	Coiled coil, Leucine rich repeats, NB-ARC	1.58	0
INNBLQX01CNUJ5	Disease resistance rpp13-like protein 2	Coiled coil, Leucine rich repeats, NB-ARC	−1.00	0
INNBLQX01B7G0R	Disease resistance rpp13-like protein 3-like	Coiled coil, Leucine rich repeats, NB-ARC	0	−1.74
INNBLQX02ITIJ1	Disease resistance rpp13-like protein 1-like isoform x2	Coiled coil, Leucine rich repeats, NB-ARC	0	−0.74
pm_c19464	Disease resistance rpp13-like protein 4	Coiled coil, Leucine rich repeats, NB-ARC	0	−1.74
pm_c15317	Disease resistance protein rpp13-like isoform x1	Coiled coil, Leucine rich repeats, NB-ARC	0	−0.74
pm_c34958	Disease resistance protein rga3-like isoform x1	Coiled coil, Leucine rich repeats, NB-ARC	0	−0.74
INNBLQX01A9IWX	Disease resistance protein rga3-like isoform x1	Coiled coil, Leucine rich repeats, NB-ARC	0	−2.32
pm_c12557	Disease resistance protein rga3-like isoform x1	Coiled coil, Leucine rich repeats, NB-ARC	0.42	0.26
INNBLQX01BA29P	Disease resistance protein rga4-like	Coiled coil, Leucine rich repeats, NB-ARC	−1.00	0
INNBLQX01DD3SZ	Disease resistance protein rga4	Coiled coil, Leucine rich repeats, NB-ARC	0.00	0.26
INNBLQX01A9IWX	Disease resistance protein rga3-like isoform x1	Coiled coil, Leucine rich repeats, NB-ARC	−2.00	0
pm_c45828	Disease resistance protein rga1-like	Leucine rich repeats, NB-ARC and P-loop NTPase	1.00	0
pm_c26661	lz-nbs-lrr class rga	Leucine rich repeats, NB-ARC and P-loop NTPase	−1.58	−0.74
INNBLQX02JN1C8	Leucine-rich repeat-containing protein	Recognize and transmit pathogen-derived signals	3.17	−0.74
pm_c20365	nbs-lrr disease resistance protein homolog	Recognize and transmit pathogen-derived signals	1.58	0
pm_c12696	nbs-lrr class disease resistance protein	Recognize and transmit pathogen-derived signals	0.58	0
pm_c28200	nbs resistance partial	Recognize and transmit pathogen-derived signals	1.00	0
pm_c19586	nbs-lrr type resistance protein	Recognize and transmit pathogen-derived signals	1.32	0.26
pm_c27783	Leucine-rich repeat family protein	Recognize and transmit pathogen-derived signals	1.00	0
INNBLQX01ECXST	Probable disease resistance protein rf45-like	P loop and NB-ARC	1.58	0
pm_c30156	npr disease resistance protein	Ankyrin_rpt-contain_dom., NONEXPRESSOR OF PR GENES	−1.00	0
pm_c8238	f-box lrr-repeat protein 13-like	F-box/LRR-repeat protein 13-like, regulate salicylic acid-dependent gene expression during systemic acquired resistance.	0.81	0
INNBLQX01A2WWG	f-box lrr-repeat protein 3-like	F-box/LRR-repeat protein 13-like, regulate salicylic acid-dependent gene expression during systemic acquired resistance	0.58	0.26
pm_c26024	mlo-like protein 1-like	Seven transmembrane domains and calmodulin binding domain	2.70	1.26
INNBLQX02G8SE7	mlo-like protein 14	Seven transmembrane domains and calmodulin binding domain	1.58	−0.74
pm_c17303	nb-arc domain containing expressed	NB, ARC1, and ARC2, regulate activity of the resistance protein	1.00	0.26
INNBLQX01ADNB1	nb-arc domain-containing protein	NB, ARC1, and ARC2, regulate activity of the resistance protein	1.32	0
pm_c49493	Disease resistance protein at1g58400-like isoform x3	CC-NBS-LRR class family	0.57	0.12

Positive sign indicate Up regulation, negative sign indicate Down regulation, n and 0 indicate no/undetectable transcript expression.

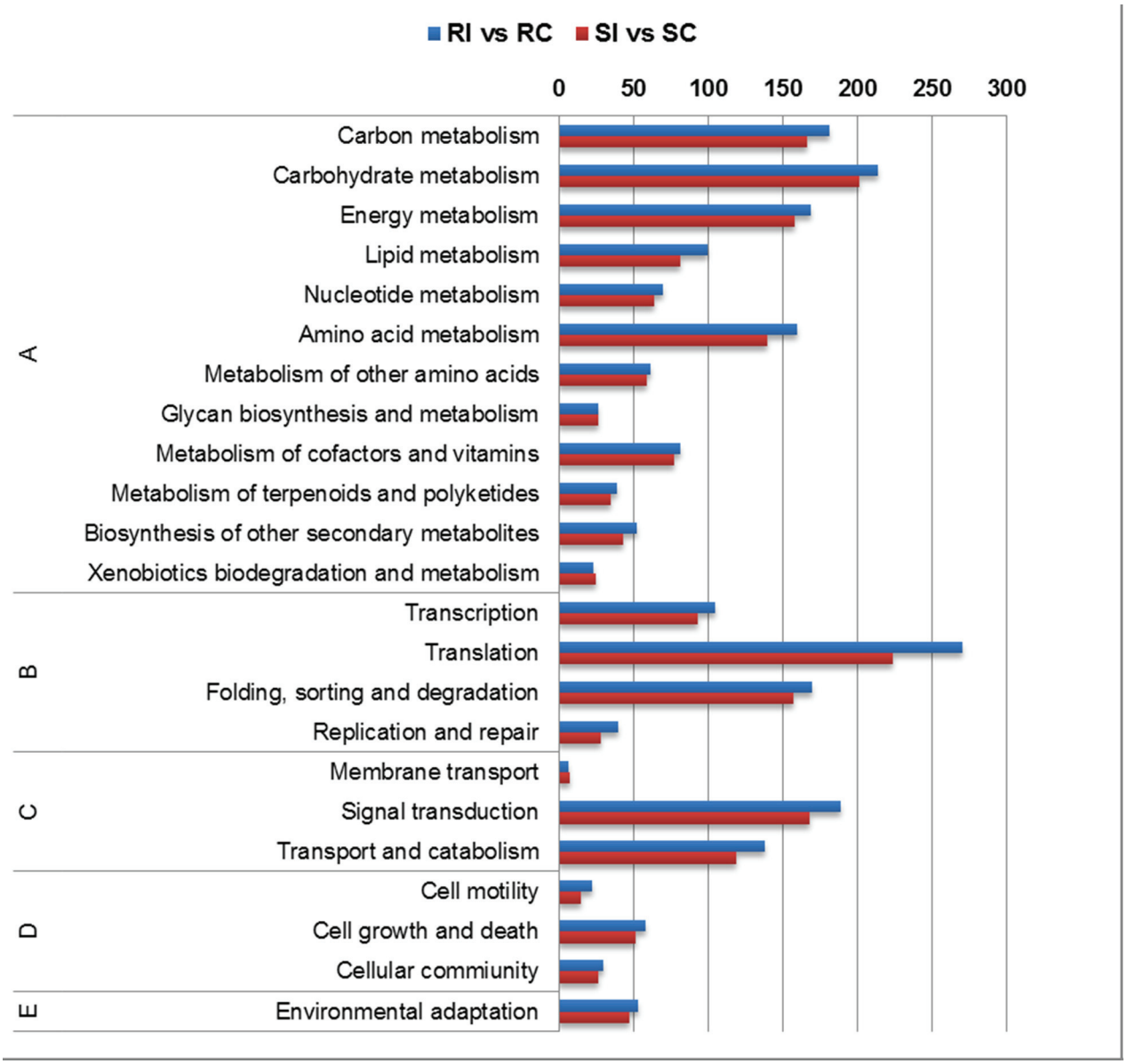

FIGURE 6 | Pathway enrichment of differentially expressed transcripts using KAAS annotation server (A) Metabolism; (B) Genetic Information Processing; (C) Environmental Information Processing; (D) Cellular Processes; (E) Organismal Systems.

transcripts was observed in RI and SI along with their respective controls (**Figure 7**). The lipoxygenase, MYB, and MAPK were among the highly up regulated transcripts in RI compared to SI. Up regulation of the defense related transcripts was also observed in SI but with lower expression than that in RI. Comparison of transcript expression levels between transcriptome data and qRT-PCR depicted positive correlation although the values for log2 fold change did not exactly match but remained consistent in expression (**Figure 8**).

DISCUSSION

The 454 Roche sequencing has been extensively employed for transcriptome sequencing and is well-suitable for both model and non-model plants with better performance than conventional methods of gene expression (Chen et al., 2013). In the present study, the sequencing throughput (684.97 Mb) and average length (433.99 bp) was consistent with the characteristic throughput and moderate read length of 454 GS FLX Titanium. It is very crucial to obtain cleaned, high-quality reads for further processing toward assembling, analysis of gene expression and hence, pre-processing was carried out on the raw sequencing reads (Martin and Wang, 2011; Vijay et al., 2013). Pre-processing removed 18% of the raw reads in the form of low complexity, low length, duplicate, and rRNA reads. To get a non-redundant data, duplicate reads were removed before assembling the reads into transcripts but were employed for back mapping while analyzing gene expression to decipher the level of transcript expression.

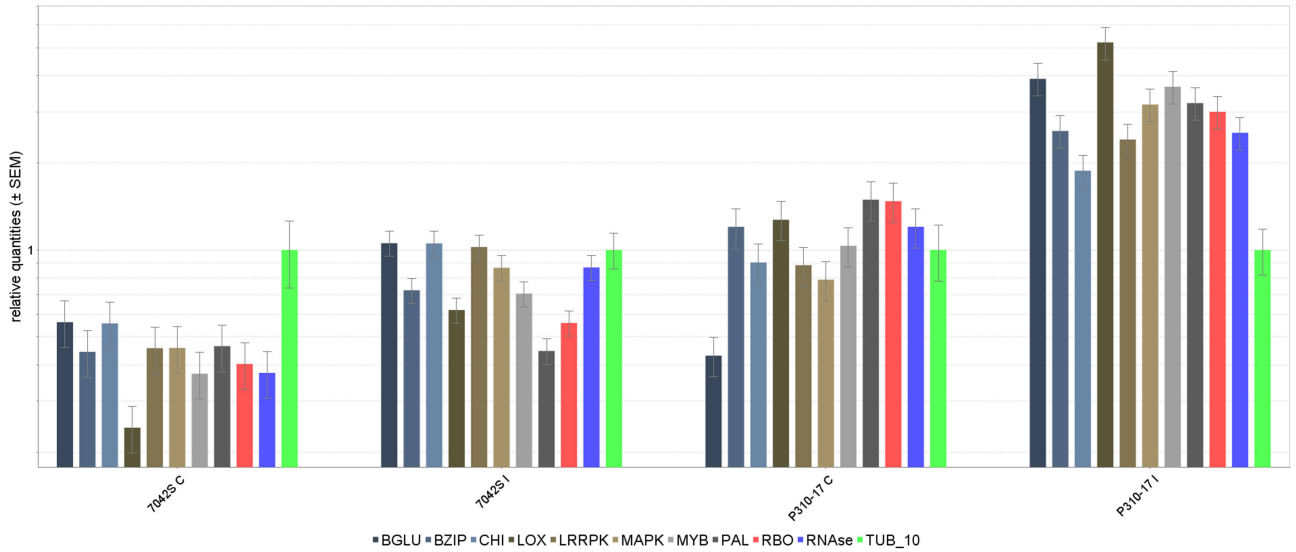

FIGURE 7 | Log2 fold differential gene expression of transcripts through Real- time PCR. Bars on top show the standard deviation of three biological replications. Expression normalized with endogenous gene: Tubulin. 1. β Glucanase, 2. Basal zipper protein (BZIP), 3. Chitinase (CHI), 4. Lipoxygenase (LOX), 5. Leucine rich repeat protein kinase (LRRPK), 6. Mitogen activated protein kinase (MAPK), 7. MYB, 8. Phenylalanine ammonia lyase, (PAL) 9. Respiratory burst oxidase (RBO), 10. Ribonuclease (RNase).

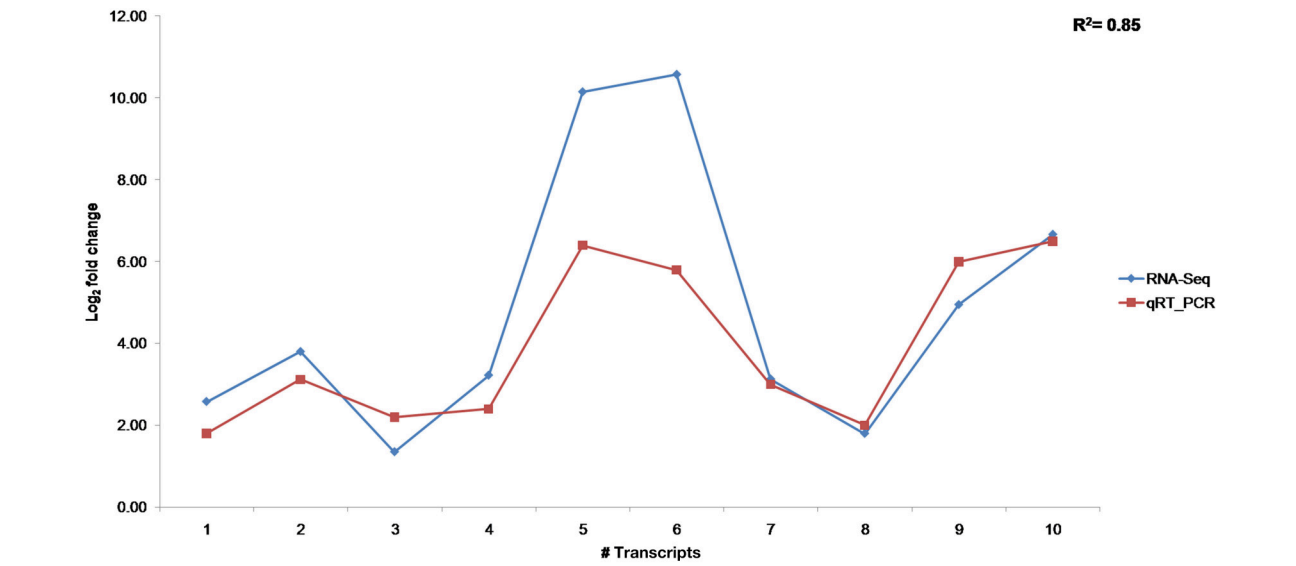

FIGURE 8 | Correlation of transcript expression between RNA-seq and qRT-PCR.

We presented much attention to assembling the reads as it forms an essential view to determine how best to evaluate assemblies, particularly in light of the variety of options available and absence of reference genome (O'Neil and Emrich, 2013). For optimal generation of transcripts, it becomes compelling to compare more than one assembler for assembling the sequencing reads (Kumar and Blaxter, 2010). From the assembly comparisons of pearl millet transcriptome, it could be inferred that the assembler, MIRA performed well as compared to other three assemblers for the 454 data. This corroborates with the earlier studies wherein MIRA generated the maximum number of contigs, largest contig size and depicted the maximum similarity with relative species proteome (Garg et al., 2011; Guimaraes et al., 2012; Zhou et al., 2012). Appropriate usage of sequencing data was reflected as MIRA emanated in the maximum number of reads utilized for assembling. The assembly assessment forms a critical step for annotating and analyzing the transcriptome data and depends on the individual data sets and species in consideration (Garg

et al., 2011). In addition, studies on transcriptome sequencing without reference genome stressed on assembly optimization step for better assembly (Chen et al., 2013). Generally, Newbler has been considered as the choice for assembling sequences generated from 454 Pyro sequencer and most of the previous studies on 454 transcriptome sequencing employed exclusively one assembler without any optimization (Kumar and Blaxter, 2010; Garg et al., 2011; Chen et al., 2013). Although, the N50 value was less for MIRA, N50 value has more significance in context of genome sequencing data than the transcriptome data. Moreover, the crucial aspect in transcriptome is number of relevant transcripts having meaningful annotation or function. The proteome coverage reflected the quality and significance of transcript formation for selection of best suitable assembly for pearl millet reads (O'Neil and Emrich, 2013). The length of the transcripts was also better represented in MIRA assembly resulting in 78.21% of transcripts having length more than 500 bp. The coverage of expressed transcripts compared with the closely related and completely sequenced crop, *S. italica* excogitated with 47.94% of transcripts having more than 80% coverage. The data is also supported by evidences of chromosomal relationships between pearl millet, foxtail millet, sorghum, and rice (Devos et al., 2000; Zhang et al., 2012). Also, in blast hit, the maximum number of pearl millet transcripts showed blast hits with foxtail millet which may point toward their ancestry and conservation of gene sequences within the Poacae family (Devos et al., 2000; Lata and Prasad, 2013). Blast hits with related oomycete species demonstrated the involvement of downy mildew transcripts in compatible interaction with host (Fawke et al., 2015). It depicted dual transcriptome wherein in compatible reaction the host and pathogen sequences were obtained (Kawahara et al., 2012; Westermann et al., 2012; Schulze et al., 2015). Withal, genome sequence information is not available for *S. graminicola*, homology of downy mildew transcripts involved in virulence or pathogenicity with other oomycetes species annotated in pathogen host interaction database was observed as avirulence determinant, reduced virulence, and unaffected pathogenicity but no further in detail analysis was performed (Jiang and Tyler, 2012).

Gene for Gene Interaction

A compatible interaction between pearl millet and downy mildew culminates into a vegetative structure instead of reproductive structure i.e., panicle, drastically bringing down its productivity. The invasion of pathogen commences at an early stage followed by morphological changes in case of compatible and incompatible interactions. Subsequent upon the infection of pearl millet seedlings with downy mildew pathogen, the appearance of brown streaks was comparatively early in resistant inoculated seedlings about eight hpi than in susceptible seedlings in which it appeared after 12–15 hpi. This can be attributed to the hypersensitive response (HR) which could have mounted as a local defense mechanism against the downy mildew pathogen (Heath, 2000). The HR has been already reported in pearl millet-downy mildew interaction (Shivakumar et al., 2003). Resistance in the form of early hypersensitive response has been recorded in relative oomycetes pathogens (Kamoun et al., 1999). There are reports published on pearl-millet downy mildew interaction describing the histological studies in downy mildew resistant genotype after inoculation, in susceptible genotype and also in case of induced resistance in resistant genotypes (Kumudini et al., 2001; Shivakumar et al., 2003; Prabhu et al., 2012).

The disease resistance or R genes are key players in defense responses involved in the gene for gene interaction i.e., the R-Avr recognition and play critical role in recognition and PAMP based response (Gururani et al., 2012). Transcript for SGT1 was highly up regulated in the resistant genotype upon infection. It has been well-established that the SGT1 complex along with HSP90 and RAR1 protein is responsible for regulation of defense responses (Spoel and Dong, 2012). Other defense related transcripts like rpp gene, *Hyaloperonospora parasitica* resistance genes identified in Arabidopsis-downy mildew interaction were also found to be expressed. Interestingly, homology can be observed between the genes expressed in plants in response to classes of downy mildew causing pathogens (Asai et al., 2014). Upregulation of antioxidant enzymes, respiratory burst oxidase and superoxide dismutase (SOD) lined up with the occurrence of HR (Babitha et al., 2002; Mahatma et al., 2011). The upregulation of respiratory burst oxidase in RI was also confirmed by qRT-PCR. Dodds et al. (2009) reviewed that oomycetes express host translocated effectors and the R-Avr interaction leads to the primary response of HR.

Global Resistance Machinery

In the present study, involvement of PR proteins in pearl millet-downy mildew interaction corroborated with the earlier studies (Shivakumar et al., 2000; Prabhu et al., 2012). PR proteins are induced locally and also activated as a response of systemic acquired resistance (SAR), in the present study also, transcripts for classes of PR proteins were expressed differentially. Expression of PR proteins has also been reported in various plant-oomycetes interactions (Van Loon and Van Strien, 1999; Glazebook, 2005). Of greater interest was purothionin, which was highly up regulated in resistant inoculated than the susceptible one. Although the PR proteins showed up-regulation in the susceptible inoculated sample, its expression was less than that in the resistant one. The expression of thionin (a cysteine rich polypeptide), thaumatin, Bowman-Birk type trypsin inhibitor-like protein can be extrapolated to have its role in anti-downy mildew activity (Chilosi et al., 2000; Chandrashekhara et al., 2010; Perazzolli et al., 2012). Expression of PR proteins has also been reported in various plant-fungal interactions including grape-downy mildew, Arabidopsis-downy mildew, foxtail-powdery mildew (Wu et al., 2010; Caillaud et al., 2013; Weng et al., 2014; Li et al., 2015). The transcript for oxalate oxidase was up-regulated and it is reported to be involved in plant defense (Zhang et al., 2013). Recently, in Arabidopsis-downy mildew interaction, it has been demonstrated that a downy mildew effector (RxLR) suppressed PR1 expression in cells containing haustoria and attenuated the salicylic acid–triggered immunity by interacting with the host mediator complex (Caillaud et al., 2013). Thus, it might be deduced that these PR proteins work in concert in bestowing resistance to pearl millet upon downy mildew infection. Moreover, the expression level of

representative transcripts for PR protein was in concurrence with expression pattern in real time PCR.

Various families of transcription factors (TFs) were upregulated upon infection (Olga et al., 2014). Higher number of MYB and WRKY transcription factors corroborated with the earlier studies on plant-pathogen interaction (Djami-Tchatchou et al., 2012; Ambawat et al., 2013; Weng et al., 2014). The expression of MYB TFs in pearl millet-downy mildew might also indicate its involvement in defense and in HR (Vailleau et al., 2002). It has been shown in barley-powdery mildew interaction that WRKY transcription factors (HvWRKY1 and HvWRKY2) activated immediately followed by Avr recognition suggesting role of WRKY (De Wit et al., 2009). The activation of Myb and WRKY TFs corroborated well with earlier studies in rice-smut, rice-blast, sorgum-sorghicola, grape-downy mildew (Bagnaresi et al., 2012; Kawahara et al., 2012; Yazawa et al., 2013; Chao et al., 2014). Furthermore, WRKY, MYB, bhlh and bZIP regulate and/or interact with phenylpropanoid pathway biosynthetic genes potentially involved in defense (Dixon et al., 2002). The high level of expression of the transcription factors, MYB and bhlh was also in line with the relatively high expression in qRT-PCR. The HSP TF was observed to be up regulated, extending the hypothesis that heat shock protein families might be expressed in pearl millet to stabilize the proteins and membranes and to assist in protein refolding under stress condition initiated by downy mildew fungus.

The up-regulation of several classes of protein kinases *viz*, wall associated kinases, calcium-dependent protein kinases, LRR receptor-like protein kinases, serine threonine protein kinases, lrr serine threonine protein kinases, MAPKs suggested a strong activation of signal transduction machinery mediated by Ca^{2+} permeable channels following positive regulation by phosphorylation of kinase domains of the protein kinases (Heath, 2000; Hammond-Kosack and Parker, 2003; White and Broadley, 2003; King et al., 2014). The relative up-regulation of MAPK upon inoculation through quantitative validation suggested its potential role as signal carrying mediator in pearl millet downy mildew interaction (Melvin et al., 2014).

The hydroxyproline rich glycoproteins (HRGPs) constitute one of the important structural components of the cell wall involved in defense against plant pathogens. The HGRPs and related proteins of its superfamily *viz*., extensins, and proline-rich proteins were expressed in the transcriptome and co-related with studies of Sujeeth et al. (2010, 2012) in pearl millet-downy mildew interaction. The transcript for polygalacturonase inhibitor protein (PGIP), cell wall glycoprotein was expressed in the resistant genotype upon inoculation which corroborated with the previous reports of Prabhu et al. (2012) in pearl millet-downy mildew and that of Wu et al. (2010) in grape-downy mildew interaction. The PGIPs, concerned as defense proteins comprise of an extra cytoplasmic leucine rich repeats (eLRR) that specifically bind and inhibit fungal polygalacturonases, thus preventing cell wall invasion of fungus into host tissue (Di Matteo et al., 2006).

The plant defense responses are multi component in nature. With regards to systemic acquired resistance, salicylic acid is principally responsible for local and systemic responses (Kachroo and Robin, 2013). Recently, study of SAR in Arabidopsis suggested that a cluster of genes including signaling, secretory, and transducing compounds are up-regulated (Gruner et al., 2013). The rate limiting enzyme, PAL was up-regulated in RI than that in SI and also affirmed with the upregulation in RI through qRT-PCR. The transcription factors mainly, WRKY, MYB, and bHLH are mainly involved in the regulation of phenyl propanoid pathway and PR proteins (Dangl and Jones, 2001; Dixon et al., 2002). Significantly higher number of transcripts belonging to phenylalanine metabolic pathway was consistent with the activation SAR in pearl millet as a defense mechanism toward downy mildew. Moreover, it has been well-established from the previous studies on plant-oomycetes interaction that phenylalanine metabolic pathway is chiefly activated and SAR provides broad-spectrum resistance against oomycetes in addition to conferring immune memory (Naoumkina et al., 2010; Orłowska et al., 2012; Kachroo and Robin, 2013; Qiu et al., 2015; Serba et al., 2015).

It can be inferred from the results that defense mechanism in the host, pearl millet in response to downy mildew could be activated in the form of hypersensitive response carried by signal transducing molecules like lrr/serine-threonine/MAP kinases followed by the activation of the pathogenesis related proteins and phenylpropanoid pathway enzymes as a part of systemic acquired resistance. Thus, through transcriptome sequencing of downy mildew resistant and susceptible genotypes, we have comprehensively presented a snapshot of differential gene expression occurring in the cell at the time of downy mildew infection. The transcripts responsible for defense resistance can be characterized further through candidate gene based approach for identification of QTL for resistance breeding. Engineering pearl millet to over-express the enzymes that were up-regulated in the resistant genotype or genome editing would be a novel and effective strategy for enhancing resistance against downy mildew pathogen.

AUTHOR CONTRIBUTIONS

YS and CJ conceived, planned and designed the study. KK, HZ, and TB carried work, analyzed, interpreted data, and prepared the manuscript. MP, HZ executed the data analysis. SK, RF, YS, and SN critically revised and edited the manuscript.

FUNDING

The funds for research work was granted by Centre of Excellence in Agricultural Biotechnology, Anand Agricultural University, Anand, Gujarat (Grant number: Budget Head 12011).

ACKNOWLEDGMENTS

The authors express gratitude to ICRISAT, Patancheru, India for providing pearl millet seed material used in the study. Authors thank Dr. J. A. Patel and Dr. Y. M. Rojasara, Regional Research Station, Anand for providing space for planting in

field. KK and HZ highly acknowledge DST INSPIRE programme and UGC RGNF respectively for providing fellowships during their doctoral research work. Technical assistance in data analysis by Sarang Sapre, Amit Bikram and Tejas Shah is duly admitted.

SUPPLEMENTARY MATERIAL

The Supplementary Material for this article can be found online at: http://journal.frontiersin.org/article/10.3389/fpls.2016.00847

Supplementary Figure 1 | Schematic representation of workflow.

Supplementary Figure 2 | Length wise distribution of pearl millet high quality reads.

Supplementary Table 1 | List of primers of transcripts used for qRT-PCR.

Supplementary Table 2 | Assembly assessment by BlastX with *Setaria italica* (Foxtail millet) proteome.

Supplementary Table 3 | Annotation of pearl millet transcripts assembled by MIRA (XLSX).

Supplementary Table 4 | Evaluation of endogenous reference genes in pearl millet under downy mildew stress using RefFinder.

REFERENCES

Ambawat, S., Sharma, P., Yadav, N. R., and Yadav, R. C. (2013). MYB transcription factor genes as regulators for plant responses: an overview. *Physiol. Mol. Biol. Plants* 19, 307–321. doi: 10.1007/s12298-013-0179-1

Anders, S., and Huber, W. (2010). Differential expression analysis for sequence count data. *Genome Biol.* 11:R106. doi: 10.1186/gb-2010-11-10-r106

Asai, S., Rallapalli, G., Piquerez, S. J. M., Caillaud, M.-C., Furzer, O. J., Ishaque, N., et al. (2014). Expression profiling during arabidopsis/downy mildew interaction reveals a highly-expressed effector that attenuates responses to salicylic acid. *PLoS Pathog.* 10:e1004443. doi: 10.1371/journal.ppat.1004443

Babitha, M. P., Bhat, S. G., Prakash, H. S., and Shetty, H. S. (2002). Differential induction of superoxide dismutase in downy mildew-resistant and susceptible genotypes of pearl millet. *Plant Pathol.* 51, 480–486. doi: 10.1046/j.1365-3059.2002.00733.x

Bagnaresi, P., Biselli, C., Orru, L., Urso, S., Crispino, L., Abbruscato, P., et al. (2012). Comparative transcriptome profiling of the early response to Magnaporthe oryzae in durable resistant vs susceptible rice (*Oryza sativa* L.) genotypes. *PLoS ONE* 7:e51609. doi: 10.1371/journal.pone.0051609

Boyd, L. A., Ridout, C., O'Sullivan, D. M., Leach, J. E., and Leung, H. (2013). Plant-pathogen interactions: disease resistance in modern agriculture. *Trends Genet.* 29, 233–240. doi: 10.1016/j.tig.2012.10.011

Cai, H., Chen, H., Yi, T., Daimon, C. M., Boyle, J. P., Peers, C., et al. (2013). VennPlex-a novel Venn diagram program for comparing and visualizing datasets with differentially regulated datapoints. *PLoS ONE* 8:e53388. doi: 10.1371/journal.pone.0053388

Caillaud, M. C., Asai, S., Rallapalli, G., Piquerez, S., Fabro, G., Jonathan, D., et al. (2013). A downy mildew effector attenuates salicylic acid-triggered immunity in Arabidopsis by interacting with the host mediator complex. *PLoS Biol.* 11:e1001732. doi: 10.1371/journal.pbio.1001732

Chandrashekhara, Niranjan-Raj, S., Deepak, S., Manjunath, G., and Shetty, H. S. (2010). Thionins (PR protein-13) mediate pearl millet downy mildew disease resistance. *Arch. Phytopathol. Plant Protect.* 43, 1356–1366. doi: 10.1080/03235400802476393

Chao, J., Jin, J., Wang, D., Han, R., Zhu, R., Zhu, Y., et al. (2014). Cytological and transcriptional dynamics analysis of host plant revealed stage-specific biological processes related to compatible Rice-Ustilaginoidea virens interaction. *PLoS ONE* 9:e91391. doi: 10.1371/journal.pone.0091391

Chen, X., Zhu, W., Azam, S., Li, H., Zhu, F., Li, H., et al. (2013). Deep sequencing analysis of the transcriptomes of peanut aerial and subterranean young pods identifies candidate genes related to early embryo abortion. *Plant Biotechnol. J.* 11, 115–127. doi: 10.1111/pbi.12018

Chilosi, G., Caruso, C., Caporale, C., Leonardi, L., Bertini, L., Buzi, A., et al. (2000). Antifungal activity of a Bowman-Birk type trypsin inhibitor from wheat kernel. *J. Phytopathol.* 148, 477–481. doi: 10.1046/j.1439-0434.2000.00527.x

Conesa, A., Gotz, S., Garcıa-Gomez, J. M., Terol, J., Talon, M., and Robles, M. (2005). Blast2GO: a universal tool for annotation, visualization and analysis in functional genomics research. *Bioinformatics* 21, 3674–3676. doi: 10.1093/bioinformatics/bti610

Dangl, J. L. and Jones, J. D. (2001). Plant pathogens and integrated defence responses to infection. *Nature* 411, 826–833. doi: 10.1038/35081161

De Wit, P. J. G. M., Mehrabi, R., Van-den-Burg, H. A., and Stergiopoulos, I. (2009). Fungal effector proteins: past, present and future. *Mol. Plant. Pathol.* 10, 735–747. doi: 10.1111/j.1364-3703.2009.00591.x

Devos, K. M., Pittaway, T. S., Reynolds, A., and Gale, M. D. (2000). Comparative mapping reveals a complex relationship between the pearl millet genome and those of foxtail millet and rice. *Theor. Appl. Genet.* 100, 190–198. doi: 10.1007/s001220050026

Di Matteo, A., Bonivento, D., Tsernoglou, D., Federici, L., and Cervone, F. (2006). Polygalacturonase-inhibiting protein (PGIP) in plant defence: a structural view. *Phytochemistry* 67, 528–533. doi: 10.1016/j.phytochem.2005.12.025

Dixon, R. A., Achnine, L., Kota, P., Liu, C. J., Reddy, M. S., and Wang, L. (2002). The phenylpropanoid pathway and plant defence-a genomics perspective. *Mol Plant Pathol.* 3, 371–390. doi: 10.1046/j.1364-3703.2002.00131.x

Djami-Tchatchou, A. T., Straker, C. J., and Allie, F. (2012). 454 Sequencing for the identification of genes differentially expressed in avocado fruit (cv. Fuerte) infected by *Colletotrichum gloeosporioides*. *J. Phytopathol.* 160, 449–460. doi: 10.1111/j.1439-0434.2012.01925.x

Dodds, P. N., and Rathjen, J. P. (2010). Plant immunity: towards an integrated view of plant-pathogen interactions. *Nat. Rev. Genet.* 11, 539–548. doi: 10.1038/nrg2812

Dodds, P. N., Rafiqi, M., Gan, P. H., Hardham, A. R., Jones, D. A. and Ellis, J. G. (2009). Effectors of biotrophic fungi and oomycetes: pathogenicity factors and triggers of host resistance. *New Phytol.* 183, 993–1000. doi: 10.1111/j.1469-8137.2009.02922.x

Fawke, S., Doumane, M. and Schornack, S. (2015). Oomycete interactions with plants: infection strategies and resistance principles. *Microbiol. Mol. Biol. Rev.* 79, 263–280. doi: 10.1128/MMBR.00010-15

Gao, L., Tu, Z. J., Millett, B. P., and Bradeen, J. M. (2013). Insights into organ-specific pathogen defense responses in plants: RNA-seq analysis of potato tuber-Phytophthora infestans interactions. *BMC Genomics* 14:340. doi: 10.1186/1471-2164-14-340

Garg, R., Patel, R. K., Tyagi, A. K., and Jain, M. (2011). *De novo* assembly of chickpea transcriptome using short reads for gene discovery and marker identification. *DNA Res.* 18, 53. doi: 10.1093/dnares/dsq028

Glazebook, J. (2005). Contrasting mechanisms of defense against biotrophic and necrotrophic pathogens. *Annu. Rev. Phytopathol.* 43, 205–227. doi: 10.1146/annurev.phyto.43.040204.135923

Gruner, K., Griebel, T., Navarova, H., Attaran, E., and Zeier, J. (2013). Reprogramming of plants during systemic acquired resistance. *Front. Plant Sci.* 4:252. doi: 10.3389/fpls.2013.00252

Guimaraes, P. M., Brasileiro, A. C. M., Morgante, C. V., Martins, A. C. Q., Pappas, G. Jr., Togawa, R., et al. (2012). Global transcriptome analysis of two wild relatives of peanut under drought and fungi infection. *BMC Genomics* 13:387. doi: 10.1186/1471-2164-13-387

Gururani, M. A., Venkatesh, J., Upadhyaya, C. P., Nookaraju, A., Pandey, S. K., and Park, S. W. (2012). Plant disease resistance genes: current status and future directions. *Physiol. Mol. Plant Pathol.* 78, 51–65. doi: 10.1016/j.pmpp.2012.01.002

Haas, B. J., Papanicolaou, A., Yassour, M., Grabherr, M., Blood, P. D., Bowden, J., et al. (2013). *De novo* transcript sequence reconstruction from RNA-seq using the Trinity platform for reference generation and analysis. *Nat protoc.* 8, 1494–1512. doi: 10.1038/nprot.2013.084

Hammond-Kosack, K. E., and Parker, J. E. (2003). Deciphering plant-pathogen communication: fresh perspectives for molecular resistance breeding. *Curr. Opin. Biotechnol.* 14, 177–193. doi: 10.1016/S0958-1669(03)00035-1

Hayden, K. J., Garbelotto, M., Knaus, B. J., Cronn, R. C., Rai, H., and Wright, J. W. (2014). Dual RNA-seq of the plant pathogen Phytophthora ramorum and its tanoak host. *Tree Genet. Genomes* 10, 489–502. doi: 10.1007/s11295-014-0698-0

Heath, M. C. (2000). Nonhost resistance and nonspecific plant defences. *Curr. Opin. Biotechnol.* 3, 315–319. doi: 10.1016/S1369-5266(00)00087-X

ICAR-AICPMIP Project co-ordinator review (2015). *50th Annual Group Meeting, All India Coordinated Research Project on Pearl millet (AICRPPM)*. Coimbatore. Available online at: http://www.aicrpmip.res.in

Jiang, R. H., and Tyler, B. M. (2012). Mechanisms and evolution of virulence in oomycetes. *Annu. Rev. Phytopathol.* 50, 295–318. doi: 10.1146/annurev-phyto-081211-172912

Jones, E. S., Breese, W. A., and Shaw, D. S. (2001). Inoculation of pearl millet with the downy mildew pathogen, *Sclerospora graminicola*: chilling inoculum to delay zoospore release and avoid spray damage to zoospores. *Plant Pathol.* 50, 310–316. doi: 10.1046/j.1365-3059.2001.00572.x

Kachroo, A., and Robin, G. P. (2013). Systemic signaling during plant defense. *Curr. Opin. Biotechnol.* 16, 527–533. doi: 10.1016/j.pbi.2013.06.019

Kale, S. D. (2012). Oomycete and fungal effector entry, a microbial Trojan horse. *New Phytol.* 193, 874–881. doi: 10.1111/j.1469-8137.2011.03968.x

Kamoun, S., Furzer, O., Jones, J. D. G., Judelson, H. S., Ali, G. S., Dalio, R. D. J., et al. (2015). The top 10 oomycete pathogens in molecular plant pathology. *Mol. Plant Pathol.* 16, 413–434. doi: 10.1111/mpp.12190

Kamoun, S., Huitema, E., and Vleeshouwers, V. G. (1999). Resistance to oomycetes: a general role for the hypersensitive response. *Trends Plant Sci.* 4, 196–200. doi: 10.1016/S1360-1385(99)01404-1

Kawahara, Y., Oono, Y., Kanamori, H., Matsumoto, T., Itoh, T., and Minami, E. (2012). Simultaneous RNA-Seq analysis of a mixed transcriptome of rice and blast fungus interaction. *PLoS ONE* 7:e49423. doi: 10.1371/journal.pone.0049423

King, S. R. F., McLellan, H., Boevink, P. C., Armstrong, M. R., Bukharov, T., Sukarta, O., et al. (2014). Phytophthora infestans RXLR effector PexRD2 interacts with host MAPKKKε to suppress plant immune signaling. *Plant Cell* 26, 1345–1359. doi: 10.1105/tpc.113.120055

Kumar, S., and Blaxter, M. L. (2010). Comparing *de novo* assemblers for 454 transcriptome data. *BMC Genomics* 11:571. doi: 10.1186/1471-2164-11-571

Kumudini, B. S., Vasanthi, N. S., and Shetty, H. S. (2001). Hypersensitive response, cell death and histochemical localisation of hydrogen peroxide in host and non-host seedlings infected with the downy mildew pathogen *Sclerospora graminicola*. *Ann. Appl. Biol.* 139, 217–225. doi: 10.1111/j.1744-7348.2001.tb00398.x

Langmead, B., and Salzberg, S. L. (2012). Fast gapped-read alignment with Bowtie2. *Nat. Methods* 9, 357–359. doi: 10.1038/nmeth.1923

Lata, C., and Prasad, M. (2013). Setaria genome sequencing: an overview. *J. Plant Biochem. Biotechnol.* 22, 257–260. doi: 10.1007/s13562-013-0216-8

Li, Y. Z., Wang, N., Dong, L., Bai, H., Quan, J. Z., Liu, L., et al. (2015). Differential gene expression in Foxtail Millet during incompatible interaction with Uromyces setariae-italicae. *PLoS ONE* 10:e0123825. doi: 10.1371/journal.pone.0123825

Liang, H., Statonb, M., Xua, Y., Xua, T., and LeBoldus, J. (2014). Comparative expression analysis of resistant and susceptible Populus clones inoculated with Septoria musiva. *Plant Sci.* 223, 69–78. doi: 10.1016/j.plantsci.2014.03.004

Mahatma, M. K., Bhatnagar, R., Mittal, G. K., and Mahatma, L. (2011). Antioxidant metabolism in pearl millet genotypes during compatible and incompatible interaction with downy mildew pathogen. *Arch. Phytopathol. Plant Protect.* 44, 911–924. doi: 10.1080/03235401003633923

Margulies, M., Egholm, M., Altman, W. E., Attiya, S., Bader, J. S., Bemben, L. A., et al. (2005). Genome sequencing in microfabricated high-density picolitre reactors. *Nature* 437, 376–380. doi: 10.1038/nature03959

Martel, E., DeNay, D., Siljak-Yakovlev, S., Brown, S., and Sarr, A. (1997). Genome size variation and basic chromosome number in pearl millet and fourteen related Pennisetum species. *J. Hered.* 88, 13–143. doi: 10.1093/oxfordjournals.jhered.a023072

Martin, J. A., and Wang, Z. (2011). Next-generation transcriptome assembly. *Nat. Rev. Genet.* 12, 671–682. doi: 10.1038/nrg3068

Melvin, P., Prabhu, S. A., Anup, C. P., Shailasree, S., Shetty, H. S., and Kini, K. R. (2014). Involvement of mitogen-activated protein kinase signalling in pearl millet-downy mildew interaction. *Plant Sci.* 214, 29–37. doi: 10.1016/j.plantsci.2013.09.008

Metzker, M. L. (2010). Sequencing technologies-the next generation. *Nat. Rev. Genet.* 11, 31–46. doi: 10.1038/nrg2626

Meyer, F. E., Shuey, L. S., Ramsuchit, S., Mamni, T., Berger, D. K., Van Den, B., et al. (2016). Dual RNA-sequencing of Eucalyptus nitens during Phytophthora cinnamomi challenge reveals pathogen and host factors influencing compatibility. *Front. Plant Sci.* 7:191. doi: 10.3389/fpls.2016.00191

Naoumkina, M. A., Zhao, Q., Gallego-Giraldo, L., Dai, X., Zhao, P. X., and Dixon, R. A. (2010). Genome-wide analysis of phenylpropanoid defence pathways. *Mol. Plant Pathol.* 11, 829–846. doi: 10.1111/j.1364-3703.2010.00648.x

O'Neil, S. T., and Emrich, S. J. (2013). Assessing *de novo* transcriptome assembly metrics for consistency and utility. *BMC Genomics.* 14:465. doi: 10.1186/1471-2164-14-465

Olga, A. P., Shao, J., and Nemchinov, L. G. (2014). *In silico* identification of transcription factors in *Medicago sativa* using available transcriptomic resources. *Mol. Genet. Genomics* 289, 457–468. doi: 10.1007/s00438-014-0823-7

Orłowska, E., Fiil, A., Kirk, H. G., Llorente, B., and Cvitanich, C. (2012). Differential gene induction in resistant and susceptible potato cultivars at early stages of infection by Phytophthora infestans. *Plant Cell Rep.* 31, 187–203. doi: 10.1007/s00299-011-1155-2

Ozsolak, F., and Milos, P. M. (2011). RNA sequencing: advances, challenges and opportunities. *Nat. Rev. Genet.* 12, 87–98. doi: 10.1038/nrg2934

Perazzolli, M., Moretto, M., Fontana, P., Ferrarini, A., Velasco, R., Delledonne, M., et al. (2012). Downy mildew resistance induced by Trichoderma harzianum T39 in susceptible grapevines partially mimics transcriptional changes of resistant genotypes. *BMC Genomics* 13:660. doi: 10.1186/1471-2164-13-660

Prabhu, S. A., Kini, K. R., Raj, S. N., Moerschbacher, B. M., and Shetty, H. S. (2012). Polygalacturonase-inhibitor proteins in pearl millet: possible involvement in resistance against downy mildew. *Acta Biochim. Biophys. Sin.* 44, 415–423. doi: 10.1093/abbs/gms015

Qiu, W., Feechan, A., and Dry, I. (2015). Current understanding of grapevine defense mechanisms against the biotrophic fungus (Erysiphe necator), the causal agent of powdery mildew disease. *Hortic. Res.* 2:15020. doi: 10.1038/hortres.2015.20

Rajaram, V., Nepolean, T., Senthilvel, S., Varshney, R. K., Vadez, V., Srivastava, R. K., et al. (2013). Pearl millet [*Pennisetum glaucum* (L.) *R. Br.]* consensus linkage map constructed using four RIL mapping populations and newly developed EST-SSRs.*BMC Genomics* 14:159. doi: 10.1186/1471-2164-14-159

Reeksting, B. J., Coetzer, N., Mahomed, W., Engelbrecht, J., and van den Berg, N. (2014). *De novo* sequencing, assembly and analysis of the root transcriptome of Persea americana (Mill.) in response to Phytophthora cinnamomi and flooding. *PLoS ONE* 9:e86399. doi: 10.1371/journal.pone.0086399

Saeed, A. I., Sharov, V., White, J., Li, J., Liang, W., Bhagabati, N., et al. (2003). TM4: a free, open-source system for microarray data management and analysis. *Biotechniques* 34, 374–378.

Safeeulla, K. M. (1976). *Biology and Control of the Downy Mildews of Pearl Millet, Sorghum and Finger Millet*. Mysore: Downy Mildew Research Laboratory; Mysore University.

Schmieder, R., and Edwards, R. (2011). Quality control and preprocessing of metagenomic datasets. *Bioinformatics* 27, 863–864. doi: 10.1093/bioinformatics/btr026

Schmieder, R., Lim, Y. W., and Edwards, R. (2012). Identification and removal of ribosomal RNA sequences from metatranscriptomes. *Bioinformatics* 28, 433–435. doi: 10.1093/bioinformatics/btr669

Schulze, S., Henkel, S. G., Driesch, D., Guthke, R., and Linde, J. (2015). Computational prediction of molecular pathogen-host interactions based on dual transcriptome data. *Front. Microbiol.* 6:65. doi: 10.3389/fmicb.2015.00065

Serba, D. D., Uppalapati, S. R., Mukherjee, S., Krom, N., Tang, Y., Mysore, K. S., et al. (2015). Transcriptome profiling of rust resistance in Switchgrass using RNA-Seq analysis. *Plant Genome* 8, 1–12. doi: 10.3835/plantgenome2014.10.0075

Shetty, H. S. (1987). "Biology and epidemiology of downy mildew of pearl millet," in *Proceedings of the International Pearl Millet Workshop* (Patencheru), 147–160.

Shivakumar, P. D., Geetha, H. M. and Shetty, H. S. (2003). Peroxidase activity and isozyme analysis of pearl millet seedlings and their implications in downy mildew disease resistance. *Plant Sci.* 164, 85–93. doi: 10.1016/S0168-9452(02)00339-4

Shivakumar, P. D., Vasanthi, N. S., Shetty, H. S., and Smedegaard-Petersen, V. (2000). Ribonucleases in the seedlings of pearl millet and their involvement in resistance against downy mildew disease. *Eur. J. Plant Pathol.* 106, 825–836. doi: 10.1023/A:1008775806087

Spoel, S. H., and Dong, X. N. (2012). How do plants achieve immunity? *Defence without specialized immune cells. Nat. Rev. Immunol.* 12, 89–100. doi: 10.1038/nri3141

Sujeeth, N., Deepak, S., Shailasree, S., Kini, R. K., Shetty, S. H., and Hille, J. (2010). Hydroxyproline-rich glycoproteins accumulate in pearl millet after seed treatment with elicitors of defense responses against *Sclerospora graminicola*. *Physiol. Mol. Plant. Pathol.* 74, 230–237. doi: 10.1016/j.pmpp.2010.03.001

Sujeeth, N., Kini, R. K., Shailasree, S., Wallaart, E., Shetty, S. H., and Hille, J. (2012). Characterization of a hydroxyproline-rich glycoprotein in pearl millet and its differential expression in response to the downy mildew pathogen *Sclerospora graminicola*. *Acta Physiol. Plant.* 34, 779–791. doi: 10.1007/s11738-011-0879-5

Tan, G., Liu, K., Kang, J., Xu, K., Zhang, Y., Hu, L., et al. (2015). Transcriptome analysis of the compatible interaction of tomato with Verticillium dahliae using RNA-sequencing. *Front. Plant Sci.* 6:428. doi: 10.3389/fpls.2015.00428

Thakur, R. P., Rai, K. N., Khairwal, I. S., and Mahala, R. S. (2008). Strategy for downy mildew resistance breeding in pearl millet in India. *J. SAT Agric. Res.* 6. 1–11. Available online at: http://oar.icrisat.org/2686/1/Strategy_for_downy_mildew_resistance_breeding_in_pearl_millet_in_India.pdf

Thakur, R. P., Rao, V. P., and Sharma, R. (2007). Evidence for temporal virulence change in pearl millet downy mildew pathogen populations in India. *J. SAT Agric. Res.* 3, 1–3. Available online at: http://oar.icrisat.org/2591/1/Evidence_for_temporal.pdf

Thakur, R. P., Sharma, R., and Rao, V. P. (2011). *Screening Techniques for Pearl Millet Diseases. Information Bulletin No. 89*. Patancheru: International Crops Research Institute for the Semi-Arid Tropics.

Vailleau, F., Daniel, X., Tronchet, M., Montillet, J. L., Triantaphylides, C., and Roby, D. (2002). A R2R3-MYB gene, AtMYB30, acts as a positive regulator of the hypersensitive cell death program in plants in response to pathogen attack. *Proc. Natl. Acad. Sci. U.S.A.* 99, 10179–10184. doi: 10.1073/pnas.152047199

Van Loon, and Van Strien, (1999). "Occurrence and properties of plant pathogenesis-related proteins," in *Pathogenesis-Related Proteins in Plants,* eds S. K. Datta, S. Muthukrishnan, (Boca Raton, FL: CRC Press LLC), 1–19.

Varshney, R. K., Nayak, S. N., May, G. D., and Jackson, S. A. (2009). Next-generation sequencing technologies and their implications for crop genetics and breeding. *Trends Biotechnol.* 27, 522–530. doi: 10.1016/j.tibtech.2009.05.006

Varshney, R. K. (2014). "*Towards developing a reference genome sequence of pearl millet (Pennisetum glaucum L.)*," in *International Plant and Animal Genome Conference*. (San Diego, CA). Available online at: www.intlpag.org

Veena, M., Melvin, P., Prabhu, S. A., Shailasree, S., Shetty, H. S., and Kini, K. R. (2016). Molecular cloning of a coiled-coil-nucleotide-binding-site-leucine rich repeat gene from pearl millet and its expression pattern in response to the downy mildew pathogen. *Mol Biol Rep.* 43, 117–128. doi: 10.1007/s11033-016-3944-8

Vijay, N., Poelstra, J. W., Kunstner, A., and Wolf, J. B. W. (2013). Challenges and strategies in transcriptome assembly and differential gene expression quantification. A comprehensive *in silico* assessment of RNA-seq experiments. *Mol. Ecol.* 22, 620–634. doi: 10.1111/mec.12014

Wang, X., Shi, W., and Rinehart, T. (2015). Transcriptomes that confer to plant defense against powdery mildew disease in Lagerstroemia indica. *Int. J. Genomics* 2015, 12. doi: 10.1155/2015/528395

Weng, K., Li, Z. Q., Liu, R. Q., Wang, L., Wang, Y. J., and Xu, Y. (2014). Transcriptome of Erysiphe necator-infected Vitis pseudoreticulata leaves provides insight into grapevine resistance to powdery mildew. *Hortic. Res.* 1:14049. doi: 10.1038/hortres.2014.49

Westermann, A. J., Gorski, S., and Vogel, J. (2012). Dual RNA-seq of pathogen and host. *Nat. Rev. Microbiol.* 10, 618–630. doi: 10.1038/nrmicro2852

White, P. J., and Broadley, M. R. (2003). Calcium in plants. *Ann. Bot.* 92, 487–511. doi: 10.1093/aob/mcg164

Winnenburg, R., Baldwin, T. K., Urban, M., Rawlings, C., Kohler, J., and Hammond-Kosack, K. E. (2006). PHI-base: a new database for pathogen host interactions. *Nucleic Acids Res.* 34, D459–D464. doi: 10.1093/nar/gkj047

Wu, J., Zhang, Y., Zhang, H., Huang, H., Folta, K. M., and Lu, J. (2010). Whole genome wide expression profiles of Vitis amurensis grape responding to downy mildew by using Solexa sequencing technology. *BMC Plant Biol.* 10:234. doi: 10.1186/1471-2229-10-234

Xie, F., Xiao, P., Chen, D., Xu, L., and Zhang, B. (2012). miRDeepFinder: a miRNA analysis tool for deep sequencing of plant small RNAs. *Plant. Mol. Biol.* 80, 75–84. doi 10.1007/s11103-012-9885-2

Yadav, R., Hash, C. T., Howarth, C., Witcombe, J. R., and Khairwal, I. S. (2013). "Successful marker-assisted selection for disease resistance and drought tolerance in pearl millet in India," in *Biotechnologies at Work for Smallholders: Some Experiences from Developing Countries in Crops, Livestock and Fish*, eds J. Ruane, J. Dargie, C. Mba, P. Boettcher, H. P. S. Makkar, D. M. Bartley and A. Sonnino (Rome: Food and Agricultural organizations (FAO) of the United Nations).

Yazawa, T., Kawahigashi, H., Matsumoto, T., and Mizuno, H. (2013). Simultaneous transcriptome analysis of Sorghum and Bipolaris sorghicola by using RNA-seq in combination with *de novo* transcriptome assembly. *PLoS ONE* 8:e62460. doi: 10.1371/journal.pone.0062460

Ye, J., Fang, L., Zheng, H., Zhang, Y., Chen, J., Zhang, Z., et al. (2006). WEGO: a web tool for plotting GO annotations. *Nucleic Acids Res.* 34, 293–297. doi: 10.1093/nar/gkl031

You, F. M., Huo, N., Gu, Y. Q., Luo, M. C., Ma, Y., Hane, D., et al. (2008). BatchPrimer3: a high throughput web application for PCR and sequencing primer design. *BMC Bioinformatics* 29:253. doi: 10.1186/1471-2105-9-253.

Zhang, X. Y., Nie, Z. H., Wang, W. J., Leung, D. W. M., Xu, D. G., Chen, B. N., et al. (2013). Relationship between disease resistance and rice oxalate oxidases in transgenic rice. *PLoS ONE* 8:e78348. doi: 10.1371/journal.pone.0078348

Zhang, Y., Ma, P., and Li, D. (2012). High-throughput sequencing of six bamboo chloroplast genomes: phylogenetic implications for temperate woody bamboos (Poaceae: Bambusoideae). *PLoS ONE* 6:e20596. doi: 10.1371/journal.pone.0020596

Zhou, Y., Gao, F., Liu, R., Feng, J., and Li, H. (2012). *De novo* sequencing and analysis of root transcriptome using 454 pyrosequencing to discover putative genes associated with drought tolerance in Ammopiptanthus mongolicus. *BMC Genomics* 13:266. doi: 10.1186/1471-2164-13-266

Conflict of Interest Statement: The authors declare that the research was conducted in the absence of any commercial or financial relationships that could be construed as a potential conflict of interest.

frontiers in Microbiology

ORIGINAL RESEARCH
published: 30 March 2016
doi: 10.3389/fmicb.2016.00408

Transcriptomes of Arbuscular Mycorrhizal Fungi and Litchi Host Interaction after Tree Girdling

*Bo Shu, Weicai Li, Liqin Liu, Yongzan Wei and Shengyou Shi**

Key Laboratory of Tropical Fruit Biology, Ministry of Agriculture, South Subtropical Crops Research Institute, Chinese Academy of Tropical Agricultural Science, Zhanjiang, China

Trunk girdling can increase carbohydrate content above the girdling site and is an important strategy for inhibiting new shoot growth to promote flowering in cultivated litchi (*Litchi chinensis* Sonn.). However, girdling inhibits carbohydrate transport to the root in nearly all of the fruit development periods and consequently decreases root absorption. The mechanism through which carbohydrates regulate root development in arbuscular mycorrhiza (AM) remains largely unknown. Carbohydrate content, AM colonization, and transcriptome in the roots were analyzed to elucidate the interaction between host litchi and AM fungi when carbohydrate content decreases. Girdling decreased glucose, fructose, sucrose, quebrachitol, and starch contents in the litchi mycorrhizal roots, thereby reducing AM colonization. RNA-seq achieved approximately 60 million reads of each sample, with an average length of reads reaching 100 bp. Assembly of all the reads of the 30 samples produced 671,316 transcripts and 381,429 unigenes, with average lengths of 780 and 643 bp, respectively. Litchi (54,100 unigenes) and AM fungi unigenes (33,120 unigenes) were achieved through sequence annotation during decreased carbohydrate content. Analysis of differentially expressed genes (DEG) showed that flavonoids, alpha-linolenic acid, and linoleic acid are the main factors that regulate AM colonization in litchi. However, flavonoids may play a role in detecting the stage at which carbohydrate content decreases; alpha-linolenic acid or linoleic acid may affect AM formation under the adaptation process. Litchi trees stimulated the expression of defense-related genes and downregulated symbiosis signal-transduction genes to inhibit new AM colonization. Moreover, transcription factors of the AP2, ERF, Myb, WRKY, bHLH families, and lectin genes altered maintenance of litchi mycorrhizal roots in the post-symbiotic stage for carbohydrate starvation. Similar to those of the litchi host, the E3 ubiquitin ligase complex SCF subunit scon-3 and polyubiquitin of AM fungi were upregulated at the perceived stages. This occurrence suggested that ubiquitination plays an important role in perceiving carbohydrate decrease in AM fungi. The transcription of cytochrome b-245 and leucine-rich repeat was detected in the DEG database, implying that the transcripts were involved in AM fungal adaptation under carbohydrate starvation. The transcriptome data might suggest novel functions of unigenes in carbohydrate shortage of mycorrhizal roots.

Keywords: litchi, carbohydrates, arbuscular mycorrhizal colonization, RNA-seq, transcripts

OPEN ACCESS

Edited by:
Pietro Daniele Spanu, Imperial College London, UK

Reviewed by:
Raffaella Balestrini, Consiglio Nazionale delle Ricerche, Italy
Biswapriya Biswavas Misra, University of Florida, USA

****Correspondence:***
Shengyou Shi
ssy7299@163.com

Specialty section:
This article was submitted to Plant Biotic Interactions, a section of the journal Frontiers in Microbiology

Received: *13 January 2016*
Accepted: *14 March 2016*
Published: *30 March 2016*

Citation:
Shu B, Li W, Liu L, Wei Y and Shi S (2016) Transcriptomes of Arbuscular Mycorrhizal Fungi and Litchi Host Interaction after Tree Girdling. Front. Microbiol. 7:408. doi: 10.3389/fmicb.2016.00408

INTRODUCTION

Arbuscular mycorrhiza represents widespread mutualistic association between soil-borne fungi of the Phylum Glomeromycota and most land plants. AM fungi play a key role in the life of host plants; the fungi supply mineral nutrients to the roots (biofertilizers), influence plant development (bioregulators), and enable mycorrhizal plants to overcome biotic and abiotic stresses (bioprotectors; Parniske, 2008; Smith and Read, 2008). The host plant provides carbohydrates to obligate biotrophic fungi to enable the fungi to complete their life cycle. Plants could allocate up to 30% of their photosynthetic carbohydrates to AM fungi, which in return, provides up to 80% of plant phosphate and nitrogen. Moreover, the two partners guarantee a "fair trade" of mineral nutrients against carbohydrates (Kiers et al., 2011; Fellbaum et al., 2012). Although carbohydrates provided by host plants play important roles in the life cycle of AM fungi, knowledge on processes involved in the host carbohydrate regulation for AM fungi colonization remains limited.

Litchi (*Litchi chinensis* Sonn.), which belongs to the Sapindaceae family, is an important woody mycorrhizal fruit tree in southern China. The area for cultivation of litchi reached 553,000 ha in 2015. The main cultivars of litchi (*L. chinensis* Sonn. Feizixiao and *L. chinensis* Sonn. Guiwei) normally flower in March and mature in June in the Guangdong province of China. Trunk girdling increases carbohydrate content above the girdling site and decreases the uptake of water and mineral nutrition; this strategy is important to inhibit new shoot growth and promote flowering in cultivated litchi (Yuan and Huang, 1993; Huang et al., 2003). Trunk girdling is generally performed in the second half of November before the period of flower-bud differentiation and wound healing in half a year. However, girdling adversely affects carbohydrate transport to the root of litchi, thereby restricting litchi mycorrhizal root development. This technique also reduces mycorrhizal root absorption, consequently decreasing the quality of fruit or inducing fruit drop during fruit development. Hence, the coping strategy of litchi mycorrhizal root under carbohydrate starvation must be elucidated to improve culture techniques.

Carbohydrates in plant tissues are diverse throughout evolution; the different kinds of carbohydrates include glucose, fructose, sucrose, sorbitol, and starch in the roots of the apple tree (Tromp, 1983) as well as glucose, fructose, sucrose, quebrachitol, and starch in the root of the litchi tree (Wang et al., 2013). All types of carbohydrates starvation may affect the pre- and post-symbiotic interactions of the AM fungi and the host plant. To date, several molecular signals are identified and used to recognize AM fungi and host plant in the pre-symbiotic period. Flavonols, strigolactones, and hydroxy fatty acids from the host plant and lipochito-oligosaccharides, short-chain chitin oligomers, and steroids from the AM fungi are dialog components (Bécard et al., 1992; Besserer et al., 2008; Maillet et al., 2011; Nagahashi and Douds, 2011; Genre et al., 2013; Bucher et al., 2014; Sun et al., 2015). Molecules and related genes in the post-symbiotic stage are more complex than those in the pre-symbiotic period. Genes, which are related to phytohormone biosynthesis and signal transduction, transport systems of nutrient and carbohydrate, transcription factor, and other processes, all participate in the post-symbiotic stages (De Hoff et al., 2009; Hogekamp et al., 2011; Handa et al., 2015). To analyze the influence of carbohydrate starvation on the litchi mycorrhizal root, this study focused on mycorrhizal root carbohydrates (glucose, fructose, sucrose, quebrachitol, and starch) to determine the degree of carbohydrate decrease and measure AM colonization rate to clarify whether carbohydrates reduce AM colonization. Based on the above analysis, this study also tested the transcriptome data to screen for interesting transcripts involved in the interaction between AM fungi and host litchi under carbohydrate starvation.

Abbreviations: AM, arbuscular mycorrhiza; COG, cluster of orthologous groups of proteins; CYP, cytochrome P450; DEG, differentially expressed gene; FDR, false discovery rate; FPKM, fragments per kilobase of exon per million fragments mapped; Gloin1, *Rhizophagus irregularis* genome assembly; GO, gene ontology; HPLC, high-performance liquid chromatography; KEGG, Kyoto Encyclopedia of Genes and Genomes; LRR, leucine-rich repeats; nr, NCBI non-redundant (nr) database.

MATERIALS AND METHODS

Plant Material and Cultivation Conditions

Six litchi trees with middle growth vigor were selected from 200 trees (cultivar Feizixiao, grafted on 12-year-old Huaizhi rootstock) and cultivated in the experimental orchard of the South Subtropical Crops Research Institute, Zhanjiang, China (mineral nutrition is shown in Supplementary Table 1). The trees received standard horticultural practices (such as weeding and irrigating) as well as disease and insect control. Three of the six trees were girdled in November (The girdling picture was shown in **Supplementary Figure S1**), and the remaining trees were used as control. Root (diameter < 1.5 mm) was sampled to 20–30 cm soil thickness, where fibrous roots were overdispersed, from the four directions of each tree; duplicate samples were obtained from each tree. The root samples were immediately obtained after girdling treatment (0 day, 0 D) as well as 1 week, 2 weeks, 1 month, and 2 months (1 W, 2 W, 1 M, and 2 M, respectively) thereafter. Thirty samples were acquired in the experiment. The samples were washed with sterile water, wiped dry with gauze at harvest, frozen in liquid nitrogen, and then immediately stored at $-80°C$.

Root Mycorrhizal Colonization

A fraction of the fresh roots was fixed in formalin/acetic acid/ethanol (FAA, 13:5:200 [v/v/v]) for 24 h to determine the degree of AM colonization. The roots were cleared in 10% (w/v) KOH at 99°C for 1.5 h and stained with 0.05% (w/v) trypan blue in lactophenol by using methods previously described by Phillips and Hayman (1970). The structures of AM fungi were examined under a compound light microscope (Olympus-BH-2). Fungal colonization was estimated using magnified intersection method (McGonigle et al., 1990). Total AM and arbuscule colonization rate were quantified by examining 200 intersections for each sample.

Measurements of Soluble Sugars and Starch

Soluble sugars were measured using HPLC analyses. Determinations were performed as described by Wang et al. (2013) and Wang T.D. et al. (2014). About 1 g of the roots were homogenized, extracted three times with 85% (v/v) ethanol (3 mL each), and then centrifuged at 6000 × *g* for 10 min. The pooled supernatant was rotary evaporated to dryness and resuspended in 4 mL of distilled water. The precipitate was then analyzed for starch content. Sugars were detected by Agilent 1200 HPLC system (Agilent Technologies, Waldbronn, Germany) equipped with a refractive index detector and a transgenomic CARB Sep Coregel 87C column (CHO-99-5860). The ultra-pure water was the mobile phase at a flow rate of 0.8 mL/min. The sugars were identified by comparing their retention times with those of authentic standards. The concentrations of individual sugars were quantified using peak areas and calibration curves derived from the standards.

The precipitates were combined with 2 mL of water, and the mixture was gelatinized for 15 min in boiled water. The mixture was cooled to 20°C and then added with 2 mL of 9.2 M perchloric acid. The mixture was stirred for 15 min, combined with 4 mL of water, and centrifuged at 3500 × *g* for 10 min. The supernatant was transferred to a 50 mL volumetric flask. The precipitate was combined with 2 mL of 4.6 M perchloric acid, and the resulting mixture was stirred for 15 min. The mixture was added with 5 mL of water and centrifuged at 3500 × *g* for 10 min. The supernatant was then transferred to the same 50 mL volumetric flask. The precipitate was washed twice with 5 mL of water, and the water was also transferred to a 50 mL volumetric flask. The solution in the 50 mL volumetric flask was analyzed for starch content according to Wang T.D. et al. (2014).

Total RNA Extraction and RNA Sequencing

Total RNA was isolated from the mycorrhizal root of litchi by using TRIzol reagent (Invitrogen, USA) and treated with DNase I to eliminate genomic DNA contamination. Three biological replicates were prepared for each treatment, and RNA of 30 samples was obtained. RNA quality was determined using Agilent 2100 Bioanalyzer. After the total RNA extraction and DNase I treatment, magnetic beads with Oligo (dT) were used to isolate mRNA. The isolated mRNA was mixed with the fragmentation buffer and then fragmented into short fragments. cDNA was synthesized using the mRNA fragments as templates. Short fragments were purified and resolved with elution buffer for end reparation and addition of single nucleotide A (adenine). The short fragments were connected with adapters. Suitable fragments were selected for PCR amplification as templates. During the quality control, Agilent 2100 Bioanalyzer and ABI StepOnePlus Real-Time PCR System were used for quantification and qualification of the sample library. Finally, 30 libraries were sequenced using the Illumina HiSeq 2000 system.

Transcript Assembly and Functional Annotation

Prior to bioinformatic analysis, the raw sequences were filtered to remove reads that contained only the adaptor sequences, those with more than 5% unknown nucleotides, and the low-quality reads with more than 20% bases having a quality value ≤ 10. Because litchi genome has not been published and multiplex types of AM fungi which might show sequence difference from *Rhizophagus irregularis* are existed in litchi mycorrhizal root, *de novo* assembly was performed by the Beijing Genomics Institute using the short-read assembly program for both litchi and AM fungi by using the Trinity software (version 2.0.6; Grabherr et al., 2011). The Blast software (version 2.2.30+) with evalue 1e-3 -num_alignments 1 was used for separating the transcript of litchi and AM fungi by against the genome (*R. irregularis* DAOM 197198, Gloin1[1]) and nr database[2].

TransDecoder software (version r20140704) was employed to predict the transcript open reading frame with -m50 setting. Functional annotation of the unigenes was performed using the nr database, the Swiss-Prot protein database[3], the KEGG database[4], uniref 90[5], and Gloin1 by using BLASTx with an *E*-value $< 10^{-5}$ by Trinotate software (version 20140708). When a unigene did not align to any of the above databases, Hmmscan (HMMER) software (version 3.1) was used for annotation through functional domain prediction (Grabherr et al., 2011).

Read Mapping and Quantification of Gene Expression

Reads containing adaptors, reads with more than 10% unknown nucleotides, and low-quality reads with more than 50% bases with a quality value ≤ 5 were removed to obtain uncontaminated sequences. The uncontaminated sequences from each sample were mapped to the assembly transcripts by using Bowtie software (version: 1.0.1; parameters: mismatch = 2). The files of the bam format were achieved and used to calculate for the number of reads mapped on the transcript by RSEM software (version: v1.2.17). The number of mapped and filtered reads for each unigene was calculated to obtain the corresponding FPKM values (Li and Dewey, 2011). DEGs between two samples were determined using the FDR threshold of <0.001, an absolute log twofold change value of >1.0, and a *P*-value of <0.01 by Edger (version: 3.10.2). The GO and KEGG pathway analyses of DEGs were accomplished using GOseq software (version: 3.0) and KOBAS software (version: 2.0; Young et al., 2010; Xie et al., 2011). The heat maps of the selected DEGs from litchi and AM fungi were constructed using mev software (v4.9.0). The flow chart for RNA-seq analysis was shown in **Supplementary Figure S2**.

[1]http://genome.jgi.doe.gov/Gloin1/Gloin1.home.html

[2]http://www.ncbi.nlm.nih.gov

[3]http://www.expasy.ch/sprot

[4]http://www.genome.jp/kegg

[5]http://www.uniprot.org/uniref/?query=&fil=identity:0.9

Statistical Analysis

Experimental data were statistically analyzed using ANOVA through SAS 8.1 software (SAS Institute, Cary, NC, USA). The probabilities of significance were used to determine significance among the treatments, and the least-significant difference ($p < 0.05$) was used to compare the data.

RESULTS

Carbohydrates

The HPLC results showed that sucrose concentration (1.59–46.96 mg/g·FW) was higher than the other carbohydrate contents in the litchi mycorrhizal roots. Variation in glucose, fructose, sucrose, and quebrachitol contents in the control and girdled mycorrhizal roots exhibited the same pattern. This finding revealed that continuous decrease began at 0 D to 2 W after girdling and then remained stable from 2 W to 2 M. The concentrations of glucose, fructose, sucrose, and quebrachitol in the control were significantly higher than those in the girdled group from 1 W to 2 M. In contrast to other carbohydrates, starch concentration in the girdling treatment continuously decreased and significantly differed from 1 to 2 M compared with that of the control (**Figure 1**).

Root Mycorrhizal Colonization

The rates of total, arbuscular, and vesicular colonization rates of litchi were 15.33–36.00%, 3.97–10.43%, and 3.10–3.90%, respectively, under field conditions. Variation in the total and arbuscular colonization rates continuously decreased from 0 D to 2 M. The total and arbuscular colonization rates were significantly higher in the control than those in the girdling treatment at 1 and 2 M. Vesicular colonization was not significantly different from total and arbuscular colonizations after girdling (**Figure 2**).

Sequence Assembly and Annotation

Thirty samples were sequenced using the Illumina genome analyzer Hiseq 2000. After quality checking and data cleaning, approximately 60 million reads of each sample were obtained, with average lengths reaching 100 bp and GC content of 44–46% (Supplementary Table 2). Assembly of all the reads of the 30 samples generated 671,316 transcripts and 381,429 unigenes, with average lengths of 780 and 643 bp, respectively. A total of 308824 unigenes were annotated among all unigenes (**Table 1**). These transcriptome data were submitted to sequence read archive of NCBI with the NO. SRX1518711.

Approximately 262,619 unique sequences were annotated through BLASTx (cut-off *E*-value10^{-5}) search of four public databases, namely, nr, Swiss-Prot protein, KEGG, and uniref 90. Of the sequences, 260,019 unique sequences were annotated with reference to the nr database, whereas 2,600 unigenes were annotated using the other databases (**Figure 3A**). The results of the annotation indicated that 9.66% (25,137) of the annotated sequences exhibited "very strong homology" (E-value $< 10^{-100}$), 15.08% (39,623) exhibited "strong homology" ($10^{-100} < E$-value $< 10^{-50}$), and 70.26% (174,042) displayed "homology" ($10^{-50} < E$-value $< 10^{-5}$) to the available sequences (**Figure 3B**). The unique sequences of AM fungi achieved top matches to sequences from *R. irregularis* DAOM181602 and *R. irregularis* DAOM197198w. The unique sequences of litchi exhibited top matches to sequences from *Citrus sinensis* and *Citrus clementina* (**Figure 3C**).

The nr, GO, KEGG, and uniref 90 databases were used to classify the functions of the predicted unigenes. The unigenes of litchi (54,100 unigenes) and AM fungi (33,120 unigenes) were classified into three main categories as follows: "cellular component," "molecular function," and "biological process" (**Figure 4**). Meanwhile, the host litchi and AM fungi obtained numerous unigenes annotated as "cell and organelle" in the "cellular component" category; "binding" and "catalytic activities" in the "molecular function" category; and "metabolic process," "cellular process," "response to stimulus," and "biological regulation" as four subcategories in the "biological process" category. However, the rates of the same subcategories differed between litchi and AM fungi. Within the "cellular component," the subcategory "extracellular region part" attained a rate of less than 1% in litchi but more than 1% in fungi. The subcategory "symplost" showed more than 1% rate in litchi but less than 1% in AM fungi. Within the "molecular function" category, the subcategory of "chemoattractant" resulted in 0.01% rate in fungi but was not found in the litchi component. The subcategory of "nutrition reviser" was more than 0.01% in litchi and less than 0.01% in AM fungi. Within "biological process," the subcategory of "immune system process" in litchi unigenes was more than 1% but less than 1% in fungi (**Figure 4**).

Differential Gene Expression Analysis

The DEGs after girdling were assessed by pair-wise comparisons of all time points with the expression fold (log 2 Ratio ≥ 1) and FDR $\leq 10^{-3}$ as the thresholds in litchi and AM fungi (**Table 2**). The number of DEGs increased with prolonged girdling. Thirty-four DEGs of litchi (34 upregulated and 0 upregulated) and only one DEG of AM fungi (1 upregulated and 0 downregulated) were detected between 0 D and 1 W. Moreover, 442 DEGs of litchi (286 upregulated and 156 downregulated) and 742 DEGs of AM fungi (742 upregulated and 0 downregulated) were identified at 0 D and 2 M after pair-wise comparison (**Table 2**).

KEGG Pathway Enrichment Analysis of Differentially Expressed Genes

The main biological process and related unigenes were screened from host litchi and AM fungi during carbohydrate starvation. Most upregulated DEGs at 0 D versus those at 1 W as well as at 0 D versus those at 2 W were mapped to carbohydrate metabolism, organismal systems (plant–pathogen interaction), and amino-acid metabolism for litchi. In particular, the upregulated DEGs were mapped to carbohydrate metabolism pathways, such as pyruvate metabolism (ko00620), amino sugar and nucleotide sugar metabolism (ko00520), and starch and sucrose metabolism (ko00500). For organismal systems, the upregulated DEGs were mapped to the plant–pathogen interactions (ko04626). The amino-acid metabolism,

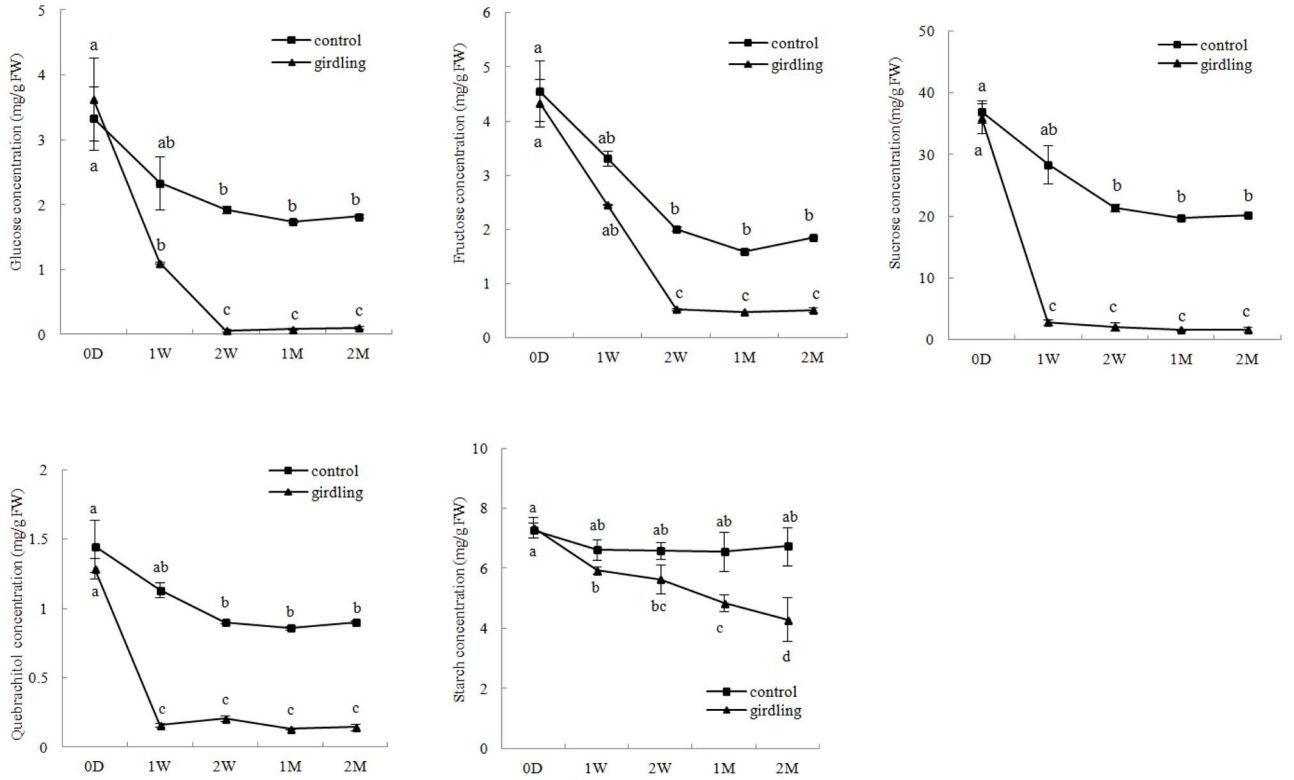

FIGURE 1 | Carbohydrate variation in the litchi mycorrhizal roots after girdling treatment. The C represents control, and the G represents girdling; 0 D, 1 W, 2 W, 1 M, 2 M represent the time after treatment (0 day, 1 week, 2 weeks, 1 month, and 2 months).

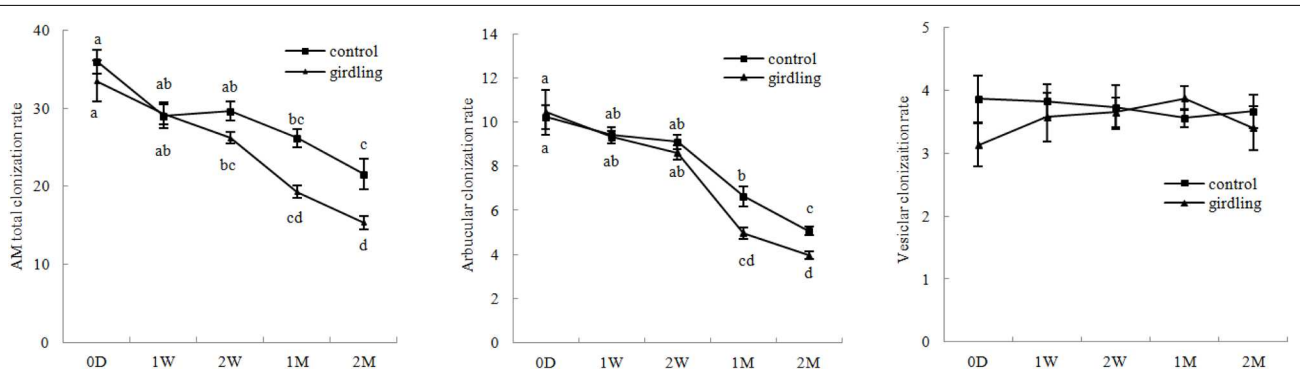

FIGURE 2 | AM colonization variation in the litchi mycorrhizal roots after girdling treatment. The C represents control, and the G represents girdling; 0 D, 1 W, 2 W, 1 M, 2 M represent the time after treatment (0 day, 1 week, 2 weeks, 1 month, and 2 months).

such as phenylalanine metabolism (ko00360) as well as valine, leucine, and isoleucine biosynthesis (ko00290) were upregulated (Supplementary Table 3). The downregulated DEGs at 0 D versus those at 1 W and at 0 D versus those at 2 W were clustered into biosynthesis of other secondary metabolites, carbohydrate metabolism, and endocrine system. Most downregulated transcripts were then mapped to the biosynthesis of other secondary metabolites in flavonoid biosynthesis (ko00941), flavone and flavonol biosynthesis (ko00944), and phenylpropanoid biosynthesis (ko00940); carbohydrate metabolism, including starch and sucrose metabolism (ko00500); and amino sugar and nucleotide sugar metabolism (ko00520; Supplementary Table 3). In the adaptation process, most upregulated DEGs at 0 D versus those at 1 M and at 0 D versus those at 2 M in litchi were clustered into lipid metabolism and biosynthesis of other secondary metabolites. The upregulated transcripts mapped to lipid metabolism were grouped under alpha-linolenic acid metabolism (ko00592), linoleic acid metabolism (ko00591), and sphingolipid metabolism (ko00600). The biosynthesis of other

TABLE 1 | Summary of read numbers based on the RNA-Seq data from the mycorrhizal roots of litchi after girdling treatment.

Item	Unigenes	Transcripts
Total number	381,429	671,316
N20	2,113	2,507
Median length	390	469
Average length	643	780
Total length	245,635,054	524,004,633
Item	**Number of genes**	**Percentage**
All	381429	100.00%
Annotated	308824	80.97%
Blast hit	253077	66.35%
Pfam	138101	36.21%
Gene ontology	157447	41.28%
Eggnog	82759	21.70%
SignalP	15636	4.10%
TmHMM	43358	11.37%

secondary metabolites, including phenylpropanoid (ko00940); stilbenoid, diarylheptanoid, gingerol (ko00945); and flavonoids, (ko00941) were also upregulated. The downregulated DEGs were mapped to several clusters under carbohydrate metabolism and immunity. The transcripts mapped to carbohydrate metabolism were grouped under starch and sucrose metabolism (ko00500), amino sugar and nucleotide sugar metabolism (ko00520), and pentose phosphate pathway (ko00030). Meanwhile, the transcripts mapped to the immune system were grouped under antigen processing and presentation (ko04612) and the NOD-like receptor signaling pathway (ko04621; Supplementary Table 3).

The upregulated DEGs at 0 D versus 1 W and at 0 D versus 2 W in AM fungi were mapped to several pathways under genetic information processing and carbohydrate metabolism. Genetic information processing included protein processing in the endoplasmic reticulum (ko04141) and ribosome (ko03010), as well as ubiquitin-mediated proteolysis (ko00290). Under carbohydrate metabolism, glyoxylate and dicarboxylate metabolism (ko00630), citrate cycle (tricarboxylic acid cycle; ko00020), and pyruvate metabolism (ko00620) were noted. The upregulated DEGs at 0 D versus those at 1 M and at 0 D versus those at 2 M in the AM fungi were mapped to genetic information processing, amino acid metabolism, lipid metabolism, and signal transduction. The genetic information processing included RNA transport (ko03013), RNA degradation (ko03018), mismatch repair (ko03430), protein processing in the endoplasmic reticulum (ko04141), and ubiquitin-mediated proteolysis (ko04120). Meanwhile, amino acid metabolism included alanine, aspartate, and glutamate metabolism (ko00250) as well as arginine and proline metabolism (ko00330). For lipid metabolism, fatty-acid biosynthesis (ko00061), alpha-linolenic acid metabolism (ko00592), and biosynthesis of unsaturated fatty acids (ko01040) were found. For signal transduction, MAPK (ko04011), Ras (ko04014), and sphingolipid signaling pathways (ko04071) were noted. The downregulated DEGs of the AM fungi were few; these DEGs were noted at 1 W versus those at 2 W (TR92985| c2_g2, putative cruciform DNA binding protein), at 1 W versus those at 2 M (TR92985| c2_g2, putative cruciform DNA binding protein), at 2 W versus those at 2 M (TR5997| c0_g2, putative protein far1-related sequence 10; TR155121| c0_g1, putative pyruvate decarboxylase; TR146357| c0_g2 and TR95299| c0_g2 uncharacterized protein), and at 1 M versus those at 2 M (TR92985| c2_g2, putative cruciform DNA

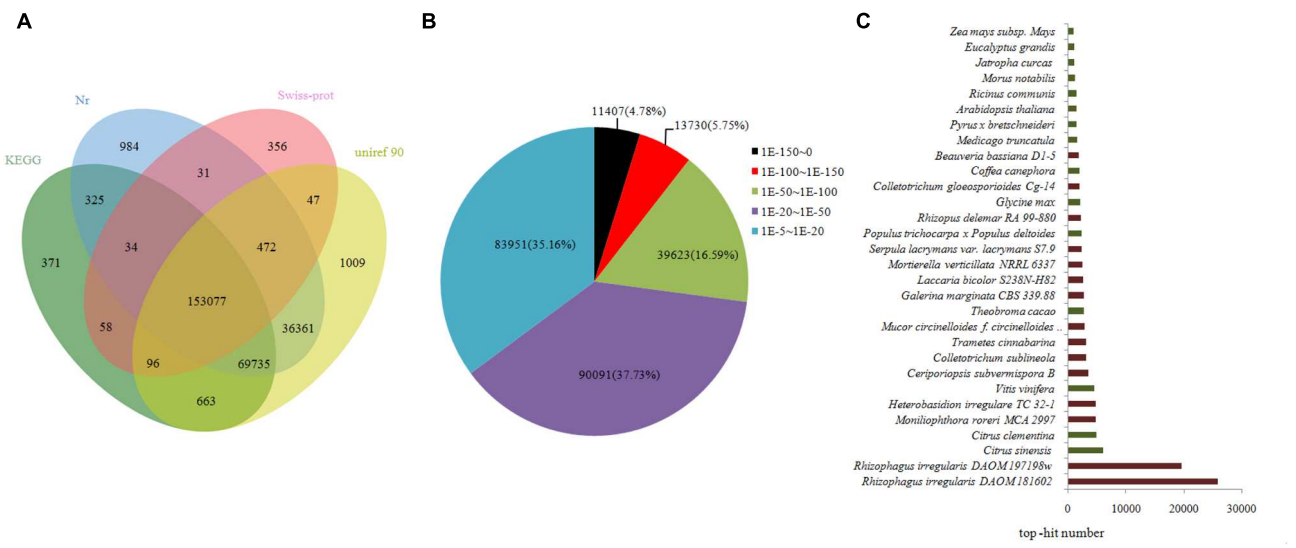

FIGURE 3 | Outcome of homology search of unigenes against the nr, KEGG, Swiss-prot, and uniref 90 databases. (A) Venn diagram of unigene numbers annotated by BLASTx with an *E*-value threshold of 10^{-5} against protein databases. The numbers in the circles indicate unigenes numbers annotated by single or multiple databases. **(B)** *E*-value distribution of the top BLAST hits for each unique sequence. **(C)** Species distribution of the top BLAST hits for all homologous sequences. Those indicated in brown denote AM fungi, and those in green correspond to litchi in **(C)**.

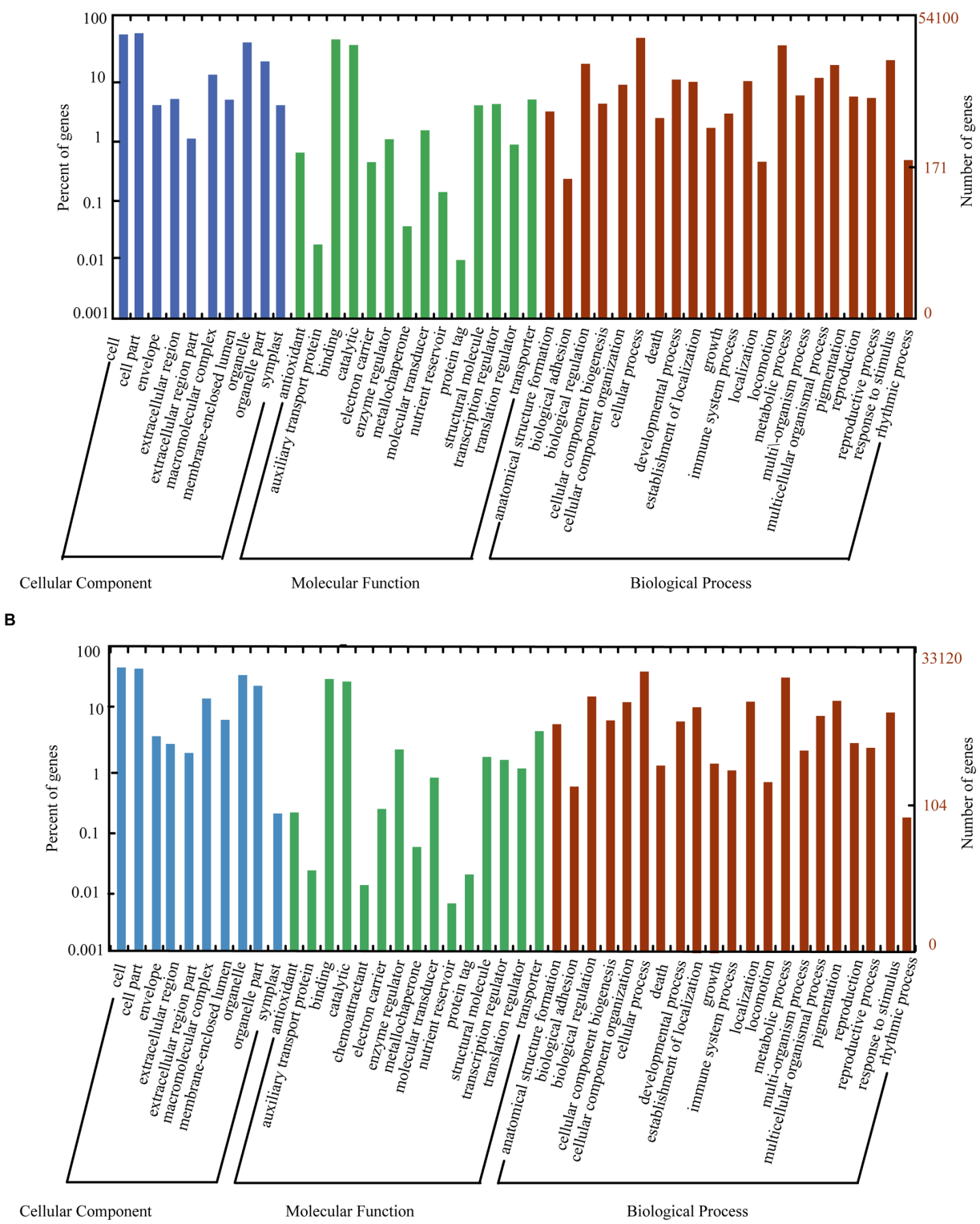

FIGURE 4 | Histogram of GO classifications for litchi (A) and AM fungi (B) transcripts in mycorrhizal roots. The unigenes corresponded to three main categories: "biological process," "cellular component," and "molecular function." The left- and right-hand *y*-axes indicate the percentage and number of annotated unigenes, respectively.

TABLE 2 | The quantity of DEGs in litchi mycorrhizal roots after girdling treatment.

	0 Day		1 Week		2 Week		1 Month		2 Month	
	Up	Down	Up	Down	Up	Down	Up	Down	Up	Down
0 D	0/0	0/0	34/1	0/0	99/41	108/0	54/190	106/0	286/742	156/0
1 W			0/0	0/0	10/5	27/1	2/4	47/0	135/244	23/1
2 W					0/0	0/0	6/5	12/0	507/79	91/4
1 M							0/0	0/0	218/19	30/2
2 M									0/0	0/0

The constitution of each value was 'DEG number of litchi/DEG number of AM fungi.'

binding protein; TR95299| c0_g2, uncharacterized protein). Only TR155121| c0_g1 was mapped to the glycolysis/gluconeogenesis pathway (ko00010; Supplementary Table 3).

Genes Including Ubiquitination, Transcription Factor, and with Repeated Domain

Ubiquitination-related unigenes, transcription factor, and unigenes with repeated domains in the host litchi were selected to construct heat map A. Ubiquitination-related unigenes, transcription factor, unigenes with repeated domains, and unigenes related to chitin synthesis in the AM fungi were used to construct heat map B. The heat map of the host litchi revealed that all selected unigenes were divested into three main subclusters. Unigenes in subcluster I were upregulated by girdling on 2 W and 1 M; unigenes in subcluster II were induced by girdling on 2 M; and unigenes in subcluster III were downregulated by girdling from 0 D to 2 M (**Figure 5A**). The heat map of AM fungi showed that all of the selected unigenes were clustered into three main subclusters. Unigenes in subcluster I were downregulated by girdling from 0 D to 1 W but were upregulated from 2 W to 2 M. Unigenes in subcluster II were downregulated by girdling on 1 W but upregulated from 2 W to 2 M. Furthermore, unigenes in subcluster III were upregulated by girdling on 2 M (**Figure 5B**).

Clustering Results of Time-Course Data from RNA-Seq by STEM Analysis

DEGs with similar expression patterns were clustered into six distinct subclusters for AM fungi and host litchi, and DEGs grouped in the same subcluster may be functionally correlated. Most DEGs in the host litchi were clustered into subclusters I and II, which were upregulated in the girdling treatment (**Figure 6A**). The expression levels of DEGs in subcluster III were stable in the control but downregulated in the girdling treatment. The expression levels of DEGs in subcluster IV were stable in the control but induced in girdling at 2 W. The expression of DEGs in subcluster V were similar to those in the control and girdling treatment from 0 D to 1 M, but the expression levels in the latter were strong upregulated at 2 M. The expression levels of DEGs in subcluster VI of the control were downregulated from 0 D to 2 M but were induced by girdling at 2 M (**Figure 6A**). Similar to those in the host litchi, the numbers of genes assigned among the six clusters in the AM fungi were statistically significant (**Figure 6B**). The DEGs of subcluster I were upregulated from 1 W in the girdling treatment, and those of subcluster II were upregulated from 2 W. The expression patterns of DEGs in subcluster III were upregulated after 2 W of girdling and then downregulated from 2 W to 2 M. The expression patterns of DEGs in subcluster IV were also upregulated after 2 W of girdling and maintained at high levels from 2 W to 2 M. The expression levels of DEGs in subcluster V were lower than those in the control from 0 D to 2 W but were induced by girdling from 2 W to 2 M. The expression patterns of DEGs in subcluster VI showed the same patterns in the control and girdling groups, but the expression levels in the latter were higher than those in the former (**Figure 6B**; Unigenes of each subcluster were displayed in Supplementary Table 4).

DISCUSSION

RNA-seq is a technique used to detect low-expressing reads (Garber et al., 2011; Wang C. et al., 2014) and identify novel transcripts in AM with DEG screening (Fiorilli et al., 2015; Handa et al., 2015). In the present experiment, transcripts obtained from each sample included litchi- and fungi-derived transcript as well as transcripts that originated from other microorganisms. The *R. irregularis* genome, genomes of model plants, and those stored in other databases were used to distinguish the transcripts, whether they were derived from litchi, AM fungi, or other organisms, through BlastP prediction (Tisserant et al., 2013). RNA-seq analysis showed approximately 60 million reads for each sample, with average read length of 100 bp. The assembly of all reads of the 30 samples produced 671,316 transcripts and 381,429 unigenes, with average lengths of 780 and 643 bp, respectively. BlastX analysis revealed that 10.85% (25,920) of the unigenes were top matched to sequences from AM fungus *R. irregularis* DAOM 181602, and 8.22% (19,627) were matched to sequences from AM fungus *R. irregularis* DAOM 197198. The unigenes of litchi (54,100 unigenes) and AM fungi (33,120 unigenes) were identified by sequence annotation during the last period of carbohydrate decrease (**Figure 4**). More than 1,300 DEGs from host litchi and 1,000 DEGs from AM fungi were noted for the corresponding carbohydrate decrease (**Supplementary Figure S2**; Supplementary Table 4). The researches on transcriptome-related AM symbiosis were obtained by different methods, such as SuperSAGE analysis, Genechip and RNA-seq. SuperSAGE analysis showed 32,808 SuperSAGE Tag sequences matched to *Nicotiana attenuata* transcriptome

FIGURE 5 | Heat map of the genes including ubiquitination, transcription factor and repeated domain expression for litchi (A); heat map of the genes including ubiquitination, transcription factor, repeated domain expression, and chitin synthesis for AM fungi (B). The C represents control and the G represents girdling; 0 D, 1 W, 2 W, 1 M, 2 M represent the time after treatment (0 day, 1 week, 2 weeks, 1 month, and 2 months). The heat map was constructed based on the FPKM values which showed on the top of the figures by the software mev (v4.9.0).

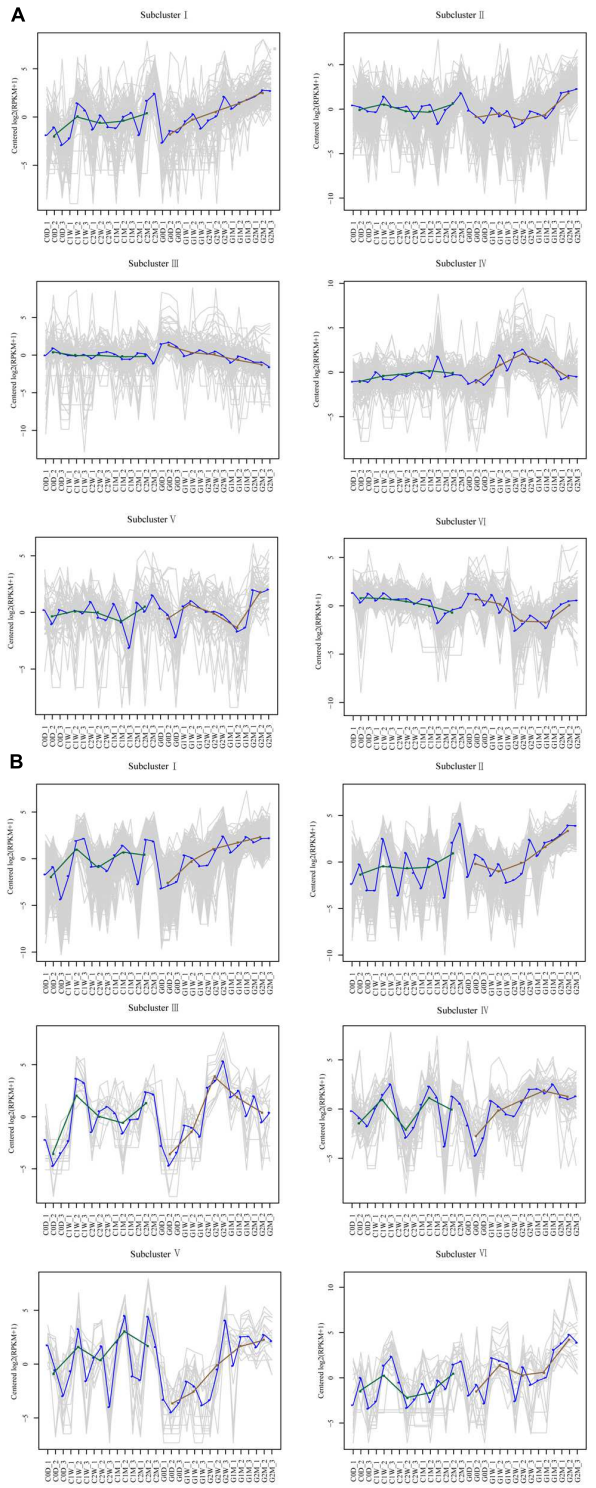

FIGURE 6 | Clustering results of time-course data from RNA-seq by short time-series expression miner analysis for litchi (A) and AM fungi (B). Each box corresponds to one of the model temporal expression profiles, and the unigene belonging to each corresponding subcluster is shown in Supplementary Table 4. The C represents control, and the G represents girdling; 0 D, 1 W, 2 W, 1 M, 2 M represent the time after treatment (0 day, 1 week, 2 weeks, 1 month, and 2 months).

database and 3,698 Tag sequences matched to *R. irregularis*. Genechip was used for DEGs screening in transcriptome of *Medicago truncatula* and *Solanum lycopersicum* mycorrhizal root (Gaude et al., 2012; Ruzicka et al., 2012; Bonneau et al., 2013; Hogekamp and Küster, 2013). It identified 512 DEGs between AM colonized and non-colonized cells in *M. truncatula* root (Gaude et al., 2012); 174 DEGs between mycorrhizal wild-type and non-mycorrhizal *rmc* roots irrespective of the N treatment of *Solanum lycopersicum* under field condition (Ruzicka et al., 2012). RNA-seq analysis identified 2,210 fungal and tomato sequence assemblies from mycorrhizal roots through comparing the wild-type and *rmc* root samples under field condition (Ruzicka et al., 2013); 3,641 genes differentially expressed during AM development in *Lotus japonicus* and approximately 80% of which were upregulated (Handa et al., 2015); 3,949 DEGs between mycorrhizal roots of large lateral roots and fine lateral roots in *Oryza sativa* (Fiorilli et al., 2015). The numbers of annotated sequences of host litchi and AM fungi in present study compared with those annotated sequences and DEGs in the biological process of AM fungi and other host plants as well as DEGs involved in carbohydrate starvation suggested that RNA-seq is an effective method for identifying transcript variation in litchi mycorrhizal roots under decreased carbohydrate conditions (**Table 2**).

Previous research suggested that plants can detect, discriminate, and reward the optimal fungal partners with high carbohydrate contents. Moreover, the fungal partners encourage cooperation by increasing nutrient transfer to the hosts to provide high amounts of carbohydrates (Kiers et al., 2011; Fellbaum et al., 2012). Mineral nutrients against carbohydrates between partners were characteristic of both sucrose starvation and hexose-enhanced conditions. Sucrose is the main sugar for transport in *M. truncatula*; the lines displayed up to 10-fold reduction in the expression levels of the *M. truncatula* sucrose synthase gene (*MtSucS1*) in the roots (Baier et al., 2010). The lines exhibited decreased numbers of internal hyphae, vesicles, and arbuscules, which caused an overall stunted aboveground growth under inorganic phosphorus limitations (Baier et al., 2010). Hexoses, especially glucose, are the main carbohydrates for mineral nutrition from AM fungi (Helber et al., 2011). Invertase derived from overexpressing yeast (*Saccharomyces cerevisiae*) in tobacco (*N. tabacum*) *alc::cwINV* increased the hexose concentration in the root. However, the colonization of *Glomus intraradices* and the level of fungus-specific palmitvaccenic acid, which indicate fungal carbohydrate supply, or plant phosphate content, did not increase (Schaarschmidt et al., 2007). These results implied that sufficient carbohydrates are available in mycorrhizal roots under normal conditions, but carbohydrate starvation inhibited AM development. As predicted, girdling decreased starch concentration as well as monosaccharide, disaccharide, and sugar alcohol contents after the treatment. AM colonization rate matched carbohydrate variation, which continuously decreased after the girdling treatment from 2 W to 2 M (**Figures 1** and **2**). Besides decreased carbohydrate content and AM colonization, DEGs generated by girdling also suggested that both the litchi root and AM fungi underwent carbohydrate starvation. Biological processes

related to carbohydrate metabolism varied after the girdling treatment; these processes include glyoxylate and dicarboxylate metabolism (ko00630), citrate cycle (ko00020), and pentose phosphate pathway (ko00030) in AM fungi; as well as starch and sucrose metabolism (ko00500) and amino sugar and nucleotide sugar metabolism (ko00520) in litchi (Supplementary Table 3). The results, including carbohydrate content, AM colonization, and pathways in both host plant and AM fungi, suggested that girdling regulated litchi mycorrhizal root development by decreasing carbohydrate loss.

Carbohydrate shortage in symbiotic roots lowers AM fungi colonization and decreases the proportion of functional arbuscules (Hayman, 1974; Vierheilig et al., 2002). Girdling inhibits mycorrhizal development in both symbiotic partners. We speculate that upregulated DEGs are required for the detection and adaptation of carbohydrate stress. By contrast, downregulated DEGs in symbiotic partners may be related to carbohydrate exchange under normal conditions. Flavonoids are not strictly required for all combinations of host plant and AM fungi recognition (Bécard et al., 1995). However, the downregulated DEGs at 0 D versus 1 W and at 0 D versus 2 W in host litchi were clustered into flavonoid, flavone, and flavonol biosynthesis as systemic processes. The evidence may suggest that flavonoid was the main factor that regulated AM formation in litchi. Compared with the downregulated DEGs, most of the upregulated DEGs were clustered into stress-inducible and resistance-related pathways, which included the NADP-dependent malic enzyme gene, endochitinase PR4, the basic form of the pathogenesis-related protein 1 LRR receptor-like serine/threonine-protein kinase EFR, cyclic nucleotide-gated ion channel 1, lignin-forming anionic peroxidase, and peroxidase 72 (Gallou et al., 2012; Tromas et al., 2012; Miyata et al., 2014). These data implied that the host litchi stimulated defense-related genes in response to fungal disease when its seceded carbohydrates decreased. In the adaptation process, the downregulated DEGs were mapped to several clusters, including antigen processing and presentation (heat shock protein 82; Heat shock 70 kDa protein; putative heat shock protein HSP 90-beta-3; nuclear transcription factor Y subunit A-2), plant hormone signal transduction (transcription factor MYC4; probable protein phosphatase 2C 24; regulatory protein NPR5), NOD-like receptor signaling pathway (heat shock protein 82; putative heat shock protein HSP 90-beta-3), and MAPK signaling pathway (heat shock 70 kDa protein). The data showed that when carbohydrate shortage, the litchi might downregulate the symbiosis signal-transduction genes. The most upregulated DEGs at 0 D versus those at 1 M and at 0 D versus those at 2 M in the litchi were system clustered into lipid metabolism processes, such as alpha-linolenic acid and linoleic acid metabolism (linoleate 13S-lipoxygenase 2-1; allene oxide cyclase 2; linoleate 13S-lipoxygenase 2-1; 4-coumarate–CoA ligase-like 5; linoleate 13S-lipoxygenase 2-1; TR107818| c4_g1, cytochrome P450 83A1; Supplementary Table 3 and **Figure 6**). Certain 2-hydroxy fatty acids comprise the putative categories of root exudate signals perceived by *Gigaspora* species; several genes related to fatty-acid and lipid metabolism that are highly upregulated in AM roots were identified (Gaude et al., 2012). Whether alpha-linolenic acid and linoleic acid could regulate AM colonization under decreased carbohydrate conditions in litchi mycorrhizal tree requires additional study. In addition to the signal molecules and defense-related genes in the symbiotic process, the DEGs involved in AM maintenance, such as transcription factors (**Figure 5A**), lectin and chitinase genes were also screened (**Figure 6A**; Supplementary Table 4). The functions of the transcription factors in the AP2, ERF, Myb, WRKY, and bHLH families as well as lectin genes were involved in cellular reprogramming during AM development (De Hoff et al., 2009; Hogekamp et al., 2011; Handa et al., 2015). This finding suggested that carbohydrate shortage potentially influence AM formation, maintenance, and systematic functioning from pre-symbiotic to post-symbiotic periods in litchi roots.

For AM fungal component, the E3 ubiquitin ligase complex SCF subunit scon-3 and putative ubiquitin thioesterase otu1 were identified in the upregulated DEGs at 0 D versus those at 1 W and at 0 D versus those at 2 W. The E3 ubiquitin ligase was found to ubiquitinate *Arabidopsis* receptor kinase flagellin sensing 2, which was also identified as agents interacting with symbiotic RLKs in *L. japonicus* (Robatzek et al., 2006; Mbengue et al., 2010; Den Herder et al., 2012). Both the genes encoding the E3 ubiquitin ligase complex SCF subunit scon-3 and putative ubiquitin thioesterase otu1 were upregulated in AM fungi upon recognition of carbohydrate decrease, which illustrated the ubiquitination was important in the process of AM fungi perceived carbohydrate decreased. The KEGG pathway of upregulated DEGs at 0 D versus those at 1 M and at 0 D versus those at 2 M in the AM fungi suggested that AM fungi not only relied on the variation of carbohydrate metabolism for the adaptation process but also upregulated the transcription in arginine and proline metabolism, alanine, aspartate, and glutamate metabolism and lipid metabolism for adopting carbohydrate starvation (Supplementary Table 3). The unigenes mapped to lipid metabolism and genes encoding chitin syntheses varied during fungal adaptation under carbohydrate starvation (**Figure 6**). The two categories of unigenes possibly related to lipochito-oligosaccharides, short-chain chitin oligomers, and thyroid, which may be correlated to the recognition of host plant and AM fungi (Bates et al., 2012; Kobae et al., 2014; Wewer et al., 2014). Interestingly, the transcripts of cytochrome b-245 and LRR were noted in the DEGs of AM fungi (Supplementary Table 3; **Figure 6**). *R. irregularis* possesses over 200 CYPs according to domain prediction using the InterPro database (Park et al., 2008; Moktali et al., 2012; Tisserant et al., 2013). This number is relatively large for CYPs of a fungal species. Previous studies showed that CYPs include heme–thiolate proteins, which are located in the endoplasmic reticulum and catalyze the oxidation of various organic compounds, such as lipids and sterols (Črešnar and Petrič, 2011). The members of the CYP51 family are well-conserved housekeeping genes that participate in the 14-demethylation of sterol precursors (van den Brink et al., 1998; Črešnar and Petrič, 2011). The CYP diversification may be related to various metabolic processes and possible fungal adaptation to the soil environment and host plant roots. In addition to CYPs, LRR transcripts were noted in the DEG database entries on AM fungi. Various surfaces of the leucine-rich repeat LRR

ectodomain superstructure are utilized for interaction with the cognate ligand in both plant and animal receptors. *Arabidopsis* LRR receptor-like kinase FLS2 and rice receptor kinase-like protein Xa21 possess large ectodomains that comprise 28 LRRs and 23 LRRs, respectively (Song et al., 1995; Gómez-Gómez and Boller, 2000), and are directly involved in elicitor binding (Chinchilla et al., 2006; Lee et al., 2009). Because the LRRs form versatile binding domains for plant proteins were involved in the process of plant–microbe interaction, the LRRs in the AM fungi binding the secreted proteins from host plant needed further study.

CONCLUSION

Girdling decreased the glucose, fructose, sucrose, quebrachitol, and even starch concentrations in the litchi mycorrhizal roots, which induced a decrease in AM colonization. In this study, we revealed the gene expression profiles of both host litchi and AM fungi during the decreased carbohydrate conditions by RNA-seq analysis. Both transcripts of litchi (54,100 unigenes) and AM fungi (33,120 unigenes) were identified in the period of decreased carbohydrates. The DEG analysis of transcriptomes identified potential novel unigenes of both host litchi and AM fungi. DEG analysis showed that flavonoids, alpha-linolenic acid, and linoleic acid were the main factors that regulated AM colonization in litchi. However, the flavonoids might play a role in the recognition of the stages of decreasing carbohydrate content, and alpha-linolenic acid or linoleic acid may affect AM formation under the process of adaptation. Litchi trees stimulated the expression of the defense-related genes (NADP-dependent malic enzyme gene, endochitinase PR4, basic form of pathogenesis-related protein 1, LRR receptor-like serine/threonine-protein kinase EFR, cyclic nucleotide-gated ion channel 1, lignin-forming anionic peroxidase, and peroxidase 72) and downregulated the symbiosis signal-transduction genes (heat-shock protein 82, heat-shock 70 kDa protein, putative heat-shock protein HSP 90-beta-3, transcription factor MYC4, probable protein phosphatase 2C 24, and regulatory protein NPR5) to inhibit new AM colonization. In addition to new AM colonization, carbohydrate shortage changed the transcription factor in the AP2, ERF, Myb, WRKY, bHLH families and lectin genes of litchi, which influenced AM maintenance in the post-symbiotic stage. Similar to those of the litchi host, the E3 ubiquitin ligase complex SCF subunit scon-3 and polyubiquitin of AM fungi were all upregulated at the perceived stages. This occurrence suggested that the ubiquitination process plays an important role in the AM fungal recognition of carbohydrate decrease. The transcription of cytochrome b-245 and LRRs were noted in the DEGs database, implying that these transcripts play important roles in the process of AM fungal adaptation under carbohydrate starvation despite the gene function still being largely unknown.

AUTHOR CONTRIBUTIONS

The data was interpreted and the article was drafted by BS. The manuscript was revised by SS. Meanwhile, the experiments were conceived and designed by BS and SS. BS, LL, and YW performed the experiments. BS and WL analyzed the data.

ACKNOWLEDGMENTS

This work was supported by the National Natural Science Fund of China (Project No. 31401818) and founded on the Basic Scientific Research Project of Non-profit Central Research Institutions (No. SSCRI-1630062014006) and the China Litchi and Longan Industry Technology Research System (Project No. CARS-33-11).

SUPPLEMENTARY MATERIAL

The Supplementary Material for this article can be found online at: http://journal.frontiersin.org/article/10.3389/fmicb.2016.00408

FIGURE S1 | The girdling litchi trees in the experimental orchard. The girdling wound was deep to xylem with 0.5 cm width.

FIGURE S2 | Flow chart of RNA-seq analysis.

REFERENCES

Baier, M. C., Keck, M., Gödde, V., Niehaus, K., Küster, H., and Hohnjec, N. (2010). Knockdown of the symbiotic sucrose synthase MtSucS1 affects arbuscule maturation and maintenance in mycorrhizal roots of *Medicago truncatula*. *Plant Physiol.* 152, 1000–1014. doi: 10.1104/pp.109.149898

Bates, P. D., Fatihi, A., Snapp, A. R., Carlsson, A. S., Browse, J., and Lu, C. (2012). Acyl editing and headgroup exchange are the major mechanisms that direct polyunsaturated fatty acid flux into triacylglycerols. *Plant Physiol.* 160, 1530–1539. doi: 10.1104/pp.112.204438

Bécard, G., Douds, D. D., and Pfeffer, P. E. (1992). Extensive in vitro hyphal growth of vesicular-arbuscular mycorrhizal fungi in the presence of CO_2 and flavonols. *Appl. Environ. Microbiol.* 58, 821–825.

Bécard, G., Taylor, L. P., Douds, D. D., Pfeffer, P. E., and Doner, L. W. (1995). Flavonoids are not necessary plant signal compounds in arbuscular mycorrhizal symbioses. *Mol. Plant Microbe Ineract.* 8, 252–258. doi: 10.1094/mpmi-8-0252

Besserer, A., Bécard, G., Jauneau, A., Roux, C., and Séjalon-Delmas, N. (2008). GR24, a synthetic analog of strigolactones, stimulates the mitosis and growth of the arbuscular mycorrhizal fungus *Gigaspora rosea* by boosting its energy metabolism. *Plant Physiol.* 148, 402–413. doi: 10.1104/pp.108.121400

Bonneau, L., Huguet, S., Wipf, D., Pauly, N., and Truong, H. N. (2013). Combined phosphate and nitrogen limitation generates a nutrient stress transcriptome favorable for arbuscular mycorrhizal symbiosis in *Medicago truncatula*. *New Phytol.* 199, 188–202. doi: 10.1111/nph.12234

Bucher, M., Hause, B., Krajinski, F., and Küster, H. (2014). Through the doors of perception to function in arbuscular mycorrhizal symbioses. *New Phytol.* 204, 833–840. doi: 10.1111/nph.12862

Chinchilla, D., Bauer, Z., Regenass, M., Boller, T., and Felix, G. (2006). The *Arabidopsis* receptor kinase FLS2 binds flg22 and determines the specificity of flagellin perception. *Plant Cell* 18, 465–476. doi: 10.1105/tpc.105.036574

Črešnar, B., and Petrič, S. (2011). Cytochrome P450 enzymes in the fungal kingdom. *BBA-Proteins Proteom.* 1814, 29–35. doi: 10.1016/j.bbapap.2010.06.020

De Hoff, P. L., Brill, L. M., and Hirsch, A. M. (2009). Plant lectins: the ties that bind in root symbiosis and plant defense. *Mol. Genet. Genom.* 282, 1–15. doi: 10.1007/s00438-009-0460-8

Den Herder, G., Yoshida, S., Antolín-Llovera, M., Ried, M. K., and Parniske, M. (2012). *Lotus japonicus* E3 ligase SEVEN IN ABSENTIA4 destabilizes the symbiosis receptor-like kinase SYMRK and negatively regulates rhizobial infection. *Plant Cell* 24, 1691–1707. doi: 10.1105/tpc.110.082248

Fellbaum, C. R., Gachomo, E. W., Beesetty, Y., Choudharib, S., Strahanc, G. D., Pfefferc, P. E., et al. (2012). Carbon availability triggers fungal nitrogen uptake and transport in arbuscular mycorrhizal symbiosis. *Proc. Natl. Acad. Sci. U.S.A.* 109, 2666–2671. doi: 10.1073/pnas.1118650109

Fiorilli, V., Vallino, M., Biselli, C., Faccio, A., Bagnaresi, P., and Bonfante, P. (2015). Host and non-host roots in rice: cellular and molecular approaches reveal differential responses to arbuscular mycorrhizal fungi. *Front. Plant Sci.* 6:636. doi: 10.3389/fpls.2015.00636

Gallou, A., Declerck, S., and Cranenbrouck, S. (2012). Transcriptional regulation of defence genes and involvement of the WRKY transcription factor in arbuscular mycorrhizal potato root colonization. *Funct. Integr. Genomic* 12, 183–198. doi: 10.1007/s10142-011-0241-4

Garber, M., Grabherr, M. G., Guttman, M., and Trapnell, C. (2011). Computational methods for transcriptome annotation and quantification using RNA-seq. *Nat. Methods* 8, 469–477. doi: 10.1038/nmeth.1613

Gaude, N., Bortfeld, S., Duensing, N., Lohse, M., and Krajinski, F. (2012). Arbuscule-containing and non-colonized cortical cells of mycorrhizal roots undergo a massive and specific reprogramming during arbuscular mycorrhizal development. *Plant J.* 69, 510–528. doi: 10.1111/j.1365-313x.2011.04810.x

Genre, A., Chabaud, M., Balzergue, C., Puech-Pagès, V., Novero, M., Rey, T., et al. (2013). Short-chain chitin oligomers from arbuscular mycorrhizal fungi trigger nuclear Ca2+ spiking in *Medicago truncatula* roots and their production is enhanced by strigolactone. *New Phytol.* 198, 190–202. doi: 10.1111/nph.12146

Gómez-Gómez, L., and Boller, T. (2000). FLS2: an LRR receptor–like kinase involved in the perception of the bacterial elicitor flagellin in *Arabidopsis*. *Mol. Cell.* 5, 1003–1011. doi: 10.1016/S1097-2765(00)80265-8

Grabherr, M. G., Haas, B. J., Yassour, M., Levin, J. Z., Thompson, D. A., Amit, I., et al. (2011). Full-length transcriptome assembly from RNA-Seq data without a reference genome. *Nat. Biotechnol.* 29, 644–652. doi: 10.1038/nbt.1883

Handa, Y., Nishide, H., Takeda, N., Suzuki, Y., Kawaguchi, M., and Saito, K. (2015). RNA-seq transcriptional profiling of an arbuscular mycorrhiza provides insights into regulated and coordinated gene expression in *Lotus japonicus* and *Rhizophagus irregularis*. *Plant Cell Physiol.* 56, 1490–1511. doi: 10.1093/pcp/pcv071

Hayman, D. S. (1974). Plant growth responses to vesicular-arbuscular mycorrhiza.VI. Effect of light and temperature. *New Phytol.* 73, 71–80.

Helber, N., Wippel, K., Sauer, N., Schaarschmidt, S., Hause, B., and Requena, N. (2011). A versatile monosaccharide transporter that operates in the arbuscular mycorrhizal fungus *Glomus* sp is crucial for the symbiotic relationship with plants. *Plant Cell* 23, 3812–3823. doi: 10.1105/tpc.111.089813

Hogekamp, C., Arndt, D., Pereira, P., Becker, J. D., Hohnjec, N., and Küster, H. (2011). Laser microdissection unravels cell-type-specific transcription in arbuscular mycorrhizal roots, including CAAT-Box transcription factor gene expression correlating with fungal contact and spread. *Plant Physiol.* 157, 2023–2043. doi: 10.1104/pp.111.186635

Hogekamp, C., and Küster, H. (2013). A roadmap of cell-type specific gene expression during sequential stages of the arbuscular mycorrhiza symbiosis. *BMC Genomics* 14:306. doi: 10.1186/1471-2164-14-306

Huang, X. M., Wang, H. C., and Yuan, W. Q. (2003). Effects of twig girdling at different stages on new shoot growth and carbon nutrient reservation. *Acta Hortic. Sin.* 30, 192–194.

Kiers, E. T., Duhamel, M., Beesetty, Y., Mensah, J. A., Franken, O., Verbruggen, E., et al. (2011). Reciprocal rewards stabilize cooperation in the mycorrhizal symbiosis. *Science* 333, 880–882. doi: 10.1126/science.1208473

Kobae, Y., Gutjahr, C., Paszkowski, U., Kojima, T., Fujiwara, T., and Hata, S. (2014). Lipid droplets of arbuscular mycorrhizal fungi emerge in concert with arbuscule collapse. *Plant Cell Physiol.* 55, 1945–1953. doi: 10.1093/pcp/pcu123

Lee, S. W., Han, S. W., Sririyanum, M., Park, C. J., Seo, Y. S., and Ronald, P. C. (2009). A type I–secreted, sulfated peptide triggers XA21-mediated innate immunity. *Science* 326, 850–853. doi: 10.1126/science.1173438

Li, B., and Dewey, C. N. (2011). RSEM: accurate transcript quantification from RNA-Seq data with or without a reference genome. *BMC Bioinformatics* 12:323. doi: 10.1186/1471-2105-12-323

Maillet, F., Poinsot, V., André, O., Puech-Pagès, V., Haouy, A., Gueunier, M., et al. (2011). Fungal lipochitooligosaccharide symbiotic signals in arbuscular mycorrhiza. *Nature* 469, 58–63. doi: 10.1038/nature09622

Mbengue, M., Camut, S., de Carvalho-Niebel, F., Deslandes, L., Froidure, S., Klaus-Heisen, D., et al. (2010). The *Medicago truncatula* E3 ubiquitin ligase PUB1 interacts with the LYK3 symbiotic receptor and negatively regulates infection and nodulation. *Plant Cell* 22, 3474–3488. doi: 10.1105/tpc.110.075861

McGonigle, T. P., Miller, M. H., Evans, D. G., Fairchild, G. L., and Swan, J. A. (1990). A new method which gives an objective measure of colonization of roots by vesicular-arbuscular mycorrhizal fungi. *New Phytol.* 115, 495–501. doi: 10.1111/j.1469-8137.1990.tb00476.x

Miyata, K., Kozaki, T., Kouzai, Y., Ozawa, K., Ishii, K., Asamizu, E., et al. (2014). The bifunctional plant receptor, OsCERK1, regulates both chitin-triggered immunity and arbuscular mycorrhizal symbiosis in rice. *Plant Cell Physiol.* 55, 1864–1872. doi: 10.1093/pcp/pcu129

Moktali, V., Park, J., Fedorova-Abrams, N., Park, B., Choi, J., Lee, Y. H., et al. (2012). Systematic and searchable classification of cytochrome P450 proteins encoded by fungal and oomycete genomes. *BMC Genomics* 13:525. doi: 10.1186/1471-2164-13-525

Nagahashi, G., and Douds, D. D. (2011). The effects of hydroxy fatty acids on the hyphal branching of germinated spores of AM fungi. *Fungal Boil.* 115, 351–358. doi: 10.1016/j.funbio.2011.01.006

Park, J., Lee, S., Choi, J., Ahn, K., Park, B., Park, J., et al. (2008). Fungal cytochrome P450 database. *BMC Genomics* 9:402. doi: 10.1186/1471-2164-9-402

Parniske, M. (2008). Arbuscular mycorrhiza: the mother of plant root endosymbioses. *Nat. Rev. Microbiol.* 6, 763–775. doi: 10.1038/nrmicro1987

Phillips, J. M., and Hayman, D. S. (1970). Improved procedures for clearing roots and staining parasitic and vesicular-arbuscular mycorrhizal fungi for rapid assessment of infection. *Trans. Br. Mycol. Soc.* 55, 158–161. doi: 10.1016/s0007-1536(70)80110-3

Robatzek, S., Chinchilla, D., and Boller, T. (2006). Ligand-induced endocytosis of the pattern recognition receptor FLS2 in *Arabidopsis*. *Gene Dev.* 20, 537–542. doi: 10.1101/gad.366506

Ruzicka, D. R., Chamala, S., Barriosmasias, F. H., Martin, F., Smith, S., Jackson, L. E., et al. (2013). Inside arbuscular mycorrhizal roots – molecular probes to understand the symbiosis. *Plant Genome* 6, 494–494. doi: 10.3835/plantgenome2012.06.0007

Ruzicka, D. R., Hausmann, N. T., Barrios-Masias, F. H., Jackson, L. E., and Schachtman, D. P. (2012). Transcriptomic and metabolic responses of mycorrhizal roots to nitrogen patches under field conditions. *Plant Soil* 350, 145–162. doi: 10.1007/S11104-011-0890-Z

Schaarschmidt, S., González, M. C., Roitsch, T., Strack, D., Sonnewald, U., and Hause, B. (2007). Regulation of arbuscular mycorrhization by carbon. The symbiotic interaction cannot be improved by increased carbon availability accomplished by root-specifically enhanced invertase activity. *Plant Physiol.* 143, 1827–1840. doi: 10.1104/pp.107.096446

Smith, S. E., and Read, D. J. (2008). *Mycorrhizal Symbiosis*, 3nd Edn. New York, NY: Academic Press. doi: 10.1016/B978-012370526-6.50003-9

Song, W. Y., Wang, G. L., Chen, L. L., Kim, H. S., Pi, L. Y., Holsten, T., et al. (1995). A receptor kinase-like protein encoded by the rice disease resistance gene, XA21. *Science* 270, 1804–1806. doi: 10.1126/science.270.5243.1804

Sun, J., Miller, J. B., Granqvist, E., Wiley-Kalil, A., Gobbato, E., Maillet, F., et al. (2015). Activation of symbiosis signaling by arbuscular mycorrhizal fungi in legumes and rice. *Plant Cell* 27, 828–838. doi: 10.1105/tpc.114.131326

Tisserant, E., Malbreil, M., Kuo, A., Kohler, A., Symeonidi, A., Balestrini, R., et al. (2013). Genome of an arbuscular mycorrhizal fungus provides insight into the oldest plant symbiosis. *Proc. Natl. Acad. Sci. U.S.A.* 110, 20117–20122. doi: 10.1073/pnas.1313452110

Tromas, A., Parizot, B., Diagne, N., Champion, A., Hocher, V., Cissoko, M., et al. (2012). Heart of endosymbioses: transcriptomics reveals a conservedgenetic program among arbuscular mycorrhizal, actinorhizal and legume-rhizobial symbioses. *PLoS ONE* 7:e44742. doi: 10.1371/journal.pone.0044742

Tromp, J. (1983). Nutrient reserves in roots of fruit trees, in particular carbohydrates and nitrogen. *Plant Soil.* 71, 401–413 doi: 10.1007/BF02182682

van den Brink, H. M., van Gorcom, R. F. M., van den Hondel, C. A. M. J. J., and Punt, P. J. (1998). Cytochrome P450 enzyme systems in fungi. *Fungal Genet. Biol.* 23, 1–17. doi: 10.1006/fgbi.1997.1021

Vierheilig, H., Bago, B., Lerat, S., and Piché, Y. (2002). Shoot-produced, light dependent factors are partially involved in the expression of the arbuscular mycorrhizal (AM) status of AM host and non-host plants. *J. Plant Nutr. Soil Sci.* 165, 21–25. doi: 10.1002/1522-2624(200202)165:1<21::AID-JPLN21>3.0.CO;2-9

Wang, H. C., Wu, Z. H., Huang, X. M., Hu, G. B., and Chen, H. B. (2013). Determination of quebrachitol *Litchi chinensis* and *Dimocarpus longan* in sapindacea family. *J. S. China Agric. Univ.* 34, 315–319.

Wang, C., Gong, B., Bushel, P. R., Thierry-Mieg, J., Thierry-Mieg, D., Xu, J., et al. (2014). The concordance between RNA-seq and microarray data depends on chemical treatment and transcript abundance. *Nat. Biotechnol.* 32, 926–932. doi: 10.1038/nbt.3001

Wang, T. D., Zhang, H. F., Wu, Z. C., Li, J. G., Huang, X. M., and Wang, H. C. (2014). Sugar uptake in the aril of litchi fruit depends on the apoplasmic post-phloem transport and the activity of proton pumps and the putative transporter LcSUT4. *Plant Cell Physiol.* 56, 377–387. doi: 10.1093/pcp/pcu173

Wewer, V., Brands, M., and Dörmann, P. (2014). Fatty acid synthesis and lipid metabolism in the obligate biotrophic fungus *Rhizophagus irregularis* during mycorrhization of *Lotus japonicus*. *Plant J.* 79, 398–412. doi: 10.1038/nbt.3001

Xie, C., Mao, X., Huang, J., Ding, Y., Wu, J., Dong, S., et al. (2011). KOBAS 2.0: a web server for annotation and identification of enriched pathways and diseases. *Nucleic Acids Res.* 39, W316–W322. doi: 10.1093/nar/gkr483

Young, M. D., Wakefield, M. J., Smyth, G. K., and Oshlack, A. (2010). Method Gene Ontology Analysis for RNA-Seq: accounting for selection bias. *Genome Biol.* 11:R14. doi: 10.1186/gb-2010-11-2-r14

Yuan, R. C., and Huang, H. B. (1993). Regulation of roots and shoots growth and fruit-drop of young litchi trees by trunk girdling in view of source-sink relationships. *J. Fruit Sci.* 10, 195–198.

Conflict of Interest Statement: The authors declare that the research was conducted in the absence of any commercial or financial relationships that could be construed as a potential conflict of interest.

frontiers in Plant Science

ORIGINAL RESEARCH
published: 15 December 2016
doi: 10.3389/fpls.2016.01836

An LRR/Malectin Receptor-Like Kinase Mediates Resistance to Non-adapted and Adapted Powdery Mildew Fungi in Barley and Wheat

*Jeyaraman Rajaraman[1†], Dimitar Douchkov[1†], Götz Hensel[2], Francesca L. Stefanato[3], Anna Gordon[3], Nelzo Ereful[3], Octav F. Caldararu[4], Andrei-Jose Petrescu[4], Jochen Kumlehn[2], Lesley A. Boyd[3] and Patrick Schweizer[1]**

[1] Pathogen-Stress Genomics, Leibniz Institute of Plant Genetics and Crop Plant Research (IPK), Stadt Seeland, Germany, [2] Plant Reproductive Biology, Leibniz Institute of Plant Genetics and Crop Plant Research (IPK), Stadt Seeland, Germany, [3] National Institute of Agricultural Botany, Cambridge, UK, [4] Department of Bioinformatics and Structural Biochemistry, Institute of Biochemistry of the Romanian Academy, Bucharest, Romania

OPEN ACCESS

Edited by:
Vincenzo Lionetti,
Sapienza University of Rome, Italy

Reviewed by:
Hans Thordal-Christensen,
University of Copenhagen, Denmark
Raffaella Balestrini,
National Research Council, Italy

***Correspondence:**
Patrick Schweizer
schweiz@ipk-gatersleben.de

†Joint first authors

Specialty section:
This article was submitted to Plant Biotic Interactions, a section of the journal Frontiers in Plant Science

Received: 04 August 2016
Accepted: 21 November 2016
Published: 15 December 2016

Citation:
Rajaraman J, Douchkov D, Hensel G, Stefanato FL, Gordon A, Ereful N, Caldararu OF, Petrescu A-J, Kumlehn J, Boyd LA and Schweizer P (2016) An LRR/Malectin Receptor-Like Kinase Mediates Resistance to Non-adapted and Adapted Powdery Mildew Fungi in Barley and Wheat. Front. Plant Sci. 7:1836. doi: 10.3389/fpls.2016.01836

Pattern recognition receptors (PRRs) belonging to the multigene family of receptor-like kinases (RLKs) are the sensing devices of plants for microbe- or pathogen-associated molecular patterns released from microbial organisms. Here we describe *Rnr8* (for *Required for non-host resistance 8*) encoding HvLEMK1, a LRR-malectin domain-containing transmembrane RLK that mediates non-host resistance of barley to the non-adapted wheat powdery mildew fungus *Blumeria graminis* f.sp. *tritici*. Transgenic barley lines with silenced *HvLEMK1* allow entry and colony growth of the non-adapted pathogen, although sporulation was reduced and final colony size did not reach that of the adapted barley powdery mildew fungus *B. graminis* f.sp. *hordei*. Transient expression of the barley or wheat *LEMK1* genes enhanced resistance in wheat to the adapted wheat powdery mildew fungus while expression of the same genes did not protect barley from attack by the barley powdery mildew fungus. The results suggest that *HvLEMK1* is a factor mediating non-host resistance in barley and quantitative host resistance in wheat to the wheat powdery mildew fungus.

Keywords: pathogen recognition receptor, PRR, 3D model, co-evolution, *Hordeum vulgare*, *Triticum aestivum*, *Blumeria graminis*

INTRODUCTION

Plants recognize interacting beneficial or parasitic organisms via pathogen recognition receptors (PRRs) belonging to the highly complex and functionally diversified superfamily of receptor-like kinases (RLKs) that are also involved in plant development and abiotic-stress signaling (Macho and Zipfel, 2014). PRRs bind to microbe-associated molecular patterns, of with pathogen-associated molecular patterns (PAMPs) form a subgroup, and to damage-associated molecular patterns consisting of, for example, plant cell-wall degradation products. RLKs typically contain extracellular ligand-binding, transmembrane and cytoplasmic kinase domains. They are grouped into several sub-families depending on the presence of specific sequence motifs in their extracellular ligand binding domain, including leucine-rich repeats (LRRs), LysM, lectin-like, cysteine-rich or malectin domains, most of which bind to a corresponding class of ligands

(Wu and Zhou, 2013). Upon ligand binding and activation, RLKs phosphorylate themselves or substrate proteins, which triggers signaling cascades such as the interacting mitogen-associated protein kinase kinase kinases cascade and leads to the execution of developmental or defense-related programs including the PAMP-triggered immunity (PTI) pathway (Jones and Dangl, 2006).

PAMP-triggered immunity is probably the underlying mechanism of a good number of cases of quantitative host resistance and of non-host resistance providing race-non-specific and durable disease resistance that ranges from partial to complete in the case of quantitative host resistance and non-host resistance, respectively (Kou and Wang, 2010; Fan and Doerner, 2012). Quantitative host resistance is usually less efficient than non-host resistance probably because pathogen-derived effector molecules (secreted proteins or non-proteinaceous small molecules) inhibit defense responses or stimulate pathogen accommodation by the host, which is referred to as effector-triggered susceptibility (ETS) (Deslandes and Rivas, 2012; Wawra et al., 2012; Giraldo and Valent, 2013). One of the preferred models for the efficiency and durability of non-host resistance states that, after host speciation, lack of co-evolution leads to gradual erosion of effector functionality in terms of their capacity to manipulate factors for defense or pathogen accommodation of previous host(s).

The genome of the barley powdery mildew fungus *Blumeria graminis* f.sp. *hordei* (*Bgh*) has been proposed to encode a set of over 500 candidate secreted effector proteins (CSEPs) with yet mostly unknown function (Pennington et al., 2016). A small proportion of these candidate effectors was recently tested functionally, which led to the discovery of a small family of RNAse-like proteins that appears to be important for initial host invasion (Pliego et al., 2013). The genome of the wheat powdery mildew fungus *B. graminis* f.sp. *tritici* (*Bgt*) encodes an even larger set of 602 CSEPs, which were defined by similar criteria as those from *Bgh* (Wicker et al., 2013). Most of the *Bgh* CSEPs share close homologs (orthologs) in *Bgt*, which suggests functional conservation of a large proportion of the host-invasion machinery by the two closely related pathogens. Until present only very few CSEPs have been described that interact with host-encoded proteins (Zhang et al., 2012; Schmidt et al., 2014). Therefore, a more or less comprehensive picture of the host-invasion mechanisms of powdery-mildew fungi is still missing.

Here we validate *Rnr8* (for *required for non-host resistance 8*) and present structural and functional data of the encoded protein HvLEMK1, an RLK of the LRR/malectin-domain sub-family. *HvLEMK1* was discovered in a transient-induced gene silencing (TIGS) screen for candidate genes of non-host resistance in barley to the non-adapted wheat powdery mildew fungus (Douchkov et al., 2014). The gene was silenced in transgenic barley plants and also transiently expressed in barley and wheat epidermal cells that were challenge-inoculated by adapted or non-adapted powdery mildew pathogens. The results suggest an important role for *LEMK1* in non-host resistance of barley and in quantitative host resistance of wheat to the wheat powdery mildew fungus.

MATERIALS AND METHODS

Plant and Fungal Material

For the TIGS and transient over-expression experiments 7-day-old seedlings of the *Bgh*-susceptible spring barley cv. Maythorpe were used. Stable transgenic barley plants of cv. Golden Promise were generated as described (Hensel et al., 2008). Transient over-expression in wheat was done by using 7-day-old seedlings of the *Bgt*-susceptible cv. Kanzler. Bombarded leaf segments or transgenic plants were inoculated with Swiss *Bgt* field isolate FAL 92315, or Swiss *Bgh* field isolate CH4.8 throughout the study.

cDNA Cloning of Wheat LEMK1 Orthologs

Initial searches of the NCBI[1] and RIKEN EST[2] databases, using *HvLEMK1* as the query sequence identified the best match to be the full-length EST TPLB0008D17, with a nucleotide similarity of 94%. Using this sequence, primers were designed using the software CLC DNA workbench, targeting a region upstream of the predicted start codon and downstream of the predicted stop codon: TaLEMK1_FL1_f1, TaLEMK1_FL1_r1, TaLEMK1_FL1_f2, TaLEMK1_FL1_r2 (Supplementary Table S1). The cDNA synthesis was performed using SuperScript III (Invitrogen) and the specific primer TaLEMK1_FL1_r2 with a mixture of RNAs from the wheat cultivar Renan. Renan was inoculated with the adapted (*Bgt*) and non-adapted (*Bgh*) pathogens of powdery mildew to ensure high levels of expression of TaLEMK1 transcripts. RNA was extracted 24 h after inoculation. Long range PCR was performed using the "Expand Long Template PCR system" from Roche Co. and following the manufacturer's recommendation for cDNA templates between 0.5 and 9 kb. DNA fragments of the desired length were gel purified and cloned into pGEMT-easy. Colonies where tested for *TaLEMK1* inserts by colony PCR. Plasmids with expected insert size where verified by sequencing. For allele comparison between wheat genotypes, seedlings (14 days after sowing) of the winter wheat varieties Arran, Brock, Cadenza, Pastiche, Vault, and Zebedee were inoculated with *Bgh* (isolate CH4.8), and RNA was extracted 24 h after inoculation. The Illumina, RNA-seq pair-end reads from each of the six varieties were assembled into contigs using a compiled hexaploid wheat reference sequence (TGAC, Norwich, UK). Transcripts were assembled using this reference sequence. *TaLEMK1.1* (clone 7) and *TaLEMK1.2* (clone 12) were used as query sequences in BlastN searches against the assembled transcripts of the six winter wheat varieties.

TIGS and Transient Over-Expression

Transient-induced gene silencing constructs were generated and transferred by particle bombardment into leaf epidermal cells of 7-day-old barley seedlings as described (Douchkov et al., 2005). Leaf segments were inoculated 3 days after the bombardment with *Bgh* at a density of 180–200 conidia mm^{-2}.

[1] http://www.ncbi.nlm.nih.gov/

[2] http://barleyflc.dna.affrc.go.jp/bexdb/

Transformed GUS-stained epidermal cells as well as haustoria-containing transformed (susceptible) cells were counted 48 h after inoculation, and TIGS effects on the susceptibility index (SI) were statistically analyzed as described in (Spies et al., 2012). For transient (over)expression, the *HvLEMK1*-containing BAC clone HvMRXALLhA0027N11 was bombarded into leaf segments of barley cv. Maythorpe or wheat cv. Kanzler, followed by challenge inoculation with the corresponding adapted pathogen *Bgh* or *Bgt* at a density of 180–200 conidia mm^{-2} 4 h after the bombardment and microscopic assessment of SI 48 h after inoculation. For the verification of *HvLEMK1* transgene effects, a 17.4 Kb *HvLEMK1*-containing BAC sub-clone (GenBank Acc. KR610392) was excised as StuI/SphI fragment and inserted into SmaI/SphI sites of transient expression vector pIPKTA09. In addition, barley and wheat cDNAs were excised and inserted as NotI fragment into to the multiple cloning site of pIPKTA09 (Zimmermann et al., 2006). The resulting sequence-verified constructs were bombarded into barley or wheat as described for BAC clones. Relative SI to empty BAC clone or to empty pIPKTA09 was calculated, log(2) transformed and tested for statistically significant deviation from the hypothetical control value "0" by a 1-sample *t*-test, 2-tailed.

Inoculation and Evaluation of Transgenic Plants

Barley cv. Golden Promise was transformed with pIPKb009_HvLEMK1 (Himmelbach et al., 2007) as described (Hensel et al., 2008). Phenotypic evaluation of *Bgh* and *Bgt* interactions was done microscopically on second, detached leaves of 12–14 day-old T1 plants placed on phytoagar plates (23,2 cm × 23,2 cm) and inoculated at a spore density of 30–40 conidia mm^{-2}. Leaf segments inoculated with either *Bgh* or *Bgt* were incubated strictly separated from each other in order to prevent cross-contamination. Golden Promise azygous T1 segregants served as internal negative controls. Inoculated leaf segments were incubated for 48 h (*Bgh*) or 7 days (*Bgt*) followed by staining with Coomassie brilliant blue R 250 (Schweizer et al., 1993). The number of growing *Bgt* colonies/leaf area was counted manually under a standard light microscope at 100× magnification. In case of *Bgh,* colonies were counted using the HyphArea software (Baum et al., 2011). Because of variability of residual *Bgt* susceptibility of the azygous control plants between the different inoculation experiments, we normalized the number of *Bgt* colonies to the average number of *Bgt* colonies on the azygous control in the corresponding experiment. Statistics: For *Bgt* susceptibility, non-normally distributed values from transgenic- or azygous control plants (a combined pool of null-allelic segregant plants from all T1 families) were subjected to Mann–Whitney test (2-tailed) for significant differences from the wildtype control. Data were obtained in three independent inoculation experiments. In the case of *Bgh* infection, data were normally distributed and tested by non-paired *t*-test against azygous control plants (2-tailed). Azygous control plants were used here as control because they were significantly more susceptible than wildtype plants, for unknown reasons. Data were obtained in two independent inoculation experiments.

To determine *HvLEMK1* transcript amounts in transgenic plants, total RNA was isolated from the 4th leaf using the RNeasy Plant Mini Kit with on-column DNase digestion (Qiagen, Hilden, Germany). Two micrograms of total RNA from 11 to 18 transgenic T1 progeny plants per primary transformant, or from a total of 32 azygous segregants, were reverse-transcribed using iScript™ cDNA Synthesis Kit (Bio-Rad Laboratories, Inc.). Transcripts of *HvLEMK1* were quantified in triplicates by using TaqMan probes in a reaction volume of 10 µL (Maxima Probe qPCR Mastermix;Thermo Fisher Scientific, Waltham, MA, USA). Amplification and detection of fluorescent signal was performed in three technical replicates per cDNA sample on a 7900 HT Fast Real-Time PCR system (Life Technologies/Applied Biosystems, Darmstadt, Germany). To determine transcript amounts of proposed non-host-resistance marker genes, plants were grown in 22.5 cm × 18 cm pots in a plant incubator (Panasonic, Hamburg, Germany) at 20°C constant temperature, 60% relative humidity and 16 h illumination (intensity level 5) provided by daylight fluorescent tubes. Twelve-day-old plants were inoculated with *Bgt* spores (20–30 conidia/mm^2), and second leaves were collected at respective time points for RNA isolation. Primary leaves were used for the hygromycin assay to identify azygous plants. RNA isolation, cDNA synthesis and qRT-PCR were done as mentioned earlier except a BRYT Green® dye (Promega Corporation, USA) based system was used instead of TaqMan probes. Primer sequences for all PCR reactions are provided in Supplementary Table S1. Thermal cycling conditions consisted of initial denaturation at 95°C for 10 min followed by 30 cycles of (95°C/15 s, 55°C/40 s, 72°C/35 s). Ubiquitin conjugating enzyme 2 (*HvUBC*, Acc. AY220735) was used as internal normalization standard. To quantify the transcript levels in each sample, a standard curve for each gene with a serial dilution series was made from pooled RNA samples with three technical replicates each. Transcript quantities were determined using the SDS.2.4 software (Life Technologies GmbH, Darmstadt, Germany). For both *HvLEMK1*- and PTI-marker transcript quantification, two independent biological replicates were analyzed using plants grown on different dates.

Subcellular Localization of Fluorescent Proteins

For subcellular localization, the full-length sequence of *HvLEMK1* was N- and C-terminally fused in-frame to *yellow fluorescent protein* (*YFP*) gene in pIPKTA48 and pIPKTA49 vectors, respectively, using Gateway® cloning technology (Thermo Fischer Scientific, New York, NY, USA) (Supplementary Figure S1; Supplementary Table S1). Resulting YFP-fusion constructs were transiently expressed in 7-day-old leaf segments of barley cv. Golden Promise by particle bombardment and examined after 24 h of incubation without *B. graminis* inoculation using confocal laser scanning microscopy. The plasma-membrane marker *aquaporin* (*AtPIP2A*) of *Arabidopsis thaliana* (plasmid pm-rk CD3-1007), or the endoplasmic-reticulum (ER) marker *Wall-associated kinase 2* (*AtWAK2*; plasmid ER-rk CD3-959), both fused to mCherry as described in Nelson et al. (2007), were mixed in an equimolar concentration

and co-bombarded for co-localization experiments. For plasmolysis of epidermal cells, leaf segments were floated on 15% glycerol for 5–10 min, immediately prior to microscopy.

Transcript Regulation

Seven-day-old barley plants of cv. Vada or wheat plants of cv. Renan were inoculated with *Bgh* or *Bgt*, and the abaxial epidermis of inoculated primary leaves or from non-inoculated control leaves was peeled at 6–74 h after inoculation, as described (Zellerhoff et al., 2010; Spies et al., 2012). Total, quality-controlled RNA was hybridized to Agilent Gene Expression 44K microarrays (design ID: 020599 for barley and 022297 for wheat; Agilent) as described (Chen X. et al., 2011). Single-channel array processing was utilized followed by data normalization with default parameters, and significant transcript-regulation events were determined by using GeneSpring GX (v11.5.1) software (Agilent Technologies, Waldbronn, Germany). Transcripts were assumed to be significantly regulated if *p*-values corrected for false-positive rate (FDR, Benjamini-Hochberg method) were smaller than 0.05 and if regulation factors between inoculated and corresponding control samples harvested in parallel exceeded 2.0. All quantile-normalized signal intensities of the analyzed candidate genes are shown in Supplementary Table S1, and the raw data from the corresponding array slides were deposited at ArrayExpress [Accession Nr. E-MTAB-2916 for barley and E-MTAB-3803 for wheat]. Array procedures followed MIAME guidelines throughout (Brazma et al., 2001).

For the analysis of PAMP-induced *TaLEMK1* expression, wheat leaf segments were placed into 2 ml tubes submerged in H_2O and pre-infiltrated by vacuum three times for 45 s. Leaf segments were left to recover in the growth cabinet for 16 h to avoid gene expression response to water infiltration. After this time, water was replaced by fresh water (control) or 1 mg/ml chitin (Yaizu Suisankagaku Industry Co., Ltd). Samples were drained, snap-frozen in liquid N_2 at different time points and stored at −80°C. RNA was extracted using Qiagen RNAeasy Plant kit followed by removal of genomic DNA by DNase Turbo DNA-Free (Ambion). For quantitative real-time PCR (qPCR) analysis, first-strand cDNA was synthesized from 1 μg of total RNA using the SuperScript III First Strand Synthesis System. Quantitative RT-PCR (RT-qPCR) analysis of *TaLEMK1*, *TaCMPG1*-like and *TaPub23*-like was conducted as described in Tufan et al. (2009) using gene-specific primers (Supplementary Table S1).

Modeling of HvLEMK1 Protein

Domain delineation, LRR repeat delineation, sequence analysis, and molecular modeling of the three domains of HvLEMK1 protein core were performed as described in Sela et al. (2012) and Slootweg et al. (2013). For model refinement an iterative procedure consisting in global simulated annealing with harmonic restraints on backbone atoms found in definite secondary structure states, followed by model quality assessment with MetaMQAP (Pawlowski et al., 2013). In order to optimize the HvLEMK1-LRR scaffold the Joint Fragment Remote Homology Modeling procedure (Sela et al., 2012; Slootweg et al., 2013) had to be used. The resulting 3D model was brought within 2.8 Å RMSD by repeated rounds of local remodeling from an optimal polypeptide path and a GDT_TS score of 60 according to MetaMQAP.

Sequence propensity analysis resulted in the following template selection for the three globular domains of (a) HvLEMK1-LRR: the LRR domain from FLS2 (PDB code: 4MN8) with sequence identity = 31%, confidence = 99; (b) HvLEMK1-malectin: the malectin from *Xenopus laevis* (PDB code: 2KR2) with sequence identity = 22%, confidence = 100; and (c) HvLEMK1-kinase: the kinase domains from BAK1 (PDB code: 3TL8) with sequence identity = 45%, confidence = 100 and from IRAK1 (PDB code: 2NRU) with sequence identity = 40%, confidence = 100. In addition the Joint Fragment Remote Homology Modeling procedure (Sela et al., 2012; Slootweg et al., 2013) was used to optimize the scaffold for Rnr8-LRR domain generation.

RESULTS

Structure and Conservation of HvLEMK1

The *Rnr8* gene encodes for an LRR/malectin-domain RLK designated *Hv*LEMK1 that contains also a transmembrane and a C-terminal full-length protein-kinase domain (**Figure 1A**). Transient silencing of *HvLEMK1* was reported to weaken non-host resistance of barley to the wheat powdery mildew fungus *Bgt*, and therefore we searched for the presence of an orthologous protein in wheat, which is the natural host for *Bgt* (Douchkov et al., 2014). By PCR we identified two genes, *TaLEMK1_1* (Acc. KX529076) and *TaLEMK1_2* (Acc. KX529077), differing by five predicted amino acids in the LRR domain (**Figure 1B**; Supplementary Figure S2). Comparison of the full length sequences of *TaLEMK1* to the wheat chromosomes on URGI database[3] revealed that the gene is located on the group 5 chromosomes, in syntenic position to the barley orthologous gene (Douchkov et al., 2014). Although exhibiting 94% nucleotide identify to *HvLEMK1*, evolutionary separation of the genus *Hordeum* and *Triticum* approximately 12 MY ago led to the accumulation of a total of 31 non-conservative amino-acid exchanges between the wheat and barley orthologs, which corresponds to approximately 3% of the protein (Supplementary Figure S2). Extending the search for close homologs of HvLEMK1 in more distantly related plants revealed the existence of HvLEMK1-like proteins in all analyzed species, and the conservation of the intron/exon structure suggested the existence of true orthologs (**Figure 1C**; Supplementary Figure S3). *TaLEMK1_1* and *TaLEMK1_2* were most closely related to genes on hexaploid wheat chromosome 5A and 5D, respectively, suggesting that they represent homeologs from the A and the D genomes of wheat. Because some of the non-*Triticum* plant species are not infected by any known powdery mildew fungus, *HvLEMK1* might function in sensing stress-related endogenous signals or highly conserved PAMPs present in different pathogens, or act as co-receptor in RLK complexes.

The putative ligand-binding LRR domain of HvLEMK1 has a homogeneous repeat length of 24. In order to put

[3]http://wheat-urgi.versailles.inra.fr/Tools/dbWFA

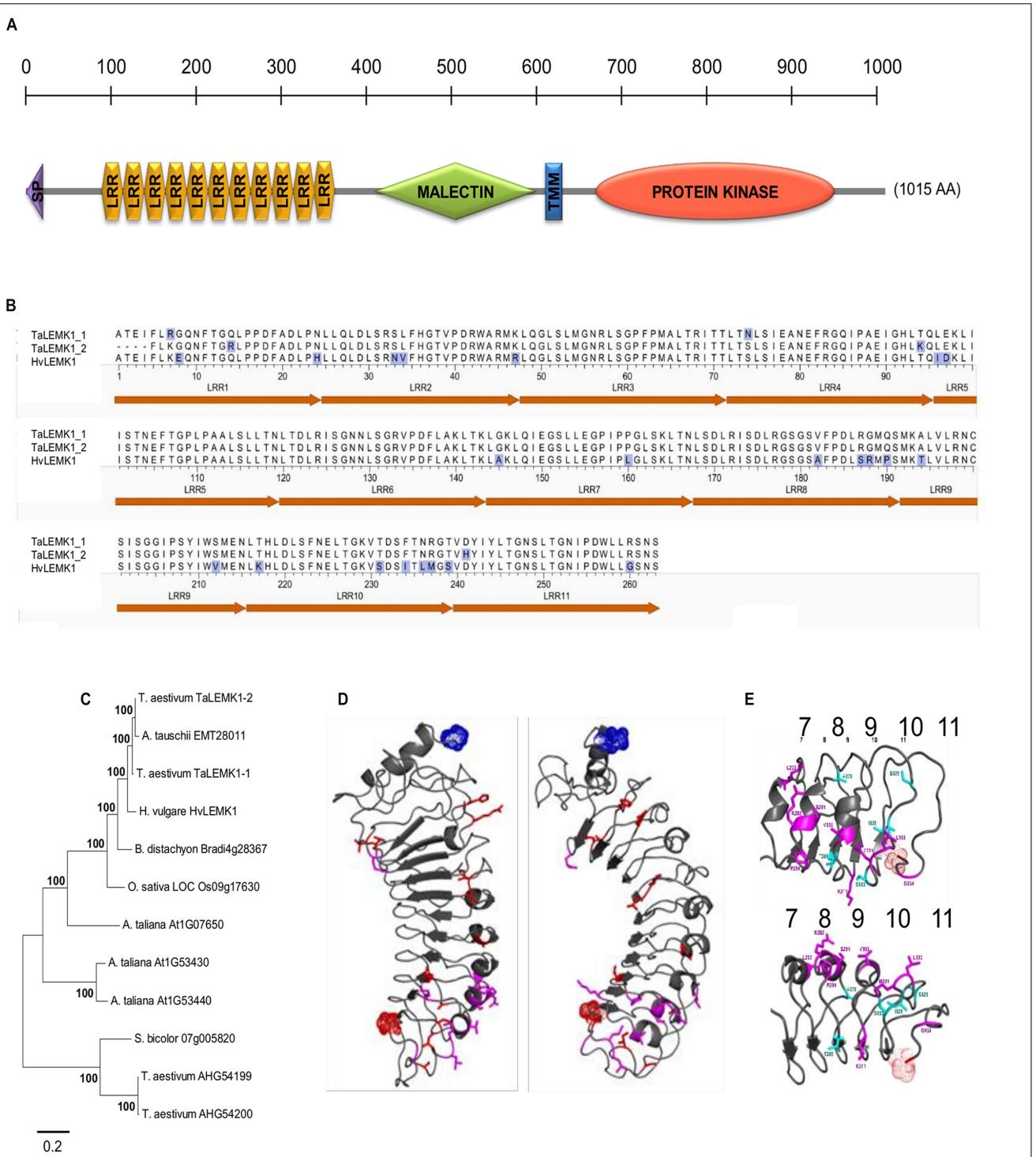

FIGURE 1 | Structure and conservation of *HvLEMK1*. (A) Schematic representation of HvLEMK1 protein domains (drawn to scale). SP, signal peptide; TMM, transmembrane domain. **(B)** Amino-acid comparison of the LRR-repeat domain between barley and wheat LEMK1 proteins. Amino-acid exchanges are highlighted with blue shading. **(C)** Nearest-neighbor joining tree of full-length LEMK1-like protein sequences across monocot and dicot species. Most closely related homologs (putative orthologs) to HvLEMK1 from *Triticum aestivum* (bread wheat), *Aegilops tauschii* (wild wheat, donor of the D genome), *Brachypodium distachyon*, *Oryza sativa* (cultivated rice), *Sorghum bicolor*, and *Arabidopsis thaliana* were included. In addition, two more distantly related proteins from *T. aestivum* were included as outgroup. **(D)** Location of conservative and non-conservative amino-acid substitutions in red and magenta, respectively, among the 11 predicted LRRs. **(E)** Close-up of most variable repeats 7–11 between barley and wheat orthologs highlighting conservative and non-conservative amino-acid exchanges in light blue and magenta, respectively. The clustering of non-conservative site exchanges on the backside of the repeat structure is clearly visible in the lower part of the panel.

differences between the orthologous barley and wheat proteins into a structural context, a three-dimensional (3D) model was generated starting from the LRR domain of FLS2, a RLK protein from *Arabidopsis*, which contains repeats of the same length as HvLEMK1 (**Figure 1D**). Variable residues between HvLEMK1-LRR and TaLEMK1_2-LRR were mapped onto the 3D structure. The overall set of variable amino acids is shown here in red and magenta. Of these only those shown in magenta are mutations that might alter locally the structure and/or the interaction potential of the LRR domain. All these variable sites are clustered in the C-terminal region of the LRR domain pointing to a possible interaction surface with pathogen- or plant interaction partners. More specifically this cluster is located on the backside of repeats 8, 9, and 10 (**Figure 1E**). The malectin domain presents a conserved ordered beta core and a more unstructured N-terminal subdomain which hosts the lectinic site involved in glycan recognition of the malectin prototype protein in animals (Supplementary Figure S4A) (Chen Y. et al., 2011). Due to low sequence identity between HvLEMK1-malectin and the template protein, the 3D structure is still a rough model, with a current RMSD of 4 Å and a GDT_TS of ∼50. Finally, the HvLEMK1-kinase represented in Supplementary Figure S4B shows high sequence similarity with both plant RLK Bak1 and with human IRAK1, not only in the secondary structure patterns but also in the enzymatic active-site region. The model was brought within less than 3 Å RMSD from an optimal polypeptide path with an overall quality GDT_TS score of 58.

Sub-Cellular Localization

The encoded HvLEMK1 protein contains a transmembrane domain between malectin- and kinase domains, suggesting plasma-membrane localization, as has been shown for other RLKs. To verify this prediction, *HvLEMK1* cDNA was fused with its 3′-end to *YFP* and bombarded into barley epidermal cells. The resulting C-terminal fusion protein was tested for co-localization with an aquaporin:mCherry fusion protein that was used as plasma membrane marker, and with a AtWAK2:mCherry fusion protein used as marker for localization to the endoplasmic reticulum (ER) (**Figure 2**). This experiment revealed co-localization of HvLEMK1 with the plasma membrane marker in turgescent- and in plasmolyzed cells, and also in Hechtian strands (**Figures 2a–h**). In addition, we could co-localize a fraction of the protein with the ER marker (**Figures 2i–l**). It is known that plasma membrane-localized RLKs such as the malectin-domain protein Ferronia are retained in the ER, through which they are delivered to the cell periphery, if folding and quality-control chaperones in the ER are limiting or missing (Li C. et al., 2016b). Therefore ER-localization of part of the HvLEMK1:YFP protein pool may reflect overloading of the secretory system by transient over-expression under the control of the strong CaMV 35S promoter. However, because malectin is known to be ER-localized (Chen Y. et al., 2011) we cannot exclude a dual role of HvLEMK1 in both compartments. Finally, another fraction of HvLEMK1:YFP appeared to be localized to the nucleus, without a ring as seen with the mCherry ER marker (inset in **Figure 2k**) This unexpected result therefore awaits further functional examination.

Regulation of LEMK1 Transcripts

Although RLKs are expected to exhibit a basal level of expression in order to fulfill their function in signal-perception, we often found their transcripts to be up-regulated upon pathogen attack of barley (Douchkov et al., 2014). We therefore interrogated two transcript-profiling datasets of leaf epidermal peels from barley and wheat challenged with *Bgh* and *Bgt*, which corresponds to a reciprocal set of host- and non-host interactions, by using

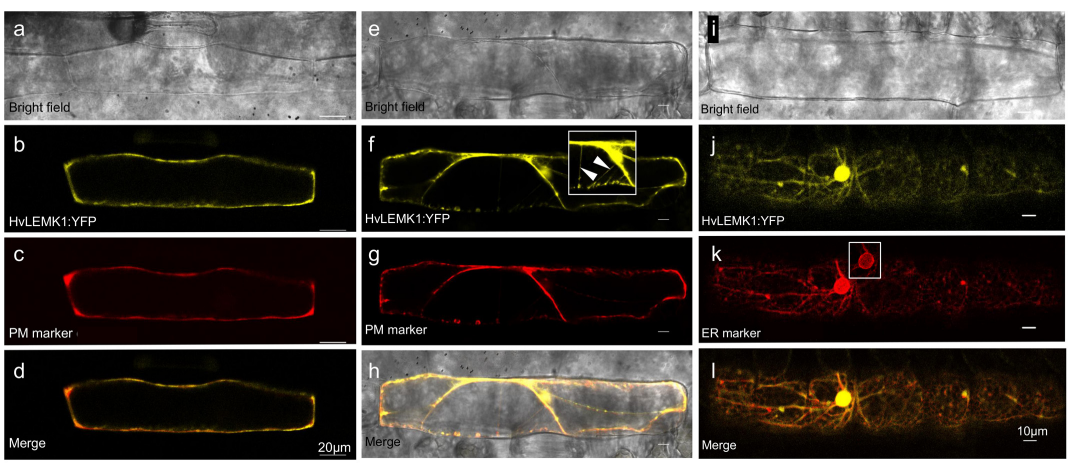

FIGURE 2 | Localization of C-terminal *Hv*LEMK1:YFP fusion protein in barley epidermal cells. Barley leaf segments were co-bombarded with plasmids encoding HvLEMK1:YFP and the plasma-membrane localization marker pm-rk CD3-1007 (encoding aquaporin) or the endoplasmic reticulum-localization (ER) marker ER-rk CD3-959 (encoding *AtWAK2*) (Nelson et al., 2007). Confocal laser-scanning microscopy of non-inoculated cells was performed 24 h after the bombardment. **(a–d)** co-localization with the plasma-membrane marker. **(e–h)** plasma-membrane localization confirmed in plasmolysed cells. The inset in **(f)** corresponds to an over-exposed section of **(f)**, showing localization to Hechtian strands (arrowheads). **(i–l)** Co-localization with the ER marker. The inset in **(k)** corresponds to the cell nucleus imaged with reduced brightness in order to reveal the expected accumulation of the ER-marker at the nuclear border.

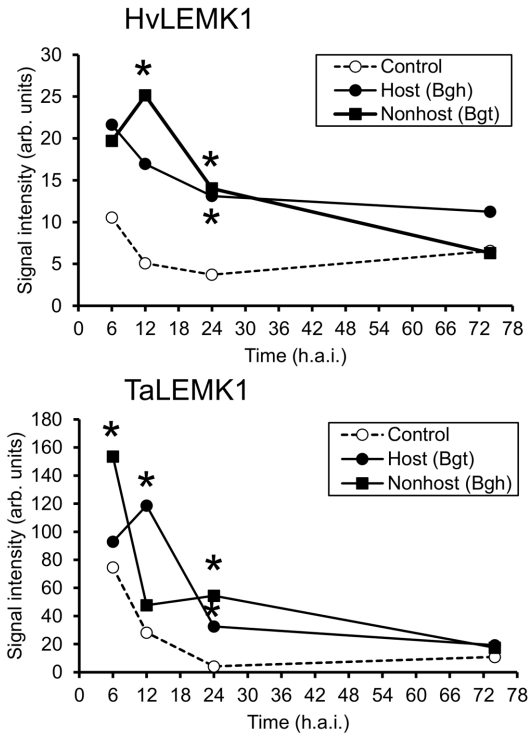

FIGURE 3 | Rapid transcriptional up-regulation of *LEMK1* in wheat and barley epidermis following inoculation with adapted or non-adapted powdery mildew fungi. Data of three independent inoculation experiments were derived from Agilent 44K oligonucleotide microarrays, as described in section "Materials and Methods." Asterisks indicate significant transcript regulation between inoculated and non-inoculated control plants (FDR-corrected p-value < 0.05). h.a.i., hours after inoculation.

the Agilent 44K Gene Expression Arrays of the two species. As shown in **Figure 3**, both *HvLEMK1* and *TaLEMK1* were up-regulated upon powdery-mildew attack. Interestingly, *Bgh* triggered maximum transcript levels at 6 h after inoculation in both plant species whereas the maximum response to *Bgt* attack was relatively delayed by 6 h. Therefore the different induction kinetics appears to be determined by the behavior of the respective pathogen (race) such as the kinetics of PAMP release, rather than by the host-vs. non-host status of barley or wheat.

Transgenic Barley Silenced in *HvLEMK1*

We stably transformed barley with an RNAi construct against *HvLEMK1* and identified 24 primary transgenic plants carrying intact versions of the silencing cassette. These were tested in the T1 generation for an altered interaction phenotype with *Bgt* (Supplementary Figure S5). T1 families with enhanced colony- or conidiospore formation of the non-adapted fungus in the first experiment were selected for subsequent tests in two more inoculation experiments, and for the quantification of target-transcript levels (**Figures 4A,B**). The susceptibility phenotype to *Bgt* could be confirmed in a statistically significant manner for four T1 families, and these also showed significant reduction of *HvLEMK1* transcript levels. On the other hand, we observed no difference of quantitative host resistance against *Bgh* in any of these four families (**Figure 4C**) suggesting no effect of *HvLEMK1* in quantitative host resistance. The microscopic inspection of *Bgt* development 7 days after inoculation (d.a.i.) of *HvLEMK1*-silenced leaves revealed the presence of colonies that, however, remained smaller than those of *Bgh* from parallel inoculations and were not visible to the naked eye (**Figure 4D**). Importantly, conidial chain formation of *Bgt* (highlighted by red arrows) was found in all four selected RNAi T1 families but never in the rare micro-colonies that were formed by *Bgt* on wildtype or azygous control plants (**Figures 4D,E**). We conclude that silencing of *HvLEMK1* resulted in a partial breakdown of non-host resistance to *Bgt*. Because the *HvLEMK1*-silenced plants showed no visible growth abnormalities or stress symptoms (Supplementary Figure S6) we assume that the *HvLEMK1* gene does not have essential developmental or housekeeping functions.

We characterized transcriptional induction of five proposed marker genes of non-host resistance in the RNAi transgenic families. These genes were selected because their transcripts were more strongly induced at 6–12 h after inoculation in non-host resistant- compared to host susceptible interactions of barley and wheat with *B. graminis*. By contrast, they showed no differential induction between barley lines carrying the *Mla6* major R-gene or being mutated at the locus (*mla6*) (Supplementary Figure S9; Supplementary Table S2). As shown in **Figure 5**, three of the five candidate markers were less induced in *HvLEMK1*-silenced T1 populations at 12 h after *Bgt*-inoculation, compared to azygous segregant plants. At 24 h after inoculation the difference between azygous and transgenic plants had disappeared.

Transient Expression of *LEMK1* Genes in Wheat and Barley

We next tested the option that heterologous expression of the barley ortholog in wheat and *vice versa* might confer non-host-like resistance across species borders due to, for example, reduced functional suppression by one or several effectors from the corresponding non-adapted powdery mildew pathogen (Deslandes and Rivas, 2012; Feng et al., 2012; Mentlak et al., 2012). Bombardment of wheat-leaf segments with either a BAC clone carrying the *HvLEMK1* gene, the coding part of the gene under the control of the CaMV 35S promoter, or a full-coding sequence cDNA clone significantly enhanced resistance, as compared to a control BAC clone containing no annotated genes or to the empty over-expression vector pIPKTA9 (**Figure 6**). Transient over-expression of the two closely related *homoeo*-alleles in wheat revealed a protective effect of *TaLEMK1_2* comparable to the barley gene, whereas *TaLEMK1_1* showed no significant effect. One possible explanation to this observation is that the TaLEMK1_2 but not TaLEMK1_1 protein is free from functional suppression by a hypothetical *Bgt*-encoded effector. Attempts to transiently silence *TaLEMK1_1* and *TaLEMK1_2* for further clarifying their function in quantitative host resistance to *Bgt* and non-host resistance to *Bgh* failed because the bombarded wheat-leaf segments built up a strong

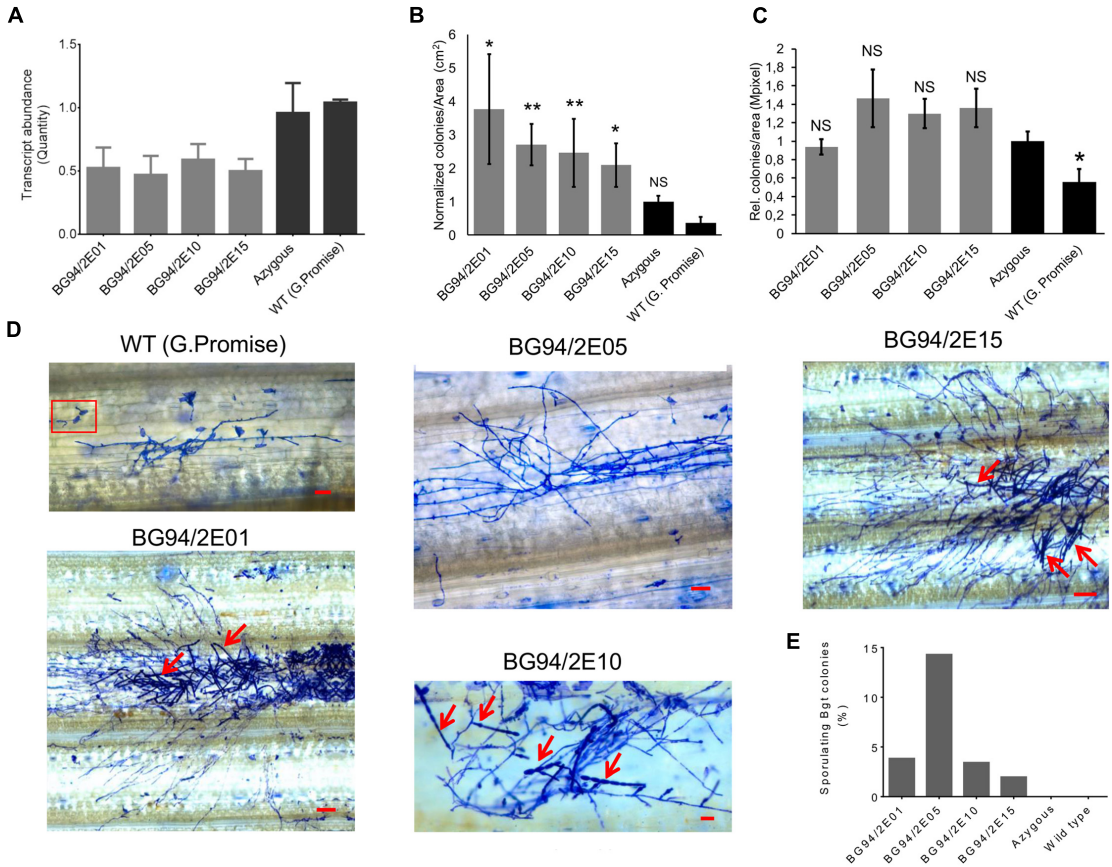

FIGURE 4 | Phenotype of RNAi transgenic T1 plants of barley with reduced *HvLEMK1* expression. (A) RT-qPCR of *HvLEMK1* in selected T1 families. Mean values ± SE from two independent experiments (batches of plants sown on different dates, non-inoculated) are shown. **(B)** Reduced non-host resistance of transgenic events against *Bgt*. Mean values ± SE of manual microscopic colony counting 7 d.a.i. from three independent inoculation experiments, normalized to the mean value of the azygous control group, are shown. Statistical significance are indicated by asterisks. *$p < 0.05$, **$p < 0.005$. n, total number of analyzed plants per event. **(C)** No change in quantitative host resistance against *Bgh* of most of the T1 families shown in **(A)**. Mean values ± SE of automated microscopic colony counting by the HyphArea software at 48 h after inoculation (two independent inoculation experiments) are shown. Asterisk indicates statistical significance. *$p < 0.05$; n, total number of analyzed plants per T1 family; NS, not-significant. **(D)** Examples of enhanced colony growth including sporulation (red arrows) of *Bgt* on leaves of *HvLEMK1*-silenced T1 plants. Panel "WT (Golden Promise)" shows examples of frequently failed penetration (inside red frame) plus one of the rarely observed, non-sporulation *Bgt* micro-colonies. Scale bars = 50 μm. **(E)** Percentage of sporulating *Bgt* colonies (mean values from two independent experiments).

resistance to *Bgt* within the minimum required incubation period of 2 days after bombardment that was required for effective TIGS. This bombardment-induced resistance, possibly due to mechanical stress, resulted in an average haustorial index of 0.006 from five independent experiments using the empty vector control. Stable transgenic RNAi lines of wheat would therefore be required to address the role of *TaLEMK1* genes in non-host resistance. In summary, at least the TaLEMK1_2 protein appears to quantitatively contribute to host resistance in wheat while its role in non-host resistance is currently unclear. In the light of the enhanced resistance caused by over-expression of endogenous *TaLEMK1_2* in wheat, the partial protection observed after transient expression of the heterologous *HvLEMK1* transgene might also be due to its over-expression rather than transgenomic functional complementation, even when bombarded as a BAC clone under the control of its own promoter.

DISCUSSION

Current models for non-host resistance suggest a range of defense-related proteins to be involved, in many cases belonging to the same families as those identified as major components of host PTI or ETI (Collins et al., 2003; Lipka et al., 2005; Stein et al., 2006; Sohn et al., 2012; Lee et al., 2014; Vega-Arreguin et al., 2014; Douchkov et al., 2016). It therefore appears plausible that non-host resistance in many instances is conferred by the robust execution of a host-defense program, which might be very diverse depending on the molecular, cellular, and physiological characteristics of a given non-host plant-pathogen interaction. A recent general model proposes that the recognition of non-adapted pathogens shortly after host speciation is mediated mostly by the robust combinations of NB-LRR-type effector recognition proteins triggering ETI whereas in more ancient non-host interactions,

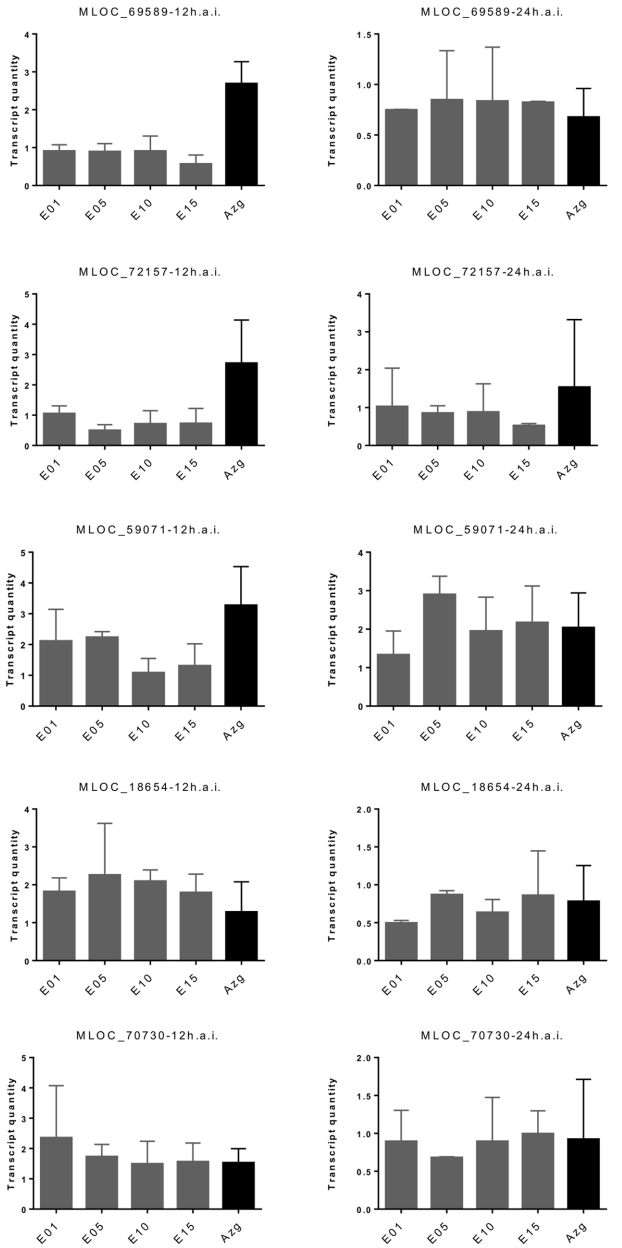

FIGURE 5 | Redued induction of proposed PTI marker genes in *HvLEMK1*-silenced barley plants. Wildtype plants or selected transgenic T1 families were inoculated with *Bgt*, followed by RNA extraction 12 and 24 h after inoculation and quantification of transcript amounts by RT-qPCR. Mean values ± SE from two independent experiments (batches of plants sown on different dates) using a total of 10–14 transgenic plants are shown. Proposed protein functions: MLOC_69589, PR17-like secreted protein; MLOC_72157, SERK1-like RLK; MLOC_59071, putative leucoanthocyanidin dioxygenase; MLOC_18654, hypothetical protein; MLOC_70730, caffeoyl-CoA-*O*-methyltransferase.

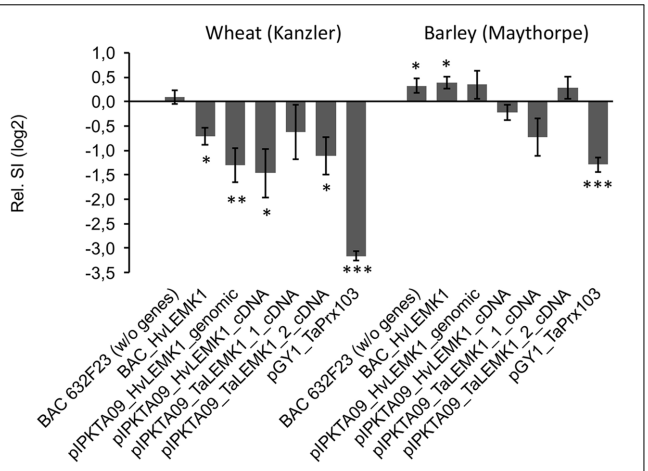

FIGURE 6 | Effect of transiently expressing *LEMK1* genes in barley and wheat on quantitative host resistance against adapted powdery mildew fungi. Barley and wheat orthologs of *LEMK1* were transiently expressed in bombarded barley and wheat leaf segments, followed by inoculation with the adapted powdery mildew fungi *Bgh* and *Bgt*, respectively. In the case of *HvLEMK1*, the gene was expressed under the control of its own promoter by bombarding an *HvLEMK1*-containing BAC clone, and under the control of the CaMV 35S promoter as genomic BAC sub-clone (pIPKTA09_HvLEMK1_genomic) or full-length cDNA clone (pIPKTA09_HvLEMK1_cDNA). The corresponding wheat orthologs *TaLEMK1_1* and *TaLEMK1_2* were only expressed as full-length cDNA clones under the control of the CaMV 35S promoter (pIPKTA09_TaLEMK1_1_cDNA; pIPKTA09_TaLEMK1_2_cDNA). pGY1_TaPrx103 for over-expression of a pathogen-induced wheat class III peroxidase (Schweizer, 2008) and BAC632F23 containing no annotated genes served as positive and negative controls, respectively. SI values were normalized to the empty over-expression vector pIPKTA09 and log(2) transformed. Mean values ± SEM of 5–10 independent experiments (pGY1_TaPrx103 in barley, 21 experiments) are shown. $*p < 0.05$, $**p < 0.01$, $***p < 0.0001$ (1-sample *t*-test against the hypothetical control value "0," 2-tailed).

strong PTI responses are activated by PAMP-recognizing PRRs for the inhibition of which the non-adapted pathogen had lost functional effectors (Schulze-Lefert and Panstruga, 2011).

Here we propose LEMK1, an LRR/malectin-domain RLK, to mediate non-host resistance in barley and quantitative host resistance in wheat against the wheat powdery-mildew fungus *Bgt*. As suggested from the presence of an N-terminal transmembrane domain and from the localization of a *Hv*LEMK1:YFP fusion protein, HvLEMK1 appears to reside in the cell membrane probably transmitting an extracellular signal. It possesses 11 predicted LRRs, and this number of repeats corresponds, for example, to the R-protein encoded by the barley *Mla1* gene conferring resistance to *Bgh*. However, repeat number is lower than in many other reported R-proteins including wheat *Pm3b* for resistance to *Bgt* (Meyers et al., 2003; Yahiaoui et al., 2004). The malectin domain, which is related to the endoplasmic reticulum-localized, high mannose glycan-binding lectin malectin of animals (Galli et al., 2011), has been involved in RLK cleavage resulting in release from steric hindrance of heteroduplex formation and in fine tuning of RLK turnover (Lindner et al., 2012; Antolin-Llovera et al., 2014a,b). However, because the conserved GDPC motif required for cleavage of the malectin domain is missing from the predicted HvLEMK1 protein its function might be rather related to extracellular mannan-rich carbohydrate perception, as proposed

for *Catharanthus roseus* RLK1-like kinases (CrRLK1Ls) including the fertilization and defense-related Ferronia protein (Lindner et al., 2012). It is interesting to note here that a highly active, secreted PAMP of *Bgt* was characterized as a glucomannan, with the mannan-residues being important for elicitor activity (Schweizer et al., 2000). Future biochemical work will have to address this possibility. Also, besides the possibility that HvLEMK1 recognizes an extracellular PAMP or a damage-associated molecular pattern, which would suggest it to act as PRR, it could function as co-receptor to PAMP receptors similar to the LRR/malectin RLK IOS1 recently characterized in *A. thaliana*, (Chinchilla et al., 2007; Niehl et al., 2016; Yeh et al., 2016). An analysis of allelic diversity of the LRR domain among different barley and wheat genotypes revealed a very high degree of intra-species conservation within each species (Supplementary Figure S7). Although this result might be strongly influenced by a breeders-driven selection for specific alleles, it supports the view that *LEMK1* is not engaged in a co-evolutionary arms race for pathogen-effector recognition but may mediate the recognition of more conserved (PAMP) signals or be a co-receptor to endogenous PRRs. This hypothesis is also in line with the observed inter-species variability in amino-acid sequences between barley and wheat, which might reflect the selection for optimal interaction with such conserved interaction partners in each species.

Further support for a role in PAMP-mediated signaling comes from transcript regulation data in wheat showing induction by chitin (Supplementary Figure S8), a well-established PAMP in many plant-pathogen interactions (Kaku et al., 2006). It is known that PRRs are transcriptionally up-regulated by PAMPs (New et al., 2015; Li B. et al., 2016a). The induction of *TaLEMK1* by chitin does not, however, qualify this LRK as chitin receptor because single PAMPs were found to induce more than one PRR (New et al., 2015). The observed, delayed accumulation of three of the five candidate markers in *HvLEMK1*-silenced T1 populations at 12 h after *Bgt*-inoculation, compared to azygous segregant plants, also suggest a role at the RLK in defense-regulated gene expression. At 24 h after inoculation the difference between azygous and transgenic plants had disappeared, which might indicate signal redundancy between different RLKs or the overriding of the RNAi effect by *HvLEMK1* transcript induction. The two non-affected transcripts from genes MLOC_18654 and MLOC_70730 might be regulated by an independent signaling pathway. In summary, the PAMP-mediated induction of *TaLEMK1* transcripts, and the *HvLEMK1*-dependent induction of non-host marker genes suggest that *LEMK1* is involved in two manifestations of PTI: quantitative host resistance and non-host-resistance (Fan and Doerner, 2012).

Transient over-expression of *TaLEMK1_2* as well as *HvLEMK1* enhanced resistance in wheat to *Bgt* but not in barley against *Bgh* suggesting that *Bgt* is more strongly affected by increased levels of the LEMK1 protein. Two possible explanations might apply to these different *LEMK1* effects in the two *B. graminis formae specialis*: *Bgh* but not *Bgt* might possess an effector controlling HvLEMK1 function, or the fungus might degrade or mask some PAMP molecule(s) as has been described before for other pathogens (van den Burg et al., 2004). Which of

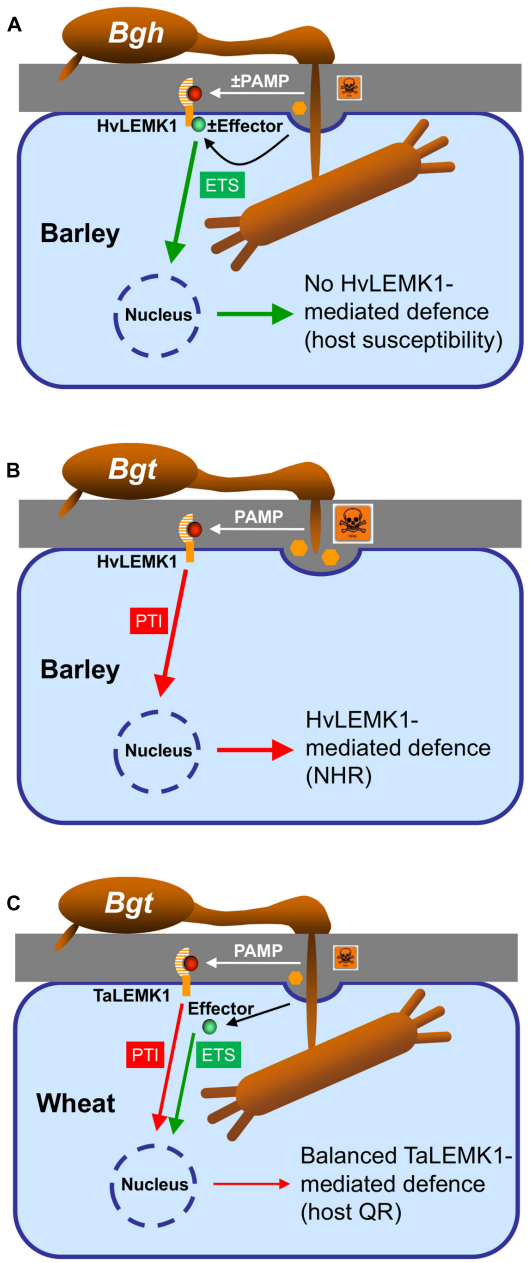

FIGURE 7 | Model of the role of LEMK1 in non-host resistance of barley and quantitative host resistance of wheat to *Bgt*. (A) In the susceptible host interaction, *Bgh* either prevents or masks the release of a PAMP (highlighted by "±," which otherwise would be recognized by HvLEMK1, or it releases an effector suppressing HvLEMK1-triggered PTI. **(B)** In the non-host-resistant interaction of barley with *Bgt*, HvLEMK1 recognizes the same/similar conserved PAMP without attenuation by an effector and triggers a strong PTI response. **(C)** During the interaction of wheat with *Bgt*, TaLEMK1 also recognizes the corresponding PAMP with high efficiency, but PTI is partially inhibited by other effector(s) from *Bgt*. **(A–C)** For simplicity the model only includes a proposed role of LEMK1 as PAMP receptor and ignores the possibility that it acts as co-receptor together with another RLK. In both scenarios, however, the outcome of the presence/absence of a PAMP or of a LEMK1-suppressing effector would be the same. NHR, non-host resistance; host QR, host quantitative resistance.

these possibilities that are summarized in the model shown in **Figure 7** are true remains to be further examined in the future.

HvLEMK1 and *TaLEMK1_2* were discovered as factors mediating non-host resistance in barley to *Bgt* and quantitative host resistance in wheat to the same pathogen indicating that *Triticeae* species share components of quantitative host-and non-host resistance. This supports the idea that non-host resistance is an extremely strong manifestation of quantitative host resistance, which is difficult for a non-adapted pathogen to overcome because it would require incremental increases of pathogenicity or aggressiveness, which cannot be selected for in the absence of reproductive cycles on the non-host. Finally, the discovery and validation of non-host resistance components of barley may provide valuable leads for quantitative host resistance improvement by allelic optimization of orthologs in wheat, or by introgression across species borders by genetic engineering (Lacombe et al., 2010).

AUTHOR CONTRIBUTIONS

LB designed research and wrote the article. OC performed research (modeling). DD performed research (transgenic plant analysis). NE performed research (gene cloning and analysis). AG performed research (gene cloning and analysis). GH performed research (plant transformation). JK designed research. A-JP designed and performed research (modeling). JR performed research and wrote the article (gene cloning, transient expression, sub-cellular localization, transgenic plant analysis, transcript profiling). FS performed research (gene cloning and sequencing). PS designed research and wrote the article.

FUNDING

This work was supported by the German Ministry of Education and Research (BMBF, project PRO-GABI, to PS and JK), by BASF Plant Science GmbH (project GABI-non-host II, to PS) and by German DFG (project ERA-CAPS DURESTrit, to PS). OC and A-JP acknowledge financial support for this work from the Romanian Academy program 3 and UEFISCDI grant PN-II-ID-PCE-2011-3-0342. LAB and FS were supported by the UK Biotechnology and Biological Sciences Research Council (BBSRC) award BB/G024987/1.

ACKNOWLEDGMENTS

We thank Stefanie Lück, Cornelia Marthe, and Gabi Brantin for excellent technical assistance. We also acknowledge Agilent array hybridizations carried out by Steve Hedley (James Hutton Institute).

SUPPLEMENTARY MATERIAL

The Supplementary Material for this article can be found online at: http://journal.frontiersin.org/article/10.3389/fpls.2016.01836/full#supplementary-material

REFERENCES

Antolin-Llovera, M., Petutsching, E. K., Ried, M. K., Lipka, V., Nurnberger, T., Robatzek, S., et al. (2014a). Knowing your friends and foes - plant receptor-like kinases as initiators of symbiosis or defence. *New Phytol.* 204, 791–802. doi: 10.1111/nph.13117

Antolin-Llovera, M., Ried, M. K., and Parniske, M. (2014b). Cleavage of the SYMBIOSIS RECEPTOR-LIKE KINASE ectodomain promotes complex formation with nod factor receptor 5. *Curr. Biol.* 24, 422–427. doi: 10.1016/j.cub.2013.12.053

Baum, T., Navarro-Quezada, A., Knogge, W., Douchkov, D., Schweizer, P., and Seiffert, U. (2011). HyphArea-automated analysis of spatiotemporal fungal patterns. *J. Plant Physiol.* 168, 72–78. doi: 10.1016/j.jplph.2010.08.004

Brazma, A., Hingamp, P., Quackenbush, J., Sherlock, G., Spellman, P., Stoeckert, C., et al. (2001). Minimum information about a microarray experiment (MIAME)—toward standards for microarray data. *Nat. Genet.* 29, 365–371. doi: 10.1038/ng1201-365

Chen, X., Hedley, P. E., Morris, J., Liu, H., Niks, R. E., and Waugh, R. (2011). Combining genetical genomics and bulked segregant analysis-based differential expression: an approach to gene localization. *Theor. Appl. Genet.* 122, 1375–1383. doi: 10.1007/s00122-011-1538-3

Chen, Y., Hu, D., Yabe, R., Tateno, H., Qin, S. Y., Matsumoto, N., et al. (2011). Role of malectin in Glc(2)Man(9)GlcNAc(2)-dependent quality control of alpha 1-antitrypsin. *Mol. Biol. Cell* 22, 3559–3570. doi: 10.1091/mbc.E11-03-0201

Chinchilla, D., Zipfel, C., Robatzek, S., Kemmerling, B., Nurnberger, T., Jones, J. D. G., et al. (2007). A flagellin-induced complex of the receptor FLS2 and BAK1 initiates plant defence. *Nature* 448, 497–500. doi: 10.1038/nature05999

Collins, N. C., Thordal-Christensen, H., Lipka, V., Bau, S., Kombrink, E., Qiu, J. L., et al. (2003). SNARE-protein-mediated disease resistance at the plant cell wall. *Nature* 425, 973–977. doi: 10.1038/nature02076

Deslandes, L., and Rivas, S. (2012). Catch me if you can: bacterial effectors and plant targets. *Trends Plant Sci.* 17, 644–655. doi: 10.1016/j.tplants.2012.06.011

Douchkov, D., Lück, S., Johrde, A., Nowara, D., Himmelbach, A., Rajaraman, J., et al. (2014). Discovery of genes for affecting resistance of barley to adapted and non-adapted powdery mildew fungi. *Genome Biol.* 15:518. doi: 10.1186/s13059-014-0518-8

Douchkov, D., Lueck, S., Hensel, G., Kumlehn, J., Rajaraman, J., Johrde, A., et al. (2016). The barley (*Hordeum vulgare*) cellulose synthase-like D2 gene (HvCslD2) mediates penetration resistance to host-adapted and nonhost isolates of the powdery mildew fungus. *New Phytol.* 212, 421–433. doi: 10.1111/nph.14065

Douchkov, D., Nowara, D., Zierold, U., and Schweizer, P. (2005). A high-throughput gene-silencing system for the functional assessment of defense-related genes in barley epidermal cells. *Mol. Plant Microbe Interact.* 18, 755–761. doi: 10.1094/MPMI-18-0755

Fan, J., and Doerner, P. (2012). Genetic and molecular basis of nonhost disease resistance: complex, yes; silver bullet, no. *Curr. Opin. Plant Biol.* 15, 400–406. doi: 10.1016/j.pbi.2012.03.001

Feng, F., Yang, F., Rong, W., Wu, X. G., Zhang, J., Chen, S., et al. (2012). A Xanthomonas uridine 5 '-monophosphate transferase inhibits plant immune kinases. *Nature* 485, 114–118. doi: 10.1038/nature10962

Galli, C., Bernasconi, R., Solda, T., Calanca, V., and Molinari, M. (2011). Malectin Participates in a backup glycoprotein quality control pathway in the mammalian ER. *PLoS ONE* 6:e16304. doi: 10.1371/journal.pone.0016304

Giraldo, M. C., and Valent, B. (2013). Filamentous plant pathogen effectors in action. *Nat. Rev. Microbiol.* 11, 800–814. doi: 10.1038/nrmicro3119

Hensel, G., Valkov, V., Middlefell-Williams, J., and Kumlehn, J. (2008). Efficient generation of transgenic barley: the way forward to modulate plant-microbe interactions. *J. Plant Physiol.* 165, 71–82. doi: 10.1016/j.jplph.2007.06.015

Himmelbach, A., Zierold, U., Hensel, G., Riechen, J., Douchkov, D., Schweizer, P., et al. (2007). A set of modular binary vectors for transformation of cereals. *Plant Physiol.* 145, 1192–1200. doi: 10.1104/pp.107.111575

Jones, J. D. G., and Dangl, J. L. (2006). The plant immune system. *Nature* 444, 323–329. doi: 10.1038/nature05286

Kaku, H., Nishizawa, Y., Ishii-Minami, N., Akimoto-Tomiyama, C., Dohmae, N., Takio, K., et al. (2006). Plant cells recognize chitin fragments for defense signaling through a plasma membrane receptor. *Proc. Natl. Acad. Sci. U.S.A.* 103, 11086–11091. doi: 10.1073/pnas.0508882103

Kou, Y. J., and Wang, S. P. (2010). Broad-spectrum and durability: understanding of quantitative disease resistance. *Curr. Opin. Plant Biol.* 13, 181–185. doi: 10.1016/j.pbi.2009.12.010

Lacombe, S., Rougon-Cardoso, A., Sherwood, E., Peeters, N., Dahlbeck, D., Van Esse, H. P., et al. (2010). Interfamily transfer of a plant pattern-recognition receptor confers broad-spectrum bacterial resistance. *Nat. Biotechnol.* 28, 365–369. doi: 10.1038/nbt.1613

Lee, H.-A., Kim, S.-Y., Oh, S.-K., Yeom, S.-I., Kim, S.-B., Kim, M.-S., et al. (2014). Multiple recognition of RXLR effectors is associated with nonhost resistance of pepper against Phytophthora infestans. *New Phytol.* 203, 926–938. doi: 10.1111/nph.12861

Li, B., Meng, X., Shan, L., and He, P. (2016a). Transcriptional regulation of pattern-triggered immunity in plants. *Cell Host Microbe* 19, 641–650. doi: 10.1016/j.chom.2016.04.011

Li, C., Wu, H. M., and Cheung, A. Y. (2016b). FERONIA and her pals: functions and mechanisms. *Plant Physiol.* 171, 2379–2392.

Lindner, H., Mueller, L. M., Boisson-Dernier, A., and Grossniklaus, U. (2012). CrRLK1L receptor-like kinases: not just another brick in the wall. *Curr. Opin. Plant Biol.* 15, 659–669. doi: 10.1016/j.pbi.2012.07.003

Lipka, V., Dittgen, J., Bednarek, P., Bhat, R., Wiermer, M., Stein, M., et al. (2005). Pre- and postinvasion defenses both contribute to nonhost resistance in *Arabidopsis*. *Science* 310, 1180–1183. doi: 10.1126/science.1119409

Macho, A. P., and Zipfel, C. (2014). Plant PRRs and the activation of innate immune signaling. *Mol. Cell* 54, 263–272. doi: 10.1016/j.molcel.2014.03.028

Mentlak, T. A., Kombrink, A., Shinya, T., Ryder, L. S., Otomo, I., Saitoh, H., et al. (2012). Effector-mediated suppression of chitin-triggered immunity by magnaporthe oryzae is necessary for rice blast disease. *Plant Cell* 24, 322–335. doi: 10.1105/tpc.111.092957

Meyers, B. C., Kozik, A., Griego, A., Kuang, H. H., and Michelmore, R. W. (2003). Genome-wide analysis of NBS-LRR-encoding genes in *Arabidopsis*. *Plant Cell* 15, 809–834. doi: 10.1105/tpc.009308

Nelson, B. K., Cai, X., and Nebenfuhr, A. (2007). A multicolored set of in vivo organelle markers for co-localization studies in *Arabidopsis* and other plants. *Plant J.* 51, 1126–1136. doi: 10.1111/j.1365-313X.2007.03212.x

New, S. A., Piater, L. A., and Dubery, I. A. (2015). In silico characterization and expression analysis of selected *Arabidopsis* receptor-like kinase genes responsive to different MAMP inducers. *Biol. Plant.* 59, 18–28. doi: 10.1007/s10535-014-0478-6

Niehl, A., Wyrsch, I., Boller, T., and Heinlein, M. (2016). Double-stranded RNAs induce a pattern-triggered immune signaling pathway in plants. *New Phytol.* 211, 1008–1019. doi: 10.1111/nph.13944

Pawlowski, M., Bogdanowicz, A., and Bujnicki, J. M. (2013). QA-RecombineIt: a server for quality assessment and recombination of protein models. *Nucleic Acids Res.* 41, W389–W397. doi: 10.1093/nar/gkt408

Pennington, H. G., Gheorghe, D. M., Damerum, A., Pliego, C., Spanu, P. D., Cramer, R., et al. (2016). Interactions between the powdery mildew effector BEC1054 and barley proteins identify candidate host targets. *J. Proteome Res.* 15, 826–839. doi: 10.1021/acs.jproteome.5b00732

Pliego, C., Nowara, D., Bonciani, G., Gheorghe, D. M., Xu, R., Surana, P., et al. (2013). Host-induced gene silencing in barley powdery mildew reveals a class of ribonuclease-like effectors. *Mol. Plant Microbe Interact.* 26, 633–642. doi: 10.1094/MPMI-01-13-0005-R

Schmidt, S. M., Kuhn, H., Micali, C., Liller, C., Kwaaitaal, M., and Panstruga, R. (2014). Interaction of a *Blumeria graminis* f. sp hordei effector candidate with a barley ARF-GAP suggests that host vesicle trafficking is a fungal pathogenicity target. *Mol. Plant Pathol.* 15, 535–549. doi: 10.1111/mpp.12110

Schulze-Lefert, P., and Panstruga, R. (2011). A molecular evolutionary concept connecting nonhost resistance, pathogen host range, and pathogen speciation. *Trends Plant Sci.* 16, 117–125. doi: 10.1016/j.tplants.2011.01.001

Schweizer, P. (2008). Tissue-specific expression of a defence-related peroxidase in transgenic wheat potentiates cell death in pathogen-attacked leaf epidermis. *Mol. Plant Pathol.* 9, 45–57. doi: 10.1111/j.1364-3703.2007.00446.x

Schweizer, P., Gees, R., and Mosinger, E. (1993). Effect of jasmonic acid on the interaction of barley (*Hordeum vulgare* L) with the powdery mildew erysiphe-graminis f.sp. hordei. *Plant Physiol.* 102, 503–511. doi: 10.1104/pp.102.2.503

Schweizer, P., Kmecl, A., Carpita, N., and Dudler, R. (2000). A soluble carbohydrate elicitor from *Blumeria graminis* f. sp tritici is recognized by a broad range of cereals. *Physiol. Mol. Plant Pathol.* 56, 157–167. doi: 10.1006/pmpp.2000.0259

Sela, H., Spiridon, L. N., Petrescu, A.-J., Akerman, M., Mandel-Gutfreund, Y., Nevo, E., et al. (2012). Ancient diversity of splicing motifs and protein surfaces in the wild emmer wheat (*Triticum dicoccoides*) LR10 coiled coil (CC) and leucine-rich repeat (LRR) domains. *Mol. Plant Pathol.* 13, 276–287. doi: 10.1111/j.1364-3703.2011.00744.x

Slootweg, E. J., Spiridon, L. N., Roosien, J., Butterbach, P., Pomp, R., Westerhof, L., et al. (2013). Structural determinants at the interface of the ARC2 and leucine-rich repeat domains control the activation of the plant immune receptors Rx1 and Gpa2. *Plant Physiol.* 162, 1510–1528. doi: 10.1104/pp.113.218842

Sohn, K. H., Saucet, S. B., Clarke, C. R., Vinatzer, B. A., O'brien, H. E., Guttman, D. S., et al. (2012). HopAS1 recognition significantly contributes to *Arabidopsis* nonhost resistance to *Pseudomonas syringae* pathogens. *New Phytol.* 193, 58–66. doi: 10.1111/j.1469-8137.2011.03950.x

Spies, A., Korzun, L., Bayles, R., Rajaraman, J., Himmelbach, A., Hedley, P. E., et al. (2012). Allele mining in barley genetic resources reveals genes of race-nonspecific powdery mildew resistance. *Front. Plant Sci.* 2:113. doi: 10.3389/fpls.2011.00113

Stein, M., Dittgen, J., Sanchez-Rodriguez, C., Hou, B. H., Molina, A., Schulze-Lefert, P., et al. (2006). *Arabidopsis* PEN3/PDR8, an ATP binding cassette transporter, contributes to nonhost resistance to inappropriate pathogens that enter by direct penetration. *Plant Cell* 18, 731–746. doi: 10.1105/tpc.105.038372

Tufan, H. A., Mcgrann, G. R. D., Magusin, A., Morel, J.-B., Miche, L., and Boyd, L. A. (2009). Wheat blast: histopathology and transcriptome reprogramming in response to adapted and nonadapted *Magnaporthe* isolates. *New Phytol.* 184, 473–484. doi: 10.1111/j.1469-8137.2009.02970.x

van den Burg, H. A., Spronk, C., Boeren, S., Kennedy, M. A., Vissers, J. P. C., Vuister, G. W., et al. (2004). Binding of the AVR4 elicitor of *Cladosporium fulvum* to chitotriose units is facilitated by positive allosteric protein-protein interactions - The chitin-binding site of AVR4 represents a novel binding site on the folding scaffold shared between the invertebrate and the plant chitin-binding domain. *J. Biol. Chem.* 279, 16786–16796.

Vega-Arreguin, J. C., Jalloh, A., Bos, J. I., and Moffett, P. (2014). Recognition of an Avr3a homologue plays a major role in mediating nonhost resistance to *Phytophthora capsici* in *Nicotiana* Species. *Mol. Plant Microbe Interact.* 27, 770–780. doi: 10.1094/MPMI-01-14-0014-R

Wawra, S., Belmonte, R., Loebach, L., Saraiva, M., Willems, A., and Van West, P. (2012). Secretion, delivery and function of oomycete effector proteins. *Curr. Opin. Microbiol.* 15, 685–691. doi: 10.1016/j.mib.2012.10.008

Wicker, T., Oberhaensli, S., Parlange, F., Buchmann, J. P., Shatalina, M., Roffler, S., et al. (2013). The wheat powdery mildew genome shows the unique evolution of an obligate biotroph. *Nat. Genet.* 45, 1092–1096. doi: 10.1038/ng.2704

Wu, Y., and Zhou, J.-M. (2013). Receptor-like kinases in plant innate immunity. *J. Integr. Plant Biol.* 55, 1271–1286. doi: 10.1111/jipb.12123

Yahiaoui, N., Srichumpa, P., Dudler, R., and Keller, B. (2004). Genome analysis at different ploidy levels allows cloning of the powdery mildew resistance gene Pm3b from hexaploid wheat. *Plant J.* 37, 528–538. doi: 10.1046/j.1365-313X.2003.01977.x

Yeh, Y. H., Panzeri, D., Kadota, Y., Huang, Y. C., Huang, P. Y., Tao, C. N., et al. (2016). The *Arabidopsis* Malectin-Like/LRR-RLK IOS1 is critical for BAK1-dependent and BAK1-independent pattern-triggered immunity. *Plant Cell* 28, 1701–1721. doi: 10.1105/tpc.16.00313

Zellerhoff, N., Himmelbach, A., Dong, W. B., Bieri, S., Schaffrath, U., and Schweizer, P. (2010). Nonhost resistance of barley to different fungal pathogens is associated with largely distinct, quantitative transcriptional responses. *Plant Physiol.* 152, 2053–2066. doi: 10.1104/pp.109.151829

Zhang, W. J., Pedersen, C., Kwaaitaal, M., Gregersen, P. L., Morch, S. M., Hanisch, S., et al. (2012). Interaction of barley powdery mildew effector candidate CSEP0055 with the defence protein PR17c. *Mol. Plant Pathol.* 13, 1110–1119. doi: 10.1111/j.1364-3703.2012.00820.x

Zimmermann, G., Baumlein, H., Mock, H. P., Himmelbach, A., and Schweizer, P. (2006). The multigene family encoding germin-like proteins of barley. Regulation and function in basal host resistance. *Plant Physiol.* 142, 181–192.

Conflict of Interest Statement: The authors declare that the research was conducted in the absence of any commercial or financial relationships that could be construed as a potential conflict of interest.

frontiers in Plant Science

PERSPECTIVE
published: 01 March 2016
doi: 10.3389/fpls.2016.00241

Avirulence Genes in Cereal Powdery Mildews: The Gene-for-Gene Hypothesis 2.0

*Salim Bourras, Kaitlin E. McNally, Marion C. Müller, Thomas Wicker and Beat Keller**

Institute of Plant and Microbial Biology, University of Zurich, Zurich, Switzerland

The gene-for-gene hypothesis states that for each gene controlling resistance in the host, there is a corresponding, specific gene controlling avirulence in the pathogen. Allelic series of the cereal mildew resistance genes *Pm3* and *Mla* provide an excellent system for genetic and molecular analysis of resistance specificity. Despite this opportunity for molecular research, avirulence genes in mildews remain underexplored. Earlier work in barley powdery mildew (*B.g. hordei*) has shown that the reaction to some *Mla* resistance alleles is controlled by multiple genes. Similarly, several genes are involved in the specific interaction of wheat mildew (*B.g. tritici*) with the *Pm3* allelic series. We found that two mildew genes control avirulence on *Pm3f*: one gene is involved in recognition by the resistance protein as demonstrated by functional studies in wheat and the heterologous host *Nicotiana benthamiana*. A second gene is a suppressor, and resistance is only observed in mildew genotypes combining the inactive suppressor and the recognized *Avr*. We propose that such suppressor/avirulence gene combinations provide the basis of specificity in mildews. Depending on the particular gene combinations in a mildew race, different genes will be genetically identified as the "avirulence" gene. Additionally, the observation of two LINE retrotransposon-encoded avirulence genes in *B.g. hordei* further suggests that the control of avirulence in mildew is more complex than a canonical gene-for-gene interaction. To fully understand the mildew–cereal interactions, more knowledge on avirulence determinants is needed and we propose ways how this can be achieved based on recent advances in the field.

Keywords: wheat, powdery mildew, resistance gene, avirulence gene, barley

OPEN ACCESS

Edited by:
Pietro Daniele Spanu, Imperial College London, UK

Reviewed by:
Guus Bakkeren, Agriculture and Agri-Food Canada, Canada
Guido Van Den Ackerveken, Utrecht University, Netherlands

****Correspondence:***
Beat Keller
bkeller@botinst.uzh.ch

Specialty section:
This article was submitted to Plant Biotic Interactions, a section of the journal Frontiers in Plant Science

Received: *29 December 2015*
Accepted: *12 February 2016*
Published: *01 March 2016*

Citation:
Bourras S, McNally KE, Müller MC, Wicker T and Keller B (2016) Avirulence Genes in Cereal Powdery Mildews: The Gene-for-Gene Hypothesis 2.0. Front. Plant Sci. 7:241. doi: 10.3389/fpls.2016.00241

AVIRULENCE GENES IN FUNGAL PLANT PATHOGENS

The identification of avirulence (*Avr*) genes in plant pathogenic fungi has been accelerating in recent years due to rapid advances in 'omics' technologies. At present, at least 35 *Avrs* have been cloned from filamentous fungi infecting a wide variety of agronomically important crops. Examples of *Avrs* fitting the gene-for-gene model are found in *Cladosporium fulvum* and *Leptosphaeria maculans*, where single *Avrs* are recognized by their cognate resistance (*R*) genes (Wulff et al., 2009; Hayward et al., 2012). However, in *Magnaporthe oryzae* and *Melampsora lini*, there are cases of single *Avrs* recognized by multiple *R* genes, as it was found for *Avr-Pik/km/kp* (Yoshida et al., 2009), *AvrL567*, and *AvrP123* (Barrett et al., 2009; Ravensdale et al., 2012). Another level of complexity has been described in *Fusarium oxysporum* f. sp. *lycopersici*, which encodes *Avr1* that is recognized by the tomato *R* gene *I-1*, but also acts as a suppressor of the recognition of *Avr2* and *Avr3* by *I-2* and *I-3*, respectively (Houterman et al., 2008).

Thus far, most cloned avirulence genes encode a typical effector protein (63–314 amino acids) with a predicted signal peptide for secretion, with *Ace1* (4034 amino acids) from *Magnaporthe grisea* being one of three exceptions (the other two are *AvrMla* genes, see below). *Ace1* encodes a hybrid polyketide synthase non-ribosomal peptide synthetase involved in the biosynthesis of the actual avirulence factor (Boehnert et al., 2004). In contrast to AVR proteins from Oomycetes that contain few or no cysteines, fungal AVRs are often cysteine-rich, which confers stability in the leaf apoplast. Most AVRs cloned from fungal pathogens forming specialized infection structures (e.g., *Blumeria graminis, M. lini, M. grisea*) appear to contain fewer cysteines than AVRs from fungal pathogens that invade exclusively with hyphae (for a summary, see Rouxel and Balesdent, 2010). Thus, differences in cysteine content might reflect the mechanistic differences between these two infection strategies.

AVIRULENCE IN CEREAL MILDEWS: GENETIC ANALYSIS IN SEGREGATING POPULATIONS

The genetic basis of *Avr–R* interactions in cereal powdery mildews was investigated using classical genetic approaches in eleven crosses of *B.g. hordei* (see Skamnioti et al., 2008, for a summary), two of *B.g. tritici* (Bourras et al., 2015; Parlange et al., 2015) and at least in one cross of *B.g. secalis* and *B.g. tritici* hybrids (Tosa, 1994). In the resulting haploid F_1 progeny, each genetic locus from the parental genotypes is expected to segregate in a 1:1 ratio, so that only one of the two parental alleles is present per locus and per individual. Deviations of *Avr* segregation from the classical 1:1 single gene model were frequently observed, indicating the involvement in avirulence of at least two or three genes (see **Table 1** for a summary and **Figures 1B–D**). Thus, in addition to the single gene control of avirulence that is commonly observed in plant pathogenic fungi, there are more complex genetic situations in cereal powdery mildews. Furthermore, classical genetic studies have often reported the emergence of additional phenotypic classes in the segregating progeny, where a quantitative variation in virulence contrasting with the parental phenotypes was observed (**Table 1**; Brown and Jessop, 1995; Bourras et al., 2015; Parlange et al., 2015). For instance, in the cross between the avirulent *B.g. tritici* isolate 96224, and the virulent isolate JIW2, 33 progeny showed consistent intermediate phenotype on wheat lines containing the mildew resistance gene *Pm3c* (**Table 1**). Similar examples were reported in segregating progeny growing on the mildew resistance genes *Pm3b*, *Pm3d*, and *Mla7* (**Table 1**). Thus, in cereal powdery mildews there is a quantitative component in race-specific *Avr–R* interactions that is reminiscent of a polygenic, quantitative trait.

In addition to studies of inheritance, linkage between different *Avr* encoding loci was resolved for 15 *Avr–R* interactions in *B.g. hordei* and six in *B.g. tritici* (Skamnioti et al., 2008; Bourras et al., 2015). In both *formae speciales*, two genetically unlinked regions in the genome that commonly control several *Avr* specificities were reported (see **Table 1** for some examples). In

TABLE 1 | Non-canonical segregation of race-specific avirulence in the F_1 progeny of wheat and barley powdery mildew crosses.

			Progeny phenotypes[3]			Genetic segregation[4]					
Host	Resistance[1]	Mildew crosses[2]	A	I	V	Ratio	Nbr. Loci	χ^2	*p*-Value	Genet. Map.[5]	Source[6]
Wheat	Pm3b	96224 × 94202	108	17	33	5:1:2	3	2.319	0.313	2	Bourras et al., 2015
	Pm3c	96224 × JIW2	78	33	42	2:1:1	2	0.107	0.743	2	Parlange et al., 2015
	Pm3d	96224 × 94202	44	18	96	2:1:5	3	0.744	0.689	2	Bourras et al., 2015
	Pm3f	96224 × 94202	46	2	119	1:0:3	2	0.745	0.388	2	Bourras et al., 2015
Barley	Mla6	CC151 × DH14	30	–	10	3:0:1	2	0.000	1.000	1	Brown et al., 1996
	Mla7	CC107 × DH14	26	13	12	2:1:1	2	0.120	0.942	2	Brown and Jessop, 1995
	Mla13	CC52 × DH14	46	–	20	3:0:1	2	1.320	0.251	2	Caffier et al., 1996

(1) Powdery mildew resistance genes in wheat (Pm) and barley (Ml) on which non-canonical segregation of avirulence was reported. (2) Wheat and barley powdery mildew crosses used for genetic studies. Crosses are indicated as parent_1 × parent_2. All crosses were done with isolates from the same forma specialis. (3) Progeny phenotypes are indicated as "A" for avirulent, "V" for virulent, and "I" for intermediate virulence that is referred to as "intermediate leaf coverage" in wheat powdery mildew or "intermediate infection types" in barley powdery mildew (for details on phenotype scoring please refer to the literature cited in the last column). (4) Genetic segregation is given as the theoretical ratio of A:I:V as reported in the literature cited in the last column. The number of loci/genes involved is indicted. Deviation of phenotype numbers from the theoretical ratios was tested with the χ^2 test for goodness of fit. The degree of freedom was assigned as the "Number of phenotypic classes – 1." The probability value for the χ^2 test is indicated. $P < 0.05$ would indicate significant deviation from the theoretical ratios. (5) The number of loci genetically mapped among the ones inferred from the genetic ratios, as described in Skamnioti et al. (2008) and Bourras et al. (2015). (6) Literature from which phenotype segregation data was extracted.

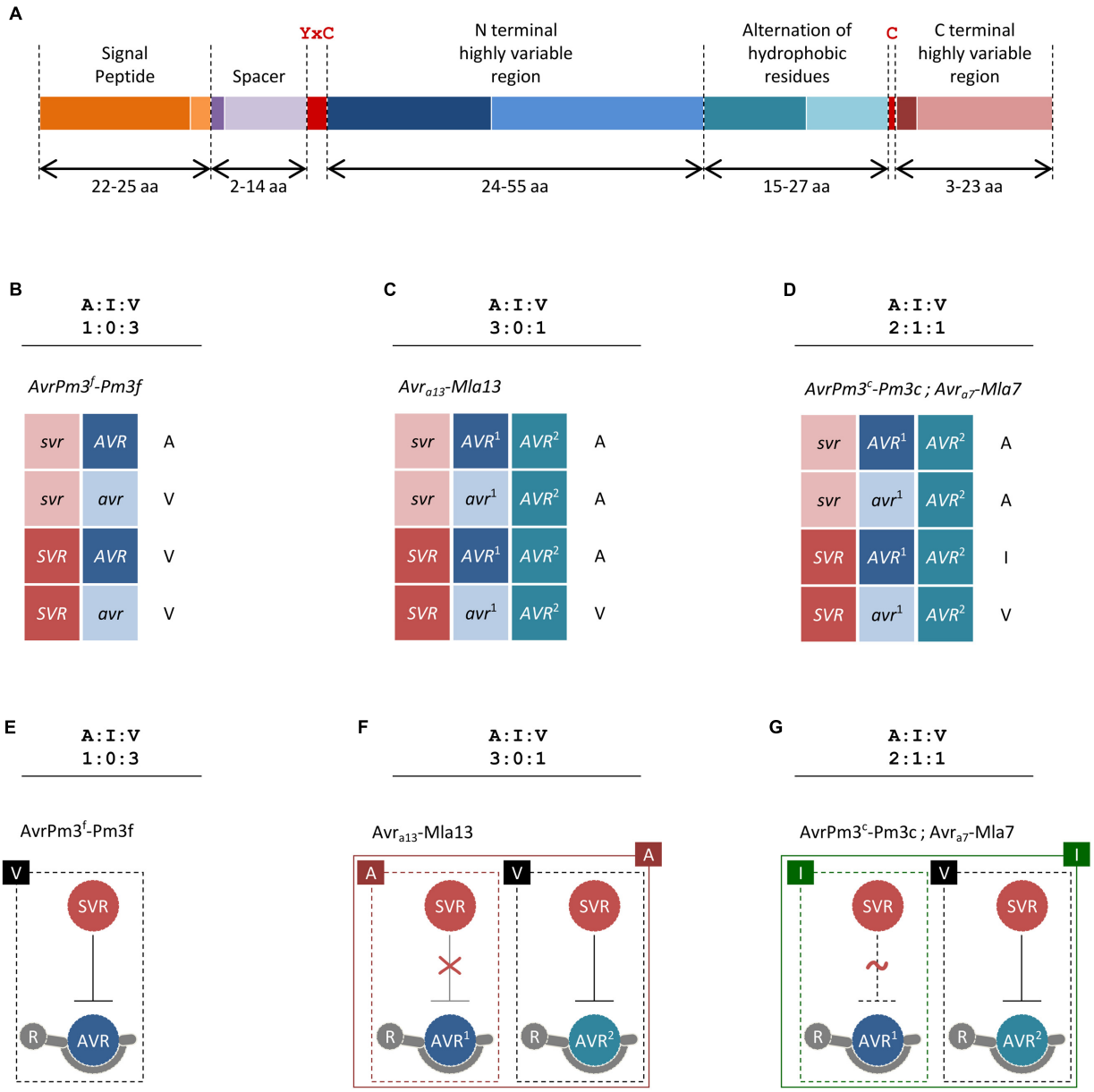

FIGURE 1 | Proposed models for *Avr–R–Svr* interactions in cereal powdery mildews. (A) Structure of the AvrPm3$^{a2/f2}$ effector family. Minimum and maximum sizes of each region as observed among family members are given in amino acids (aa) and differentiated with dark and light color shades, respectively. The YxC motif and the conserved cysteines are indicated in red. **(B–D)** Proposed *Avr-R-Svr* genetic models for the interpretation of genetic segregation ratios deviating from the canonical 1:1 single gene hypothesis. For readability, active and inactive alleles are distinguished with upper and lower case. Here, we have only considered examples of mildew *Avr–R* interactions where genetic segregation ratios and mapping data were consistent with at least two genetically independent loci being involved in avirulence. **(B)** Considering the *Avr-R-Svr* model and a genetic segregation ratio of 1:0:3, avirulence results from a combination of an inactive suppressor allele (*svr*) and an active avirulence allele (*AVR*). In the presence of the active *SVR* and the active *AVR*, the interaction result in virulence. A molecular model for this suppression scenario is depicted in **(E)**. **(C)** Considering the *Avr-R-Svr* model, a genetic segregation ratio of 3:0:1 can be explained by a model involving one suppressor locus and two loci for avirulence (*AVR*^{1} and *AVR*^{2}). Importantly, the second locus for avirulence (*AVR*^{2}) is not polymorphic in this cross, thus only the active allele (*AVR*^{2}) is present. In this model, the active *SVR* is only effective in suppressing *AVR*^{2} but not *AVR*^{1}. A molecular model for this suppression scenario is depicted in **(F)**. **(D)** Considering the *Avr-R-Svr* model, a genetic segregation ratio of 2:1:1 can be explained by a model involving one suppressor locus and two loci for avirulence (*AVR*^{1} and *AVR*^{2}). Importantly, the second locus for avirulence (*AVR*^{2}) is not polymorphic in this cross, thus only the active allele (*AVR*^{2}) is present. In this model, the active *SVR* can fully suppress *AVR*^{2} but is only partially effective on *AVR*^{1}, thus resulting in avirulence in the first case and intermediate virulence in the second. A molecular model for this suppression scenario is depicted in **(G)**. **(E–G)** Proposed suppression scenarios based on the genetic models described in **(B–D)** and resulting in three major phenotypic classes of avirulence 'A,' virulence 'V,' and intermediate virulence 'I.' Only active suppressor and avirulence proteins are shown. For simplicity, AVR–R interactions are represented as physical binding. Absence of suppression is depicted as a red "X" sign. Partial suppression is depicted as a dotted line and a red "∼" sign. The phenotype resulting from single and combined interactions is indicated.

B.g. hordei there is the AVR_{a10} locus controlling the AVR_{a10}, AVR_{k1}, AVR_{a22}, AVR_{a9}, $AVR_{a13\text{-}1}$, AVR_g and possibly AVR_{a6} and AVR_{a7-2} specificities. There is also the AVR_{a12} locus comprised of AVR_{a6}, AVR_{a12}, AVR_{P17}, and AVR_{La}. Similarly in *B.g. tritici* there is *locus_1* controlling the $AvrPm3^a$, $AvrPm3^{b1}$, $AvrPm3^{c1}$, $AvrPm3^{d1}$, $AvrPm3^{f1}$, and $AvrPm3^e$ specificities, and *locus_3* for $AvrPm3^{b2}$, $AvrPm3^{c2}$, and $AvrPm3^{d2}$. However, while in *B.g. hordei* the AVR_{a10} and the AVR_{a12} loci were described as clusters of linked but recombining *Avr* genes (Skamnioti et al., 2008), *locus_1* in *B.g. tritici* was characterized as encoding for a single *Avr* factor commonly involved in the interaction with six alleles of the *Pm3* resistance genes (Bourras et al., 2015; Parlange et al., 2015). Considering the $AvrPm3^{a/f}$-*Pm3a/f* interaction involving *locus_1* and *locus_2* in *B.g. tritici*, it was found that specificity is only encoded by *locus_2*, while *locus_1* encodes a factor acting unspecifically on several *AvrPm3–Pm3* interactions. Assuming this genetic model stands true for *B.g. hordei*, it is possible that the AVR_{a10} and AVR_{a12} loci encode for general factors that are reminiscent of the *B.g. tritici locus_1*, while the actual avirulence proteins are encoded within specific loci outside of these clusters.

GENES ENCODING CSEPs IN CEREAL MILDEWS: THE PRIMARY CANDIDATES FOR AVIRULENCE GENES

Genes encoding so-called candidate secreted effector proteins (CSEPs; Spanu et al., 2010) have been suggested as major determinants of the mildew–host interaction and as good candidates for avirulence proteins. Refined analyses of the CSEP complement in the *Blumeria* genomes indicated there are close to 500 of such genes in *B.g. hordei* (Pedersen et al., 2012) and over 600 in *B.g. tritici* (Fabrizio Menardo, personal communication), hence much more than initially predicted (Spanu et al., 2010; Wicker et al., 2013). Pedersen et al. (2012) showed that many CSEPs are highly expressed in haustoria, and thus expected to be released from the haustorial membrane into the extrahaustorial matrix. How effector proteins subsequently enter the plant cell is still unclear, although data from site directed mutagenesis suggest that specific conserved protein motifs such as the HRxxH motif in the CSEP BEC1019 may mediate translocation of the effector through the plant membrane (Whigham et al., 2015).

Beyond the common features described above, CSEPs have very limited sequence similarity and only a few common protein motifs are found (e.g., the YxC motif, **Figure 1A**), suggesting they may target different proteins in the host and fulfill different functions (Pedersen et al., 2012; Wicker et al., 2013). One group of predicted CSEP proteins share structural similarities to ribonucleases (Pedersen et al., 2012), which is why they are suspected to mimic and compete with plant proteins involved in pathogen defense. Furthermore, several CSEPs have homology to enzymes that could be involved in processes of plant–pathogen interaction such as cell-wall remodeling or protein degradation (Pliego et al., 2013). Indeed, a *B.g. hordei* CSEP of the latter type (BEC1019) was recently shown to suppress plant cell death (Whigham et al., 2015). In summary, our understanding of the actual 'effects' of CSEPs is very limited, but we can expect that data from comparative analyses and functional assays will soon shed more light on this large class of fungal proteins.

THE IDENTIFICATION OF Avr_{a10} AND Avr_{k1}: A NOVEL CLASS OF AVIRULENCE GENES ENCODED BY LINE RETROTRANSPOSONS

The two avirulence genes Avr_{a10} and Avr_{k1} were isolated by map-based cloning from *B.g. hordei* by Ridout et al. (2006). Both encode unusual avirulence proteins as they lack signal peptides. Avr_{k1} was functionally validated by bombardment assays that demonstrated induction of cell death in a *Mlk*-resistance gene dependent manner, as well as enhanced infection on susceptible varieties after transient expression. It was found that recognition of AVR_{a10} by MLA10 induced nuclear associations between the immune receptor and WRKY transcription factors (Shen et al., 2007). Furthermore, Nowara et al. (2010) described that silencing of Avr_{a10} resulted in reduced fungal development in the absence but not in the presence of the cognate resistance gene *Mla10*.

In *B.g. hordei* Avr_{a10} and Avr_{k1} were found to map only 0.7 cM from Avr_{a22} (Skamnioti et al., 2008), and the evolutionary origin of these *Avr* genes has been subject of intense debate. Recent genome-wide analysis and comparisons with LINE elements from animals and plants made clear that Avr_{a10} and Avr_{k1} are derived from non-LTR retrotransposons (also known as Long Interspersed Nuclear Elements or LINEs). These retro-elements usually consist of two open reading frames (ORFs), where ORF2 encodes a reverse transcriptase and RNaseH (RT/RH), while ORF1 is thought to encode a protein that mediates the transfer of retrovirus-like particles into the nucleus, at least in the human L1 element. Avr_{a10} and Avr_{k1} are both derivatives of ORF1, but their homology at the DNA and protein level is very limited, thus indicating that both genes arose independently from distantly related LINE families (Amselem et al., 2015). Since LINEs are among the most abundant types of transposable elements in the *Blumeria* genomes (Parlange et al., 2011), it is not surprising that more than a thousand Avr_{a10} and Avr_{k1} homologs were originally interpreted as a very large gene family that happened to co-evolve with the RT/RH domain of LINEs (Sacristán et al., 2009). The evolutionary origin of Avr_{a10} and Avr_{k1} from LINEs has the intriguing implication that the large amount of repetitive DNA found in powdery mildew genomes serves as raw material from which new proteins and regulatory regions can emerge (Amselem et al., 2015).

THE IDENTIFICATION OF $SvrPm3^{A1/F1}$ AND $AvrPm3^{A2/F2}$ IN *B.g. tritici*: TWO CSEPS INVOLVED IN *Pm3*-MEDIATED AVIRULENCE

The identification of the first *Avr* gene in wheat powdery mildews was enabled by a combination of new genomic tools,

next generation sequencing and high-throughput genotyping technologies (Bourras et al., 2015). Analysis of the two loci controlling the $AvrPm3^{a/f}$–$Pm3^{a/f}$ interaction resulted in the cloning of $AvrPm3^{a2/f2}$, a typical CSEP encoded within *locus_2* (**Figure 1A**). The avirulent allele is specifically recognized by *Pm3a* and *Pm3f*, whereas the virulent allele differing by two amino acid polymorphisms escapes recognition. Similarly, $SvrPm3^{a1/f1}$, also a typical CSEP gene encoded within the general *locus_1* was cloned (Parlange et al., 2015). Most likely, this gene acts as a suppressor (*Svr)* of the *AvrPm3–Pm3* mediated avirulence (Bourras et al., 2015). Thus, in the *AvrPm3–Pm3* interaction model, a second layer of regulation is provided by a suppression mechanism. Here, in the presence of an active SVR suppressor, primary recognition of the avirulence effector by the cognate resistance protein is not sufficient to induce a resistance response. In this model, it is possible for the pathogen to maintain an unaltered and active AVR effector while still escaping *R* gene recognition which represents an evolutionary advantage on the long term.

It was shown that both *Avr* and *Svr* genes have the same kinetics of expression with a peak at 2 days after mildew inoculation (Bourras et al., 2015). This time point coincides with the formation of the haustorium, a fungal feeding structure involved in effector delivery, and a milestone for successful infection. It was also shown that *Avr* and *Svr* regulation is inherited in a parent-of-origin-specific manner in progeny from a cross between the *Pm3a/f* avirulent isolate 96224 and the *Pm3a/f* virulent isolate 94202 (Bourras et al., 2015). Considering these parental isolates and the critical time point of 2 days, it was found that the *Avr* gene is upregulated in the avirulent parent while the *Svr* suppressor is downregulated, and the exact opposite situation was found in the virulent parent. This situation can be explained by mechanisms such as epiallelic variation, mutations in *cis*-elements, alteration of trans-acting factors, or epigenetic modulation, all of which can affect effector protein accumulation without altering protein sequence (Bakkeren and Valent, 2014; Gijzen et al., 2014). Thus, in addition to sequence polymorphism distinguishing *Avr* and *avr* alleles, and the presence of an active (*Svr*) or inactive (*svr*) suppressor, there is a third layer of regulation of the *AvrPm3–Pm3* interaction at the gene expression level.

Based on these results, an extension of Flor's gene-for-gene model that accounts for a suppressor locus was proposed as the *Avr-R-Svr* genetic model (**Figures 1B–D**). Here, resistance is mediated by an interaction involving an allele-specific avirulence effector (*Avr)*, a resistance gene allele (*R*), and an allele-unspecific pathogen-encoded suppressor of avirulence (*Svr*). At the molecular level, recognition and suppression of recognition are determined by sequence polymorphism as well as gene expression levels differentiating *Avr vs. avr* and *Svr vs. svr* alleles. Thus, resistance can only occur if the suppressor is inactive and the AVR protein is produced in sufficient amounts for *R* gene activation.

HOW IS RESISTANCE SPECIFICITY TO ALLELIC SERIES OF RESISTANCE GENES CONTROLLED BY POWDERY MILDEW?

The recent studies on the *Pm3a* and *Pm3f* resistance genes (Stirnweis et al., 2014) on the host side, as well as the identification of $AvrPm3^{a2/f2}$ on the pathogen side (Bourras et al., 2015) have given a first insight into the control of molecular specificity. Considering these two *Pm3* alleles, *Pm3a* is a stronger form of *Pm3f* as *Pm3a* recognizes all isolates which are recognized by *Pm3f*, plus some additional ones (Brunner et al., 2010). It was found that activation efficiency through the ARC2 domain controls the difference in the recognition spectrum of these two alleles, and there is no difference in recognition specificity (Stirnweis et al., 2014). Furthermore, there is strong evidence that specificity in the allelic interactions is based on the recognition of different *AvrPm3* or *AvrMla* genes. $AvrPm3^{a2/f2}$ is not recognized by any of the other *Pm3* alleles and genetic mapping (Bourras et al., 2015) and mutant analysis (Parlange et al., 2015) have revealed at least three additional genetic loci controlling recognition specificity toward *Pm3* alleles in *B.g. tritici*. In *B.g. hordei* also, the complex genetic ratios of avirulence inheritance indicate the involvement of many genes (**Table 1**). Thus, the corresponding avirulence genes seem to be quite different from each other, a surprising finding given that some allelic PM3 protein variants differ only by two amino acids in the LRR domain. Finally, resistance specificity also involves the pathogen encoded $SvrPm3^{a1/f1}$ suppressor of the *Pm3* resistance (**Figures 1B–G**) (Bourras et al., 2015). In *B.g. hordei*, the molecular basis of recognition specificity of the Avr_{a10} and Avr_{k1} alleles is not yet understood. As discussed below, there are several ways to further explore the function of these genes. In addition, it will be essential to characterize at the protein level the determinants of recognition, and also to isolate more *AvrMla* genes for the many members of the *Mla* allelic series (Seeholzer et al., 2010) to get further insight into this interaction.

Clearly, genetic studies in mildew are greatly simplified by haploid inheritance, but haploid genetics has the disadvantage that dominant and recessive traits cannot easily be distinguished. Thus, based on genetics only it is not possible to predict whether an "avirulence gene" actually encodes for an AVR that is recognized by the cognate resistance protein, or an inactive suppressor that is ineffective in inhibiting AVR-R recognition and/or resistance signaling. In addition to this first layer of complexity, gene expression possibly plays an important regulatory role in the determination of specificity (Bourras et al., 2015). Therefore, differences in gene expression levels between different *B.g. tritici* or *B.g. hordei* isolates might actually give important hints on functional avirulence and suppressor genes. In this context, we propose that comparative RNAseq studies in many isolates might be useful to detect such diagnostic expression differences.

NEXT STEPS IN THE CHARACTERIZATION OF CEREAL POWDERY MILDEW AVIRULENCE

Despite the progress in the characterization of mildew avirulence genetics and genomics described above, there are large remaining gaps in our knowledge. Considering the identified components of avirulence in mildew, the specific interactions leading to $AvrPm3^{a2/f2}$ recognition/suppression need to be studied at the molecular and biochemical level. In addition, the role of the LINE encoded *B.g. hordei* avirulence genes Avr_{a10} and Avr_{k1} needs to be clarified. It is also possible that these two genes are not recognized by the resistance genes (in a situation similar to $SvrPm3^{a1/f1}$ in the case of *B.g. tritici*) but rather play a different, molecularly unknown role as activators or suppressors of avirulence. In this context, it will be important to isolate more *AvrPm3* and *AvrMla* genes to understand the molecular basis of specificity in cereal mildews.

So far, all known *Avr* loci in *Blumeria* were isolated by map-based cloning approaches which are solid but very time-consuming. The *B.g. tritici* and *B.g. hordei* reference genomes should be improved by new sequencing technologies such as PacBio (Eid et al., 2009) which would greatly support map-based cloning and pave the way for genome-wide association studies (GWAS), an attractive alternative for *Avr* identification. The decreased costs of next-generation sequencing allow us to sequence a large number of isolates which is the basis for GWAS. However, it remains to be seen if GWAS approaches will be capable of identifying mildew *Avrs*, where avirulence seems to result from complex genetic networks and epistatic interactions.

A largely unexplored area of research is the identification of specific mutants in avirulence genes. Such mutants should theoretically be easy to identify by mutagenizing avirulent races and selecting for growth on a barley or wheat genotype containing the cognate resistance gene. Two such mutants at new and still uncharacterized genetic loci have been identified for loss-of-recognition by *Pm3a* and *Pm3f*, with no impact on the other *Pm3* alleles (Parlange et al., 2015). Based on whole genome sequencing of pools from segregants of mapping populations, and considering the haploid nature of the mildew genome, it should be straightforward to identify the causative mutations and we suggest that larger screens for many different *Avr* mutants should be performed. Given that there are relatively few gene families in mildew (with the exception of rapidly diverging CSEP families, Wicker et al., 2013) genetic redundancy should be a minor problem for mutant identification. $AvrPm3^{a2/f2}$ belongs to a family of 36 members identified *in silico*. Twenty-three of these members, including the most homologous paralogs by protein sequence, PU_24 (61%) and PU_23 (59%), were functionally tested, but none of them was recognized by *Pm3a/f* (Bourras et al., 2015; our unpublished data).

Finally, there is a need for additional systems to study gene function. Particle bombardment has been a successful system to study *Avr* gene function, either directly or by host-induced gene silencing (Ridout et al., 2006; Nowara et al., 2010; Bourras et al., 2015), but it is time-consuming and needs practice and optimization in individual labs. In the case of the $AvrPm3^{a2/f2}$ avirulence gene, transient expression studies after infiltration of the heterologous species *N. benthamiana* have been successful (Bourras et al., 2015). However, it remains to be seen how broadly this system is suitable for mildew avirulence research. Therefore, alternative delivery approaches for functional studies, e.g., by bacterial vectors (Upadhyaya et al., 2014) should be developed for mildew. In addition, further work should be invested into the development of a highly reproducible mildew transformation system. This would then allow us to fully exploit the current rapid development in mildew avirulence biology and fully understand the interaction of this fascinating obligate biotroph and the co-evolution with its host.

In a more applied perspective, knowledge on the molecular interactions between *R* and *Avr* genes could be highly productive to develop pathogen-informed strategies for resistance improvement in the host. On the pathogen side, information on the allelic diversity of *Avrs* and *Svrs* in mildew populations can guide the spatio-temporal deployment of *R* genes in the field. On the molecular level, the identification of novel sources of resistance should be facilitated by the characterization of the genes and gene networks involved in resistance activation by AVR proteins *vs.* resistance suppression by the pathogen encoded suppressor. In particular, synthetic modification of wheat proteins co-opted by mildew suppressors might provide a strategy to achieve durable resistance.

AUTHOR CONTRIBUTIONS

All authors reviewed literature and contributed to writing the manuscript. SB and BK coordinated the manuscript.

FUNDING

This work was supported by a grant from the Swiss National Science Foundation: 310030_163260.

ACKNOWLEDGMENT

We acknowledge the technical support of Gerhard Herren, Helen Zbinden, Gabriele Buchmann, Linda Lüthi, and Simon Flückiger.

REFERENCES

Amselem, J., Vigouroux, M., Oberhaensli, S., Brown, J. K., Bindschedler, L. V., Skamnioti, P., et al. (2015). Evolution of the EKA family of powdery mildew avirulence-effector genes from the ORF 1 of a LINE retrotransposon. *BMC Genomics* 16:917. doi: 10.1186/s12864-015-2185-x

Bakkeren, G., and Valent, B. (2014). Do pathogen effectors play peek-a-boo? *Front. Plant Sci.* 5:731. doi: 10.3389/fpls.2014.00731

Barrett, L. G., Thrall, P. H., Dodds, P. N., van der Merwe, M., Linde, C. C., Lawrence, G. J., et al. (2009). Diversity and evolution of effector loci in natural populations of the plant pathogen *Melampsora lini*. *Mol. Biol. Evol.* 26, 2499–2513. doi: 10.1093/molbev/msp166

Boehnert, H. U., Fudal, I., and Dioh, W., Tharreau, D., Notteghem, J.-L., and Lebrun, M.-H. (2004). A putative polyketide synthase peptide synthetase from *Magnaporthe grisea* signals pathogen attack to resistant rice. *Plant Cell* 16, 2499–2513. doi: 10.1105/tpc.104.022715

Bourras, S., McNally, K. E., Ben-David, R., Parlange, F., Roffler, S., Praz, C. R., et al. (2015). Multiple avirulence loci and allele-specific effector recognition control the pm3 race-specific resistance of wheat to powdery mildew. *Plant Cell* 27, 2991–3012.

Brown, J. K. M., and Jessop, A. C. (1995). Genetics of avirulences in *Erysiphe graminis* f. sp. *hordei*. *Plant Pathol.* 44, 1039–1049. doi: 10.1111/j.1365-3059.1995.tb02663.x

Brown, J. K. M., Le Boulaire, S., and Evans, N. (1996). Genetics of responses to morpholine-type fungicides and of avirulences in *Erysiphe graminis* f. sp. *hordei*. *Eur. J. Plant Pathol.* 102, 479–490. doi: 10.1007/BF01877142

Brunner, S., Hurni, S., Streckeisen, P., Mayr, G., Albrecht, M., Yahiaoui, N., et al. (2010). Intragenic allele pyramiding combines different specificities of wheat Pm3 resistance alleles. *Plant J.* 64, 433–445. doi: 10.1111/j.1365-313X.2010.04342.x

Caffier, V., de Vallavieille-Pope, C., and Brown, J. K. M. (1996). Segregation of avirulences and genetic basis of infection types in *Erysiphe graminis* f. sp. hordei. *Phytopathology* 86, 1112–1121. doi: 10.1094/Phyto-86-1112

Eid, J., Fehr, A., Gray, J., Luong, K., Lyle, J., Otto, G., et al. (2009). Real-time DNA sequencing from single polymerase molecules. *Science* 323, 133–138. doi: 10.1126/science.1162986

Gijzen, M., Ishmael, C., and Shrestha, S. D. (2014). Epigenetic control of effectors in plant pathogens. *Front. Plant Sci.* 5, 1–4. doi: 10.3389/fpls.2014.00638

Hayward, A., McLanders, J., Campbell, E., Edwards, D., and Batley, J. (2012). Genomic advances will herald new insights into the Brassica: *Leptosphaeria maculans* pathosystem. *Plant Biol.* 14, 1–10. doi: 10.1111/j.1438-8677.2011.00481.x

Houterman, P. M., Cornelissen, B. J. C., and Rep, M. (2008). Suppression of plant resistance gene-based immunity by a fungal effector. *PLoS Pathog.* 4:e1000061. doi: 10.1371/journal.ppat.1000061

Nowara, D., Gay, A., Lacomme, C., Shaw, J., Ridout, C., Douchkov, D., et al. (2010). HIGS: host-induced gene silencing in the obligate biotrophic fungal pathogen *Blumeria graminis*. *Plant Cell* 22, 3130–3141. doi: 10.1105/tpc.110.077040

Parlange, F., Oberhaensli, S., Breen, J., Platzer, M., Taudien, S., Simková, H., et al. (2011). A major invasion of transposable elements accounts for the large size of the *Blumeria graminis* f.sp. tritici genome. *Funct. Integr. Genomics.* 11, 671–677. doi: 10.1007/s10142-011-0240-5

Parlange, F., Roffler, S., Menardo, F., Ben-David, R., Bourras, S., McNally, K. E., et al. (2015). Genetic and molecular characterization of a locus involved in avirulence of *Blumeria graminis* f. sp. tritici on wheat Pm3 resistance alleles. *Fungal Genet. Biol.* 82, 181–192. doi: 10.1016/j.fgb.2015.06.009

Pedersen, C., Ver Loren van Themaat, E., McGuffin, L. J., Abbott, J. C., Burgis, T. A., Barton, G., et al. (2012). Structure and evolution of barley powdery mildew effector candidates. *BMC Genomics* 13:694. doi: 10.1371/journal.ppat.1000061

Pliego, C., Nowara, D., Bonciani, G., Gheorghe, D. M., Xu, R., Surana, P., et al. (2013). Host-induced gene silencing in barley powdery mildew reveals a class of ribonuclease-like effectors. *Mol. Plant Microbe Interact.* 26, 633–642. doi: 10.1094/MPMI-01-13-0005-R

Ravensdale, M., Bernoux, M., Ve, T., Kobe, B., Thrall, P. H., Ellis, J. G., et al. (2012). Intramolecular interaction influences binding of the flax L5 and L6 resistance proteins to their AvrL567 ligands. *PLoS Pathog.* 8:e1003004. doi: 10.1371/journal.ppat.1003004

Ridout, C. J, Skamnioti, P., Porritt, O., Sacristan, S., Jones, J. D. G., and Brown, J. M. K. (2006). Multiple avirulence paralogous in cereal powdery mildew fungi may contribute to parasite fitness and defeat of plant resistance. *Plant Cell* 18, 2402–2414. doi: 10.1105/tpc.106.043307

Rouxel, T., and Balesdent, M.-H. (2010). "Avirulence Genes," in *Encyclopedia of Life Sciences (ELS),* (Chichester: John Wiley & Sons, Ltd). doi: 10.1002/9780470015902.a0021267

Sacristán, S., Vigouroux, M., Pedersen, C., Skamnioti, P., Thordal-Christensen, H., Micali, C., et al. (2009). Coevolution between a family of parasite virulence effectors and a class of LINE-1 retrotransposons. *PLoS ONE* 4:e7463. doi: 10.1371/journal.pone.0007463

Seeholzer, S., Tsuchimatsu, T., Jordan, T., Bieri, S., Pajonk, S., Yang, W., et al. (2010). Diversity at the Mla powdery mildew resistance locus from cultivated barley reveals sites of positive selection. *Mol. Plant. Microbe. Interact.* 23, 497–509. doi: 10.1094/MPMI-23-4-0497

Shen, Q.-H., Saijo, Y., Mauch, S., Biskup, C., Bieri, S., Keller, B., et al. (2007). Nuclear activity of MLA immune receptors links isolate-specific and basal disease-resistance responses. *Science* 315, 1098–1103. doi: 10.1126/science.1136372

Skamnioti, P., Pedersen, C., Al-Chaarani, G. R., Holefors, A., Thordal-Christensen, H., Brown, J. K., et al. (2008). Genetics of avirulence genes in *Blumeria graminis* f.sp. hordei and physical mapping of AVR(a22) and AVR(a12). *Fungal Genet. Biol.* 45, 243–252. doi: 10.1016/j.fgb.2007.09.011

Spanu, P. D., Abbott, J. C., Amselem, J., Burgis, T. A., Soanes, D. M., Stüber, K., et al. (2010). Genome expansion and gene loss in powdery mildew fungi reveal tradeoffs in extreme parasitism. *Science* 330, 1543–1546. doi: 10.1126/science.1194573

Stirnweis, D., Milani, S. D., Jordan, T., Keller, B., and Brunner, S. (2014). Substitutions of two amino acids in the nucleotide-binding site domain of a resistance protein enhance the hypersensitive response and enlarge the PM3F resistance spectrum in wheat. *Mol. Plant. Microbe. Interact.* 27, 265–276. doi: 10.1094/MPMI-10-13-0297-FI

Tosa, Y. (1994). Gene-for-gene interactions between the rye mildew fungus and wheat cultivars. *Genome.* 37, 758–762. doi: 10.1139/g94-108

Upadhyaya, N. M., Mago, R., Staskawicz, B. J., Ayliffe, M. A., Ellis, J. G., and Dodds, P. N. (2014). A bacterial type III secretion assay for delivery of fungal effector proteins into wheat. *Mol. Plant Microbe Interact.* 27, 255–264. doi: 10.1094/MPMI-07-13-0187-FI

Whigham, E., Qi, S., Mistry, D., Surana, P., Xu, R., Fuerst, G., et al. (2015). Broadly conserved fungal effector bec1019 suppresses host cell death and enhances pathogen virulence in powdery mildew of barley (*Hordeum vulgare* L.). *Mol. Plant Microbe Interact.* 28, 968–983. doi: 10.1094/MPMI-02-15-0027-FI

Wicker, T., Oberhaensli, S., Parlange, F., Buchmann, J. P., Shatalina, M., Roffler, S., et al. (2013). The wheat powdery mildew genome shows the unique evolution of an obligate biotroph. *Nat. Genet.* 45, 1092–1096. doi: 10.1038/ng.2704

Wulff, B. B. H., Chakrabarti, A., and Jones, D. A. (2009). Recognitional specificity and evolution in the tomato-*Cladosporium fulvum* pathosystem. *Mol. Plant. Microbe. Interact.* 22, 1191–1202. doi: 10.1094/MPMI-22-10-1191

Yoshida, K., Saitoh, H., Fujisawa, S., Kanzaki, H., Matsumura, H., Yoshida, K., et al. (2009). Association genetics reveals three novel avirulence genes from the rice blast fungal pathogen *Magnaporthe oryzae*. *Plant Cell* 21, 1573–1591. doi: 10.1105/tpc.109.066324

Conflict of Interest Statement: The authors declare that the research was conducted in the absence of any commercial or financial relationships that could be construed as a potential conflict of interest.

frontiers in Plant Science

ORIGINAL RESEARCH
published: 11 March 2015
doi: 10.3389/fpls.2015.00132

Biological control of the cucurbit powdery mildew pathogen *Podosphaera xanthii* by means of the epiphytic fungus *Pseudozyma aphidis* and parasitism as a mode of action

*Aviva Gafni[1], Claudia E. Calderon[1], Raviv Harris[1], Kobi Buxdorf[1], Avis Dafa-Berger[1], Einat Zeilinger-Reichert[2] and Maggie Levy[1]**

[1] Plant Pathology and Microbiology, Hebrew University of Jerusalem, Jerusalem, Israel, [2] The Interdepartmental Equipment Facility, The Robert H. Smith Faculty of Agriculture, Food and Environment, Hebrew University of Jerusalem, Jerusalem, Israel

OPEN ACCESS

Edited by:
Ralph Panstruga, RWTH Aachen University, Germany

Reviewed by:
Richard Belanger, Université Laval, Canada
Alejandro Perez-Garcia, University of Malaga, Spain

***Correspondence:**
Maggie Levy, Department of Plant Pathology and Microbiology, The Robert H. Smith Faculty of Agriculture, Food and Environment, The Hebrew University of Jerusalem, Lautreman Building, Herzel St. No. 1, PO Box 12, Rehovot 76100, Israel
maggie.levy@mail.huji.ac.il

Specialty section:
This article was submitted to Plant-Microbe Interaction, a section of the journal Frontiers in Plant Science

Received: 13 November 2014
Accepted: 18 February 2015
Published: 11 March 2015

Citation:
Gafni A, Calderon CE, Harris R, Buxdorf K, Dafa-Berger A, Zeilinger-Reichert E and Levy M (2015) Biological control of the cucurbit powdery mildew pathogen Podosphaera xanthii by means of the epiphytic fungus Pseudozyma aphidis and parasitism as a mode of action. Front. Plant Sci. 6:132. doi: 10.3389/fpls.2015.00132

Epiphytic yeasts, which colonize plant surfaces, may possess activity that can be harnessed to help plants defend themselves against various pathogens. Due to their unique characteristics, epiphytic yeasts belonging to the genus *Pseudozyma* hold great potential for use as biocontrol agents. We identified a unique, biologically active isolate of the epiphytic yeast *Pseudozyma aphidis* that is capable of inhibiting *Botrytis cinerea* via a dual mode of action, namely induced resistance and antibiosis. Here, we show that strain L12 of *P. aphidis* can reduce the severity of powdery mildew caused by *Podosphaera xanthii* on cucumber plants with an efficacy of 75%. Confocal and scanning electron microscopy analyses demonstrated *P. aphidis* proliferation on infected tissue and its production of long hyphae that parasitize the powdery mildew hyphae and spores as an ectoparasite. We also show that crude extract of *P. aphidis* metabolites can inhibit *P. xanthii* spore germination *in planta*. Our results suggest that in addition to its antibiosis as mode of action, *P. aphidis* may also act as an ectoparasite on *P. xanthii*. These results indicate that *P. aphidis* strain L12 has the potential to control powdery mildew.

Keywords: dimorphism, biocontrol, powdery mildew, phytopathogens, parasitism

Introduction

Plant pathogens challenge our efforts to maximize crop production. Fungi, bacteria and other pathogens attack various parts of crop plants, inducing diseases that reduce the plant's growth rate, suppress plant development and reduce yield. Agronomists use chemical-based pesticides to control the spread of pathogens and pests and help ensure stable and prosperous agricultural systems. Nevertheless, constant selective pressures from multiple applications has led to the development of pathogens and pests that are resistant to chemical pesticides and consequently efforts are being made to develop novel techniques and tools to control these pests and pathogens (Denholm and Rowland, 1992; Leroux et al., 2002). Among these tools, fungal biocontrol agents have attracted much attention as a viable and important alternative to conventional pesticides. Biological control

may involve one or a combination of mechanisms, such as antibiosis, mycoparasitism, competition and the induction of generalized resistance in the host plant (Elad and Freeman, 2002; Shoresh et al., 2010). These mechanisms can hinder pathogen growth and development, thereby reducing disease. The complex modes of action of biocontrol agents, unlike those of chemical agents, reduce the likelihood of pathogens developing resistance to these agents, which increases the appeal of biocontrol agents as an alternative to conventional chemical products in the battle against pests and pathogens.

Epiphytic yeasts that colonize different plant surfaces (Pusey et al., 2009; Fernandez et al., 2012) are thought to possess biocontrol activity and to provide a natural barrier against certain plant pathogens (Avis et al., 2001; Urquhart and Punja, 2002; Bleve et al., 2006; Jacobsen, 2006; Robiglio et al., 2011). Epiphytes usually produce extracellular polysaccharides, which are thought to help them survive on aerial plant surfaces that are exposed to the elements. Phylloplane yeasts can also metabolize a wide variety of nutrient sources and tolerate a variety of chemical-based fungicides (Barnett et al., 2000; Buck and Burpee, 2002), characteristics which could potentially contribute to their utility as biocontrol agents.

The genus *Pseudozyma* is a small group of yeast-like fungi classified among the *Ustilaginales* (Boekhout, 1995). They are mostly epiphytic or saprophytic and they are non-pathogenic to plants, animals and insects (Avis and Belanger, 2002). *Pseudozyma rugulosa* and *Pseudozyma flocculosa* have both been reported to exhibit biological activity against the different powdery mildews with which they are associated (Dik et al., 1998; Hammami et al., 2010, 2011) (for review see Kiss, 2003). *P. flocculosa*, for example, does not penetrate powdery mildew cells, but has been found to secrete an unusual fatty acid that has an antibiotic effect against powdery mildew and other pathogens (Hajlaoui et al., 1994; Benyagoub et al., 1996; Avis and Belanger, 2001; Avis et al., 2001). Recently the genome and transcriptome of the biocontrol agent *P. flocculosa* was published and compared to the related plant pathogen *Ustilago maydis* and other Ustilaginales pathogens (Lefebvre et al., 2013). Genome comparison demonstrated high similarity of genomes, including the mating-type loci, meiosis loci and pathogenicity components, suggesting *P. flocculosa* used to be a virulent smut pathogen. Furthermore, it was shown that *P. flocculosa* has lost a subset of secreted effectors reported to influence virulence while acquiring other genes coding for secreted proteins, not found in the pathogenic fungi, that probably contribute to its biocontrol nature (Lefebvre et al., 2013). In agreement with these findings, the genome and transcriptome of *P. antarctica*, that did not demonstrate biocontrol ability against powdery mildew (Avis et al., 2001), shares a high degree of syntany to the pathogenic fungus *U. maydis*. However, the transcriptome analysis reveals significant differences regarding pathogenicity and metabolism, indicating *P. antarctica* has an oleaginous nature which is relevant to its non-pathogenic characteristics (Morita et al., 2013b, 2014).

Pseudozyma aphidis is a close relative of the powdery mildew biocontrol agent *P. rugulosa* (Begerow et al., 2000). *P. aphidis* was first isolated from aphid secretions (Henninger and Windisch, 1975) and later identified on plant surfaces as well (Allen et al., 2004). Recently the sequence of *P. aphidis* isolate DSM70725 that was isolated from aphid secretions was published (Lorenz et al., 2014). Previous studies on another *P. aphidis* strain that was also isolated from aphid secretions (isolate CBS517.83) indicated that this species does not produce any unique fungitoxic fatty acids (Avis and Belanger, 2001) and is not associated with the collapse of powdery mildew colonies [*Podosphaera xanthii* formerly *Sphaerotheca fuliginea* (Schlechtend.:Fr.) Pollacci].

We recently reported on a unique active isolate of *P. aphidis* that was identified on the surface of strawberry leaves in association with powdery mildew collapse (designated isolate L12). We demonstrated this isolate's activity against *Botrytis cinerea* colonization and spread on tomato (*Solanum lycopersicum*) and *Arabidopsis thaliana* plants. That observed biocontrol effect was based on a dual mode of action: antibiosis and induced resistance (Buxdorf et al., 2013a,b). The induced resistance was found to be both SA/NPR1- and JAR1/EIN2-independent (Buxdorf et al., 2013a,b).

Powdery mildew is the most common disease of cucurbits and a serious threat in many countries. *P. xanthii* is considered to be the main causal agent of powdery mildew on cucurbits, one of the most important limiting factors for cucurbit production (Bélanger et al., 2002; Perez-Garcia et al., 2009). The constant fungicide application in the field to control this pathogen has led to the development of resistance to various chemicals, thereby reducing the effectiveness of these treatments (McGrath, 2001; Hollomon et al., 2002). Thus, efforts are being made to develop novel techniques to control powdery mildew in the field.

Here, we present a potentially efficient biological control agent against cucurbit powdery mildew that relies on the biologically active *P. aphidis* strain (isolate L12). We demonstrate in the current work the ability of this isolate to antagonized powdery mildew on cucumber plants, using parasitism and antibiosis as modes of action.

Materials and Methods

Propagation of *P. aphidis* and Pathogens

Pseudozyma aphidis strain L12 was maintained on potato dextrose agar (PDA; Difco, France) at 25°C. An indigenous population of *Podosphaera xanthii* was maintained on squash (*Cucurbita maxima*) plants under field conditions.

Propagation of Plants

Cucumber (*Cucumis sativus* cv. Saphi) plants were grown at 25°C under 40% relative humidity in the greenhouse.

Fluorescence Microscopy

A GFP-labeled *P. aphidis* (see Supplementary Figure 1 and Supplementary Methods) was used to visualize colonization of healthy and infected tissue. Ten-day-old cucumber cotyledons were sprayed with either water or GFP-*P. aphidis* (10^8 cells/ml of sterile, deionized water). Three days after treatment the cotyledons were placed on tap water agar medium and then inoculated with *P. xanthii*. Inoculation with *P. xanthii* was done by brushing cucumber cotyledons at several points with a brush that had been

vigorously rubbed on squash (*Cucurbita maxima*) leaves that had been intensely colonized by *P. xanthii*.

The inoculated cucumber cotyledons were layered on agar trays and placed in a controlled-environment chamber where they were kept at 22°C at 80–90% relative humidity and under fluorescent and incandescent light with a photofluency rate of approximately 120 μmol/m^2s and a 12-h photoperiod. Two–seven days after inoculation with *P. xanthii*, the cotyledons were examined with a stereomicroscope (Nikon SMZ 1500) with an epifluorescence attachment (Nikon P-FLA-2). The intensity of the green fluorescence produced by excitation at 488 nm was measured and a GFP filter was used for visualization (Nikon, GFP-B). Images were taken using a Nikon Ds-Ri1camera and processed with NIS elements BR 3.10 software. Cotyledons were also examined with confocal laser scanning microscope (TCS SP8, Leica) 7 days after inoculation with *P. xanthii*; GFP was excited using a 488 nm laser and maximum emission was set at 500 nm. Cucumber cotyledons were also treated with 1mg/ml propidium iodide that was excited using a 514 nm laser and maximum emission was set at 610 nm. The images were analyzed in the LAS AF (Leica) computer program, at a resolution of 1024 × 1024 pixels. The experiments were repeated three times.

Inhibition of Powdery Mildew on Cucumber Seedlings

Two-week-old greenhouse-grown (25°C and 40% relative humidity) cucumber seedlings (with two true leaves) were sprayed with *P. aphidis* cells suspended in water (10^8 cells/ml) or water ($n = 10$) 3 days before they were inoculated with *P. xanthii*. Inoculation with *P. xanthii* was performed by brushing cucumber leaves with a brush that had been vigorously rubbed on squash (*Cucurbita maxima*) leaves that were intensely colonized by *P. xanthii*. Infection severity was scored 11, 12, and 16 days post-inoculation by evaluating the percentage of the infected area on each of the first two leaves. The experiment was concluded after 16 days when the first leaf of the control treatment was fully coved with powdery mildew. Percentage of powdery mildew coverage (PMC) was estimate and disease severity was scored using the 12-grade scale described by Horsfall and Barratt (1945) with minor modifications: 0 = 0%, 1 = 0–3%, 2 = 3–6%, 3 = 6–12%, 4 = 12–25%, 5 = 25–50%, 6 = 50–75%, 7 = 75–87%, 8 = 87–94%, 9 = 94–97%, 10 = 97–100%, 11 = 100% disease. A mean disease-severity index value (DSI) was calculated for each treatment by adding up the scores of the 20 leaves in the treatment and then expressing that sum as a percentage using the formula described by Raupach et al. (1996): Disease Severity Index = [$\sum$(rating no. × no. of plants in rating) × 100%]/(total no. of plants × highest rating). Biocontrol efficacy was calculated as: Efficacy = [(disease rate in control − disease rate in treatment)/disease rate in control] × 100. The entire experiment was performed three times with similar results.

Scanning Electron Microscopy

For scanning electron microscopy (SEM), *P. aphidis*-treated and powdery mildew-inoculated cucumber cotyledons were collected 1–4 days after inoculation and fixed with glutaraldehyde using standard protocols (Weigel and Glazebrook, 2002). Samples were mounted on aluminum stubs and sputter-coated with AU-Pd. SEM was performed using a Jeol JEM 5410 at 20 kV.

Transmission Electron Microscopy

For transmission electron microscopy (TEM), cucumber cotyledons were treated with *P. aphidis* inoculated with *P. xanthii* 3 days later, and collected 8 days post-inoculation and processed using a standard protocol (Chuartzman et al., 2008). Epon-embedded samples were sectioned using a diamond knife on an LKB 3 microtome (Leica, Bensheim, Germany) and ultrathin sections (80 nm) were collected onto 200 Mesh, thin bar copper grids. The sections on grids were sequentially stained with Uranyl acetate and Lead citrate for 10 min each and observed with a Technai T12 TEM 100 kV (Phillips, Eindhoven, the Netherlands).

Antibiosis Assays Using Crude Extract of *P. aphidis* Metabolites

Metabolites were extracted from *P. aphidis* cells using ethyl acetate. One and a half liters of PDB medium in a 3-l Erlenmeyer flask were inoculated with two 1-cm^2 blocks of PDA carrying mycelia and/or spores of *P. aphidis* and grown for 10 days at 27°C, in dark with constant agitation at 150 rpm. We then spun down the fungal cells (5 min at 7000 rpm) and extracted them with a 3-l of ethyl-acetate. The ethyl-acetate fraction was collected and evaporated in a rotor evaporator (Buchi, Flawil, Switzerland) at 42°C (Paz et al., 2007). Evaluation of the inhibitory effect of the metabolites extracted from *P. aphidis* on *P. xanthii* conidia germination was carried out using cucumber cotyledons from 1-week-old plants. Cotyledons disks (15 mm in diameter) were disinfected with 0.1% NaOCl (w/v) for 2 min, and rinsed twice in sterile distilled water. The crude extract (200 mg/ml in ethyl-acetate) was diluted with distilled water (1:15 v/v) and poured into sterile six-well plates. Distilled water and an ethyl acetate diluted in distilled water (1:15 v/v) were used as controls. The cotyledon disks were placed in these dilutions upside down and incubated at room temperature for 10 min. After incubation, the disks were transferred onto solid medium (40 g sucrose, 30 mg benzimidazole, 10 g agar, 1-l distilled water) in 5 cm diameter Petri dishes, and the upper side of the disks was inoculated with conidia of *P. xanthii* with a brush. After 24 h of incubation (22°C and 16 h of daylight), disks were cleared in boiling absolute ethanol for 20 min in a water bath, followed by a final wash in glycerol: lactic acid: water (1:1:1 v/v) overnight. The disks were then incubated for 2 min in aniline blue (0.2%) followed by rinsing in distilled water, and then examined under a bright-field microscope. The percentage of spore-inhibition was calculated in relation to untreated control with distilled water. Spore germination in water ranged between 98 and 100%. For each experiment the means of the distilled water control values were considered as a 100% germination; all other values were divided by these values and multiplied by a 100 for obtaining the percentage of spore germination. To obtain percentage of spore inhibition the percentage of spore germination was reduced from a 100.

Chitinase Activity

To evaluate chitinase activity, *P. aphidis* was grown on tap water agar plates (TWA; 2% agar) or TWA supplemented with 0.1%

(w/v) chitin (Sigma-Aldrich, USA). Colony diameter was measured 8 and 17 days post-inoculation.

Data Analysis

Student's *t*-test was performed only when data were normally distributed and the sample variances were equal. Significance was accepted at $P < 0.05$, as noted in the text or table captions. All experiments described here are representative of at least two independent experiments with the same pattern of results.

Results

Antagonistic Effect of *P. aphidis* Against Powdery Mildew *in Planta*

We first demonstrated the ability of *P. aphidis* to maintain a stable population on cucumber (*C. sativus*) seedlings. Specifically, we treated 10-day-old seedlings with a *P. aphidis* suspension and monitored the number of CFU appearing over a period of 21 days post-inoculation. The size of the *P. aphidis* remained stable for 18-days on plants maintained under controlled conditions (Supplementary Figure 2). Foliar application of *P. aphidis* (10^8 cells/ml) to cucumber plants did not result in any symptoms of pathogenicity or phytotoxicity, such as chlorosis. Furthermore, following application of GFP-expressing *P. aphidis* (Supplementary Figure 1) to healthy cucumber cotyledons, we observed minor spreading of the green fluorescence cells throughout the cotyledons (**Figure 1A**). When *P. aphidis*-treated cucumber cotyledons were then inoculated with *P. xanthii*, a stronger, denser and more uniform green fluorescent signal was observed in the inoculated area (**Figure 1B**), indicating the close association of *P. aphidis* with *P. xanthii*.

We then tested the ability of *P. aphidis* to control cucumber powdery mildew *in vivo*. Greenhouse-grown cucumber seedlings (two leaves) were sprayed with *P. aphidis* cells or with water as a control and 3 days later, seedlings were inoculated with *P. xanthii*. The application of *P. aphidis* significantly reduced the severity of powdery mildew disease symptoms on the treated cucumber plants as compared with control untreated infected plants (**Table 1**). Sixteen days after inoculation, almost all first two leaves of the untreated plants showed close to 100% coverage with powdery mildews, compared to only 17% coverage on the treated plants (**Table 1** and Supplementary Figure 3). Moreover, the appearance of disease symptoms was delayed by 12 days on the treated plants as compared to the untreated ones. After 11 days, there was 45% powdery mildew coverage of the untreated leaves, whereas all of the treated leaves were still symptomless (**Table 1**). Disease severity 12 days post-inoculation was 15% for plants treated with *P. aphidis* as compared to 88% for control plants, and 16 days post-inoculation, 31% for *P. aphidis*-treated plants vs. 98% for untreated control plants (**Table 1**). The efficacy of *P. aphidis* treatment was 75% on day 16 post-inoculation (**Table 1**).

Morphological Yeast-to-Hypha Transition and Ectoparasitism of *P. aphidis*

We demonstrated *in vitro* that *P. aphidis* is a dimorphic yeast-like fungus that grows mainly as a yeast in PDB medium but can form hyphae when grown in different media, such as YMPD

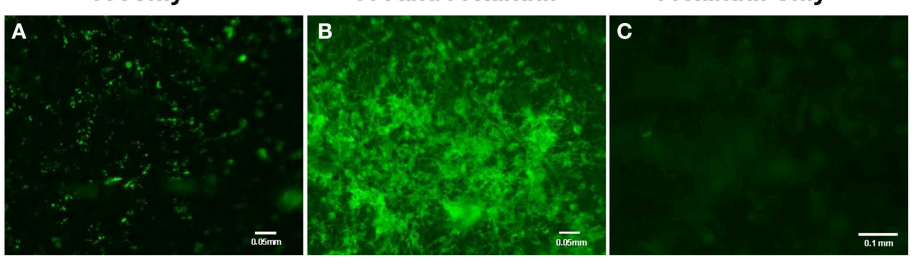

FIGURE 1 | Imaging of *P. aphidis* proliferation on infected cucumber cotyledons. Fluorescence microscopy analysis of cucumber cotyledons treated with GFP-tagged *P. aphidis* **(A)** followed by successive inoculation (3 days after *P. aphidis* treatment) with *P. xanthii* **(B)** or treated with water and inoculated with *P. xanthii* **(C)**. Images were recorded 5 days after inoculation *P. xanthii*. Shown are representative pictures taken of one cotyledon out of 5 from each treatment in one representative experiment. The entire experiment was performed three times with similar results.

TABLE 1 | Effect of *P. aphidis* treatment on severity of disease symptoms caused by *P. xanthii*.

Treatment	DSI (%)			PMC (%)			Efficacy (%)		
	11 dpi	12 dpi	16 dpi	11 dpi	12 dpi	16 dpi	11 dpi	12 dpi	16 dpi
PA-treated	0	15	31	0*	3.2 ± 1.7*	16.9 ± 9.1*	100	88	75
Control	67	88	98	46.5 ± 4.7	56.5 ± 4.7	98.7 ± 2.5			

Disease severity index (DSI) and P. xanthii average leaf coverage (PMC) were calculated 11, 12 and 16 days post-inoculation (dpi) as described by Raupach et al. (1996). PA, P. aphidis. Means and standard errors of PMC are presented. Means of DSI followed by asterisks is significantly different from inoculated water-treated control according to Student's t-test; $P < 0.05$; $n = 20$ leaves from 10 different plants.

or MS (Supplementary Figure 4). Using confocal microscopy, we demonstrated the morphological yeast-to-hypha transition (dimorphism) of *P. aphidis in planta* (**Figure 2**). *P. aphidis* was mainly in yeast form on uninfected tissue (**Figure 2** Left), whereas on *P. xanthii*-infected tissue, it was mainly in hyphal form (**Figure 2** Right). SEM revealed that the areas infected with powdery mildew were covered with *P. aphidis* (**Figure 3**), and that the powdery mildew's hyphae were significantly shorter (by 27%, Supplementary Table 1) when they were associated with *P. aphidis* at infection initiation 2 dpi (**Figure 3C**). *P. aphidis*, on the other hand, formed long hyphae that branched when associated with *P. xanthii* and attached to the powdery mildew hyphae by coiling around them as seen by SEM analysis (**Figures 3A,B**). We observed inhibition of growth and sporulation of powdery mildew on the plants that were treated with *P. aphidis* as compared to control (**Figure 3D**). We also observed accumulation of extracellular matrix in the area of interaction between *P. aphidis* and powdery mildew, and that the hyphae of *P. aphidis* extending from one powdery mildew hypha to another one were thinner (**Figures 3A,B** and Supplementary Figure 5). Furthermore, *P. aphidis* behave like an ectoparasite, as demonstrated by confocal and TEM microscopy. We could not detect any GFP fluorescence or *P. aphidis* cells inside the powdery mildew hyphae using confocal microscopy or TEM, respectively (**Figures 4**, **5** and Supplementary Movies 1, 2). TEM analysis of powdery mildew cells associated with *P. aphidis* showed numerous abnormalities: increased vacuolation, deformation of the cell wall and disorganization of the cytoplasm. These abnormalities eventually lead to collapse of the powdery mildew cells (**Figure 5**). Accumulation of extracellular matrix surrounding *P. aphidis* was also observed (**Figure 5**).

P. aphidis Metabolites Inhibit *P. xanthii* Spore Germination *in Planta* and Poses Chitinase Activity

While the precise biochemical nature of the pinkish substance secreted by *P. aphidis* is still unknown, we hypothesized that *P. aphidis* secretes antibiotics and enzymes, such as chitinase, that can inhibit and degrade fungal cell walls. For antibiosis activity, we used *P. aphidis* extract and revealed that crude extract of *P. aphidis* metabolites can almost completely inhibit *P. xanthii* spore germination on intact cucumber cotyledons (**Table 2**). We also demonstrated that the vast majority of spores that are germinated on extract form a one germination tube and not hypha (Supplementary Figure 6).

For chitinase activity verification we grew *P. aphidis* on TWA plates supplemented with chitin as sole carbon source. On TWA plates supplemented with chitin, *P. aphidis* colony diameter was

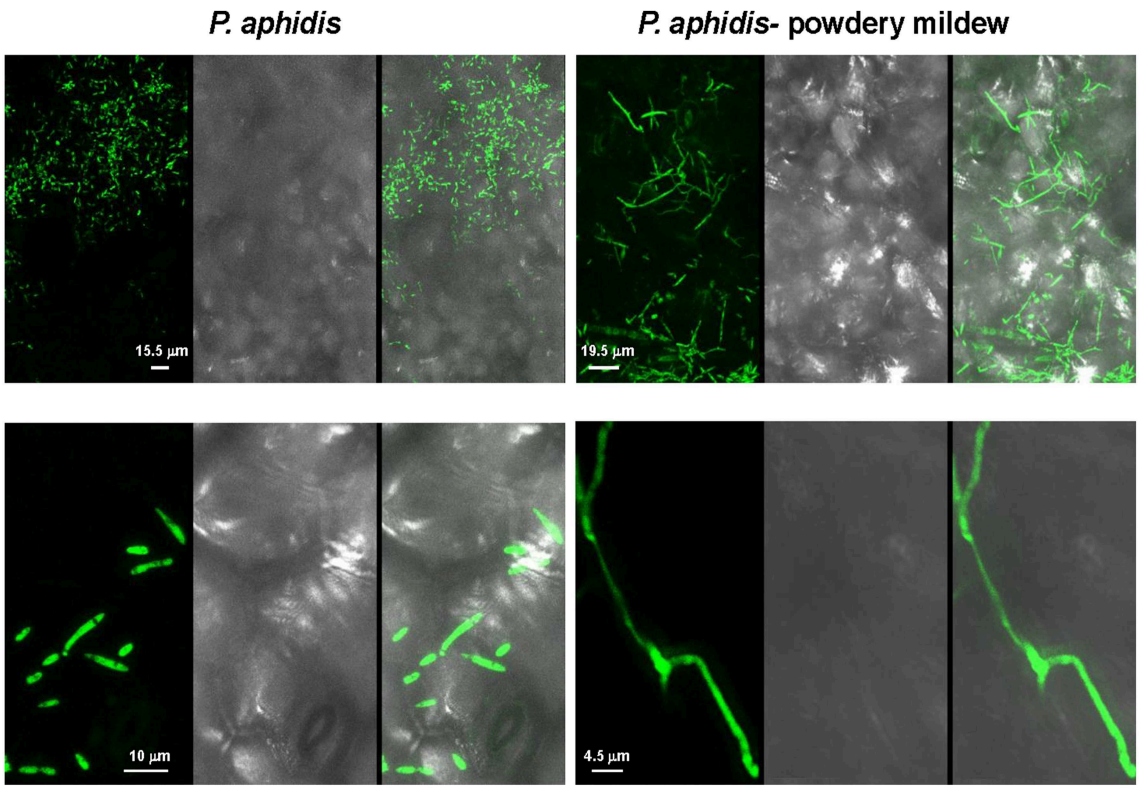

FIGURE 2 | *P. aphidis* forms long hyphae when interacting with powdery mildew. Confocal microscopy observations of cucumber cotyledons treated with GFP-tagged *P. aphidis* (PA-GFP). PA-GFP-treated cotyledons 4 days after inoculation with *Podosphaera xanthii* (*P. aphidis*-powdery mildew) or water (*P. aphidis*). The panels, from left to right, depict fluorescence, white light, and overlay images, respectively, for each of the treatments.

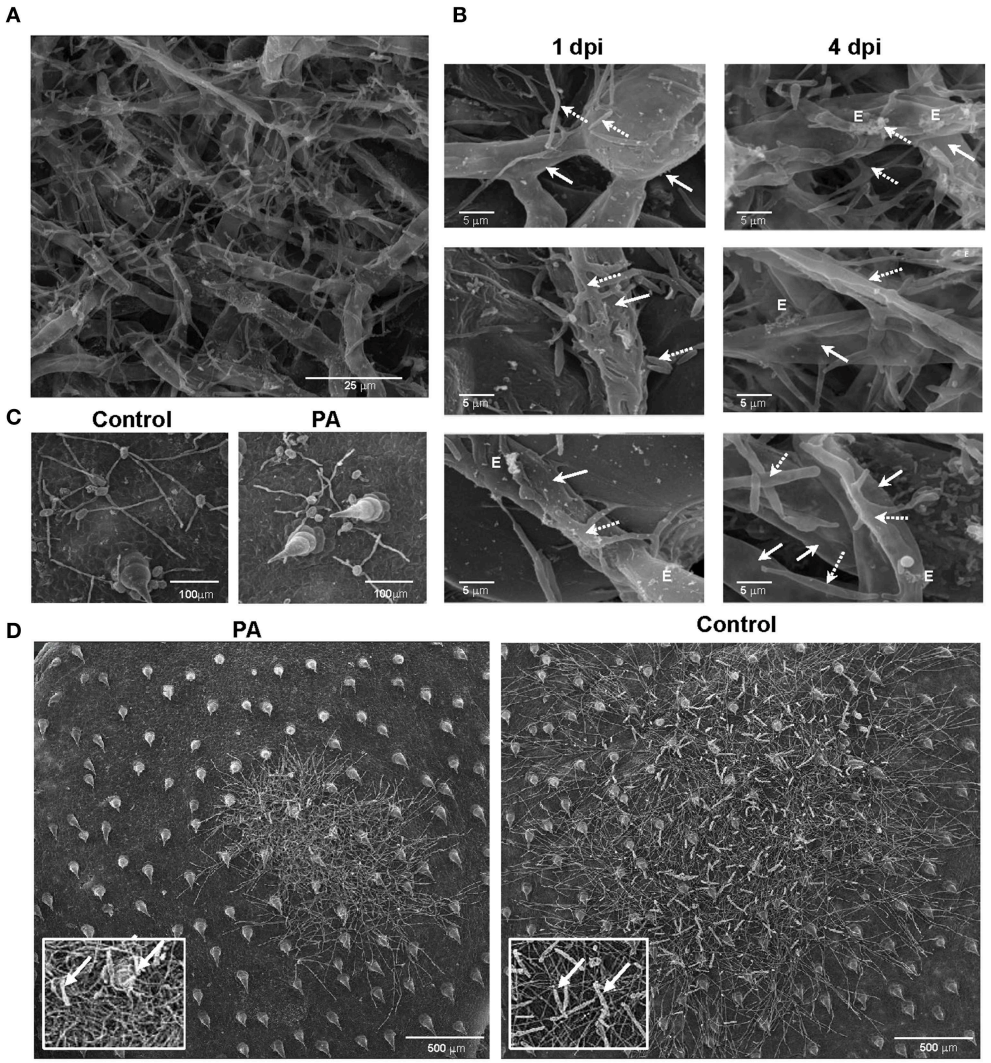

FIGURE 3 | *P. aphidis*–powdery mildew interactions on cucumber cotyledons. SEM microscopy of cucumber cotyledons treated with *P. aphidis* and infected with *Podosphaera xanthii*. **(A)** Cucumber cotyledons treated with *P. aphidis* 4 days post-infection with *P. xanthii*. **(B)** Closer look at the interaction of *P. aphidis* and *P. xanthii* mycelium and spores 1 and 4 days post-infection with *P. xanthii*. Cucumber cotyledons treated with *P. aphidis* (PA) or with water (Control) 1 day post-inoculation **(C)** and 10 days post-inoculation with *P. xanthii* **(D)** (sporulation marked with white arrows). **(A–C)** *P. xanthii* mycelium and spores are indicated with white arrows and *P. aphidis* cells and hyphae with dashed arrows; E, extracellular matrix.

21.8 mm as compared to 9.1 mm on TWA alone (**Figure 6**). These findings suggest that *P. aphidis* can secrete chitinase to utilize chitin as a carbon source.

Discussion

Fungal biocontrol agents are important for disease control and can provide a viable alternative for chemical-based pesticides. Yet the number of fungal biocontrol agents that are currently used for practical applications is minuscule as compared with the use of chemical-based agents. We recently identified a unique isolate of *P. aphidis* (isolate L12) from strawberry leaves associated with powdery mildew collapse and demonstrated that this isolate can reduce *B. cinerea* infection of tomato and *Arabidopsis* plants (Buxdorf et al., 2013a,b). That biocontrol effect against *B. cinerea* was found to proceed via a dual mode of action, antibiosis and induced resistance that is SA/NPR1- and JA/ET-independent (Buxdorf et al., 2013a,b). Here, we studied the ability of this isolate to control the growth of another pathogen. We demonstrated that *P. aphidis* can colonize healthy plant leaf surfaces and that it can proliferate on powdery mildew infected cucumber cotyledons (**Figures 1–3**, and Supplementary Figure 2), as was also demonstrated for its close relative *Pseudozyma flocculosa*, which can colonize cucumber leaves that have been inoculated with powdery mildew (Hammami et al., 2011).

The *P. aphidis* isolate studied in this work was found to control powdery mildew (**Table 1**) via parasitism (**Figures 3–5**) and

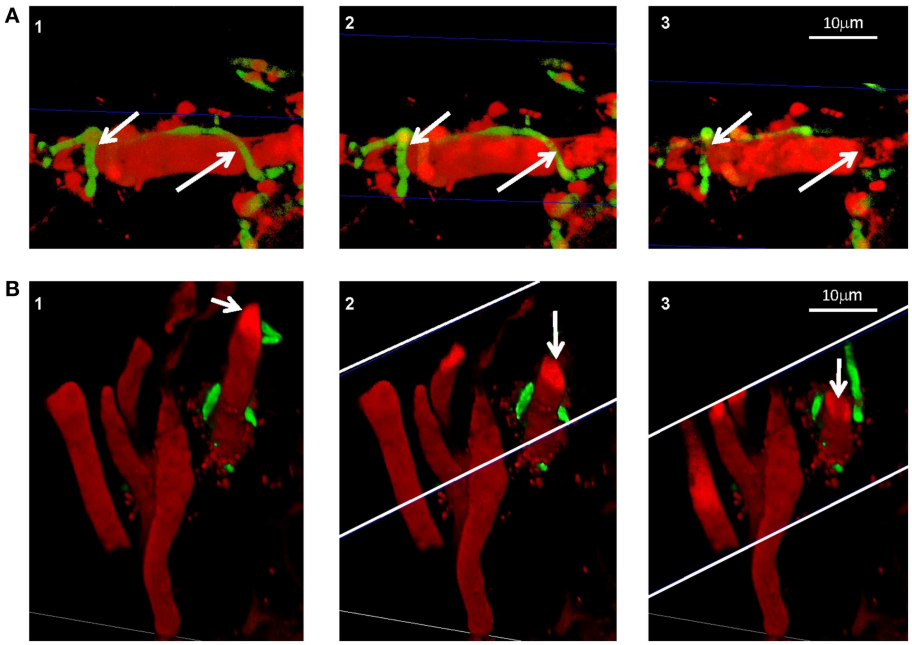

FIGURE 4 | *P. aphidis* as an ectoparasite. Confocal microscopic analysis of cucumber cotyledons treated with propidium iodide 10 days after treatment with GFP-tagged *P. aphidis* (green) and 7 days after inoculation with *P. xanthii* (red). **(A)** Reconstructed 3D images demonstrating *P. aphidis* (green; marked with white arrows) coiling around the powdery mildew hyphae and cross-sections (marked with blue thin lines) demonstrating no fluorescence inside the powdery mildew hypha. See Supplemental Movie 1 for whole series of sections. **(B)** Reconstructed 3D cross-section images. The white thin lines marked the area of the cross-sections, while the white arrows point to the sectioned powdery mildew hypha. See Supplemental Movie 2 for whole series of sections.

antibiosis (**Table 2**). This is in contrast to the findings reported in previous studies by Avis et al. (2001). The difference between our findings and those of Avis et al. (2001) is likely due to the different isolates used. It is particularly noteworthy that the application of *P. aphidis* prior to pathogen inoculation significantly reduced the severity of powdery mildew on greenhouse-grown cucumber plants with an efficacy of 75% (**Table 1**). We and others have previously reported that applying a biocontrol agent before pathogen infection can indeed improve biocontrol activity (Filonow et al., 1996; Buxdorf et al., 2013a,b), but other reports have suggested otherwise (Chalutz and Wilson, 1990; Cook et al., 1997).

We demonstrated that *P. aphidis* occupies the same niches as powdery mildew (**Figures 1**–**3**), as also observed previously with *B. cinerea* (Buxdorf et al., 2013b) and similar to observations made with its close relative the biocontrol agent *P. flocculosa* in association with powdery mildew (Hammami et al., 2011). *P. aphidis* isolate L12 was also shown to have a dimorphic morphology, forming yeast-like structures and short pseudo-hyphae on plant surfaces or when interacting with *B. cinerea* (Buxdorf et al., 2013b). Here we demonstrated that *P. aphidis* mainly forms yeast-like structures on uninfected leaves and hyphae on infected tissue that lengthen with infection development (**Figures 2**, **3**). Similarly, Hammami et al. (2010, 2011) demonstrated pseudo-hyphal growth of *P. flocculosa* under stress conditions as compared to yeast-like growth under control conditions (Hammami et al., 2010, 2011). In many other dimorphic fungi, the morphological choice of yeast or mycelium is associated with quorum sensing, inoculum size, stress conditions and secreted molecules (Hornby et al., 2001, 2004; Hogan, 2006; Nickerson et al., 2006; Berrocal et al., 2014). Since we did not observed coiling or the formation of long hyphae when *P. aphidis* interacted with *B. cinerea*, we assume that the interaction with powdery mildew triggers this yeast–mycelia transition, probably involving molecule secretion or other cues that activate gene expression and need to be further characterized. We demonstrated that *P. aphidis* attaches by coiling around the powdery mildew hyphae, forming a hyphal network. While we could observe strong attachments of *P. aphidis* to the powdery mildew hyphae and appressorium-like structures using SEM (**Figure 3**), we did not observed *P. aphidis* inside the powdery mildew hypha using confocal or TEM microscopy (**Figures 4**, **5** and Supplementary Movies 1, 2). This suggests that *P. aphidis* is an ectoparasite of *P. xanthii*, as also demonstrated with *Trichoderma* spp. on *Pythium*, *Rhizoctonia solani*, *Sclerotium rolfsii,* and *Sclerotinia sclerotium* (Chet et al., 1981; Elad et al., 1983; Hubbard et al., 1983; Inbar et al., 1996). Although we could not observe any penetration of *P. aphidis* into the powdery mildew hyphae (**Figures 4**, **5** and Supplementary Movies 1, 2), we could demonstrate chitinase activity *in vitro* (**Figure 6**). It has been shown that attachment of an antagonist to a pathogen plays a major role in the former's biological activities, enabling cell wall degrading enzymes to be effective (Jones, 1994; Askary et al., 1997; Cook et al., 1997).

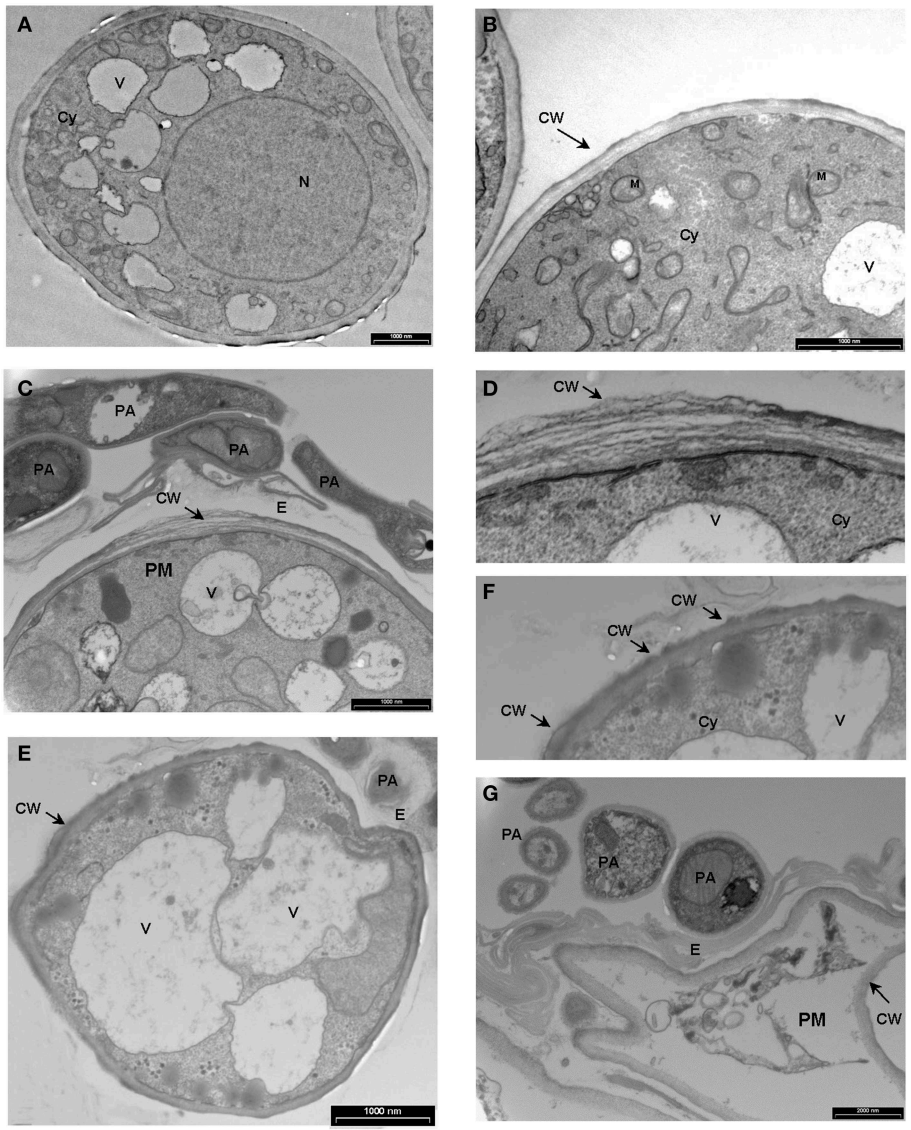

FIGURE 5 | Transmission electron micrographs depicting the interaction between *P. Xanthii* and *P. aphidis* on cucumber leaves. (A,B) Ultrastructure of *P. xanthii* (PM) hypha on cucumber leaves 8 days post-inoculation. Hyphal cells are surrounded by an intact cell wall (CW) and show a dense polyribosome—rich cytoplasm (Cy), with numerous organelles inside, including mitochondria (M), nucleus (N) and vacuoles (V). **(C–G)** Ultrastructure of *P. xanthii* and *P. aphidis* (PA) interactions on cucumber leaves 8 days post-inoculation and 11 days post-treatment with *P. aphidis*. **(C)** *P. aphidis* cells encircle the *P. xanthii* hyphae causing deformation of the cell wall (CW), also seen at higher magnification in **(D)**. **(E)** Increased vacuolation is accompanied by deformation of the cell wall and disorganization of the cytoplasm, also seen at higher magnification in **(F)**. **(G)** *P. xanthii* cells are markedly collapsed. E, extracellular matrix.

The abundance of *P. aphidis* on *P. xanthii* (**Figures 1**, **2**), its coiling around *P. xanthii* as demonstrated by SEM (**Figure 3**), and its chitinase activity demonstrated *in vitro* (**Figure 6**), suggest that *P. aphidis* parasitizes the powdery mildew hyphae. *P. aphidis* probably disrupts the pathogen's tissue via the chitinase activity and releases the nutrients required for abundant growth of *P. aphidis*. Moreover we were able to demonstrate antibiosis of *P. aphidis* crude extract against *P. xanthii in planta* (**Table 2**). This might contribute to its biocontrol ability by damaging and even killing powdery mildew cells. This is the first case, as far as we know, that mycoparasitism is demonstrated as a mode of action of a yeast-like biocontrol agent against powdery mildew. The literature mostly describes antibiosis as a mode of action of yeast-like biocontrol agents such as *P. flocculosa* (Bélanger et al., 1994; Hajlaoui et al., 1994; Benyagoub et al., 1996; Avis and Belanger, 2001; Avis et al., 2001; Hammami et al., 2010, 2011) and *Tilletiopsis* species (Urquhart and Punja, 1997, 2002) against powdery mildew. While mycoparasitism against powdery mildew was demonstrated as a mode of action used by biocontrol fungi such as *Veticillium lecanii* (Askary et al., 1997, 1998) and

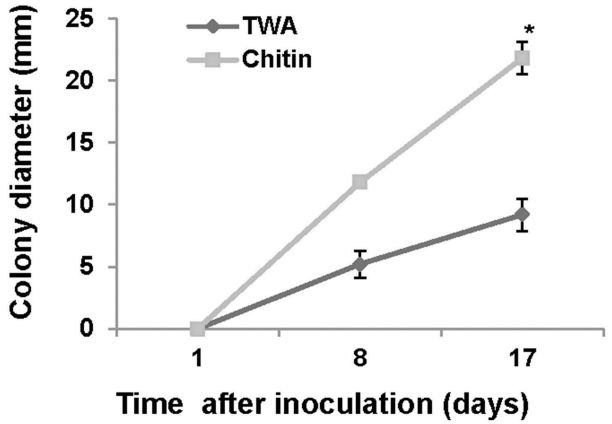

FIGURE 6 | Chitinase activity. Growth of *P. aphidis* on 0.1% chitin as compared to TWA. Averages of five samples are presented with standard-error bars. Asterisks indicate a significant difference as determined by Student's *t*-test; $P < 0.05$.

TABLE 2 | Inhibition of spore germination by. *P. aphidis* crude extract.

Treatment	Inhibition of spore germination (%)
PA	97.5 ± 1.7*
Control	2.3 ± 4.3

Percentage of spore inhibition after 24 h on cucumber cotyledon disks covered with P. aphidis crude extract (PA) or EtOAc (Control). Data represent the means ± standard deviation. Value followed by an asterisk is significantly different from the control according to Student's t-test; P < 0.001; n = 7 replicates per treatment with 100 spores each.

by *Ampelomyces quisiqualis* on cucumber plants (Rotem et al., 1999).

The chitinase activity of *P. aphidis* L12 (**Figure 6**), is supported also by recently released DNA sequence of *P. aphidis* (isolate DSM 70725) demonstrating one chitinase gene and two other candidate genes that are related to chitinase (Lorenz et al., 2014). Furthermore, the sequenced isolate contains one extracellular aspartic proteinase and eight potential glucanases (Lorenz et al., 2014); these cell wall-degrading enzymes might be involved in degradation of the pathogen cell wall, but the availability and intactness of those genes and their protein activity must be further characterized in our isolate. Furthermore, genome and transcriptome analysis of the biocontrol agent *P. flocculosa* demonstrated differences from the pathogenic related fungi *U. maydis* in genes related to fungal cell wall degradation and other gene families related to *P. flocculosa*'s epiphytic and antagonistic characteristics, such as lipases, chitinases and chitin binding proteins (Lefebvre et al., 2013).

The released sequences of the genomes of *Pseudozyma* spp. provide further support for antibiosis as they reveal the presence of gene clusters regulating synthesis of glycolipids, some of which have an antibiosis ability (Lefebvre et al., 2013; Morita et al., 2013a, 2014; Lorenz et al., 2014; Saika et al., 2014). Flocculosin, synthesized by *P. flocculosa* is an example of such glycolipid (Teichmann et al., 2007, 2011a,b). We speculate *P. aphidis* isolate L12 also has the ability to produce glycolipid/s with antibiosis ability. However, antibiosis as a mode of action *in vivo* is still questionable since *U. maydis*, which synthesize ustilagic acid, an antifungal compound very similar to flocculosin, does not have any antagonistic effect against powdery mildew (Hammami et al., 2011).

Collectively, our data show that the *P. aphidis* isolate L12 has potential for use as a biocontrol agent against powdery mildew via mycoparasitism. We also suggest antibiosis as a possible mechanism based on our observation that spore-germination of powdery mildew is inhibited *in planta* by the crude extract of metabolites of *P. aphidis*. We show morphological yeast-to-hypha transition of *P. aphidis* that parasitize the powdery mildew. However, to extend our knowledge, it is important to identify the cues causing *P. aphidis* dimorphism in association with *P. xanthii*.

Author Contributions

ML designed the experiments. AG, KB, CC, RH, and AD performed the experiments. EZ preform the confocal microscopy analysis. ML analyzed the results and wrote the manuscript. All authors read and approved the final manuscript.

Acknowledgments

We thank Prof. Regine Khamann from the Max Plank Institute (Germany) for providing us the GFP construct. This work was supported by the Chief Scientist of the Ministry of Agriculture, Israel, grant 823-0209-14.

Supplementary Material

The Supplementary Material for this article can be found online at: http://www.frontiersin.org/journal/10.3389/fpls.2015.00132/abstract

References

Allen, T. W., Quayyum, H. A., Burpee, L. L., and Buck, J. W. (2004). Effect of foliar disease on the epiphytic yeast communities of creeping bentgrass and tall fescue. *Can. J. Microbiol.* 50, 853–860. doi: 10.1139/w04-073

Askary, H., Benhamou, N., and Brodeur, J. (1997). Ultrastructural and cytochemical investigations of the antagonistic effect of *Verticillium lecanii* on cucumber powdery mildew. *Phytopathology* 87, 359–368. doi: 10.1094/PHYTO.1997.87.3.359

Askary, H., Carriere, Y., Bélanger, R., and Brodeur, J. (1998). Pathogenicity of the fungus *Verticillium lecanii* to aphids and powdery mildew. *Biocont. Sci. Technol.* 8, 23–32. doi: 10.1080/09583159830405

Avis, T. J., and Belanger, R. R. (2001). Specificity and mode of action of the antifungal fatty acid cis-9-heptadecenoic acid produced by *Pseudozyma flocculosa*. *Appl. Environ. Microbiol.* 67, 956–960. doi: 10.1128/AEM.67.2.956-960.2001

Avis, T. J., and Belanger, R. R. (2002). Mechanisms and means of detection of biocontrol activity of *Pseudozyma* yeasts against plant-pathogenic fungi. *FEMS Yeast Res.* 2, 5–8. doi: 10.1016/S1567-1356(01)00058-7

Avis, T. J., Caron, S. J., Boekhout, T., Hamelin, R. C., and Belanger, R. R. (2001). Molecular and physiological analysis of the powdery mildew antagonist *Pseudozyma flocculosa* and related fungi. *Phytopathology* 91, 249–254. doi: 10.1094/PHYTO.2001.91.3.249

Barnett, J. A., Payne, R. W., and Yarrow, D. (2000). *Yeasts: Characteristics and Identification*. Cambridge: Cambridge University Press

Begerow, D., Bauer, R., and Boekhout, T. (2000). Phylogenetic placements of ustilaginomycetous anamorphs as deduced from nuclear LSU rDNA sequences. *Mycol. Res.* 104, 53–60. doi: 10.1017/S0953756299001161

Bélanger, R. R., Labbé, C., and Jarvis, W. R. (1994). Commercial-scale control of rose powdery mildew with a fungal antagonist. *Plant Dis.* 78, 420–424. doi: 10.1094/PD-78-0420

Bélanger, R. R., Bushnell, W. R., Dik, A. J., and Carver, T. L. W. (2002). *The Powdery Mildews: A Comprehensive Treatise*. St. Paul, MN: American Phytopatholgical Society Press.

Benyagoub, M., Willemot, C., and Bélanger, R. R. (1996). Influence of a subinhibitory dose of antifungal fatty acids from *Sporothrix flocculosa* on cellular lipid composition in fungi. *Lipids* 31, 1077–1082. doi: 10.1007/BF02522465

Berrocal, A., Oviedo, C., Nickerson, K. W., and Navarrete, J. (2014). Quorum sensing activity and control of yeast-mycelium dimorphism in *Ophiostoma floccosum*. *Biotechnol. Let.* 36, 1503–1513. doi: 10.1007/s10529-014-1514-5

Bleve, G., Grieco, F., Cozzi, G., Logrieco, A., and Visconti, A. (2006). Isolation of epiphytic yeasts with potential for biocontrol of *Aspergillus carbonarius* and *A. niger* on grape. *Int. J. Food Microbiol.* 108, 204–209. doi: 10.1016/j.ijfoodmicro.2005.12.004

Boekhout, T. (1995). *Pseudozyma Bandoni* emend. *Boekhout*, a genus for yeast-like anamorphs of Ustilaginales. *Gen. Appl. Microbiol.* 41, 359–366. doi: 10.2323/jgam.41.359

Buck, J. W., and Burpee, L. L. (2002). The effects of fungicides on the phylloplane yeast populations of creeping bentgrass. *Can. J. Microbiol.* 48, 522–529. doi: 10.1139/w02-050

Buxdorf, K., Rahat, I., Gafni, A., and Levy, M. (2013a). The epiphytic fungus *Pseudozyma aphidis* induces jasmonic acid- and salicylic acid/nonexpressor of PR1-independent local and systemic resistance. *Plant Physiol.* 161, 2014–2022. doi: 10.1104/pp.112.212969

Buxdorf, K., Rahat, I., and Levy, M. (2013b). *Pseudozyma aphidis* induces ethylene-independent resistance in plants. *Plant Signal. Behav.* 8:e26273. doi: 10.4161/psb.26273

Chalutz, E., and Wilson, C. L. (1990). Postharvest biocontrol of green and blue mold and sour rot of citrus fruit by *Debaryomyces hansenii*. *Plant Dis.* 74, 134–137. doi: 10.1094/PD-74-0134

Chet, I., Harman, G., and Baker, R. (1981). *Trichoderma hamatum*: its hyphal interactions with *Rhizoctonia solani* and *Pythium* spp. *Microb. Ecol.* 7, 29–38. doi: 10.1007/BF02010476

Chuartzman, S. G., Nevo, R., Shimoni, E., Charuvi, D., Kiss, V., Ohad, I., et al. (2008). Thylakoid membrane remodeling during state transitions in Arabidopsis. *Plant Cell* 20, 1029–1039. doi: 10.1105/tpc.107.055830

Cook, D. W. M., Long, P. G., Ganesh, S., and Cheah, L. H. (1997). Attachment microbes antagonistic against *Botrytis cinerea*—biological control and scanning electron microscope studies *in vivo*. *Ann. Appl. Biol.* 131, 503–518. doi: 10.1111/j.1744-7348.1997.tb05177.x

Denholm, I., and Rowland, M. W. (1992). Tactics for managing pesticide resistance in arthropods: theory and practice. *Annu. Rev. Entomol.* 37, 91–112. doi: 10.1146/annurev.en.37.010192.000515

Dik, A. J., Verhaar, M. A., and Bélanger, R. R. (1998). Comparison of three biological control agents against cucumber powdery mildew (*Sphaerotheca fuliginea*) in semi-commercial-scale glasshouse trials. *Eur. J. Plant Pathol.* 104, 413–423. doi: 10.1023/A:1008025416672

Elad, Y., Chet, I., Boyle, P., and Henis, Y. (1983). Parasitism of *Trichoderma* spp. on *Rhizoctonia solani* and *Sclerotium rolfsii*-scanning electron microscopy and fluorescence microscopy. *Phytopathology* 73, 85–88. doi: 10.1094/Phyto-73-85

Elad, Y., and Freeman, S. (2002). "Biological control of fungal plant pathogens," in *The Mycota, A Comprehensive Treatise on Fungi as Experimental Systems for Basic and Applied Research. XI. Agricultural Applications*, ed F. Kempken (Heidelberg: Springer), 93–109

Fernandez, N. V., Mestre, M. C., Marchelli, P., and Fontenla, S. B. (2012). Yeast and yeast-like fungi associated with dry indehiscent fruits of *Nothofagus nervosa* in Patagonia, Argentina. *FEMS Microbiol. Ecol.* 80, 179–192. doi: 10.1111/j.1574-6941.2011.01287.x

Filonow, A. B., Vishniac, H. S., Anderson, J. A., and Janisiewicz, W. J. (1996). Biological control of *Botrytis cinerea* in apple by yeasts from various habitats and their putative mechanisms of antagonism. *Biol. Cont.* 7, 212–220. doi: 10.1006/bcon.1996.0086

Hajlaoui, M. R., Traquair, J. A., Jarvis, W. R., and Bélanger, R. R. (1994). Antifungal activity of extracellular metabolites produced by *Sporothrix flocculosa*. *Biocontrol Sci. Technol.* 4, 229–237. doi: 10.1080/09583159409355331

Hammami, W., Castro, C. Q., Remus-Borel, W., Labbe, C., and Belanger, R. R. (2011). Ecological basis of the interaction between *Pseudozyma flocculosa* and powdery mildew fungi. *Appl. Environ. Microbiol.* 77, 926–933. doi: 10.1128/AEM.01255-10

Hammami, W., Chain, F., Michaud, D., and Bélanger, R. R. (2010). Research Proteomic analysis of the metabolic adaptation of the biocontrol agent *Pseudozyma flocculosa* leading to glycolipid production. *Proteome Sci.* 8:7 doi: 10.1186/1477-5956-8-7

Henninger, W., and Windisch, S. (1975). *Pichia lindnerii* sp. n., a new methanol assimilating yeast from soil. *Arch. Microbiol.* 105, 47–48. doi: 10.1007/BF00447111

Hogan, D. A. (2006). Talking to themselves: autoregulation and quorum sensing in fungi. *Eukaryot Cell* 5, 613–619. doi: 10.1128/EC.5.4.613-619.2006

Hollomon, D., Wheeler, I., Bélanger, R., Bushnell, W., Dik, A., and Carver, T. (2002). *Controlling powdery mildews with chemistry*. St. Paul, MN: American Phytopathology Society Press.

Hornby, J. M., Jacobitz-Kizzier, S. M., McNeel, D. J., Jensen, E. C., Treves, D. S., and Nickerson, K. W. (2004). Inoculum size effect in dimorphic fungi: extracellular control of yeast-mycelium dimorphism in *Ceratocystis ulmi*. *Appl. Environ. Microbiol.* 70, 1356–1359. doi: 10.1128/AEM.70.3.1356-1359.2004

Hornby, J. M., Jensen, E. C., Lisec, A. D., Tasto, J. J., Jahnke, B., Shoemaker, R., et al. (2001). Quorum sensing in the dimorphic fungus *Candida albicans* is mediated by farnesol. *Appl. Environ. Microbiol.* 67, 2982–2992. doi: 10.1128/AEM.67.7.2982-2992.2001

Horsfall, J. G., and Barratt, R. W. (1945). An improved grading system for measuring plant disease. *Phytopathology* 35, 655.

Hubbard, J., Harman, G., and Hadar, Y. (1983). Effect of soilborne *Pseudomonas* spp. on the biological control agent, *Trichoderma hamatum*. on pea seeds. *Phytopathology* 73, 655–659. doi: 10.1094/Phyto-73-655

Inbar, J., Menendez, A., and Chet, I. (1996). Hyphal interaction between *Trichoderma harzianum* and *Sclerotinia sclerotiorum* and its role in biological control. *Soil Biol. Biochem.* 28, 757–763. doi: 10.1016/0038-0717(96)00010-7

Jacobsen, B. (2006). "Biological control of plant disease by phyllosphere applied biological control agents," in *Microbial Ecology, Aerial Plant Surfaces*, eds M. Bailey, A. Lilley, T. Timms-Wilson, and P. Spencer-Philips (London: CABI international), 133–147.

Jones, E. (1994). Fungal adhesion. *Mycol. Res.* 98, 961–981. doi: 10.1016/S0953-7562(09)80421-8

Kiss, L. (2003). A review of fungal antagonists of powdery mildews and their potential as biocontrol agents. *Pest Manag. Sci.* 59, 475–483. doi: 10.1002/ps.689

Lefebvre, F., Joly, D. L., Labbé, C., Teichmann, B., Linning, R., Belzile, F., et al. (2013). The transition from a phytopathogenic smut ancestor to an anamorphic biocontrol agent deciphered by comparative whole-genome analysis. *Plant Cell* 25, 1946–1959. doi: 10.1105/tpc.113.113969

Leroux, P., Fritz, R., Debieu, D., Albertini, C., Lanen, C., Bach, J., et al. (2002). Mechanisms of resistance to fungicides in field strains of *Botrytis cinerea*. *Pest Manag. Sci.* 58, 876–888. doi: 10.1002/ps.566

Lorenz, S., Guenther, M., Grumaz, C., Rupp, S., Zibek, S., and Sohn, K. (2014). Genome Sequence of the Basidiomycetous fungus *Pseudozyma aphidis* DSM70725, an efficient producer of biosurfactant mannosylerythritol lipids. *Genome Announc.* 2. doi: 10.1128/genomeA.00053-14

McGrath, M. T. (2001). Fungicide resistance in cucurbit powdery mildew: experiences and challenges. *Plant Dis.* 85, 236–245. doi: 10.1094/PDIS.2001.85.3.236

Morita, T., Fukuoka, T., Imura, T., and Kitamoto, D. (2013a). Accumulation of cellobiose lipids under nitrogen−limiting conditions by two ustilaginomycetous yeasts, *Pseudozyma aphidis* and *Pseudozyma hubeiensis*. *FEMS Yeast Res.* 13, 44–49. doi: 10.1111/1567-1364.12005

Morita, T., Koike, H., Hagiwara, H., Ito, E., Machida, M., Sato, S., et al. (2014). Genome and transcriptome analysis of the Basidiomycetous yeast *Pseudozyma*

antarctica producing extracellular glycolipids, mannosylerythritol lipids. *PLoS ONE* 9:e86490. doi: 10.1371/journal.pone.0086490

Morita, T., Koike, H., Koyama, Y., Hagiwara, H., Ito, E., Fukuoka, T., et al. (2013b). Genome sequence of the basidiomycetous yeast *Pseudozyma antarctica* T-34, a producer of the glycolipid biosurfactants mannosylerythritol lipids. *Genome Announc*. 1:e0006413. doi: 10.1128/genomeA.00064-13

Nickerson, K. W., Atkin, A. L., and Hornby, J. M. (2006). Quorum sensing in dimorphic fungi: farnesol and beyond. *Appl. Environ. Microbiol*. 72, 3805–3813. doi: 10.1128/AEM.02765-05

Paz, Z., Burdman, S., Gerson, U., and Sztejnberg, A. (2007). Antagonistic effects of the endophytic fungus Meira geulakonigii on the citrus rust mite Phyllocoptruta oleivora. *J. Appl. Microbiol*. 103, 2570–2579. doi: 10.1111/j.1365-2672.2007.03512.x

Perez-Garcia, A., Romero, D., Fernandez-Ortuno, D., Lopez-Ruiz, F., De Vicente, A., and Tores, J. A. (2009). The powdery mildew fungus *Podosphaera fusca* (synonym *Podosphaera xanthii*), a constant threat to cucurbits. *Mol. Plant Pathol*. 10, 153–160. doi: 10.1111/j.1364-3703.2008.00527.x

Pusey, P. L., Stockwell, V. O., and Mazzola, M. (2009). Epiphytic bacteria and yeasts on apple blossoms and their potential as antagonists of *Erwinia amylovora*. *Phytopathology* 99, 571–581. doi: 10.1094/PHYTO-99-5-0571

Raupach, G. S., Liu, L., Morphy, J. F., Tuzun, S., and Kloepper, J. W. (1996). Induced systemic resistance in cucumber and tomato against cucumber mosaic cucumovirus using plant growth-promoting rhizobacteria (PGPR). *Plant Dis*. 80, 891–894. doi: 10.1094/PD-80-0891

Robiglio, A., Sosa, M. C., Lutz, M. C., Lopes, C. A., and Sangorrin, M. P. (2011). Yeast biocontrol of fungal spoilage of pears stored at low temperature. *Int. J. Food Microbiol*. 147, 211–216. doi: 10.1016/j.ijfoodmicro.2011.04.007

Rotem, Y., Yarden, O., and Sztejnberg, A. (1999). The mycoparasite *Ampelomyces quisqualis* expresses *exgA* encoding an exo-β-1, 3-glucanase in culture and during mycoparasitism. *Phytopathology* 89, 631–638. doi: 10.1094/PHYTO.1999.89.8.631

Saika, A., Koike, H., Hori, T., Fukuoka, T., Sato, S., Habe, H., et al. (2014). Draft genome sequence of the yeast *Pseudozyma antarctica* type strain JCM10317, a producer of the glycolipid biosurfactants, mannosylerythritol lipids. *Genome Announc*. 2:e00878-14. doi: 10.1128/genomeA.00878-14

Shoresh, M., Harman, G. E., and Mastouri, F. (2010). Induced systemic resistance and plant responses to fungal biocontrol agents. *Annu. Rev. Phytopathol*. 48, 21–43. doi: 10.1146/annurev-phyto-073009-114450

Teichmann, B., Labbé, C., Lefebvre, F., Bölker, M., Linne, U., and Bélanger, R. R. (2011a). Identification of a biosynthesis gene cluster for flocculosin a cellobiose lipid produced by the biocontrol agent *Pseudozyma flocculosa*. *Mol. Microbiol*. 79, 1483–1495. doi: 10.1111/j.1365-2958.2010.07533.x

Teichmann, B., Lefebvre, F., Labbé, C., Bölker, M., Linne, U., and Bélanger, R. R. (2011b). Beta hydroxylation of glycolipids from *Ustilago maydis* and *Pseudozyma flocculosa* by an NADPH-dependent β-hydroxylase. *Appl. Environ. Microbiol*. 77, 7823–7829. doi: 10.1128/AEM.05822-11

Teichmann, B., Linne, U., Hewald, S., Marahiel, M. A., and Bölker, M. (2007). A biosynthetic gene cluster for a secreted cellobiose lipid with antifungal activity from *Ustilago maydis*. *Mol. Microbiol*. 66, 525–533. doi: 10.1111/j.1365-2958.2007.05941.x

Urquhart, E. J., and Punja, Z. K. (2002). Hydrolytic enzymes and antifungal compounds produced by Tilletiopsis species, phyllosphere yeasts that are antagonists of powdery mildew fungi. *Can. J. Microbiol*. 48, 219–229. doi: 10.1139/w02-008

Urquhart, E., and Punja, Z. (1997). Epiphytic growth and survival of Tilletiopsis pallescens, a potential biological control agent of Sphaerotheca fuliginea, on cucumber leawes. *Can. J. Bot*. 75, 892–901. doi: 10.1139/b97-099

Weigel, D., and Glazebrook, J. (2002). *Arabidopsis: A Laboratory Manual*. Cold Spring Harbor, NY: Cold Spring Harbor Laboratory Press.

Conflict of Interest Statement: The authors declare that the research was conducted in the absence of any commercial or financial relationships that could be construed as a potential conflict of interest.

frontiers in Plant Science

REVIEW
published: 21 June 2016
doi: 10.3389/fpls.2016.00906

Extracellular Recognition of Oomycetes during Biotrophic Infection of Plants

*Tom M. Raaymakers and Guido Van den Ackerveken**

Plant–Microbe Interactions, Department of Biology, Faculty of Science, Utrecht University, Utrecht, Netherlands

Extracellular recognition of pathogens by plants constitutes an important early detection system in plant immunity. Microbe-derived molecules, also named patterns, can be recognized by pattern recognition receptors (PRRs) on the host cell membrane that trigger plant immune responses. Most knowledge on extracellular pathogen detection by plants comes from research on bacterial and fungal pathogens. For oomycetes, that comprise some of the most destructive plant pathogens, mechanisms of extracellular pattern recognition have only emerged recently. These include newly recognized patterns, e.g., cellulose-binding elicitor lectin, necrosis and ethylene-inducing peptide 1-like proteins (NLPs), and glycoside hydrolase 12, as well as their receptors, e.g., the putative elicitin PRR elicitin response and the NLP PRR receptor-like protein 23. Immunity can also be triggered by the release of endogenous host-derived patterns, as a result of oomycete enzymes or damage. In this review we will describe the types of patterns, both pathogen-derived exogenous and plant-derived endogenous ones, and what is known about their extracellular detection during (hemi-)biotrophic oomycete infection of plants.

Keywords: oomycete pathogens, pattern recognition, MAMP/DAMP, plant disease resistance, secreted proteins, extracellular recognition

OPEN ACCESS

Edited by:
Pietro Daniele Spanu, Imperial College London, UK

Reviewed by:
Sebastian Schornack, University of Cambridge, UK
Helen Grace Pennington, The Sainsbury Laboratory, UK

***Correspondence:**
Guido Van den Ackerveken
g.vandenackerveken@uu.nl

Specialty section:
This article was submitted to Plant Biotic Interactions, a section of the journal Frontiers in Plant Science

Received: *03 May 2016*
Accepted: *08 June 2016*
Published: *21 June 2016*

Citation:
Raaymakers TM and Van den Ackerveken G (2016) Extracellular Recognition of Oomycetes during Biotrophic Infection of Plants. Front. Plant Sci. 7:906. doi: 10.3389/fpls.2016.00906

INTRODUCTION

Most plant pathogens are able to penetrate host tissues but essentially grow in the plant apoplast or extracellular space. Even haustoria, feeding structures formed by many biotrophic fungi and oomycetes that invaginate host cells, remain separated from the plant cell cytoplasm by the plant-derived extrahaustorial membrane (Parniske, 2000). It, therefore, comes as no surprise that a first line of pathogen recognition is extracellular and mediated by membrane-bound receptors that detect microbe- or host damage-derived molecules or patterns. Over the last decades, many pattern-recognition receptors mediating immunity to patterns of bacteria and fungi have been reported. Well known examples include the *Arabidopsis* receptor-like kinase (RLK) FLAGELLIN-SENSITIVE 2 (FLS2) that mediates recognition of bacterial flagellin, and the RLK, CHITIN ELICITOR RECEPTOR KINASE 1 (CERK1) involved in detection of fungal chitin (Zipfel, 2014). Flagellin and chitin are considered microbe-associated molecular patterns (MAMPs), while their cognate receptors are termed pattern-recognition receptors (PRRs; Jones and Dangl, 2006; Hein et al., 2009; Dodds and Rathjen, 2010). MAMPs are generally considered conserved molecules that occur in all species of a given taxon. There are, however, many examples of patterns that are species-specific or that are less well conserved, e.g., apoplastic effectors that are recognized by cognate resistance gene-encoded membrane-bound receptors (Thomma et al., 2011).

In this review we, therefore, refer to all extracellular molecules that trigger immunity as patterns (Cook et al., 2015). In older papers the term "elicitor" is most often used, but many of these can be regarded as patterns too (Boller and Felix, 2009; Cook et al., 2015). Although numerous oomycete patterns have been described, knowledge on the mechanism of their extracellular recognition has only emerged recently for some of them.

Oomycetes are filamentous organisms that belong to the Stramenopiles, a taxon that also encompasses the diatoms and brown algae. Many oomycetes are free-living saprobes in soils or aquatic environments. The best known oomycetes, or the most infamous ones, are species that are pathogenic on plants, e.g., the potato late blight pathogen *Phytophthora infestans* and the grape downy mildew *Plasmopara viticola* (Haas et al., 2009; Kamoun et al., 2015). Five main taxa of phytopathogenic oomycetes can be distinguished: (i) the genus *Phytophthora*, (ii) the downy mildews, (iii) the white blister rusts, (iv) the genus *Pythium*, and (v) the genus *Aphanomyces* (Thines and Kamoun, 2010).

In this review, we focus on the extracellular recognition of (hemi-)biotrophic oomycetes, on patterns that trigger immunity, and on mechanisms of pattern recognition. A broad range of molecules or patterns are released during oomycete infection of plants, either exogenous ones derived from the pathogen, or endogenous ones that are released from the plant host (**Figure 1**). The distinction between exogenous and endogenous signals can also be referred to as non-self and modified-self patterns (Schwessinger and Zipfel, 2008). Endogenous patterns, also known as damage-associated molecular patterns (DAMPs), either result from oomycete enzyme activities, or from lysis or disruption of host cells during the infection process. Oomycete patterns and other elicitors can be grouped based on their cellular origin (oomycete cell wall/membrane, or pathogen secreted). We will review the different patterns, their cellular origin, and what is known about the detection mechanisms that have evolved to recognize such patterns, and trigger the plant immune system.

OOMYCETE PATTERNS TRIGGERING IMMUNITY

Plants can sense a wide variety of extracellular oomycete-derived patterns. These molecules can be secreted by oomycetes during infection, or released from the invading pathogens by host-derived enzymes (**Table 1**). Several oomycete patterns are derived from the pathogen's cell wall or membrane, whereas others are secreted to the extracellular environment before being detected by the plant immune system. Below we discuss the different extracellular patterns, where they derive from, and what is known about their function.

Cell Wall/Membrane-Derived Patterns

β-Glucans

The most abundant constituents of oomycete cell walls are glucans, polysaccharides that consist of linked glucose units (Aronson et al., 1967; Sietsma et al., 1969). β-1,3 and β-1,6-glucan are the major components of oomycete cell walls, whereas cellulose, a β-1,4-glucan, forms a relatively small fraction (Aronson et al., 1967). β-1,6-Glucan is only found in oomycetes and fungi, whereas cellulose and β-1,3-glucan are present in plant cell walls too (Fesel and Zuccaro, 2015).

A β-glucan-triggered response, i.e., the accumulation of the phytoalexin glyceollin, was first observed when soybean (*Glycine max*) was treated with glucans isolated from cell walls of *Phytophthora sojae* (previously *P. megasperma* f. sp. *glycinea* and *P. megasperma* var. *sojae*) (Ayers et al., 1976). β-Glucans also trigger phytoalexin production in several other fabaceous species, and in potato (*Solanum tuberosum*), although this is a weaker response (Cline et al., 1978; Cosio et al., 1996). A purified β-1,3/1,6-glucan heptaglucoside was found to be one of the active molecules in eliciting production of phytoalexins in soybean (Sharp et al., 1984a,b). Laminarin, an oligomeric β-1,3-glucan with β-1,6-glucan branches isolated from the marine brown alga *Laminaria digitata*, is another pattern that can induce a plethora of defense-associated responses in *Nicotiana tabacum*, grapevine (*Vitis vinifera*), and the monocots rice (*Oryza sativa*) and wheat (*Triticum aestivum*; Inui et al., 1997; Klarzynski et al., 2000; Aziz et al., 2003). Furthermore, *Arabidopsis thaliana* is responsive to the β-glucan laminarin, although it does not respond to the oomycete-derived heptaglucoside elicitor. *Arabidopsis* responses to laminarin are mediated by the plant hormone ethylene, and do not seem to involve the well-known defense hormone salicylic acid (SA). In contrast, when *Arabidopsis* or tobacco plants are treated with a sulfated form of laminarin the expression of the SA-induced marker gene *PR1* is induced (Ménard et al., 2004). Taken together, responses to β-glucans vary greatly depending on the specific β-glucan and plant species. Therefore, different plant species might have different receptors involved in the recognition of different β-glucan patterns.

Phytophthora-derived β-1,3-glucan was shown to bind soybean membranes (Yoshikawa et al., 1983). The glucan-binding protein (GBP) from soybean was identified and it was demonstrated that, when expressed in tobacco and *Escherichia coli*, GBP conferred β-glucan-binding activity. Furthermore, an antibody raised against GBP inhibited β-glucan-binding activity in soybean and reduced phytoalexin accumulation (Umemoto et al., 1997). Interestingly, GBP also shows β-glucanase activity and might release β-glucans from the pathogen's cell wall (Fliegmann et al., 2004). After heterologous expression of soybean GBP in tomato, high affinity binding of the β-1,3/1,6-glucan heptaglucoside was observed. However, this did not result in activation of downstream defense responses in tomato (Mithöfer et al., 2000; Fliegmann et al., 2004). These data suggest that additional, probably membrane-bound, proteins are required to recognize the β-glucan patterns (Mithöfer et al., 2000).

Glucan-Chitosaccharides

Recently, glucan-chitosaccharides were isolated from the cell wall of the root oomycete *Aphanomyces euteiches* and were found as novel patterns that triggered calcium oscillations in the nucleus of root cells and induced defense genes in *Medicago truncatula* (Nars et al., 2013). How these molecules are perceived is not yet known, but there is a role for the nod factor perception (NFP) protein, a lysin motif (LysM)-RLK. NFP is

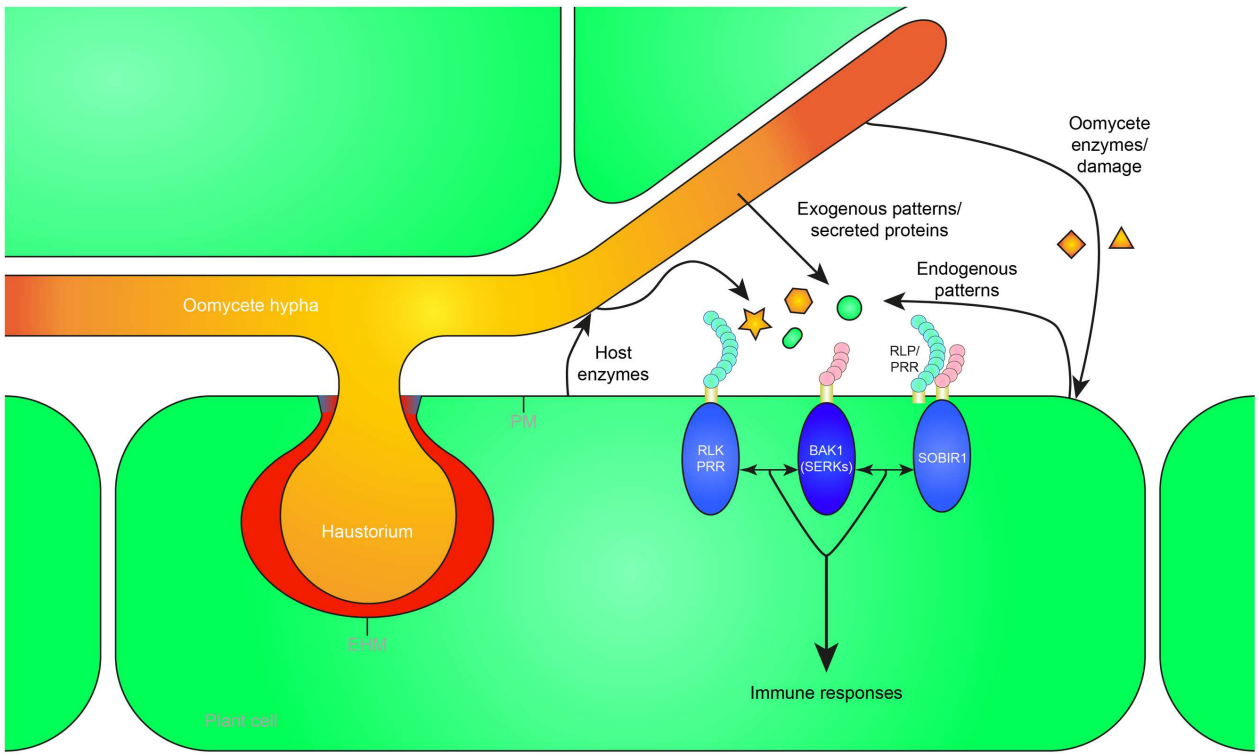

FIGURE 1 | Recognition of exogenous and endogenous patterns during oomycete infection leads to the activation of plant immunity. Oomycete pathogens secrete proteins in the apoplast (white) and extrahaustorial matrix (red) which can be perceived as exogenous patterns by pattern recognition receptors (PRRs) in the plant plasma membrane (PM) or extrahaustorial membrane (EHM). Furthermore, pathogen-derived cell wall or membrane fragments are released during infection, possibly by host enzymes, and recognized as patterns by the host. Mechanical damage or damage caused by oomycete secreted enzymes can release endogenous patterns that trigger immunity. The receptor-like kinase (RLK) BRI1-ASSOCIATED RECEPTOR KINASE 1 (BAK1), a member of the SOMATIC EMBRYOGENESIS RECEPTOR KINASE (SERK) family, functions as a central hub of RLK and receptor-like protein (RLP) triggered immunity. RLPs form a bimolecular receptor kinase with the RLK SUPPRESSOR OF BIR1 1 (SOBIR1). RLKs and RLPs bound to SOBIR1 associate with BAK1 to activate pattern-triggered immunity upon perception of exogenous or endogenous patterns. The haustorial callosic neckband that is sometimes formed in oomycete–plant interactions is depicted in blue. Oomycete-derived patterns and proteins are depicted in orange, plant-derived patterns in green.

involved in the recognition of microbial *N*-acetylglucosamine patterns and is required for nodule formation in interaction with *Rhizobium* bacteria. An *nfp* mutant was more susceptible to *A. euteiches*, whereas overexpression of *NFP* led to increased resistance, demonstrating its involvement in the perception of *A. euteiches* by *M. truncatula* (Rey et al., 2013). However, NFP was not required for the glucan-chitosaccharide-induced calcium oscillations, suggesting a regulatory function in defense for NFP rather than direct recognition (Nars et al., 2013).

Transglutaminases (Pep-13)

Transglutaminases (TGases) are a widespread family of enzymes, found in prokaryotes and eukaryotes, that facilitate cross-linking between glutamine and lysine residues in proteins, thereby strengthening structures, e.g., cell walls (Lorand and Graham, 2003; Martins et al., 2014). The formation of a covalent bond between amino acid residues confers high resistance to proteolysis (Reiss et al., 2011). In oomycetes, TGases could protect cell walls from hydrolytic host enzymes. A 42-kDa TGase cell wall glycoprotein (GP42) of *P. sojae* functions as a potent elicitor of phytoalexin synthesis in the non-host parsley (*Petroselinum crispum*) (Parker et al., 1991). A 13-amino acid peptide fragment (Pep-13) derived from GP42 was found responsible for triggering immunity and was shown to bind to purified plasma membranes of parsley. Furthermore, Pep-13 elicits a multitude of defense responses, e.g., expression of defense-related genes and phytoalexin production (Nürnberger et al., 1994, 1995; Hahlbrock et al., 1995). Interestingly, Pep-13 treatment of potato resulted in a similar defense activation, with the distinct difference that it induced a hypersensitive response (HR; Halim et al., 2004).

GP42 homologs are only found in oomycetes and some marine bacteria belonging to the genus *Vibrio* that are pathogenic on fish and several marine invertebrates (Reiss et al., 2011). It is thought that an ancestral oomycete, from which species of *Phytophthora*, *Pythium* and downy mildews have evolved, acquired GP42 from *Vibrio* bacteria through horizontal gene transfer, giving an selective advantage over oomycetes that lack this TGase (Reiss et al., 2011). A 100 kDa monomeric plasma membrane protein from parsley was shown to bind to the Pep-13 ligand and thus may be part of the putative receptor complex (Nennstiel et al., 1998).

TABLE 1 | Oomycete patterns that activate plant immunity.

Elicitor[a]	Source	Type	(Putative) Receptor[b]	Receptor type[c]	Co-receptors[d]	Reference
β-Glucans	Cell wall	Carbohydrate	GBP, additional components required	GH16		Fesel and Zuccaro, 2015
Glucan-chitosaccharides	Cell wall	Carbohydrate	Unknown			Nars et al., 2013
Pep-13	Cell wall	Peptide	Unknown monomeric 100 kDa integral plasma membrane protein			Reiss et al., 2011
Eicosapolyenoic acids	Membrane	Fatty acid	Unknown			Robinson and Bostock, 2015
GH12 (XEG1)	Secreted protein	Protein	Unknown		SERK3/BAK1 required	Ma et al., 2015
nlp20/nlp24	Secreted protein	Peptide	RLP23	RLP	BAK1 and SOBIR1 required	Albert et al., 2015
Elicitins	Secreted protein	Protein	ELR	RLP	BAK1 and SOBIR1 required	Du et al., 2015
CBM1/CBEL	Secreted protein	Protein	Unknown		partially requires BAK1	Larroque et al., 2013
OPEL	Secreted protein	Protein	Unknown			Chang et al., 2015

[a]*GH12 = glycoside hydrolase family 12; XEG1 = xyloglucanspecific endo-β-1,4-glucanase; nlp = necrosis and ethylene-inducing peptide 1-like protein; CBM1 = carbohydrate binding module 1; CBEL = cellulose-binding elicitor lectin.*
[b]*GBP = Glucan Binding Protein; RLP23 = receptor-like protein 23; ELR = elicitin response.*
[c]*GH16 = glycoside hydrolase family 16; RLP = receptor-like protein.*
[d]*SERK3 = SOMATIC EMBRYOGENESIS RECEPTOR-LIKE KINASE 3; BAK1 = BRI1-ASSOCIATED RECEPTOR KINASE; SOBIR1 = SUPPRESSOR OF BIR1 1.*

Eicosapolyenoic Acids

Application of mycelial extracts from *P. infestans* to potato tubers led to necrosis and accumulation of phytoalexins, predominantly rishitin, and lubimin. The molecules responsible for triggering this response were identified as the eicosapolyenoic acids (EPs), arachidonic acid (AA), and eicosapentaenoic acid (EPA; Bostock et al., 1981). Treating potato tuber slices with AA greatly reduced or even arrested growth of *P. infestans* (Bostock et al., 1982). EPs are components of *Phytophthora* cells and are seemingly not present in other microbial classes nor are they produced by higher plants (Robinson and Bostock, 2015). Interestingly, the downy mildew *Hyaloperonospora arabidopsidis* has lost the genes required for AA synthesis (Baxter et al., 2010). It is tempting to speculate that *H. arabidopsidis* has lost this ability through evolution as a way to avoid recognition.

Eicosapolyenoic acids induce the accumulation of antimicrobial compounds in many plant species, ranging from many solanaceous species, e.g., potato and tomato, to bean (*Phaseolus vulgaris*) and avocado (*Persea americana*) (Longland et al., 1987; Romero-Correa et al., 2014; Robinson and Bostock, 2015). Furthermore, in potato application of AA induced accumulation of reactive oxygen species (ROS), that could be involved in mediating synthesis of the phytoalexin rishitin from lubimin (Yoshioka et al., 2001).

EPs are able to trigger systemic acquired resistance in several plants species to different pathogens. The hormonal regulation of these responses seems to differ among plant species; in some the SA pathway is elicited, whereas in other species responses seem to rely on jasmonic acid (JA) or ethylene. It is postulated that this may be due to the concentration of EPs in the treatment (Robinson and Bostock, 2015). For example, *Arabidopsis* plants made to produce low levels of EP showed increased resistance to *Botrytis cinerea*, *P. capsici* and aphid feeding, but higher susceptibility to *Pseudomonas syringae* pv. *tomato* (DC3000). This was associated with higher levels of JA and enhanced expression of JA-related genes, but decreased SA levels and reduced expression of SA-related genes. Furthermore, low levels of AA administered to tomato leaves resulted in increased JA levels and decreased SA levels and higher resistance against *Botrytis cinerea* (Savchenko et al., 2010).

How, exactly, EPs are perceived remains to be resolved. EPs could be recognized directly by a membrane-bound receptor, leading to the activation of plant immunity. Another possibility is that plant membranes that readily incorporate AA (Ricker and Bostock, 1992), are perturbed leading to the release of endogenous patterns from the host cell cytoplasm. Or alternatively, AA can be used as a substrate for lipoxygenases, e.g., the potato LOX1, thereby producing oxylipin signals that trigger plant immunity. In the latter two scenarios recognition would be independent of plant PRRs (Robinson and Bostock, 2015).

Interestingly, treating potato with a combination of AA and β-1,3-glucans strongly increased the response to AA. β-glucans alone, however, did not trigger a response in potato (Preisig and Kuć, 1988).

Secreted Proteins

Glycoside Hydrolase 12 Proteins

Recently, the XEG1 (xyloglucanspecific endo-β-1,4-glucanase) protein was isolated from *P. sojae* culture filtrates (Ma et al., 2015). This secreted protein elicits cell death in *N. benthamiana*, *N. tabacum*, pepper (*Capsicum annuum*), tomato (*S. lycopersicon*) and soybean but not in maize (*Zea mays*) and cotton (*Gossypium hirsutum*). Analysis of the XEG1 protein sequence revealed that it belongs to the glycoside hydrolase GH12 family that is widespread amongst prokaryotic and eukaryotic microbes, especially in plant-associated microorganisms. Within the *Phytophthora* genus many GH12 proteins are found of which half trigger cell death in *N. benthamiana.* The downy

mildew *H. arabidopsidis* also has three GH12 genes, however, none of them encode a protein that elicits cell death (Ma et al., 2015). Previously, it was demonstrated that fungal GH12 proteins are able to degrade β-glucan (Karlsson et al., 2002) and xyloglucan, a hemicellulose found in the plant cell wall (Master et al., 2008). Recombinant XEG1 protein partially released reducing sugars from both glucans, but was most active with a xyloglucan substrate. Mutations in the catalytic site of XEG1 strongly decreased xyloglucanase activity and abolished β-glucanase activity. In contrast, XEG1 enzyme activity was not required for the induction of cell death in *N. benthamiana* and soybean. Moreover, active and inactive recombinant XEG1 were able to induce resistance against *P. sojae* and *Phytophthora parasitica* var. *nicotianae* to a similar extent in soybean and *N. benthamiana,* respectively. Silencing as well as overexpression of XEG1 in *P. sojae* both led to reduced virulence on soybean through distinct mechanisms. Silenced *P. sojae* lines showed reduced virulence, but did not activate a stronger defense response in soybean, suggesting that XEG1 has a role in virulence, possibly through breakdown of cell wall components. XEG1 overexpression transformants induced more ROS accumulation and callose deposition compared to wildtype *P. sojae*, confirming the idea that XEG1 acts as a MAMP. A XEG1 PRR has not been identified but XEG1 requires the co-receptor SOMATIC EMBRYOGENESIS RECEPTOR-LIKE KINASE 3/BRI1-ASSOCIATED RECEPTOR KINASE (SERK3/BAK1) for triggering cell death, suggesting that a SERK3/BAK1-associated RLK or RLP recognizes XEG1 (Ma et al., 2015).

Necrosis and Ethylene-Inducing Peptide 1 (Nep1)-Like Proteins

Necrosis and ethylene-inducing peptide 1 (Nep1)-like proteins (NLPs) form a family of secreted proteins mainly found in plant-associated microorganisms, and cytotoxic members are well known to induce necrosis and ethylene production in dicot plants (Bailey, 1995; Oome and Van den Ackerveken, 2014). Three types of NLPs have been identified: type 1 NLPs are found in bacteria, oomycetes and fungi, type 2 NLPs are found in fungi and bacteria and the newly identified type 3 NLPs are only present in fungi (Oome and Van den Ackerveken, 2014). Although many members of the NLP family are cytotoxic to plants, in recent years many non-cytoxic NLPs have been identified in fungal and oomycete species with a (hemi-)biotrophic lifestyle (Cabral et al., 2012; Dong et al., 2012; Zhou et al., 2012). In search of the function of 10 non-cytotoxic NLPs of the obligate biotrophic downy mildew *H. arabidopsidis* (HaNLPs) it was found that NLPs activate plant immunity in *Arabidopsis* (Oome et al., 2014). Expression of *HaNLPs* in *Arabidopsis* led to a severe growth reduction and increased resistance to *H. arabidopsidis* for 7 out of 10 HaNLPs. Only a small fragment of the tested HaNLP3 protein was sufficient to activate plant defense responses and immunity to downy mildew. This 20–24 amino acid fragment (nlp20/nlp24) contains two conserved regions. The second region is the heptapeptide motif GHRHDWE which is highly conserved in all NLPs (Oome and Van den Ackerveken, 2014). The first motif that starts with the AIMY amino acid sequence is highly conserved in type 1 NLPs (Oome et al., 2014). Treatment of *Arabidopsis* plants with synthetic nlp24 peptides corresponding to an oomycete, fungal and bacterial type 1 NLP resulted in the increased production of the defense-related phytohormone ethylene and high resistance to downy mildew. Conversely, a synthetic peptide of a type 2 NLP from the bacterial pathogen *Pectobacterium carotovorum* that lacks the AIMY motif was unable to elicit a response in *Arabidopsis*. Taken together, this demonstrated that the first motif contains the immunogenic part of nlp24 (Oome et al., 2014). Furthermore, nlp20, a peptide based on *Pp*NLP, a cytotoxic *P. parasitica* type 1 NLP, was sufficient for MAPK activation, production of ROS, and increased callose deposition in *Arabidopsis*, but did not have any cytotoxic effect (Böhm et al., 2014). Other plant species were tested for their ability to respond to nlp peptides, revealing that nlp-triggered ethylene production was observed in several closely related Brassicaceae species, and also in more distantly related lettuce plants (*Lactuca sativa*), but not in solanaceous species such as tomato, potato, and *N. benthamiana* (Böhm et al., 2014).

In a screen for nlp20 sensitivity, a collection of T-DNA insertion mutants corresponding to 29 RLKs and 44 RLPs were tested for loss of nlp20-induced ethylene production. Furthermore, 135 natural accessions of *Arabidopsis* were also tested for the loss of nlp20 sensitivity. Two T-DNA insertion alleles of *RLP23*, *rlp23-1*, and *rlp23-2* that were unable to express the receptor-like protein as well as three *Arabidopsis* accessions that carried a frameshift mutation resulting in a premature stop codon in *RLP23* coding sequence were insensitive to nlp20. It was shown that the RLP23 LRR domain physically interacts with nlp20 *in vitro* and *in planta* (Albert et al., 2015). RLP23 lacks a cytoplasmic signaling domain but was shown to require the RLK SUPPRESSOR OF BIR1 1 (SOBIR1) for signaling. RLP23 and SOBIR1 interact in the absence of nlp peptides (Bi et al., 2014; Albert et al., 2015), whereas a second RLK, BAK1, was recruited only in presence of the ligand (Albert et al., 2015). *Arabidopsis sobir1* and *bak1-5/bkk1* mutants lost nlp20-responsiveness, indicating that SOBIR1 and BAK1 are required for RLP23 to function. Moreover, it was demonstrated that RLP23 is required for nlp peptide-induced resistance. Unlike wildtype *Arabidopsis*, nlp24-treatment of *rlp23* mutants did not result in an increased resistance to *H. arabidopsidis* (Albert et al., 2015).

Elicitins

Many oomycete pathogens secrete small 10 kDa proteins called elicitins. The first proteins from this family identified were cryptogein and capsicein from *Phytophthora cryptogea* and *Phytophthora capsici,* respectively. These proteins were found to elicit necrosis, induce resistance, and cause increased production of ethylene as well as the phytoalexin capsidiol in tobacco plants (Ricci et al., 1989; Milat et al., 1991). Elicitin responses were observed in all tested *Nicotiana* spp., but not in other solanaceous species, such as tomato and eggplant. Furthermore, some Brassicaceae species also respond to elicitin; most radish cultivars (*Raphanus sativus*) and one turnip cultivar (*Brassica campestris*), but not *Arabidopsis*, showed necrosis after elicitin treatment (Kamoun et al., 1993). The gene encoding for *P. infestans* elicitin INF1 was found to be downregulated during early infection of

potato. However, in the necrotrophic phase of infection *inf1* expression was upregulated (Kamoun et al., 1997). Interestingly, *N. benthamiana*, a nonhost of *P. infestans*, gained susceptibility after silencing of *inf1*, demonstrating that the recognition of INF1 contributes to resistance (Kamoun et al., 1998).

Members of the Peronosporales, e.g., *Phytophthora* spp. and downy mildews are unable to synthesize sterols and must, therefore, acquire them during pathogenesis. Elicitin and elicitin-like sequences are also found in downy mildew pathogens, but no functional analysis has been performed on these proteins (Baxter et al., 2010; Cabral et al., 2011; Stassen et al., 2012; Sharma et al., 2015). Dehydroergosterol binding activity was shown for several elicitins *in vitro*. Furthermore, elicitins are able to catalyze sterol transfer between liposomes (Mikes et al., 1998). However, *in vivo* sterol-binding activity of elicitins has not been demonstrated. Interestingly, the oomycete pathogen *A. euteiches* is able to synthesize sterols and seems to lack elicitin genes (Gaulin et al., 2008, 2010).

The putative elicitin receptor was recently cloned from a wild potato (*Solanum*) that responds to the *P. infestans* elicitin INF1. A *S. microdontum* ecotype showed a clear cell-death response when *inf1* was transiently expressed. Crosses with an unresponsive *S. microdontum* subspecies and further screening and genetic mapping resulted in the identification of the RLP ELR (elicitin response). Stable expression of ELR in *S. tuberosum* cv. Désirée conferred the cell death response after expression of *inf1*. Furthermore, ELR mediated a broad-spectrum response to elicitins of oomycetes: most tested elicitins induced a cell-death response in transgenic ELR potato, even though there is often low sequence similarity between elicitins (Du et al., 2015). Recognition might therefore be based on structural similarity rather than a small conserved peptide. ELR was shown to bind to SERK3/BAK1, but binding of the putative receptor to the RLP adaptor protein SOBIR1 or the elicitin ligand was not tested (Du et al., 2015). Intracellular perception, however, cannot be ruled out as elicitins have, anecdotally, been reported to be detected inside plant cells, e.g., the immunocytochemical localization of the elicitin quercinin in oak (*Quercus robur*) root cells infected with *P. quercina* (Brummer et al., 2002). ELR is thought to mediate extracellular recognition of elicitins, but direct binding to confirm the receptor function of ELR still needs to be demonstrated (Du et al., 2015). Previously, studies in tobacco suggested that INF1 binds to the cytoplasmic domain of a lectin RLK from *N. benthamiana*, NbLRK1 (Kanzaki et al., 2008). Silencing of *NbLRK1* resulted in reduced INF1 responsiveness suggesting the RLK contributes to defense signaling. Although no ELR has been identified in tobacco yet, SERK3/BAK1 and SOBIR1 were found to be required for elicitin-triggered cell death in *N. benthamiana* (Chaparro-Garcia et al., 2011; Peng et al., 2015). It is, therefore, likely that ELR acts similar to RLP23 (Albert et al., 2015) and tomato Cf-4 (Postma et al., 2016), in that it requires both a BAK1-like RLK and SOBIR1-like RLK for pattern-triggered immunity.

Cellulose-Binding Elicitor Lectin

A 34 kDa glycoprotein was isolated from *P. parasitica* var. *nicotianae* mycelium that triggered enhanced lipoxygenase activity as well as accumulation the defense-related cell wall hydroxyproline-rich glycoproteins in tobacco. This protein was localized to the internal and external layers of the hyphal cell wall (Séjalon-Delmas et al., 1997). The protein sequence revealed two cellulose-binding domains belonging to the carbohydrate binding module 1 (CBM1) family similar to that of fungal glycanases (Mateos et al., 1997; Gaulin et al., 2006). This putative function was corroborated by demonstrating protein binding to fibrous cellulose and plant cell walls. Furthermore, the protein was shown to have lectin-like activities; human red blood cells were readily agglutinated by this protein. Therefore, it was designated cellulose-binding elicitor lectin (CBEL). Moreover, CBEL was able to elicit necrosis, activate defense gene expression, and trigger immunity to *P. parasitica* var. *nicotianae*. No enzymatic activities for CBEL were observed, suggesting it acts as a pattern (Mateos et al., 1997).

Silencing of *CBEL* resulted in a severe reduction of adhesive abilities of *P. parasitica* var. *nicotianae* to cellulosic surfaces, but did not affect pathogenicity. Interestingly, knockdown mutants showed dispersed abnormal cell wall thickenings, indicating that CBEL might be involved in cell wall deposition in the pathogen (Gaulin et al., 2002). CBEL activity as a pattern is not limited to tobacco, as infiltration of CBEL in *Arabidopsis* leaves resulted in defense responses differentially dependent on the phytohormones SA, JA, and ethylene (Khatib et al., 2004). CBEL-induced necrosis was lost in JA-insensitive *coi1* and ethylene-insensitive *ein2* mutant plants, whereas *PR1* and *WAK1* expression, accumulation hydroxyproline-rich glycoproteins, and peroxidase activity was greatly reduced or abolished in an *Arabidopsis NahG* mutant that metabolizes SA (Khatib et al., 2004). Transient expression of *CBEL* as well as infiltration of recombinant CBEL in tobacco leaves resulted in rapid development of necrotic lesions. Immunocytochemistry revealed that the delivered CBEL was bound to the plant cell wall. Substitution of aromatic residues in CBEL that are possibly involved in cellulose binding reduced the necrosis-inducing activity. Necrosis-induction in tobacco was lost for three recombinant CBEL proteins (Y52A, Y188A, and Y52A_Y188A), that were also unable to induce defense-related genes at similar concentrations as native CBEL. Recently, it was shown that CBM1-1 is the main determinant in the interaction with cellulose; a mutation in CBM1-2 (Y188A) only showed a slight decrease in cellulose binding compared to wild type CBEL, whereas a mutation in CBM1-1 (Y52A) strongly decreased the binding capacity of CBEL and the double mutant (Y52A_Y188A) entirely lost the ability to bind cellulose (Martinez et al., 2015). Taken together, these data show amino acids in the two CBM1s, that were predicted to be important for cellulose binding, are important for elicitor activity.

To define the minimum CBEL pattern that triggers immunity, synthetic peptides of CBM1-1 and CBM1-2 were generated. CBM1-1synt and CBM1-2synt were sufficient to activate plant defense in tobacco and *Arabidopsis*, respectively. Intriguingly, recombinant CBEL but not recombinant CBEL_Y52A_Y188A, induced calcium fluxes in tobacco cells but not in protoplasts. This demonstrates that the plant cell wall and unmodified

CBM1s are important for CBEL perception (Gaulin et al., 2006).

CBM1s are probably not essential for pathogens with an obligate biotrophic lifestyle; only one was detected in the *Albugo laibachii* genome and no clear CBM1-encoding genes were found in *H. arabidopsidis*, whereas *Pythium ultimum* and *Phytophthora* spp. contain multiple CBM1-encoding genes (Larroque et al., 2012). It has been proposed that adhesion of CBEL or its CBM1s perturb the cellulose status, and the perception of this disturbance leads to defense activation, but this remains to be proven (Dumas et al., 2008). The fact that BAK1 and RESPIRATORY BURST OXIDASE HOMOLOGUE (RBOH) D and F proteins are required for some of the CBEL-induced defense responses suggests that a PRR might be involved (Larroque et al., 2013). The oxidative burst triggered by pattern recognition is mediated by the NADPH oxidases RBOH D and F (Suzuki et al., 2011). Necrosis-induction by CBEL in *bak1-4* and the *rbohD/F* double mutant was similar to the Col-0 *Arabidopsis* wildtype. However, no ROS production was detected in *bak1-4* and *rbohD/F* and activation of MAP kinases was reduced in *bak1-4* and delayed in *rbohD/F* compared to Col-0. The expression of JA-responsive genes *WRKY11* and *PDF1.2*, but not the expression of the SA-responsive gene *PR1,* was also reduced in these mutant lines (Larroque et al., 2013). The dependence of some CBEL-induced responses on BAK1 suggests a role for an RLK or RLP in the perception of CBEL. Three *Arabidopsis* accessions were found that are unresponsive to CBEL, and may therefore offer a way to decipher CBEL-triggered immunity (Larroque et al., 2013).

OPEL

A secreted apoplastic protein from *P. parasitica* called OPEL was recently discovered to trigger a plant immune response (Chang et al., 2015). OPEL contains a thaumatin-like domain, a glycine-rich domain, and a glycosyl hydrolase (GH) domain that has a putative laminarinase active site. OPEL seems to be oomycete specific; homologues were only found in *Phytophthora* spp. and other oomycetes such as *H. arabidopsidis, Py. ultimum* and *A. laibachii*. OPEL is expressed during early infection stages of *P. parasitica*, rapidly increasing transcript levels within 12 hours after inoculation on *N. benthamiana*. Furthermore, infiltration of *N. tabacum* with recombinant OPEL protein resulted in cell death, increased callose deposition, ROS accumulation, induction of defense-related genes and systemic acquired resistance against several pathogens. Moreover, transient expression of *OPEL* in *N. benthamiana* enhanced resistance to *P. parasitica*. It was shown that the GH domain was essential for the increased callose deposition and increased accumulation of ROS in *N. tabacum*. Although the OPEL GH domain contains a laminarinase signature active site motif, no laminarin or β-1,3-glucan enzymatic activity was detected in OPEL recombinant protein. Mutation of the putative laminarinase active site motif in the predicted GH domain abolished elicitor activity of OPEL, which suggests enzymatic activity of OPEL is required for triggering the defense response (Chang et al., 2015). The OPEL substrate has not been identified but is likely a polysaccharide in the plant cell wall. OPEL-released degradation products might, therefore, be perceived by plants as DAMPs.

ENDOGENOUS PATTERNS

Next to exogenous patterns, host-derived molecules that are released upon pathogen infection can serve as danger signals (**Table 2**). Several endogenous patterns, also known as DAMPs, have been described that are plant cell wall derived or that are released from the host cytosol (Boller and Felix, 2009; Yamaguchi and Huffaker, 2011). The release of these patterns is promoted by a plethora of hydrolytic enzymes that are produced by pathogens (Baxter et al., 2010; Blackman et al., 2015). Interestingly, the downy mildew *H. arabidopsidis* has fewer hydrolases than the hemibiotrophic *Phytophthora* spp., probably as adaptation to its obligate biotrophic lifestyle (Baxter et al., 2010).

Oligogalacturonides (OGs) are released from the plant cell wall after mechanical damage or by pathogen-secreted hydrolytic enzymes through degradation of homogalacturonan (Ferrari et al., 2013). OGs bind to several members of the cell wall-associated kinase (WAK) family, which consequently leads to the activation of immunity (Brutus et al., 2010; Ferrari et al., 2013). Also cutin, the main constituent of the plant cuticle (Heredia, 2003), can be degraded to cutin monomers by pathogen released cutinases. Cutin monomers are potent elicitors of defense in several plant species (Schweizer et al., 1996; Fauth et al., 1998). However, it remains unknown how cutin monomers are recognized by plants.

Damage patterns could also be released from the plant cytosol during oomycete infection. These include members of the plant elicitor peptide (Pep) family. The cytosolic precursors of Peps, PROPEPS are released and cleaved when the plant cell is damaged, resulting in the production of endogenous

TABLE 2 | Plant-derived patterns that trigger plant immunity.

Elicitor[a]	Type	Receptor[b]	Receptor type[c]	Source	Reference
Oligogalacturonides	Carbohydrate	WAK1	EGF-like	Cell wall	Ferrari et al., 2013
Cutin monomers	Fatty alcohol	Unknown		Cell wall	Fauth et al., 1998
Peps	Peptide	PEPR1/PEPR2	RLK	Cytosol	Bartels and Boller, 2015
Extracellular ATP	Nucleoside triphosphate	DORN1/LecRK-I.9	LecRK	Cytosol	Choi et al., 2014

[a]*ATP = Adenosine triphosphate.*
[b]*WAK1 = CELL WALL-ASSOCIATED KINASE 1; PEPR1/PEPR2 = PEP1 RECEPTOR 1/PEP1 RECEPTOR 2; DORN1 = Does Not Respond to Nucleotides 1; LecRK-I.9 = lectin receptor kinase clade 1.9.*
[c]*EGF = epidermal growth factor; RLK = receptor-like kinase; LecRK = lectin receptor kinase.*

patterns. The receptors for Peps have been identified, the RLKs PEP1 RECEPTOR 1 (PEPR1) and PEP1 RECEPTOR 2 (PEPR2) recognized Peps and contributed to immune responses against several pathogens (Yamaguchi et al., 2006, 2010; Krol et al., 2010; Yamaguchi and Huffaker, 2011; Albert, 2013; Bartels et al., 2013; Bartels and Boller, 2015).

Furthermore, extracellular adenosine triphosphate (eATP) could be perceived as a damage pattern. Treatment of *Arabidopsis* with ATP induced a similar set of genes as wounding did (Choi et al., 2014). In a screen for ATP-insensitivity, a *dorn1* (Does Not Respond to Nucleotides 1) mutant was identified that is defective in the lectin receptor kinase LecRK-I.9. LecRK-I.9 binds to ATP with high affinity and is required for the activation of several ATP-induced responses, demonstrating it is an ATP receptor (Choi et al., 2014). Previously, *lecrk-I.9* mutants were shown to be more susceptible to two *Phytophthora* species than wildtype *Arabidopsis*. Conversely, overexpression of *LecRK-I.9* led to increased resistance to *P. brassicae* (Bouwmeester et al., 2011).

Finally, it has been proposed that recognition of the exogenous pattern β-1,3-glucan could have evolved as an endogenous danger signal; callose could be degraded by host or pathogen-derived β-1,3-glucanases, thereby eliciting a defense response (Klarzynski et al., 2000).

PUTATIVE RECEPTOR PROTEINS

Plant genomes encode many RLKs and RLPs. The *Arabidopsis* genome, for example, encodes more than 600 RLKs and 57 RLPs (Shiu et al., 2004; Wang et al., 2008). For most of these proteins the function is unknown. We expect that several of these receptor proteins have a role in the perception of oomycete pathogens. Recently, it was shown that many *RLP* genes are upregulated after treatment with *P. infestans* and the *P. infestans* NLP NPP1, suggesting a role for these RLPs during oomycete infection (Wu et al., 2016). Several RLKs are also reported to affect the interaction with oomycete pathogens. For example, other LecRKs, next to the aforementioned LecRK-I.9 and NbLRK1, influence the defense response against *Phytophthora* in *Arabidopsis*, tomato and *N. benthamiana* (Wang et al., 2014, 2015b,a). Silencing of several LecRKs in tomato and *N. benthamiana* led to increased susceptibility to *P. capsici* and *P. infestans*, respectively (Wang et al., 2015b). Two *Arabidopsis* LecRKs from the same clade (IX) were shown to affect *Phytophthora* resistance in a similar way (Wang et al., 2015a). Finally, the *Arabidopsis* LecRK-VI.2A positively regulates the MAMP-triggered immunity response (Singh et al., 2012). Although, some RLKs and RLPs partly regulate the defense response against oomycetes, the patterns or molecules that are recognized by these proteins are still largely unknown.

CONCLUSIONS AND PERSPECTIVES

Recent discoveries in extracellular recognition of oomycete patterns have provided new insight in how plants detect early infection of these (hemi-)biotrophic pathogens. Novel PRRs for elicitins and NLPs have been identified and mechanisms of how these exogenous patterns are perceived by plants have been elucidated. The scientific progress described in this review provides interesting leads for resistance breeding of crops. For example, transgenic expression of the PRRs ELR and RLP23 in cultivated potato resulted in increased resistance to the late blight pathogen *P. infestans* that is known to produce elicitins and NLPs (Haas et al., 2009; Albert et al., 2015; Du et al., 2015). Classical resistance breeding has mainly focused on the introgression of resistance genes encoding cytoplasmic NB-LRR receptors, which are rapidly broken by new emerging strains of the pathogen. The use of PRRs, many of which recognize conserved microbial patterns, for breeding a new generation of disease resistant crops could offer a more durable solution, especially if PRRs and resistance genes are stacked (Dangl et al., 2013; Schwessinger et al., 2015). A great example is the expression of the *Arabidopsis* PRR EFR in tomato that resulted in broad spectrum resistance to different bacterial pathogens that all produce the EF-Tu pattern that is recognized by EFR (Lacombe et al., 2010). As many of the described oomycete patterns are broadly distributed, expression of the cognate PRRs in crops could reduce plant disease and aid in securing our future food.

AUTHOR CONTRIBUTIONS

All authors listed, have made substantial, direct and intellectual contribution to the work, and approved it for publication.

FUNDING

The authors of this review are supported by the Less is More grant no. 847.13.006 of the Netherlands Organization for Scientific Research.

REFERENCES

Albert, I., Böhm, H., Albert, M., Feiler, C. E., Imkampe, J., Wallmeroth, N., et al. (2015). An RLP23–SOBIR1–BAK1 complex mediates NLP-triggered immunity. *Nat. Plants* 1:15140. doi: 10.1038/nplants.2015.140

Albert, M. (2013). Peptides as triggers of plant defence. *J. Exp. Bot.* 64, 5269–5279. doi: 10.1093/jxb/ert275

Aronson, J. M., Cooper, B. A., and Fuller, M. S. (1967). Glucans of oomycete cell walls. *Science* 155, 332–335. doi: 10.1126/science.155.3760.332

Ayers, A. R., Ebel, J., Valent, B., and Albersheim, P. (1976). Host-pathogen interactions X. fractionation and biological activity of an elicitor isolated from the mycelial walls of *Phytophthora megasperma* var. *sojae*. *Plant Physiol.* 57, 760–765. doi: 10.1104/pp.57.5.760

Aziz, A., Poinssot, B., Daire, X., Adrian, M., Bézier, A., Lambert, B., et al. (2003). Laminarin elicits defense responses in grapevine and induces protection against *Botrytis cinerea* and *Plasmopara viticola*. *Mol. Plant Microbe Interact.* 16, 1118–1128. doi: 10.1094/MPMI.2003.16.12.1118

Bailey, B. A. (1995). Purification of a protein from culture filtrates of *Fusarium oxysporum* that induces ethylene and necrosis in leaves of *Erythroxylum coca*. *Phytopathology* 85:1250. doi: 10.1094/Phyto-85-1250

Bartels, S., and Boller, T. (2015). Quo vadis, pep? Plant elicitor peptides at the crossroads of immunity, stress, and development. *J. Exp. Bot.* 66, 5183–5193. doi: 10.1093/jxb/erv180

Bartels, S., Lori, M., Mbengue, M., van Verk, M., Klauser, D., Hander, T., et al. (2013). The family of Peps and their precursors in *Arabidopsis*: differential expression and localization but similar induction of pattern-triggered immune responses. *J. Exp. Bot.* 64, 5309–5321. doi: 10.1093/jxb/ert330

Baxter, L., Tripathy, S., Ishaque, N., Boot, N., Cabral, A., Kemen, E., et al. (2010). Signatures of adaptation to obligate biotrophy in the *Hyaloperonospora arabidopsidis* genome. *Science* 330, 1549–1551. doi: 10.1126/science.1195203

Bi, G., Liebrand, T. W., Cordewener, J. H., America, A. H., Xu, X., and Joosten, M. H. (2014). *Arabidopsis thaliana* receptor-like protein *At*RLP23 associates with the receptor-like kinase *At*SOBIR1. *Plant Signal. Behav.* 9:e27937. doi: 10.4161/psb.27937

Blackman, L. M., Cullerne, D. P., Torreña, P., Taylor, J., and Hardham, A. R. (2015). RNA-seq analysis of the expression of genes encoding cell wall degrading enzymes during infection of lupin (*Lupinus angustifolius*) by *Phytophthora parasitica*. *PLoS ONE* 10:e0136899. doi: 10.1371/journal.pone.0136899

Böhm, H., Albert, I., Oome, S., Raaymakers, T. M., Van den Ackerveken, G., and Nürnberger, T. (2014). A conserved peptide pattern from a widespread microbial virulence factor triggers pattern-induced immunity in *Arabidopsis*. *PLoS Pathog.* 10:e1004491. doi: 10.1371/journal.ppat.1004491

Boller, T., and Felix, G. (2009). A renaissance of elicitors: perception of microbe-associated molecular patterns and danger signals by pattern-recognition receptors. *Annu. Rev. Plant Biol.* 60, 379–406. doi: 10.1146/annurev.arplant.57.032905.105346

Bostock, R. M., Kuc, J. A., and Laine, R. A. (1981). Eicosapentaenoic and arachidonic acids from *Phytophthora infestans* elicit fungitoxic sesquiterpenes in the potato. *Science* 212, 67–69. doi: 10.1126/science.212.4490.67

Bostock, R. M., Laine, R. A., and Kuć, J. A. (1982). Factors affecting the elicitation of sesquiterpenoid phytoalexin accumulation by eicosapentaenoic and arachidonic acids in potato. *Plant Physiol.* 70, 1417–1424. doi: 10.1104/pp.70.5.1417

Bouwmeester, K., de Sain, M., Weide, R., Gouget, A., Klamer, S., Canut, H., et al. (2011). The lectin receptor kinase LecRK-I.9 is a novel *Phytophthora* resistance component and a potential host target for a RXLR effector. *PLoS Pathog.* 7:e1001327. doi: 10.1371/journal.ppat.1001327

Brummer, M., Arend, M., Fromm, J., Schlenzig, A., and Oßwald, W. (2002). Ultrastructural changes and immunocytochemical localization of the elicitin quercinin in *Quercus robur* L. roots infected with *Phytophthora quercina*. *Physiol. Mol. Plant Pathol.* 61, 109–120. doi: 10.1006/pmpp.2002.0419

Brutus, A., Sicilia, F., Macone, A., Cervone, F., and De Lorenzo, G. (2010). A domain swap approach reveals a role of the plant wall-associated kinase 1 (WAK1) as a receptor of oligogalacturonides. *Proc. Natl. Acad. Sci. U.S.A.* 107, 9452–9457. doi: 10.1073/pnas.1000675107

Cabral, A., Oome, S., Sander, N., Küfner, I., Nürnberger, T., and Van den Ackerveken, G. (2012). Nontoxic Nep1-like proteins of the downy mildew pathogen *Hyaloperonospora arabidopsidis*: repression of necrosis-inducing activity by a surface-exposed region. *Mol. Plant Microbe Interact.* 25, 697–708. doi: 10.1094/MPMI-10-11-0269

Cabral, A., Stassen, J. H. M., Seidl, M. F., Bautor, J., Parker, J. E., and Van den Ackerveken, G. (2011). Identification of *Hyaloperonospora arabidopsidis* transcript sequences expressed during infection reveals isolate-specific effectors. *PLoS ONE* 6:e19328. doi: 10.1371/journal.pone.0019328

Chang, Y.-H., Yan, H.-Z., and Liou, R.-F. (2015). A novel elicitor protein from *Phytophthora parasitica* induces plant basal immunity and systemic acquired resistance. *Mol. Plant Pathol.* 16, 123–136. doi: 10.1111/mpp.12166

Chaparro-Garcia, A., Wilkinson, R. C., Gimenez-Ibanez, S., Findlay, K., Coffey, M. D., Zipfel, C., et al. (2011). The receptor-like kinase SERK3/BAK1 is required for basal resistance against the late blight pathogen *Phytophthora infestans* in *Nicotiana benthamiana*. *PLoS ONE* 6:e16608. doi: 10.1371/journal.pone.0016608

Choi, J., Tanaka, K., Cao, Y., Qi, Y., Qiu, J., Liang, Y., et al. (2014). Identification of a plant receptor for extracellular ATP. *Science* 343, 290–294. doi: 10.1126/science.343.6168.290

Cline, K., Wade, M., and Albersheim, P. (1978). Host-pathogen interactions: XV. Fungal glucans which elicit phytoalexin accumulation in soybean also elicit the accumulation of phytoalexins in other plants. *Plant Physiol.* 62, 918–921. doi: 10.1104/pp.62.6.918

Cook, D. E., Mesarich, C. H., and Thomma, B. P. H. J. (2015). Understanding plant immunity as a surveillance system to detect invasion. *Annu. Rev. Phytopathol.* 53, 541–563. doi: 10.1146/annurev-phyto-080614-120114

Cosio, E. G., Feger, M., Miller, C. J., Antelo, L., and Ebel, J. (1996). High-affinity binding of fungal ß-glucan elicitors to cell membranes of species of the plant family Fabaceae. *Planta* 200, 92–99. doi: 10.1007/BF00196654

Dangl, J. L., Horvath, D. M., and Staskawicz, B. J. (2013). Pivoting the plant immune system from dissection to deployment. *Science* 341, 746–751. doi: 10.1126/science.1236011

Dodds, P. N., and Rathjen, J. P. (2010). Plant immunity: towards an integrated view of plant-pathogen interactions. *Nat. Rev. Genet.* 11, 539–548. doi: 10.1038/nrg2812

Dong, S., Kong, G., Qutob, D., Yu, X., Tang, J., Kang, J., et al. (2012). The NLP toxin family in *Phytophthora sojae* includes rapidly evolving groups that lack necrosis-inducing activity. *Mol. Plant Microbe Interact.* 25, 896–909. doi: 10.1094/MPMI-01-12-0023-R

Du, J., Verzaux, E., Chaparro-Garcia, A., Bijsterbosch, G., Keizer, L. C. P., Zhou, J., et al. (2015). Elicitin recognition confers enhanced resistance to *Phytophthora infestans* in potato. *Nat. Plants* 1:15034. doi: 10.1038/nplants.2015.34

Dumas, B., Bottin, A., Gaulin, E., and Esquerré-Tugayé, M.-T. (2008). Cellulose-binding domains: cellulose associated-defensive sensing partners? *Trends Plant Sci.* 13, 160–164. doi: 10.1016/j.tplants.2008.02.004

Fauth, M., Schweizer, P., Buchala, A., Markstädter, C., Riederer, M., Kato, T., et al. (1998). Cutin monomers and surface wax constituents elicit H_2O_2 in conditioned cucumber hypocotyl segments and enhance the activity of other H_2O_2 elicitors. *Plant Physiol.* 117, 1373–1380. doi: 10.1104/pp.117.4.1373

Ferrari, S., Savatin, D. V., Sicilia, F., Gramegna, G., Cervone, F., and Lorenzo, G. D. (2013). Oligogalacturonides: plant damage-associated molecular patterns and regulators of growth and development. *Front. Plant Sci.* 4:49. doi: 10.3389/fpls.2013.00049

Fesel, P. H., and Zuccaro, A. (2015). β-glucan: crucial component of the fungal cell wall and elusive MAMP in plants. *Fungal Genet. Biol.* 90, 53–60. doi: 10.1016/j.fgb.2015.12.004

Fliegmann, J., Mithöfer, A., Wanner, G., and Ebel, J. (2004). An ancient enzyme domain hidden in the putative ß-glucan elicitor receptor of soybean may play an active part in the perception of pathogen-associated molecular patterns during broad host resistance. *J. Biol. Chem.* 279, 1132–1140. doi: 10.1074/jbc.M308552200

Gaulin, E., Bottin, A., and Dumas, B. (2010). Sterol biosynthesis in oomycete pathogens. *Plant Signal. Behav.* 5, 258–260. doi: 10.4161/psb.5.3.10551

Gaulin, E., Dramé, N., Lafitte, C., Torto-Alalibo, T., Martinez, Y., Ameline-Torregrosa, C., et al. (2006). Cellulose binding domains of a *Phytophthora* cell wall protein are novel pathogen-associated molecular patterns. *Plant Cell* 18, 1766–1777. doi: 10.1105/tpc.105.038687

Gaulin, E., Jauneau, A., Villalba, F., Rickauer, M., Esquerré-Tugayé, M.-T., and Bottin, A. (2002). The CBEL glycoprotein of *Phytophthora parasitica* var. *nicotianae* is involved in cell wall deposition and adhesion to cellulosic substrates. *J. Cell Sci.* 115, 4565–4575. doi: 10.1242/jcs.00138

Gaulin, E., Madoui, M.-A., Bottin, A., Jacquet, C., Mathé, C., Couloux, A., et al. (2008). Transcriptome of *Aphanomyces euteiches*: new oomycete putative pathogenicity factors and metabolic pathways. *PLoS ONE* 3:e1723. doi: 10.1371/journal.pone.0001723

Haas, B. J., Kamoun, S., Zody, M. C., Jiang, R. H. Y., Handsaker, R. E., Cano, L. M., et al. (2009). Genome sequence and analysis of the Irish potato famine pathogen *Phytophthora infestans*. *Nature* 461, 393–398. doi: 10.1038/nature08358

Hahlbrock, K., Scheel, D., Logemann, E., Nürnberger, T., Parniske, M., Reinold, S., et al. (1995). Oligopeptide elicitor-mediated defense gene activation in cultured parsley cells. *Proc. Natl. Acad. Sci. U.S.A.* 92, 4150–4157. doi: 10.1073/pnas.92.10.4150

Halim, V. A., Hunger, A., Macioszek, V., Landgraf, P., Nürnberger, T., Scheel, D., et al. (2004). The oligopeptide elicitor Pep-13 induces salicylic acid-dependent and -independent defense reactions in potato. *Physiol. Mol. Plant Pathol.* 64, 311–318. doi: 10.1016/j.pmpp.2004.10.003

Hein, I., Gilroy, E. M., Armstrong, M. R., and Birch, P. R. J. (2009). The zig-zag-zig in oomycete-plant interactions. *Mol. Plant Pathol.* 10, 547–562. doi: 10.1111/j.1364-3703.2009.00547.x

Heredia, A. (2003). Biophysical and biochemical characteristics of cutin, a plant barrier biopolymer. *Biochim. Biophys. Acta* 1620, 1–7. doi: 10.1016/S0304-4165(02)00510-X

Inui, H., Yamaguchi, Y., and Hirano, S. (1997). Elicitor actions of *N*-acetylchitooligosaccharides and laminarioligosaccharides for chitinase and L-phenylalanine ammonia-lyase induction in rice suspension culture. *Biosci. Biotechnol. Biochem.* 61, 975–978. doi: 10.1271/bbb.61.975

Jones, J. D. G., and Dangl, J. L. (2006). The plant immune system. *Nature* 444, 323–329. doi: 10.1038/nature05286

Kamoun, S., Furzer, O., Jones, J. D. G., Judelson, H. S., Ali, G. S., Dalio, R. J. D., et al. (2015). The Top 10 oomycete pathogens in molecular plant pathology. *Mol. Plant Pathol.* 16, 413–434. doi: 10.1111/mpp.12190

Kamoun, S., van West, P., de Jong, A. J., de Groot, K. E., Vleeshouwers, V. G. A. A., and Govers, F. (1997). A gene encoding a protein elicitor of *Phytophthora infestans* is down-regulated during infection of potato. *Mol. Plant Microbe Interact.* 10, 13–20. doi: 10.1094/MPMI.1997.10.1.13

Kamoun, S., van West, P., Vleeshouwers, V. G. A. A., de Groot, K. E., and Govers, F. (1998). Resistance of *Nicotiana benthamiana* to *Phytophthora infestans* is mediated by the recognition of the elicitor protein INF1. *Plant Cell* 10, 1413–1426. doi: 10.2307/3870607

Kamoun, S., Young, M., Glascock, C. B., and Tyler, B. M. (1993). Extracellular protein elicitors from *Phytophthora*: host-specificity and induction of resistance to bacterial and fungal phytopathogens. *Mol. Plant Microbe Interact.* 6, 15–25. doi: 10.1094/MPMI-6-015

Kanzaki, H., Saitoh, H., Takahashi, Y., Berberich, T., Ito, A., Kamoun, S., et al. (2008). NbLRK1, a lectin-like receptor kinase protein of *Nicotiana benthamiana*, interacts with *Phytophthora infestans* INF1 elicitin and mediates INF1-induced cell death. *Planta* 228, 977–987. doi: 10.1007/s00425-008-0797-y

Karlsson, J., Siika-aho, M., Tenkanen, M., and Tjerneld, F. (2002). Enzymatic properties of the low molecular mass endoglucanases Cel12A (EG III) and Cel45A (EG V) of *Trichoderma reesei*. *J. Biotechnol.* 99, 63–78. doi: 10.1016/S0168-1656(02)00156-6

Khatib, M., Lafitte, C., Esquerré-Tugayé, M.-T., Bottin, A., and Rickauer, M. (2004). The CBEL elicitor of *Phytophthora parasitica* var. *nicotianae* activates defence in *Arabidopsis thaliana* via three different signalling pathways. *New Phytol.* 162, 501–510. doi: 10.1111/j.1469-8137.2004.01043.x

Klarzynski, O., Plesse, B., Joubert, J. M., Yvin, J. C., Kopp, M., Kloareg, B., et al. (2000). Linear ß-1,3 glucans are elicitors of defense responses in tobacco. *Plant Physiol.* 124, 1027–1038. doi: 10.1104/pp.124.3.1027

Krol, E., Mentzel, T., Chinchilla, D., Boller, T., Felix, G., Kemmerling, B., et al. (2010). Perception of the *Arabidopsis* danger signal peptide 1 involves the pattern recognition receptor *At*PEPR1 and its close homologue *At*PEPR2. *J. Biol. Chem.* 285, 13471–13479. doi: 10.1074/jbc.M109.097394

Lacombe, S., Rougon-Cardoso, A., Sherwood, E., Peeters, N., Dahlbeck, D., van Esse, H. P., et al. (2010). Interfamily transfer of a plant pattern-recognition receptor confers broad-spectrum bacterial resistance. *Nat. Biotechnol.* 28, 365–369. doi: 10.1038/nbt.1613

Larroque, M., Barriot, R., Bottin, A., Barre, A., Rougé, P., Dumas, B., et al. (2012). The unique architecture and function of cellulose-interacting proteins in oomycetes revealed by genomic and structural analyses. *BMC Genomics* 13:605. doi: 10.1186/1471-2164-13-605

Larroque, M., Belmas, E., Martinez, T., Vergnes, S., Ladouce, N., Lafitte, C., et al. (2013). Pathogen-associated molecular pattern-triggered immunity and resistance to the root pathogen *Phytophthora parasitica* in *Arabidopsis*. *J. Exp. Bot.* 64, 3615–3625. doi: 10.1093/jxb/ert195

Longland, A. C., Slusarenko, A. J., and Friend, J. (1987). Arachidonic and Linoleic acids elicit isoflavonoid phytoalexin accumulation in *Phaseolus vulgaris* (French bean). *J. Phytopathol.* 120, 289–297. doi: 10.1111/j.1439-0434.1987.tb00492.x

Lorand, L., and Graham, R. M. (2003). Transglutaminases: crosslinking enzymes with pleiotropic functions. *Nat. Rev. Mol. Cell Biol.* 4, 140–156. doi: 10.1038/nrm1014

Ma, Z., Song, T., Zhu, L., Ye, W., Wang, Y., Shao, Y., et al. (2015). A *Phytophthora sojae* Glycoside Hydrolase 12 protein is a major virulence factor during soybean infection and is recognized as a PAMP. *Plant Cell* 27, 2057–2072. doi: 10.1105/tpc.15.00390

Martinez, T., Texier, H., Nahoum, V., Lafitte, C., Cioci, G., Heux, L., et al. (2015). Probing the functions of carbohydrate binding modules in the CBEL protein from the Oomycete *Phytophthora parasitica*. *PLoS ONE* 10:e0137481. doi: 10.1371/journal.pone.0137481

Martins, I. M., Matos, M., Costa, R., Silva, F., Pascoal, A., Estevinho, L. M., et al. (2014). Transglutaminases: recent achievements and new sources. *Appl. Microbiol. Biotechnol.* 98, 6957–6964. doi: 10.1007/s00253-014-5894-1

Master, E. R., Zheng, Y., Storms, R., Tsang, A., and Powlowski, J. (2008). A xyloglucan-specific family 12 glycosyl hydrolase from *Aspergillus niger*: recombinant expression, purification and characterization. *Biochem. J.* 411, 161–170. doi: 10.1042/BJ20070819

Mateos, F. V., Rickauer, M., and Esquerré-Tugayé, M. T. (1997). Cloning and characterization of a cDNA encoding an elicitor of *Phytophthora parasitica* var. *nicotianae* that shows cellulose-binding and lectin-like activities. *Mol. Plant Microbe Interact.* 10, 1045–1053. doi: 10.1094/MPMI.1997.10.9.1045

Ménard, R., Alban, S., de Ruffray, P., Jamois, F., Franz, G., Fritig, B., et al. (2004). ß-1,3 glucan sulfate, but not ß-1,3 glucan, induces the salicylic acid signaling pathway in tobacco and *Arabidopsis*. *Plant Cell* 16, 3020–3032. doi: 10.1105/tpc.104.024968

Mikes, V., Milat, M. L., Ponchet, M., Panabières, F., Ricci, P., and Blein, J. P. (1998). Elicitins, proteinaceous elicitors of plant defense, are a new class of sterol carrier proteins. *Biochem. Biophys. Res. Commun.* 245, 133–139. doi: 10.1006/bbrc.1998.8341

Milat, M. L., Ricci, P., Bonnet, P., and Blein, J. P. (1991). Capsidiol and ethylene production by tobacco cells in response to cryptogein, an elicitor from *Phytophthora cryptogea*. *Phytochemistry* 30, 2171–2173. doi: 10.1016/0031-9422(91)83608-N

Mithöfer, A., Fliegmann, J., Neuhaus-Url, G., Schwarz, H., and Ebel, J. (2000). The hepta-ß-glucoside elicitor-binding proteins from legumes represent a putative receptor family. *Biol. Chem.* 381, 705–713. doi: 10.1515/BC.2000.091

Nars, A., Lafitte, C., Chabaud, M., Drouillard, S., Mélida, H., Danoun, S., et al. (2013). *Aphanomyces euteiches* cell wall fractions containing novel glucan-chitosaccharides induce defense genes and nuclear calcium oscillations in the plant host *Medicago truncatula*. *PLoS ONE* 8:e75039. doi: 10.1371/journal.pone.0075039

Nennstiel, D., Scheel, D., and Nürnberger, T. (1998). Characterization and partial purification of an oligopeptide elicitor receptor from parsley (*Petroselinum crispum*). *FEBS Lett.* 431, 405–410. doi: 10.1016/S0014-5793(98)00800-X

Nürnberger, T., Nennstiel, D., Hahlbrock, K., and Scheel, D. (1995). Covalent cross-linking of the *Phytophthora megasperma* oligopeptide elicitor to its receptor in parsley membranes. *Proc. Natl. Acad. Sci. U.S.A.* 92, 2338–2342. doi: 10.1073/pnas.92.6.2338

Nürnberger, T., Nennstiel, D., Jabs, T., Sacks, W. R., Hahlbrock, K., and Scheel, D. (1994). High affinity binding of a fungal oligopeptide elicitor to parsley plasma membranes triggers multiple defense responses. *Cell* 78, 449–460. doi: 10.1016/0092-8674(94)90423-5

Oome, S., Raaymakers, T. M., Cabral, A., Samwel, S., Böhm, H., Albert, I., et al. (2014). Nep1-like proteins from three kingdoms of life act as a microbe-associated molecular pattern in *Arabidopsis*. *Proc. Natl. Acad. Sci. U.S.A.* 111, 16955–16960. doi: 10.1073/pnas.1410031111

Oome, S., and Van den Ackerveken, G. (2014). Comparative and functional analysis of the widely occurring family of Nep1-like proteins. *Mol. Plant Microbe Interact.* 27, 1081–1094. doi: 10.1094/MPMI-04-14-0118-R

Parker, J. E., Schulte, W., Hahlbrock, K., and Scheel, D. (1991). An extracellular glycoprotein from *Phytophthora megasperma* f. sp. *glycinea* elicits phytoalexin

synthesis in cultured parsley cells and protoplasts. *Mol. Plant Microbe Interact.* 4, 19–27. doi: 10.1094/MPMI-4-019

Parniske, M. (2000). Intracellular accommodation of microbes by plants: a common developmental program for symbiosis and disease? *Curr. Opin. Plant Biol.* 3, 320–328. doi: 10.1016/S1369-5266(00)00088-1

Peng, K.-C., Wang, C.-W., Wu, C.-H., Huang, C.-T., and Liou, R.-F. (2015). Tomato *SOBIR1/EVR* homologs are involved in elicitin perception and plant defense against the oomycete pathogen *Phytophthora parasitica*. *Mol. Plant Microbe Interact.* 28, 913–926. doi: 10.1094/MPMI-12-14-0405-R

Postma, J., Liebrand, T. W. H., Bi, G., Evrard, A., Bye, R. R., Mbengue, M., et al. (2016). Avr4 promotes Cf-4 receptor-like protein association with the BAK1/SERK3 receptor-like kinase to initiate receptor endocytosis and plant immunity. *New Phytol.* 210, 627–642. doi: 10.1111/nph.13802

Preisig, C. L., and Kuć, J. A. (1988). Metabolism by potato tuber of arachidonic acid, an elicitor of hypersensitive resistance. *Physiol. Mol. Plant Pathol.* 32, 77–88. doi: 10.1016/S0885-5765(88)80007-9

Reiss, K., Kirchner, E., Gijzen, M., Zocher, G., Löffelhardt, B., Nürnberger, T., et al. (2011). Structural and phylogenetic analyses of the GP42 transglutaminase from *Phytophthora sojae* reveal an evolutionary relationship between oomycetes and marine *Vibrio* bacteria. *J. Biol. Chem.* 286, 42585–42593. doi: 10.1074/jbc.M111.290544

Rey, T., Nars, A., Bonhomme, M., Bottin, A., Huguet, S., Balzergue, S., et al. (2013). NFP, a LysM protein controlling Nod factor perception, also intervenes in *Medicago truncatula* resistance to pathogens. *New Phytol.* 198, 875–886. doi: 10.1111/nph.12198

Ricci, P., Bonnet, P., Huet, J. C., Sallantin, M., Beauvais-Cante, F., Bruneteau, M., et al. (1989). Structure and activity of proteins from pathogenic fungi *Phytophthora* eliciting necrosis and acquired resistance in tobacco. *Eur. J. Biochem.* 183, 555–563. doi: 10.1111/j.1432-1033.1989.tb21084.x

Ricker, K. E., and Bostock, R. M. (1992). Evidence for release of the elicitor arachidonic acid and its metabolites from sporangia of *Phytophthora infestans* during infection of potato. *Physiol. Mol. Plant Pathol.* 41, 61–72. doi: 10.1016/0885-5765(92)90049-2

Robinson, S. M., and Bostock, R. M. (2015). β-glucans and eicosapolyenoic acids as MAMPs in plant-oomycete interactions: past and present. *Front. Plant Sci.* 5:797. doi: 10.3389/fpls.2014.00797

Romero-Correa, M. T., Villa-Gómez, R., Castro-Mercado, E., and García-Pineda, E. (2014). The avocado defense compound phenol-2,4-bis (1,1-dimethylethyl) is induced by arachidonic acid and acts via the inhibition of hydrogen peroxide production by pathogens. *Physiol. Mol. Plant Pathol.* 87, 32–41. doi: 10.1016/j.pmpp.2014.05.003

Savchenko, T., Walley, J. W., Chehab, E. W., Xiao, Y., Kaspi, R., Pye, M. F., et al. (2010). Arachidonic acid: an evolutionarily conserved signaling molecule modulates plant stress signaling networks. *Plant Cell* 22, 3193–3205. doi: 10.1105/tpc.110.073858

Schweizer, P., Felix, G., Buchala, A., Müller, C., and Métraux, J. P. (1996). Perception of free cutin monomers by plant cells. *Plant J.* 10, 331–341. doi: 10.1046/j.1365-313X.1996.10020331.x

Schwessinger, B., Bahar, O., Thomas, N., Holton, N., Nekrasov, V., Ruan, D., et al. (2015). Transgenic expression of the dicotyledonous pattern recognition receptor EFR in rice leads to ligand-dependent activation of defense responses. *PLoS Pathog.* 11:e1004809. doi: 10.1371/journal.ppat.1004809

Schwessinger, B., and Zipfel, C. (2008). News from the frontline: recent insights into PAMP-triggered immunity in plants. *Curr. Opin. Plant Biol.* 11, 389–395. doi: 10.1016/j.pbi.2008.06.001

Séjalon-Delmas, N., Mateos, F. V., Bottin, A., Rickauer, M., Dargent, R., and Esquerré-Tugayé, M. T. (1997). Purification, elicitor activity, and cell wall localization of a glycoprotein from *Phytophthora parasitica* var. *nicotianae*, a fungal pathogen of tobacco. *Phytopathology* 87, 899–909. doi: 10.1094/PHYTO.1997.87.9.899

Sharma, R., Xia, X., Cano, L. M., Evangelisti, E., Kemen, E., Judelson, H., et al. (2015). Genome analyses of the sunflower pathogen *Plasmopara halstedii* provide insights into effector evolution in downy mildews and *Phytophthora*. *BMC Genomics* 16:741. doi: 10.1186/s12864-015-1904-7

Sharp, J. K., Albersheim, P., Ossowski, P., Pilotti, A., Garegg, P., and Lindberg, B. (1984a). Comparison of the structures and elicitor activities of a synthetic and a mycelial-wall-derived hexa(ß-D-glucopyranosyl)-D-glucitol. *J. Biol. Chem.* 259, 11341–11345.

Sharp, J. K., McNeil, M., and Albersheim, P. (1984b). The primary structures of one elicitor-active and seven elicitor-inactive hexa(ß-D-glucopyranosyl)-D-glucitols isolated from the mycelial walls of *Phytophthora megasperma* f. sp. *glycinea*. *J. Biol. Chem.* 259, 11321–11336.

Shiu, S.-H., Karlowski, W. M., Pan, R., Tzeng, Y.-H., Mayer, K. F. X., and Li, W.-H. (2004). Comparative analysis of the receptor-like kinase family in *Arabidopsis* and rice. *Plant Cell* 16, 1220–1234. doi: 10.1105/tpc.020834

Sietsma, J. H., Eveleigh, D. E., and Haskins, R. H. (1969). Cell wall composition and protoplast formation of some oomycete species. *Biochim. Biophys. Acta* 184, 306–317. doi: 10.1016/0304-4165(69)90033-6

Singh, P., Kuo, Y.-C., Mishra, S., Tsai, C.-H., Chien, C.-C., Chen, C.-W., et al. (2012). The lectin receptor kinase-VI.2 is required for priming and positively regulates *Arabidopsis* pattern-triggered immunity. *Plant Cell* 24, 1256–1270. doi: 10.1105/tpc.112.095778

Stassen, J. H. M., Seidl, M. F., Vergeer, P. W. J., Nijman, I. J., Snel, B., Cuppen, E., et al. (2012). Effector identification in the lettuce downy mildew *Bremia lactucae* by massively parallel transcriptome sequencing. *Mol. Plant Pathol.* 13, 719–731. doi: 10.1111/j.1364-3703.2011.00780.x

Suzuki, N., Miller, G., Morales, J., Shulaev, V., Torres, M. A., and Mittler, R. (2011). Respiratory burst oxidases: the engines of ROS signaling. *Curr. Opin. Plant Biol.* 14, 691–699. doi: 10.1016/j.pbi.2011.07.014

Thines, M., and Kamoun, S. (2010). Oomycete-plant coevolution: recent advances and future prospects. *Curr. Opin. Plant Biol.* 13, 427–433. doi: 10.1016/j.pbi.2010.04.001

Thomma, B. P. H. J., Nürnberger, T., and Joosten, M. H. A. J. (2011). Of PAMPs and effectors: the blurred PTI-ETI dichotomy. *Plant Cell* 23, 4–15. doi: 10.1105/tpc.110.082602

Umemoto, N., Kakitani, M., Iwamatsu, A., Yoshikawa, M., Yamaoka, N., and Ishida, I. (1997). The structure and function of a soybean ß-glucan-elicitor-binding protein. *Proc. Natl. Acad. Sci. U.S.A.* 94, 1029–1034. doi: 10.1073/pnas.94.3.1029

Wang, G., Ellendorff, U., Kemp, B., Mansfield, J. W., Forsyth, A., Mitchell, K., et al. (2008). A genome-wide functional investigation into the roles of receptor-like proteins in *Arabidopsis*. *Plant Physiol.* 147, 503–517. doi: 10.1104/pp.108.119487

Wang, Y., Bouwmeester, K., Beseh, P., Shan, W., and Govers, F. (2014). Phenotypic analyses of *Arabidopsis* T-DNA insertion lines and expression profiling reveal that multiple L-type lectin receptor kinases are involved in plant immunity. *Mol. Plant Microbe Interact.* 27, 1390–1402. doi: 10.1094/MPMI-06-14-0191-R

Wang, Y., Cordewener, J. H. G., America, A. H. P., Shan, W., Bouwmeester, K., and Govers, F. (2015a). *Arabidopsis* lectin receptor kinases LecRK-IX.1 and LecRK-IX.2 are functional analogs in regulating *Phytophthora* resistance and plant cell death. *Mol. Plant Microbe Interact.* 28, 1032–1048. doi: 10.1094/MPMI-02-15-0025-R

Wang, Y., Weide, R., Govers, F., and Bouwmeester, K. (2015b). L-type lectin receptor kinases in *Nicotiana benthamiana* and tomato and their role in *Phytophthora* resistance. *J. Exp. Bot.* 66, 6731–6743. doi: 10.1093/jxb/erv379

Wu, J., Liu, Z., Zhang, Z., Lv, Y., Yang, N., Zhang, G., et al. (2016). Transcriptional regulation of receptor-like protein genes by environmental stresses and hormones and their overexpression activities in *Arabidopsis thaliana*. *J. Exp. Bot.* 67, 3339–3351. doi: 10.1093/jxb/erw152

Yamaguchi, Y., and Huffaker, A. (2011). Endogenous peptide elicitors in higher plants. *Curr. Opin. Plant Biol.* 14, 351–357. doi: 10.1016/j.pbi.2011.05.001

Yamaguchi, Y., Huffaker, A., Bryan, A. C., Tax, F. E., and Ryan, C. A. (2010). PEPR2 is a second receptor for the Pep1 and Pep2 peptides and contributes to defense responses in *Arabidopsis*. *Plant Cell* 22, 508–522. doi: 10.1105/tpc.109.068874

Yamaguchi, Y., Pearce, G., and Ryan, C. A. (2006). The cell surface leucine-rich repeat receptor for *At*Pep1, an endogenous peptide elicitor in *Arabidopsis*, is functional in transgenic tobacco cells. *Proc. Natl. Acad. Sci. U.S.A.* 103, 10104–10109. doi: 10.1073/pnas.0603729103

Yoshikawa, M., Keen, N. T., and Wang, M. C. (1983). A receptor on soybean membranes for a fungal elicitor of phytoalexin accumulation. *Plant Physiol.* 73, 497–506. doi: 10.1104/pp.73.2.497

Yoshioka, H., Sugie, K., Park, H. J., Maeda, H., Tsuda, N., Kawakita, K., et al. (2001). Induction of plant gp91 *phox* homolog by fungal cell wall, arachidonic acid, and salicylic acid in potato. *Mol. Plant Microbe Interact.* 14, 725–736. doi: 10.1094/MPMI.2001.14.6.725

Zhou, B.-J., Jia, P.-S., Gao, F., and Guo, H.-S. (2012). Molecular characterization and functional analysis of a necrosis- and ethylene-inducing, protein-encoding gene family from *Verticillium dahliae*. *Mol. Plant Microbe Interact.* 25, 964–975. doi: 10.1094/MPMI-12-11-0319

Zipfel, C. (2014). Plant pattern-recognition receptors. *Trends Immunol.* 35, 345–351. doi: 10.1016/j.it.2014.05.004

Conflict of Interest Statement: The authors declare that the research was conducted in the absence of any commercial or financial relationships that could be construed as a potential conflict of interest.

frontiers in Plant Science

ORIGINAL RESEARCH
published: 06 April 2016
doi: 10.3389/fpls.2016.00380

Genome-Wide Study of the Tomato *SlMLO* Gene Family and Its Functional Characterization in Response to the Powdery Mildew Fungus *Oidium neolycopersici*

Zheng Zheng[1†], Michela Appiano[2†], Stefano Pavan[3], Valentina Bracuto[3], Luigi Ricciardi[3], Richard G. F. Visser[2], Anne-Marie A. Wolters[2] and Yuling Bai[2]*

[1] Institute of Vegetables and Flowers, Chinese Academy of Agricultural Sciences, Beijing, China, [2] Wageningen UR Plant Breeding, Wageningen University and Research Centre, Wageningen, Netherlands, [3] Section of Genetics and Plant Breeding, Department of Plant, Soil and Food Science, University of Bari Aldo Moro, Bari, Italy

OPEN ACCESS

Edited by:
Ralph Panstruga,
RWTH Aachen University, Germany

Reviewed by:
Ralph Hückelhoven,
Technische Universität München, Germany
Thomas Debener,
Leibniz University of Hanover, Germany

***Correspondence:**
Yuling Bai
bai.yuling@wur.nl

[†]These authors have contributed equally to this work.

Specialty section:
This article was submitted to Plant Biotic Interactions, a section of the journal Frontiers in Plant Science

Received: 23 December 2015
Accepted: 12 March 2016
Published: 06 April 2016

Citation:
Zheng Z, Appiano M, Pavan S, Bracuto V, Ricciardi L, Visser RGF, Wolters A-MA and Bai Y (2016) Genome-Wide Study of the Tomato SlMLO Gene Family and Its Functional Characterization in Response to the Powdery Mildew Fungus Oidium neolycopersici. Front. Plant Sci. 7:380. doi: 10.3389/fpls.2016.00380

The *MLO* (*Mildew Locus O*) gene family encodes plant-specific proteins containing seven transmembrane domains and likely acting in signal transduction in a calcium and calmodulin dependent manner. Some members of the *MLO* family are susceptibility factors toward fungi causing the powdery mildew disease. In tomato, for example, the loss-of-function of the *MLO* gene *SlMLO1* leads to a particular form of powdery mildew resistance, called *ol-2*, which arrests almost completely fungal penetration. This type of penetration resistance is characterized by the apposition of papillae at the sites of plant-pathogen interaction. Other *MLO* homologs in Arabidopsis regulate root response to mechanical stimuli (*AtMLO4* and *AtMLO11*) and pollen tube reception by the female gametophyte (*AtMLO7*). However, the role of most *MLO* genes remains unknown. In this work, we provide a genome-wide study of the tomato *SlMLO* gene family. Besides *SlMLO1*, other 15 *SlMLO* homologs were identified and characterized with respect to their structure, genomic organization, phylogenetic relationship, and expression profile. In addition, by analysis of transgenic plants, we demonstrated that simultaneous silencing of *SlMLO1* and two of its closely related homologs, *SlMLO5* and *SlMLO8*, confer higher level of resistance than the one associated with the *ol-2* mutation. The outcome of this study provides evidence for functional redundancy among tomato homolog genes involved in powdery mildew susceptibility. Moreover, we developed a series of transgenic lines silenced for individual *SlMLO* homologs, which lay the foundation for further investigations aimed at assigning new biological functions to the *MLO* gene family.

Keywords: *MLO* gene family, tomato, susceptibility, powdery mildew disease

INTRODUCTION

Many important crop species can be affected by the powdery mildew (PM) disease, resulting in great yield losses in agricultural settings. In barley, recessive loss-of-function mutations occurring in the *HvMLO* (*Hordeum vulgare Mildew Resistance Locus O*) gene confer resistance to all known isolates of the PM fungus *Blumeria graminis* f.sp *hordei*. Therefore, natural

or induced *mlo*-mutant alleles are in use for about seven decades to introduce resistance in spring barley breeding programs (Jørgensen, 1992; Büschges et al., 1997; Reinstädler et al., 2010).

Biochemical analysis showed that the barley HvMLO protein contains seven transmembrane domains integral to the plasma membrane, with an extracellular amino-terminus and an intracellular carboxy-terminus. The latter harbors a calmodulin-binding domain likely involved in sensing calcium influxes into cells (Devoto et al., 1999). Although the domain structure of MLO proteins is related to that of metazoan G-protein coupled receptors (GPCRs), several studies could not confirm the role of MLO proteins as canonical GPCRs (Kim et al., 2002; Lorek et al., 2013). Despite further intensive efforts to explain the biochemical function of the HvMLO protein, its core activity remains elusive (Panstruga, 2005). However, HvMLO might be exploited by the fungus to impair vesicle-associated defense mechanism at plant-pathogen interaction sites, thus facilitating its penetration (Panstruga and Schulze-Lefert, 2003; Opalski et al., 2005; Miklis et al., 2007). This feature makes *HvMLO* a typical representative of susceptibility genes (*S*-genes) (Miklis et al., 2007; van Schie and Takken, 2014).

The robustness of barley *mlo*-resistance, due to its non-race-specific spectrum and durability, led in the last years to an extensive quest for identification and functional characterization of the *MLO* genes in other species affected by the PM disease. The search resulted in the identification of multiple *MLO* gene families, ranging from 12 to 39 members in Arabidopsis, rice, grapevine, cucumber, apple, peach, woodland strawberry, tobacco, and soybean (Devoto et al., 2003; Feechan et al., 2008; Liu and Zhu, 2008; Shen et al., 2012; Zhou et al., 2013; Pessina et al., 2014; Appiano et al., 2015). Moreover, specific homologs were shown to play a major role in plant-pathogen interactions (Consonni et al., 2006).

A detailed phylogenetic analysis distinguished up to eight clades in which Angiosperm MLO proteins can be found (Feechan et al., 2008; Acevedo-Garcia et al., 2014; Pessina et al., 2014). The MLO homologs involved in the interaction with PM pathogens (Arabidopsis AtMLO2, AtMLO6, AtMLO12, tomato SlMLO1, pea Er1/PsMLO1, grapevine VvMLO3 and VvMLO4, tobacco NtMLO1, pepper CaMLO2, cucumber CsaMLO8, *Lotus japonicus* LjMLO1, and barrel clover MtMLO1) are grouped into clade V. On the other hand, all the known monocot MLO homologs acting as susceptibility factors (barley HvMLO, rice OsMLO3, and wheat TaMLO_A1 and TaMLO_B1) do not cluster in clade V, but in clade IV, which is primarily but not exclusively represented by monocot MLO proteins. For example, grapevine VvMLO14, strawberry FvMLO17, and peach PpMLO12 belong also to clade IV (Elliott et al., 2002; Feechan et al., 2008; Acevedo-Garcia et al., 2014; Pessina et al., 2014).

In Arabidopsis, the PM resistance conferred by the loss-of-function of *AtMLO2* is incomplete and only mutations in all the three *AtMLO* homologs in clade V can completely prevent fungal entry (Consonni et al., 2006). In addition, more recent studies in Arabidopsis indicated that other members of the *MLO* gene family play a role in different biological processes. The homologs *AtMLO4* and *AtMLO11* are together involved in root thigmomorphogenesis, i.e., root responses to mechanical stimuli (Chen et al., 2009), while *AtMLO7* regulates pollen tube reception from the synergid cells during fertilization (Kessler et al., 2010). The biological roles of other *MLO* homologs still remain elusive.

Tomato (*Solanum lycopersicum*) is one of the most economically important vegetables in the world. It can be host of three PM species, namely *Oidium neolycopersici*, *Oidium lycopersici,* and *Leveillula taurica* (Seifi et al., 2014). Since 1996, when it was found that all the tomato cultivars were susceptible to *O. neolycopersici*, extensive researches were conducted by our group for sources of resistance (Seifi et al., 2014). An allele containing a 19 bp deletion in the coding region of the PM susceptibility gene *SlMLO1* was found in a wild accession of *S. lycopersicum* var. *cerasiforme*. This mutant allele, named *ol-2*, was shown to confer recessively inherited broad-spectrum resistance to a series of isolates of *O. neolycopersici* (Bai et al., 2005, 2008). Through histological analysis, it was shown that its mechanism of resistance is based on the early abortion of fungal pathogenesis at the sites of attempted penetration (Bai et al., 2005). This type of penetration resistance is characterized by papillae apposition, the same as described also for the PM resistance in the *Atmlo2* mutant of Arabidopsis (Consonni et al., 2006). Although papilla formation can significantly reduce fungal development at the host cell entry level, fungal penetration was not fully prevented in the *ol-2* mutant (Bai et al., 2005).

In this study, we exploited tomato sequence information, derived from the tomato genome sequencing Heinz 1706 and the 150 tomato genome resequencing projects (Tomato Genome Consortium, 2012; The 100 Tomato Genome Sequencing Consortium et al., 2014), in order to identify tomato *MLO* homologs (*SlMLO*). These were characterized with respect to (1) their genomic organization, (2) relation with *MLO* homologs from other species, (3) occurrence of tissue-specific differentially spliced variants, (4) expression in different tissues in axenic condition and (5) upon inoculation with the powdery mildew pathogen *O. neolycopersici*. Finally, an RNAi-based reverse genetic approach was followed to investigate the possibility that *SlMLO* homologs other than *SlMLO1* could play additional roles in the interaction with *O. neolycopersici*.

RESULTS

In silico Identification and Sequencing of the Tomato *SlMLO* Gene Family

A total of 17 tomato *MLO*-like loci were identified through BLAST interrogation of the tomato genomic sequence database (SGN), using AtMLO protein sequences as query. Two of them (referred to as Solyc09g18830 and Solyc09g18840 in the SGN database) were noticeably shorter than other predicted *MLO* homologs and physically close to each other, suggesting they are different parts of the same gene (**Table 1**). Search in the tomato EST database and gene prediction analysis in the *S. pimpinellifolium* genome with the FGENESH software allowed identifying a hypothetical full-length *MLO* transcript encompassing Solyc09g18830 and Solyc09g18840. PCR from leaf of the tomato cultivar Moneymaker (MM) confirmed the presence of this transcript, which was named *SlMLO7* (Supplementary Figure 1). The other 15 predicted *SlMLO* genes

TABLE 1 | Features of the *SlMLO* gene family as inferred by the Sol Genomics Network Database.

SGN locus name	*MLO* gene	Chromosome	Position	ORF lenght (aa)	Introns
Solyc04g049090	*SlMLO1*	4	SL2.40ch04:38700445..38705951	507	14
Solyc08g015870	*SlMLO2*	8	SL2.40ch08:6074040..6078983	504	13
Solyc06g010030	*SlMLO3*	6	SL2.40ch06:4786764..4792828	591	14
Solyc00g007200	*SlMLO4*	2?	SL2.40ch00:6816892..6823417	554	14
Solyc03g095650	*SlMLO5*	3	SL2.40ch03:50279919..50288063	517	14
Solyc02g082430	*SlMLO6*	2	SL2.40ch02:40694608..40700995	553	14
Solyc09g018830 Solyc09g018840	*SlMLO7*	9	SL2.40ch09:17564555..17568214	270	10
Solyc11g069220	*SlMLO8*	11	SL2.40ch11:50939533..50946726	506	13
Solyc06g082820	*SlMLO9*	6	SL2.40ch06:44779673..44784035	511	13
Solyc02g083720	*SlMLO10*	2	SL2.40ch02:41596474..41602413	533	14
Solyc01g102520	*SlMLO11*	1	SL2.40ch01:83071860..83075439	475	13
Solyc08g067760	*SlMLO12*	8	SL2.40ch08:53957062..53962884	532	14
Solyc10g044510	*SlMLO13*	10	SL2.40ch10:22128868..22135940	558	14
Solyc07g063260	*SlMLO14*	7	SL2.40ch07:62995345..63002900	563	14
Solyc02g077570	*SlMLO15*	2	SL2.40ch02:37045094..37050486	375	10
Solyc06g010010	*SlMLO16*	6	SL2.40ch06:4699552..4706571	477	14

TABLE 2 | Types of differentially spliced events observed in cloned *SlMLO* homologs from different tissues of the tomato cv. Moneymaker.

SlMLO	Plant tissue	Type of alternative splicing			
		Intron retention	Exon skipping	Alternative 5′ splice site	Alternative 3′ splice site
SlMLO1	Flower				√
*SlMLO5**	Fruit	√			
SlMLO6	Leaf			√	√
SlMLO9	Leaf		√		
*SlMLO11**	Root	√			
SlMLO13	Leaf		√		√
SlMLO15	Fruit		√	√	
*SlMLO15**	Root	√	√	√	
*SlMLO15**	Flower	√	√	√	

The asterisk (*) indicates SlMLO transcripts that can be either incompletely spliced or alternatively spliced.

were named from *SlMLO1* to *SlMLO6*, and from *SlMLO8* to *SlMLO16*, as reported in **Table 1**. For all of them, information is available with respect to putative amino acid length and number of introns.

With the exception of *SlMLO4*, information on chromosomal localization could also be inferred (**Table 1**). Most *SlMLO* homologs are scattered throughout the tomato genome, thus suggesting that segmental duplication events have been a major source for the evolution of the *SlMLO* gene family. Exceptions are represented by two physical gene clusters, one containing *SlMLO6*, *SlMLO10,* and *SlMLO15* on chromosome 2, and the other containing *SlMLO3* and *SlMLO16* on chromosome 6.

Sequence and expression of all the predicted *SlMLO* homologs were verified by PCR amplification of cDNAs derived from four different tissues (leaf, root, flower, and ripened fruit) of MM. All the *SlMLO* homologs could be amplified at least from one plant tissue. In total, 15 *SlMLO* homologs could be cloned from leaf (with the exception of *SlMLO12*), 10 from flower, nine from fruit and eight from root (Supplementary Table 1).

Sequence alignment of cloned *SlMLO* transcripts with corresponding SGN predicted coding sequence (CDS), derived from the cultivar Heinz 1706, revealed polymorphisms for *SlMLO7*, *SlMLO8*, *SlMLO10,* and *SlMLO15* (Supplementary Figure 1). The 1339 bp *SlMLO7* cloned transcript corresponds to a short open reading frame (ORF) due to a stop codon at 137–139 bp (Supplementary Figure 1). The SGN predicted CDS of *SlMLO8* misses part of the third, seventh, eighth, and ninth exon present in the corresponding transcript cloned from MM leaf; compared to the SGN predicted CDS of *SlMLO10*, the transcript cloned from MM fruit contains a base change at the beginning of the fifth exon, which results in a stop codon (Supplementary Figure 1). Also the predicted ORF of *SlMLO15* is shorter (375 aa) than the average ORF length of other SlMLOs (**Table 1**). The sequence cloned from MM leaf has a longer ORF (459 aa) compared to the predicted SGN sequence (**Table 3A**).

In other cases, sequence alignments of cloned *SlMLO* from the different tissues with their corresponding genomic regions showed various types of splice variants, consisting of intron retention, exon skipping and alternative 5′ and 3′ splice sites, according to the types of alternative splicing described by Keren et al. (2010) (**Table 2** and Supplementary Figure 1).

Characterization of Conserved Amino Acids and Motifs of the SlMLO Proteins

To examine sequence features of the tomato SlMLO proteins, a multiple sequence alignment was performed using sequences obtained by the conceptual translation of transcripts cloned in different tissues. When no deviating transcripts were observed for a *SlMLO* gene, the sequence obtained from leaf was used for translation, with the exception of *SlMLO12* which is the only homolog that was not cloned from leaf but from flower.

TABLE 3A | Features and motifs distribution occurring in SlMLO proteins obtained from *in silico* translation of leaf, root, flower, and fruit transcripts of the tomato cv. Moneymaker.

		ORF Length (aa)	MOTIF 1	MOTIF 2	MOTIF 3	MOTIF4	MOTIF 5	MOTIF 6	MOTIF 7	MOTIF 8	MOTIF 9	MOTIF10
SlMLO1	Leaf	507	√	√	√	√	√	√				
	Root	507	√	√	√	√	√	√				
	Flower	491	√	√	√	√	√					
SlMLO2	Leaf	504	√	√	√	√	√					
SlMLO3	Leaf	591	√			√		√				
SlMLO4	Leaf	554	√	√	√	√		√	√	√		
SlMLO5	Leaf	517	√	√	√	√		√				
	Flower	517	√	√	√	√		√				
	Fruit	540	√	√	√	√		√				
SlMLO6	Leaf	549	√	√	√	√			√	√		
	Root	553	√	√	√	√		√	√	√		
	Flower	553	√	√		√		√	√	√		
	Fruit	553	√	√	√	√		√	√	√		
SlMLO7	Leaf	61										
SlMLO8	Leaf	561	√	√	√	√		√				
SlMLO9	Leaf	448	√		√	√	√	√		√		
	Flower	511	√	√	√	√	√	√		√		
	Fruit	511	√	√	√	√	√	√		√		
SlMLO10	Leaf	533	√	√	√	√	√	√			√	
	Root	533	√	√	√	√	√	√			√	
	Flower	533	√	√	√	√	√	√			√	
	Fruit	178		√							√	
SlMLO11	Leaf	475	√	√	√	√	√	√		√		
	Root	70										
	Flower	475	√	√	√	√	√	√		√		
	Fruit	475	√	√	√	√	√	√		√		
SlMLO12	Flower	532	√	√		√		√		√		
SlMLO13	Leaf	63	√									
	Root	558	√	√		√		√			√	√
	Flower	558	√	√		√		√			√	√
	Fruit	558	√	√		√		√			√	√
SlMLO14	Leaf	563	√	√	√	√	√					
SlMLO15	Leaf	459	√		√		√			√		
	Root	56										
	Flower	70										
	Fruit	84								√		
SlMLO16	Leaf	477	√		√	√	√					

When no deviating transcripts are present for one SlMLO, the one from leaf has been used for motif analysis. Cells highlighted in gray indicate the absence of the corresponding motif.

TABLE 3B | Features details of the consensus motifs reported in Table 3A as predicted by the MEME software package (http://meme-suite.org/tools/meme).

	Sequence consensus	Width	e-value	Location
MOTIF 1	NAFQMAFFFWIWWEYGWKSCFWDNFIPIIIRLVMGVKVQVWCSYMTLPLYARVTQM	56	6.5e-1021	TM6
MOTIF 2	PTWAVAMVCAVIVAISIFIERIIHKLGKWLKKKNKKALYEALEKIKEELMLLGFISLLLTVCQDYISQIC	70	1.5e-1076	TM1
MOTIF 3	LLWIVCFFRQFYRSVNKSDYLTLRHGFIMAHCAPNNYNNFDYYMYRMREDDFDF	54	3.9e-840	2 IC
MOTIF 4	EGKVPFASYEALHQLHIFIFVLAVAHVLYCCTTMWLGMAKMRQWRAWEDETKT	53	6.7e-823	TM3
MOTIF 5	VGISWYLWIFVVLCLLLNINGWHSYFWIPFFPLILILLVGTKLEHIITQMAVEIAE	56	1.0e-402	TM5
MOTIF 6	GSTMKKSIFDENVRDALRKWHMTVKKRKKHKYDRSNTTRSNCPACSMAMDGPNHP	55	8.8e-386	CaMBD
MOTIF7	HRYKTTGHSSRFQGYSDQEASDLENDPTTPMTRAEIATTHIDHDDTEIHVHIPQNGESTRNEDDFSFVKP	70	2.50E-178	C-term
MOTIF 8	PPNVADTMLPCPPNNKDQAKEEEHCRHLGWYERRHLACNE	40	6.30E-149	2 EC
MOTIF9	VNSSAVSSHFYPCSPPDNDMKSAITRDAIHGSSYSNHSTS	40	1.90E-114	2 EC
MOTIF 10	SPCSSRGSFNHLDEKVLSNDHQEDCIVETTNQPGHELSFRNSEVLVTDAEEIVDDEADKIETLFELFQKT	70	2.80E-89	C-term

For each motif, the MEME e-value for significance and the position of each motif in one of the MLO protein domains (transmembrane –TM-, extracellular –EC-, intracellular –IC-, C-terminus –C-term-, calmodulin-binding –CaMBD- domain) is indicated.

The aligned amino acid sequences of the tomato SlMLO protein family showed a high degree of conservation (92%) of the 30 amino acid residues previously described to be invariable throughout the whole MLO protein family (Supplementary Figure 2; Elliott et al., 2005).

Due to aberrant transcripts, the protein sequences of SlMLO7 and SlMLO13 in leaf, SlMLO11 in root, and SlMLO15 in root, flower and fruit, were severely truncated (**Table 3A**). The predicted ORF of SlMLO8 in leaf was longer than the one deriving from the SGN prediction, which is missing important domains of the translated MLO protein. The protein sequence of *SlMLO9* in leaf was shorter (448 aa length) than the ones obtained from the other two tissues (512 aa length) and it is predicted to have five transmembrane (TM) domains, instead of seven as in fruit and flower (**Table 3A**).

Finally, the SlMLO protein family was also used as input to search for conserved motifs. Ten patterns of consecutive amino acids, having a length ranging from 40 to 70 and shared by at least three MLO sequences (**Table 3B**), were found. Interestingly, four of these motifs included transmembrane domains, while the others were located in the second intracellular and extracellular domains, in the C-terminus and in the calmodulin-binding domain. The motifs seven and nine were shared only by SlMLO4/SlMLO6 and SlMLO10/SlMLO13 respectively while the motif ten was only present in the amino acid sequences of SlMLO13 of root, flower, and fruit. Those motifs might indicate regions of peculiar importance for the specific function of these homologs.

Phylogenetic Analysis of the Tomato SlMLO Protein Family

A phylogenetic analysis was carried out in order to establish the relationships between SlMLO proteins and MLO proteins of other plant species (Arabidopsis AtMLO1-15, pea PsMLO1, *Lotus japonicus* LjMLO1, barrel clover MtMLO1, pepper CaMLO2, tobacco NtMLO1, cucumber CsaMLO8, apple MdMLO18 and MdMLO20, strawberry FvMLO13 and FvMLO15, peach PpMLO9 and PpMLO13, barley HvMLO, rice OsMLO3, and wheat TaMLOA1b and TaMLOB1a). The resulting tree contains eight different clades (**Figure 1**). These were named by Roman numerals from I to VIII, in accordance with previous studies performing phylogenetic analysis on the Arabidopsis and apple MLO protein families (Devoto et al., 2003; Pessina et al., 2014).

Five clades, namely clade I, II, III, V, and VI, contain both tomato and Arabidopsis homologs; clade IV contains only the monocot MLO homologs that were selected for this study; clade VII contains only SlMLO15 together with apple, peach and strawberry MLO proteins (MdMLO18, PpMLO9, and FvMLO15, respectively). No SlMLO homologs could be assigned to clade VIII, which only contains Rosaceae MLO homologs (**Figure 1**).

Three tomato MLO homologs, SlMLO3, SlMLO5, and SlMLO8, cluster together with SlMLO1 in clade V, containing all the known eudicot MLO homologs functionally related to powdery mildew susceptibility (AtMLO2, AtMLO6, AtMLO12, PsMLO1, LjMLO1, MtMLO1, CsaMLO8, NtMLO1, and CaMLO2; **Figure 1**; Elliott et al., 2005; Consonni et al., 2006; Bai et al., 2008; Pavan et al., 2009; Humphry et al., 2011; Várallyay et al., 2012; Zheng et al., 2013; Appiano et al., 2015; Berg et al., 2015).

The tomato homologs SlMLO4, SlMLO6, and SlMLO12 group in clade III together with AtMLO7, which regulates Arabidopsis pollen tube reception by the synergid cells, whereas SlMLO10, SlMLO13, and SlMLO14 are the closest tomato homologs to the root thigmomorphogenesis regulating proteins, AtMLO4 and AtMLO11, in clade I (**Figure 1**).

Finally, clade II includes four tomato SlMLO homologs (SlMLO2, SlMLO7, SlMLO9, and SlMLO11) together with three Arabidopsis proteins (AtMLO1, AtMLO13, and AtMLO15) and clade VI harbors only AtMLO3 and tomato SlMLO16 (**Figure 1**).

Expression Profiles of *SlMLO* Homologs in Axenic Conditions and Upon Powdery Mildew Challenge

The expression level of *SlMLO* genes was determined in four different tissues (leaf, root, flower, and ripened fruit). These were found to vary considerably among *SlMLO* genes, and it was not

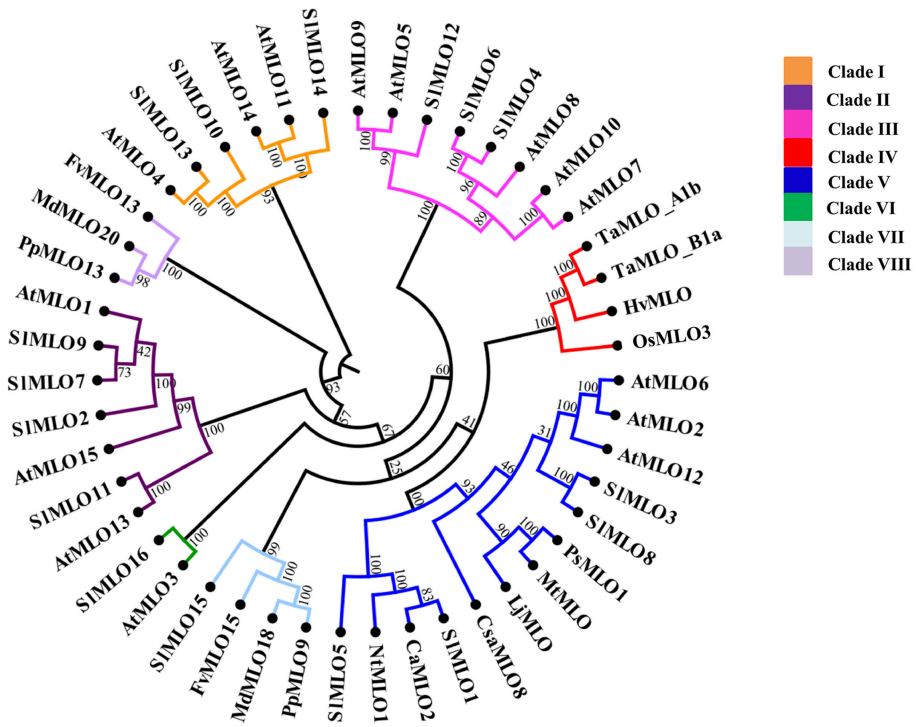

FIGURE 1 | Rooted circular cladogram showing the phylogenetic relationships of the tomato SlMLO proteins. A UPGMA-based tree comprises all the sequences of the MLO protein family of Arabidopsis (At) and tomato (Sl). Individual sequences of apple (Md), tobacco (Nt), cucumber (Csa), pea (Ps), *Lotus japonicus* (Lj), barrel clover (Mt), pepper (Ca), barley (Hv), rice (Os), and wheat (Ta) are included. Numbers on each node represent bootstrap values based on 100 replicates. Phylogenetic clades are designated with colors and Roman numbers according to the position of AtMLO homologs and apple MdMLO, as indicated by Pessina et al. (2014). The tomato SlMLO protein sequences used for this tree derived all from the translation of the transcripts cloned from leaf of the cv. Moneymaker, except for SlMLO12, which corresponds to the translated sequence of flower. Accession numbers of the sequences used, other than tomato SlMLO, are listed in Supplementary Table 2.

possible to assign clade-specific expression patterns (**Figure 2**). Concerning clade V, *SlMLO5* and *SlMLO8* were found to be characterized by very low expression levels in all the tissues. Interestingly, *SlMLO1* was found to be less expressed in leaves compared to flowers. Our results are supported by the collection of RNA-seq data, as shown by the FPKM (fragments per kilobase of exon per million fragments mapped) values for the four tissues under investigation of each homolog represented into graphs of Supplementary Figure 3.

Next, we investigated the expression profile of the *SlMLO* gene family in response to *O. neolycopersici*, using L33 as a reference gene (**Figure 3**). *SlMLO1* expression significantly increased at 6 and 10 h after pathogen challenge. No other *SlMLO* homolog in clade V (*SlMLO3*, *SlMLO5*, *SlMLO8*) showed pathogen-dependent up-regulation.

On the other hand, a significant upregulation in response to *O. neolycopersici* was observed for *SlMLO* homologs outside clade V, namely *SlMLO2*, *SlMLO4*, *SlMLO7*, *SlMLO10*, *SlMLO13*, *SlMLO14,* and *SlMLO16*. In particular, the expression of *SlMLO4* and *SlMLO14* at 10 h after inoculation was comparable to the one of *SlMLO1*, and ∼four-fold and ∼three-fold higher than the one of control plants, respectively.

Similar results were obtained repeating the expression analysis using Ef 1α as reference gene (Supplementary Figure 4).

In order to confirm the strong up-regulation of the above mentioned genes, a second inoculation experiment was carried out, sampling leaf tissues at the same time points (0, 6, and 10 hpi). The results presented in Supplementary Figure 5 indicate that indeed *SlMLO1*, *SlMLO4,* and *SlMLO14* show a statistically significant up-regulated expression due to the *O. neolycopersici* challenge. The slight down-regulated expression of *SlMLO3* observed after the first pathogen inoculation was not confirmed in the second experiment.

Functional Characterization of Clade V *SlMLO* Homologs

Based on their relatedness with eudicot *MLO* homologs predisposing to PM susceptibility, including *SlMLO1*, the newly identified *SlMLO* homologs in clade V (*SlMLO3*, *SlMLO5,* and *SlMLO8*, **Figure 1**) were further investigated with respect to their role in the interaction with *O. neolycopersici*. Therefore, specific RNAi silencing constructs for these three homologs were developed, which were used to transform the susceptible cultivar Moneymaker (MM) (Supplementary Figure 6 and Supplementary Table 3). A silencing construct targeting *SlMLO1* was included as control, which was expected to lead to a resistant phenotype.

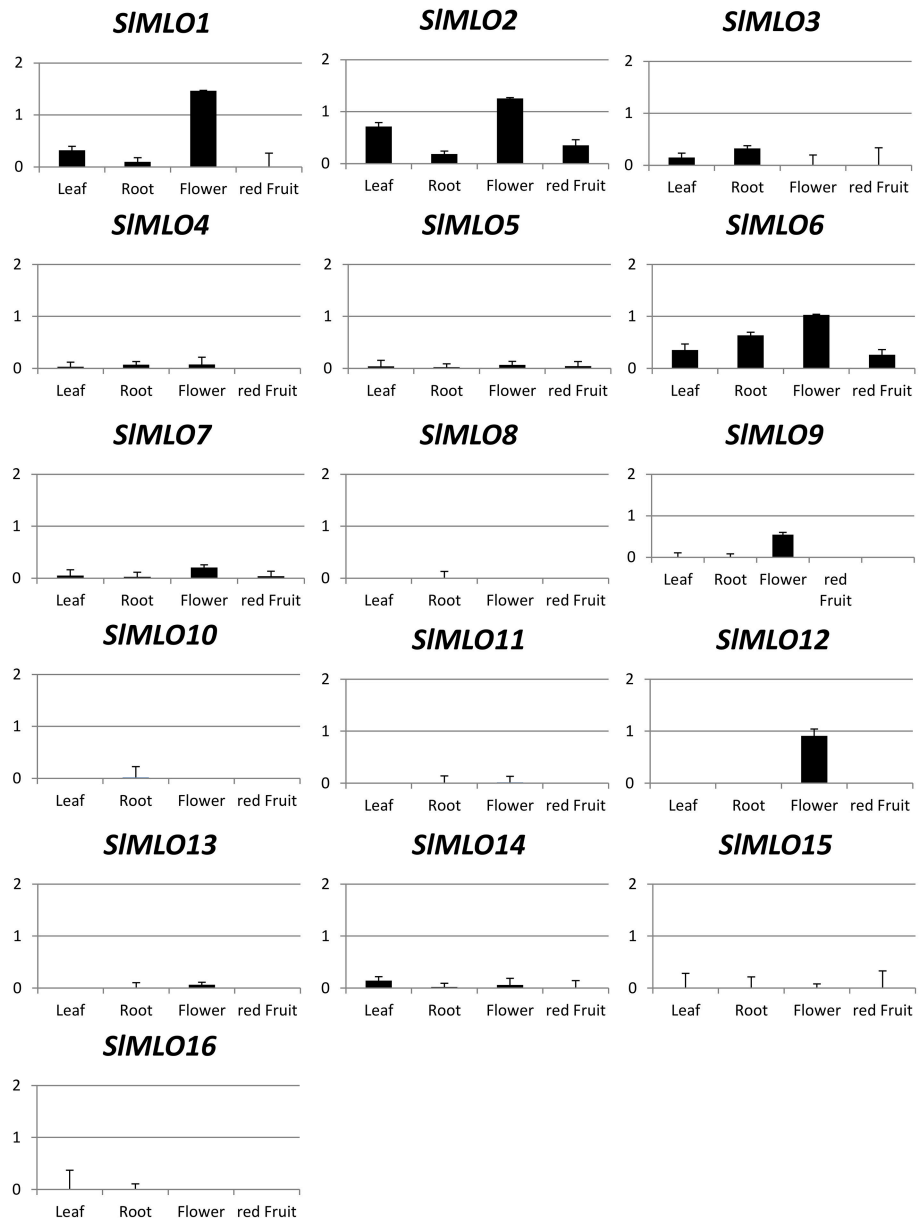

FIGURE 2 | Relative expression level of *SlMLO* transcripts evaluated in four different tissues (leaf, root, flower, and mature fruit) of the tomato cv. Moneymaker in axenic condition. The expression level of each gene is compared to the abundance of Ef1α which was used as reference gene. Bars show standard errors based on three technical replicates. Similar trends are reported in Supplementary Figure 3.

Ten to 20 T_1 plants were obtained for each silencing construct. The expression of the target genes was assessed by means of real-time qPCR (Supplementary Figure 7) and T_1 plants with a reduced level of expression of the target gene were allowed to self-pollinate to develop T_2 families. In total, two independent T_2 families (each segregating for the presence of the silencing construct) were developed for *SlMLO1* and *SlMLO8*, and three were obtained for *SlMLO3* and *SlMLO5*. Transgenic individuals of each family were further assessed for the silencing levels of target genes and other clade V homologs. This revealed successful silencing of each target genes and no unwanted co-silencing in transgenic RNAi::*SlMLO3*, *SlMLO5,* and *SlMLO8* individuals (**Figures 4B–D**). Conversely, T_2 transgenic plants of two T_2 families carrying the RNAi::*SlMLO1* silencing construct were characterized by the simultaneous silencing of *SlMLO1*, *SlMLO5,* and *SlMLO8* (**Figure 4A** and Supplementary Figure 8).

As expected, T_2 progenies carrying the RNAi::*SlMLO1* construct segregated for PM resistance: T_2 plants carrying the silencing construct [T_2_*SlMLO1*_NPT(+)] were resistant, whereas non-transgenic plants [T_2_*SlMLO1*_NPT(-)] were susceptible as MM (**Figure 5A**). In contrast, all T_2 progenies segregating for *SlMLO3*, *SlMLO5,* and *SlMLO8* silencing

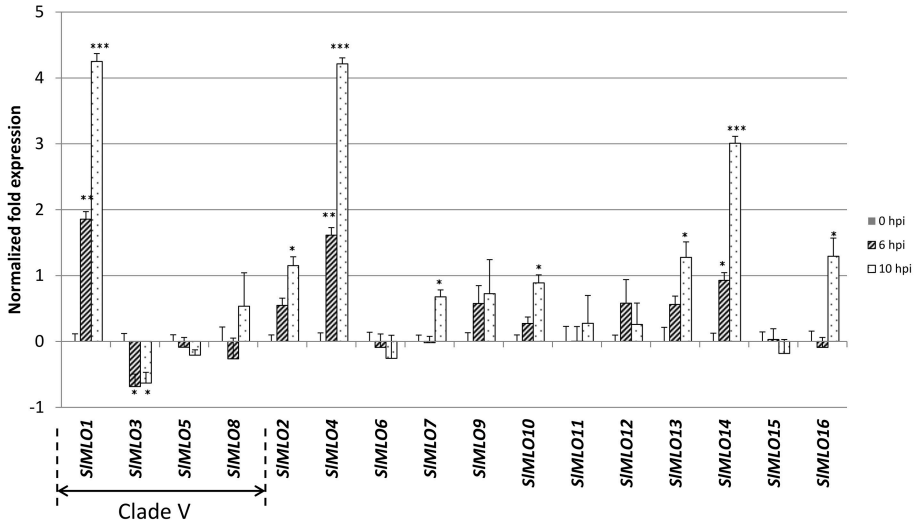

FIGURE 3 | Relative expression level of the *SlMLO* gene family in response to *O. neolycopersici* inoculation. Samples were collected at 0, 6, and 10 h after inoculation (hpi). Transcript abundance of each *SlMLO* homolog was normalized against the transcription level of the 60S ribosomal protein L33 used as reference gene. Bars show standard errors based on four biological replicates. Asterisks refer to significant differences with respect to non-inoculated plants (0 hpi), inferred by mean comparisons with a Student's *t*-test (*$p < 0.05$, **$p < 0.01$, ***$p < 0.001$). The *SlMLO* genes harbored in clade V, based on the phylogenetic tree of **Figure 1**, are indicated by an arrow spanning their corresponding bars. Similar results were obtained by using the elongation factor Ef1α as housekeeping gene (Supplementary Figure 4).

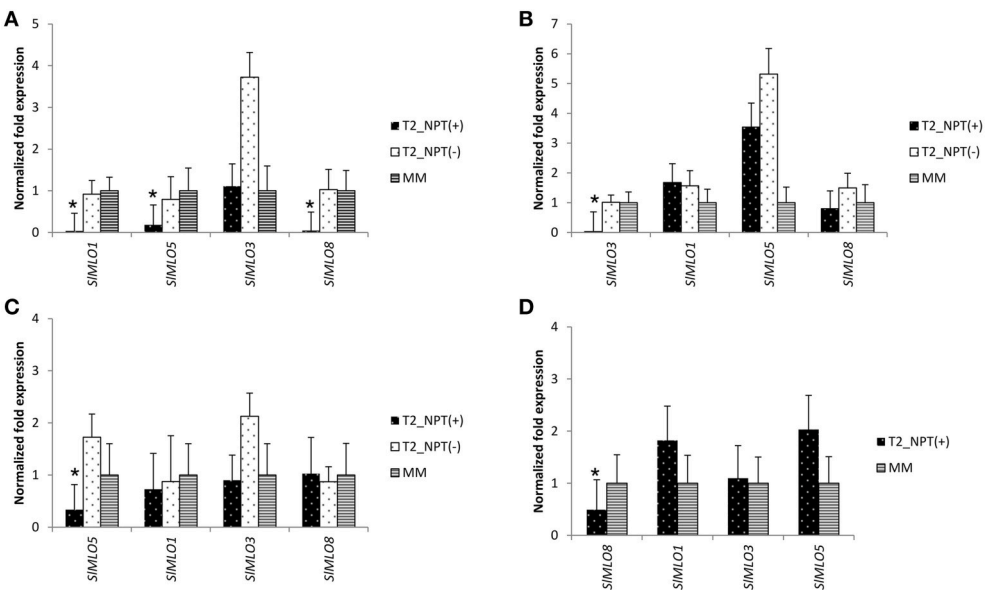

FIGURE 4 | Evaluation of the silencing effect of the RNAi constructs designed to target *SlMLO1*, *SlMLO3*, *SlMLO5,* and *SlMLO8* in segregating T_2 families of the tomato cv. Moneymaker. Panels **(A–D)** show the expressions of clade V *SlMLO* homologs in plants of T_2 families, derived from different transformation events and segregating for the presence [T_2_NPT(+)] or absence [T_2_NPT(-)] of the RNAi::*SlMLO1*, RNAi::*SlMLO3*, RNAi::*SLMLO5,* and RNAi::*SlMLO8* constructs, respectively. In **(A)** bars and standard errors refer to eight plants T_2_NPT(+) and four plants T_2_NPT(-) of two T_2 families and four Moneymaker (MM) plants. In **(B)** bars and standard errors refer to ten plants T_2_NPT(+) and five plants T_2_NPT(-) of three T_2 families and four MM individuals. In **(C)** bars and standard errors refer to ten plants T_2_NPT(+) and five plants T_2_NPT(-) of three T_2 families and four MM individuals. In **(D)** bars and standard errors refer to 10 T_2_NPT(+) of two T_2 families and four MM individuals.

constructs visually appeared to be fully susceptible to *O. neolycopersici* (**Figure 5A**). The quantification of disease severity on these lines using real-time qPCR supported phenotypic observations, as no significant difference was found between T_2_*SlMLO3*_NPT(+), T_2_*SlMLO5*_NPT(+), T_2_*SlMLO8*_NPT(+) plants, and MM (**Figure 5B** and

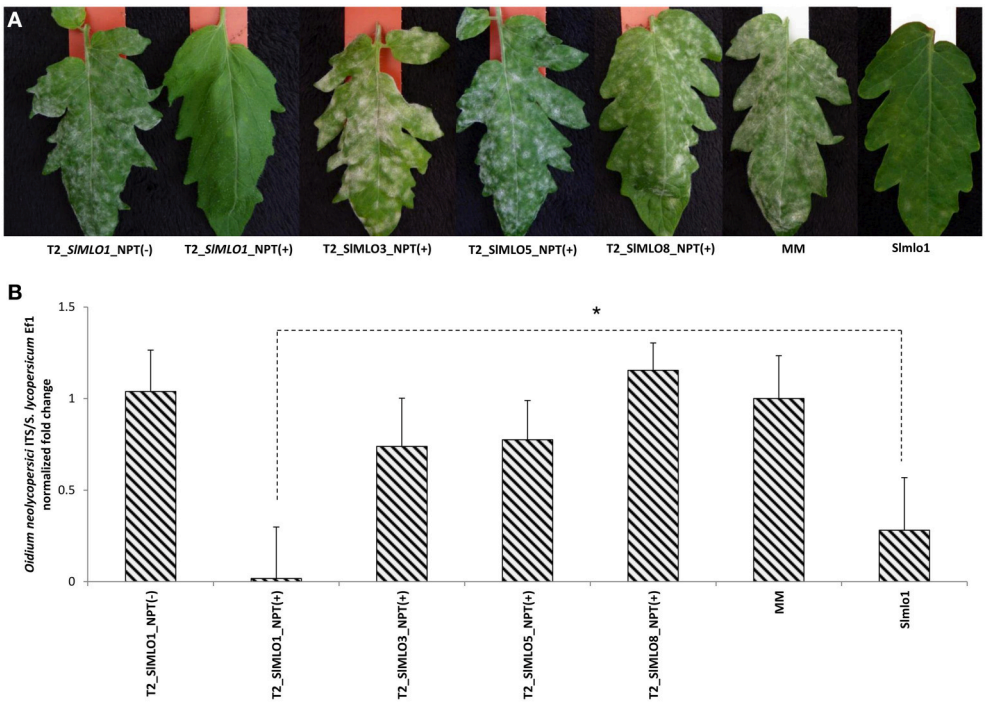

FIGURE 5 | Powdery mildew evaluation on plants of segregating T_2 families obtained with silencing constructs targeting *SlMLO* genes to attest their involvement in *O. neolycopersici* susceptibility. Panel **(A)** shows the phenotypic evaluation of the powdery mildew growth on leaves of different T_2 individuals that have been evaluated for the (from left to right) absence of the RNAi::*SlMLO1*, presence of the RNAi::*SlMLO1*, presence of the RNAi::*SlMLO3,* presence of the RNAi::*SlMLO5,* and presence of the RNAi::*SlMLO8* silencing constructs, followed by one individual of the cv Moneymaker (MM) and one of the Slmlo1 line carrying a loss-of-function mutation in the *SlMLO1* gene. Panel **(B)** shows the relative quantification of the ratio between *Oidium neolycopersici* and plant gDNAs in transgenic individuals [NPT(+)] and not transgenic individuals [NPT(-)] segregating in T_2 families obtained with the silencing constructs above described. Bars and standard errors refer to (from left to right) four individuals of two independent T_2 families not carrying the RNAi::*SlMLO1*, eight individuals of the same two T_2 families carrying the RNAi::*SlMLO1*, 18 individuals of three independent T_2 segregating families carrying the RNAi::*SlMLO3* construct, 18 individuals of three independent T_2 segregating families carrying the RNAi::*SlMLO5* construct and 20 individuals of two T_2 segregating families carrying the RNAi::*SlMLO8* construct, next to 10 MM plants and 10 plants of the Slmlo1 line. The asterisk refers to the significant difference in susceptibility between individuals of the T_2_SlMLO1_NPT(+) and Slmlo1, inferred by mean comparisons with a Student's *t*-test (*$p < 0.05$).

Supplementary Figure 9). For each T_2 family, transgenic and non-transgenic plants were phenotypically indistinguishable.

The Slmlo1 line, harboring a loss-of-function mutation in the *SlMLO1* gene (Bai et al., 2008), is resistant to PM, however lower leaves displayed PM symptoms (**Figure 5A**). Compared to the plants of the Slmlo1 line, RNAi plants carrying the RNAi::*SlMLO1* construct [T_2_*SlMLO1*_NPT(+) plants] showed no PM symptom and also a significantly lower amount of fungal biomass (**Figure 5B** and Supplementary Figure 9A). Therefore, further microscopic observations were carried out to study the fungal growth on the Slmlo1 line and T_2_*SlMLO1*_NPT(+) plants.

Since the two T_2 families carrying the RNAi::*SlMLO1* construct showed no difference with respect to the level of reduced expression of the *SlMLO* homologs and fungal biomass quantification (Supplementary Figures 8, 9), we used one T_2 family for microscopic study. Compared to MM, fungal growth was significantly reduced in both Slmlo1 and T_2_RNAi::*SlMLO1*_NPT(+) individuals due to the formation of a papilla beneath the appressorium (**Figure 6**). Interestingly, the rate of papilla formation in T_2_RNAi::*SlMLO1*_NPT(+) (93.3% of the infection units) was significantly higher than in Slmlo1 (64.4% of the infection units; **Table 4**). In some cases, *O. neolycopersici* was still able to penetrate epidermal cells and form haustoria with a rate of 48.9% in Slmlo1 and 30% in T_2_RNAi::*SlMLO1*_NPT(+) (**Table 4** and **Figure 6**). The general development of the spores on the two genotypes was strikingly different: while on the Slmlo1 line the fungus could produce mostly up to two secondary hyphae (in 36.7% of the total infection units), on T_2_RNAi::*SlMLO1*_NPT(+) individuals fungal growth was significantly reduced after producing a germination tube (**Table 4** and **Figure 6**).

DISCUSSION

Structure and Evolution of the *SlMLO* Gene Family

In this study, we followed an *in silico* approach to assign 16 homologs to the tomato *MLO* gene family. This is consistent with the results of previous studies reporting the *MLO* gene families of several diploid species made of a number of homologs variable from 13 to 21 (Devoto et al., 2003; Feechan et al., 2008; Liu and

TABLE 4 | Development of *Oidium neolycopersici* growth on the susceptible genotype Moneymaker and on the two resistant genotypes, Slmlo1 carrying a loss-of-function *SlMLO1* gene and plants of a T_2 family selected to carry the RNAi::*SlMLO1* silencing construct which can effectively silence *SlMLO1*, *SlMLO5,* and *SlMLO8*.

Genotype	Percentage of infection units (IU)					Hyphae per IU				
	Primary AP	Primary papilla	Primary HS	Secondary Papilla	Secondary HS	1	2	3	4	5
MM	100	0	90.2	0	68.3	76.8	67.1	35.4	6.1	0
Slmlo1	100	64.4	48.9	23.3	14.4	43.3	36.7	18.9	3.3	0
T_2_RNAi::*SlMLO1*_NPT(+)	100	93.3*	30.0	2.2	0.0	11.1	7.8	3.3	0.0	0

*AP, appressorium; HS, haustorium; *$p < 0.05$ compared to Slmlo1.*

Zhu, 2008; Shen et al., 2012; Pessina et al., 2014; Schouten et al., 2014; Appiano et al., 2015). This suggests that a similar number of *MLO* homologs is likely to be retrieved in future genome-wide investigations involving diploid eudicot species.

Information on chromosomal localization was available for all the *SlMLO* homologs with the exception of *SlMLO4*. However, potato and tomato genomes are highly syntenic (Tomato Genome Consortium, 2012) and the closest *SlMLO4* homolog in potato (Sotub02g007200) is positioned on chromosome 2, thus suggesting that *SlMLO4* is also located on tomato chromosome 2.

Cloning of the *SlMLO* gene family from different tissues of the cultivar MM revealed the occurrence of transcripts deviating from predictions available at the SGN database, indicating that, despite the efforts of the tomato resequencing project, the assembly of genomic regions and the prediction of certain loci are not correct yet. Moreover, several cases of differentially spliced variants among plant tissues were observed, mostly due to intron retention and exon skipping, as it is in the case of *SlMLO5*, *SlMLO9*, *SlMLO11, SlMLO13,* and *SlMLO15*. Due to the method used in this study to amplify the *SlMLO* homologs, we cannot exclude that the intron retention is the result of the amplification of non-mature mRNA. However, intron retention was previously reported to be a very common type of alternative splicing in Arabidopsis and rice (Ner-Gaon et al., 2007). There is also a well-documented evidence indicating organ-specific regulation of alternative splicing in plants (Palusa et al., 2007). More studies need to be performed to unravel its complexity and functional significance. Certainly, alternative forms of splicing, such as the ones found in this study, can lead to aberrant mRNA isoforms that cause the loss-of-function of a *MLO* gene. An example is reported by a recent study conducted by Berg et al. (2015) in cucumber. They show that the integration of a transposable element in the genomic region of the *CsaMLO8* leads to an aberrant splicing that causes the loss-of-function of this susceptibility gene in a resistant cucumber genotype.

The identification of protein motifs conserved in transmembrane domains of specific SlMLO homologs (**Tables 3A,B**) corroborates previous findings in Solanaceae plant species (Appiano et al., 2015). This indicates that transmembrane domains, which are thought to provide a common scaffold invariable for the whole MLO family (Devoto et al., 1999), might also be involved in conferring specific functions to MLO homologs. Future functional studies of targeted mutagenesis of transmembrane MLO protein regions can help to unravel their actual role.

All the SlMLO proteins were found to group in six phylogenetic clades together with other eudicot MLO homologs, including the complete Arabidopsis AtMLO family and certain members of the apple, peach and strawberry MLO family. No SlMLO homolog could be assigned to clade IV, previously shown to contain monocot MLO homologs and a few eudicot homologs (grapevine VvMLO14, strawberry FvMLO17, and peach PpMLO12) (Feechan et al., 2008; Pessina et al., 2014).

Based on their sequence relatedness with Arabidopsis AtMLO proteins of known function, it is logical to argue that one or more of the tomato SlMLO homologs in clade III and clade I could regulate the processes of root response to mechanical stimuli and pollen tube reception, respectively. The RNAi silenced lines of several *SlMLO* homologs generated in this study could be useful to assign new functions to MLO proteins which have gone unnoticed by the evaluation of the available panel of Arabidopsis *Atmlo* mutants.

Possible Pleiotropic Effects and Co-functioning of SlMLO Homologs

RNA-seq data, RT-PCR and real-time qPCR of the *SlMLO* gene family confirmed the expression of all the 16 *SlMLO* homologs. Often, it was possible to detect high level of transcript of the same *SlMLO* homolog in more than one of the four tissues under study (leaf, root, flower, and mature fruit). This is in line with the findings of the previous study of Chen et al. (2006), investigating the expression pattern of the Arabidopsis *AtMLO* gene family in several tissues. Overall, this body of evidence suggest that: (a) different *MLO* homologs may have synergistic or antagonistic roles in regulating the same biological process; (b) *MLO* homologs may have pleiotropic effects on different biological processes. Co-functioning between *MLO* homologs has been demonstrated to occur in Arabidopsis, where different *AtMLO* genes co-participate in the same tissue to determine powdery mildew susceptibility and root response to mechanical stimuli (Consonni et al., 2006; Chen et al., 2009). A yet unidentified additional biological function could be hypothesized for the *SlMLO1*, previously shown to act as a susceptibility gene toward *O. neolycopersici* (Pavan et al., 2009). This gene was found to exhibit its strongest expression level in tomato flower and moderate expression in root,

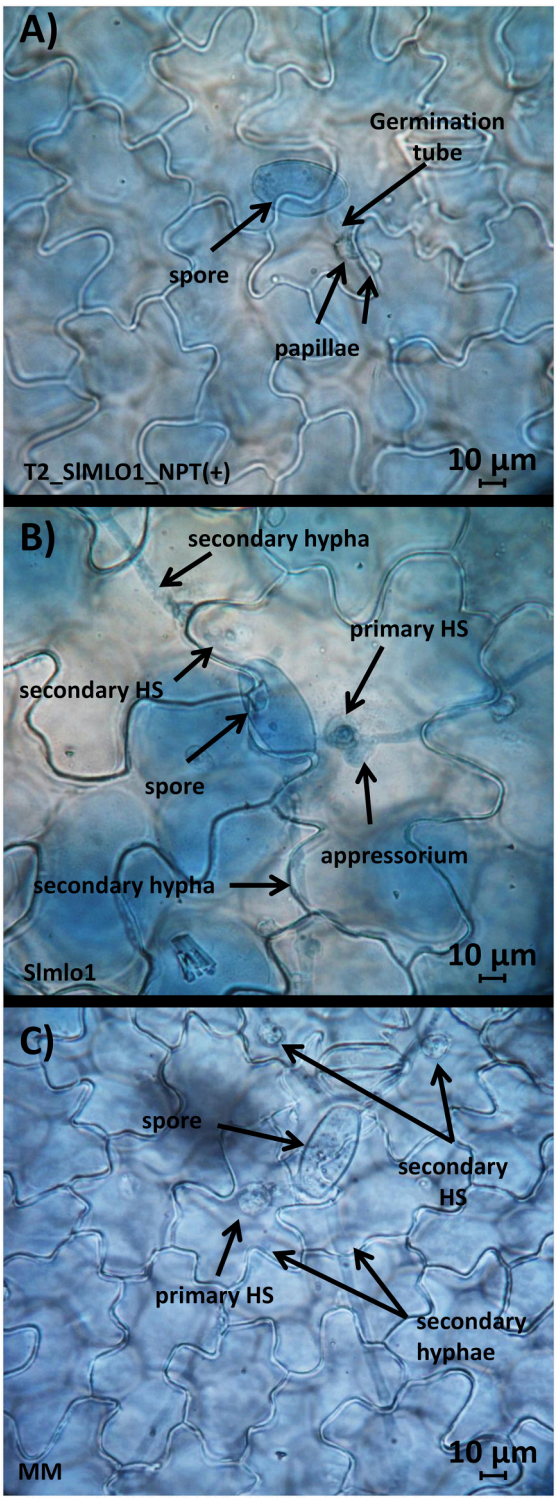

FIGURE 6 | Effect of the silencing of *SlMLO1*, *SlMLO5,* and *SlMLO8* in tomato cv Moneymaker background compared with the Slmlo1 line harboring a loss-of-function of the *SlMLO1* gene. Panel **(A)** refers to a transgenic plant carrying the RNAi::*SlMLO1* construct, Panel **(B)** a plant of the Slmlo1 line and **(C)** a plant of the tomato cv. Moneymaker. Panels **(A–C)** show fungal structures (spores, germination tube, appressorium, haustorium –HS-, and hyphae) and the plant cellular reaction of papilla apposition at the sites of fungal penetration.

two tissues which are less or not attacked by the fungus, respectively. Moreover, additional biological roles for *SlMLO1* would explain why this gene has not been excluded from evolution, despite promoting susceptibility to PM pathogen. Interestingly, evidence shows that the *SlMLO1* orthologs in barley and Arabidopsis are involved in the interaction with pathogens other than powdery mildews, such as necrotrophs and hemibiotroph (Jarosch et al., 1999; Kumar et al., 2001; Consonni et al., 2006). Thus, it is worthwhile to test the RNAi::*SlMLO1* plants with more pathogens to broaden its role in plant-pathogen interactions.

SlMLO Homologs Involved in Powdery Mildew Susceptibility

In this study, we mainly focused on the *SlMLO* genes grouped in the clade V containing all the *MLO* homologs associated with PM susceptibility in eudicots. The presence of multiple tomato homologs in clade V is in accordance with the existence of three Arabidopsis proteins (AtMLO2, AtMLO6, and AtMLO12) associated with increased fungal penetration (Consonni et al., 2006).

We showed that tomato *SlMLO3*, *SlMLO5,* and *SlMLO8*, differently from *SlMLO1*, do not increase their expression upon *O. neolycopersici* challenge. Furthermore, strong silencing of the same homologs in a susceptible tomato background (Moneymaker) did not result in a significant reduction of disease symptoms (**Figures 3**–**5**).

Plants transformed with a construct meant to silence *SlMLO1* showed co-silencing of *SlMLO5* and *SlMLO8*, due to sequence relatedness between these genes (**Figure 4**). Interestingly, these plants were also significantly more resistant than plants of the Slmlo1 line (**Figure 5**). Since the Slmlo1 line is only a BC_3S_2 line carrying the *Slmlo1*mutation (the *ol-2* gene) in MM background, we cannot fully exclude background effects from the *ol-2* donor, the resistant line LC-95 of *S. lycopersicum* var. *cerasiforme*, which might add to partial susceptibility phenotype of the Slmlo1 line. On the other hand, our scenario is reminiscent of the one reported in Arabidopsis, where *Atmlo2* single mutant displays partial PM resistance, whereas *Atmlo2/Atmlo6/Atmlo12* triple mutant is fully resistant (Consonni et al., 2006). Also in grape, more than one *VvMLO* genes are involved in susceptibility to powdery mildew (Feechan et al., 2008, 2013). Taken together with the knowledge of functional redundancy in Arabidopsis and grape, our data suggest that in tomato *SlMLO1*, *SlMLO5,* and *SlMLO8* are functionally redundant as PM susceptibility factors with *SlMLO1* playing a major role. Our results showed that the contribution of *SlMLO5* and *SlMLO8* is too small to be observed with an RNAi approach silencing individual genes, but a complementation experiment using the Slmlo1 line could be more suitable to observe their minor role.

It cannot be excluded yet that the other clade V tomato homolog, *SlMLO3*, is also involved in plant-pathogen interactions. However, it is worthwhile to notice that the SlMLO3 protein is missing three of the six motifs contained in SlMLO1, two of which are also present in SlMLO5 and SlMLO8 (**Table 3B**). The motif three in **Table 3B** is located in the second

intracellular domain, which is known to be involved together with the third intracellular domain in the protein functionality (Elliott et al., 2005). This would suggest that *SlMLO3* might miss important features to be fully functional as susceptibility factor. Overexpressing *SlMLO3* in the Slmlo mutant may provide a better evidence on its eventual role as a functional susceptibility gene.

Interestingly, we noticed that *SlMLO4* and *SlMLO14*, which do not belong to clade V, are up-regulated upon *O. neolycopersici* infection (**Figure 3** and Supplementary Figures 4, 5). *SlMLO14* is closely related to *AtMLO4* and *AtMLO11,* which are involved in root thigmomorphogenesis (Chen et al., 2009), while *SlMLO4* is related to *AtMLO7*, involved in pollen tube reception (Kessler et al., 2010). In Arabidopsis, mutation of *AtMLO4*, *AtMLO7,* and *AtMLO11* does not result in PM resistance. Thus, we expected that silencing of *SlMLO4* and *SlMLO14* in tomato will not lead to PM resistance too. The up-regulated expression of *SlMLO4* and *SlMLO14* after challenge with *O. neolycopersici* might be the result of shared regulatory cis-acting elements. We used a 2 kb region located upstream the starting codon of *SlMLO1*, *SlMLO4,* and *SlMLO14* coding sequences to search for shared regulatory elements through the online database Plant Care (http://bioinformatics.psb.ugent.be/webtools/plantcare/html/) (Lescot et al., 2002). We found at least five common motifs which are associated with upregulation by multiple biotic and/or abiotic stresses: ABRE (CACGTG), involved in abscisic acid responsiveness, CGTCA- and TGACG-motifs, involved in the MeJA responsiveness, HSE (AAAAAATTC), involved in heat stress responsiveness, and TCA (CCATCTTTTT/GAGAAGAATA) element, involved in salicylic acid response. It is intriguing whether *SlMLO4* and *SlMLO14* can act as a susceptibility gene to PM. Till now, only clade IV and clade V *MLO* genes have been studied for their role as a susceptibility gene. To further study these PM-induced non-clade V *SlMLO* genes, a complementation test using the Slmlo mutant could be performed.

In conclusion, this study provides a comprehensive characterization of the *MLO* gene family in tomato by analyzing their genomic structure, expression profile and predicted protein motifs. In tomato, there are 17 *MLO* genes which can be grouped into six clades. The expression of these *MLO* genes can be tissue specific and some *MLO* genes show alternative splicing variants in different tissues. The *SlMLO1* in clade V is confirmed to be the major PM susceptibility factor. In addition, two clade V genes, *SlMLO5* and *SlMLO8*, are suggested to have a partial redundant function, as described in Arabidopsis for *AtMLO2, 6,* and *12* genes (Consonni et al., 2006). To label an *MLO* gene as a PM susceptibility gene, it is recommended to combine phylogenetic analysis and expression profile to select candidates of clade IV (for monocot) and V (for dicot) that are induced by PM infection. However, the upregulation of *MLO* genes outside clade V in response to PM, as shown in this study and in Pessina et al. (2014), raises the possibility that they may act as susceptibility genes. Finally, the RNAi lines generated in this study are useful materials for further assigning new biological functions to the *MLO* gene family members.

MATERIALS AND METHODS

Plant Material, Fungal Material, and Inoculation

In this study, we used the susceptible *S. lycopersicum* cultivar Moneymaker (MM), the Slmlo1 line and transgenic T_2 families in which individual *SlMLO* gene was silenced via RNAi in MM background. The Slmlo1 mutant (the *ol-2* gene) was a natural mutation discovered in the resistant line LC-95 of *S. lycopersicum* var. *cerasiforme*. The LC-95 line was crossed with the susceptible tomato *S. lycopersicum* cv. Super Marmande and the F2 progeny was used for mapping in 1998 (Ciccarese et al., 1998). Later, we introgressed the *ol-2* allele into *S. lycopersicum* cv Moneymaker (MM) by backcrossing and one BC3S2 line homozygous for the *ol-2* allele (the tomato Slmlo1 line) was used in the experiment.

The powdery mildew disease assay was performed by artificial inoculation in the greenhouse. For this, the Wageningen isolate of *O. neolycopersici* (*On*) was used (Bai et al., 2008). A suspension of *O. neolycopersici* conidia was prepared, by rinsing freshly sporulating leaves of infected tomato plants with tap water. This suspension was immediately sprayed on 1 month-old tomato plants. Ten plants for each of the T_2 progenies obtained from the transformation of each silencing construct, 10 Slmlo1 plants and 10 MM plants were used for disease assay. The scoring of powdery mildew symptoms was done 10 days after inoculation, inspecting and collecting the third and fourth true leaves for each plant.

For the evaluation of the expression of the *SlMLO* gene family, two independent inoculations were set up. In both cases, we used the cultivar MM, four and three biological replicates for each of the three time points (0, 6, and 10 h post inoculation –*hpi*-) during the first and the second inoculation, respectively.

Identification and Cloning of the *SlMLO* Gene Family

Putative tomato MLO protein sequences were identified in the Sol Genomics Network (SGN) (http://solgenomics.net/) database by using the BLASTP and TBLASTN algorithms with Arabidopsis AtMLO protein sequences as query. Chromosomal localization, sequences of the corresponding genes and introns/exons boundaries were inferred by annotations from the International Tomato Annotation Group (ITAG).

Aiming at cloning and sequencing the *SlMLO* gene family from the cultivar MM, total RNA from leaf, root, flower and ripened fruit was isolated (RNeasy® mini kit, Qiagen). The different tissues were collected from five MM plants and pooled together to obtain enough material for the RNA isolation. For each individual *SlMLO* homolog, two primer pairs specifically amplifying overlapping products of around 800 bp of the predicted coding sequences (CDS) were designed using the Primer3 plus online software (http://www.bioinformatics.nl/cgi-bin/primer3plus/primer3plus.cgi; Rozen and Skaletsky, 2000). The forward primer and the reverse primer of product A and product B, respectively, are located in the respective UTR regions to ensure the cloning of the complete CDS. A one-step PCR was performed to obtain

the desired product (SuperScript® III One-Step RT-PCR System, Invitrogen; Supplementary Table 1). Its high sensitivity and specificity ensured the amplification of these very lowly expressed genes. Indeed, a PCR performed on a cDNA obtained with oligo$(dT)_{20}$ primers did not yield any product for many of the homologs under investigation. The use of sequence-specific primers in the one-step PCR, on the other hand, allowed the binding of only the desired mRNA sequences.

Corresponding amplicons were visualized on agarose gel and cloned into the pGEM®-T Easy vector (Promega). Recombinant plasmids were sequenced by using universal T7 and SP6 primers.

In order to reveal gene structures and polymorphisms, *SlMLO* sequences obtained by cloned amplicons were merged using the package Seqman of the software DNASTAR® Lasergene8. The obtained consensus was aligned with the coding region of the *SlMLO* identified *in silico* and the corresponding genomic region using the CLC 7.6.1 sequence viewer software (www.clcbio.com).

Finally, for the motif analysis, the MEME (http://meme.nbcr.net/) package was used to predict consensus patterns of consecutive conserved amino acids in the SlMLO proteins deriving from the *in silico* translation of the cloned transcripts from leaf, root, flower, and fruit of the cultivar MM (Bailey et al., 2015).

Comparative Analysis

The corresponding SlMLO protein sequences of translated cloned CDS obtained from leaf and flower (in the case of *SlMLO12*) were used as dataset in the CLC 7.6.1 sequence viewer software (www.clcbio.com) for ClustalW alignment and the obtainment of an UPGMA-based comparative tree (bootstrap value was set equal to 100), together with those of the 15 Arabidopsis AtMLO homologs. Moreover, MLO proteins experimentally shown to be required for PM susceptibility were added, namely pea PsMLO1, barley HvMLO, wheat TaMLO_A1b and TaMLO_B1a, rice OsMLO3, pepper CaMLO2, tobacco NtMLO1, cucumber CsaMLO8, *Lotus japonicus* LjMLO1, and barrel clover MtMLO1. Moreover, MLO homologs of the Rosaceae species that cluster in clade VII (FvMLO15, MdMLO18, PpMLO9) and VIII (FvMLO13, MdMLO20, and PpMLO13) were included (Supplementary Table 2). The obtained UPGMA-comparative tree was then displayed as circular rooted cladogram with CLC software.

Expression Analysis of the *SlMLO* Gene Family in Response to *O. neolycopersici*

Tissue samples from the third and fourth true leaf of 1 month-old tomato plants were collected immediately before fungal inoculation and at two time points after inoculation (6 and 10 h). The RNA isolation was performed with MagMAX-96 Total RNA Isolation kit (Applied Biosystem), following the manufacturer's instructions. Included in the protocol is a DNase treatment using the TURBO™ DNase. An aliquot of the RNA isolated was run on denaturing agarose gel to assess its integrity. Purity and concentration were determined by measuring its absorbance at 260 and 280 nm using the NanoDrop® 1000A spectrophotometer. Following this protocol for RNA isolation, intact and pure RNA was obtained and the concentration was variable between 200 and 250ng/μl.

cDNAs were synthesized by using the SuperScript III first-strand synthesis kit (Invitrogen) using the oligo$(dT)_{20}$ primer, starting from the same amount of RNA (200 ng/μl). Specific primer pairs for each of the 16 *SlMLO* homologs, amplifying fragments ranging from 70 to 230 bp, were designed as described above (Supplementary Table 3). The amplification of single fragments of the expected size for each homolog was verified by agarose gel electrophoresis and by the observation of the melting pick. Four tomato reference genes were tested for expression stability in order to determine which ones could be suitable for normalization of the expression of *SlMLO* homologs. These included the 60S ribosomal protein L33 (GeneBank number Q2MI79), the elongation factor 1α (GeneBank number X14449), actin (Genebank XP_004236747), and ubiquitin (GeneBank number XP_004248311) (Schijlen et al., 2007; Løvdal and Lillo, 2009). Gene expression stability was assayed with the BestKeeper program (Pfaffl et al., 2004), determining as best reference genes the ribosomal protein L33 and the elongation factor 1α. The cDNAs were diluted 10-fold and used in real-time qPCR with a Bio-Rad CFX96TM thermal cycler. The thermal cycling conditions used were 95°C for 1 min, followed by 40 cycles at: 95°C for 15 s, 60°C for 1 min, and 72°C for 30 s, followed by a melt cycle of 0.5°C increment per min from 65 to 95°C. Comparable amplification efficiencies between target and reference genes were determined using the LinRegPCR software (Karlen et al., 2007). Normalization was performed according to the $\Delta\Delta C_t$ method (Livak and Schmittgen, 2001). Four biological replicates and two technical replicates were used in this experiment. Student's *t*-tests were applied in order to assess significant differences between the treatments.

SlMLO Family Expression Analysis in Different Tissues

To analyze *MLO* gene expression in leaf, root, flower and ripened fruit approximately equal amount of tissues from five MM plants were pooled and used for RNA isolation and cDNA synthesis as described in the previous paragraph. Before using them as templates, cDNAs were diluted 10-fold. Real-time qPCR was performed using the set of primers reported in Supplementary Table 3 to amplify each homolog in the four tissues above mentioned. Elongation factor 1α was used as reference gene. Data analysis was performed according to the ΔC_t method (Livak and Schmittgen, 2001). Three technical replicates for each sample were performed.

Generation of RNAi Silencing Lines

Four primer pairs were designed to amplify and clone fragments from *SlMLO1*, *SlMLO3*, *SlMLO5,* and *SlMLO8* into the Gateway-compatible vector pENTR D-TOPO (Invitrogen) (Supplementary Table 3). The cloned sequences of the *SlMLO1*, *SlMLO3*, *SlMLO5,* and *SlMLO8* genes are highlighted in Supplementary Figure 6. After cloning in *E. coli* (strain DH5α), the kanamycin-resistant colonies were assessed for the presence of constructs by colony PCR. Positive recombinant plasmids were further analyzed by restriction enzyme digestion

and sequencing. Next, amplicons were transferred by LR recombination reaction into the pHELLSGATE12 vector for hairpin-induced RNAi (Wielopolska et al., 2005) following the instructions provided by the manufacturer (Invitrogen), and cloned again in *E. coli* DH5α. Bacterial colonies growing on a spectinomycin-containing medium were selected for the presence of the silencing construct by colony PCR and sequencing. Recombinant plasmids were transferred into the AGL1+virG strain of *Agrobacterium tumefaciens* (Lazo et al., 1991) by electroporation, and transformed bacterial cells were selected on a medium containing 100 mg/ml^{-1} spectinomycin, 50 mg/ml^{-1} carbenicillin, and 50 mg/ml^{-1} chloramphenicol. Single colonies of *A. tumefaciens* were picked and the presence of the insert was confirmed by colony PCR. Ten-fold dilutions of overnight culture from single positive colonies were re-suspended in MSO medium (4.3 g/l MS basal salt mixture, 30 g/l sucrose, 0.4 mg/l thiamine, 100 mg/l myoinositol, pH 5.8) to a final OD_{600} of 0.5 and used for transformation.

The transformation procedure for tomato cotyledons was carried out similarly to the method described by Appiano et al. (2015).

Silencing efficiency was assessed, for each of the four constructs, on 10–20 T_1 plants and on selected T_2 lines by real-time qPCR, as described for the analysis of the *SlMLO* gene family expression in response to *O. neolycopersici*. In addition, the T_2 lines were assessed for the presence of the NPTII marker gene and the 35S promoter by PCR, using the primer pair NPTII_Fw (5′ACTGGGCACAACAGACAATC3′)/NPTII_Rev (5′ TCGTCCTGCAGTTCATTCAG 3′) and 35S-Fw (5′-GCTCCTACAAATGCCATCA-3′)/35S-Rev (5′- GATAGTGG GATTGTGCGTCA-3′), and visualizing the products on agarose gel.

Disease Quantification on Silenced Lines

T_2 lines originating from selfing of T_1 plants showing high level of silencing were inoculated with *O. neolycopersici* (*On*) by spraying 4 weeks old plants with a suspension of conidiospores obtained from freshly sporulating leaves of heavily infected plants and adjusted to a final concentration of 4×10^4 spores/ml. Inoculated plants were grown in a greenhouse compartment at 20 ± 2°C with 70 ± 15% relative humidity and day length of 16 h. Two weeks later, infected tissues from the third and fourth true leaf were visually scored and sampled. Plant and fungal DNAs were extracted by using the DNeasy DNA extraction kit (Qiagen). In total, 15 ng of DNA was used as template for amplification with the primer pair *On*-Fw (5′-CGCCAAAGACCTAACCAAAA-3′) and *On*-Rev (5′-AGCCAAGAGATCCGTTGTTG-3′), designed on *On*-specific internal transcribed spacer sequences (GenBank accession number EU047564). The tomato Ef1α primers (Supplementary Table 3) were used as reference to determine fungal biomass relative to host plant DNA by $\Delta\Delta C_t$ method.

Disease Tests for Microscopic Evaluation in Histological Study

Spores of the Wageningen isolate of *O. neolycopersici* grown in a climate chamber at 20 ± 1°C, with 70 ± 10% RH and a 16-h photoperiod were water-sprayed on the third leaf of 1-month old tomato plants of the susceptible tomato cv. MM, the resistant line Slmlo1 and transgenic plants of one T_2 family selected by PCR for the presence of the NPTII and 35S marker genes of the RNAi::*SlMLO1* silencing construct. The concentration of the spore suspension was 3×10^5 conidia ml^{-1}. After 65 h, a 4 cm^2 segment was cut from the inoculated leaves. Three samples were taken from four plants of each genotype and from five plants of the T_2 family, bleached in a 1:3 (v/v) acetic acid/ethanol solution and 48 h later stained in 0.005% trypan blue as described by Pavan et al. (2008). For each genotype, a total of 90 infection units (IU), defined as a germinated spore that produced, at least, a primary appressorium, were counted. Observations were performed using a Zeiss Axiophot bright field microscope and pictures were taken with an Axiocam ERc5s. For each IU, the number of hyphae, the presence/absence of a primary and secondary haustoria and presence/absence of papillae were recorded.

AUTHOR CONTRIBUTIONS

Conceived and designed the experiments: ZZ, MA, SP, and VB. Performed the experiments: MA, ZZ, VB. Analyzed the data: MA, ZZ, VB. Contributed reagents/materials/ analysis tools: LR, RV. Wrote and edited the paper: SP, MA, ZZ, AW, and VB.

FUNDING

The work of ZZ is supported by the Chinese Academy of Agricultural Sciences Fundamental Research Budget Increment Project (Grant No. 2015ZL008), The Agricultural Science and Technology Innovation Program (Grant No. CAAS-ASTIP-2013-IVFCAAS) and the Merit-based Scientific Research Foundation of the State Ministry of Human Resources and Social Security of China for Returned Overseas Chinese Scholars (Grant No. 2015-192). The work of SP, VB, and LR was supported by the Italian Ministry of University and Research (GenHORT project).

SUPPLEMENTARY MATERIAL

The Supplementary Material for this article can be found online at: http://journal.frontiersin.org/article/10.3389/fpls.2016.00380

REFERENCES

Acevedo-Garcia, J., Kusch, S., and Panstruga, R. (2014). Magical mystery tour: MLO proteins in plant immunity and beyond. *New Phytol.* 204, 273–281. doi: 10.1111/nph.12889

Appiano, M., Pavan, S., Catalano, D., Zheng, Z., Bracuto, V., Lotti, C., et al. (2015). Identification of candidate MLO powdery mildew susceptibility genes in cultivated Solanaceae and functional characterization of tobacco NtMLO1. *Transgenic Res.* 24, 847–858. doi: 10.1007/s11248-015-9878-4

Bai, Y., Pavan, S., Zheng, Z., Zappel, N. F., Reinstädler, A., Lotti, C., et al. (2008). Naturally occurring broad-spectrum powdery mildew resistance in a Central American tomato accession is caused by loss of Mlo function. *Mol. Plant Microbe Interact.* 21, 30–39. doi: 10.1094/MPMI-21-1-0030

Bai, Y., Van Der Hulst, R., Bonnema, G., Marcel, T. C., Meijer-Dekens, F., Niks, R. E., et al. (2005). Tomato defense to *Oidium neolycopersici*: dominant OI genes confer isolate-dependent resistance via a different mechanism than recessive oI-2. *Mol. Plant Microbe Interact.* 18, 354–362. doi: 10.1094/MPMI-18-0354

Bailey, T. L., Johnson, J., Grant, C. E., and Noble, W. S. (2015). The MEME suite. *Nucleic Acids Res.* 37, W202–W208. doi: 10.1093/nar/gkv416

Berg, J., Appiano, M., Santillán Martínez, M., Hermans, F., Vriezen, W., Visser, R., et al. (2015). A transposable element insertion in the susceptibility gene CsaMLO8 results in hypocotyl resistance to powdery mildew in cucumber. *BMC Plant Biol.* 15:243. doi: 10.1186/s12870-015-0635-x

Büschges, R., Hollricher, K., Panstruga, R., Simons, G., Wolter, M., Frijters, A., et al. (1997). The barley Mlo gene: a novel control element of plant pathogen resistance. *Cell* 88, 695–705. doi: 10.1016/S0092-8674(00)81912-1

Chen, Z., Hartmann, H. A., Wu, M. J., Friedman, E. J., Chen, J. G., Pulley, M., et al. (2006). Expression analysis of the AtMLO gene family encoding plant-specific seven-transmembrane domain proteins. *Plant Mol. Biol.* 60, 583–597. doi: 10.1007/s11103-005-5082-x

Chen, Z., Noir, S., Kwaaitaal, M., Hartmann, H. A., Wu, M. J., Mudgil, Y., et al. (2009). Two seven-transmembrane domain MILDEW RESISTANCE LOCUS O proteins cofunction in arabidopsis root thigmomorphogenesis. *Plant Cell* 21, 1972–1991. doi: 10.1105/tpc.108.062653

Ciccarese, F., Amenduni, M., Schiavone, D., and Cirulli, M. (1998). Occurrence and inheritance of resistance to powdery mildew (*Oidium lycopersici*) in *Lycopersicon* species. *Plant Pathol.* 47, 417–419. doi: 10.1046/j.1365-3059.1998.00254.x

Consonni, C., Humphry, M. E., Hartmann, H. A., Livaja, M., Durner, J., Westphal, L., et al. (2006). Conserved requirement for a plant host cell protein in powdery mildew pathogenesis. *Nat. Genet.* 38, 716–720. doi: 10.1038/ng1806

Devoto, A., Hartmann, H. A., Piffanelli, P., Elliott, C., Simmons, C., Taramino, G., et al. (2003). Molecular phylogeny and evolution of the plant-specific seven-transmembrane MLO family. *J. Mol. Evol.* 56, 77–88. doi: 10.1007/s00239-002-2382-5

Devoto, A., Piffanelli, P., Nilsson, I., Wallin, E., Panstruga, R., von Heijne, G., et al. (1999). Topology, subcellular localization, and sequence diversity of the Mlo family in plants. *J. Biol. Chem.* 274, 34993–35004. doi: 10.1074/jbc.274.49.34993

Elliott, C., Müller, J., Miklis, M., Bhat, R. A., Schulze-Lefert, P., and Panstruga, R. (2005). Conserved extracellular cysteine residues and cytoplasmic loop-loop interplay are required for functionality of the heptahelical MLO protein. *Biochem. J.* 385, 243–254. doi: 10.1042/BJ20040993

Elliott, C., Zhou, F., Spielmeyer, W., Panstruga, R., and Schulze-Lefert, P. (2002). Functional conservation of wheat and rice Mlo orthologs in defense modulation to the powdery mildew fungus. *Mol. Plant Microbe Interact.* 15, 1069–1077. doi: 10.1094/MPMI.2002.15.10.1069

Feechan, A., Jermakow, A. M., Ivancevic, A., Godfrey, D., Pak, H., Panstruga, R., et al. (2013). Host cell entry of powdery mildew is correlated with endosomal transport of antagonistically acting VvPEN1 and VvMLO to the papilla. *Mol. Plant Microbe Interact.* 26, 1138–1150. doi: 10.1094/MPMI-04-13-0091-R

Feechan, A., Jermakow, A. M., Torregrosa, L., Panstruga, R., and Dry, I. B. (2008). Identification of grapevine MLO gene candidates involved in susceptibility to powdery mildew. *Funct. Plant Biol.* 35, 1255–1266. doi: 10.1071/FP08173

Humphry, M., Reinstädler, A., Ivanov, S., Bisseling, T., and Panstruga, R. (2011). Durable broad-spectrum powdery mildew resistance in pea er1 plants is conferred by natural loss-of-function mutations in PsMLO1. *Mol. Plant Pathol.* 12, 866–878. doi: 10.1111/j.1364-3703.2011.00718.x

Jarosch, B., Kogel, K. H., and Schaffrath, U. (1999). The ambivalence of the barley Mlo locus: mutations conferring resistance against powdery mildew (*Blumeria graminis* f. sp. hordei) enhance susceptibility to the rice blast fungus *Magnaporthe grisea*. *Mol. Plant Microbe Interact.* 12, 508–514.

Jørgensen, I. H. (1992). Discovery, characterization and exploitation of Mlo powdery mildew resistance in barley. *Euphytica* 63, 141–152. doi: 10.1007/BF00023919

Karlen, Y., McNair, A., Perseguers, S., Mazza, C., and Mermod, N. (2007). Statistical significance of quantitative PCR. *BMC Bioinformatics* 8:131. doi: 10.1186/1471-2105-8-131

Keren, H., Lev-Maor, G., and Ast, G. (2010). Alternative splicing and evolution: diversification, exon definition and function. *Nat. Rev. Genet.* 11, 345–355. doi: 10.1038/nrg2776

Kessler, S. A., Shimosato-Asano, H., Keinath, N. F., Wuest, S. E., Ingram, G., Panstruga, R., et al. (2010). Conserved molecular components for pollen tube reception and fungal invasion. *Science* 330, 968–971. doi: 10.1126/science.1195211

Kim, M. C., Panstruga, R., Elliott, C., Müller, J., Devoto, A., Yoon, H. W., et al. (2002). Calmodulin interacts with MLO protein to regulate defence against mildew in barley. *Nature* 416, 447–451. doi: 10.1038/416447a

Kumar, J., Hückelhoven, R., Beckhove, U., Nagarajan, S., and Kogel, K. H. (2001). A compromised Mlo pathway affects the response of barley to the necrotrophic fungus *Bipolaris sorokiniana* (Teleomorph: *Cochliobolus sativus*) and its toxins. *Phytopathology* 91, 127–133. doi: 10.1094/PHYTO.2001.91.2.127

Lazo, G. R., Stein, P. A., and Ludwig, R. A. (1991). A DNA transformation-competent Arabidopsis genomic library in Agrobacterium. *Nat. Biotechnol.* 9, 963–967. doi: 10.1038/nbt1091-963

Lescot, M., Déhais, P., Thijs, G., Marchal, K., Moreau, Y., Van De Peer, Y., et al. (2002). PlantCARE, a database of plant cis-acting regulatory elements and a portal to tools for *in silico* analysis of promoter sequences. *Nucleic Acids Res.* 30, 325–327. doi: 10.1093/nar/30.1.325

Liu, Q., and Zhu, H. (2008). Molecular evolution of the MLO gene family in *Oryza sativa* and their functional divergence. *Gene* 409, 1–10. doi: 10.1016/j.gene.2007.10.031

Livak, K. J., and Schmittgen, T. D. (2001). Analysis of relative gene expression data using real-time quantitative PCR and the 2 -ΔΔCT method. *Methods* 25, 402–408. doi: 10.1006/meth.2001.1262

Lorek, J., Griebel, T., Jones, A. M., Kuhn, H., and Panstruga, R. (2013). The role of Arabidopsis heterotrimeric G-protein subunits in MLO2 function and MAMP-triggered immunity. *Mol. Plant Microbe Interact.* 26, 991–1003. doi: 10.1094/MPMI-03-13-0077-R

Løvdal, T., and Lillo, C. (2009). Reference gene selection for quantitative real-time PCR normalization in tomato subjected to nitrogen, cold, and light stress. *Anal. Biochem.* 387, 238–242. doi: 10.1016/j.ab.2009.01.024

Miklis, M., Consonni, C., Bhat, R. A., Lipka, V., Schulze-Lefert, P., and Panstruga, R. (2007). Barley MLO modulates actin-dependent and actin-independent antifungal defense pathways at the cell periphery. *Plant Physiol.* 144, 1132–1143. doi: 10.1104/pp.107.098897

Ner-Gaon, H., Leviatan, N., Rubin, E., and Fluhr, R. (2007). Comparative cross-species alternative splicing in plants. *Plant Physiol.* 144, 1632–1641. doi: 10.1104/pp.107.098640

Opalski, K. S., Schultheiss, H., Kogel, K. H., and Hückelhoven, R. (2005). The receptor-like MLO protein and the RAC/ROP family G-protein RACB modulate actin reorganization in barley attacked by the biotrophic powdery mildew fungus *Blumeria graminis* f.sp. hordei. *Plant J.* 41, 291–303. doi: 10.1111/j.1365-313X.2004.02292.x

Palusa, S. G., Ali, G. S., and Reddy, A. S. N. (2007). Alternative splicing of pre-mRNAs of Arabidopsis serine/arginine-rich proteins: regulation by hormones and stresses. *Plant J.* 49, 1091–1107. doi: 10.1111/j.1365-313X.2006.03020.x

Panstruga, R. (2005). Serpentine plant MLO proteins as entry portals for powdery mildew fungi. *Biochem. Soc. Trans.* 33, 389–392. doi: 10.1042/BST0330389

Panstruga, R., and Schulze-Lefert, P. (2003). Corruption of host seven-transmembrane proteins by pathogenic microbes: a common theme in animals and plants? *Microbes Infect.* 5, 429–437. doi: 10.1016/S1286-4579(03)00053-4

Pavan, S., Jacobsen, E., Visser, R. G. F., and Bai, Y. (2009). Loss of susceptibility as a novel breeding strategy for durable and broad-spectrum resistance. *Mol. Breed.* 25, 1–12. doi: 10.1007/s11032-009-9323-6

Pavan, S., Zheng, Z., Borisova, M., Van Den Berg, P., Lotti, C., De Giovanni, C., et al. (2008). Map- vs. homology-based cloning for the recessive gene ol-2 conferring resistance to tomato powdery mildew. *Euphytica* 162, 91–98. doi: 10.1007/s10681-007-9570-8

Pessina, S., Pavan, S., Catalano, D., Gallotta, A., Visser, R. G., Bai, Y., et al. (2014). Characterization of the MLO gene family in Rosaceae and gene expression analysis in Malus domestica. *BMC Genomics* 15:618. doi: 10.1186/1471-2164-15-618

Pfaffl, M. W., Tichopad, A., Prgomet, C., and Neuvians, T. P. (2004). Determination of stable housekeeping genes, differentially regulated target genes and sample integrity: bestkeeper - Excel-based tool using pair-wise correlations. *Biotechnol. Lett.* 26, 509–515. doi: 10.1023/B:BILE.0000019559.84305.47

Reinstädler, A., Müller, J., Czembor, J. H., Piffanelli, P., and Panstruga, R. (2010). Novel induced mlo mutant alleles in combination with site-directed mutagenesis reveal functionally important domains in the heptahelical barley Mlo protein. *BMC Plant Biol.* 10:31. doi: 10.1186/1471-2229-10-31

Rozen, S., and Skaletsky, H. (2000). Primer3 on the WWW for general users and for biologist programmers. *Methods Mol. Biol.* 132, 365–386. doi: 10.1385/1-59259-192-2:365

Schijlen, E. G. W. M., de Vos, C. H. R., Martens, S., Jonker, H. H., Rosin, F. M., Molthoff, J. W., et al. (2007). RNA interference silencing of chalcone synthase, the first step in the flavonoid biosynthesis pathway, leads to parthenocarpic tomato fruits. *Plant Physiol.* 144, 1520–1530. doi: 10.1104/pp.107.100305

Schouten, H., Krauskopf, J., Visser, R. F., and Bai, Y. (2014). Identification of candidate genes required for susceptibility to powdery or downy mildew in cucumber. *Euphytica* 200, 475–486. doi: 10.1007/s10681-014-1216-z

Seifi, A., Gao, D., Zheng, Z., Pavan, S., Faino, L., Visser, R. F., et al. (2014). Genetics and molecular mechanisms of resistance to powdery mildews in tomato (*Solanum lycopersicum*) and its wild relatives. *Eur. J. Plant Pathol.* 138, 641–665. doi: 10.1007/s10658-013-0314-4

Shen, Q., Zhao, J., Du, C., Xiang, Y., Cao, J., and Qin, X. (2012). Genome-scale identification of MLO domain-containing genes in soybean (Glycine max L. Merr.). *Genes Genet. Syst.* 87, 89–98. doi: 10.1266/ggs.87.89

The 100 Tomato Genome Sequencing Consortium, Aflitos, S., Schijlen, E., De Jong, H., De Ridder, D., Smit, S., et al. (2014). Exploring genetic variation in the tomato (Solanum section Lycopersicon) clade by whole-genome sequencing. *Plant J.* 80, 136–148. doi: 10.1111/tpj.12616

Tomato Genome Consortium (2012). The tomato genome sequence provides insights into fleshy fruit evolution. *Nature* 485, 635–641. doi: 10.1038/nature11119

van Schie, C. C. N., and Takken, F. L. W. (2014). Susceptibility genes 101: how to be a good host. *Annu. Rev. Phytopathol.* 52, 551–581. doi: 10.1146/annurev-phyto-102313-045854

Várallyay, É., Giczey, G., and Burgyán, J. (2012). Virus-induced gene silencing of Mlo genes induces powdery mildew resistance in *Triticum aestivum*. *Arch. Virol.* 157, 1345–1350. doi: 10.1007/s00705-012-1286-y

Wielopolska, A., Townley, H., Moore, I., Waterhouse, P., and Helliwell, C. (2005). A high-throughput inducible RNAi vector for plants. *Plant Biotechnol. J.* 3, 583–590. doi: 10.1111/j.1467-7652.2005.00149.x

Zheng, Z., Nonomura, T., Appiano, M., Pavan, S., Matsuda, Y., Toyoda, H., et al. (2013). Loss of function in Mlo orthologs reduces susceptibility of pepper and tomato to powdery mildew disease caused by *Leveillula taurica*. *PLoS ONE* 8:e70723. doi: 10.1371/journal.pone.0070723

Zhou, S. J., Jing, Z., and Shi, J. L. (2013). Genome-wide identification, characterization, and expression analysis of the MLO gene family in *Cucumis sativus*. *Genet. Mol. Res.* 12, 6565–6578. doi: 10.4238/2013.december.11.8

Conflict of Interest Statement: The authors declare that the research was conducted in the absence of any commercial or financial relationships that could be construed as a potential conflict of interest.

frontiers in Plant Science

ORIGINAL RESEARCH
published: 31 May 2016
doi: 10.3389/fpls.2016.00742

Reduction of Growth and Reproduction of the Biotrophic Fungus *Blumeria graminis* in the Presence of a Necrotrophic Pathogen

*Elizabeth S. Orton and James K. M. Brown**

Crop Genetics, John Innes Centre, Norwich, UK

Crops are attacked by many potential pathogens with differing life-history traits, which raises the question of whether or not the outcome of infection by one pathogen may be modulated by a change in the host environment brought on by infection by another pathogen. We investigated the host-mediated interaction between the biotroph *Blumeria graminis* f.sp. *tritici* (*Bgt*), the powdery mildew pathogen of wheat, and the necrotroph *Zymoseptoria tritici*, which has a long latent, endophytic phase following which it switches to a necrotrophic phase, resulting in the disease symptoms of Septoria tritici blotch. Both diseases are potentially severe in humid temperate climates and are controlled by fungicides and by growing wheat varieties with partial resistance. The compatible interaction between *Z. tritici* and the host reduced the number, size, and reproductive capacity of mildew colonies that a normally virulent *Bgt* isolate would produce but did not significantly alter the early development of *Bgt* on the leaf. The effect on virulent *Bgt* was elicited only by viable spores of *Z. tritici*. Notably, this effect was seen before the necrotic foliar symptoms induced by *Z. tritici* were visible, which implies there is a physiological interaction during the latent, endophytic period of *Z. tritici*, which either takes place directly between this fungus and *Bgt* or is mediated by the wheat leaf. Information on how different pathogens interact in host plants may allow plant breeders and others to improve the design of screening trials and selection of germplasm.

Keywords: powdery mildew, *Blumeria graminis*, *Zymoseptoria tritici*, co-infection, wheat, biotrophic pathogens, necrotrophic pathogens

OPEN ACCESS

Edited by:
Pietro Daniele Spanu, Imperial College London, UK

Reviewed by:
William Underwood, United States Department of Agriculture-Agricultural Research Service, USA
Jan A. L. Van Kan, Wageningen University, Netherlands

****Correspondence:***
James K. M. Brown
james.brown@jic.ac.uk

Specialty section:
This article was submitted to Plant Biotic Interactions, a section of the journal Frontiers in Plant Science

Received: *31 March 2016*
Accepted: *16 May 2016*
Published: *31 May 2016*

Citation:
Orton ES and Brown JKM (2016) Reduction of Growth and Reproduction of the Biotrophic Fungus Blumeria graminis *in the Presence of a Necrotrophic Pathogen. Front. Plant Sci. 7:742. doi: 10.3389/fpls.2016.00742*

INTRODUCTION

Plants are exposed to many different microbes including potential pathogens. Studies of disease on crop pathology tend to focus on individual diseases, but when environmental conditions are conducive to more than one parasite, plants must defend themselves against several species, often with different life histories. Understanding interactions between multiple pathogens on a host plant is essential for being able to control multiple diseases simultaneously in a crop. Disease control on arable crops generally requires the combined use of pesticides and resistant varieties (Torriani et al., 2015). While some groups of fungicides have broad-spectrum activity against several diseases,

the scope for relying on them is diminishing because of the evolution of insensitivity in important pathogens (Lucas et al., 2015) and increased regulation of the marketing and use of agrochemicals (Hillocks, 2012; Jess et al., 2014). Regarding breeding for disease resistance, a cultivar has little value to farmers if it has good resistance to one disease but high susceptibility to another disease which is also important in the same environment. Efforts to breed crop varieties resistant to multiple pathogens will be assisted by information on how important pathogens interact with each other and the mechanisms behind their interaction. This will support the design of disease screening trials and the choice of parental germplasm.

The disease outcome of infection by one pathogen may be mediated by a change in host environment brought on by infection by another pathogen. Both induction and suppression of a plant's defenses by prior contact with a pathogen has been reported. In the early mid 20th century several authors noted that cereals attacked by one pathogen predisposed them to attack by another (Bensaude, 1926; Chester, 1944; Yarwood, 1959; Brokenshire, 1974). More recently in tests in controlled environment conditions, it has been shown that biotrophic pathogens can suppress a plant's resistance to both biotrophic and non-biotrophic pathogens; *Albugo candida* suppresses innate immunity allowing infection by avirulent *Hyaloperonospora arabidopsidis* (Cooper et al., 2008) while *Pseudomonas syringae* pv. t*omato* (*Pst*) induces salicylic acid-mediated defenses and suppresses the jasmonic acid-mediated defense pathway normally induced in plants infected with *Alternaria brassicicola* (Spoel et al., 2007).

A reduction in disease severity has also been noted in field conditions. The non-biotrophic fungus *Parastagonospora nodorum* reduced the disease severity of powdery mildew (*Blumeria graminis*) although the presence of *B. graminis* increased the accumulated disease severity caused by *P. nodurum* (Weber et al., 1994). In a glasshouse trial, the non-biotrophic fungal pathogen *Zymoseptoria tritici* reduced the incidence of *Puccinia striiformis*, thought to be due to competition between the two pathogens (Madariaga and Scharen, 1986). Under controlled conditions, Lyngkjær and Carver (1999) found that an initial successful infection by a virulent isolate of *B. graminis* can render cells accessible to future attacks by other, normally avirulent isolates of this fungus but equally, inaccessibility to future infection could be induced if the initial attack failed. Aghnoum and Niks (2012), investigating interactions between virulent *P. hordei* and *B. graminis* f.sp. *hordei* isolates on barley, found that pre-inoculation with the rust isolate induced increased resistance to both isolates of *B. graminis* by preventing haustorium formation.

These previous studies demonstrate that the interactions between pathogens are not yet predictable and that there are many underlying factors in the outcome of infection. The aim of this research was to investigate how infection of wheat with *Z. tritici* affects the wheat plant's response to *B. graminis* f.sp. *tritici* (*Bgt*). *Z. tritici* causes the disease Septoria tritici blotch, currently the most common foliar disease of wheat in temperate areas in much of the world (Fones and Gurr, 2015). Efficacy of fungicides is declining for control of this disease as the population develops insensitivity to triazole and strobulurin fungicides (Fraaije et al., 2005, 2007) while there has been a recent report of insensitivity to succinate dehydrogenase fungicides (Teagasc, 2015). Currently a combination of several fungicides still gives good control of Septoria on moderately resistant wheat varieties (Torriani et al., 2015). Breeding is improving the level of resistance to Septoria, but not to the extent that fungicides can be dispensed with (Brown, 2015). There is also widespread insensitivity of wheat powdery mildew to broad-spectrum fungicides but it is generally well-controlled by a combination of specific anti-mildew fungicides (AHDB, 2016) and partial resistance, which is generally durable (Brown, 2015).

The two pathogens have very different modes of infection. *Z. tritici* enters the leaf through the stomata (Kema et al., 1996) and no differences have been seen in the penetration ability of avirulent and virulent *Z. tritici* spores (Shetty et al., 2003). This is followed by a long latent, apparently endophytic period (Orton et al., 2011; Sánchez-Vallet et al., 2015) in which the fungus remains within the substomatal cavity for at least 7 days after inoculation (dai) before symptoms appear on the leaf (reviewed by Steinberg, 2015). During this latent period there is no detectable increase in fungal biomass (Keon et al., 2007; Shetty et al., 2007). A compatible interaction is initiated with the onset of host cell collapse and growth of the fungus in the mesophyll layer between 10 and 14 dai, after which pycnidia are formed, emerging through the stoma after at least 14 days (Kema et al., 1996; Shetty et al., 2003; Keon et al., 2007). In an incompatible interaction, no increase in fungal biomass is seen (Shetty et al., 2007) and there is no evidence for macro- or microscopic symptoms indicative of a hypersensitive reaction (Hammond-Kosack and Rudd, 2008). *Bgt*, by contrast, grows on the epidermis, infecting cells from appressoria formed approximately 12 h after inoculation (hai). Haustoria are formed from 24 hai onwards within host cells, enabling the fungus to feed (Zhang et al., 2005). Except for the haustoria, which occupy the epidermal cells, the fungus grows on the surface of the leaf throughout its lifecycle. Asexual conidiophores are produced on the surface of the leaf from 5 to 10 dai. The hypersensitive response which forms during an incompatible interaction is a critical aspect of resistance to mildew (Boyd et al., 1995).

As these two pathogens cause widespread foliar diseases of wheat which often occur in the same mild, humid environments but have strongly contrasting lifestyles, their interaction is potentially of profound importance for attempts to control a broad spectrum of diseases by a combination of resistance breeding and chemical applications. We investigated the effect of a compatible interaction between the necrotroph *Z. tritici* and the wheat host on inhibiting the growth and development of a virulent isolate of the obligately biotrophic *Bgt*. This effect occurred several days before necrotic Septoria lesions formed, implying that signals which form during the early stages of the wheat-*Z. tritici* interaction, not the later formation of necrotic lesions, are responsible for inhibiting *Bgt*. Conversely, we tested if the maintenance of green leaf tissue during the incompatible interaction of Septoria-resistant wheat with an

avirulent *Z. tritici* isolate (Kema et al., 1996; Shetty et al., 2003) promoted greater susceptibility of the leaf to an avirulent *Bgt* isolate, possibly by overriding the hypersensitive response to avirulent *Bgt*.

MATERIALS AND METHODS

Plant and Fungal Material

The wheat varieties Longbow and Flame were used throughout these experiments. Flame has the mildew resistance gene *Pm4b* and Longbow carries *Pm2*. The *Bgt* isolate JIW11 is avirulent to both these genes while JIW48 is virulent to both of them. The mildew-susceptible cultivar Cerco was used as a control. Longbow, which has the Septoria resistance gene *Stb15*, is susceptible to *Z. tritici* isolate IPO323 while Flame, which has *Stb6*, is resistant.

Wheat plants were grown in a growth room with temperatures set to 18°C for 16 h light and 12°C in the dark for 8 h. *Z. tritici* isolate IPO323 (Kema and van Silfhout, 1997) was grown on YPD+ agar. For plant inoculation, the second leaves of 14 days old seedlings were attached adaxial side up to Perspex sheets using double-sided tape (Keon et al., 2007). The leaves were inoculated evenly with a fungal spore solution at a density of 10^7 spores per mL of water using a swab stick with a cotton sterile tip (Fisher Scientific, Loughborough, Leicestershire, UK; Keon et al., 2007). Plants inoculated with *Z. tritici* were placed in trays with plastic lids and under black plastic sheeting, to achieve dark conditions with high relative humidity for 24 h. Control leaves were mock inoculated with water only. A method using detached leaves (Arraiano et al., 2001) was modified to test infection of wheat by two pathogens. The bottom of rectangular clear polystyrene boxes were filled with 50 mL 1% water agar with 100 mg L^{-1} benzimidazole. After 24 h in the dark the inoculated leaves were placed into the boxes and the cut ends of the leaves were covered with a layer of benzimidazole agar. *Bgt* isolates JIW11 and JIW48 were maintained on the wheat cultivar Cerco and were inoculated by blowing fresh spores into settling towers placed over the plant material (Boyd et al., 1994). For all experiments control boxes to check for mildew colony formation and *Z. tritici* sporulation were set up. Boxes were placed in a controlled environment cabinet at 14°C 9 h light supplemented with UV light and 15 h dark at 9°C.

Effect of Decreasing Concentrations of *Z. tritici*

To observe if there is a dosage effect of *Z. tritici* spores on the number of colonies formed by virulent *Bgt*, leaves of Longbow were inoculated with decreasing concentrations of the *Z. tritici* IPO323 and placed into detached leaf boxes before inoculation with *Bgt*. The dilution series started at 10^7 spores per mL and inoculum was successively diluted 2.5-fold down to 100 spores per mL (Keon et al., 2007). Each detached leaf box contained a leaf of Cerco and 10 leaves of Longbow encompassing the whole dilution series. The boxes were inoculated with the virulent *Bgt* isolate JIW48 under settling towers, 4 days after inoculation with *Z. tritici*. Colony formation was assessed by counting visible colonies under a 2× magnifying lens after 8–10 days. The experiment was done in three replicates.

Requirement for Living *Z. tritici* Spores

To produce non-viable spores, a spore suspension of *Z. tritici* (IPO323) was autoclaved at 121°C at 15 psi for 15 min. The spore suspension was then inoculated onto leaves of Flame and Longbow and the leaves placed into detached leaf boxes, along with mock-inoculated leaves, before being inoculated with *Bgt* at 1 day after and 10 days after inoculation with the autoclaved *Z. tritici*. Two leaves of each treatment were included in each box and the experiment was carried out a total of three times.

Early Development of *B. graminis*

To investigate the development of *Bgt* spores at the early stages of development on leaves preinoculated with *Z. tritici*, Longbow and Flame leaves inoculated with IPO323 or mock-inoculated were placed in detached leaf boxes along with leaves of Cerco, which were not inoculated with *Z. tritici*. Leaves were inoculated with the mildew isolate JIW48, 1 or 6 days after *Z. tritici* inoculation. Each of three replicate experiments consisted of three independent replicate detached

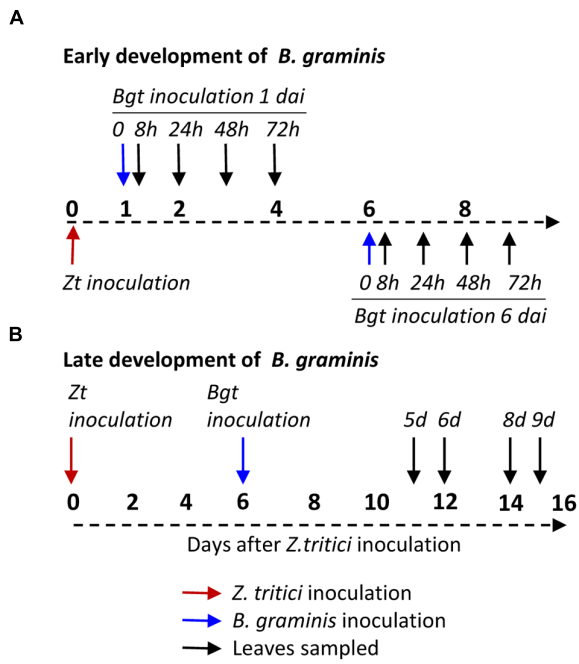

FIGURE 1 | Experimental design to investigate early and late development of *Blumeria graminis* f.sp. *tritici* on wheat leaves after inoculation with *Zymoseptoria tritici*. (A) Inoculation and data collection points to study the early development of *Bgt* on wheat leaves after inoculation with *Z. tritici* at day 0. **(B)** Inoculation and data collection points to study the late development of *Bgt* on wheat leaves after inoculation with a *Z. tritici* at day 0. In this figure, dai refers to days after inoculation with *Z. tritici*. h and d refer to hours or days at which leaves were sampled following inoculation with *Bgt*.

leaf boxes, with each box containing one leaf of each variety given each treatment. Leaves were destructively sampled at 8 h, 24 or 32, 48, and 72 h after infection (hai) with *Bgt* (**Figure 1A**). After the first replicate was assessed at 24 h, it was decided that 32 h would be a better timepoint to sample at as more development of the *Bgt* germlings had taken place. In terms of mildew development, the 24 and 32 h time points are fairly close and in the statistical analysis each replicate was treated as a block effect. The sampled leaves were placed onto filter paper soaked in 3:1 ethanol: acetic acid until they had cleared and were stored in lactoglycerol (1:1:1 solution of lactic acid, glycerol and water) until assessment by microscopy. To visualize fungal spores, the leaves were placed on a glass slide and Aniline Blue 0.1% (made up in lactoglycerol) was pipetted onto them. On each leaf, 30 *Bgt* spores were assessed for growth and development at the following stages; no germination, primary germ tube, appressorial germ tube, appressorium, balloon haustorium, digitate haustorium, or elongating secondary hyphae (ESH). Only spores that were isolated, undamaged and not infecting the same cell as another spores were assessed. Observations were made using a Nikon Microphot-SA (2) general light microscope. Haustoria were visualized under differential interference contrast (DIC) microscopy where necessary.

Separate statistical analyses were conducted on the data at each timepoint. The categories of *Bgt* development were formed into groups. At 8 h, the number of spores that had germinated with either a primary germ tube or an appressorium was studied as a

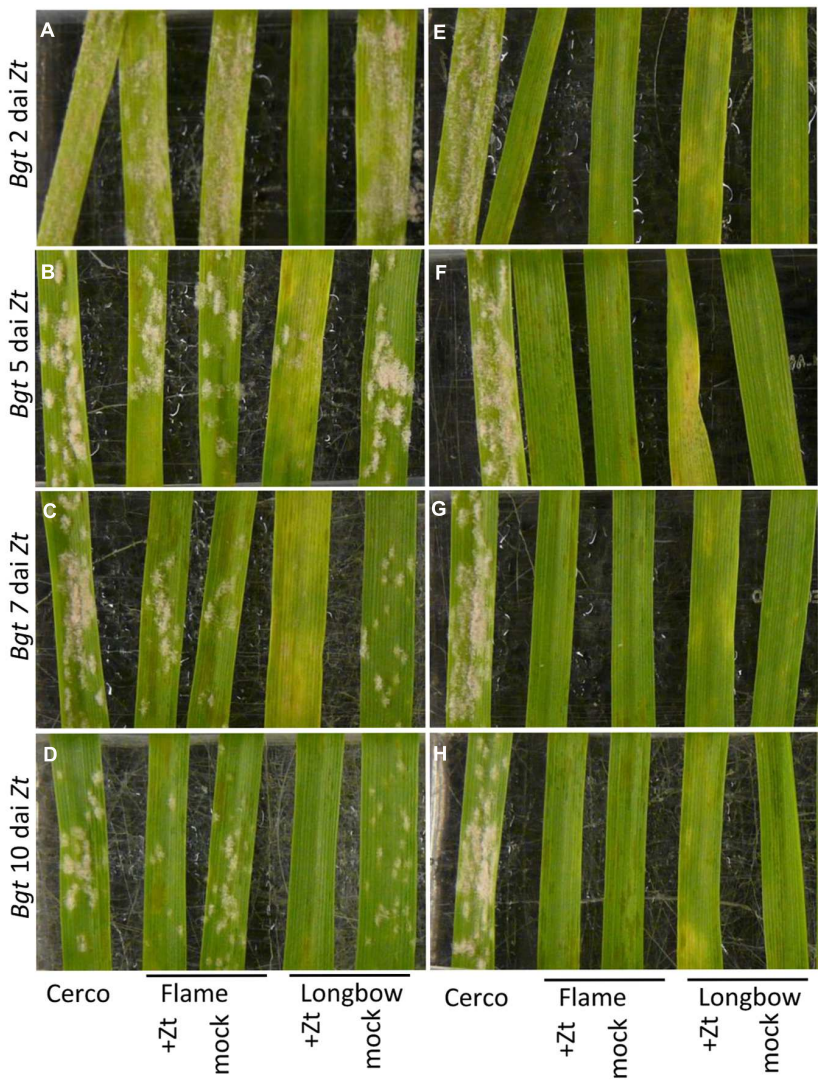

FIGURE 2 | Leaves of wheat varieties Flame and Longbow inoculated first with *Z. tritici* isolate IPO323 then with either avirulent or virulent isolates of *B. graminis* f.sp. *tritici* (*Bgt*). Order of leaves in each photograph (L to R): Cerco, Flame + IPO323, mock-inoculated Flame, Longbow + IPO323, Longbow mock. **(A–D)** Inoculated with virulent *Bgt* isolate JIW48. **(E–H)** Inoculated with avirulent *Bgt* isolate JIW11. Leaves were inoculated with *Bgt* 2 days after inoculation (dai) with *Z. tritici* **(A,E)**, 5 dai **(B,F)**, 7 dai **(C,G)** or 10 dai **(D,H)**. Photographed 20 days after inoculation with *Z. tritici*.

proportion of the total spores counted. The 24/32 h timepoints were combined and the proportion of spores that had infected the host, having formed at least a haustorium, was analyzed as a proportion of all germinated spores. At 48 and 72 h, the categories were grouped to analyze spores that had developed ESH as a proportion of the total number of infecting spores. For each timepoint, a logistic regression model was fitted with a binomial distribution, the model being Replicate + Day*Treatment, where the crossing operator (*) indicates that both the main effects and the interaction of the factors were estimated. Treatments were Longbow inoculated with IPO323, Flame inoculated with IPO323 or mock-inoculated Longbow. Standard errors were calculated on a logit scale and back-transformed predicted means were calculated for the purposes of presentation.

Later Development of *B. graminis*

To investigate the effect of pre-inoculation with virulent *Z. tritici* on the later stages of development of *Bgt* colonies, leaves of Longbow were inoculated either with *Z. tritici* isolate IPO323 or mock inoculated, in the same way as the early stage development inoculations. Leaves were subsequently inoculated with virulent *Bgt* isolate JIW48, 6 dai with *Z. tritici*. Each box contained two leaves of each treatment. Two leaves of each treatment were sampled at 5, 6, 8, and 9 days after infection (dai) with *Bgt* (**Figure 1B**). The experiment was done in three replicates.

All mildew colonies on the leaves were measured using a graticule at 100× magnification. The area of the colony was calculated by assessing the area as that of an ellipse $\pi(ab)$ where a and b are half the ellipse's major and minor axes, respectively. The number of conidiophores was assessed on a scale of 0–4: (0 = zero, 1 = < 5, 2 = 5–10, 3 = 11–30, and 4 = 30+ conidiophores per colony). The data were analyzed using linear modeling using the model Treatment*Day, where the Treatment factor indicated whether the leaves were inoculated with IPO323 or mock-inoculated. Colony sizes were transformed to square

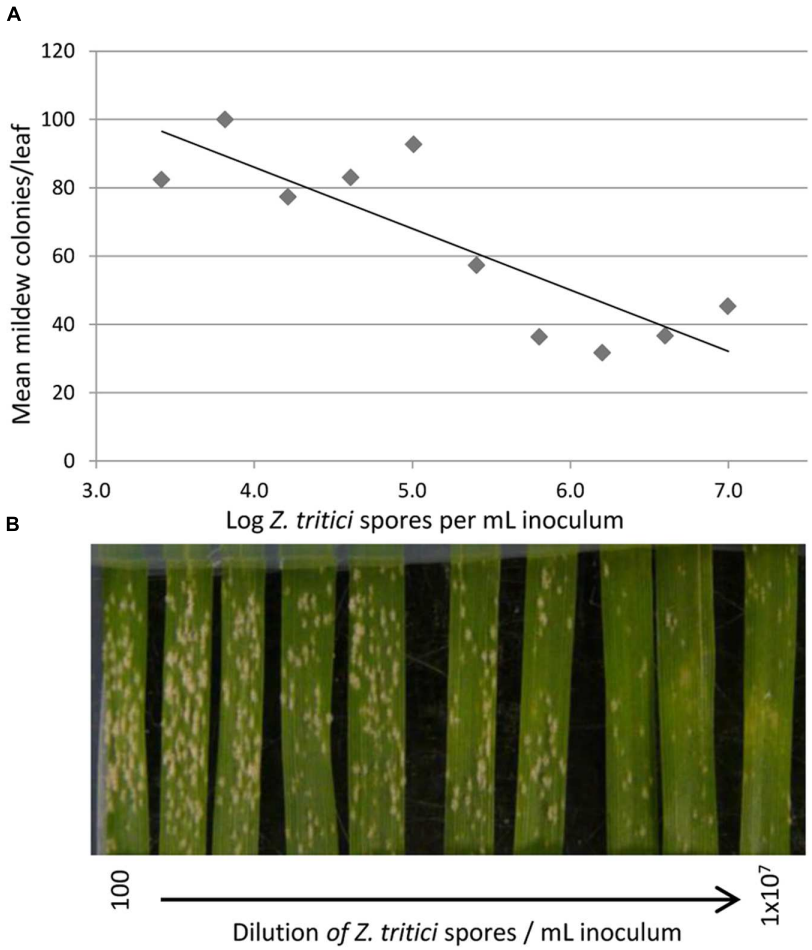

FIGURE 3 | The effect of different concentrations of virulent *Z. tritici* inoculum on the number of visible colonies of virulent *B. graminis* f.sp. *tritici*. Leaves of Longbow were inoculated with decreasing concentrations of *Z. tritici* spores, from 1×10^7/mL down to 100/mL. **(A)** A reduction of 18 mildew colonies per leaf was seen for every 10-fold increase in *Z. tritici* spores: the regression equation of the number of *Bgt* colonies **(B)** on the $\log_{10}$-concentration of *Z. tritici* (Z) was $B = 158\text{-}18Z$, $R^2 = 0.71$. ($P = 0.002$ for linear regression). **(B)** Effect of increasing *Z. tritici* concentration on mildew colony formation. Photographed 14 days after inoculation with *Z. tritici*; 10 days after inoculation with *Bgt*.

roots for statistical analysis. This normalized the variance and made it independent of fitted values. In addition, this procedure reflects the constant radial growth rate of mildew colonies. Least significant differences of predicted means were calculated at the 5% level.

DNA Quantification to Determine *Bgt* Biomass

To determine the relative biomass of *Bgt*, DNA of infected wheat leaves was extracted and the amount of mildew DNA quantified using a Taqman probe assay (Fraaije et al., 2006). To check that isolate JIW48 contained the same cytochrome *b* gene fragment that is amplified by the primers, the fragment was cloned and sequenced. DNA was extracted from leaves with visible sporulating mildew colonies of isolate JIW48 using a Qiagen DNeasy kit (Qiagen, Valencia, CA, USA). A 136bp fragment of the cytochrome *b* gene was amplified with primers PMR1 (5′-TTACTGCATTCCTGGGTTATGTATTG-3′) and PMS1 (5′-CAGAGAAACCTCCTCAAAGGAACT -3′; Fraaije et al., 2006). The fragments amplified were cloned into pGEM-T easy vector (Promega, Madison, WI, USA) following the manufacturer's protocol. The vector was transformed into OneShot TOP10/P3 competent cells (Invitrogen, Carlsbad, CA, USA) following the manufacturer's protocol using a heat shock transformation procedure. Blue/white colony selection was used to select for transformed cells, which were purified using Qiagen MinElute plasmid purification kit (Qiagen, Valencia, CA, USA) and sent for sequencing at TGAC, Norwich, UK. Sequences were aligned using WebPrank using the default settings[1] to four known *Bgt* cytochrome *b* sequences from different isolates available on the NCBI database[2]: Fel08 (AF343442.1), Fel12 (AF343441.1), JAS501 (AJ293567.1), and W26 (AJ293566.1).

Longbow leaves were inoculated with *Bgt* either 1 or 6 days after inoculation with *Z. tritici* and samples collected at 5 and 10 days after *Bgt* inoculation. Total DNA was quantified on a Picodrop spectrophotometer (Picodrop Ltd, Hinxton, UK) and diluted so each sample contained 10 ng/μL. The reaction mixture for qPCR contained 0.5 μM forward primer (PMR1), 0.3 μM reverse primer (PMS1), 0.1 μM of 5′-CY5/3′-BHQ2-labeled probe (5′-CTTGTCCTATTCATGGTATAGCGCTCATTAGG-3′) and 20 ng of DNA sample and 10 μL iQ supermix (Bio-Rad, Hemel Hempstead, Herts, UK) to a volume of 20 μL. A standard curve was produced by plotting known amounts of DNA against Cq values. The reaction cycle was: 2 min at 50°C, 2 min 95°C followed by 50 cycles of 15 s at 95°C and 1 min at 60°C. The increase in fluorescence from the probe was recorded at 60°C during every cycle.

A logistic regression model was fitted: Interval*daiBg*Trt where the * operator indicates that both the main effects and the interaction of the factors were estimated. Interval indicates

[1]http://www.ebi.ac.uk/goldman-srv/webprank/

[2]http://www.ncbi.nlm.nih.gov

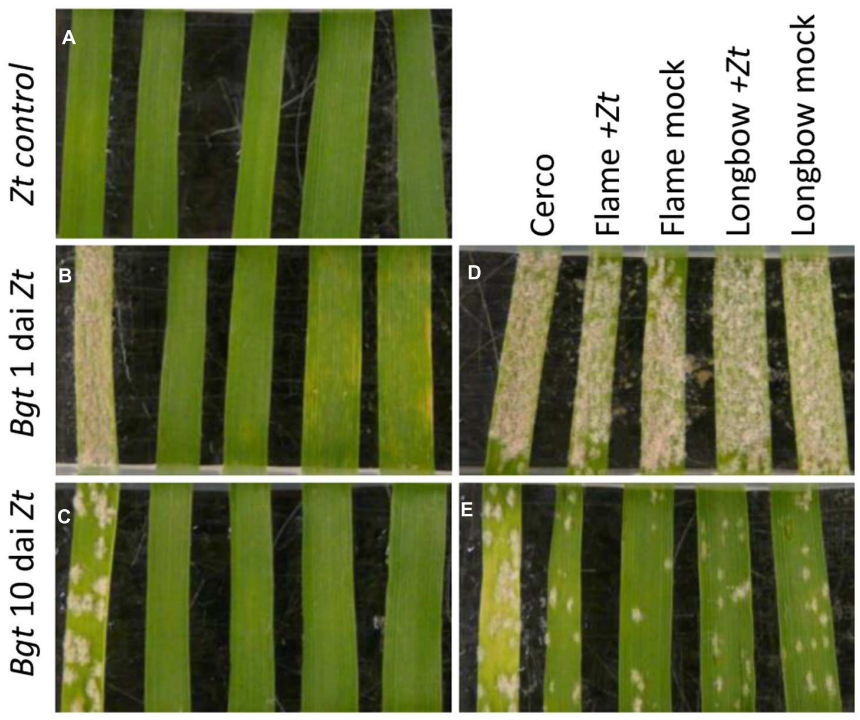

FIGURE 4 | The effect of non-viable *Z. tritici* spores on mildew colony development. Order of leaves in each photograph, from left: Cerco, Flame IPO323, Flame mock, Longbow IPO323, Longbow mock. **(A)** Inoculated only with non-viable *Z. tritici* spores. **(B)** and **(C)** Inoculated with non-viable *Z. tritici* then with avirulent *B. graminis* f.sp. *tritici* (*Bgt*) isolate JIW11. **(D)** and **(E)** Inoculated with non-viable *Z. tritici* virulent *Bgt* isolate JIW48. **(B)** and **(D)** Inoculated with *Bgt* 1 day after *Z. tritici* inoculation. **(C)** and **(E)** inoculated with *Bgt* 10 days after *Z. tritici* inoculation. Photographed 21 days after inoculation with *Z. tritici*.

the amount of time between inoculation with *Z. tritici* and inoculation with *Bgt* (either 1 or 6 days). DaiBg is the time that the samples were taken, either 5 or 10 days after *Bgt* inoculation. Trt is the treatment of *Z. tritici* or mock inoculation. Standard errors were calculated using least significant differences of predicted means on a log10 scale and back-transformed for the purposes of presentation.

RESULTS

Suppression of Mildew by Preinoculation with *Z. tritici*

When Longbow was inoculated first with *Z. tritici* isolate IPO323 and subsequently with the virulent *Bgt* isolate JIW48, fewer or no mildew colonies were visible on the leaf than on the mock-inoculated controls. This result was consistent, regardless of whether the *Bgt* inoculation was carried out 2, 5, 7 or 10 dai with *Z. tritici*. When Flame was pre-inoculated with IPO323, and subsequently inoculated with JIW48, the number of mildew colonies on pre-inoculated leaves across all replicates was similar to that on mock-inoculated leaves (**Figures 2A–D**). When Flame and Longbow were pre-inoculated with *Z. tritici* and subsequently inoculated with an avirulent *Bgt* isolate, JIW11, no colonies of mildew formed (**Figures 2E–H**). Some chlorotic flecking was seen on leaves of Longbow inoculated first with *Z. tritici*, consistent with an incompatible response to avirulent *B. graminis* (**Figure 2F**).

When Longbow was inoculated with a dilution series of the virulent *Z. tritici* isolate, higher concentrations of *Z. tritici* spores hindered the formation of colonies formed by a virulent *Bgt* isolate more strongly (**Figure 3**, $P = 0.002$). The regression equation of the number of *Bgt* colonies (B) on the $\log_{10}$-concentration of *Z. tritici* (Z) was $B = 158\text{-}18Z$, implying that for every 10-fold reduction in *Z. tritici* spores, there were 18 more mildew colonies per leaf on average.

When Flame and Longbow were inoculated with a suspension of non-viable spores of IPO323, the appearance of mildew colonies on the leaves was similar to that on the mock inoculated leaves (**Figure 4**). The leaves were either inoculated after 1 or 10 dai with the non-viable *Z. tritici* spores; at 10 days, less mildew developed on all the leaves inoculated with the virulent mildew including the control cultivar Cerco.

Early Development of *B. graminis*

To assess the progress of *Bgt* spore development at the early stages of infection on leaves pre-inoculated with *Z. tritici*, leaves were sampled 8, 24/32, 48, and 72 hai after inoculation with *Bgt*, the leaves having been inoculated with *Z. tritici* either 1 or 6 days previously. At 8 hai, *Bgt* germination rates (spores scored as having at least a PGT) on leaves of all varieties and treatments ranged from 60 to 74.9% for leaves inoculated with *Bgt* 1 dai with *Z. tritici* and 62.3% to 77.8% for leaves inoculated 6 dai with *Z. tritici* (**Figure 5A**). There were no significant differences in the proportion of spores that had germinated between the treatments: Longbow with compatible *Z. tritici* IPO323, Longbow and Flame with a mock inoculation and Flame with incompatible IPO323 ($P = 0.8$; Supplementary Table S1). There were also no significant differences between the leaves inoculated with *Bgt* at 1 or 6 dai with *Z. tritici* ($P = 0.68$).

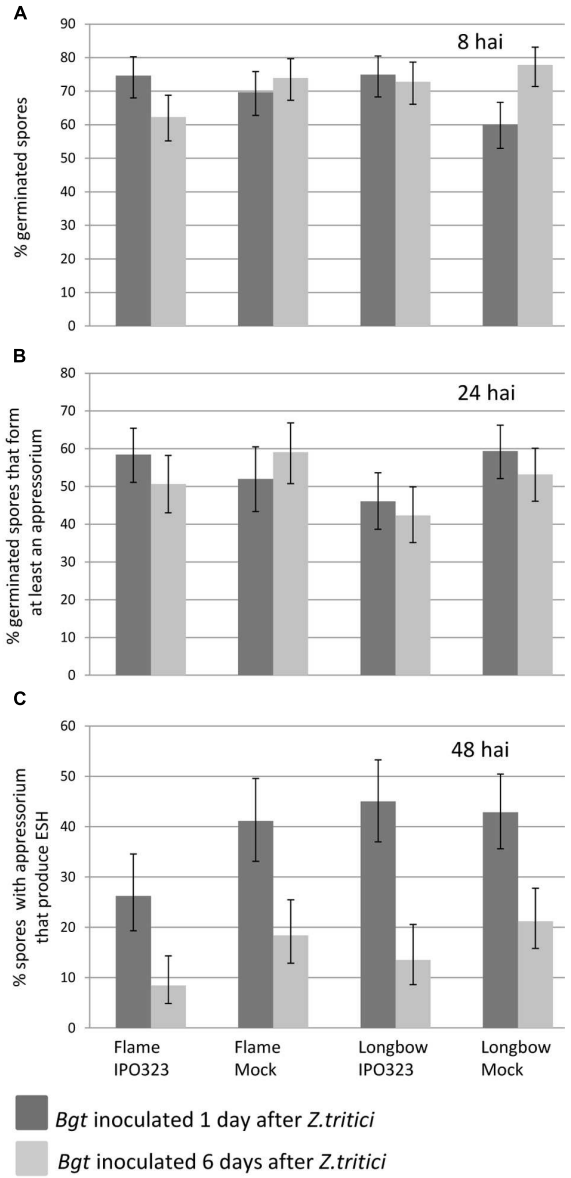

FIGURE 5 | The effect of inoculation with virulent *Z. tritici* on the early development of *B. graminis* f.sp. *tritici* (*Bgt*) on wheat leaves. **(A)** Percentage of germinated spores 8 h after inoculation (hai) with *Bgt*. **(B)** Percentage of germinated spores that form at least an appressorium up to 24/32 hai with *Bgt*. **(C)** Percentge of spores which form an appressorium that produce elongated secondary hyphae (ESH) at 48 hai with *Bgt*. Error bars indicate ±1 standard error of predicted mean.

At 24/32 hai, a proportion of *Bgt* spores had attempted infection or succeeded in infecting the host, producing appressoria and occasionally haustoria and hyphae. The percentage of germinated spores that had formed at least an

appressorium ranged from 46.0 to 59.4% on leaves inoculated with *Bgt* 1 dai with *Z. tritici* and from 42.3 to 59.0% on leaves inoculated with *Bgt* 6 dai with *Z. tritici* (**Figure 5B**). No significant differences in the proportion of germinated spores which had infected the plant were seen either between treatments ($P = 0.3$) or between days ($P = 0.6$).

At 48 hai, the percentage of *Bgt* spores which had formed an appressorium that had then gone on to form ESH ranged from 26.2 to 42.9% at 1 dai with *Z. tritici* and 8.4 to 21.1% at 6 dai with *Z. tritici* (**Figure 5C**). There were no significant differences between treatments ($P = 0.2$), but there was a significant effect of day ($P < 0.001$): consistently fewer *Bgt* spores produced ESH when infected with *Bgt* 6 dai with *Z. tritici* than 1 dai with *Z. tritici*. The data at 72 hai (not shown) were very similar to 48 hai.

Later Development of *B. graminis*

To assess the effect of pre-inoculation with *Z. tritici* on the later stages of mildew colony development on the variety Longbow, the area of each mildew colony formed was measured at 5, 6, 8, and 9 days after inoculation with *Bgt*. At 5 and 6 days, pre-inoculation with virulent *Z. tritici* had no effect on the area of the colonies produced. By 8 days, the difference between the two treatments was significant and by 9 days, the gap between the two treatments was wider, with a difference of 605 μm^2 between them (**Figure 6**). At 8 and 9 days after inoculation with *Bgt*, the number of conidiophores produced by the colonies on mock inoculated leaves was significantly greater than on the pre-inoculated leaves (**Figure 6**). At 9 days, the mock inoculated leaves produced between 10 and 30 conidiophores per colony, while the pre-inoculated leaves only produced up to 10 conidiophores per colony.

DNA Quantification to Determine *Bgt* Biomass

RT-qPCR was used to determine the concentration of *Bgt* DNA on infected leaves as a proportion of total DNA. The timing of *Z. tritici* inoculation (1 or 6 days), the treatment (*Z. tritici* or mock) and the number of days after *Bgt* inoculation that the samples were taken (5 or 10) all had a significant effect on the level of fungal biomass in the leaves (**Table 1**). The amount of *Bgt* DNA was greater in all samples collected 10 days after inoculation than in those collected after 5 days ($P < 0.001$). In samples inoculated with *Bgt* 6 dai with *Z. tritici*, there was less *Bgt* than in those inoculated with *Bgt* 1 dai with *Z. tritici* ($P < 0.01$). In the 10 days

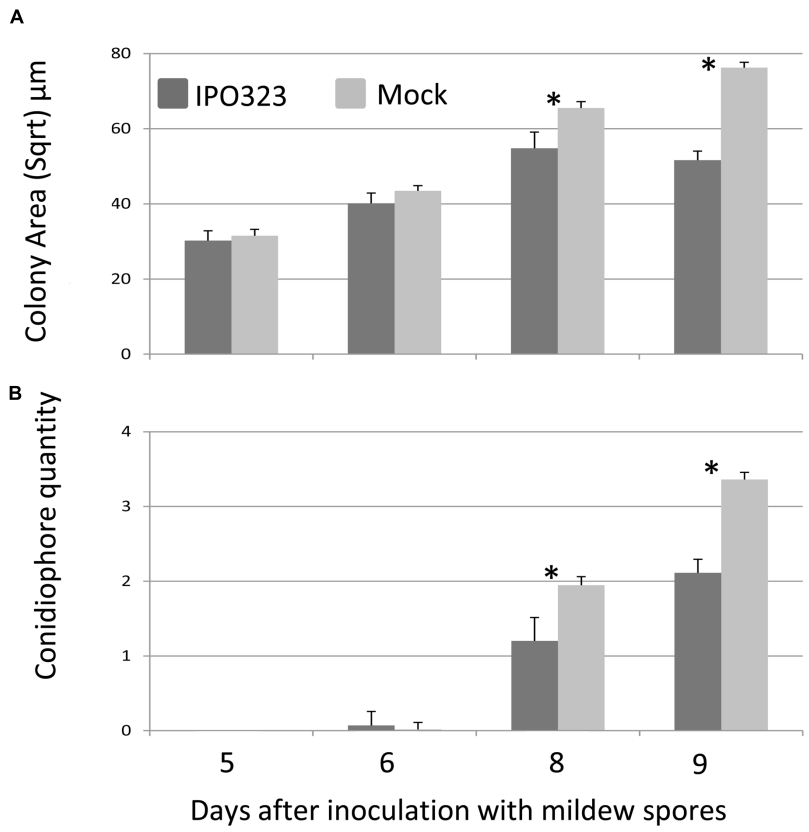

FIGURE 6 | Effect of pre-inoculation with virulent *Z. tritici* on the late stages of development of *B. graminis* f.sp. *tritici* (*Bgt*). Leaves of Longbow were sampled 5–9 days after inoculation with *Bgt*, after either pre-inoculation with *Z. tritici* isolate IPO323 or mock-inoculation. **(A)** Mean square root of colony area (µm) where the square root of the area is proportional to the length of the axis of the ellipse formed by the colony. **(B)** Mean number of conidiophores per colony (0–4 scale). Error bars are ±1 SE of predicted means. *$P < 0.05$ (Fisher's protected least significant difference).

TABLE 1 | Accumulated analysis of variance table from logistic regression model: interval*daiBg*trt where the * operator indicates that both the main effects and the interaction of the factors were estimated.

Change	d.f.	m.s.	v.r.	F pr
Interval	1	1.3589	8.85	0.007
daiBg	1	2.9516	19.23	< 0.001
trt	1	1.8015	11.74	0.002
Interval.daiBg	1	1.1335	7.38	0.012
Interval.trt	1	0.0756	0.49	0.49
daiBg.trt	1	0.278	1.81	0.191
Interval.daiBg.trt	1	0.0679	0.44	0.512
Residual	24	0.1535		
Total	31	0.3662		

Interval indicates the amount of time after inoculation with Z. tritici that Bgt inoculation occurred (either 1 or 6 days). DaiBg is the time that the samples were taken, either 5 or 10 days after Bgt inoculation. Trt is the treatment of Z. tritici or mock inoculation.

samples, there was significantly less *Bgt* in samples inoculated with *Bgt* at both 1 and 6 dai with *Z. tritici* than in the mock samples ($P < 0.001$). At 5 days this difference was only apparent in the samples inoculated with *Bgt* at 6 dai with *Z. tritici* ($P < 0.01$; **Figure 7**).

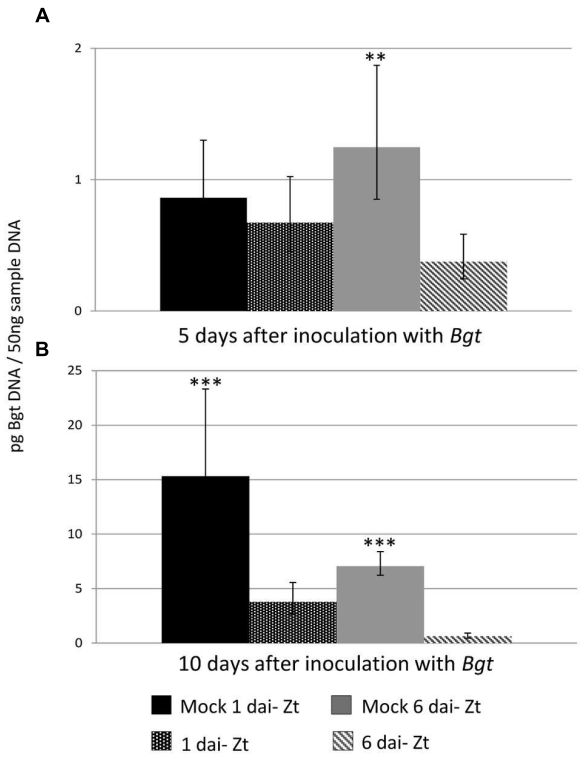

FIGURE 7 | Biomass of *B. graminis* f.sp. *tritici* (*Bgt*) on wheat leaves, measured as *Bgt* DNA as a proportion of total DNA. Leaves of Longbow were pre-inoculated with virulent *Z. tritici* IPO323 or mock inoculated either 1 or 6 days before inoculation with virulent *Bgt* isolate JIW48. Samples were taken at 5 **(A)** and 10 days **(B)** after mildew inoculation. *Bgt* DNA (pg per 50 ng sample DNA) was determined by RT-qPCR using a Taqman probe. $^{**}P < 0.1$, $^{***}P < 0.001$ based on least significant differences of predicted means.

DISCUSSION

We investigated the three-way interaction between wheat and two economically important, specialist fungal pathogens: an obligate biotroph, *B. graminis* f.sp. *tritici* and a necrotroph, *Z. tritici*. The experiments established a laboratory system to allow these two pathogens to infect the same host plant simultaneously. The main findings are that a compatible interaction between *Z. tritici* and the wheat leaf reduces the number, size, and reproductive capacity of mildew colonies that a normally virulent *Bgt* isolate produces but does not significantly alter the early development of *Bgt* on the leaf. Conversely, an incompatible interaction between *Z. tritici* and the wheat leaf has no apparent effect on the ability of a virulent *Bgt* isolate to form mildew colonies and does not detectably alter the susceptibility of the leaf to an avirulent *Bgt* isolate. The effect on virulent *Bgt* was not elicited by non-viable spores of *Z. tritici*. Increased resistance to *Bgt* is therefore elicited specifically by infection with virulent *Z. tritici*. This occurs before Septoria symptoms are visible on the leaf, implying that the effect involves a physiological interaction during the latent, endophytic period of *Z. tritici*, which either takes place directly between this fungus and *Bgt* or is mediated by the wheat leaf.

Priming of plant defenses which are induced in response to one pathogen and are effective against future attack by another pathogen has been suggested as a mechanism which inhibits subsequent pathogen growth (e.g., Lyngs Jørgensen et al., 1998; Lyngkjær and Carver, 2000; Aghnoum and Niks, 2012). Here, *Bgt* spores were able to infect and develop appressoria, haustoria, and ESH but were hindered in subsequent growth and reproductive ability at the later stages of fungal development. This implies that the suppressive effect of *Z. tritici* is not effective against the early stages of development of *Bgt*. The inhibition of *Bgt* by *Z. tritici* was consistent regardless of the length of the interval between the inoculations with the two fungi, which implies that the effect is unlikely to be a specific effect of the later developmental stages of *Z. tritici*. In particular, it is presumably an effect of the early, endophytic phase of the *Z. tritici* life cycle, not the later, necrotrophic phase, because *Bgt* was inhibited before Septoria symptoms were visible. The lack of a detectable effect of non-viable spores of *Z. tritici* on mildew colony formation could mean that MAMPs delivered to the surface of the wheat leaf are not sufficient to inhibit growth and development of *Bgt*. The method is not sensitive enough to determine if proteinaceous MAMPs are involved as these may be destroyed by the autoclaving process. Additionally, during the period of symptomless colonization there is no apparent nutrient acquisition from the host (Rudd et al., 2015), which means that *Bgt* is unlikely to be hindered in obtaining nutrients from the plant.

An explanation for the inhibition of *Bgt* through pre-infection of wheat by *Z. tritici* may concern the very different roles of host responses to the two diseases. In powdery mildew, the hypersensitive response, involving death of infected epidermal

cells and subtending mesophyll cells, plays a critical role in inhibition of avirulent *B. graminis* (Boyd et al., 1995) whereas *Bgt*, as an obligate biotroph, requires living host tissue for its growth, development, and reproduction. In Septoria, by contrast, fungal development in a compatible interaction occurs in necrotic tissue but in an incompatible interaction, the host plant keeps its leaf tissue alive, possibly by suppressing the hypersensitive response and thus preventing transition of *Z. tritici* to the necrotrophic phase (Keon et al., 2007; Jing et al., 2008). It has been proposed that *Z. tritici* hijacks disease resistance signaling pathways (Hammond-Kosack and Rudd, 2008), causing its host to express a response which is typical of resistance to biotrophic pathogens but elicits susceptibility to the necrotrophic *Z. tritici*. We propose that as yet unknown early signaling events during the latent phase of the interaction between wheat and the virulent genotype of *Z. tritici*, prior to the necrotic stage, can lead to the suppression of the obligate biotroph *Bgt*.

Higher inoculum levels of *Z. tritici* reduced the number of mildew colonies formed on the leaf in a dosage dependent manner. The severity of Septoria symptoms is itself closely correlated with inoculum load (Fones et al., 2015), which is consistent with the response of wheat to *Z. tritici* being localized rather than systemic within the leaf (Rudd et al., 2008). At higher doses of *Z. tritici*, therefore, it is expected that a larger proportion of the leaf is involved in the proposed early signaling events. The greater the number of *Z. tritici* infection sites, the larger the impact on the mildew colonies will be as *Bgt* spores are dispersed over the entire leaf. This is consistent with the hypothesis that infection by *Z. tritici* may predispose leaf tissue around the site of infection to become necrotic and thus to have reduced susceptibility to *Bgt*.

By contrast, the incompatible *Z. tritici* isolate had no effect on the outcome of *Bgt* infection. This may be because early, endophytic infection by avirulent *Z. tritici* does not yet induce the plant's mechanism which suppresses the necrotising response to *Z. tritici* infection (Hammond-Kosack and Rudd, 2008) or because any such host response does not further increase the susceptibility of wheat leaf tissue to *Bgt*.

The ability of *Bgt* to form appressoria and haustoria and to produce secondary hyphae despite the inhibition of later development by pre-inoculation with virulent *Z. tritici* contrasts with the interaction between *Z. tritici* and *P. striiformis*. In the latter case, germination of urediniospores was reduced by the presence of *Z. tritici* and rust development was restricted to areas of the leaf not infected by *Z. tritici* (Madariaga and Scharen, 1986), suggesting the rust pathogen could not compete for resources in the face of *Z. tritici* infection.

Longer incubation periods of the detached leaves prior to inoculation with *Bgt* has a significant negative impact on *Bgt* infection, as is apparent from both colony number and fungal biomass quantification. It is likely that this is due to deterioration of the leaf tissue once it is detached from the plant. All the experiments presented here included appropriate mock-inoculated controls which also showed a reduction in colony formation in each treatment. Detached leaves were used because they allow many treatment combinations to be tested in replicate in controlled conditions (Arraiano et al., 2001).

The results presented here indicate that because susceptibility to *Z. tritici* inhibits powdery mildew, breeding efforts should focus on increasing resistance to Septoria whilst maintaining the current level of moderately high partial resistance to powdery mildew in many winter wheat breeding programs (Brown, 2015). Resistance to *Z. tritici* had no effect on *Bgt*, so focusing attention on breeding for Septoria resistance should not have a detrimental effect on mildew resistance. In the U.K., breeding for mildew resistance has taken place for many years, whereas breeding for resistance to Septoria has been relatively recent but is now one of the main targets for new winter wheat varieties (Brown, 2015). Breeders and farmers require acceptable resistance to all diseases so more information on how different pathogens interact with each other is desirable when breeding new varieties, especially in the face of growing government and public concern over fungicides (Torriani et al., 2015). There is little value in having good resistance to one disease if its resistance to another is poor as this will not reduce demand for pesticides. Speculatively, long term breeding for resistance to powdery mildew may have meant that wheat is now well adapted to defense against biotrophic pathogens, but less well adapted to defense against necrotrophic pathogens.

We have shown that a non-biotrophic pathogen has a negative impact on a biotrophic pathogen. Histology of powdery mildew development shows that *Z. tritici* infection inhibits growth and reproductive capacity of *Bgt*, the powdery mildew fungus. This effect is apparent before necrotic symptoms indicative of Septoria disease are visible. Understanding the interactions of host responses to diverse pathogens with differing life-histories will underpin efforts to breed crop varieties with durable resistance to several diseases that occur simultaneously.

AUTHOR CONTRIBUTIONS

EO and JB planned the research, analyzed the data, and wrote the paper. ESO did the experiments.

FUNDING

This research was supported by a BBSRC Targeted Priority Studentship (EO) and the BBSRC Biotic Interactions institute strategic programme (JB).

ACKNOWLEDGMENTS

The data included in this article first appeared in EO's doctoral thesis (Orton, 2012). The authors thank Miss Mathilde Calliau and Mrs Margaret Corbitt for assistance with the microscopy work and Dr Jason Rudd for co-supervision of EO's PhD.

SUPPLEMENTARY MATERIAL

The Supplementary Material for this article can be found online at: http://journal.frontiersin.org/article/10.3389/fpls.2016.00742

REFERENCES

Aghnoum, R., and Niks, R. E. (2012). Compatible *Puccinia hordei* infection in barley induces basal defense to subsequent infection by *Blumeria graminis*. *Physiol. Mol. Plant Pathol.* 77, 17–22. doi: 10.1016/j.pmpp.2011.10.003W

AHDB (2016). *Wheat Disease Management Guide*. Available at: http://cereals.ahdb.org.uk/media/176167/g63-wheat-disease-management-guide-february-2016.pdf

Arraiano, L. S., Brading, P. A., and Brown, J. K. M. (2001). A detached seedling leaf technique to study resistance to *Mycosphaerella graminicola* (anamorph *Septoria tritici*) in wheat. *Plant Pathol.* 50, 339–346. doi: 10.1046/j.1365-3059.2001.00570.x

Bensaude, M. (1926). Notes on wheat diseases in Portugal. *Bol. Soc. Brot.* 4:92.

Boyd, L. A., Smith, P. H., and Brown, J. K. M. (1994). Molecular and cellular expression of quantitative resistance in barley to powdery mildew. *Physiol. Mol. Plant Pathol.* 45, 47–58. doi: 10.1016/S0885-5765(05)80018-9

Boyd, L. A., Smith, P. H., Foster, E. M., and Brown, J. K. M. (1995). The effects of allelic variation at the Mla resistance locus in barley on the early development of *Erysiphe graminis* f. sp. hordei and host responses. *Plant J.* 7, 959–968. doi: 10.1046/j.1365-313X.1995.07060959.x

Brokenshire, T. (1974). Predisposition of wheat to *Septoria* infection following attack by *Erysiphe*. *T. Brit. Mycol. Soc.* 63, 393–397. doi: 10.1016/S0007-1536(74)80188-9

Brown, J. K. M. (2015). Durable resistance of crops to disease: a Darwinian perspective. *Annu. Rev. Phytopathol.* 53, 513–539. doi: 10.1146/annurev-phyto-102313-045914

Chester, K. S. (1944). Low incidence of wheat leaf rust associated with late winter weather or antagonism of *Septoria tritici*. *Plant Dis. Rep.* 8, 280–287.

Cooper, A. J., Latunde-Dada, A. O., Woods-Tor, A., Lynn, J., Lucas, J. A., Crute, I. R., et al. (2008). Basic compatibility of *Albugo candida* in *Arabidopsis thaliana* and *Brassica juncea* causes broad-spectrum suppression of innate immunity. *Mol. Plant Microbe Interact.* 21, 745–756. doi: 10.1094/MPMI-21-6-0745

Fones, H., and Gurr, S. (2015). The impact of *Septoria tritici* blotch disease on wheat: an EU perspective. *Fungal Genet. Biol.* 79, 3–7. doi: 10.1016/j.fgb.2015.04.004

Fones, H. N., Steinberg, G., and Gurr, S. J. (2015). Measurement of virulence in *Zymoseptoria tritici* through low inoculum-density assays. *Fungal Genet. Biol.* 79, 89–93. doi: 10.1016/j.fgb.2015.03.020

Fraaije, B., Burnett, F., Clark, W., Motteram, J., and Lucas, J. (2005). QoI resistance in *Mycosphaerella graminicola*: role of inoculum, effect of different anti-resistance strategies and current status in UK. *Phytopathol.* 95, S30.

Fraaije, B. A., Burnett, F. J., Clark, W. S., and Lucas, J. A. (2006). *Development and Field Testing of Fungicide Anti-Resistance Strategies, with Particular Reference to Strobilurin QoI Group of Fungicides*. London: HGCA Publications.

Fraaije, B. A., Cools, H. J., Kim, S. H., Motteram, J., Clark, W. S., and Lucas, J. A. (2007). A novel substitution I381V in the sterol 14 alpha-demethylase (CYP51) of *Mycosphaerella graminicola* is differentially selected by azole fungicides. *Mol. Plant Pathol.* 8, 245–254. doi: 10.1111/j.1364-3703.2007.00388.x

Hammond-Kosack, K., and Rudd, J. J. (2008). Plant resistance signalling hijacked by a necrotrophic fungal pathogen. *Plant Signal. Behav.* 3, 993–995.

Hillocks, R. J. (2012). Farming with fewer pesticides: EU pesticide review and resulting challenges for UK agriculture. *Crop Prot.* 31, 85–93. doi: 10.1016/j.cropro.2011.08.008

Jess, S., Kildea, S., Moody, A., Rennick, G., Murchie, A. K., and Cooke, L. R. (2014). European Union policy on pesticides: implications for agriculture in Ireland. *Pest Manag. Sci.* 70, 1646–1654. doi: 10.1002/ps.3801

Jing, H. C., Lovell, D., Gutteridge, R., Jenk, D., Kornyukhin, D., Mitrofanova, O. P., et al. (2008). Phenotypic and genetic analysis of the *Triticum monococcum*-*Mycosphaerella graminicola* interaction. *New Phytol.* 179, 1121–1132. doi: 10.1111/j.1469-8137.2008.02526.x

Kema, G. H. J., and van Silfhout, C. H. (1997). Genetic variation for virulence and resistance in the wheat-*Mycosphaerella graminicola* pathosystem III. Comparative seedling and adult plant experiments. *Phytopathology* 87, 266–272. doi: 10.1094/PHYTO.1997.87.3.266

Kema, G. H. J., Yu, D. Z., Rijkenberg, F. H. J., Shaw, M. W., and Baayen, R. P. (1996). Histology of the pathogenesis of *Mycosphaerella graminicola* in wheat. *Phytopathology* 86, 777–786. doi: 10.1094/Phyto-86-777

Keon, J., Antoniw, J., Carzaniga, R., Deller, S., Ward, J. L., Baker, J. M., et al. (2007). Transcriptional adaptation of *Mycosphaerella graminicola* to programmed cell death (PCD) of its susceptible wheat host. *Mol. Plant. Microbe Interact.* 20, 178–193. doi: 10.1094/MPMI-20-2-0178

Lucas, J. A., Hawkins, N. J., and Fraaije, B. A. (2015). The evolution of fungicide resistance. *Adv. Appl. Microbiol.* 90, 29–92. doi: 10.1016/bs.aambs.2014.09.001

Lyngkjær, M. F., and Carver, T. L. W. (1999). Induced accessibility and inaccessibility to *Blumeria graminis* f. sp. hordei in barley epidermal cells attacked by a compatible isolate. *Physiol. Mol. Plant Pathol.* 55, 151–162. doi: 10.1006/pmpp.1999.0211

Lyngkjær, M. F., and Carver, T. L. W. (2000). Conditioning of cellular defence resposnes to powdery mildew in cereal leaves by prior attack. *Mol. Plant Pathol.* 1, 41–49. doi: 10.1046/j.1364-3703.2000.00006.x

Lyngs Jørgensen, H. J. L., Lübeck, P. S., Thordal-Christensen, H., de Neergaard, E., and Smedegaard-Petersen, V. (1998). Mechanisms of induced resistance in barley against *Drechslera teres*. *Phytopathology* 88, 698–707. doi: 10.1094/PHYTO.1998.88.7.698

Madariaga, R. B., and Scharen, A. L. (1986). Interactions of *Puccinia striiformis* and *Mycosphaerella graminicola* on wheat. *Plant Dis.* 70, 651–654. doi: 10.1094/PD-70-651

Orton, E. S. (2012). *Responses of Wheat to Infection by Mycosphaerella graminicola*. Ph.D. thesis, University of East Anglia/John Innes Centre, UK.

Orton, E. S., Deller, S., and Brown, J. K. M. (2011). *Mycosphaerella graminicola*: from genomics to disease control. *Mol. Plant Pathol.* 12, 413–424. doi: 10.1111/j.1364-3703.2010.00688.x

Rudd, J. J., Kanyuka, K., Hassani-Pak, K., Andongabo, A., Devonshire, J., Lysenko, A., et al. (2015). Transcriptome and metabolite profiling of the infection cycle of *Zymoseptoria tritici* on wheat reveals a biphasic interaction with plant immunity involving differential pathogen chromosomal contributions and a variation on the hemibiotrophic lifestyle definition. *Plant Physiol.* 167, 1158–1185. doi: 10.1104/pp.114.255927

Rudd, J. J., Keon, J., and Hammond-Kosack, K. E. (2008). The wheat mitogen-activated protein kinases TaMPK3 and TaMPK6 are differentially regulated at multiple levels during compatible disease interactions with *Mycosphaerella graminicola*. *Plant Physiol.* 147, 802–815. doi: 10.1104/pp.108.119511

Sánchez-Vallet, A., McDonald, M. C., Solomon, P. S., and McDonald, B. A. (2015). Is *Zymoseptoria tritici* a hemibiotroph? *Fungal Genet. Biol.* 79, 29–32. doi: 10.1016/j.fgb.2015.04.001

Shetty, N. P., Kristensen, B. K., Newman, M.-A., Moller, K., Gregersen, P. L., and Jorgensen, H. J. L. (2003). Association of hydrogen peroxide with restriction of *Septoria tritici* in resistant wheat. *Physiol. Mol. Plant Pathol.* 62, 333–346. doi: 10.1016/S0885-5765(03)00079-1

Shetty, N. P., Mehrabi, R., Lütken, H., Haldrup, A., Kema, G. H. J., Collinge, D. B., et al. (2007). Role of hydrogen peroxide during the interaction between the hemibiotrophic fungal pathogen *Septoria tritici* and wheat. *New Phytol.* 174, 637–647. doi: 10.1111/j.1469-8137.2007.02026.x

Spoel, S. H., Johnson, J. S., and Dong, X. (2007). Regulation of tradeoffs between plant defenses against pathogens with different lifestyles. *Proc. Natl. Acad. Sci. U.S.A.* 104, 18842–18847. doi: 10.1073/pnas.0708139104

Steinberg, G. (2015). Cell biology of *Zymoseptoria tritici*: pathogen cell organization and wheat infection. *Fungal Genet. Biol.* 79, 17–23. doi: 10.1016/j.fgb.2015.04.002

Teagasc (2015). *SDHI Resistant Septoria Found in the Field*. Available at: http://www.teagasc.ie/news/2015/201512-03.asp

Torriani, S. F., Melichar, J. P., Mills, C., Pain, N., Sierotzki, H., and Courbot, M. (2015). *Zymoseptoria tritici*: a major threat to wheat production, integrated approaches to control. *Fungal Genet. Biol.* 79, 8–12. doi: 10.1016/j.fgb.2015.04.010

Weber, G. E., Gulec, S., and Kranz, J. (1994). Interactions between *Erysiphe graminis* and *Septoria nodurum* on wheat. *Plant Pathol.* 43, 158–163. doi: 10.1111/j.1365-3059.1994.tb00565.x

Yarwood, C. E. (1959). "Predisposition," in *Plant Pathology: an Advanced Treatise*, Vol. 1, eds J. G. Horsfall and A. E. Dimond (New York, NY: Academic Press), 521–562.

Zhang, Z., Henderson, C., Perfect, E., Carver, T. L. W., Thomas, B. J., Skamnioti, P., et al. (2005). Of genes and genomes, needles and haystacks: *Blumeria graminis* and functionality. *Mol. Plant Pathol.* 6, 561–575. doi: 10.1111/j.1364-3703.2005.00303.x

Conflict of Interest Statement: The authors declare that the research was conducted in the absence of any commercial or financial relationships that could be construed as a potential conflict of interest.

frontiers in Plant Science

ORIGINAL RESEARCH
published: 08 December 2016
doi: 10.3389/fpls.2016.01850

Structure and Function of the TIR Domain from the Grape NLR Protein RPV1

Simon J. Williams[1,2†], Ling Yin[3,4,5†], Gabriel Foley[1], Lachlan W. Casey[1], Megan A. Outram[1], Daniel J. Ericsson[6], Jiang Lu[5,7], Mikael Boden[1], Ian B. Dry[3,4*] and Bostjan Kobe[1*]*

[1] School of Chemistry and Molecular Biosciences, Institute for Molecular Bioscience and Australian Infectious Diseases Research Centre, University of Queensland, Brisbane, QLD, Australia, [2] Research School of Biology, The Australian National University, Canberra, ACT, Australia, [3] Guangxi Crop Genetic Improvement and Biotechnology Key Lab, Guangxi Academy of Agricultural Sciences, Nanning, China, [4] Commonwealth Scientific and Industrial Research Organisation, Urrbrae, SA, Australia, [5] College of Food Science and Nutritional Engineering, China Agricultural University, Beijing, China, [6] Australian Synchrotron, Clayton, VIC, Australia, [7] Department of Plant Science, Shanghai Jiao Tong University, Shanghai, China

The N-terminal Toll/interleukin-1 receptor/resistance protein (TIR) domain has been shown to be both necessary and sufficient for defense signaling in the model plants flax and *Arabidopsis*. In examples from these organisms, TIR domain self-association is required for signaling function, albeit through distinct interfaces. Here, we investigate these properties in the TIR domain containing resistance protein RPV1 from the wild grapevine *Muscadinia rotundifolia*. The RPV1 TIR domain, without additional flanking sequence present, is autoactive when transiently expressed in tobacco, demonstrating that the TIR domain alone is capable of cell-death signaling. We determined the crystal structure of the RPV1 TIR domain at 2.3 Å resolution. In the crystals, the RPV1 TIR domain forms a dimer, mediated predominantly through residues in the αA and αE helices ("AE" interface). This interface is shared with the interface discovered in the dimeric complex of the TIR domains from the *Arabidopsis* RPS4/RRS1 resistance protein pair. We show that surface-exposed residues in the AE interface that mediate the dimer interaction in the crystals are highly conserved among plant TIR domain-containing proteins. While we were unable to demonstrate self-association of the RPV1 TIR domain in solution or using yeast 2-hybrid, mutations of surface-exposed residues in the AE interface prevent the cell-death autoactive phenotype. In addition, mutation of residues known to be important in the cell-death signaling function of the flax L6 TIR domain were also shown to be required for RPV1 TIR domain mediated cell-death. Our data demonstrate that multiple TIR domain surfaces control the cell-death function of the RPV1 TIR domain and we suggest that the conserved AE interface may have a general function in TIR-NLR signaling.

Keywords: nucleotide-binding oligomerisation domain (NOD)-like receptor (NLR), toll/interleukin-1 receptor (TIR), *Muscadinia rotundifolia*, *Plasmopara viticola*, grapevine downy mildew, plant disease resistance, X-ray crystallography

OPEN ACCESS

Edited by:
Ralph Panstruga, RWTH Aachen University, Germany

Reviewed by:
Mark James Banfield, John Innes Centre – Biotechnology and Biological Sciences Research Council, UK
Frank L. W. Takken, University of Amsterdam, Netherlands
Thomas Kroj, French National Institute for Agricultural Research, France

***Correspondence:**
Simon J. Williams
simon.williams@anu.edu.au
Bostjan Kobe
b.kobe@uq.edu.au
Ian B. Dry
ian.dry@csiro.au

† These authors have contributed equally to this work.

Specialty section:
This article was submitted to Plant Biotic Interactions, a section of the journal Frontiers in Plant Science

Received: *05 August 2016*
Accepted: *23 November 2016*
Published: *08 December 2016*

Citation:
Williams SJ, Yin L, Foley G, Casey LW, Outram MA, Ericsson DJ, Lu J, Boden M, Dry IB and Kobe B (2016) Structure and Function of the TIR Domain from the Grape NLR Protein RPV1. Front. Plant Sci. 7:1850. doi: 10.3389/fpls.2016.01850

INTRODUCTION

To detect pathogens and activate defense responses, plants utilize multi-domain receptor proteins that resemble mammalian innate immunity NLRs [nucleotide-oligomerisation (NOD)-like receptors] (Dangl et al., 2013). In plants, NLRs can interact directly with effector proteins secreted by the invading pathogen, or perceive the presence of effector proteins by monitoring host proteins that are targeted and modified during infection (Dodds et al., 2006; Jones and Dangl, 2006; van Der Hoorn and Kamoun, 2008). This process generally occurs within the plant cell, whereby effector-recognition and subsequent activation of the NLR stimulates an immune response known as the hypersensitive response (HR). The activation of a HR generally culminates in programmed cell death of the infected cell and immunity at the whole plant level in a process commonly referred to as effector-triggered immunity (Dodds and Rathjen, 2010).

The multi-domain architecture of plant NLRs generally involves a C-terminal leucine-rich repeat (LRR) domain, a central nucleotide-binding (NB) domain and either a coiled-coil (CC) domain or Toll-interleukin receptor (TIR) domain at the N-terminus. The LRR domain was originally defined as the effector recognition domain, but this has only been demonstrated for a handful of NLR-effector pairs (Dodds et al., 2006; Krasileva et al., 2010). Subsequent evidence from a number of plant NLR systems suggests a more general regulatory role (Moffett et al., 2002; Ade et al., 2007; Slootweg et al., 2010). While no plant NLR structure is currently available, the crystal structure of the autoinhibited mammalian NLR protein NLRC4 supports an inhibitory role for the LRR domain (Hu et al., 2013). The central NB domain controls the activation of NLR proteins through the binding of adenosine nucleotide di- or tri-phosphate (ADP/ATP; Tameling et al., 2002; Williams et al., 2011). Mutations within conserved motifs that mediate nucleotide binding prevent proper NLR function in most cases. A number of autoactive mutations locate to the NB domain and change the dynamics of, or preference for, ADP/ATP binding (Tameling et al., 2002; Williams et al., 2011). The N-terminal CC and TIR domains have both been implicated in effector-independent activation of cell-death pathways and are therefore generally implicated in NLR signaling (Frost et al., 2004; Swiderski et al., 2009; Krasileva et al., 2010; Bernoux et al., 2011; Collier et al., 2011; Maekawa et al., 2011). However, it has been shown that this cell-death function is not universal. Collier et al. (2011) observed CC domain-dependent cell death from the helper-NLR protein NRG1 but not the canonical solanaceous CC-NLR resistance proteins they tested.

Our current understanding of the molecular and structural basis of plant NLR protein activation and function comes from analyses of the N-terminal domains, and lacks reference to a full-length structure. To date, structures of the CC domains from the barley NLR MLA10, potato NLR Rx and wheat NLR Sr33 have been solved (Maekawa et al., 2011; Hao et al., 2013; Casey et al., 2016), and five crystal structures of plant TIR domains have been published (Chan et al., 2010; Bernoux et al., 2011; Williams et al., 2014). Four TIR domain structures originate from *Arabidopsis* proteins, and include AtTIR, a protein of unknown function, and the TIR domains from the NLRs RRS1 ($RRS1^{TIR}$), RPS4 ($RPS4^{TIR}$) and a heterodimer complex between the two (Chan et al., 2010; Williams et al., 2014). The remaining TIR domain structure is from the flax NLR L6 ($L6^{TIR}$; Bernoux et al., 2011). The known plant TIR domains all share a common fold. They also appear to share functional features, as both L6 and RPS4 TIR domains require self-association for cell-death signaling, albeit through distinct interfaces (Bernoux et al., 2011; Williams et al., 2014). However, in the crystal structures of AtTIR, $RRS1^{TIR}$, $RPS4^{TIR}$ and the $RRS1^{TIR}$:$RPS4^{TIR}$ complex, a common TIR:TIR domain interface has been observed. This interface was shown to control heterodimerisation between the TIR domains from RPS4 and RRS1, which has significant functional consequences for the activation of dual NLR protein resistance provided by these proteins in *Arabidopsis* (Williams et al., 2014). We previously reported that residues within the dimerisation interface of RPS4 and RRS1 that facilitate the interaction are conserved in other plant TIR-NLR proteins but that their function in other NLR proteins was not yet known.

In an effort to understand TIR domain function further, we investigated the TIR domain from the *Muscadinia rotundifolia* TIR-NLR protein RPV1 (resistance to *Plasmopara viticola* 1). *M. rotundifolia* is a wild North American grape species closely related to the cultivated grapevine species *Vitis vinifera*, and RPV1 confers resistance to the oomycete *Plasmopara viticola*, the casual agent of downy mildew in cultivated grapevines (Feechan et al., 2013). Here we report the crystal structure of the TIR domain of RPV1 (residues 20–193; $RPV1^{TIR20-193}$) at 2.3 Å resolution. In the crystal structure we observe a molecular interface within the asymmetric unit involving residues within the αA and αE helices that resembles the interface previously observed for AtTIR, $RRS1^{TIR}$, $RPS4^{TIR}$ and $RRS1^{TIR}$:$RPS4^{TIR}$ structures. A thorough assessment of sequencing data from the plant Phytozome resource (Goodstein et al., 2012) reveals that surface-exposed residues within the αA and αE helices involved in molecular contacts in the RPV1 TIR domain crystal structures are well conserved among plant species. We demonstrate that the integrity of this interface is important for the autoactive signaling function of RPV1 TIR domain in a *Nicotiana tabacum* transient expression system. Additionally, we show that mutations in other distinct protein surfaces, including a region analogous to that required for $L6^{TIR}$ self-association and signaling, also disrupts cell-death signaling. In light of these observations, we suggest that in addition to its role in the dual-NLR protein function in *Arabidopsis*, the AE interface may play a more general functional role in TIR-NLR protein function and that multiple, distinct protein surfaces in plant TIR domains influence TIR domain signaling.

MATERIALS AND METHODS

Vectors and Constructs

Truncation constructs coding for the RPV1 TIR domain were prepared by amplification of the corresponding fragments from a plasmid template of *MrRPV1* full-length cDNA (Feechan et al., 2013) with primers containing Gateway attB sites, using polymerase chain reaction (PCR). The PCR

products were cloned into the donor vector pDONR223 (Invitrogen) using BP clonase. To create protein fusions with yellow fluorescent protein (YFP) tags, the desired entry clone and destination vector (pEarlyGate100-L-YFP) containing attR1 and attR2 sites were recombined by LR reaction. The vector pEarlygate100-L-YFP was derived from pEarlyGate100 (Earley et al., 2006) by the introduction of an AvrII-SpeI GA linker-vYFP fragment from ER082 (Tucker et al., 2012). All MrRPV1 TIR domain mutants were created from the plasmid of the entry clone with the QuikChange Site-Directed Mutagenesis Kit (Agilent Technologies) according to the manufacturer's instructions. The desired mutations were recombined into pEarlygate100-L-YFP by LR reaction. For yeast-two-hybrid (Y2H) studies, $RPV1^{TIR1-193}$ was recombined into the Gateway-compatible Y2H vectors based on pGADT7 and pGBKT7 (Clontech) kindly provided by Dr Maud Bernoux (CSIRO Agriculture, Canberra). All constructs were sequenced for verification. All primers used to generate the above constructs are listed in Supplementary Table S1.

Transient Expression and Yeast-2-Hybrid Assays

Tobacco (*N. tabacum* cv. White Burley) plants were grown in a greenhouse at the Commonwealth Scientific and Industrial Research Organisation (CSIRO), Adelaide, Australia. Agrobacterium (strain EHA105) cells were in grown in yeast extract peptone (YEP) media supplemented with 25 μg/mL rifampicin and 50 μg/mL kanamycin at 28°C for 2 days. Approximately 0.5 ml culture was inoculated into 50 ml of YM+MES (pH 5.6) media supplemented with 20 μM acetosyringone and 50 μg/mL kanamycin and grown at 28°C until the $OD_{600\,nm}$ was >0.5. Cells were pelleted and resuspended in infiltration medium (10 mM $MgCl_2$, 10 mM MES pH 5.6, 200 μM acetosyringone) to give a final $OD_{600\,nm}$ of 0.5 and incubated at room temperature for 2–3 h. Infiltration of rapidly expanding tobacco leaves was carried out with a blunt needleless syringe. Plants were maintained at a constant temperate of 23°C for 48 h before being transferred to the glasshouse.

Yeast transformation and growth assays were performed essentially as described in the Yeast Protocols Handbook (Clontech). Yeast cells (AH109) were co-transformed with the prey and bait vectors using a lithium acetate-based protocol. Transformants were first spread on CSM-Trp-Leu plates, and then co-transformed positive colonies were grown on CSM-Trp-Leu-His + 5 mM 3-AT plates to detect activation of the *HIS3* reporter gene. Prey and bait vectors containing the $L6^{TIR29-233}$ (Bernoux et al., 2011) were used as a positive control. Empty prey and bait vectors were used as a negative control.

Immunoblot Analysis

Leaf tissue (∼1 cm diameter disk) was collected from the middle of an infiltrated area 48 h after agroinfiltration. Tissue was ground up in 100 μl of 2X Laemmli extraction buffer, centrifuged at 23,000 x *g* for 10 min at 4°C and the supernatant fraction collected. Proteins were separated by SDS-PAGE and transferred to nitrocellulose membranes (Pall). Membranes were blocked in 5% skim milk and probed with anti-GFP (Roche) followed by goat anti-mouse antibodies conjugated with horseradish peroxidase (Thermo Scientific). Labeling was detected with a SuperSignal West Pico chemiluminescence kit (Thermo Scientific) following the manufacturer's instructions. Membranes were stained with Ponceau S staining solution for protein loading.

Cloning, Expression and Protein Purification

$RPV1^{TIR20-193}$ and $RPV1^{TIR20-193\ H42A}$ were amplified from plasmid templates described above using the primer combinations $RPV1^{TIR}$20-F and $RPV1^{TIR}$193-R (Supplementary Table S1). The PCR product was cloned into the *Escherichia coli* expression vector pMCSG7 (Stols et al., 2002) by ligation-independent cloning and verified by sequencing. The proteins were expressed in *E. coli* BL21 (DE3) cells using the autoinduction method (Studier, 2005). All media was supplemented with 100 μg/mL ampicillin for plasmid selection. An overnight culture was used to inoculate large-scale cultures. Cells were grown by continuous shaking at 37°C in 2 L flasks containing 500 mL of media until the $OD_{600\,nm}$ reached 0.6–0.8. At this point, the temperature was reduced to 20°C and the cells were grown for an additional 18 h before harvesting by centrifugation.

Cells expressing the protein of interest were resuspended in a lysis buffer containing 50 mM HEPES (pH 8.0), 300 mM NaCl and 1 mM DTT. The cells were lysed using sonication, clarified by centrifugation and the resulting supernatant was applied to a 5 mL HisTrap FF column (GE Healthcare). The column was washed with the lysis buffer supplemented with 30 mM imidazole to remove non-specifically bound proteins. The bound protein was eluted using a linear gradient of imidazole from 30 to 250 mM. Fractions containing the protein of interest were pooled, concentrated and buffer-exchanged (to remove imidazole) into 50 mM Tris pH 8.0, 250 mM NaCl, 1 mM DTT and 0.1 mM EDTA for overnight treatment with His-tagged TEV protease at 4°C. The cleaved protein was reapplied to the HisTrap FF column to remove the histidine tag, TEV protease and other contaminants and the flow-through was concentrated and separated further on a Superdex 75 HiLoad 26/60 gel-filtration column (GE Healthcare) pre-equilibrated with the gel filtration buffer containing 10 mM HEPES (pH 7.5), 150 mM NaCl and 1 mM DTT. The peak fractions were pooled and concentrated to 10 mg/mL. Protein was stored in aliquots at −80°C for future biophysical and crystallization studies.

Crystallization and Crystallography

Initial screening was prepared using a Mosquito robot (TTP LabTech, UK) in a 96-well format. The hanging drop vapor-diffusion method of crystallization was used, and drops consisting of 100 nl protein solution and 100 nl reservoir solution were equilibrated against 80 μl reservoir solution. Eight commercial screens were utilized: Index, PEG/Ion and PEGRx (Hampton Research), Morpheus, ProPlex, JCSG Plus, PACT Premier (Molecular Dimensions) and Precipitant Synergy (Jena

Biosciences). A number of single crystals were observed in the screening plates and these were harvested directly from the screens and after cryo-protection with 20% glycerol in well solution the crystals were vitrified in liquid nitrogen. The crystals were subjected to X-ray radiation at the Australian Synchrotron MX1 beamline. X-ray diffraction data to approximately 2.3 Å resolution was obtained from a crystal (approximate dimensions 200 μm × 30 μm × 30 μm) harvested from the PEG/Ion screen, grown in condition 16% PEG3350, 0.1 M Tris pH 8.5 and 2% Tacsimate. Data was collected using a wavelength of 0.9537 Å with a detector distance of 200 mm. The resulting dataset was indexed and integrated with XDS (Kabsch, 2010) and scaled with Aimless (Evans and Murshudov, 2013). Molecular replacement was performed using the program phaser (McCoy et al., 2007) using the $RPS4^{TIR}$ structure (PDB ID 4c6r) as a template. Automated model building was performed in the Phenix package using autobuild, while phenix refine combined with manual inspection and corrections using coot (Emsley et al., 2010) were combined to produce the final atomic model.

Biophysical Studies

Multi-angle laser light scattering (MALS) and small-angle x-ray scattering (SAXS) were used in conjunction with size-exclusion chromatography (SEC) to assess the molecular mass of $RPV1^{TIR20-193}$ in solution. SEC-SAXS was performed at the SAXS/WAXS beamline of the Australian Synchrotron. A Pilatus 1M detector at a sample-to-detector distance of 1.6 m and an energy of 12 keV yielded data over a q-range of 0.007–0.361 $Å^{-1}$, where $q=4\pi.\sin(\theta)/\lambda$. 1 mg of both $RPV1^{TIR}$ and $RPV1^{TIR20-193}$H34A were separated over an inline 3 mL Superdex S200 5/150 GL Increase column (GE Healthcare) at 16°C, at a flow rate of 0.2 mL/min in 10 mM HEPES (pH 7.5), 150 mM NaCl buffer with 1 mM DTT. Frames were collected in 2 s exposures. Data reduction and subtraction was performed using scatterBrain[1]. 100 frames immediately preceding each peak were summed and normalized to obtain buffer blanks, which were subtracted from each individual frame across the peak. Values of R_g and $I(0)$ were calculated from each frame via Autorg in the PRIMUS suite (Petoukhov et al., 2012), and molecular masses were calculated from the volume of correlation for points where $0 < q < 0.3$ $Å^{-1}$ (Rambo and Tainer, 2013).

Sequence-Level Analysis of Conservation

To gain insight into whether the AE interface is conserved across a wider sample of plant species, TIR domain-annotated sequences from Pfam version 29.0 (Finn et al., 2016) were aligned and used to construct profile Hidden Markov Models (profile HMMs). These profile HMMs were then used to search plant genomes from the more extensive Phytozome database (**Supplementary Figure S1**). Pfam sequences were mapped to four clades and four individual sequences within Phytozome in order to include representative sequences from a greater number of plant species than present in Pfam (**Supplementary Figure S2**). We were able to uncover a larger set of TIR domains by expanding the search from Pfam to Phytozome, except in the cases of *Arabidopsis thaliana* and *V. vinifera*, in which mapping to the Phytozome database resulted in fewer proteins than originally identified within Pfam (Supplementary Table S2 and Supplementary Data Sheet 1).

The Pfam description of TIR domains (PF01582) does not always account for the entire sequence of the domain, judging from the available structures, with sequences often truncated at the C-terminus of the domain (*i.e.,* missing the αE helix). To address these errors, the full-length protein sequences for each Pfam entry were retrieved from UniProt (UniProt, 2015).

When an individual sequence had multiple annotated TIR domains, it was divided into regions that maximized the length of each region. If an individual region's new length was below 100 amino-acids, it was deemed unlikely to represent a true TIR domain and was re-joined with the neighboring region in the sequence. If two or more neighboring region's new lengths were greater than 100 amino-acids the original sequence was split at the boundary and the regions were included as separate sequences within the set.

The previously reported AE interface within RPS4 (Williams et al., 2014) was used as a reference to exclude sequences that did not contain the αA and αE regions. As RPS4 was only present within the Malvids clade and Pentapetalae clade, for all other sets RPS4 was manually added and aligned to identify a new sequence that aligned to RPS4 in the AE interface regions and could serve as a reference sequence for its set. After identification of this reference sequence, RPS4 was removed from the alignments for subsequent analysis.

The sequences were clustered using CD-HIT (Li and Godzik, 2006) at 100% identity to identify any duplicate sequences and remove them. Sequences were aligned using MAFFT (Katoh and Standley, 2013) with the default FFT-NS-2 strategy. Any sequence in the alignment that had less than 50% of positions containing an amino-acid in either the αA or αE regions defined by the reference sequence were tentatively excluded. The remaining sequences were realigned and this exclusion process was repeated until no sequences were present in the alignment that had less than 50% of positions containing an amino-acid in either of these regions.

Excluded sequences were checked for the possibility of truncation of the UniProt record. A BLAST search was conducted that only accepted hits longer than the query sequence but that otherwise exactly matched the query sequence. The results from this BLAST search were realigned to the set of sequences without 50% or higher gaps in the αA or αE regions, and all sequences with 50% or higher gaps were definitively excluded.

The remaining sequences within these clades were aligned and used to build four profile HMMs specific to their containing sequences. To identify TIR domains in species not annotated by Pfam, the characteristic profile HMMs were used to query sets of predicted proteins from primary transcripts of genomes found in the Phytozome database. The primary transcripts were from clades containing the original sets of species used to derive each profile.

[1]http://www.synchrotron.org.au/index.php/aussyncbeamlines/saxswaxs/software-saxswaxs

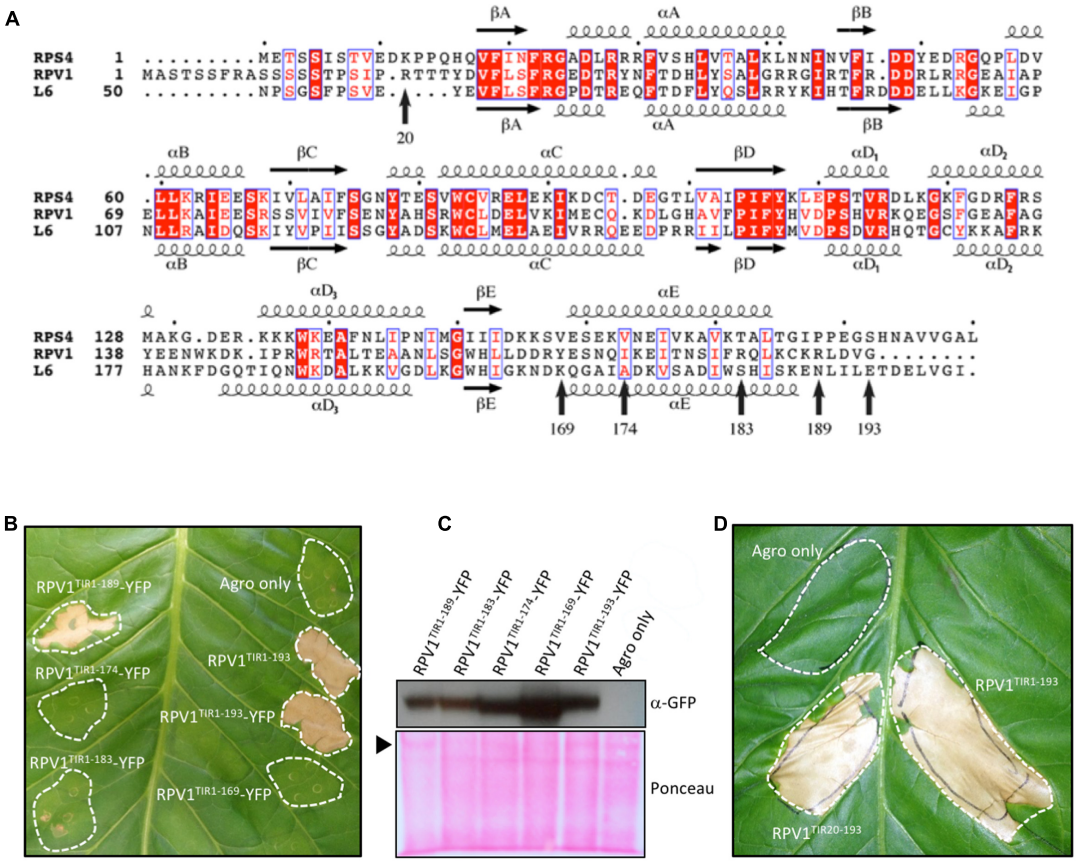

FIGURE 1 | RPV1^{TIR} cell-death signaling. (A) Multiple sequence alignment containing RPS4 (residues 1–193), RPV1 (1–193) and L6 (50–240). The alignment was formatted using the program ESPript (Robert and Gouet, 2014). The secondary structure shown above and below the alignment is derived from the RPS4^{TIR} (PDB ID 4c6r) and L6^{TIR} (PDB ID 3ozi) structures, respectively. Arrows indicate residue positions corresponding to the various RPV1 constructs tested in **(B,D)**. **(B,D)** *Nicotiana tabacum* leaves 5 days after infiltration with *A. tumefaciens* alone or *A. tumefaciens* expressing RPV1^{TIR} constructs. **(B)** Comparison of the RPV1^{TIR} truncations fused to YFP. **(C)** Protein extracts of tobacco-leaf tissue **(B)**, sampled from agroinfiltrated areas 2 days after agroinfiltration, were immunoblotted with anti-GFP antibodies, demonstrating RPV1^{TIR}-YFP protein expression. The arrow indicates Ponceau staining of the large RuBisCO subunit. **(D)** Autoactivity is observed with both RPV1$^{TIR1-193}$ and RPV1$^{TIR20-193}$ constructs without YFP. Agro only, corresponds to agrobacterium transformed with a vector without an insert.

A profile HMM was constructed using HMMER 3.1b2 (Eddy, 2011) and used to search the relevant subset of the Phytozome database. Hits from the profile HMM search of the Phytozome databases with an *E*-value cut-off of 1*e*−5 were used to construct a multiple sequence alignment following the previous protocol of clustering at 100% identity with CD-HIT, identification of a reference sequence, alignment with MAFFT FFT-NS-2 strategy, and exclusion of sequences missing characters at over 50% of the reference sequence's designated αA or αE regions. The resulting multiple sequence alignments were trimmed of columns that had gaps in 75% or more of the sequences, and visualized as sequence logos. Note that residues at positions 18–20 representing the start of the αE region are presented here in the sequence logos for completeness; however, there is a higher presence of gaps in the alignments at positions 18–20 and alignment error could account for the differences of amino-acids at these positions.

In order to highlight patterns occurring at the species level, individual species from the four clades were chosen—*A. thaliana*, *Glycine max*, *P. persica*, *Populus trichocarpa*, and *V. vinifera*. The same search procedure as for the larger sets was repeated for each of these species. Alignments and profile HMMs were constructed specific to each individual species and the subsets of the Phytozome database used for the more extensive search were restricted to sequences from each individual species.

RESULTS

The RPV1 TIR Domain Causes Cell Death in Tobacco

The *RPV1* gene from *M. rotundifolia* encodes a TIR-NB-LRR protein that confers resistance to the oomycete pathogen *P. viticola* (Feechan et al., 2013). Based on the protein structures of RPS4^{TIR} and L6^{TIR} (Bernoux et al., 2011; Williams et al., 2014), the TIR domain is predicted to be located between residues 20 and 188 (**Figure 1A**). As TIR-domain autoactivity has been demonstrated for a number of plant NLR proteins (Frost et al., 2004; Swiderski et al., 2009; Krasileva et al., 2010; Bernoux

et al., 2011), we tested whether the RPV1 TIR domain was also autoactive. Agroinfiltration experiments confirmed that RPV1$^{TIR1-193}$ and RPV1$^{TIR20-193}$ were capable of causing rapid cell death in *N. tabacum* (**Figures 1B,D**). To determine the minimal functional region of RPV1 required for autoactivity, we tested a series of RPV1^{TIR} truncated fragments fused to YFP for autoactivity in tobacco. The addition of the YFP tag had no effect on RPV1$^{TIR1-193}$ autoactivity (**Figure 1B**). Truncation of the αE helix led to a significant decrease in RPV1^{TIR} autoactivity (**Figure 1B**), in agreement with similar results obtained with L6^{TIR} (Bernoux et al., 2011). However, whereas corresponding truncations in the αE helix of L6^{TIR} were found to affect protein stability, this was not the case for the truncated RPV1^{TIR} proteins (**Figure 1C**). These results strongly support the secondary-structure predictions, suggesting that RPV1^{TIR} is located between residues 20–188.

Crystal Structure of RPV1 TIR Domain Reveals a Conserved Dimeric Interface

On the basis of these results, we expressed the N-terminal residues 20–193 of RPV1 (designated RPV1$^{TIR20-193}$) in *E. coli* and purified it to homogeneity. Crystals of RPV1$^{TIR20-193}$ diffracted x-rays to 2.3 Å resolution and the structure was solved by molecular replacement (**Table 1**, **Figure 2**). The RPV1$^{TIR20-193}$ structure resembles closely the AtTIR (PDB ID 3jrn), L6^{TIR} (3ozi) and RPS4^{TIR} (4c6r; Chan et al., 2010; Bernoux et al., 2011; Williams et al., 2014) structures with an overall Cα RMSD (root-mean-square-distance) value of ∼1.2, ∼1.3, ∼1.6 Å (for 141, 147, 148 superimposed residues), respectively. Within the asymmetric unit, we observe a dimer (**Figure 2A**) that resembles the heterodimer of the TIR domains from *Arabidopsis* RRS1 and RPS4 (Williams et al., 2014). This interaction involves the αA and αE helices and the loop regions that precede both helices (**Figure 2A**); we consequently define this protein-protein interface as the AE interface. Analysis of the RPV1^{TIR} structure using the program PISA (Krissinel and Henrick, 2007) identified that the AE interface was the largest crystal lattice contact, contributing a combined buried surface area of ∼1340 Å^2 (∼670 Å^2 from each molecule). This is similar to the combined ∼1300 Å^2 buried surface in the RRS1^{TIR}:RPS4^{TIR} heterodimer (Williams et al., 2014). Within the AE interface, 17 surface-exposed amino-acids from each RPV1$^{TIR20-193}$ monomer are buried within the dimer and contribute to the interaction (**Figure 2B**). At the core of the interface, His42 forms an important stacking interaction between the two monomers and hydrogen bonds with Glu170 from the opposing monomer (**Figure 2C**). Hydrogen bonding between Asp41 and Ser171 is also prominent and these equivalent residues were also important in the RPS4^{TIR}:RRS1^{TIR} interaction (Williams et al., 2014).

RPV1 TIR Domain-Mediated Cell Death Is Dependent on the Conserved AE Interface

Based on the analysis of the crystal structure of RPV1$^{TIR20-193}$, we were interested to understand further the potential role of the AE interface in RPV1 function. To do this, we generated mutations to specific residues in the core and peripheral regions of the AE interface of RPV1$^{TIR1-193}$ (fused to YFP) and assessed the impact of these mutations on autoactivity. Mutations of residues His42 and Asp41 to alanine within the core of the AE interface, were found to abolish and markedly reduce, RPV1$^{TIR1-193}$-YFP mediated cell death in tobacco. Mutation of R49 to alanine at the periphery of the interface had no effect on RPV1$^{TIR1-193}$ autoactivity (**Figure 2D**), while mutation of R36 to alanine, which is also on the periphery of the interface, abolished cell death.

Importantly, these results could not be explained by differences in protein stability. Indeed, levels of RPV1$^{TIR1-193}$-YFP protein recovered from tobacco-leaf tissue agroinfiltrated for the loss-of-function mutants (R36A, D41A and H42A) appeared higher, 48 h post-infiltration, than from the constructs that displayed strong necrosis at day 5 (**Figure 2E**), potentially due to the impact of cell death on protein yield from agroinfiltrated sectors. These results demonstrate that residues R36, D41, and H42 within the AE interface play a key role in the RPV1^{TIR} signaling.

TABLE 1 | Crystallographic data.

	RPV1$^{TIR20-193}$
Data collection	
Space group	P 2 2_1 2_1
a, b, c (Å)	41.855 89.117 113.858
α, β, γ (°)	90 90 90
Resolution (Å)	37.95–2.3 (2.38–2.3)[a]
Rmeas (%)[b]	0.098 (0.997)
Rpim (%)[c]	0.036 (0.366)
$<I/\sigma(I)>$	19.6 (2.2)
$CC_{1/2}$ [d]	0.99 (0.78)
Completeness (%)	100 (100)
Multiplicity	7.2 (7.4)
Wilson plot B (Å^2)	27.5
Observations	142338 (13863)
Unique reflections	19672 (1881)
Refinement	
Rwork (%)	17.9
Rfree (%)	23.5
Average B-factor (Å^2)	48.9
R.m.s deviations	
Bond lengths (Å)	0.008
Bond angles (°)	1.03
Ramachandran plot (%)[e]	
Favored	99.1
Allowed	0.9
Outliers	0

[a] *Values within parentheses indicate the highest resolution bin.*

[b] $R_{meas} = \sum_{hkl}\{N(hkl)/[N(hkl)-1]\}^{1/2}\sum_i |I_i(hkl) - <I(hkl)>| / \sum_{hkl}\sum_i I_i(hkl)$, *where* $I_i(hkl)$ *is the intensity of the ith measurement of an equivalent reflection with indices hkl.*

[c] $R_{pim} = \sum_{hkl}\{1/[N(hkl)-1]\}^{1/2}\sum_i |I_i(hkl) - <I(hkl)>| / \sum_{hkl}\sum_i I_i(hkl)$.

[d] *Calculated with the program Aimless (Evans and Murshudov, 2013).* [e] *As calculated by MolProbity (Chen et al., 2010).*

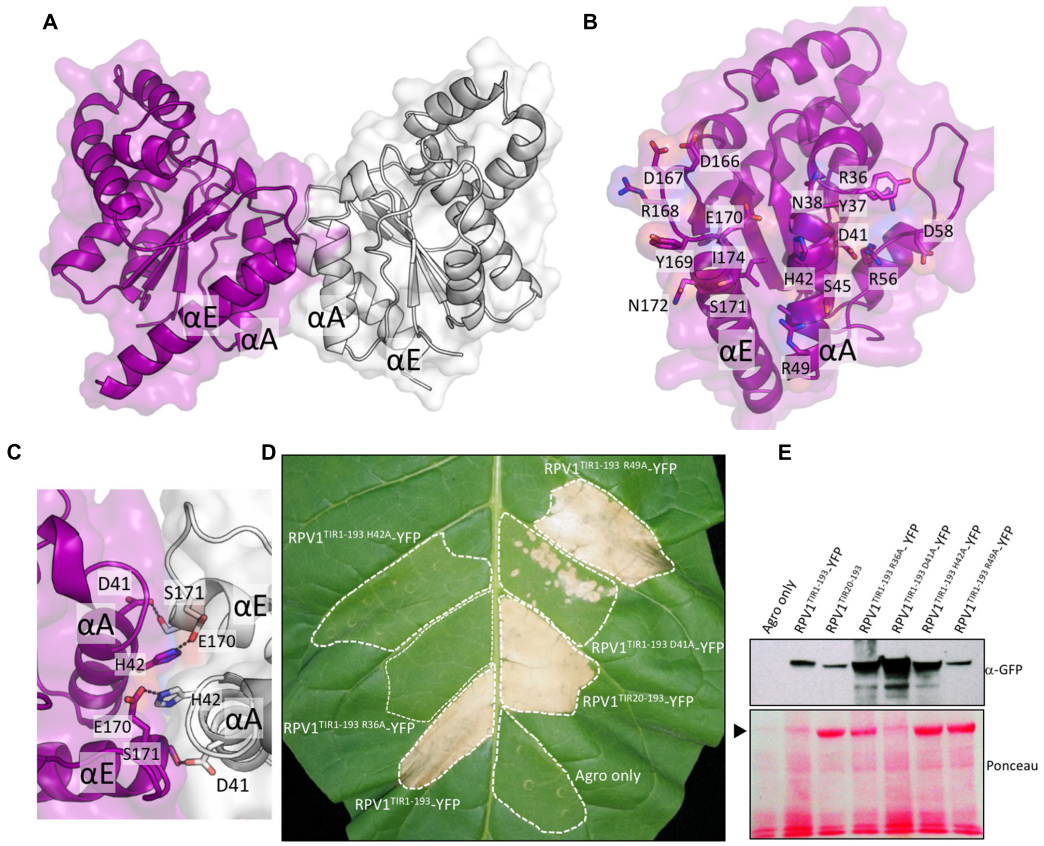

FIGURE 2 | RPV1^{TIR} cell-death signaling is dependent on the integrity of the conserved interface revealed by the RPV1$^{TIR20-193}$ crystal structure. **(A)** Structure of the dimer of RPV1 observed in the asymmetric unit of the crystals, shown in cartoon representation with transparent surface (chain A and B are colored purple and gray, respectively). **(B)** The dimer interface with chain A facing the plane of the page. Buried residues are displayed in stick representation and labeled. **(C)** The conserved histidine stacking within the interface. **(D)** *N. tabacum* plants 5 days after infiltration with *A. tumefaciens* strains expressing the RPV1$^{TIR1-193}$ and mutants fused to YFP, and RPV1$^{TIR20-193}$ analogous to the protein used for structural analysis. **(E)** Immunoblot detection of RPV1^{TIR}-YFP fusions with anti-GFP antibodies, 2 days after agroinfiltration into *N. tabacum* leaves. Ponceau staining of the membrane used for western analysis, with the large RuBisCO subunit identified with an arrow. Agro only, corresponds to agrobacterium transformed with a vector without an insert.

RPV1 TIR Domain-Mediated Cell Death Is Dependent on Regions Outside the AE Interface

The crystal structure of L6^{TIR} revealed an interface that is spatially distinct to the AE interface, involving the αD and αE helices and the βE strand. In L6^{TIR}, this region was shown to be important in mediating L6^{TIR} self-association, which is a requirement for the cell death signaling function of the L6^{TIR} (Bernoux et al., 2011). To investigate if residues in this region affect RPV1^{TIR} signaling, we generated mutations P121Y, R125A and G161R (**Figure 3A**); equivalent to P160Y, R164A and G201R in L6^{TIR}, and found that these mutants were compromised in their ability to mediate cell death in tobacco (**Figure 3B**). In the case of L6^{TIR}, cell-death signaling was shown to be compromised when residues outside the L6^{TIR} self-association interface were mutated (Bernoux et al., 2011). We also observed disruption of cell-death signaling in W94A and C95S RPV1$^{TIR1-193}$-YFP constructs (equivalent to W131A and C132S in L6^{TIR}), consistent with findings for L6. Importantly not all mutations to surface-exposed residues disrupted cell-death signaling, as demonstrated by the fact that mutation of the non-conserved L108 to a valine did not affect the protein (**Figures 3A,B**). All mutated RPV1$^{TIR1-193}$YFP proteins were detectable by western-blot analysis (**Figure 3C**), suggesting that these results are not influenced by *in planta* protein stability.

Solution Studies of the RPV1 TIR Domain

Homo- and hetero-meric TIR:TIR domain interactions are responsible for the biological functions of TIR domains (Ve et al., 2014). Interactions have been observed in the TIR domains from RRS1, RPS4, and L6 by both Y2H assays and by studies in solution with recombinant proteins (Bernoux et al., 2011; Williams et al., 2014). For RPV1$^{TIR1-193}$, we did not observe an interaction in Y2H assays (**Supplementary Figure S3**) under the conditions tested, despite observing self-association of L6$^{TIR29-233}$, which was consistent with previous observations (Bernoux et al., 2011). Solution studies using SEC-coupled MALS and SAXS suggested that only limited self-interaction of RPV1$^{TIR20-193}$ may be

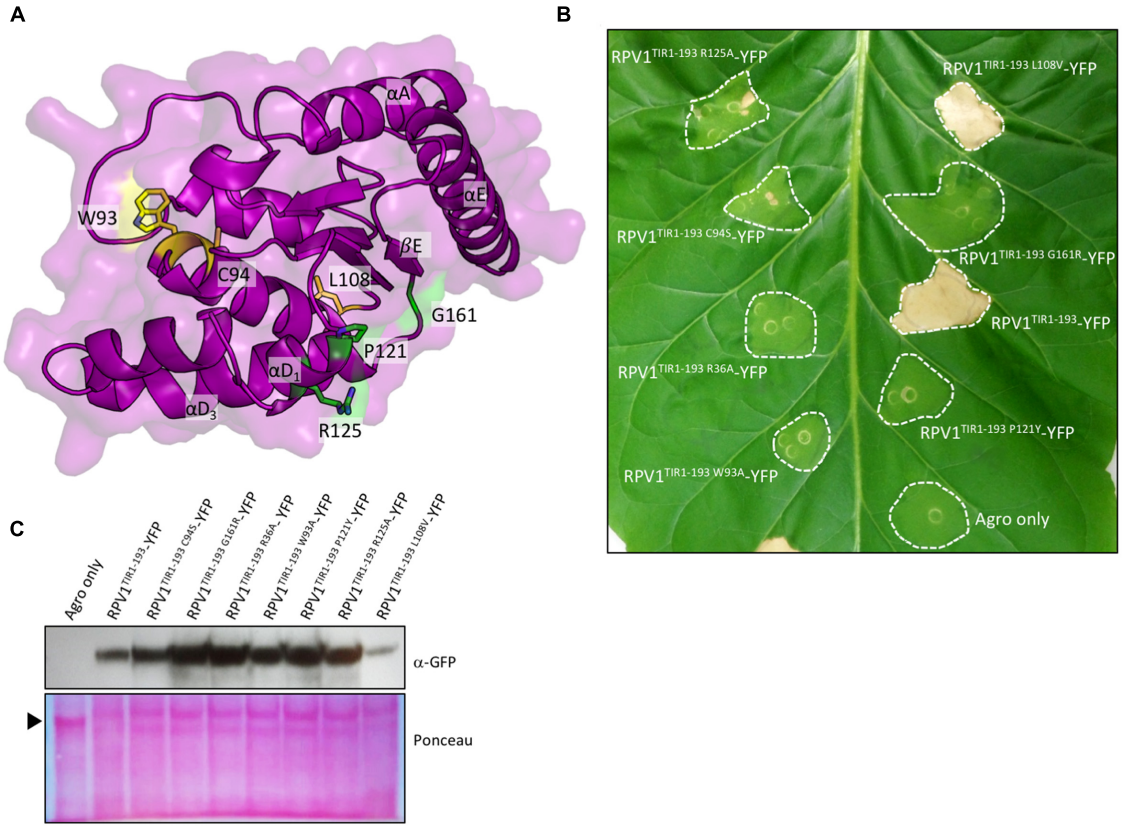

FIGURE 3 | RPV1^{TIR} cell-death signaling is dependent on regions outside of the AE interface. (A) Structure of the RPV1$^{TIR20-193}$, highlighting residues mutated in regions outside of the AE interface. Residues colored green represent residues important in L6^{TIR} self-association and autoactivity, while residues colored yellow represent residues outside of this region and the AE interface. **(B)** *N. tabacum* plants 5 days after infiltration with *A. tumefaciens* strains expressing the RPV1$^{TIR1-193}$ and mutants fused to YFP. RPV1$^{TIR1-193}$ and RPV1$^{TIR1-193R36A}$ are included as positive and negative controls. **(C)** Immunoblot detection of RPV1^{TIR}-YFP fusions with anti-GFP antibodies, 2 days after agroinfiltration into *N. tabacum* leaves. The arrow indicates Ponceau staining of the large RuBisCO subunit.

present (**Figure 4**). The average SEC-MALS-derived molecular mass of RPV1$^{TIR20-193}$ was 22.3 kDa, while the theoretical molecular mass of RPV1$^{TIR20-193}$ is 20.7 kDa. We also tested, by SEC-MALS, the recombinant RPV1$^{TIR20-193}$ protein carrying an alanine mutation at position H42 (RPV1$^{TIR20-193H42A}$). The equivalent mutation in RPS4^{TIR} had previously been shown to disrupt RPS4^{TIR}:RRS1^{TIR} dimerisation and inhibited RPS4^{TIR} self-association. This analysis produced a molecular mass of 20.8 kDa, slightly lower than that of RPV1$^{TIR20-193}$ (**Figure 4A**). Using SEC-SAXS, the averaged molecular masses observed for both proteins were lower than masses determined by SEC-MALS, 19.6 kDa for RPV1$^{TIR20-193}$ and 18.7 kDa for RPV1$^{TIR20-193H42A}$, and small shifts in elution time between RPV1$^{TIR20-193}$ and RPV1$^{TIR20-193H42A}$ were also observed (**Figure 4B**). Molecular masses higher than monomer were previously observed in L6, RPS4, and RRS1 by SEC-MALS (Bernoux et al., 2011; Williams et al., 2014) and in these cases, this behavior could be convincingly linked to self-association. However, in the case of RPV1^{TIR}, the absolute difference in molecular mass is small and may be beyond the sensitivity of these scattering techniques. Therefore, while these data do not exclude the possibility that the RPV1^{TIR} domain can self-associate, a link to this function cannot be made based on the Y2H and in-solution experiments presented here.

Conservation of a Functional Interface in Plants

We previously highlighted the potential conservation of surface-exposed residues in the AE interface after defining its role in RPS4 and RRS1 defense signaling (Williams et al., 2014). In light of our findings presented here for RPV1, we embarked on a more extensive analysis to characterize the conservation of the AE interface across a broader range of plant species. We created species-specific profiles to capture >2000 TIR domain-containing sequences from across 29 plant species and used profile HMMs to create and inspect TIR-domain sequence logos across this wide species range with a focus on the AE interface (See Supplementary Table S2, Supplementary Data Sheet 1, and Materials and Methods). Sequences identified from Pfam were collated into four clades for comparison based on the species tree from Phytozome (**Supplementary Figure S2**):

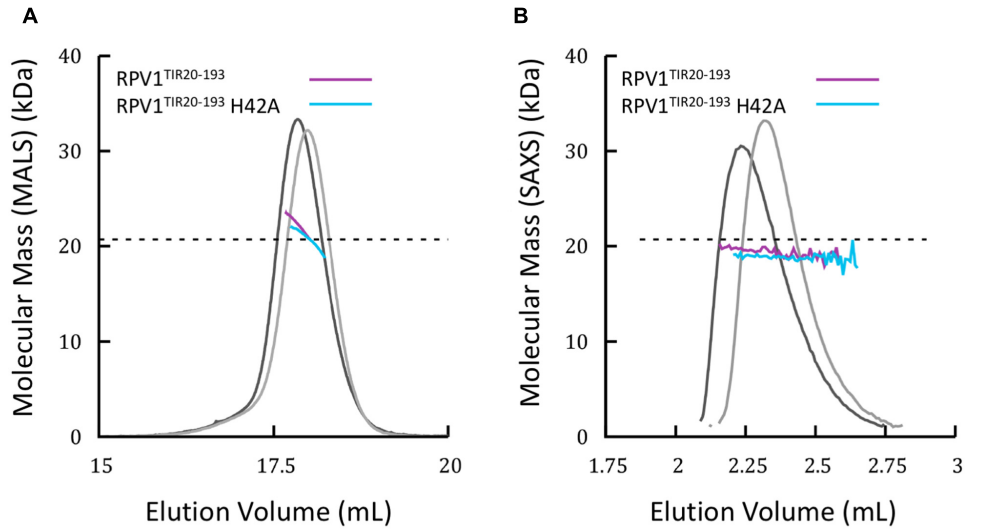

FIGURE 4 | Solution properties of RPV1$^{TIR20-193}$ (A) Size-exclusion chromatography (SEC)/ multi-angle laser light scattering (MALS) analysis of RPV1$^{TIR20-193}$ (purple) and RPV1$^{TIR20-193}$H42A (sky blue). Purified proteins were separated over an inline Superdex 200 10/300 GL column and the molecular mass (MM) was calculated across the elution peak by MALS. Colored lines under the peaks correspond to the averaged MM (*y*-axis) distributions across that peak, while gray lines indicate the normalized refractive index trace (nominal units). A dotted black line denotes the expected monomeric molecular mass of RPV1$^{TIR20-193}$. **(B)** SEC/small-angle x-ray scattering (SAXS) analysis of RPV1$^{TIR20-193}$ and RPV1$^{TIR20-193}$H42A. Purified proteins were separated on an in-line Superdex Increase 200 5/150 GL SEC column. MM was calculated using the volume of correlation (Rambo and Tainer, 2013). Colored lines under the peak correspond to the molecular mass (*y*-axis) across the peak. Gray lines indicate the zero angle scattering, *I*(0), arbitrarily scaled onto the molecular mass for visualization.

Malvids, containing *A. thaliana*, *A. lyrata*, *Brassica rapa*, and *Eutrema salsugineum*; Fabales, containing *G. max* and *P. persica*; Malpighiales, containing *P. trichocarpa* and *Ricinus communis*; and Pentapetalae, that contained all of the three previous sets, plus *Solanum lycopersicum*, *S. tuberosum*, and *V. vinifera*—representing all classified TIR domain sequences from Pfam within the Pentapetalae clade (**Figure 5B**). We also undertook a more specific analysis into five individual species to highlight residue differences occurring at the species level (**Figure 5C**).

Conservation of residues across a wide range of species in the αA and αE regions showed that the αA region (positions 1–17) was more conserved than the αE region (positions 18–30). A number of hydrophobic residues are highly conserved, including positions 7, 11, 15, 26, 29, and 30 (**Figures 5A–C**). These residues are mostly buried and appear to assist in stabilizing the positioning of the αA and αE helices. The well-conserved position 26 (RPV1 Ile174) is surface-exposed and contributes to a pocket that in the RPV1$^{TIR20-193}$ structure is occupied by His42 from the interacting RPV1$^{TIR20-193}$ protomer. The most important surface-exposed residues in the AE interface are at positions 9, 10, and 22, which form the core of the AE interface (**Figures 5A** and **2C**). This analysis reveals that at these positions, there is conservation of histidine and glutamate at position 10 and 22, respectively (RPV1 His42 and Glu170). The amino-acid distribution at position 9 (RPV1 Asp41) is more varied across the clades (**Figure 5B**), with evidence of species-specific conservation, for example the conservation of serine in *A. thaliana* (**Figure 5C**). There is also a general trend for position 23 to contain a small amino-acid such as alanine or serine. While histidine at position 10 is well conserved, there is minor representation of aromatic residues including phenylalanine and tyrosine. Interestingly, in the case of AtTIR, a phenylalanine occupies this position, indicating that phenylalanine is compatible with dimerisation through the AE interface, at least within the context of AtTIR crystals. At the species level, *G. max* (soybean) appeared to deviate most significantly of the species compared across the important AE interface residues. *G. max* appears to have a similar preference for histidine and asparagine at position 10 (**Figure 5C**) and at position 22, the negatively charged residue glutamate is replaced by aspartate and glutamine in some instances. In general, there is significant variation in other interface interacting residues at both the clade and species levels, with the exception of position 4, which is essentially an invariant arginine.

DISCUSSION

Toll-interleukin receptor domains are protein scaffolds that regulate pathogen defense-related pathways in plants and animals through TIR:TIR domain interactions (Ve et al., 2014). Of the five structures currently available for plant TIR domains, four originate from *Arabidopsis* and one from flax. All the crystal structures of TIR domains from *Arabidopsis* proteins show an analogous interaction interface (designated here the AE interface). We previously hypothesized that this interface would have broad functional relevance, beyond signaling in *Arabidopsis* (Williams et al., 2014). Here, our crystal structure of the *M. rotundifolia* RPV1$^{TIR20-193}$ domain reveals a dimer interaction that is mediated by the AE interface. We demonstrate

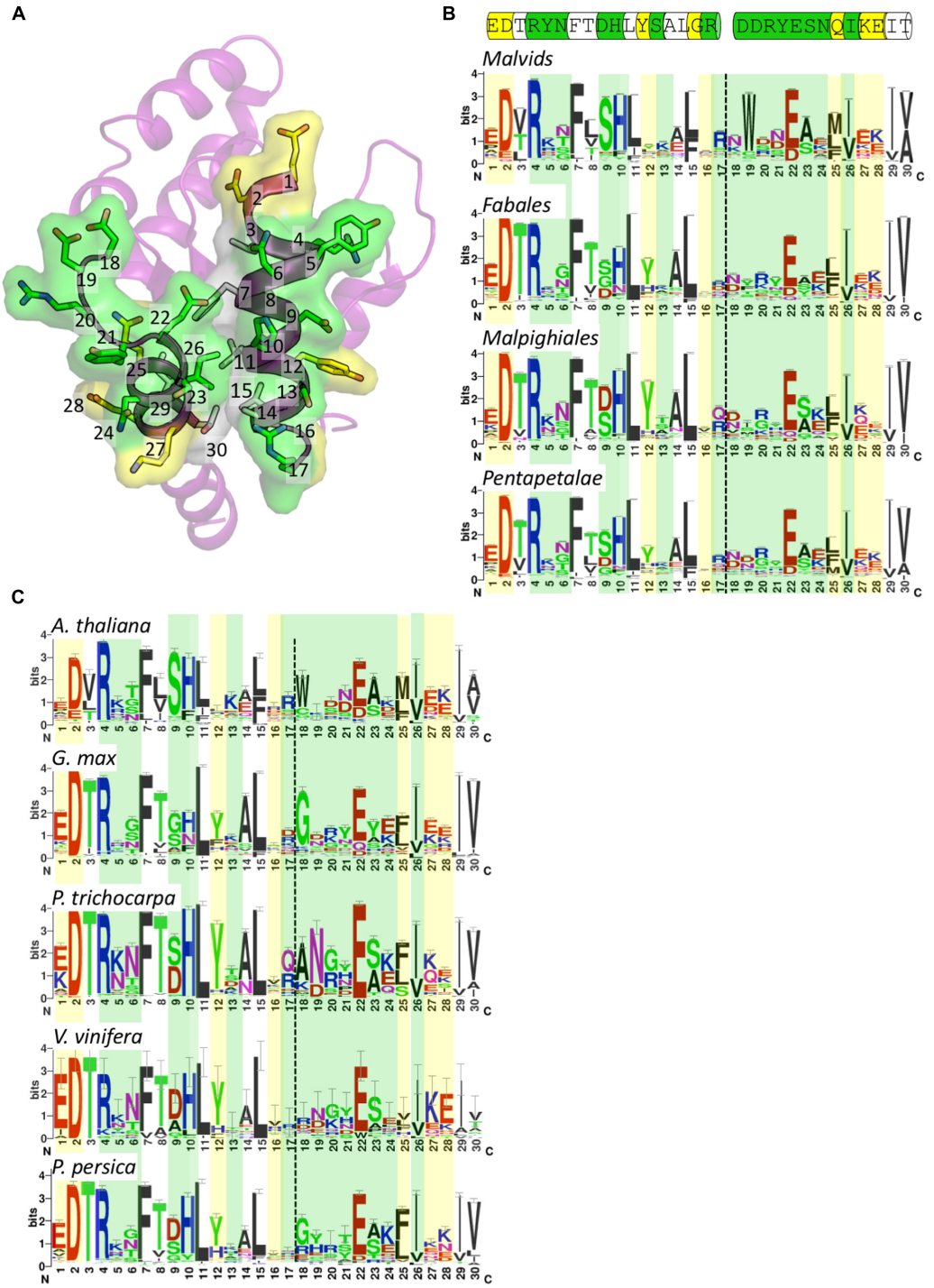

FIGURE 5 | Conservation of surface-exposed residues within the AE interface. (A) Crystal structure of RPV1 shown in ribbon representation with the face of the AE interface oriented toward the page. The AE interface residues are presented as sticks and are included in the sequence logos presented in **(B,C)**. The numbering corresponds to position in the logos. Surface-exposed residues involved in interface interactions are colored green, surface-exposed residues not involved in interface interactions are colored yellow, and residues that are not surface-exposed are colored white. **(B)** Sequence logos of the AE interface in the families Malvids, Fabales, Malipighiales and Pentapetalae. Coloring as defined for **(A)**. Dotted lines represent the division between the αA and αE regions. Cartoon above the logos represents the sequence of this region in RPV1 as shown in **(A)**. **(C)** Sequence logos of the AE interface in the species *A. thaliana, G. max, P. trichocarpa, V. vinifera,* and *P. persica* colored and labeled as in **(B)**.

that the conserved surface-exposed residues in the AE interface are required for the autoactive cell-death phenotype exhibited by the TIR domain of RPV1 when transiently expressed in *N. tabacum*. In addition, we demonstrate that the integrity of residues that map to the $L6^{TIR}$ self-association interface and residues that are outside of both interfaces are also required for the autoactive cell-death in *N. tabacum*. These observations combined with the conservation of this region across a broad range of plant species strongly suggest that this protein interface plays a general role in plant TIR-domain signaling.

The presence of an interface within a crystal structure does not, in itself, support a functional role for this interface (Kobe et al., 2008). However, the presence of a dimer mediated by the analogous AE interface in five of the six available plant TIR domain crystal structures is striking (**Supplementary Figure S4**). We have previously demonstrated that the AE interface is biologically relevant. The AE interface is responsible for the strong heterodimeric interaction between $RPS4^{TIR}$ and $RRS1^{TIR}$, and also that self-association of the $RPS4^{TIR}$, suggesting that competition between these two interactions is important for the regulation in the full-length NLR (Williams et al., 2014). In the case of $RPV1^{TIR20-193}$, biophysical characterisation suggests that self-association, is absent or very weak in solution. SEC-MALS yielded an averaged molecular mass only slightly higher than that predicted for a monomer and while the interface-disrupting mutant $RPV1TIR^{20-193}$H42A did restore the theoretical monomeric molecular mass of RPV1 in SEC-MALS, the difference between the mutant and wild-type protein is less than 10% of the mass and therefore within potential error associated with this technique. Consequently, from the experiments used we were unable to confirm self-association of $RPV1^{TIR}$. Despite this, it is clear that the AE interface plays a crucial role in autoactivity of the RPV1 TIR domain. Mutations that alter the surface characteristics in the core of the AE interface were found to significantly reduce cell-death signaling *in planta*, demonstrating that the interface is functionally relevant in RPV1 TIR-domain cell-death signaling. This disruption is unlikely to be due to misfolding, as these proteins were expressed *in planta*. We also show that regions outside the AE interface are important for this cell-death signaling. $RPV1^{TIR}$ autoactivity is also prevented by mutations of conserved residues within the interface identified in $L6^{TIR}$ (the DE interface) to be required for self-association and signaling. Interestingly, a similar observation was recently made in studies of the *Arabidopsis* NLR protein RPP1, whereby residues in both the AE and DE interfaces played were important for RPP1 TIR domain mediated cell death signaling (Schreiber et al., 2016).

An interesting feature of the cell death induced by RPV1 is that the region that encompasses the TIR domain structure is, itself, sufficient to induce cell death. To the best of our knowledge, this is the first demonstration that the TIR domain alone can signal autoactive cell death. In previous studies, amino-acid sequences that extended beyond the structural borders of the TIR domain were included when assaying for autoactivity *in planta*. For example, the available $L6^{TIR}$ structure encompasses residues 59–228; however, residues 1–233 were used in functional experiments to demonstrate cell death (Bernoux et al., 2011). Similarly, the available $RPS4^{TIR}$ structure includes residues 10–178; however, the minimal cell death-inducing construct used in functional experiments comprised residues 1–235 (Williams et al., 2014). Furthermore, in the case of NdA allele of RPP1, autoactive cell death was induced in *N. tabacum* when the first 254 residues were used, while the TIR domain alone (residues 90–254) did not induce this phenotype (Schreiber et al., 2016). In all these cases, the integrity of residues in the structured region of the TIR domain was established to be critical for the cell-death function, demonstrating that the TIR domain was required for cell death. Also, in all cases, a strong correlation between self-association (measured *in vitro*) and cell-death function was observed.

The RPV1 TIR domain represents the first instance of a lack of obvious correlation between self-association (measured *in vitro*) and *in planta* autoactive cell-death function. Previous studies involving the WsB allele of RPP1 (residues 1–266) demonstrated that the weak dimerisation propensity of the C-terminal GFP tag was required to cause autoactive cell death (Krasileva et al., 2010). In the case of $RPV1^{TIR}$, the inclusion of the YFP had no consequence on the autoactive cell-death phenotype (**Figure 1**). It is plausible that $RPV1^{TIR}$ self-association is stabilized by other proteins when overexpressed in *N. tabacum*; however, it is also possible that $RPV1^{TIR}$ can interact with other TIR-only, TIR-NLR proteins in *N. tabacum* or a yet to be identified signaling protein in order to initiate cell-death. Regardless of the mechanisms of cell-death activation, the integrity of the AE interface is required.

Our comparison of the AE interfaces across plant species shows that surface-exposed residues that occupy the central region of the interface are highly conserved, while residues further away from the center are generally variable. We suggest that this gives the AE interface a conserved core to facilitate interactions, while the variable exterior residues control the specificity of TIR:TIR domain interactions. An exception to this is the highly conserved arginine at position 4 (**Figure 5**), which is at the periphery of the AE interface. Mutation of this residue to in alanine in $RPV1^{TIR}$ prevented TIR domain dependent cell death, which was also observed previously for $L6^{TIR}$ and $RPS4^{TIR}$ (Swiderski et al., 2009; Bernoux et al., 2011). While this residue has only a minor involvement in the AE interface, it does appear to associate with a slight kinking of the αA helix in the known plant TIR-domain structures and likely influences the positing of the αA helix. The comparison between species also highlights that the functionally important histidine is highly preferred in *Arabidopsis* (*A. thaliana*), poplar (*P. trichocarpa*), grape (*V. vinifera*) and peach (*P. persica*) but less so in soybean (*G. max*). It will be interesting to characterize further these divergent residues at conserved positions in terms of TIR domain autoacitivity and NLR function in the future.

Overall, the data presented here highlights that the AE interface is likely to be functionally important across a broad range of plant species and is not limited to *Arabidopsis* TIR domains. Our work also confirms that the TIR domain is the minimal region required for cell-death signaling. We suggest

the available data build a general paradigm of structure-function relationships in plant TIR domains, where the AE interface and other spatially distinct protein surfaces in plant TIR domains play key roles in the signaling mechanism of plant TIR-NLR proteins.

AUTHOR CONTRIBUTIONS

SW, BK, ID, MB, LY, and GF conceived and designed the experiments, SW, LY, GF, LC, MO, and DE performed the experiments, all authors analyzed the data and SW, LY, BK, ID, GF, and LC wrote the paper. All authors reviewed and edited the paper.

FUNDING

This research was supported by the Australian Research Council (ARC) Discovery Projects DP120100685 and DP160102244. BK is a NHMRC Research Fellow (1003325 and 1110971). SW is funded by ARC DECRA (DE160100893).

ACKNOWLEDGMENTS

We thank Angelica Jermakow and Nayana Arunasiri for excellent technical assistance. We acknowledge the use of the University of Queensland Remote Operation Crystallization and X-ray Diffraction Facility (UQ ROCX). The X-ray diffraction data collection was undertaken on the MX and SAXS-WAXS beamlines at the Australian Synchrotron. We thank beamline staff for their help and advice with data collection. The crystal structure of RPV1$^{TIR20-193}$ and data used to derive the structure has been deposited with the Protein Data Bank with accession numbers 5KU7.

SUPPLEMENTARY MATERIAL

The Supplementary Material for this article can be found online at: http://journal.frontiersin.org/article/10.3389/fpls.2016.01850/full#supplementary-material

FIGURE S1 | Workflow diagram. Key steps involved in the sequence-level analysis of conservation.

FIGURE S2 | Species tree representing species and clades investigated in the sequence-level analysis of conservation. Colored triangles indicate individual species retrieved from Pfam that comprised the four clades used to build the profile HMMs. Colored circles on the tree indicate the subtree from Phytozome that was queried with the profile HMM built from the equivalently colored triangle. Yellow squares represent the individual species used to build species-level profile HMMs to query the respective species from Phytozome.

FIGURE S3 | Analysis of TIR dimerization in Y2H assays. Growth of yeast cells co-expressing GAL4-BD and GAL4-AD empty vector (Negative), RPV1^{TIR} and L6^{TIR} domain fusions on synthetic media lacking tryptophan and leucine (-TL) or on selective media lacking tryptophan, leucine and histidine and containing 5 mM 3AT. Growth on media lacking tryptophan and leucine (-TL) confirms yeast viability, while growth on media lacking histidine (-HTL) indicates expression of the HIS3 reporter gene due to interaction between the fusion proteins.

FIGURE S4 | Published TIR-domain structures that feature the AE interface. (A) RPV1 (PDB ID 5KU7) chain A and B. **(B)** RRS1-RPS4 heterodimer (PDB ID 4c6t) chain A and B. **(C)** RPS4 (PDB ID 4c6r) chain A and D (symmetry operator $x, y-1, z$). **(D)** RRS1 (PDB ID 4c6s) chain A and A (symmetry operator $y+1, -x+1, -z+5/2$). **(E)** AtTIR (PDB ID 3jrn) chain A and A (symmetry operator $-y+1, -x+1, -z+1/2$). **(F)** L6 (PDB ID 3OZI) chain A (yellow) and B (wheat) mediated by αD and αE helices and orientated as in **(A–E)** for comparison.

REFERENCES

Ade, J., Deyoung, B. J., Golstein, C., and Innes, R. W. (2007). Indirect activation of a plant nucleotide binding site-leucine-rich repeat protein by a bacterial protease. *Proc. Natl. Acad. Sci. U.S.A.* 104, 2531–2536. doi: 10.1073/pnas.0608779104

Bernoux, M., Ve, T., Williams, S., Warren, C., Hatters, D., Valkov, E., et al. (2011). Structural and functional analysis of a plant resistance protein TIR domain reveals interfaces for self-association, signaling, and autoregulation. *Cell Host Microbe* 9, 200–211. doi: 10.1016/j.chom.2011.02.009

Casey, L. W., Lavrencic, P., Bentham, A., Cesari, S., Ericsson, D. J., Croll, T. I., et al. (2016). The CC domain structure from the wheat stem rust resistance protein Sr33 challenges paradigms for dimerization in plant NLR proteins. *Proc. Natl. Acad. Sci. U.S.A.* 113, 12856–12861. doi: 10.1073/pnas.1609922113

Chan, S. L., Mukasa, T., Santelli, E., Low, L. Y., and Pascual, J. (2010). The crystal structure of a TIR domain from *Arabidopsis thaliana* reveals a conserved helical region unique to plants. *Protein Sci.* 19, 155–161. doi: 10.1002/pro.275

Chen, V. B., Arendall, W. B., Headd, J. J., Keedy, D. A., Immormino, R. M., Kapral, G. J., et al. (2010). MolProbity: all-atom structure validation for macromolecular crystallography. *Acta Crystallogr. D Biol. Crystallogr.* 66, 12–21. doi: 10.1107/S0907444909042073

Collier, S. M., Hamel, L.-P., and Moffett, P. (2011). Cell death mediated by the N-terminal domains of a unique and highly conserved class of NB-LRR protein. *Mol. Plant Microbe Interact.* 24, 918–931. doi: 10.1094/MPMI-03-11-0050

Dangl, J. L., Horvath, D. M., and Staskawicz, B. J. (2013). Pivoting the plant immune system from dissection to deployment. *Science* 341, 746–751. doi: 10.1126/science.1236011

Dodds, P. N., Lawrence, G. J., Catanzariti, A.-M., Teh, T., Wang, C.-I. A., Ayliffe, M. A., et al. (2006). Direct protein interaction underlies gene-for-gene specificity and coevolution of the flax resistance genes and flax rust avirulence genes. *Proc. Natl. Acad. Sci. U.S.A.* 103, 8888–8893. doi: 10.1073/pnas.0602577103

Dodds, P. N., and Rathjen, J. P. (2010). Plant immunity: towards an integrated view of plant-pathogen interactions. *Nat. Rev. Genet.* 11, 539–548. doi: 10.1038/nrg2812

Earley, K. W., Haag, J. R., Pontes, O., Opper, K., Juehne, T., Song, K. M., et al. (2006). Gateway-compatible vectors for plant functional genomics and proteomics. *Plant J.* 45, 616–629. doi: 10.1111/j.1365-313X.2005.02617.x

Eddy, S. R. (2011). Accelerated profile HMM searches. *PLoS Comput. Biol.* 7:e1002195. doi: 10.1371/journal.pcbi.1002195

Emsley, P., Lohkamp, B., Scott, W. G., and Cowtan, K. (2010). Features and development of Coot. *Acta Crystallogr. D Biol. Crystallogr.* 66, 486–501. doi: 10.1107/S0907444910007493

Evans, P. R., and Murshudov, G. N. (2013). How good are my data and what is the resolution? *Acta Crystallogr. D Biol. Crystallogr.* 69, 1204–1214. doi: 10.1107/S0907444913000061

Feechan, A., Anderson, C., Torregrosa, L., Jermakow, A., Mestre, P., Wiedemann-Merdinoglu, S., et al. (2013). Genetic dissection of a TIR-NB-LRR locus from the wild North American grapevine species *Muscadinia rotundifolia identifies paralogous genes conferring resistance to major fungal and oomycete pathogens in cultivated grapevine. *Plant J.* 76, 661–674. doi: 10.1111/tpj.12327

Finn, R. D., Coggill, P., Eberhardt, R. Y., Eddy, S. R., Mistry, J., Mitchell, A. L., et al. (2016). The Pfam protein families database: towards a more sustainable future. *Nucleic Acids Res.* 44, D279–D285. doi: 10.1093/nar/gkv1344

Frost, D., Way, H., Howles, P., Luck, J., Manners, J., Hardham, A., et al. (2004). Tobacco transgenic for the flax rust resistance gene L expresses allele-specific activation of defense responses. *Mol. Plant Microbe Interact.* 17, 224–232. doi: 10.1094/MPMI.2004.17.2.224

Goodstein, D. M., Shu, S., Howson, R., Neupane, R., Hayes, R. D., Fazo, J., et al. (2012). Phytozome: a comparative platform for green plant genomics. *Nucleic Acids Res.* 40, D1178–D1186. doi: 10.1093/nar/gkr944

Hao, W., Collier, S. M., Moffett, P., and Chai, J. (2013). Structural basis for the interaction between the potato virus X resistance protein (Rx) and its cofactor Ran GTPase-activating protein 2 (RanGAP2). *J. Biol. Chem.* 288, 35868–35876. doi: 10.1074/jbc.M113.517417

Hu, Z., Yan, C., Liu, P., Huang, Z., Ma, R., Zhang, C., et al. (2013). Crystal structure of NLRC4 reveals its autoinhibition mechanism. *Science* 341, 172–175. doi: 10.1126/science.1236381

Jones, J. D. G., and Dangl, J. L. (2006). The plant immune system. *Nature* 444, 323–329. doi: 10.1038/nature05286

Kabsch, W. (2010). XDS. *Acta Crystallogr. D Biol. Crystallogr.* 66, 125–132. doi: 10.1107/S0907444909047337

Katoh, K., and Standley, D. M. (2013). MAFFT multiple sequence alignment software version 7: improvements in performance and usability. *Mol. Biol. Evol.* 30, 772–780. doi: 10.1093/molbev/mst010

Kobe, B., Guncar, G., Buchholz, R., Huber, T., Maco, B., Cowieson, N., et al. (2008). Crystallography and protein-protein interactions: biological interfaces and crystal contacts. *Biochem. Soc. Trans.* 36, 1438–1441. doi: 10.1042/BST0361438

Krasileva, K. V., Dahlbeck, D., and Staskawicz, B. J. (2010). Activation of an *Arabidopsis* resistance protein is specified by the in planta association of its leucine-rich repeat domain with the cognate oomycete effector. *Plant Cell* 22, 2444–2458. doi: 10.1105/tpc.110.075358

Krissinel, E., and Henrick, K. (2007). Inference of macromolecular assemblies from crystalline state. *J. Mol. Bol.* 372, 774–797. doi: 10.1016/j.jmb.2007.05.022

Li, W., and Godzik, A. (2006). Cd-hit: a fast program for clustering and comparing large sets of protein or nucleotide sequences. *Bioinformatics* 22, 1658–1659. doi: 10.1093/bioinformatics/btl158

Maekawa, T., Cheng, W., Spiridon, L. N., Töller, A., Lukasik, E., Saijo, Y., et al. (2011). Coiled-coil domain-dependent homodimerization of intracellular barley immune receptors defines a minimal functional module for triggering cell death. *Cell Host Microbe* 9, 187–199. doi: 10.1016/j.chom.2011.02.008

McCoy, A. J., Grosse-Kunstleve, R. W., Adams, P. D., Winn, M. D., Storoni, L. C., and Read, R. J. (2007). Phaser crystallographic software. *J. Appl. Crystallogr.* 40, 658–674. doi: 10.1107/S0021889807021206

Moffett, P., Farnham, G., Peart, J., and Baulcombe, D. C. (2002). Interaction between domains of a plant NBS-LRR protein in disease resistance-related cell death. *EMBO J.* 21, 4511–4519. doi: 10.1093/emboj/cdf453

Petoukhov, M. V., Franke, D., Shkumatov, A. V., Tria, G., Kikhney, A. G., Gajda, M., et al. (2012). New developments in the ATSAS program package for small-angle scattering data analysis. *J. Appl. Crystallogr.* 45, 342–350. doi: 10.1107/S0021889812007662

Rambo, R. P., and Tainer, J. A. (2013). Accurate assessment of mass, models and resolution by small-angle scattering. *Nature* 496, 477–481. doi: 10.1038/nature12070

Robert, X., and Gouet, P. (2014). Deciphering key features in protein structures with the new ENDscript server. *Nucleic Acids Res.* 42, 320–324. doi: 10.1093/nar/gku316

Schreiber, K. J., Betham, A., Williams, S. J., Kobe, B., and Staskawicz, B. J. (2016). Multiple domain associations within the *Arabidopsis* immune receptor RPP1 regulate the activation of programmed cell death. *PLoS Pathog.* 12:e1005769. doi: 10.1371/journal.ppat.1005769

Slootweg, E., Roosien, J., Spiridon, L. N., Petrescu, A.-J., Tameling, W., Joosten, M., et al. (2010). Nucleocytoplasmic distribution is required for activation of resistance by the potato NB-LRR receptor Rx1 and is balanced by Its functional domains. *Plant Cell* 22, 4195–4215. doi: 10.1105/tpc.110.077537

Stols, L., Gu, M., Dieckman, L., Raffen, R., Collart, F. R., and Donnelly, M. I. (2002). A new vector for high-throughput, ligation-independent cloning encoding a tobacco etch virus protease cleavage site. *Protein Expr. Purif.* 25, 8–15. doi: 10.1006/prep.2001.1603

Studier, F. W. (2005). Protein production by auto-induction in high density shaking cultures. *Protein Expr. Purif.* 41, 207–234. doi: 10.1016/j.pep.2005.01.016

Swiderski, M. R., Birker, D., and Jones, J. D. G. (2009). The TIR domain of TIR-NB-LRR resistance proteins is a signaling domain involved in cell death induction. *Mol. Plant Microbe Interact.* 22, 157–165. doi: 10.1094/MPMI-22-2-0157

Tameling, W. I. L., Elzinga, S. D. J., Darmin, P. S., Vossen, J. H., Takken, F. L. W., Haring, M. A., et al. (2002). The tomato R gene products I-2 and MI-1 are functional ATP binding proteins with ATPase activity. *Plant Cell* 14, 2929–2939. doi: 10.1105/tpc.005793

Tucker, M. R., Okada, T., Hu, Y. K., Scholefield, A., Taylor, J. M., and Koltunow, A. M. G. (2012). Somatic small RNA pathways promote the mitotic events of megagametogenesis during female reproductive development in *Arabidopsis*. *Development* 139, 1399–1404. doi: 10.1242/dev.075390

UniProt, C. (2015). UniProt: a hub for protein information. *Nucleic Acids Res.* 43, 204–212. doi: 10.1093/nar/gku989

van Der Hoorn, R. A. L., and Kamoun, S. (2008). From guard to decoy: a new model for perception of plant pathogen effectors. *Plant Cell* 20, 2009–2017. doi: 10.1105/tpc.108.060194

Ve, T., Williams, S. J., and Kobe, B. (2014). Structure and function of Toll/interleukin-1 receptor/resistance protein (TIR) domains. *Apoptosis* 20, 250–261. doi: 10.1007/s10495-014-1064-2

Williams, S. J., Sohn, K. H., Wan, L., Bernoux, M., Sarris, P. F., Segonzac, C., et al. (2014). Structural basis for assembly and function of a heterodimeric plant immune receptor. *Science* 344, 299–303. doi: 10.1126/science.1247357

Williams, S. J., Sornaraj, P., Decourcy-Ireland, E., Menz, R. I., Kobe, B., Ellis, J., et al. (2011). An autoactive mutant of the M flax rust resistance protein has a preference for binding ATP, while wild-type M protein has a preference for binding ADP. *Mol. Plant Microbe Interact.* 24, 897–906. doi: 10.1094/MPMI-03-11-0052

Conflict of Interest Statement: The authors declare that the research was conducted in the absence of any commercial or financial relationships that could be construed as a potential conflict of interest.

frontiers in Plant Science

ORIGINAL RESEARCH
published: 18 January 2016
doi: 10.3389/fpls.2015.01214

TaADF3, an Actin-Depolymerizing Factor, Negatively Modulates Wheat Resistance Against *Puccinia striiformis*

Chunlei Tang[‡], *Lin Deng*[†‡], *Dan Chang*, *Shuntao Chen*, *Xiaojie Wang*[*] *and Zhensheng Kang*[*]

State Key Laboratory of Crop Stress Biology for Arid Areas and College of Plant Protection, Northwest A&F University, Yangling, China

OPEN ACCESS

Edited by:
Ralph Panstruga, RWTH Aachen University, Germany

Reviewed by:
Lei Zhang, Washington State University, USA
Elena Prats, Consejo Superior de Investigaciones Científicas, Spain

***Correspondence:**
Xiaojie Wang
wangxiaojie@nwsuaf.edu.cn;
Zhensheng Kang
kangzs@nwsuaf.edu.cn

[†]**Present Address:**
Lin Deng, Department of Biological Chemistry and Molecular Pharmacology, Harvard Medical School, Boston, Massachusetts 02115, USA; Department of Pediatric Oncology, Dana-Farber Cancer Institute, Boston, Massachusetts 02215, USA

[‡]*These authors have contributed equally to this work.*

Specialty section:
This article was submitted to Plant Biotic Interactions, a section of the journal Frontiers in Plant Science

Received: *03 November 2015*
Accepted: *17 December 2015*
Published: *18 January 2016*

Citation:
Tang C, Deng L, Chang D, Chen S, Wang X and Kang Z (2016) TaADF3, an Actin-Depolymerizing Factor, Negatively Modulates Wheat Resistance Against Puccinia striiformis. Front. Plant Sci. 6:1214. doi: 10.3389/fpls.2015.01214

The actin cytoskeleton has been implicated in plant defense against pathogenic fungi, oomycetes, and bacteria. Actin depolymerizing factors (ADFs) are stimulus responsive actin cytoskeleton modulators. However, there is limited evidence linking ADFs with plant defense against pathogens. In this study, we have isolated and functionally characterized a stress-responsive ADF gene (*TaADF3*) from wheat, which was detectable in all examined wheat tissues. *TaADF3* is a three-copy gene located on chromosomes 5AL, 5BL, and 5DL. A particle bombardment assay in onion epidermal cells revealed the cytoplasmic and nuclear localization of TaADF3. The expression of *TaADF3* was inducible by abscisic acid (ABA), as well as various abiotic stresses (drought and cold) and virulent *Puccinia striiformis* f. sp. *tritici* (*Pst*) but was down regulated in response to avirulent *Pst*. Virus-induced silencing of *TaADF3* copies enhanced wheat resistance to avirulent *Pst*, with decreased reactive oxygen species (ROS) accumulation and hypersensitive response (HR). Upon treatment with virulent *Pst*, *TaADF3*-knockdown plants exhibited reduced susceptibility, which was accompanied by increased ROS production and HR. Interestingly, the silencing of *TaADF3* resulted in hindered pathogen penetration and haustoria formation for both avirulent and virulent *Pst*. Moreover, the array and distribution of actin filaments was transformed in *TaADF3*-knockdown epidermal cells, which possibly facilitated attenuating the fungus penetration. Thus, our findings suggest that *TaADF3* positively regulates wheat tolerance to abiotic stresses and negatively regulates wheat resistance to *Pst* in an ROS-dependent manner, possibly underlying the mechanism of impeding fungal penetration dependent on the actin architecture dynamics.

Keywords: actin depolymerizing factors, wheat, *Puccinia striiformis* f. sp. *tritici*, abiotic stress, ROS, fungal penetration, actin filaments

INTRODUCTION

Actin is one of the most abundant and highly conserved proteins in eukaryotic cells. The dynamic reorganization and rearrangement of the actin cytoskeleton is associated with various important cellular processes that are essential for cell growth, differentiation, division, membrane organization, motility, cold acclimation, and wound repair (Pollard et al., 2000; Wasteneys and Galway, 2003; Day et al., 2011). Increasing evidence has shown that the actin cytoskeleton is

precisely regulated to function as a contributing factor to plant immunity against pathogen ingress (Hardham et al., 2007; Tian et al., 2009; Henty-Ridilla et al., 2013). Pharmacological perturbation of the cytoskeleton compromised the basal defense and non-host resistance of a range of plants species by increasing the incidence of pathogen entry (Kobayashi et al., 1997a; Yun et al., 2003; Shimada et al., 2006; Miklis et al., 2007). The actin cytoskeleton also plays a role in race-specific resistance (Skalamera and Heath, 1998; Tian et al., 2009). The actin-based cytoskeleton is modulated by a plethora of actin-binding proteins (ABPs), among which the actin-depolymerizing factors (ADFs) and the cofilins form a single family called the ADF/cofilins (Bamburg, 1999). They are abundant and essential in almost every eukaryotic cell type and are responsible for the high turnover rates of actin filaments *in vivo* (Staiger et al., 1997; Dos Remedios et al., 2003; Van Troys et al., 2008). The interaction between actin and ADF/cofilins is controlled by reversible phosphorylation, ubiquitination, pH, oxidation, phosphoinositides, and specific proteins (Ayscough, 1998).

Whereas most non-plant organisms contain only one or two genes encoding ADF proteins, plant species appear to express larger families of ADF genes (Meagher et al., 1999). In terms of phylogenetic relationships, plant ADF/cofilins are classified into at least four groups (Mun et al., 2000). Group I is composed exclusively of dicots except for a rice ADF gene, whereas Group IV is proposed to be exclusive to the monocots (Danyluk et al., 1996). Group II and Group III are expressed in both dicots and monocots, although Group II is pollen specific (Lopez et al., 1996). Higher-plant ADFs exhibit specific temporal and spatial expression patterns, and the preferential tissue existence seems to be related to their distinct roles in different biological processes. Pollen-specific ADFs in Group II serve to bind and remodel F-actin in pollen grains in cooperation with other actin binding proteins (Lopez et al., 1996; Allwood et al., 2002; Chen et al., 2003). ADFs in root hairs function to increase the turnover of actin filaments (Jiang et al., 1997; Dong et al., 2001). In Arabidopsis, 12 ADFs in four ancient subclasses exhibit distinct tissue-specific and developmental expression and have been proposed to have different functions (Ruzicka et al., 2007). The diverse expression patterns and functions of ADFs appear to co-evolve with the ancient and divergent actin isovariants.

Corresponding to the regulatory role of the actin cytoskeleton in plants against various environmental stimuli, plant ADFs have been shown to play an important role in response to biological invasion and abiotic stress. ADFs from Arabidopsis, barley and wheat were found to be related to plant resistance to various pathogens (Miklis et al., 2007; Tian et al., 2009; Fu et al., 2014). The ectopic expression of barley *HvADF3* effectively impedes actin cytoskeleton integrity, thereby enhancing the susceptibility of the *Mlo* genotype to barley powdery mildew and partially breaks down *mlo* resistance with an elevated incidence of fungal entry (Miklis et al., 2007). The Arabidopsis AtADF4 is potentially targeted by the bacterial effector protein AvrPphB under the control of the cognate resistance gene RPS5-mediated resistance to *Pseudomonas syringae* (Porter et al., 2012). *AtADF4* mediated both effector-triggered immunity (ETI) and PAMP-triggered immunity (PTI) signaling due to its activity in actin rearrangement modulation or translocation of the cytoskeleton into the nucleus through the nuclear localization signal (NLS), where these triggers function as gene expression regulators (Tian et al., 2009; Porter et al., 2012; Henty-Ridilla et al., 2014). In wheat, *TaADF7* contributes to resistance against *Puccinia striiformis* f. sp. *tritici* (*Pst*) by modulating the cytoskeleton dynamics to influence ROS accumulation and HR (Fu et al., 2014). During cold acclimation, another wheat ADF protein, TaADF, accumulated to higher levels in freeze-tolerant but not sensitive wheat cultivars (Ouellet et al., 2001). Ectopic overexpression of *OsADF3* conferred enhanced drought/osmotic stress tolerance on transgenic Arabidopsis by modulating several downstream abiotic stress-responsive target genes related to drought responses (Huang et al., 2012).

As one of the top 10 plant-pathogenic fungi, *Pst* causes destructive wheat stripe rust disease worldwide (Dean et al., 2012). In response to *Pst* infection, wheat shows race-specific resistance accompanied with hypersensitive response (HR), rapid cell death at neighboring mesophyll cells and infected sites. As *Pst* is an obligate biotrophic basidiomycete, which could not be cultured *in vitro*, the wheat-*Pst* interaction mechanism has been largely hindered. The expanded understanding of the profound regulation of ADF/cofilins and the multifaceted functions of these ADF/cofilins in physiological changes has led to the conclusion that ADF/cofilin proteins are a functional node in cell biology (Bernstein and Bamburg, 2010). Despite their multiple and essential roles, there is still limited evidence linking ADFs with host pathogen defense, especially in the wheat-*Pst* interaction phytosystem, except for *TaADF7* (Fu et al., 2014). Similar to the presence of 12 ADF genes in the entire rice and Arabidopsis genomes, the wheat genome also encodes a large ADF family consisting of multiple ADF genes. In this study, we isolated a novel ADF gene, *TaADF3*, that encodes a protein sharing only 57.55% similarity to TaADF7. To investigate the function of *TaADF3* in wheat, we analyzed its spatial and temporal expression patterns under various exogenous stresses. Furthermore, knockdown of *TaADF3* in wheat was performed to analyze whether and how *TaADF3* participates in wheat resistance to *Pst*. Our results demonstrated that *TaADF3* positively regulates wheat tolerance to drought and cold, possibly by participating in the abscisic acid (ABA) signaling pathway. Further silencing analyses revealed that *TaADF3* negatively regulated wheat resistance to *Pst,* most likely by hindering fungus entry in an reactive oxygen species (ROS)-dependent manner. These findings provide new insight into the role of ADFs in host immunity to biotrophic fungal pathogens.

MATERIALS AND METHODS

Plant and Fungal Material

Wheat (*Triticum aestivum* L.) genotype Suwon 11 and *Pst* pathotypes CYR23 and CYR31 were used for this study. Wheat cv. Suwon 11 contains the stripe rust resistance gene *YrSu* (Cao et al., 2002) and is resistant to CYR23 but highly susceptible to CYR31. Wheat seedlings were grown, inoculated and maintained as described by Kang and Li (1984). *Pst* pathotypes CYR23

and CYR31 were maintained on wheat cv. Mingxian 169 and Suwon 11, respectively. The fresh uredinospores of CYR23 and CYR31 were inoculated on the first leaves of wheat cv. Suwon 11 at the first leaf stage. Parallel mock control plants were inoculated with sterile water. After inoculation, plants were kept in a dark chamber with 100% humidity for 24 h and subsequently transferred to a growth chamber at 15°C with a 16 h photoperiod under fluorescent white light. Wheat leaves were sampled at 0, 12, 18, 24, 48, 72, and 120 h post-inoculation (hpi).

For chemical treatment, 2-week-old wheat seedlings were sprayed with 2 mM salicylic acid (SA), 100 mM methyl jasmonate (MeJA), 100 mM ethepon, and 100 mM abscisic acid (ABA) dissolved in 0.1% (v/v) ethanol. Mock control plants were treated with 0.1% ethanol. The first leaves that were treated with chemicals along with the control plants were sampled at 0, 0.5, 2, 6, 12, and 24 h post-treatment (hpt). For various abiotic stresses, the roots of wheat seedlings were soaked in 200 mM NaCl or 20% PEG6000 for high salinity or drought treatment. To cause wounding, the first wheat leaves of 2-week-old seedlings were scraped with a sterilized needle. Low-temperature treatment was performed by transferring the wheat seedlings to a 4°C chamber. The first leaves of the treated plants and mock control plants were collected at 0, 2, 6, 12, 24, and 48 hpt. Intact tissues of different wheat organs from 2-week-old seedlings were collected for tissue-specific expression analysis, except for glume, which was collected at the adult stage of wheat seedlings.

All the freshly collected samples were immediately frozen into liquid nitrogen and stored at −80°C prior to the extraction of total RNA or DNA. For each time point, three independent biological replications were performed.

RNA/DNA Isolation and qRT-PCR

Genomic DNA of wheat leaves was extracted using the DNeasy Plant Mini Kit (Qiagen). Total RNA from wheat leaves treated with chemicals, challenged by abiotic stresses and *Pst*, and different wheat tissues were extracted using the RNeasy Plant Mini Kit (Qiagen) and treated with DNase I to remove the contaminating DNA. First strand cDNA was synthesized from 2 μg of total RNA using the SuperScript First-strand Synthesis System (Invitrogen, Carlsbad, CA, USA). The expression of the *TaADF3* gene was controlled using the wheat elongation factor *TaEF-1α* gene (GenBank accession no. Q03033). Quantitative RT-PCR was performed on a 7500 Real-time PCR system (Applied Biosystems, Foster City, CA, USA), and the relative gene expression was quantified using the comparative $2^{-\Delta\Delta CT}$ method (Livak and Schmittgen, 2001). All reactions were performed in triplicate. The primers used for qRT-PCR are listed in **Table S1**.

Cloning of *TaADF3* and Sequence Analyses

Based on the EST sequence (TA54178_4565) in the TIGR Wheat Genome Database, a set of primers TaADF3-cDNA-F and TaADF3-cDNA-R were designed to amplify *TaADF3* from the cDNA of wheat leaves. The DNA sequence was obtained by genomic PCR using the total DNA of wheat leaves as the template. The physical characteristics of the deduced protein encoded by the obtained cDNA were computed using the Compute pI/MW Tool. Multiple sequence alignments and phylogenetic analysis were conducted using DNAMAN and MEGA (version 4.0) software, respectively. The phylogram was constructed using the neighbor-joining method, in which bootstrap support values were based on 1000 replicates.

Plasmid Construction

For subcellular localization in onion cells, the TaADF3 protein-encoding sequence was amplified and inserted into the *Hin*dIII and *Nco*I sites of the *pCaMV35S::GFP* vector to generate the *pCaMV35S::TaADF3-GFP* fusion vector.

The plasmids used for the silencing of *TaADF3* in the barley stripe mosaic virus (BSMV)—mediated virus-induced gene silencing (VIGS) experiment were constructed as described previously (Holzberg et al., 2002). A cDNA fragment derived from the coding sequence and the 3′ untranslated region (416–592) was inserted into the *Not*I and *Pac*I sites to replace the phytoene desaturase (PDS) gene fragment of γ:*PDS* and generate the recombinant γ:*TaADF3*. To guarantee the specificity of gene silencing, the cDNA sequence of *TaADF3* was aligned with the *T. aestivum* cv. Chinese Spring (CS) genome using the service provided by the International Wheat Genome Sequencing Consortium (http://wheat-urgi.versailles.inra.fr/Seq-Repository/BLAST). The fragments that showed the highest polymorphism within the gene family and the lowest sequence similarity to other genes were chosen for constructing γRNA-based derivative plasmids.

Subcellular Localization

The fusion *pCaMV35S::TaADF3-GFP* construct and the control plasmid *pCaMV35S::GFP* were transformed into onion epidermal cells by particle bombardment at a helium pressure of 1100 psi using the PDS-1000/He system (Bio-Rad, Hercules, CA, USA). The transformed onion epidermal cells were cultured on MS medium plates at 28°C for 18–24 h in a dark chamber. Fluorescent signals were observed using a Zeiss LSM 510 confocal laser microscope (Zeiss, Germany) with a 480-nm filter.

BSMV-Mediated Silencing of *TaADF3* in Wheat cv. Suwon 11

By *in vitro* transcription using a high-yield capped RNA transcription kit (mMESSAGE mMACHINE; Ambion), BSMV RNAs were prepared from linearized plasmids. For inoculation, the RNA transcripts were diluted four times, and 2.5 μL of each transcript, including the BSMV RNA α, β, and γ (γ-*TaPDS*, γ-*TaADF3*) transcripts, were mixed with 42.5 μL of FES buffer (Pogue et al., 1998). The mixture was inoculated into the second leaves of wheat seedlings at the two-leaf stage by gently rubbing the surface with a gloved finger (Scofield et al., 2005). BSMV: 00 and BSMV: *TaPDS* were used as controls for BSMV infection. Wheat seedlings inoculated with FES buffer were used as the mock controls. The virus-infected wheat seedlings were kept in a growth chamber at 25 ± 2°C under a 16 h photoperiod. Ten days post BSMV inoculation, the fourth leaves were further inoculated with fresh uredinospores of *Pst* pathotype CYR23 or CYR31, and the plants were subsequently maintained as described above. Three independent sets of plants were prepared for each assay.

The disease phenotype of the fourth leaves was observed and photographed 14 days post-inoculation of *Pst*.

Expression Level of *TaADF3* and Pathogenesis Related Genes in *TaADF3*-Knockdown Plants

The fourth leaves inoculated with BSMV:00 or BSMV:*TaADF3* were collected at 0, 24, 48, and 120 h post-inoculation (hpi) with CYR23 or CYR31, as well as the mock control plants. The relative expression of *TaADF3* was analyzed by qRT-PCR in each assay to assess the silencing efficiency compared to the control plants. The relative transcription levels of pathogenesis-related protein (PR) genes *TaPR1* (AAK60565), *TaPR2* (DQ090946), and *TaPR5* (FG618781) in the *TaADF3*-silenced leaves were confirmed by qRT-PCR.

Histological Observation of Host Defense and Fungal Growth in *TaADF3*-Knockdown Plants

The defense response and fungal growth in *TaADF3*-knockdown plants were observed microscopically. For histological observation, leaf segments (1.5 cm in length) were fixed and decolorized in ethanol/ acetic acid (1:1 v/v). The specimens were cleared in saturated chloral hydrate until leaf tissue became translucent. The autofluorescence of the attacked mesophyll cells was observed under a fluorescence microscope (excitation filter 485 nm, dichromic mirror 510 nm, barrier filter 520 nm) and measured using DP-BSW software to determine the necrotic cell area. The H_2O_2 that accumulated in the infection sites was stained using 3,3′-diaminobenzidine (DAB; Amresco, Solon, OH, USA; Wang et al., 2007), viewed under differential interference contrast optics and measured using DP-BSW software. The infection structure of stripe rust fungus was stained by wheat germ agglutinin (WGA) conjugated to Alexa 488 (Invitrogen, Carlsbad, CA, USA), as previously described (Ayliffe et al., 2011). Leaf segements were autoclaved in 1 M KOH and 0.05% Silwet L-77 (Hood and Shew, 1996). After washing in 50 mM Tris (pH 7.5) twice, leaf tissue was stained with WGA-alexa (20 μg/ml) for 15 min. Then the tissues were rinsed with 50 mM Tris (pH 7.5) and mounted in 50 mM Tris (pH 7.5) to be examined under blue light excitation. The hyphal length, haustoria, and infection area were observed and calculated using DP-BSW software. Only infection sites where substomatal vesicles had formed underneath stomata were considered to be successful penetration and were microscopically evaluated the infection hyphae, haustoria, and infection area. Penetration success was calculated as the number of infection sites that exhibited one or multiple haustoria in relation to the total number of infection sites. Standard deviations and Student's *t*-test were applied for statistical analysis.

Fungal Biomass Analyses in *TaADF3*-Knockdown Plants

Absolute quantification of the wheat stripe rust fungus in infected wheat leaves was analyzed by qRT-PCR. First-strand cDNA was synthesized using 2 μg of total RNA from *Pst* CYR31 uredinospores or *Pst*-infected leaves pre-inoculated with BSMV:00 or BSMV:*TaADF3*. The cDNA of uredinospores of *Pst* CYR31 diluted in a gradient was used to generate the standard

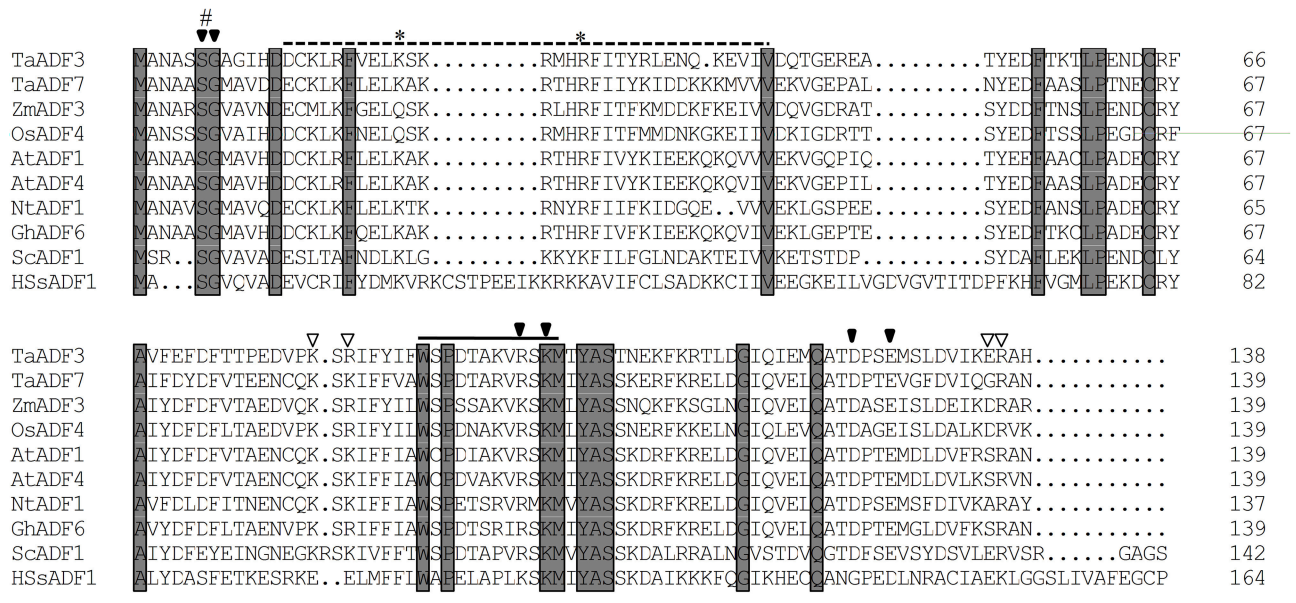

FIGURE 1 | Multiple alignment of TaADF3 against ADF/cofilins from other species. Each ADF/cofilin contains preserved phosphorylation sites on serine (#) and a nucleus localization signal (*). The solid arrow and open arrow indicate the binding site of G-actin and F-actin, respectively. The dotted line represents the CAM combining region and the solid line indicates the PIP2/actin-binding domain. Ta, *Triticum aestivum*; Os, *Oryza sativa*; Zm, *Zea mays*; At, *Arabidopsis thaliana*; Nt, *Nicotiana tomentosiformis*; Gh, *Gossypium hirsutum*; Sc, *Saccharomyces cerevisiae*; Hs, *Homo sapiens*.

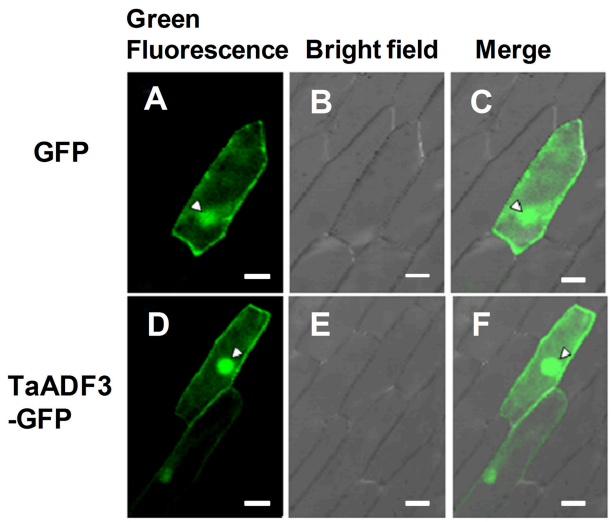

FIGURE 2 | Subcellular localization of TaADF3 in onion cells. Green fluorescent protein (GFP) **(A–C)** or TaADF3-GFP fusion protein **(D–F)** was transiently expressed in onion epidermal cells under the control of the cauliflower mosaic virus (CaMV) 35S promoter by particle bombardment. The green fluorescence was observed under a confocal microscope and imaged using a 488-laser excitation light source **(A,D)**. The corresponding cell morphology photos were taken under bright field **(B,E)**. Bar, 50 μm.

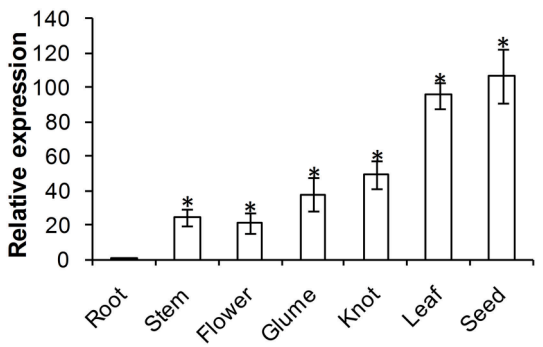

FIGURE 3 | Expression patterns of *TaADF3* in different wheat tissues. Samples were collected from root, stem, flower, glume, knot, leaf, and seed. The relative expression level was analyzed by qRT-PCR and normalized to the wheat elongation factor *TaEF-1α* gene. Three independent biological replications were performed. Asterisks indicate a significant difference ($P < 0.05$) from the root using Student's *t*-test.

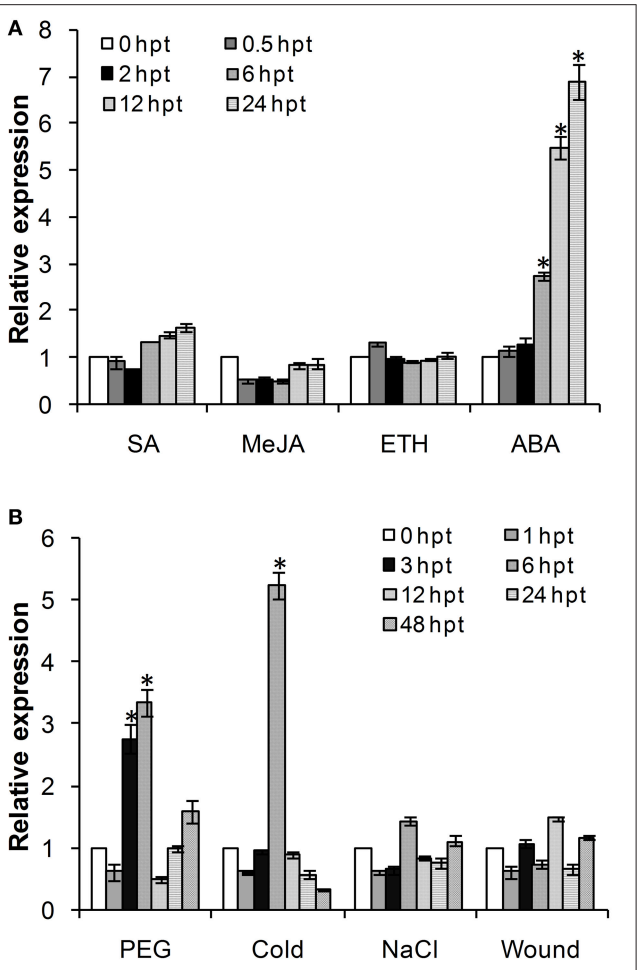

FIGURE 4 | Expression profile of *TaADF3* in response to exogenous hormones (A) and abiotic stresses (B). Three independent biological replications were performed. The expression levels were normalized to *TaEF-1α*, and the results are shown as the mean ± standard deviation of three biological replications. Asterisks indicate a significant difference ($P < 0.05$) from 0 hpt using Student's *t*-test. SA, salicylic acid; MeJA, methyl jasmonate; ETH, ethylene; ABA, abscisic acid.

curve. The cDNA of the *Pst* infected leaves of BSMV:00- or BSMV:*TaADF3*-inoculated plants at 24, 48, and 120 hpi were adjusted to 300 ng/μL. For the quantification of wheat stripe rust fungus, the constitutively expressed wheat stripe rust elongation factor gene *Pst-EF* was used (Yin et al., 2011). The standard curve was used to perform the absolute quantification of *Pst* in planta.

Actin Filament Staining

Actin microfilaments were stained as described previously (Kobayashi et al., 1997b) with slight modifications (Opalski et al., 2005). Ten days post-virus inoculation, the fourth leaves of the virus-infected plants were collected. The leaf segments (5 × 5 mm in size) were fixed in 3.7% formaldehyde in 25 mM piperazine-N,N′-bis (2-ethanesulfonic acid) buffer (PIPES, pH 6.8), with 2 mM EGTA, 2 mM $MgCl_2$, and 0.05% Tween 20 (v/v) at room temperature for 1 h. After washing in 25 mM PIPES and 25 mM phosphate buffer (PBS, pH 6.8), leaf segments were treated with 0.5% Triton X-100 in 25 mM PBS (pH 6.8) at room temperature for 1 h. The specimens were washed with 25 mM PBS (pH 6.8), then with 25 mM PBS (pH 7.4) for three times. Then leaf segments were stained with Alexa-Fluor 488 phalloidin (0.66 μM in 25 mM PBS, pH 7.4). Vacuum infiltration was performed three times for 20 s at 27 mm Hg to promote uptake of the dye. Subsequently, samples were stored at room temperature for 3 h in darkness. Finally, leaves were rinsed with 25 mM PBS (pH 7.4), mounted in 25 mM PBS (pH 7.4) on glass slides and observed by fluorescence microscopy. Three biological replications were performed and approximately five leaf segments were observed for each repliation.

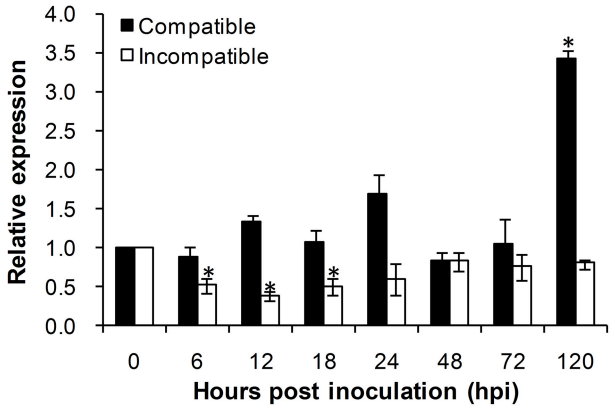

FIGURE 5 | Transcript profile of *TaADF3* in wheat leaves inoculated with virulent and avirulent *Pst* races. In compatible interaction, wheat cultivar Suwon 11 was inoculated with virulent *Pst* CYR31, and in incompatible interaction, wheat Suwon 11 was challenged by avirulent *Pst* CYR23. The data were normalized to wheat *TaEF-1α* gene, and the results were obtained from three independent replicates. Vertical bars represent the standard deviation. Asterisks indicate a significant difference ($P < 0.05$) from 0 hpt using Student's *t*-test.

Statistical Analyses

Mean values and standard errors were calculated with Microsoft Excel software. Statistical significance was assessed by one-tailed Student's *t*-test with unequal variance and between control and treatment.

RESULTS

TaADF3 Encodes an Actin Depolymerizing Factor

Based on the EST sequence (TA54178_4565) in the wheat TIGR genome database, a cDNA fragment of 795 bp in length was obtained with an open reading frame (ORF) of 417 bp, which shows the highest similarity (97.83%) to the actin-depolymerizing factor 3 (GenBank no. AIZ95472.1) of *T. aestivum*. PCR amplification using the same primers obtained a genomic sequence of 1858 bp, consisting of three exons split by two introns with lengths of 972 bp and 91 bp. The first exon exclusively encodes the first start codon (methionine), typically found in ADF genes (**Figure S1**). BlastN analyses in the *T. aestivum* cv. Chinese spring (CS) genome sequence showed that there are three copies of this gene in the wheat genome, located on the long arms of chromosomes 5A, 5B, and 5D (**Figure S1**). The ADF gene obtained in this study and wheat actin-depolymerizing factor 3 in the NCBI Database exhibited the highest identity with the copies on chromosome 5BL and 5AL, respectively. The results indicate that these two genes are actually two homologous genes located on different chromosomes. Thus, here, we designated the ADF gene as *TaADF3*. The two copies of *TaADF3* on 5AL and 5DL encode the same protein, showing one residue variation from 5BL (**Figure S2**), although there were variations at 18 nucleotide positions in the open reading frames of the three copies (**Figure S3**).

The deduced TaADF3 protein encoded 138 amino acid residues with a molecular weight of 16.10 kDa and an isoelectric point (PI) of 5.65. Multi-alignment of TaADF3 and ADFs from other higher plants revealed a preserved Ser6 in plant ADFs (Ser3 in animal) that could be phosphorylated. TaADF3 contained a bipartite NLS—Lys22 and Arg28 close to the amino terminus; Ser6, Gly7, Arg97, Lys99, Asp124, and Glu127 could bind to actin monomers (G-actin); Lys81, Arg83, Glu135, and Arg136 could specifically bind to microfilaments (F-actin). A CAM combining region (Asp13—Val42) and a PIP2 (phospholipid phosphatidylinositol -4, 5-bisphosphate) binding domain (Trp89—Met100) were also included in the sequence (**Figure 1**). The results indicate the conservation of ADF proteins across different higher plant species.

Based on the spatial and temporal expression pattern, the ADF proteins in higher plants were categorized into four groups. As shown in **Figure S4**, the majority of Group I ADF members are from dicotyledon plants, except for the ADF7 proteins from wheat, barley and *Brachypodium distachyon*. Group II contains pollen-specific ADFs, which can then be sub-grouped into the monocot group and the dicot group. Group III includes ADFs from both monocotyledons and dicotyledons. In contrast to the other groups, Group IV, to date, exclusively contains monocot ADFs and is most closely related to animal ADF/cofilins (**Figure S4**). Phylogenetic analyses showed that TaADF3 was homologous to rice OsADF4 and corn ZmADF3, with 67.63 and 62.59% similarity, respectively. In the phylogram, all of them belong to Group IV of the ADF/cofilin family.

TaADF3 is Localized in Both Cytoplasm and Nucleus

To determine the subcellular localization of TaADF3, the fusion construct pCaMV35S::TaADF3-GFP was transiently expressed in onion epidermal cells by particle bombardment. Laser-scanning confocal micrographs showed the green fluorescence of fusion TaADF3-GFP protein in both cytoplasm and nucleus, the same as the distribution of GFP alone (**Figure 2**).

Tissue-Specific Expression of *TaADF3*

ADF protein in higher plants is reported to show tissue specific expression patterns. To examine the physiological role of *TaADF3*, the transcript of *TaADF3* in different wheat tissues was examined by qRT-PCR. The result showed that *TaADF3* was detectable in all tested wheat tissues, with the lowest level in the root. The *TaADF3* transcript is most abundant in wheat leaf and the developing seed by ∼95 and 106 times the amount in the root. *TaADF3* transcript is also highly abundant in wheat stem, flower, glume and knot, although less than in leaf and seed (**Figure 3**).

TaADF3 is Upregulated in Response to Abiotic Stresses

Considering the involvement of ADFs in the response to various abiotic stresses, we investigated the effects of exogenous hormone chemicals and abiotic stresses on the expression of *TaADF3*.

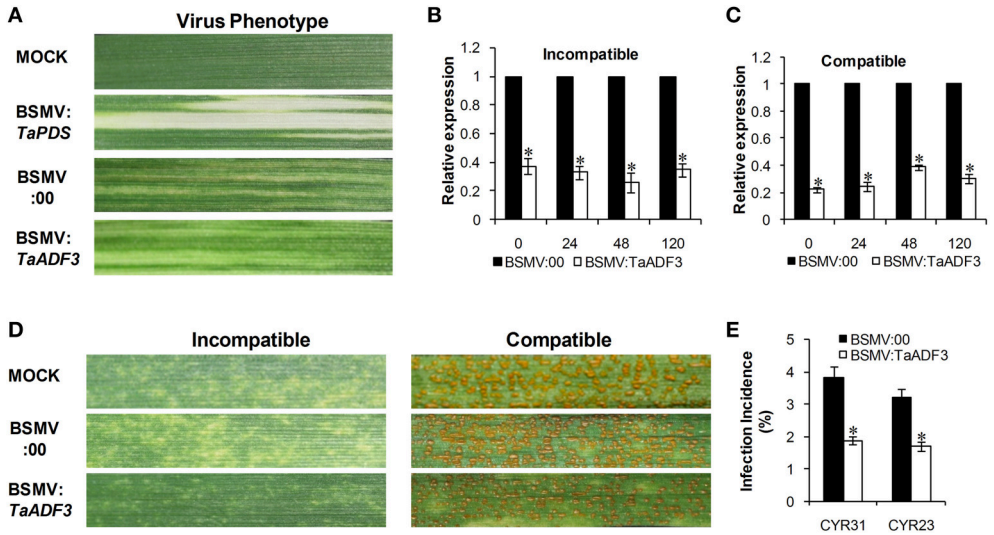

FIGURE 6 | Functional characterization of *TaADF3* during interaction of wheat and *Pst* by BSMV-mediated gene silencing. (A) Photobleaching was evident on the fourth leaves of wheat plants inoculated with BSMV:*TaPDS*. Mild chlorotic virus symptoms were observed on the fourth leaves of wheat seedlings inoculated with BSMV:00 or BSMV:*TaADF3*. MOCK: wheat leaves inoculated with FES buffer. Silencing efficiency of *TaADF3* in the fourth leaves of *TaADF3*-knockdown plants in incompatible **(B)** or compatible **(C)** interaction. Wheat leaves inoculated with BSMV:00 and further challenged by stripe rust fungus were used as the controls. The data were normalized to the *TaEF-1*α gene. **(D)** Disease phenotypes of the fourth leaves further challenged by avirulent CYR23 or virulent CYR31. Photos were taken 14 days post pathogen inoculation. **(E)** Silencing of *TaADF3* attenuated infection of the virulent *Pst* CYR31 and the avirulent *Pst* CYR23. Only infection sites where substomatal vesicle formed were considered as successful penetration. The number of successful infection sites per 100 stoma was calculated. Three independent biological replications were performed, and 20 sets of infection incidence were measured for each biological replication. Asterisks indicate a significant difference ($P < 0.05$) from BSMV:00 using Student's *t*-test.

As shown in **Figure 4A**, *TaADF3* was mainly induced by ABA treatment but showed no significant response to the other treatments. In ABA treatment, the expression of *TaADF3* was continuously increased after 6 hpt (hour post-treatment) and peaked at 24 hpt with approximate 7-fold expression. These results suggested that *TaADF3* may be related to the ABA-dependent signaling pathway.

The transcriptional levels of *TaADF3* were also induced by some abiotic elicitors (**Figure 4B**). PEG6000 treatment and low temperature (4°C) could significantly upregulate the expression of *TaADF3*. Both treatments reached the peak at 6 hpt with approximately 3-fold and 5-fold increases, respectively. Compared with cold treatment, *TaADF3* was induced earlier under PEG6000 treatment. In contrast, under wounding and high salinity treatments, the expression of *TaADF3* did not exhibit any significant changes.

TaADF3 is Induced Upon Virulent *Pst* Attack

To investigate the role of *TaADF3* in plant-pathogen interactions, the transcriptional profile of *TaADF3* was determined in Suwon 11 wheat leaves inoculated with *Pst* pathotypes CYR31 and CYR23 for compatible and incompatible interactions, respectively. During wheat-*Pst* interaction, the transcript level of *TaADF3* was induced at 120 hpi in wheat leaves challenged by the virulent *Pst* pathotype CYR31, reaching a level 2.4-fold higher than that in the control plants (**Figure 5**). In wheat leaves challenged by the avirulent *Pst* pathotype CYR23, *TaADF3* was repressed as soon as the plants were infected by CYR23 (6 hpi) and had the lowest expression level (∼0.4-fold) at 12 hpi. The significant difference between compatible and incompatible interactions (particularly at 12, 18, and 120 hpi) suggested that *TaADF3* may be a negative regulator in wheat defense against stripe rust fungus.

Silencing of *TaADF3* Enhances Wheat Resistance to *Pst*

To further characterize the function of *TaADF3* in the wheat defense response to stripe rust fungus, BSMV-mediated VIGS was used to silence the expression of *TaADF3*. Ten days after BSMV inoculation, mild chlorotic mosaic symptoms appeared on the fourth leaves of infected wheat seedlings, and the BSMV:*TaPDS* inoculated plants exhibited strong photobleaching (**Figure 6A**). Fourteen days post pathogen infection, the disease phenotype was observed.

Silencing efficiency assessment by qRT-PCR showed that the expression level of *TaADF3* was greatly reduced to different extents in *TaADF3*-knockdown plants compared with the control plants, with an approximate reduction as high as 80% (**Figures 6B,C**). The fragment used for silencing is shown in **Figure S1**. Due to the high identity among the three copies, the three copies should be silenced simultaneously.

With the significantly repressed *TaADF3* expression, less necrosis was observed on wheat leaves from *TaADF3*-knockdown plants inoculated with *Pst* race CYR23, in contrast to the high necrosis observed in control plants (**Figure 6D**). When

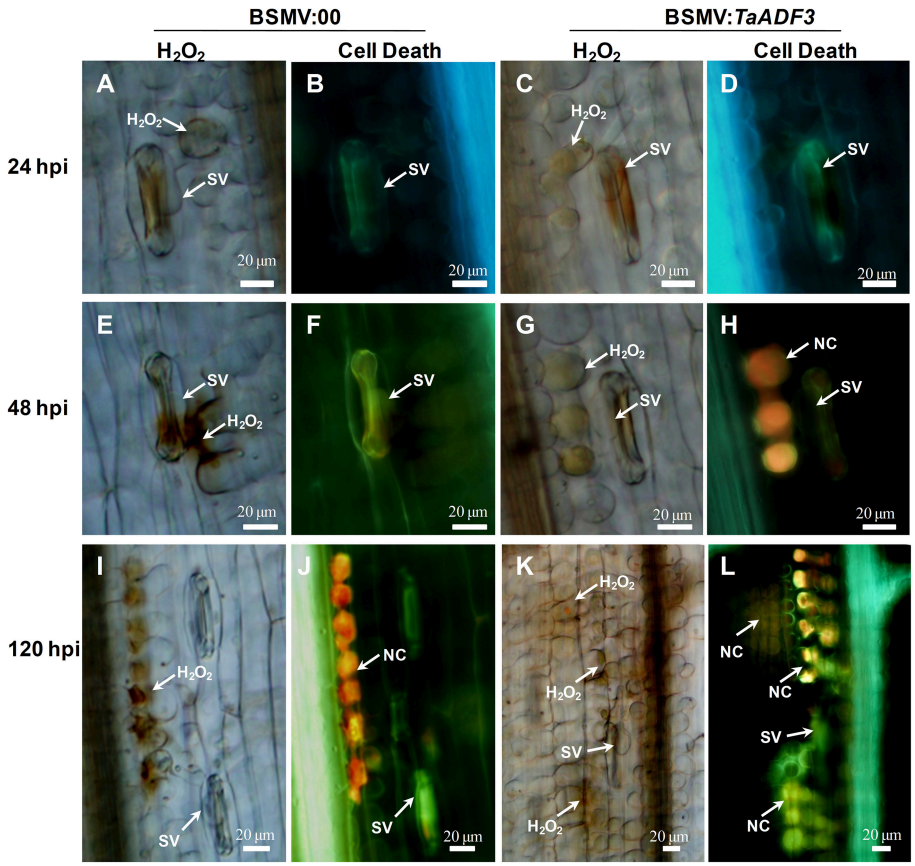

FIGURE 7 | Histological observation of the defense response in *TaADF3*-knockdown plants against the virulent *Pst* CYR31. Wheat leaves that were pre-infected with BSMV:00 or recombinant BSMV:*TaADF3* were followed by *Pst* CYR31 inoculation. H_2O_2 burst and necrosis were observed in wheat leaves inoculated with BSMV:00 or BSMV:*TaADF3* at 24 hpi **(A–D)**, 48 hpi **(E–H),** and 120 hpi **(I–L)**. Histochemical H_2O_2 accumulation at infection sites was stained using 3,3′-diaminobenzidine (DAB) staining and viewed under differential interference contrast optics. The autofluorescence of the attacked mesophyll cells at the same infection site was observed under a fluorescence microscope (excitation filter 485 nm, dichromic mirror 510 nm, barrier filter 520 nm). SV, substomatal vesicle; NC, necrotic cell death.

challenged by *Pst* race CYR31, leaves from the wild-type plants and BSMV:00-infected plants exhibited a fully susceptible phenotype. Leaves of the *TaADF3*-knockdown plants also exhibited a susceptible phenotype, but obvious necrotic cell death was observed, accompanied by reduced sporulation (**Figure 6D**).

The incidence of sites with substomatal vesicle formation underneath stoma was assessed in *TaADF3*-knockdown plants at 24 hpi. As shown in **Figure 6E**, in compatible interaction, the successful infection incidence of *Pst* CYR31 in *TaADF3*-knockdown plants was 1.89%, which was significantly lower than that in the control plants (3.83%). In incompatible interaction, the infection incidence of *Pst* CYR23 was also reduced by 1.51% compared to the controls (**Figure 6E**).

Elevated Defense Response in *TaADF3*-Knockdown Plants

Based on the observed enhanced resistance phenotype, the host response was further analyzed. We measured the H_2O_2 accumulation and necrotic cell death areas per infection site at 24, 48, and 120 hpi. In compatible interaction, H_2O_2 accumulation mainly occurred in the guard cells in the early stage, and the H_2O_2 amount in *TaADF3*-knockdown plants was not affected (**Figures 7**, **8A**). At 24 and 48 hpi, H_2O_2 seldom occurred in mesophyll cells in mock control plants, which was also the case in *TaADF3*-knockdown plants at 24 hpi (**Figure 7**). However, at 48 hpi, 8.51% of the infection sites exhibited H_2O_2 production in attacked mesophyll cells when *TaADF3* was silenced, which was significantly higher than that in control plants (**Figure S5A**). Much more abundant H_2O_2 was accumulated in the attacked mesophyll cells (**Figures 7**, **8B**). Along with the increased H_2O_2 at 48 hpi, the occurrence of necrosis and the corresponding necrosis area were significantly elevated (**Figure 8C** and **Figure S5B**). At 120 hpi, in control plants, obvious accumulation was already observed, but significantly increased H_2O_2 was accumulated in *TaADF3*-knockdown plants (**Figures 7**, **8C**). The necrotic cell death observed by auto-fluorescence exhibited a similar increased pattern to the H_2O_2 accumulation (**Figures 7**, **8C**).

In incompatible interaction, the H_2O_2 accumulation in guard cells was also not affected (**Figure S6A**), but the

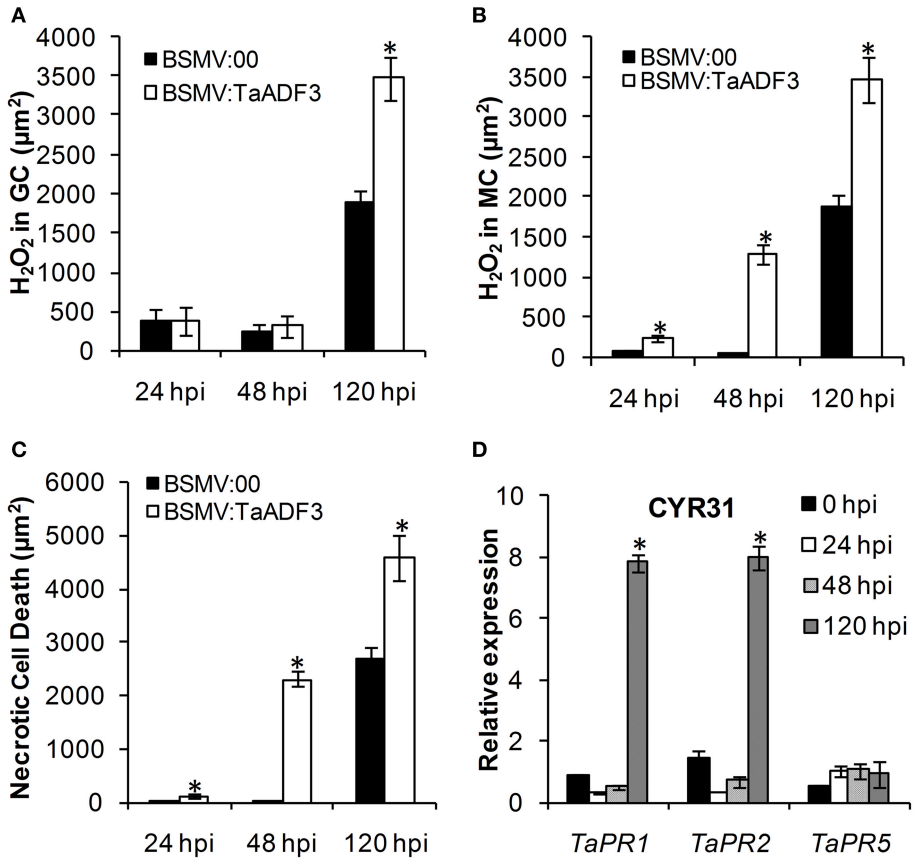

FIGURE 8 | Enhanced wheat defense response in *TaADF3*-knockdown plants attacked by virulent *Pst* CYR31. The amount of H_2O_2 production was measured by calculating the DAB staining area at each infection site using the DP-BSW software **(A,B)**. The area of autofluorescence was measured to determine the necrotic cell death **(C)**. H_2O_2 produced in the guard cells (GC) and the attacked mesophyll cells (MC) was calculated. All results were obtained from 50 infection sites. **(D)** The expression profiles of three pathogenesis-related proteins were assessed in *TaADF3*-knockdown plants compared with the mock control plants. The data were normalized to the wheat *TaEF-1α* gene. Three independent biological replications were performed. Asterisks indicate a significant difference ($P < 0.05$) from BSMV:00 using Student's *t*-test.

H_2O_2 accumulation in attacked mesophyll cells was decreased in *TaADF3*-knockdown plants, as was the necrosis area (**Figures S6B,C**). Lower occurrence of H_2O_2 production and cell death in mesophyll cells was observed in *TaADF3*-knockdown plants compared to the controls (**Figures S5C,D**). The reductions in observed cell death occurrence and area appear to correlate with the smaller observed necrosis.

Aside from the altered ROS accumulation and cell death, qRT-PCR analyses showed that *TaPR1* and *TaPR2* were sharply induced at 120 hpi in *TaADF3*-knockdwon plants attacked by either virulent CYR31 or avirulent CYR23 (**Figure 8D** and **Figure S6D**). In contrast to this dramatic induction, *TaPR5* was slightly induced only in the interaction with CYR23 (**Figure 8D** and **Figure S6D**). Taken together, all results suggested that the silencing of *TaADF3* enhanced the wheat defense response to *Pst*.

Fungal Entry and Haustoria Formation are Impeded in *TaADF3*-Knockdown Plants

To test whether the enhanced resistance of wheat affected the survival of wheat stripe rust fungus, the growth and development of *Pst* were assessed through histological observation. As shown in **Figure 9**, in compatible interaction, the silencing of *TaADF3* greatly decreased the number of haustoria at 48 hpi (**Figures 9A–D,G**). Hyphal growth and infection area were not significantly affected at 24 and 48 hpi (**Figures 9H,I**). By 120 hpi, when haustoria formed in great numbers, the infected area of *Pst* was significantly smaller than in the controls (**Figure 9I**). Absolute quantification revealed less fungus in planta throughout the examined infection stages when *TaADF3* was silenced (**Figure 9J**).

In incompatible interaction, the knockdown of *TaADF3* caused decreased haustoria formation numbers at 48 hpi (**Figure S7A**), and the hyphal length and infection area were not affected at all (**Figures S7B,C**). The qRT-PCR analyses revealed a slight decrease in the fungal amount in infected *TaADF3*-knockdown plants (**Figure S7D**).

Furthermore, in compatible interaction, the fungal entry of *Pst* CYR31 in *TaADF3*-knockdown plants was reduced by 12.4% at 48 hpi and unchanged at 24 hpi (**Figure 10A**). In incompatible interaction, the successful entry of *Pst* CYR23

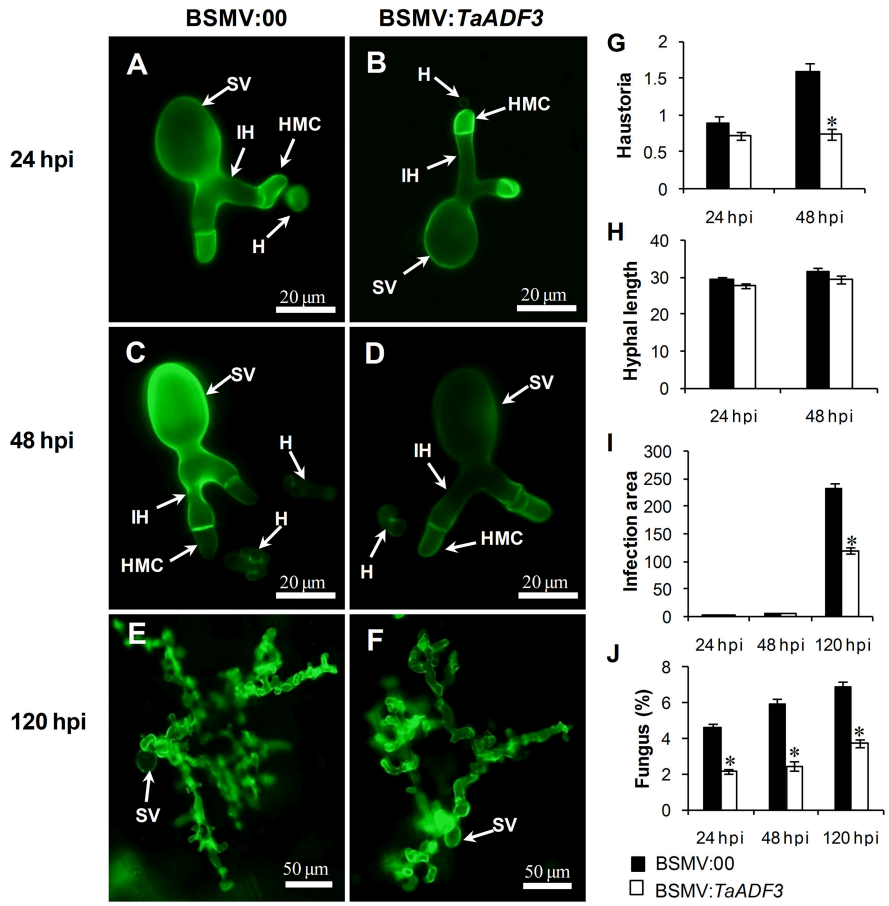

FIGURE 9 | Histological observation of fungal growth in *TaADF3*-knockdown plants challenged by virulent *Pst* CYR31. The fungal structure was stained with wheat germ agglutinin (WGA). The fungal growth of *Pst* pathotype CYR31 in wheat leaves inoculated with BSMV:00 or BSMV:*TaADF3* at 24 hpi **(A,B)**, 48 hpi **(C,D),** and 120 hpi **(E,F)** was observed under a fluorescence microscope. The average number of haustoria **(G)** of *Pst* in each infection site were counted. **(H)** Hyphal length, which is the average distance from the junction of the substomatal vesicle and the hypha to the tip of the hypha, was measured using DP-BSW software (unit in μm). **(I)** Infection area, the average area of the expanding hypha, was calculated using DP-BSW software (units of 10^3 μm^2). All results were obtained from 50 infection sites, and three biological replications were performed. **(J)** Quantification of fungus in *Pst* infected wheat leaves. The ratio of *Pst* CYR31 mRNA to total wheat mRNA was evaluated by qRT-PCR. Asterisks indicate a significant difference ($P < 0.05$) from BSMV:00-inoculated plants using a one-tailed Student's *t*-test. SV, substomatal vesicle; HMC, haustorial mother cell; IH, infection hypha; H, haustorium.

was reduced by 12.5 and 21.9% at 24 and 48 hpi, respectively (**Figure 10B**).

Actin Architecture Rearrangement in *TaADF3*-Knockdown Plants

To examine whether silencing of *TaADF3* affects the actin cytoskeleton in wheat cells, 10 days post-virus inoculation, the fourth leaves were sampled for Alexa-Fluor 488 phalloidin staining. Alexa-Fluor-stained actin filaments were observed in wheat epidermal cells (**Figures 11A,B**) and mesophyll cells (**Figures 11C,D**). In epidermal cells, the actin filaments were observed in two different array patterns, as thin filamentous structures arranged almost longitudinally or obliquely to the longitudinal axes of the cells (**Figure 11A**), or formed parallel arrays arranged obliquely or transversely to the longitudinal axis of the cells (**Figure 11B**). In BSMV:00 infected cells, the actin filamentous in 78.4% of the observed epidermal cells was arranged in the longitudinal array, only 21.6% in transversal array (**Figure 11E**). In contrast, the transversely arranged actin filaments were observed in ∼39.8% of the *TaADF3*-knockdown cells (**Figure 11E**), almost one-fold higher than that in control cells. Besides, the actin filaments appear to be more abundant in transversal array. In mesophyll cells, staining of actin filaments revealed an intact actin filament network in control cells (**Figure 11C**). Similarly, integrate caged actin architecture in *TaADF3*-knockdown plants was observed (**Figure 11D**).

DISCUSSION

ADFs are among the most highly expressed actin binding proteins that regulate actin dynamics. The four classified groups of ADFs in higher plants implies the functional divergence in the ADF family (Mun et al., 2002). The specific existence of Group

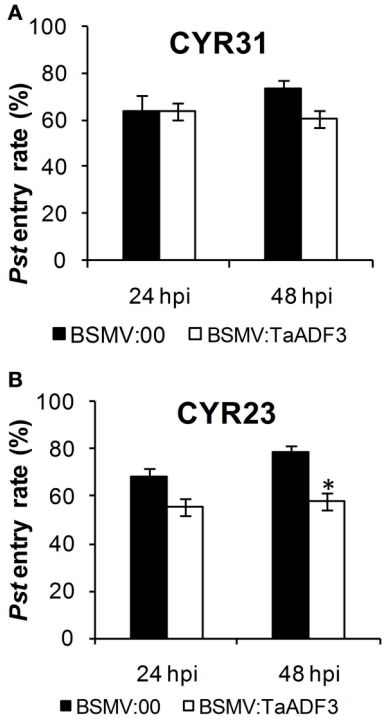

FIGURE 10 | Knockdown of the expression of *TaADF3* compromised fungus entry. Successful fungus entry was assessed in *TaADF3*-knockdown plants, which were subsequently infected with virulent *Pst* CYR31 **(A)** or avirulent *Pst* CYR31 **(B)**. Only infection sites where substomatal vesicles had formed over stomata were considered successful penetration and were microscopically observed for the presence or absence of haustoria. Entry success was calculated as the number of penetration sites that exhibited one or multiple haustoria in relation to the total number of infection sites. The data shown represent the mean ±SD from at least three experiments in which, as a minimum, 50 successful penetration sites each were evaluated. Asterisks beside columns indicate $P < 0.05$ (Student's *t*-test) compared with the negative control (BSMV:00).

IV ADF members in monocot plants may suggest their distinct roles (Maciver and Hussey, 2002). In this study, we isolated a wheat ADF gene, *TaADF3*, belonging to Group IV. The induced expression of *TaADF3* under PEG6000 treatment and low temperature indicated the involvement of *TaADF3* in enhancing plant acclimation to abiotic stresses. It has been reported that a wheat ADF member (TaADF) contributes to wheat cold acclimation regulated by genes located on chromosome 5A that are associated with cold hardiness (Ouellet et al., 2001). In addition, TaADF functions as a substrate for a wheat kinase, the activity of which is modulated by low temperature (Lopez et al., 1996). It is possible that *TaADF3* contributes to cold tolerance by interacting with other proteins to modulate cell cytoskeleton dynamics.

Plants perceive and respond adaptively to abiotic stress imposed by salt, cold, drought, and wounding, and the adaptive process is controlled mainly by the phytohormone ABA, which acts as an endogenous messenger in the regulation of plant water status (Swamy and Smith, 1999; Tuteja, 2007). The induction of *TaADF3* upon exogenous ABA application suggested that *TaADF3* may function as the downstream component in the ABA signaling pathway to elevate plant tolerance to abiotic stresses. ABA treatment is believed to result in stomatal closure through the disassembly of actin filaments (Eun and Lee, 1997). Thus, it can be assumed that *TaADF3* may participate in the ABA signaling pathway under abiotic stresses through regulating the actin dynamics in wheat stomatal movement. The ABA-dependent stomatal closure is also likely to function as a pre-invasive defense barrier against pathogens. Despite of the positive role of ABA in pre-invasive defense, its role in post-invasive defense seems to be mostly negative (Ton et al., 2009). Taking into account of the induced expression pattern of *TaADF3* under virulent *Pst*, it is reasonable that *TaADF3* is engaged in the negative regulation of post-invasive defense against *Pst* mediated by ABA, rather than contribute to the early pre-invasive defense.

ADFs have been implicated to play an important role in determining plant resistance against pathogenic microbes (Hardham et al., 2007). *HvADF3* was demonstrated to mediate race-specific immune responses in barley to an appropriate powdery mildew pathogen (Miklis et al., 2007). In the wheat-*Pst* interaction pathosystem, *TaADF7* was demonstrated to positively contribute to wheat resistance to *Pst* (Fu et al., 2014). In contrast to *TaADF7*, *TaADF3* function as a negative regulator in wheat resistance to *Pst*. Silencing of *TaADF3* enhanced race-specific immunity to *Pst* in *TaADF3*-knockdown plants. In response to the virulent *Pst* CYR31, *TaADF3*-knockdown plants was less susceptible with increased HR cell death, ROS accumulation and less sporulation. Previous histological and cytological observations revealed the oxidative bursts in the early (12–24 h) and late (96–120 h) infection stages of *Pst* (Wang et al., 2007). The induced *TaADF3* expression at 120 hpi in compatible interaction may be responsible for the suppression of ROS production. Thus, silencing of *TaADF3* led to increased ROS accumulation in *TaADF3*-kncokdown plants. It seemed that *TaADF3* negatively regulated wheat resistance in an ROS-dependent manner. Nevertheless, upon avirulent *Pst* infection, *TaADF3*-kncokdown plants retained complete resistance, but with less HR and ROS, which is closer to the immune response. The Arabidopsis *AtADF1-4* RNAi lines exhibited suppressed HR mediated by AvrPphB but retained the disease resistance phenotype (Tian et al., 2009). It appeared that HR can be uncoupled from resistance and that HR is not always for gene-for gene resistance. However, it is still possible that *TaADF3* may function in a dose-dependent manner to amplify defense signals. According to the hypothesis described by Jones and Dangl (2006), effective resistance or HR is achieved only when the amplitude of the defense signal reaches a certain threshold. We infer that the residual transcript of *TaADF3* was sufficient to sustain disease resistance but insufficient to attain the threshold for eliciting strong HR, as observed for *AtADF4* (Tian et al., 2009).

It has been documented that the actin cytoskeleton plays a crucial role in resistance during early stages of fungal penetration (Hardham et al., 2007; Miklis et al., 2007). The ectopic expression of *HvADF3* in barley leaf epidermal cells confers enhanced fungal entry of the powdery mildew fungus by interfering with the

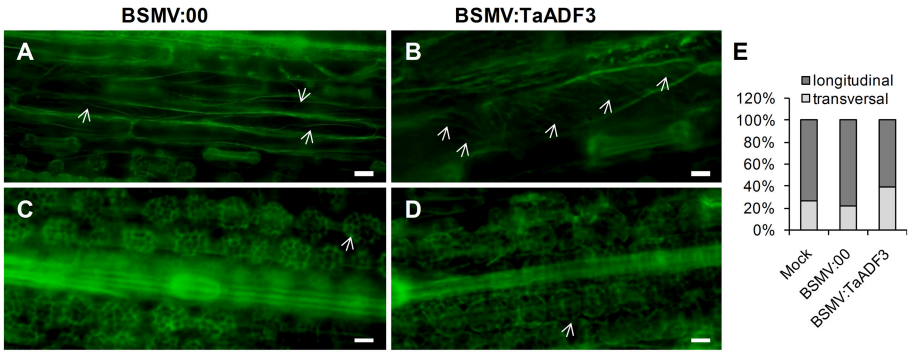

FIGURE 11 | Actin filament patterns in *TaADF3*-knockdown wheat cells. Ten days post-virus inoculation, the fourth leaves of BSMV:00 or BSMV:TaADF3 inoculated plants were collected and stained with Alexa-Fluor 488 phalloidin, and observed under fluorescence microscopy. The stained F-actin was observed in epidermal cells **(A,B)** and mesophyll cells **(C,D)**. In epidermal cells, the actin filaments were arranged almost longitudinally or obliquely to the longitudinal axes of the cells **(A)**, or formed parallel arrays arranged obliquely or transversely to the longitudinal axis of the cells **(B)**. In mesophyll cells, the actin architecture in *TaADF3*-knockdown plants **(D)** did not seem to change significantly compared to the control cells **(C)**. **(E)** The proportion of actin filaments arranged in longitudinal array and transversal array was calculated. The data were obtained from at least 100 epidermal cells of five leaf segments and three biological replications were performed. The arrows indicate the Alexa-Fluor -labeled F-actin. Bar = 20 μm.

integrity of the plant actin cytoskeleton (Miklis et al., 2007). In our study, silencing of *TaADF3* resulted in transformed array of the actin filaments, which presumably serve as tracks for deposition of callose, secretion of antimicrobial products and delivery of vectorial vesicle (Henty-Ridilla et al., 2014). Based on the finding that *Pst* germinates on the leaf surface and penetrate through the stoma, it is tempting to speculate that the altered actin architecture partially attenuated *Pst* infection. The observed decreased haustoria number may be partially attributed to the impeded fungal entry. As the unique infection structure of biotrophic pathogens in host cells, the haustorium makes intimate contact with the host cell membrane and allows nutrient uptake and effector release into host cells (Voegele and Mendgen, 2003). The resulting compromised haustoria formation of *Pst* in *TaADF3*-knockdown plants would lead to a repressed nutrient supply, further limiting the growth and expansion of *Pst*. Whether the hindered *Pst* entry was due to the role of *TaADF3* on actin architecture is still unclear, although it seems that no detectable change was observed in mesophyll cells actin filaments.

In conclusion, this study demonstrated that *TaADF3* can positively modulate plant acclimation to abiotic stresses, possibly as a downstream component of ABA signaling pathway. Moreover, it suggested that *TaADF3* functions as a negative regulator in wheat resistance to *Pst* dependent on interfering the actin architecture, via limiting ROS release and hindering pathogen penetration. Nevertheless, the exact functional mechanism of *TaADF3* still needs further exploration.

AUTHOR CONTRIBUTIONS

CT, LD, and ZK designed the experiment. CT, LD, DC and SC performed the experiments and analyzed the data. XW helped with data interpretation and article editing. CT wrote the manuscript.

ACKNOWLEDGMENTS

For critical reading of the manuscript we thank Prof. Brett M. Tyler from Oregon State University. This study was supported financially by the National Basic Research Program of China (Grant No. 2013CB127700), the National Natural Science Funds of China (Grant No. 31401693), the Key Grant Project of Chinese Ministry of Education (No. 313048), and China Postdoctoral Science Foundation (2015T81056 and 2014M550514).

SUPPLEMENTARY MATERIAL

The Supplementary Material for this article can be found online at: http://journal.frontiersin.org/article/10.3389/fpls.2015.01214

Table S1 | Oligonucleotides used for PCR and plasmid construction.

Figure S1 | Gene structure of *TaADF3*. TaADF3, the full-length cDNA sequence amplified from cDNA of wheat Suwon 11; TaADF3-Genome, the genomic DNA sequence amplified from the total genomic DNA of wheat Suwon 11. The genome sequences of the three copies of *TaADF3* on chromosomes 5AL, 5BL, and 5DL were obtained from the wheat UGRI genome database of the wheat cultivar Chinese Spring. The full genome sequence of *TaADF3* contains three exons and two introns. The start codon and stop codon are indicated by red boxes, and the two introns are indicated by blue boxes. The specific fragment used for silencing is indicated by a red line.

Figure S2 | Multi-alignment of the deduced protein of the three copies of *TaADF3*.

Figure S3 | Multi-alignment of the encoding sequence of the three copies of *TaADF3*.

Figure S4 | Phylogenetic analyses of *TaADF3* and ADF members in other species. Branches are labeled with protein names and GenBank accession numbers. Ta, *Triticum aestivum*; Bd, *Brachypodium distachyon*; Os, *Oryza sativa*; Zm, *Zea mays*; At, *Arabidopsis thaliana*; Nt, *Nicotiana tomentosiformis*; Gh, *Gossypium hirsutum*; Ph, *Petunia x hybrid*; Sc, *Saccharomyces cerevisiae*; Hs, *Homo sapiens*.

Figure S5 | Incidence of H_2O_2 production and cell death in *Pst* infected *TaADF3*-knockdown plants. The fourth leaves of wheat seedlings inoculated

with BSMV:00 or BSMV:*TaADF3* were further challenged by virulent or avirulent *Pst*. The H_2O_2 accumulation in attacked mesophyll cells in each infection site was observed under differential interference contrast optics through DAB staining. Necrotic cell death of the mesophyll cells at the same infection site was viewed under a flurorescence microscope. The number of infection sites with H_2O_2 accumulation and necrosis in attacked mesophyll cells among 50 infection sites was calculated. The incidence of H_2O_2 production and necrosis in mesophyll cells attacked by virulent Pst CYR31 **(A,B)** or avirulent Pst CYR23 **(C,D)** was measured. Three independent biological replications were performed. Asterisks indicate a significant difference ($P < 0.05$) from BSMV:00 using Student's *t*-test.

Figure S6 | Decreased H_2O_2 production and cell death in *TaADF3*-knockdown plant challenged by avirulent *Pst* CYR23. The amount of H_2O_2 production was measured by calculating the DAB staining area at each infection site using DP-BSW software **(A,B).** The area of autofluorescence was measured to determine the necrotic cell death **(C).** H_2O_2 produced in guard cells (GC) and the attacked mesophyll cells (MC). All results were obtained from 50 infection sites. **(D)** The expression profiles of three pathogenesis-related proteins were assessed in *TaADF3*-knockdown plants compared withmock control plants. The data were normalized to the wheat *TaEF-1*α gene. Three independent biological replications were performed. Asterisks indicate a significant difference ($P < 0.05$) from BSMV:00 using Student's *t*-test.

Figure S7 | Fungal growth in *TaADF3*-knockdown plant challenged by avirulent *Pst* CYR23. (A) Average numbers of haustoria of *Pst* CYR23 in each infection site were counted. **(B)** Hyphal length, which is the average distance from the junction of the substomatal vesicle and the hypha to the tip of the hypha, was measured using DP-BSW software (unit in μm). **(C)** Infection area, the average area of the expanding hypha, was calculated using DP-BSW software (units of 10^3 μm^2). All results were obtained from 50 infection sites, and three biological replications were performed. **(D)** Quantification of fungus in *Pst*-infected wheat leaves. The ratio of *Pst* CYR23 mRNA to total wheat mRNA was evaluated by qRT-PCR. Asterisks indicate a significant difference ($P<0.05$) from BSMV:00-inoculated plants using a one-tailed Student's *t*-test.

REFERENCES

Allwood, E. G., Anthony, R. G., Smertenko, A. P., Reichelt, S., Drobak, B. K., Doonan, J. H., et al. (2002). Regulation of the pollen-specific actin-depolymerizing factor *LlADF1*. *Plant Cell* 14, 2915–2927. doi: 10.1105/tpc.005363

Ayliffe, M., Devilla, R., Mago, R., White, R., Talbot, M., Pryor, A., et al. (2011). Nonhost resistance of rice to rust pathogens. *Mol. Plant-Microbe Interact.* 24, 1143–1155. doi: 10.1094/MPMI-04-11-0100

Ayscough, K. R. (1998). *In vivo* functions of actin-binding proteins. *Curr. Opin. Cell Biol.* 10, 102–111. doi: 10.1016/S0955-0674(98)80092-6

Bamburg, J. R. (1999). Proteins of the ADF/cofilin family: essential regulators of actin dynamics. *Annu. Rev. Cell Dev. Biol.* 15, 185–230. doi: 10.1146/annurev.cellbio.15.1.185

Bernstein, B. W., and Bamburg, J. R. (2010). ADF/cofilin: a functional node in cell biology. *Trends Cell Biol.* 20, 187–195. doi: 10.1016/j.tcb.2010.01.001

Cao, Z., Jing, J., Wang, M., Shang, H., and Li, Z. (2002). Relation analysis of stripe rust resistance gene in wheat important cultivar Suwon 11, Suwon 92 and hybrid 46. *Acta Bot. BorealiOccident. Sin.* 23, 64–68.

Chen,Y.-H., Cheung, A. Y., and Wu, H.-M. (2003). Actin-depolymerizing factor mediates Rac/Rop GTPase–regulated pollen tube growth. *Plant Cell* 15, 237–249. doi: 10.1105/tpc.007153

Danyluk, J., Carpentier, E., and Sarhan, F. (1996). Identification and characterization of a low temperature regulated gene encoding an actin-binding protein from wheat. *FEBS Lett.* 389, 324–327. doi: 10.1016/0014-5793(96)00599-6

Day, B., Henty, J. L., Porter, K. J., and Staiger, C. J. (2011). The pathogen-actin connection: a platform for defense signaling in plants. *Annu. Rev. Phytopathol.* 49, 483–506. doi: 10.1146/annurev-phyto-072910-095426

Dean, R., Van Kan, J. A., Pretorius, Z. A., Hammond−Kosack, K. E., Di Pietro, A., Spanu, P. D., et al. (2012). The top 10 fungal pathogens in molecular plant pathology. *Mol. Plant Pathol.* 13, 414–430. doi: 10.1111/j.1364-3703.2011.00783.x

Dong, C. H., Xia, G. X., Hong, Y., Ramachandran, S., Kost, B., and Chua, N. H. (2001). ADF proteins are involved in the control of flowering and regulate F-actin organization, cell expansion, and organ growth in Arabidopsis. *Plant Cell* 13, 1333–1346. doi: 10.1105/tpc.13.6.1333

Dos Remedios, C. G., Chhabra, D., Kekic, M., Dedova, I. V., Tsubakihara, M., Berry, D. A., et al. (2003). Actin binding proteins: regulation of cytoskeletal microfilaments. *Physiol. Rev.* 83, 433–473. doi: 10.1152/physrev.00026.2002

Eun, S. O., and Lee, Y. (1997). Actin filaments of guard cells are reorganized in response to light and abscisic acid. *Plant Physiol.* 115, 1491–1498. doi: 10.1104/pp.115.4.1491

Fu, Y., Duan, X., Tang, C., Li, X., Voegele, R. T., Wang, X., et al. (2014). TaADF7, an actin-depolymerizing factor, contributes to wheat resistance against *Puccinia striiformis* f. sp. *tritici*. *Plant J.* 78, 16–30. doi: 10.1111/tpj.12457

Hardham, A. R., Jones, D. A., and Takemoto, D. (2007). Cytoskeleton and cell wall function in penetration resistance. *Curr. Opin. Plant Biol.* 10, 342–348. doi: 10.1016/j.pbi.2007.05.001

Henty-Ridilla, J. L., Li, J., Day, B., and Staiger, C. J. (2014). ACTIN DEPOLYMERIZING FACTOR4 regulates actin dynamics during innate immune signaling in Arabidopsis. *Plant Cell* 26, 340–352. doi: 10.1105/tpc.113.122499

Henty-Ridilla, J. L., Shimono, M., Li, J., Chang, J. H., Day, B., and Staiger, C. J. (2013). The plant actin cytoskeleton responds to signals from microbe-associated molecular patterns. *PLoS Pathog.* 9:e1003290. doi: 10.1371/journal.ppat.1003290

Holzberg, S., Brosio, P., Gross, C., and Pogue, G. P. (2002). Barley stripe mosaic virus-induced gene silencing in a monocot plant. *Plant J.* 30, 315–327. doi: 10.1046/j.1365-313X.2002.01291.x

Hood, M., and Shew, H. (1996). Applications of KOH-aniline blue fluorescence in the study of plant-fungal interactions. *Phytopathology* 86, 704–708. doi: 10.1094/Phyto-86-704

Huang, Y. C., Huang, W. L., Hong, C. Y., Lur, H. S., and Chang, M. C. (2012). Comprehensive analysis of differentially expressed rice actin depolymerizing factor gene family and heterologous overexpression of *OsADF3* confers *Arabidopsis thaliana* drought tolerance. *Rice* 5:33. doi: 10.1186/1939-8433-5-33

Jiang, C. J., Weeds, A. G., and Hussey, P. J. (1997). The maize actin-depolymerizing factor, ZmADF3, redistributes to the growing tip of elongating root hairs and can be induced to translocate into the nucleus with actin. *Plant J.* 12, 1035–1043. doi: 10.1046/j.1365-313X.1997.12051035.x

Jones, J. D., and Dangl, J. L. (2006). The plant immune system. *Nature* 444, 323–329. doi: 10.1038/nature05286

Kang, Z., and Li, Z. (1984). Discovery of a normal T. type new pathogenic strain to Lovrin10. *Acta Cllegii Septentrionali Occident. Agric.* 4, 18–28.

Kobayashi, T., Shimanuki, S., Saitoh, S., and Yamashita, Y. (1997a). Improved growth of large lead zinc niobate titanate piezoelectric single crystals for medical ultrasonic transducers. *Jpn. J. Appl. Phys.* 36, 6035.

Kobayashi, Y., Kobayashi, I., Funaki, Y., Fujimoto, S., Takemoto, T., and Kunoh, H. (1997b). Dynamic reorganization of microfilaments and microtubules is necessary for the expression of non-host resistance in barley coleoptile cells. *Plant J.* 11, 525–537.

Livak, K. J., and Schmittgen, T. D. (2001). Analysis of relative gene expression data using real-time quantitative PCR and the $2^{-\Delta\Delta CT}$ method. *Methods* 25, 402–408. doi: 10.1006/meth.2001.1262

Lopez, I., Anthony, R. G., MacIver, S. K., Jiang, C. J., Khan, S., Weeds, A. G., et al. (1996). Pollen specific expression of maize genes encoding actin depolymerizing factor-like proteins. *Proc. Natl. Acad. Sci. U.S.A.* 93, 7415–7420. doi: 10.1073/pnas.93.14.7415

Maciver, S. K., and Hussey, P. J. (2002). The ADF/cofilin family: actin-remodeling proteins. *Genome Biol.* 3, 3007.3001–3007.3012. doi: 10.1186/gb-2002-3-5-reviews3007

Meagher, R. B., McKinney, E. C., and Vitale, A. V. (1999). The evolution of new structures: clues from plant cytoskeletal genes. *Trends Genet.* 15, 278–284. doi: 10.1016/S0168-9525(99)01759-X

Miklis, M., Consonni, C., Bhat, R. A., Lipka, V., Schulze-Lefert, P., and Panstruga, R. (2007). Barley MLO modulates actin-dependent and actin-independent antifungal defense pathways at the cell periphery. *Plant Physiol.* 144, 1132–1143. doi: 10.1104/pp.107.098897

Mun, J. H., Lee, S. Y., Yu, H. J., Jeong, Y. M., Shin, M. Y., Kim, H., et al. (2002). Petunia actin-depolymerizing factor is mainly accumulated in vascular tissue and its gene expression is enhanced by the first intron. *Gene* 292, 233–243. doi: 10.1016/S0378-1119(02)00646-7

Mun, J. H., Yu, H. J., Lee, H. S., Kwon, Y. M., Lee, J. S., Lee, I., et al. (2000). Two closely related cDNAs encoding actin-depolymerizing factors of petunia are mainly expressed in vegetative tissues. *Gene* 257, 167–176. doi: 10.1016/S0378-1119(00)00412-1

Opalski, K. S., Schultheiss, H., Kogel, K. H., and Hückelhoven, R. (2005). The receptor-like MLO protein and the RAC/ROP family G-protein RACB modulate actin reorganization in barley attacked by the biotrophic powdery mildew fungus *Blumeria graminis* f. sp. *hordei*. *Plant J.* 41, 291–303. doi: 10.1111/j.1365-313X.2004.02292.x

Ouellet, F., Carpentier, É., Cope, M. J. T., Monroy, A. F., and Sarhan, F. (2001). Regulation of a wheat actin-depolymerizing factor during cold acclimation. *Plant Physiol.* 125, 360–368. doi: 10.1104/pp.125.1.360

Pogue, G. P., Lindbo, J. A., Dawson, W. O., and Turpen, T. H. (1998). "Tobamovirus transient expression vectors: tools for plant biology and high-level expression of foreign proteins in plants," in *Plant Molecular Biology Manual*, ed S. B. Gelvin (Dordrecht: Springer), 67–93.

Pollard, T. D., Blanchoin, L., and Mullins, R. D. (2000). Molecular mechanisms controlling actin filament dynamics in nonmuscle cells. *Annu. Rev. Biophys. Biomol. Struct.* 29, 545–576. doi: 10.1146/annurev.biophys.29.1.545

Porter, K., Shimono, M., Tian, M., and Day, B. (2012). Arabidopsis Actin-Depolymerizing Factor-4 links pathogen perception, defense activation and transcription to cytoskeletal dynamics. *PLoS Pathog.* 8:e1003006. doi: 10.1371/journal.ppat.1003006

Ruzicka, D. R., Kandasamy, M. K., McKinney, E. C., Burgos-Rivera, B., and Meagher, R. B. (2007). The ancient subclasses of Arabidopsis ACTIN DEPOLYMERIZING FACTOR genes exhibit novel and differential expression. *Plant J.* 52, 460–472. doi: 10.1111/j.1365-313X.2007.03257.x

Scofield, S. R., Huang, L., Brandt, A. S., and Gill, B. S. (2005). Development of a virus-induced gene-silencing system for hexaploid wheat and its use in functional analysis of the *Lr21*-mediated leaf rust resistance pathway. *Plant Physiol.* 138, 2165–2173. doi: 10.1104/pp.105.061861

Shimada, C., Lipka, V., O'Connell, R., Okuno, T., Schulze-Lefert, P., and Takano, Y. (2006). Nonhost resistance in Arabidopsis-*Colletotrichum* interactions acts at the cell periphery and requires actin filament function. *Mol. Plant-Microbe Interact.* 19, 270–279. doi: 10.1094/MPMI-19-0270

Skalamera, D., and Heath, M. C. (1998). Changes in the cytoskeleton accompanying infection-induced nuclear movements and the hypersensitive response in plant cells invaded by rust fungi. *Plant J.* 16, 191–200. doi: 10.1046/j.1365-313x.1998.00285.x

Staiger, C. J., Gibbon, B. C., Kovar, D. R., and Zonia, L. E. (1997). Profilin and actin-depolymerizing factor: modulators of actin organization in plants. *Trends Plant Sci.* 2, 275–281. doi: 10.1016/S1360-1385(97)86350-9

Swamy, P., and Smith, B. (1999). Role of abscisic acid in plant stress tolerance. *Curr. Sci.* 76, 1220–1227.

Tian, M., Chaudhry, F., Ruzicka, D. R., Meagher, R. B., Staiger, C. J., and Day, B. (2009). Arabidopsis actin-depolymerizing factor *AtADF4* mediates defense signal transduction triggered by the *Pseudomonas syringae* effector AvrPphB. *Plant Physiol.* 150, 815–824. doi: 10.1104/pp.109.137604

Ton, J., Flors, V., and Mauch-Mani, B. (2009). The multifaceted role of ABA in disease resistance. *Trends Plant Sci.* 14, 310–317. doi: 10.1016/j.tplants.2009.03.006

Tuteja, N. (2007). Abscisic acid and abiotic stress signaling. *Plant Signal. Behav.* 2, 135–138. doi: 10.4161/psb.2.3.4156

Van Troys, M., Huyck, L., Leyman, S., Dhaese, S., Vandekerkhove, J., and Ampe, C. (2008). Ins and outs of ADF/cofilin activity and regulation. *Eur. J. Cell Biol.* 87, 649–667. doi: 10.1016/j.ejcb.2008.04.001

Voegele, R. T., and Mendgen, K. (2003). Rust haustoria: nutrient uptake and beyond. *New Phytol.* 159, 93–100. doi: 10.1046/j.1469-8137.2003.00761.x

Wang, C. F., Huang, L. L., Buchenauer, H., Han, Q. M., Zhang, H. C., and Kang, Z. S. (2007). Histochemical studies on the accumulation of reactive oxygen species (O^{-2} and H_2O_2) in the incompatible and compatible interaction of wheat: *Puccinia striiformis* f. sp. *tritici*. *Physiol. Mol. Plant Pathol.* 71, 230–239. doi: 10.1016/j.pmpp.2008.02.006

Wasteneys, G. O., and Galway, M. E. (2003). Remodeling the cytoskeleton for growth and form: an overview with some new views. *Annu. Rev. Plant Biol.* 54, 691–722. doi: 10.1146/annurev.arplant.54.031902.134818

Yin, C., Jurgenson, J. E., and Hulbert, S. H. (2011). Development of a host-induced RNAi system in the wheat stripe rust fungus *Puccinia striiformis* f. sp. *tritici*. *Mol. Plant-Microbe Interact.* 24, 554–561. doi: 10.1094/MPMI-10-10-0229

Yun, B. W., Atkinson, H. A., Gaborit, C., Greenland, A., Read, N. D., Pallas, J. A., et al. (2003). Loss of actin cytoskeletal function and EDS1 activity, in combination, severely compromises non-host resistance in Arabidopsis against wheat powdery mildew. *Plant J.* 34, 768–777. doi: 10.1046/j.1365-313X.2003.01773.x

Conflict of Interest Statement: The authors declare that the research was conducted in the absence of any commercial or financial relationships that could be construed as a potential conflict of interest.

frontiers in Plant Science

ORIGINAL RESEARCH
published: 21 April 2016
doi: 10.3389/fpls.2016.00544

TaSYP71, a Qc-SNARE, Contributes to Wheat Resistance against *Puccinia striiformis* f. sp. *tritici*

Minjie Liu, Yan Peng, Huayi Li, Lin Deng, Xiaojie Wang and Zhensheng Kang**

State Key Laboratory of Crop Stress Biology for Arid Areas and College of Plant Protection, Northwest A&F University, Xiangyang, China

N-ethylmaleimide-sensitive factor attachment protein receptors (SNAREs) are involved in plant resistance; however, the role of SYP71 in the regulation of plant–pathogen interactions is not well known. In this study, we characterized a plant-specific SNARE in wheat, TaSYP71, which contains a Qc-SNARE domain. Three homologs are localized on chromosome 1AL, 1BL, and 1DL. Using *Agrobacterium*-mediated transient expression, TaSYP71 was localized to the plasma membrane in *Nicotiana benthamiana*. Quantitative real-time PCR assays revealed that *TaSYP71* homologs was induced by NaCl, H_2O_2 stress and infection by virulent and avirulent *Puccinia striiformis* f. sp. *tritici* (*Pst*) isolates. Heterologous expression of TaSYP71 in *Schizosaccharomyces pombe* elevated tolerance to H_2O_2. Meanwhile, H_2O_2 scavenging gene (*TaCAT*) was downregulated in *TaSYP71* silenced plants treated by H_2O_2 compared to that in control, which indicated that *TaSYP71* enhanced tolerance to H_2O_2 stress possibly by influencing the expression of *TaCAT* to remove the excessive H_2O_2 accumulation. When *TaSYP71* homologs were all silenced in wheat by the virus-induced gene silencing system, wheat plants were more susceptible to *Pst*, with larger infection area and more haustoria number, but the necrotic area of wheat mesophyll cells were larger, one possible explanation that minor contribution of resistance to *Pst* was insufficient to hinder pathogen extension when *TaSYP71* were silenced, and the necrotic area was enlarged accompanied with the pathogen growth. Of course, later cell death could not be excluded. In addition, the expression of pathogenesis-related genes were down-regulated in *TaSYP71* silenced wheat plants. These results together suggest that TaSYP71 play a positive role in wheat defense against *Pst*.

Keywords: *Puccinia striiformis* f. sp. *tritici*, wheat, SNARE, plasma membrane, virus-induced gene silencing, resistance, H_2O_2 tolerance

OPEN ACCESS

Edited by:
Ralph Panstruga,
RWTH Aachen University, Germany

Reviewed by:
Elena Prats,
Consejo Superior de Investigaciones Científicas, Spain
Chian Kwon,
Dankook University, South Korea

****Correspondence:***
Zhensheng Kang
kangzs@nwsuaf.edu.cn;
Xiaojie Wang
wangxiaojie@nwsuaf.edu.cn

Specialty section:
This article was submitted to Plant Biotic Interactions, a section of the journal Frontiers in Plant Science

Received: *28 January 2016*
Accepted: *06 April 2016*
Published: *21 April 2016*

Citation:
Liu M, Peng Y, Li H, Deng L, Wang X and Kang Z (2016) TaSYP71, a Qc-SNARE, Contributes to Wheat Resistance against Puccinia striiformis f. sp. tritici. Front. Plant Sci. 7:544. doi: 10.3389/fpls.2016.00544

INTRODUCTION

Eukaryotes have evolved a specialized class of proteins, the soluble *N*-ethylmaleimide-sensitive factor attachment protein receptors (SNAREs), that functions as mediators of vesicle membrane fusion with specific organelles. Based on the amino acid residues (glutamine or arginine) in the center of the SNARE motif, SNAREs can be grouped as Q- and R-SNAREs. Generally, Q-SNAREs localize to the membrane of target organelles (t-SNAREs), whereas R-SNAREs localize to the transport vesicles (v-SNAREs). Three distinct t-SNAREs and one v-SNARE form a four-helix

hetero-oligomeric complex to mediate membrane fusion between vesicles and target membranes, including vesicles, organelles of the endomembrane system, and the plasma membrane (PM). Based on their positions within the assembled four-helix bundle, Q-SNAREs can be classified as Qa-SNARE motifs (occupy the syntaxin position), Qb-SNARE (SNAP-25 N-terminal) and Qc-SNARE (SNAP-25 C-terminal) (Bock et al., 2001).

Recent findings indicate that SNARE functions in plants resistance pathogen against various pathogens (Inada and Ueda, 2014). *Arabidopsis thaliana* syntaxin (At)SYP121 (PEN1, encoding a Qa-SNARE) and its barley (*Hordeum vulgare*) ortholog, HvSYP121 (ROR2), contribute to either non-host resistance or basal penetration resistance against barley powdery mildew (*Blumeria graminis* f. sp. *hordei*) by cell wall reinforcements to avoid penetration (Collins et al., 2003). AtSNAP33 (Qa + Qb-SNARE) forms a ternary SNARE complex with AtSYP121 and AtVAMP721/722 at the PM that is necessary for pre-invasive immune responses in barley and *Arabidopsis* (Kwon et al., 2008). Tobacco (*N. tabacum*) PM SNARE SYP132 has been shown to contribute to defense against bacterial pathogens by mediating the secretion of pathogenesis-related protein 1 (Kalde et al., 2007). Golgi SNARE AtMEMB12 is targeted by miR393b* and regulates the exocytosis of an antimicrobial pathogenesis-related protein, PR1 (Zhang et al., 2011). AtSYP4 proteins localized to the trans-Golgi network (TGN) contribute to extracellular resistance against fungal pathogens and protect the chloroplasts from salicylic acid-dependent biotic stress (Uemura et al., 2012). In wheat (*Triticum aestivum*), knocking down *TaNPSN11* (Qb-SNARE) expression reduced the resistance of wheat to an avirulent isolate of *Puccinia striiformis* f. sp. *tritici* (*Pst*) (Wang et al., 2014).

SYP7 is one of the SNARE subfamilies unique to plants. The SYP7 subfamily belongs to the Qc-SNAREs and contains SYP71, SYP72, and SYP73. SYP71 is the most studied member of this family. The *Lotus japonicus* SYP71 expressed in vascular tissues has been shown to be involved in symbiotic nitrogen fixation with rhizobia (Hakoyama et al., 2012). Recently, SYP71 has been reported to participate in plant defense against various pathogens. *Arabidopsis* SYP71 is essential for successful viral infection by mediating the fusion of the turnip mosaic potyvirus (TuMV)-induced 6K2 vesicles with chloroplasts during TuMV infection (Wei et al., 2013). Overexpression of OsSYP71 in rice enhanced tolerance to oxidative stress and resistance to rice blast (Bao et al., 2012). However, the exact role of the SYP7 family in defense against biotrophic obligate fungi is limited known.

Wheat stripe rust, caused by *P. striiformis* f. sp. *tritici*, is a devastating worldwide disease. The fungus is strictly biotrophic and cannot survive without the host plant, making it difficult to study the interaction between wheat and *Pst*. In addition, the complex hexaploid nature of the wheat genome makes genetic and functional analyses extremely challenging. In this study, we isolated a wheat SYP71 homolog fragment from the incompatible cDNA library previously constructed by our laboratory, implying a possible role in *Pst* resistance. To find out whether TaSYP71 is involved in wheat resistance, we analyzed its expression patterns under various stresses. Overexpression of TaSYP71 in fission yeast enhanced the ability of the yeast to survive in hydrogen peroxide. Knocking down the expression of *TaSYP71* by a virus-induced gene silencing (VIGS) system reduced the resistance of wheat to CYR23. Therefore, we demonstrated that TaSYP71 plays a positive role in plant resistance possibly through influencing H_2O_2 signaling pathways.

MATERIALS AND METHODS

Plant Materials, *Pst* Isolates, and Chemical Treatments

Triticum aestivum cultivar Suwon 11 containing the *YrSu* resistance gene was grown at 16°C with a 16 h photoperiod. *N. benthamiana,* which was used for transient expression, was kept at 25°C with a light regime of 16 h light/8 h darkness. *P. striiformis* f. sp. *tritici* (*Pst*) pathotypes CYR23 (avirulent to Suwon 11) and CYR31 (virulent to Suwon 11) were used in this study for wheat and *Pst* interaction assays. Inoculation of *Pst* was performed as described (Kang and Li, 1984).

To study expression levels of *TaSYP71*, wheat leaves were infected with CYR31 or CYR23, and leaf tissues were then sampled at 0, 6, 12, 24, 48, 72, and 120 h post-inoculation (hpi) based on the histological study of the interactions between Suwon11 and CYR23 or CYR31 (Wang et al., 2007). Parallel mock-inoculated control plants were brushed with sterile water. Three biological replicates were performed independently for each assay.

To study expression levels of *TaSYP71* following various chemicals and stress elicitors, wheat leaves were sampled at 0, 6, 12, 24, 48 h post-treatment (hpt). For high salinity and H_2O_2 treatment, wheat seedlings were removed from soil, and their roots were soaked in 200 mM NaCl and 10 mM H_2O_2, respectively. Osmotic stress was imposed by application of 20% polyethylene glycol 6000 (PEG 6000) in the nutrient solution. All samples were immediately frozen in liquid nitrogen and stored at −80°C. Three biological replicates were performed independently for each assay.

RNA Extraction, cDNA Synthesis and qRT-PCR Analysis

Total RNA was extracted using the RNeasy Plant Mini Kit (Qiagen) and treated with DNase I according to the manufacturer's instructions. RNA was reverse transcribed into cDNA with an oligo$(dT)_{18}$ primer using an RT-PCR system (Promega, Madison, WI, USA). The expression patterns of *TaSYP71* under different conditions as described above were detected by qRT-PCR following the procedure previously described (Wang et al., 2009) using a 7500 Real-Time PCR System (Applied Biosystems, Foster City, CA, USA). The wheat elongation factor *TaEF-1a* gene (GenBank accession no. Q03033) was used as the internal reference for all qRT-PCR assays. The relative transcript levels of the pathogenesis-related (PR) protein genes (*TaPR1*, AAK60565; *TaPR2*, DQ090946; and *TaPR5*, FG618781), and reactive oxygen

species- scavenging genes (catalase, *TaCAT*, X94352) were also confirmed using qRT-PCR. Primers used in these assays were listed in Supplementary Table S1. The comparative $2^{-\Delta\Delta CT}$ method was used to quantify relative gene expression (Livak and Schmittgen, 2001). Three biological replicates were performed independently.

Cloning of *TaSYP71* and Sequence Analyses

Specific primers for *TaSYP71* were designed based on the sequence from the cDNA library of the wheat-*Pst* incompatible interaction constructed by our laboratory (Wang et al., 2008). The fragment was cloned into the pMD18-T simple vector and sequenced.

The ORF of *TaSYP71* was aligned with the *T. aestivum* cv. Chinese Spring genome using the International Wheat Genome Sequencing Consortium[1]. The domain structure of the TaSYP71 protein was analyzed using InterProScan (Jones et al., 2014). TMHMM 3.0 was used for transmembrane domain prediction (Krogh et al., 2001). Multiple sequence alignment was performed, and a neighbor joining tree was created using Clustal W (Larkin et al., 2007) and MEGA 6 (Tamura et al., 2013), respectively.

Subcellular Localization of TaSYP71 in *N. benthamiana*

In the subcellular localization assay, the pCAMBIA1302: TaSYP71-eGFP fusion vector was constructed. pCAMBIA1302: eGFP was used as a control. These two constructs were separately introduced into the *Agrobacterium tumefaciens* strain GV3101 by electroporation. Transformants were selected using kanamycin (50 μg ml^{-1}) and rifampicin (20 μg ml^{-1}). For infiltration of leaves, recombinant strains of *A. tumefaciens* were grown in LB medium with proper antibiotics to late-log phase, collected, suspended in an infiltration media (10 mM $MgCl_2$, 10 mM MES, pH 5.6 and 150 mM acetosyringone), and then maintained at room temperature for 1–3 h before infiltration. *A. tumefaciens* suspensions were infiltrated at an OD_{600} of 0.8 into leaves of 4- to 6-week-old *N. benthamiana* plants using a syringe without a needle. Tissue samples were harvested at 2 or 3 days after infiltration from the infiltration area and directly imaged with an Olympus BX-51 microscope (Olympus Corporation, Japan). Every experiment was repeated at least three times, with each assay consisting of at least three tobacco plants.

Overexpression of TaSYP71 in *Schizosaccharomyces pombe*

In the overexpression assay, pREP3x: *TaSYP71* was constructed as described (He et al., 1997). The pREP3x: TaSYP71 and pREP3x empty vector were transformed into *S. pombe* by electroporation. Thiamine was used as the repressor of the nmt promoter in the pREP3x vector at a concentration of 2 μg/mL. For assessment of yeast cell sensitivity to H_2O_2, cells were removed from logarithmic cultures after 24 h of growth, collected by centrifugation, washed twice with sterile distilled water and finally diluted to densities of $OD_{600} = 0.2$ with leucine dropout medium containing 20 mM H_2O_2. The incubated fission yeast cells were sampled at 4, 8, 12, 16, 20, 24, 28, and 32 h pi. Fission yeast cell growth was also assayed on yeast solid media plates (-leu dropout) with 0, 20, and 60 mM H_2O_2 in inducing (without thiamine) or repressing (thiamine) medium. Photos were taken 3–5 days later. Three biological replicates were performed for each assay.

For the western blot analysis, protein was extracted from *S. pombe* as described previously (Moreno et al., 1991). Protein was then separated on a 12% SDS-polyacrylamide gel (SDS-PAGE). The protein was subsequently transferred onto a nitrocellulose membrane using a Semi-Phor Semi-Dry Transfer Unit. The immuno-blot analysis was conducted using the monoclonal antibody raised against GFP (Roche) as the primary antibody and goat anti-mouse IgG-peroxidase conjugate (Sigma–Aldrich, Saint Louis, MO, USA) as the secondary antibody. The immuno-reactivity was detected using an ECL Western Blotting Substrate kit (Thermo scientific, Meridian, Rockford, USA) and photographed.

BSMV-Mediated *TaSYP71* Gene Silencing

The VIGS system is an effective reverse genetics tool in wheat. The plasmids used for gene silencing were constructed as described by Holzberg et al. (2002). To guarantee the specificity of gene silencing, we searched for silencing fragments that showed the lowest sequence similarities with other genes. Possible silencing off-target effects of these VIGS constructs were tested by si-Fi software (version 3.2) as previously described (Nowara et al., 2010). Based on the criteria described above, a 147-bp cDNA fragment containing part of the 5′ untranslated region and part of the coding sequence and a 126-bp fragment derived from the partial coding sequence to the 3′ untranslated region were used to construct the recombinant *TaSYP71-1* and *TaSYP71-2* plasmids, respectively. Primers used are listed in Supplementary Table S1.

Infectious BSMV RNA was prepared from each linearized plasmid by *in vitro* transcription using a high-yield capped T7 transcription kit (mMESSAGE mMACHINE; Ambion). Three independent sets of wheat plants were used. The second leaves of two-leaf wheat seedlings were inoculated with BSMV transcripts. The BSMV inoculum was made by combining an equimolar ratio of α, β, and γ transcripts with excess inoculation buffer containing a wounding agent (Fes buffer) as previously described (Holzberg et al., 2002). The mock control was inoculated with 1× Fes buffer. BSMV: *TaPDS* and BSMV: γ empty vector were used as controls for the BSMV infection. BSMV-treated wheat plants were kept in a cultivation chamber at 25 ± 2°C. When the virus phenotype was observed (∼10 days after BSMV treatment), the fourth leaves of these plants were inoculated with fresh urediniospores of CYR23. The fourth leaves were sampled at 0, 24, 48, and 120 h p-i for histological observation and RNA isolation. The silencing efficiency for each of the BSMV constructs compared with BSMV: γ was examined by qRT-PCR. The phenotypes of the fourth leaves were observed and photographed 14 days after *Pst* inoculation.

[1]http://wheat-urgi.versailles.inra.fr/Seq-Repository/BLAST

Histological Observation of Fungal Growth and Host Response

Samples leaves were fixed and cleared as described Wang et al. (2007). For microscopic observations, leaf segments were kept in 50% glycerol and examined using differential interference contrast microscopy. The germinated urediospores enter into the host leaf tissue through stomata and form substomatal vesicle. Infection hyphae arising from the substomatal vesicle attempt to penetrate mesophyll cell wall and form haustoria for sustaining further fungal growth. Only infection sites with substomatal vesicles were considered for assessment. The autofluorescence of attacked mesophyll cells was captured using Olympus BX51 fluorescence microscope. H_2O_2 accumulation in mesophyll cells was stained by DAB as described (Thordal-Christensen et al., 1997). The area of necrotic cells and DAB stained H_2O_2 accumulation cells were measured by DP-BSW program (Olympus) connected with the microscope which can measure the area of closed polygon.

Fungal structures were then specifically stained using wheat germ agglutinin conjugated to Alexa-488 (Invitrogen) as described (Ayliffe et al., 2011). Stained tissue was examined under blue light excitation (excitation wavelength 450–480 nm, emission wavelength 515 nm). The *Pst* hyphae were observed using an Olympus BX-51 microscope, the number of branches and haustoria number were counted, the lengths and the infection area (indicating the ability of fungal expansion) were calculated by DP-BSW software.

RESULTS

TaSYP71 Cloning and Sequence Analysis

A cDNA fragment (938 bp) with a SNARE domain was first isolated from the wheat-*Pst* incompatible cDNA library constructed by our laboratory. The complete open reading frame (ORF) was obtained from cDNA of wheat cultivar Suwon11 infected by CYR23. This gene shared high similarity with *SYP71*, so we designated it as *TaSYP71* (GenBank accession no. KF683945.1). The predicted ORF length of *TaSYP71* is 813 bp, encoding a protein of 270 amino acid residues, with a molecular weight of 30.03 kDa.

Sequence alignment with the *Triticum aestivum* cv. Chinese Spring genome sequence from the UGRI database showed that the sequence was identical with the sequence on long arm of chromosomes 1A. Two other homologs were located on long arm of chromosomes 1B and 1D. The first 154 bp of the ORF was missing in chromosome 1D (**Supplementary Figure S1A**). Only one amino acid residue variation was found between chromosomes 1A and 1B (**Supplementary Figure S1B**), although there were nine nucleotide variations in the ORF of the two copies (**Supplementary Figure S1A**). In addition, only few nucleotide variations were found in 5′ and 3′ UTR region (**Supplementary Figure S1A**).

As predicted by TMHMM 3.0, a transmembrane helix located at the C-terminal of TaSYP71. The structural analysis of the TaSYP71 protein showed a Qc-SNARE motif located adjacent to the C-terminal transmembrane anchor. A multiple sequence alignment of TaSYP71 with homologs from other species showed the highest similarity with HvSYP71 (97.78%) in *Hordeum vulgare*. However, TaSYP71 had only 66.67% identity with AtSYP71 in *Arabidopsis* (**Figure 1A**). Phylogenetic analysis revealed that TaSYP71 and its homologs from monocotyledonous were clustered into one large clade in which HvSYP71 showed the highest similarity to TaSYP71. Homologs from dicotyledonous were clustered into another large clade (**Figure 1B**).

TaSYP71 Was Localized to the Plasma Membrane by Transient Expression in Tobacco

Previous studies of SYP71 in other organisms have shown that SYP proteins are mainly located in the PM or endoplasmic reticulum membrane. To determine the subcellular localization of wheat SYP71, a TaSYP71-eGFP fusion protein was expressed in *N. benthamiana* using *A. tumefaciens* infiltration. Observation by fluorescence microscopy revealed that, in contrast to eGFP alone, which exhibited fluorescence in both the cytoplasm and the nucleus, TaSYP71-eGFP was restricted to the PM (**Figure 2**).

TaSYP71 is Upregulated Following NaCl, H_2O_2 and *Pst* Treatment

Quantitative real-time PCR (qRT-PCR) was used to determine the transcript profile of *TaSYP71*. For abiotic stresses, wheat seedlings were treated with polyethylene glycol 6000 (PEG 6000), NaCl, and H_2O_2. As shown in **Figure 3A**, following treatment by H_2O_2, expression levels of *TaSYP71* showed a significant upregulation from 6 h pthpt to 24 hpt and peaked at 12 hpt with an approximately 12-fold increase in expression. Following NaCl treatment, *TaSYP71* expression was dramatically elevated at 12 hpt with an approximately eightfold increase. However, *TaSYP71* did not show any significant induction by PEG 6000 treatment.

We also examined whether *TaSYP71* was induced by biotic stresses. During wheat and *Pst* interaction, *TaSYP71* was upregulated both in the compatible and incompatible interaction by 2- to 13-fold during infection. In the compatible interaction, the relative transcript level of *TaSYP71* was dramatically elevated at 12 hpi, followed by a slight decrease at 24 and 48 hpi and finally, a gradual increase at 72 and 120 hpi. The expression of *TaSYP71* in the incompatible interaction showed a similar pattern to the compatible interaction, except for the first peak at 24 hpi, which was later than the compatible interaction (**Figure 3B**).

Overexpression of TaSYP71 in Fission Yeast Enhanced the Yeast Tolerance to H_2O_2 Stress

To elucidate the exact role for TaSYP71 in response to H_2O_2 stress, we heterologously overexpressed TaSYP71 in *S. pombe*. The non-transformed yeast and empty vector pREP3X was used as a negative control. Yeast cells were cultured in medium with thiamine (repressing) or without thiamine (inducing) for 20 h. At the same H_2O_2 concentration (0 or 20 mM), the thiamine

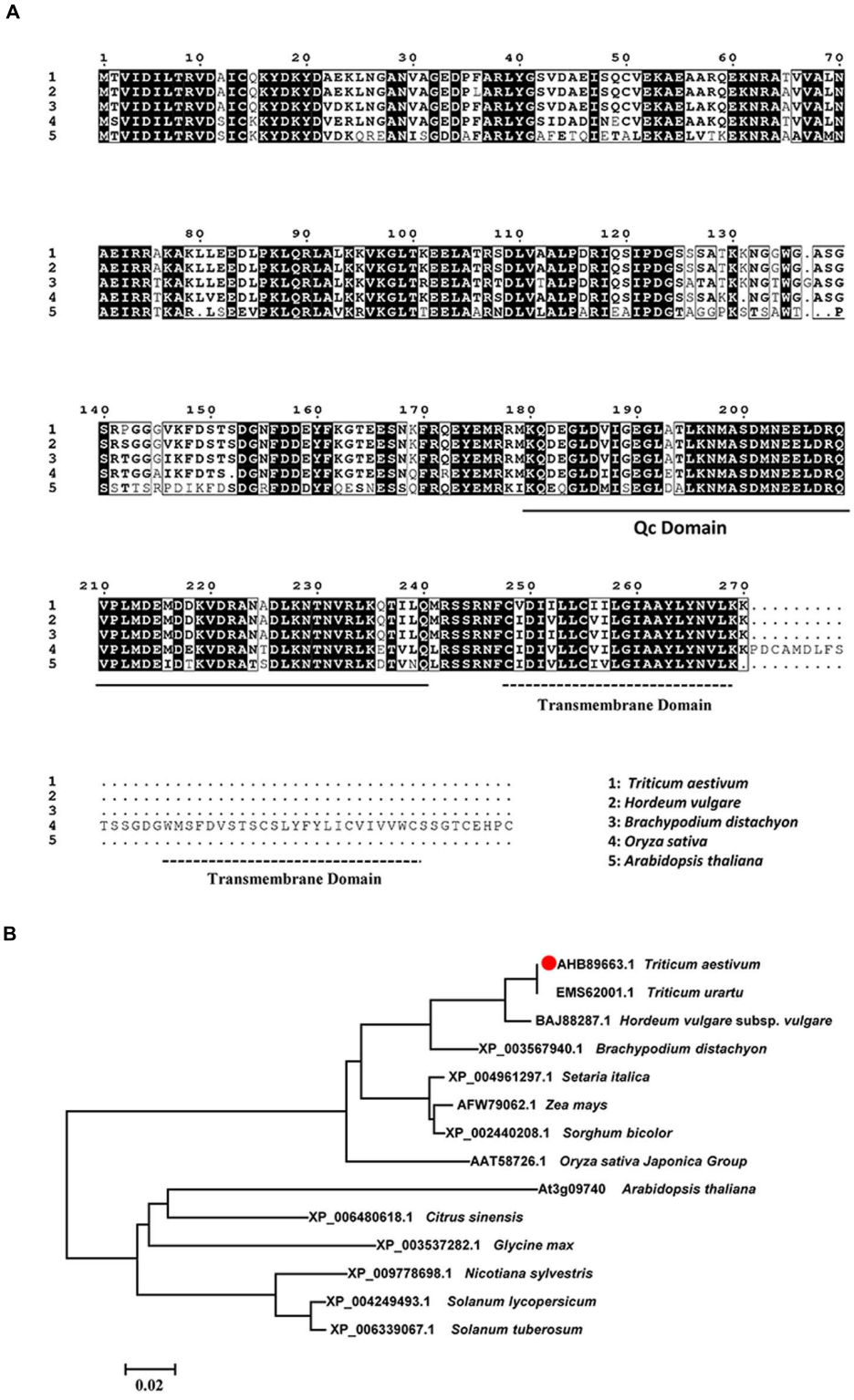

FIGURE 1 | Multiple sequence alignment and phylogenetic analysis of *TaSYP71* and its homologs from other species. (A) Multiple sequence alignment of amino acids. Identical amino acid residues are shaded in black. Black underline indicates the Qc-SNARE motif, and dotted lines indicate the transmembrane domain conserved in the SYP71 family. **(B)** Phylogenetic analysis of *TaSYP71* and homologs in other plant species. Multiple sequence alignments and the neighbor joining tree were created using the MUSCLE method by MEGA 6.0.

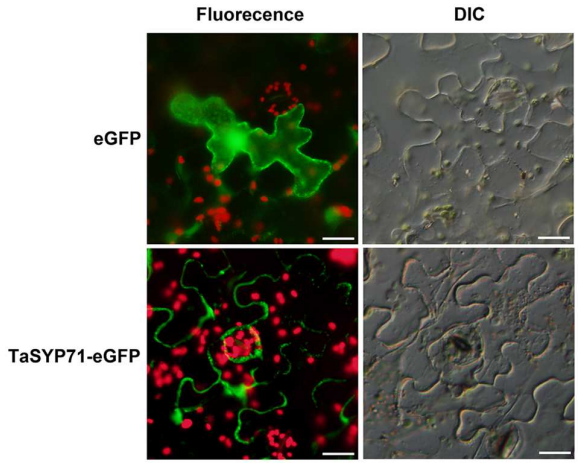

FIGURE 2 | Subcellular localization of TaSYP71 in *Nicotiana benthamiana* (tobacco). Enhanced green fluorescent protein (eGFP) (control) and the TaSYP71-eGFP fusion protein were expressed in *N. benthamiana* by transient agro-infiltration assays. The green fluorescence was observed with fluorescence microscopy. The corresponding cell morphology was observed with a differential interference contrast microscope (DIC). Bar = 20 μm.

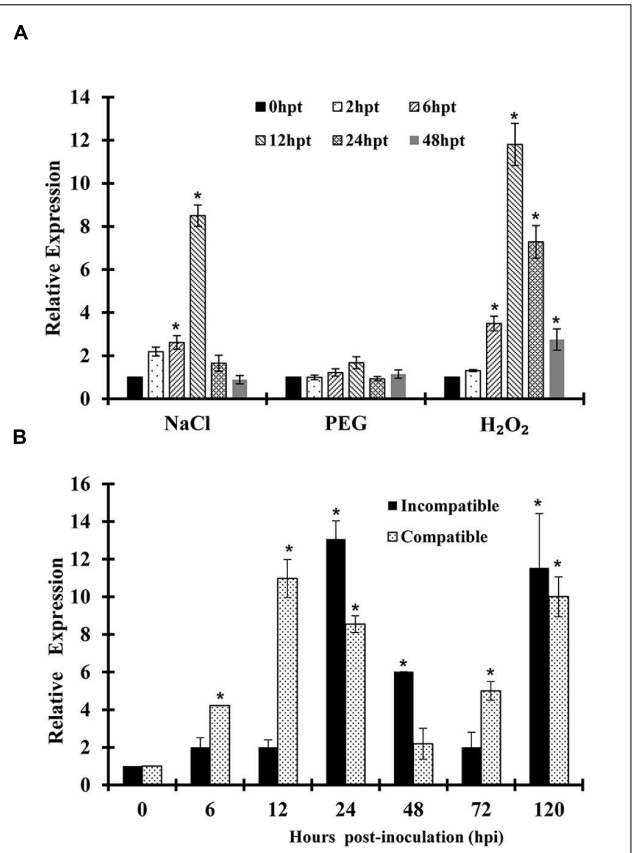

FIGURE 3 | Expression profiles of *TaSYP71* in response to abiotic and biotic stresses. Expression levels were normalized to the wheat elongation factor *TaEF-1a* gene. The results are shown as the mean ± standard deviation of three biological replicates. **(A)** Wheat leaves were separately treated with PEG 6000, NaCl, or H_2O_2 and sampled at 0, 2, 6, 12, 24, 48 hpt. **(B)** Wheat leaves inoculated with CYR23 (incompatible) or CYR31 (compatible) were sampled at 0, 6, 12, 24, 48, 72, and 120 hpi. Asterisks indicate a significant difference ($p < 0.05$) from 0 hpi or hpt using Student's *t*-test.

did not influence yeast growth in both controls (Supplementary Table S3). The number of colonies was reduced on the plate with 20 mM H_2O_2, which indicated that yeast growth, was inhibited by H_2O_2 treatment. No yeast cells survived when treated with 60 mM H_2O_2 in both controls. Moreover, yeast cells expressing pREP3X: eGFP showed fluorescence (**Supplementary Figure S2**) and the expression of eGFP was detected by western blot with anti-GFP antibody, which indicated that the system was feasible for protein expression. We used equal concentrations of yeast cells on the leucine dropout plates. As shown in **Figure 4A**, on H_2O_2 plate, the number of fission yeast cells expressing pREP3X: TaSYP71 in the absence of thiamine (− VB) was greater than the number of the control cells with thiamine (+ VB). Fission yeast cells survived even on the plate with a high concentration of H_2O_2 (60 mM). These results clearly demonstrated that overexpression of TaSYP71 in the fission yeast enhanced tolerance to H_2O_2.

The assay in leucine dropout liquid medium showed similar results. Regardless of the presence of thiamine, the OD_{600} of the group without H_2O_2 was much higher than that with H_2O_2. Without H_2O_2 treatment, there was no significant difference between yeast cells treated with thiamine and untreated cells. Following treatment with H_2O_2, fission yeast cells expressing TaSYP71 in the absence of thiamine (− VB) significantly increased ($p < 0.05$) compared to those in the presence of thiamine (+ VB) from 20 to 32 h after incubation (**Figure 4B**).

TaSYP71 Knockdown Wheat Plants Show Enhanced Susceptibility to *Pst*

As *TaSYP71* was isolated from the wheat-*Pst* incompatible interaction, a VIGS system was applied to characterize the role of *TaSYP71* during the wheat-*Pst* incompatible interaction. None of the VIGS constructs was predicted to possess effective off-targets or cross silencing other SNARE transcripts in wheat as determined by the si-Fi software (Supplementary Table S2). BSMV: *TaPDS* (wheat phytoene desaturase gene) was used as a positive control for the gene silencing system. As shown in **Figure 5A**, photobleaching was presented in the fourth leaves of the BSMV: *TaPDS*-inoculated plants.

To determine the efficiency of silencing, qRT-PCR assays were performed on RNA samples extracted from the fourth leaves of wheat seedlings 0, 24, 48, and 120 hpi with the CYR23. These leaves were pre-infected with BSMV: γ, BSMV: *TaSYP71-1*, and BSMV: *TaSYP71-2*. Compared to the BSMV: γ control, the abundance of *TaSYP71* transcripts was greatly reduced to different extents (20–40%) in *TaSYP71* knockdown plants (**Figure 5B**).

Fourteen days after inoculation of CYR23, several necrotic spots were observed on the BSMV: γ and mock-inoculated wheat leaves. However, there were many necrotic spots and sporadic urediniospores on *TaSYP71*-knockdown plants. Resistance was

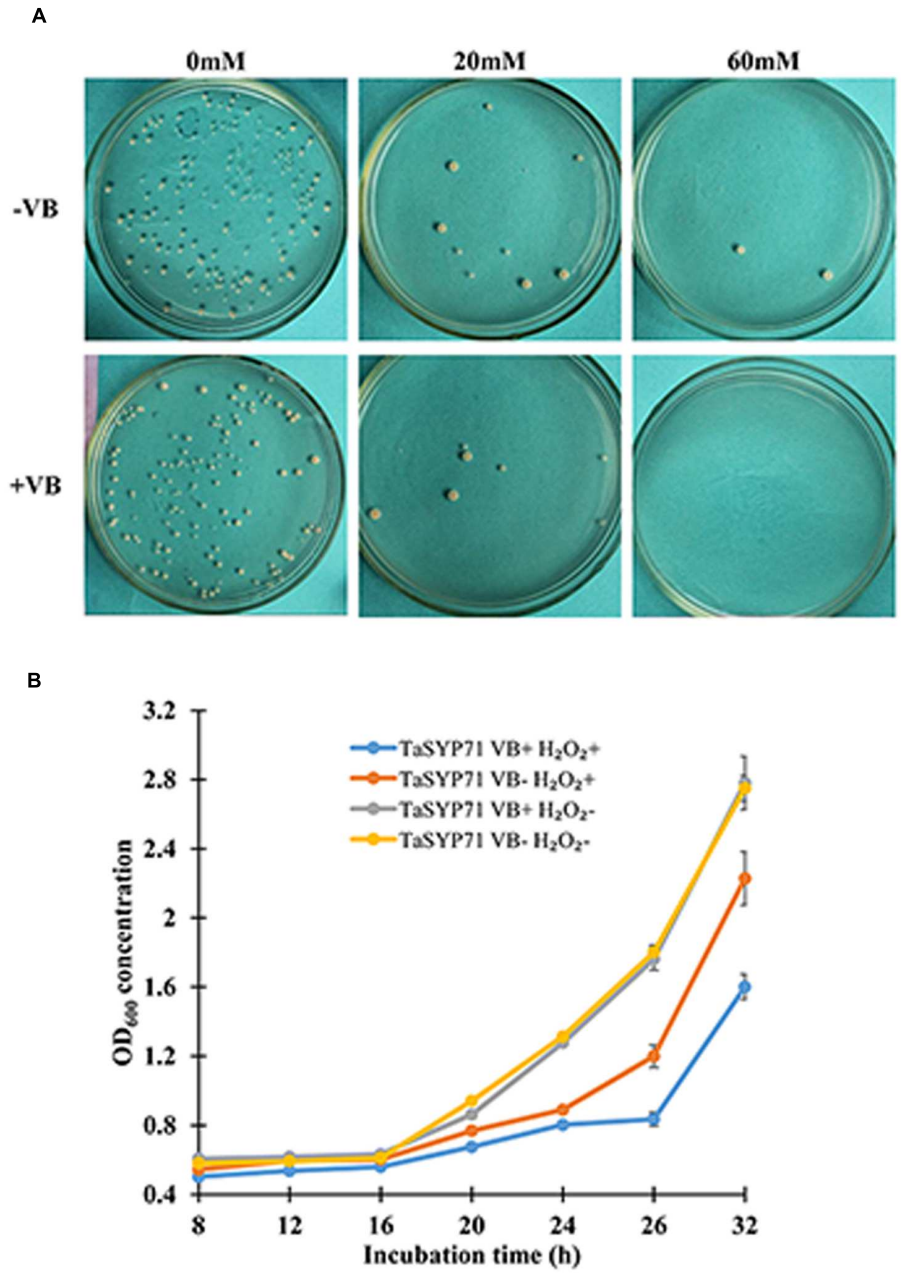

FIGURE 4 | Overexpression of TaSYP71 in fission yeast enhanced the ability of yeast to survive in H_2O_2 stress. (A) Yeast cells expressing TaSYP71 were spotted on leucine dropout solid medium at the same concentration. The media contained 0, 20, and 60 mM H_2O_2 with (+VB) or without (−VB) thiamine. **(B)** Yeast cells carrying pREP3X-TaSYP71 were incubated in leucine dropout liquid medium with 20 mM H_2O_2, and the OD_{600} was measured at 12, 16, 20, 24, 28, and 32 h p-i.

greatly reduced in *TaSYP71*-knockdown wheat plants (shown in **Figure 5A**).

Histological Changes of *Pst* Growth and Host Response

To observe the histological changes associated with the enhanced susceptibility to *Pst* in these silenced plants, leaf segments from at least three plants inoculated with the CYR23 were harvested from each treatment. The phenolic autofluorogen accumulations per infection site in BSMV: *TaSYP71* pre-infected wheat leaves were significantly ($p < 0.01$) greater than the control at both 48 and 120 hpi (**Figure 6**; **Table 1**), indicating that knockdown of *TaSYP71* expression decreases plant defense reactions at infection sites. The H_2O_2 area stained by DAB was larger in *TaSYP71* knockdown plants than in the control 24 hpi of *Pst* (**Figure 6**;

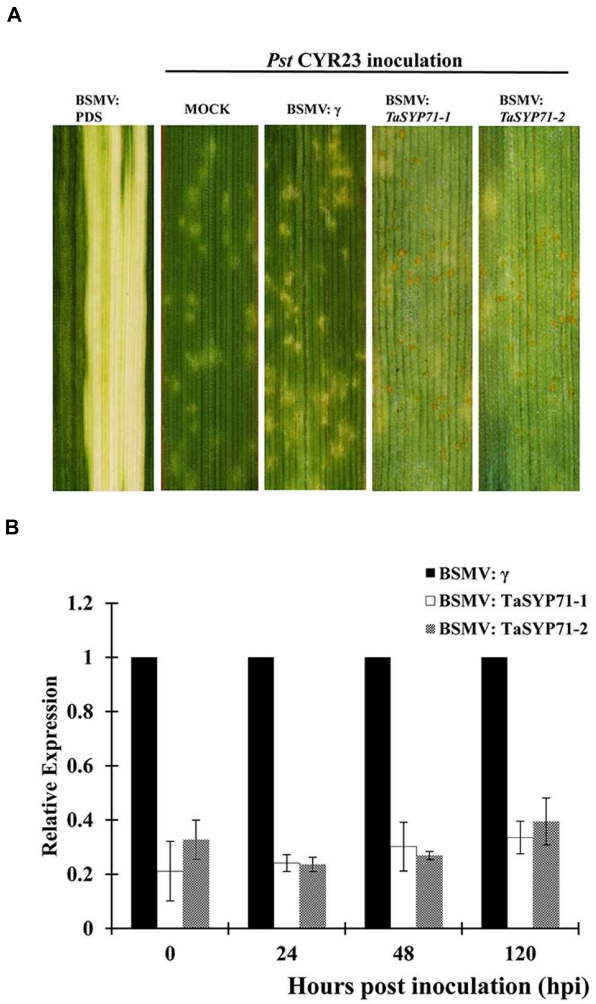

FIGURE 5 | Functional analyses of TaSYP71 during the incompatible interaction using a BSMV-mediated virus-induced gene silencing system. (A) Photobleaching was evident on the fourth leaves of plants infected with BSMV: *TaPDS*. After inoculation of CYR23, disease phenotypes of the fourth leaves were assessed and are shown from the left: mock, pre-inoculated with BSMV: γ, BSMV: *TaSYP71*-1, and BSMV: *TaSYP71*-2. **(B)** Silencing efficiency assessment of the two segments of *TaSYP71* in the fourth leaves of *TaSYP71* knockdown plants compared with BSMV: γ during incompatible interaction. The data were normalized to the *TaEF-1a* expression level. The transcript levels of *TaSYP71* in BSMV: γ at each time point were set to one. Error bars represent variations among three independent replicates.

Table 1). The leaf samples were further stained using wheat germ agglutinin conjugated to the fluorophore Alexa-488 to facilitate rust hyphal observation. The *Pst* hyphal lengths in BSMV: *TaSYP71* pre-infected wheat leaves were significantly ($p < 0.01$) longer than those observed in BSMV: γ -infected leaves at 24 and 48 hpi (**Figure 6**; **Table 1**). The haustoria number of *TaSYP71* silenced plants were more than that in control plants (**Table 1**, $p < 0.05$). Meanwhile, the infection area 120 hpi was larger in *TaSYP71* knockdown plants (**Figure 6**; **Table 1**, $p < 0.05$). The hyphal branches showed no significant change following BSMV: *TaSYP71* treatment.

Furthermore, we examined the expression of defense related genes (*TaPR1*, *TaPR2* and *TaPR5*) in CYR23 inoculated *TaSYP71* knockdown wheat plants by qRT-PCR. The transcript level of *TaPR1* was gradually induced in BSMV: γ control wheat plants, however, expression was reduced or not changed in *TaSYP71* knockdown wheat plants. Although the expression of *TaPR2* was induced 24 hpi in *TaSYP71* knockdown, the induction intensity was lower than that in control wheat plants, and the transcript levels were sharply reduced 48 and 120 hpi (**Figure 7**). In control wheat plants, the expression of *TaPR5* was significantly induced 24 hpi. But the expression of *TaPR5* in *TaSYP71* knockdown wheat plants was reduced during *Pst* infection (**Figure 7**). Hence, we inferred that the expressions of *TaPRs* were reduced in *TaSYP71* knockdown plants challenged with the CYR23 compared to control, further suggesting that TaSYP71 is involved in the resistance of wheat to *Pst*.

H_2O_2 Scavenging Gene Was Reduced by H_2O_2 Treatment in *TaSYP71* Knockdown Plants

To test whether TaSYP71 involved in H_2O_2 scavenging, we assayed the transcript level of H_2O_2 scavenging related gene *TaCAT* in *TaSYP71* knockdown plants after H_2O_2 treatment. Compared with control plants that the expression of *TaCAT* was significantly induced 12 hpt, the transcript levels of *TaCAT* were almost unchanged or dropped a little in *TaSYP71* silenced plants (**Figure 8**), which partially uncovers that TaSYP71 is relevant to H_2O_2 scavenging.

DISCUSSION

SNARE proteins mediate intracellular vesicle fusion, which is an essential cellular process of eukaryotic cells. Along with membrane fusion, SNARE proteins also regulate many plant biological processes. In this study, from a wheat-*Pst* incompatible interaction cDNA library, we isolated a *SYP71* homolog, which has a Qc-SNARE domain and C-terminal transmembrane domain. However, this gene has no close relatives in other kingdoms; in other words, SYP71 is unique to the plant kingdom. Moreover, SYP71 was also found in the green algae *Chlamydomonas reinhardtii* and the moss *Physcomitrella patens,* suggesting that an essential role for plant-specific biological processes evolved early (Lipka et al., 2007). In *Arabidopsis*, SYP71 knockout mutant embryos and seedlings displayed strong morphological abnormalities (El Kasmi et al., 2013). Meanwhile, AtSYP71 also contributed to TuMV infection as reported previously (Wei et al., 2013). These indicate that SYP71 indeed contributes to diverse crucial biological processes. In this study, we focused on the involvement of wheat SYP71 protein in defense against biotrophic fungi. Three homologous were located in the A, B, and D genome, and the amino acid sequences of homoeoloci are conserved with only one residue difference (**Supplementary Figure S1**), which indicate that the function of these three copies might be similar and reduntant (Brenchley et al., 2012). Hence, it is necessary that all three copies will be silenced to further study their function.

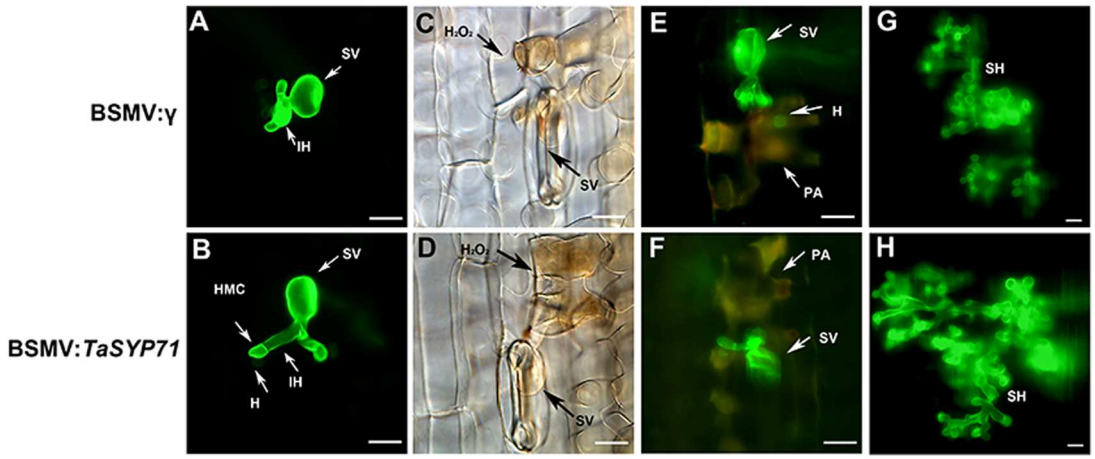

FIGURE 6 | Histological observation of fungal growth and host response during the incompatible interaction using a BSMV-mediated virus-induced gene silencing system. *Pst* hypha were observed in leaf segments after staining by wheat germ agglutinin conjugated to the fluorophore Alexa-488. The fungal growth of *Pst* CYR23 in wheat leaves that were inoculated with BSMV: γ, BSMV:*TaSYP71* at 24 hpi **(A,B)**, 48 hpi **(E,F)** and 120 hpi **(G,H)** was observed under a fluorescence microscope. The accumulation of H_2O_2 at the infection site was observed in leaf segments sampled at 24 hpi after DAB staining **(C,D)**. SV, substomatal vesicle; IH, initial hyphae; PA, phenolic autofluorogens; H_2O_2, specific staining of H_2O_2 accumulation using DAB; HMC, haustorial mother cell; H, haustorium, SH, secondary hyphae. Bar = 20 μm.

TABLE 1 | Histological analysis of the incompatible interaction between wheat and *Pst* in *TaSYP71* knockdown plants.

Treatment	H_2O_2 area per infection site (μm²)	Necrotic area per infection site (μm²)		Hyphal length (μm)		Hyphal branches		Haustoria number		Infection area per infection site(μm²)
	24 hpi	48 hpi	120 hpi	24 hpi	48 hpi	24 hpi	48 hpi	24 hpi	48 hpi	120 hpi
BSMV: γ	249.7	690.2	822.5	15.5	17.5	1.8	2.26	1.26	1.53	16167.91
BSMV: *TaSYP71-1*	317.2**	936.1**	1107*	18.6**	21.7**	1.9	2.38	1.57*	1.83*	23641.72*
BSMV: *TaSYP71-2*	354.1**	1046**	1305**	25.4**	28.8**	2.1**	2.60	1.65*	1.95*	26909.49*

*Wheat leaves were inoculated with BSMV: γ and two TaSYP71 knockdown fragments, respectively, and then inoculated with CYR23. H_2O_2 area per infection site, necrotic cell area and the infection area were calculated by DP-BSW software. Hyphae length was measured from the junction of the substomatal vesicle and hypha to the tip of the hypha. All data were calculated from at least 50 infection sites. Significance was measured according to a paired sample t-test method. *$p < 0.05$; **$p < 0.01$.*

In previous studies in *Arabidopsis*, AtSYP71 was localized to both the endoplasmic reticulum (ER) and the PM. When GFP-AtSYP71 was transiently expressed in the protoplasts of *Arabidopsis* suspension cultured cells, AtSYP71 was found to be localized to the ER (Uemura et al., 2004). However, AtSYP71 was mainly localized to the PM in transgenic *Arabidopsis* expressing GFP-AtSYP71 under its native promoter, although it was also localized to the ER in dividing regions (Suwastika et al., 2008). In our study, we showed that TaSYP71 was localized to the PM by transient expression of TaSYP71-eGFP in tobacco cells, suggesting that SYP71 might be involved in membrane trafficking to the PM. Fujiwara et al. (2014) employed immunoprecipitation and mass spectrometry and found that SYP71 interacts with Qa-SNARE SYP121, SYP122, and SYP132, which were located at the PM (Fujiwara et al., 2014). However, we cannot exclude the possibility of other location sites, which will need to be further analyzed in different physiological conditions.

An increasing body of evidence has suggested that SNARE genes are induced by various abiotic stresses. *NtSyp121* was strongly and transiently induced in tobacco leaves by ABA, drought, salt and wounding (Leyman et al., 1999). SYP61 has been reported to function in both salinity and osmotic stress tolerance as T-DNA mutant line *osm1* (*AtSYP61* disruption) exhibited increased sensitivity to both salinity and osmotic stress in a root-bending assay (Zhu et al., 2002). The expression pattern of *TaSYP71* in response to various abiotic stresses showed that SYP71 was induced by H_2O_2 and NaCl treatments; however, the expression pattern was unaffected when treated with PEG 6000, which may indicate that TaSYP71 is involved in salt and oxidative stress but not in drought stress. The expression pattern results support a similar but distinct function for TaSYP71 compared with other SNAREs. Because *TaSYP71* was induced following H_2O_2 treatment, we hypothesized a role for TaSYP71 in resistance to oxidative stress. To interpret the role of TaSYP71 in oxidative stress, we overexpressed TaSYP71 in fission yeast. Compared to the control, TaSYP71-overexpressing fission yeast showed more tolerance to H_2O_2 stress, which confirmed the role of TaSYP71 in oxidative stress. Furthermore, the assay for H_2O_2 treatment in *TaSYP71* silenced wheat plants indicates that TaSYP71 enhanced tolerance to H_2O_2 stress possibly by influencing the expression of *TaCAT* to remove the excessive

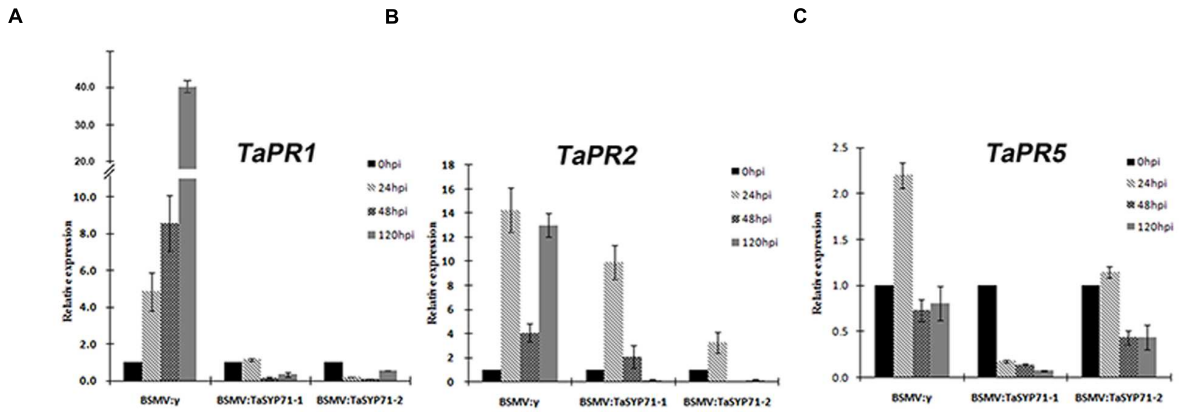

FIGURE 7 | The expression profiles of three pathogenesis-related genes *TaPR1* (A), *TaPR2* (B), and *TaPR5* (C) were assessed 0, 24, 48, 120 h post *Pst* inoculation in *TaSYP71* knockdown plants in BSMV-inoculated plants. The data were normalized to the wheat *TaEF-1a* expression level. The transcript levels of each gene at 0 hpi were set to one. Error bars represent variations among three independent replicates.

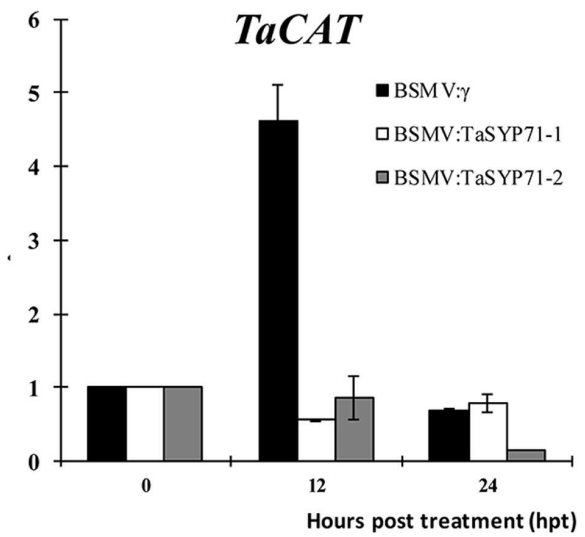

FIGURE 8 | The expression profiles of *TaCAT* was assessed 0, 12, and 24 h post 10 mM H_2O_2 treatment in *TaSYP71* knockdown plants. The data were normalized to the wheat *TaEF-1a* expression level. The transcript levels of *TaCAT* at 0 hpt were set to one. Error bars represent variations among three independent replicates.

H_2O_2 accumulation. One possibility is that SYP71 may enhance the ability of plants to remove ROS. Previous studies have confirmed that SNAREs could prevent H_2O_2-induced apoptosis (Levine et al., 2001). In our study, the transcript level of *TaSYP71* was peaked at 12 and 120 hpi in compatible interaction, representing the period of formation of haustoria and large amount of secondary hyphae respectively, which might indicate that stripe rust pathogen try to remove H_2O_2 accumulation by regulating the expression of *TaSYP71* to extend in its host. Meanwhile, the expression of *TaSYP71* was also induced during wheat infected by avirulent isolate CYR23, possibly suggesting its role in wheat resistance to *Pst* attack. Taken together, we inferred that vesicles containing H_2O_2 may fuse with the PM easily and exhaust outside of the plant cells to relieve the damage to the cells, and during the wheat-*Pst* interactions, ROS is key arm for pathogen or host to survive. However, the enigma that how TaSYP71 performs its role still needs to be excavated.

Accumulating evidence has indicated that plant endo- and exocytotic processes play crucial roles in plant-microbe interactions (Lipka et al., 2007). SYP71 was reported to participate in plant defense against various pathogens. The SNARE protein Syp71 is essential for turnip mosaic virus infection by mediating fusion of virus-induced vesicles with chloroplasts. OsSYP71-overexpressing transgenic lines grew better than wild type plants, and the expression of PR-1b and peroxidase was significantly enhanced after rice blast inoculation, which demonstrated that OsSYP71 confers resistance to rice blast (Bao et al., 2012). However, there has been limited evidence for the role of SYP71 in plant defense against biotrophic fungi. In this study, to determine the role of TaSYP71 in wheat-*Pst* interactions, the expression of *TaSYP71* was suppressed by a BSMV-mediated VIGS system. *TaSYP71* knockdown plants were more susceptible, the hyphal length was longer, the infection area was larger and more haustoria were formed in *TaSYP71* knockdown plants compared with control plants. Additionally, the expression of PR genes was down-regulated in *TaSYP71* silenced wheat plants. These results reported here indicate that TaSYP71 participates in wheat defense against *Pst* infection.

Surprisingly, in *TaSYP71* knockdown plants, the necrotic area per infection site was increased compared with that in control plants associated to higher infection areas. One possibility is that when *TaSYP71* was suppressed, H_2O_2 containing vesicle trafficing was tardy and inefficient, which lead to a later cell death insufficient to restrict fungal infection. Of course, we could not exclude the possibility that there are other redundant apoptotic factors that function in the interaction. In addition, we

found that the accumulation of H_2O_2 was enhanced in *TaSYP71* knockdown plants compared to control 24 hpi, which was the peak period of oxidative bursts as shown by previous histological and cytological observations. At optimal concentrations, H_2O_2 acts as a second messenger for the induction of defense genes, but excessive accumulation of ROS is detrimental to plants. Considering the role of TaSYP71 in H_2O_2 stress, we speculated that TaSYP71 might regulate the H_2O_2 balance in host cells and H_2O_2–induced signaling pathways, thereby contributing to *Pst* resistance. Localized at the PM, TaSYP71 facilitates signaling H_2O_2 -containing vesicles moving from host cells to extracellular regions, thus conferring *Pst* resistance.

In sum, we speculate that there are correlations between enhanced H_2O_2 tolerance and *Pst* resistance. This may be related to vesicle fusion and trafficking. However, the regulation of TaSYP71 in wheat under *Pst* stresses may be more complex than currently understood. Our study confirmed the positive role of TaSYP71 in host defense against *Pst*. Stable transgenic SNARE RNAi wheat should be used for further studies to explore the precise mechanism of how TaSYP71 modulates host defense.

AUTHOR CONTRIBUTIONS

ML, HL, XW, and ZK designed the experiment. ML, YP, and HL performed the experiments and analyzed the data. XW and LD helped with data interpretation and article editing. ML wrote the manuscript.

ACKNOWLEDGMENTS

This study was supported financially by the National Basic Research Program of China (Grant No. 2013CB127700), the National Natural Science Funds of China (Grant No. 31471733), and the 111 Project from the Ministry of Education of China (No. B07049).

SUPPLEMENTARY MATERIAL

The Supplementary Material for this article can be found online at: http://journal.frontiersin.org/article/10.3389/fpls.2016.00544

FIGURE S1 | Multi-sequence alignment of *TaSYP71* copies. The sequence of 1AL is the sequence we obtained. **(A)** Multi-alignment of the mRNA sequence of the three copies of *TaSYP71*. Black underline indicates 5′ and 3′ UTR region as shown in the figure. **(B)** Alignment of amino acid sequence of the two copies of *TaSYP71* (on chromosome 1A and 1B).

FIGURE S2 | Over-expression of TaSYP71 in fission yeast cells. The fluorescence of fission yeast cells carrying pREP3X-eGFP was observed at Olympus DP71 fluorescence microscope **(A)** and the corresponding cell morphology was observed under bright field **(B)**. Western blot analysis of eGFP expression levels in yeast cells with anti-GFP antibody **(C)**.

REFERENCES

Ayliffe, M., Devilla, R., Mago, R., White, R., Talbot, M., Pryor, A., et al. (2011). Nonhost resistance of rice to rust pathogens. *Mol. Plant Microbe Interact.* 24, 1143–1155. doi: 10.1094/MPMI-04-11-0100

Bao, Y.-M., Sun, S.-J., Li, M., Li, L., Cao, W.-L., Luo, J., et al. (2012). Overexpression of the Qc-SNARE gene OsSYP71 enhances tolerance to oxidative stress and resistance to rice blast in rice (*Oryza sativa* L.). *Gene* 504, 238–244. doi: 10.1016/j.gene.2012.05.011

Bock, J. B., Matern, H. T., Peden, A. A., and Scheller, R. H. (2001). A genomic perspective on membrane compartment organization. *Nature* 409, 839–841. doi: 10.1038/35057024

Brenchley, R., Spannagl, M., Pfeifer, M., Barker, G. L., D'Amore, R., Allen, A. M., et al. (2012). Analysis of the bread wheat genome using whole-genome shotgun sequencing. *Nature* 491, 705–710. doi: 10.1038/nature11650

Collins, N. C., Thordal-Christensen, H., Lipka, V., Bau, S., Kombrink, E., Qiu, J.-L., et al. (2003). SNARE-protein-mediated disease resistance at the plant cell wall. *Nature* 425, 973–977. doi: 10.1038/nature02076

El Kasmi, F., Krause, C., Hiller, U., Stierhof, Y.-D., Mayer, U., Conner, L., et al. (2013). SNARE complexes of different composition jointly mediate membrane fusion in *Arabidopsis cytokinesis*. *Mol. Biol. Cell* 24, 1593–1601. doi: 10.1091/mbc.E13-02-0074

Fujiwara, M., Uemura, T., Ebine, K., Nishimori, Y., Ueda, T., Nakano, A., et al. (2014). Interactomics of Qa-SNARE in *Arabidopsis thaliana*. *Plant Cell Physiol.* 55, 781–789. doi: 10.1093/pcp/pcu038

Hakoyama, T., Oi, R., Hazuma, K., Suga, E., Adachi, Y., Kobayashi, M., et al. (2012). The SNARE protein SYP71 expressed in vascular tissues is involved in symbiotic nitrogen fixation in *Lotus japonicus* nodules. *Plant Physiol.* 160, 897–905. doi: 10.1104/pp.112.200782

He, X., Patterson, T. E., and Sazer, S. (1997). The *Schizosaccharomyces pombe* spindle checkpoint protein mad2p blocks anaphase and genetically interacts with the anaphase-promoting complex. *Proc. Natl. Acad. Sci. U.S.A.* 94, 7965–7970. doi: 10.1073/pnas.94.15.7965

Holzberg, S., Brosio, P., Gross, C., and Pogue, G. P. (2002). Barley stripe mosaic virus-induced gene silencing in a monocot plant. *Plant J.* 30, 315–327. doi: 10.1046/j.1365-313X.2002.01291.x

Inada, N., and Ueda, T. (2014). Membrane trafficking pathways and their roles in plant–microbe interactions. *Plant Cell Physiol.* 55, 672–686. doi: 10.1093/pcp/pcu046

Jones, P., Binns, D., Chang, H.-Y., Fraser, M., Li, W., McAnulla, C., et al. (2014). InterProScan 5: genome-scale protein function classification. *Bioinformatics* 30, 1236–1240. doi: 10.1093/bioinformatics/btu031

Kalde, M., Nühse, T. S., Findlay, K., and Peck, S. C. (2007). The syntaxin SYP132 contributes to plant resistance against bacteria and secretion of pathogenesis-related protein 1. *Proc. Natl. Acad. Sci. U.S.A.* 104, 11850–11855. doi: 10.1073/pnas.0701083104

Kang, Z., and Li, Z. (1984). Discovery of a normal T. type new pathogenic strain to Lovrin10. *Acta Cllegii Septent. Occident. Agric.* 4, 18–28.

Krogh, A., Larsson, B., Von Heijne, G., and Sonnhammer, E. L. (2001). Predicting transmembrane protein topology with a hidden Markov model: application to complete genomes. *J. Mol. Biol.* 305, 567–580. doi: 10.1006/jmbi.2000.4315

Kwon, C., Neu, C., Pajonk, S., Yun, H. S., Lipka, U., Humphry, M., et al. (2008). Co-option of a default secretory pathway for plant immune responses. *Nature* 451, 835–840. doi: 10.1038/nature06545

Larkin, M. A., Blackshields, G., Brown, N., Chenna, R., McGettigan, P. A., McWilliam, H., et al. (2007). Clustal W and Clustal X version 2.0. *Bioinformatics* 23, 2947–2948. doi: 10.1093/bioinformatics/btm40

Levine, A., Belenghi, B., Damari-Weisler, H., and Granot, D. (2001). Vesicle-associated membrane protein of *Arabidopsis* suppresses Bax-induced apoptosis in yeast downstream of oxidative burst. *J. Biol. Chem.* 276, 46284–46289. doi: 10.1074/jbc.M107375200

Leyman, B., Geelen, D., Quintero, F. J., and Blatt, M. R. (1999). A tobacco syntaxin with a role in hormonal control of guard cell ion channels. *Science* 283, 537–540. doi: 10.1126/science.283.5401.537

Lipka, V., Kwon, C., and Panstruga, R. (2007). SNARE-ware: the role of SNARE-domain proteins in plant biology. *Annu. Rev. Cell Dev. Biol.* 23, 147–174. doi: 10.1146/annurev.cellbio.23.090506.123529

Livak, K. J., and Schmittgen, T. D. (2001). Analysis of relative gene expression data using real-time quantitative PCR and the $2^{-\Delta\Delta CT}$ method. *Methods* 25, 402–408. doi: 10.1006/meth.2001.1262

Moreno, S., Klar, A., and Nurse, P. (1991). Molecular genetic analysis of fission yeast *Schizosaccharomyces pombe*. *Methods Enzymol.* 194, 795–823. doi: 10.1016/0076-6879(91)94059-L

Nowara, D., Gay, A., Lacomme, C., Shaw, J., Ridout, C., Douchkov, D., et al. (2010). HIGS: host-induced gene silencing in the obligate biotrophic fungal pathogen *Blumeria graminis*. *Plant Cell* 22, 3130–3141. doi: 10.1105/tpc.110.077040

Suwastika, I. N., Uemura, T., and Shiina, T. (2008). SYP71, a plant-specific Qc-SNARE protein, reveals dual localization to the plasma membrane and the endoplasmic reticulum in *Arabidopsis*. *Cell Struct. Funct.* 33, 185–192. doi: 10.1247/csf.08024

Tamura, K., Stecher, G., Peterson, D., Filipski, A., and Kumar, S. (2013). MEGA6: molecular evolutionary genetics analysis version 6.0. *Mol. Biol. Evol.* 30, 2725–2729. doi: 10.1093/molbev/mst197

Thordal-Christensen, H., Zhang, Z., Wei, Y., and Collinge, D. B. (1997). Subcellular localization of H_2O_2 in plants. H_2O_2 accumulation in papillae and hypersensitive response during the barley-powdery mildew interaction. *Plant J.* 11, 1187–1194. doi: 10.1046/j.1365-313X.1997.11061187.x

Uemura, T., Kim, H., Saito, C., Ebine, K., Ueda, T., Schulze-Lefert, P., et al. (2012). Qa-SNAREs localized to the trans-Golgi network regulate multiple transport pathways and extracellular disease resistance in plants. *Proc. Natl. Acad. Sci. U.S.A.* 109, 1784–1789. doi: 10.1073/pnas.1115146109

Uemura, T., Ueda, T., Ohniwa, R. L., Nakano, A., Takeyasu, K., and Sato, M. H. (2004). Systematic analysis of SNARE molecules in *Arabidopsis*: dissection of the post-Golgi network in plant cells. *Cell Struct. Funct.* 29, 49–65. doi: 10.1247/csf.29.49

Wang, C.-F., Huang, L.-L., Buchenauer, H., Han, Q.-M., Zhang, H.-C., and Kang, Z.-S. (2007). Histochemical studies on the accumulation of reactive oxygen species (O_2^- and H_2O_2) in the incompatible and compatible interaction of wheat- *Puccinia striiformis* f. sp. *tritici*. *Physiol. Mol. Plant Pathol.* 71, 230–239. doi: 10.1016/j.pmpp.2008.02.006

Wang, X., Tang, C., Zhang, G., Li, Y., Wang, C., Liu, B., et al. (2009). cDNA-AFLP analysis reveals differential gene expression in compatible interaction of wheat challenged with *Puccinia striiformis* f. sp. *tritici*. *BMC Genomics* 10:289. doi: 10.1186/1471-2164-10–289

Wang, X., Wang, X., Deng, L., Chang, H., Dubcovsky, J., Feng, H., et al. (2014). Wheat TaNPSN SNARE homologues are involved in vesicle-mediated resistance to stripe rust (*Puccinia striiformis* f. sp. *tritici*). *J. Exp. Bot.* 65, 4807–4820. doi: 10.1093/jxb/eru241

Wang, Y., Qu, Z., Zhang, Y., Ma, J., Guo, J., Han, Q., et al. (2008). Construction of a cDNA library and analysis of expressed sequence tags in association with the incompatible interaction between wheat and *Puccinia striiformis*. *Sci. Agric. Sin.* 41, 3376–3381. doi: 10.3864/j.issn.0578-1752.2008.10.061

Wei, T., Zhang, C., Hou, X., Sanfaçon, H., and Wang, A. (2013). The SNARE protein Syp71 is essential for turnip mosaic virus infection by mediating fusion of virus-induced vesicles with chloroplasts. *PLoS Pathog.* 9:e1003378. doi: 10.1371/journal.ppat.1003378

Zhang, X., Zhao, H., Gao, S., Wang, W.-C., Katiyar-Agarwal, S., Huang, H.-D., et al. (2011). *Arabidopsis Argonaute* 2 regulates innate immunity via miRNA393*-mediated silencing of a Golgi-localized SNARE gene MEMB12. *Mol. Cell.* 42, 356–366. doi: 10.1016/j.molcel.2011.04.010

Zhu, J., Gong, Z., Zhang, C., Song, C. -P., Damsz, B., Inan, G., et al. (2002). OSM1/SYP61: a syntaxin protein in *Arabidopsis* controls abscisic acid–mediated and non-abscisic acid–mediated responses to abiotic stress. *Plant Cell* 14, 3009–3028. doi: 10.1105/tpc.006981

Conflict of Interest Statement: The authors declare that the research was conducted in the absence of any commercial or financial relationships that could be construed as a potential conflict of interest.

frontiers in Plant Science

ORIGINAL RESEARCH
published: 21 June 2016
doi: 10.3389/fpls.2016.00873

TaTypA, a Ribosome-Binding GTPase Protein, Positively Regulates Wheat Resistance to the Stripe Rust Fungus

Peng Liu†, Thwin Myo†, Wei Ma, Dingyun Lan, Tuo Qi, Jia Guo, Ping Song, Jun Guo and Zhensheng Kang**

State Key Laboratory of Crop Stress Biology for Arid Areas, College of Plant Protection, Northwest A&F University, Yangling, China

Tyrosine phosphorylation protein A (TypA/BipA) belongs to the ribosome-binding GTPase superfamily. In many bacterial species, TypA acts as a global stress and virulence regulator and also mediates resistance to the antimicrobial peptide bactericidal permeability-increasing protein. However, the function of *TypA* in plants under biotic stresses is not known. In this study, we isolated and functionally characterized a stress-responsive *TypA* gene (*TaTypA*) from wheat, with three copies located on chromosomes 6A, 6B, and 6D, respectively. Transient expression assays indicated chloroplast localization of TaTypA. The transcript levels of *TaTypA* were up-regulated in response to treatment with methyl viologen, which induces reactive oxygen species (ROS) in chloroplasts through photoreaction, cold stress, and infection by an avirulent strain of the stripe rust pathogen. Knock down of the expression of *TaTypA* through virus-induced gene silencing decreased the resistance of wheat to stripe rust accompanied by weakened ROS accumulation and hypersensitive response, an increase in *TaCAT* and *TaSOD* expression, and an increase in pathogen hyphal growth and branching. Our findings suggest that *TaTypA* contributes to resistance in an ROS-dependent manner.

Keywords: TypA, *Puccinia striiformis* f. sp. *tritici*, ROS, virus-induced gene silencing, *Triticum aestivum*, tyrosine phosphorylation

OPEN ACCESS

Edited by:
Pietro Daniele Spanu, Imperial College London, UK

Reviewed by:
Raffaella Balestrini, Consiglio Nazionale delle Ricerche, Italy
Marc Tad Nishimura, Colorado State University, Fort Collins, USA

****Correspondence:***
Jun Guo
guojunwgq@nwsuaf.edu.cn;
Zhensheng Kang
kangzs@nwsuaf.edu.cn

† These authors have contributed equally to this work.

Specialty section:
This article was submitted to Plant Biotic Interactions, a section of the journal Frontiers in Plant Science

Received: *18 March 2016*
Accepted: *02 June 2016*
Published: *21 June 2016*

Citation:
Liu P, Myo T, Ma W, Lan D, Qi T, Guo J, Song P, Guo J and Kang Z (2016) TaTypA, a Ribosome-Binding GTPase Protein, Positively Regulates Wheat Resistance to the Stripe Rust Fungus. Front. Plant Sci. 7:873. doi: 10.3389/fpls.2016.00873

INTRODUCTION

During the growth of plants that are subjected to different environmental stresses, including drought, salinity, chilling, and metal toxicity as well as pathogen attack. In these biotic and abiotic stresses, reactive oxygen species (ROS) are generated in plants due to a disruption of cellular homeostasis (Sharma and Dubey, 2005; Srivastava and Dubey, 2011). ROS are comprised of free radicals, such as superoxide anion ($O_2^{\cdot -}$) and hydroxyl radical ($^{\cdot}OH$), as well as non-radical molecules, like hydrogen peroxide (H_2O_2) and singlet oxygen ($^1O_2$; Sharma and Dubey, 2005). Diverse mechanisms have been shown to be involved in pathogen-induced ROS production, including peroxidases and different oxidases (oxalate oxidase, amine oxidase, and NADPH oxidase; Pugin et al., 1997; Wojtaszek, 1997; Rea et al., 1998). The increased production of ROS during biotic and abiotic stresses can pose a threat to plant cells by causing oxidation of proteins, peroxidation of lipids, damage to nucleic acids, inhibition of enzymes, activation of the programmed cell death (PCD) pathway, and ultimately lead to death of the cells. ROS act as more likely cofactors in redox reactions taking part in various roles in plant defenses (Torres, 2010). For example, ROS have been characterized as primary signaling molecules modulating multiple physiological processes during

plant growth and development (De Tullio, 2010). Intriguingly, evolutionary considerations based on the NADPH gene family imply that mechanisms detoxifying ROS were acquired before the plants used ROS as signaling molecules (Mittler et al., 2011). The reasons that make ROS important signaling regulators are: (i) rapid control over the production and scavenging of ROS in individual cells, allowing a dynamic control of ROS levels; (ii) accumulation of ROS in different subcellular organelles, resulting in an efficient intracellular control; (iii) rapid propagation of ROS-induced signaling from the origin of the stimuli to nearby cells; (iv) interaction and modification of a variety of targets by ROS (Mittler et al., 2011). Remarkably, plants exploit this versatility of ROS when responding to the environment and during biotic interactions (Scheler et al., 2013).

Tyrosine phosphorylation protein A (TypA/BipA) is a member of the ribosome-binding GTPase superfamily. GTPases are widely distributed molecular switches found across all bacterial species (Robinson, 2008) and are involved in the regulation of multiple cellular processes, including protein translocation, translation, tRNA modification, ribosome biogenesis and assembly, cell polarity, cell division and diverse signaling events (Verstraeten et al., 2011). Translational GTPases (trGTPases) are involved in GTPase activity that is induced by the large ribosomal subunit of bacterial species (Ramakrishnan, 2002; Nilsson and Nissen, 2005; Margus et al., 2007). A few members of trGTPases family, such as EF-G, EF-Tu, IF2 and RF3, bind to an overlapping site on the ribosome (Sergiev et al., 2005). TypA/BipA was firstly identified in *Salmonella typhimurium* as a protein induced by the antimicrobial peptide bactericidal permeability-increasing protein (BPI; Qi et al., 1995). Previous studies suggested that TypA has an effect on expression of the global regulator Fis by destabilizing unusually strong interactions between the 5′-untranslated region of *fis* mRNA and the ribosome. TypA binding to ribosomes at a site in accordance with that of EF-G indicated that GTPase activity of TypA is sensitive to high GDP:GTP ratios (Owens et al., 2004). Several studies showed that TypA is involved in regulating diverse virulence-related mechanisms in *Escherichia coli*, including flagella-mediated cell motility and cytoskeletal rearrangements in host epithelial cells (Farris et al., 1998), capsule synthesis and expression of genes from different pathogenicity islands (Grant et al., 2003). TypA is necessary for survival of *Sinorhizobium meliloti* under some stress conditions, such as low pH, low temperature, and treatment with sodium dodecyl sulfate (SDS; Kiss et al., 2004) and is required for growth of *E. coli* K12 at low temperatures (Pfennig and Flower, 2001). TypA are widely distributed in plants and are present in green algae, mosses, liverworts, gymnosperms, and angiosperms (Barak and Trebitsh, 2007). Recently, Atkinson (2015) identified a previously unreported TypA subfamily (mTypA) which are mitochondrially targeted according to transit peptide predictions in some Archaeplastida, Amoebozoa, and fungi (Atkinson, 2015). *TypA* genes also have roles in pollen tube growth in *Arabidopsis* (Lalanne et al., 2004) and in development of male reproductive organs in cucumber (Barak and Trebitsh, 2007). SsTypA was proposed as a new member of the ROS-scavenging system in the chloroplast of *Suaeda salsa* when subjected to environmental stress (Wang et al., 2008). However, little is known about the functions of *TypA* gene in plant defense against pathogens.

Wheat stripe rust, caused by *Puccinia striiformis* f. sp. *tritici* (*Pst*), is a destructive disease of wheat (*Triticum aestivum*) worldwide (Hau and de Vallavieille-Pope, 2006). The fungus is a strict biotroph and is dependent on living host cells for growth and survival. This life style has hindered study of the molecular mechanisms involved in the wheat-*Pst* interaction. In a previous study, to isolate defense-related genes against the fungus, we constructed an incompatible suppression subtractive hybridization (SSH) cDNA library of wheat leaves infected by *Pst* and identified a cDNA fragment exhibiting high homology to the rice TypA protein (Yu et al., 2010). In the present work, we identified a wheat *TypA* homolog, designated *TaTypA*. The transcript profile of *TaTypA* was analyzed in wheat seedlings inoculated with *Pst* and in plants subjected to environmental stimuli, and the subcellular localization of *TaTypA* was determined. Furthermore, knock down of *TaTypA* in wheat was performed to analyze whether and how *TaTypA* participates in resistance to stripe rust. Our results demonstrated that *TaTypA* performs a positive function in resistance by regulating ROS-induced signaling.

MATERIALS AND METHODS

Plant Materials, Fungal Pathogens, and Treatments

Wheat cv. Suwon 11 (Su11) and isolates of *Pst* pathotypes CYR23 (avirulent) and CYR31 (virulent) were used in the study. Su11, carrying the *YrSu* resistance gene, expresses a typical hypersensitive response (HR) to CYR23, but is susceptible to CYR31 (Cao et al., 2002). Wheat seedlings were grown, inoculated and maintained following procedures and conditions described previously (Kang et al., 2002). For RNA isolation wheat leaves were collected at 0, 12, 24, 36, 48, 72, 96, and 120 h post-inoculation (hpi) with CRY23 or CYR31. The time points were selected based on a microscopic study of the interactions between Su11 with CYR23 and CYR31 (Kang et al., 2002; Wang et al., 2007). A methyl viologen (MV) concentration gradient assay was conducted to induce oxidative stress, whereby 10-days-old wheat seedlings were sprayed with 0.1, 1, or 5 mM MV. Samples were collected at 0, 4, 6, 8, 12, and 24 h hpt. Control wheat seedlings were treated with sterile distilled water in both treatments. Ten-days-old wheat seedlings were placed in a 4°C chamber for low-temperature treatment. Roots of 10-days-old wheat seedlings were soaked in 20% PEG 6000 for the drought stress treatment, or in 200 mM NaCl to induce salt stress. The first leaves of the treated and control plants treated with sterile distilled water were collected at 0, 6, 12, and 24 hpt. Three biological replicates were included in each assay. Tissues harvested from all treatments were immediately frozen in liquid nitrogen and stored at −80°C until the extraction of total RNA.

Identification and Sequence Analysis of the *TaTypA* Gene

A 433-bp unisequence (GenBank accession number EV253998) exhibiting high homology to a putative TypA *Oryza sativa* GTP-binding protein was obtained from the *Pst*-induced SSH cDNA library (Yu et al., 2010) and used as a query sequence to screen EST databases of wheat constructed in our laboratory (Ma et al., 2009). Homologous wheat EST clones were retrieved and assembled, and according to the assembled sequence, we designed the TaTypA-F and TaTypA-R primers (**Supplementary Table S1**) to amplify *TaTypA*. The amplified product was cloned into the pGEM-T Easy Vector (Promega, Madison, WI, USA) for sequencing. This cDNA product was aligned with the wheat cv. Chinese Spring (CS) genome using data of the International Wheat Genome Sequencing Consortium[1]. The predicted chromosomal location and related sequences were also obtained from this website. The cDNA sequences were analyzed with ORF Finder[2] and the BLAST[3] programs. The amino acid sequence was analyzed with Pfam[4], InterProScan[5] and PROSITE Scan[6] to identify conserved domains. Multiple sequence alignment was performed with ClustalW2.0 (Chenna et al., 2003) and DNAMAN7.0 software (Lynnon Biosoft, USA), and a phylogenetic tree of alignment of amino acid sequences was generated with Mega 5.0 software (Tamura et al., 2011).

RNA Extraction, cDNA Synthesis, and qRT-PCR

Total RNA was extracted with the Trizol^{TM} Reagent (Invitrogen, Carlsbad, CA, USA) following the manufacturer's instructions. Three μg of RNA were subjected to first strand cDNA synthesis with the Promega RT-PCR system (Promega, Madison, WI, USA) and Oligo (dT) 18 primer. Relative quantification of *TaTypA* expression was performed with a SYBR Green qRT-PCR mixture on an ABI prism 7500 sequence detection system (Applied Biosystems, USA). Specific primers (**Supplementary Table S1**) were designed and qRT-PCR was conducted according to previously described procedures (Wang et al., 2009). The wheat translation elongation factor *TaEF-1α* (GenBank Accession number Q03033) was used as an internal reference for normalization. Dissociation curves were produced for each reaction to ensure specific amplification. Threshold Ct values were generated from the ABI PRISM 7500 Software Tool (Applied Biosystems) to quantify relative gene expression. Transcript levels of *TaTypA* were calculated by the comparative $2^{-\Delta\Delta CT}$ method (Livak and Schmittgen, 2001). Transcript abundance was assessed from three independent biological replicates.

[1]http://wheat-urgi.versailles.inra.fr/Seq-Repository/BLAST

[2]http://www.ncbi.nlm.nih.gov/gorf/gorf.html

[3]http://www.ncbi.nlm.nih.gov/blast/

[4]http://pfam.xfam.org/

[5]http://www.ebi.ac.uk/interpro/search/sequence-search

[6]http://prosite.expasy.org/scanprosite/

Subcellular Location of TaTypA-GFP Fusion Protein and Western Blotting

Protoplasts for subcellular localization of TaTypA protein were isolated from mesophyll tissue of 1-week-old wheat seedlings as previously described (Li et al., 2015). A recombinant plasmid, pCaMV35S::TaTypA::GFP, was constructed by cloning full-length cDNA and of *TaTypA* into a pCaMV35S::GFP vector by PCR using primers TaTyPA-163-F and TaTyPA-163-R (**Supplementary Table S1**). For analysis of the chloroplast transit peptide in TaTypA, the partial coding sequence (positions 1–240, 240 nt) at N-terminal was fused into pCaMV35S::GFP vector by PCR using primers TaTyPA-163-F and TaTyPA-163-R_N (**Supplementary Table S1**; pCaMV35S::TaTypA-N_{1-80}::GFP). Wheat mesophyll protoplasts were then transformed by the polyethylene glycol (PEG) transfection method using the plasmid DNA of pCaMV35S::TaTypA::GFP and pCaMV35S::TaTypA-N_{1-80}::GFP, pCaMV35S::GFP as the control. The PEG-transfected mesophyll protoplasts were incubated in W5 solution in a dark chamber at 23°C for 18 h, and GFP fluorescence was observed under a confocal laser scanning microscope (Zeiss LSM 700, Germany) as previously described (Ito and Shinozaki, 2002).

The total protein in the protoplast pellet was extracted with protein extraction kits (Solarbio, Beijing, China) following the manufacturer's instructions. Western blotting assays were performed using the total protein by 12% SDS-PAGE. After the proteins were transferred to nitrocellulose membranes (Millipore), the membranes were incubated in blocking buffer (0.05% Tween 20 and 5% non-fat milk powder in TBS). GFPs were detected using mouse-derived GFP-antibodies (Sungene, Tianjing, China) diluted in blocking buffer at 1:5000 overnight at 4°C. Membranes were washed and incubated with horseradish peroxidase-conjugated antimouse secondary antibody (Sungene, Tianjing, China) diluted at 1:10,000 and chemiluminescence substrate for detection (Sigma, Tokyo, Japan).

BSMV-Mediated TaTypA Gene Silencing

cDNA fragments of *TaTypA* with *Not*I and *Pac*I restriction sites were obtained by reverse transcription PCR to modify the original BSMV:γ vector for gene silencing as previously described (Holzberg et al., 2002). The fragments show no similarity with any other wheat gene in BLAST analyses, indicating their specificity. Capped *in vitro* transcripts of BSMV RNAs were prepared from the linearized plasmids (Petty et al., 1990) γ-TaPDS-as, γ-TaTypA-as, γ, α, β using a Message T7 *in vitro* transcription kit (Ambion, Austin, TX, USA) according to the manufacturer's protocol; 2.5 μl of each transcript, including BSMV RNAs α, β and genetically modified γ, were added to 42.5 μl of FES buffer (0.1 M glycine, 0.06 M K_2HPO_4, 1% w/v tetrasodium pyrophosphate, 1% w/v bentonite, and 1% w/v celite, pH 8.5) and inoculated into the second leaves of two-leaf wheat seedlings by gentle rubbing of the surface with a gloved finger (Scofield et al., 2005). After 24 h of incubation in a dark, humid environment, the seedlings were maintained in a growth chamber at 25°C with a 16 h photoperiod, and virus symptoms were

monitored at regular intervals. Recombinant virus BSMV:TaPDS-as was used as a positive control in all experiments. Mock-treated plants were inoculated with 1× Fes buffer as a negative control. When virus symptoms were observed at 10 days post-viral inoculation, symptom phenotypes were photographed, and the fourth seedling leaves were inoculated with fresh urediniospores of *Pst* pathotypes CYR23 or CYR31. For RNA isolation and histological observation, leaves were sampled at 0, 24, 48, and 120 hpi with CYR23. The *Pst* infection phenotypes were also photographed at 15 dpi. This experiment was conducted with three independent biological replications.

Histology of Fungal Growth and Host Response

Wheat leaves infected with BSMV were sampled at 24, 48, and 120 hpi with *Pst* and stained as described (Wang et al., 2007). The fourth leaves pre-infected with BSMV were sampled at 24, 48, and 120 hpi with *Pst* race CYR23. The areas of necrosis in infected leaves were estimated by auto-fluorescence of mesophyll cells. Hyphal length and hyphal branches were examined under blue light excitation by epi-fluorescence microscopy (excitation filter, 485 nm; dichromic mirror, 510 nm; and barrier filter, 520 nm). H_2O_2 accumulation was detected by staining with 3,3′-diaminobenzidine (DAB; Amresco, Solon, OH, USA) as previously described (Wang et al., 2007), then viewed by differential interference contrast optics. Only a site where an appressorium had formed over a stoma was considered to be successfully penetrated. At least 50 infection sites were examined on each of five randomly selected leaf segments for each treatment. Necrotic areas, areas of H_2O_2 accumulation, and hyphal length were observed with an Olympus BX-53 microscope (Olympus, Corp., Tokyo) and estimated with DP2-TWAIN/DP2-BSW software. Statistical analysis was performed by Tukey's HSD test ($P < 0.05$) with the use of SPSS software (SPSS, Inc., Chicago, IL, USA).

RESULTS

Cloning and Structural Features of *TaTypA*

A wheat 2,278-bp homolog of tyrosine phosphorylation protein A, first identified *in silico*, was obtained. It had an open reading frame (ORF) of 2,028 bp and was designated as *TaTypA* (GenBank accession number KF309066). Sequence alignment in the Chinese Spring genome database indicated that each sub-genome (A, B, or D) contained more than three sequences, each lacking the full *TaTypA* coding sequence likely due to incomplete Chinese Spring genome sequences. However, all sub-genomic sequences were localized on the long arm of chromosomes 6A, 6B, and 6D (data not shown). To better understand *TaTypA* characteristics in the wheat genome, the exon of each sub-genomic sequence was selected and assembled artificially, designated *TaTypA-6A*, *TaTypA-6B,* and *TaTypA-6D*, respectively (**Supplementary Figure S1**). The *TaTypA* gene from wheat cv. Su11 exhibited 98.67, 77.78 and 98.52% identities with the sequences from *TaTypA-6A*, *TaTypA-6B,* and *TaTypA-6D*, respectively (**Supplementary Figure S1**). TaTypA-6A and TaTypA-6D contain only a few amino acid variations relative to TaTypA from Su11, whereas TaTypA-6B contains 101- and 48-aa deletions (**Supplementary Figure S2**). We concluded that the wheat genome contains three homologous copies of *TaTypA* located on the long arms of chromosomes 6A, 6B, and 6D.

Sequence analysis indicated that *TaTypA* encodes a putative protein composed of 675 amino acid residues, a molecular weight of 74.25 kDa, and an isoeletric point (pI) of 5.65. Multi-sequence alignment with TypA from other higher plants showed that Su11 TaTypA shares highest identity (94.09%) with TypA from *Brachypodium distachyon*. In addition, TaTypA shared 89, 75, and 74% identity with OsTypA, SsTypA1, and AtTypA, respectively (**Supplementary Figure S3**). Structural analysis showed that TaTypA has three conserved regions, including an ATP/GTP-binding motif, a GTP-binding elongation factor signature, and a putative ribosome-binding domain (**Supplementary Figure S3**). Conserved tyrosine residues were also present.

TypA/BipA proteins from different organisms were selected to study the evolutionary relationships of TypA homologs. The neighbor-joining phylogenetic tree (**Figure 1**) showed that the proteins share a common ancestor with bacterial TypA and can be grouped into four groups. Plant TypA proteins formed a monophyletic group containing monocot and eudicot subgroups. TaTypA, together with OsTypA from *Oryza sativa* and BdTypA from *B. distachyon*, constituted a monocot subgroup. Homologous proteins from dicotyledonous plants clustered into another group. The short branch length (**Figure 1**) indicated that TypA proteins from different organisms share close evolutionary relationships.

TaTypA Is Mainly Localized in Chloroplasts of Wheat Cells

To determine the subcellular localization of TaTypA in wheat, recombinant pCaMV35S::TaTypA::GFP and pCaMV35S::TaTypA-N_{1-80}::GFP were transfected into wheat mesophyll protoplasts by transfection. The empty pCaMV35S::GFP vector was used as a control. GFP was ubiquitously distributed throughout the cell, including in the nucleus (**Figure 2**). pCaMV35S::TaTypA::GFP and pCaMV35S::TaTypA-N_{1-80}::GFP fusion proteins were mainly targeted to the chloroplasts of wheat cells (**Figure 2**). To further confirm this result, a Western blot was performed using GFP antibodies on the subcellular fractions of pCaMV35S::GFP, pCaMV35S::TaTypA::GFP, and pCaMV35S::TaTypA-N_{1-80}::GFP transfected wheat protoplasts. Bands of 28-, 107-, and 35-kDa were detected, suggesting that GFP, TapA-GFP and TaTypA-N_{1-80}-GFP was expressed in wheat cells (**Supplementary Figure S4**). These results from fluorescence microscope and Western blot analysis indicated that TaTypA-GFP was targeted to wheat chloroplast.

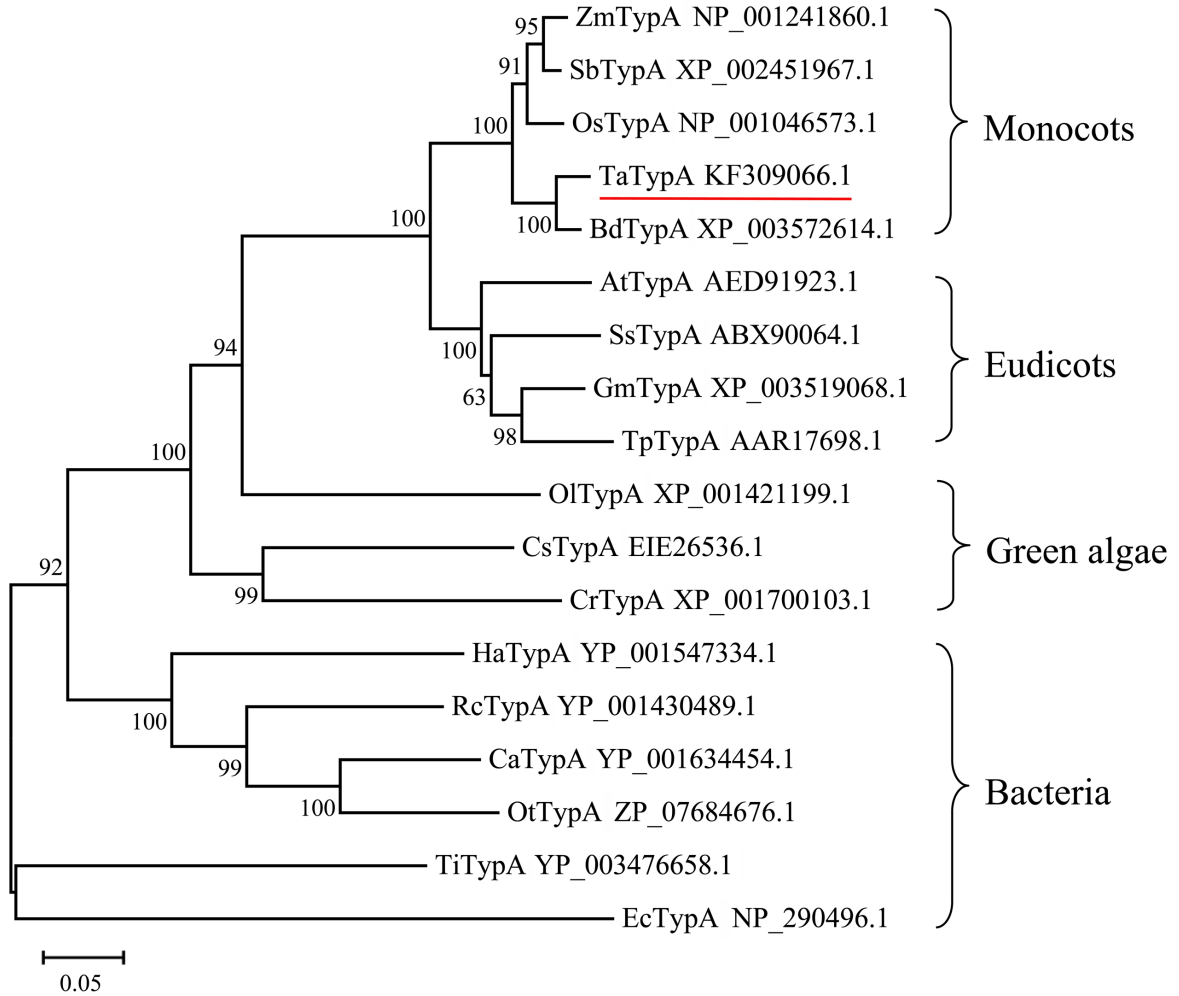

FIGURE 1 | Neighbor-joining tree of TypA protein sequences based on multiple alignments. The number above the internal branches indicates bootstrap values estimated based on 1,000 replications. Scale bar represents the estimated number of amino acid substitutions per site. Branches are labeled with protein names and GenBank accession numbers. Ta, *Triticum aestivum*; Bd, *Brachypodium distachyon*; Os, *Oryza sativa*; Zm, *Zea mays*; Sb, *Sorghum bicolor*; Gm, *Glycine max*; Ss, *Suaeda salsa*; At, *Arabidopsis thaliana*; Tp, *Trifolium pretense*; Ol, *Ostreococcus lucimarinus*; Cs, *Coccomyxa subellipsoidea*; Cr, *Chlamydomonas reinhardtii*; Ca, *Chloroflexus aurantiacus*; Rc, *Roseiflexus castenholzii*; Ha, *Herpetosiphon aurantiacus*; Ot, *Oscillochloris trichoides*; Ti, *Thermoanaerobacter italicus*; Ec, *Escherichia coli*.

Transcript Profiles of *TaTypA* in Response to Oxidative Stress and Abiotic Stress

When treated with MV, a superoxide anion propagator, the wheat seedlings wilted due to oxidative stress (**Supplementary Figure S5**). Wheat seedlings treated with 5 mM MV rapidly showed damping off symptoms, whereas seedlings treated with 0.1 mM MV were only slightly affected up to 12 hpt. However, seedlings treated with 1 mM MV expressed intermediate symptoms. Therefore, 1 mM MV was selected as a suitable concentration for the oxidative stress treatment. *TaTypA* transcripts were up-regulated and peaked as early as 4 hpt at a level approximately sixfold higher. The transcript level subsequently fell reaching the basal level at 6 and 8 hpt, but increased again at 12 hpt until 24 hpt (**Figure 3A**).

Considering the involvement of *TypA* in response to various abiotic stresses in *S. salsa*, we investigated the effects of various abiotic stresses on expression of *TaTypA*. The transcript level of *TaTypA* increased threefold at 6 h after low-temperature treatment and reached a maximum of about sevenfold higher than the base level at 12 hpt (**Figure 3B**). No significant change (less than twofold, $P > 0.05$) in *TaTypA* transcript was detected in wheat leaves after treatment with salt or PEG (**Figure 3B**).

Transcript Analysis of *TaTypA* in Response to *Pst*

To investigate whether *TaTypA* is involved in response to *Pst*, quantitative RT-PCR was used to analyze *TaTypA* transcript profiles in both compatible and incompatible interactions. In the incompatible combination, transcript levels were induced at 36

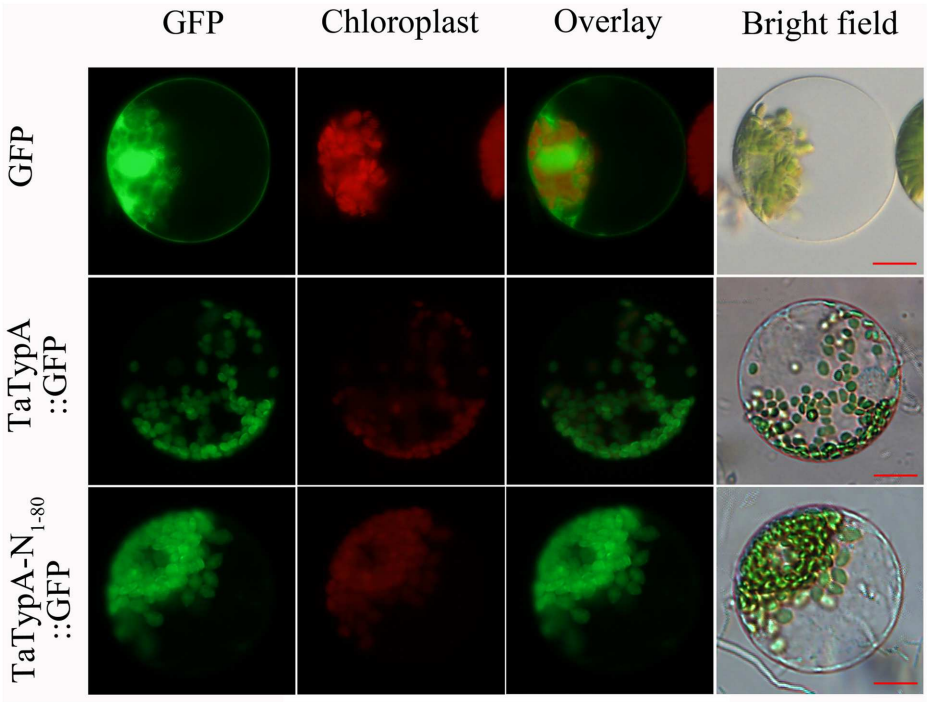

FIGURE 2 | Subcellular localization of TaTypA protein in wheat protoplasts. GFP signals are indicated by green color. All images were observed with a fluorescence microscope. Bar, 20 μm.

hpi and reached the highest level of 2.5-fold higher that in control plants at 96 hpi. In the compatible combination there was no significant change in relative *TaTypA* expression (**Figure 4**).

Suppression of *TaTypA* Enhances Susceptibility of Wheat to *Pst*

Virus-induced gene silencing (VIGS) is a rapid and effective reverse genetics approach in barley and wheat (Holzberg et al., 2002; Cakir and Scofield, 2008). To characterize in more detail the effect of the *TaTypA* gene in stripe rust response, BSMV-mediated VIGS was employed to silence the *TaTypA* gene(s). Su11 seedlings inoculated with BSMV:TaPDS-as exhibited strong photobleaching symptoms at 10 dpi. The presence of non-symptomatic new leaves in plants treated with Fes buffer under the same conditions indicated that silencing of *TaPDS* occurred specifically in BSMV:TaPDS-as infected plants. All wheat seedlings inoculated with BSMV: γ and BSMV:TypA-as displayed mild chlorotic mosaic symptoms on the third leaf at 10 dpi (**Figure 5A**), confirming that the BSMV-mediated gene silencing system functioned correctly and could be used in further experiments. Silencing efficiency assessed by qRT-PCR showed that *TaTypA* transcript levels were significantly reduced in *TaTypA* knock-down plants compared to control plants, with a reduction as high as 80% (**Figure 5B**). When fourth leaves of wheat plants were inoculated with the avirulent or virulent *Pst* races, an obvious HR was elicited by the avirulent CYR23 race on leaves pre-infected with BSMV:γ, BSMV:TaTypA-as and on mock-inoculated seedlings. Nevertheless, only limited fungal sporulation had occurred around the necrotic spots on leaves pre-infected with BSMV:TaTypA-as after 15 dpi compared to the other two treatments (**Figure 5C**). By contrast, wheat seedlings inoculated with virulent CYR31 showed normal disease development and numerous uredinia (**Figure 5D**). The specific fragment used in silencing is shown in **Supplementary Figure S1**. However, due to the high identity and similarity among the three copies, the silencing efficiency of each copy on A, B, and D could not be determined.

Pst Growth and Host Response

Leaf segments from at least three plants inoculated with CYR23 were harvested from each sample to examine detailed histological changes associated with the enhanced susceptibility in *TaTypA* knock-down plants. Areas of cell death were obvious at 24, 48, and 120 hpi by microscopy and were estimated by DP-BSW software (**Figure 6A**). The areas were significantly less in *TaTypA* knock-down plants than in BSMV:γ-infected plants at 48 and 120 hpi (**Figure 6B**). There was no obvious difference in hyphal growth and branching at 24 hpi between *TaTypA* knock-down and BSMV:γ plants (**Figures 6C,D**). However, hyphal length and branch number in BSMV:TaTypA-as infected leaves were significantly ($P < 0.05$) increased relative to those in BSMV:γ infected leaves at 48 and 120 hpi, respectively (**Figures 6C,D**). The collective histological results suggest that silencing of *TaTypA* weakened

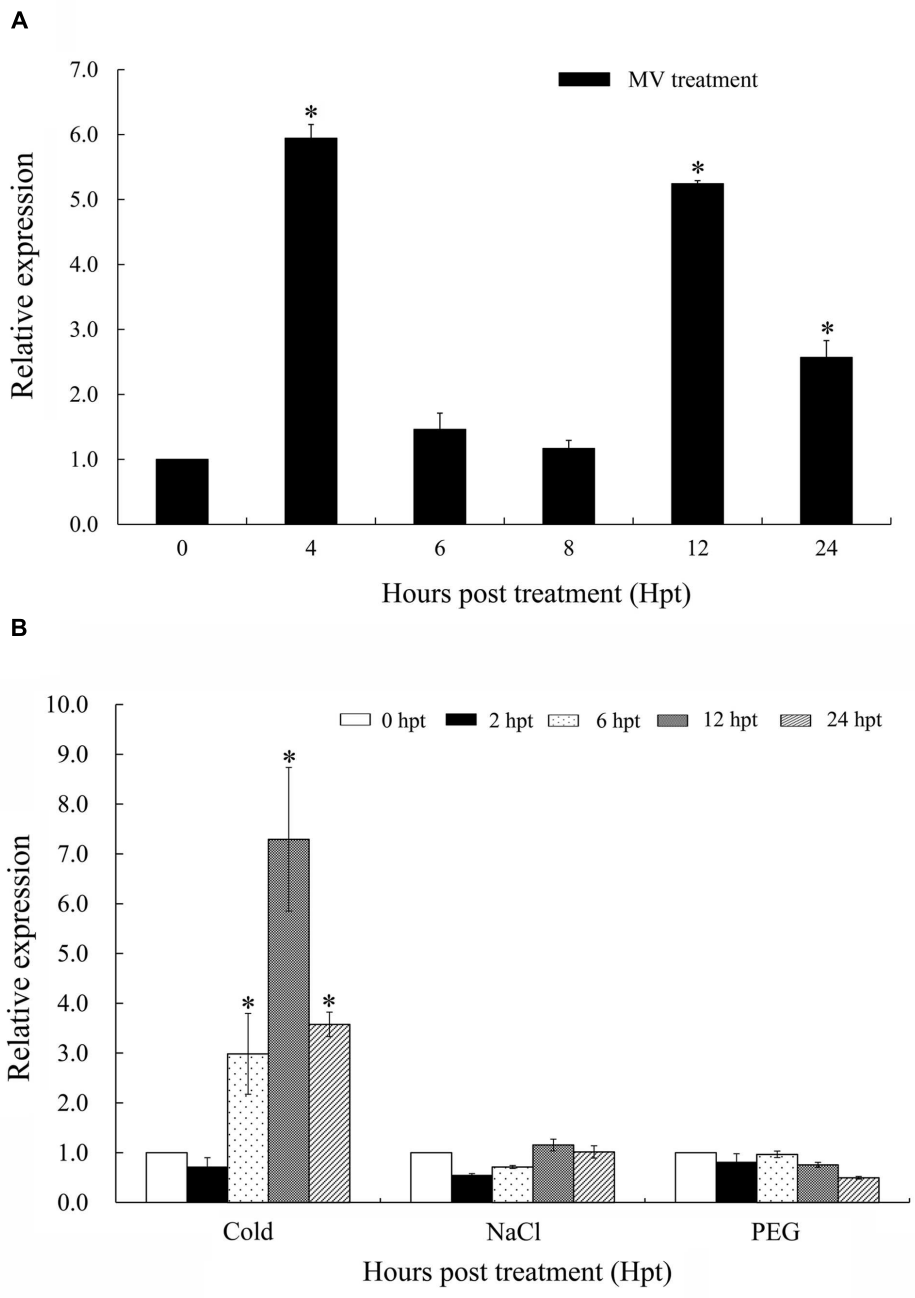

FIGURE 3 | Expression patterns of *TaTypA* in wheat leaves based on qRT-PCR analyses. (A) Expression levels of *TaTypA* in wheat leaves in response to MV treatment. **(B)** Expression profiles of TaTypA in wheat leaves after treatment with environmental stresses: low temperature (4°C), salt (NaCl), and drought (PEG). The expression levels were analyzed by qRT-PCR and normalized to the wheat elongation factor *TaEF-1a* gene. Means and standard deviations were based on three independent biological replicates. Asterisks indicate a significant difference ($P < 0.05$) from 0 hpt by Tukey's HSD test.

the resistance of in Su11 and permitted enhanced hyphal growth and branching. The transcription level of SA-induced marker gene *TaPR1* was significantly reduced in CYR23-infected *TaTypA* knock-down plants at 48 and 120 hpi, indicating a concurrent effect on defense-related gene expression (**Figure 6E**).

Weakened ROS Accumulation in *TaTypA* Knock-down Plants

Reactive oxygen species accumulation with the occurrence of HR occurs in the resistance response to rust fungi in wheat (Wang et al., 2007). The induction of H_2O_2 by infection in *TaTypA* knock-down plants was analyzed by histochemical

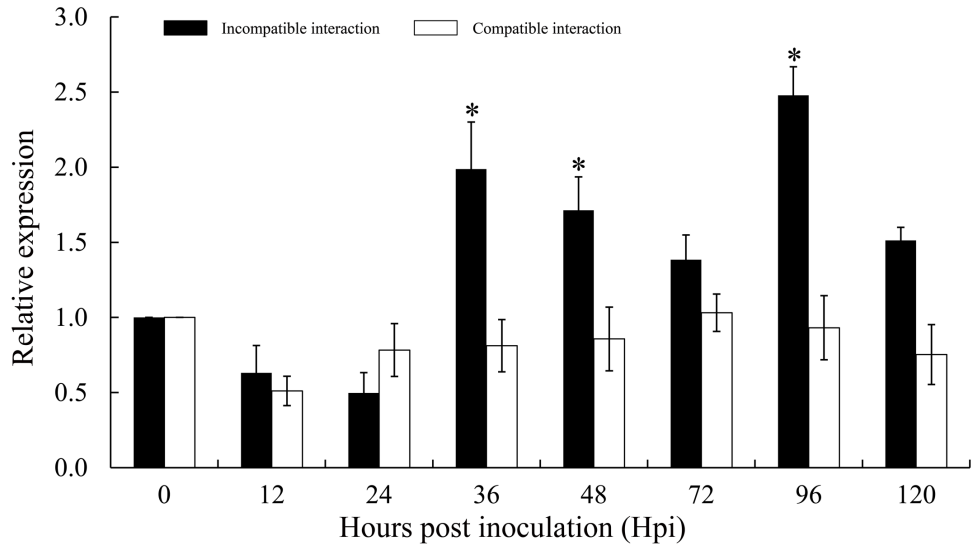

FIGURE 4 | Expression profiles of *TaTypA* in wheat leaves in response to virulent and avirulent *Pst* races. Wheat leaves inoculated with *Pst* isolates CYR23 (avirulent) and CYR31 (virulent) were sampled at 0, 6, 12, 24, 48, and 120 h post-inoculation. The data were normalized to the wheat *TaEF-1a* gene, and error bars represent the variation among three independent replicates. Asterisks indicate significant differences from 0 hpi using Tukey's HSD test ($P < 0.05$).

observation and colorimetric determination. H_2O_2 accumulation was significantly decreased in *TaTypA* knock-down plants compared to BSMV:γ infected plants at 48 and 120 hpi (**Figures 7A,B**). In addition, expression levels of the *TaCAT* and *TaSOD* genes involved in ROS-scavenging were significantly up-regulated in *TaTypA* knock down plants infected with CYR23 (**Figure 7C**).

DISCUSSION

TypA proteins are a novel class of stress tolerance-related proteins in all species ranging from prokaryotes to higher eukaryotes (Wang et al., 2008). In this study, we conducted molecular and functional analyses of wheat TaTypA in a wheat-*Pst* pathosystem.

As many as 87% of the genes in hexaploid wheat are triplicated across the A, B, and D sub-genomes (Pumphrey et al., 2009). Therefore, not unexpectedly there were three copies of *TaTypA* in the wheat genome. However, sequence alignment of three genomic copies of *TaTypA* showed that *TaTypA-6A*, *TaTypA-6B* and *TaTypA-6D* differed by sequence variation and deletion (**Supplementary Figure S1**). As described in previous reports, newly formed polyploids undergo a speciation process driven by combined effects of chromosomal re-patterning, gene deletion, mutation, suppression (silencing), or acquisition of modified gene function (Wendel, 2000). Thus, the differences in the three genomic copies of *TaTypA* are consistent with such events. Sequence analysis revealed that TaTypA is a typical member of the ribosome-binding GTPase superfamily, which is characterized by a ATP/GTP-binding motif, a GTP-binding elongation factor signature, and a putative ribosome-binding domain (Kiss et al., 2004). Phylogenetic analysis indicated that TypA proteins in plants form a monophyletic group, within which TaTypA and rice OsTypA constitute a subgroup (**Figure 1**). The presence of different subgroups within and between monocots and eudicots indicate possibilities for functional divergence between species and, in the case of allopolyploid plants, between sub-genomes.

In *S. salsa*, the SsTypA1-GFP fusion protein localized in the chloroplasts, and structural analysis revealed a chloroplast transit peptide sequence at the N-terminal part of the SsTypA1 protein (Wang et al., 2008). Without a chloroplast transit peptide the chloroplast localization of the protein was unexpected (Shi and Theg, 2013). In this study, we proved that the N-terminal region and the full length of TaTypA have the same subcellular localization as SsTypA1, indicating that the N-terminal region of TaTypA does contain a chloroplast transit peptide sequence. It has been confirmed that chloroplasts play a significant role in defense responses (de Torres Zabala et al., 2015). The chloroplast is a major source of ROS in plant cells and is responsible for producing the two signaling molecules required for pathogen responses, SA and jasmonic acid (Almagro et al., 2009). In addition, a few reports have shown that the resistance proteins are targeted to this organelle. For example, wheat stripe rust resistance protein WKS1 localized in chloroplasts and reduced the ability of the thylakoid-associated ascorbate peroxidase to detoxify ROS (Gou et al., 2015), and the chloroplastic/cytoplasmic protein NRIP1, which associated with the NB-LRR immune receptor "N", was shown to be responsible for *tobacco mosaic virus* recognition and resistance in *Nicotiana* (Caplan et al., 2008). In this study, ROS accumulation was reduced during *Pst* infection in TaTypA-knock down plants. Our data suggest that TaTypA is a new chloroplast-localized defense protein, which is involved in wheat resistance to *Pst*.

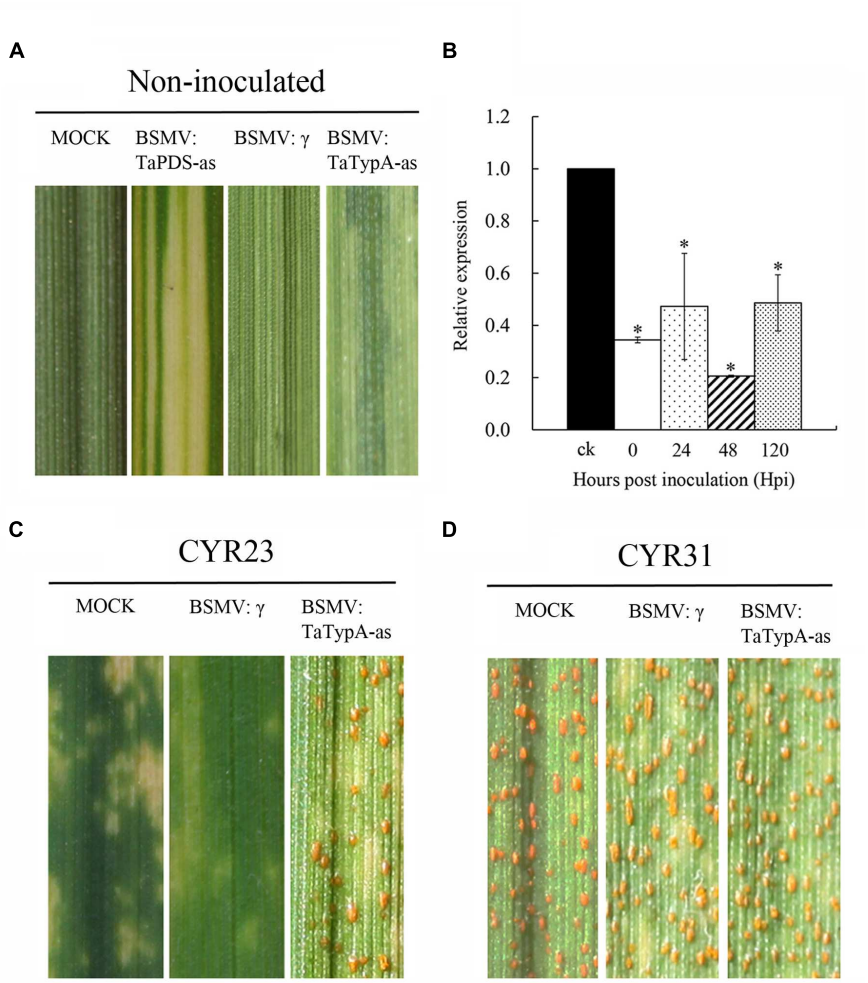

FIGURE 5 | Functional characterization of the *TaTypA* gene during interaction of wheat and *Pst* by BSMV-mediated gene silencing. (A) Mild chlorotic mosaic symptoms on the fourth leaves of seedlings inoculated with BSMV:γ, BSMV:TaPDS-as, and BSMV:TaTypA-as at 10 dpi. Mock: wheat leaves treated with 1× Fes buffer. **(B)** Relative transcript levels of *TaTypA* in *TaTypA* knock-down plants inoculated with CYR23. The data were normalized to the *TaEF-1a* gene. CK indicates BSMV:γ. Asterisks indicate significant differences from BSMV:γ using Tukey's HSD test ($P < 0.05$). Photographs of fourth leaves further inoculated with urediniospores of avirulent race CYR23 **(C)** or virulent race CYR31 **(D)**. Typical leaves were photographed at 15 dpi.

Reactive oxygen species can be produced in chloroplasts through photoreaction of the herbicide MV, a superoxide anion propagator (Scarpeci et al., 2008). Wheat not only wilted when treated with certain concentrations of MV (**Supplementary Figure S4**), but transcript levels of *TaTypA* were significantly elevated in wheat seedlings exposed to MV (**Figure 3A**). This response is similar to that of *SsTypA*, which showed pronounced activation in response to H_2O_2 treatment (Wang et al., 2008). ROS, such as superoxide, hydrogen peroxide, and hydroxyl radicals, were induced by drought, salt, and cold stress. The increased expression of *TaTypA* in response to cold stress (**Figure 3B**) may result from the excessive ROS generated. However, the transcript level of *TaTypA* was not significantly changed under salt or drought stress. As previous studies showed, the biphasic production of ROS consists of a primary phase that occurs within minutes and a secondary phase that occurs within hours/days under abiotic stress (Mittler et al., 2011). It seems that *TaTypA* was not involved in primary phase of ROS production under drought and cold stress. On the contrary, *SsTypA1* was induced by NaCl and mannitol (drought stress) treatments as early as 6 and 4 hpt, respectively (Wang et al., 2008). These differences in expression of *TaTypA* and *SsTypA1* may be associated with divergence of monocots and dicots or different treatment methods used. Different plant species are highly variable in response to environmental factors; an environmental condition that is harmful to one species may not be stressful for another (Munns and Tester, 2008). This is also evidenced by the multitude of different stress-response mechanisms. Hence, we propose that the functions of *TaTypA* and *SsTypA1* differ when plants are subjected to the same environmental stresses.

TypA/BipA proteins are widely distributed in all organisms. However, there has been little research on the functions of TypA proteins in plant disease responses. Our results in the present study indicated that *TaTypA* positively regulates

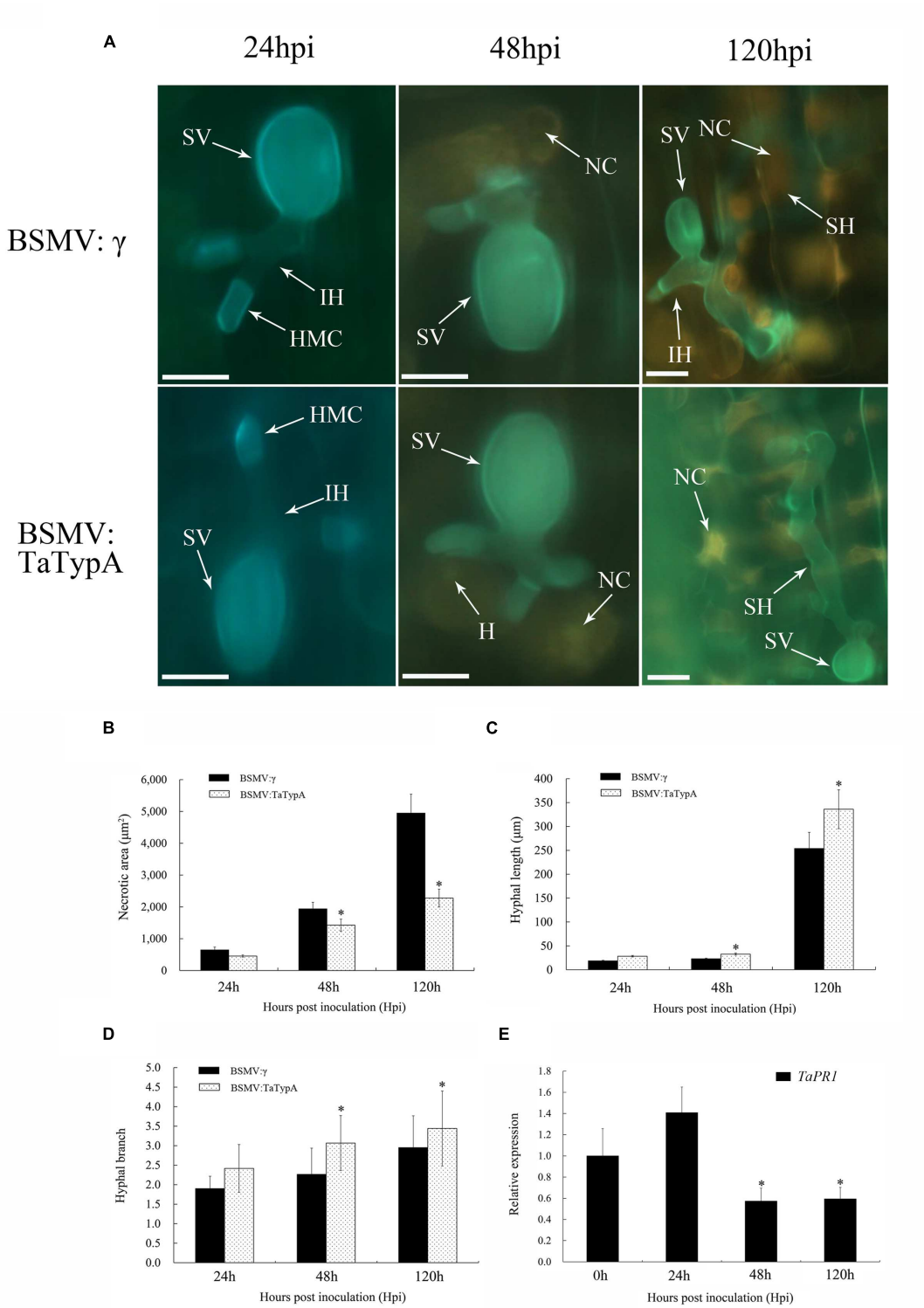

FIGURE 6 | Weakened wheat defense response in *TaTypA* knock-down plants challenged by avirulent *Pst* race CYR23. Wheat leaves previously treated with recombinant BSMV:γ or BSMV:TaTypA were inoculated with race CYR23. **(A)** Typical leaves were examined at 24, 48 and 120 hpi. The infection sites were observed by epifluorescence. HMC, haustorial mother cell; SV, substomatal vesicle; NC, necrotic cell death; IH, primary hyphae; SH, secondary hyphae. All results were obtained from 50 infection sites. Bar, 20 μm. **(B)** Necrotic cell death was quantified as the area of autofluorescence. **(C)** Hyphal lengths are means of the average distance from the junction of the substomatal vesicle to the hyphal tip. **(D)** Hyphal branch values are means of average numbers of primary hyphae. **(E)** Expression of *TaPR1* was assayed in *TaTypA* knock-down plants compared to controls. The data were normalized to the wheat *TaEF-1a* gene. Asterisks indicate a significant differences ($P < 0.05$) from BSMV:γ using the Tukey's HSD test.

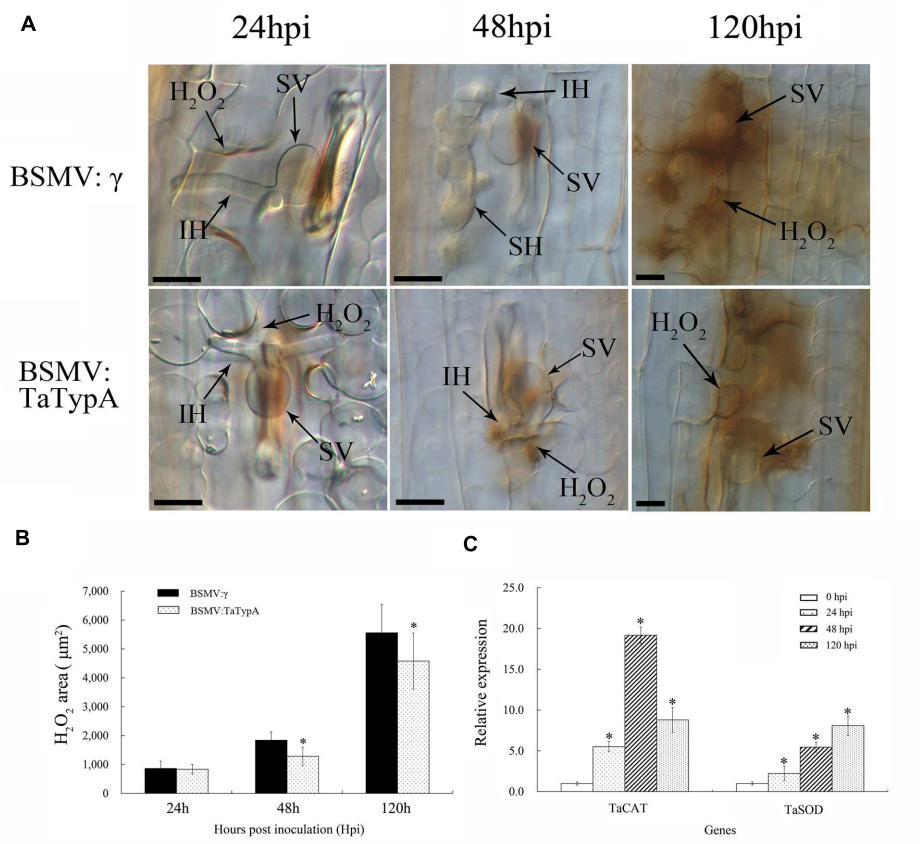

FIGURE 7 | Reduced H_2O_2 accumulation in *TaTypA* knock-down plants challenged by avirulent race CYR23. (A) Wheat leaves previously treated with recombinant BSMV:γ or BSMV:TaTypA were inoculated with *Pst* race CYR23. H_2O_2 accumulation at infection sites was detected by staining with 3,3′-diaminobenzidine (DAB). Infection sites were observed by light microscopy. SV, substomatal vesicle; IH, initial hyphae; SH, secondary hyphae. Bar, 20 μm. **(B)** The amount of H_2O_2 production was measured by calculating the DAB-stained area at each infection site using DP-BSW software. Values represent mean ± standard errors of three independent assays. **(C)** Expressions of two ROS-scavenging enzyme genes were assayed in *TaTypA* knock-down plants compared to control plants. The data were normalized to wheat the *TaEF-1a* gene. Asterisks indicate significant difference ($P < 0.05$) from BSMV:γ using Tukey's HSD test.

the response of wheat to *Pst*. Silencing of *TaTypA* reduced the level of race-specific immunity to *Pst* in *TaTypA* knock-down plants. In response to the avirulent *Pst* race CY23, *TaTypA* knock-down Su11 wheat plants expressed weakened resistance characterized by decreased necrotic area, reduced ROS accumulation and increased uredinia production. Previous histological and cytological observations revealed oxidative bursts during the early (12–24 h) and late (96–120 h) stages of infection in incompatible interactions between wheat and *Pst* (Wang et al., 2007). In contrast, the hyphae of *Pst* rapidly colonized host tissues during the compatible interaction without any detectable $O_2^{\cdot-}$ and H_2O_2 accumulation or HR. *TaTypA* expression was induced as early as 36 hpi and peaked at 96 hpi in the incompatible interaction, suggesting that *TaTypA* may be responsible for ROS accumulation and protection of host cells from *Pst* infection. Thus, silencing of *TaTypA* led to decreased ROS accumulation in *TaTypA*-knock-down plants. Superoxide dismutase (SOD) and catalase (CAT) are major ROS-scavenging enzymes (Mittler et al., 2004). H_2O_2 can be eliminated by increased catalase and superoxidase activities. The accumulation of *TaSOD* and *TaCAT* in *TaTypA* knock-down plants was induced by CYR23 infection, suggesting that *TaTypA* is an important factor in the ROS-scavenging system. Decreased catalase and ascorbate peroxidase activities in tobacco resulted in plants with increased resistance to pathogens (Mittler et al., 1999), whereas overexpression of catalase resulted in plants that were more susceptible (Polidoros et al., 2001). These results suggest that the ROS-scavenging systems have an important role in managing ROS generated in response to pathogens. Our results suggest that *TaTypA* positively regulates resistance to stripe rust in a ROS-dependent manner.

Hyphal length and number of branches are measures the ability of the pathogen to colonize the host under the stress imposed by HR at infection sites. The necrotic area triggered by infection of avirulent race CYR23 was used to represent the level of the HR, which is probably triggered by generation of ROS (Wang et al., 2007; Zurbriggen et al., 2010). In *TaTypA* knock-down plants, ROS accumulation was reduced in CYR23 infection at 48 and 120 hpi, coinciding with decreased hyphal length, necrotic area and hyphal branch number, suggesting that

increased colonizing ability of the pathogen is a consequence of decreased host resistance. ROS are the well-characterized second messengers in a variety of cellular processes in plants, including tolerance to environmental stress (Desikan et al., 2001). ROS has been shown to regulate different plant hormone signaling pathways, plant-biotic interactions and developmental processes by redox-dependent regulation of transcription factors (Barna et al., 2012). One of the most thoroughly characterized defense-signaling pathways regulated by oxidation events is the induction of salicylic acid (SA)-dependent responses (Fu and Dong, 2013). In the present study, *TaPR1*, the marker gene of the SA pathway, was significantly decreased by CYR23 infection at 48 and 120 hpi. We infer that *TaTypA*, functions in the SA-signaling pathway via ROS-dependent signals and thereby contributes to systemic acquired resistance.

To our knowledge this is the first report to confirm that *TypA* functions in biotic stress. Knock-down of *TaTypA* demonstrated its positive role in regulation of hypersensitive cell death and in resistance of wheat to stripe rust. On the basis of our results, we believe that TypA has an important role in plant disease resistance, but determination of the precise functional mechanism of *TaTypA* requires further investigation.

AUTHOR CONTRIBUTIONS

JG and ZK designed the experiment. PL, TM, WM, DL, TQ, and JG performed the experiments and analyzed the data. PL, TM, JG, and ZK wrote the manuscript.

FUNDING

This study was financially supported by National Basic Research Program of China (No. 2013CB127700), National Natural Science Foundation of China (No. 31371889 and 31171795), the Program for New Century Excellent Talents in University (NCET-12-0471), the 111 Project from the Ministry of Education of China (No. B07049), the Natural Science Foundation of Shaanxi Province (2014JM3059) and the Fundamental Research Funds for the Central Universities of China (YQ2013001).

ACKNOWLEDGMENTS

We thank Professor Larry Dunkle from the USDA-Agricultural Research Service at Purdue University, USA and Professor Robert Mcintosh from University of Sydney, Australia for critical reading of the manuscript.

SUPPLEMENTARY MATERIAL

The Supplementary Material for this article can be found online at: http://journal.frontiersin.org/article/10.3389/fpls.2016.00873

FIGURE S1 | Multi-alignment of the encoding sequence of the three copies of *TaTypA*. *TaTypA* cDNA, the full-length cDNA sequence amplified from cDNA of wheat cv. Suwon 11. The cDNA sequences of three *TaTypA* copies from chromosomes 6AL, 6BL, and 6DL were obtained from the wheat UGRI genome database of wheat cv Chinese Spring. The red and blue boxes indicate the initiation codon (ATG) and termination codon (TAG), respectively.

FIGURE S2 | Multi-alignment of the deduced TaTypA proteins from wheat cv. Suwon11 and Chinese Spring genome database. Identical and similar amino acid residues are shaded in black and light gray, respectively.

FIGURE S3 | Multi-sequence alignment of *TaTypA* against TypA from other species. Identical and similar amino acid residues are shaded in black and light gray, respectively. Motifs indicated in the sequence: (I) ATP/GTP binding site; (II) GTP-binding elongation factor signature; (III) putative ribosome binding domain. Triangles indicate conserved tyrosine residues in all nine proteins. Ta, *Triticum aestivum*; Bd, *Brachypodium distachyon*; Os, *Oryza sativa*; Zm, *Zea mays*; Sb, *Sorghum bicolor*; Gm, *Glycine max*; Ss, *Suaeda salsa*; At, *Arabidopsis thaliana*; Tp, *Trifolium pretense*.

FIGURE S4 | The expression of GFP, TaTypA::GFP and TaTypA-N_{1-80}::GFP proteins was determined by Western blot analysis using GFP antibody. The GFP antibody was diluted in blocking buffer at 1:5000. The graph shows the relative band using image Lab 3.0 software.

FIGURE S5 | Symptoms of wheat seedlings treated with MV. Ten-days-old wheat seedlings were sprayed with 0.1, 1, and 5 mM MV under the normal growing conditions. CK, wheat seedlings sprayed with water.

TABLE S1 | Primers used for TaTypA analyses.

REFERENCES

Almagro, L., Gómez Ros, L. V., Belchi-Navarro, S., Bru, R., Ros Barceló, A., and Pedreño, M. A. (2009). Class III peroxidases in plant defence reactions. *J. Exp. Bot.* 60, 377–390. doi: 10.1093/jxb/ern277

Atkinson, G. C. (2015). The evolutionary and functional diversity of classical and lesser-known cytoplasmic and organellar translational GTPases across the tree of life. *BMC Genomics* 16:1. doi: 10.1186/s12864-015-1289-7

Barak, M., and Trebitsh, T. (2007). A developmentally regulated GTP binding tyrosine phosphorylated protein A-like cDNA in cucumber (*Cucumis sativus* L.). *Plant Mol. Biol.* 65, 829–837. doi: 10.1007/s11103-007-9246-8

Barna, B., Fodor, J., Harrach, B., Pogány, M., and Király, Z. (2012). The Janus face of reactive oxygen species in resistance and susceptibility of plants to necrotrophic and biotrophic pathogens. *Plant Physiol. Biochem.* 59, 37–43. doi: 10.1016/j.plaphy.2012.01.014

Cakir, C., and Scofield, S. (2008). Evaluating the ability of the barley stripe mosaic virus-induced gene silencing system to simultaneously silence two wheat genes. *Cereal Res. Commun.* 36, 217–222. doi: 10.1556/CRC.36.2008.Suppl.B.18

Cao, Z., Jing, J., Wang, M., Shang, H., and Li, Z. (2002). Relation analysis of stripe rust resistance gene in wheat important cultivar Suwon 11, Suwon 92 and Hybrid 46. *Acta Bot. Boreal-Occident Sin.* 23, 64–68.

Caplan, J. L., Mamillapalli, P., Burch-Smith, T. M., Czymmek, K., and Dinesh-Kumar, S. P. (2008). Chloroplastic protein NRIP1 mediates innate immune receptor recognition of a viral effector. *Cell* 132, 449–462. doi: 10.1016/j.cell.2007.12.031

Chenna, R., Sugawara, H., Koike, T., Lopez, R., Gibson, T. J., Higgins, D. G., et al. (2003). Multiple sequence alignment with the clustal series of programs. *Nucleic Acids Res.* 31, 3497–3500. doi: 10.1093/nar/gkg500

de Torres Zabala, M., Littlejohn, G., Jayaraman, S., Studholme, D., Bailey, T., Lawson, T., et al. (2015). Chloroplasts play a central role in plant

defence and are targeted by pathogen effectors. *Nat. Plants* 1:15074. doi: 10.1038/nplants.2015.74

De Tullio, M. C. (2010). Antioxidants and redox regulation: changing notions in a changing world. *Plant Physiol. Biochem.* 48, 289–291. doi: 10.1016/j.plaphy.2010.02.011

Desikan, R., Soheila, A. H., Hancock, J. T., and Neill, S. J. (2001). Regulation of the *Arabidopsis* transcriptome by oxidative stress. *Plant Physiol.* 127, 159–172. doi: 10.1104/pp.127.1.159

Farris, M., Grant, A., Richardson, T. B., and O'Connor, C. D. (1998). BipA: a tyrosine-phosphorylated GTPase that mediates interactions between enteropathogenic *Escherichia coli* (EPEC) and epithelial cells. *Mol. Microbiol.* 28, 265–279. doi: 10.1046/j.1365-2958.1998.00793.x

Fu, Z. Q., and Dong, X. (2013). Systemic acquired resistance: turning local infection into global defense. *Annu. Rev. Plant Biol.* 64, 839–863. doi: 10.1146/annurev-arplant-042811-105606

Gou, J. Y., Li, K., Wu, K., Wang, X., Lin, H., Cantu, D., et al. (2015). Wheat stripe rust resistance protein WKS1 reduces the ability of the thylakoid-associated ascorbate peroxidase to detoxify reactive oxygen species. *Plant Cell* 27, 1755–1770. doi: 10.1105/tpc.114.134296

Grant, A. J., Farris, M., Alefounder, P., Williams, P. H., Woodward, M. J., and O'Connor, C. D. (2003). Co-ordination of pathogenicity island expression by the BipAGTPase in enteropathogenic *Escherichia coli* (EPEC). *Mol. Microbiol.* 48, 507–521. doi: 10.1046/j.1365-2958.2003.t01-1-03447.x

Hau, B., and de Vallavieille-Pope, C. (2006). "Wind-dispersed diseases," in *The Epidemiology of Plant Diseases*, ed. B. M. Cooke (Dordrecht: Springer), 387–416.

Holzberg, S., Brosio, P., Gross, C., and Pogue, G. P. (2002). Barley stripe mosaic virus-induced gene silencing in a monocot plant. *Plant J.* 30, 315–327. doi: 10.1046/j.1365-313X.2002.01291.x

Ito, T., and Shinozaki, K. (2002). The MALE STERILITY1 gene of *Arabidopsis*, encoding a nuclear protein with a PHD-finger motif, is expressed in tapetal cells and is required for pollen maturation. *Plant Cell Physiol.* 43, 1285–1292. doi: 10.1093/pcp/pcf154

Kang, Z., Huang, L., and Buchenauer, H. (2002). Ultrastructural changes and localization of lignin and callose in compatible and incompatible interactions between wheat and *Puccinia striiformis*. *J. Plant Dis. Prot.* 109, 25–37.

Kiss, E., Huguet, T., Poinsot, V., and Batut, J. (2004). The typA gene is required for stress adaptation as well as for symbiosis of *Sinorhizobium meliloti* 1021 with certain *Medicago truncatula* lines. *Mol. Plant Microbe Interact.* 17, 235–244. doi: 10.1094/MPMI.2004.17.3.235

Lalanne, E., Michaelidis, C., Moore, J. M., Gagliano, W., Johnson, A., Patel, R., et al. (2004). Analysis of transposon insertion mutants highlights the diversity of mechanisms underlying male progamic development in *Arabidopsis*. *Genetics* 167, 1975–1986. doi: 10.1534/genetics.104.030270

Li, C., Lin, H., and Dubcovsky, J. (2015). Factorial combinations of protein interactions generate a multiplicity of florigen activation complexes in wheat and barley. *Plant J.* 84, 70–82. doi: 10.1111/tpj.12960

Livak, K. J., and Schmittgen, T. D. (2001). Analysis of relative gene expression data using real-time quantitative PCR and the $2^{-\Delta\Delta CT}$ method. *Methods* 25, 402–408. doi: 10.1006/meth.2001.1262

Ma, J., Huang, X., Wang, X., Chen, X., Qu, Z., Huang, L., et al. (2009). Identification of expressed genes during compatible interaction between stripe rust (*Puccinia striiformis*) and wheat using a cDNA library. *BMC Genomics* 10:1. doi: 10.1186/1471-2164-10-586

Margus, T., Remm, M., and Tenson, T. (2007). Phylogenetic distribution of translational GTPases in bacteria. *BMC Genomics* 8:15. doi: 10.1186/1471-2164-8-15

Mittler, R., Herr, E. H., Orvar, B. L., Van Camp, W., Willekens, H., Inzé, D., et al. (1999). Transgenic tobacco plants with reduced capability to detoxify reactive oxygen intermediates arehyper-responsive to pathogen infection. *Proc. Natl. Acad. Sci. U.S.A.* 96, 14165–14170. doi: 10.1073/pnas.96.24.14165

Mittler, R., Vanderauwera, S., Gollery, M., and Van Breusegem, F. (2004). Reactive oxygen gene network of plants. *Trends Plant Sci.* 9, 490–498. doi: 10.1016/j.tplants.2004.08.009

Mittler, R., Vanderauwera, S., Suzuki, N., Miller, G., Tognetti, V. B., Vandepoele, K., et al. (2011). ROS signaling: the new wave? *Trends Plant Sci.* 16, 300–309. doi: 10.1016/j.tplants.2011.03.007

Munns, R., and Tester, M. (2008). Mechanisms of salinity tolerance. *Annu. Rev. Plant Biol.* 59, 651–681. doi: 10.1146/annurev.arplant.59.032607.092911

Nilsson, J., and Nissen, P. (2005). Elongation factors on the ribosome. *Curr. Opin. Struct. Biol.* 15, 349–354. doi: 10.1016/j.sbi.2005.05.004

Owens, G. K., Kumar, M. S., and Wamhoff, B. R. (2004). Molecular regulation of vascular smooth muscle cell differentiation in development and disease. *Physiol. Rev.* 84, 767–801. doi: 10.1152/physrev.00041.2003

Petty, I. T., French, R., Jones, R., and Jackson, A. (1990). Identification of barley stripe mosaic virus genes involved in viral RNA replication and systemic movement. *EMBO J.* 9, 3453–3457.

Pfennig, P., and Flower, A. (2001). BipA is required for growth of *Escherichia coli* K12 at low temperature. *Mol. Genet. Genomics* 266, 313–317. doi: 10.1007/s004380100559

Polidoros, A., Mylona, P., and Scandalios, J. (2001). Transgenic tobacco plants expressing the maize Cat2 gene have altered catalase levels that affect plant-pathogen interactions and resistance to oxidative stress. *Transgenic Res.* 10, 555–569. doi: 10.1023/A:1013027920444

Pugin, A., Frachisse, J. M., Tavernier, E., Bligny, R., Gout, E., Douce, R., et al. (1997). Early events induced by the elicitor cryptogein in tobacco cells: involvement of a plasma membrane NADPH oxidase and activation of glycolysis and the pentose phosphate pathway. *Plant Cell* 9, 2077–2091. doi: 10.2307/3870566

Pumphrey, M., Bai, J., Laudencia-Chingcuanco, D., Anderson, O., and Gill, B. S. (2009). Nonadditive expression of homoeologous genes is established upon polyploidization in hexaploid wheat. *Genetics* 181, 1147–1157. doi: 10.1534/genetics.108.096941

Qi, S. Y., Li, Y., Szyroki, A., Giles, I. G., Moir, A., and O'connor, C. (1995). Salmonella typhimurium responses to a bactericidal protein from human neutrophils. *Mol. Microbiol.* 17, 523–531. doi: 10.1111/j.1365-2958.1995

Ramakrishnan, V. (2002). Ribosome structure and the mechanism of translation. *Cell* 108, 557–572. doi: 10.1016/S0092-8674(02)00619-0

Rea, D. K., Snoeckx, H., and Joseph, L. H. (1998). Late Cenozoic eolian deposition in the North Pacific: asian drying, Tibetan uplift, and cooling of the northern hemisphere. *Paleoceanography* 13, 215–224. doi: 10.1029/98PA00123

Robinson, V. L. (2008). *Salmonella enterica* serovar Typhimurium BipA exhibits two distinct ribosome binding modes. *J. Bacteriol.* 190, 5944–5952. doi: 10.1128/JB.00763-08

Scarpeci, T. E., Zanor, M. I., Carrillo, N., Mueller-Roeber, B., and Valle, E. M. (2008). Generation of superoxide anion in chloroplasts of *Arabidopsis* thaliana during active photosynthesis: a focus on rapidly induced genes. *Plant Mol. Biol.* 66, 361–378. doi: 10.1007/s11103-007-9274-4

Scheler, C., Durner, J., and Astier, J. (2013). Nitric oxide and reactive oxygen species in plant biotic interactions. *Curr. Opin. Plant Biol.* 16, 534–539. doi: 10.1016/j.pbi.2013.06.020

Scofield, S. R., Huang, L., Brandt, A. S., and Gill, B. S. (2005). Development of a virus-induced gene-silencing system for hexaploid wheat and its use in functional analysis of the Lr21-mediated leaf rust resistance pathway. *Plant Physiol.* 138, 2165–2173. doi: 10.1104/pp.105.061861

Sergiev, P. V., Lesnyak, D. V., Kiparisov, S. V., Burakovsky, D. E., Leonov, A. A., Bogdanov, A. A., et al. (2005). Function of the ribosomal E-site: a mutagenesis study. *Nucleic Acids Res.* 33, 6048–6056. doi: 10.1093/nar/gki910

Sharma, P., and Dubey, R. S. (2005). Drought induces oxidative stress and enhances the activities of antioxidant enzymes in growing rice seedlings. *Plant Growth Regul.* 46, 209–221. doi: 10.1007/s10725-005-0002-2

Shi, L. X., and Theg, S. M. (2013). The chloroplast protein import system: from algae to trees. *Biochim. Biophys. Acta* 1833, 314–331. doi: 10.1016/j.bbamcr.2012.10.002

Srivastava, S., and Dubey, R. (2011). Manganese-excess induces oxidative stress, lowers the pool of antioxidants and elevates activities of key antioxidative enzymes in rice seedlings. *Plant Growth Regul.* 64, 1–16. doi: 10.1007/s10725-010-9526-1

Tamura, K., Peterson, D., Peterson, N., Stecher, G., Nei, M., and Kumar, S. (2011). MEGA5: molecular evolutionary genetics analysis using maximum likelihood, evolutionary distance, and maximum parsimony methods. *Mol. Biol. Evol.* 28, 2731–2739. doi: 10.1093/molbev/msr121

Torres, M. A. (2010). ROS in biotic interactions. *Physiol. Plant.* 138, 414–429. doi: 10.1111/j.1399-3054.2009.01326.x

Verstraeten, N., Fauvart, M., Versées, W., and Michiels, J. (2011). The universally conserved prokaryotic GTPases. *Microbiol. Mol. Biol. Rev.* 75, 507–542. doi: 10.1128/MMBR.00009-11

Wang, C. F., Huang, L. L., Buchenauer, H., Han, Q. M., Zhang, H. C., and Kang, Z. S. (2007). Histochemical studies on the accumulation of reactive oxygen species (O2- and H2O2) in the incompatible and compatible interaction of wheat-*Puccinia striiformis* f. *sp.* tritici. *Physiol. Mol. Plant Pathol.* 71, 230–239. doi: 10.1016/j.pmpp.2008.02.006

Wang, F., Zhong, N. Q., Gao, P., Wang, G. L., Wang, H. Y., and Xia, G. X. (2008). SsTypA1, a chloroplast-specific TypA/BipA-type GTPase from the halophytic plant Suaeda salsa, plays a role in oxidative stress tolerance. *Plant Cell Environ.* 31, 982–994. doi: 10.1111/j.1365-3040.2008.01810.x

Wang, X., Tang, C., Zhang, G., Li, Y., Wang, C., Liu, B., et al. (2009). cDNA-AFLP analysis reveals differential gene expression in compatible interaction of wheat challenged with *Puccinia striiformis* f. *sp. tritici*. *BMC Genomics* 10:289. doi: 10.1186/1471-2164-10-289

Wendel, J. F. (2000). Genome evolution in polyploids. *Plant Mol. Biol.* 42, 225–249. doi: 10.1007/978-94-011-4221-2_12

Wojtaszek, P. (1997). Mechanisms for the generation of reactive oxygen species in plant defence response. *Acta Physiol. Plant.* 19, 581–589. doi: 10.1007/s11738-997-0057-y

Yu, X., Wang, X., Wang, C., Chen, X., Qu, Z., Yu, X., et al. (2010). Wheat defense genes in fungal (*Puccinia striiformis*) infection. *Funct. Integr. Genomics* 10, 227–239. doi: 10.1007/s10142-010-0161-8

Zurbriggen, M. D., Carrillo, N., and Hajirezaei, M. R. (2010). ROS signaling in the hypersensitive response: when, where and what for? *Plant Signal. Behav.* 5, 393–396. doi: 10.4161/psb.5.4.10793

Conflict of Interest Statement: The authors declare that the research was conducted in the absence of any commercial or financial relationships that could be construed as a potential conflict of interest.

frontiers in Plant Science

ORIGINAL RESEARCH
published: 04 June 2015
doi: 10.3389/fpls.2015.00409

The knottin-like *Blufensin* family regulates genes involved in nuclear import and the secretory pathway in barley-powdery mildew interactions

Weihui Xu[1‡], *Yan Meng*[1†‡], *Priyanka Surana*[1,2], *Greg Fuerst*[1,3], *Dan Nettleton*[4] *and Roger P. Wise*[1,3*]

[1] *Department of Plant Pathology and Microbiology, Center for Plant Responses to Environmental Stresses, Iowa State University, Ames, IA, USA,* [2] *Bioinformatics and Computational Biology Graduate Program, Iowa State University, Ames, IA, USA,* [3] *Corn Insects and Crop Genetics Research Unit, U.S. Department of Agriculture-Agricultural Research Service, Iowa State University, Ames, IA, USA,* [4] *Department of Statistics, Iowa State University, Ames, IA, USA*

Plants have evolved complex regulatory mechanisms to control a multi-layered defense response to microbial attack. Both temporal and spatial gene expression are tightly regulated in response to pathogen ingress, modulating both positive and negative control of defense. BLUFENSINs, small knottin-like peptides in barley, wheat, and rice, are highly induced by attack from fungal pathogens, in particular, the obligate biotrophic fungus, *Blumeria graminis* f. sp. *hordei (Bgh)*, causal agent of barley powdery mildew. Previous research indicated that *Blufensin1* (*Bln1*) functions as a negative regulator of basal defense mechanisms. In the current report, we show that BLN1 and BLN2 can both be secreted to the apoplast and *Barley stripe mosaic virus* (*BSMV*)-mediated overexpression of *Bln2* increases susceptibility of barley to *Bgh*. Bimolecular fluorescence complementation (BiFC) assays signify that BLN1 and BLN2 can interact with each other, and with calmodulin. We then used *BSMV*-induced gene silencing to knock down *Bln1*, followed by Barley1 GeneChip transcriptome analysis, to identify additional host genes influenced by *Bln1*. Analysis of differential expression revealed a gene set enriched for those encoding proteins annotated to nuclear import and the secretory pathway, particularly Importin α1-b and Sec61 γ subunits. Further functional analysis of these two affected genes showed that when silenced, they also reduced susceptibility to *Bgh*. Taken together, we postulate that *Bln1* is co-opted by *Bgh* to facilitate transport of disease-related host proteins or effectors, influencing the establishment of *Bgh* compatibility on its barley host.

Keywords: knottin, nuclear import, secretory pathway, powdery mildew, calmodulin, BSMV-VIGS, gene expression, negative regulator

OPEN ACCESS

Edited by:
Xin Li,
University of British Columbia, Canada

Reviewed by:
Erik Limpens,
Wageningen University, Netherlands
Hugo Germain,
Université du Québec à Trois-Rivières, Canada

****Correspondence:***
Roger P. Wise,
Corn Insects and Crop Genetics Research Unit, U.S. Department of Agriculture-Agricultural Research Service and Department of Plant Pathology and Microbiology, Iowa State University, 351 Bessey Hall, Ames, IA 50011–1020, USA
roger.wise@ars.usda.gov

†Present Address:
Yan Meng,
Department of Agriculture, Alcorn State University, Lorman, USA

‡These authors have contributed equally to this work.

Specialty section:
This article was submitted to Plant-Microbe Interaction, a section of the journal Frontiers in Plant Science

Received: *03 October 2014*
Accepted: *21 May 2015*
Published: *04 June 2015*

Citation:
Xu W, Meng Y, Surana P, Fuerst G, Nettleton D and Wise RP (2015) The knottin-like Blufensin family regulates genes involved in nuclear import and the secretory pathway in barley-powdery mildew interactions. Front. Plant Sci. 6:409. doi: 10.3389/fpls.2015.00409

Introduction

Obligate fungal biotrophs, i.e., pathogens that require their host to survive, are a major threat to crop production worldwide. To establish biotrophy, the fungus must penetrate cell walls, suppress defense, and establish haustoria for nutrient acquisition (Dodds et al., 2004; Micali et al., 2011; Mentlak et al., 2012). In general, these pathogens interfere with recognition

at the host plasma membrane or secrete effector proteins, often through feeding structures termed haustoria, into the plant cell cytosol that alter resistance signaling or the downstream manifestation of resistance responses. Many cloned effectors are small proteins of unknown function containing a signal for secretion into the apoplast; how these effectors gain entry into host cells and contribute to pathogen colonization has been a major focus to understand the underlying mechanisms determining pathogenicity (Rovenich et al., 2014; Stotz et al., 2014).

The host responds with an integrated multi-layer defense system. Typically, pathogen-associated molecular patterns (PAMPs) trigger the initial activation of non-specific, innate immune responses, currently termed PAMP Triggered Immunity (PTI) (Macho and Zipfel, 2014). These include the transcription of thousands of stress-related genes, as well as production of antimicrobial metabolites and peptides during early stages of pathogen invasion. A second layer, designated Effector-Triggered Immunity (ETI) generally follows gene-for-gene interactions, in which specific resistance (R) proteins initiate a signal cascade when they recognize, either directly or indirectly, corresponding effectors delivered by the pathogen (Bent and Mackey, 2007; Jacob et al., 2013; Cesari et al., 2014).

Host factors that are activated and recruited by pathogen effectors interfere with different layers of the plant defense response. These plant factors are either called negative regulators of plant defense or susceptibilty factors, which are co-opted by the pathogen to optimize growth and parasitism; both are encoded by susceptibility (*S*) genes (Vogel et al., 2002, 2004; Hückelhoven et al., 2013; Lapin and Van Den Ackerveken, 2013; Van Schie and Takken, 2014). Mutation of an *S* gene has the potential to alter the plants susceptibility and lead to resistance, an important feature that is often used in breeding. For example, the cell wall has long been recognized as a major barrier against pathogen infection (Bellincampi et al., 2014; Malinovsky et al., 2014). PMR5 and PMR6 are two potential susceptibility factors identified in Arabidopsis. Mutations in *pmr5* [defective in a gene encoding a predicted endoplasmic reticulum (ER) protein] and *pmr6* (defective in a cell wall-degrading pectate lyase-like gene) genes both affect pectin composition of the cell wall, thus increasing Arabidopsis resistance to powdery mildew (Vogel et al., 2002, 2004). Other examples include *xa5*, encoding a subunit of transcription factor IIA (Iyer and McCouch, 2004; Jiang et al., 2006), and *xa13*, encoding a plasma membrane protein and essential for pollen development (Chu et al., 2006). Both loss-of-function mutants to bacterial blight have been used successfully in rice cultivation (Iyer-Pascuzzi and McCouch, 2007).

A classic case in barley is the well-characterized *Mlo* gene that encodes a transmembrane protein, which negatively regulates penetration resistance to powdery mildew (Büschges et al., 1997). Loss of function *mlo* mutants result in durable and broad-spectrum resistance, which has been wildly adapted for cultivation in Europe (Büschges et al., 1997; Panstruga, 2005; Acevedo-Garcia et al., 2014). MLO2, an *Arabidopsis thaliana* homolog of the barley *S*-gene *Mlo*, was found to be the target of the *Pseudomonas syringae* effector HopZ2 (Lewis et al., 2012).

BAX INHIBITOR-1 (BI-1) inhibits BAX-induced PCD in yeast and Arabidopsis; additionally, BI-1 modulates cell-wall-associated defense and contributes to establishing full compatibility of barley with the obligate biotrophic fungus, *Blumeria graminis* f. sp. *hordei* (*Bgh*), causal agent of powdery mildew disease (Eichmann et al., 2010). Interestingly, overexpression of BI-1 was found to negatively regulate penetration resistance mediated by *mlo* and almost restored the penetration efficiency (PE) of *Bgh* to wild-type levels (Hückelhoven et al., 2003), suggesting these genes have important roles in a complex interconnected network. The MLO protein in barley negatively regulates the actin-dependent resistance pathway, and the actin cytoskeleton is thought to contribute to the establishment of effective barriers at the cell periphery against fungal access (Miklis et al., 2007). The RAC/ROP family G-protein RACB, another potential host susceptibility factor, is also involved in the modulation of actin reorganization and cell polarity in the interaction of barley with *Bgh* (Opalski et al., 2005).

We previously reported the discovery of the monocot-specific Blufensin family of cysteine-rich, peptides, which negatively impact plant defense (Meng et al., 2009). The *Bln1* and *Bln2* transcripts are highly upregulated in response to infection by a wide array of fungal pathogens, including *Blumeria*, *Puccinia*, *Cochliobolus,* and *Fusarium* spp., as compared to uninfected control plants. The genes that encode these peptides are so far unique to the cereal grain crops barley, wheat, and rice, and the resulting proteins are similar to knottins, a diverse family of proteins characterized by a unique disulfide through disulfide knot (Gracy et al., 2008).

In the work described herein, we used BLN-GFP fusion constructs to demonstrate that BLN1 and BLN2 can be secreted into the apoplast. Bimolecular fluorescence complementation (BiFC) assays (Kerppola, 2006) suggest that BLN1 and BLN2 interact with calmodulin, as well as each other. *Barley stripe mosaic virus* (*BSMV)*-mediated *Bln* overexpression increased susceptibility of barley to *Bgh*. BSMV–Virus Induced Gene Silencing (VIGS) coupled with a Barley1 GeneChip transcriptome analysis, identified additional genes in the *Blufensin1* (*Bln1*) network. These candidates appear to have key roles in *R*-gene mediated and innate immunity networks, thus, the functional identification of their precise roles will be a significant step in understanding plant defense.

Results

BLN1 and BLN2 can be Secreted into the Apoplast

In previous research, BSMV-VIGS of *Bln1* decreased barley susceptibility to *Bgh* in compatible interactions. Likewise, single cell transient overexpression of *Bln1* significantly increased accessibility toward virulent *Bgh*. Moreover, silencing of *Bln1* in plants harboring the *Mildew locus o* (*Mlo)* susceptibility factor decreased accessibility to *Bgh*, suggesting BLN1 functions in parallel with or upstream of MLO to modulate penetration resistance (Meng et al., 2009).

Computational analysis of the BLN1 and BLN2 signal peptides (SP) predicted that BLN could be secreted into the apoplast, and thus, may act as ligands to generate a signal transduction cascade, influencing *Bgh* accessibility (Meng et al., 2009). To test this hypothesis, six different *Bln-GFP* fusion constructs were assembled for bombardment into onion epidermal cells, [BLN1 or 2 minus SP (35S:BLN1/2–SP), BLN1 or 2 plus SP (35S:BLN1/2 + SP), and BLN1 or 2 SP only (35S:BLN1/2 SP only)] (**Figure 1A**).

Because GFP is unstable at low pH, to visualize its expression in the apoplast, onion epidermal cells were treated with 20 mM Pipes-KOH (pH 7.0) to neutralize the pH according to Genovesi et al. (2008) (see Materials and Methods). The pH 7.0 medium neutralizes the normally acidic apoplast, facilitating

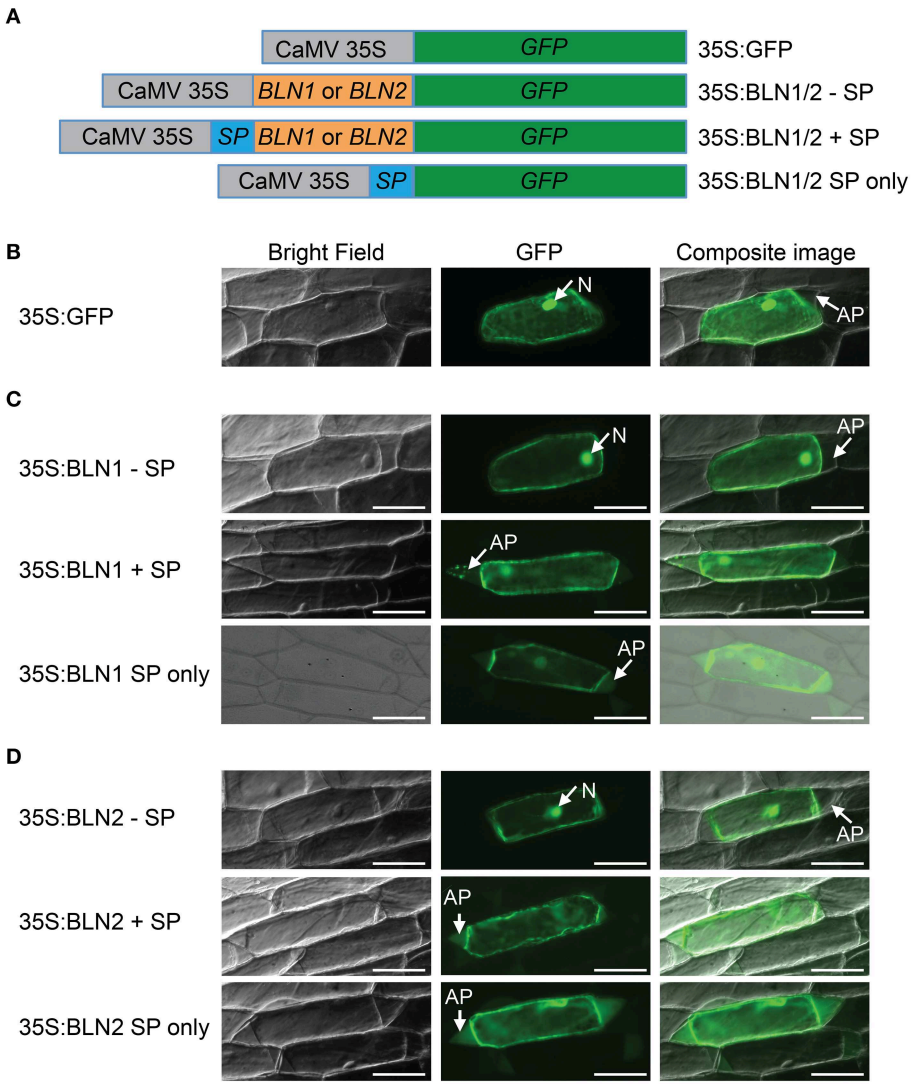

FIGURE 1 | Subcellular localization of BLN1 and BLN2. (A) Schematic diagram of expression constructs. Gray boxes represent *Cauliflower Mosaic Virus* (CaMV) 35S promoter; the green, orange, and the blue boxes represent coding regions for GFP, mature BLN1/BLN2, and BLN1/BLN2 signal peptides, respectively. The CaMV 35S promoter was used to drive gene expression. The GFP coding sequence is fused to *Bln1* and *Bln2* without signal peptide-coding region (35S:BLN1/2—SP), to *Bln1* and *Bln2* with signal peptide-coding region (35S:BLN1/2 + SP), and to BLN1/2 signal peptide-coding region only (35S:BLN1/2 SP only). The construct harboring GFP coding sequence alone was used as a subcellular localization control. **(B)** Microscopic observation of GFP signal in onion epidermal cells after plasmolysis. GFP signal was observed in the cytoplasm and nucleus region in cells expressing GFP alone. No GFP signal was observed in apoplast region. **(C,D)** Microscopic observation of GFP signal in onion epidermal cells after plasmolysis. GFP signal was observed in apoplast when GFP was fused to full-length BLN1 or BLN2 with signal peptide (35S:BLN1 + SP, 35S:BLN2 + SP), as well as in cells expressing GFP fused to signal peptides from BLN1 and BLN2 (35S:BLN1 SP only, 35S:BLN2 SP only). By contrast, no GFP signal was observed in the apoplastic region in cells expressing GFP fused to BLN1 or BLN2 without signal peptides from BLN1 and BLN2 (35S:BLN1-SP, 35S:BLN2-SP). Left column: bright field images; middle column: fluorescence microscopic images of GFP; right column: composite images of the GFP and bright light images. AP, apoplast; N, Nucleus. Bar = 100 μm.

the visualization of GFP-mediated fluorescence. As illustrated in **Figures 1C,D** (middle panel), GFP fluorescence was detected in the apoplast, cytoplasm and nuclei of plasmolysed cells when transformed with the full-length *Bln1* or *Bln2* ORFs fused with GFP. Similar results were obtained when constructs harboring *GFP* fused with coding sequences for signal peptides from BLN1 or BLN2 (**Figures 1C,D**, lower panel). By contrast, GFP fluorescence was found only in the cytoplasm or the nucleus when onion epidermal cells were bombarded with constructs absent the signal peptides (**Figures 1C,D**, upper panel), similar to the GFP-only control (**Figure 1B**); no visible fluorescent signal was observed in the apoplastic region. The above results indicate that the BLN1 and BLN2 signal peptides can direct protein secretion, and both BLN1 and BLN2 can be secreted from the cytoplasm into the apoplast.

BSMV-VOX: A New *BSMV*-mediated Overexpression System for Functional Analysis of *Bln1* and *Bln2*

As described above, we developed a bombardment based BSMV-VIGS system for high-throughput silencing of candidate genes involved in interactions with the barley powdery mildew fungus (Meng et al., 2009). To complement these gene-silencing studies, we further developed *BSMV* as a transient overexpression system (BSMV-VOX) for functional analysis in both host and pathogen. To generate the expected cleavage products from the artificial fusion proteins, a 54-nucleotide sequence encoding the 18 amino-acid foot and mouth virus peptide (FMDV-2A) was inserted in front of the 5′ end of BSMV:γ ORF B. The ORF encoding GFP was inserted between the *Stu*I and *Bam*H1 sites before FMDV 2A as a visible marker to monitor overexpression (**Figure 2A**). These GFP and BSMV:γB coding regions are fused in-frame via the FMDV 2A coding sequence. The FMDV 2A peptide mediates the primary *cis*-"cleavage" of the FMDV polyprotein in a cascade of processing events that ultimately generate the mature FMDV proteins. Subsequently, FMDV 2A efficiently generates the expected cleavage products from the artificial fusion proteins in cells (Furler et al., 2001). The *BSMV*-mediated overexpression construct (pBSMV-OEx) was then co-bombarded with BSMV:α and BSMV:β to barley cultivar Black Hulless, which is susceptible to *BSMV*. Overexpression of *GFP* (pBSMV-OEx:GFP) was used to examine the efficacy of overexpression with this approach. Microscopic observation showed that all leaves with *BSMV* infected stripe and mosaic symptoms also exhibit green fluorescence as detected by UV microscopy (**Figure 2B**), signifying the robustness of BSMV-VOX system for transient gene overexpression. In addition, due to the systemic infection of *BSMV*, the BSMV-VOX system results in transient gene overexpression throughout *BSMV*-infected barley leaves (Lee et al., 2012), as compared to single-cell-overexpression in epidermal cells (Meng et al., 2009). Therefore, the infection phenotypes can be observed by the naked eye, hyphal growth and associated symptoms can be quantified digitally, and the target gene expression levels can be assayed by quantitative real-time reverse transcriptase PCR (qRT-PCR), in the absence of stable transformation.

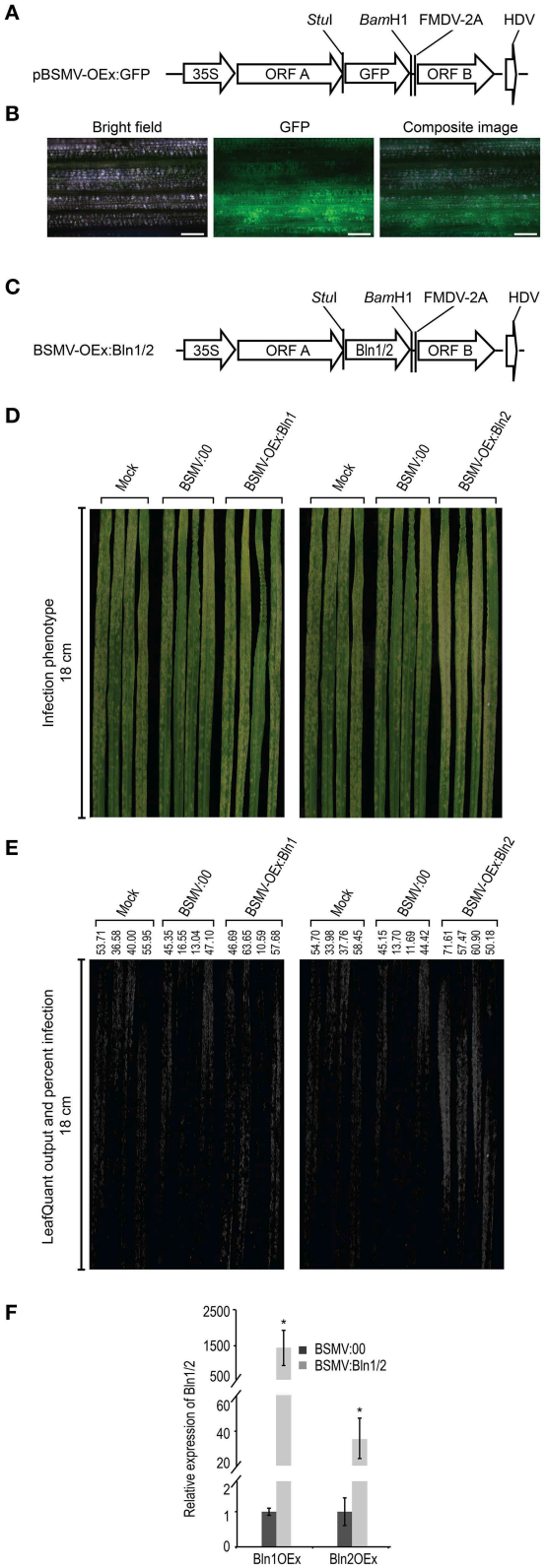

FIGURE 2 | *BSMV*-mediated over-expression of *Bln1/2*. (A) Schematic diagram of *BSMV*-mediated GFP over-expression (VOX) construct. The coding

(Continued)

FIGURE 2 | Continued
sequence for the fusion protein of GFP and foot- and-mouth disease virus (*FMDV*)-2A self-cleavage peptide was digested by *Bgl*II and *Kpn*I, ligated into the construct BSMV: γ, which harbors the BSMV γ-subgenome. Subsequent digestion with *Bgl*II and *Kpn*I, resulted in *BSMV*-mediated GFP over-expression construct pBSMV-OEx:GFP. **(B)** Microscopic observation of GFP signal (middle column) in barley leaves (black hull-less) co-bombarded with *BSMV*-mediated GFP over-expression construct pBSMV-OEx:GFP, BSMV:α, and BSMV:β. The efficacy of the observed GFP signal is 100% in leaves that showed *BSMV* infection symptom. Bar = 100 μm. **(C)** Schematic diagram of *BSMV*-mediated BLN1/2 over-expression construct pBSMV-OEx:Bln1/2. PCR amplified fragments for Bln1/2 coding regions were digested by *Stu*I and *Bam*H1 and inserted into *Stu*I and *Bam*H1 digested pBSMV-OEx:GFP, generating constructs pBSMV-OEx:Bln1 and pBSMV-OEx:Bln2. **(D)** Phenotype of *Bgh* infected leaves treated with buffer (Mock), BSMV:00 control, and pBSMV-OEx:Bln1 (*Bln1* over-expression) (left column); buffer (Mock), BSMV:00 control, and *Bln2* over-expression (pBSMV-OEx:Bln2) (right column). **(E)** LeafQuant infection phenotype images and quantification of *Bgh* hyphal growth on leaves treated with buffer (mock), BSMV:00 control, and over-expression for *Bln1* and *Bln2* (See **Table 1**). **(F)** Quantitative RT-PCR analyses for *Bln1* and *Bln2* levels in leaves treated by BSMV-mediated over-expression Bln1OEx and BlnOEx. Bars represent standard error calculated from at least four independent plants for each treatment from two replicate experiments shown in this figure. The average *Bln1* and *Bln2* levels in BSMV:00 control were set to 1.00 (* designates that $p < 0.05$).

Overexpression of *Bln2* Increases Susceptibility in Compatible Interactions

Our newly developed BSMV-VOX system (described above) was adopted to further corroborate the function of *Bln* genes in barley immunity to *Bgh*. Full-length *Bln1-1* and *Bln2* ORFs were substituted in place of *GFP* in the BSMV-VOX vector, pBSMV-OEx:GFP, to create the expression constructs BSMV-OEx:Bln1 and BSMV-OEx:Bln2 (**Figure 2C**). pBSMV-OEx:Bln1 or pBSMV-OEx:Bln2 plasmids were then co-bombarded with the BSMV:α and BSMV:β separately into 7 day old Black Hulless seedlings. After 7 days, sap from *BSMV* infected barley leaves was used to mechanically inoculate barley cultivar HOR11358 (*Mla9*). Twelve days after overexpression, plants were subsequently challenged with the virulent *Bgh* isolate 5874 (avr_{a9}). Control bombardments were performed with the BSMV:00 construct (see Materials and Methods). Systemic overexpression of *Bln2* in whole barley leaves significantly increased susceptibility in compatible barley-*Bgh* interactions ($p = 0.0194$). Although one can observe a small increase in *Bgh* colony proliferation on *Bln1*-OEx barley leaves, this did not result in a significant difference in quantifiable growth (**Figures 2D,E**, **Table 1**). This contrasts with our previous result using transient single-cell-overexpression in barley epidermal cells (Meng et al., 2009), and may be due to the differential resistance of barley genotypes to *BSMV* (Hein et al., 2005), which could further influence the phenotypic effects of *BSMV*-mediated overexpression, as opposed to single cell bombardment assays (which contain no *BSMV*).

Transcript accumulation of *Bln1* and *Bln2* was assayed to monitor the level of gene overexpression. Third leaves of BSMV-treated plants were used for qRT-PCR assays at 24 HAI with *Bgh*. Barley *Actin* mRNA was used as an internal quantitative control for all samples. Results of qRT-PCR demonstrated the distinct induction of *Bln1* and *Bln2* transcripts in *Bgh* inoculated leaves that harbored overexpression constructs as compared to BSMV:00 inoculated plants (**Figure 2F**).

Interaction of BLN1 and BLN2

Next, we were interested to see if the BLN1 and BLN2 secreted small peptides could physically interact as BLN complexes to facilitate cellular signaling. To test this hypothesis, bimolecular fluorescent complementation (BiFC) assays (Kerppola, 2006) were performed to test the interaction between BLN1 and BLN2. *Bln1* and *Bln2* full-length open reading frames were fused to both N-terminal and C-terminal halves of yellow fluorescent protein (YFP), respectively, and co-expressed in onion epidermal cells. As shown in **Figure 3A** and **Table 2**, the interaction of N-terminal BLN2 and C-terminal BLN1 re-comprised YFP activity. We did not observe YFP fluorescence in tests with the reciprocal (N-terminal BLN1 and C-terminal BLN2) constructs, implying some conformational constraints on successful interactions (**Table 2**). This may be due to the orientation of the GFP tag in relation to the interacting interface. This non-reciprocity was also observed in BiFC interaction experiments among *Bgh* effector proteins and barley small heat shock proteins (Ahmed et al., 2015).

DISULFIND software (Ceroni et al., 2006) predicted that the cysteines in BLN1 and BLN2 form disulfide bonds; these are expected to stabilize knottin protein structures, which may be critical for interactions with other proteins (Combelles et al., 2008; Gracy et al., 2008). To test if these two conserved cysteines may be involved in the interaction interface between BLN1 and BLN2 (Kerppola, 2006), Cys36 and Cys45 in BLN1 and Cys37 and Cys47 in BLN2 were mutated to Gly and the resulting BiFC constructs were co-bombarded into onion epidermal cells. As shown in **Table 2**, the average number of observed fluorescent cells from three independent replications was significantly reduced (adjusted $p < 0.0016$). The reciprocal construct described above, as well as each of the BLN1 and BLN2 site-directed mutants also serve as negative controls for non-specific interactions (Kerppola, 2006). Interestingly, co-bombardment of constructs harboring BLN1 fused to the N-terminal and C-terminal halves of YFP also showed YFP activity (**Figure 3B**); similar results were also observed for BLN2 (**Figure 3C**). These results suggest that BLN family members can not only interact with each other, but also dimerize or polymerize with themselves. Even so, mutations in conserved residues may compromise protein stability, thus, this preliminary result should be viewed with caution without direct evidence that the mutant proteins actually accumulate.

Interactions between BLN Family Members and Calmodulin

Calmodulin (CaM) plays a pivotal role in controlling an abundance of Ca^{2+}-based cellular signaling events (Berridge et al., 2003) and functions in response to changes in cellular calcium levels by interacting with various targets, including those in plant immunity (Yamniuk and Vogel, 2004; Du et al., 2009). These targets include IQ (isoleucine-glutamine;

TABLE 1 | Linear model analysis of BSMV induced gene overexpression and silencing on *Bgh* infection[a].

Treatment[b]	Control	Percent infection[c]		Standard error[d]	*T*-value	Adjusted *p*-value[e]
		Treatment	Control			
Bln1						
BSMV:00	Mock	30.510	46.560	12.850	−1.249	0.3890
12219 p1 OEx	BSMV:00	44.653	30.510	12.850	1.101	0.4680
Bln2						
BSMV:00	Mock	28.780	46.223	9.756	−1.792	0.1812
26496 p1 OEx	BSMV:00	60.040	28.780	9.756	3.208	0.0194
Imp α-1b						
3615 p1	BSMV:00	30.401	65.812	6.625	−5.345	0.0007
Sec61 γ[f]						
3680 p2	BSMV:00	35.771	77.311	8.751	−4.747	0.0020

[a] *A linear model analysis was performed relative to BSMV with empty vector using the MULTCOMP package in R.*
[b] *Mock and BSMV with indicated silencing or overexpression plasmids were compared against BSMV with empty vector; OEx, overexpression.*
[c] *LeafQuant-VIGS distinguishes white Bgh hyphae from dark green leaves as a quantitative measure of Bgh associated hyphal growth (see Materials and Methods). LeafQuant-VIGS converts the images to gray scale and outputs histograms of the hyphal distribution per leaf, which then reports mean, median, and quantiles of the results as a csv (comma separated values) file for further processing (Whigham et al., 2015). The average of percent infection for each treatment across replicates is shown here.*
[d] *Standard error is the estimate of how far the sample mean is likely to be from the population mean.*
[e] *p-values were adjusted for multiple testing using the Dunnett method (Dunnett, 1955). Treatments with adjusted $p \leq 0.05$ were considered significantly different from the control.*
[f] *The results for mock samples compared to empty vector were not significant for Sec61.*

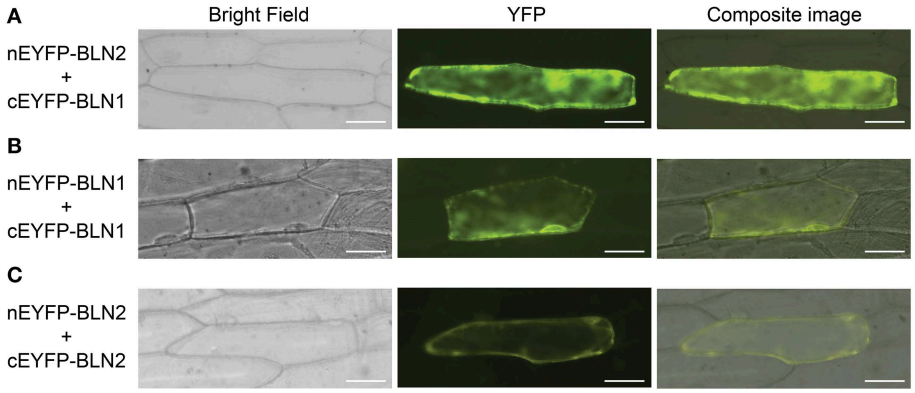

FIGURE 3 | Bimolecular fluorescence complementation (BiFC) assay for BLN1 and BLN2 interactions. The *Bln1* and *Bln2* full length ORFs were PCR-amplified and cloned into *Eco*RI-*Bam*HI sites of pSAT4-nEYFP-C1 or pSAT4-cEYFP-C1 to generate pSAT4-nEYFP-Bln1, pSAT4-nEYFP-Bln2, pSAT4-cEYFP-Bln1 pSAT4-cEYFP-Bln2 respectively. The designated plasmid combinations were co-bombarded into onion epidermal cells. The bright field and fluorescent images were taken using the Zeiss Axiovert 100 microscope equipped with the appropriate YFP filter. Statistical analysis of YFP count data is presented in **Table 2**. **(A)** Microscopic observation for interaction between BLN1 and BLN2. **(B)** Microscopic observation for BLN1 self-interaction. **(C)** Microscopic observation for BLN2 self-interaction.

consensus sequence = [FILV]Qxxx[RK]Gxxx[RK])- (Rhoads and Friedberg, 1997; Bahler and Rhoads, 2002) and partial-IQ-motif containing proteins (Houdusse and Cohen, 1995; Munshi et al., 1996; Sienaert et al., 2002). As shown in **Figure 4**, sequence alignments indicate that BLN family members contain partial IQ motifs. Moreover, previous results from silencing and overexpression experiments suggested that BLN family members possess an *S*-gene function somewhat similar to MLO, a calmodulin (CaM)-binding protein in plant defense (Kim et al., 2002). Thus, we were interested to investigate if BLN1 or BLN2 could physically interact with CaM. Both *Bln1* and *Bln2* full-length open reading frames were fused to the N-terminal half of YFP, *CaM* was fused to C-terminal half, and co-expressed in onion epidermal cells. As illustrated in **Figures 5A,B** and **Table 3**, significant YFP fluorescence was observed, indicating a possible interaction of BLN1/BLN2 with CaM. To further examine the function of glutamine residues in the BLN1 and BLN2 partial IQ motifs, Gln30 and Gln42 in BLN1, and Gln30 and Gln44 in BLN2 were mutated to Gly. Quantification for fluorescent cells indicated that these mutations significantly reduced the numbers of observed interactions between BLN and CaM (adjusted $p < 5.43^{E-04}$), suggesting that these two glutamine residues in BLN1 and BLN2 are necessary to facilitate the full-strength interaction with CaM (**Table 3**). Interestingly,

TABLE 2 | Mixed linear analysis of mutations in the BLN1 and BLN2 IQ domain and cysteines and their effect on forming heteroduplexes[a].

Treatment	Mean YFP cell counts[b]	Estimate[c]	*T*-value	Adjusted *P*-value[d]
BLN1 and BLN2[e]	0.00	–	–	–
BLN1-C36G and BLN2	0.33	−0.33	−0.38	0.9855
BLN1-C45G and BLN2	1.00	−1.00	−1.13	0.6421
BLN1-Q30G and BLN2	2.33	−2.33	−2.63	0.0891
BLN1-Q42G and BLN2	0.67	−0.67	−0.75	0.8632
BLN2 and BLN1	8.00	–	–	–
BLN2-C37G and BLN1	1.00	7.00	5.63	0.0016
BLN2-C47G and BLN1	0.00	8.00	6.44	0.0007
BLN2-Q30G and BLN1	0.33	7.67	6.17	0.0009
BLN2-Q44G and BLN1	2.00	6.00	4.83	0.0042

[a] *A mixed linear model analysis was done using PROC MIXED of the SAS Software. Contrasts were designed to test the differences between the control and the treatment with cell counts as the response.*

[b] *Represents mean of total cells exhibiting YFP from three independent biological replications. The appearance of YFP fluorescing cells was equivalent among mutant or wild-type bombarded constructs.*

[c] *Difference between least square means for the total YFP cells in control vs. the treatment.*

[d] *P-values were adjusted for multiple testing using the methods of Dunnett (1980) and Hsu (1992). Treatments with adjusted $p \leq 0.05$ were considered significantly different from the BLN1 and BLN2 wild-type control interactions.*

[e] *These BLN1 and BLN2 reciprocal constructs serve as internal negative controls for non-specific (background) interactions.*

the Gln mutations in BLN2 also negatively impacted BLN1-BLN2 interactions (**Table 2**, adjusted $p < 0.0042$).

Both BLN1 and BLN2 are cysteine-rich small peptides (Meng et al., 2009). These cysteines are positioned in or close to the partial IQ motifs (**Figure 4**). It is predicted that these cysteines may form inter- or intra-molecular disulfide bonds to maintain a structure supporting protein-protein interactions and cysteines in CaM targets are important for CaM-target interactions (Moore et al., 1999). To investigate the possible function of these two cysteines in the interaction between BLN and CaM, the Cys to Gly site-directed mutants described above were used in pairings with CaM, resulting in significantly reduced fluorescence activity (adjusted $p < 4.19^{E-04}$) (**Table 3**). These data indicate that these cysteines play a role, either directly or indirectly, in the interaction between BLN protein and CaM.

Identification of *Bln*-mediated Response Pathways

The data presented above, combined with previous functional studies (Meng et al., 2009), indicate that the monocot-specific, BLN small secreted peptides negatively regulate barley-*Bgh* interactions. To identify genes influenced by *Bln1* function, we took a mutational approach and used the BSMV-VIGS system to knock down *Bln1* (Contig12219_at). We then performed Barley1 GeneChip expression profiling on the silenced plants to discover additional genes that impact *Bln1*-mediated regulation of immunity.

Figure 6 illustrates the basic matrix of the experiment. Key contrasts were designed to compare differences in transcript accumulation among *Bln1*-silenced plants relative to BSMV:00 (empty vector) controls. Comparison of BSMV:00 to mock (buffer-treated) controls enabled us to detect possible confounding effects of BSMV. To account for background-specific differences, we utilized two host genotypes; both compatible with our *Bgh* 5874 isolate and previously demonstrated to be good hosts for BSMV-VIGS experiments (Hein et al., 2005; Meng et al., 2009; Meng and Wise, 2012).

We performed five independent biological replications of a split-plot experimental design (shown in **Figure 6**) with replications as blocks, *Bgh* treatment as the whole-plot factor, and all combinations of genotype [Clansman (*Mla13*), HOR11358 (*Mla9*)] and VIGS treatment [Buffer control (mock), BSMV:00 (empty vector), BSMV:$Bln1_{248}$] as the split-plot factor for a total of 60 GeneChip hybridizations. Ten seedlings were used as a split-plot experimental unit. Twelve days after VIGS treatment, plants were transferred to a growth chamber where half of the plants in each replication were challenged with the compatible *Bgh* isolate 5874; the other half remained un-inoculated. At 32 h after inoculation (HAI), 5 of the 10 leaves from each treatment were harvested for RNA isolation; this timepoint has the highest differential *Bln1* transcript accumulation in prior experiments (Meng et al., 2009), and is after initial establishment of the perihaustorial interface (Caldo et al., 2004). The remaining 5 leaves were used to document infection phenotypes 7 days after inoculation (representative experiments shown in **Figure 6**).

To interrogate the GeneChip data, we conducted mixed linear model analyses of the normalized signal intensities for each of the 22,840 Barley1 probe sets (Caldo et al., 2004, see Materials and Methods). Using a stringent threshold $p < 0.0001$ and false discovery rate (FDR) < 5%, 47 genes were suppressed or induced in BSMV:$Bln1_{248}$ silenced plants as compared to the BSMV:00 controls in the HOR11358 (*Mla9*) background. Using the same threshold criteria, 48 genes were similarly affected in the Clansman (*Mla13*) background (**Figure 7**). Many of the genes affected by silencing *Bln1* in HOR11358, as opposed to Clansman, had dissimilar annotations; this could be due to genotype-specific silencing, genotype-specific probe-set efficiency, or it could reflect the threshold *p*-value we selected (i.e., genes in one background may still be significant, but at a less conservative threshold). Nevertheless, six of these genes were suppressed in common, including the *Bln1* target, represented by Barley1 Contig12219_at [$p = 4.66^{E-19(HOR11358)}$/$p = 8.30^{E-06(Clansman)}$] (**Figure 8A**; Supplemental Table S1). *Bln2* (Contig26496_at; $p = 4.99^{E-06}$) was suppressed along with *Bln1* in the HOR11358 (*Mla9*) background (**Figure 8B**), but was not significant at the selected threshold $p < 0.0001$ in the Clansman (*Mla13*) background.

The experiment also yielded many genes that were influenced by infection with BSMV:00, in addition to BSMV:$Bln1_{248}$ (Supplemental Table S1). This may be due to an overlap in general defense gene functions, or may represent strictly *BSMV*-dependent responses. Although one must be cautious regarding overlap in general defense-gene functions, *BSMV* has been shown not to interfere with infection of *Blumeria graminis* f. sp. *tritici*, the causal agent of powdery mildew in wheat (Tufan et al., 2011).

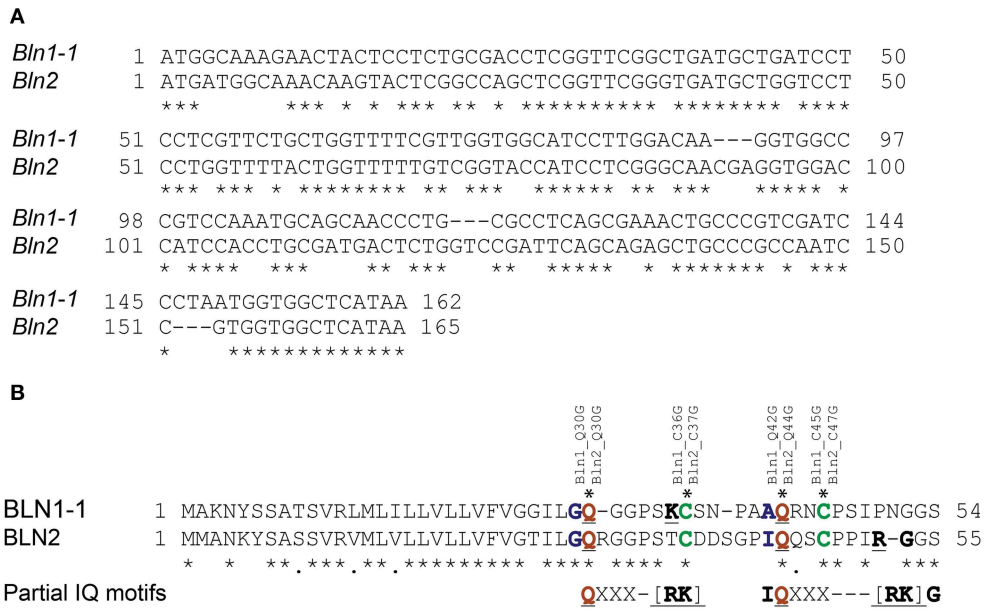

FIGURE 4 | Alignment of *Bln1* and *Bln2* with the positions of conserved cysteines and potential partial IQ motifs. (A) Nucleotide alignment of *Bln1* and *Bln2* open reading frames. A "*" indicates conserved nucleotides. **(B)** Amino acid alignment of BLN1 and BLN2. The conserved glutamines (Q) in the partial IQ motifs are shown in red (with blue adjacent), cysteines (C) are shown in green. The conserved amino acids in potential partial IQ motifs (compared to the complete consensus [FILV]Qxxx[RK]Gxxx[RK]) are underlined. For BLN1, Q to G mutations were inserted at amino acid residues 30 and 42, and C to G mutations at residues 36 and 45. For BLN2, Q to G mutations were inserted at amino acid residues 30 and 44, and C to G mutations at residues 37 and 47.

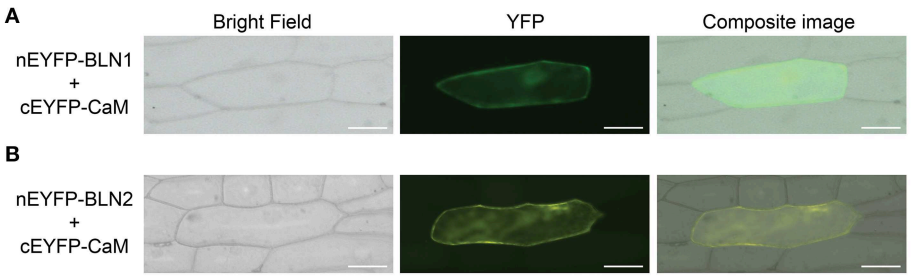

FIGURE 5 | Bimolecular fluorescence complementation (BiFC) assay for interaction between BLN1/2 and CaM. The *Bln1* and *Bln2* full length ORFs were PCR-amplified and cloned into *Eco*RI-*Bam*HI sites of *Eco*RI-*Bam*HI sites of pSAT4-nEYFP-C1 or pSAT4-cEYFP-C1 to generate pSAT4-nEYFP-Bln1, pSAT4-nEYFP-Bln2, pSAT4-cEYFP-CaM respectively. The designated plasmid combinations were co-bombarded into onion epidermal cells. The bright-field and fluorescent images were taken using the Zeiss Axiovert 100 microscope equipped with appropriate YFP filter. Statistical analysis of YFP count data is presented in **Table 3**. **(A)** Microscopic observation for interaction between BLN1 and CaM. **(B)** Microscopic observation for interaction between BLN2 and CaM.

However, to specifically understand *Bln1*-regulated targets, we restricted our follow-up functional assays to genes with no confounding effects (Mock vs. BSMV:00 $p > 0.01$).

In addition to the newly identified genes, we also discovered that *Bln2* (Contig26496_at) was suppressed in *Bln1* silenced plants (**Figure 8B**). Sequence comparison of *Bln1* and *Bln2* indicates that these two genes share significant identity (**Figure 4**; Meng et al., 2009). Although the *Bln1* silencing construct was designed across a 3′ divergent region, the two *Bln* family members share 13 contiguous nucleotides, indicating that *Bln2* might be unintentionally silenced (Jackson et al., 2003).

Functional Characterization of Conserved Genes Suppressed Upon *Bln1* Silencing

Analysis of the cohorts described above should provide mechanistic clues to the function of *Bln1* in innate immunity. For example, the most significant candidate from this comparison is Barley1 Contig3615_at [$p = 4.85^{E\text{-}11(HOR11538)}$/$p = 1.0^{E\text{-}8(Clansman)}$], representing the gene encoding Importin subunit α-1b, which is suppressed in BSMV:$Bln1_{248}$ silenced plants (**Figure 8C**). Importin subunit α-1b localizes to the perinuclear region of the cytoplasm, where it binds specifically to substrates containing a nuclear localization signal (NLS)

and promotes docking of these substrates to the nuclear envelope for subsequent import (Jiang et al., 2001). A homolog of Importin α is also involved in innate immunity in Arabidopsis (Palma et al., 2005). Silencing of *Bln1* also results in the suppression of genes encoding components in the protein secretory pathway, including Sec61 γ, represented by Contig3680_at [$p = 2.89^{E-05(HOR11538)}/p = 9.31^{E-05(Clansman)}$] (**Figure 8D**). Sec61 γ protein is a component of the SEC61 complex that is a conserved protein-conducting channel for secretory protein translocation across the endoplasmic reticulum (ER) membrane (Osborne et al., 2005). Also represented in the common set of six is a gene encoding a putative cysteine protease inhibitor (HV10C01u_s_at). This protein is similar to maize CC9, an apoplastic cysteine protease inhibitor that suppresses host immunity to *Ustilago maydis* (Van Der Linde et al., 2012). Another gene in the conserved set (Contig12608_at) encodes a protein of unknown function but with a classic nuclear localization signal (Dinkel et al., 2014). Genes represented by Contig12219_at (*Bln1*), Contig3680_at (*Sec61* γ), HS16M03u_x_at (unknown), and HV10C01u_s_at (cysteine protease inhibitor) are induced by

TABLE 3 | Mixed linear analysis of mutations in the BLN1 and BLN2 IQ domain and cysteines and their effect on binding with CaM[a].

Treatment	Mean YFP cell counts[b]	Estimate[c]	*T*-value	Adjusted *P*-value[d]
BLN1 and CaM	57.00	–	–	–
BLN1-C36G and CaM	2.33	54.67	17.28	4.37E-07
BLN1-C45G and CaM	0.33	56.67	17.91	3.30E-07
BLN1-Q30G and CaM	8.33	48.67	15.38	1.08E-06
BLN1-Q42G and CaM	2.67	54.33	17.17	4.59E-07
BLN2 and CaM	32.33	–	–	–
BLN2-C37G and CaM	1.00	31.33	6.13	3.85E-04
BLN2-C47G and CaM	1.33	31.00	6.06	4.19E-04
BLN2-Q30G and CaM	0.00	32.33	6.32	2.99E-04
BLN2-Q44G and CaM	2.33	30.00	5.87	5.43E-04

[a] *A mixed linear model analysis was done using PROC MIXED of the SAS Software. Contrasts were designed to test the differences between the control and the treatment with cell counts as the response.*

[b] *Represents mean of total cells exhibiting YFP from three independent biological replications. The appearance of YFP fluorescing cells were equivalent among mutant or wild-type bombarded constructs.*

[c] *Difference between the least square means for the total YFP cells in control vs. the treatment.*

[d] *P-values were adjusted for multiple testing the methods of Dunnett (1980) and Hsu (1992). Treatments with adjusted $p \leq 0.05$ were considered significantly different from the BLN1, BLN2, and CaM wild-type control interactions.*

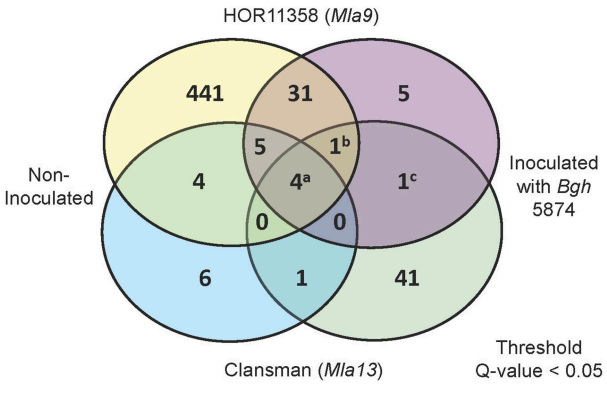

FIGURE 7 | Summary of differentially expressed genes in *Bln1*-silenced leaves as compared to BSMV:00 controls. Venn diagram represents differentially expressed genes (Threshold: $q < 0.05$) with and without inoculation with *Bgh* for both HOR11358 (*Mla9*; upper circles) and Clansman (*Mla13*; lower circles) background plants. Contrasts were assessed between empty vector (BSMV:00) and *Bln1* silenced (BSMV:$Bln1_{248}$) plants. Superscripts (a) Contig12608_at, HS16M03u_x_at, HV10C01u_s_at, Contig3615_at (*Importin α-1b*); (b) Contig12219_at (*Bln1*); (c) Contig3680_s_at (*Sec61 γ*).

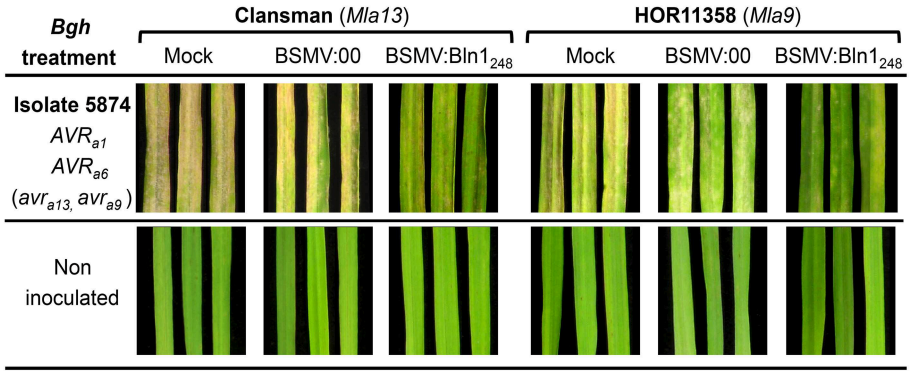

FIGURE 6 | Barley1 GeneChip expression profiling design and phenotypes upon *Bgh* infection. Transcript profiling was based a split-plot design with 5 replications as blocks, *Bgh* treatment as the whole-plot factor, and all combinations of genotype [cv. Clansman (*Mla13*) and cv. HOR11358 (*Mla9*)] and VIGS treatment [Buffer control (mock), BSMV:00 (empty vector), and BSMV:$Bln1_{248}$] as the split-plot factor for a total of 60 Barley1 GeneChip hybridizations. Seven-day-old plants were treated with Mock, BSMV:00, and BSMV:$Bln1_{248}$. Twelve days after buffer and *BSMV* treatments, plants were inoculated with the compatible *Bgh* isolate 5874 (AVR_{a1}, AVR_{a6}, avr_{a9}, avr_{a13}), or non-inoculated. Leaves were harvested at 32 h after *Bgh* inoculation. Five leaves for each treatment were used for phenotyping 7 days after *Bgh* inoculation.

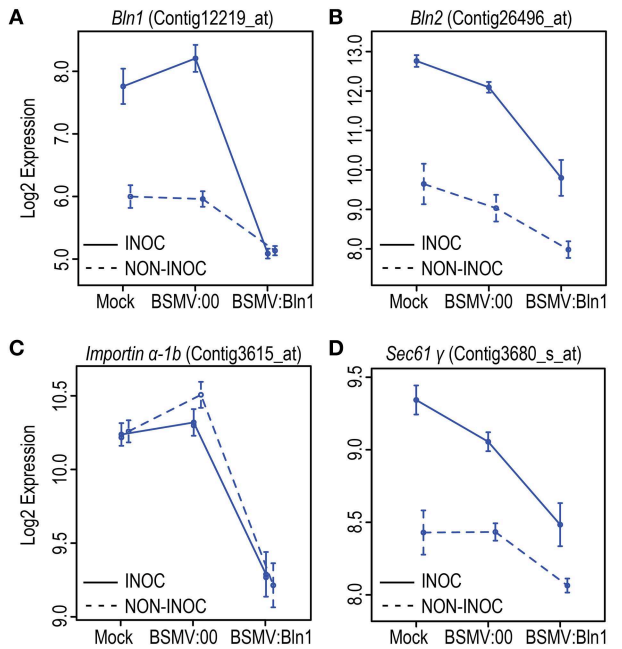

FIGURE 8 | Log2 expression level results from Barley1 GeneChip profiling of *Bln1*, *Bln2*, *Importin* α-1b, and *Sec61* γ in *Bln1*-silenced leaves. *Barley stripe mosaic virus* (*BSMV*)-Virus Induced Gene silencing was performed on HOR11358 (*Mla9*) plants as described in **Figure 6**. Twelve days after buffer and *BSMV* treatments, plants were inoculated with the compatible *Bgh* isolate 5874 (AVR_{a1}, AVR_{a6}, avr_{a9}, avr_{a13}). Log2 expression levels for *Bln1* **(A)**, *Bln2* **(B)**, *Importin α-1b* **(C)**, and *Sec61* γ **(D)** are plotted in graphs. INOC, inoculation; NON-INOC, Non-inoculated. Error bars represent the standard errors (SE).

Bgh infection, whereas, Contig3615_at (*Importin α-1b*) and Contig12608_at (NLS protein) are not. Nevertheless, transcript accumulation of all six is suppressed in *Bln1*-silenced plants (**Figure 7**).

Based on these predicted annotations, we then selected a sub-set for functional analysis via *BSMV*-mediated gene silencing. Both *Importin α-1b* (Contig3615_at) and *Sec61* γ (Contig3680_s_at), were introduced into the BSMV-VIGS system as BSMV:Imp α-1b$_{319}$ and BSMV:Sec61γ_{319}, respectively, and plants were subjected to silencing as described above. To alleviate off-target silencing, the chosen genes were aligned to the barley genome resource (Mayer et al., 2012). Subsequently, unique, single-copy regions of each target gene were used to design BSMV-VIGS primers (Supplemental Table S2), and each construct was bombarded in at least two independent replicates of 10 plants each. As shown in **Figure 9**, both of these genes impact powdery mildew development, as demonstrated by significantly less fungal colonies and hyphal growth on the surface of epidermal cells, as compared to BSMV:00 controls (**Figures 9A,B**, **Table 1**). qRT-PCR on RNA isolated from the silenced leaves as well as BSMV:00 controls confirmed that transcript accumulation for the target genes was suppressed (**Figure 9C**). These data suggest that both *Importin α-1b* and *Sec61* γ play negative roles in barley innate immunity to *Bgh*.

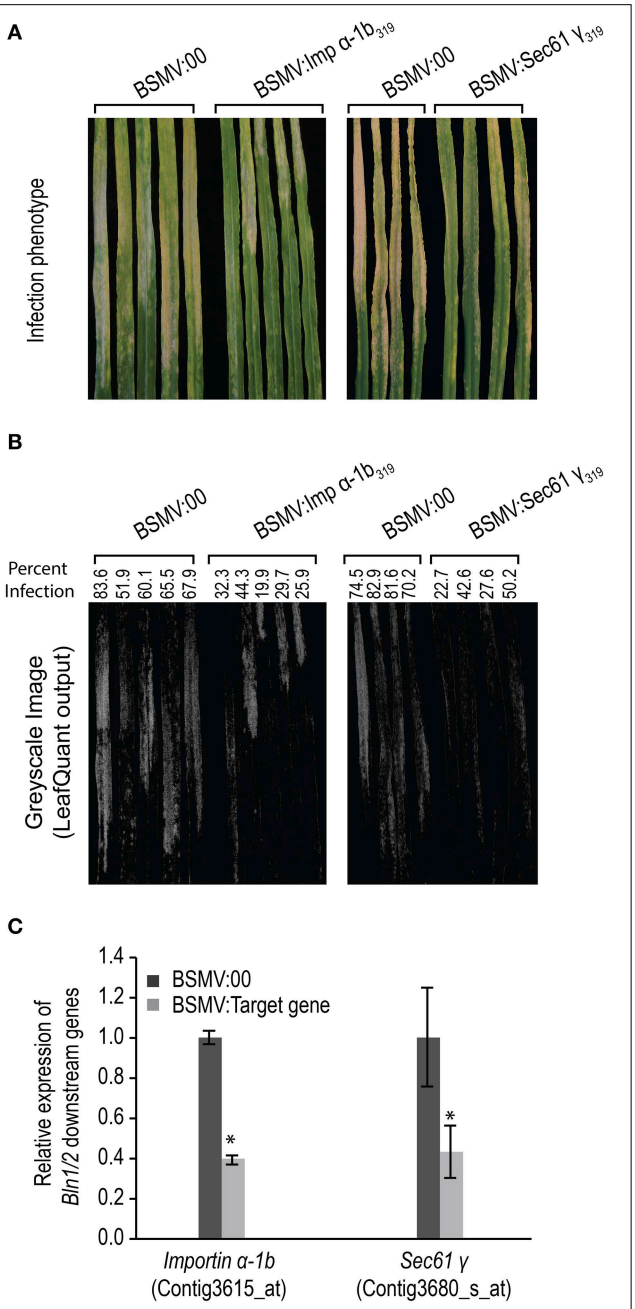

FIGURE 9 | Infection phenotype of *Blumeria graminis* f. sp. *hordei* (*Bgh*) for leaves silenced for *Importin α-1b* and *Sec61* γ. Gene silencing was performed on HOR11358 (*Mla9*) plants and mediated by *Barley stripe mosaic virus* (*BSMV*). Seven-day-old plants were treated with buffer and *BSMV*. Twelve days after buffer and *BSMV* treatments, plants were inoculated with compatible *Bgh* isolate 5874 (AVR_{a1}, AVR_{a6}, avr_{a9}, avr_{a13}). The infection phenotypes were photographed 7 days after inoculation and hyphal growth area for each leaf was quantified by LeafQuant-VIGS software (**Table 1**). RNA samples for gene expression analysis were prepared from the same quantified leaves and gene levels were analyzed by quantitative reverse-transcriptase polymerase chain reaction analysis on transcript accumulation. The amount of RNA in each reaction was normalized using primers specific for barley Actin. The $2^{-\Delta CT}$ method was used to calculate the target gene expression for each individual silencing construct as compared with BSMV:00 treated plants

(Continued)

FIGURE 9 | Continued
(Schmittgen and Livak, 2008). Fold change due to silencing is calculated by dividing the expression mean value for the targeted gene in silenced plants by the mean value measured in BSMV:00-treated plants (* designates that $p < 0.05$). Bars represent standard error calculated from at least five independent plants from two replicate experiments. The average value in BSMV:00 samples was set to 1.0. **(A)** Infection phenotype of *Bgh* on *Importin α-1b* and *Sec61 γ* silenced leaves. **(B)** LeafQuant outputs and quantification fungal infection. **(C)** Relative expression of *Importin α-1b* and *Sec61 γ* in *BMSV* induced gene silenced leaves.

Discussion

BLUFENSIN1 (BLN1) and BLUFENSIN2 (BLN2), two members in a monocot-specific family of cysteine-rich peptides, are barley susceptibility factors to powdery mildew (Meng et al., 2009). Both BLN1 and BLN2 reveal structural and sequence similarities to knottins, small disulfide-rich proteins characterized by a unique "disulfide through disulfide knot" (Combelles et al., 2008). *Bln* family members are highly upregulated upon fungal infection and BLN proteins can be secreted into the apoplast. Although silencing *Bln* does not break *Mla* [Nucleotide binding, Leucine rich repeat (NLR)]-mediated resistance, knockdown of *Bln1* increases barley innate immune responses and overexpression renders the barley host supersusceptible in compatible interactions.

Based on these observations, we postulate that BLN family members are potential signal molecules co-opted by *Bgh* effectors to bypass innate immune systems and colonize the host. In turn, interactors or partners of BLN would also be expected to play key roles in mediating the plant immune response. This hypothesis is supported by the observed interaction between BLN1 and BLN2, and barley calmodulin (CaM) (**Figure 5**). CaM, as a universal Ca^{2+} sensor, plays essential roles in regulating numerous intracellular processes, including plant defense (Kim et al., 2002; Reddy et al., 2011; Bender and Snedden, 2013). The BLN protein may function as a ligand to interact with CaM and change its conformation to alter downstream CaM signaling (**Figure 10**). Alternatively, BLN may interact with barley partner(s) or *Bgh* effector(s) to favor basic compatibility.

Nuclear Import and the Secretory Pathway—Pathogen Effector Import Systems in Host Plants

Negative regulation of the basal defense pathway prevents unchecked potentiation of the response and deleterious effects on normal cell functions (Ge et al., 2007). Forty-seven and forty-eight genes were identified in HOR11358 (*Mla9*) and Clansman (*Mla13*), respectively, that are significantly differentially expressed ($p < 0.0001$) when *Bln1* is silenced (**Figure 7**, Supplemental Table S1). Six of these genes were suppressed in common between the two backgrounds. Of these, *Importin α-1b* and *Sec61 γ* are involved in protein trafficking, the CC9 homolog (HV10C01u_s_at) is a putative apoplastic cysteine protease inhibitor, and finally, the gene represented by Contig12608_at, encodes an unknown protein with a classic nuclear localization signal (Dinkel et al., 2014). Silencing two (*Importin α-1b* and *Sec61 γ*) of the conserved set of six genes significantly reduced host susceptibility in compatible interactions of barley and *Bgh* (**Figure 9**), and CC9 suppresses host immunity to *Ustilago maydis* in maize (Van Der Linde et al., 2012), suggesting that transcription of these plant genes is essential for the fungus to successfully colonize host cells.

It has become evident that the interaction of pathogen effectors and resistance proteins in the nucleus is critical to *R*-gene-mediated resistance (Burch-Smith et al., 2007; Shen et al., 2007; Tameling and Baulcombe, 2007; Wirthmueller et al., 2007; Liu and Coaker, 2008; Tameling et al., 2010). Data presented here indicates that translocation of protein into the nucleus is a key step in innate immunity as well. Importin α in pepper was shown to interact with AvrBs3, a type III-secreted effector from *Xanthomonas campestris* pv. *vesicatoria*, both in yeast and *in vitro* through a nuclear localization signal (NLS) (Szurek et al., 2001). Given that the gene encoding Importin subunit α-1b (Contig3615_at) is significantly down-regulated in *Bln1*-silenced plants, we postulate that a function of BLN1, even in the absence of *Bgh* infection (**Figure 8C**), could be to sustain transcript accumulation of Importin. Induction of BLN1 by *Bgh* may enhance the translocation of select effectors from the apoplast to the nucleus, which might be necessary for the fungus to colonize its barley host.

Such a scenario, though not reported before in cereal-fungal interactions, is not without precedent. In the interaction of Arabidopsis with *Agrobacterium*, a historically important pathogen most widely know for its role in plant transformation (McCullen and Binns, 2006), multiple Importin α proteins interact with both *Agrobacterium* VirD2 and VirE2. However, Importin α-4 appears to be the most crucial isoform for transfer of Vir proteins to the plant cell nucleus (Bhattacharjee et al., 2008).

It should also be noted that although two full-length Importin α isoforms have been identified in barley (Importin α-1a and Importin α-1b, represented by probe sets Contig4129_at and Contig3615_at, respectively), only expression of Importin α-1b is significantly affected by *Bln1* silencing. This indicates that Importin α-1b is specifically involved in BLN-mediated resistance to barley powdery mildew.

Nonetheless, Importin α-1b in barley and Importin α3 in Arabidopsis (Palma et al., 2005) have opposite effects on plant defense against pathogens. This suggests that different isoforms of Importin α have substrate-specific recognition to differentially regulate plant immunity. Substrate-specific recognition of Importin has also been observed for nuclear import of proteins involved in rice photomorphogenesis (Jiang et al., 2001) and for neural differentiation of mouse embryonic stem cells (Goldfarb et al., 2004; Yasuhara et al., 2007, 2013), signifying the diverse temporal and spatial regulation influenced by Importin isoforms in plant and animal systems.

Silencing of *Bln1* also results in the coordinate suppression of genes encoding components in the protein secretory pathway, including the SEC61 complex. The SEC61 complex is a conserved protein-conducting channel for translocation across the endoplasmic reticulum (ER) membrane (Osborne et al.,

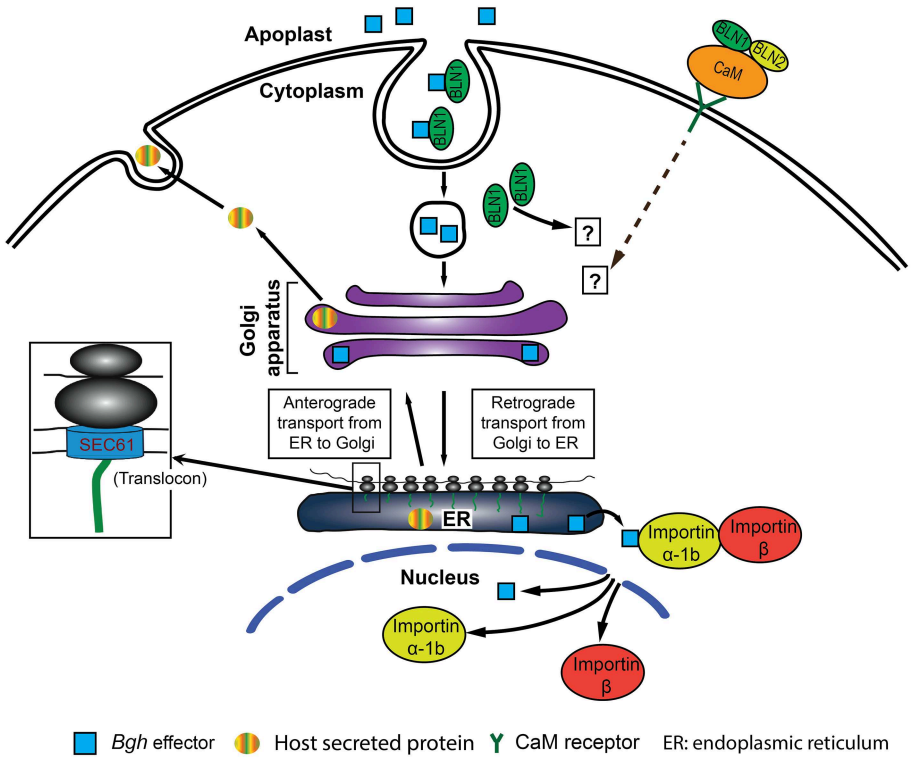

FIGURE 10 | Predictive model for BLN1 and BLN2 function in the barley immune system. (1) BLN (green filled circle) can function as a ligand and binds with effectors in the apoplast to promote barley-*Bgh* compatible interactions. (2) The BLN-effector complex then can enter plant cells by endocytic routes, and move to the ER region through a retrograde secretory pathway. (3) Subsequently, effectors could be released into the cytoplasm through the SEC61 pore-forming complex and picked up by Importin α-1b and translocated into the nucleus by the Importin complex to regulate gene expression. (4) The level of BLN1-effector complex may be the positive force regulating the expression of Importin α-1b and Sec61 γ to titrate the BLN-effector level. Alternatively, BLN binds CaM, a Ca^{2+} sensor, in the apoplast and changes CaM conformation to alternate the interaction of CaM with its receptor in the plasma membrane (Cui et al., 2005; Wang et al., 2009) to positively regulate the state-steady levels of Importin α-1b and Sec61 γ. In both cases, BLN, Importin α-1b, and Sec61 γ proteins are positive regulators for barley-*Bgh* compatible interactions (or negative regulators for innate immunity). Silencing of *Bln1* results in the suppression of *Importin α-1b* and *Sec61 γ*, impairing protein anterograde and retrograde trafficking as well as translocation into the nucleus required for barley-*Bgh* compatible interaction.

2005; Kelkar and Dobberstein, 2009; Park and Rapoport, 2012) and is required for induction of systemic aquired resistance to *Pseudomonas syringae* pv. *maculicola* in Arabidopsis (Wang et al., 2005). Recently, the Sec61 β subunit in barley has been shown to be an ER protein transporting pore that is required for host susceptibility to powdery mildew (Zhang et al., 2013).

Does BLN1 Drive Protein Trafficking?

The protein secretory pathway starts with insertion of protein into the SEC61 translocon complex and involves a series of steps by which proteins are transported between organelles in anterograde or retrograde directions. Protein trafficking into the nucleus includes the interaction of transported targets with the Importin complex. The secretory pathway plays a vital role in plant disease resistance (Kwon et al., 2008a,b; Rojo and Denecke, 2008; Wang and Dong, 2011). Down-regulation of multiple components in the secretory pathway in *Bln1* silenced plants point to a role of *Bln1* in the regulation of this pathway. One possibility is that BLN1 may interact with host-secreted proteins required for pathogen-host interaction. Silencing of *Bln1* may reduce the amount of these BLN1 interacting host-secreted proteins, resulting in down-regulation of anterograde protein transport. Alternatively, interaction of BLN1 with *Bgh* or host secreted proteins could signal the entry of BLN interactors into the host cell via the retrograde pathway (Spooner et al., 2006; Johannes and Popoff, 2008; Dong et al., 2013; Drerup and Nechiporuk, 2013; Koyuncu et al., 2013). Silencing of *Bln1* reduces these interactions and therefore release the demand for components involved in protein trafficking pathway, such as Sec61 γ and Importin α-1b. A third scenario may involve BLN1 interacting with a specific signal molecule, such as the Ca^{2+} sensor CaM, to positively regulate transcript accumulation of genes encoding components involved in protein trafficking, such as *Sec61 γ and Importin α-1b*. Knock down of *Bln1* would suppress the expression of genes encoding these components (**Figure 10**). All three hypotheses are supported by the observation that *Bln* family members regulate the expression of genes implicated in protein trafficking, overexpression of

Bln renders barley more susceptible to *Bgh* (**Figure 2**), and that silencing of *Bln1*, *Importin α-1b*, and *Sec61 γ* increases barley innate immunity (**Figures 6**, **9**). Thus, BLN proteins may modulate protein transport in barley-*Bgh* interactions and BLN levels influence protein trafficking in infected barley cells.

Summary: Are BLN1 and BLN2-potential Host-targeting Signals for *Bgh*?

In the interaction between barley and *Bgh,* transfer of signals may be expected to occur between host and pathogen during formation of the perihaustorial interface (Dodds et al., 2004, 2006).

From an evolutionary standpoint, genes in redundant networks with an incredible level of buffering capacity imply minimal selective pressures acting on these genes. One example was discussed by Xu et al. (2006), where *Atwrky18*/*Atwrky40* and *Atwrky18*/*Atwrky60* double mutants were more resistant to *Pseudomonas syringae* DC3000 but more susceptible to *Botrytis cinerea* infection, but single *Atwrky* mutants behaved similar to wild-type plants. BLN1 and BLN2 are potentially part of a redundant set of negative regulators for plant defense.

Both BLN1 and BLN2 are highly induced upon *Bgh* inoculation and transient overexpression increases barley plants susceptibility; these results are consistent with the silencing results. We further identified that BLN proteins could be secreted into the apoplast and interact with each other and CaM in plant cells. Thus, BLN could act as potential host-targeting signals for *Bgh* to colonize in plant cells; the interactions between BLN and *Bgh* effectors could fine-tune sets of protein pathways, which might be involved in transporting fungal proteins into the host cells.

Materials and Methods

Plant Materials and Fungal Isolates

Seedlings of barley lines Black Hulless, CI 16151 (*Mla6*), HOR11358 (*Mla9*), and Clansman (*Mla13*) were used for functional analysis. Virus infected barley was maintained in a growth chamber with a 16 h photoperiod with light intensity at 550 μmol m^{-2} s^{-1} and a daytime temperature of 24°C and dark temperature of 20°C. *Bgh* isolate 5874 (AVR_{a1}, AVR_{a6}, avr_{a9}, avr_{a13}) was propagated on *H. vulgare* cv. Manchuria (CI 2330) in a controlled growth chamber at 18°C (16 h light/8 h darkness).

BLN1 and BLN2 Subcellular Localization

Total RNA was extracted from CI 16151 (*Mla6*) plants 20 hai with *Bgh* isolate 5874 (AVR_{a6}) according to the method of Caldo et al. (2004). First-strand cDNA was synthesized using 2 μg of total RNA, oligo$(dT)_{20}$ primer and Superscript reverse transcriptase III (Invitrogen, Carlsbad, CA). Subsequently, first strand cDNA was used as the template to amplify *Bln1* and *Bln2* coding sequences with/without signal peptides or the signal peptide regions; Primers were designed according to *Bln1* EST sequence (GeneBank Accession no. is FJ156737) and *Bln2* EST sequence (GeneBank Accession no. is FJ156745) and listed in Supplemental Table S2.

BLN-GFP chimeric constructs were made using overlapping PCR. First, full length *Bln1* was amplified using primer pair Bln1-NcoN_pf1 and Bln1-C_pr1; *GFP* was amplified with pEGFP (Clontech Laboratories, Inc., Mountain View, CA) as template and primer pair GFP-FKS_pf1 and GFP-Bam_pr1. The final PCR was performed using PCR products of the previous two reactions as template and primer pair Bln1-NcoN_pf1 and GFP-Bam_pr1. The final PCR product was digested with *Nco*I and *Bam*HI and ligated into similarly treated pTRL2 (Restrepo et al., 1990) to yield p35S:BLN1+SP, harboring coding regions for full-length BLN1 and GFP. A similar strategy was adopted to make the *Bln1* signal peptide-GFP construct, p35S:BLN1_SP only, as well as *Bln1*-GFP construct absent the *Bln1* signal peptide, p35S:BLN1-SP. When making corresponding Bln2-GFP constructs (p35S:BLN2+SP, p35S:BLN2_SP only and p35S:BLN2-SP), PCR products were digested with *Nco*I and *Sma*I and inserted into similarly treated pBLN1+SP.

These constructs were delivered into onion epidermal cells by using biolistic PDS-1000/he system (Bio-Rad, Hercules, CA, USA) as described by Elling et al. (2007). After bombardment, epidermal peels were incubated for 24 h in the dark at 20–25°C. Plasmolysis of onion epidermal cells was attained by soaking the peels in 1 M sucrose solution for 20 min. A Zeiss Axio Imager M.1 microscope (Zeiss, Inc., Thornwood, NY) was used for observation. At least three independent replicate experiments were conducted.

To visualize GFP in the apoplast, onion epidermal cells were incubated in agar medium supplemented with 3% sucrose (Murashige and Skoog, 1962) for 20 h, and transferred to 20 mM Pipes-KOH (pH 7.0) for 4 h on half-concentrated Murashige and Skoog (1962) agar medium supplemented with 1% sucrose (Genovesi et al., 2008). The pH 7.0 medium neutralizes the normally acidic apoplast in order to observe the fluorescence patterns.

Overexpression of *Bln1* and *Bln2* by Using the *BSMV* system

To introduce a foot- and-mouth disease virus (FMDV)-2A self-cleavage peptide and GFP for expression of foreign gene, pBPMV-IA-V5 (Zhang et al., 2010) was used as template with primer pair BS3-G4F1 and BS3-G4R1 for PCR to produce DNA fragment A, which was used as template with primer pair BS3-G4F2 and BS3-G4R2 to produce DNA fragment B. BSMV:γ (Meng et al., 2009) was used as template with primer pair BSMV-R3-F3 and BS3-4Rev for PCR to produce DNA fragment C. DNA fragments B and C were then used for overlapping PCR with primer pair BSMV-R3-F3 and BS3-G4R2 for PCR to produce DNA fragment D. Product D was digested with *Bgl*II and *Kpn*I and ligated into BSMV: γ digested by *Bgl*II and *Kpn*I to produce pBSMV-OEx:GFP.

To make *Bln1* and *Bln2* overexpression constructs, *Bln1* and *Bln2* cDNA described above were used as templates and primer pairs BSBln1Ov_pf1/BSBln1Ov_pr1 or BSBln2Ov_pf1/BSBln2Ov_pr1 were used respectively (Supplemental Table S2). PCR fragments contained an introduced *Stu*I and *Bam*H1 recognition sites at the 5′ and 3′ ends, respectively and were inserted into the *Stu*I and *Bam*H1

sites of pBSMV-OEx:GFP, the resulting vectors were designated as pBSMV-OEx:Bln1 and pBSMV-OEx:Bln2, respectively.

DNA bombardment and subsequent virion mechanical infection on HOR11358 (*Mla9*) plants was performed according to Meng et al. (2009). A Zeiss Axio Imager M.1 microscope (Zeiss, Inc., Thornwood, NY) was used for observation the GFP. At least two independent replicate experiments were performed.

BLN1 and BLN2 Interactions Via Bimolecular Fluorescence Complementation (BiFC)

Site-directed mutagenesis was carried out on *Bln1* and *Bln2* full length ORFs using QuickChange™ site-directed mutagenesis kit (Stratagene, La Jolla, CA). Primers used for amplification and mutagenesis are listed in Supplemental Table S2. From the BLN1 start codon, amino acid residues 30 and 42 were changed from Q to G and residues 36 and 45 were changed from C to G. For BLN2, amino acid residues 30 and 44 were changed from Q to G and residues 37 and 47 were changed from C to G. The resulting products contained *Eco*RI and *Bam*HI restriction sites respectively, and cloned into *Eco*RI-*Bam*HI sites of pSAT4-nEYFP-C1 or pSAT4-cEYFP-C1 to generate pSAT4-nEYFP-Bln1, pSAT4-nEYFP-Bln2, pSAT4-cEYFP-Bln1, and pSAT4-cEYFP-Bln2, respectively. For coexpression, particle bombardment was performed using onion epidermal cells. Gold particles (1.6 μm diameter) (Bio-Rad) were washed with 100% ethanol and coated with 1.25 μg of each DNA using standard procedures. cDNA-coated gold particles were bombarded at 1100 p.s.i. and 9 cm distance using a Biolistic Particle Delivery System PDS-1000/He (Bio-Rad). Bombarded tissues were incubated at 25°C in darkness for ∼24 h before being assayed for YFP activity. The bright-field and fluorescent images were taken using the Zeiss Axiovert 100 microscope with appropriate YFP filter.

BLN Interactions with Calmodulin Via Bimolecular Fluorescence Complementation (BiFC)

Calmodulin full length ORFs were PCR-amplified using primers listed in Supplemental Table S2. The resulting product containing *Eco*RI and *Bam*HI restriction sites was cloned into *Eco*RI-*Bam*HI sites of pSAT4-cEYFP-C1 to generate pSAT4-cEYFP-CaM. This was combined with Bln1 or Bln2 pSAT4 constructs as described above for bombardment and microscopic observation. At least three independent replicate experiments were conducted.

Statistical Analysis of YFP Cell Count Data

All cells exhibiting YFP were counted for each of the 3 independent biological replications. A mixed linear model analysis of observed YFP cell count data was conducted using PROC MIXED in SAS software. The model used total YFP cell count as the response and included random effect for replications. Four contrasts in SAS software were used to compare different controls (*Bln1* and *CaM*, *Bln2* and *CaM*, *Bln1* and *Bln2*, *Bln2* and *Bln1*) with their respective treatments. The least square means were correlated and when the *p*-values were adjusted using the Dunnett (1980) method, PROC MIXED used the factor-analytic covariance approximation described in Hsu (1992).

Target Synthesis and GeneChip Hybridization

Total RNA was isolated using a hot (60°C) phenol/guanidine thiocyanate method described by Caldo et al. (2004). Trizol-like reagent was made from 38% saturated phenol (pH 4.3), 0.8M guanidine thiocyanate, 0.4M ammonium thiocyanate, 0.1M sodium acetate (pH 5.0) and 5% glycerol (Fisher Scientific, Pittsburg, PA). RNA was purified further using RNeasy columns (Qiagen, Valencia, CA). Probe synthesis, labeling, and hybridization to Barley1 GeneChip probe arrays (Affymetrix #900515; Close et al., 2004) were performed using One Cycle and GeneChip IVT labeling protocols based on the Affymetrix manual (Affymetrix, Santa Clara, CA) at the Iowa State University GeneChip Core facility.

Normalization and Mixed Linear Model Analysis of Barley1 GeneChip Data

As described previously (Caldo et al., 2004; Wise et al., 2007), we conducted mixed linear model analyses of the normalized signal intensities for each of the 22,840 Barley1 probe sets (Wolfinger et al., 2001). RMA normalization and data transformation was done using package affy in BioConductor/R. Mixed linear model analysis was conducted using PROC MIXED in SAS software. The model used RMA normalized expression values as the response, replication, inoculation and treatment (genotype*vector) as fixed factors, and replication*inoculation and replication*treatment as random factors. Contrasts in SAS software (SAS Institute Inc., Cary, NC, U.S.A.) were used to compare transcript levels between treatments (Mock vs. BSMV:00; BSMV:00 vs. BSMV:$Bln1_{248}$) of a specific genotype [HOR11538 (*Mla9)* or Clansman (*Mla13*)] after infection with *Bgh* 5874. *Q*-values were estimated using the smoother method described in Storey and Tibshirani (2003). From these analyses, we expected to identify sets of genes involved in *Bln1*-mediated compatibility or incompatibility, and also genes that are perturbed in response to *BSMV* infection, in both *Bgh* inoculated vs. non-inoculated reference plants.

BSMV-VIGS

Inserts for BSMV-VIGS were amplified by PCR using primers that add *Pac*I and *Not*I restriction sites to the 5′ end and 3′ end, respectively (Supplemental Table S2). These sites enable ligation of the fragment in antisense orientation into the BSMV:γ vector. Silencing experiments were performed as described previously (Meng et al., 2009; Xi et al., 2009; Meng and Wise, 2012; Xu et al., 2014). Plants were maintained for 12 days in a growth chamber (Percival Scientific, Perry, IA, USA) with 16 h of light at 24°C (550 μmol m^{-2} s^{-1}) and 8 h darkness at 20°C. Plants were then inoculated with *Bgh* isolate 5874 (avr_{a9}) conidiospores [compatible interaction with HOR 11358 (*Mla9*)] and maintained in a growth chamber 16 h of light/ 8 h of darkness at 18°C. The infection phenotype was monitored for 7 days.

Quantitative Real-time PCR

Barley leaves were pulverized in liquid nitrogen and total RNA extracted using Trizol-like reagent (Caldo et al., 2004). Genomic

DNA was degraded by RNase-free DNase I (Ambion, Austin, TX, U.S.A.). SuperScript III reverse transcriptase (Invitrogen, Carlsbad, CA, USA) was used to synthesize first strand cDNA using 2 μg total RNA and oligo(dT)$_{20}$ primer. This cDNA was used as a template for qRT-PCR to determine expression of various target genes to barley Actin. The qRT-PCR was performed using a Bio-Rad iCycler (Bio-Rad, Hercules, CA, USA). Conditions for 20 μL reactions using PerfeCTa® SYBR® Green FastMix® for iQ (Quanta Biosciences, Gaithersburg, MD) were 95°C for 3 min, followed by 40 cycles of 95°C for 15 sec and 60°C for 1 min, then a melt curve was determined by starting at 55°C for 10 s and then increasing by 0.5°C every 10 s for 80 cycles. Three technical replicates for each biological sample in addition to four or five biological samples per treatment were included in each experiment. Target gene expression was calculated using the $2^{-\Delta CT}$ method for the BSMV:target gene and BSMV:00-treated plants. The fold change due to silencing was calculated by dividing the expression value for each BSMV:target gene treated leaves by the mean value measured in BSMV:00 treated plants (Schmittgen and Livak, 2008).

Imaging of *Bgh* Infection Phenotypes

At seven days after powdery mildew inoculation, third leaves of *BSMV* treated plants were randomly selected and photographed at high resolution (2592 pixels × 3456 pixels, i.e., 9 Megapixel at 4:3 aspect ratio) using a Canon PowerShot SX110 IS and the Vidpro professional Photo and Video LED light kit model Z-96K. The leaves were set on black felt for uniform, high contrast background. Subsequent images were analyzed using an in-house pattern-recognition software, designated LeafQuant-VIGS, developed using MathWorks® MATLAB® 7.14 and Image Processing Toolbox™ 8.0. Starting with high-resolution RGB images of each leaf, LeafQuant-VIGS first defines the edges, then detects the background and converts it to uniformly true black, converts the high-resolution color RGB image to an 8-bit gray-scale image with 256 shades of gray, and outputs histograms of the hyphal distribution per leaf, which then reports mean, median, and quantiles of the results as a csv (comma separated values) file for further processing (Whigham et al., 2015). Because elongating secondary hyphae (ESH), an indicator of functional haustoria (Ellingboe, 1972), are white and the barley leaf is green, these differences can be used to quantify fungal growth in terms of percent infection. LeafQuant-VIGS software is offered under MIT license via Github at http://git.io/leafquant.

Analysis of LeafQuant-VIGS Data

A separate linear model analysis of the LeafQuant-VIGS data was conducted for each silencing and over-expression construct using the package MULTCOMP in R programming language (Hothorn et al., 2008). All models used percent infection as the response. The model was used to compare the mean percent infection of BSMV:00 treated leaves to the mean percent infection for mock and BSMV:construct treated leaves. *P*-values were adjusted for multiple testing using the Dunnett method (Dunnett, 1955).

Data Access

All detailed data and data from expression profiling have been deposited as Accession number BB101 in PLEXdb (http://plexdb.org/) (Dash et al., 2012). Files can be downloaded as batch files in MAGE-ML, CSV, CEL, DAT, or expression data formats at the Download Center or downloaded as individual CEL, CHP, DAT, or EXP files under "browse experiments." Data has also been deposited as Accession number GSE61644 at NCBI-GEO.

Author Contributions

Conceived and designed the experiments: YM, WX, DN, and RW. Performed the experiments: YM, WX, GF, and RW. Analyzed the data: WX, YM, PS, GF, DN, and RW. Contributed reagents/materials/ analysis tools: YM, WX, PS, GF, DN, and RW. Wrote and edited the paper: WX, YM, PS, GF, and RW.

Acknowledgments

We thank Matt Moscou for initial analysis of the Barley1 GeneChip dataset. This research was supported by National Science Foundation Plant Genome grants 05-00461, 09-22746, and 13-39348. This article is a joint contribution of the Iowa Agriculture and Home Economics Experiment Station and the Corn Insects and Crop Genetics Research Unit, USDA-Agricultural Research Service. Mention of trade names or commercial products in this publication is solely for the purpose of providing specific information and does not imply recommendation or endorsement by the U.S. Department of Agriculture or the National Science Foundation.

Supplementary Material

The Supplementary Material for this article can be found online at: http://journal.frontiersin.org/article/10.3389/fpls.2015.00409/abstract

References

Acevedo-Garcia, J., Kusch, S., and Panstruga, R. (2014). Magical mystery tour: MLO proteins in plant immunity and beyond. *New Phytol.* 204, 273–281. doi: 10.1111/nph.12889

Ahmed, A. A., Pedersen, C., Schultz-Larsen, T., Kwaaitaal, M., Jørgensen, H. J., and Thordal-Christensen, H. (2015). The barley powdery mildew candidate secreted effector protein CSEP0105 inhibits the chaperone activity of a small heat shock protein. *Plant Physiol.* 168, 321–333. doi: 10.1104/pp.15.00278

Bahler, M., and Rhoads, A. (2002). Calmodulin signaling via the IQ motif. *FEBS Lett.* 513, 107–113. doi: 10.1016/S0014-5793(01)03239-2

Bellincampi, D., Cervone, F., and Lionetti, V. (2014). Plant cell wall dynamics and wall-related susceptibility in plant-pathogen interactions. *Front. Plant Sci.* 5:228. doi: 10.3389/fpls.2014.00228

Bender, K. W., and Snedden, W. A. (2013). Calmodulin-related proteins step out from the shadow of their namesake. *Plant Physiol.* 163, 486–495. doi: 10.1104/pp.113.221069

Bent, A. F., and Mackey, D. (2007). Elicitors, effectors, and *R* genes: the new paradigm and a lifetime supply of questions. *Annu. Rev. Phytopathol.* 45, 399–436. doi: 10.1146/annurev.phyto.45.062806.094427

Berridge, M. J., Bootman, M. D., and Roderick, H. L. (2003). Calcium signalling: dynamics, homeostasis and remodelling. *Nat. Rev. Mol. Cell Biol.* 4, 517–529. doi: 10.1038/nrm1155

Bhattacharjee, S., Lee, L.-Y., Oltmanns, H., Cao, H., Veena, C. J., and Gelvin, S. B. (2008). IMPa-4, an *Arabidopsis* importin α isoform, is preferentially involved in *Agrobacterium*-mediated plant transformation. *Plant Cell* 20, 2661–2680. doi: 10.1105/tpc.108.060467

Burch-Smith, T. M., Schiff, M., Caplan, J. L., Tsao, J., Czymmek, K., and Dinesh-Kumar, S. P. (2007). A novel role for the TIR domain in association with pathogen-derived elicitors. *PLoS Biol.* 5:e68. doi: 10.1371/journal.pbio.0050068

Büschges, R., Hollricher, K., Panstruga, R., Simons, G., Wolter, M., Frijters, A., et al. (1997). The barley *Mlo* Gene: a novel control element of plant pathogen resistance. *Cell* 88, 695–705. doi: 10.1016/S0092-8674(00)81912-1

Caldo, R. A., Nettleton, D., and Wise, R. P. (2004). Interaction-dependent gene expression in *Mla*-specified response to barley powdery mildew. *Plant Cell* 16, 2514–2528. doi: 10.1105/tpc.104.023382

Ceroni, A., Passerini, A., Vullo, A., and Frasconi, P. (2006). DISULFIND: a disulfide bonding state and cysteine connectivity prediction server. *Nucleic Acids Res.* 34, W177–W181. doi: 10.1093/nar/gkl266

Cesari, S., Bernoux, M., Moncuquet, P., Kroj, T., and Dodds, P. N. (2014). A novel conserved mechanism for plant NLR protein pairs: the 'integrated decoy' hypothesis. *Front. Plant Sci.* 5:606. doi: 10.3389/fpls.2014.00606

Chu, Z., Yuan, M., Yao, J., Ge, X., Yuan, B., Xu, C., et al. (2006). Promoter mutations of an essential gene for pollen development result in disease resistance in rice. *Genes Dev.* 20, 1250–1255. doi: 10.1101/gad.1416306

Close, T. J., Wanamaker, S. I., Caldo, R. A., Turner, S. M., Ashlock, D. A., Dickerson, J. A., et al. (2004). A new resource for cereal genomics: 22K barley GeneChip comes of age. *Plant Physiol.* 134, 960–968.

Combelles, C., Gracy, J., Heitz, A., Craik, D. J., and Chiche, L. (2008). Structure and folding of disulfide-rich miniproteins: insights from molecular dynamics simulations and MM-PBSA free energy calculations. *Proteins* 73, 87–103. doi: 10.1002/prot.22054

Cui, S. J., Guo, X. Q., Chang, F., Cui, Y. W., Ma, L. G., Sun, Y., et al. (2005). Apoplastic calmodulin receptor-like binding proteins in suspension-cultured cells of *Arabidopsis thaliana*. *J. Biol. Chem.* 280, 31420–31427. doi: 10.1074/jbc.M501349200

Dash, S., Van Hemert, J., Hong, L., Wise, R. P., and Dickerson, J. A. (2012). PLEXdb: gene expression resources for plants and plant pathogens. *Nucleic Acids Res.* 40, D1194–D1201. doi: 10.1093/nar/gkr938

Dinkel, H., Van Roey, K., Michael, S., Davey, N. E., Weatheritt, R. J., Born, D., et al. (2014). The eukaryotic linear motif resource ELM: 10 years and counting. *Nucleic Acids Res.* 42, D259–D266. doi: 10.1093/nar/gkt1047

Dodds, P. N., Lawrence, G. J., Catanzariti, A.-M., Ayliffe, M. A., and Ellis, J. G. (2004). The *Melampsora lini AvrL567* avirulence genes are expressed in haustoria and their products are recognized inside plant cells. *Plant Cell* 16, 755–768. doi: 10.1105/tpc.020040

Dodds, P. N., Lawrence, G. J., Catanzariti, A. M., Teh, T., Wang, C. I., Ayliffe, M. A., et al. (2006). Direct protein interaction underlies gene-for-gene specificity and coevolution of the flax resistance genes and flax rust avirulence genes. *Proc. Natl. Acad. Sci. U.S.A.* 103, 8888–8893. doi: 10.1073/pnas.0602577103

Dong, B., Kakihara, K., Otani, T., Wada, H., and Hayashi, S. (2013). Rab9 and retromer regulate retrograde trafficking of luminal protein required for epithelial tube length control. *Nat. Commun.* 4:1358. doi: 10.1038/ncomms2347

Drerup, C. M., and Nechiporuk, A. V. (2013). JNK-interacting protein 3 mediates the retrograde transport of activated c-Jun N-terminal kinase and lysosomes. *PLoS Genet.* 9:e1003303. doi: 10.1371/journal.pgen.1003303

Du, L. Q., Ali, G. S., Simons, K. A., Hou, J. G., Yang, T. B., Reddy, A. S. N., et al. (2009). Ca2+/calmodulin regulates salicylic-acid-mediated plant immunity. *Nature* 457, 1154–U1116. doi: 10.1038/nature07612

Dunnett, C. W. (1955). A multiple comparison procedure for comparing several treatments with a control. *J. Am. Statist. Ass.* 50, 1096–1121.

Dunnett, C. W. (1980). Pairwise multiple comparisons in the unequal variance case. *J. Am. Statist. Ass.* 75, 796–800.

Eichmann, R., Bischof, M., Weis, C., Shaw, J., Lacomme, C., Schweizer, P., et al. (2010). BAX INHIBITOR-1 is required for full susceptibility of barley to powdery mildew. *Mol. Plant Microbe Interact.* 23, 1217–1227. doi: 10.1094/MPMI-23-9-1217

Elling, A. A., Davis, E. L., Hussey, R. S., and Baum, T. J. (2007). Active uptake of cyst nematode parasitism proteins into the plant cell nucleus. *Int. J. Parasitol.* 37, 1269–1279. doi: 10.1016/j.ijpara.2007.03.012

Ellingboe, A. H. (1972). Genetics and physiology of primary infection by *Erysiphe graminis*. *Phytopathology* 62, 401–406. doi: 10.1094/Phyto-62-401

Furler, S., Paterna, J. C., Weibel, M., and Bueler, H. (2001). Recombinant AAV vectors containing the foot and mouth disease virus 2A sequence confer efficient bicistronic gene expression in cultured cells and rat substantia nigra neurons. *Gene Ther.* 8, 864–873. doi: 10.1038/sj.gt.3301469

Ge, X., Li, G.-J., Wang, S.-B., Zhu, H., Zhu, T., Wang, X., et al. (2007). AtNUDT7, a negative regulator of basal immunity in Arabidopsis, modulates two distinct defense response pathways and is involved in maintaining redox homeostasis. *Plant Physiol.* 145, 204–215. doi: 10.1104/pp.107.103374

Genovesi, V., Fornalé, S., Fry, S. C., Ruel, K., Ferrer, P., Encina, A., et al. (2008). ZmXTH1, a new xyloglucan endotransglucosylase/hydrolase in maize, affects cell wall structure and composition in *Arabidopsis thaliana*. *J. Exp. Bot.* 59, 875–889. doi: 10.1093/jxb/ern013

Goldfarb, D. S., Corbett, A. H., Mason, D. A., Harreman, M. T., and Adam, S. A. (2004). Importin α: a multipurpose nuclear-transport receptor. *Trends Cell Biol.* 14, 505–514. doi: 10.1016/j.tcb.2004.07.016

Gracy, J., Le-Nguyen, D., Gelly, J.-C., Kaas, Q., Heitz, A., and Chiche, L. (2008). KNOTTIN: the knottin or inhibitor cystine knot scaffold in 2007. *Nucl. Acids Res.* 36, D314–D319. doi: 10.1093/nar/gkm939

Hein, I., Barciszewska-Pacak, M., Hrubikova, K., Williamson, S., Dinesen, M., Soenderby, I. E., et al. (2005). Virus-Induced Gene Silencing-based functional characterization of genes associated with powdery mildew resistance in barley. *Plant Physiol.* 138, 2155–2164. doi: 10.1104/pp.105.062810

Hothorn, T., Bretz, F., and Westfall, P. (2008). Simultaneous inference in general parametric models. *Biom. J.* 50, 346–363. doi: 10.1002/bimj.200810425

Houdusse, A., and Cohen, C. (1995). Target sequence recognition by the calmodulin superfamily—Implications from light-chain binding to the regulatory domain of scallop myosin. *Proc. Natl. Acad. Sci. U.S.A.* 92, 10644–10647. doi: 10.1073/pnas.92.23.10644

Hsu, J. C. (1992). The factor analytic approach to simultaneous inference in the general linear model. *J. Comp. Graph. Statist.* 1, 151–168.

Hückelhoven, R., Dechert, C., and Kogel, K. H. (2003). Overexpression of barley *BAX inhibitor 1* induces breakdown of *mlo*-mediated penetration resistance to *Blumeria graminis*. *Proc. Natl. Acad. Sci. U.S.A.* 100, 5555–5560. doi: 10.1073/pnas.0931464100

Hückelhoven, R., Eichmann, R., Weis, C., Hoefle, C., and Proels, R. K. (2013). Genetic loss of susceptibility: a costly route to disease resistance? *Plant Pathol.* 62, 56–62. doi: 10.1111/ppa.12103

Iyer, A. S., and McCouch, S. R. (2004). The rice bacterial blight resistance gene *xa5* encodes a novel form of disease resistance. *Mol. Plant Microbe Interact.* 17, 1348–1354. doi: 10.1094/MPMI.2004.17.12.1348

Iyer-Pascuzzi, A. S., and McCouch, S. R. (2007). Recessive resistance genes and the *Oryza sativa-Xanthomonas oryzae* pv. *oryzae* pathosystem. *Mol. Plant Microbe Interact.* 20, 731–739. doi: 10.1094/MPMI-20-7-0731

Jackson, A. L., Bartz, S. R., Schelter, J., Kobayashi, S. V., Burchard, J., Mao, M., et al. (2003). Expression profiling reveals off-target gene regulation by RNAi. *Nat. Biotech.* 21, 635–637. doi: 10.1038/nbt831

Jacob, F., Vernaldi, S., and Maekawa, T. (2013). Evolution and conservation of plant NLR functions. *Front. Immunol.* 4:297. doi: 10.3389/fimmu.2013.00297

Jiang, C.-J., Shoji, K., Matsuki, R., Baba, A., Inagaki, N., Ban, H., et al. (2001). Molecular cloning of a novel Importin alpha homologue from rice, by which constitutive photomorphogenic 1 (COP1) nuclear localization signal (NLS)-protein Is preferentially nuclear imported. *J. Biol. Chem.* 276, 9322–9329. doi: 10.1074/jbc.M006430200

Jiang, G. H., Xia, Z. H., Zhou, Y. L., Wan, J., Li, D. Y., Chen, R. S., et al. (2006). Testifying the rice bacterial blight resistance gene *xa5* by genetic complementation and further analyzing *xa5* (*Xa5*) in comparison with its homolog *TFIIAγ1*. *Mol. Genet. Genomics* 275, 354–366. doi: 10.1007/s00438-005-0091-7

Johannes, L., and Popoff, V. (2008). Tracing the retrograde route in protein trafficking. *Cell* 135, 1175–1187. doi: 10.1016/j.cell.2008.12.009

Kelkar, A., and Dobberstein, B. (2009). Sec61β, a subunit of the Sec61 protein translocation channel at the endoplasmic reticulum, is involved in the transport of Gurken to the plasma membrane. *BMC Cell Biol.* 10:11. doi: 10.1186/1471-2121-10-11

Kerppola, T. K. (2006). Design and implementation of bimolecular fluorescence complementation (BiFC) assays for the visualization of protein interactions in living cells. *Nat. Protoc.* 1, 1278–1286. doi: 10.1038/nprot.2006.201

Kim, M. C., Panstruga, R., Elliott, C., Muller, J., Devoto, A., Yoon, H. W., et al. (2002). Calmodulin interacts with MLO protein to regulate defence against mildew in barley. *Nature* 416, 447–451. doi: 10.1038/416447a

Koyuncu, O. O., Perlman, D. H., and Enquist, L. W. (2013). Efficient retrograde transport of pseudorabies virus within neurons requires local protein synthesis in axons. *Cell Host Microbe* 13, 54–66. doi: 10.1016/j.chom.2012.10.021

Kwon, C., Bednarek, P., and Schulze-Lefert, P. (2008a). Secretory pathways in plant immune responses. *Plant Physiol.* 147, 1575–1583. doi: 10.1104/pp.108.121566

Kwon, C., Neu, C., Pajonk, S., Yun, H. S., Lipka, U., Humphry, M., et al. (2008b). Co-option of a default secretory pathway for plant immune responses. *Nature* 451, 835–840. doi: 10.1038/nature06545

Lapin, D., and Van Den Ackerveken, G. (2013). Susceptibility to plant disease: more than a failure of host immunity. *Trends Plant Sci.* 18, 546–554. doi: 10.1016/j.tplants.2013.05.005

Lee, W. S., Hammond-Kosack, K. E., and Kanyuka, K. (2012). *Barley Stripe Mosaic Virus*-mediated tools for investigating gene function in cereal plants and their pathogens: virus-induced gene silencing, host-mediated gene silencing, and virus-mediated overexpression of heterologous protein. *Plant Physiol.* 160, 582–590. doi: 10.1104/pp.112.203489

Lewis, J., Wan, J., Ford, R., Gong, Y., Fung, P., Nahal, H., et al. (2012). Quantitative Interactor Screening with next-generation Sequencing (QIS-Seq) identifies Arabidopsis thaliana MLO2 as a target of the *Pseudomonas syringae* type III effector HopZ2. *BMC Genomics* 13:8. doi: 10.1186/1471-2164-13-8

Liu, J., and Coaker, G. (2008). Nuclear trafficking during plant innate immunity. *Mol. Plant* 1, 411–422. doi: 10.1093/mp/ssn010

Macho, A. P., and Zipfel, C. (2014). Plant PRRs and the activation of innate immune signaling. *Mol. Cell* 54, 263–272. doi: 10.1016/j.molcel.2014.03.028

Malinovsky, F. G., Fangel, J. U., and Willats, W. G. T. (2014). The role of the cell wall in plant immunity. *Front. Plant Sci.* 5:178. doi: 10.3389/fpls.2014.00178

Mayer, K., Waugh, R., Langridge, P., Close, T. J., Wise, R. P., Graner, A., et al. (2012). A physical, genetic and functional sequence assembly of the barley genome. *Nature* 491, 711–716. doi: 10.1038/nature11543

McCullen, C. A., and Binns, A. N. (2006). *Agrobacterium tumefaciens* and plant cell interactions and activities required for interkingdom macromolecular transfer. *Annu. Rev. Cell Dev. Biol.* 22, 101–127. doi: 10.1146/annurev.cellbio.22.011105.102022

Meng, Y., Moscou, M. J., and Wise, R. P. (2009). *Blufensin1* negatively impacts basal defense in response to barley powdery mildew. *Plant Physiol.* 149, 271–285. doi: 10.1104/pp.108.129031

Meng, Y., and Wise, R. P. (2012). HvWRKY10, HvWRKY19, and HvWRKY28 Regulate *Mla*-triggered immunity and basal defense to barley powdery mildew. *Mol. Plant Microbe Interact.* 25, 1492–1505. doi: 10.1094/MPMI-04-12-0082-R

Mentlak, T. A., Kombrink, A., Shinya, T., Ryder, L. S., Otomo, I., Saitoh, H., et al. (2012). Effector-mediated suppression of chitin-triggered immunity by *Magnaporthe oryzae* Is necessary for rice blast disease. *Plant Cell* 24, 322–335. doi: 10.1105/tpc.111.092957

Micali, C. O., Neumann, U., Grunewald, D., Panstruga, R., and O'Connell, R. (2011). Biogenesis of a specialized plant–fungal interface during host cell internalization of *Golovinomyces orontii* haustoria. *Cell. Microbiol.* 13, 210–226. doi: 10.1111/j.1462-5822.2010.01530.x

Miklis, M., Consonni, C., Bhat, R. A., Lipka, V., Schulze-Lefert, P., and Panstruga, R. (2007). Barley MLO modulates actin-dependent and actin-independent antifungal defense pathways at the cell periphery. *Plant Phys.* 144, 1132–1143. doi: 10.1104/pp.107.098897

Moore, C. P., Zhang, J. Z., and Hamilton, S. L. (1999). A role for cysteine 3635 for RYR1 in redox modulation and calmodulin binding. *J. Biol. Chem.* 274, 36831–36834. doi: 10.1074/jbc.274.52.36831

Munshi, H. G., Burks, D. J., Joyal, J. L., White, M. F., and Sacks, D. B. (1996). Ca2+ regulates calmodulin binding to IQ motifs in IRS-1. *Biochemistry* 35, 15883–15889. doi: 10.1021/bi962107y

Murashige, T., and Skoog, F. (1962). A revised medium for rapid growth and bio assays with tobacco tissue cultures. *Physiol. Plant.* 15, 473–497. doi: 10.1111/j.1399-3054.1962.tb08052.x

Opalski, K. S., Schultheiss, H., Kogel, K.-H., and Hückelhoven, R. (2005). The receptor-like MLO protein and the RAC/ROP family G-protein RACB modulate actin reorganization in barley attacked by the biotrophic powdery mildew fungus *Blumeria graminis* f. sp. *hordei*. *Plant J.* 41, 291–303. doi: 10.1111/j.1365-313X.2004.02292.x

Osborne, A. R., Rapoport, T. A., and Van Den Berg, B. (2005). Protein translocation by the Sec61/SecY channel. *Annu. Rev. Cell Dev. Biol.* 21, 529–550. doi: 10.1146/annurev.cellbio.21.012704.133214

Palma, K., Zhang, Y., and Li, X. (2005). An Importin α homolog, MOS6, plays an important role in plant innate immunity. *Curr. Biol.* 15, 1129–1135. doi: 10.1016/j.cub.2005.05.022

Panstruga, R. (2005). Serpentine plant MLO proteins as entry portals for powdery mildew fungi. *Biochem. Soc. Trans.* 33, 389–392. doi: 10.1042/bst0330389

Park, E., and Rapoport, T. A. (2012). Mechanisms of Sec61/SecY-mediated protein translocation across membranes. *Annu. Rev. Biophys.* 41, 21–40. doi: 10.1146/annurev-biophys-050511-102312

Reddy, A. S., Ali, G. S., Celesnik, H., and Day, I. S. (2011). Coping with stresses: roles of calcium- and calcium/calmodulin-regulated gene expression. *Plant Cell* 23, 2010–2032. doi: 10.1105/tpc.111.084988

Restrepo, M. A., Freed, D. D., and Carrington, J. C. (1990). Nuclear transport of plant potyviral proteins. *Plant Cell* 2, 987–998. doi: 10.1105/tpc.2.10.987

Rhoads, A. R., and Friedberg, F. (1997). Sequence motifs for calmodulin recognition. *Faseb J.* 11, 331–340.

Rojo, E., and Denecke, J. (2008). What is moving in the secretory pathway of plants? *Plant Physiol.* 147, 1493–1503. doi: 10.1104/pp.108.124552

Rovenich, H., Boshoven, J. C., and Thomma, B. P. H. J. (2014). Filamentous pathogen effector functions: of pathogens, hosts and microbiomes. *Curr. Opin. Plant Biol.* 20, 96–103. doi: 10.1016/j.pbi.2014.05.001

Schmittgen, T. D., and Livak, K. J. (2008). Analyzing real-time PCR data by the comparative CT method. *Nat. Protoc.* 3, 1101–1108. doi: 10.1038/nprot.2008.73

Shen, Q. H., Saijo, Y., Mauch, S., Biskup, C., Bieri, S., Keller, B., et al. (2007). Nuclear activity of MLA immune receptors links isolate-specific and basal disease-resistance responses. *Science* 315, 1098–1103. doi: 10.1126/science.1136372

Sienaert, I., Kasri, N. N., Vanlingen, S., Parys, J. B., Callewaert, G., Missiaen, L., et al. (2002). Localization and function of a calmodulin-apocalmodulin-binding domain in the N-terminal part of the type 1 inositol 1,4,5-trisphosphate receptor. *Biochem. J.* 365, 269–277. doi: 10.1042/BJ20020144

Spooner, R. A., Smith, D. C., Easton, A. J., Roberts, L. M., and Lord, J. M. (2006). Retrograde transport pathways utilised by viruses and protein toxins. *Virol. J.* 3:26. doi: 10.1186/1743-422X-3-26

Storey, J. D., and Tibshirani, R. (2003). Statistical significance for genomewide studies. *Proc. Natl. Acad. Sci. U.S.A.* 100, 9440–9445. doi: 10.1073/pnas.1530509100

Stotz, H. U., Mitrousia, G. K., De Wit, P. J. G. M., and Fitt, B. D. L. (2014). Effector-triggered defence against apoplastic fungal pathogens. *Trends Plant Sci.* 19, 491–500. doi: 10.1016/j.tplants.2014.04.009

Szurek, B., Marois, E., Bones, U., and Van den Ackerveken, G. (2001). Eukaryotic features of the Xanthomonas type III effector AvrBs3: protein domains involved in transcriptional activation and the interaction with nuclear import receptors from pepper. *Plant J.* 26, 523–534.

Tameling, W. I. L., and Baulcombe, D. C. (2007). Physical association of the NB-LRR resistance protein Rx with a ran GTPase-activating protein is required for extreme resistance to Potato virus X. *Plant Cell* 19, 1682–1694. doi: 10.1105/tpc.107.050880

Tameling, W. I. L., Nooijen, C., Ludwig, N., Boter, M., Slootweg, E., Goverse, A., et al. (2010). RanGAP2 mediates nucleocytoplasmic partitioning of the NB-LRR immune receptor Rx in the Solanaceae, thereby dictating Rx function. *Plant Cell Online* 22, 4176–4194. doi: 10.1105/tpc.110.077461

Tufan, H. A., Stefanato, F. L., McGrann, G. R., Maccormack, R., and Boyd, L. A. (2011). The *Barley stripe mosaic virus* system used for virus-induced gene silencing in cereals differentially affects susceptibility to fungal pathogens in wheat. *J. Plant Physiol.* 168, 990–994. doi: 10.1016/j.jplph.2010.11.019

Van Der Linde, K., Hemetsberger, C., Kastner, C., Kaschani, F., Van Der Hoorn, R. A. L., Kumlehn, J., et al. (2012). A maize cystatin suppresses host Immunity

by inhibiting apoplastic cysteine proteases. *Plant Cell* 24, 1285–1300. doi: 10.1105/tpc.111.093732

Van Schie, C. C. N., and Takken, F. L. W. (2014). Susceptibility genes 101: how to be a good host. *Annu. Rev. Phytopathol.* 52, 551–581. doi: 10.1146/annurev-phyto-102313-045854

Vogel, J. P., Raab, T. K., Schiff, C., and Somerville, S. C. (2002). PMR6, a pectate lyase-like gene required for powdery mildew susceptibility in Arabidopsis. *Plant Cell* 14, 2095–2106. doi: 10.1105/tpc.003509

Vogel, J. P., Raab, T. K., Somerville, C. R., and Somerville, S. C. (2004). Mutations in PMR5 result in powdery mildew resistance and altered cell wall composition. *Plant J.* 40, 968–978. doi: 10.1111/j.1365-313X.2004.02264.x

Wang, D., and Dong, X. N. (2011). A highway for war and peace: the secretory pathway in plant-microbe interactions. *Mol. Plant* 4, 581–587. doi: 10.1093/mp/ssr053

Wang, D., Weaver, N. D., Kesarwani, M., and Dong, X. N. (2005). Induction of protein secretory pathway is required for systemic acquired resistance. *Science* 308, 1036–1040. doi: 10.1126/science.1108791

Wang, Q. L., Chen, B., Liu, P., Zheng, M. Z., Wang, Y. Q., Cui, S. J., et al. (2009). Calmodulin binds to extracellular sites on the plasma membrane of plant cells and elicits a rise in intracellular calcium concentration. *J. Biol. Chem.* 284, 12000–12007. doi: 10.1074/jbc.M808028200

Whigham, E., Qi, S., Mistry, D., Surana, P., Xu, R., Fuerst, G. S., et al. (2015). Broadly conserved fungal effector BEC1019 suppresses host cell death and enhances pathogen virulence in powdery mildew of barley (*Hordeum vulgare* L.). *Mol. Plant Microbe Interact.* doi: 10.1094/MPMI-02-15-0027-FI. [Epub ahead of print].

Wirthmueller, L., Zhang, Y., Jones, J. D. G., and Parker, J. E. (2007). Nuclear accumulation of the Arabidopsis immune receptor RPS4 is necessary for triggering EDS1-dependent defense. *Curr. Biol.* 17, 2023–2029. doi: 10.1016/j.cub.2007.10.042

Wise, R. P., Moscou, M. J., Bogdanove, A. J., and Whitham, S. A. (2007). Transcript profiling in host-pathogen interactions. *Ann. Rev. Phytopathol.* 45, 329–369.

Wolfinger, R. D., Gibson, G., Wolfinger, E. D., Bennett, L., Hamadeh, H., Bushel, P., et al. (2001). Assessing gene significance from cDNA microarray expression data via mixed models. *J. Comput. Biol.* 8, 625–637. doi: 10.1089/106652701753307520

Xi, L., Moscou, M. J., Meng, Y., Xu, W., Caldo, R. A., Shaver, M., et al. (2009). Transcript-based cloning of *RRP46*, a regulator of rRNA processing and *R* gene-independent cell death in barley-powdery mildew interactions. *Plant Cell* 21, 3280–3295. doi: 10.1105/tpc.109.066167

Xu, W., Meng, Y., and Wise, R. P. (2014). *Mla*- and *Rom1*-mediated control of microRNA398 and chloroplast copper/zinc superoxide dismutase regulates cell death in response to the barley powdery mildew fungus. *New Phytol.* 201, 1396–1412. doi: 10.1111/nph.12598

Xu, X., Chen, C., Fan, B., and Chen, Z. (2006). Physical and functional interactions between pathogen-induced *Arabidopsis* WRKY18, WRKY40, and WRKY60 transcription factors. *Plant Cell* 18, 1310–1326. doi: 10.1105/tpc.105.037523

Yamniuk, A. P., and Vogel, H. J. (2004). Calmodulin's flexibility allows for promiscuity in its interactions with target proteins and peptides. *Mol. Biotechnol.* 27, 33–57. doi: 10.1385/MB:27:1:33

Yasuhara, N., Shibazaki, N., Tanaka, S., Nagai, M., Kamikawa, Y., Oe, S., et al. (2007). Triggering neural differentiation of ES cells by subtype switching of importin-α. *Nat. Cell Biol.* 9, 72–79. doi: 10.1038/ncb1521

Yasuhara, N., Yamagishi, R., Arai, Y., Mehmood, R., Kimoto, C., Fujita, T., et al. (2013). Importin α subtypes determine differential transcription factor localization in embryonic stem cells maintenance. *Dev. Cell* 26, 123–135. doi: 10.1016/j.devcel.2013.06.022

Zhang, C., Bradshaw, J. D., Whitham, S. A., and Hill, J. H. (2010). The development of an efficient multipurpose *Bean pod mottle virus* viral vector set for foreign gene expression and RNA silencing. *Plant Physiol.* 153, 52–65. doi: 10.1104/pp.109.151639

Zhang, W.-J., Hanisch, S., Kwaaitaal, M., Pedersen, C., and Thordal-Christensen, H. (2013). A component of the Sec61 ER protein transporting pore is required for plant susceptibility to powdery mildew. *Front. Plant Sci.* 4:127. doi: 10.3389/fpls.2013.00127

Conflict of Interest Statement: The authors declare that the research was conducted in the absence of any commercial or financial relationships that could be construed as a potential conflict of interest.

frontiers in Plant Science

ORIGINAL RESEARCH
published: 17 February 2016
doi: 10.3389/fpls.2016.00097

The Poplar Rust-Induced Secreted Protein (RISP) Inhibits the Growth of the Leaf Rust Pathogen *Melampsora larici-populina* and Triggers Cell Culture Alkalinisation

Benjamin Petre[1,2,3], Arnaud Hecker[1,2], Hugo Germain[4], Pascale Tsan[5,6], Jan Sklenar[3], Gervais Pelletier[7], Armand Séguin[7], Sébastien Duplessis[1,2] and Nicolas Rouhier[1,2]**

[1] Institut National de la Recherche Agronomique, Centre INRA Nancy Lorraine, UMR 1136 Interactions Arbres/Microorganismes, Champenoux, France, [2] Faculté des Sciences et Technologies, UMR 1136 Interactions Arbres/Microorganismes, Université de Lorraine, Vandoeuvre-lès-Nancy, France, [3] The Sainsbury Laboratory, Norwich, UK, [4] Groupe de Recherche en Biologie Végétale, Université du Québec à Trois-Rivières, Trois-Rivières, QC, Canada, [5] CRM^2, Equipe BioMod, Faculté des Sciences et Technologies, UMR 7036, Université de Lorraine, Vandoeuvre-lès-Nancy, France, [6] CNRS, CRM^2, Equipe BioMod, Faculté des Sciences et Technologies, UMR 7036, Vandoeuvre-lès-Nancy, France, [7] Natural Resources Canada, Canadian Forest Service, Laurentian Forestry Centre, Québec, QC, Canada

OPEN ACCESS

Edited by:
Ralph Panstruga,
RWTH Aachen University, Germany

Reviewed by:
Peter Dodds,
Commonwealth Scientific and Industrial Research Organisation, Australia
Carsten Pedersen,
University of Copenhagen, Denmark

***Correspondence:**
Nicolas Rouhier
nicolas.rouhier@univ-lorraine.fr;
Sébastien Duplessis
duplessi@nancy.inra.fr

Specialty section:
This article was submitted to Plant Biotic Interactions, a section of the journal Frontiers in Plant Science

Received: 11 November 2015
Accepted: 18 January 2016
Published: 17 February 2016

Citation:
Petre B, Hecker A, Germain H, Tsan P, Sklenar J, Pelletier G, Séguin A, Duplessis S and Rouhier N (2016) The Poplar Rust-Induced Secreted Protein (RISP) Inhibits the Growth of the Leaf Rust Pathogen Melampsora larici-populina and Triggers Cell Culture Alkalinisation. Front. Plant Sci. 7:97. doi: 10.3389/fpls.2016.00097

Plant cells secrete a wide range of proteins in extracellular spaces in response to pathogen attack. The poplar rust-induced secreted protein (RISP) is a small cationic protein of unknown function that was identified as the most induced gene in poplar leaves during immune responses to the leaf rust pathogen *Melampsora larici-populina*, an obligate biotrophic parasite. Here, we combined *in planta* and *in vitro* molecular biology approaches to tackle the function of RISP. Using a RISP-mCherry fusion transiently expressed in *Nicotiana benthamiana* leaves, we demonstrated that RISP is secreted into the apoplast. A recombinant RISP specifically binds to *M. larici-populina* urediniospores and inhibits their germination. It also arrests the growth of the fungus *in vitro* and on poplar leaves. Interestingly, RISP also triggers poplar cell culture alkalinisation and is cleaved at the C-terminus by a plant-encoded mechanism. Altogether our results indicate that RISP is an antifungal protein that has the ability to trigger cellular responses.

Keywords: antifungal activity, peptide elicitor, plant immunity, *Populus trichocarpa*, rust fungus, obligate biotroph

INTRODUCTION

Plant cells respond to changes in their environment by secreting peptides in their extracellular space (Krause et al., 2013; Matsubayashi, 2014; Simon and Dresselhaus, 2015). Understanding how these peptides function is key to understanding plant responses. Secreted peptides belong to two main categories: the antimicrobial peptides (AMPs) that directly interfere with invaders, and the peptide hormones that function as signal molecules which coordinate further responses.

Antimicrobial peptides constitute a major component of the inducible plant immune system (Dodds and Rathjen, 2010). Their gene expression is tightly controlled and usually induced upon pathogen infection (Tao et al., 2003). AMPs exert a direct toxic effect against microbial parasites, often through the disruption of their cell integrity (van Loon et al., 2006; Poon et al., 2014). The

antimicrobial activities of these peptides are commonly characterized using *in vitro* assays which consist in applying purified peptides to microbial cultures and then in evaluating growth reduction (Vasconcelos et al., 2011; Poon et al., 2014). At the structural level, plant AMPs typically present rigid 3D structures whereas many AMPs from other eukaryotes are intrinsically disordered in aqueous solutions (Zasloff, 2002; Haney et al., 2009; Pelegrini et al., 2011).

Peptide hormones (also known as peptide elicitors) are signaling molecules involved in cell-to-cell communication for coordinating plant development or stress responses (Butenko et al., 2009; Fuglsang et al., 2014; Tabata and Sawa, 2014; Bartels and Boller, 2015). These are usually small peptides, with a size comprised between 11 and 50 amino acids, and which are often released by the cleavage of larger protein precursors (or pro-proteins). They function in the apoplast where they bind to cell-surface receptors to trigger cellular responses (Monaghan and Zipfel, 2012; Krause et al., 2013; Haruta et al., 2014). Cell culture alkalinisation assays, during which extracellular pH shifts toward basic values, are used as proxies to detect plant cellular responses to peptides (Yamaguchi and Huffaker, 2011). Complementary assays measuring ROS levels, MAP kinase activation, gene expression or levels of plant hormones are often used to determine the exact nature of the responses (activation of immune responses for example).

Poplar trees are used in agroforestry for wood production, but their susceptibility to the leaf rust fungus *Melampsora larici-populina*, an obligate biotrophic pathogen, causes severe losses in plantations (Duplessis et al., 2009). Since the release of the poplar (*Populus trichocarpa*) genome sequence, many research efforts have been devoted to the identification of components of the poplar immune system that govern resistance to *M. larici-populina* (Duplessis et al., 2009; Hacquard et al., 2011). Notably, Rinaldi et al. (2007) reported that the *Rust-induced secreted protein* (*RISP*) gene is highly induced in poplar leaves challenged by an avirulent isolate of *M. larici-populina*. RISP is a small (82 amino acids), cationic (pI 9.5), cysteine-rich (4) protein predicted to be secreted in the apoplast. These observations prompted the authors to hypothesize that RISP is a component of the poplar immune system, possibly working as an antifungal agent. More recently, *RISP* gene position in the *P. trichocarpa* genome was refined and it was found at close vicinity of a leucine-rich repeat receptor-like protein (LRR-RLP) gene (Petre et al., 2014). Interestingly, both genes present similar promoter regions and expression profiles in response to *M. larici-populina* infection. Considering that LRR-RLPs are cell-surface receptors, we recently suggested that RISP could also be a peptide hormone or a precursor of such peptide (Petre et al., 2014).

In the present study, we have tested whether RISP (i) is a secreted protein, (ii) is an AMP that can inhibit the growth of *M. larici-populina,* and (iii) is a peptide hormone able to trigger cellular responses in poplar. We assessed the first point by determining the subcellular localisation of a RISP-mCherry fusion transiently expressed in *Nicotiana benthamiana*. After producing a recombinant RISP and investigating its biochemical and structural properties, we addressed the second question by examining RISP interaction with *M. larici-populina* urediniospores and evaluating its ability to inhibit fungal growth. In order to test the third hypothesis, we measured the capacity of RISP to promote poplar cell culture alkalinisation.

MATERIALS AND METHODS

Biological Material, Growth Conditions, and Inoculation Procedures

Hybrid poplar cultivar 'Beaupré' (*Populus trichocarpa* x *Populus deltoides*) and *M. larici-populina* isolates 98AG31 (pathotype 3-4-7) and 93ID6 (pathotype 3-4), were grown and used as previously detailed (Rinaldi et al., 2007). *Laccaria bicolor* strain S238N was maintained at 25°C in dark conditions on Pachlewsky P5 medium (Di Battista et al., 1996), with transfer to fresh media every 4 weeks. *Magnaporthe oryzae* strain Guy11 was maintained at 25°C in the dark on complete medium (Talbot et al., 1993), with transfer to fresh media every 2 weeks. For longer storage, mycelium fragments were conserved on sterile Whatman paper at −20°C. For spore production, a frozen-stock was inoculated on complete medium. Spores were retrieved after 12 days by raking the mycelium in sterile water and purified by filtration on sterile Joseph paper, washed twice in 50 mL sterile water by gentle centrifugation and immediately used.

Sequence Analyses and Bioinformatic Procedures

Sequences were retrieved from the *P. trichocarpa* 'Nisqually-1' genome sequence hosted on the Phytozome portal (version 2.2, currently v3 assembly[1]). Sequence alignments were performed using the online programs Multalin[2] and ClustalW[3]. Intrinsically disordered regions were predicted using Globplot online[4]. Protein signal peptides were predicted on the SignalP 3.0 server[5] and protein parameters were calculated with the Protparam program[6]. Disulfide bonds were predicted using the diANNA 1.1 Web server[7].

RNA Isolation and RT-qPCR Analyses

Time-course infection of poplar leaves by either virulent or avirulent isolates of *M. larici-populina* as well as water-agar (mock-inoculated treatment), RNA isolation and cDNA synthesis were performed previously (Petre et al., 2011). A pair of primers (forward: GCGGTAGTAGCAAACAAAGT; reverse: CTCCTAAGCACGTATACAAC) was designed to specifically amplify RISP transcripts (GenBank accession number: XP_006379231, Phytozome ID Potri.T160900.1 in *P. trichocarpa* v3.0, POPTR_0580s00210.1 in v2.2). We

[1]http://www.phytozome.net/poplar
[2]http://multalin.toulouse.inra.fr/multalin/
[3]http://www.genome.jp/tools/clustalw/
[4]http://globplot.embl.de
[5]http://www.cbs.dtu.dk/services/SignalP-3.0/
[6]http://web.expasy.org/protparam/
[7]http://clavius.bc.edu/~clotelab/DiANNA/

experimentally determined the efficiency of this primer pair to be 1.89, i.e., 89%. Reverse transcription-quantitative polymerase chain reaction (RT-qPCR) experiments were carried out as previously described (Hacquard et al., 2010), and included two biological and two technical replicates. For each biological replicate, the average value of the two technical replicates was used, provided that the two values differed by less than one Ct. Transcript expression was normalized to a reference ubiquitin transcript as previously reported (Rinaldi et al., 2007).

Cloning and Transient Expression of a RISP-mCherry Fusion in *N. benthamiana* Leaf Cells

The open reading frame (ORF) encoding the full-length RISP (i.e., with the signal peptide) was amplified by polymerase chain reaction (PCR) from Beaupré leaf cDNA and cloned into the golden gate level 0 vector pICSL01005 (AATG/TTCG compatible overhangs[8]). The DNA fragment was then assembled with an ORF coding the mCherry (pICSL50004, TTCG/GCTT compatible overhangs) into the golden gate level 1 binary vector pICH86988 (AATG/GCTT compatible overhangs) in order to create a RISP-mCherry fusion expressed under the control of a 35S promoter (see Supplementary Table S1). The transient transformation of *N. benthamiana* leaf cells by *Agrobacterium tumefaciens* was performed as previously described (Win et al., 2011). Leaves were collected 2 days post-infiltration and pavement cells were observed with a Leica DM6000B/TCS SP5 microscope (Leica Microsystems, Bucks, UK). The mCherry was excited at 561 nm. mCherry and chlorophyll fluorescent signals were retrieved between 580–620 nm and 680–710 nm, respectively. Plasmolysis was induced with 1 M NaCl. Image analysis was performed with Fiji[9].

Cloning, Expression, and Purification of Recombinant Proteins

The ORF sequence encoding mature RISP (devoid of the first 23 amino acids) was amplified from *P. trichocarpa* cDNAs and cloned into pET3d and pET15b (Novagen) for producing a protein without tag or with an N-terminal His-tag respectively. For generating the RISP-GFP-His fusion, the mature RISP sequence was cloned into pCK S65T (Menand et al., 1998) for a C-terminal in-frame fusion with GFP S65T, and then subcloned into pET28a to insert a His-tag at the C-terminus of the GFP. Primers, plasmid construction and corresponding expressed proteins are presented in Supplementary Table S1. His-tagged or untagged recombinant RISP were produced in *Escherichia coli* strains BL21(DE3) pSBET or Rosetta2(DE3) pLysS, purified following a procedure previously described (Couturier et al., 2014) and dialyzed against 30 mM Tris-HCl, 1 mM EDTA pH 8.0 (TE) buffer. As a final purification step, recombinant RISP proteins were eventually incubated 10 min at 95°C to remove residual *E. coli* contaminants that precipitated upon heating. Protein concentrations were measured by spectrophotometry using a molar extinction coefficient at 280 nm of 1,640 M^{-1} cm^{-1}. All the experiments involving recombinant RISP were performed with freshly prepared proteins because they precipitated upon freezing. Other recombinant proteins (His-AtBolA2, AtGrxC1, poplar His-Trxh1 and *Neisseria meningitidis* Grx) were produced and purified as previously described (Rouhier and Jacquot, 2003; Rouhier et al., 2007; Couturier et al., 2014). These proteins, used as negative controls in the antifungal and cleavage assays, were selected due to their similarity to RISP in terms of size, stability, and production/purification procedure. For ^{15}N-labeled RISP production, bacteria were grown in M9 minimal synthetic medium containing $^{15}NH_4Cl$ (1 g/L) as previously described (Bouillac et al., 2004).

In Vitro Antifungal Assays

To assess the ability of recombinant proteins to inhibit the germination of *M. larici-populina* urediniospores, 15,000 urediniospores stored at −80°C (isolate 98AG31) were resuspended in 1 mL of sterile water under vigorous agitation for 1 h, then put in contact with protein solution (the protein concentration in the tube is indicated everywhere relevant) and spread on water-agar (20 g/L) in Petri dishes. After 5 h of incubation (constant light 25 μmol/s/m^2, 21°C), urediniospores were observed under a binocular and the percentage of germination was calculated on a minimum of 300 urediniospores for each replicate. To assess the ability of recombinant proteins to inhibit the elongation of *M. larici-populina* germ tubes, urediniospores were spread on water-agar (20 g/L) and were allowed to germinate for 4 h. Then, protein solutions were gently deposited on agar surface to avoid germ tube breaking and Petri dishes were incubated for 4 more hours. Pictures were taken after 4 and 8 h under a binocular microscope and germinating tube length was measured using the AnalySIS^B software (Olympus, Tokyo, Japan). To assess the ability of recombinant proteins to inhibit the mycelium growth of *L. bicolor* and *M. oryzae in vitro*, 10 μL of 100 μM recombinant RISP or control solutions were placed at the margins of growing mycelium colonies on paper disks or directly onto the medium and growth was recorded after 3 and 7 days for *M. oryzae* and *L. bicolor*, respectively. Phenotype of the hyphae was estimated by light microscopy. Alternatively, 2 mm^3 fungal explants were transferred on appropriate fresh media and 100 μL of 100 μM recombinant RISP or control solutions were directly deposited on the explants. Growth of the fungi was recorded after 8 days. To assess the ability of recombinant proteins to inhibit the germination of *M. oryzae* spores, the latter were allowed to germinate in glass cupules with 100 μM recombinant RISP or control solutions. Germination was recorded after 6 and 24 h under a light microscope.

Antifungal Assay on Poplar Leaves

Beaupré leaves were inoculated with a mix of *M. larici-populina* (isolate 98AG31, virulent on Beaupré) urediniospores (100,000 spores/mL) and 100 μM recombinant proteins in TE buffer, TE buffer alone or double-distilled water (ddHOH). Inoculation was performed on entire leaves as previously described (Rinaldi

[8]http://synbio.tsl.ac.uk/

[9]http://fiji.sc/Fiji

et al., 2007) or with a pipette on 5 cm^2 leaf disks. Pictures were taken 7–10 days post-inoculation (dpi) unless otherwise stated. For pre-treatments by recombinant RISP prior to inoculation, 1 mL of 100 μM recombinant protein or controls were deposited with a pipette on 3 cm^2 areas of Beaupré leaves and then inoculated with *M. larici-populina* urediniospores (100,000 spores/mL, isolate 98AG31) immediately, or 3 or 5 days later. Orange uredinia pustules were tracked from 8 up to 20 dpi.

Recombinant Protein Reduction and Thiol Titration

Recombinant proteins were reduced with a 100-fold excess of dithiothreitol (DTT, 10 mM for 100 μM recombinant proteins) for 1 h at room temperature. DTT was removed by desalting on G25 columns (GE Healthcare, Little Chalfont, UK). For thiol titration, 20 μM of untreated and pre-reduced recombinant proteins prepared in a TE or TE-SDS 1% buffer were reacted with 100 μM 5,5′-dithiobis-2-nitrobenzoic acid (DTNB) for 1 h in the dark. Absorbance was measured at 412 nm and free-thiol content was calculated using a TNB− molar extinction coefficient of 13,600 M^{-1} cm^{-1} as previously reported (Rouhier et al., 2004).

Structural Analyses

For CD analyses, His-RISP was adjusted to 50–200 μM in a 10 mM phosphate buffer pH 7.0, and spectra were recorded on a CD6 spectropolarimeter (HORIBA Jobin Yvon, Longjumeau, France) in triplicates at 20°C with 0.2 nm wavelength increments from 190 to 250 nm, using a 0.1 cm path length cuvette. The spectra were corrected from the buffer baseline. CD spectra of the reduced proteins were performed with 10 mM DTT added 10 min prior to analyses. For experiments with trifluoroethanol (TFE), 50 or 80% TFE was added to recombinant proteins 1 h prior to analyses. Secondary structure abundance was determined after deconvolution of the spectra with Selcon3 and ContinII softwares.

Nuclear magnetic resonance (NMR) spectra of His-RISP were obtained on a 600 MHz Bruker Avance III spectrometer equipped with a TCI cryoprobe. COSY, TOCSY (mixing time of 60 ms) and NOESY (mixing time of 150 and 300 ms) experiments were recorded on a 1 mM His-RISP sample in a 4:1 (v/v) mixture of deuterated trifluoroethanol (TFE-d3) and 5 mM phosphate buffer at pH 7.4 and 25°C. Spectra were processed in Topspin3.0 (Bruker) and referenced to TFE residual signal at 3.88 ppm.

One hundred and sixty-five distance restraints were derived from NOESY experiments. These restraints were applied in an iterative structure calculation and a simulated annealing protocol with water refinement using ARIA2.3 (Rieping et al., 2007) and CNS1.21 (Brünger et al., 1998; Brünger, 2007). Eighty structures were generated and the 20 structures of lowest energy were kept. The global backbone RMSD among the 20 lowest-energy structures is 0.63 and 1.62 Å for the 1–9 and 10–15 segments, respectively.

Poplar Cell Suspension Alkalinisation Assay

Poplar cell suspensions (*P. trichocarpa* x *P. deltoides*; H11-11 hybrid) were maintained in Murashige and Skoog medium (pH 5.6, adjusted with KOH) by weekly transferring 10 mL of cells to 30 mL of fresh media. Cells were grown in dark conditions, at 20°C and under shaking at 160 rpm. For the alkalinisation assay, cells were used 4 days after transfer. The day before each alkalinisation assay, 5 mL of cells were aliquoted in sterile opened 50 mL centrifuge tubes and allowed to equilibrate overnight at room temperature at 160 rpm in the dark. Prior to the alkalinisation assay, cultures equilibrated 2 additional hours under room-light conditions. A constant volume of 20 μL of recombinant proteins or TE buffer adjusted to various concentrations was added and pH variations were recorded thereafter. TE buffer treatment remained stable at a pH of 4.2 during the experiment and was used to calculate the pH ratio for each time-point.

Leaf Protein Isolation and Western Blotting Analyses

Frozen leaves were ground with a mortar and a pestle in liquid nitrogen. The powder was resuspended into the following extraction buffer [50 mM Tris-HCl pH 8.0, 1 mM phenylmethanesulfonylfluoride (PMSF), 50 mM β-mercaptoethanol] and incubated for 20 min under shaking at 4°C. After centrifugation (15 min at 30,000 *g*), the supernatant (i.e., soluble proteins) was precipitated overnight at −20°C into 80% cold acetone whereas the pellet was resuspended into another extraction buffer (50 mM Tris-HCl pH 8.0, 1% SDS) to recover insoluble proteins. After 20 min incubation and a similar centrifugation, the supernatant containing denatured insoluble proteins was also precipitated overnight at −20°C into 80% cold acetone. Proteins were recovered by centrifugation (10 min at 35,000 *g*), the pellet was resupended into 50 μL SDS 0.2% and the proteins were quantified using a BCA (bicinchoninic acid) assay. The protein concentration was adjusted to 2 μg/μL in a Laemmli buffer, denatured 10 min at 95°C and stored at −20°C. For total protein extraction, leaf powder was directly resuspended into a denaturing extraction buffer (7 M urea, 2 M thiourea, 4% [m/v] CHAPS, 0.4% [v/v] triton X-100, 10 mM DTT) and incubated for 1 h under shaking at 4°C. After centrifugation (15 min at 30,000 *g*), the supernatant corresponding to total proteins was precipitated overnight at −20°C into 80% cold acetone. Proteins were retrieved, quantified and adjusted into Laemmli buffer as specified above.

Western blotting analyses were performed as previously described (Pégeot et al., 2014). Polyclonal antibodies raised in rabbit against recombinant His-RISP were purified from the immune serum by affinity chromatography as described previously, using a CnBr sepharose bound untagged RISP (Rouhier et al., 2001). Pre-immune and depleted sera were used as controls to ensure the specificity of the signal.

Time-Course Cleavage of Recombinant Proteins by Poplar Soluble Protein Extracts

Five percent (v/v) of purified RISP, His-RISP, or poplar His-Trxh1 were incubated with soluble protein extracts from poplar leaves for up to 24 h at room temperature under gentle shaking and with 1 mM PMSF to avoid rapid and unspecific protein degradation. The incubation was arrested by denaturing and reducing the samples (i.e., by adding Laemmli buffer and boiling the samples for 10 min at 95°C). Protein integrity was followed by western blot analyses as described above.

Pull-Down of RISP with *M. larici-populina* Urediniospores

Urediniospores from the *M. larici-populina* (isolate 98AG31) were resuspended in sterile ddHOH with 0.05% Tween20 under vigorous agitation for 30 min. Five hundred micrograms of resuspended urediniospores were incubated with 50 μg of recombinant proteins for 5 min under gentle agitation in ddHOH. Urediniospores were washed twice with 1 mL of ddHOH by centrifugation at 13,000 *g* for 30 s. Finally, urediniospores were incubated in 100 μL of Laemmli buffer, incubated 10 min at 95°C and centrifuged again (the supernatant being the final elution). The presence of recombinant proteins in the different fractions was estimated by 15% SDS-PAGE and Coomassie blue staining. Recombinant proteins that were obtained following similar procedures used for RISP were used as negative controls.

RESULTS

A RISP-mCherry Fusion Accumulates in the Apoplast in *N. benthamiana*

Rust-induced secreted protein carries a predicted N-terminal signal peptide for secretion (**Figure 1A**). In order to verify the functionality of the predicted signal peptide, a RISP-mCherry fusion was transiently expressed in *N. benthamiana* leaf pavement cells by the agro-infiltration method and the mCherry fluorescence was observed by live-cell imaging. A specific signal was detected around the cells. Plasmolysis experiments confirmed that the mCherry signal was exclusively observed in the apoplast (**Figure 1B**). We concluded that RISP signal

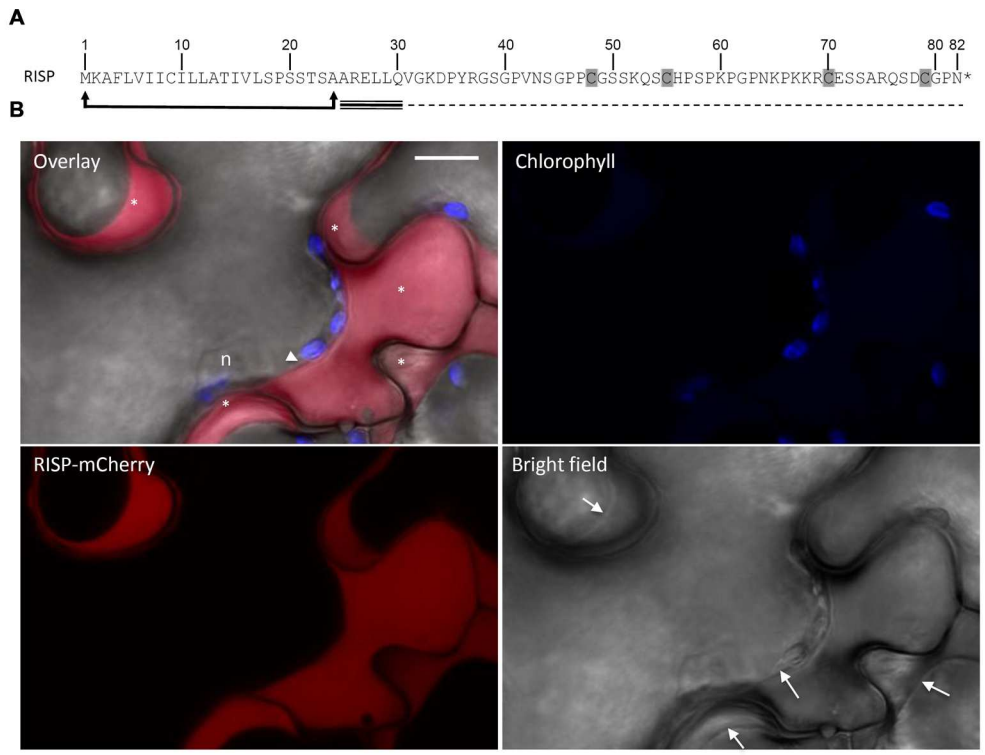

FIGURE 1 | Rust-induced secreted protein (RISP) is secreted into the apoplast. (A) RISP amino acid sequence. The predicted secretory peptide is delimited by arrows and the four cysteines are shaded. The predicted intrinsically disordered region and the predicted α-helix are indicated with dotted and triple lines respectively. **(B)** A RISP-mCherry fusion was transiently expressed into *Nicotiana benthamiana* leaf pavement cells by the agro-infiltration method. Cells were plasmolysed with 1 M NaCl 5 min before observation. The mCherry signal was observed by live-cell imaging 2 days post-infiltration. Excitation: 561 nm. Signal collection: mCherry (red, 580–620 nm); chlorophyll (blue, 680–710 nm). Scale bar: 10 μM. n: nucleus. The white arrowhead marks a tiny space of cytosol, whereas the asterisks indicate the apoplastic space of different cell cavities. Arrows within the bright field image indicate cell plasma membranes.

peptide is functional and efficiently targets the protein to the apoplast.

RISP Can be Overexpressed in *Escherichia coli* Cytosol and Purified as a Monomer

The predicted mature form of RISP was expressed in *E. coli* with an N-terminal hexahistidine tag (His-RISP) or without (RISP). The proteins were purified to homogeneity by affinity chromatography (His-RISP) or by ammonium sulfate fractionation, gel filtration, and ion exchange chromatography (RISP; Supplementary Figure S1A). Given the presence of four cysteine residues and the prediction that residues 48–70 and 55–79 would form disulfide bonds, we assessed the RISP redox state by thiol titration experiments. No thiol group was titrated in the purified protein, even under denaturing conditions, whereas 3.57 ± 0.35 free thiol groups per protein were titrated using a pre-reduced protein (Supplementary Figure S1B). This indicated that RISP was completely oxidized at the end of the purification. Mass spectrometry analyses of an untreated RISP protein identified a single peak corresponding to the size of a RISP monomer. The absence of disulfide-bridged oligomers indicated that the protein contained two intramolecular disulfide bridges.

Rust-induced secreted protein structural properties have been further analyzed using circular dichroism (CD) and NMR spectroscopy. Although recombinant tagged and untagged RISP can be purified without any sign of precipitation or insolubility, the CD spectrum of a His-RISP indicated that the protein has no detectable secondary structure (**Figure 2A**). This was corroborated with the poor spectral dispersion and the very few NOESY correlations observed in the NMR spectra of a ^{15}N-labeled RISP recorded in phosphate buffer at various pH values (4.9–7.0) and temperatures (15–50°C; Supplementary Figure S2A). The reduction of His-RISP had a negligible effect on the CD spectrum, which indicated that the disordered state of RISP is independent of the cysteine redox state (Supplementary Figure S2B). Interestingly, in the presence of 80% trifluoroethanol (TFE), a solvent classically used to promote the acquisition of protein secondary structures, the His-RISP CD spectrum was consistent with a partial folding; the protein showing up to 34%

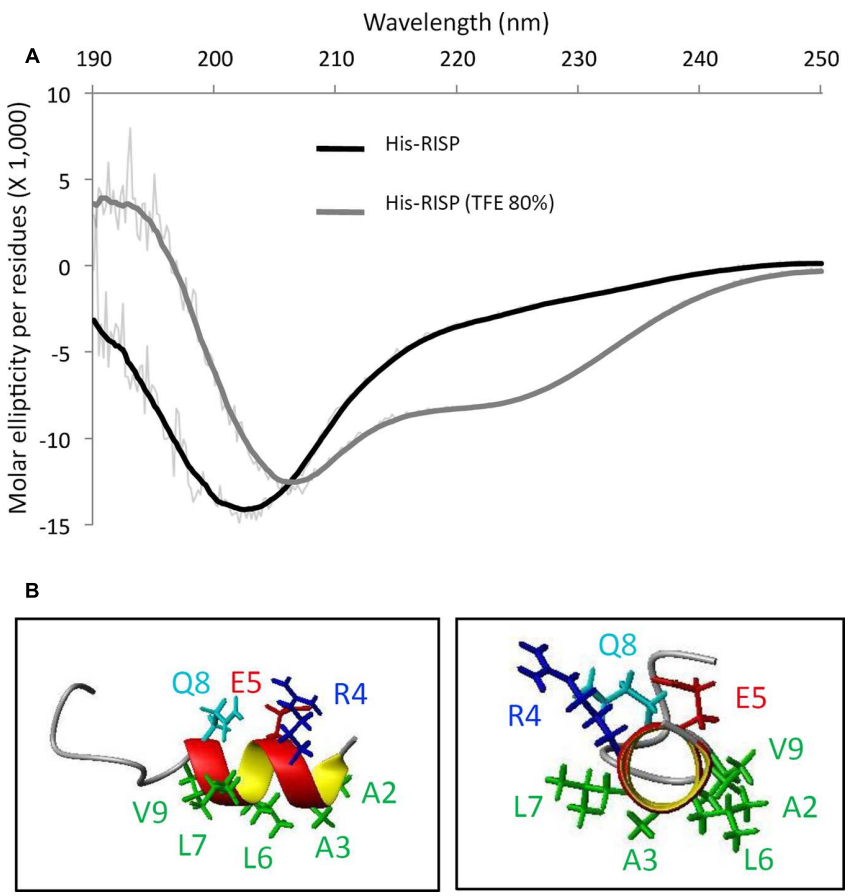

FIGURE 2 | RISP is intrinsically disordered and adopts α-helices in TFE. (A) Circular dichroism (CD) spectra of His-RISP in aqueous solution (phosphate buffer pH 7.0, in black) or in 80% trifluoroethanol (TFE; in gray). Thick lines: smoothed curves ($n = 25$), thin lines: curves established with raw CD data. **(B)** Nuclear magnetic resonance (NMR) model of the 15 N-terminal residues of His-RISP in 80% TFE-d_3/20% phosphate buffer pH 7.4, at 25°C. Side chains of residues 2–9 are represented in green (hydrophobic side chains), dark blue (positively charged side chain), red (negatively charged side chain) or light blue (polar side chain).

of predicted α-helices (**Figure 2A**; Supplementary Table S2). In 80% TFE, albeit most residues gave only broad unresolved peaks in the H^{α}/amide region, some residues displayed numerous and relatively sharp NOESY correlations in the aliphatic/amide region as well as in the amide/amide region (Supplementary Figure S3). This has enabled the assignment of the first 15 residues. Residues 2–8 (AARELLQ, which correspond to residues 24–30 in **Figure 1A** including the leader sequence) appeared to show typical correlations for helical structure, i.e., medium-range correlations in the aliphatic/amide region, together with medium H^N(i)- H^N(i+1) and weak H^N (i)- H^N (i+2) correlation peaks in the amide-amide region (Supplementary Figure S3). The solution structure of the 15 assignable N-terminal residues of His-RISP was modeled using NMR distance restraints. Polar or charged side-chains of this helix appeared to be located on the opposite side to the hydrophobic ones (**Figure 2B**), resulting in an amphiphilic character. The presence of structural order limited to the N-terminal region was coherent with the prediction of secondary structure and of intrinsically disordered regions made by the Globplot software (**Figure 1A**, Supplementary Figure S3). The unfolded nature of the protein prompted us to investigate its thermosolubility. After 10 min incubation at 95°C, both His-RISP and RISP remained soluble. We concluded from this set of experiments that RISP is thermosoluble and in a disordered state in aqueous solution, but can acquire some secondary structures in specific conditions.

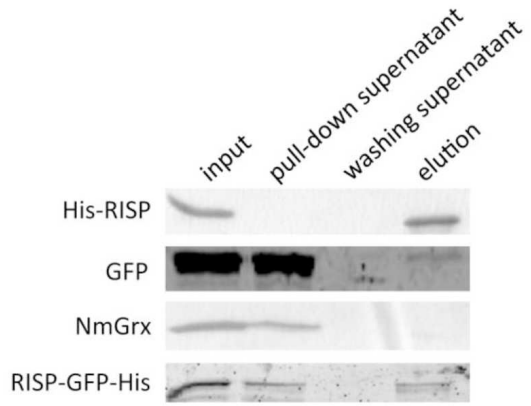

FIGURE 3 | RISP interacts with *M. larici-populina* urediniospores *in vitro*. Recombinant His-RISP, RISP-GFP-His, GFP and *Neisseria meningitidis* Grx were included in a pull-down assay with *M. larici-populina* urediniospores (isolate 98AG31). Recombinant proteins from the different fractions of the pull-down assay were visualized on 15% SDS-PAGE. Input: protein solution before centrifugation. Pull-down supernatant: supernatant after the first centrifugation. Washing supernatant: supernatant after the second centrifugation for washing. Elution: supernatant after incubation at 95°C in Laemmli buffer.

RISP Binds to *M. larici-populina* Urediniospores and Inhibits Germination and Germ Tube Elongation *In Vitro*

Several eukaryotic AMPs are cationic and intrinsically disordered in aqueous solution. Their positively charged residues and amphipathic nature usually promote interaction with microbial structures (Melo et al., 2009). The fact that RISP has comparable properties prompted us to investigate whether RISP can attach to *M. larici-populina* urediniospores *in vitro*. We developed a pull-down assay by mixing urediniospores with RISP and with several recombinant proteins used as controls. His-RISP co-precipitated with urediniospores whereas other recombinant proteins, such as a GFP or a *Neisseria meningitidis* glutaredoxin, remained mostly in the supernatant (**Figure 3**). For visualizing the RISP-urediniospore interaction, we produced and purified a His-tagged GFP fusion protein (RISP-GFP-His). However, only very few RISP-GFP-His did co-precipitate with urediniospores (**Figure 3**). We concluded that RISP stably interacts with *M. larici-populina* urediniospores whereas the GFP-fusion only weakly binds spores, the GFP tag likely preventing full binding.

Then, an antifungal assay was set up to evaluate the capacity of purified recombinant proteins to inhibit the germination of *M. larici-populina* urediniospores *in vitro* (**Figure 4A**). Both His-RISP and RISP impaired urediniospore germination at 10 μM and almost completely abolished germination at 100 μM (**Figures 4A,B**). In contrast, BSA or other recombinant proteins did not affect urediniospore germination (**Figure 4B**). The ability to inhibit urediniospore germination was still observed after heating oxidized or reduced recombinant RISP for 10 min at 95°C, indicating that its antifungal activity is insensitive to the temperature and independent of the protein redox state (**Figure 4C**). To assess whether RISP can also affect germ tube elongation, His-RISP was added to germinating urediniospores (incubated for 4 h) and germ tube length was measured after 4 additional hours (**Figure 5A**). His-RISP reduced germ tube elongation to 75% compared to controls (**Figure 5B**). We concluded that RISP possesses an antifungal activity *in vitro* against *M. larici-populina*.

We investigated whether RISP antifungal activity could be extended to other microbes by testing the ability of purified RISP to inhibit *in vitro* mycelium growth of the mycorrhizal basidiomycete *L. bicolor* and both mycelium growth and spore germination of the rice blast ascomycete *M. oryzae*. However, RISP neither inhibited the growth nor the germination of these fungi (Supplementary Figure S4). This suggests that RISP antifungal activity is not effective against a wide range of fungi and may be specifically targeted to *M. larici-populina*.

RISP Inhibits *M. larici-populina* Growth on Poplar Leaves

To further validate the antifungal activity observed *in vitro* and to assess whether RISP can inhibit *M. larici-populina* growth directly on leaves, purified RISP was applied simultaneously with urediniospores of a virulent isolate onto poplar leaves. The level of fungal growth was then evaluated by analyzing the final number of uredinia, i.e., orange pustules containing newly formed urediniospores, produced after 10 days on the leaf surface. As shown in **Figure 6A**, RISP strongly inhibited fungal development

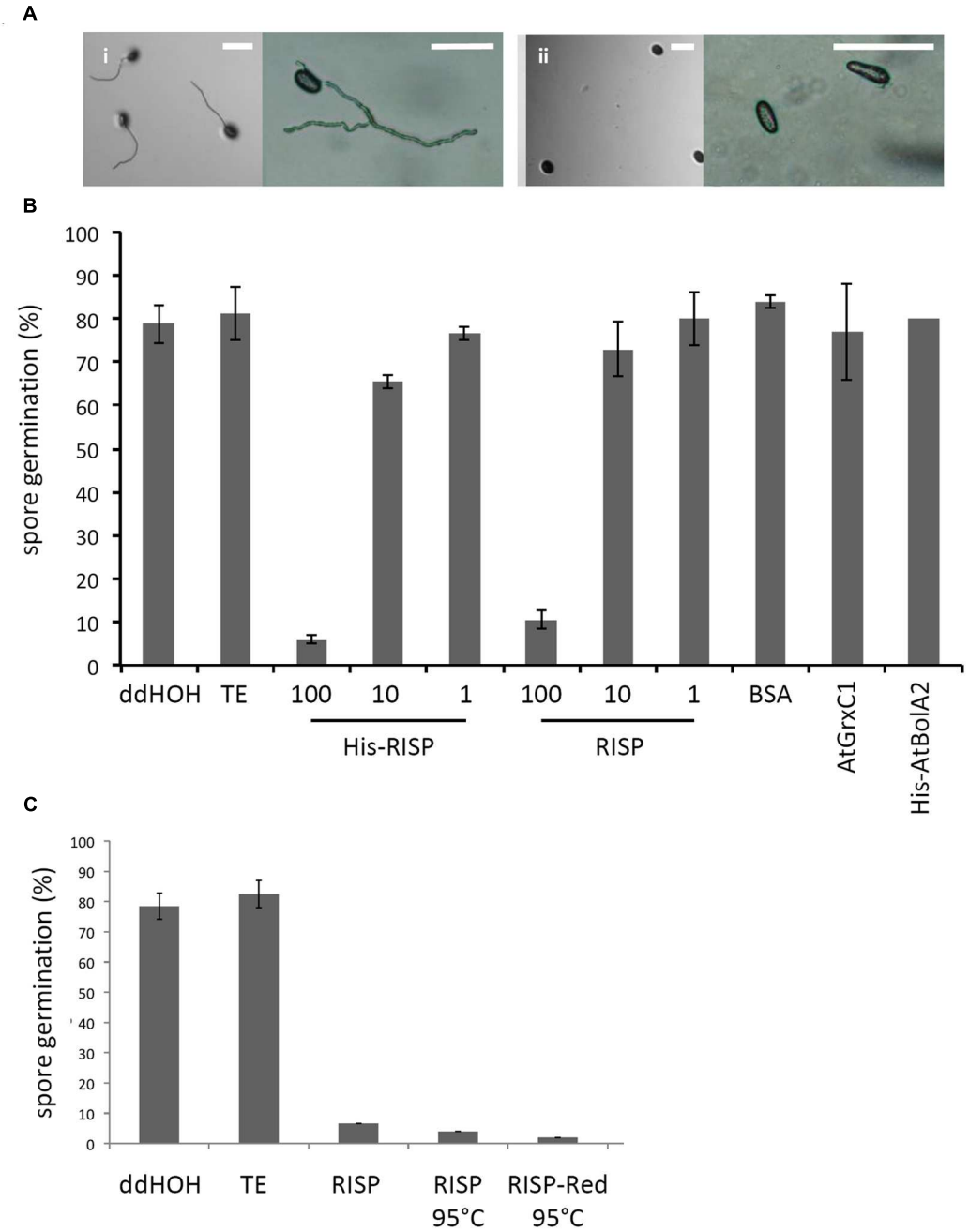

FIGURE 4 | RISP inhibits *M. larici-populina* spore germination *in vitro*. **(A)** *M. larici-populina* urediniospores were deposited on water-agar Petri dishes with (i) TE pH 8.0 buffer (i.e., control without protein) or (ii) His-RISP and pictures were taken after 5 h. Scale bar: 100 μM. **(B)** *M. larici-populina* urediniospores were deposited on water-agar Petri dishes with RISP, His-RISP, BSA, AtGrxC1, His-AtBolA2, TE pH 8.0 buffer (i.e., control without protein) or ddHOH. After 5 h, a minimum of 300 urediniospores were observed and considered to calculate a percentage of germination. RISP concentration is indicated in μM. BSA, AtGrxC1, and His-AtBolA2 were used at a concentration of 100 μM. Error bar: SE, $n \geq 3$ (His-AtBolA2, $n = 2$). **(C)** As in B, with 100 μM RISP, 100 μM RISP boiled for 10 min (RISP 95°C) or 100 μM RISP DTT-reduced and boiled for 10 min (RISP-red 95°C). Error bar: SE of independent repeats, $n \geq 2$.

compared to the control. As an alternative method, RISP was locally deposited on specific leaf areas and the whole leaf was inoculated with urediniospores either immediately or after 3 or 5 days. In all cases, RISP-treated areas remained free of uredinia up to 3 weeks after inoculation (**Figure 6B**; Supplementary Figures S5A,B). Similar results have been obtained with His-RISP (Supplementary Figure S5C). We concluded that RISP presents an antifungal activity against *M. larici-populina* both *in vitro* and on the surface of poplar leaves.

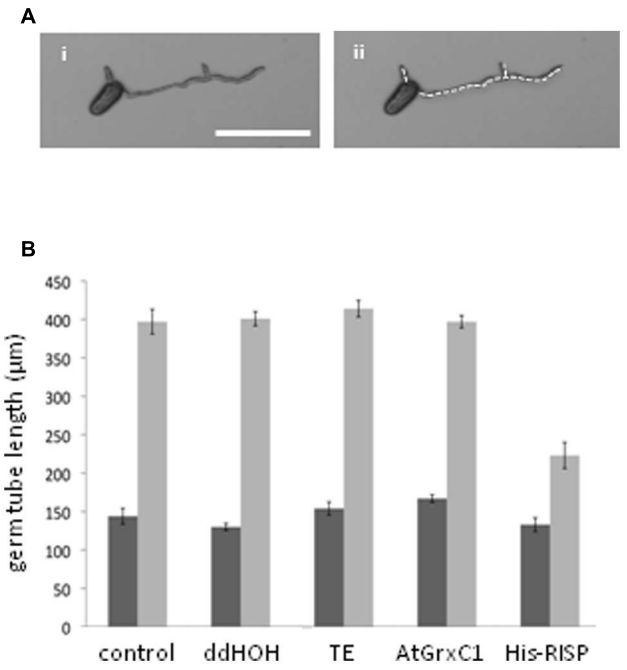

FIGURE 5 | RISP inhibits *M. larici-populina* germinating tube elongation *in vitro*. **(A)** Pictures of *M. larici-populina* urediniospores that germinated 4 h on water-agar in Petri dishes. (ii) Same picture as (i) with the white dotted line marking the measured length of the germ tubes. Scale bar: 100 µM. **(B)** Inhibitory effect of RISP on the elongation of germinating tube *in vitro*. *M. larici-populina* urediniospores germinated for 4 h on water-agar in Petri dishes, then 100 µM His-RISP, 100 µM AtGrxC1, TE pH 8.0 buffer or ddHOH were carefully deposited onto the medium and left 4 additional hours. 'Control' indicates non-treated urediniospores. Pictures were taken under a binocular microscope 4 h (dark gray bars) and 8 h (light gray bars) after the beginning of the experiment and were used to measure the total length of germ tube(s) of a minimum of 15 spores for each repetition. Error bar: SE, $n = 5$.

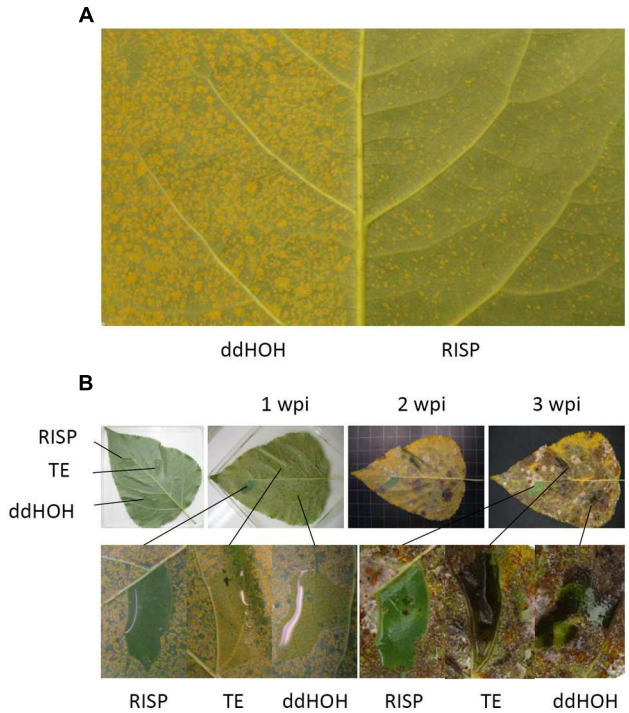

FIGURE 6 | RISP inhibits *M. larici-populina* growth on poplar leaves. **(A)** The left part of a Beaupré leaf was inoculated with *M. larici-populina* urediniospores (isolate 98AG31, virulent on Beaupré) mixed with TE pH 8.0 buffer, whereas the right part was inoculated with the same batch of urediniospores mixed with 100 µM recombinant RISP. Pictures were taken at 10 dpi. **(B)** Selected areas of a Beaupré leaf were treated with 1 mL of ddHOH, TE pH 8.0 buffer or 100 µM RISP, and then the whole leaf was immediately inoculated by pulverization with *M. larici-populina* urediniospores (isolate 98AG31). Pictures were taken just after inoculation as well as 1, 2, or 3 weeks post-inoculation (wpi).

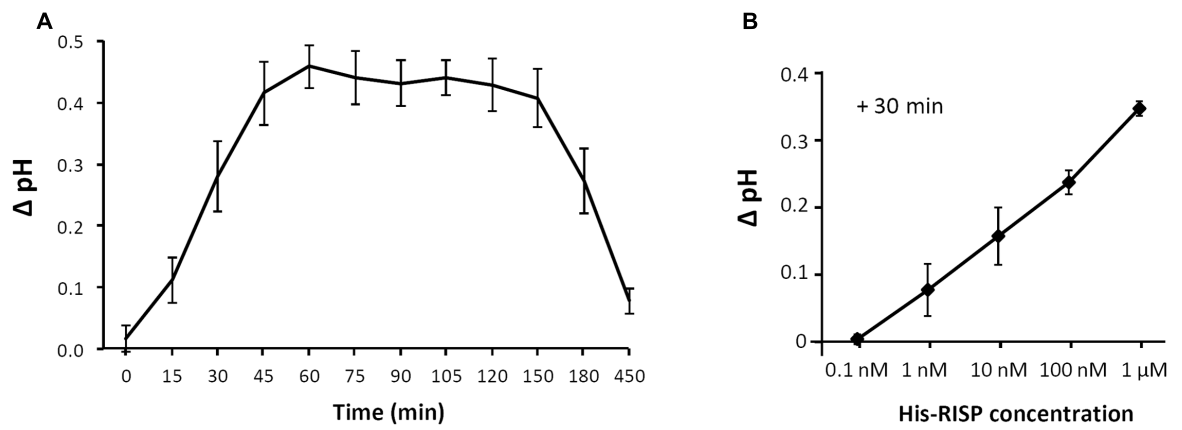

FIGURE 7 | RISP induces poplar cell culture alkalinisation. **(A)** His-RISP was added to poplar cell suspensions (*P. trichocarpa* x *P. deltoides* H11-11 hybrid) at a concentration of 1 µM and the pH was recorded at regular times as indicated. A control without protein was performed with TE pH 8.0 buffer. Error bars: SE, $n = 3$. **(B)** His-RISP was added to the H11-11 cell suspensions at concentrations ranging from 0.1 nM to 1 µM and the pH was recorded after 30 min. Error bars: SE, $n = 3$. TE buffer values (stable at pH 4.2 during the experiment) were used to calculate the pH ratio for each time-point.

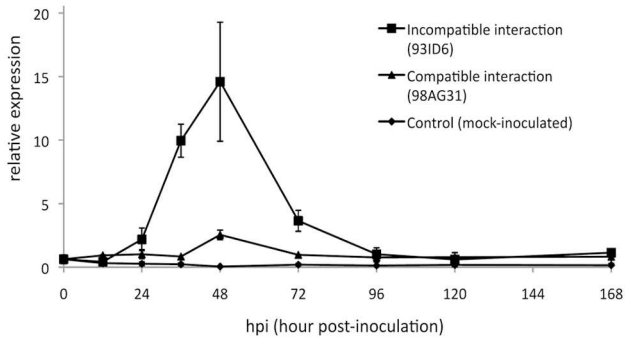

FIGURE 8 | RISP transcripts accumulate in poplar leaves during immune responses. Reverse transcription-quantitative polymerase chain reaction (RT-qPCR) expression profile of *RISP* transcripts during a time-course infection of 'Beaupré' leaves with either virulent (compatible interaction) or avirulent (incompatible interaction) isolates of *M. larici-populina*. Mock-inoculated leaves were used as a control treatment and transcript expression was normalized to a poplar ubiquitin transcript. Error bar: standard deviation of the values from two biological replicates.

RISP Induces Poplar Cell Culture Alkalinisation

The recent observation that the *RISP* gene is adjacent to a *LRR-RLP* gene in the poplar genome sequence and that both genes are co-expressed upon *M. larici-populina* infection led to the hypothesis that RISP may function as an elicitor of cellular responses through this specific receptor-like protein (Petre et al., 2014). To test the ability of RISP to elicit a plant response, we used a poplar cell culture medium alkalinisation assay (Haruta and Constabel, 2003). When added to poplar cell cultures at a final concentration of 1 μM, His-RISP induced a shift of 0.5 pH units after 45 min whereas no pH shift was observed with the buffer alone (**Figure 7A**). An alkalinisation was still observed by decreasing His-RISP concentration to 1 nM, although the pH shift was lower (**Figure 7B**). To rule out the possibility that an *E. coli* contaminant co-purified with the protein triggered cell culture alkalinisation, the assay was repeated with a concentrated protein extract consisting of IMAC-retained proteins from the *E. coli* production strain (Supplementary Figure S6). These contaminants did not affect the pH of the cell culture, indicating that RISP specifically induced cell culture alkalinisation. We concluded that RISP is able to rapidly elicit plant cell responses in a dose-dependent manner.

RISP Transcript Accumulation During Poplar Immune Responses to *M. larici-populina* is Not Reflected at the Protein Level

Previous analyses showed that *RISP* transcripts strongly accumulate at 48 h post-inoculation (hpi), a time-point corresponding to the establishment of poplar defense responses and to the arrest of the growth of an avirulent isolate of *M. larici-populina* (Rinaldi et al., 2007). We used RT-qPCR to further examine *RISP* transcripts accumulation during a complete infection cycle on poplar leaves with virulent and avirulent isolates of *M. larici-populina*. This time-course included key time-points such as 12 hpi (penetration through the stomata), 24 hpi (formation of the first haustorial infection structures), 48 hpi (arrest of avirulent isolate growth), and 168 hpi (formation of uredinia symptoms by the virulent isolate and urediniospores release) (Hacquard et al., 2011). In leaves infected with the avirulent isolate, *RISP* transcripts strongly accumulated between 36 and 72 hpi, with a peak of expression at 48 hpi (**Figure 8**). In contrast, transcript levels remained basal along the whole time-course experiment in either mock-inoculated leaves or leaves infected by a virulent isolate. Hence, by refining the expression pattern of *RISP*, we confirmed that it is specifically induced in poplar leaves during immune responses against *M. larici-populina*, as previously reported (Rinaldi et al., 2007; Petre et al., 2014).

In order to test whether RISP also accumulates at the protein level during an incompatible interaction with *M. larici-populina*, we performed western blotting experiments with a polyclonal antibody raised against the recombinant His-RISP. The antibody efficiently labeled the recombinant His-RISP as well as the endogenous RISP in a total leaf protein extract consisting of an equal mixture of soluble and insoluble proteins (**Figure 9A**). However, RISP was surprisingly not detected in poplar leaves over a time-course infection with an avirulent isolate (**Figures 9A,B**). All subsequent attempts that aimed at identifying RISP by western blot during the incompatible interaction, in particular between 48 and 96 hpi, failed (e.g., by extracting total proteins in a denaturing buffer, by adding a protease inhibitor cocktail, or by performing an enrichment with soluble and thermostable proteins; Supplementary Figure S7). The anti-RISP antibody was also used in co-immunoprecipitation experiments from soluble proteins isolated from *M. larici-populina*-infected poplar leaves as well as immunolocalisation experiments performed on the same tissues (data not shown). In all cases, we were unable to detect RISP at the protein level. This indicated that RISP transcript and protein levels do not correlate during immune responses to *M. larici-populina*, raising the question of a possible modification (degradation or cleavage) of RISP in leaves.

RISP C-Terminus is Cleaved by a Plant-Encoded Mechanism

An approach that has been successfully used to detect the cleavage of protein precursors is to incubate them with plant protein extracts (Guo et al., 2011). To determine whether RISP can be subject to a plant-driven processing, purified RISP and His-RISP were incubated with soluble proteins isolated from poplar leaves, and their integrity assessed by western blot. After 30 min of incubation, a band with a smaller apparent molecular mass appeared for both RISP and His-RISP (**Figure 9C**). In order to better delineate the dynamics of RISP cleavage, the time-course incubation was extended over 24 h with His-RISP. Following 30 min of incubation, the lower band gradually appeared concomitantly with the disappearance of the upper

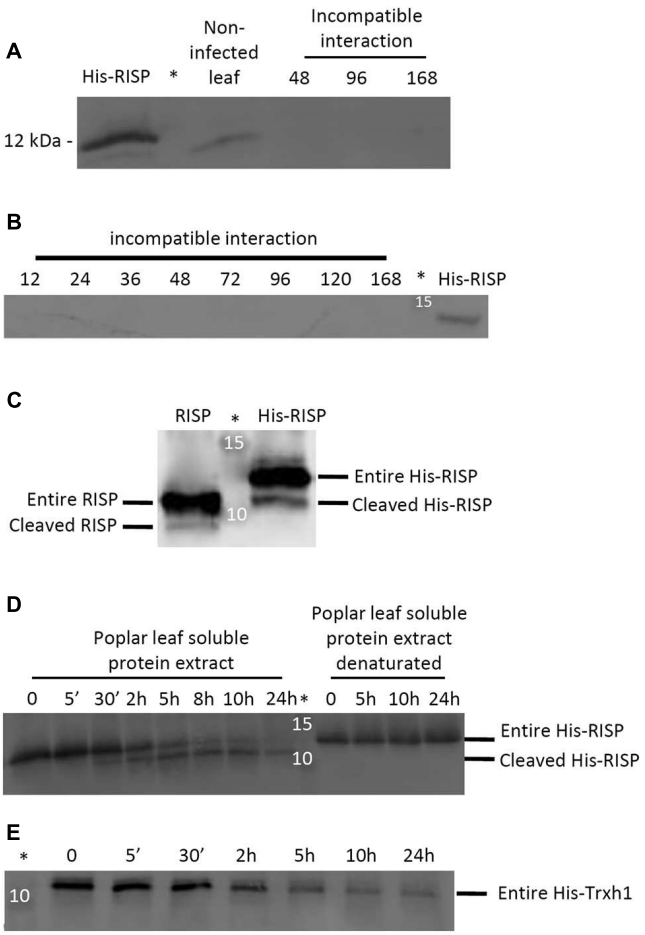

FIGURE 9 | RISP is not detected in poplar leaves during immune responses and its C-terminus is cleaved by a plant-encoded mechanism. (A) Western blot showing the expression of RISP in non-infected poplar leaves and at three time-points of poplar leaves during an incompatible interaction with *M. larici-populina* (see main text for details). **(B)** Western blot showing the expression of RISP over the whole time-course experiments of poplar leaves during an incompatible interaction with *M. larici-populina*. In A and B, proteins isolated from poplar leaves (30 μg: 15 μg of soluble proteins + 15 μg of insoluble proteins) were separated on 15% SDS-PAGE and transferred on nitrocellulose membrane. The His-RISP recombinant protein (20 ng in A and 10 ng in B) was used as a reference. Anti-RISP polyclonal antibodies were used for primary detection of RISP. Numbers presented indicate hpi. **(C)** Five percent (w/w) of purified RISP and His-RISP were incubated with soluble protein extracts from poplar leaves for 30 min at room temperature under gentle agitation and with 1 mM phenylmethanesulfonylfluoride (PMSF). **(D)** RISP time-course incubation with soluble protein extracts from poplar leaves. Five percent (w/w) of purified His-RISP was incubated with untreated or denatured soluble protein extracts from poplar leaves for up to 24 h at room temperature under gentle agitation and with 1 mM PMSF. **(E)** His-tagged thioredoxin h1 (His-Trxh1) time-course incubation with soluble protein extracts from poplar leaves. Five percent (w/w) of purified His-Trxh1 was incubated with soluble protein extracts from poplar leaves for up to 24 h at room temperature under gentle agitation and with 1 mM PMSF. Protein integrity was followed by western blot. *Indicates the lane occupied by the molecular weight marker.

band corresponding to the entire protein (**Figure 9D**). Incubation with heat-denatured soluble protein extracts prevented His-RISP cleavage, suggesting that it was triggered by some thermo-sensitive plant protease activity. Since both untagged and N-terminally His-tagged proteins were cleaved, we favored the idea that the cleavage occurred at the C-terminus. To ensure that the lower band observed with His-RISP was not due to the cleavage of the His-tag, we used an N-terminally His-tagged thioredoxin h1 (His-Trxh1) as a negative control (**Figure 9E**). As a complementary experiment, we have re-purified a mixture of the entire and processed forms of His-RISP using IMAC. After SDS-PAGE separation, the band corresponding to the processed form was digested by trypsin and analyzed by mass spectrometry. Peptides encompassing the His-tag have been unambiguously identified in this sample (data not shown). From these experiments, we concluded that a thermo-sensitive agent (likely a protease) present in poplar leaves promoted the cleavage of the C-terminal end of RISP.

DISCUSSION

In this study, we reported the biochemical, structural, and functional characterisation of the RISP from poplar. We showed that RISP is secreted into the apoplast when transiently expressed in *N. benthamiana* leaf pavement cells. The predicted N-terminal

signal peptide of RISP probably mediates the targeting to the extracellular space through the ER-Golgi secretory pathway. The absence of a fluorescent signal in the cytosol and of any sign of aggregation in the ER-Golgi suggests an efficient secretion. The apoplastic localisation is particularly suited for the two demonstrated roles of RISP, i.e., inhibition of the growth of the fungal pathogen *M. larici-populina*, and elicitation of cellular responses. The dual function of RISP is further discussed below.

RISP Possesses an Antifungal Activity Against *M. larici-populina*

We have shown that RISP co-precipitates with *M. larici-populina* urediniospores in pull-down assays and inhibits their germination. It is noteworthy that the inhibitory effect of RISP on spore germination was used as a proxy to detect its antifungal activity, but may not happen upon natural infections. Indeed, *RISP* expression is induced at 48 hpi by an avirulent strain, a time-point at which fungal structures have already developed inside the leaves. The only possibility is that enough RISP protein persists on leaves until another cycle of infection. For this reason, an assay measuring the capacity of RISP to inhibit the elongation of germinating tubes (a structure sharing the topology of infection hyphae exploring the leaf apoplast during infections) has been set up. It revealed that RISP was also able to inhibit the elongation of *M. larici-populina* germinating tubes *in vitro*. Altogether, these findings suggest that, during leaf infection, RISP is likely secreted in the apoplast where it can directly interact with fungal structures to restrict their development.

An important issue in these bioassays is the concentration of RISP (100 μM) that fully prevented *M. larici-populina* urediniospore germination, since it is in the upper range of what can be found in the literature about plant antifungal proteins (Silva et al., 2014). It is worthy to mention that the indicated concentrations correspond to the initial concentrations of the protein stock solution. For instance, the use of solid media through which proteins diffuse prevents us from rigorously determining the exact concentration of RISP active in these assays. For this reason, the RISP concentration exerting an antimicrobial activity is likely much lower. Concerning the co-inoculation experiments of the virulent strain of *M. larici-populina* with RISP on poplar leaves, it is first important to specify that the absence of rust disease symptoms is likely attributed to the fact that RISP inhibits the germination of urediniospores present on the surface of the leaves as observed in the *in vitro* system. Other important aspects to consider are that high spore concentrations are used and that a single spore is sufficient to generate an infection and produce a uredinia. Thus, the fact that we observed no lesions on leaves treated with 100 μM RISP suggests that RISP prevented the germination of almost 100% of the spores, which was never observed in the tests performed *in vitro*. Hence, RISP seems to be a more potent inhibitor of spore germination on poplar leaves. A possible explanation is that part of the protein can diffuse through the wax and prevent the growth of the fungal structures that have invaded the leaf, either directly as observed *in vitro* through the inhibition of germ tube elongation or by eliciting some cellular responses. Nevertheless, this explanation is unlikely considering the existence of a very thick and impermeable cuticle in leaves of this poplar cultivar. A more plausible explanation is that contrary to *in vitro* experiments where protein solutions are rapidly diluted into the agar, the RISP solution remains as a drop on leaves and spores are continuously exposed to a high RISP concentration for hours.

Known plant AMPs are usually structured proteins (Pelegrini et al., 2011) whereas we have observed that RISP is in a disordered state in aqueous solutions (**Figure 2A**). The fact that it can partially fold in the presence of TFE suggests that RISP might fold in particular conditions, for example in contact with target molecules. From the co-precipitation assay with *M. larici-populina* urediniospores (**Figure 3**) some external molecules present at the surface of the urediniospores constitute one of these targets. The disruption of membrane integrity by AMPs can be due to the formation of toroidal pores formed by a supramolecular assembly of peptides and lipids, as well as to the accumulation of high concentrations of peptides whose amphipathic structures align parallel to the membrane surface (Bechinger and Salnikov, 2012). In accordance with this need to form structures with a particular arrangement, we observed that the presence of a GFP tag precluded RISP interaction with the spores.

RISP Elicits Cellular Responses Upon Incubation with Poplar Cells

Besides its antifungal properties, the genomic proximity and co-regulation of the *RISP* gene with a gene encoding a LRR-RLP prompted us to investigate a possible elicitor function (Petre et al., 2014). Cell-culture alkalinisation assays have been widely used to identify and characterize plant elicitors in a number of species (Pearce and Ryan, 2003; Scheer et al., 2003; Huffaker et al., 2006; Pearce et al., 2009, 2010; Chang et al., 2013). Haruta and Constabel (2003) previously reported the use of the poplar cell line H11-11 (*P. trichocarpa* x *P. deltoides*) to characterize poplar rapid-alkalinisation factor 1 (RALF1). The alkalinisation profile observed with His-RISP is similar to the one previously reported for RALF1, reaching a maximal alkalinisation of approximately 4.7 pH units. Maximal cell alkalinisation was obtained with a concentration of 1 μM. This concentration is higher than those usually reported for RALF or other peptides in cell cultures from different plant species (Haruta and Constabel, 2003; Yamaguchi et al., 2011) but we noticed that an effect is still visible at 1 nM with His-RISP (**Figure 7B**).

One hypothesis that may explain the requirement for higher concentrations is that the RISP form used in these experiments is not similar to the native protein, i.e., the one produced *in planta*. For instance, while disulfide bond formation into inceptin has no effect on its biological activity (Schmelz et al., 2007), it was observed that the *in vitro* oxidation of a synthetic tobacco RALF peptide leads to the formation of different oxidized forms that are more or less active (Pearce et al., 2001). Considering the presence of four cysteines in RISP, variations in its redox state may explain

this difference. However, RISP structure and antifungal activity is not affected by disulfide bond reduction. Another hypothesis to explain the high concentration of RISP required for these elicitor activity assays is that we have used a precursor protein and not the bioactive peptide. It is well-documented that peptide hormones are often released from their precursors upon cleavage (Germain et al., 2006; Matsubayashi, 2014). Consistently, we have observed that a plant mechanism promoted the specific cleavage of several amino acids from the C-terminus of RISP. In parallel, the absence of RISP detection in infected poplar leaves, whereas the polyclonal anti-RISP antibodies efficiently detected nanograms of recombinant proteins, also supports the view that RISP is a cleavable precursor. Of course, we cannot completely exclude that other factors prevented RISP detection. Secreted peptide hormones might undergo post-translational modifications (Matsubayashi, 2014). In the case of RISP, it may mask the recognized epitopes. It may also be that protein accumulation occurs at spatially restricted sites making it almost undetectable using destructive approaches (Caillaud et al., 2013). However, we were unable to detect any specific signal in intact infected tissues using fluorescent immunolocalisation.

Although the cell culture alkalinisation assay revealed that RISP is able to trigger cellular responses, the nature of these responses remains unknown. In model plants such as *Arabidopsis thaliana*, alkalinisation assays are often associated with other bioassays such as MAP-kinase activation, ROS formation, callose deposition or activation of defense genes (Schwessinger et al., 2011; Lloyd et al., 2014). However, such assays cannot be established in our poplar species primarily because gene activation measurement in response to RISP is prevented by the difficulty to perform appropriate infiltration of poplar leaves. Note also that no or very low amounts of ROS are produced during poplar defense responses (Rinaldi et al., 2007). Hence, future investigations could rather consist in evaluating RISP elicitor activity in model plant species ectopically expressing the candidate LRR-RLP receptor associated with RISP (Petre et al., 2014).

CONCLUSION

Rust-induced secreted protein combines both antimicrobial and elicitor activities. Growing evidence suggest that many AMPs of animals, fungi and plants are multifunctional peptides, which fulfill other biological functions related to immunity or not (Hegedus and Marx, 2013; Woriedh et al., 2015). For instance in animals, defensins are well-known AMPs with a wide range of secondary functions (Selsted and Ouellette, 2005; Yeung et al., 2011). In plants, *Capsicum annuum* antimicrobial protein 1 or *Prunus domestica* PR5-1 stimulate defense responses when ectopically over-expressed in *A. thaliana* (El-kereamy et al., 2011; Lee et al., 2011). Also, Chang et al. (2013) recently isolated a 16 amino acid peptide from sweet potato leaves that is able to induce tomato cell culture alkalinisation. This peptide corresponds to the N-terminus of a thaumatin-like protein (Chang et al., 2013), an antimicrobial protein belonging to the PR5 family (Petre et al., 2011). Future work should aim at determining the nature of the cellular responses triggered by RISP, the hypothesis being that these responses participate in immunity against *M. larici-populina*. Contrasting with most of the AMPs and peptide hormones that are often conserved in plants, there is no protein similar to RISP in other plant species. The study of RISP may reveal novel mechanisms that poplar developed to resist *M. larici-populina*.

AUTHOR CONTRIBUTIONS

BP, HG, AS, SD, and NR conceived and designed the experiments; BP, AH, HG, PT, JS, GP, SD, and NR performed the experiments and analyzed the data; BP, SD, and NR wrote the manuscript.

ACKNOWLEDGMENTS

This work was supported by a grant overseen by ANR as part of the "Investissements d'Avenir" program (ANR-11-LABX-0002-01, Lab of Excellence ARBRE) and by funding from Région Lorraine and INRA, including the CJS contract for BP salary. A 1 month visit of BP at the LFC in Quebec was funded by the INRA EFPA department. BP has received the support of the European Union, in the framework of the Marie-Curie FP7 COFUND People Program, through the award of an AgreenSkills' fellowship (under grant agreement n° 267196). Research in The Sainsbury Laboratory is supported by the Gatsby Charitable Foundation, the European Research Council, and the Biotechnology and Biological Sciences Research Council (BBSRC). The authors thank Claire Veneault-Fourrey (INRA, France) for her help with *M. oryzae* spore isolation, Pascal Frey and Bénédicte Fabre (INRA, France) for their advice on poplar culture in greenhouses and *M. larici-populina* inoculations as well as for providing rust fungus material, Patrice Vion and Christine Delaruelle (INRA, France) for technical help, Stéphane Hacquard (MPI, Germany) for helpful discussions about RT-qPCR, Meriem Benchabane (LFC, Canada) for her help with poplar cell cultures, Francis Martin (INRA, France), Sophien Kamoun's group and Frank Menke (TSL, UK) for helpful discussions. Access to the Bruker Avance III 600 spectrometers (NMR facilities of the SCBIM – FR3209-CNRS "Bioingénierie Moléculaire, Cellulaire et Thérapeutique" Université de Lorraine) was appreciated.

SUPPLEMENTARY MATERIAL

The Supplementary Material for this article can be found online at: http://journal.frontiersin.org/article/10.3389/fpls.2016.00097

REFERENCES

Bartels, S., and Boller, T. (2015). Quo vadis, Pep? Plant elicitor peptides at the crossroads of immunity, stress, and development. *J. Exp. Bot.* 66, 5183–5193. doi: 10.1093/jxb/erv180

Bechinger, B., and Salnikov, E. S. (2012). The membrane interactions of antimicrobial peptides revealed by solid-state NMR spectroscopy. *Chem. Phys. Lipids* 165, 282–301. doi: 10.1016/j.chemphyslip.2012.01.009

Bouillac, S., Rouhier, N., Tsan, P., Jacquot, J.-P., and Lancelin, J.-M. (2004). Letter to the Editor: 1H, 13C and 15N NMR assignment of the homodimeric poplar phloem type II peroxiredoxin. *J. Biomol. NMR* 30, 105–106. doi: 10.1023/B:JNMR.0000042965.46172.1b

Brünger, A. (2007). Version 1.2 of the Crystallography and NMR system. *Nat. Protoc.* 2, 2728–2733. doi: 10.1038/nprot.2007.406

Brünger, A. T., Adams, P. D., Clore, G. M., DeLano, W. L., Gros, P., Grosse-Kunstleve, R. W., et al. (1998). Crystallography & NMR system: a new software suite for macromolecular structure determination. *Acta Crystallogr. D Biol. Crystallogr.* 54, 905–921. doi: 10.1107/S0907444998003254

Butenko, M. A., Vie, A. K., Brembu, T., Aalen, R. B., and Bones, A. M. (2009). Plant peptides in signalling: looking for new partners. *Trends Plant Sci.* 14, 255–263. doi: 10.1016/j.tplants.2009.02.002

Caillaud, M. C., Asai, S., Rallapalli, G., Piquerez, S., Fabro, G., and Jones, J. D. (2013). A downy mildew effector attenuates salicylic acid-triggered immunity in Arabidopsis by interacting with the host mediator complex. *PLoS Biol.* 11:e1001732. doi: 10.1371/journal.pbio.1001732

Chang, V. H.-S., Yang, D. H.-A., Lin, H.-H., Pearce, G., Ryan, C. A., and Chen, Y.-C. (2013). IbACP, a sixteen-amino-acid peptide isolated from *Ipomoea batatas* leaves, induces carcinoma cell apoptosis. *Peptides* 47, 148–156. doi: 10.1016/j.peptides.2013.02.005

Couturier, J., Wu, H. C., Dhalleine, T., Pégeot, H., Sudre, D., Gualberto, J. M., et al. (2014). Monothiol glutaredoxin-BolA interactions: redox control of *Arabidopsis thaliana* BolA2 and SufE1. *Mol. Plant* 7, 187–205. doi: 10.1093/mp/sst156

Di Battista, C., Selosse, M. A., Bouchard, D., Stenstrom, E., and Le Tacon, F. (1996). Variations in symbiotic efficiency, phenotypic characters and ploidy level among different isolates of the ectomycorrhizal basidiomycete *Laccaria bicolor* strain S 238. *Mycol. Res.* 100, 1315–1324. doi: 10.1016/S0953-7562(96)80058-X

Dodds, P. N., and Rathjen, J. P. (2010). Plant immunity: towards an integrated view of plant-pathogen interactions. *Nat. Rev. Genet.* 11, 539–548. doi: 10.1038/nrg2812

Duplessis, S., Major, I., Martin, F., and Séguin, A. (2009). Poplar and pathogen interactions: insights from *Populus* genome-wide analyses of resistance and defense gene families and gene expression profiling. *Crit. Rev. Plant Sci.* 28, 309–334. doi: 10.1080/07352680903241063

El-kereamy, A., El-sharkawy, I., Ramamoorthy, R., Taheri, A., Errampalli, D., Kumar, P., et al. (2011). *Prunus domestica* pathogenesis-related protein-5 activates the defense responses pathway and enhances the resistance to fungal infection. *PLoS ONE* 6:e17973. doi: 10.1371/journal.pone.0017973

Fuglsang, A. T., Kristensen, A., Cuin, T. A., Schulze, W. X., Persson, J., Thuesen, K. H., et al. (2014). Receptor kinase-mediated control of primary active proton pumping at the plasma membrane. *Plant J.* 80, 951–964. doi: 10.1111/tpj.12680

Germain, H., Chevalier, E., and Matton, D. P. (2006). Plant bioactive peptides: an expanding class of signaling molecules. *Can. J. Bot.* 84, 1–19. doi: 10.1139/b05-162

Guo, Y., Ni, J., Denver, R., Wang, X., and Clark, S. E. (2011). Mechanisms of molecular mimicry of plant CLE peptide ligands by the parasitic nematode *Globodera rostochiensis*. *Plant Physiol.* 157, 476–484. doi: 10.1104/pp.111.180554

Hacquard, S., Petre, B., Frey, P., Hecker, A., Rouhier, N., and Duplessis, S. (2011). The poplar-poplar rust interaction: insights from genomics and transcriptomics. *J. Pathog.* 2011, 716041. doi: 10.4061/2011/716041

Hacquard, S., Veneault-Fourrey, C., Delaruelle, C., Frey, P., Martin, F., and Duplessis, S. (2010). Validation of *Melampsora larici-populina* reference genes for in planta RT-quantitative PCR expression profiling during time-course infection of poplar leaves. *Physiol. Mol. Plant Pathol.* 75, 106–112. doi: 10.1016/j.pmpp.2010.10.003

Haney, E. F., Hunter, H. N., Matsusaki, K., and Vogel, H. J. (2009). Solution NMR studies of amphibian antimicrobial peptides: linking structure to function? *Biochim. Biophys. Acta* 1788, 1639–1655. doi: 10.1016/j.bbamem.2009.01.002

Haruta, M., and Constabel, P. (2003). Rapid alkalinization factors in poplar cell cultures. Peptide isolation, cdna cloning, and differential expression in leaves and methyl jasmonate-treated cells. *Plant Physiol.* 131, 814–823. doi: 10.1104/pp.014597

Haruta, M., Sabat, G., Stecker, K., Minkoff, B. B., and Sussman, M. R. (2014). A peptide hormone and its receptor protein kinase regulate plant cell expansion. *Science* 343, 408–411. doi: 10.1126/science.1244454

Hegedüs, N., and Marx, F. (2013). Antifungal proteins: more than antimicrobials? *Fungal Biol. Rev.* 26, 132–145. doi: 10.1016/j.fbr.2012.07.002

Huffaker, A., Pearce, G., and Ryan, C. A. (2006). An endogenous peptide signal in *Arabidopsis* activates components of the innate immune response. *Proc. Natl. Acad. Sci. U.S.A.* 26, 10098–10103. doi: 10.1073/pnas.0603727103

Krause, C., Richter, S., Knoll, C., and Jurgens, G. (2013). Plant secretome – From cellular process to biological activity. *Biochim. Biophys. Acta* 1834, 2429–2441. doi: 10.1016/j.bbapap.2013.03.024

Lee, S. C., Hwang, I. S., and Hwang, B. K. (2011). Overexpression of the pepper antimicrobial protein CaAMP1 regulates the oxidative stress– and disease-related proteome in *Arabidopsis*. *Planta* 234, 1111–1125. doi: 10.1007/s00425-011-1473-1

Lloyd, S. R., Schoonbeek, H. J., Trick, M., Zipfel, C., and Ridout, C. J. (2014). Methods to study PAMP-triggered immunity in *Brassica* species. *Mol. Plant Microbe Interact.* 3, 286–295. doi: 10.1094/MPMI-05-13-0154-FI

Matsubayashi, Y. (2014). Posttranslationally modified small-peptide signals in plants. *Annu. Rev. Plant Biol.* 65, 385–413. doi: 10.1146/annurev-arplant-050312-120122

Melo, M. N., Ferre, R., and Castanho, A. R. B. (2009). Antimicrobial peptides: linking partition, activity and high membrane-bound concentrations. *Nat. Rev. Microbiol.* 7, 245–250. doi: 10.1038/nrmicro2095

Menand, B., Marechal-Drouard, L., Sakamoto, W., Dietrich, A., and Wintz, H. (1998). A single gene of chloroplast origin codes for mitochondrial and chloroplastic methionyl-tRNA synthetase in *Arabidopsis thaliana*. *Proc. Natl. Acad. Sci. U.S.A.* 95, 11014–11019. doi: 10.1073/pnas.95.18.11014

Monaghan, J., and Zipfel, C. (2012). Plant pattern recognition receptor complexes at the plasma membrane. *Curr. Opin. Plant Biol.* 15, 1–9. doi: 10.1016/j.pbi.2012.05.006

Pearce, G., Bhattacharya, R., Chen, Y. C., Barona, G., Yamaguchi, Y., and Ryan, C. A. (2009). Isolation and characterization of hydroxyproline-rich glycopeptide signals in black nightshade leaves. *Plant Physiol.* 3, 1422–1433. doi: 10.1104/pp.109.138669

Pearce, G., Munske, G., Yamaguchi, Y., and Ryan, C. A. (2010). Structure-activity studies of GmSubPep, a soybean peptide defense signal derived from an extracellular protease. *Peptides* 12, 2159–2164. doi: 10.1016/j.peptides.2010.09.004

Pearce, G., Moura, D. S., Stratmann, J., and Ryan, C. A., Jr. (2001). "RALF, a 5-kDa ubiquitous polypeptide in plants, arrests root growth and development," in *Proceedings of the National Academy of Sciences of the United States of America* 98, 12843–12847.

Pearce, G., and Ryan, C. A. (2003). Systemic signaling in tomato plants for defense against herbivores. *J. Biol. Chem.* 278, 30044–30050. doi: 10.1074/jbc.M304159200

Pégeot, H., Koh, C. S., Petre, B., Mathiot, S., Duplessis, S., Hecker, A., et al. (2014). The poplar Phi class glutathione transferase: expression, activity and structure of GSTF1. *Front. Plant Sci.* 5:712. doi: 10.3389/fpls.2014.00712

Pelegrini, P. B., del Sarto, R. P., Silva, O. N., Franco, O. L., and Grossi-de-Sa, M. F. (2011). Antibacterial peptides from plants: what they are and how they probably work. *Biochem. Res. Int.* 2011, 250349. doi: 10.1155/2011/250349

Petre, B., Hacquard, S., Duplessis, S., and Rouhier, N. (2014). Genome analysis of poplar LRR-RLP gene clusters reveals RISP, a defense-related gene coding a candidate endogenous peptide elicitor. *Front. Plant Sci.* 5:111. doi: 10.3389/fpls.2014.00111

Petre, B., Major, I., Rouhier, N., and Duplessis, S. (2011). Genome-wide analysis of eukaryote thaumatin-like proteins (TLPs) with an emphasis on poplar. *BMC Plant Biol.* 11:33. doi: 10.1186/1471-2229-11-33

Poon, I. K. H., Baxter, A. A., Lay, F. T., Mills, G. D., Adda, C. G., Payne, J. A. E., et al. (2014). Phosphoinositide-mediated oligomerization of a defensin induces cell lysis. *Elife* 3, e01808. doi: 10.7554/eLife.01808

Rieping, W., Habeck, M., Bardiaux, B., Bernard, A., Malliavin, T. E., and Nilges, M. (2007). ARIA2: automated NOE assignment and data integration in NMR structure calculation. *Bioinformatics* 23, 381–382. doi: 10.1093/bioinformatics/btl589

Rinaldi, C., Kohler, A., Frey, P., Duchaussoy, F., Ningre, N., Couloux, A., et al. (2007). Transcript profiling of poplar leaves upon infection with compatible and incompatible strains of the foliar rust *Melampsora larici-populina*. *Plant Physiol.* 144, 347–366. doi: 10.1104/pp.106.094987

Rouhier, N., Gelhaye, E., Gualberto, J., Jordy, M.-N., de Fäy, E., Hirasawa, M., et al. (2004). Poplar peroxiredoxin Q. A thioredoxin-linked chloroplast antioxidant functional in pathogen defense. *Plant Physiol.* 134, 1–12. doi: 10.1104/pp.900099

Rouhier, N., Gelhaye, E., Sautiere, P.-E., Brun, A., Laurent, P., Tagu, D., et al. (2001). Isolation and characterization of a new peroxiredoxin from poplar sieve tubes that uses either glutaredoxin or thioredoxin as a proton donor. *Plant Physiol.* 127, 1299–1309. doi: 10.1104/pp.010586

Rouhier, N., and Jacquot, J.-P. (2003). Molecular and catalytic properties of a peroxiredoxin-glutaredoxin hybrid from *Neisseria meningitidis*. *FEBS Lett.* 554, 149–153. doi: 10.1016/S0014-5793(03)01156-6

Rouhier, N., Unno, H., Bandyopadhyay, S., Masip, L., Kim, S. K., Hirasawa, M., et al. (2007). Functional, structural, and spectroscopic characterization of a glutathione-ligated [2Fe-2S] cluster in poplar glutaredoxin C1. *Proc. Natl. Acad. Sci. U.S.A.* 104, 7379–7384. doi: 10.1073/pnas.0702268104

Scheer, J. M., Pearce, G., and Ryan, C. A. (2003). Generation of systemin signaling in tobacco by transformation with the tomato systemin receptor kinase gene. *Proc. Natl. Acad. Sci. U.S.A.* 17, 10114–10117. doi: 10.1073/pnas.1432910100

Schmelz, E. A., Leclere, S., Carroll, M. J., Alborn, H. T., and Teal, P. E. (2007). Cowpea chloroplastic ATP synthase is the source of multiple plant defense elicitors during insect herbivory. *Plant Physiol.* 144, 793–805. doi: 10.1104/pp.107.097154

Schwessinger, B., Roux, M., Kadota, Y., Ntoukakis, V., Sklenar, J., Jones, A., et al. (2011). Phosphorylation-dependent differential regulation of plant growth, cell death, and innate immunity by the regulatory receptor-like kinase BAK1. *PLoS Genet.* 4:e1002046. doi: 10.1371/journal.pgen.1002046

Selsted, M. E., and Ouellette, A. J. (2005). Mammalian defensins in the antimicrobial immune response. *Nat. Immunol.* 6, 551–557. doi: 10.1038/ni1206

Silva, P. M., Goncalves, S., and Santos, N. C. (2014). Defensins: antifungal lessons from eukaryotes. *Front. Microbiol.* 5:97. doi: 10.3389/fmicb.2014.00097

Simon, R., and Dresselhaus, T. (2015). Peptides take centre stage in plant signalling. *J. Exp. Bot.* 66, 5135–5138. doi: 10.1093/jxb/erv376

Tabata, R., and Sawa, S. (2014). Maturation processes and structures of small secreted peptides in plants. *Front. Plant Sci.* 5:311. doi: 10.3389/fpls.2014.00311

Talbot, N. J., Ebbole, D. J., and Hamer, J. E. (1993). Identification and characterization of MPG1, a gene involved in pathogenicity from the rice blast fungus *Magnaporthe grisea*. *Plant Cell* 11, 1575–1590. doi: 10.2307/3869740

Tao, Y., Xie, Z., Chen, W., Glazebrook, J., Chang, H. S., Han, B., et al. (2003). Quantitative nature of Arabidopsis responses during compatible and incompatible interactions with the bacterial pathogen *Pseudomonas syringae*. *Plant Cell* 15, 317–330. doi: 10.1105/tpc.007591

van Loon, L. C., Rep, M., and Pieterse, C. M. J. (2006). Significance of inducible defense-related proteins in infected plants. *Annu. Rev. Phytopathol.* 44, 135–162. doi: 10.1146/annurev.phyto.44.070505.143425

Vasconcelos, E. A. R., Santana, C. G., Godoy, C. V., Seixas, C. D. S., Silva, M. S., Moreira, L. R. S., et al. (2011). A new chitinase-like xylanase inhibitor protein (XIP) from coffee (*Coffea arabica*) affects Soybean Asian rust (*Phakopsora pachyrhizi*) spore germination. *BMC Biotechnol.* 11:14. doi: 10.1186/1472-6750-11-14

Win, J., Kamoun, S., and Jones, A. M. (2011). Purification of effector-target protein complexes via transient expression in *Nicotiana benthamiana*. *Methods Mol. Biol.* 712, 181–194. doi: 10.1007/978-1-61737-998-7_15

Woriedh, M., Merkl, R., and Dresselhaus, T. (2015). Maize EMBRYO SAC family peptides interact differentially with pollen tubes and fungal cells. *J. Exp. Bot.* 66, 5205–5216. doi: 10.1093/jxb/erv268

Yamaguchi, Y., Barona, G., Ryan, C. A., and Pearce, G. (2011). GmPep914, an eight-amino acid peptide isolated from soybean leaves, activates defense-related genes. *Plant Physiol.* 156, 932–942. doi: 10.1104/pp.111.173096

Yamaguchi, Y., and Huffaker, A. (2011). Endogenous peptide elicitors in higher plants. *Curr. Opin. Plant Biol.* 14, 1–7. doi: 10.1016/j.pbi.2011.05.001

Yeung, A. T. Y., Gellatly, S. L., and Hancock, R. E. W. (2011). Multifunctional cationic host defence peptides and their clinical applications. *Cell. Mol. Life Sci.* 13, 2161–2176. doi: 10.1007/s00018-011-0710-x

Zasloff, M. (2002). Antimicrobial peptides of multicellular organisms. *Nature* 415, 389–395. doi: 10.1038/415389a

Conflict of Interest Statement: The authors declare that the research was conducted in the absence of any commercial or financial relationships that could be construed as a potential conflict of interest.

frontiers in Plant Science

ORIGINAL RESEARCH
published: 27 October 2016
doi: 10.3389/fpls.2016.01546

cAMP Signaling Regulates Synchronised Growth of Symbiotic *Epichloë* Fungi with the Host Grass *Lolium perenne*

Christine R. Voisey[1], Michael T. Christensen[2], Linda J. Johnson[1], Natasha T. Forester[1], Milan Gagic[1], Gregory T. Bryan[1], Wayne R. Simpson[1], Damien J. Fleetwood[3], Stuart D. Card[1], John P. Koolaard[4], Paul H. Maclean[5] and Richard D. Johnson[1]*

[1] Forage Science, AgResearch Ltd., Grasslands Research Centre, Palmerston North, New Zealand, [2] Formally of Forage Improvement, AgResearch Ltd., Grasslands Research Centre, Palmerston North, New Zealand, [3] Biotelliga Ltd., Institute for Innovation in Biotechnology, Auckland, New Zealand, [4] Bioinformatics and Statistics Team, AgResearch Ltd., Grasslands Research Centre, Palmerston North, New Zealand, [5] Bioinformatics and Statistics Team, AgResearch Ltd., Lincoln Research Centre, Christchurch, New Zealand

OPEN ACCESS

Edited by:
Ralph Panstruga, RWTH Aachen University, Germany

Reviewed by:
Paul Tudzynski, Westfälische Wilhelms-Universität Münster, Germany
Matthew Agler, Max Planck Institute for Plant Breeding Research, Germany
Daigo Takemoto, Nagoya University, Japan

***Correspondence:**
Christine R. Voisey
christine.voisey@agresearch.co.nz

Specialty section:
This article was submitted to Plant Biotic Interactions, a section of the journal Frontiers in Plant Science

Received: *28 April 2016*
Accepted: *03 October 2016*
Published: *27 October 2016*

Citation:
Voisey CR, Christensen MT, Johnson LJ, Forester NT, Gagic M, Bryan GT, Simpson WR, Fleetwood DJ, Card SD, Koolaard JP, Maclean PH and Johnson RD (2016) cAMP Signaling Regulates Synchronised Growth of Symbiotic Epichloë Fungi with the Host Grass Lolium perenne. Front. Plant Sci. 7:1546. doi: 10.3389/fpls.2016.01546

The seed-transmitted fungal symbiont, *Epichloë festucae,* colonizes grasses by infecting host tissues as they form on the shoot apical meristem (SAM) of the seedling. How this fungus accommodates the complexities of plant development to successfully colonize the leaves and inflorescences is unclear. Since adenosine 3′, 5′-cyclic monophosphate (cAMP)-dependent signaling is often essential for host colonization by fungal pathogens, we disrupted the cAMP cascade by insertional mutagenesis of the *E. festucae* adenylate cyclase gene (*acyA*). Consistent with deletions of this gene in other fungi, *acyA* mutants had a slow radial growth rate in culture, and hyphae were convoluted and hyper-branched suggesting that fungal apical dominance had been disrupted. Nitro blue tetrazolium (NBT) staining of hyphae showed that cAMP disruption mutants were impaired in their ability to synthesize superoxide, indicating that cAMP signaling regulates accumulation of reactive oxygen species (ROS). Despite significant defects in hyphal growth and ROS production, *E. festucae* Δ*acyA* mutants were infectious and capable of forming symbiotic associations with grasses. Plants infected with *E. festucae* Δ*acyA* were marginally less robust than the wild-type (WT), however hyphae were hyper-branched, and leaf tissues heavily colonized, indicating that the tight regulation of hyphal growth normally observed in maturing leaves requires functional cAMP signaling.

Keywords: *Epichloë festucae*, *Lolium perenne*, symbiosis, cAMP signaling, reactive oxygen species, hyphal branching

INTRODUCTION

Temperate grasses such as *Lolium perenne* (Poaceae, subfamily Pooideae) often host mutualistic endophytic fungi in the genus *Epichloë* of the family Clavicipitaceae (Christensen and Voisey, 2009; Card et al., 2014; Leuchmann et al., 2014; Simpson et al., 2014). This genus became prominent when these endophytes were proven to be agents of chronic circulatory and neurological disorders in livestock feeding on infected forage (Bacon et al., 1977; Ball and Prestidge, 1993; Leuchmann et al., 2014). Several classes of endophyte metabolites with mammalian and insect toxicity, as

well as invertebrate deterrent effects, have been characterized (Schardl and Phillips, 1997; Schardl et al., 2007, 2013). *Epichloë* infection can also elevate the tolerance of grasses to certain abiotic stresses (Arachevaleta et al., 1989; Malinowski and Belesky, 2000; Vázquez-de-Aldana et al., 2013). Given these attributes, these fungi are often prevalent in native grass habitats, but are also essential for persistence of forage in managed pastoral farming systems where insect pressure is high, as in New Zealand, Australia, and the Americas (Johnson et al., 2013a).

Epichloë hyphae within host tissues are confined to the intercellular spaces and do not invade cells (Christensen et al., 2008). They are notable for their complex biotrophic lifecycle which is synchronized with growth and development of the host from seedling to mature plant. Colonization of the plant by the endophyte proceeds through discrete modes of hyphal growth that alternate between apical extension and branch formation of hyphae in the shoot apical meristem (SAM), intercalary hyphal growth along the length of the filament in expanding host structures, and a phase in mature plant tissues where the fungus stops growing but remains metabolically active (Christensen et al., 2008; Christensen and Voisey, 2009; Voisey, 2010; Eaton et al., 2011). Each phase of vegetative hyphal development is seemingly initiated in response to changes in host development. For example, the transition between plant cell division and extension in developing leaves correlates with repression of hyphal lateral branch formation and initiation of intercalary hyphal extension; and maturation (cessation of growth) of host leaves correlates with a transition from hyphal intercalary growth to little or no extension or tip (polar) growth. The developmental switch from polar to intercalary hyphal growth is a critical stage in host colonization, and is achieved through initiation of the full cell cycle within intercalary hyphal compartments, including mitosis, the laying down of new septa, and cell expansion, a mechanism of growth rarely observed in vegetative filamentous fungi (Christensen et al., 2008; Christensen and Voisey, 2009; Voisey, 2010). Growth of *Epichloë* hyphae in plants is therefore restricted to developing plant tissues, particularly those arising from the SAM, axillary meristems (from which new tillers form) and floral meristems; and plant structures undergoing cell expansion such as developing leaves and floral spikes. How *Epichloë* colonization processes are synchronized with host development is likely mediated through hyphal sensing of changes in host development that induce corresponding changes in fungal development. *E. festucae* genes in the stress-activated mitogen-activated protein kinase (*sakA*) (Eaton et al., 2010), pH-sensing (*pacC*) (Lukito et al., 2015) and striatin-interacting phosphatase and kinase complex (*mobC*) (Green et al., 2016) are required for regulation of hyphal growth in *L. perenne*, and their deletion induces aberrant hyphal distribution in plants and alters host growth and development. Production of reactive oxygen species (ROS) by *E. festucae* in culture and *in planta* is also vital for establishment of normal symbiotic associations between these organisms. Superoxide ions regulate many processes in fungal morphogenesis and growth, and deletion of *E. festucae* genes encoding proteins of the NADPH oxidase complex responsible for superoxide synthesis, including *noxA*, *noxR*, *racA*, and *bemA* also disrupts the phenotype of both the endophyte and the host during symbiosis (Takemoto et al., 2006, 2011; Tanaka et al., 2006, 2008).

The ubiquitous signaling molecule, adenosine 3′5′- cyclic AMP (cAMP) is an integral component of signaling in most organisms. Accumulation of cAMP in the cytoplasm is modulated through the activities of adenylate cyclase (AC) and phosphodiesterase enzymes that synthesize or degrade cAMP respectively. The main target of cAMP in fungi is cAMP-dependent protein kinase (PKA) which mediates many of the physiological effects (D'Souza and Heitman, 2001) by phosphorylating target proteins such as protein kinases, ion channels, and transcription factors. Recently however, other unidentified target(s) of cAMP have been detected, such as those shown to be involved in the regulation of the *Fusarium fujikuroi* secondary metabolite, fusarubin (Studt et al., 2013). To date fungi have been shown to possess a single adenylate cyclase gene that encodes a large membrane-bound enzyme that is stimulated by a variety of environmental signals, and acts down-stream of heterotrimeric G proteins (Ivey and Hoffman, 2005; Kamerewerd et al., 2008) and CO_2 or HCO_3^- (Bahn and Mühlschlegel, 2006; Mogensen et al., 2006). This versatility contrasts with mammalian cells that possess several adenylate cyclase enzymes, both cytosolic and plasma-membrane localized, each responding to specific stimuli (McDonough and Rodriguez, 2012). The implication of this is that the single fungal AC enzyme has many interaction partners and is highly interconnected with other pathways to mediate its effects.

Although highly conserved across the fungal kingdom, the components of the cAMP-PKA signaling pathway regulate functionally diverse processes including hyphal growth, secondary metabolite biosynthesis (García-Martínez et al., 2012), conidiation (Mukherjee et al., 2007), reaction to oxidative stress (Choi and Xu, 2010; Deveau et al., 2010), and virulence (Kohut et al., 2010; García-Martínez et al., 2012; McDonough and Rodriguez, 2012). Disruption of AC can have opposing effects in different fungi, even in closely related species (McDonough and Rodriguez, 2012). For example, in *F. fujikuroi*, deletion of the adenylate cyclase gene increases colony sensitivity to oxidative stress (García-Martínez et al., 2012) while in *F. proliferatum* and *F. verticillioides* the mutants are less sensitive than wild-type (Choi and Xu, 2010; Kohut et al., 2010). Similarly, disruption in cAMP signaling has no impact on virulence of *F. fujikuroi* on tomato (García-Martínez et al., 2012), while in *F. proliferatum* virulence on tomato and maize is reduced (Kohut et al., 2010). Generally however, AC is indispensable for virulence in many pathogenic fungi, or nearly so (Klimpel et al., 2002), including the pathogens of insects (Liu et al., 2012), fungi (Mukherjee et al., 2007), humans (Bahn and Sundstrom, 2001; Brakhage and Liebmann, 2005) and plants (Kulkarni and Dean, 2004; Martínez-Espinoza et al., 2004; Yamauchi et al., 2004; Mukherjee et al., 2007; Choi and Xu, 2010; Kohut et al., 2010; Bormann et al., 2014). Reduction in virulence in AC pathway deletion mutants is largely due to the pleiotropic effects of cAMP on the development and functionality of specialized infection structures (Adachi and Hamer, 1998; Yamauchi et al., 2004) or alterations in secondary metabolite biosynthesis (Brakhage and

Liebmann, 2005; Sugui et al., 2007; Gallagher et al., 2012) and other virulence factors (Alspaugh et al., 2002).

The cAMP pathway is also important in fungal growth and development. Deletion of the adenylate cyclase gene reduces radial growth and produces a more compact colony in *F. verticilloides*, *F. proliferatum* and *F. fujikuroi* (Choi and Xu, 2010; Kohut et al., 2010; García-Martínez et al., 2012). Cyclic-AMP also regulates the transition from yeast to filamentous forms in *Candida albicans* (Xu et al., 2008), *Ustilago maydis* (Martínez-Espinoza et al., 2004), and *Paracoccidioides brasiliensis* (Chen et al., 2007) and can either increase (Kohut et al., 2010) or decrease (Choi and Xu, 2010) production of conidia, and delay conidial germination (Kohut et al., 2010).

Despite extensive investigation of the multiple processes influenced by cAMP signaling in pathogens, the role of this pathway in regulating colonization and symbiosis by mutualistic fungi is currently unknown. Here we describe the role of cAMP signaling in the establishment and maintenance of a symbiotic partnership between *E. festucae* and the temperate grass species *Lolium perenne* (perennial ryegrass). We report on disruption of the adenylate cyclase gene (herein designated *acyA*) and consequent defects in hyphal growth and morphology in colonies growing in axenic culture, and the requirement for functional cAMP signaling in *E. festucae* for accumulation of ROS. We also show that *E. festucae* cAMP signaling, unlike most pathogens, appears to modulate growth of the fungus in plants, limiting over-colonization and enabling the symbionts to grow synchronously with plants during development.

MATERIALS AND METHODS

Fungal Strains

The adenylate cyclase gene (*acyA*) was originally cloned and sequenced from *E. festucae* var. *lolii*, previously *Neotyphodium lolii* (Leuchmann et al., 2014), strain Lp19, isolated from *L. perenne*. Gene disruption experiments were performed on the closely related strain *E. festucae* Fl1, isolated from *Festuca trachyphylla* (Hack.) Krajina. The strains used in this study are presented in **Table 1**.

Fungal and Plant Growing Conditions

Fungi were cultured on potato dextrose agar (PDA, Difco, Le Pont, De Claix, France) at 22°C in an 8 h light, 16 h dark cycle. *L. perenne* cv. Nui or Samson plants infected with *E. festucae* Fl1 wild-type or mutant strains were maintained in glasshouse conditions under ambient light and temperature.

Identification and Sequencing of *Epichloë acyA* Genes

We previously cloned and sequenced a 300 bp *acyA* PCR product from *E. festucae* var. *lolii* strain Lp19 (Johnson et al., 2007). The DNA fragment was used as a probe to screen an Lp19 genomic DNA lambda library (Fleetwood et al., 2007) to recover a larger fragment of the gene for functional analysis. A single lambda clone (designated 6163) with homology to the adenylate cyclase gene fragment was recovered (Genbank accession KR815911). Sequencing of the 6047 bp insert indicated the presence of 5819 bp of the adenylate cyclase open reading frame (ORF) plus 228 bp of the *acyA* 3' region. The first 1419 bp of the open reading frame was missing. This sequence was used to design the gene disruption vector. Later, *de novo* sequencing of the *E. festucae* Fl1 genome by Schardl et al. (2013) enabled a complete genomic *acyA* sequence (gene model Fl1M3.048730, http://www.endophyte.uky.edu/) to be recovered. BLASTn was used to recover the *acyA* gene from other haploid *Epichloë* species (**Table 2**).

The *acyA* genes from allopolyploids AR3046 (*E. baconii/amarillans* × *E. bromicola*) and AR1006 (*E. typhina* × *E. bromicola*) were recovered by mapping their genome read pairs (unpublished) to 7 kb genomic scaffolds (containing the *acyA* gene) of extant strains of their parental species using the "aln" algorithm BWA version 0.7.9a-r786. For AR3046, 43,768,368 78 bp read pairs with an insert size of ∼290 bp were individually mapped to *E. baconii* strain ATCC 200745 and *E. bromicola* strain AL0434 (Schardl et al., 2014). For AR1006, 21,293,733 100 bp read pairs with an insert size of ∼160 bp were mapped to *E. typhina* strain ATCC 200736 and *E. bromicola* strain AL0434. The mapped reads were extracted using SAMtools (Li et al., 2009) version 0.1.19-44428cd and imported into Geneious V8.1 (Biomatters, http://www.geneious.com) (Kearse et al., 2012) and consensus sequences for each mapping file were generated based on a threshold of 95% identity.

Vector Construction

The *acyA* disruption vector (pCRVacyhph) was constructed using the Multisite Gateway system (ThermoFisher Scientific, Walden, MA, USA) following the manufacturer's instructions. The entry vector pDONR221/hygromycin, containing the *hph* cassette from pAN7-1 (Punt et al., 1987), was constructed as previously described (Fleetwood et al., 2007). Two further Multisite Gateway entry vectors, pDONRP2R-P3/AC3′ and pDONRP4-P1R/AC5′ containing a 5′ (3002 bp) and 3′ (3064 bp) region respectively, flanking the integration site in *acyA*, were created. PCR products were amplified from *E. festucae* var. *lolii* Lp19 genomic DNA using primer pairs AC5′-attB4 and AC5′-attB1 (for the 5′ flank) and AC3′-attB2 and AC3′-attB3 (for the 3′ flank) using Platinum Pfx DNA polymerase (ThermoFisher Scientific) according to the manufacturer's instructions. Primer sequences are listed in Supplementary Table 1. The PCR products were purified using the QIAquick PCR Purification Kit (Qiagen, Hilden, Germany), and the products quantified by fluorometric quantitation using the Qubit system (ThermoFisher Scientific). The PCR fragments were then recombined into Gateway donor vectors pDONRP4-P1R and pDONRP2R-P3 using Gateway BP Clonase II. The resulting vectors, pDONRP4-P1R/AC5′and pDONRP2R-P3/AC3,′ along with pDONR221/hygromycin, were then recombined into the destination vector pDESTR4-R3 using Gateway LR Clonase II Plus, to create pCRVacyhph.

Disruption of *E. festucae acyA*

Gene disruption experiments were originally designed to disrupt *acyA* in strain *E. festucae* var. *lolii* Lp19, however as this strain proved to be relatively intractable to homologous recombination the closely-related strain *E. festucae* Fl1 was used instead.

TABLE 1 | *E. festucae* strains used in this study.

Strain	Genotype	References
E. festucae var. lolii Lp19	wild type	Christensen et al., 1993
E. festucae Fl1	wild type	Leuchtmann, 1994; Moon et al., 1999
E. festucae Fl1 EGFP	*pTef::EGFP::GA; hph*	Christensen et al., 2008
E. festuae Fl1 *acyA19*	Ectopic insertion of acyA	This study
E. festuae Fl1 *acyA49*	Ectopic insertion of acyA	This study
E. festuae Fl1 Δ*acyA*34	Δ*acy::hph*	This study
E. festuae Fl1 Δ*acyA*42	Δ*acy::hph*	This study
E. festuae Fl1 Δ*acyA*47	Δ*acy::hph*	This study
E. festuae Fl1 Δ*acyA*34/*acyA*	Δ*acy::hph; acyA, gen*	This study
E. festuae Fl1 Δ*acyA*42/*acyA*	Δ*acy::hph; acyA, gen*	This study
E. festuae Fl1 Δ*acyA*42/EGFP	Δ*acy; hph; pTef::EGFP::GA, gen*	This study

TABLE 2 | Copy number of *acyA* in haploid and allopolyploid *Epichloë* species.

Species	Parental species	Strain	No. of genomes	*acyA* copy number	Genome References
E. festucae	n/a	E2368	1	1	Schardl et al., 2013
E. festucae	n/a	Fl1	1	1	Schardl et al., 2013
E. brachyelytri	n/a	E4804	1	1	Schardl et al., 2013
E. glyceriae	n/a	E277	1	1	Schardl et al., 2013
E. amarillans	n/a	ATCC 200744	1	1	Schardl et al., 2013
E. typhina	n/a	ATCC 200736	1	1	Schardl et al., 2013
E. typhina	n/a	E5819	1	1	Schardl et al., 2013
Epichloë sp.	*E. baconii/amarillans* x *E. bromicola*	AR3046*	2	2	unpublished
E. uncinata	*E. typhina* x *E. bromicola*	AR1006*	2	2	unpublished

**allopolyploid strains, n/a is not applicable.*

Homologous recombinants were obtained by PEG-mediated transformation of protoplasts. Protoplasts were prepared using the method of Young et al. (1998), except that 10 mg/ml of Glucanex (InterSpex Products, San Mateo, CA, USA) was used to digest cell walls for 3 h at 30°C with shaking (100 rpm). *E. festucae* Fl1 was transformed using 5 μg of each plasmid by the method of Vollmer and Yanofsky (1986) with modifications (Itoh et al., 1994). Protoplasts were co-transformed with plasmid pCRVacyhph (see above) or pTEFEGFP (EGFP fused to the *tef2* promoter from *Aureobasidium pullulans*) (Vanden Wymelenberg et al., 1997) plus either pPN1688 (Young et al., 2005) or pII99 (Namiki et al., 2001) for resistance against hygromycin B or geneticin (both Gibco, ThermoFisher Scientific) respectively. Transgenic colonies were selected on PDA containing 150 μg/mL or 200 μg/mL of hygromycin B or geneticin respectively, and regenerating colonies were purified to homogeneity by sub-culturing hyphal tips onto fresh selective media three times. A number of colonies were analyzed by Southern-blot hybridization to confirm that each contained a single integration of the hygromycin resistance cassette at the desired locus. Genomic DNA was extracted from putative recombinant strains using the method of Byrd et al. (1990) and 2 μg of DNA was digested to completion with *Hin*dIII. The DNA was subjected to standard agarose gel (0.8% w/v) electrophoresis, transferred to nylon (Hybond N^+, GE Healthcare, Buckinghamshire, UK) and the membrane hybridized independently against two dideoxygenin-labeled probes following the manufacturer's instructions (Roche, Basel, Switzerland). Probe 1 (482 bp) was amplified by PCR using the TripleMaster polymerase system (Eppendorf, Hamburg, Germany) using primers ACseqrev4120/ACseqfor3657 and probe 2 (644 bp) was synthesized using primers AC SeqIntRev2/ACM13ForRev (see Supplementary Table 1 for primer sequences).

To complement the mutation, the full length wild-type *acyA* was PCR-amplified from *E. festucae* Fl1genomic DNA using Platinum Pfx Polymerase (ThermoFisher Scientific) and primers AcyAF and AcyAR. The 8371 bp fragment comprising 859 bp upstream of the putative start site, 7170 bp of the open reading frame and 342 bp of the 3′ un-translated region was purified according to the manufacturer's instructions (DNA Clean and Concentrator -5, Zymo Research, Irvine, CA, USA) and protoplasts of Δ*acyA*34 and Δ*acyA*42 disruption mutants transformed as described above. Ectopic integration of wild-type *acyA* was confirmed by PCR using primers ACKOF/R (data not shown).

Fungal Growth on Media Supplemented with cAMP

Mycelial sections (approximately 1 mm^2) were inoculated onto PDA plates supplemented with 2.5, 5.0 or 7.5 mM cAMP sodium

salt (Sigma-Aldrich, St. Louis, MO, USA). Three control strains (*E. festucae* Fl1 wild-type plus two strains with ectopic insertions, *acyA*19 and *acyA*49*)* and three independent disruption mutants (Δ*acyA*34, Δ*acyA*42, and Δ*acyA*47) were inoculated in triplicate onto each medium supplemented with cAMP (including a no-cAMP control) in a randomized design. The radial measurement (mm) of the colony was taken at approximately 24 h intervals over 165 h. The first measurement was taken 20 h after the colonies were inoculated. The growth rate of each strain was obtained by least squares regression and the slope of the line used to represent the rate of radial growth in mm/h. Analysis of variance was used to estimate the effects of strain and cAMP concentration, and their interaction. Means for each strain and cAMP combination were obtained, together with the least significant difference (LSD—calculated at the 5% significance level) between means. The residual plot from the ANOVA was checked and displayed no evidence of heterogeneity of variance, thus the pooled LSD was used for comparing means at the same level of cAMP.

Infection of *L. perenne* with *E. festucae* Fl1

Mycelial sections were inoculated into incisions created in the SAM of sterile 5 days old *L. perenne* seedlings growing on 1.5% (w/v) water agar, according to the method of Latch and Christensen (1985). Strains inoculated included the wild-type, mutants Δ*acyA*34, Δ*acyA*42 and Δ*acyA*47, plus two independent complementation strains, Δ*acyA*34/*acyA* and Δ*acyA*42/*acyA*. Inoculated plants were then maintained at 22°C in the dark for 7 days, followed by 22°C in the light for 7 days, before being transplanted into potting mix and maintained under glasshouse conditions. After 12 weeks, six tillers from each plant were tested for endophyte infection by tissue print immuno-assay using an *Epichloë*-specific polyclonal anti-serum (Simpson et al., 2012). Plants were inoculated as described on two independent occasions.

Light Microscopy

E. festucae Fl1 wild-type and *acyA* deletion mutants were grown in triplicate on potato dextrose broth (PDB, Difco, Le Pont, De Claix, France), either 1X or diluted 1:100 in water, containing 0.8% (w/v) agarose. The broths were inoculated and grown for 5 days at 22°C in continuous light. Alternatively, cultures were grown on the same medium on sterile microscope slides and incubated as described above. If grown in a culture dish, 0.5 cm^2 of agar was cut from the outer edge of the colony, mounted onto a microscope slide, and a drop of water and a cover glass placed directly onto the specimen. If grown on a microscope slide, a drop of water was added to the mycelium and a cover glass applied. Cultures were imaged by bright field microscopy using a BX50 fluorescent microscope (Olympus, Tokyo, Japan) and a 40X UPLANFLN objective with a 0.75 numerical aperture. Images were taken using an Olympus Colorview III camera with AnalySIS^B image processing software. Endophytes in the epidermal layer of the host leaf sheath were stained with 0.15% (w/v) aniline blue and examined by bright field microscopy as described previously (Christensen et al., 2008). Leaf sheaths from two tillers per plant, and at least three infected plants per strain in each inoculation experiment, were examined.

Confocal Laser Scanning Microscopy (CLSM)

To examine hyphae in the host shoot apex, semi-thin (0.5–1 mm) longitudinal or transverse sections were taken through the shoot apex and true stem of at least six independent *L. perenne* tillers infected with each strain and mounted on a microscope slide in water. CLSM images were captured on an inverted FluoView FV10i Confocal Laser Scanning Microscope (Olympus). For visualizing EGFP the excitation wavelength was 457 nm and detection wavelength was between 465 and 565 nm. Two dimensional images were taken using the 10x phase contrast objective, numerical aperture 0.4 (equivalent to UPLSAPO 10x). To examine hyphal morphology in the expansion zone of the developing leaf, young leaves of approximately 5 cm in length were dissected from tillers and cut in half along the midrib. A 1 cm section from the base of a halved blade was mounted in water on a microscope slide for imaging as described above. For each image, the optimal depth to show the most hyphae possible in a sample was selected, and the laser sensitivity then adjusted to immediately below saturation levels.

Transmission Electron Microscopy (TEM)

Endophyte-infected pseudostem material from two plants each infected with wild-type, Δ*acyA*34, Δ*acyA*42, or Δ*acyA*34/*acyA*, was dissected from *L. perenne* plants 0.5 cm above the tiller crown, and 0.5 mm transverse sections fixed in 2% (w/v) formaldehyde and 3% (w/v) glutaraldehyde in 0.1 M sodium/potassium phosphate (pH 7.2) for 2 h at room temperature. The samples were washed three times in 0.1 M sodium/potassium phosphate (pH 7.2) and post-fixed in 1% (w/v) osmium tetroxide in the same buffer for 1 h. After washing again as described above, the samples were subjected to a graded acetone/water series with 10 min each in 25, 50, 75, and 95% (v/v) acetone, followed by concentrated acetone for 2 h. The samples were embedded in Procure 812 resin (ProSciTech, Kirwan, Qld. Australia):acetone (50:50) overnight under constant stirring and then in 100% resin overnight. The resin was refreshed for a further 8 h and then mounted in 100% resin at 60°C for 48 h. Ultra-thin sections were collected onto a copper grid and stained with saturated uranyl acetate in 50% (v/v) ethanol for 4 min and then in lead citrate for a further 4 min. Specimens were examined at 46 000X magnification on a Philips CM10 (Philips Electron Optics, Eindhoven, The Netherlands) transmission electron microscope. Micrographs of at least 12 hyphae in developing leaves and in the second mature leaf sheath were captured. The thickness of hyphal cell walls was measured at eight equidistant positions around the circumference of each hypha using open source ImageJ 1.45 s software (Wayne Rasband, National Institutes of Health, USA). The cell wall thickness measurements were analyzed using one way ANOVA to compare the strains. The least significant differences ($P = 0.05$ level) between means were calculated.

Detection of ROS

Superoxide radicals in *E. festucae* in axenic culture were stained using NBT (Sigma-Aldrich) as described by Tanaka et al. (2006). Three replicates for each strain were included in the analysis and the experiment was repeated twice. Strains were grown on PDA for 1 week at 22°C under 8 h light and 16 h dark, and mycelia stained for 5 h at 22°C in continuous light by incubation in 20 μL of 0.05% (w/v) NBT dissolved in 0.05 M sodium phosphate pH 7.5. The reaction was stopped by removing the stain and adding 40 μL of absolute ethanol. The ethanol was removed after 5 min, and mycelia were analyzed at 400X magnification under bright field illumination using an Olympus BX50 compound microscope with a 40X UPLANFLN objective and a 0.75 numerical aperture. Images were taken using an Olympus Colorview III camera with AnalySIS^{B} image processing software.

Quantitation of Hyphal Biomass

Genomic DNA was extracted from freeze-dried pseudostems (leaf and blade tissue between the crown and the first ligule of a tiller) dissected from three tillers of each plant using the DNAeasy Plant Kit (Qiagen). The plants were infected with either the wild-type or Δ*acyA*42 mutant strain. There were three replicate plants per strain. Hyphal biomass (expressed as endophyte concentration) was determined by quantitative PCR of the single copy *E. festucae* NRPS-1 gene (EFM3.005350, http://www.endophyte.uky.edu/) from 1 ng of genomic DNA using a MyiQ^{TM} cycler (Bio-Rad Laboratories, Hercules, California, USA), with primers 1-1F, and 1-1R (Supplementary Table 1) as described (Rasmussen et al., 2007; Liu et al., 2011). Hyphal biomass between strains was compared using one way ANOVA. The least significant differences ($P = 0.05$ level) between means was calculated.

RESULTS

The *E. festucae acyA* Gene

A partial *acyA* gene (1419–5816 bp) was initially recovered from *E. festucae* var. *lolii* (Lp19). Subsequent to functional characterization of this gene in *E. festucae* Fl1 (reported here), the Fl1 genome became available and the full length *acyA* gene recovered (gene model Fl1M3.048730, http://www.endophyte.uky.edu/). Analysis of the partial and full length conceptual AcyA proteins from the Lp19 and Fl1 strains respectively, confirmed the presence of the key motifs consistent with fungal Class III adenylate cyclases, including the domains for adenylate cyclase G-alpha binding (IPR013716), ras association (IPR000159), leucine rich repeats (IPR001611, IPR003591, IPR025875), protein phosphatase 2C-like (IPR001932), and the adenylate cyclase (IPR001054) catalytic core (**Figure 1A**). The *E. festucae* var. *lolii acyA* sequence contains a 66 bp indel that is not present in the *E. festucae* Fl1 *acyA*. Consistent with other fungal species, Southern-blot hybridization confirmed that *E. festucae* Fl1 contains a single *acyA* gene (**Figure 1C**) and BLASTn analysis of the genomes of other *Epichloë* species (Schardl et al., 2013) also suggests the presence of a single *acyA* gene in the haploid strains examined (**Table 2**).

Since genome hybridization has been a relatively common occurrence in the *Epichloë* genus, we investigated whether two recently-sequenced allopolyploid strains had retained both copies of the *acyA* gene from their progenitors, with the attendant prospects for neofunctionalisation (as is observed in mammals). Reads from the genomes of strains AR1006 (*E. uncinata*) and AR3046 (*Epichloë* sp.) were mapped independently to the haploid genomes of extant strains related to the original progenitors. *E. uncinata* (AR1006) is a hybrid between *E. bromicola* and *E. typhina* (Craven et al., 2001; Moon et al., 2004), and AR3046 is a hybrid between *E. bromicola* and the *E. baconii*/ *E. amarillans* clade (unpublished). Two *acyA* genes were recovered from each allopolyploid genome examined (**Table 2**), consistent with a gene originating from each of the species that contributed to the allopolyploid. The *acyA* homeologs from AR3046 (KT732649 and KT732650) and AR1006 (KT732647 and KT732648) were then mapped back to the genomes of the predicted progenitor species, which confirmed that each *acyA* gene mapped with higher identity to one or the other of the species that contributed the genes to the allopolyploid (Supplementary Table 2A). The *acyA* genes from AR3046 encoded conceptual full-length proteins indicating that both genes had the potential to be functional, however in AR1006 one of the genes (KT732647) encoded a full length protein while the other, KT732648, encoded a conceptual protein truncated after amino acid position 686. This gene has also lost a triplet 232–234 bp from the start codon and sustained a number of other deletions relative to the presumed parent *E. typhina* (Supplementary Table 2B). Alignment of *acyA* genes within each allopolyploid strain indicated they had no more identity between each other than was found in the comparisons between genes from other species (Supplementary Table 2C) confirming that the genes came together through a genome hybridization event and was not the result of gene duplication.

Disruption of *E. festucae* Fl1 *acyA*

An *acyA* gene disruption vector (pCRVacyhph) was constructed using flanking regions designed from the partial *E. festucae* var. *lolii* Lp19 sequence, and gene disruption experiments were performed in strain Fl1 as the frequency of homologous recombination in Lp19 is extremely low. Insertion of the hygromycin cassette introduced a stop codon into the *acyA* open reading frame upstream of the catalytic core domain (**Figures 1A,B**). Three colonies (Δ*acyA*34, Δ*acyA*42, and Δ*acyA*47), each with a single gene disruption event and no ectopic insertions, were identified by PCR and confirmed by Southern-blot hybridization (**Figure 1C**). The recombination breakpoints of the mutant strains differed with respect to the presence or absence of the 66 bp indel (**Figure 1C**), presumably due to differences in the recombination site during homologous recombination in the disruption mutants. *E. festucae* Δ*acyA*34 contained the insertion, while Δ*acyA*42 and Δ*acyA*47 did not. The integrity of each gene immediately flanking the disrupted *acyA* was checked by PCR to ensure that the disruption event was confined to the *acyA* gene. Two primer pairs spanning the

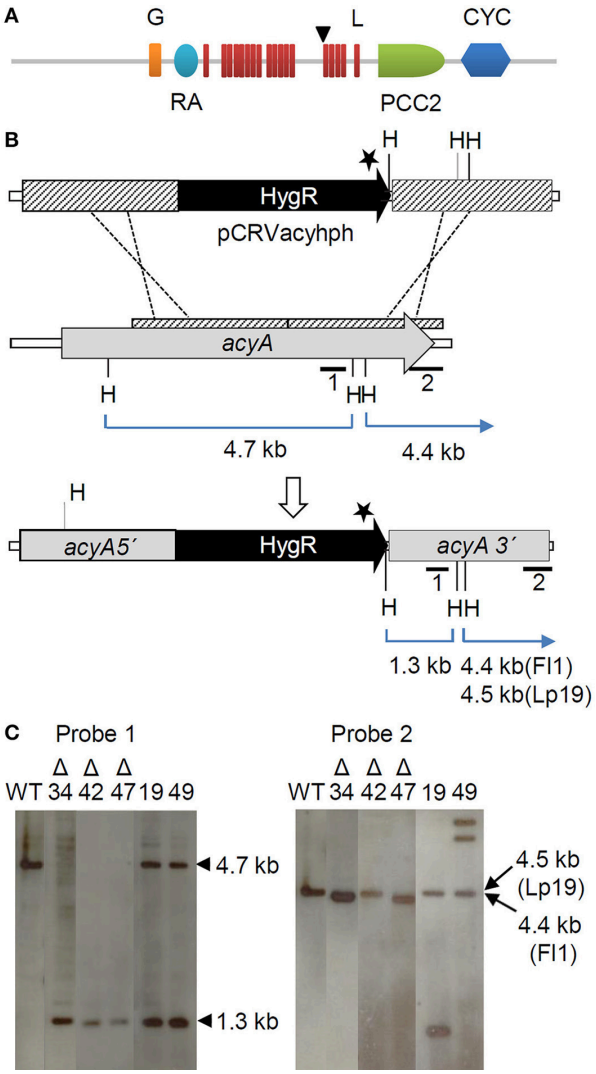

FIGURE 1 | Disruption of *acyA* in *E. festucae* Fl1. (A) Domain architecture of AcyA in relation to the insertion site of the hygromycin resistance cassette (HygR). The protein contains the domains for G-alpha binding (G), ras association (RA), leucine rich repeats (L), protein phosphatase 2C (PP2C), and catalytic cyclic nucleotide biosynthesis (CYC) (Baker and Kelly, 2004). The HygR cassette was inserted (arrow) upstream of the phosphatase 2C (PPC2) and catalytic (CyC) domains. **(B)** Diagram of the *acyA* disruption locus in *E. festucae* Fl1. In vector pCRVacyhph, the HygR cassette is flanked by approximately 3 kb of DNA from the partial *acyA* gene (hatched) cloned from *E. festucae* var. *lolii* Lp19 (KR815911). The stop codon in the hygromycin resistance gene is indicated (⋆). The regions of homology between the Lp19 flanking regions and the corresponding Fl1 *acyA* sequence (hatched) is shown immediately above the Fl1 *acyA* gene, gene model Fl1M3.048730 (http://www.endophyte.uky.edu). Probes 1 and 2 (solid bars) were used in Southern-blot hybridization experiments **(C)** to confirm that the endogenous *acyA* gene had been disrupted and to ascertain the number of *acyA* copies in each strain respectively. **(C)** Southern-blot hybridization to confirm *acyA* insertion mutants. Genomic DNA was isolated from the wild-type (WT) plus a number of putative insertional mutants, and digested with *Hin*dIII. Probe 1 bound to the predicted 4.7 kb fragment in the wild-type *acyA* also in ectopic integrants *acyA*19 and *acyA*49 and to the 1.3 kb *Hin*dIII fragment of the disrupted *acyA* gene in ectopic integrants *acyA*19 & *acyA*49 and insertional

(Continued)

FIGURE 1 | Continued
mutants Δ*acyA*34 (Δ34), Δ*acyA*42 (Δ42) and Δ*acyA*47 (Δ47). Probe 2 was used to determine copy number, and bound to either a 4.4 kb or 4.5 kb *Hin*dIII fragment depending on whether the recombination locus was before or after the 66 bp indel in the Lp19 *acyA*.

intergenic region and the flanking gene 5′ and 3′ of the *acyA* were used. No evidence of untargeted rearrangements were detected (Supplementary Figure 1). Two further colonies (*acyA*19 and *acyA*49) retained the intact *acyA* gene plus an ectopic insertion of the gene replacement vector and were used as transformation controls.

Regulation of Radial Growth by cAMP Signaling in *E. festucae* in Axenic Culture

The three independent *E. festucae* mutants, Δ*acyA*42, Δ*acyA*34, and Δ*acyA*47, grew more slowly in axenic culture compared with the wild-type, or control strains *acyA*19 and *acyA*49 (**Figure 2A**). The mutant colonies were also highly compact compared to the controls. The radial growth rates of Δ*acyA*42, Δ*acyA*34, and Δ*acyA*47 increased in a dose-dependent manner in response to supplementation of the media with exogenous cAMP (**Figure 2B**). The growth rates of *E. festucae* Δ*acyA*42 and Δ*acyA*47 were statistically indistinguishable from wild-type when the medium was supplemented with 7.5 mM cAMP. *E. festucae* Δ*acyA*34 grew more slowly than the other strains under all conditions; however its growth rate on PDA containing 7.5 mM cAMP was almost 2 fold higher than when growing on PDA alone. The growth rates of the control strains (wild-type, *acyA*19 and *acyA*49) were not altered by cAMP supplementation (**Figure 2B**) indicating that endogenous cAMP does not limit growth of strains with functional AC enzymes.

E. festucae Δ*acyA*47 produced a faster-growing sector (named Δ*acyA*47var) on PDA supplemented with 150 μg/mL hygromycin. Southern-blot hybridization confirmed that the sector was identical to Δ*acyA*47 at the disruption locus (data not shown). Strains Δ*acyA*34 and Δ*acyA*42 did not produce overt spontaneous growth revertants, however if repeatedly sub-cultured onto fresh media, gradually grew faster until their growth rates were similar to wild-type (data not shown). PCR (using primers ACKO F and ACKO R) was used to check the fidelity of the integration locus during this period (data not shown). We saw no evidence of a loss of the integrated DNA over time in these colonies suggesting that the changes in phenotype were due to mutations or epigenetic changes at other loci.

Regulation of Hyphal Branching in *E. festucae* Growing in Axenic Culture

We next examined the hyphal morphology of *acyA* disruption mutants in culture by bright field microscopy. In wild-type cultures, hyphae were long and straight, relatively sparsely branched and produced lateral branches at the proximal end of compartments immediately adjacent to septa several compartments behind the tip (**Figure 3**). Conversely, the hyphae of *E. festucae* Δ*acyA*34, Δ*acyA*42, and Δ*acyA*47 were highly

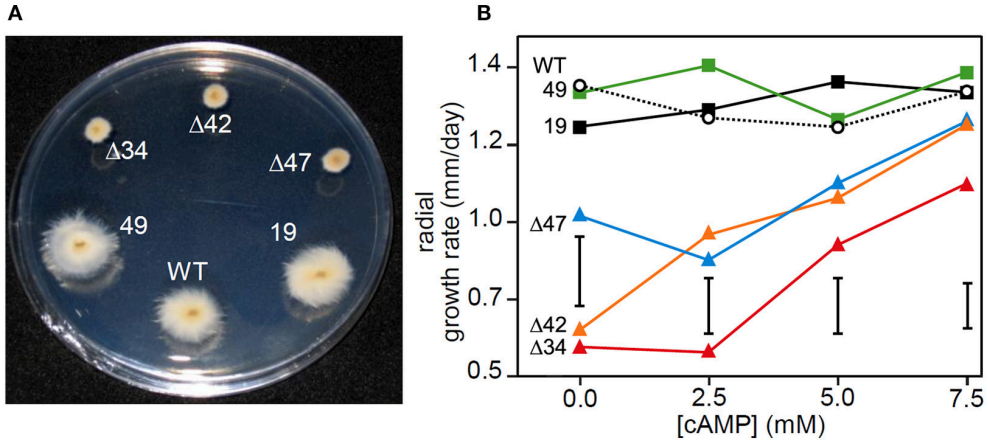

FIGURE 2 | Growth of *E. festucae acyA* disruption mutants in axenic culture. (A) Growth of wild-type, disruption mutants Δ*acyA*34 (Δ34), Δ*acyA*42 (Δ42), ΔacyA47 (Δ47), and colonies with an intact *acyA* gene plus an ectopic insertion(s) of the transformation vector, *acyA*19, *acyA*49 on PDA (22°C for 7 days). **(B)** The effect of exogenous cAMP on the radial growth rate of the same strains. The mean growth rate of each strain (with three clonal replicates) at each cAMP concentration is shown. Analysis of variance was used to compare the growth rate of strains between and within each concentration of cAMP. The vertical bar represents the least significant differences (LSD) between means at the 5% significance level when comparing strains at the same concentration of cAMP.

convoluted, sometimes forming thick aggregates or cables, and produced multiple lateral branches. Excessive lateral branches accounted for the compact nature of the mutant colonies. The morphology of strains complemented with the wild-type *acyA* gene were similar to the wild-type strain (**Figure 3**) confirming the role of cAMP in suppressing lateral branches. This phenotype was reproducible, however similarly to the observations on effects of AC disruption on colony growth rate, hyphal morphology in mutant colonies was not stable over time and reverted to the wild-type form if the cultures were maintained continuously in axenic culture.

Regulation of ROS in *E. festucae* Growing in Axenic Culture

Synthesis of ROS is essential for mutualism in the *E. festucae* Fl1/*L. perenne* interaction, and disruption results in hyper-colonization of host tissues, stunting and premature leaf senescence (Tanaka et al., 2006, 2008). In order to determine whether the morphology of the *E. festucae* Δ*acyA* disruption mutants was linked to changes in ROS production, strains were grown in culture on microscope slides and stained with NBT. NBT forms a blue precipitate on exposure to superoxide ions, and blue deposits were typically observed in the hyphal apices of the *E. festucae* Fl1 wild-type (**Figure 4**) and occasionally in some compartments behind the tip (data not shown). NBT staining of *E. festucae acyA* disruption mutants revealed a substantial reduction in superoxide radicals relative to the wild-type strain (**Figure 4**). The localization of superoxide radicals was similar between the wild-type and mutants, however superoxide ions were not detectable in the majority of mutant hyphae (**Figure 4**). Strains complemented with the wild-type *acyA* gene were able to produce ROS at similar or higher levels than the wild-type confirming that cAMP signaling directly or indirectly regulates accumulation of superoxide ions in *E. festucae*.

Regulation of *E. festucae* Growth by cAMP during Colonization of *L. perenne*

To determine the role of fungal cAMP signaling in *E. festucae* during mutualistic interactions with *L. perenne*, mycelia of strains carrying the disrupted gene were inoculated though a small incision into young seedlings. In each inoculation experiment, between 25 and 50% of inoculated plants ($n = 25$) became infected with wild-type, Δ*acyA*34, Δ*acyA*42, and the complementation strains, however despite repeated attempts ($n > 75$ plants), no plants infected with the original *E. festucae* Δ*acyA*47 strain were obtained. It is unclear why this strain was apparently incapable of host colonization since the *acyA* locus was identical to Δ*acyA*34 and Δ*acyA*42. Inoculation of plants with *E. festucae* Δ*acyA*47var produced infected plants with similar frequency to the other strains. This strain was not included in further experiments due to its unstable phenotype.

We next investigated whether a functional fungal cAMP signaling pathway is required for a mutualistic interaction between the symbionts and the host grass. Three to five independent plants for each strain were examined. Consistent differences in the growth and phenotype of plants infected with wild-type, Δ*acyA*, or Δ*acy/acyA* complemented strains were not observed, although plants infected with mutant strains did express a variable marginally-stunted phenotype (Supplementary Figure 2). After 3 months, hyphae within the mature leaf sheaths of infected plants were stained with aniline blue and analyzed by bright field microscopy. Wild-type hyphae in this tissue were long and straight, seldom branched, and oriented in the direction of leaf growth. In contrast, hyphae of the two independent *acyA* mutants were highly branched and convoluted (**Figure 5**). The phenotypes of Δ*acyA*34 and 42 in all the plants examined (at least three plants per strain per experiment) were highly consistent. The complementation strains Δ*acyA*34/*acyA* and Δ*acyA*42/*acyA* both resembled the wild type (**Figure 5**).

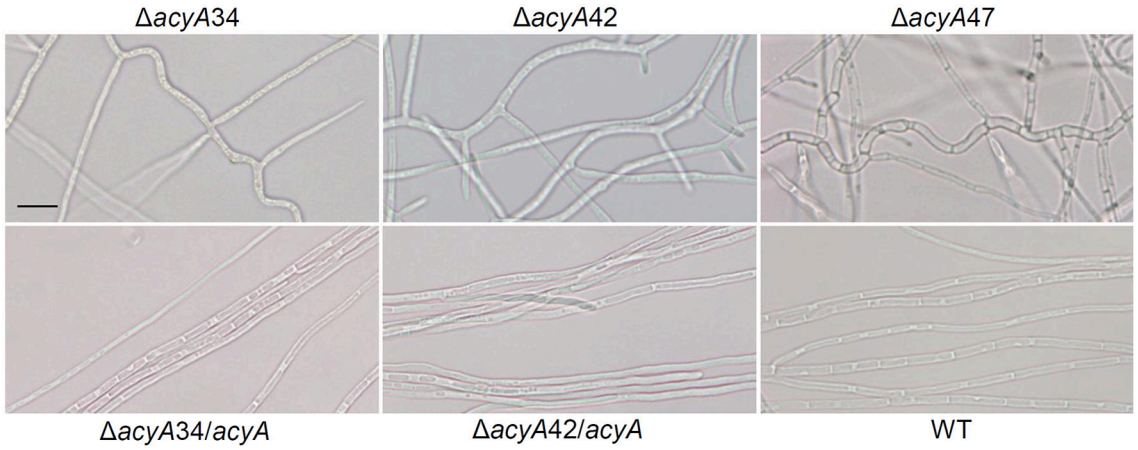

FIGURE 3 | Effects of *acyA* disruption on *E. festucae* hyphal morphology in axenic culture. Bright field images of *E. festucae* Fl1 hyphae growing on water agar at 22°C for 7 days (bar, 10 μM). Images were taken approximately 3 mm behind the colony margin. Hyphae of all independent mutants (Δ*acyA*34, Δ*acyA*42, and Δ*acyA*47) were convoluted, irregular in diameter (Δ*acyA*47) and heavily branched compared to the wild-type. Ectopic integration of the wild-type *acyA* gene into Δ*acyA*34 and Δ*acyA*42 resulted in a reversion to the wild-type phenotype to greater or lesser extents dependent on the individual strain (Δ*acyA*34/*acyA*, Δ*acyA*42/*acyA*). Gross morphology at the hyphal tips appeared similar in mutants and wild-type.

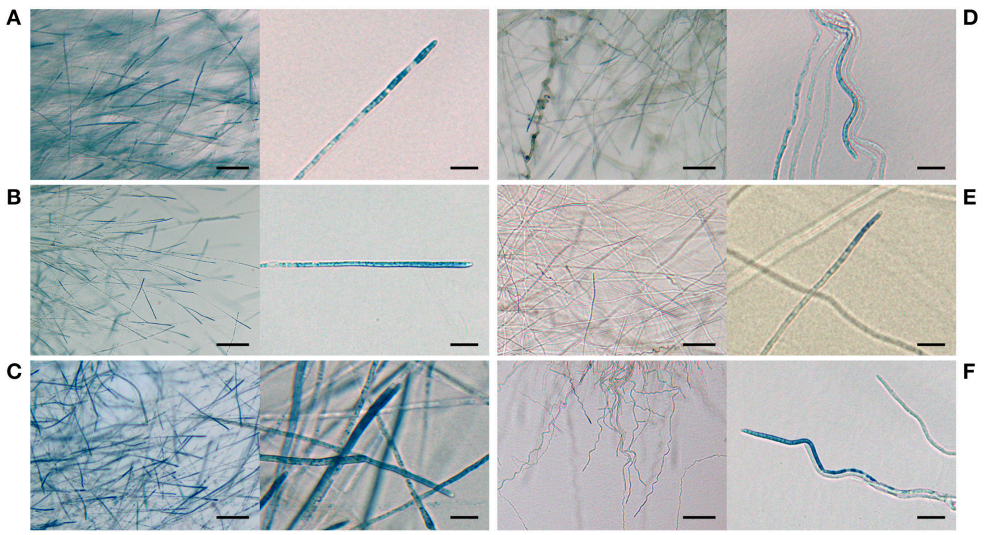

FIGURE 4 | Influence of *acyA* disruption on production of ROS in *E. festucae* Fl1 hyphae in axenic culture. Bright field images of *E. festucae* Fl1 growing on PDA at 22°C for 7 days and stained with NBT. Included is a low (scale bar = 50 μm) and high (scale bar = 5 μm) resolution image of the wild-type **(A)** plus mutants Δ*acyA*34 **(D)**, Δ42 **(E)**, and Δ47 **(F)**, and complementation strains Δ*acyA*34/*acyA* **(B)** and Δ*acyA*42/*acyA* **(C)**.

To further investigate the role of cAMP signaling in endophyte colonization of the host at different developmental stages, we transformed Δ*acyA*42 with vector pTEFEGFP (for constitutive EGFP expression in *E. festucae*) and inoculated EGFP-expressing strains into *L. perenne* seedlings for examination by confocal microscopy. Wild-type *E. festucae* Fl1 transformed with the same plasmid was used as a control. An EGFP-expressing *acyA*-complemented strain was not included in this experiment as it was not technically feasible to conduct a third transformation on this mutant strain. We first examined the hyphae in longitudinal sections taken through the shoot apex at the base of the tiller. In host tissues immediately below the meristem, and in the youngest developing leaves, the mycelial density of Δ*acyA*42/EGFP was similar to wild-type controls (**Figures 6I,J**), however in young leaf sheaths above the shoot meristem (lower leaf sheath), hyphae of the mutant strain appeared more numerous than wild-type (**Figures 6E–H**). A key feature of *E. festucae-L. perenne* mutualism is that once host tissues are mature and have stopped expanding, colonizing endophytes also cease growing (Tan et al., 2001). To determine whether *E. festucae* Δ*acyA*42/EGFP was still capable of responding to host developmental cues, and to stop growing, epidermal peels from mature (upper) leaf sheaths

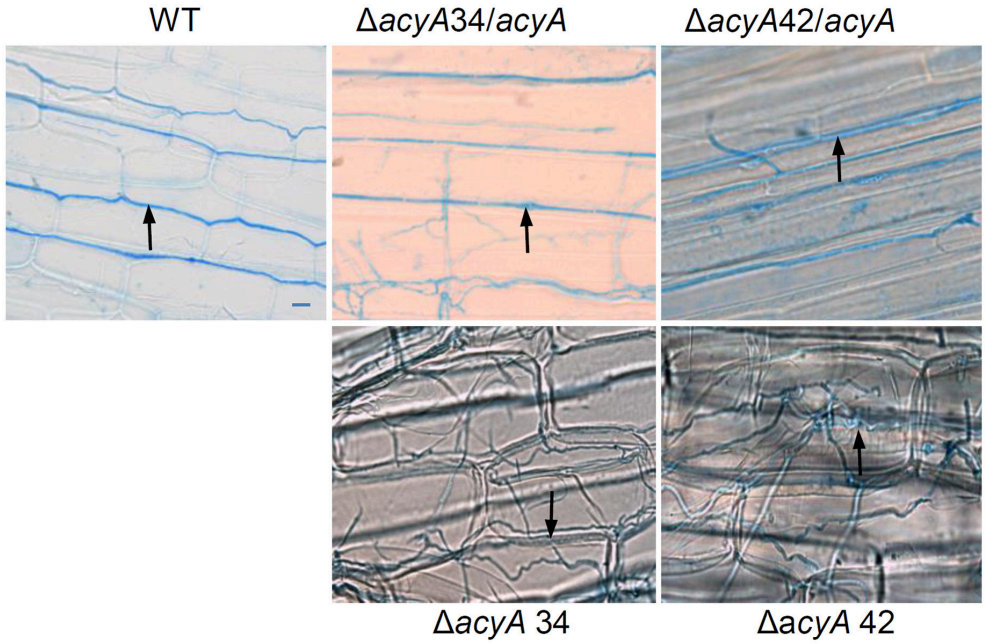

FIGURE 5 | Morphology of *E. festucae* Δ*acyA* in *L. perenne.* Aniline blue-stained hyphae (arrows) in the mature second leaf sheath of *L. perenne* infected with the wild-type and strains Δ*acyA*34 and Δ*acyA*42. The morphology of the mutant strains after complementation (Δ*acyA*34/*acyA* and Δ*acyA*42/*acyA*) with the wild-type gene is also shown. All images are at the same magnification. The scale bar is 5 μm.

were examined. Contrary to the uniform appearance of wild-type hyphae in this tissue, disruption of the cAMP signaling pathway resulted in a dense and heavily-branched mycelium (**Figures 6A–D**). To confirm the microscopy observations, the biomass of the wild-type and Δ*acyA*42 strains in the pseudostem of these plants was determined by quantitative PCR of a single copy *E. festucae* gene. Hyphal biomass (expressed as endophyte concentration) was an average of 2081 (SE 222.7) gene copies per ng of plant and endophyte genomic DNA for wild-type, and 3949 (SE 226.1) for the Δ*acyA*42 mutant, 1.9 fold higher than wild-type (**Figure 7**). The means of the technical replicates for each biological replicate per strain were compared using the Student's *T*-test. The *T*-test indicated that the mean hyphal biomass of the mutant strain was significantly greater than the wild-type ($P = 0.004$).

The impact of *acyA* disruption on hyphal ultrastructure *in planta* was investigated by TEM of infected *L. perenne* tillers. Tillers are comprised of bundles of leaves ranging in development from the most immature (in the middle of the tiller) to the fully mature outer leaf sheath. Transverse sections through the base of tillers were fixed and embedded. Ultra-thin sections of tillers infected with wild-type, Δ*acyA*34, Δ*acyA*42, and the Δ*acyA*34/*acyA* complementation strains were stained with osmium tetroxide and examined by TEM. The thickness of the cell wall was measured at eight equidistant positions around 12 hyphae from the immature leaf blade (**Figure 8A**) and the second fully mature leaf sheath (**Figure 8B**) of each tiller. In immature leaves, where both the plant and endophyte grow by intercalary growth, mean cell wall thickness of Δ*acyA*34 and Δ*acyA*42 was 70.3 and 62.8 nm respectively, significantly thinner ($P \leq 0.05$) than the wild-type which had an average thickness of 111.3 nm (**Figure 8A**). The phenotype was nearly fully restored in the Δ*acyA*34/*acyA* complemented strain which had a mean cell wall thickness of 101.04 nm, indicating that cAMP signaling positively regulates cell wall biogenesis during intercalary growth. Conversely, in the fully developed leaf sheath where plant and fungal cells are no longer growing, there were no significant differences in cell wall thickness between any of the strains (**Figure 8B**). Cell walls of wild-type *E. festucae* hyphae in the leaf sheath were thicker than those in the immature leaf (139 nm vs. 111.3 nm respectively, $P \leq 0.001$) confirming previous reports of thinner cell walls in *E. festucae* Fl1 hyphae in developing vs. mature host tissues (Christensen et al., 2008).

DISCUSSION

In this study we tested the hypothesis that cAMP signaling is required for regulated growth of the mutualistic fungal endophyte *E. festucae* in host grasses, and for compatibility between the host and endophyte. Our data show that disruption of the *acyA* gene severely reduced *E. festucae* radial colony growth in axenic culture, however this growth defect did not affect initial plant infection processes. The *acyA* mutant strains were hyper-branched in culture and unable to accumulate superoxide radicals. When infecting plants, the mycelia became progressively more dense compared to wild-type as plant tissues aged. Disruption of cAMP synthesis therefore disrupted the ability of the endophyte to grow in synchrony with developing leaves, an attribute which prevents overgrowth of the host during symbiosis.

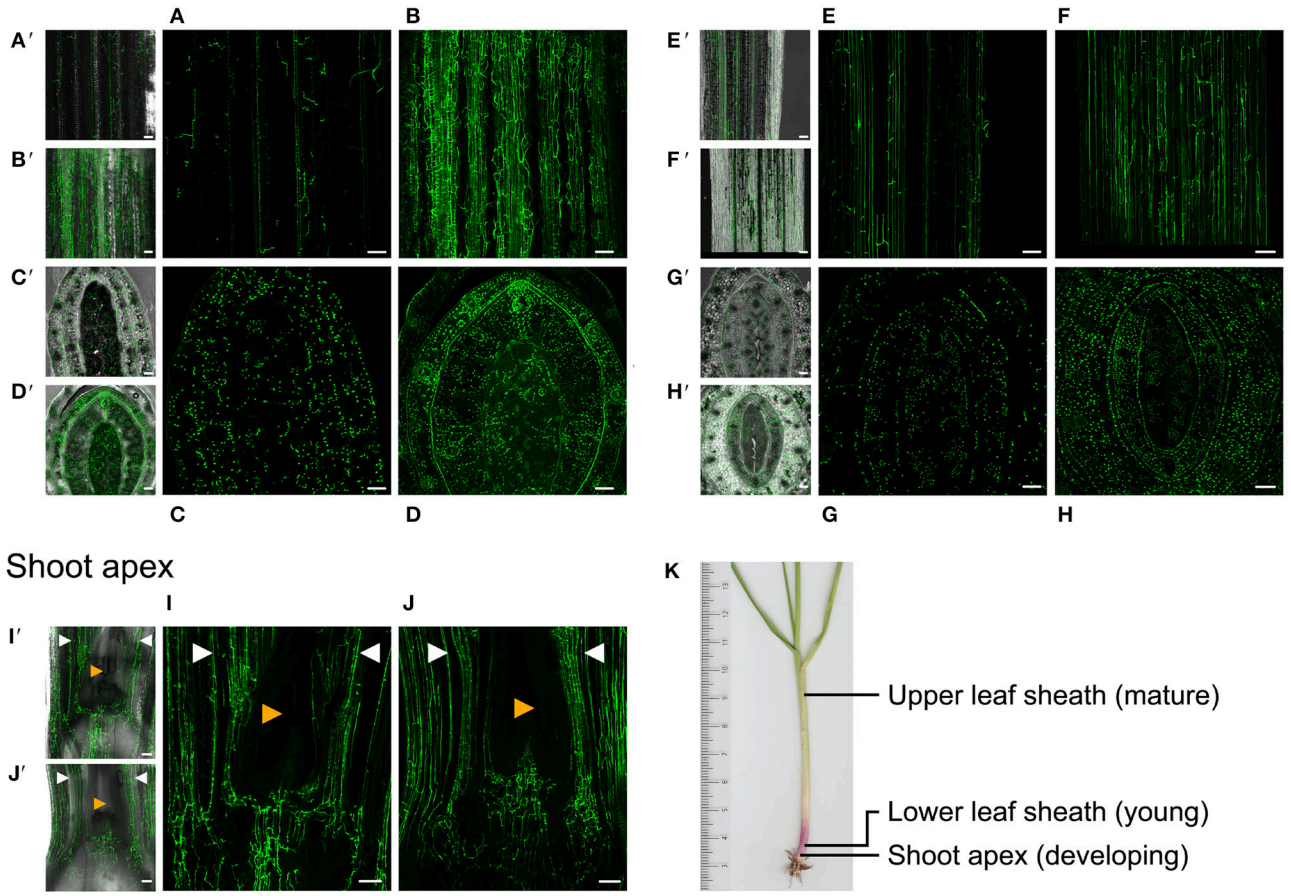

FIGURE 6 | Disruption of *E. festucae acyA* deregulates hyphal branching during host colonization. (A–J). Confocal laser scanning micrographs (CLSM) of *E. festucae* hyphae at three stages of host development. *L. perenne* leaves infected with the wild-type and disruption mutant Δ*acyA*42 are shown. Both strains are transformed with plasmid pTEFEGFP and constitutively express EGFP. **(A′–J′)**, CSLM overlaid on corresponding phase contrast images of the same field of view. **(K)** *L. perenne* tiller showing the positions at which the tissue sections were taken. A/B, CLSM of a longitudinal section of the mature upper leaf sheath of the pseudostem 3.5 cm above the crown (base) of the tiller showing colonization by WT and Δ*acyA*42 hyphae respectively. **(C,D)** CLSM of a transverse section though the tiller at the same position as **(A,B)**. The youngest developing leaf is in the center of the section and is enclosed by progressively older leaf sheaths. **(E,F)** CLSM of a longitudinal section of a young developing leaf sheath immediately above the crown of the tiller. (**G,H)** CLSM of a transverse section through the pseudostem at the same position as (**E,F)**. **(I,J)** CSLM of a longitudinal section through the crown showing the position of hyphae relative to the shoot apex. The shoot apex (red arrow) is a small dome of overlapping leaf primordia visible only in the phase contract images **(I′, J′)**. Hyphae are either not detectable in this tissue by confocal microscopy or are not present. Hyphae in the youngest leaves emerging from the shoot apex are marked by white arrows.

The reduction in colony radial growth rate of *E. festucae acyA* mutants is consistent with deletion of the AC gene in plant pathogenic fungi such as *F. verticillioides* (Choi and Xu, 2010), *F. fujikuroi* (García-Martínez et al., 2012), *F. proliferatum* (Kohut et al., 2010) and *Botrytis cinerea* (Klimpel et al., 2002). Complementation of the mutant phenotype with cAMP confirmed that the relatively slow radial growth rate in the mutants was due to cAMP depletion. Significantly, strains Δ*acyA*34 and Δ*acyA*42 had similar radial growth rates in the absence of exogenous cAMP, while Δ*acyA*47 grew at a faster rate despite having an identical *acyA* disruption locus. Similar spontaneous revertants have been obtained from adenylate cyclase *MAC1* mutants of *Magnaporthe oryzae* (Adachi and Hamer, 1998) and *cr-1* mutants of *Neurospora crassa* (Garnjobst and Tatum, 1970). This phenomenon has also been reported in *B. cinerea* where the slow radial growth rate of the AC mutants reverted to wild-type levels over time (Klimpel et al., 2002). The reason for this phenomenon was not investigated in our study but is speculated to be due to the accumulation of suppressor mutations that complement the mutant growth phenotype. By-pass suppressors of the *MAC1* (AC) phenotype (*sum*) that fully restore growth and morphogenesis in *M. oryzae* have been identified (Adachi and Hamer, 1998). One such mutation in the PKA catalytic subunit (*sum1–99*) alters a conserved amino acid in the cAMP binding domain (Adachi and Hamer, 1998). As shown here and reported elsewhere, the fungal cAMP signaling

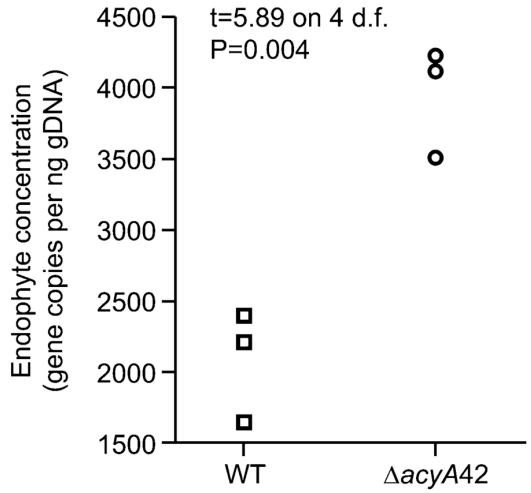

FIGURE 7 | Effects of *acyA* disruption on biomass of *E. festucae* in host grasses. Comparison of hyphal biomass in the pseudostem (the region between the crown and the first ligule of a tiller) of plants infected with either the wild-type or Δ*acyA*42 mutant strains. Hyphal biomass (expressed as endophyte concentration) was determined by quantitative PCR of a single copy gene from 1 ng of genomic DNA. Hyphal biomass between strains was compared using the Students' *T*-test. The means of the two treatments were significantly different ($P = 0.004$).

pathway is highly responsive to AC deletion/disruption and perturbations in cAMP synthesis. Suppressor mutations mask AC deletion phenotypes and confound the interpretation of cAMP signaling experiments, potentially contributing to the diversity in morphology and growth rates reported in different fungi.

Microscopic examination of *E. festucae* Δ*acyA* strains in culture revealed that the cAMP signaling pathway plays a significant role in colony architecture. Mutant hyphae were aggregated, convoluted and hyper-branched. The cAMP cascade therefore enforces apical dominance in this species by preventing development of new hyphal branch points near the apex. The morphology of the *acyA* mutant colonies quite closely resembled the *E. festucae* small GTPase *racA* mutant (Tanaka et al., 2008) which also had a slower growth rate compared to the wild-type, had convoluted hyphae, produced lateral branches with higher frequency, and formed branches at atypical sites. Notably, similarly to the *E. festucae* Δ*acyA* phenotype, hyphal morphology and colony size in the Δ*racA* reverted to wild-type over time in culture (Kayano et al., 2013). RacA is a small GTPase of the Rho subfamily involved in hyphal growth and morphogenesis (Zhang et al., 2013). Production of superoxide from molecular oxygen by the plasma membrane-localized NADPH oxidase complex is important in regulating polar growth in *E. festucae* as exemplified by deletion of several genes encoding proteins of the NADPH oxidase complex (Takemoto et al., 2007; Scott and Eaton, 2008; Eaton et al., 2011; Tanaka et al., 2012), *noxA* (Tanaka et al., 2006), *noxR* (Takemoto et al., 2006), *racA* (Tanaka et al., 2008), and *bemA* (Takemoto et al., 2011). *E. festucae* RacA GTPase binds to NoxR, a regulator of NADPH oxidase, and activates the NADPH oxidase complex that synthesizes superoxide (Tanaka et al., 2008). A further similarity in morphology between the *E. festucae racA* and *acyA* mutants in culture was the absence of ROS in hyphal tips. In the strains complemented with the wild-type *acyA* gene, superoxide levels were the same as, or more concentrated than wild-type, confirming that cAMP signaling positively regulates superoxide accumulation in *E. festucae*. This result contrasts with the *E. festucae* Fl1 *sakA* mutant where deletion of the stress-activated mitogen-activated protein (MAP) kinase resulted in elevated H_2O_2, both in culture and in plants (Eaton et al., 2008, 2010) suggesting the stress-activated MAP kinase and cAMP pathways play opposing roles in ROS regulation. Transcriptomics analysis of the *sakA* mutant demonstrated that genes for 27 ROS decomposition enzymes such as peroxidases and catalases are also more highly expressed in relation to the wild-type, possibly in response to the elevated ROS produced by this mutant (Eaton et al., 2010). Regulation of ROS by cAMP has also been reported in *C. albicans* where cAMP negatively regulates oxidative stress response genes such as *MCR1* (cytochrome b_5 reductase), *SOD2* (Mn superoxide dismutase), *HSP12* (heat shock protein) and *CCP1* (cytochrome *c* peroxidase) (Bahn et al., 2007). Likewise, repression of the Ras-cAMP-PKA cascade by farnesol (a small signaling molecule) results in up-regulation of catalase and superoxide dismutase, with a consequential increase in resistance against oxidative stress (Deveau et al., 2010). Increased resistance to H_2O_2 has also been observed in *F. proliferatum* after deletion of *FpacyA* (Kohut et al., 2010). Despite similarities between *racA* and *acyA* mutants in morphology and ROS regulation during saprotrophic growth, deletion of *noxA*, *noxA/noxB*, *noxR,* or *bemA* in *E. festucae* results in only a slight reduction in colony growth on PDA and no marked effects on hyphal morphology (Tanaka et al., 2006; Kayano et al., 2013) indicating that the substantial reduction in radial colony growth rate and the hyper-branched phenotype of the *acyA* mutants on PDA is therefore not mediated through ROS but through other, yet unidentified, mechanisms. This is also true for traits associated with apical dominance in other fungi where apical dominance and polar growth is not overcome by disruption of NADPH oxidase genes when growing on enriched media (Scott and Eaton, 2008; Semighini and Harris, 2008). In *E. festucae noxA*, *noxA/noxB,* and *noxR* (but not *bemA*) are critical for regulation of apical dominance and hyphal organization during growth on water agar suggesting that ROS regulation of hyphal branching is more important in nutrient limited conditions (Kayano et al., 2013).

The cAMP signaling cascade regulates key processes in fungal pathogenesis, and in most pathogenic fungi AC deletion attenuates or eliminates virulence in animal and plant pathogens (Choi and Dean, 1997; Klimpel et al., 2002; Kohut et al., 2010), although others report the virulence unchanged, as in *F. fujikuroi* (Δ*acyA*) on tomato (García-Martínez et al., 2012). In contrast with most fungal pathogens, AC was not required for establishment of a stable symbiosis between *E. festucae* and *L. perenne*. Only Δ*acyA*34 and 42 were competent to form a symbiosis, and Δ*acyA*47 did not appear to be infectious, despite growing more rapidly in culture as mentioned above. The spontaneous growth revertant, Δ*acyA*47var, was capable of forming compatible interactions with host plants. We speculate

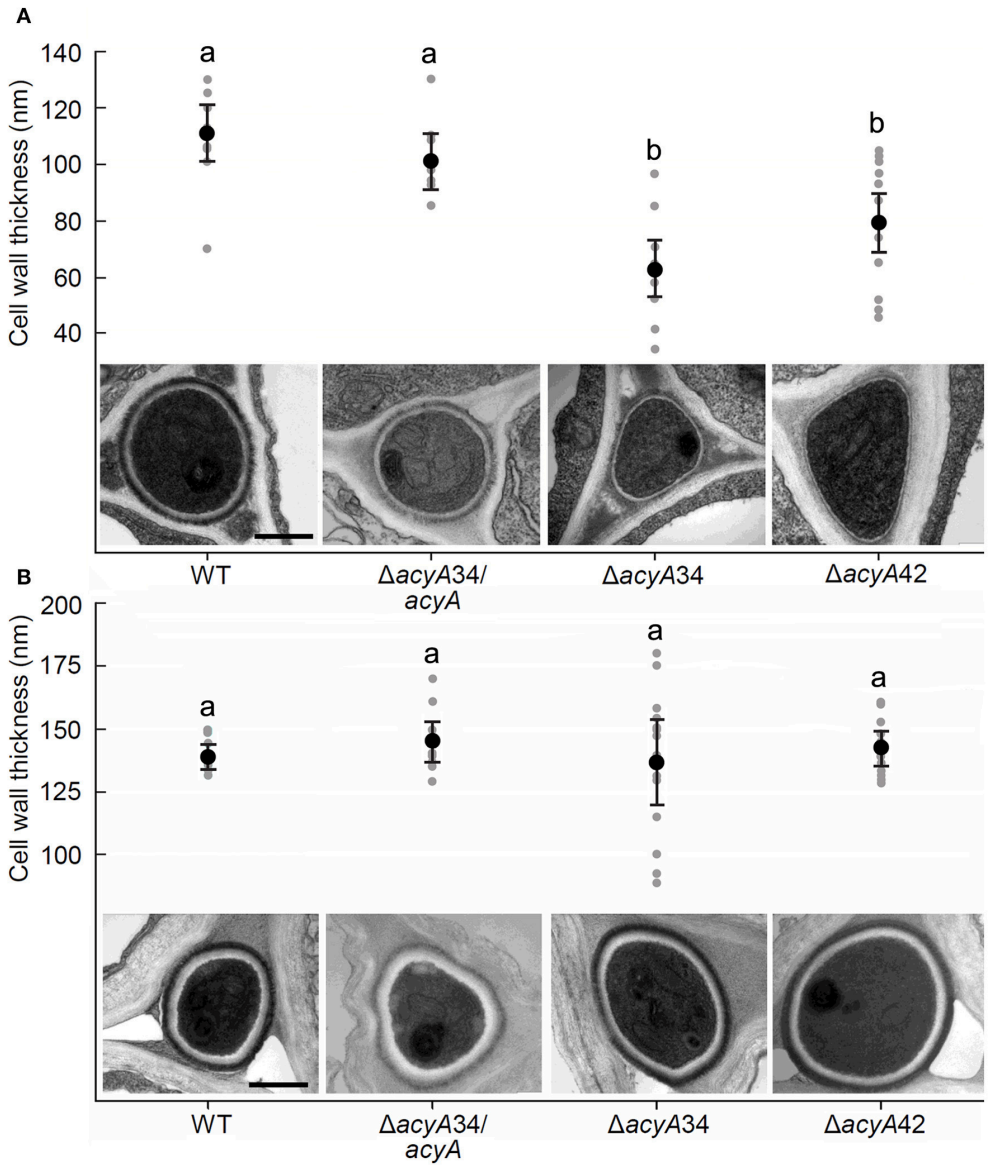

FIGURE 8 | Regulation of hyphal cell wall synthesis by cAMP during leaf colonization. The cell wall of 12 hyphae each from developing leaves **(A)** and mature second leaf sheaths **(B)** of *L. perenne* was measured at eight positions around each hypha. The gray symbols represent the average cell wall thickness of each hypha. The overall mean cell wall thickness and its 95% confidence interval is presented for each strain. Analysis of variance was used to compare the strains. Within each plant tissue **(A,B)**, different letters indicate means that are different at the 5% significance level. Transmission electron micrographs show representative hyphae of *E. festucae* wild-type, mutants Δ*acyA*34, and Δ*acyA*42, and the complementation strain Δ*acyA*34/*acyA* strain in the two host tissue types. All images are at the same magnification. The scale bar is 500 nm.

that this change in infectivity was also due to suppressor mutation(s). The hyphae of *acyA* mutants in plants were hyper-branched in mature host tissues, suggesting that the endophytes produced many more hyphal apices in plants, as they did in culture. This phenotype largely reverted to wild-type in strains complemented with the functional *acyA* gene. *E. festucae* is predominantly a foliar symbiont, and infects aerial plant tissues as they are developing on the host SAM at the base of the plant. The youngest host (and endophyte) tissues are those nearest the SAM while the older tissues are those furthest from it (the tips of the leaves for example). Hyphae were visible between meristematic cells at the base of developing leaves, and morphology and distribution of Δ*acyA*42/EGFP appeared similar to the wild-type in this very young tissue. However hyphal biomass appeared to increase at each successive stage in leaf development examined. This contrasts with the wild-type colonization process where branching is mostly confined to hyphae colonizing meristematic host tissues, and is quite tightly

constrained during intercalary growth in the host expansion zone (Christensen et al., 2008).

It is not possible to deduce whether breakdown in regulated control of hyphal biomass during host colonization through cAMP disruption was a consequence of lower ROS levels as this was not tested directly. However, *E. festucae* strains with deletions in components of the NADPH oxidase complex exhibit similar hyper-colonization phenotypes (Takemoto et al., 2006, 2011; Tanaka et al., 2006, 2008) suggesting that changes in ROS accumulation should be considered as one potential contributor to the *E. festucae* cAMP disruption phenotype in plants. Another *E. festucae* Fl1 mutant (Δ*sidN*, deficient in the biosynthesis of the iron-chelating siderophore epichloënin A), also phenocopies the defective polarized growth of the *E. festucae racA* and *acyA* deletion mutants, but under iron depleted conditions (Johnson et al., 2013b). Deletion of Δ*sidN* in *E. festucae* reduced *racA* transcripts between 2.2 and 3.3 fold in infected plants and the mutants also over colonized the host (Johnson et al., 2013b). Iron homeostatic regulation of the NADPH oxidase complex is therefore another layer of complexity potentially involved in ROS regulation of hyphal branching. Whether there are direct interactions between the NADPH oxidase complex, *racA*, iron homeostasis and the cAMP pathway remains to be determined. Unlike the other *acyA* phenotypes which revert to wild-type over time in culture, ROS suppression in *acyA* deletion mutants was highly stable. Cyclic AMP may therefore exert its effect on ROS accumulation through a different downstream mechanism to those used to regulate other traits such as colony growth and hyphal morphology.

The hyphal walls of the *E. festucae* Δ*acyA* mutants were significantly thinner compared to wild-type or *acyA*-complemented mutant strains, however this was only the case for hyphae in developing host tissues (where the endophytes grow by intercalary extension). This suggests that, while cell wall growth is slower in the *acyA* mutants vs. the wild-type, the differential is sufficiently small to enable them to maintain cell walls of similar thickness once hyphal and plant growth has ceased (in mature leaves). These data indicate that, similar to the wild-type, cell wall synthesis in *acyA* mutant strains also continues after extension growth has ceased.

The mutant strains had a small but variable impact on the morphology of host plants (Supplementary Figure 2). In contract to the results presented here, excessive hyphal branching by *E. festucae* mutants in plants almost always induces abnormalities in host morphology, such as stunted tillers (Takemoto et al., 2006, 2011; Tanaka et al., 2008; Eaton et al., 2010; Johnson et al., 2013b; Green et al., 2016). We assume that the *acyA* mutants did not stunt the host because hyphal distribution in the shoot apex was similar to the wild-type. The architecture of grasses is largely regulated by this tissue (where the leaves, inflorescences and tillers are differentiated) and competition for resources, hyphal overgrowth or disruption of host cell organization at this critical stage in development is likely to have a negative impact on host morphology. Since the distribution of hyphae in the shoot apex has not been investigated for many *E. festucae* mutants the discrepancy between hyphal branching and host morphology disturbance is unresolved.

Most fungi contain a single AC gene, however ancestral interspecific hybridizations between different *Epichloë* species have generated a number of strains with additional genomes (Schardl et al., 1994; Kuldau et al., 1999). Analyses of allopolyploids AR3046, and AR1006 (Craven et al., 2001; Moon et al., 2004) indicates that these strains each have two homeologs of *acyA*. A report describing the consequences of genomic and transcriptomics shock in a third relatively recent natural *Epichloë* hybrid (Lp1) suggests that both homeologs of most genes in the parental strains are also retained in this hybrid, and that there is little evidence for higher expression levels in one homeolog vs. the other (Cox et al., 2014). Similarly, in AR1006 one of the *acyA* genes was truncated and is likely a pseudogene, while in AR3046 both genes appear functional. Allopolyploids are often more competitive than their parental progenitors (Cox et al., 2014) and duplicate copies of key signaling pathway genes may, if both are retained, provide allopolyploid *E. festucae* strains (all asexual) resilience against mutations or allow for the evolution of new functions.

In summary, the cAMP cascade regulates saprotrophic growth of *E. festucae* in culture, with a role in enforcing the dominance of the hyphal apex and restricting development of lateral branches. Although ROS accumulation in *E. festucae* on PDA is positively regulated through cAMP, depletion of ROS alone cannot account for the hyper-branched phenotype in *E. festucae* Δ*acyA* as ROS synthesis mutants of *E. festucae* (Δ*racA* excepted) have a wild type phenotype when growing on PDA. In plants, wild-type *E. festucae* hyphal growth is tightly regulated and hyphal overgrowth is often observed in antagonistic *Epichloë-L. perenne* symbioses, such as those with disruptions in ROS synthesis (Takemoto et al., 2006; Tanaka et al., 2006). *E. festucae* Δ*acyA* mutants produce progressively more hyphae in host leaves as they age, presumably through the continued production of new hyphal tips that are normally restricted in wild type strains. Cyclic AMP is therefore critical in restricting potential overgrowth of the symbiont during colonization of developing host tissues, and in regulating the synchronicity in growth of the two organisms.

AUTHOR CONTRIBUTIONS

CV, RJ, GB, LJ, and JK conceived the ideas for the study. All the authors participated in data analysis and interpretation, and contributed to the writing and editing of the manuscript. CV, MC, LJ, NF, SC, MG and WS contributed to the experimentation.

FUNDING

This research was supported by Core Funding from AgResearch Ltd., and the New Zealand Ministry of Business and Primary Industries (to CV).

ACKNOWLEDGMENTS

We thank Kelly Dunstan, Sophie Borchert, Charlotte Gaborit, Jennifer Pratt, Catherine Tootle, Nadia Houssain and Lydia

Koolaard for technical services, Pauline Hunt for preparation of the figures, and Rosemary Van Essen and Joy Dick for library services (all AgResearch Ltd., Grasslands Research Centre, New Zealand). Transmission electron microscopy services were provided by Jianyu Chen and Jordan Taylor (Manawatu Microscopy and Imaging Centre, Massey University, New Zealand). We also gratefully acknowledge Professor Chris Schardl (University of Kentucky) for providing generous early access to the genome sequences of *E. festucae* and other fungi of the Clavicipitaceae.

SUPPLEMENTARY MATERIAL

The Supplementary Material for this article can be found online at: http://journal.frontiersin.org/article/10.3389/fpls.2016.01546/full#supplementary-material

REFERENCES

Adachi, K., and Hamer, J. E. (1998). Divergent cAMP signaling pathways regulate growth and pathogenesis in the rice blast fungus *Magnaporthe grisea*. *Plant Cell Online* 10, 1361–1373. doi: 10.1105/tpc.10.8.1361

Alspaugh, J. A., Pukkila-Worley, R., Harashima, T., Cavallo, L. M., Funnell, D., Cox, G. M., et al. (2002). Adenylyl cyclase functions downstream of the G alpha protein Gpa1 and controls mating and pathogenicity of *Cryptococcus neoformans*. *Eukaryot. Cell* 1, 75–84. doi: 10.1128/EC.1.1.75-84.2002

Arachevaleta, M., Bacon, C. W., Hoveland, C. S., and Radcliffe, D. E. (1989). Effect of the tall fescue endophyte on plant response to environmental stress. *Agron. J.* 81, 83–90. doi: 10.2134/agronj1989.00021962008100010015x

Bacon, C. W., Porter, J. K., Robbins, J. D., and Luttrell, E. S. (1977). *Epichloë typhina* from toxic tall fescue grasses. *Appl. Environ. Microbiol.* 34, 576–581.

Bahn, Y.-S., Molenda, M., Staab, J. F., Lyman, C. A., Gordon, L. J., and Sundstrom, P. (2007). Genome-wide transcriptional profiling of the cyclic AMP-Dependent signaling pathway during morphogenic transitions of *Candida albicans*. *Eukaryot. Cell* 6, 2376–2390. doi: 10.1128/EC.00318-07

Bahn, Y. S., and Mühlschlegel, F. A. (2006). CO2 sensing in fungi and beyond. *Curr. Opin. Microbiol.* 9, 572–578. doi: 10.1016/j.mib.2006.09.003

Bahn, Y. S., and Sundstrom, P. (2001). CAP1, an adenylate cyclase-associated protein gene, regulates bud-hypha transitions, filamentous growth, and cyclic AMP levels and is required for virulence of *Candida albicans*. *J. Bacteriol.* 183, 3211–3223. doi: 10.1128/JB.183.10.3211-3223.2001

Baker, D. A., and Kelly, J. M. (2004). Structure, function and evolution of microbial adenylyl and guanylyl cyclases. *Mol. Microbiol.* 52, 1229–1242. doi: 10.1111/j.1365-2958.2004.04067.x

Ball, O. J.-P., and Prestidge, R. A. (1993). Endophyte-associated alkaloids, insect resistance and animal disorders: an interrelated complex. *N.Z. Vet. J.* 41, 216.

Bormann, J., Boenisch, M. J., Brückner, E., Firat, D., and Schäfer, W. (2014). The adenylyl cyclase plays a regulatory role in the morphogenetic switch from vegetative to pathogenic lifestyle of *Fusarium graminearum* on wheat. *PLoS ONE* 9:e91135. doi: 10.1371/journal.pone.0091135

Brakhage, A., and Liebmann, B. (2005). *Aspergillus fumigatus* conidial pigment and cAMP signal transduction: significance for virulence. *Med. Mycol.* 43, S75–S82. doi: 10.1080/13693780400028967

Byrd, A. D., Schardl, C. L., Songlin, P. J., Mogen, K. L., and Siegel, M. R. (1990). The β-tubulin gene of *Epichloë typhina* from perennial ryegrass (*Lolium perenne*). *Curr. Genet.* 18, 347–354. doi: 10.1007/BF00318216

Card, S. D., Faville, M. J., Simpson, W. R., Johnson, R. D., Voisey, C. R., de Bonth, A. C. M., et al. (2014). Mutualistic fungal endophytes in the Triticeae–survey and description. *FEMS Microbiol. Ecol.* 88, 94–106. doi: 10.1111/1574-6941.12273

Chen, D., Janganan, T. K., Chen, G., Marques, E. R., Kress, M. R., Goldman, G. H., et al. (2007). The cAMP pathway is important for controlling the morphological switch to the pathogenic yeast form of *Paracoccidioides brasiliensis*. *Mol. Microbiol.* 65, 761–779. doi: 10.1111/j.1365-2958.2007.05824.x

Choi, W., and Dean, R. A. (1997). The adenylate cyclase gene MAC1 of *Magnaporthe grisea* controls appressorium formation and other aspects of growth and development. *Plant Cell* 9, 1973–1983. doi: 10.1105/tpc.9.11.1973

Choi, Y.-E., and Xu, J. -R. (2010). The cAMP Signaling pathway in *Fusarium verticillioides* is important for conidiation, plant infection, and stress responses but not fumonisin production. *Mol. Plant Microbe Interact.* 23, 522–533. doi: 10.1094/MPMI-23-4-0522

Christensen, M. J., Bennett, R. J., Ansari, H. A., Koga, H., Johnson, R. D., Bryan, G. T., et al. (2008). *Epichloë* endophytes grow by intercalary hyphal extension in elongating grass leaves. *Fungal Genet. Biol.* 45, 84–93. doi: 10.1016/j.fgb.2007.07.013

Christensen, M. J., and Voisey, C. R. (2009). "Tall Fescue-endophyte symbiosis," in *Tall Fescue for the Twenty-first Century. Agronomy Monologue, Vol 53*, eds H. A. Fribourg, D. B, Hannaway, and C. P. West (Madison, WI: Book and Multimedia Publishing), 251–272.

Christensen, M., Leuchtmann, A., Rowan, D., and Tapper, B. (1993). Taxonomy of *Acremonium* endophytes of tall fescue (*Festuca arundinacea*), meadow fescue (*F. pratensis*), and perennial rye-grass (*Lolium perenne*). *Mycol. Res.* 97, 1083–1092. doi: 10.1016/S0953-7562(09)80509-1

Cox, M. P., Dong, T., Shen, G., Dalvi, Y., Scott, D. B., and Ganley, A. R. D. (2014). An interspecific fungal hybrid reveals cross-kingdom rules for allopolyploid gene expression patterns. *PLoS Genet.* 10:e1004180. doi: 10.1371/journal.pgen.1004180

Craven, K. D., Blankenship, J. D., Leuchtmann, A., Hignight, K., and Schardl, C. L. (2001). Hybrid fungal endophytes symbiotic with the grass *Lolium pratense*. *Sydowia* 53, 44–73.

Deveau, A., Piispanen, A. E., Jackson, A. A., and Hogan, D. A. (2010). Farnesol induces hydrogen peroxide resistance in *Candida albicans* yeast by inhibiting the Ras-Cyclic AMP signaling pathway. *Eukaryot. Cell* 9, 569–577. doi: 10.1128/EC.00321-09

D'Souza, C. A., and Heitman, J. (2001). Conserved cAMP signaling cascades regulate fungal development and virulence. *Fems Microbiol. Rev.* 25, 349–364. doi: 10.1111/j.1574-6976.2001.tb00582.x

Eaton, C. J., Cox, M. P., Ambrose, B., Becker, M., Hesse, U., Schardl, C. L., et al. (2010). Disruption of signaling in a fungal-grass symbiosis leads to pathogenesis. *Plant Physiol.* 153, 1780–1794. doi: 10.1104/pp.110.158451

Eaton, C. J., Cox, M. P., and Scott, B. (2011). What triggers grass endophytes to switch from mutualism to pathogenism? *Plant Sci.* 180, 190–195. doi: 10.1016/j.plantsci.2010.10.002

Eaton, C. J., Jourdain, I., Foster, S. J., Hyams, J. S., and Scott, B. (2008). Functional analysis of a fungal endophyte stress-activated MAP kinase. *Curr. Genet.* 53, 163–174. doi: 10.1007/s00294-007-0174-6

Fleetwood, D. J., Scott, D. B., Lane, G. A., Tanaka, A., and Johnson, R. D. (2007). A Complex ergovaline gene cluster in *Epichloë* endophytes of grasses. *Appl. Environ. Microbiol.* 73, 2571–2579. doi: 10.1128/AEM.00257-07

Gallagher, L., Owens, R. A., Dolan, S. K., O'Keeffe, G., Schrettl, M., Kavanagh, K., et al. (2012). The *Aspergillus fumigatus* Protein GliK protects against oxidative stress and is essential for gliotoxin biosynthesis. *Eukaryot. Cell* 11, 1226–1238. doi: 10.1128/EC.00113-12

García-Martínez, J., Ádám, A. L., and Avalos, J. (2012). Adenylyl cyclase plays a regulatory role in development, stress resistance and secondary metabolism in *Fusarium fujikuroi*. *PLoS ONE* 7:e28849. doi: 10.1371/journal.pone.0028849

Garnjobst, L., and Tatum, E. L. (1970). New crisp genes and crisp-modifiers in *Neurospora crassa*. *Genetics* 66, 281–290.

Green, K. A., Becker, Y., Fitzsimons, H. L., and Scott, B. (2016). An *Epichloë festucae* homologue of MOB3, a component of the STRIPAK complex, is required for the establishment of a mutualistic symbiotic interaction with *Lolium perenne*. *Mol. Plant Pathol.* doi: 10.1111/mpp.12443. [Epub ahead of print].

Itoh, Y., Johnson, R., and Scott, B. (1994). Integrative transformation of the mycotoxin-producing fungus, *Penicillium paxilli*. *Curr. Genet.* 25, 508–513. doi: 10.1007/BF00351670

Ivey, F. D., and Hoffman, C. S. (2005). Direct activation of fission yeast adenylate cyclase by the Gpa2 Gα of the glucose signaling pathway. *Proc. Natl. Acad. Sci. U.S.A.* 102, 6108–6113. doi: 10.1073/pnas.0502270102

Johnson, L. J., De Bonth, A. C. M., Briggs, L. R., Caradus, J. R., Finch, S. C., Fleetwood, D. J., et al. (2013a). The exploitation of epichloae endophytes for agricultural benefit. *Fungal Divers* 60, 171–188. doi: 10.1007/s13225-013-0239-4

Johnson, L. J., Koulman, A., Christensen, M., Lane, G. A., Fraser, K., Forester, N., et al. (2013b). An extracellular siderophore is required to maintain the mutualistic interaction of *Epichloë festucae* with *Lolium perenne*. *PLoS Pathog.* 9:e1003332. doi: 10.1371/journal.ppat.1003332

Johnson, R., Voisey, C., Johnson, L., Pratt, J., Fleetwood, D., Khan, A., et al. (2007). Distribution of NRPS gene families within the *Neotyphodium*/*Epichloë* complex. *Fungal Genet. Biol.* 44, 1180–1190. doi: 10.1016/j.fgb.2007.04.009

Kamerewerd, J., Jansson, M., Nowrousian, M., Pöggeler, S., and Kück, U. (2008). Three α-subunits of heterotrimeric G proteins and an adenylyl cyclase have distinct roles in fruiting body development in the homothallic fungus *Sordaria macrospora*. *Genetics* 180, 191–206. doi: 10.1534/genetics.108.091603

Kayano, Y., Tanaka, A., Akano, F., Scott, B., and Takemoto, D. (2013). Differential roles of NADPH oxidases and associated regulators in polarized growth, conidiation and hyphal fusion in the symbiotic fungus *Epichloë festucae*. *Fungal Genet. Biol.* 56, 87–97. doi: 10.1016/j.fgb.2013.05.001

Kearse, M., Moir, R., Wilson, A., Stones-Havas, S., Cheung, M., Sturrock, S., et al. (2012). Geneious Basic: an integrated and extendable desktop software platform for the organization and analysis of sequence data. *Bioinformatics* 28, 1647–1649. doi: 10.1093/bioinformatics/bts199

Klimpel, A., Gronover, C. S., Williamson, B., Stewart, J. A., and Tudzynski, B. (2002). The adenylate cyclase (BAC) in *Botrytis cinerea* is required for full pathogenicity. *Mol. Plant Pathol.* 3, 439–450. doi: 10.1046/j.1364-3703.2002.00137.x

Kohut, G., Oláh, B., Ádám, A. L., García-Martínez, J., and Hornok, L. (2010). Adenylyl cyclase regulates heavy metal sensitivity, bikaverin production and plant tissue colonization in *Fusarium proliferatum*. *J. Basic Microbiol.* 50, 59–71. doi: 10.1002/jobm.200900113

Kuldau, G. A., Tsai, H.-F., and Schardl, C. L. (1999). Genome sizes of *Epichloë* species and anamorphic hybrids. *Mycologia* 91, 776–782. doi: 10.2307/3761531

Kulkarni, R. D., and Dean, R. A. (2004). Identification of proteins that interact with two regulators of appressorium development, adenylate cyclase and cAMP-dependent protein kinase A, in the rice blast fungus *Magnaporthe grisea*. *Mol. Genet. Genomics* 270, 497–508. doi: 10.1007/s00438-003-0935-y

Latch, G. C. M., and Christensen, M. T. (1985). Artificial infection of grasses with endophytes. *Ann. Appl. Biol.* 107, 17–24. doi: 10.1111/j.1744-7348.1985.tb01543.x

Leuchmann, A., Bacon, C. W., Schardl, C. L., White, J. F. JR., and Tadych, M. (2014). Nomenclatural realignment of *Neotyphodium* species with genus *Epichloë*. *Mycologia* 106, 202–215. doi: 10.3852/13-251

Leuchtmann, A. (1994). Isozyme relationships of *Acremonium* endophytes from twelve *Festuca* species. *Mycol. Res.* 98, 25–33. doi: 10.1016/S0953-7562(09)80331-6

Li, H., Handsaker, B., Wysoker, A., Fennell, T., Ruan, J., Homer, N., et al. (2009). The sequence alignment/map format and SAMtools. *Bioinformatics* 25, 2078–2079. doi: 10.1093/bioinformatics/btp352

Liu, Q., Parsons, A. J., Xue, H., Fraser, K., Ryan, G. D., Newman, J. A., et al. (2011). Competition between foliar *Neotyphodium lolii* endophytes and mycorrhizal *Glomus* spp. fungi in *Lolium perenne* depends on resource supply and host carbohydrate content. *Funct. Ecol.* 25, 910–920. doi: 10.1111/j.1365-2435.2011.01853.x

Liu, S., Peng, G., and Xia, Y. (2012). The adenylate cyclase gene MaAC is required for virulence and multi-stress tolerance of *Metarhizium acridum*. *BMC Microbiol* 12:163. doi: 10.1186/1471-2180-12-163

Lukito, Y., Chujo, T., and Scott, B. (2015). Molecular and cellular analysis of the pH response transcription factor PacC in the fungal symbiont *Epichloë festucae*. *Fungal Genet. Biol.* 85, 25–37. doi: 10.1016/j.fgb.2015.10.008

Malinowski, D. P., and Belesky, D. P. (2000). Adaptations of endophyte-infected cool-season grasses to environmental stresses: mechanisms of drought and mineral stress tolerance. *Crop Sci.* 40, 923–940. doi: 10.2135/cropsci2000.404923x

Martínez-Espinoza, A. D., Ruiz-Herrera, J., León-Ramírez, C. G., and Gold, S. E. (2004). MAP kinase and cAMP signaling pathways modulate the pH-induced yeast-to-mycelium dimorphic transition in the corn smut fungus *Ustilago maydis*. *Curr. Microbiol.* 49, 274–281. doi: 10.1007/s00284-004-4315-6

McDonough, K. A., and Rodriguez, A. (2012). The myriad roles of cyclic AMP in microbial pathogens, from signal to sword. *Nat. Rev. Microbiol.* 10, 27–38. doi: 10.1038/nrmicro2688

Mogensen, E. G., Janbon, G., Chaloupka, J., Steegborn, C., Man, S. F., Moyrand, F., et al. (2006). *Cryptococcus neoformans* senses CO2 through the carbonic anhydrase Can2 and the adenylyl cyclase Cac1. *Eukaryot. Cell* 5, 103–111. doi: 10.1128/EC.5.1.103-111.2006

Moon, C. D., Craven, K. D., Leuchtmann, A., Clement, S. L., and Schardl, C. L. (2004). Prevalence of interspecific hybrids amongst asexual fungal endophytes of grasses. *Mol. Ecol.* 13, 1455–1467. doi: 10.1111/j.1365-294X.2004.02138.x

Moon, C. D., Tapper, B. A., and Scott, B. (1999). Identification of epichloë endophytes in planta by a microsatellite-based PCR fingerprinting assay with automated analysis. *Appl. Environ. Microbiol.* 65, 1268–1279.

Mukherjee, M., Mukherjee, P. K., and Kale, S. P. (2007). cAMP signaling is involved in growth, germination, mycoparasitism and secondary metabolism in *Trichoderma virens*. *Microbiology* 153, 1734–1742. doi: 10.1099/mic.0.2007/005702-0

Namiki, F., Matsunaga, M., Okuda, M., Inoue, I., Nishi, K., Fujita, Y., et al. (2001). Mutation of an arginine biosynthesis gene causes reduced pathogenicity in *Fusarium oxysporum* f. *sp. melonis*. *Mol. Plant Microbe Interact.* 14, 580–584. doi: 10.1094/MPMI.2001.14.4.580

Punt, P. J., Oliver, R. P., Dingemanse, M. A., Pouwels, P. H., and van den Hondel, C. A. (1987). Transformation of *Aspergillus* based on the hygromycin B resistance marker from *Escherichia coli*. *Gene* 56, 117–124. doi: 10.1016/0378-1119(87)90164-8

Rasmussen, S., Parsons, A. J., Bassett, S., Christensen, M. J., Hume, D. E., Johnson, L. J., et al. (2007). High nitrogen supply and carbohydrate content reduce fungal endophyte and alkaloid concentration in *Lolium perenne*. *New Phytol.* 173, 787–797. doi: 10.1111/j.1469-8137.2006.01960.x

Schardl, C. L., Grossman, R. B., Nagabhyru, P., Faulkner, J. R., and Mallik, U. P. (2007). Loline alkaloids: currencies of mutualism. *Phytochemistry* 68, 980–996. doi: 10.1016/j.phytochem.2007.01.010

Schardl, C. L., Leuchtmann, A., Tsai, H. F., Collett, M. A., Watt, D. M., and Scott, D. B. (1994). Origin of a fungal symbiont of perennial ryegrass by interspecific hybridization of a mutualist with the ryegrass choke pathogen, *Epichloe typhina*. *Genetics* 136, 1307–1317.

Schardl, C. L., and Phillips, T. D. (1997). Protective grass endophytes. Where are they from and where are they going? *Plant Dis.* 81, 430–438. doi: 10.1094/PDIS.1997.81.5.430

Schardl, C. L., Young, C. A., Hesse, U., Amyotte, S. G., Andreeva, K., Calie, P. J., et al. (2013). Plant-symbiotic fungi as chemical engineers: multi-genome analysis of the Clavicipitaceae reveals dynamics of alkaloid loci. *PLoS Genet.* 9:e1003323. doi: 10.1371/journal.pgen.1003323

Schardl, C. L., Young, C. A., Moore, N., Krom, N., Dupont, P.-Y., Pan, J., et al. (2014). "Chapter ten - genomes of plant-associated clavicipitaceae," in *Adv Bot Res, Vol 70*, ed M. M. Francis (London: Academic Press), 291–327.

Scott, B., and Eaton, C. J. (2008). Role of reactive oxygen species in fungal cellular differentiations. *Curr. Opin. Microbiol.* 11, 488–493. doi: 10.1016/j.mib.2008.10.008

Semighini, C. P., and Harris, S. D. (2008). Regulation of apical dominance in *Aspergillus nidulans* hyphae by reactive oxygen species. *Genetics* 179, 1919–1932. doi: 10.1534/genetics.108.089318

Simpson, W. R., Faville, M. J., Moraga, R. A., Williams, W. M., McManus, M. T., and Johnson, R. D. (2014). *Epichloë* fungal endophytes and the formation of synthetic symbioses in *Hordeeae* (=*Triticeae*) grasses. *J. Syst. Evol.* 52, 794–806. doi: 10.1111/jse.12107

Simpson, W. R., Schmid, J., Singh, J., Faville, M. J., and Johnson, R. D. (2012). A morphological change in the fungal symbiont *Neotyphodium lolii* induces dwarfing in its host plant *Lolium perenne*. *Fungal Biol.* 116, 234–240. doi: 10.1016/j.funbio.2011.11.006

Studt, L., Humpf, H.-U., and Tudzynski, B. (2013). Signaling governed by G proteins and cAMP is crucial for growth, secondary metabolism and sexual development in *Fusarium fujikuroi*. *PLoS ONE* 8:e58185. doi: 10.1371/journal.pone.0058185

Sugui, J. A., Pardo, J., Chang, Y. C., Zarember, K. A., Nardone, G., Galvez, E. M., et al. (2007). Gliotoxin is a virulence factor of *Aspergillus fumigatus*: gliP deletion attenuates virulence in mice immunosuppressed with hydrocortisone. *Eukaryot. Cell* 6, 1562–1569. doi: 10.1128/EC.00141-07

Takemoto, D., Kamakura, S., Saikia, S., Becker, Y., Wrenn, R., Tanaka, A., et al. (2011). Polarity proteins Bem1 and Cdc24 are components of the filamentous fungal NADPH oxidase complex. *Proc. Natl. Acad. Sci. U.S.A.* 108, 2861–2866. doi: 10.1073/pnas.1017309108

Takemoto, D., Tanaka, A., and Scott, B. (2006). A p67Phox-like regulator is recruited to control hyphal branching in a fungal–grass mutualistic symbiosis. *Plant Cell* 18, 2807–2821. doi: 10.1105/tpc.106.046169

Takemoto, D., Tanaka, A., and Scott, B. (2007). NADPH oxidases in fungi: diverse roles of reactive oxygen species in fungal cellular differentiation. *Fungal Genet. Biol.* 44, 1065–1076. doi: 10.1016/j.fgb.2007.04.011

Tan, Y. Y., Spiering, M. J., Scott, V., Lane, G. A., Christensen, M. J., and Schmid, J. (2001). *In planta* regulation of extension of an endophytic fungus and maintenance of high metabolic rates in its mycelium in the absence of apical extension. *Appl. Environ. Microbiol.* 67, 5377–5383. doi: 10.1128/AEM.67.12.5377-5383.2001

Tanaka, A., Christensen, M. J., Takemoto, D., Park, P., and Scott, B. (2006). Reactive oxygen species play a role in regulating a fungus-perennial ryegrass mutualistic interaction. *Plant Cell* 18, 2807–2821. doi: 10.1105/tpc.105.039263

Tanaka, A., Takemoto, D., Chujo, T., and Scott, B. (2012). Fungal endophytes of grasses. *Curr. Opin. Plant Biol.* 15, 462–468. doi: 10.1016/j.pbi.2012.03.007

Tanaka, A., Takemoto, D., Hyon, G.-S., Park, P., and Scott, B. (2008). NoxA activation by the small GTPase RacA is required to maintain a mutualistic symbiotic association between *Epichloë festucae* and perennial ryegrass. *Mol. Microbiol.* 68, 1165–1178. doi: 10.1111/j.1365-2958.2008.06217.x

Vanden Wymelenberg, A. J., Cullen, D., Spear, R. N., Schoenike, B., and Andrews, J. H. (1997). Expression of green fluorescent protein in *Aureobasidium pullulans* and quantification of the fungus on leaf surfaces. *BioTechniques* 23, 686–690.

Vázquez-de-Aldana, B. R., García-Ciudad, A., García-Criado, B., Vicente-Tavera, S., and Zabalgogeazcoa, I. (2013). Fungal endophyte (*Epichloë festucae*) alters the nutrient content of *Festuca rubra* regardless of water availability. *PLoS ONE* 8:e84539. doi: 10.1371/journal.pone.0084539

Voisey, C. R. (2010). Intercalary growth in hyphae of filamentous fungi. *Fungal Biol. Rev.* 24, 123–131. doi: 10.1016/j.fbr.2010.12.001

Vollmer, S. J., and Yanofsky, C. (1986). Efficient cloning of genes of *Neurospora crassa*. *Proc. Natl. Acad. Sci. U.S.A.* 83, 4869–4873. doi: 10.1073/pnas.83.13.4869

Xu, X. L., Lee, R. T., Fang, H. M., Wang, Y. M., Li, R., Zou, H., et al. (2008). Bacterial peptidoglycan triggers *Candida albicans* hyphal growth by directly activating the adenylyl cyclase Cyr1p. *Cell Host Microbe* 4, 28–39. doi: 10.1016/j.chom.2008.05.014

Yamauchi, J., Takayanagi, N., Komeda, K., Takano, Y., and Okuno, T. (2004). cAMP-pKA signaling regulates multiple steps of fungal infection cooperatively with Cmk1 MAP kinase in *Colletotrichum lagenarium*. *Mol. Plant Microbe Interact.* 17, 1355–1365. doi: 10.1094/MPMI.2004.17.12.1355

Young, C. A., Bryant, M. K., Christensen, M. J., Tapper, B. A., Bryan, G. T., and Scott, B. (2005). Molecular cloning and genetic analysis of a symbiosis-expressed gene cluster for lolitrem biosynthesis from a mutualistic endophyte of perennial ryegrass. *Mol. Genet. Genomics* 274, 13–29. doi: 10.1007/s00438-005-1130-0

Young, C., Itoh, Y., Johnson, R., Garthwaite, I., Miles, C., Munday-Finch, S., et al. (1998). Paxilline-negative mutants of *Penicillium paxilli* generated by heterologous and homologous plasmid integration. *Curr. Genet.* 33, 368–377. doi: 10.1007/s002940050349

Zhang, C., Wang, Y., Wang, J., Zhai, Z., Zhang, L., Zheng, W., et al. (2013). Functional characterization of Rho family small GTPases in *Fusarium graminearum*. *Fungal Genet. Biol.* 61, 90–99. doi: 10.1016/j.fgb.2013.09.001

Conflict of Interest Statement: The authors declare that the research was conducted in the absence of any commercial or financial relationships that could be construed as a potential conflict of interest.

frontiers in Plant Science

OPINION
published: 16 February 2016
doi: 10.3389/fpls.2016.00096

Does a Common Pathway Transduce Symbiotic Signals in Plant–Microbe Interactions?

Andrea Genre and Giulia Russo*

Department of Life Sciences and Systems Biology, University of Turin, Turin, Italy

Recent years have witnessed major advances in our knowledge of plant mutualistic symbioses such as the rhizobium-legume symbiosis (RLS) and arbuscular mycorrhizas (AM). Some of these findings caused the revision of longstanding hypotheses, but one of the most solid theories is that a conserved set of plant proteins rules the transduction of symbiotic signals from beneficial glomeromycetes and rhizobia in a so-called common symbiotic pathway (CSP). Nevertheless, the picture still misses several elements, and a few crucial points remain unclear. How does one common pathway discriminate between – at least – two symbionts? Can we exclude that microbes other than AM fungi and rhizobia also use this pathway to communicate with their host plants? We here discuss the possibility that our current view is biased by a long-lasting focus on legumes, whose ability to develop both AM and RLS is an exception among plants and a recent innovation in their evolution; investigations in non-legumes are starting to place legume symbiotic signaling in a broader perspective. Furthermore, recent studies suggest that CSP proteins act in a wider scenario of symbiotic and non-symbiotic signaling. Overall, evidence is accumulating in favor of distinct activities for CSP proteins in AM and RLS, depending on the molecular and cellular context where they act.

Keywords: plant–microbe interactions, symbiosis, arbuscular mycorrhiza, legume nodulation, signaling pathways

OPEN ACCESS

Edited by:
Pietro Daniele Spanu, Imperial College London, UK

Reviewed by:
Christian Staehelin, Sun Yat-sen University, China
Liliana Maria Cano, North Carolina State University, USA

****Correspondence:***
Andrea Genre
andrea.genre@unito.it

Specialty section:
This article was submitted to Plant Biotic Interactions, a section of the journal Frontiers in Plant Science

Received: *02 November 2015*
Accepted: *18 January 2016*
Published: *16 February 2016*

Citation:
Genre A and Russo G (2016) Does a Common Pathway Transduce Symbiotic Signals in Plant–Microbe Interactions? Front. Plant Sci. 7:96. doi: 10.3389/fpls.2016.00096

INTRODUCTION

Our understanding of the major beneficial plant–microbe interactions – the rhizobium-legume symbiosis (RLS) and arbuscular mycorrhizas (AM) – has changed over the last decade in the light of breakthrough discoveries on the role of hormones, the exchange of symbiotic signals, or the lifetime of intraradical structures (Gutjahr and Parniske, 2013; Oldroyd, 2013; Schmitz and Harrison, 2014). AM fungi were once believed to open their way across the root apoplast thanks to cell wall degrading enzymes: genomic sequencing (Tisserant et al., 2013; Lin et al., 2014) suggests this is not the case and cellular evidence (Genre et al., 2005, 2008; Rich et al., 2014) has shown that host cell responses are critical for fungal colonization. Similarly, rhizobium entry in root hairs has been ascribed to the action of bacterial enzymes (Gage, 2004; Robledo et al., 2008); nevertheless, evidence is accumulating in favor of a plant-driven meltdown of the wall surrounding the 'infection chamber,' which then expands into the growing infection thread as one semi-solid compartment, where bacteria proliferate and slide (Fournier et al., 2008, 2015).

The demonstration that host plants have major control over such interactions has supported the results of genetic studies, where single plant gene mutations were shown to block both bacterial and fungal penetration of the root (Kistner et al., 2005). Such studies on legume mutants gave rise to the hypothesis that AM and RLS share one signal transduction pathway (Oldroyd, 2013). This common symbiotic pathway, or CSP, is proposed to act downstream of both fungal and rhizobial signal perception and upstream of the activation of the appropriate response to either symbiont (**Figure 1**).

THE COMMON SYMBIOTIC PATHWAY

Research on plant symbioses has largely been focussed on legumes. The culturability of rhizobia and their amenable genetics – compared to far less manageable glomeromycetes – is probably the main reason why research has progressed more rapidly in the field of RLS than AM. When our knowledge of RLS was later applied to AM, legumes were the obvious biological system for such studies.

A number of legume mutants had been selected for their RLS-defective phenotype (Catoira et al., 2000; Sandal et al., 2006); some of them were later found to display a mycorrhizal phenotype too, either blocking fungal entry at the epidermis surface or altering fungal development inside the root tissues (Kistner et al., 2005; Parniske, 2008; Oldroyd, 2013). The corresponding genes have been characterized and, based on their functions, positioned along a signal transduction pathway, the CSP, transducing glomeromycotan or rhizobial signal perception from the plasma membrane into the nucleus (**Figure 1**).

In *Lotus japonicus,* CSP gene products include the receptor-like kinase SYMRK; three nucleoporins, NUP85, NUP133, and NENA; CASTOR and POLLUX, cationic channels located on the nuclear envelope; a nuclear calcium- and calmodulin-dependent kinase CCaMK; and a CCaMK substrate, CYCLOPS (Oldroyd, 2013 and references therein). Furthermore, HMGR1, a key enzyme in the mevalonate biosynthetic pathway, and MCA8, a SERCA-type Ca^{2+}-ATPase localized on the nuclear envelope, have been characterized in *Medicago truncatula* as additional members of the CSP (Kevei et al., 2007; Capoen et al., 2011). Secondary messengers such as mevalonate and Ca^{2+} have also been demonstrated to act within the CSP, either as a product of HMGR1 or an activator of CCaMK, respectively (Levy et al., 2004; Venkateshwaran et al., 2015).

In spite of its reassuring name, though, not all evidence confirms that CSP genes actually encode a signal transduction pathway that is common and restricted to RLS and AM.

Pathway

While a solid link between signal perception and gene expression is a frequent feature in CSP representations (**Figure 1A**), evidence only supports a connection between sub-sets of the CSP members (**Figure 1B**).

A first set of CSP proteins includes the membrane-bound receptor-like kinase SYMRK (interacting with other proteins, like the Nod factor receptors NFR1 and NFR5) and the enzyme

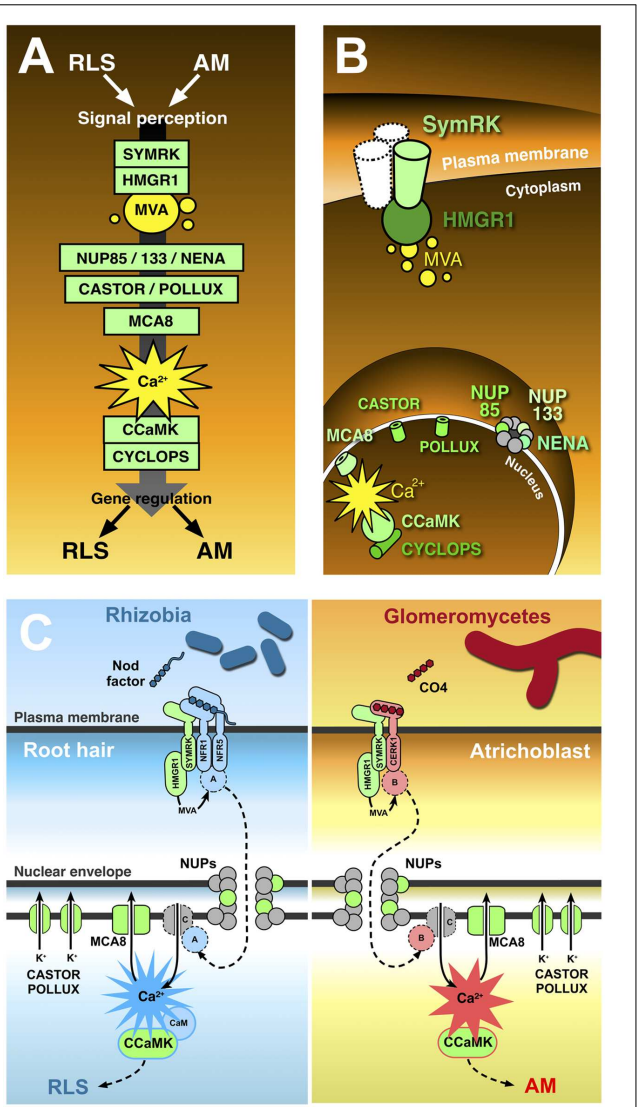

FIGURE 1 | The common symbiotic pathway. Ten proteins (in green) have been identified as essential for both RLS and AM. In contrast with the conventional representation of signal transduction along the common symbiotic pathway **(A)**, CSP protein location in different plant cell districts **(B)** highlights the existence of significant discontinuities between three subsets of CSP members. The receptor-like kinase SYMRK is believed to interact with other co-receptors (such as NFR1 and NFR5) at the cell membrane; its cytoplasmic domain binds the mevalonate (MVA) biosynthetic enzyme HMGR1(3-Hydroxy-3-Methylglutaryl CoA Reductase 1), linking SYMRK activation to MVA synthesis in the vicinity of the plasmalemma. Three nucleoporins (NUP85, NUP133, and NENA) localize at the nuclear pore complex, but their role in signal transduction as well as their functional connection with the previous set of CSP proteins remains unclear. The final stretch of the CSP localizes to the nucleoplasm: here, repeated oscillations in Ca^{2+} concentration (spiking) are generated with the contribution of MCA8 (a nuclear envelope-bound ATP-powered Ca^{2+} pump) and the potassium channels encoded by *CASTOR* and *POLLUX* genes. Such Ca^{2+}-mediated signals are believed to activate the nuclear kinase CCaMK. In turn, CYCLOPS phosphorylation by CCaMK preludes to the regulation of gene expression. **(C)** Presents a proposal model of receptor complex assortment and CSP protein role in two separate pathways for the transduction of Nod factors or chito-tetraose in legume root hairs and atrichoblasts, respectively.

(*Continued*)

FIGURE 1 | Continued

Localized on the plasma membrane of root hairs (left), the extracellular LysM domain of NFR1 and NFR5 directly bind Nod factors (Broghammer et al., 2012). NFR1 and NFR5 form a complex with SYMRK (Ried et al., 2014) and HMGR1 (Kevei et al., 2007). MVA, produced upon HMGR1 activation (Venkateshwaran et al., 2015) is small enough to diffuse through the nuclear pore complex without the involvement of nucleoporins (NUPs); nevertheless, the inclusion of three NUPs in the CSP opens the possibility that at least one additional unknown protein **(A)** is involved, which could be activated as a consequence of MVA production and translocated to the nucleus through the action of NUPs. Ca^{2+} spiking activation in the nucleoplasm is generated by the recursive release of Ca^{2+} through unidentified channel proteins **(C)** in the nuclear envelope, combined with the continuous action of ATP-powered Ca^{2+} pumps like MCA8 (Engstrom et al., 2002; Capoen et al., 2011). To consider a minimal number of unidentified proteins, we can assume Ca^{2+} channels are directly activated by nuclear-imported A. CASTOR/POLLUX has been proposed to act in concert with Ca^{2+} channels (Oldroyd, 2013). The resulting Ca^{2+} spiking activates CCaMK through a RLS-specific conformational change requiring calmodulin (Shimoda et al., 2012; Poovaiah et al., 2013), which then modulates the activity of gene expression regulators, allowing the establishment of RLS (Oldroyd, 2013). A parallel pathway acts in atrichoblasts (right), where chito-tetraose (CO4) released by glomeromycetes is recognised by a complex possibly including CERK1 (Miyata et al., 2014), SYMRK, and HMGR1. Also in this case an additional protein **(B)** is proposed to be activated by MVA. B is then translocated to the nucleoplasm, where it activates Ca^{2+} spiking signals with a distinct, AM-specific signature (Kosuta et al., 2008; Russo et al., 2013). Consequently, CCaMK is activated in an AM-specific mode (Shimoda et al., 2012; Poovaiah et al., 2013), and its activity regulates AM-specific gene expression.

HMGR1 (Madsen et al., 2003; Kevei et al., 2007; Lefebvre et al., 2010). As a consequence of HMGR1 activation, mevalonate production can also be localized in the vicinity of the cytoplasmic face of the plasma membrane (Venkateshwaran et al., 2015).

A second cluster of CSP proteins is located in the nuclear pore complex: it is composed of three nucleoporins (NUP133, NUP85, and NENA), each of which is responsible for a strong symbiotic phenotype (Kanamori et al., 2006; Saito et al., 2007; Groth et al., 2010). This suggests that the nuclear pore must be controlling the import of an unknown key CSP component. This is not likely to be mevalonate, whose small size should allow nucleoporin-independent diffusion across the nuclear pore (Evans et al., 2004).

Also bound to the nuclear envelope are the ATP-powered Ca^{2+} pump MCA8 (Capoen et al., 2011) and the cationic channel encoded by CASTOR and POLLUX genes in *L. japonicus* (Ané et al., 2004; Charpentier et al., 2008). Both proteins contribute to the intense oscillations in nuclear Ca^{2+} concentration (spiking) that are observed during both AM and RLS establishment (Ehrhardt et al., 1996; Kosuta et al., 2008; Chabaud et al., 2011; Sieberer et al., 2012). In detail, so far unidentified channels are hypothesized to release Ca^{2+} from the nuclear envelope lumen. This release is sustained by the opposite flow of potassium ions (K^+) through CASTOR/POLLUX, in a charge compensation mechanism (Parniske, 2008; Venkateshwaran et al., 2012); concomitant MCA8 activity contributes to the re-establishment of basic nuclear Ca^{2+} concentration at the end of each peak. Intriguingly, the nuclear pore has been proposed to play a role in flipping membrane-bound proteins from the outer to the inner nuclear membrane (Capoen et al., 2011), shedding light on the possible function of CSP nucleoporins in the targeting of CASTOR, POLLUX, MCA8, and Ca^{2+} channels.

The last group of CSP proteins whose direct interaction has been demonstrated resides in the nucleoplasm: Ca^{2+} spiking is supposed to activate CCaMK with the help of calmodulin, through a complex conformational change (Shimoda et al., 2012; Miller et al., 2013; Poovaiah et al., 2013); the enzyme can thus phosphorylate CYCLOPS, a CCaMK-interacting protein (Yano et al., 2008). Phosphorylated CYCLOPS regulates gene expression either directly, as in the case of the NIN promoter (Singh et al., 2014) or through the action of other transcription factors like NSP1, NSP2, and RAM1 (Oldroyd, 2013).

This topological review of the CSP highlights the gaps that uncouple each set of proteins from the next one: with so much missing information, depicting signal transduction along the CSP requires some extrapolation.

On the front of secondary messengers, reactive species of oxygen (Salzer et al., 1999; Pauly et al., 2006) and nitrogen (Meilhoc et al., 2010; Calcagno et al., 2012; Zhang et al., 2013) have also been associated with RLS and AM signaling, although their role in relation to the CSP remains unclear. Furthermore, growing evidence hints at the existence of symbiotic signal transduction pathways that bypass or run parallel to the CSP (Gutjahr et al., 2008, 2009; Bonfante and Requena, 2011), indicating that the plant's perception of rhizobia and glomeromycetes could rely on multiple signaling routes.

In this context, the information we are still missing will critically challenge the CSP hypothesis: new data will either demonstrate that the CSP is indeed a pathway, or show that the remaining elements differ for each interaction, and what we had imagined as a straight line is rather a core of conserved, yet disconnected, protein functions.

Symbiotic

Even if the concept of symbiosis can be extended to any interaction between organisms that live together (De Bary, 1879), the CSP concept is mostly restricted to RLS and AM, where the requirement for CSP genes was initially described (Stougaard, 2001; Kistner et al., 2005). Nevertheless, a third symbiosis also requires *SYMRK* (Gherbi et al., 2008), nuclear Ca^{2+} signals (Granqvist et al., 2015; Chabaud et al., 2016) and *CCaMK* (Svistoonoff et al., 2013): nitrogen-fixing actinorrhizas (**Supplementary Figure S1**).

In addition, non-symbiotic interactions have been shown to depend on CSP members. Parasitic interactions with root-knot nematodes involve *NFR1*, *NFR5*, and *SYMRK* (Weerasinghe et al., 2005). An intriguing role for *SYMRK* and *CCaMK* was also described during the colonization of *Pisum sativum* by the parasitic plant *Orobanche crenata* (Fernández-Aparicio et al., 2009): in this case *symrk* and *ccamk* mutants were more severely infected, indicating an unprecedented role for these CSP genes in inhibiting (rather than allowing) root colonization.

Furthermore, a key role in the regulation of gene expression has been demonstrated for *M. truncatula CCaMK* during interaction with the rhizobacterium *Pseudomonas fluorescens* (Sanchez et al., 2005).

The infection of *M. truncatula* by the pathogens *Phytophthora palmivora* (Huisman et al., 2015; Rey et al., 2015), *Aphanomyces euteiches,* and *Colletotrichum trifolii* (Rey et al., 2013) has been proposed to partially depend on Nod factor receptors, albeit the involvement of the CSP core was not highlighted. Nevertheless, *M. truncatula* mutants in *CCaMK* ortholog *DMI3* did not develop any cytoplasmic aggregation – a common defense response – upon *Phoma medicaginis* or *C. trifolii* attack (Genre et al., 2009), and displayed an anticipation of necrotrophic fungal growth.

Lastly, CSP homologs are found in mosses, Charophytes and Chlorophytes clades (Wang et al., 2010; Delaux et al., 2013b, 2015): the lack of known naturally occurring symbiotic interactions in such organisms (Field et al., 2015), and the tight phylogenetic relationship between Charales and land plants, might suggest the existence of conserved non-symbiotic functions for CSP proteins throughout the plant clade.

Overall, as research explores additional aspects of plant interactions, the functions of CSP genes appear to be growing in diversity, and extending well beyond the range of symbioses (**Supplementary Figure S1**).

Common

There is no question CSP genes are essential for both legume endosymbiosis, but can we conclude that the signal transduction process involving CSP proteins is shared? Over the years, such a hypothesis has raised several questions (Bonfante and Requena, 2011), the most striking being: how can one pathway discern two signals, and activate distinct sets of downstream responses?

The foundations of the CSP hypothesis are built on the categorical results of forward genetic approaches: mutant phenotyping has shown that each CSP protein is indispensable for both RLS and AM establishment (Kistner et al., 2005). Nevertheless, signal transduction is not just a matter of protein presence/absence; finer aspects, such as the intensity of enzyme activation in response to each symbiont, could not be revealed by genetic investigations. In fact, recent biochemical analyses indicate that calmodulin binding is dispensable for CCaMK activation during mycorrhization, but essential for nodulation, suggesting that CCaMK is activated in two distinct modes during the perception of rhizobial versus glomeromycotan signals (Shimoda et al., 2012; Poovaiah et al., 2013). Along the same lines, evidence is accumulating in favor of different 'signatures' in the Ca^{2+}-mediated signals, which can be responsible for such differential activation of CCaMK at the core of the CSP (Kosuta et al., 2008; Russo et al., 2013).

These studies strongly suggest that the same molecular actors can be playing different biochemical scripts in each interaction. The case of the GRAS-type transcription factor NSP2 (Kaló et al., 2005) is enlightening: NSP2 has been proposed to form a transcription regulator complex with other RLS- or AM-specific factors (NSP1 and RAM1, respectively); it has therefore been described as a CSP protein (Oldroyd, 2013). Nevertheless, *in vitro* interaction experiments support a model where NSP2 performs distinct symbiotic functions, depending on its interactors (Maillet et al., 2011; Gobbato et al., 2012, 2013; Lauressergues et al., 2012).

Importantly, cellular investigations on model legumes have demonstrated that rhizobia preferentially attach to and penetrate through root hair cells (Gage, 2004), whereas AM fungi contact and enter non-hair cells (atrichoblasts; Genre et al., 2005). Consequently, the study of early plant responses to rhizobial and glomeromycotan signaling only has a biological meaning when this specialization in root epidermal cell types is taken into account: while one pathway including all the necessary proteins could theoretically be designed based on legume genomes, it is likely that each cell type complements the expression of CSP genes with a set AM- or RLS-specific proteins, assembling two spatially and functionally distinct pathways (**Figure 1C**).

PROVIDING CONTEXT TO CSP PROTEINS

Even if legumes remain the most important model plants for the study of symbiotic interactions, a growing number of publications is providing significant advancements on AM signal perception in non-legumes (Gutjahr et al., 2009; Miyata et al., 2014; Sun et al., 2015; Zhang et al., 2015).

A particular interest has recently been raised by rice mutants in *CERK1* (Miya et al., 2007; Sánchez-Vallet et al., 2015), a well-characterized LysM-type chitin receptor involved in defense responses: *cerk1* mutants display a strong mycorrhizal phenotype, blocking AM hyphae at the surface of the root epidermis (Miyata et al., 2014). RNAi-based knock-down of *CERK1* also induced a significant reduction in AM colonization (Zhang et al., 2015). Involving chitin receptors in symbiotic signaling is very intriguing: chitin-based molecules secreted by AM fungi activate the CSP and downstream responses (Maillet et al., 2011; Czaja et al., 2012; Genre et al., 2013; Giovannetti et al., 2015; Sun et al., 2015). Such Myc factors include lipo-chito-oligosaccharides (LCOs), structurally similar to Nod factors (Maillet et al., 2011), and short undecorated chito-oligosaccharides, or COs (Genre et al., 2013). LCOs appear to be particularly active in legumes, where they trigger a range of responses that are generally common to Nod Factor perception, such as lateral root formation or gene regulation (Maillet et al., 2011; Czaja et al., 2012; Sun et al., 2015), suggesting that some degree of overlap exists between legume perception of Nod and Myc factors. By contrast COs trigger CSP-dependent Ca^{2+} spiking in both legumes and non-legumes at concentrations as low as 10^{-8} M (Genre et al., 2013; Sun et al., 2015) and can be considered universal pre-symbiotic AM signals (Sun et al., 2015; Zhang et al., 2015).

Overall, a model is emerging where the assembly of different membrane-residing receptor complexes (Oldroyd, 2013; Liang et al., 2014; Gobbato, 2015; Limpens et al., 2015; Shinya et al., 2015) depends on which receptors are expressed by each cell type and possibly which signaling molecule is present. In the case of defense responses to pathogenic fungi, CERK1/CERK1 (as in *Arabidopsis*) or CERK1/CEBIP receptor dimers (as in

rice) are hypothesized to bind long oligomers such as chito-octaose (CO8), half of the CO8 molecule fitting in to each receptor's LysM domain (Wan et al., 2008; Shimizu et al., 2010; Liu et al., 2012; Shinya et al., 2015). The perception of shorter COs such as chito-tetraose could rather rely on monomeric receptors (Miyata et al., 2014; Shinya et al., 2015). In legumes, a further level of specificity results in their ability to respond to COs as well as LCOs (such as Nod factors), which fits with the proliferation of legume LysM and LysM-related receptor families through gene duplication events (Zhang et al., 2007).

It is reasonable to speculate that each receptor complex interacts with a corresponding set of cytoplasmic proteins (Asai et al., 2002). At present, information is very limited, but in analogy to SYMRK interaction with HMGR1, we can hypothesize that other proteins associate with each receptor, generating a signal-specific composition in the cytoplasmic moiety of the signaling complex. MAP kinases (Chen et al., 2012) may be playing a role; sensitivity to mevalonate appears as a stringent requisite for the selection of other candidates.

In such a scenario, CSP proteins would represent a conserved backbone in distinct AM and RLS signaling pathways that legumes localize in different cell types: atrichoblasts or root hairs, respectively. Symbiont-specific signal transduction and downstream responses would rather depend on the specific subsets of proteins that act in association with CSP members in each cell, as hypothesized in the schemes of **Figure 1C**.

CONCLUSION

The history of life is rich in examples of so-called evolutionary tinkering: processes in evolution where new functions are obtained through small modifications of a pre-existing biological mechanism. Evolutionary tinkering consists of two opposite processes: on the one hand, gene duplication and neo-functionalization produce new proteins for the novel functions; on the other hand, all those genes that play the same function in both conditions are conserved. The hypothesis that RLS has evolved by redirecting AM responses toward bacterial accommodation is widely accepted and explains the numerous similarities that exist between these two interactions (Bonfante and Genre, 2008; Parniske, 2008). In particular, several features of plant cell restructuring (e.g., symbiotic interface biogenesis) are strikingly similar (Parniske, 2008). In this context, conserved genes should be much more numerous than just the few currently listed in the CSP; not surprisingly, *common symbiotic* genes have already been identified which do not fit into the *pathway*. To mention just a few examples, VAPYRIN (Pumplin et al., 2010) is a partially characterized protein featuring a Major Sperm Protein domain and several ankyrin repeats, likely involved in membrane dynamics; CERBERUS (Yano et al., 2009) is an E3 ubiquitin ligase. Both are required for symbiont accommodation, but more likely in cellular remodeling and interface development than in signaling. On the same line, a group of SNARE proteins belonging to the VAMP72 family has been involved in symbiotic interface assembly for both interactions (Ivanov et al., 2012). It is reasonable to conclude that CSP proteins belong to this array of conserved genes, and act in a complex mix of common and interaction-specific processes, required for the establishment of each symbiosis.

Further indications may come from detailed analyses of AM phenotypes in available mutants. The legume transcription factor *NSP1* was originally described as indispensable for rhizobial, but not fungal, colonization (Catoira et al., 2000; Smit et al., 2005). Nevertheless, a recent study showed that *nsp1* mutation significantly slows down AM infection (Delaux et al., 2013a). Similarly, a partial involvement of Nod factor receptors *NFR1* and *NFR5* has been described in the induction of common symbiotic responses such as root branching and gene regulation (Maillet et al., 2011; Czaja et al., 2012; Zhang et al., 2015). Such studies suggest that fine phenotypic analyses, reaching cellular and molecular detail, can be crucial for completing the picture.

In conclusion, the CSP lives on as a precious genetic reference in our simplistic models of plant-microbe signaling. Nevertheless, we have sufficient clues to suspect the existence of a more complex scenario of CSP protein localization and activity. Studying symbiotic signaling in non-legumes appears today as a very promising approach to address such questions (Watts-Williams and Cavagnaro, 2015): working on a biological system that intrinsically excludes the cross-talk of two evolutionarily related interactions such as RLS and AM will deliver crucial knowledge that can then be applied to decipher the multiple symbiotic system of legumes.

AUTHOR CONTRIBUTIONS

AG conceived the general layout of the manuscript and was primarily involved in text writing and figure preparation. GR contributed to text writing, and gave a major contribution to literature search and figure elaboration. Both AG and GR contributed to critical literature reviewing and model elaboration.

ACKNOWLEDGMENTS

The authors are very grateful to David Barker and Mireille Chabaud for fruitful discussion; to Paola Bonfante for her constructive criticism of the manuscript; and to Dan Chamberlain for his revision of the English language.

SUPPLEMENTARY MATERIAL

The Supplementary Material for this article can be found online at: http://journal.frontiersin.org/article/10.3389/fpls.2016.00096

FIGURE S1 | The role of CSP proteins in different plant interactions. CSP and CSP-related proteins have been shown to play several roles beyond RLS and AM. SYMRK is required for the establishment of actinorhizal symbiosis and the parasitic interaction with root knot nematodes; furthermore it has been implicated in host defense against root colonization by parasitic plants. *CCaMK* is also necessary for actinorhizal symbiosis and defense responses to parasitic plants; in addition, it has a role in responses to pathogenic fungi. Beside CSP proteins, a

few receptors that act upstream of the CSP have also been assigned with multiple roles. Nod factor receptors *NFR1* and *NFR5* are required for the establishment of actinorhizas and root knot nematode parasitism, and both have also been assigned a limited role in AM signaling. Finally, the chitin receptor *CERK1* is required for both defense responses to pathogenic fungi and the accommodation of AM fungi. Overall, a survey of the literature data suggests that CSP and CSP-related genes have a diverse spectrum of functions in several plant interactions.

REFERENCES

Ané, J. M., Kiss, G. B., Riely, B. K., Penmetsa, R. V., Oldroyd, G. E. D., Ayax, C., et al. (2004). *Medicago truncatula* DMI1 required for bacterial and fungal symbioses in legumes. *Science* 303, 1364–1367. doi: 10.1126/science.1092986

Asai, T., Tena, G., Plotnikova, J., Willmann, M. R., Chiu, W. L., Gomez-Gomez, L., et al. (2002). MAP kinase signalling cascade in *Arabidopsis* innate immunity. *Nature* 415, 977–983. doi: 10.1038/415977a

Bonfante, P., and Genre, A. (2008). Plants and arbuscular mycorrhizal fungi: an evolutionary-developmental perspective. *Trends Plant Sci.* 13, 492–498. doi: 10.1016/j.tplants.2008.07.001

Bonfante, P., and Requena, N. (2011). Dating in the dark: how roots respond to fungal signals to establish arbuscular mycorrhizal symbiosis. *Curr. Opin. Plant Biol.* 14, 451–457. doi: 10.1016/j.pbi.2011.03.014

Broghammer, A., Krusell, L., Blaise, M., Sauer, J., Sullivan, J. T., Maolanon, N., et al. (2012). Legume receptors perceive the rhizobial lipochitin oligosaccharide signal molecules by direct binding. *Proc. Natl. Acad. Sci. U.S.A.* 109, 13859–13864. doi: 10.1073/pnas.1205171109

Calcagno, C., Novero, M., Genre, A., Bonfante, P., and Lanfranco, L. (2012). The exudate from an arbuscular mycorrhizal fungus induces nitric oxide accumulation in *Medicago truncatula* roots. *Mycorrhiza* 22, 259–269. doi: 10.1007/s00572-011-0400-4

Capoen, W., Sun, J., Wysham, D., Otegui, M. S., Venkateshwaran, M., Hirsch, S., et al. (2011). Nuclear membranes control symbiotic calcium signaling of legumes. *Proc. Natl. Acad. Sci. U.S.A.* 108, 14348–14353. doi: 10.1073/pnas.1107912108

Catoira, R., Galera, C., de Billy, F., Penmetsa, R. V., Journet, E. P., Maillet, F., et al. (2000). Four genes of *Medicago truncatula* controlling components of a nod factor transduction pathway. *Plant Cell* 12, 1647–1666. doi: 10.1105/tpc.12.9.1647

Chabaud, M., Genre, A., Sieberer, B. J., Faccio, A., Fournier, J., Novero, M., et al. (2011). Arbuscular mycorrhizal hyphopodia and germinated spore exudates trigger Ca^{2+} spiking in the legume and nonlegume root epidermis. *New Phytol.* 189, 347–355. doi: 10.1111/j.1469-8137.2010.03464.x

Chabaud, M., Gherbi, H., Pirolles, E., Vaissayre, V., Fournier, J., Moukouanga, D., et al. (2016). Chitinase-resistant hydrophilic symbiotic factors secreted by Frankia activate both Ca^{2+} spiking and NIN gene expression in the actinorhizal plant *Casuarina glauca*. *New Phytol.* 209, 86–93. doi: 10.1111/nph.13732

Charpentier, M., Bredemeier, R., Wanner, G., Takeda, N., Schleiff, E., and Parniske, M. (2008). *Lotus japonicus* CASTOR and POLLUX are ion channels essential for perinuclear calcium spiking in legume root endosymbiosis. *Plant Cell* 20, 3467–3479. doi: 10.1105/tpc.108.063255

Chen, T., Zhu, H., Ke, D., Cai, K., Wang, C., Gou, H., et al. (2012). A MAP kinase kinase interacts with SymRK and regulates nodule organogenesis in *Lotus japonicus*. *Plant Cell* 24, 823–838. doi: 10.1105/tpc.112.095984

Czaja, L. F., Hogekamp, C., Lamm, P., Maillet, F., Martinez, E. A., Samain, E., et al. (2012). Transcriptional responses toward diffusible signals from symbiotic microbes reveal MtNFP- and MtDMI3-dependent reprogramming of host gene expression by arbuscular mycorrhizal fungal lipo-chitooligosaccharides. *Plant Physiol.* 159, 1671–1685. doi: 10.1104/pp.112.195990

De Bary, A. (1879). *Die Erscheinung der Symbiose*. Strassburg: Verlag von Karl J. Trubner.

Delaux, P. M., Bécard, G., and Combier, J. P. (2013a). NSP1 is a component of the Myc signaling pathway. *New Phytol.* 199, 59–65. doi: 10.1111/nph.12340

Delaux, P. M., Séjalon-Delmas, N., Bécard, G., and Ané, J. M. (2013b). Evolution of the plant-microbe symbiotic "toolkit." *Trends Plant Sci.* 18, 298–304. doi: 10.1016/j.tplants.2013.01.008

Delaux, P. M., Radhakrishnan, G. V., Jayaraman, D., Cheema, J., Malbreil, M., Volkening, J. D., et al. (2015). Algal ancestor of land plants was preadapted for symbiosis. *Proc. Natl. Acad. Sci. U.S.A* 112, 13390–13395. doi: 10.1073/pnas.1515426112

Ehrhardt, D. W., Wais, R., and Long, S. R. (1996). Calcium spiking in plant root hairs responding to Rhizobium nodulation signals. *Cell* 85, 673–681. doi: 10.1016/S0092-8674(00)81234-9

Engstrom, E. M., Ehrhardt, D. W., Mitra, R. M., and Long, S. R. (2002). Pharmacological analysis of nod factor-induced calcium spiking in *Medicago truncatula*. Evidence for the requirement of type IIA calcium pumps and phosphoinositide signaling. *Plant Physiol.* 128, 1390–1401. doi: 10.1104/pp.010691

Evans, D. E., Hutchison, C. J., and Bryant, J. A. (2004). *The Nuclear Envelope*. Oxford: Taylor and Francis Bios.

Fernández-Aparicio, M., Rispail, N., Prats, E., Morandi, D., García-Garrido, J. M., Dumas-Gaudot, E., et al. (2009). Parasitic plant infection is partially controlled through the symbiotic pathways. *Weed Res.* 50, 76–82. doi: 10.1111/j.1365-3180.2009.00749.x

Field, K. J., Pressel, S., Duckett, J. G., Rimington, W. R., and Bidartondo, M. I. (2015). Symbiotic options for the conquest of land. *Trends Ecol. Evol.* 30, 477–486. doi: 10.1016/j.tree.2015.05.007

Fournier, J., Teillet, A., Chabaud, M., Ivanov, S., Genre, A., Limpens, E., et al. (2015). Remodeling of the infection chamber prior to infection thread formation reveals a two-step mechanism for rhizobial entry into the host legume root hair. *Plant Physiol.* 167, 1233–1242. doi: 10.1104/pp.114.253302

Fournier, J., Timmers, A. C. J., Sieberer, B. J., Jauneau, A., Chabaud, M., and Barker, D. G. (2008). Mechanism of infection thread elongation in root hairs of *Medicago truncatula* and dynamic interplay with associated rhizobial colonization. *Plant Physiol.* 148, 1985–1995. doi: 10.1104/pp.108.125674

Gage, D. J. (2004). Infection and invasion of roots by symbiotic, nitrogen-fixing rhizobia during nodulation of temperate legumes. *Microbiol. Mol. Biol. Rev.* 68, 280–300. doi: 10.1128/MMBR.68.2.280-300.2004

Genre, A., Chabaud, M., Balzergue, C., Puech-Pagès, V., Novero, M., Rey, T., et al. (2013). Short-chain chitin oligomers from arbus- cular mycorrhizal fungi trigger nuclear Ca^{2+} spiking in *Medicago truncatula* roots and their production is enhanced by strigolactone. *New Phytol.* 198, 190–202. doi: 10.1111/nph.12146

Genre, A., Chabaud, M., Faccio, A., Barker, D. G., and Bonfante, P. (2008). Prepenetration apparatus assembly precedes and predicts the colonization patterns of arbuscular mycorrhizal fungus within the root cortex of both *Medicago truncatula* and *Daucus carota*. *Plant Cell* 20, 1407–1420. doi: 10.1105/tpc.108.059014

Genre, A., Chabaud, M., Timmers, T., Bonfante, P., and Barker, D. G. (2005). Arbuscular mycorrhizal fungi elicit a novel intracellular apparatus in *Medicago truncatula* root epidermal cells before infection. *Plant Cell* 17, 3489–3499. doi: 10.1105/tpc.105.035410

Genre, A., Ortu, G., Bertoldo, C., Martino, E., and Bonfante, P. (2009). Biotic and abiotic stimulation of root epidermal cells reveals common and specific responses to arbuscular mycorrhizal fungi. *Plant Physiol.* 149, 1424–1434. doi: 10.1104/pp.108.132225

Gherbi, H., Markmann, K., Svistoonoff, S., Estevan, J., Autran, D., Giczey, G., et al. (2008). SymRK defines a common genetic basis for plant root endosymbioses with arbuscular mycorrhiza fungi, rhizobia, and Frankia bacteria. *Proc. Natl. Acad. Sci. U.S.A.* 105, 4928–4932. doi: 10.1073/pnas.0710618105

Giovannetti, M., Mari, A., Novero, M., and Bonfante, P. (2015). Early *Lotus japonicus* root transcriptomic responses to symbiotic and pathogenic fungal exudates. *Front. Plant Sci.* 6:480. doi: 10.3389/fpls.2015.00480

Gobbato, E. (2015). Recent developments in arbuscular mycorrhizal signaling. *Curr. Opin. Plant Biol.* 26, 1–7. doi: 10.1016/j.pbi.2015.05.006

Gobbato, E., Marsh, J. F., Vernié, T., Wang, E., Maillet, F., Kim, J., et al. (2012). A GRAS-type transcription factor with a specific function in mycorrhizal signalling. *Curr. Biol.* 22, 2236–2241. doi: 10.1016/j.cub.2012.09.044

Gobbato, E., Wang, E., Higgins, G., Bano, S. A., Henry, C., Schultze, M., et al. (2013). RAM1 and RAM2 function and expression during arbuscular mycorrhizal symbiosis and *Aphanomyces euteiches* colonization. *Plant Signal. Behav.* 8:e26049. doi: 10.4161/psb.26049

Granqvist, E., Sun, J., den Camp, R., Pujic, P., Hill, L., Normand, P., et al. (2015). Bacterial-induced calcium oscillations are common to nitrogen-fixing associations of nodulating legumes and nonlegumes. *New Phytol.* 207, 551–558. doi: 10.1111/nph.13464

Groth, M., Takeda, N., Perry, J., Uchida, H., Dräxl, S., Brachmann, A., et al. (2010). NENA, a *Lotus japonicus* homolog of Sec13, is required for rhizodermal infection by arbuscular mycorrhiza fungi and rhizobia but dispensable for cortical endosymbiotic development. *Plant Cell* 22, 2509–2526. doi: 10.1105/tpc.109.069807

Gutjahr, C., Banba, M., Croset, V., An, K., Miyao, A., An, G., et al. (2008). Arbuscular mycorrhiza-specific signaling in rice transcends the common symbiosis signaling pathway. *Plant Cell* 20, 2989–3005. doi: 10.1105/tpc.108.062414

Gutjahr, C., Casieri, L., and Paszkowski, U. (2009). *Glomus intraradices* induces changes in root system architecture of rice independently of common symbiosis signaling. *New Phytol.* 182, 829–837. doi: 10.1111/j.1469-8137.2009.02839.x

Gutjahr, C., and Parniske, M. (2013). Cell and developmental biology of arbuscular mycorrhiza symbiosis. *Ann. Rev. Cell Dev. Biol.* 29, 593–617. doi: 10.1146/annurev-cellbio-101512-122413

Huisman, R., Bouwmeester, K., Brattinga, M., Govers, F., Bisseling, T., and Limpens, E. (2015). Haustorium formation in *Medicago truncatula* roots infected by *Phytophthora palmivora* does not involve the common endosymbiotic program shared by AM fungi and rhizobia. *Mol. Plant Microbe Interact.* 28, 1271–1280. doi: 10.1094/MPMI-06-15-0130-R

Ivanov, S., Fedorova, E. E., Limpens, E., De Mita, S., Genre, A., Bonfante, P., et al. (2012). Rhizobium-legume symbiosis shares an exocytotic pathway required for arbuscule formation. *Proc. Natl. Acad. Sci. U.S.A.* 109, 8316–8321. doi: 10.1073/pnas.1200407109

Kaló, P., Gleason, C., Edwards, A., Marsh, J., Mitra, R. M., Hirsch, S., et al. (2005). Nodulation signaling in legumes requires NSP2, a member of the GRAS family of transcriptional regulators. *Science* 308, 1786–1789. doi: 10.1126/science.1110951

Kanamori, N., Madsen, L. H., Radutoiu, S., Frantescu, M., Quistgaard, E. M., Miwa, H., et al. (2006). A nucleoporin is required for induction of Ca^{2+} spiking in legume nodule development and essential for rhizobial and fungal symbiosis. *Proc. Natl. Acad. Sci. U.S.A.* 103, 359–364. doi: 10.1073/pnas.0508883103

Kevei, Z., Lougnon, G., Mergaert, P., Horvath, G. V., Kereszt, A., Jayaraman, D., et al. (2007). 3-hydroxy-3-methylglutaryl coenzyme A reductase1 interacts with NORK and is crucial for nodulation in *Medicago truncatula*. *Plant Cell* 19, 3974–3989. doi: 10.1105/tpc.107.053975

Kistner, C., Winzer, T., Pitzschke, A., Mulder, L., Sato, S., Kaneko, T., et al. (2005). Seven *Lotus japonicus* genes required for transcriptional reprogramming of the root during fungal and bacterial symbiosis. *Plant Cell* 17, 2217–2229. doi: 10.1105/tpc.105.032714

Kosuta, S., Hazledine, S., Sun, J., Miwa, H., Morris, R. J., Downie, J. A., et al. (2008). Differential and chaotic calcium signatures in the symbiosis signaling pathway of legumes. *Proc. Natl. Acad. Sci. U.S.A.* 105, 9823–9828. doi: 10.1073/pnas.0803499105

Lauressergues, D., Delaux, P.-M., Formey, D., Lelandais-Brière, C., Fort, S., Cottaz, S., et al. (2012). The microRNA miR171h modulates arbuscular mycorrhizal colonization of *Medicago truncatula* by targeting SP2. *Plant J.* 72, 512–522. doi: 10.1111/j.1365-313X.2012.05099.x

Lefebvre, B., Timmers, T., Mbengue, M., Moreau, S., Hervé, C., Tóth, K., et al. (2010). A remorin protein interacts with symbiotic receptors and regulates bacterial infection. *Proc. Natl. Acad. Sci. U.S.A.* 107, 2343–2348. doi: 10.1073/pnas.0913320107

Levy, J., Bres, C., Geurts, R., Chalhoub, B., Kulikova, O., Duc, G., et al. (2004). A putative Ca^{2+} and calmodulin-dependent protein kinase required for bacterial and fungal symbioses. *Science* 303, 1361–1364. doi: 10.1126/science.1093038

Liang, Y., Tóth, K., Cao, Y., Tanaka, K., Espinoza, C., and Stacey, G. (2014). Lipochitooligosaccharide recognition: an ancient story. *New Phytol.* 204, 289–296. doi: 10.1111/nph.12898

Limpens, E., van Zeijl, A., and Geurts, R. (2015). Lipochitooligosaccharides modulate plant host immunity to enable endosymbioses. *Annu. Rev. Phytopathol.* 53, 311–334. doi: 10.1146/annurev-phyto-080614-120149

Lin, K., Limpens, E., Zhang, Z., Ivanov, S., Saunders, D. G. O., Desheng, M., et al. (2014). Single nucleus genome sequencing reveals high similarity among nuclei of an endomycorrhizal fungus. *PLoS Genet.* 10:e1004078. doi: 10.1371/journal.pgen.1004078

Liu, T., Liu, Z., Song, C., Hu, Y., Han, Z., She, J., et al. (2012). Chitin-induced dimerization activates a plant immune receptor. *Science* 336, 1160–1164. doi: 10.1126/science.1218867

Madsen, E. B., Madsen, L. H., Radutoiu, S., Olbryt, M., Rakwalska, M., Szczyglowski, K., et al. (2003). A receptor kinase gene of the LysM type is involved in legume perception of rhizobial signals. *Nature* 425, 637–640. doi: 10.1038/nature02045

Maillet, F., Poinsot, V., Andre, O., Puech-Pages, V., Haouy, A., Gueunier, M., et al. (2011). Fungal lipochitooligosaccharide symbiotic signals in arbuscular mycorrhiza. *Nature* 469, 58–63. doi: 10.1038/nature09622

Meilhoc, E., Cam, Y., Skapski, A., and Bruand, C. (2010). The response to nitric oxide of the nitrogen-fixing symbiont *Sinorhizobium meliloti*. *Mol. Plant Microbe Interact.* 23, 748–759. doi: 10.1094/MPMI-23-6-0748

Miller, J. B., Pratap, A., Miyahara, A., Zhou, L., Bornemann, S., Morris, R. J., et al. (2013). Calcium/Calmodulin-dependent protein kinase is negatively and positively regulated by calcium, providing a mechanism for decoding calcium responses during symbiosis signaling. *Plant Cell* 25, 5053–5066. doi: 10.1105/tpc.113.116921

Miya, A., Albert, P., Shinya, T., Desaki, Y., Ichimura, K., Shirasu, K., et al. (2007). CERK1, a LysM receptor kinase, is essential for chitin elicitor signaling in *Arabidopsis*. *Proc. Natl. Acad. Sci. U.S.A.* 104, 19613–19618. doi: 10.1073/pnas.0705147104

Miyata, K., Kozaki, T., Kouzai, Y., Ozawa, K., Ishii, K., Asamizu, E., et al. (2014). The bifunctional plant receptor, OsCERK1, regulates both chitin-triggered immunity and arbuscular mycorrhizal symbiosis in rice. *Plant Cell Physiol.* 55, 1864–1872. doi: 10.1093/pcp/pcu129

Oldroyd, G. E. D. (2013). Speak, friend, and enter: signalling systems that promote bene?cial symbiotic associations in plants. *Nat. Rev. Microbiol.* 11, 252–263. doi: 10.1038/nrmicro2990

Parniske, M. (2008). Arbuscular mycorrhiza: the mother of plant root endosymbioses. *Nat. Rev. Microbiol.* 6, 763–775. doi: 10.1038/nrmicro1987

Pauly, N., Pucciariello, C., Mandon, K., Innocenti, G., Jamet, A., Baudouin, E., et al. (2006). Reactive oxygen and nitrogen species and glutathione: key players in the legume–Rhizobium symbiosis. *J. Exp. Bot.* 57, 1769–1776. doi: 10.1093/jxb/erj184

Poovaiah, B. W., Du, L., Wang, H., and Yang, T. (2013). Recent advances in calcium/calmodulin-mediated signaling with an emphasis on plant: microbe interactions. *Plant Physiol.* 163, 531–542. doi: 10.1104/pp.113.220780

Pumplin, N., Mondo, S. J., Topp, S., Starker, C. G., Gantt, J. S., and Harrison, M. J. (2010). *Medicago truncatula* Vapyrin is a novel protein required for arbuscular mycorrhizal symbiosis. *Plant J.* 61, 482–494. doi: 10.1111/j.1365-313X.2009.04072.x

Rey, T., Chatterjee, A., Buttay, M., Toulotte, J., and Schornack, S. (2015). *Medicago truncatula* symbiosis mutants affected in the interaction with a biotrophic root pathogen. *New Phytol.* 206, 497–500. doi: 10.1111/nph.13233

Rey, T., Nars, A., Bonhomme, M., Bottin, A., Huguet, S., Balzergue, S., et al. (2013). NFP, a LysM protein controlling Nod factor perception, also intervenes in *Medicago truncatula* resistance to pathogens. *New Phytol.* 198, 875–886. doi: 10.1111/nph.12198

Rich, M. K., Schorderet, M., and Reinhardt, D. (2014). The role of the cell wall compartment in mutualistic symbioses of plants. *Front. Plant. Sci.* 5:238. doi: 10.3389/fpls.2014.00238

Ried, M. K., Antolín-Llovera, M., and Parniske, M. (2014). Spontaneous symbiotic reprogramming of plant roots triggered by receptor-like kinases. *eLife* 3:e03891. doi: 10.7554/eLife.03891

Robledo, M., Jiménez-Zurdo, J., Velázquez, E., Trujillo, M. E., Zurdo-Piñeiro, J. L., Ramírez-Bahena, M. H., et al. (2008). Rhizobium cellulase $CelC_2$ is essential for primary symbiotic infection of legume host roots. *Proc. Natl. Acad. Sci. U.S.A.* 105, 7064–7069. doi: 10.1073/pnas.0802547105

Russo, G., Spinella, S., Sciacca, E., Bonfante, P., and Genre, A. (2013). Automated analysis of calcium spiking profiles with CaSA software: two case studies from root-microbe symbioses. *BMC Plant Biol.* 13:224. doi: 10.1186/1471-2229-13-224

Saito, K., Yoshikawa, M., Yano, K., Miwa, H., Uchida, H., Asamizu, E., et al. (2007). NUCLEOPORIN85 is required for calcium spiking, fungal and bacterial symbioses, and seed production in *Lotus japonicus*. *Plant Cell* 19, 610–624. doi: 10.1105/tpc.106.046938

Salzer, P., Corbiere, H., and Boller, T. (1999). Hydrogen peroxide accumulation in *Medicago truncatula* roots colonized by the arbuscular mycorrhiza-forming fungus *Glomus intraradices*. *Planta* 208, 319–325. doi: 10.1007/s004250050565

Sanchez, L., Weidmann, S., Arnould, C., Bernard, A. R., Gianinazzi, S., and Gianinazzi-Pearson, V. (2005). *Pseudomonas fluorescens* and *Glomus mosseae* trigger DMI3-dependent activation of genes related to a signal transduction pathway in roots of *Medicago truncatula*. *Plant Physiol.* 139, 1065–1077. doi: 10.1104/pp.105.067603

Sánchez-Vallet, A., Mesters, J. R., and Thomma, B. P. H. J. (2015). The battle for chitin recognition in plant-microbe interactions. *FEMS Microbiol. Rev.* 39, 171–183. doi: 10.1093/femsre/fuu003

Sandal, N., Petersen, T. R., Murray, J., Umehara, Y., Karas, B., Yano, K., et al. (2006). Genetics of symbiosis in *Lotus japonicus*: recombinant inbred lines, comparative genetic maps, and map position of 35 symbiotic loci. *Mol. Plant Microbe Interact.* 19, 80–91. doi: 10.1094/MPMI-19-0080

Schmitz, A. M., and Harrison, M. J. (2014). Signalling events during initiation of arbuscular mycorrhizal symbiosis. *J. Integr. Plant Biol.* 56, 250–261. doi: 10.1111/jipb.12155

Shimizu, T., Nakano, T., Takamizawa, D., Desaki, Y., Ishii-Minami, N., Nishizawa, Y., et al. (2010). Two LysM receptor molecules, CEBiP and OsCERK1, cooperatively regulate chitin elicitor signaling in rice. *Plant J.* 64, 204–214. doi: 10.1111/j.1365-313X.2010.04324.x

Shimoda, Y., Han, L., Yamazaki, T., Suzuki, R., Hayashi, M., and Imaizumi-Anraku, H. (2012). Rhizobial and fungal symbioses show different requirements for calmodulin binding to calcium calmodulin-dependent protein kinase in *Lotus japonicus*. *Plant Cell* 24, 304–321. doi: 10.1105/tpc.111.092197

Shinya, T., Nakagawa, T., Kaku, H., and Shibuya, N. (2015). Chitin-mediated plant–fungal hiding and handshaking. *Curr. Opin. Plant Biol.* 26, 64–71. doi: 10.1016/j.pbi.2015.05.032

Sieberer, B. J., Chabaud, M., Fournier, J., Timmers, A. C., and Barker, D. G. (2012). A switch in Ca^{2+} spiking signature is concomitant with endosymbiotic microbe entry into cortical root cells of *Medicago truncatula*. *Plant J.* 69, 822–830. doi: 10.1111/j.1365-313X.2011.04834.x

Singh, S., Katzer, K., Lambert, J., Cerri, M., and Parniske, M. (2014). CYCLOPS, A DNA-Binding transcriptional activator, orchestrates symbiotic root nodule development. *Cell Host Microbe* 15, 139–152. doi: 10.1016/j.chom.2014.01.011

Smit, P., Raedts, J., Portyanko, V., Debellé, F., Gough, C., Bisseling, T., et al. (2005). NSP1 of the GRAS protein family is essential for rhizobial Nod factor-induced transcription. *Science* 308, 1789–1791. doi: 10.1126/science.1111025

Stougaard, J. (2001). Genetics and genomics of root symbiosis. *Curr. Opin. Plant Biol.* 4, 328–335. doi: 10.1016/S1369-5266(00)00181-3

Sun, J., Miller, J. B., Granqvist, E., Wiley-Kalil, A., Gobbato, E., Maillet, F., et al. (2015). Activation of symbiosis signaling by arbuscular mycorrhizal fungi in legumes and rice. *Plant Cell* 27, 823–838. doi: 10.1105/tpc.114.131326

Svistoonoff, S., Benabdoun, F. M., Nambiar-Veetil, M., Imanishi, L., Vaissayre, V., Cesari, S., et al. (2013). The independent acquisition of plant root nitrogen-fixing symbiosis in Fabids recruited the same genetic pathway for nodule organogenesis. *PLoS ONE* 8:e64515. doi: 10.1371/journal.pone.0064515

Tisserant, E., Malbreil, M., Kuo, A., Kohlera, A., Symeonidid, A., Balestrini, R., et al. (2013). Genome of an arbuscular mycorrhizal fungus provides insight into the oldest plant symbiosis. *Proc. Natl. Acad. Sci. U.S.A.* 110, 20117–20122. doi: 10.1073/pnas.1313452110

Venkateshwaran, M., Cosme, A., Han, L., Banba, M., Satyshur, K. A., Schleiff, E., et al. (2012). The recent evolution of a symbiotic ion channel in the legume family altered ion conductance and improved functionality in calcium signaling. *Plant Cell* 24, 2528–2545. doi: 10.1105/tpc.112.098475

Venkateshwaran, M., Jayaraman, D., Chabaud, M., Genre, A., Balloon, A. J., Maeda, J., et al. (2015). A role for the mevalonate pathway in early plant symbiotic signaling. *Proc. Natl. Acad. Sci. U.S.A.* 112, 9781–9786. doi: 10.1073/pnas.1413762112

Wan, J., Zhang, X.-C., and Stacey, G. (2008). Chitin signaling and plant disease resistance. *Plant Signal. Behav.* 3, 831–833. doi: 10.4161/psb.3.10.5916

Wang, B., Yeun, L. H., Xue, J. Y., Liu, Y., Ané, J.-M., and Qiu, Y. L. (2010). Presence of three mycorrhizal genes in the common ancestor of land plants suggests a key role of mycorrhizas in the colonization of land by plants. *New Phytol.* 186, 514–525. doi: 10.1111/j.1469-8137.2009.03137.x

Watts-Williams, S. J., and Cavagnaro, T. R. (2015). Using mycorrhiza-defective mutant genotypes of non-legume plant species to study the formation and functioning of arbuscular mycorrhiza: a review. *Mycorrhiza* 25, 587–597. doi: 10.1007/s00572-015-0639-2

Weerasinghe, R. R., Bird, D., and Allen, N. S. (2005). Root-knot nematodes and bacterial Nod factors elicit common signal transduction events in *Lotus japonicus*. *Proc. Natl Acad. Sci. U.S.A.* 102, 3147–3152. doi: 10.1073/pnas.0407926102

Yano, K., Shibata, S., Chen, W. L., Sato, S., Kaneko, T., Jurkiewicz, A., et al. (2009). CERBERUS, a novel U-box protein containing WD-40 repeats, is required for formation of the infection thread and nodule development in the legume-Rhizobium symbiosis. *Plant J.* 60, 168–180. doi: 10.1111/j.1365-313X.2009.03943.x

Yano, K., Yoshida, S., Muller, J., Singh, S., Banba, M., Vickers, K., et al. (2008). CYCLOPS, a mediator of symbiotic intracellular accommodation. *Proc. Natl. Acad. Sci. U.S.A.* 105, 20540–20545. doi: 10.1073/pnas.0806858105

Zhang, R.-Q., Zhu, H.-H., Zhao, H.-Q., and Yao, Q. (2013). Arbuscular mycorrhizal fungal inoculation increases phenolic synthesis in clover roots via hydrogen peroxide, salicylic acid and nitric oxide signaling pathways. *J. Plant Physiol.* 170, 74–79. doi: 10.1016/j.jplph.2012.08.022

Zhang, X., Dong, W., Sun, J., Feng, F., Deng, Y., He, Z., et al. (2015). The receptor kinase CERK1 has dual functions in symbiosis and immunity signalling. *Plant J.* 81, 258–267. doi: 10.1111/tpj.12723

Zhang, X. C., Wu, X., Findley, S., Wan, J., Libault, M., Nguyen, H. T., et al. (2007). Molecular evolution of lysin motif-type receptor-like kinases in plants. *Plant Physiol.* 144, 623–636. doi: 10.1104/pp.107.097097

Conflict of Interest Statement: The authors declare that the research was conducted in the absence of any commercial or financial relationships that could be construed as a potential conflict of interest.

frontiers in Plant Science

REVIEW
published: 16 February 2016
doi: 10.3389/fpls.2016.00170

How Phytohormones Shape Interactions between Plants and the Soil-Borne Fungus *Fusarium oxysporum*

*Xiaotang Di, Frank L. W. Takken and Nico Tintor**

Molecular Plant Pathology, Faculty of Science, Swammerdam Institute for Life Sciences, University of Amsterdam, Amsterdam, Netherlands

Plants interact with a huge variety of soil microbes, ranging from pathogenic to mutualistic. The *Fusarium oxysporum* (*Fo*) species complex consists of ubiquitous soil inhabiting fungi that can infect and cause disease in over 120 different plant species including tomato, banana, cotton, and Arabidopsis. However, in many cases *Fo* colonization remains symptomless or even has beneficial effects on plant growth and/or stress tolerance. Also in pathogenic interactions a lengthy asymptomatic phase usually precedes disease development. All this indicates a sophisticated and fine-tuned interaction between *Fo* and its host. The molecular mechanisms underlying this balance are poorly understood. Plant hormone signaling networks emerge as key regulators of plant-microbe interactions in general. In this review we summarize the effects of the major phytohormones on the interaction between *Fo* and its diverse hosts. Generally, Salicylic Acid (SA) signaling reduces plant susceptibility, whereas Jasmonic Acid (JA), Ethylene (ET), Abscisic Acid (ABA), and auxin have complex effects, and are potentially hijacked by *Fo* for host manipulation. Finally, we discuss how plant hormones and *Fo* effectors balance the interaction from beneficial to pathogenic and *vice versa*.

Keywords: plant immunity, root pathogen, vascular wilt disease, effectors, endophyte

OPEN ACCESS

Edited by:
Ralph Panstruga, RWTH Aachen University, Germany

Reviewed by:
Kemal Kazan, Commonwealth Scientific and Industrial Research Organization, Australia
Louise Thatcher, Commonwealth Scientific and Industrial Research Organization, Australia

****Correspondence:***
Nico Tintor
N.Tintor@uva.nl

Specialty section:
This article was submitted to Plant Biotic Interactions, a section of the journal Frontiers in Plant Science

Received: *18 December 2015*
Accepted: *01 February 2016*
Published: *16 February 2016*

Citation:
Di X, Takken FLW and Tintor N (2016) How Phytohormones Shape Interactions between Plants and the Soil-Borne Fungus Fusarium oxysporum. Front. Plant Sci. 7:170. doi: 10.3389/fpls.2016.00170

INTRODUCTION

Fusarium oxysporum (*Fo*), one of the most relevant plant pathogens in global agriculture, is a widespread soil-borne fungus that invades roots and causes vascular wilt disease through colonization of xylem tissue (Tjamos and Beckman, 1989). Pathogenic *Fo* strains have been classified in more than 120 *formae speciales* (ff.spp.), which refers to a specific plant host, as a particular isolate typically produces disease only within a limited range of host species (Armstrong and Armstrong, 1981; Katan and Di Primo, 1999; **Table 1**). The infection process occurs following attachment to the root surface and subsequent penetration and colonization of the plant root and proliferation within the xylem vessels, leading to both local and systemic induction of a broad spectrum of plant defense responses (Berrocal-Lobo and Molina, 2008). Vascular browning, stunting, progressive wilting, and eventually plant death are typical disease symptoms in infected plants (Pietro et al., 2003; Agrios, 2005). In contrast to the potential of pathogenic *Fo* isolates to cause destructive plant diseases, many *Fo* strains are non-pathogenic and survive either saprophytically in the soil, as non-invasive colonizer of the rhizosphere, or as endophyte inside plant tissues (Kuldau and Yates, 2000; Edel-Hermann et al., 2015; Imazaki and Kadota, 2015). There is relatively little known about the lifestyle

TABLE 1 | *Fo* strains and their host described in the manuscript.

Abbreviations	*Formae speciales*	Host
Foal	*Fusarium oxysporum* f.sp. *albedinis*	Date palm
Focn	*Fusarium oxysporum* f.sp. *conglutinans*	Cabbage, Arabidopsis
Focb	*Fusarium oxysporum* f.sp. *cubense*	Banana
Fol	*Fusarium oxysporum* f.sp. *lycopersici*	Tomato
Fomt	*Fusarium oxysporum* f.sp. *matthioli*	Garden stock, Arabidopsis
Foph	*Fusarium oxysporum* f.sp. *phaseoli*	Common bean
Forp	*Fusarium oxysporum* f.sp. *raphani*	Radish, Arabidopsis
Forl	*Fusarium oxysporum* f.sp. *radicis-lycopersici*	Tomato

strategies of these inconspicuous endophytic strains, but some of them have been successfully employed in biocontrol strategies to combat plant diseases (Alabouvette et al., 2009; Vos et al., 2014).

Based on their lifestyle plant pathogenic fungi have been classified as biotrophs and necrotrophs. Biotrophic pathogens derive nutrients from living cells and deploy complex manipulation strategies to exploit their hosts while keeping them alive. In contrast, necrotrophic pathogens generally kill host cells and feed on their contents, resulting in extensive necrosis, tissue maceration, and plant rot (Glazebrook, 2005). A third type, termed hemi-biotrophs, displays both forms of nutrient acquisition, shifting from a biotrophic phase early in infection to necrotrophy at later stages. These pathogens typically produce toxins only at later stages of disease development in order to kill the host cells and to complete their life cycle on dead tissues (Horbach et al., 2011). The strategy of different pathogenic *Fo* strains can vary, but is usually best described by a hemi-biotrophic lifestyle (Michielse and Rep, 2009). Consistently, the *Fo* genomes show an expansion of genes that encode small, secreted proteins as well as cell-wall degrading enzymes, a feature shared by many hemi-biotrophic fungi (Lo Presti et al., 2015). Analysis of the xylem sap proteome from *Fol*-infected tomato plants identified numerous fungal proteins, termed Secreted in Xylem (Six) protein. For several Six proteins a contribution to virulence has been demonstrated, designating them as *bona fide* effectors (Takken and Rep, 2010; de Sain and Rep, 2015). However, their molecular mode of action and putative virulence targets remain unknown.

Phytohormones such as SA, JA, and ET, are known to play major roles in regulating plant defense responses against various pathogens. Generally, SA signaling triggers resistance against biotrophic and hemibiotrophic pathogens, whereas a combination of JA and ET signaling activates resistance against necrotrophic pathogens (Glazebrook, 2005). All these hormones are part of a larger signaling network that integrates environmental inputs and provides robustness against microbial manipulations (Katagiri and Tsuda, 2010; Pieterse et al., 2012). Additional hormones such as auxins, abscisic acid (ABA), gibberellic acids (GAs), and brassinosteroids (BRs) have also been reported to be involved in plant immunity and to fine-tune immunity and growth/development in plants (**Table 2**; Robert-Seilaniantz et al., 2011). In this review, we summarize the current knowledge on the role of phytohormones in plant disease and resistance triggered by different *Fo* ff.spp. to uncover how they shape the outcome of this widespread plant-fungal interaction.

SA PROMOTES RESISTANCE TO *FO*

Defense to biotrophic or hemibiotrophic pathogens is frequently mediated via SA signaling (Glazebrook, 2005). Arabidopsis plants with impaired SA accumulation showed increased susceptibility to *Fo* f.sp. *conglutinans* (*Focn*), but not to *Fo* f.sp. *raphani* (*Forp*) pointing to an isolate-specific role of SA-dependent defense responses (**Table 2**; Berrocal-Lobo and Molina, 2004; Diener and Ausubel, 2005; Trusov et al., 2009; Cole et al., 2014). Interestingly, mutants of the SA master-signaling regulator NPR1 showed wildtype (WT)-like susceptibility to *Focn* when 2–3-week-old soil grown plants were examined (Diener and Ausubel, 2005; Trusov et al., 2009). In contrast, when seedlings were infected on sterile agar plates *npr1* mutants displayed clearly enhanced susceptibility in comparison to WT (Berrocal-Lobo and Molina, 2004). SA accumulation and signaling is also influenced by the nucleo-cytoplasmic proteins PAD4 and EDS1. Soil-grown *pad4*, but not *eds1*, Arabidopsis showed increased susceptibility, whereas sterile grown *pad4* seedlings behaved like WT (Berrocal-Lobo and Molina, 2004; Diener and Ausubel, 2005; Trusov et al., 2009). Thus, the influence of SA signaling regulators depends on growth and inoculation conditions, plant age and the *Fo* isolate used. It appears that at least in soil-grown plants, SA enhances immunity to *Fo* via NPR1- and EDS1-independent pathways.

Consistent with its defense promoting role in Arabidopsis, exogenous application of SA, or synthetic SA analogs reduced *Fo* disease symptoms in a broad range of tested plants including tomato, common bean, date palm, and Arabidopsis (Edgar et al., 2006; Mandal et al., 2009; Dihazi et al., 2011; Xue et al., 2014). Furthermore, stable overexpression of Arabidopsis *NPR1* in tomato reduced disease symptoms as well as *Fo* f.sp. *lycopersici* (*Fol*) colonization of the stem (Lin et al., 2004). Similarly, preventing SA volatilization by silencing of a *Salicylic Acid Methyltransferase* reduced tomato susceptibility to *Fol*, however without significantly changing overall SA levels (Ament et al., 2010). How exactly Methyl-SA levels influence tomato defense to *Fol* remains to be addressed.

Despite a clear effect of SA on disease severity, global transcriptome profiling of Arabidopsis plants inoculated with *Focn* revealed relatively mild changes in the expression of known SA marker genes (Kidd et al., 2011; Zhu et al., 2013; Chen et al., 2014; Lyons et al., 2015). In fact, expression of *PR1* was even slightly down regulated both in roots and shoots of inoculated plants (Kidd et al., 2011). It is possible that activation of SA signaling occurs at rather late stages, which would be missed by the present studies that focus on the time points 1–6 days-post-inoculation (dpi). Alternatively, SA signaling could activate previously uncharacterized defense mechanisms, in line with the

TABLE 2 | Phytohormone mutants involved in the defense response against *Fo* infection.

Hormones	Mutants and transgenic lines	Process affected	Plant species	Susceptibility	References
SA	*NahG*	SA accumulation	Arabidopsis	Increased to *Focn* and *Fol*	Berrocal-Lobo and Molina, 2004; Diener and Ausubel, 2005; Thatcher et al., 2009; Trusov et al., 2009
	sid2-1	SA biosynthesis	Arabidopsis	Increased to *Focn* and *Fol*	Berrocal-Lobo and Molina, 2004; Diener and Ausubel, 2005
	eds1-1, eds1-22	SA signaling	Arabidopsis	Unaltered to *Focn* and *Fol*	Berrocal-Lobo and Molina, 2004; Trusov et al., 2009
	eds3, eds4, eds10	SA signaling	Arabidopsis	Increased to *Focn*	Diener and Ausubel, 2005
	eds5-1	SA biosynthesis	Arabidopsis	Increased to *Focn* and *Fol*	Berrocal-Lobo and Molina, 2004; Diener and Ausubel, 2005; Thatcher et al., 2009; Trusov et al., 2009
	pad4-1	SA signaling	Arabidopsis	Unaltered to *Focn* and *Fol*	Berrocal-Lobo and Molina, 2004
	pad4			Increased to *Focn*	Diener and Ausubel, 2005
	npr1-1	SA perception	Arabidopsis	Increased to *Focn* and *Fol*	Berrocal-Lobo and Molina, 2004
	npr1-1, npr1-2, npr1-3, npr1-4	SA perception	Arabidopsis	Unaltered to *Focn*	Diener and Ausubel, 2005; Trusov et al., 2009
	35S::NPR1	SA perception	Tomato	Reduced to *Fol*	Lin et al., 2004
	hpSAMT	SA metabolism	Tomato	Reduced to *Fol*	Ament et al., 2010
JA	*aos, fad3-2, opr3 fad7-1 fad8*	JA biosynthesis	Arabidopsis	Unaltered to *Focn*	Thatcher et al., 2009
	coi1, coi1-21	JA perception	Arabidopsis	Reduced to *Focn* and *Fomt*,	Thatcher et al., 2009; Trusov et al., 2009; Cole et al., 2014
	jar1-1	JA-Ile biosynthesis	Arabidopsis	Increased to *Focn* and *Fol*	Berrocal-Lobo and Molina, 2004; Trusov et al., 2009
	jar1-1			Unaltered to *Focn*	Thatcher et al., 2009
	jin1-9(atmyc2-3), jin1-9/myc2	JA signaling	Arabidopsis	Reduced to *Focn*	Anderson et al., 2004; Trusov et al., 2009
	35S::AtERF2	Positive regulator of MeJA response	Arabidopsis	Reduced to *Focn*	McGrath et al., 2005
	35S::AtERF4	Negative regulator of MeJA response	Arabidopsis	Increased to *Focn*	McGrath et al., 2005
	pft1-1, med8	JA signaling	Arabidopsis	Reduced to *Focn*	Kidd et al., 2009
	def1	JA biosynthesis	Tomato	Increased to *Forl* and *Fol*	Thaler et al., 2004; Kavroulakis et al., 2007
	jai1	JA perception (Coi1 homolog)	Tomato	Unaltered to *Fol*	Cole et al., 2014
ET	*ein2-1*	ET signaling	Arabidopsis	Reduced to *Focn* and *Forp*	Trusov et al., 2009; Cole et al., 2014
	ein2, etr1	ET signaling	Arabidopsis	Unaltered to *Focn*	Thatcher et al., 2009
	ein2-5	ET signaling	Arabidopsis	Increased to *Focn* and *Fol*	Berrocal-Lobo and Molina, 2004
	etr1-1	ET perception	Arabidopsis	Reduced to *Forp*	Pantelides et al., 2013
	35S::ERF1	ET signaling	Arabidopsis	Reduced to *Focn* and *Fol*	Berrocal-Lobo and Molina, 2004
	Never ripe	ET perception	Tomato	Reduced to *Fol*	Lund et al., 1998; Francia et al., 2007
	Never ripe, epinastic (epi1)	ET signaling	Tomato	Unaltered to *Forl*	Kavroulakis et al., 2007
ABA	*aba1-6, aba2-1*	ABA biosynthesis	Arabidopsis	Reduced to *Focn*	Anderson et al., 2004; Trusov et al., 2009
	aba2	ABA biosynthesis	Arabidopsis	Reduced to *Focn*	Cole et al., 2014
Auxin	*cyp79b2 cyp79b3, atr4/sur2, myb51/hig1, atr1, atr2d, pad3*	auxin biosynthesis	Arabidopsis	Unaltered to *Focn*	Kidd et al., 2011
	35S:ATR1/MYB34, atr1d, 35S:ATR2				
	axr1, axr2, axr3, sgt1b	auxin signaling	Arabidopsis	Reduced to *Focn*	Kidd et al., 2011
	tir1	auxin perception	Arabidopsis	Unaltered to *Focn*	Kidd et al., 2011
	arf1, arf2, arf1arf2	auxin signaling	Arabidopsis	Reduced to *Focn*	Lyons et al., 2015

observed NPR1- and EDS1-independency, especially in roots that are still little explored in terms of plant immunity (De Coninck et al., 2015). A third possibility has been suggested by Cole et al.: SA signaling could serve to dampen activation of JA responses that are promoting Arabidopsis infection by *Fo* (see below; Cole et al., 2014). Similar to Arabidopsis, transcriptome profiling of banana saplings infected with virulent and avirulent *Fo* f.sp. *cubense* (*Focb*) strains also failed to detect activation of typical SA marker genes, at least at the relatively early time points analyzed (Li et al., 2013). This led to the suggestion that in banana defense against *Fo* is mainly mediated via ET/JA signaling (Swarupa et al., 2014).

Taken together, SA signaling positively regulates defense to *Fo* in most tested plant species, which is in line with a predominantly hemi-biotrophic lifestyle of this pathogen (**Figure 1**). However, the exact mechanisms by which SA reduces susceptibility to *Fo* are not understood and yet unknown SA targets possibly play a role during defense to this root-infecting pathogen.

JA SIGNALING CAN PROMOTE EITHER RESISTANCE OR SUSCEPTIBILITY IN DIFFERENT HOST–*FO* INTERACTIONS

JA signaling generally mediates resistance to necrotrophic pathogens and insect herbivores. These two functions are exerted by two separate and often mutually antagonistic branches: the former is regulated by ERF transcription factors and is associated with ET signaling, whereas the latter requires MYC transcription factors and often involves ABA signaling (Pieterse et al., 2012).

In Arabidopsis JA biosynthesis is not critical for defense to *Focn* as a whole series of mutants with impaired JA accumulation behaved like WT plants (**Table 2**; Thatcher et al., 2009). Similarly, *jar1* mutants that are defective in synthesis of the bioactive JA–Isoleucine conjugate showed WT-like or slightly increased susceptibility (Thatcher et al., 2009; Trusov et al., 2009). Considering these results it was unexpected that mutations in *CORONATINE INSENSITIVE1* (*COI1*), an essential component of JA perception, strongly increased resistance to *Focn* (Thatcher et al., 2009; Trusov et al., 2009). Importantly, loss-of-function mutations in additional regulators of JA signaling that are involved in pathogen defense, such as the transcriptional regulators MYC2, PFT1, and LBD20, also resulted in increased resistance to *Focn* (Anderson et al., 2004; Kidd et al., 2009; Thatcher et al., 2012b). These findings indicate that JA signaling-capacity of the host is critical for *Fo* pathogenesis in Arabidopsis.

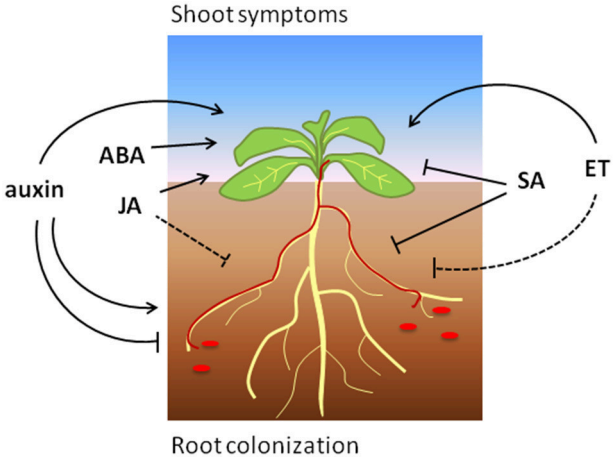

FIGURE 1 | The effects of phytohormone signaling on Arabidopsis root colonization and shoot symptoms induced by *Focn* (shown in red). Arrows and blunt ends indicate promotion and reduction, respectively. The dashed line indicates a presumed positive role of ET-signaling on (root) defense.

Hijacking the host JA signaling machinery is a common strategy employed by many (hemi-)biotrophic pathogens and often involves suppression of SA-dependent defense responses (Pieterse et al., 2012; Kazan and Lyons, 2014). However, COI1 promotes *Fo* infection in an SA-independent manner as *coi1 NahG* plants remain as resistant as *coi1* plants (Thatcher et al., 2009). This indicates that JA signaling supports *Fo* pathogenesis by mechanisms other than antagonizing SA responses. Grafting experiments demonstrated that expression of *COI1* in roots, but not in shoots, is required for *Fo* infection (Thatcher et al., 2009). Cole and co-workers observed reduced colonization of the vasculature in *coi1* plants pointing to a role of JA signaling at relatively early stages (Cole et al., 2014). Thatcher et al. detected similar levels of fungal biomass in WT and *coi1* shoots before the switch to necrotrophic growth, and hence concluded that *COI1* is predominantly required for triggering plant decay (Thatcher et al., 2009). These differences might be explained by the inoculation methods used: uprooting of plants before inoculation could have created additional entry sites leading to stronger vascular colonization (as observed in Thatcher et al., 2009). Nevertheless, the studies indicate that COI1 influences the interaction with *Fo* at several stages. Moreover, the finding that even strongly colonized *coi1* plants remain essentially symptomless reveals an uncoupling of colonization and plant disease symptoms (Thatcher et al., 2009).

Despite its strong effects on the interaction with *Fo*, it is not well-understood how the host JA signaling machinery is re-wired by the pathogen to promote disease. Cole and co-workers found that two Arabidopsis-infecting strains, *Focn* and f.sp. *matthioli* (*Fomt*) produce JA-isoleucin and JA-leucin conjugates in culture filtrates that induce senescence-like symptoms on Arabidopsis leaves in a COI1-dependent manner (Cole et al., 2014). However, it is not yet known if these fungal derived hormones are also generated during infection, and to what extent they contribute to virulence. Alternatively, *Fo* effectors could play a role in JA signaling manipulation as has been suggested for the effector SIX4 (Thatcher et al., 2012a). It will be interesting to explore which JA signaling regulators are targeted by *Fo* and how their activity is modulated.

The dependency on host JA signaling for successful colonization however, is not conserved among all *Fo* ff.spp. For instance, *Forp* colonizes WT and *coi1* Arabidopsis plants to a similar extent and this isolate does not produce bioactive JA-conjugates *in vitro*. Similarly, *Fol* seems to infect tomato without JA-signaling manipulation as this f.sp. does not produce

JAs and is not dependent on the tomato *COI1* homolog to cause disease (Cole et al., 2014). Thus, different *Fo* isolates have developed distinct infection strategies that either strongly rely on host JA signaling manipulation or involve alternative virulence mechanisms that are JA-independent.

In addition, several lines of evidence point to a role of JA in promoting resistance rather than susceptibility in plant species other than Arabidopsis. Tomato *def1* mutants that are defective in JA synthesis show enhanced susceptibility to *Fol*, which can be suppressed by exogenous JA treatment (Thaler et al., 2004). Similarly, *def1* tomato plants were more susceptible to root rot caused by *Fo* f.sp. *radicis-lycopersici* (*Forl*; Kavroulakis et al., 2007). Consistently, Sun and co-workers found that spraying of banana plants with Methyl-JA reduced disease incidence and severity caused by *Focb* Tropical Race 4 (Sun et al., 2013). In addition, resistant cultivars of strawberry and watermelon showed strong induction of the JA biosynthesis enzyme AOC upon inoculation with *Fo* f.sp. *fragariae* (Lu et al., 2011; Fang et al., 2013). A positive role of JA for defense activation was also found in date palms inoculated with *Fo* f.sp. *albenidis* (Jaiti et al., 2009).

In summary, JA signaling promotes defense to *Fo* in different plant species, but can also be hijacked to induce pathogenicity in at least Arabidopsis (**Figure 1**). Further research will be necessary to reveal via which mechanisms JA contributes to disease reduction or induction, and which function is predominant among different plant species.

DUAL ROLE OF ET IN ACTIVATION OF BOTH DEFENSE RESPONSES AND DISEASE SYMPTOMS

Generally, ET together with JA mediates the resistance response to necrotrophic pathogens. However, ET can also positively influence defense responses to hemi-biotrophs and induced systemic resistance, which is triggered by beneficial root-associated microbes (Pieterse et al., 2014; Broekgaarden et al., 2015).

Pre-treatment of Arabidopsis seedlings with either MeJA or the ET precursor 1-aminocyclopropane-1-carboxylic acid (ACC) resulted in enhanced disease symptoms upon *Focn* inoculation, indicating that both these hormones promote disease development (Trusov et al., 2009). Accordingly, the ET-insensitive Arabidopsis *ein2-1* and *etr1-1* mutants showed a reduction of disease symptoms compared to WT Col plants when inoculated with *Focn* or *Forp*, respectively (**Table 2**; Trusov et al., 2009; Pantelides et al., 2013). It is worth mentioning that enhanced disease upon MeJA treatment, as well as reduced disease in ET-insensitive plants was not observed in similar studies, indicating that these effects are either weak or depend on yet unknown factors (Edgar et al., 2006; Thatcher et al., 2009). Moreover, a different *ein2* allele (*ein2-5*) even showed markedly enhanced susceptibility to *Focn* under sterile conditions (Berrocal-Lobo and Molina, 2004). These findings point to an age- and/or condition-dependent role of ET in Arabidopsis interaction with *Fo*.

Global transcriptome profiling in Arabidopsis and banana plants inoculated with virulent *Fo* strains revealed a massive induction of ET/JA-responsive genes such as *Plant Defensins* (*PDF*s) and *Pathogenesis-Related* (*PR*) genes as well as genes encoding ethylene biosynthesis enzymes (McGrath et al., 2005; Kidd et al., 2011; Li et al., 2013; Zhu et al., 2013; Lyons et al., 2015). Furthermore, the transcriptome profiles indicated that initial activation of ET-dependent genes precedes the activation of JA, SA and ABA signaling (Li et al., 2013; Zhu et al., 2013). Altogether, these findings suggest a model in which initial ET/JA-associated defenses are mounted in response to *Fo* infection, but these are typically insufficient to stop the pathogen. At later stages however, ET signaling can rather enhance disease symptoms and possibly also pathogen proliferation. This hypothesis is further supported by the observation that Arabidopsis plants overexpressing certain *ERF* transcription factors, thereby constitutively activating ET/JA-dependent defense responses, become less susceptible to *Focn* (Berrocal-Lobo and Molina, 2004; McGrath et al., 2005). However, whether ET signaling is actively suppressed and/or at later stages co-opted by *Fo* to promote pathogenesis remains to be addressed.

The exact role of ET in other plant species is relatively little understood. The tomato *Never ripe* (*Nr*) mutant is impaired in ethylene perception and shows reduced disease symptoms upon *Fol* inoculation (Lund et al., 1998; Francia et al., 2007). Interestingly, previous work revealed a role for ET in mediating xylem occlusion through formation of gels in castor bean (Vandermolen et al., 1983). Xylem occlusion is thought to limit pathogen spread, but also to contribute to the typical wilting symptoms (Yadeta and Thomma, 2013). Thus, it is an interesting question whether *Nr* tomato plants allow systemic fungal spread and how this would correspond to the observed reduction in disease symptoms. Resistance to *Forl*, a pathogen which adopts a necrotroph-like lifestyle, was largely unaffected in two tested ET-insensitive tomato lines, *Nr* and *epinastic* (*epi*; Kavroulakis et al., 2007). However, protection mediated by an endophytic *Fusarium solani* strain was greatly reduced in *Nr* and *epi* tomato plants and hence required intact ET signaling (Kavroulakis et al., 2007).

In conclusion, the present studies underline a multifaceted role of ET signaling that strongly depends on the interaction stage, the host plant and environmental conditions (**Figure 1**).

ABA PROMOTES SHOOT DISEASE SYMPTOMS BUT NOT ROOT COLONIZATION IN ARABIDOPSIS

Besides its well-described role in development and abiotic stress responses, ABA has been increasingly recognized as a critical regulator of biotic interactions. ABA can either positively or negatively influence resistance largely depending on the encountered pathogen (Ton et al., 2009; Robert-Seilaniantz et al., 2011).

Similarly to Methyl-JA and ACC, exogenous treatment with ABA increased Arabidopsis susceptibility to *Focn* (Trusov et al., 2009). Consistently, Arabidopsis mutants in which either ABA biosynthesis or signaling is disrupted showed fewer symptoms

(**Table 2**; Anderson et al., 2004; Trusov et al., 2009). The reduced susceptibility of ABA mutants was associated with hyper-activation of ET/JA-dependent defense genes, likely due to antagonistic interactions between ABA and ET signaling (Anderson et al., 2004). ABA could also antagonize SA-dependent responses (Yasuda et al., 2008), but currently it is unknown if the interaction with other hormones explains reduced *Fo* symptoms in ABA-deficient mutants.

Interestingly, *Fo* successfully colonized the roots of ABA-deficient mutants to a similar extent as those from WT plants (Cole et al., 2014). This would point to a role of ABA during the switch to the necrotrophic phase. However, transcriptome profiling revealed activation of numerous ABA responsive genes in the roots of *Fo*-inoculated plants (Lyons et al., 2015). Previous studies indicated that ABA mediates root-to-shoot defense signaling in plants (Balmer et al., 2013). This raises the possibility that *Fo* co-opts systemic ABA signaling to manipulate root-shoot signaling. Moreover, it has been shown that, for example during defense against herbivorous insects, ABA signaling can serve to activate or enhance the MYC2-regulated branch of JA signaling (Kazan and Manners, 2013; Vos et al., 2013). However, if and how exactly *Fo* manipulates ABA signaling, is currently unknown.

AUXINS AFFECTS BOTH ROOT COLONIZATION AND SHOOT SYMPTOM DEVELOPMENT

Auxins are major regulators of plant growth and development, but have also profound effects on interactions with both pathogenic and mutualistic microbes (Robert-Seilaniantz et al., 2011; Zamioudis et al., 2013).

Exogenous application of auxin or auxin biosynthesis inhibitors did not affect disease development in *Focn*-inoculated Arabidopsis (Kidd et al., 2011). Similarly, mutants with either reduced or increased auxin levels behaved like WT plants. In contrast, *Focn*-inoculated auxin-signaling mutants showed markedly reduced symptoms relative to WT plants (**Table 2**). Additionally, alteration of polar auxin transport, either by chemical inhibitors or in mutants, resulted in increased resistance to *Focn* (Kidd et al., 2011). These data indicate that local changes of auxin levels and/or distribution are important for disease susceptibility. Indeed, histological visualization of *DR5* expression, a well-known auxin reporter gene, revealed activation of auxin signaling at root tips and lateral root initials, two preferred *Fo* entry sites in Arabidopsis (Czymmek et al., 2007; Kidd et al., 2011; Diener, 2012). Additionally, Diener revealed that fewer root tips are colonized in plants mutated in the auxin efflux carrier *PIN2/EIR1* (Diener, 2012). In contrast, *tir3* mutants which are defective in polar auxin transport show 2–3 fold higher *Fo* biomass in roots, but disease symptoms of the shoot remained strongly reduced (Kidd et al., 2011; Diener, 2012). These findings suggest that auxin signaling and transport affect several stages of the *Fo*–Arabidopsis interaction from initial root tip colonization to disease symptom expression in the shoot. However, the mechanisms by which auxin promotes colonization and symptom development are still enigmatic. Previous studies describe an antagonistic relationship between auxin and SA signaling, however the *Fo* disease phenotypes of auxin signaling mutants were not SA-dependent (Kidd et al., 2011).

Auxin accumulation, transport, and signaling are modulated by numerous different symbiotic and pathogenic organisms including bacteria, fungi, nematodes, and even parasitic plants during their interaction with roots (Grunewald et al., 2009; Kazan and Manners, 2009; Zamioudis and Pieterse, 2012). This suggests that manipulation of the host auxin signaling pathway represents a common strategy employed by diverse root colonizers resulting in either detrimental or beneficial effects for plants.

ARE PHYTOHORMONES DETERMINANTS OF *FO* LIFESTYLE?

Interestingly, changes in the phytohormone network can uncouple colonization by *Fo* from plant disease development. For instance, specific mutants with impaired JA, ABA, and auxin signaling still allow extensive root (and sometimes shoot) colonization but have greatly reduced disease symptoms (Thatcher et al., 2009; Diener, 2012; Cole et al., 2014). Similarly, resistant tomato plants that are completely free of symptoms can have their shoots and stems extensively colonized by *Fol* (Mes et al., 1999). Furthermore, a *Fol* knockout strain lacking the Six6 effector triggered vascular browning in a susceptible tomato cultivar, indicative of successful xylem colonization, but exerted almost no negative effects on plant growth and development (Gawehns et al., 2014). Altogether, these findings suggest that manipulation of plant hormone signaling rather than colonization triggers disease symptom development.

How does *Fo* manipulate the plant hormone network? One mechanism could be the production by the fungus of hormone-like secondary metabolites, including JAs, auxins, gibberellic acids, and ethylene (Hasan, 2002; Cole et al., 2014; Bitas et al., 2015). *Fo* also secretes numerous small proteins during plant infection, which might be another means to manipulate the host. For several of these proteins a virulence-promoting function has been shown designating them as effectors *sensu strictu* (Takken and Rep, 2010; de Sain and Rep, 2015). Among these, SIX4 was found to enhance JA signaling during infection of Arabidopsis (Thatcher et al., 2012a). Infection of tomato plants with *Fol* knockout strains lacking specific effectors revealed common and unique effects on the xylem proteome composition raising the possibility that each effector targets a distinct hormone signaling pathway (Gawehns et al., 2015). However, for the vast majority of *Fo* effectors their working mechanism remains unknown. It will be interesting to explore if plant hormone-synthesis or -signaling represents a recurrent virulence target of *Fo* strains on various hosts. Furthermore, it is tempting to speculate that at least a subset of the proteinacious effectors mediate immune suppression enabling (endophytic) colonization during the biotrophic phase of infection, whereas secondary metabolites with hormonal- or toxic-activity trigger plant damage/death during necrotrophic growth.

A growing body of evidence suggests that the majority of *Fo* strains survive in soil, in the rhizosphere or within plant tissues without causing disease symptoms, and some strains even confer extensive beneficial effects (Alabouvette et al., 2009; Edel-Hermann et al., 2015; Imazaki and Kadota, 2015). The existence of such a widespread and intimate co-habitation points to a finely balanced interaction between plant and fungus. The finding that also pathogenic strains can reside inside plant tissues without damaging the host indicate that one *Fo* isolate can employ diverse interaction/colonization strategies whose outcome possibly depends on the "compatibility" of a putative host plant. Thus, the "infection tools" of a *Fo* strain, likely comprised of a combination of effectors, enzymes, and secondary metabolites, determine the outcome of an interaction: either endophytic with potential beneficial effects for the host or pathogenic with various levels of disease and in extreme cases plant death. This idea is supported by the observation that transfer of one specific *Fol* chromosome, which contains most of its effector genes plus a secondary metabolite cluster, conferred pathogenicity to an endophytic strain (Ma et al., 2010).

Clearly more research in the areas of genomics and effector biology is required to understand how *Fo* manages to trick the hormonal network of its hosts, and how these interactions can have opposite outcomes ranging from pathogenesis to mutualism.

CONCLUSIONS AND OUTLOOK

Phytohormones determine colonization and disease symptom development during interactions with pathogenic *Fo* strains. However, their roles vary depending on the host plant and the fungal strain involved, suggesting that the manipulation of the host hormonal network differs between individual *Fo* strains. Genetic interference with hormone regulators mostly reduced disease symptoms, as seen for JA, ABA, and auxin, indicating that the ability to hijack plant hormone pathways is a requirement for pathogenesis. This scenario implies a strong adaptation to a particular host plant, potentially leading to the narrow host range observed in the *Fo* species complex. How exactly the manipulation of phytohormone signaling differs between *Fo* strains—and if this is indeed the key difference between pathogenic and endophytic interactions—remains an intriguing question for future research. Comparison of the respective effector repertoires as well as a better understanding of their mode of action will help answering these questions and may furthermore reveal novel approaches for plant protection, either by breeding or by optimizing *Fo* strains for biocontrol.

AUTHOR CONTRIBUTIONS

XD and NT wrote the manuscript together with input from FT. The scope and the topic were developed by XD, NT, and FT.

ACKNOWLEDGMENTS

We apologize to our colleagues whose work is not cited due to space limitation. The authors wish to thank Prof. Ben Cornelissen and Dr. Martijn Rep for critically reading and commenting on the manuscript. XD was supported by funding from the program of China Scholarship Council. FT received funding from the European Union's Horizon 2020 research and innovation programme under the Marie Skłodowska-Curie grant agreement No. 676480 (Bestpass) and from the NWO-Earth and Life Sciences funded VICI project No. 865.14.003. NT was financed from a NWO VICI grant (project No. 865.10.002) granted to Dr. Martijn Rep.

REFERENCES

Agrios, G. N. (2005). *Plant Pathology*. St. Louis, MO: Academic Press.

Alabouvette, C., Olivain, C., Migheli, Q., and Steinberg, C. (2009). Microbiological control of soil-borne phytopathogenic fungi with special emphasis on wilt-inducing *Fusarium oxysporum*. *New phytol.* 184, 529–544. doi: 10.1111/j.1469-8137.2009.03014.x

Ament, K., Krasikov, V., Allmann, S., Rep, M., Takken, F. L., and Schuurink, R. C. (2010). Methyl salicylate production in tomato affects biotic interactions. *Plant J.* 62, 124–134. doi: 10.1111/j.1365-313X.2010.04132.x

Anderson, J. P., Badruzsaufari, E., Schenk, P. M., Manners, J. M., Desmond, O. J., Ehlert, C., et al. (2004). Antagonistic interaction between abscisic acid and jasmonate-ethylene signaling pathways modulates defense gene expression and disease resistance in Arabidopsis. *Plant Cell* 16, 3460–3479. doi: 10.1105/tpc.104.025833

Armstrong, G. M., and Armstrong, J. K. (1981). "Formae speciales and races of *Fusarium oxysporum* causing wilt diseases," in *Fusarium, Diseases, Biology and Taxonomy*, eds P. E. Nelson, T. A. Toussoun, and R. J. Cook (University park, TX: Pennsylvania State University Press), 391–399.

Balmer, D., De Papajewski, D. V., Planchamp, C., Glauser, G., and Mauch-Mani, B. (2013). Induced resistance in maize is based on organ-specific defence responses. *Plant J.* 74, 213–225. doi: 10.1111/tpj.12114

Berrocal-Lobo, M., and Molina, A. (2004). Ethylene response factor 1 mediates Arabidopsis resistance to the soilborne fungus *Fusarium oxysporum*. *Mol. Plant Microb. Interact.* 17, 763–770. doi: 10.1094/MPMI.2004.17.7.763

Berrocal-Lobo, M., and Molina, A. (2008). Arabidopsis defense response against *Fusarium oxysporum*. *Trends Plant Sci.* 13, 145–150. doi: 10.1016/j.tplants.2007.12.004

Bitas, V., McCartney, N., Li, N., Demers, J., Kim, J. E., Kim, H. S., et al. (2015). Volatiles enhance plant growth via affecting Auxin transport and signaling. *Front. Microbiol.* 6:1248. doi: 10.3389/fmicb.2015.01248

Broekgaarden, C., Caarls, L., Vos, I. A., Pieterse, C. M., and Van Wees, S. C. (2015). Ethylene: traffic controller on hormonal crossroads to defense. *Plant Physiol.* 169, 2371–2379. doi: 10.1104/pp.15.01020

Chen, Y. C., Wong, C. L., Muzzi, F., Vlaardingerbroek, I., Kidd, B. N., and Schenk, P. M. (2014). Root defense analysis against *Fusarium oxysporum* reveals new regulators to confer resistance. *Sci. Rep.* 4:5584. doi: 10.1038/srep05584

Cole, S. J., Yoon, A. J., Faull, K. F., and Diener, A. C. (2014). Host perception of jasmonates promotes infection by *Fusarium oxysporum* formae speciales that produce isoleucine- and leucine-conjugated jasmonates. *Mol. Plant Pathol.* 15, 589–600. doi: 10.1111/mpp.12117

Czymmek, K. J., Fogg, M., Powell, D. H., Sweigard, J., Park, S. Y., and Kang, S. (2007). *In vivo* time-lapse documentation using confocal and multi-photon microscopy reveals the mechanisms of invasion into the Arabidopsis root vascular system by *Fusarium oxysporum*. *Fungal Genet. Biol.* 44, 1011–1023. doi: 10.1016/j.fgb.2007.01.012

De Coninck, B., Timmermans, P., Vos, C., Cammue, B. P. A., and Kazan, K. (2015). What lies beneath: belowground defense strategies in plants. *Trends Plant Sci.* 20, 91–101. doi: 10.1016/j.tplants.2014.09.007

de Sain, M., and Rep, M. (2015). The role of pathogen-secreted proteins in fungal vascular wilt diseases. *Int. J. Mol. Sci.* 16, 23970–23993. doi: 10.3390/ijms161023970

Diener, A. (2012). Visualizing and quantifying *Fusarium oxysporum* in the plant host. *Mol. Plant Microbe Interact.* 25, 1531–1541. doi: 10.1094/MPMI-02-12-0042-TA

Diener, A. C., and Ausubel, F. M. (2005). Resistance to *Fusarium oxysporum* 1, a dominant Arabidopsis disease-resistance gene, is not race specific. *Genetics* 171, 305–321. doi: 10.1534/genetics.105.042218

Dihazi, A., Serghini, M. A., Jaiti, F., Daayf, F., Driouich, A., Dihazi, H., et al. (2011). Structural and biochemical changes in salicylic-acid-treated date palm roots challenged with *Fusarium oxysporum* f. sp. *albedinis*. *J. Pathog.* 2011:280481. doi: 10.4061/2011/280481

Edel-Hermann, V., Gautheron, N., Mounier, A., and Steinberg, C. (2015). *Fusarium* diversity in soil using a specific molecular approach and a cultural approach. *J. Microbiol. Methods* 111, 64–71. doi: 10.1016/j.mimet.2015.01.026

Edgar, C. I., McGrath, K. C., Dombrecht, B., Manners, J. M., Maclean, D. C., Schenk, P. M., et al. (2006). Salicylic acid mediates resistance to the vascular wilt pathogen *Fusarium oxysporum* in the model host *Arabidopsis thaliana*. *Australas. Plant Pathol.* 35, 581–591. doi: 10.1071/AP06060

Fang, X. L., Jost, R., Finnegan, P. M., and Barbetti, M. J. (2013). Comparative proteome analysis of the strawberry-*Fusarium oxysporum* f. sp *fragariae* pathosystem reveals early activation of defense responses as a crucial determinant of host resistance. *J. Proteome Res.* 12, 1772–1788. doi: 10.1021/pr301117a

Francia, D., Demaria, D., Calderini, O., Ferraris, L., Valentino, D., Arcioni, S., et al. (2007). Wounding induces resistance to pathogens with different lifestyles in tomato: role of ethylene in cross-protection. *Plant Cell Environ.* 30, 1357–1365. doi: 10.1111/j.1365-3040.2007.01709.x

Gawehns, F., Houterman, P. M., Ichou, F. A., Michielse, C. B., Hijdra, M., Cornelissen, B. J. C., et al. (2014). The *Fusarium oxysporum* effector Six6 contributes to virulence and suppresses I-2-mediated cell death. *Mol. Plant Microb. Interact.* 27, 336–348. doi: 10.1094/MPMI-11-13-0330-R

Gawehns, F., Ma, L. S., Bruning, O., Houterman, P. M., Boeren, S., Cornelissen, B. J. C., et al. (2015). The effector repertoire of *Fusarium oxysporum* determines the tomato xylem proteome composition following infection. *Front. Plant Sci.* 6:967. doi: 10.3389/fpls.2015.00967

Glazebrook, J. (2005). Contrasting mechanisms of defense against biotrophic and necrotrophic pathogens. *Annu. Rev. Phytopathol.* 43, 205–227. doi: 10.1146/annurev.phyto.43.040204.135923

Grunewald, W., Van Noorden, G., Van Isterdael, G., Beeckman, T., Gheysen, G., and Mathesius, U. (2009). Manipulation of Auxin transport in plant roots during rhizobium symbiosis and nematode parasitism. *Plant Cell* 21, 2553–2562. doi: 10.1105/tpc.109.069617

Hasan, H. A. H. (2002). Gibberellin and auxin production by plant root-fungi and their biosynthesis under salinity-calcium interaction. *Rost. Vyroba* 48, 101–106. doi: 10.1556/amicr.49.2002.1.11

Horbach, R., Navarro-Quesada, A. R., Knogge, W., and Deising, H. B. (2011). When and how to kill a plant cell: infection strategies of plant pathogenic fungi. *J. Plant Physiol.* 168, 51–62. doi: 10.1016/j.jplph.2010.06.014

Imazaki, I., and Kadota, I. (2015). Molecular phylogeny and diversity of *Fusarium* endophytes isolated from tomato stems. *FEMS Microbiol. Ecol.* 91:fiv098. doi: 10.1093/femsec/fiv098

Jaiti, F., Verdeil, J. L., and El Hadrami, I. (2009). Effect of jasmonic acid on the induction of polyphenoloxidase and peroxidase activities in relation to date palm resistance against *Fusarium oxysporum* f. sp *albedinis*. *Physiol. Mol. Plant Pathol.* 74, 84–90. doi: 10.1016/j.pmpp.2009.09.005

Katagiri, F., and Tsuda, K. (2010). Understanding the plant immune system. *Mol. Plant Microb. Interact.* 23, 1531–1536. doi: 10.1094/MPMI-04-10-0099

Katan, T., and Di Primo, P. (1999). Current status of vegetative compatibility groups in *Fusarium oxysporum*. *Phytoparasitica* 27(Suppl.), 273–277. doi: 10.1007/BF02981483

Kavroulakis, N., Ntougias, S., Zervakis, G. I., Ehaliotis, C., Haralampidis, K., and Papadopoulou, K. K. (2007). Role of ethylene in the protection of tomato plants against soil-borne fungal pathogens conferred by an endophytic *Fusarium solani* strain. *J. Exp. Bot.* 58, 3853–3864. doi: 10.1093/jxb/erm230

Kazan, K., and Lyons, R. (2014). Intervention of phytohormone pathways by pathogen effectors. *Plant Cell* 26, 2285–2309. doi: 10.1105/tpc.114.125419

Kazan, K., and Manners, J. M. (2009). Linking development to defense: auxin in plant-pathogen interactions. *Trends Plant Sci.* 14, 373–382. doi: 10.1016/j.tplants.2009.04.005

Kazan, K., and Manners, J. M. (2013). Myc2: the master in action. *Mol. Plant* 6, 686–703. doi: 10.1093/mp/sss128

Kidd, B. N., Edgar, C. I., Kumar, K. K., Aitken, E. A., Schenk, P. M., Manners, J. M., et al. (2009). The mediator complex subunit PFT1 is a key regulator of jasmonate-dependent defense in Arabidopsis. *Plant Cell* 21, 2237–2252. doi: 10.1105/tpc.109.066910

Kidd, B. N., Kadoo, N. Y., Dombrecht, B., Tekeoglu, M., Gardiner, D. M., Thatcher, L. F., et al. (2011). Auxin signaling and transport promote susceptibility to the root-infecting fungal pathogen *Fusarium oxysporum* in Arabidopsis. *Mol. Plant Microb. Interact.* 24, 733–748. doi: 10.1094/MPMI-08-10-0194

Kuldau, G., and Yates, I. (2000). "Evidence for *Fusarium* endophytes in cultivated and wild plants,"in *Microbial Endophytes*, eds C. W. Bacon and J. F. White (New York, NY: Marcel Dekker), 85–117.

Li, C. Q., Shao, J. F., Wang, Y. J., Li, W. B., Guo, D. J., Yan, B., et al. (2013). Analysis of banana transcriptome and global gene expression profiles in banana roots in response to infection by race 1 and tropical race 4 of *Fusarium oxysporum* f. sp *cubense*. *BMC Genomics* 14:851. doi: 10.1186/1471-2164-14-851

Lin, W. C., Lu, C. F., Wu, J. W., Cheng, M. L., Lin, Y. M., Yang, N. S., et al. (2004). Transgenic tomato plants expressing the Arabidopsis NPR1 gene display enhanced resistance to a spectrum of fungal and bacterial diseases. *Transgenic Res.* 13, 567–581. doi: 10.1007/s11248-004-2375-9

Lo Presti, L., Lanver, D., Schweizer, G., Tanaka, S., Liang, L., Tollot, M., et al. (2015). Fungal effectors and plant susceptibility. *Annu. Rev. Plant. Biol.* 66, 513–545. doi: 10.1146/annurev-arplant-043014-114623

Lu, G. Y., Guo, S. G., Zhang, H. Y., Geng, L. H., Song, F. M., Fei, Z. J., et al. (2011). Transcriptional profiling of watermelon during its incompatible interaction with *Fusarium oxysporum* f. sp *niveum*. *Eur. J. Plant Pathol.* 131, 585–601. doi: 10.1007/s10658-011-9833-z

Lund, S. T., Stall, R. E., and Klee, H. J. (1998). Ethylene regulates the susceptible response to pathogen infection in tomato. *Plant Cell* 10, 371–382. doi: 10.1105/tpc.10.3.371

Lyons, R., Stiller, J., Powell, J., Rusu, A., Manners, J. M., and Kazan, K. (2015). *Fusarium oxysporum* triggers tissue-specific transcriptional reprogramming in *Arabidopsis thaliana*. *PLoS ONE* 10:e0121902. doi: 10.1371/journal.pone.0121902

Ma, L. J., Van Der Does, H. C., Borkovich, K. A., Coleman, J. J., Daboussi, M. J., Di Pietro, A., et al. (2010). Comparative genomics reveals mobile pathogenicity chromosomes in *Fusarium*. *Nature* 464, 367–373. doi: 10.1038/nature08850

Mandal, S., Mallick, N., and Mitra, A. (2009). Salicylic acid-induced resistance to *Fusarium oxysporum* f. sp *lycopersici* in tomato. *Plant Physiol. Biochem.* 47, 642–649. doi: 10.1016/j.plaphy.2009.03.001

McGrath, K. C., Dombrecht, B., Manners, J. M., Schenk, P. M., Edgar, C. I., Maclean, D. J., et al. (2005). Repressor- and activator-type ethylene response factors functioning in jasmonate signaling and disease resistance identified via a genome-wide screen of Arabidopsis transcription factor gene expression. *Plant Physiol.* 139, 949–959. doi: 10.1104/pp.105.068544

Mes, J. J., Weststeijn, E. A., Herlaar, F., Lambalk, J. J., Wijbrandi, J., Haring, M. A., et al. (1999). Biological and molecular characterization of *Fusarium oxysporum* f. sp *lycopersici* divides race 1 isolates into separate virulence groups. *Phytopathology* 89, 156–160. doi: 10.1094/PHYTO.1999.89.2.156

Michielse, C. B., and Rep, M. (2009). Pathogen profile update: *Fusarium oxysporum*. *Mol. Plant Pathol.* 10, 311–324. doi: 10.1111/j.1364-3703.2009.00538.x

Pantelides, I. S., Tjamos, S. E., Pappa, S., Kargakis, M., and Paplomatas, E. J. (2013). The ethylene receptor ETR1 is required for *Fusarium oxysporum* pathogenicity. *Plant Pathol.* 62, 1302–1309. doi: 10.1111/ppa.12042

Pieterse, C. M., Van der Does, D., Zamioudis, C., Leon-Reyes, A., and Van Wees, S. C. (2012). Hormonal modulation of plant immunity. *Annu. Rev. Cell Dev. Biol.* 28, 489–521. doi: 10.1146/annurev-cellbio-092910-154055

Pieterse, C. M., Zamioudis, C., Berendsen, R. L., Weller, D. M., Van Wees, S. C., and Bakker, P. A. (2014). Induced systemic resistance by beneficial microbes. *Annu. Rev. Phytopathol.* 52, 347–375. doi: 10.1146/annurev-phyto-082712-102340

Pietro, A. D., Madrid, M. P., Caracuel, Z., Delgado-Jarana, J., and Roncero, M. I. (2003). *Fusarium oxysporum*: exploring the molecular arsenal of a vascular wilt fungus. *Mol. Plant Pathol.* 4, 315–325. doi: 10.1046/j.1364-3703.2003.00180.x

Robert-Seilaniantz, A., Grant, M., and Jones, J. D. (2011). Hormone crosstalk in plant disease and defense: more than just jasmonate-salicylate antagonism. *Annu. Rev. Phytopathol.* 49, 317–343. doi: 10.1146/annurev-phyto-073009-114447

Sun, D. Q., Lu, X. H., Hu, Y. L., Li, W. M., Hong, K. Q., Mo, Y. W., et al. (2013). Methyl jasmonate induced defense responses increase resistance to *Fusarium oxysporum* f. sp *cubense* race 4 in banana. *Sci. Hortic.* 164, 484–491. doi: 10.1016/j.scienta.2013.10.011

Swarupa, V., Ravishankar, K. V., and Rekha, A. (2014). Plant defense response against *Fusarium oxysporum* and strategies to develop tolerant genotypes in banana. *Planta* 239, 735–751. doi: 10.1007/s00425-013-2024-8

Takken, F., and Rep, M. (2010). The arms race between tomato and *Fusarium oxysporum*. *Mol. Plant Pathol.* 11, 309–314. doi: 10.1111/j.1364-3703.2009.00605.x

Thaler, J. S., Owen, B., and Higgins, V. J. (2004). The role of the jasmonate response in plant susceptibility to diverse pathogens with a range of lifestyles. *Plant Physiol.* 135, 530–538. doi: 10.1104/pp.104.041566

Thatcher, L. F., Gardiner, D. M., Kazan, K., and Manners, J. M. (2012a). A highly conserved effector in *Fusarium oxysporum* is required for full virulence on Arabidopsis. *Mol. Plant Microb. Interact.* 25, 180–190. doi: 10.1094/MPMI-08-11-0212

Thatcher, L. F., Manners, J. M., and Kazan, K. (2009). *Fusarium oxysporum* hijacks COI1-mediated jasmonate signaling to promote disease development in Arabidopsis. *Plant J.* 58, 927–939. doi: 10.1111/j.1365-313X.2009.03831.x

Thatcher, L. F., Powell, J. J., Aitken, E. A., Kazan, K., and Manners, J. M. (2012b). The lateral organ boundaries domain transcription factor LBD20 functions in *Fusarium* wilt susceptibility and jasmonate signaling in Arabidopsis. *Plant Physiol.* 160, 407–418. doi: 10.1104/pp.112.199067

Tjamos, E. C., and Beckman, C. H. (1989). *Vascular Wilt Diseases of Plants*. Berlin: Springer-Verlag.

Ton, J., Flors, V., and Mauch-Mani, B. (2009). The multifaceted role of ABA in disease resistance. *Trends Plant Sci.* 14, 310–317. doi: 10.1016/j.tplants.2009.03.006

Trusov, Y., Sewelam, N., Rookes, J. E., Kunkel, M., Nowak, E., Schenk, P. M., et al. (2009). Heterotrimeric G proteins-mediated resistance to necrotrophic pathogens includes mechanisms independent of salicylic acid-, jasmonic acid/ethylene- and abscisic acid-mediated defense signaling.*Plant J. Cell Mol. Biol.* 58, 69–81. doi: 10.1111/j.1365-313X.2008.03755.x

Vandermolen, G. E., Labavitch, J. M., Strand, L. L., and Devay, J. E. (1983). Pathogen-induced vascular gels - ethylene as a host intermediate. *Physiol. Plantarum* 59, 573–580. doi: 10.1111/j.1399-3054.1983.tb06282.x

Vos, C. M., Yang, Y., De Coninck, B., and Cammue, B. P. A. (2014). Fungal (-like) biocontrol organisms in tomato disease control. *Biol. Control* 74, 65–81. doi: 10.1016/j.biocontrol.2014.04.004

Vos, I. A., Verhage, A., Schuurink, R. C., Watt, L. G., Pieterse, C. M., and Van Wees, S. C. (2013). Onset of herbivore-induced resistance in systemic tissue primed for jasmonate-dependent defenses is activated by abscisic acid. *Front. Plant Sci.* 4:539. doi: 10.3389/fpls.2013.00539

Xue, R. F., Wu, J., Wang, L. F., Blair, M. W., Wang, X. M., Ge, W. D., et al. (2014). Salicylic acid enhances resistance to *Fusarium oxysporum* f. sp. *phaseoli* in common beans (*Phaseolus vulgaris* L.). *J. Plant Growth Regul.* 33, 470–476. doi: 10.1007/s00344-013-9376-y

Yadeta, K., and Thomma, B. P. (2013). The xylem as battleground for plant hosts and vascular wilt pathogens. *Front. Plant Sci.* 4:97. doi: 10.3389/fpls.2013.00097

Yasuda, M., Ishikawa, A., Jikumaru, Y., Seki, M., Umezawa, T., Asami, T., et al. (2008). Antagonistic interaction between systemic acquired resistance and the abscisic acid-mediated abiotic stress response in Arabidopsis. *Plant Cell* 20, 1678–1692. doi: 10.1105/tpc.107.054296

Zamioudis, C., Mastranesti, P., Dhonukshe, P., Blilou, I., and Pieterse, C. M. (2013). Unraveling root developmental programs initiated by beneficial *Pseudomonas* spp. bacteria. *Plant Physiol.* 162, 304–318. doi: 10.1104/pp.112.212597

Zamioudis, C., and Pieterse, C. M. (2012). Modulation of host immunity by beneficial microbes. *Mol. Plant Microb. Interact.* 25, 139–150. doi: 10.1094/MPMI-06-11-0179

Zhu, Q. H., Stephen, S., Kazan, K., Jin, G. L., Fan, L. J., Taylor, J., et al. (2013). Characterization of the defense transcriptome responsive to *Fusarium oxysporum*-infection in Arabidopsis using RNA-seq. *Gene* 512, 259–266. doi: 10.1016/j.gene.2012.10.036

Conflict of Interest Statement: The authors declare that the research was conducted in the absence of any commercial or financial relationships that could be construed as a potential conflict of interest.

frontiers in Plant Science

PERSPECTIVE
published: 28 April 2016
doi: 10.3389/fpls.2016.00565

Linking Jasmonic Acid to Grapevine Resistance against the Biotrophic Oomycete *Plasmopara viticola*

Ana Guerreiro[1], Joana Figueiredo[1,2,3], Marta Sousa Silva[2,3†] and Andreia Figueiredo[1†]*

[1] Biosystems and Integrative Sciences Institute, Science Faculty of Lisbon University, Lisboa, Portugal, [2] Laboratório de FTICR e Espectrometria de Massa Estrutural, Faculdade de Ciências, Universidade de Lisboa, Lisboa, Portugal, [3] Centro de Química e Bioquímica, Faculdade de Ciências, Universidade de Lisboa, Lisboa, Portugal

Plant resistance to biotrophic pathogens is classically believed to be mediated through salicylic acid (SA) signaling leading to hypersensitive response followed by the establishment of Systemic Acquired Resistance. Jasmonic acid (JA) signaling has extensively been associated to the defense against necrotrophic pathogens and insects inducing the accumulation of secondary metabolites and PR proteins. Moreover, it is believed that plants infected with biotrophic fungi suppress JA-mediated responses. However, recent evidences have shown that certain biotrophic fungal species also trigger the activation of JA-mediated responses, suggesting a new role for JA in the defense against fungal biotrophs. *Plasmopara viticola* is a biotrophic oomycete responsible for the grapevine downy mildew, one of the most important diseases in viticulture. In this perspective, we show recent evidences of JA participation in grapevine resistance against *P. viticola*, outlining the hypothesis of JA involvement in the establishment of an incompatible interaction with this biotroph. We also show that in the first hours after *P. viticola* inoculation the levels of OPDA, JA, JA-Ile, and SA increase together with an increase of expression of genes associated to JA and SA signaling pathways. Our data suggests that, on the first hours after *P. viticola* inoculation, JA signaling pathway is activated and the outcomes of JA–SA interactions may be tailored in the defense response against this biotrophic pathogen.

Keywords: *Vitis vinifera*, biotroph, downy mildew, salicylic acid, jasmonic acid

OPEN ACCESS

Edited by:
Ralph Panstruga,
RWTH Aachen University, Germany

Reviewed by:
Rensen Zeng,
Fujian Agriculture and Forestry University, China
Hannah Kuhn,
RWTH Aachen University, Germany

***Correspondence:**
Andreia Figueiredo
aafigueiredo@fc.ul.pt

† These authors are co-senior authors.

Specialty section:
This article was submitted to Plant Biotic Interactions, a section of the journal Frontiers in Plant Science

Received: *29 December 2015*
Accepted: *12 April 2016*
Published: *28 April 2016*

Citation:
Guerreiro A, Figueiredo J, Sousa Silva M and Figueiredo A (2016) Linking Jasmonic Acid to Grapevine Resistance against the Biotrophic Oomycete Plasmopara viticola. Front. Plant Sci. 7:565. doi: 10.3389/fpls.2016.00565

GRAPEVINE DOWNY MILDEW

Grapevine is one of the most valuable crops for fruit and wine production in a global scale, representing more than 7500 kHa of cultivated area in 2014 (data from the International Organization of Vine and Wine[1]). Downy mildew is one of the most economically significant grapevine diseases worldwide. It was introduced in Europe in the 1870s (Millardet, 1881) and quickly spread to all major grape-producing regions of the world (Galet, 1977; Gessler et al., 2011). The grapevine downy mildew causal agent, *Plasmopara viticola* (Berk. et Curt.) and De Toni, is a biotrophic obligatory oomycete that obtains nutrients from living cells of hosts in order to complete its life cycle. It infects all green parts of the plant, specifically leaves and clusters (Gessler et al., 2011). Under favorable conditions, motile zoospores are released from sporangia and swim toward the stomata. Subsequently, zoospores germinate and the germ tube penetrates into the substomatal cavity,

[1] www.oiv.int

primary hypha expand into the intercellular spaces of the mesophyll tissue differentiating specialized structures known as haustoria (Diez-Navajas et al., 2008). These highly specialized structures of biotrophic oomycetes and fungi play an essential role in nutrient acquisition from the plant cells and allow intense exchanges of signals that redirect the host metabolism and suppress the defense reaction (Diez-Navajas et al., 2008).

While American and Asiatic *Vitis* spp. present genetic resistance to this pathogen, domesticated grapevine *Vitis vinifera*, presently the most cultivated on a global scale, is sensitive to downy mildew. As a control measure, several fungicide applications are necessary every year and *P. viticola* resistance has already been found to the most common groups of site specific fungicides (Chen et al., 2007; Blum et al., 2010). Only in the past few decades, resistance breeding partly replaced the chemical plant protection applied against grapevine downy mildew. Partially resistant grapevine varieties resulted from breeding programs by introgression of resistant traits from wild *Vitis* spp. (e.g., *V. labrusca, V. amurensis*). However, recent reports have shown that *P. viticola* presents a high evolutionary potential as several isolates were able to break down plant resistance of interspecific hybrids (Peressotti et al., 2010; Casagrande et al., 2011). These findings have highlighted the need to fully understand grapevine resistance mechanisms against *P. viticola*.

The signaling pathways associated to grapevine and *P. viticola* interaction are still poorly understood. In plant defense against pathogens, phytohormones such as jasmonates and salicylic acid (SA) have received considerable attention (Bari and Jones, 2009). It is generally assumed that SA is involved in the activation of defense responses against biotrophic and hemi-biotrophic pathogens as well as the establishment of systemic acquired resistance, whereas inducible defense against leaf-chewing insects and necrotrophic microbes is mediated by jasmonic acid (JA)-dependent signaling (Glazebrook, 2005). These generalities are disputed in grapevine as JA signaling has been implicated in resistance against biotrophs, such as powdery and downy mildews (Hamiduzzaman et al., 2005; Belhadj et al., 2006, 2008; Trouvelot et al., 2008).

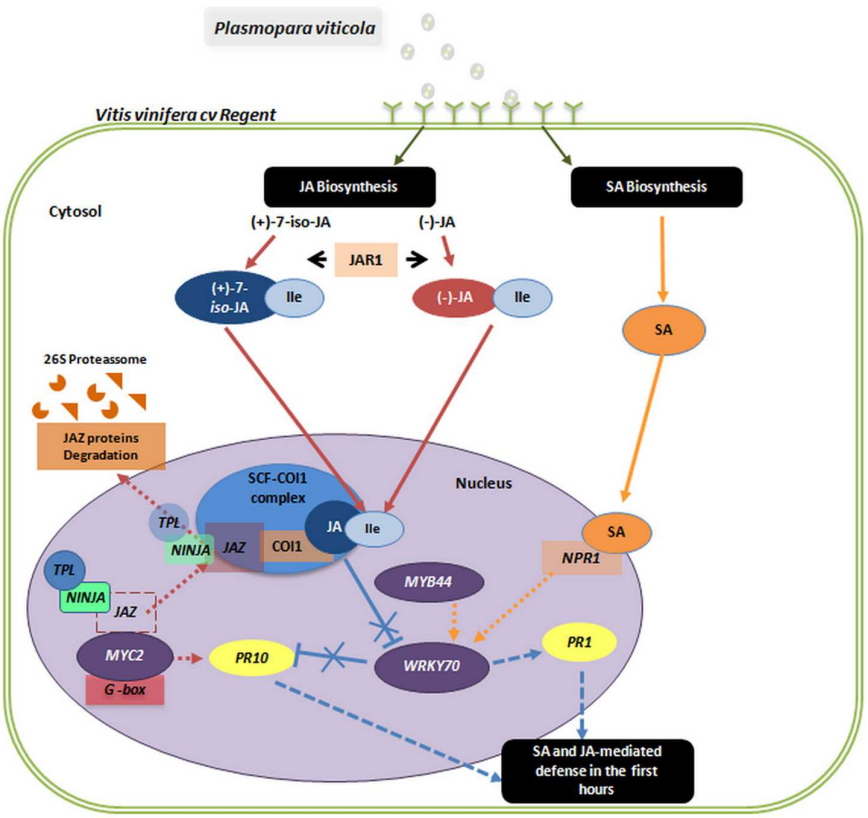

FIGURE 1 | On the first hours after *Plasmopara viticola* inoculation, the levels of SA, JA, and JA-Ile increased in *V. vinifera* cv. Regent relatively to mock inoculated control plants. Rapid accumulation of bioactive JA-Ile promotes SCF-COI1 mediated ubiquitination and subsequent degradation of JAZ proteins and corepressors TLP and NINJA via the 26S proteasome, relieving the transcription factors such as *MYC2* and promoting the expression of JA-responsive genes such as *PR10*. High levels of SA mediate a change in the cellular redox potential, resulting in the reduction of the NPR1 oligomer to its active monomeric form. Monomeric NPR1 is then translocated into the nucleus where it functions as a transcriptional co-activator of SA-responsive genes, such as *PR-1*. Both the SA and JA signaling pathways seem to be simultaneously activated on the first hours of interaction. See text for details on the molecular processes underlying both JA- and SA-signaling. Solid lines indicate established accumulation and dashed lines suggested activities.

JASMONIC ACID SIGNALING

Jasmonic acid signaling has been extensively studied in model plants such as *Arabidopsis*. Briefly, biosynthesis of JA takes place in three different cell compartments. In the chloroplast, α-linolenic acid is released from membranes and deoxygenated by 13-lipoxygenases (13-LOXs), followed by the sequential action of allene oxide synthase (AOS) and allene oxide cyclase (AOC), resulting in the synthesis of 12-oxophytodienoic acid (OPDA). OPDA is transported to the peroxisome where the cyclopentenone ring is reduced by a *cis*-OPDA reductase 3 (OPR3) and subsequently the carboxylic acid side chain is shortened by β-oxidation to generate (+)-7-*iso*-JA, which is again released into the cytosol and epimerizes to the less active (−)-JA (Dave and Graham, 2012). In 2004, it was found that the active phytohormone is not JA itself but its isoleucine conjugate (Staswick and Tiryaki, 2004). This conjugation is catalyzed by jasmonate resistant 1 (JAR1) using (+)-7-*iso*-JA as the substrate to form bioactive jasmonate (+)-7-*iso*-jasmonoyl-L-isoleucine (JA-Ile; Staswick and Tiryaki, 2004; Fonseca et al., 2009). JA-dependent gene activation involves binding of JA-Ile to the F-box protein coronatine insensitive 1 (COI1), which acts as a JA receptor in the E3 ubiquitin-ligase SKP1-Cullin-F-box complex (SCF^{COI1}). Further discovery of JASMONATE ZIM-DOMAIN (JAZ) proteins as negative regulators of JA-induced gene expression and as the true targets of SCF^{COI1} complex represented a major breakthrough in analysis of JA signaling (Chini et al., 2007; Thines et al., 2007; Yan et al., 2007). In the absence of the JA-Ile, JAZ proteins block basic helix-loop-helix leucine zipper transcription factor (MYC2) activity by recruiting the general corepressors TOPLESS (TPL) and TPL-related proteins through an interaction with the adaptor protein Novel Interactor of JAZ (NINJA; Pauwels et al., 2010). In response to JA-Ile, JAZ proteins are targeted by SCF^{COI1} for degradation, MYC2 is released activating JA-dependent gene expression and ultimately activating the regulation of various physiological processes (**Figure 1**). This model and the role of other proteins in JA perception and signaling has been widely discussed in many reviews (e.g., Wasternack, 2007; Avanci et al., 2010; Dave and Graham, 2012; Pieterse et al., 2012; Wasternack and Hause, 2013).

LINKING JASMONIC ACID SIGNALING TO GRAPEVINE RESISTANCE TO *Plasmopara viticola*

The first cues of JA role in grapevine resistance to downy mildew emerged from elicitor-based studies where it was shown that following both β-aminobutyric acid (BABA) and sulfated laminarin (PS3) application, the expression of LOX and JA responsive genes increased (Hamiduzzaman et al., 2005). Other studies also reported, that after *P. viticola* inoculation, the expression of *AOC* and *AOS* (Polesani et al., 2010), *LOXO* and *JAZ* (Marchive et al., 2013) and *JAZ1* and *AOC* increased (Gauthier et al., 2014). Other evidences pointing to the involvement of JA pathway came from the studies of Polesani et al. (2010) that showed an increase of JA and MeJA levels after inoculation, of Ali et al. (2012) that pointed out an increased α-linolenic acid content in resistant grapevine cultivars and Gauthier et al. (2014) that reported an transient increase in JA levels in b-1,3 glucan laminarin elicited plants.

Very recently, Figueiredo et al. (2015) characterized gene expression profile for the first steps of JA biosynthesis (*LOX2*, *AOC*, *AOS,* and *OPR3*), activation (*JAR1*) and signaling (*COI1*) in two *Vitis vinifera* cultivars with different degrees of resistance to *P. viticola*. These authors have shown that, following *P. viticola* inoculation, there was an early (6 and 12 hpi) up-regulation of JA biosynthesis-related enzymes (*LOXO, AOS, AOC,* and *OPR3*) and a later activation (18 and 24 hpi) of two of the key components of JA signaling, *JAR1* and *COI1* in the resistant cultivar. Simultaneously, an up-regulation of *LOX*, *JAZ,* and *PR14* genes and a higher content of JA (at 12 and 24 hpi) and SA (at 24, 48, and 72 hpi) was described for the incompatible *Vitis amurensis* cv. '*Shuanghong*'–*P. viticola* interaction (Li et al., 2015).

Altogether these studies highlighted the potential role of JA in this particular plant-biotrophic pathogen interaction. To further investigate this hypothesis we have determined OPDA, JA, JA-Ile, and SA levels and conducted a qPCR expression analysis of JA-signaling associated genes [*MYC2*, *JAZ1,* and *JAZ3*, *TOPLESS*, *NINJA,* and *PR10* (pathogenesis-related protein 10)], SA-signaling markers [*NPR1* (non-expressor of PR1); *PR1* (pathogenesis-related protein 1)] and genes involved in the crosstalk between SA and JA signaling [*WRKY70* and *MYB44* (MYB domain protein 44)]. The *V. vinifera* cv. Regent, bred at the JKI-Institute for Grapevine Breeding Geilweilerhof (Akkurt et al., 2007) presenting a high degree of resistance to both downy and powdery mildew (Anonymous, 2000) was chosen as a model. Early inoculation time-points (6, 12, and 24 hpi) were considered in order to account for signaling events related to pathogen recognition in *V. vinifera*. Briefly, between 6 and 12 hpi stomatal penetration and development of stomatal vesicles with primary hyphae occur and at 24 hpi elongated hyphae invade the intercellular space of the mesophyll progressing to the branching stage in susceptible plants and stopping the development in resistant plants (Kortekamp and Zyprian, 2003; Unger et al., 2007).

After *P. viticola* inoculation, both *JAZ* genes analyzed also increased their expression at 6 hpi (JAZ3: 2.03 ± 0.33) and 12 hpi (JAZ1: 3.85 ± 0.98), the co-repressor TOPLESS and NINJA also increased their expression at 6 hpi (NINJA: 2.77 ± 0.29) and 24 hpi (TOPLESS: 1.72 ± 0.01). These results are coherent with the release of JAZ-bound transcription factors resulting in the activation of downstream JA responses (**Figure 2B**) and with the feed-back loop model where *de novo* synthesis of JAZ repressors is described for a negative feedback control. Moreover, in the interaction of *V. amurensis* with *P. viticola*, Li et al. (2015) have also shown an up-regulation of JAZ related genes from 24 hpi and after JA-elicitor treatment Gauthier et al. (2014) have reported an up-regulation of JAZ1 at 12 hpi.

At 12 hpi with *P. viticola MYC2* expression increased (6 hpi: 1.10 ± 0.01; 12 hpi: 2.48 ± 1.00; 24 hpi: 1.06 ± 0.20), together with the expression of *PR10* (6 hpi: 1.59 ± 0.83; 12 hpi: 3.35 ± 0.45;

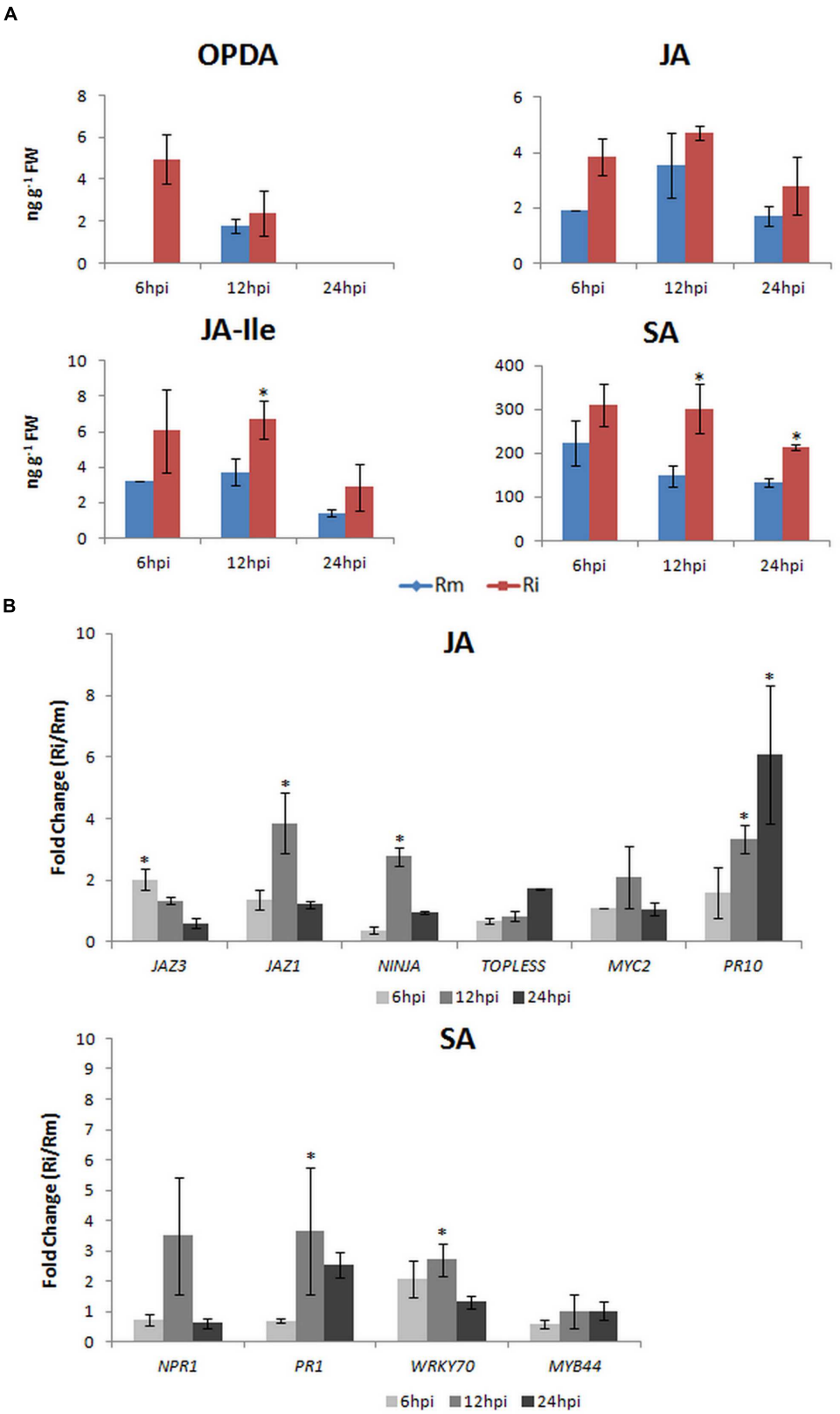

FIGURE 2 | Continued

FIGURE 2 | Continued

***Vitis vinifera* cv. Regent plants were inoculated with *P. viticola* (Ri) as described in Figueiredo et al. (2012).** Plant material was harvested at 6, 12, and 24 hpi. Mock inoculated samples (Rm) were done for each time-point. **(A)** Determination of the endogenous levels (ng g^{-1} FW) of OPDA, JA, JA-ILE, and SA. Briefly, 50 mg of lyophilized samples were used for phytohormone quantification in a 4000 QTRAP LC/MS/MS system (AB Sciex) at the Proteomics & Mass Spectrometry Facility at the Danforth Plant Science Center (USA). Phytohormone levels are represented as the mean and standard deviation of three biological replicates. **(B)** qPCR expression analysis of JA- and SA-signaling associated genes. Total RNA extraction, cDNA synthesis, and qPCR experiments were done according to Monteiro et al. (2013). Primer sequences, amplicon size, amplification efficiency, annealing and melting temperatures for each gene studied are given in Supplementary Table 1. To normalize expression data, ubiquitin conjugating enzyme (*UBQ*), Elongation factor 1α (*EF1α*) and glyceraldehyde-3-phosphate dehydrogenase (*GAPDH*) were used (Monteiro et al., 2013). Transcript abundance of inoculated samples relative to mock inoculated controls at each time point is represented as the mean and standard deviation of five biological replicates. Expression between 0 and 1 represents a down-regulation. Asterisks (*) represent significant difference ($p \leq 0.05$) between inoculated and control samples at the same time point (Mann–Whitney *U* test; SPSS Inc., USA, V20).

24 hpi: 6.19 ± 2.24), suggesting an activation of JA signaling. This activation is corroborated by the increase of JA at 6 and 12 hpi and by the significantly increase of JA-Ile levels at 12 hpi (**Figure 2A**). After *P. viticola* inoculation it was also reported a significant increase of JA levels at 12 and 24 hpi (Li et al., 2015) in *V. amurensis* and a later increase (48 hpi) of both JA and MeJA levels in *V. riparia* (Polesani et al., 2010). *PR10* levels were also shown to increase after *P. viticola* inoculation in both Benzothiadiazole-primed and control *V. vinifera* plants (Dufour et al., 2013) and in *V. vinifera* cv. Regent plants (Figueiredo et al., 2012). Altogether, our results on this pathosystem suggest that in the resistant *V. vinifera* cv. Regent, an increase in α-linolenic acid content occurs after *P. viticola* inoculation (Ali et al., 2012) which is used for the biosynthesis of JA. The conversion of JA to its bioactive form JA-Ile is corroborated by both the increase of *JAR1* expression, described by Figueiredo et al. (2015), and the increase of JA-Ile levels at 12 hpi (**Figure 2A**). The activation of JA-dependent defense responses is suggested by the increase of *MYC2* and *PR10* expression.

SA AND JA CROSSTALK IN THE INITIAL HOURS OF INTERACTION

It is generally accepted that SA activates resistance against biotrophic pathogens, while JA is critical for activation of defense against herbivorous insects and necrotrophic pathogens. Both signaling pathways are interdependent and although most reports indicate a mutually antagonistic interaction between SA- and JA-dependent signaling, synergistic interactions have been described as well (reviewed in Pieterse et al., 2012).

Signaling downstream of SA is largely controlled by the regulatory protein NPR1 that acts as a transcriptional co-activator of a large set of defense related genes, namely PR proteins (Dong, 2004) of which *PR-1* is often used as a robust marker for SA-responsive gene expression (Pieterse et al., 2012). WRKY transcription factors are important regulators of SA-dependent defense responses (reviewed in Koornneef and Pieterse, 2008) and some of them have been implicated in SA/JA cross talk, namely *WRKY70* (Li et al., 2004). *WRKY70* positively regulates SA-mediated defenses while repressing the JA response (Li et al., 2004) and in turn is transcriptionally activated by *MYB44* (Shim et al., 2013), thus both genes may be considered integrators of the cross-talk between SA and JA in plant defense responses (**Figure 1**).

After inoculation of *V. vinifera* cv. Regent with *P. viticola*, the expression of *NPR1* increased at 12 hpi (3.44 ± 1.81) decreasing afterward, when compared to mock inoculated plants (**Figure 2B**). This peak of expression at 12 hpi is accompanied by the expression of *PR1* (6 hpi: 0.70 ± 0.08; 12 hpi: 3.67 ± 2.09; 24 hpi: 2.53 ± 0.43). The levels of SA were significantly increased at both 12 and 24 hpi (**Figure 2A**). After *P. viticola* inoculation, high *PR1* levels were also described by Dufour et al. (2013) in both Benzothiadiazole-primed and control *V. vinifera* plants. Moreover, in *V. amurensis* a significant increase in SA content was also shown to occur from 24 hpi, coordinated with an increase in *PR1* expression (Li et al., 2015). Interestingly, these authors have also reported a significant increase in JA content from 12 hpi, thus both SA and JA were significantly altered at the first hours after inoculation with *P. viticola*. Although many reports describe an antagonistic interaction between the SA and JA pathways, neutral and synergistic interactions have been described as well (Mur et al., 2006). It was shown that at low concentrations SA and JA may act synergistically and at higher concentrations the effects are antagonistic, demonstrating that the outcome of the SA-JA interaction is dependent upon the relative concentration of each hormone (Mur et al., 2006).

Although WRKY70 has been implicated in SA/JA cross talk by positively regulating SA-mediated defenses while repressing the JA response (Li et al., 2004), *MYB44* shows no altered expression and *WRKY70* is slightly regulated at 6 and 12 hpi (6 hpi: 2.08 ± 0.61; 12 hpi: 2.71 ± 0.53). The expression of *WRKY70* seems to be coordinated with an increase of NPR1 and PR1 expression at 12 hpi but it does not repress the expression of *PR10*. Altogether our results suggest that at the first hours after inoculation both SA and JA pathways seem to be activated (**Figure 1**), but an antagonistic mechanism between the two pathways may be present at later inoculation time-points. The employment of synergistic/antagonistic mechanisms may represent positive and negative feedback loops allowing the tailoring of *V. vinifera* cv. Regent response to the biotrophic oomycete *P. viticola*.

CONCLUSION

To reduce the environmental impact of pesticide overuse, there is an increasing interest in the use of elicitors to induce resistance

against pathogens in crop plants. Disease control measures for grapevine downy mildew are based on the preventive use of phytochemical compounds. Elicitors of grapevine immunity such as BABA or PS3 are being extensively studied as alternatives for pesticide application. Here, we have highlighted the involvement of jasmonic and SA in grapevine resistance against *P. viticola*.

Future research efforts have to be made to characterize the effectiveness of JA as an elicitor of grapevine immunity against biotrophic fungi, namely on physiological adjustments, growth, yield and reduction of disease incidence. Also, very recently the effect of the foliar application of methyl jasmonate to Tempranillo grapevines to improve wine quality was studied (Portu et al., 2015). It was shown that the phenolic composition, namely 3-*O*-glucosides of petunidin and peonidin, *trans*-*p*-coumaroyl derivatives of cyanidin and peonidin and *trans*-piceid content increase significantly. Thus exogenous application of JA and jasmonates may be not only important as elicitors of grapevine immunity but also be a simple and accessible practice to enhance grape and wine quality.

AUTHOR CONTRIBUTIONS

AF designed the study and planned the experiment. AG and JF performed the experiments. AF, MS, AG, and JF performed data analysis. AF and MS wrote the manuscript. All authors have read and approved the manuscript.

FUNDING

This work was supported by the FCT projects PTDC/AGR-GPL/112217/2009, EXPL/BBB-BIO/0439/2013, PEst-OE/BIA/UI 4046/2014, PEst-OE/QUI/UI0612/2013 and UID/MULTI/006 12/2013, and research grant SFRH/BPD/99712/2014.

ACKNOWLEDGMENTS

The authors wish to acknowledge the Proteomics & Mass Spectrometry Facility at the Danforth Plant Science Center for its contribution on the quantification of the phytohormone levels (National Science Foundation under Grant No. DBI-1427621) and to Dr. Lisete Sousa from the Department of Statistics and Operational Research/FCUL for her advices on the statistical analysis.

SUPPLEMENTARY MATERIAL

The Supplementary Material for this article can be found online at: http://journal.frontiersin.org/article/10.3389/fpls.2016.00565

REFERENCES

Akkurt, M., Welter, L., Maul, E., Topfer, R., and Zyprian, E. (2007). Development of SCAR markers linked to powdery mildew (*Uncinula necator*) resistance in grapevine (*Vitis vinifera* L. and Vitis sp.). *Mol. Breed.* 29, 103–111. doi: 10.1007/s11032-006-9047-9

Ali, K., Maltese, F., Figueiredo, A., Rex, M., Fortes, A. M., Zyprian, E., et al. (2012). Alterations in grapevine leaf metabolism upon inoculation with *Plasmopara viticola* in different time-points. *Plant Sci.* 191, 100–107. doi: 10.1016/j.plantsci.2012.04.014

Anonymous. (2000). *Description List of Varieties–Grapes 2000*. Hannover: Landburg Verlag.

Avanci, N., Luche, D., Goldman, G., and Goldman, M. (2010). Jasmonates are phytohormones with multiple functions, including plant defense and reproduction. *Genet. Mol. Res.* 9, 484–505. doi: 10.4238/vol9-1gmr754

Bari, R., and Jones, J. (2009). Role of plant hormones in plant defence responses. *Plant Mol. Biol.* 69, 473–488. doi: 10.1007/s11103-008-9435-0

Belhadj, A., Saigne, C., Telef, N., Cluzet, S., Bouscaut, J., Corio-Costet, M., et al. (2006). Methyl jasmonate induces defense responses in grapevine and triggers protection against *Erysiphe necator*. *J. Agric. Food Chem.* 54, 9119–9125. doi: 10.1021/jf0618022

Belhadj, A., Telef, N., Saigne, C., Cluzet, S., Barrieu, F., Hamdi, S., et al. (2008). Effect of methyl jasmonate in combination with carbohydrates on gene expression of PR proteins, stilbene and anthocyanin accumulation in grapevine cell cultures. *Plant Physiol. Biochem.* 46, 493–499. doi: 10.1016/j.plaphy.2007.12.001

Blum, M., Waldner, M., and Gisi, U. (2010). A single point mutation in the novel PvCesA3 gene confers resistance to the carboxylic acid amide fungicide mandipropamid in *Plasmopara viticola*. *Fungal Genet. Biol.* 47, 499–510. doi: 10.1016/j.fgb.2010.02.009

Casagrande, K., Falginella, L., Castellarin, S., Testolin, R., and Di Gaspero, G. (2011). Defence responses in Rpv3-dependent resistance to grapevine downy mildew. *Planta* 234, 1097–1109. doi: 10.1007/s00425-011-1461-5

Chen, W., Delmotte, F., Richard-Cervera, S., Douence, L., Greif, C., and Corio-Costet, M. (2007). At least two origins of fungicide resistance in grapevine downy mildew Populations. *Appl. Environ. Microbiol.* 73, 5162–5172. doi: 10.1128/AEM.00507-07

Chini, A., Fonseca, S., Fernandez, G., Adie, B., Chico, J., Lorenzo, O., et al. (2007). The JAZ family of repressors is the missing link in jasmonate signalling. *Nature* 448, 666–671. doi: 10.1038/nature 06006

Dave, A., and Graham, I. (2012). Oxylipin signaling: a distinct role for the jasmonic acid precursor cis-(+)-12-oxo-phytodienoic acid (cis-OPDA). *Front. Plant Sci.* 3:42. doi: 10.3389/fpls.2012.00042

Diez-Navajas, A., Wiedemann-Merdinoglu, S., Greif, C., and Merdinoglu, D. (2008). Nonhost versus host resistance to the grapevine downy mildew, *Plasmopara viticola*, studied at the tissue level. *Phytopathology* 98, 776–780. doi: 10.1094/PHYTO-98-7-0776

Dong, X. (2004). NPR1, all things considered. *Curr. Opin. Plant Biol.* 7, 547–552. doi: 10.1016/j.pbi.2004.07.005

Dufour, M., Lambert, C., Bouscaut, J., Merillon, J., and Corio-Costet, M. (2013). Benzothiadiazole-primed defence responses and enhanced differential expression of defence genes in *Vitis vinifera* infected with biotrophic pathogens *Erysiphe necator* and *Plasmopara viticola*. *Plant Pathol.* 62, 370–382. doi: 10.1111/j.1365-3059.2012. 02628.x

Figueiredo, A., Monteiro, F., Fortes, A. M., Bonow-Rex, M., Zyprian, E., Sousa, L., et al. (2012). Cultivar-specific kinetics of gene induction during downy mildew early infection in grapevine. *Funct. Integr. Genomics* 12, 379–386. doi: 10.1007/s10142-012-0261-8

Figueiredo, A., Monteiro, F., and Sebastiana, M. (2015). First clues on a jasmonic acid role in grapevine resistance against the biotrophic fungus *Plasmopara viticola*. *Eur. J. Plant Pathol.* 142, 645–652. doi: 10.1007/s10658-015-0634-7

Fonseca, S., Chini, A., Hamberg, M., Adie, B., Porzel, A., Kramell, R., et al. (2009). ± 7-iso-Jasmonoyl-L-isoleucine is the endogenous bioactive jasmonate. *Nat. Chem. Biol.* 5, 344–350. doi: 10.1038/nchembio.161

Galet, P. (1977). *Mildiou*. Paris: Lavoisier.

Gauthier, A., Trouvelot, S., Kelloniemi, J., Frettinger, P., Wendehenne, D., Daire, X., et al. (2014). The sulfated laminarin triggers a stress transcriptome before priming the SA- and ROS-dependent defenses during grapevine's induced resistance against *Plasmopara viticola*. *PLoS ONE* 9:e88145. doi: 10.1371/journal.pone.0088145

Gessler, C., Pertot, I., and Perazzolli, M. (2011). *Plasmopara viticola*: a review of knowledge on downy mildew of grapevine and effective disease management. *Phytopathol. Mediter.* 50, 3–44.

Glazebrook, J. (2005). Contrasting mechanisms of defense against biotrophic and necrotrophic pathogens. *Annu. Rev. Phytopathol.* 43, 205–227. doi: 10.1146/annurev.phyto.43.040204.135923

Hamiduzzaman, M., Jakab, G., Barnavon, L., Neuhaus, J., and Mauch-Mani, B. (2005). beta-Aminobutyric acid-induced resistance against downy mildew in grapevine acts through the potentiation of callose formation and jasmonic acid signaling. *Mol. Plant Microbe Interact.* 18, 819–829. doi: 10.1094/MPMI-18-0819

Koornneef, A., and Pieterse, C. (2008). Cross talk in defense signaling. *Plant Physiol.* 146, 839–844. doi: 10.1104/pp.107.112029

Kortekamp, A., and Zyprian, E. (2003). Characterization of Plasmopara-resistance in grapevine using in vitro plants. *J. Plant Physiol.* 160, 1393–1400. doi: 10.1078/0176-1617-01021

Li, J., Brader, G., and Palva, E. (2004). The WRKY70 transcription factor: a node of convergence for jasmonate-mediated and salicylate-mediated signals in plant defense. *Plant Cell* 16, 319–331. doi: 10.1105/tpc.016980

Li, X., Wu, J., Yin, L., Zhang, Y., Qu, J., and Lu, J. (2015). Comparative transcriptome analysis reveals defense-related genes and pathways against downy mildew in *Vitis amurensis* grapevine. *Plant Physiol. Biochem.* 95, 1–14. doi: 10.1016/j.plaphy.2015.06.016

Marchive, C., Leon, C., Kappel, C., Coutos-Thevenot, P., Corio-Costet, M., Delrot, S., et al. (2013). Over-Expression of VvWRKY1 in grapevines induces expression of jasmonic acid pathway-related genes and confers higher tolerance to the downy mildew. *PLoS ONE* 8:e54185. doi: 10.1371/journal.pone.0054185

Millardet, A. (1881). *Notes sur les Vignes Américaines et Opuscules Divers sur le Même Sujet*. Bordeaux: Féret & Fils.

Monteiro, F., Sebastiana, M., Pais, M. S., and Figueiredo, A. (2013). Reference gene selection and validation for the early responses to downy mildew infection in susceptible and resistant *Vitis vinifera* cultivars. *PLoS ONE* 8:e72998. doi: 10.1371/journal.pone.0072998

Mur, L., Kenton, P., Atzorn, R., Miersch, O., and Wasternack, C. (2006). The outcomes of concentration-specific interactions between salicylate and jasmonate signaling include synergy, antagonism, and oxidative stress leading to cell death. *Plant Physiol.* 140, 249–262. doi: 10.1104/pp.105.072348

Pauwels, L., Barbero, G., Geerinck, J., Tilleman, S., Grunewald, W., Perez, A., et al. (2010). NINJA connects the co-repressor TOPLESS to jasmonate signalling. *Nature* 464, 788–791. doi: 10.1038/nature08854

Peressotti, E., Wiedemann-Merdinoglu, S., Delmotte, F., Bellin, D., Di Gaspero, G., Testolin, R., et al. (2010). Breakdown of resistance to grapevine downy mildew upon limited deployment of a resistant variety. *BMC Plant Biol.* 10:147. doi: 10.1186/1471-2229-10-147

Pieterse, C., Van Der Does, D., Zamioudis, C., Leon-Reyes, A., Van Wees, S., and Schekman, R. (2012). Hormonal modulation of plant immunity. *Annu. Rev. Cell Dev. Biol.* 28, 489–521. doi: 10.1146/annurev-cellbio-092910-154055

Polesani, M., Bortesi, L., Ferrarini, A., Zamboni, A., Fasoli, M., Zadra, C., et al. (2010). General and species-specific transcriptional responses to downy mildew infection in a susceptible (*Vitis vinifera*) and a resistant (*V. riparia*) grapevine species. *BMC Genomics* 11:117. doi: 10.1186/1471-2164-11-117

Portu, J., Santamaría, P., López-Alfaro, I., López, R., and Garde-Cerdán, T. (2015). Methyl jasmonate foliar application to Tempranillo vineyard improved grape and wine phenolic content. *J. Agric. Food Chem.* 63, 2328–2337. doi: 10.1021/jf5060672

Shim, J., Jung, C., Lee, S., Min, K., Lee, Y., Choi, Y., et al. (2013). AtMYB44 regulates WRKY70 expression and modulates antagonistic interaction between salicylic acid and jasmonic acid signaling. *Plant J.* 73, 483–495. doi: 10.1111/tpj.12051

Staswick, P., and Tiryaki, I. (2004). The oxylipin signal jasmonic acid is activated by an enzyme that conjugates it to isoleucine in *Arabidopsis*. *Plant Cell* 16, 2117–2127. doi: 10.1105/tpc.104.023549

Thines, B., Katsir, L., Melotto, M., Niu, Y., Mandaokar, A., Liu, G., et al. (2007). JAZ repressor proteins are targets of the SCFCO11 complex during jasmonate signalling. *Nature* 448, 661–665. doi: 10.1038/nature05960

Trouvelot, S., Varnier, A., Allegre, M., Mercier, L., Baillieul, F., Arnould, C., et al. (2008). A beta-1,3 glucan sulfate induces resistance in grapevine against *Plasmopara viticola* through priming of defense responses, including HR-like cell death. *Mol. Plant Microbe Interact.* 21, 232–243. doi: 10.1094/MPMI-21-2-0232

Unger, S., Bueche, C., Boso, S., and Kassemeyer, H. (2007). The course of colonization of two different vitis genotypes by *Plasmopara viticola* indicates compatible and incompatible host-pathogen interactions. *Phytopathology* 97, 780–786. doi: 10.1094/PHYTO-97-7-0780

Wasternack, C. (2007). Jasmonates: an update on biosynthesis, signal transduction and action in plant stress response, growth and development. *Ann. Bot.* 100, 681–697. doi: 10.1093/aob/mcm079

Wasternack, C., and Hause, B. (2013). Jasmonates: biosynthesis, perception, signal transduction and action in plant stress response, growth and development. an update to the 2007 review in Annals of Botany. *Bot.* 111, 1021–1058. doi: 10.1093/aob/mct067

Yan, Y., Stolz, S., Chetelat, A., Reymond, P., Pagni, M., Dubugnon, L., et al. (2007). A downstream mediator in the growth repression limb of the jasmonate pathway. *Plant Cell* 19, 2470–2483. doi: 10.1105/tpc.107.050708

Conflict of Interest Statement: The authors declare that the research was conducted in the absence of any commercial or financial relationships that could be construed as a potential conflict of interest.

The reviewer HK and handling Editor declared their shared affiliation, and the handling Editor states that the process nevertheless met the standards of a fair and objective review.

frontiers in Plant Science

ORIGINAL RESEARCH
published: 19 August 2015
doi: 10.3389/fpls.2015.00650

Phytoplasma infection in tomato is associated with re-organization of plasma membrane, ER stacks, and actin filaments in sieve elements

*Stefanie V. Buxa[1], Francesca Degola[2], Rachele Polizzotto[3], Federica De Marco[3], Alberto Loschi[3], Karl-Heinz Kogel[1], Luigi Sanità di Toppi[2], Aart J. E. van Bel[1] and Rita Musetti[3]**

[1] Department of Phytopathology and Applied Zoology, Justus Liebig University, Giessen, Germany, [2] Department of Life Sciences, University of Parma, Parma, Italy, [3] Department of Agricultural and Environmental Sciences, University of Udine, Udine, Italy

Phytoplasmas, biotrophic wall-less prokaryotes, only reside in sieve elements of their host plants. The essentials of the intimate interaction between phytoplasmas and their hosts are poorly understood, which calls for research on potential ultrastructural modifications. We investigated modifications of the sieve-element ultrastructure induced in tomato plants by '*Candidatus* Phytoplasma solani,' the pathogen associated with the stolbur disease. Phytoplasma infection induces a drastic re-organization of sieve-element substructures including changes in plasma membrane surface and distortion of the sieve-element reticulum. Observations of healthy and stolbur-diseased plants provided evidence for the emergence of structural links between sieve-element plasma membrane and phytoplasmas. One-sided actin aggregates on the phytoplasma surface also inferred a connection between phytoplasma and sieve-element cytoskeleton. Actin filaments displaced from the sieve-element mictoplasm to the surface of the phytoplasmas in infected sieve elements. Western blot analysis revealed a decrease of actin and an increase of ER-resident chaperone luminal binding protein (BiP) in midribs of phytoplasma-infected plants. Collectively, the studies provided novel insights into ultrastructural responses of host sieve elements to phloem-restricted prokaryotes.

Keywords: actin, BiP protein, endoplasmic reticulum, phloem, phytoplasmas, plasma membrane, sieve elements

OPEN ACCESS

Edited by:
Erh-Min Lai,
Academia Sinica, Taiwan

Reviewed by:
Saskia A. Hogenhout,
The John Innes Centre, UK
Jun-Yi Yang,
National Chung Hsing University, Taiwan

****Correspondence:***
Rita Musetti,
Department of Agricultural and Environmental Sciences, University of Udine, Via delle Scienze, 206, I-33100 Udine, Italy
rita.musetti@uniud.it

Specialty section:
This article was submitted to Plant Biotic Interactions, a section of the journal Frontiers in Plant Science

Received: *18 May 2015*
Accepted: *05 August 2015*
Published: *19 August 2015*

Citation:
Buxa SV, Degola F, Polizzotto R, De Marco F, Loschi A, Kogel K-H, Sanità di Toppi L, van Bel AJE and Musetti R (2015) Phytoplasma infection in tomato is associated with re-organization of plasma membrane, ER stacks, and actin filaments in sieve elements. Front. Plant Sci. 6:650. doi: 10.3389/fpls.2015.00650

Introduction

Phytoplasmas are biotrophic plant-pathogenic wall-less prokaryotes (class *Mollicutes*), phylogenetically related to the low G + C Gram-positive bacteria (Weisberg et al., 1989). Phytoplasmas are associated with several 100s of diseases affecting important crops including ornamentals, vegetables, and fruit trees (Lee et al., 2000). They occur restricted to the sieve elements of host plants and are transmitted to other plants *via* sieve-tube sap feeding leafhoppers (*Cicadellidae*), planthoppers (*Cixiidae*) or psyllids (*Psyllidae*) in a persistent manner (Hogenhout et al., 2008).

Plant–phytoplasma interactions have been poorly characterized due to a lack of techniques. Thus far, it has been impossible to transform or genetically modify phytoplasmas, or simply isolate different strains from mixtures present in nature (Seemüller et al., 2013). Methods for *in vitro* culture of phytoplasmas await further confirmation of feasibility (Contaldo et al., 2012).

Infection of plants by phytoplasmas leads to massive changes in phloem physiology associated with a severely impaired assimilate translocation (Musetti et al., 2013). This leads to characteristic symptoms such as low productivity, stunting, general decline, and reduced vigor of the host (Kartte and Seemüller, 1991). While the macroscopic consequences of phytoplasma activity on host plants have been amply described (Bertaccini, 2007), the effects phytoplasma infection on the ultrastructure of the host cells have been insufficiently examined. In particular, crucial phytopathogenic traits such as adhesion ability to sieve-element membrane (as assumed by Seemüller et al., 2013), as well as the relationship with the sieve endoplasmic reticulum (SER) and sieve-element actin have not yet been studied. Since phytoplasmas probably may exert their action on plants by binding to sieve-element components (Christensen et al., 2005), this study focused on the ability of phytoplasmas to interact with the sieve-element plasma membrane, SER, and sieve-element actin. Resin-embedded leaf sections of healthy and stolbur-affected tomato (*Solanum lycopersicum*) plants [the disease associated with the '*Candidatus* Phytoplasma solani' ('*Ca*. P. solani')] were examined by transmission electron microscopy (TEM) combined with immunogold labeling (Musetti et al., 2002).

By western blot analyses of protein extracts from midribs of healthy and '*Ca*. P. solani'-infected plants, expression levels of actin and ER-resident chaperone BiP (luminal binding protein) – the latter was chosen as marker of the ER-stress response (Lee, 2005) – were quantified.

The studies provided evidence that infection of *S. lycopersicum* with '*Ca*. P. solani' leads to abnormalities in the sieve-element plasma membrane – SER – actin network. Intimate structural links between phytoplasma body and host cell membranes seem to point to a complex interplay between host and invader during phytoplasma infection.

Materials and Methods

The preparation of plant material and the microscopy analyses have been performed according the methods previously reported by Buxa (2014).

Plant Material and Phytoplasma Inoculation

Four *S. lycopersicum* plants ('cv Micro-Tom') were infected with the stolbur phytoplasma '*Ca*. P. solani' (subgroup 16 SrXII-A, Quaglino et al., 2013) by grafting. Shoot tips from naturally infected tomato plants, grown in the field, were used as scions and grafted onto 50-days-old healthy tomato plants, in a greenhouse (27°C day, 20°C night). Four 50-days-old, uninfected tomato plants, grown in a greenhouse, were also grafted using shoot tips from healthy plants, and served as controls. Analyses were performed with the advent of symptoms, when plants were three and half months old.

Phytoplasma presence was assessed in randomly collected leaf samples by real time RT-PCR analyses. Total RNA was extracted from 1 g of frozen leaf midribs using RNeasy Plant Mini Kit (Qiagen GmbH, Hilden, Germany). RNAs were reverse-transcribed using a QuantiTect Reverse Transcription Kit (Qiagen GmbH, Hilden, Germany) with random hexamers, following the manufacturer's instructions. Real time RT-PCR analyses were performed using the primers 16S stol F2/R3 based on the 16SrRNA gene of '*Ca*. P. solani' (accession n° AF248959, Santi et al., 2013a). Real time RT-PCR reactions were set up with 2X Sso Fast^{TM} Eva Green® Supermix (Bio-Rad Laboratories Co., Hercules, CA, USA), primers at 400 nM each, and 10 ng of cDNA in a total volume of 10 μl. The reactions were performed in a CFX96 Real Time PCR Detection System (Bio-Rad Laboratories Co., Hercules, CA, USA) using the following conditions: 95°C for 2 min, 40 cycles of 95°C for 15 s and 60°C for 1 min. The melting curve was performed with a ramp from 60 to 95°C.

Conventional Transmission Electron Microscopy

Fifteen randomly chosen leaf midrib segments, sampled from the four either infected or healthy tomato plants, were cut into pieces 6–7 mm in length, fixed in a solution of 3 % glutaraldehyde in 0.1M phosphate buffer (PB), pH 7.2, for 2 h at 4°C, washed for 30 min at 4°C in PB and post-fixed for 2 h with 1% (w/v) OsO_4 in PB at 4°C (Musetti et al., 2011). Samples were dehydrated in ethanol and propylene oxide, embedded in Epon/Araldite epoxy resin (Electron Microscopy Sciences, Fort Washington, PA, USA). Serial ultrathin sections (60–70 nm) of about 60 samples from each healthy or infected plant, were cut using an ultramicrotome (Reichert Leica Ultracut E ultramicrotome, Leica Microsystems, Wetzlar, Germany) and collected on 200 mesh uncoated copper grids, stained and then observed under a Philips CM 10 (FEI, Eindhoven, The Netherlands) TEM operating at 100 kV.

Sample Preparation for Electron Microscopy of Immuno-Labeled Sections

Fifteen randomly chosen leaf midrib segments were excised from infected or healthy tomato plants. Segments were cut into small portions (6–7 mm in length), fixed in 0.2% glutaraldehyde, rinsed in 0.1 M PB, pH 7.4 and dehydrated in graded ethanol series (25-, 50-, 75%, 30 min for each step) at 4°C. After 1 h of the final 100% ethanol step, the samples were infiltrated in a hard-grade London Resin White (LRW; Electron Microscopy Sciences, Fort Washington, PA, USA)-100% ethanol mixture in the proportion 1:2 for 30 min, followed by LRW:ethanol 2:1 for 30 min, and 100% LRW overnight at room temperature (with a change 1 h after the start of the infiltration). The samples were embedded in Eppendorf tubes using fresh LRW containing benzoyl peroxide 2% (w/w) according to manufacturer's protocol and polymerized for 24 h at 60°C (Musetti et al., 2002).

Immunogold Labeling

Several serial ultrathin sections (60–70 nm) of about 60 LR-White-embedded samples from each healthy or infected plant were cut using an ultramicrotome (Reichert Leica Ultracut E ultramicrotome, Leica Microsystems, Wetzlar, Germany) and collected on carbon/formvar coated 400 mesh nickel grids (Electron Microscopy Sciences, Fort Washington, PA, USA).

To visualize the presence and distribution of actin in LR-White-embedded plant tissue, immunogold-labeling technique was performed (modified after White et al., 1994). Unspecific binding sites, were blocked placing grids carrying the sections on droplets of blocking solution containing normal goat serum (NGS) diluted 1:30 in 1% BSA in PBS, pH 7.6, for 2 h at room temperature. Subsequently, the grids were incubated overnight at 4°C with primary mouse monoclonal antibody against actin (MAB anti-actin, clone C11, Agrisera, Vännäs, Sweden) diluted 1:200 in blocking solution. Control grids were incubated in 1% BSA/PBS without primary antibody. All grids were then rinsed with PBS, and treated for 1 h at room temperature with secondary goat anti-mouse antibody coated with colloidal 5 nm gold particles (GAM 5; Auro Probe EM GAM G5 Amersham, Arlington Heights, IL, USA), diluted 1:40 in 1% BSA/PBS. After staining with 3% uranyl acetate and 0.1% lead citrate (Reynolds, 1963) samples were observed under TEM, as reported above.

To assess the subcellular distribution of actin labeling, immunogold particle number was determined in healthy and infected sieve elements. Gold spots were manually counted and recorded on plasma membrane, cytoplasm (i.e., mictoplasm, Hafke et al., 2013) and lumen of three sieve elements in three not-serial sections (Bamunusinghe et al., 2009).

Western Blot Analyses

Total proteins were extracted from *S. lycopersicum* midribs: 150 mg of fresh tissue from three healthy and three stolbur-diseased plants were frozen in liquid nitrogen with 200 ml of glass microbeads (diameter 200 mm), ground to a powder with a dental amalgamator (TAC 200/S Amalgamator, Linea TAC, Italy), and resuspended in 300 µl of lysis buffer [50 mM TRIS-HCl pH 7.5, 2 M thiourea, 7 M urea, 2% (v/v) Triton X-100, 1% dithiothreitol (DTT), 2% (w/v) polyvinylpolypyrrolidone (PVP), 1 mM PMSF, 0.2% β-mercaptoethanol]. Samples were centrifuged at 15000 × *g* for 20 min at 4°C, then the supernatant was recovered and subjected to a second centrifugation (15000 × *g* for 20 min at 4°C). The protein concentration was assessed according to Bradford (1976) using bovine serum albumin as standard (BSA, Sigma, USA). For each sample 20 µg of total protein was separated in a 12% acrylamide SDS-PAGE (Laemmli, 1970) and blotted at 100 V for 60 min to a nitrocellulose membrane (GE Healthcare Bio-Sciences AB, Uppsala, Sweden) using a Mini Trans-Blot cell apparatus (Bio-Rad Laboratories, Hercules, CA, USA). Both protein loading and transfer efficiency were verified by Ponceau-S staining. For quantitative analysis of actin and ER stress-sensor BiP, western blot analyses were performed with polyclonal antibodies raised against *Arabidopsis thaliana* actin (AS132640; Agrisera AB, Vännäs, Sweden) and BiP luminal-binding protein (AS09481; Agrisera AB, Vännäs, Sweden) diluted 1:2500 and 1:10000, respectively. Membranes were blocked 1 h in PBS 5% (w/v) skim milk, probed with primary antibodies for 1 h and with anti-rabbit IgG horseradish peroxidase conjugated antibody (GE Healthcare Bio-Sciences AB, Uppsala, Sweden) for 1 h. Chemiluminescence detection was assessed with Pierce ECL Plus Western blot Substrate system (Pierce Biotechnology, Rockford, IL, USA), according to manufacturer's instructions.

Quantification and Statistical Analysis

An ANOVA procedure with SPSS software version 21.0 (IBM SPSS Statistics, Armonk, NY, USA) evaluated differences in the number of gold particles observed in healthy and infected sieve elements. Homogeneity of variance and distributional assumptions were assessed via the Levene test. A significance level of 0.05 was used for all comparisons.

A densitometric analysis was conducted on actin and BiP Western Blot signals with Quantity One 4.6.6. Bio-Rad Software (Bio-Rad Laboratories, Hercules, CA, USA). A total of six samples for each plant were analyzed. The statistical analysis of densitometric values was performed with the unpaired *t*-test.

Results

Plant Symptom Development and Phytoplasma Molecular Detection

Control plants were regularly grown, without disease symptoms. In stolbur-infected plants, typical symptoms, such as leaf yellowing, leaf-size reduction, witches' brooms and stunting, emerged nearly 2 months after grafting (**Figure 1**). Real

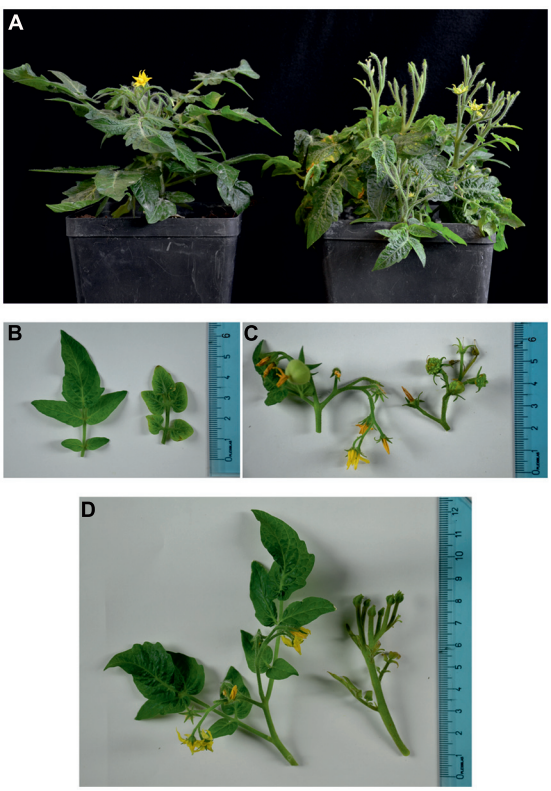

FIGURE 1 | (A–D) Images of healthy (left half of the panels) and stolbur-infected (right half) tomato Micro-Tom plants. Healthy tomato plants show regular growth, normal leaves and flowers are present, whereas in stolbur-infected plants diffuse symptoms are visible **(A)**. Leaf blades are severely reduced **(B)**. Buds are aborted; flowers are malformed with green petals **(C)**. Shoots develop witches' brooms and show a stunted habit **(D)**.

time RT-PCR of '*Ca*. P. solani' *16SrRNA* confirmed the presence of phytoplasmas in leaf samples from stolbur-infected *S. lycopersicum* before treatment for microscopic examination. Starting from 40 ng of total cDNA, stolbur phytoplasma *16SrRNA* was amplified in infected plants, whereas no amplification of the *16SrRNA* gene was obtained in control plants (**Table 1**).

Sieve-Element Membrane Structures in Control and Infected Plants

In total, 60 sections from the 15 embedded blocks have been screened by TEM. TEM images revealed the sieve-element plasma membrane appressed to the cell wall in healthy leaves (**Figure 2A**). In infected samples, the plasma membrane of the phloem cells (phloem parenchyma cells, companion cells and sieve elements – SEs) was deformed, invaginated or undulating (**Figures 2B–H**). The membrane of parietal phytoplasmas and the sieve-element plasma membrane appeared in close contact (**Figure 2D**) *via* a membrane-bound structure forming a firm connection (**Figures 2E–H**). The typical pleomorphism and the ribosomes inside the bacterial bodies (**Figure 2D**) enabled a ready discrimination between phytoplasmas and sieve-element plastids (SEPs) even though size and location were similar (see **Figure 5B** and Ehlers et al., 2000). The characteristic multiple anchoring of SEPs to the sieve-element plasma membrane (Ehlers et al., 2000) was never observed for phytoplasmas.

Sieve-Element Actin and Sieve Endoplasmic Reticulum and their Connections with Phytoplasma Cells by Transmission Electron Microscopy

Control sections (from both healthy and infected samples), incubated with buffer alone, did not show labeling (not shown). In agreement with labeling with α-actin-gold-conjugated antibodies, actin occurred along the sieve-element membrane (**Figure 3A**), in the sieve-element mictoplasm and lumen (**Figures 3B–D**), and also in companion cell cytoplasm. The existence of an actin network in sieve elements has recently been demonstrated by Hafke et al. (2013).

In infected samples, high spatial resolution images revealed a co-localization of sieve-element actin and phytoplasma cells (**Figures 4A–D**). Ultrastructural images obtained from infected samples indicated that antibody dots exclusively resided in the sieve-element lumen in association with phytoplasma cells and were always aggregated at one side of the phytoplasma membrane surface (**Figures 4A–D**). Within sieve pores too, actin was localized to phytoplasma cells (**Figure 4D**). These actin fields often co-localized with the tubular corridors between phytoplasma body and plasma membrane (e.g., **Figure 4D**).

Gold particles were counted to determine the labeling distribution in sieve-element membrane, mictoplasm and lumen. The countings were statistically analyzed (**Table 2**). In healthy sieve elements, gold particles were mainly found in the mictoplasm and in association with the membrane, whereas in the cell lumen they were significantly less abundant. In infected sieve elements, gold particles were observed, almost exclusively, in the lumen, in association with phytoplasmas. Gold spots in the lumen of phytoplasma-infected sieve elements were significantly more abundant compared to those recorded in the lumen of healthy ones (**Table 2**) which indicates a displacement of actin away from the plasma membrane. It was noteworthy that the absolute number of actin dots per sieve-element cross-section was approximately 35% lower than in control sieve elements (**Table 2**).

TEM images of healthy samples showed SER stacks mostly orientated parallel to the sieve-element plasma membrane (**Figures 5A,B**), while the SER seems to be distorted in stolbur-diseased samples (**Figures 5C–F**). In infected plants, SER stacks frequently were fragmented into lobes and vesicles intruding into the sieve-element lumen (**Figure 5F**). Besides phytoplasmas attached to sieve-element plasma membrane (as above reported and **Figure 5E**) or free-lying in the lumen (**Figure 5C**), phytoplasma cells were located near to the SER (**Figures 5C,E**), but minute anchors attaching to the SER-stacks (as reported for sieve element plastids, Ehlers et al., 2000) were absent. Strikingly, actin labeling was absent on the surface of phytoplasmas adhered to the ER. Two modes of parietal contact seem to occur: adhesion to the ER or tubular contacts with the plasma membrane which probably concur in time (**Figure 5E**).

TABLE 1 | Molecular detection of '*Candidatus* Phytoplasma solani' in tomato plants.

Well	Label	Primers	C_q
F1	Stolbur-infected *S. lyc* 1	16SRT f2r3	17.98
F2	Stolbur-infected *S. lyc* 2	16SRT f2r3	19.38
F3	Stolbur-infected *S. lyc* 3	16SRT f2r3	17.54
F4	Stolbur-infected *S. lyc* 4	16SRT f2r3	16.10
F5	C. roseus Stol+	16SRT f2r3	17.55
F6	Grapevine Stol+	16SRT f2r3	23.50
F7	Tomato C–	16SRT f2r3	None
F8	H_2O	16SRT f2r3	None

Stolbur phytoplasma 16SrRNA was detected in infected plants, whereas no amplification was obtained in control plants.
Cq: quantification cycle (the cycle in which the threshold line intersects the amplification curve of the sample in the exponential phase of the reaction).
F1–F4: stolbur-infected Solanum lycopersicum samples.
F5: stolbur-infected Catharanthus roseus, positive control.
F6: stolbur-infected grapevine, positive control.
F7: healthy S. lycopersicum, negative control.

Alteration of Actin and BiP Protein Expression in Stolbur-Diseased Tomato Midribs

Western Blot analyses (**Figures 6A–D**) were performed on midrib extracts from healthy and stolbur-diseased plants. The rationale of using midribs is that they contain the sieve elements as the phytoplasma carriers. This approach revealed that actin and BiP protein levels significantly varied in infected plants compared to the healthy ones (**Figure 6A**). Densitometric analyses indicated that the actin level in extracts from infected midribs was significantly lower than in healthy ones (**Figure 6C**). The 40% decrease (**Figure 6C**) is in agreement with the decreased actin contents measured by immuno-gold labeling (**Table 2**). By contrast, infected tissues displayed a 6.3-fold-increased BiP protein level in comparison with healthy samples (**Figure 6D**).

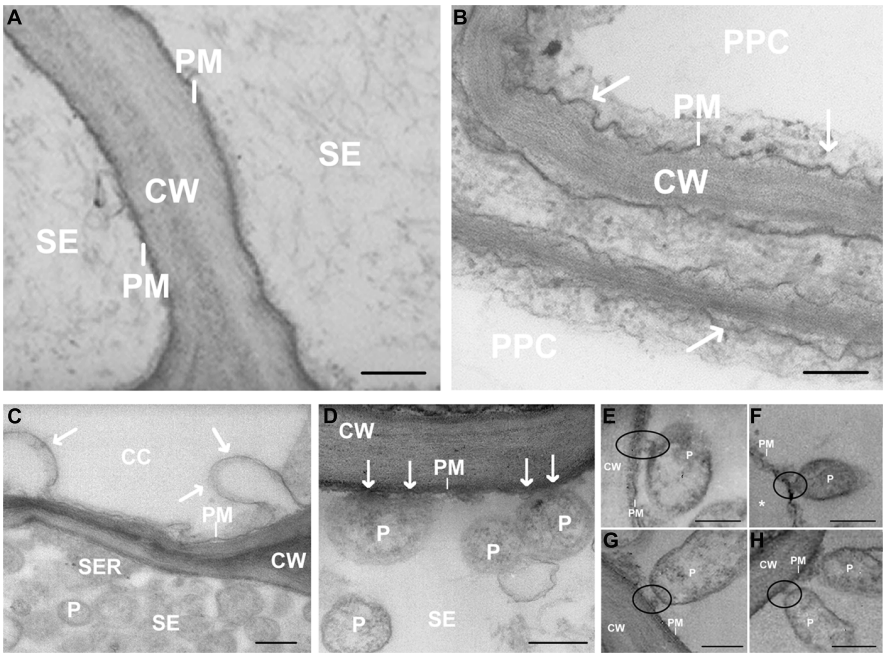

FIGURE 2 | (A–H) Transmission Electron Microscopy (TEM) micrographs of main vein cross-sections of healthy **(A)** and stolbur-diseased tomato leaves **(B–H)**. Arrows in **(B–D)** indicate cell membrane disorganization and black circles in **(E–H)** show attachment of phytoplasma body to sieve-element plasma membrane. * indicates a detachment of the SE plasma membrane from the wall. CW, cell wall; P, phytoplasma; PM, plasma membrane; CC, companion cell; PPC, phloem parenchyma cell; SE, sieve element. Scale bars **(A)** = 400 nm; **(B–H)** = 200 nm.

The densitometric differences in protein expression of both actin and BiP in healthy and infected plants turned out to be highly significant (p-value ≤ 0.001).

Discussion

It has been advanced that cytological relationships between phytoplasmas and sieve elements are essential for the establishment of pathogenic activity in the host (Christensen et al., 2005). Despite their presumptive importance, structural changes during infection have not been investigated in depth. Past and recent studies hinted at structural modifications of host tissue triggered by phytoplasma infection (Rudzińska-Langwald and Kamińska, 2001; Musetti et al., 2013; Santi et al., 2013b). Moreover different effectors providing communication in phytoplasma–plant and phytoplasma–insect interrelationships, have been described (Hoshi et al., 2007; Bai et al., 2009; Galetto et al., 2011; McLean et al., 2014; Sugio et al., 2014). The present EM studies demonstrate massive structural modifications of infected sieve elements (**Figures 2–5**), which may be accompanied by profound metabolic changes (**Figure 6**).

Interconnections between Phytoplasmas and Sieve-Element Plasma Membrane

Among the diverse traits of *Mollicutes* infecting humans and animals, adherence to host membranes is regarded as an important pathogenic factor (Razin et al., 1998). Phytoplasmas seem to be in close contact with the sieve-element plasma membrane (Marcone, 2010), but specific adherence structures to host membranes have not been described. Adherence would be feasible, since several studies demonstrated the existence of a subset of adhesin-like membrane proteins in most phytoplasmas (for a review, see Kube et al., 2012; Neriya et al., 2014).

TABLE 2 | Sieve elements of healthy and infected tomato were analyzed by immunogold labeling and electron microscopy, to assess actin subcellular distribution.

Sample	# Fields	Membrane	Lumen	Mictoplasm	Total gold particles
Healthy	9	12.00 ± 2.35 a	4.78 ± 5.09 b	16.89 ± 6.17 a	303
Infected	9	0.00 ± 0.00	23.11 ± 1.62 c	0.00 ± 0.00	210

Fields are defined as the cross sections of three sieve elements observed in three non-serial sections. Gold particles in each field were counted manually and determined for the sieve-element plasma membrane, mictoplasm and lumen. Zeros indicate subcellular domains without immunogold label. Different letters next to each standard deviation represent significant differences. P-values < 0.05.

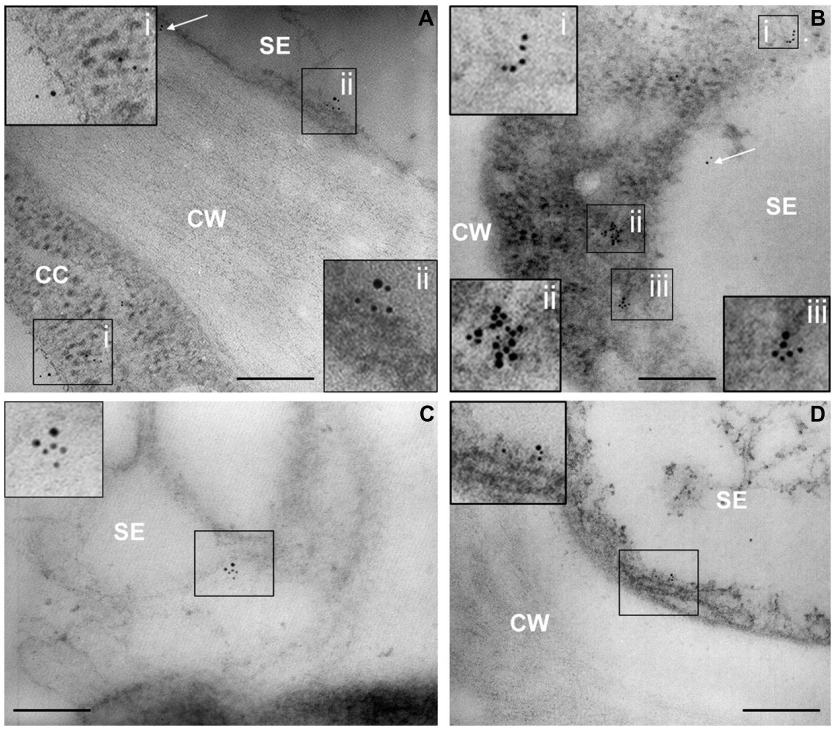

FIGURE 3 | (A–D) TEM micrographs of main-vein cross-sections of healthy tomato leaves. Gold labeling of SE actin was clustered at the plasma membrane (**A,D**, squares) and the near cytoplasm area (mictoplasm) of sieve elements (**B,C**, squares). Labeling also occurs on the proximity of cell walls (**A**, arrow), in the lumen of the SEs (**B**, arrow) and in the cytoplasm of the adjacent companion cells **(A)**. In insets, areas of interest of **(A–D)**, are magnified. CC, companion cell; CW, cell wall; SE, sieve element; Scale bars = 200 nm.

Here, TEM observations evidence major modifications of the plasma membrane in infected sieve elements. Parietally located phytoplasmas do not only adhere to the SER (**Figure 5**), but also form intimate tubular contacts toward the SE plasma membrane (**Figures 2E–H**). In some pictures (**Figures 2H** and **5E**) both forms of contact were observed side by side.

Interconnections between Phytoplasmas and Host Cytoskeleton

Both animal and plant pathogens actively interact with the host cytoskeleton to successfully enter in the host (Rottner et al., 2005; Pizarro-Cerdá and Cossart, 2006) and move inside host cells (Tilney and Portnoy, 1989; Sansonetti, 1993; Opalski et al., 2005). Phytoplasmas interact with the host cytoskeleton by means of membrane proteins (so-called antigenic membrane proteins, AMP or immunodominant membrane proteins, IMP), capable to bind to the vector (Suzuki et al., 2006; Galetto et al., 2011) or plant actin filaments (Boonrod et al., 2012).

In our study, the connection between the invader phytoplasma and sieve-element actin has been described *in situ*. Apparently, phytoplasmas impose a reorganization that anchors SE actin to the phytoplasma surface. As already known for other prokaryotes (Lybarger and Maddock, 2001; Dworkin, 2009), the connection between actin and phytoplasma turned out to be unilateral, indicating a polarity in the phytoplasma body. Unipolar acquisition and polymerization of host actin has evolved, in particular, in Gram-positive intracellular pathogenic bacteria, such as *Listeria monocytogenes*, to facilitate cell-to-cell spread (Lybarger and Maddock, 2001). A similar asymmetric polymerization of host actin may occur in phytoplasma-infected sieve elements to enable bacterial movement (Rudzińska-Langwald and Kamińska, 1999). Likewise, interaction between phytoplasmas and host actin (Boonrod et al., 2012) may facilitate bacterial spread through the narrow sieve pores *via* pleomorphic modification of phytoplasma *corpus*, as indicated by concurrent gold labeling of sieve-plate areas and phytoplasmas (**Figure 4D**). Phytoplasmas do not appear to possess actin thus far (Christensen et al., 2005), but they have contractile membrane proteins (Kakizawa et al., 2006), which might help to pass the sieve pores, which have smaller diameters (e.g., van Bel, 2003) than those of phytoplasmas (Hogenhout et al., 2008). In plant cells, movement of organelles, including plastids, depends on their interaction with cytoskeleton and ER (Schattat et al., 2011). Phytoplasmas being in the size range of plastids may use a similar actin-based mechanism of displacement.

To gain additional evidence for actin involvement in the sieve-element interaction with phytoplasmas, quantitative actin expression analyses were carried out. Western blotting and gold labeling demonstrated that the interaction between phytoplasmas and actin in infected sieve elements is associated with a

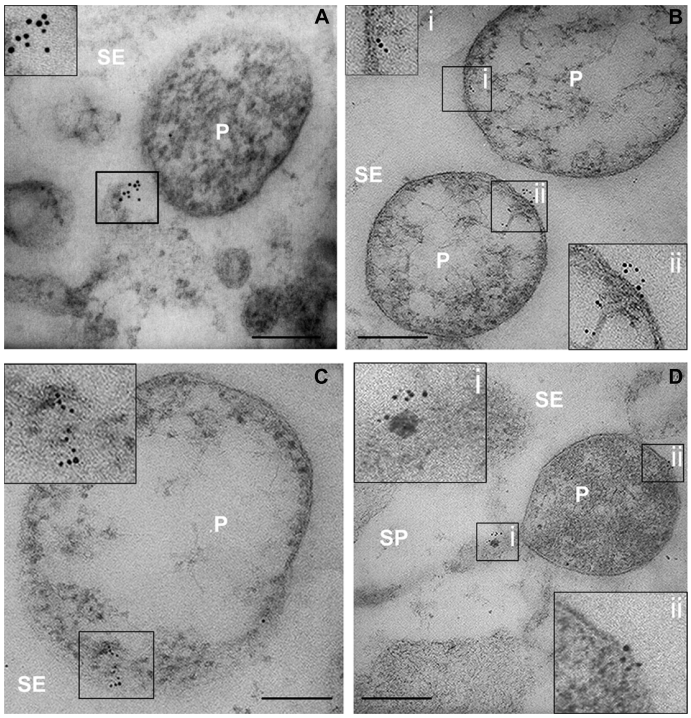

FIGURE 4 | (A–D) TEM micrographs of main-vein cross-sections of stolbur-diseased tomato leaves. Aggregated of SE actin in contact with the phytoplasma cells were evidenced by a TEM-immunogold technique. In insets, areas of interest of **(A–D)**, are magnified. P, phytoplasma; SE, sieve element; SP, sieve pore. Scale bars = 200 nm

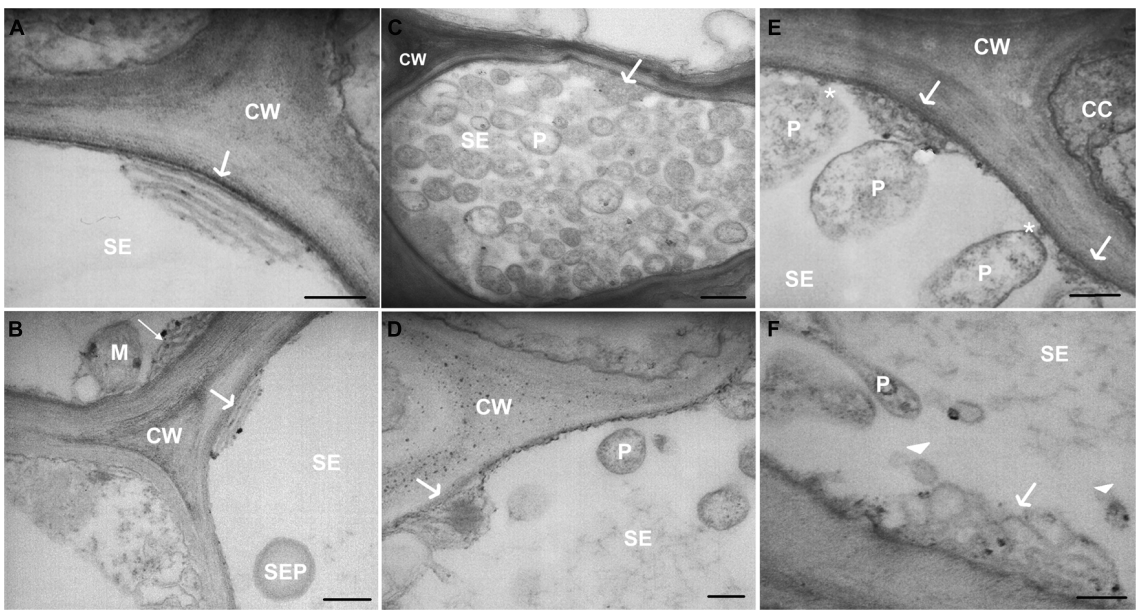

FIGURE 5 | (A–F) TEM micrographs of main veins cross-sections of healthy **(A,B)** and stolbur-diseased tomato leaves **(C–F)**. Arrows point to ER organization, asterisks indicate attachment of phytoplasma cell to sieve-element plasma membrane. In stolbur-diseased samples SER cisternae were frequently intruding into the sieve-element lumen **(C–E)** and were fragmented into lobes and vesicles **(F)**. CC, companion cell; CW, cell wall; M, mitochondria; P, phytoplasma; PM, plasma membrane; SE, sieve element; SEP, sieve-element plastid. Scale bars **(A,B,D)** = 200 nm; **(C)** = 400 nm.

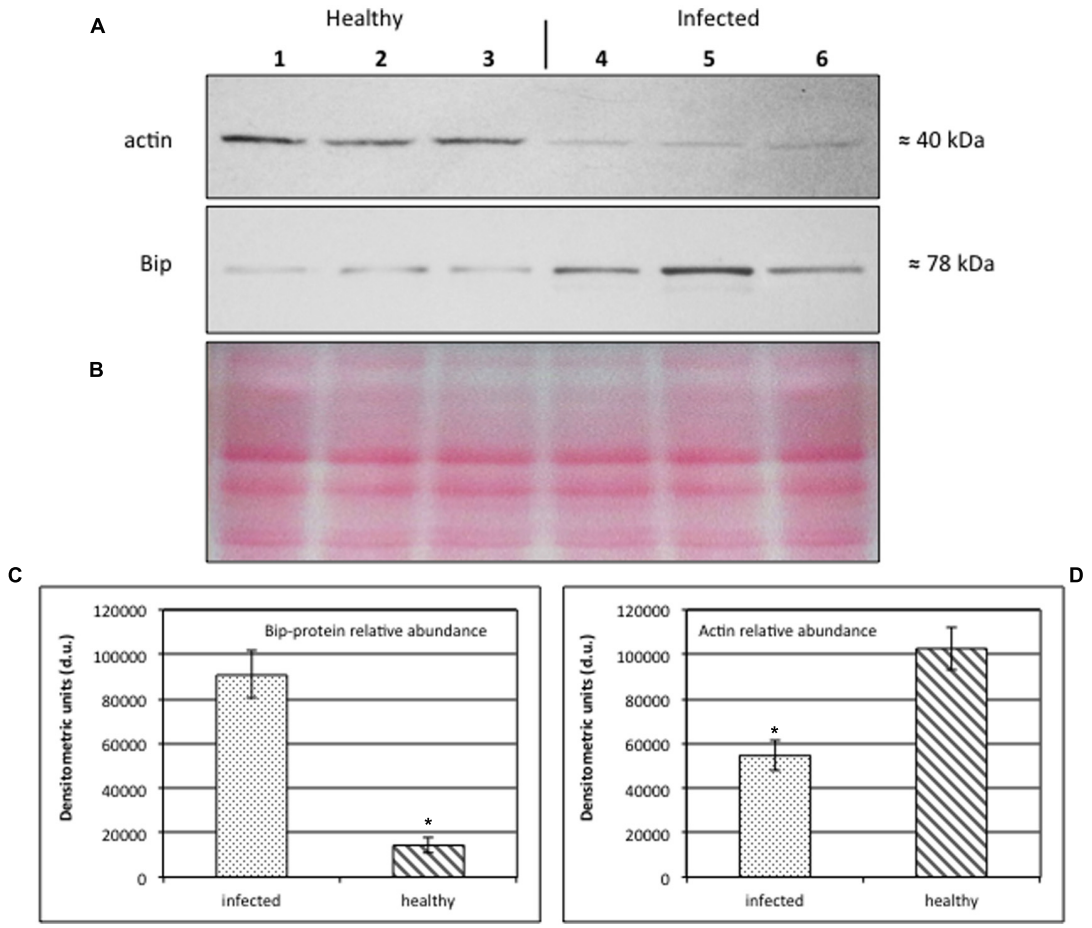

FIGURE 6 | (A–D) Western blot analyses of *S. lycopersicum* midrib extracts. Three healthy (lanes 1–3) and three infected (lanes 4–6) plants were analyzed. Immunoreactive signals corresponding to actin and ER luminal binding protein (BiP) displayed the expected molecular weights of ≈40 and ≈78 kDa, respectively **(A)**. Amount of loaded protein were checked by Ponceau-S staining **(B)**. Quantification of immunoreactive luminescence signals was achieved by densitometric scanning of the respective actin **(C)** and BiP **(D)** bands. The mean of six replicates (±SD) was calculated for each sample. Actin *T*-value: –9.977; BiP *T*-value: 15.068. * denotes significant difference of the means (P-values $\leq$ 0.001).

decrease of the amount of actin. This interpretation should be made with care, as it departs from the assumption that the changes occur in sieve elements, the exclusive location of phytoplasmas. It is not excluded that part of the changes occurs in the surrounding (vascular) cells given the use of entire midribs. Nevertheless, a similar reduction of actin content in infected cells measured in expression studies (**Figure 6**) and in immuno-labeling studies (**Table 2**) render credibility to the view that the values obtained with midribs hold for sieve elements.

Dynamic actin re-arrangement is regulated by a pool of actin-binding proteins, named actin depolarizing factors (ADFs), which sense stresses and environmental modifications and regulate the cytoskeleton through diverse biochemical activities (Hussey et al., 2006; Staiger and Blanchoin, 2006), responsible for actin turnover. High levels of ADFs confer high severing frequencies and decreased actin filament lengths and lifetimes (Henty et al., 2011) and, hence a dramatic decrease of the overall number of actin filaments (Thomas et al., 2006). These events would explain the decreased western blot signals in infected tissue.

In stolbur-diseased plants, ADF genes have been reported significantly overexpressed (Hren et al., 2009). The decrease of polymerized actin might be correlated with an activation of host defense mechanisms, since actin depolymerization is a potential inductor of plant defense responses (Kobayashi and Kobayashi, 2007). Although the manner in which actin disruption is linked with the defense response is unclear given the dynamic behavior of actin filaments in immune responses, evidence is accumulating that actin participates in cellular signaling cascades in phytoplasma–host interaction (Boonrod et al., 2012).

Furthermore, ADF activates actin-based motility of bacteria, as reported for *Listeria monocytogenes* (Carlier and Pantaloni, 2007) increasing the rate of propulsion by shortening the actin tails. Shorter actin filaments could therefore be of advantage for phytoplasma movement along the sieve-element cytoskeleton.

Phytoplasma Effects on the Structure of the Sieve-Element Reticulum

Rudzińska-Langwald and Kamińska (2001) observed that SER was often situated in the sieve-element lumen being separated from the plasma membrane and in close association with phytoplasmas in sieve elements of *Limonium sinuatum* infected by Aster Yellows. Here (**Figure 5**), SER undergoes a re-organization in infected sieve elements accompanied by a deformation of the SER stacks, resulting in expansion of the cisternae, development of the lobes and fragmentation into vesicles. Such morphological modifications have been described as part of the "unfolded protein response" (UPR; Bernales et al., 2006), characterized by the accumulation of unfolded proteins in the SER. External stimuli such as pathogen invasion, nutrient deficiency and other environmental factors exert stress on the cellular metabolism leading to aberrations in Ca^{2+} or redox regulation and protein synthesis. These responses enhance the level of misfolded proteins in the ER and trigger UPR (Ye et al., 2011). The UPR is considered important to recover the normal function of ER, to mitigate the stress exerted on the ER, and to prevent the cytotoxic impact of malformed proteins (Jelitto-Van Dooren et al., 1999; Xu et al., 2005; Slepak et al., 2007; Urade, 2007; Preston et al., 2009). In both mammals and plants, the UPR mechanism also includes increased synthesis and activity of several ER-resident proteins, such as the ER chaperone BiP. We found a sevenfold increase of BiP protein levels in stolbur-diseased plants. This suggests a phytoplasma-triggered UPR similar to what has been reported for tobacco infected with Potato Virus X (Ye et al., 2011).

Conclusion

In conclusion, our results show that stolbur-phytoplasma infection results in a significant re-organization of the sieve-element ultrastructure in phloem tissue of *S. lycopersicum*.

Despite the structural interconnections between phytoplasmas and the host sieve-element plasma membrane and actin and the massive impact of phytoplasma infection on the SER ultrastructure, the functional nature of the interactions remains largely unclear. The changes probably express a transformation that benefits growth, maintenance and transport of phytoplasmas. Phytoplasmas may effectively re-arrange the host ultrastructure to enable nutrient supply and systemic spread *via* the sieve elements, which enables a fast distribution and proliferation of bacteria inside the host plant. On the other hand, the extensive re-organization of the membrane systems and actin network in sieve elements provoked by '*Ca*. P. solani' may also be a protective answer of the plant to ensure fast defense reactions and signaling. Unlike other plant cells, the sieve elements do not contain several significant organelles (e.g., Knoblauch and van Bel, 1998) indispensable for most plant immune responses, so the release of effector proteins by phytoplasmas into other phloem cells (Bai et al., 2009) *via* plasmodesmata might induce a profound alteration of the host sieve elements.

Author Contributions

RM and SB conceived the project under the supervision of AvB and KK, SB, and RM established the protocols for the electron microscopy and performed microscopical observations. AL prepared infected tomato plants. FDM and RP performed phytoplasma detection by real-time RT-PCR on tomato leaves. FD and LS established the protocols and performed western blot analyses. SB and RM wrote the manuscript with extensive support of AvB.

Acknowledgment

This work was supported by the International Giessen Graduate Centre for the Life Sciences (GGL) founded by the Deutscher Akademischer Austauschdienst (DAAD) and by the University of Udine.

References

Bai, X. D., Correa, V. R., Toruno, T. Y., Ammar, E. D., Kamoun, S., and Hogenhout, S. A. (2009). AY-WB phytoplasma secretes a protein that targets plant cell nuclei. *Mol. Plant-Microbe Interact.* 22, 18–30. doi: 10.1094/MPMI-22-1-0018

Bamunusinghe, D., Hemenway, C. L, Nelson, R. S., Sanderfoot, A. A., Ye, C. M., Silva, M. A. T., et al. (2009). Analysis of potato virus X replicase and TGBp3 subcellular locations. *Virology* 393, 272–285. doi: 10.1016/j.virol.2009.08.002

Bernales, S., Mcdonald, K. L., and Walter, P. (2006). Autophagy counterbalances endoplasmic reticulum expansion during the unfolded protein response. *PLoS Biol.* 4:e423. doi: 10.1371/journal.pbio.0040423

Bertaccini, A. (2007). Phytoplasmas, diversity, taxonomy, and epidemiology. *Front. Biosci.* 12:673–689. doi: 10.2741/2092

Boonrod, K., Munteanu, B., Jarausch, B., Jarausch, W., and Krczal, G. (2012). An immunodominant membrane protein (Imp) of '*Candidatus* Phytoplasma mali' binds to plant actin. *Mol. Plant-Microbe Interact.* 25, 889–895. doi: 10.1094/MPMI-11-11-0303

Bradford, M. M. (1976). A rapid and sensitive method for the quantitation of microgram quantities of protein utilizing the principle of protein–dye binding. *Anal. Biochem.* 72, 248–254. doi: 10.1016/0003-2697(76)90527-3

Buxa, S. V. (2014). *Microscopic Identification of Plant Immune Responses in Phloem Tissue of Higher Plants Relating to Bacterial Infection*. Ph.D. thesis, Justus-Liebig University, Giessen.

Carlier, M. F., and Pantaloni, D. (2007). Control of actin assembly dynamics in cell motility. *J. Biol. Chem.* 282, 23005–23009. doi: 10.1074/jbc.R700020200

Christensen, N. M., Axelsen, K. B., Nicolaisen, M., and Schulz, A. (2005). Phytoplasmas and their interactions with hosts. *Trends Plant Sci.* 10, 526–535. doi: 10.1016/j.tplants.2005.09.008

Contaldo, N., Bertaccini, A., Paltrinieri, S., Windsor, H. M., and Windsor, G. D. (2012). Axenic culture of plant pathogenic phytoplasmas. *Phytopathol. Med.* 51, 607–617.

Dworkin, J. (2009). Cellular polarity in prokaryotic organisms. *Cold Spring Harb Perspect. Biol.* 1:a003368. doi: 10.1101/cshperspect.a003368

Ehlers, K., Knoblauch, M., and van Bel, A. J. E. (2000). Ultrastructural features of well-preserved and injured sieve elements: minute clamps keep the phloem transport conduits free for mass flow. *Protoplasma* 214, 80–92. doi: 10.1007/BF02524265

Galetto, L., Bosco, D., Balestrini, R., Genre, A., Fletcher, J., and Marzachì, C. (2011). The major antigenic membrane protein of '*Candidatus* Phytoplasma asteris' selectively interacts with ATP synthase and actin

of leafhopper vectors. *PLoS ONE* 6:e22571. doi: 10.1371/journal.pone.0022571

Hafke, J. B., Ehlers, K., Föller, J., Höll, S. R., Becker, S., and van Bel, A. J. E. (2013). Involvement of the sieve-element cytoskeleton in electrical responses to cold shocks. *Plant Physiol.* 162, 707–719. doi: 10.1104/pp.113.216218

Henty, J. L., Bledsoe, S. W., Khurana, P., Meagher, R. B., Day, B., Blanchoin, L., et al. (2011). *Arabidopsis* actin depolymerizing factor 4 modulates the stochastic dynamic behavior of actin filaments in the cortical array of epidermal cells. *Plant Cell* 23, 3711–3726. doi: 10.1105/tpc.111.090670

Hogenhout, S. A., Oshima, K., Ammar, E., Kakizawa, S., Kingdom, H. N., and Namba, S. (2008). Phytoplasmas: bacteria that manipulate plants and insects. *Mol. Plant Pathol.* 9, 403–423. doi: 10.1111/j.1364-3703.2008.00472.x

Hoshi, A., Ishii, Y., Kakizawa, S., Oshima, K., and Namba, S. (2007). Host-parasite interaction of phytoplasmas from a molecular biological perspective. *Bull. Insectol.* 60, 105–110.

Hren, M., Nikolic, P., Rotter, A., Blejec, A., Terrier, N., Ravnikar, M., et al. (2009). 'Bois noir' phytoplasma induces significant reprogramming of the leaf transcriptome in the field grown grapevine. *BMC Genom* 10:460. doi: 10.1186/1471-2164-10-460

Hussey, P. J., Ketelaar, T., and Deeks, M. J. (2006). Control of the actin cytoskeleton in plant cell growth. *Annu. Rev. Plant Biol.* 57, 109–125. doi: 10.1146/annurev.arplant.57.032905.105206

Jelitto-Van Dooren, E. P., Vidal, S., and Denecke, J. (1999). Anticipating endoplasmic reticulum stress. A novel early response before pathogenesis-related gene induction. *Plant Cell* 11, 1935–1944. doi: 10.1105/tpc.11.10.1935

Kakizawa, S., Oshima, K., and Namba, S. (2006). Diversity and functional importance of phytoplasma membrane proteins. *Trends Microbiol.* 14, 254–256. doi: 10.1016/j.tim.2006.04.008

Kartte, S., and Seemüller, E. (1991). Histopathology of apple proliferation in *Malus taxa* and hybrids of different susceptibility. *J. Phytopathol.* 131, 149–116. doi: 10.1111/j.1439-0434.1991.tb04740.x

Knoblauch, M., and van Bel, A. J. E. (1998). Sieve tubes in action. *Plant Cell* 10, 35–50. doi: 10.1105/tpc.10.1.35

Kobayashi, Y., and Kobayashi. I. (2007). Depolymerization of the actin cytoskeleton induces defence responses in tobacco plants. *J. Gen. Plant Pathol.* 73, 360–364. doi: 10.1007/s10327-007-0029-5

Kube, M., Mitrovic, J., Duduk, B., Rabus, R., and Seemüller, E. (2012). Current view on phytoplasma genomes and encoded metabolism. *Scientific World J.* 2012:185942. doi: 10.1100/2012/185942

Laemmli, U. K. (1970). Cleavage of structural proteins during the assembly of the head of Bacteriophage T4. *Nature* 227, 680–685. doi: 10.1038/227680a0

Lee, A. S. (2005). The ER chaperone and signaling regulator GRP78/BiP as a monitor of endoplasmic reticulum stress. *Methods* 35, 373–381. doi: 10.1016/j.ymeth.2004.10.010

Lee, I. M., Davis, R. E., and Gundersen-Rindal, D. E. (2000). Phytoplasma: phytopathogenic mollicutes. *Annu. Rev. Microbiol.* 54, 221–255. doi: 10.1146/annurev.micro.54.1.221

Lybarger, S. R., and Maddock, J. R. (2001). Polarity in action: asymmetric protein localization in bacteria. *J. Bacteriol.* 183, 3261–3267. doi: 10.1128/JB.183.11.3261-3267.2001

Marcone, C. (2010). "Movement of phytoplasmas and the development of disease in the plant," in *Phytoplasmas: Genomes, Plant Hosts and Vectors*, eds P. Jones and P. Weintraub (Wallingford: CABI Publishing), 114–131.

McLean, A. M., Orlovskis, Z., Kowitwanich, K., Zdziarska, A. M., Angenent, G. C., Immink, R. G., et al. (2014). Phytoplasma effector SAP54 hijacks plant reproduction by degrading MADS-box proteins and promotes insect colonization in a RAD23-dependent manner. *PLoS Biol.* 12:e1001835. doi: 10.1371/journal.pbio.1001835

Musetti, R., Buxa, S. V., De Marco, F., Loschi, A., Polizzotto, R., Kogel, K.-H., et al. (2013). Phytoplasma-triggered $Ca2^{+}$ influx is involved in sieve-tube blockage. *Mol. Plant-Microbe Interact.* 26, 379–386. doi: 10.1094/MPMI-08-12-0207-R

Musetti, R., Carraro, L., Loi, N., and Ermacora, P. (2002). Application of immunoelectron microscopy techniques in the diagnosis of phytoplasma diseases. *Microsc. Res. Tech.* 56, 462–464. doi: 10.1002/jemt.10061

Musetti, R., Grisan, S., Polizzotto, R., Martini, M., Paduano, C., and Osler, R. (2011). Interactions between '*Candidatus* Phytoplasma mali' and the apple endophyte *Epicoccum nigrum* in *Catharanthus roseus* plants. *J. Appl. Microbiol.* 110, 746–756. doi: 10.1111/j.1365-2672.2011.04937.x

Neriya, Y., Maejima, K., Nijo, T., Tomomitsu, T., Yusa, A., Himeno, M., et al. (2014). Onion yellow phytoplasma P38 protein plays a role in adhesion to the hosts. *FEMS Microbiol. Lett.* 361, 115–122. doi: 10.1111/1574-6968.12620

Opalski, K., Schultheiss, H., Kogel, K.-H., and Hückelhoven, R. (2005). The receptor-like MLO protein and the RAC/ROP family G-protein RACB modulate actin reorganization in barley attacked by the biotrophic powdery mildew fungus *Blumeria graminis* f.*sp. hordei*. *Plant J.* 41, 291–303. doi: 10.1111/j.1365-313X.2004.02292.x

Pizarro-Cerdá, J., and Cossart, P. (2006). Subversion of cellular functions by *Listeria monocytogenes*. *J. Pathol.* 208, 215–223. doi: 10.1002/path.1888

Preston, A. M., Gurisik, E., Bartley, C., Laybutt, D. R., and Biden, T. J. (2009). Reduced endoplasmic reticulum (ER)-to-Golgi protein trafficking contributes to ER stress in lipotoxic mouse beta cells by promoting protein overload. *Diabetologia* 52, 2369–2373. doi: 10.1007/s00125-009-1506-5

Quaglino, F., Zhao, Y., Casati, P., Bulgari, D., Bianco, P. A., Wei, W., et al. (2013). '*Candidatus* Phytoplasma solani' a novel taxon associated with stolbur and bois noir related diseases of plants. *Int. J. Syst. Evol. Microbiol.* 63, 2879–2894. doi: 10.1099/ijs.0.044750-0

Razin, S., Yogev, D., and Naot, Y. (1998). Molecular biology and pathogenicity of mycoplasmas. *Microbiol. Mol. Biol. Rev.* 62, 1094–1156.

Reynolds, E. S. (1963). The use of lead citrate at high pH as an electron-opaque stain in electron microscopy. *J. Cell Biol.* 17, 208–212. doi: 10.1083/jcb.17.1.208

Rottner, K., Stradal, T. E., and Wehland, J. (2005). Bacteria-host-cell interactions at the plasma membrane: stories on actin cytoskeleton subversion. *Dev. Cell* 9, 3–17. doi: 10.1016/j.devcel.2005.06.002

Rudzińska-Langwald, A., and Kamińska, M. (1999). Cytoypathological evidence for transport of phytoplasma in infected plants. *Acta Soc. Bot. Pol.* 68, 261–266. doi: 10.5586/asbp.1999.035

Rudzińska-Langwald, A., and Kamińska, M. (2001). Ultrastructural changes in Aster Yellows Phytoplasma affected *Limonium sinuatum* Mill. plants. I. Pathology of conducting tissues. *Acta Soc. Bot. Pol.* 70, 173–180. doi: 10.5586/asbp.2001.022

Sansonetti, P. J. (1993). Bacterial pathogens, from adherence to invasion: comparative strategies. *Med. Microbiol. Immunol.* 182, 223–232. doi: 10.1007/BF00579621

Santi, S., Grisan, S., Pierasco, A., De Marco, F., and Musetti, R. (2013a). Laser microdissection of grapevine leaf phloem infected by stolbur reveals site-specific gene responses associated to sucrose transport and metabolism. *Plant Cell Environ.* 36, 343–355. doi: 10.1111/j.1365-3040.2012.02577.x

Santi, S., De Marco, F., Polizzotto, R., Grisan, S., and Musetti, R. (2013b). Recovery from stolbur disease in grapevine involves changes in sugar transport and metabolism. *Front. Plant Sci.* 4:171–182. doi: 10.3389/fpls.2013.00171

Schattat, M., Barton, K., Baudisch, B., Klösgen, R. B., and Mathur, J. (2011). Plastid stromule branching coincides with contiguous endoplasmic reticulum dynamics. *Plant Physiol.* 155, 1667–1677. doi: 10.1104/pp.110.170480

Seemüller, E., Sule, S., Kube, M., Jelkmann, W., and Schneider, B. (2013). The AAA^{+} ATPases and HflB/FtsH proteases of '*Candidatus* Phytoplasma mali': phylogenetic diversity, membrane topology, and relationship to strain virulence. *Mol. Plant Microbe Interact.* 26, 367–376. doi: 10.1094/MPMI-09-12-0221-R

Slepak, T. I., Tang, M., Slepak, V. Z., and Lai, K. (2007). Involvement of endoplasmic reticulum stress in a novel classic galactosemia model. *Mol. Genet. Metab.* 92, 78–87. doi: 10.1016/j.ymgme.2007.06.005

Staiger, C. J., and Blanchoin, L. (2006). Actin dynamics: old friends with new stories. *Curr. Opin. Plant Biol.* 9, 554–562. doi: 10.1016/j.pbi.2006.09.013

Sugio, A., McLean, A. M., and Hogenhout, S. A. (2014). The small phytoplasma virulence effector SAP11 contains distinct domains required for nuclear targeting and CIN-TCP binding and destabilization. *New Phytol.* 202, 838–848. doi: 10.1111/nph.12721

Suzuki, S., Oshima, K., Kakizawa, S., Arashida, R., Jung, H. Y., Yamaji, Y., et al. (2006). Interaction between the membrane protein of a pathogen and insect microfilament complex determines insect-vector specificity. *Proc. Natl. Acad. Sci. U.S.A.* 103, 4252–4257. doi: 10.1073/pnas.0508668103

Thomas, C., Hoffmann, C., Dieterle, M., van Troys, M., Ampe, C., and Steinmetz, A. (2006). Tobacco WLIM1 is a novel F-actin binding protein involved in actin cytoskeleton remodeling. *Plant Cell* 18, 2194–2206. doi: 10.1105/tpc.106.040956

Tilney, L. G., and Portnoy, D. A. (1989). Actin filaments and the growth, movements, and spread of the intracellular bacterial parasite *Lysteria monocytogens*. *J. Cell Biol.* 109, 1597–1608. doi: 10.1083/jcb.109.4.1597

Urade, R. (2007). Cellular response to unfolded proteins in the endoplasmic reticulum of plants. *FEBS J.* 274, 1152–1171. doi: 10.1111/j.1742-4658.2007.05664.x

van Bel, A. J. E. (2003). The phloem, a miracle of ingenuity. *Plant Cell Environ.* 26, 125–149. doi: 10.1046/j.1365-3040.2003.00963.x

Weisberg, W. G., Tully, J. G., Rose, D. L. J., Petzel, P., Oyaizu, H., Yang, D., et al. (1989). A phylogenetic analysis of the mycoplasmas: basis for their classification. *J. Bacteriol.* 171, 6455–6467.

White, R. G., Badelt, K., Overall, R. L., and Vesk, M. (1994). Actin associated with plasmodesmata. *Protoplasma* 180, 169–184. doi: 10.1007/BF01507853

Xu, C., Bailly-Maitre, B., and Reed, J. C. (2005). Endoplasmic reticulum stress: cell life and death decisions. *J. Clin. Invest.* 115, 2656–2664. doi: 10.1172/JCI26373

Ye, C., Dickman, M. B., Whitham, S. A., Payton, M., and Verchot, J. (2011). The unfolded protein response is triggered by a plant viral movement protein. *Plant Physiol* 156, 741–755. doi: 10.1104/pp.111.174110

Conflict of Interest Statement: The authors declare that the research was conducted in the absence of any commercial or financial relationships that could be construed as a potential conflict of interest.

frontiers in Microbiology

ORIGINAL RESEARCH
published: 02 May 2016
doi: 10.3389/fmicb.2016.00630

The Pmt2p-Mediated Protein *O*-Mannosylation Is Required for Morphogenesis, Adhesive Properties, Cell Wall Integrity and Full Virulence of *Magnaporthe oryzae*

*Min Guo *†, Leyong Tan †, Xiang Nie †, Xiaolei Zhu, Yuemin Pan and Zhimou Gao*

Department of Plant Pathology, College of Plant Protection, Anhui Agricultural University, Hefei, China

Protein *O*-mannosylation is a type of *O*-glycosylation that is characterized by the addition of mannose residues to target proteins, and is initially catalyzed by evolutionarily conserved protein *O*-mannosyltransferases (PMTs). In this study, three members of PMT were identified in *Magnaporthe oryzae*, and the pathogenic roles of MoPmt2, a member of PMT2 subfamily, were analyzed. We found that MoPmt2 is a homolog of *Saccharomyces cerevisiae* Pmt2 and could complement yeast Pmt2 function in resistance to CFW. Quantitative RT–PCR revealed that *MoPmt2* is highly expressed during conidiation, and targeted disruption of *MoPmt2* resulted in defects in conidiation and conidia morphology. The *MoPmt2* mutants also showed a distinct reduction in fungal growth, which was associated with severe alterations in hyphal polarity. In addition, we found that the *MoPmt2* mutants severely reduced virulence on both rice plants and barley leaves. The subsequent examination revealed that the fungal adhesion, conidial germination, CWI and invasive hyphae growth in host cells are responsible for defects on appressorium mediated penetration, and thus attenuated the pathogenicity of *MoPmt2* mutants. Taken together, our results suggest that protein *O*-mannosyltransferase MoPmt2 plays essential roles in fungal growth and development, and is required for the full pathogenicity of *M. oryzae*.

Keywords: *Magnaporthe oryzae*, *O*-mannosylation, conidia germination, appressoria formation, cell wall integrity, pathogenicity

OPEN ACCESS

Edited by:
Pietro Daniele Spanu, Imperial College London, UK

Reviewed by:
Yasin Fatih Dagdas, The Sainsbury Laboratory, UK
Michael John Kershaw, University of Exeter, UK

****Correspondence:***
Min Guo
kandylemon@163.com

† These authors have contributed equally to this work.

Specialty section:
This article was submitted to Plant Biotic Interactions, a section of the journal Frontiers in Microbiology

Received: *22 February 2016*
Accepted: *18 April 2016*
Published: *02 May 2016*

Citation:
Guo M, Tan L, Nie X, Zhu X, Pan Y and Gao Z (2016) The Pmt2p-Mediated Protein O-Mannosylation Is Required for Morphogenesis, Adhesive Properties, Cell Wall Integrity and Full Virulence of Magnaporthe oryzae. Front. Microbiol. 7:630. doi: 10.3389/fmicb.2016.00630

INTRODUCTION

The filamentous fungus *Magnaporthe oryzae*, which causes rice blast disease, is the most destructive pathogen of cultivated rice plants worldwide (Howard and Valent, 1996). It has been developed as a model system to study fungus–plant interactions due to its economic and scientific importance (Talbot, 2003; Xu et al., 2007; Dean et al., 2012). During growing seasons, like many other phytopathogens, asexual spores play an important role in the disease cycle of *M. oryzae* (Lee et al., 2006). When landed on the plant surface, asexual spores immediately secrets conidial tip mucilage to adhere themselves on rice leaves. Under suitable condition, conidia begin to germinate, and four to 6 h later, a dome-shaped infection structure known as appressorium differentiates at the tip of the germ tube. Rice blast fungus generates enormous amount of turgor pressure (up to

8 MPa) within appressorium to penetrate the plant cuticle layer (Howard et al., 1991; Howard and Valent, 1996; Talbot, 2003), and after penetration, the fungus develops bulbous biotrophic infectious hyphae in the rice leaf cells and typical necrotic lesions on the leaf surface (Kankanala et al., 2007). After 5–7 days, newly formed pyriform conidia differentiate from the hyphae on the lesion, and serve as inocula for secondary infection cycles (Talbot, 2003). These findings suggest that the sporulation and appressorium formation are essential for successful disease development. Thus, an understanding of the molecular mechanisms involved in these processes could provide insights into the nature of the plant–fungi interaction and is of great interest in the development of antifungal strategies.

Protein glycosylation is a post-translational modification conserved in organisms from yeasts to humans, and plays a critical role in determining the structure and function of numerous secreted and membrane-bound proteins (Lehle et al., 2006). In eukaryotic cells, there are two types of protein glycosylation (*N*- and *O*-glycosylation) that are highly regulated by the activity of protein- and site-specific enzymes (Fernández-Álvarez et al., 2009). *O*-mannosylation is a type of *O*-glycosylation that is characterized by the addition of mannose residues to target proteins, and is initially catalyzed by protein *O*-mannosyltransferases (PMTs), a family of proteins that are evolutionarily conserved from yeast to humans (Strahl-Bolsinger et al., 1999; Willer et al., 2003). In fungi, the PMTs are grouped into Pmt1, Pmt2, and Pmt4 subfamilies based on phylogeny, with each subfamily having three to seven members (Girrbach et al., 2000). In *Saccharomyces cerevisiae*, seven homologous PMT proteins have been identified and divided into the Pmt1, Pmt2, and Pmt4 subfamilies, which differ in their number of genes and the protein substrate specificity (Girrbach and Strahl, 2003). However, in many other filamentous fungi, including *M. oryzae*, only a single member in each Pmt subfamily was identified (Dean et al., 2005; Fernández-Álvarez et al., 2009; Goto et al., 2009; Mouyna et al., 2010; Gonzalez et al., 2013). In the past two decades, studies of the functions of fungal PMTs has been increasing, and now it is clear that protein glycosylation contributes to the modification of proteins involved in important processes, such as cell wall integrity (CWI), sensing of environmental signals, morphogenesis and the virulence of fungal pathogens (Gentzsch and Tanner, 1996; Prill et al., 2005; Olson et al., 2007; Zhou et al., 2007; Fernández-Álvarez et al., 2009, 2012). Simultaneous disruptions of three different types of *PMT* genes in *Schizosaccharomyces pombe* were lethal (Willer et al., 2005), suggesting that each class provided a unique function for *O*-mannosylation. In *S. cerevisiae*, the *PMT* genes are not individually essential for viability, probably as a result of gene redundancy (Gentzsch et al., 1995). Deletion of *PMT1* does not affect viability but leads to cells that tend to aggregate. Inactivation of both *PMT1* and *PMT2* causes defects in growth and resistance to antifungal drug (Lussier et al., 1995), whereas triple mutants are not viable, indicating that PMT protein activity is essential in *S. cerevisiae*, although individual genes are dispensable (Tanner et al., 1996; Loibl and Strahl, 2013). In *Candida albicans* and *Cryptococcus neoformans*, *Pmt* disruption affects morphogenesis and virulence (Prill et al., 2005; Olson et al., 2007). In filamentous fungus *Aspergillus fumigatus*, deletion of *Pmt4* results in abnormal growth, defective conidiation and associated proteomic changes, while disruption of *Pmt2* results in lethal growth (Mouyna et al., 2010). In *Aspergillus nidulans*, all the single *Pmt* disruption mutants were viable, but defective in cell wall integrity, hyphal growth and asexual development (Kriangkripipat and Momany, 2009). In *Ustilago maydis*, the three Pmt orthologs play diverse roles in fungal development. The deletion of *Pmt1* doesn't affect the fungal growth and plant infection, while the mutation in *Pmt2* is not viable, indicating an essential role in fungal development. By contrast, the disruption of *Pmt4* specifically affected appressorium formation, penetration and tumor formation in maize (Fernández-Álvarez et al., 2009). In *Botrytis cinerea*, PMTs are individually required for morphogenesis, fungal adherence, cell wall integrity and virulence on plants, and deletion of *PMT2* results in defects on the stability of the cell wall, poor sporulation and attenuated virulence on plants (Gonzalez et al., 2013). In *Beauveria bassiana*, PMTs play crucial roles on fungal development, and individual *Pmt* gene deletion results in defects on growth, conidiation, stress tolerance and virulence (Wang et al., 2014). In *Penicillium digitatum*, the disruption of *Pmt2* causes pleiotropic effects, including defects on cell wall integrity, conidiogenesis, virulence and resistance to the antifungal peptide PAF26 (Harries et al., 2015). Based on the above facts, it is therefore evident that the *O*-mannosyltransferases Pmts play important roles in fungal development and pathogenesis in pathogenic fungi.

Recently, evidence that the α-1, 3-mannosyltransferase ALG3 from *M. oryzae* play a critical role in mediating the glycosylation of secreted effectors, and thus required for fungal pathogenicity on host (Chen et al., 2014), suggest that protein glycosylation may be important for the pathogenic development of *M. oryzae*. However, till now, enzymes involving *O*-mannosylation pathway has not been characterized in the rice blast fungus. Here, we describe a detailed characterization of the role of *MoPmt2* in *M. oryzae*, and our results showed that *MoPmt2* contribute to fungal morphology, growth, CWI and virulence on host plants.

MATERIALS AND METHODS

Fungal Strains and Culture Conditions

The *M. oryzae* Guy11 was used as wild-type strains throughout this work. Fungal mycelia grown in liquid complete media at 28°C for 2 days were harvested and used for genomic DNA and RNA extractions. For observing the mycelial growth, strains were inoculated in liquid CM as described in the reference (Guo et al., 2015). For conidiation, mycelial plugs were inoculated on RDC agar plates (Guo et al., 2011) and maintained at 28°C for 7 days in the dark followed 3–5 days constant fluorescent light condition to promote conidiation. For medium containing cell wall-perturbing agents, the final concentrations were 50, 100, 200 μg/mL for Congo red (CR, 860956, Sigma, China), and/or for Calcofluor white (CFW, F3543, Sigma, China), respectively. The inhibition rate was calculated by the method described in the reference (Guo et al., 2015).

Yeast *Pmt2* Mutant Complementation

S. cerevisiae BY4741Δ*YAL023c* (Δ*Pmt2*) and the strain from which it was derived, BY4741 (*MATa*; *ura3*Δ*0*; *leu2*Δ*0*; *his3*Δ*1*; *met15*Δ*0*) were purchased from Euroscarf (http://www.uni-frankfurt.de/fb15/mikro/euroscarf/). The full-length of *MoPmt2* cDNA (XM_003715348.1) from *M. oryzae* was amplified using primer pairs Pmt2-YC1/ Pmt2-YC2. The PCR products, digested with *Hind*III and *Xho*I, were cloned into pYES2 (Invitrogen) and transformed into Δpmt2 mutant (BY4741, Δ*YAL023c::kanMX4*). Positive transformants were selected on SD medium lacking uracil. For complementation assays, all tested strains were grown and treated as described by Harries et al. (2015). The cells of the tested strains were diluted to an OD600 of 0.1 and 10 μL of ten-fold serial dilutions were spotted onto SC-Ura plates containing 2% glucose with and without 12.5 μg/mL CFW or 2% galactose with 12.5 μg/mL CFW, respectively, and grown for 3 days at 30°C. The wild type strain BY4741 as well as the *Pmt2* deletion mutant BY4741ΔYAL023c expressed empty pYES2 vector were used as a control.

Multiple Sequence Alignment and Phylogenetic Analysis

The Pmt proteins from different organisms were obtained from NCBI database (http://www.ncbi.nlm.nih.gov/) using the BLAST algorithm (McGinnis and Madden, 2004). Sequence alignments were performed using the Clustal_W program (Thompson et al., 1994) and a phylogenetic tree was created with the Mega 4.0 Beta program (Tamura et al., 2007). Domain architecture was automatically provided by the SMART online software program (Letunic et al., 2012) or TMHMM Server v. 2.0 (Krogh et al., 2001).

Gene Disruption and Complementation

The gene deletion mutants were generated using the standard one step gene replacement strategy. For gene replacement construct, DNA fragments of the 1.0 kb flanking regions of the target gene were amplified with the primers Pmt2-1F/Pmt2-1R and Pmt2-2F/ Pmt2-2R (**Table S1**), then a ∼2-kb fragment containing the two flanking sequences was amplified by overlap PCR with primers Pmt2-1F / Pmt2-2R (**Table S1**), and then was inserted into the pMD19-T vector (Takara Co., Dalian, China) to generate plasmid pMDT–*MoPmt2*. The hygromycin B-resistance cassette, which was amplified with primers HPH-F/HPH-R by KOD-Plus-Neo (KOD-401, TOYOBO, Shanghai, China), was purified to insert into the *Pme*I site in plasmid pMDT–*MoPmt2* to generate deletion construct pMDT-*MoPmt2-hph*. A ∼3.4-kb fragments, which was amplified from the deletion construct with primers Pmt2-1F/Pmt2-2R, was transformed into protoplasts of wild type Guy11. To obtain *MoPmt2* null mutants, all hygromycin B-resistant transformants were screened by PCR using the primer pairs P1/P2 and P3/P4 (**Figure S1**), respectively, and were further validated by Southern blot hybridization and RT-PCR (**Figures S2D–F**). For complementation of *MoPmt2*, the fragments containing the 1.5-kb native promoter region of the gene, *MoPmt2* full-length coding region and a 0.5-kb terminator sequence were amplified using primers Pmt2-C1/Pmt2-C2 and then inserted into the pMo1102 vector (unpublished plasmid) using the yeast gap repair approach (Park et al., 2004) to generate pMo1102::*MoPmt2*. The complemental fragment was then reintroduced into the *MoPmt2-6* mutant by the *Agrobacterium* mediated transformation of *M. oryzae*, and the complemented strains were validated by semiquantitative RT-PCR.

Phenotypic Characterization of Mutants

To assess the growth rate, mycelia plugs of Guy11 and its derivative mutants were obtained from the edge of 5-day-old cultures and placed onto fresh media (CM, MM, OM, and RDC), followed by incubation in the dark condition at 28°C for 5 days (Guo et al., 2015). The conidia production of the tested strains was carried out by counting the number of conidia harvested with 5 ml of sterilized distilled water from 10-day-old RDC agar plates using a haemocytometer (Zhang et al., 2009). Conidium size was measured under a microscope as previously described (Guo et al., 2011). For conidium germination and appressorium formation, drops (20 μl) of conidial suspension (1.0×10^5 spores/ml) were inoculated onto a hydrophobic coverslip and placed under humid conditions at 28°C. Conidia germination and appressoria formation were observed by microscopic examination of at least 99 conidia per replicate at each time point. Appressorium turgor was measured by incipient cytorrhysis assay using a 1-4 molar concentration of glycerol solution (Zhang et al., 2009). For conidium adhesion assay, drops (30 μl) of conidial suspension (1.0×10^5 spores/ml) were placed on the hydrophobic surface of coverslips for 2 h in a humid box, then the coverslips were washed by pipetting 1 ml distilled water three times (each washing takes 3 s)., and the percentage of conidium adhesion was assessed as described previously (Han et al., 2015). All above experiments were independently repeated three times with three replicate each, and representative results from one experiment are shown in this study.

Pathogenicity Assay and Infectious Growth Observation

For plant infection assays, conidial suspension (4 ml, 1.0×10^5 spores/ml) containing gelatin (2%, wt/vol) were sprayed on 14-day-old rice seedlings (*Oryza sativa* cv CO-39) or drops of conidial suspension (10 μL, 1.0×10^5 spores/ml) were placed on 7-day-old barley leaves (*Hordeum vulgare* cv Golden Promise). Inoculated plants were kept in a moist chamber in dark at 28°C for first 2 h, and then were moved to a moist chamber with a photoperiod of 12 h under fluorescent lights (Guo et al., 2011). The disease development on plants was assessed at 5 days after inoculation. For pathogenicity assay on abraded rice leaves, drops (10 μl) of conidia suspension (1.0×10^5 ml^{-1}) of the tested strains were placed on wounded rice leaves and kept in a moist chamber as described above, and their virulence was evaluated at 5 days after incubation. Conidiation on the lesion was treated as described above and observed 15 days after incubation. Plant penetration assays were carried out using 7-day-old barley leaves (Chen et al., 2014). Conidial suspension (1×10^4 spores/ml) was dropped onto barley leaves and incubated at 28°C in a moistened chamber. Invasive growth inside plant cells was examined after at 48 and 72 h using a light microscopy. These experiments

were repeated three times, and representative results from one experiment are shown.

FITC-ConA and CFW Staining

FITC staining was performed with conidia collected from RDC agar plates (Zhang et al., 2009). Conidia suspension (1×10^5 conidia ml^{-1}) was inoculated on the hydrophobic surface of coverslips and then treated as described in reference (Hamer et al., 1988) at 0.5 and 24 h, respectively. Microscopic examination of stained conidia and mature appressorium (>100 conidia or appressorium) was carried out using a Nikon inverted T*i*-S epifluorescence microscope (Nikon Co., Tokyo, Japan). For CFW staining, conidia suspension (1×10^4 conidia ml^{-1}) was inoculated on glassslides covered with a thin layer of water agar and kept in a moist plate for 48 h or on hydrophobic coverslips and kept in a moist plate for 24 h, then both the vegetative hyphae and appressorium stained by CFW was observed using the Nikon inverted T*i*-S epifluorescence microscope (Nikon Co., Tokyo, Japan), respectively.

Nucleic Acid Manipulation and Southern Blotting

The standard method was used to prepare genomic DNA for both diagnostic PCR and Southern blot hybridization (Sambrook et al., 1989). A DNA hybridization probe, which is amplified by primer set Pmt2-P1/Pmt2-P2, were labeled with digoxigenin-11-dUTP using DIG-High prime according to the manufacturer's instructions (11745832910, Roche, China). Southern hybridization experiments, including restriction enzyme digestion, DNA gel blotting and hybridization were performed as described by Guo et al. (2015). Total RNA samples from mycelia, conidia and plants infectious stages (8, 24, 48, and 72 h) were extracted using the methods described in E.Z.N.A. Total RNA Kit I (R6834-01, Omega Bio-Tek, Norcross, USA).

qRT–PCR, RT–PCR, and Gene Expression Analysis

For RT-PCR and qRT-PCR, 5 μg of total RNA were reversely transcribed into first-strand cDNA using the ReverTra Ace® qPCR-RT Master Mix (FSQ-301, TOYOBO, Shanghai, China). Confirmation of deletions and reintroduction of *MoPmt2* gene was made with primer pairs Pmt2-S1/Pmt2-S2 (**Table S2**). The stable expression *actin* gene (*MGG_03982.5*) and β-*tubulin* gene (*MGG_00604.5*) amplified by primer pairs Actin-F/Actin-R and β-tubF/β-tubR, respectively, (**Table S2**) was used as internal control (Guo et al., 2015).

qRT-PCR were performed using a BIO-RAD CFX96 touch q-PCR system (BIO-RAD, Hercules, California, USA), following previously established procedures: 3 min at 95°C (one cycle) followed by 15 s at 95°C, 30 s at 60°C, and 30 s at 72°C (40 cycles). To measure the relative abundance of *MoPmt2* transcripts, the average threshold cycle (Ct) was normalized to that of *actin* gene (*MGG_03982.5*) and expressed as $2^{-\Delta Ct}$, where $-\Delta Ct = (C_{t,\text{target gene}} - C_{t,\text{actin gene}})$. Fold changes in expression during fungal development and infectious growth were calculated as $2^{-\Delta\Delta Ct}$, where $-\Delta\Delta Ct = (C_{t,\text{target gene}} - C_{t,\text{actin gene}})_{\text{testcondition}} - (C_{t,\text{target gene}} - C_{t,\text{ actin gene}})_{CM}$ (Livak and Schmittgen, 2001). Three independent pools of tissues in three sets of experimental replicates were performed and primer pairs used in this section were listed in **Table S2**.

Measurement of Enzyme Activity in Extracellular Culture Filtrate

Enzyme activity was assayed using culture filtrate from 2-day old CM liquid culture. For measurement of peroxidase and laccase activity, a reaction mixture (1 ml) containing 50 mM acetate buffer (pH 5.0) and 10 mM 2, 2′- azino-di-3-ethylbenzthiazoline-6-sulphonate (ABTS, Sigma, A1888) was mixed with the culture filtrate (200 μl) and incubated at 25°C for 5 min with or without 3 mM of H_2O_2. Absorbance was evaluated at 420 nm.

Transmission Electron Microscopy

Transmission electron microscopy was carried out using hyphae grown in liquid CM for 48 h. The hyphae were fixed in 2.5% (v/v) glutaraldehyde and 1% (v/v) osmium tetroxide. Sections were prepared and visualized using a H-7650 transmission electron microscope (Hitachi, Tokyo, Japan) as described by Xu et al. (2010).

RESULTS

Identification of Three *Pmt* Genes in *M. oryzae*

In our previous study, the *Moap1* mutants were identified as non-pathogenic to rice plants (Guo et al., 2011). To investigate the possible reason for this, a serial analysis of gene expression (SAGE) libraries for the wild type Guy11 and *Moap1* mutant were generated. In the SAGE libraries, three *O*-Mannosyltransferases encoding genes were identified with different expression patterns, with MGG_02954 and MGG_04427 showing 0.35- and 1.0-fold increased expression, respectively, while MGG_07190 showing 1.35-fold reduced expression in the *Moap1* mutants. Sequence alignment using amino acid sequences of the three *O*-Mannosyltransferases revealed the MGG_02954, a protein of 998 amino acids, showed an amino acid identity of 39% to *S. cerevisiae* Pmt1p; MGG_07190, of 737 amino acids, showed 47% identity to *S. cerevisiae* Pmt2p; and MGG_04427, of 775 amino acids, showed 45% identity to *S. cerevisiae* Pmt4p (**Table S1**; Gentzsch and Tanner, 1996). The hydropathy analysis of *M. oryzae* Pmt sequences revealed the presence of two large transmembrane domains, located in their N- and C-terminal regions and separated by a central hydrophilic region (Strahl-Bolsinger and Scheinost, 1999; **Figure 1A**). In addition, analysis of the candidate proteins showed the presence of two characteristic domains of the PMT family: the PMT domain, a region implicated in PMT complex formation and *O*-mannosyltransferase activity, found within the N-terminal transmembrane region, and the mannosyltransferase IP3 ryanodine receptor domain (MIR) composed of three submotifs, located in the hydrophilic central region (Girrbach et al., 2000; **Figure 1B**; **Table S1**). The assignment of these identified genes as protein *O*-mannosyltransferases was further confirmed by phylogenetic reconstruction with homologous

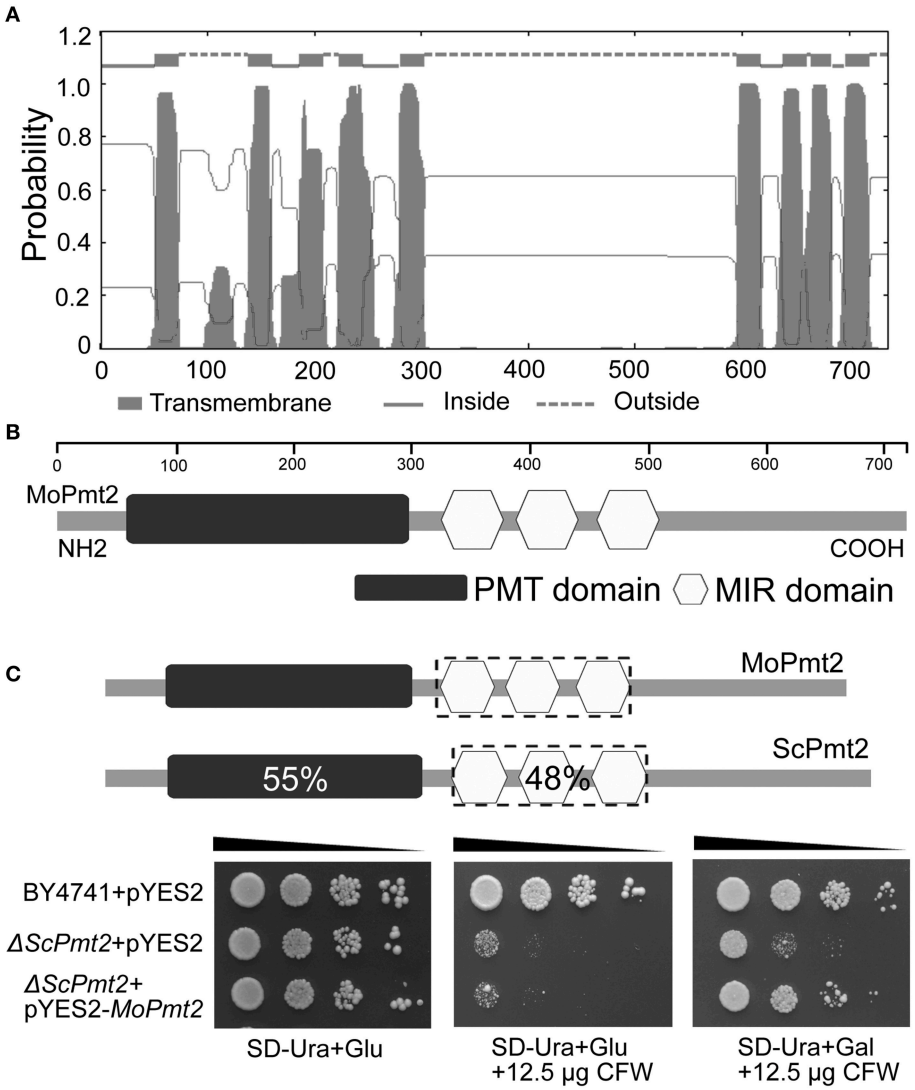

FIGURE 1 | *M. oryzae* MoPmt2 encodes a functional homolog of *S. cerevisiae* Pmt2. (A) Prediction of transmembrane structure in MoPmt2. The position of each transmembrane domain was generated by the TMHMM Server v. 2.0 online program, and the MoPmt2 possess the typical hydropathy profiles of *O*-mannosyltransferases. **(B)** Conservation of the Pmt sequence motifs in MoPmt2. Physical map of MoPmt2 revealed two conserved motifs (Pmt and MIR) of the PMT family at the N-terminal transmembrane region and central hydrophilic region. **(C)** Functional complementation of *S. cerevisiae Pmt2* mutant. Serial 10-fold dilutions of cells from wild-type strain BY4741 transformed with pYES2 and the *Pmt2* strain transformed with either pYES2 or pYES2-*Mo*Pmt2 are dotted onto SC-Ura plates with Glu or Gal supplemented with 12.5 μg/mL CFW as indicated, and incubated at 30°C for 72 h.

fungal genes, and they were grouped into each PMT subfamily (Lehle et al., 2006; **Figure S1**). Thus, consistent with their hydropathy profiles, conserved sequence motifs, and our phylogenetic analysis, we can provisionally named MGG_02954, MGG_07190 and MGG_04427 as MoPmt1, MoPmt2, and MoPmt4 respectively.

MoPmt2 Encodes Protein *O*-Mannosyltransferases

The SAGE libraries revealed that *MoPmt2* showed transcriptional reduction in the *Moap1* mutant, indicating its potential roles in regulating fungal development and pathogenicity in *M. oryzae*. Therefore, the functional roles of *MoPmt2* were characterized in this study. In *S. cerevisiae*, the *pmt2* gene is responsible for cell wall integrity, and *Δpmt2* mutant has defects in cell wall and exhibit increased sensitivity to the chitin-binding fluorophore CFW (Harries et al., 2013). To provide experimental evidence that *MoPmt2* encodes a functional homolog of *S. cerevisiae* Pmt2 with *O*-mannosyltransferase activity, we tested the ability of *MoPmt2* to complement a yeast strain lacking *pmt2*. Our results showed that the *S. cerevisiae* Δ*pmt2* mutants transformed with the expression vector pYES2-*MoPmt2* restored the resistance to CFW under induction conditions (**Figure 1C**), indicating that *M. oryzae* Pmt2 is functional homolog of the *S. cerevisiae* Pmt2. Moreover, it also confirms our phylogenetic-based assignment of PMT family members.

The Expression and Disruption of *MoPmt2* Gene in *M. oryzae*

To gain insight into the possible function of MoPmt2 in *M. oryzae*, the changes in *MoPmt2* gene expression were analyzed by quantitative RT-PCR (qRT-PCR), and found that *MoPmt2* gene is expressed during fungal vegetative growth and plant infection, with the highest induction at conidia stage (7.4-fold; **Figure S2A**), compared with the stable expression of *actin* gene.

We generated *MoPmt2* mutants using the *MoPmt2* deletion vector which contains the hygromycin resistance gene (**Figure S2B**). The transformants that confers resistance to the antibiotic hygromycin B were verified by diagnostic PCR (**Figure S2C**). The putative mutants were further confirmed by Southern blot and semiquantitative RT-PCR (RT-PCR) analysis (**Figures S2D–F**), and two deletion mutants, *MoPmt2-6* and *MoPmt2-8*, were obtained for further analysis. To ascertain that the observed phenotypes of the *MoPmt2* mutants are caused by the deletion of *MoPmt2*, a complemented strain *MoPmt2c* was generated and verified by RT-PCR (**Figure S2F**). As expected, the complemented strain recovered all the defects described in this study (**Figures 2–8**).

MoPmt2 Deletion Leads to Retarded Vegetative Growth

To investigate the role of *MoPmt2* on mycelium growth in *M. oryzae*, mycelial growth of wild type strain Guy11, the *MoPmt2* mutants and complemented strain *MoPmt2c* was compared on complete media (CM), minimal media (MM), oatmeal medium (OM), and RDC medium (Guo et al., 2015). Mycelial growth of the *MoPmt2* mutants differed from that of Guy11, with a significant reduction in radial growth on the four media, compared to Guy11 and *MoPmt2c* (**Figure 2A**; **Figure S3**). In liquid CM media, we found that mycelial growth of the *MoPmt2* mutants was more compact than that of Guy11 and *MoPmt2c* (**Figure 2B**), and a subsequent assay indicated significantly less fungal biomass for the *MoPmt2* mutants than for Guy11 and *MoPmt2c* after incubating in liquid CM for 72 and 120 h, respectively (**Figure 2C**). In view of these phenotypes, we examined the morphology of *MoPmt2* mutants by microscopy after CFW staining. Our results showed that *MoPmt2* mutants presented more septa, which were intensively stained and had shorter interseptal distances than those of Guy11 and complemented strain *MoPmt2c* (**Figures 2D,E**). In addition, The *MoPmt2* mutants also showed defects in polarity, with more branching hyphae and globular balloon-like structures (**Figure 2D**; **Figure S4A**).

MoPmt2 Plays Critical Role in Asexual Spore Development

It is clear that asexual spores play an important role in the disease cycle of *M. oryzae* (Lee et al., 2006), thus, sporulation of the Guy11, *MoPmt2* mutants (*MoPmt2-6* and *MoPmt2-8*), and the complemented strain *MoPmt2c* was compared on 14 day old RDC cultures. Our findings revealed that conidiation was dramatically reduced by approximately 12 to 14-fold in *MoPmt2* deletion mutants (*MoPmt2-6*, 12-fold; *MoPmt2-8*, 14-fold), compared with Guy11 and complemented strains *MoPmt2c* (**Figures 3A,B**). In addition, of the spores that formed in *MoPmt2-6*, most exhibited abnormal, with 49.9% in large size and 43.7% in small size, compared with Guy11 and *MoPmt2c* (**Figures 3C–E**; **Figure S5**). Combined with gene expression profiles that *MoPmt2* showed a much higher level of expression in conidia (**Figure S2A**), we concluded that MoPmt2 plays an important role in conidial development.

MoPmt2 is Responsible for Conidia Germination and Appressorium Formation

Conidia germination is the vital step during *M. oryzae* infection (Howard et al., 1991). Therefore, we measured the germination ability of conidia on a hydrophobic surface of coverslips. Our results showed that conidial germination was significantly delayed in the *MoPmt2* mutant when compared with that of Guy11 and *MoPmt2c*. By 2 h, only 4.7% of *MoPmt2* conidia germinated compared with 85.9% of the Guy11 and 85% of the *MoPmt2c*. When prolonged the inoculation time to 8 h, even though the conidial germination of the mutant gradually increased to 92.3%, it was still significantly less germination by the mutant than that of by Guy11 (**Figures 4A,B**).

The appressorium is a typical penetration structure that enables the *M. oryzae* to invade into host cells (Howard and Valent, 1996). Thus, we also evaluated the ability of appressorium formation by the mutants, and found that appressoria developed by the *MoPmt2* mutants were 75.4% by 8 h, 87.9% by 12 h, and 91.6% by 24 h, with a dramatic decrease compared with that of by Guy11 and *MoPmt2c* (**Figures 4A,C**). Meanwhile, of those appressoria formed by the mutant at each time point, only 39.7, 60.3, and 87.4% were melanic and non-reduced in size, compared with 85.2, 92.9, and 95.3% of that by Guy11 (**Figure 4D**). In addition, we also find that over 53% of the conidia were bipolar germination, compared with less than 8% of that by Guy11 and *MoPmt2c* strain at 24 hpi (**Figure 4A**; **Figures S4B,C**). Based on the above, we conclude that the *MoPmt2* is associated with both conidia germination and appressorium development in *M. oryzae*.

MoPmt2 is Essential for Pathogenic Development

To investigate the role of *MoPmt2* in pathogenic development, conidial suspension (1×10^5 conidia ml^{-1}) of the tested strains were inoculated on 14-day-old susceptible rice seedlings (*Oryza sativa* cv CO-39) and/or 7-day-old barley leaves by spraying. The wild type strain Guy11 caused numerous typical necrotic lesions, whereas the *MoPmt2* mutants developed small and restricted lesions on host plants (**Figures 5A,B**). Meanwhile, most of those lesions caused by the *MoPmt2* mutants seldom produced conidia, compared to wild type Guy11 and *MoPmt2c*. When the incubation time was extending to 15 days after inoculation, only few conidia were observed on the larger lesions (**Figure 5C**). To further determine the role of *MoPmt2* in pathogenicity, conidial suspension of the tested strains was inoculated on

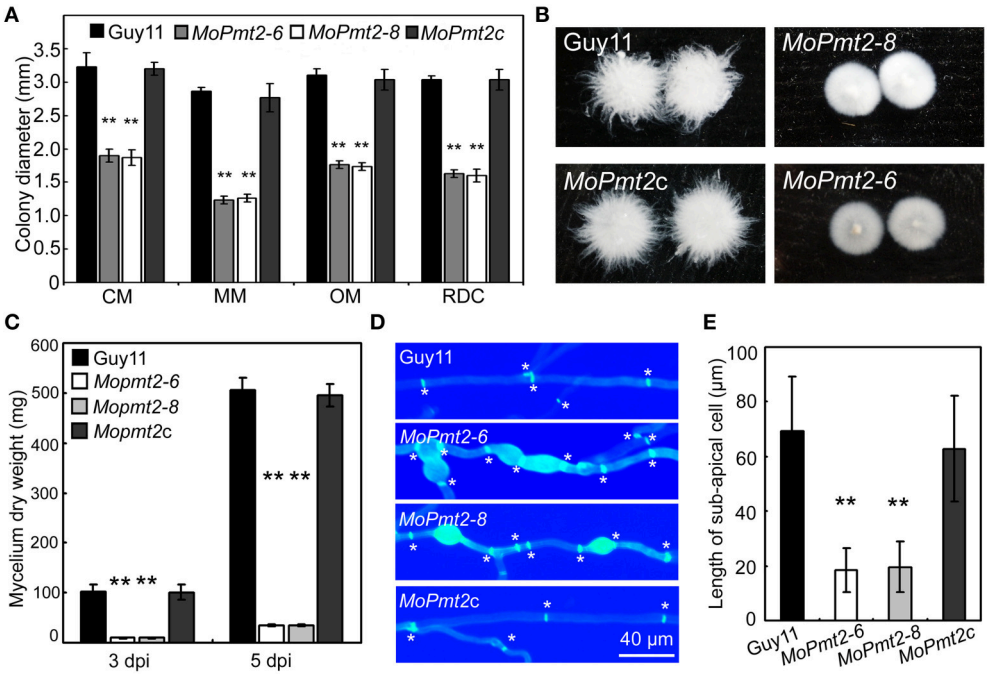

FIGURE 2 | The effect of MoPmt2 on mycelia growth of *M. oryzae*. (A) Mycelial growth is altered in the *MoPmt2* mutant. Colony diameters of the tested strains on different media were measured and statistically analyzed by Duncan analysis. **(B)** Phenotype of mycelia grown in liquid CM. All tested strains were inoculated in liquid CM for 48 h at 28°C in darkness and then photographed. **(C)** Measurement of fungal biomass. The fungal mycelia of the tested strains, grown in liquid CM for 3 and 5 days respectively, were collected and freezing dried, and were statistically analyzed. **(D)** Mycelia growth on water agar media. CFW staining of mycelia is used to show the distance of septa and swollen of mycelia. Asterisks in white color indicate septa. **(E)** The average length of the sub-apical cell of vegetative hyphae in Guy11, *MoPmt2-6*, *MoPmt2-8,* and *MoPmt2c*. The mean and standard deviations were calculated based on three independent experiments by measuring at least 50 sub-apical cells in each replicate. Error bar represents standard deviation, and asterisks in this figure indicate significant differences from the control ($P < 0.01$).

wounded rice leaves. The results revealed that the wild type Guy11 were fully pathogenic, and developed extendible and necrotic lesions, in contrast, the *MoPmt2* mutant only causes small lesions on the inoculation sites (**Figure 5D**). When the *MoPmt2* gene was reintroduced in the mutant, it recovered the pathogenicity on both rice and barley plants (**Figures 5A–D**), suggesting a potential role for the MoPmt2 in plant invasion and colonization.

MoPmt2 Deletion Results in Defects on Fungal Adhesion

In *M. oryzae*, the persistent adhesion of the three-celled conidia to the rice leaf by means of the spore tip mucilage is a prerequisite for pathogenic development (Hamer et al., 1988). Thus, to identify the reason for attenuated virulence of *MoPmt2* mutants, we firstly tested conidium adhesion to a hydrophobic surface due to the fact that the spore tip mucilage could stick to hydrophobic coverslips (Hamer et al., 1988; Han et al., 2015). Our results showed that more than 63% of conidia of the *MoPmt2* mutant were washed away from the hydrophobic surface of coverslips, whereas only 15% of those by the wild type and *MoPmt2c* (**Figures 6A,B**), indicating that *MoPmt2* plays a critical role in fungal adhesion in *M. oryzae*. As the lectin concanavalin A (ConA) conjugated to fluorescein isothiocyanate (FITC) could be used for detecting STM (Hamer et al., 1988), thus, STM secreted by Guy11, *MoPmt2* mutant and complemental strain *MoPmt2c* were compared on hydrophobic glass cover slips. At 0.5 hpi, conidia of Guy11 showed a very strong signal for STM compared with those of *MoPmt2* mutant, with 93.9 and 91.8% conidia from Guy11 and *MoPmt2c* strain, respectively, showing fluorescence, in contrast to 10.9% conidia from *MoPmt2* mutant (**Figures 6C,D**). When the incubation time was prolonged to 24 h, however, no obvious differences were observed by comparison of fluorescence signal from mature appressoria of Guy11 and *MoPmt2* mutant (**Figure S6A**).

MoPmt2 is Required for Penetration and Invasive Hyphae Growth

To further understand the role of *MoPmt2* in disease development, we carried out penetration assays on the barley leaves (**Figure 7A**). The appressoria formed by *MoPmt2* mutants could less effectively penetrate into the epidermal cells of barley leaves at 48 hpi when compared to Guy11 and *MoPmt2c*. In addition, most of the invasive hyphae developed by the penetrated appressorium of the mutants displayed extremely retarded growth in the host cells (**Figure 7A**). When infected leaves were examined after 72 hpi, most invasive hyphae of *MoPmt2* mutant had still failed to colonize the leaf epidermis beyond the first cell (**Figure 7B**). In contrast, the wild type

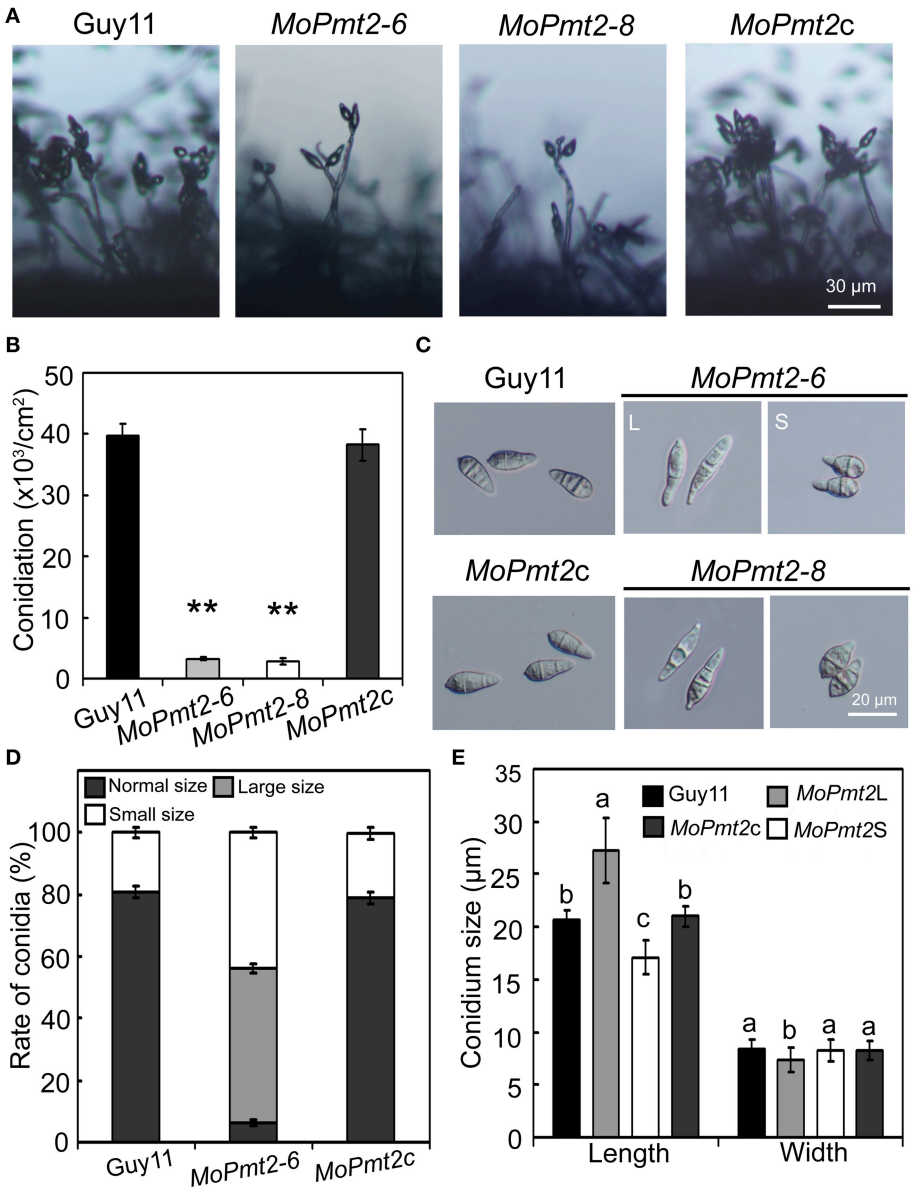

FIGURE 3 | The effect of MoPmt2 on conidiation and conidial morphology of *M. oryzae*. (A) *MoPmt2* deletion results in defects on conidiation. The development of conidia on conidiophores was examined by light microscope using strains grown on RDC medium for 7 days. Scale bar = 30 μm. **(B)** Statistical analysis of conidiation. The conidia produced by the tested strains grown on RDC medium for 14 days were measured and analyzed by Duncan analysis ($p < 0.01$). Asterisks indicate significant differences of conidiation among tested strains. Error bar represents standard deviation. **(C)** Conidial morphology comparison. Conidia of tested strains were collected from 14-day-old cultures, and then photographed under light microscope. Bars = 20 μm. **(D)** The percentage of each type of abnormal conidia. Conidia of tested strains were harvested from 14-day-old cultures, and the rate of large and small conidia was calculated and statistically analyzed, respectively. **(E)** Conidia sizes comparison. The conidia sizes were determined as width by length from 297 conidia of each strain.

and *MoPmt2c* could freely expand and successfully colonized new cells across the cell walls of the initially invaded cell (**Figures 7A,C**). These results indicated that MoPmt2 is required for appressorium-mediated penetration as well as invasive hyphae growth in host cells, and the defect on these aspects might be responsible, at least in part, for the reduction of pathogenicity.

MoPmt2 is Required for Turgor Generation and Cell Wall Integrity

In *M. oryzae*, the defects in cell wall composition can affect the accumulation of turgor pressure and impair the successful infection of rice plants (Howard et al., 1991; Howard and Valent, 1996; Thines et al., 2000). Based on penetration-defective phenotypes of the *MoPmt2* mutants, appressorium

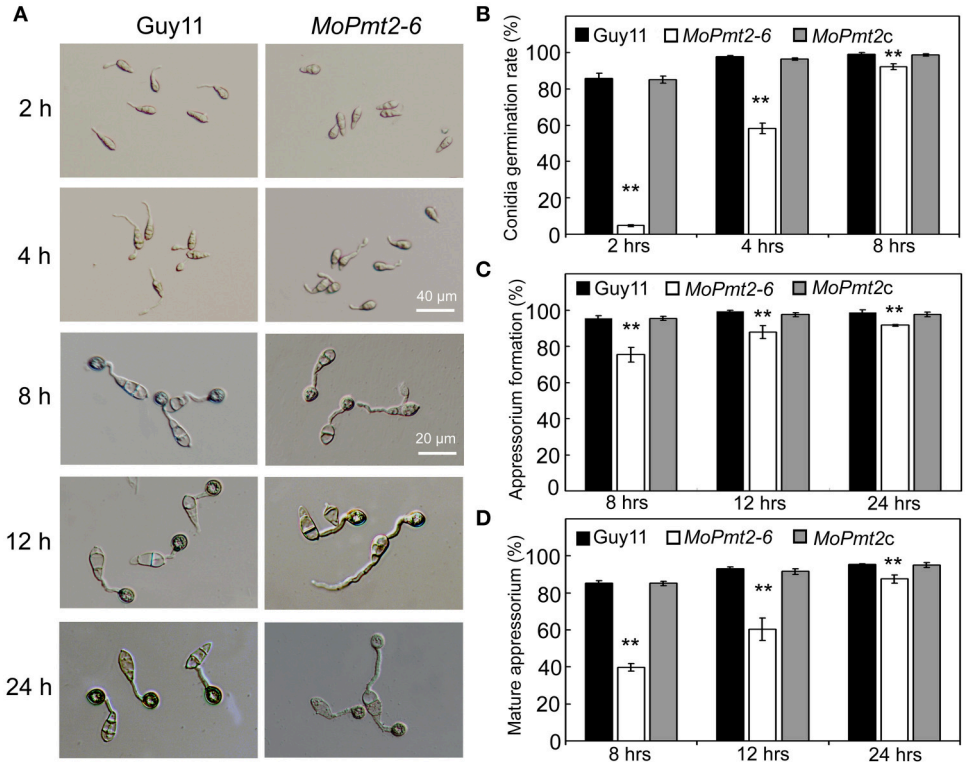

FIGURE 4 | Conidial germination and appressorium formation. (A) Delayed conidial germination and appressorium formation of the *MoPmt2* mutant. Conidia of indicated strains were harvested from 14-day-old cultures. Droplets of conidial suspension (1×10^5 ml^{-1}) were inoculated on the hydrophobic surface of the coverslips for indicated time, and then photographed. Scale bars are indicated in the figure. **(B)** Statistical analysis of conidial germination. Germinated conidia were counted at each indicated time under a light microscope, and statistically analyzed by Duncan analysis. **(C)** Statistical analysis of appressorium formation. Appressorium formed at the germ tube were counted and statistically analyzed. **(D)** Measurement of mature appressorium. Appressorium formed at the germ tube with melanin were counted, and the ratio of mature appressorium was statistically analyzed. Asterisks in this figure indicate significant differences from the control ($p < 0.01$). Error bar represents standard deviation.

turgor pressure of the *MoPmt2* mutant was compared to wild-type Guy11, and the results showed that appressoria of the *MoPmt2* mutant were in a tendency to collapse at lower glycerol concentrations, compared to those of by the Guy11 and *MoPmt2c* (**Figure 8A**), suggesting a defect in maintaining appressorium cell wall integrity in *MoPmt2* mutant. In M. oryzae, an intact cell wall is the guarantee of full virulence on rice plants (Jeon et al., 2008), we thus examined the sensitivity of the transformants to different cell wall inhibitor, and the results showed that *MoPmt2* mutants showed significantly increased sensitivity to cell wall damaging agents CFW and CR, respectively (**Figures 8B,C**). Meanwhile, CFW staining of appressorium also revealed that much stronger fluorescence signal was observed around the appressorium of Guy11 and *MoPmt2c*, compared to *MoPmt2* mutant (**Figure S6B**), indicating less chitin accumulated on the cell wall of *MoPmt2* mutant. Moreover, protoplast release by the *MoPmt2* mutant was much faster than that of Guy11 and *MoPmt2c* after enzyme treatment for 30, 60, 90, and 120 min (**Figure 8D**), suggesting that cell wall integrity was impaired in the *MoPmt2* mutants. TEM assay further confirmed this phenotype and the cell wall ultrastructures of *MoPmt2* mutants were much thinner than wild type Guy11 (**Figure 8E**), indicating CWI defect may be results in failure of accumulation of appressorium turgor pressure, and thus attenuation of pathogenicity on rice plants.

MoPmt2 Deletion Attenuates the Activity of Extracellular Peroxidases and Laccases

In *M. oryzae*, the secreted extracellular peroxidases were presumed to be responsible for CR degradation, which, as a result, could generate a bright halo around the colony (Guo et al., 2011). In the examination of cell wall integrity of the *MoPmt2* mutants, we found that the degradation halo of CR by the *MoPmt2* mutants was not as apparent as the wild type (**Figure 8B**), indicating a deficiency of the CR-degrading activity in the *MoPmt2* mutants. An enzyme activity assay using ABTS as substrate revealed that the *MoPmt2* mutant severely reduced its peroxidase activity in the extracellular culture filtrate (**Figure S7A**). In addition, the activity of additional extracellular enzyme laccases was determined and found that the decreased laccase activity was also observed in the *MoPmt2* mutant, with lower levels of laccase activity

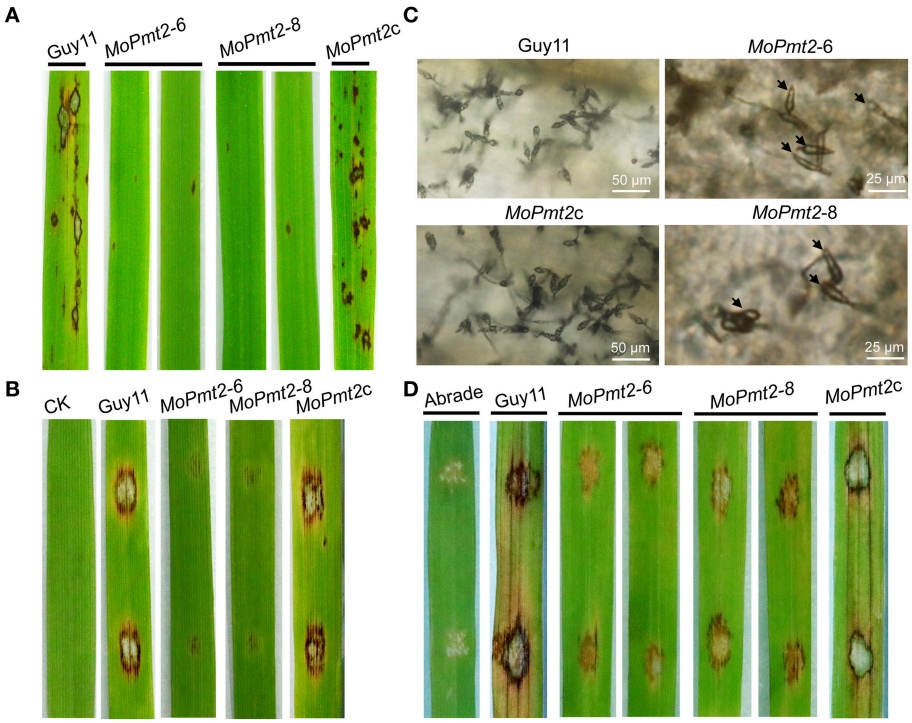

FIGURE 5 | Pathogenicity assays. (A) The pathogenic development of the mutants on rice leaves. The *MoPmt2* deletion attenuated pathogenicity on rice leaves. Diseased leaves were harvested 5 days after inoculation. **(B)** Pathogenicity assays on barley leaves. The *MoPmt2* deletion attenuated virulence on barley leaves. Diseased leaves were harvested 5 days after inoculation. **(C)** Microscopic examination of conidia produced on the lesions. Diseased leaves were harvested 15 days after inoculation and observed under a light microscope. **(D)** Pathogenicity assay on abraded rice leaves. Drops (10 μL) of conidia suspension from tested strains were inoculated on abraded rice leaves and a virulence defect was indicated in the mutants, compared with the control strains at 5 dpi.

in the culture filtrate, compared with the wild-type strain (**Figure S7B**).

DISCUSSION

In this study, three putative *O*-mannosyltransferases, with one member in each Pmt subfamily, were identified in rice blast fungus *M. oryzae*, which is consistent with findings that showed the existence of only one ortholog for each Pmt subfamily in other filamentous fungi and in the fission yeast (Willer et al., 2005; Fernández-Álvarez et al., 2009; Goto et al., 2009; Gonzalez et al., 2013; Harries et al., 2015). Amino acid sequence alignment showed that, similar to other members of the Pmt2 family in fungi, MoPmt2 contains a conserved the PMT domain in the N-terminal transmembrane region, and a MIR domain in the hydrophilic central region, which share 55 and 48% amino acid identity to the respective domains of Pmt2p from *S. cerevisiae* (Gentzsch and Tanner, 1996). Compared to *MoPmt1* and *MoPmt4*, the *MoPmt2* showed reduced transcriptional expression in the *Moap1* mutant, indicating distinctive roles during fungal development and pathogenicity. The functional analysis by complementation of yeast *Pmt2* deletion mutant demonstrated that MoPmt2 is homologous to Pmt2 from *S. cerevisiae*. These findings are also consistent with previous findings in *P. digitatum*, and suggest a conserved role of MoPmt2 in the regulation of growth and development in *M. oryzae* (Harries et al., 2015).

Previous studies revealed that the *O*-mannosyltransferase encoding gene *Pmt2* had diverse roles in fungal development (Fernández-Álvarez et al., 2009; Goto et al., 2009; Fang et al., 2010; Shimizu et al., 2014; Wang et al., 2014). In *M. oryzae*, our findings reveal that the *MoPmt2* deletion mutants are viable, but show severe defects in polarity, with more branching hyphae and septa, and globular balloon-like structures as compared to Guy11, which is similar to previous findings in *P. digitatum* and *B. cinerea* (Gonzalez et al., 2013; Harries et al., 2015). Previous studies in null *chs* mutants of *P. digitatum* revealed that the globular structures are resulted from abnormal fungal cell wall synthesis (Gandia et al., 2014). We therefore stained the cell wall of mycelia with CFW and found that these morphological defects are ascribed to production of cell enlargements with altered chitin content (**Figure 2D**), similar to results identified in *A. nidulans* (Shaw and Momany, 2002) and *P. digitatum* (Harries et al., 2015), suggesting an important role of MoPmt2 in regulating of the distribution of chitin content in *M. oryzae*. In addition, pathogenic test also revealed that *MoPmt2* mutants showed restricted invasive growth in host cells. Most invasive hyphae of *MoPmt2* mutant were confined to the host cells at early infection stage and the disease lesions (<10 days) of the *MoPmt2* mutant

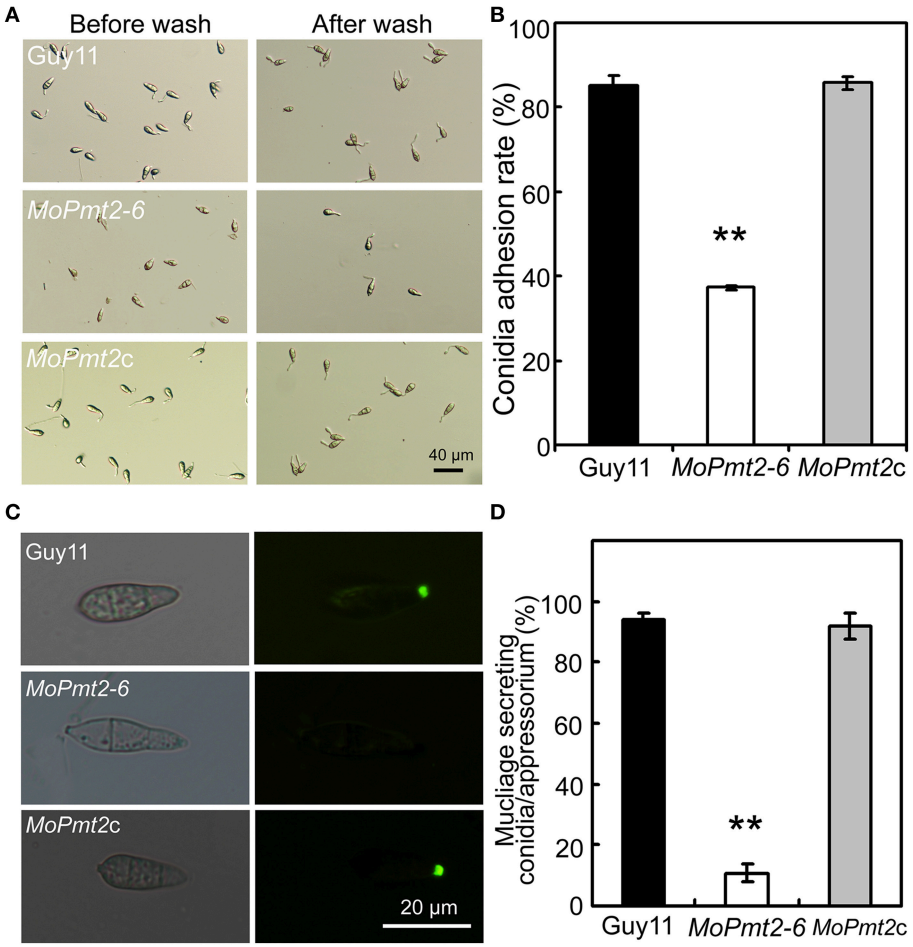

FIGURE 6 | The effect of MoPmt2 on conidia adhesion. (A) Inability of *MoPmt2* conidia to adhere to a hydrophobic surface. Conidia suspension of tested strains grew on a hydrophobic coverslips for 2 h was washed with sterilized water by pipetting and then visualized with brightfield optics of Nikon inverted Ti-S microscope. Scale bar = 40 μm. **(B)** Statistical analysis of conidia adhesion to hydrophobic coverslips. The numbers of conidia adhesive to the coverslips after wash were counted and statistically analyzed by Duncan's analysis ($p < 0.01$). Asterisks indicate significant differences of conidia adhesion among strains. Error bar represents standard deviation. **(C)** STM secretion test. STM from the conidia of Guy11, *MoPmt2* mutant and *MoPmt2c* were stained with FITC-ConA, and the fluorescence signal from the germinated conidia were visualized by a Nikon inverted Ti-S epifluorescence microscope. **(D)** Statistical analysis of conidia stained by FITC-ConA. The numbers of conidia stained by FITC-ConA were counted and statistically analyzed by Duncan's analysis ($p < 0.01$). Asterisks indicate significant differences among strains. Error bar represents standard deviation.

seldom produce conidia, indicating a possible necrotic reaction and low level invasive hyphae growth of *MoPmt2* mutants in plant cells. These above results are similar to the previous findings that deletion of a α-1, 3-Mannosyltransferase encoding gene *ALG3*, which is essential for *N*-glycosylation of secreted effector like Slp1, resulted in the arrest of secondary infection hyphae and a significant reduction in virulence, and thus made us presume that the constrained growth of *MoPmt2* mutants might be ascribed to the failure of evading host innate immunity and thus attenuated virulence on host. However, in view of the facts that the *MoPmt2* mutant is defective in polarity, and some large lesions of *MoPmt2* mutant can produce conidia, we couldn't exclude that the hindered hyphae growth might also partly affect the proliferation of invasive hyphae and lesion development by the *MoPmt2* mutants.

In *M. oryzae*, conidiogenesis is a complex process that involves a series of morphological events (Liu et al., 2010). In field condition, the severity of the disease epidemic lies on the quantity of conidia produced in the rice blast lesion, suggesting an important role of conidiation in the disease cycle. Previous studies in filamentous fungus showed that disruption of *Pmt2* genes in *A. nidulans*, *A. fumigatus* and *P. digitatum* equally led to a significant reduction of conidiation (Goto et al., 2009; Fang et al., 2010; Harries et al., 2015), whereas in the *B. cinerea*, deletion of *Pmt2* gene resulted in a complete loss of sporulation (Gonzalez et al., 2013), indicating a potential role of *Pmt2* gene in conidial development. In this study, we observed an increased expression level of *MoPmt2* in conidia, which is similar to the transcriptional pattern of *Moap1* in *M. oryzae*, demonstrating a potential role in asexual spore development (Guo et al., 2011).

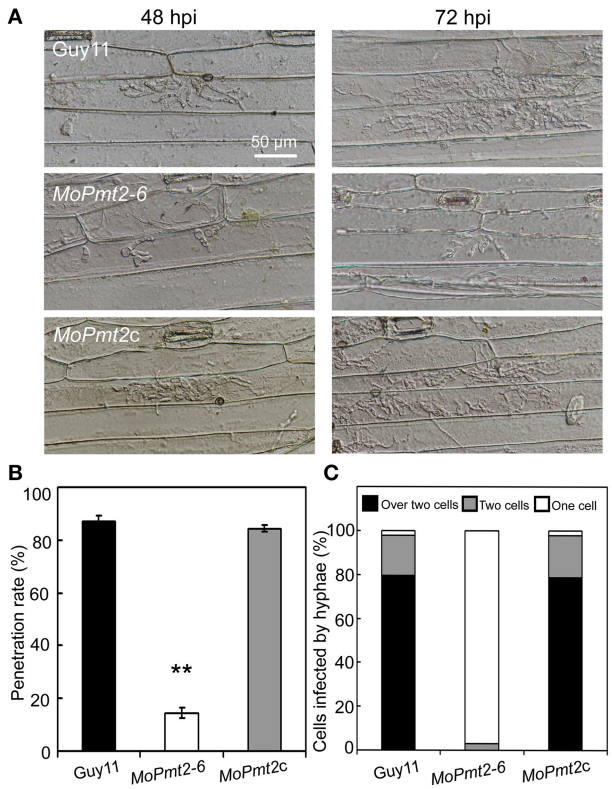

FIGURE 7 | The deletion of *MoPmt2* results in impaired appressorium penetration. (A) The *MoPmt2* mutants are defective on appressorium-mediated penetration. The *MoPmt2* mutants exhibited penetration defects on barley leaves after 48 and 72 h, respectively, in contrast with control strains. Scale bar = 50 μm. **(B)** Statistical analysis of appressorium penetrated in host cells. The appressoria that penetrated into barley epidermal cells were counted at 48 hpi, and the data were statistically analyzed. Asterisks indicate significant differences among strains. Error bar represents standard deviation. **(C)** Quantification of hyphae infection on barley epidermal cells. The percentage of infected cells occupied by infectious hyphae of tested strains at 72 hpi were measured and statistically analyzed.

This hypothesis was confirmed by the analysis of *MoPmt2* mutants, with phenotypes of significant reduction of conidiation, abnormal conidia size and delayed conidial germination, which is consistent with the identification in other fungi (Gonzalez et al., 2013; Wang et al., 2014; Harries et al., 2015), suggesting a conserved role of MoPmt2 protein in asexual spore development in *M. oryzae*. In particular, it is pointed out that conidial morphology of large conidia from the *MoPmt2* mutants, was similar to those observed in *Moap1* mutants, demonstrating that the MoPmt2 protein might function downstream of the MoAp1 and is responsible for conidial development (Guo et al., 2011).

The initial stages of infection by *M. oryzae* usually require the immediate and persistent adhesion of a conidium to the rice leaf by means of the spore tip mucilage released from the spore apex (Jelitto et al., 1994). Cell wall glycoproteins have been identified as fungal adhesives and have been implicated in host cell adhesion in many organisms (Gaur and Klotz, 1997; Frieman et al., 2002; Harries et al., 2015). *O*-mannosylation, a type of protein *O*-glycosylation with the capacity of addition of mannose residues to target proteins, have been described for fungal development, including in cell wall integrity, cell morphology and cell adhesion (Fernández-Álvarez et al., 2009; Kriangkripipat and Momany, 2009; Lommel and Strahl, 2009; Harries et al., 2015). In this study, we identified MoPmt2 as a homolog of the yeast Pmt2 protein, an *O*-mannosyltransferase from PMT2 subfamily, in *M. oryzae*. Deletion of *MoPmt2* resulted in reduced ability of conidial adhesion to hydrophobic surfaces, and thus attenuated virulence on rice plants, which agreed with the findings in *B. cinerea*, *A. fumigatus* (Kriangkripipat and Momany, 2009; Gonzalez et al., 2013), indicating a conserved role of MoPmt2 in fungal adhesion during plant infection. Our subsequent FITC-ConA staining revealed that STM secretion was not detected in the *MoPmt2* mutants, compared to wild-type Guy11, making us further confirm that *MoPmt2* might be involved in synthesis and secretion of STM in *M. oryzae*. However, this seems paradoxical to the result that secretion of STM from mature appressoria of *MoPmt2* mutant was comparable to that of Guy11. In *M. oryzae*, previous studies showed that STM is stored at the conidial apex of dormant conidia, and its release is an early event before germ tube emergence (Hamer et al., 1988). Therefore, we speculated that *MoPmt2* deletion might be lead to defects on storage and secretion of STM in *M. oryzae*, and our subsequent staining of mature appressoria with FITC-ConA might be not reflected the true STM, but newly synthesized glycosylated-proteins that were secreted outside of the appressorium cell wall of *MoPmt2* mutants and wild-type Guy11.

In *M. oryzae*, the fungal cell wall provides mechanical protection against attack from the host during host–pathogen interactions, and an intact cell wall is the guarantee for full virulence on rice plants (Jeon et al., 2008; Guo et al., 2015). In this study, we identified that defects on appressorium-mediated penetration was one of the main reasons for attenuated virulence of MoPmt2 mutants (**Figure 7B**). Our subsequent assay revealed that the MoPmt2 mutants showed increased sensitivity to CFW and CR (**Figure 8**), and more protoplast was released in the mutants as compared to Guy11, suggesting a defective CWI in the MoPmt2 mutants (**Figure 8**). This deduction was supported by the analysis of turgor pressure, with more collapsed appressorium being observed in the MoPmt2 mutants at different glycerol solutions. Together with the altered distribution of chitin content in the cell wall of both mycelia and appressorium, we concluded that the defective CWI in the mutants might be responsible for their inability to accumulate sufficient turgor pressure in appressorium, thus leading to failed penetration of host cells and attenuated pathogenicity on rice plants. Our results is consistent with the biological roles of *Pmt2* in phytopathogen like *B. cinerea*, B. bassiana and *P. digitatum*, which is critical for the stability of cell wall integrity (Gonzalez et al., 2013; Wang et al., 2014; Harries et al., 2015).

In phytopathogens, secreted peroxidases are regarded to help pathogens to detoxify host-derived ROS during plant-microbe interactions (Chi et al., 2009; Guo et al., 2010, 2011). We identified an attenuation of secreted peroxidase activity in the *MoPmt2* mutant by comparing CR discoloration and

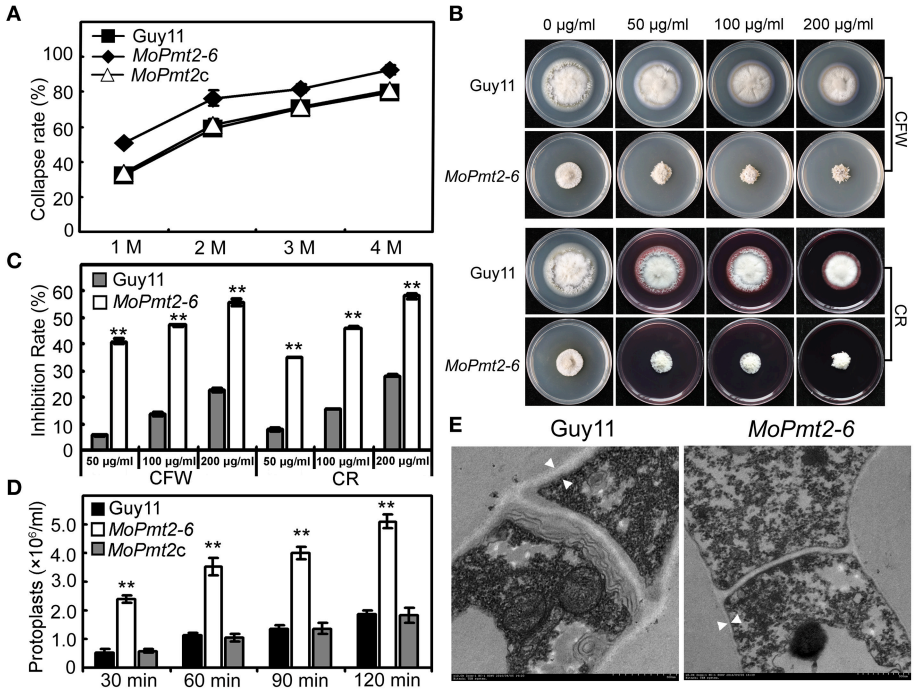

FIGURE 8 | The deletion of *MoPmt2* impaired cell wall integrity of *M. oryzae*. (A) Measurement of collapsed appressoria. The collapsed appressoria (>100) were observed at each glycerol concentration and statistically analyzed. **(B)** Sensitivity of *MoPmt2* mutants to cell wall damaging agents. All tested strains were inoculated on CM containing cell wall-perturbing agents (CR and CFW) with final concentrations of 50, 100, 200 mg/mL, respectively. **(C)** Statistical analysis of mycelial growth of the tested strains under CR and CFW. **(D)** Protoplast release assay. Protoplasts released under the treatment of lysing enzymes were counted and statistically analyzed at each indicated time. Asterisks in this figure indicate significant differences among the strains ($p < 0.01$). Error bar represents standard deviation. **(E)** Ultrastructure of the cell wall in the *MoPmt2* mutant. Cell wall ultrastructures of mycelia of wild type strain Guy11 and the *MoPmt2* mutant were observed by sectioning and TEM. Distances between the white triangles indicated the width of cell wall. Three independent experiments were carried out and representative images from one experiment were shown.

assaying the peroxidase activity in culture filtrates. Meanwhile, the secreted laccases were also reduced in enzyme activity in the culture filtrates of *MoPmt2* mutant. In *M. oryzae*, a previous study revealed that hundreds of putatively secretory proteins possessed Ser/Thr-rich regions and could be potentially *O*-glycosylated in protein posttranslational modification (Gonzalez et al., 2012), thus, combined with the observed phenotypes, we presumed that MoPmt2 may be required for the *O*-glycosylation of those secreted peroxidases and laccases, and its deletion may result in proteins modification defects, which thus reduced the enzymatic activity of the *MoPmt2* mutants.

In summary, our result reveals that the MoPmt2 play a critical role during the development of *M. oryzae*. The deletion of *MoPmt2* could result in defects on conidiation, fungal adhesion, conidia germination, CWI and invasive hyphae growth, and thus attenuated the pathogenicity of *M. oryzae* on rice plants.

AUTHOR CONTRIBUTIONS

Conceived and designed the experiments: MG, ZG. Performed the experiments: MG, LT, XN. Analyzed the data: MG, XZ, XN, YP. Wrote the paper: MG.

ACKNOWLEDGMENTS

This work was supported by the National Natural Science Foundations of China (Grant No: 31101401), the Foundation for the Author of National Excellent Doctoral Dissertation of PR China (Grant No: 201470), the Foundation for the Excellent Talents of Anhui Agricultural University (Grant No: RC2015002), and the Key Grant for Excellent Young Talents of Anhui Higher Education Institutions (gxyqZD2016037). We gratefully acknowledge Professor Zhengguang Zhang for providing the plasmids pYES2.

SUPPLEMENTARY MATERIAL

The Supplementary Material for this article can be found online at: http://journal.frontiersin.org/article/10.3389/fmicb.2016.00630

Figure S1 | The dendrogram of PMT proteins from different organisms. A phylogenetic tree of MoPmts homologs was created by the distance based minimum evolution method, based on 1000 bootstraps. *M. oryzae* sequences characterized in this study are highlighted in dotted box. Pmt proteins from different fungal organisms were obtained from NCBI database (http://www.ncbi.nlm.nih.gov/) and the accession numbers of all the sequences used in this analysis are as followings: *M. oryzae* (XP_003720753, ELQ38305, XP_003713520), *S. cerevisiae* (NP_010188, NP_009379, NP_014966,

NP_012677, NP_010190, NP_011715), *C. albicans* (XP_716993, XP_719907, XP_714280, XP_719311, XP_717283), *S. pombe* (NP_593237, NP_594135, NP_596807), *U. maydis* (XP_762320, XP_761621, XP_761580), *Drosophila melanogaster* (NP_524025, NP_569858), *Homo sapiens* (NP_009102.3, NP_037514.2), *C. neoformans* (XP_570521, XP_567365, XP_570292), *B. cinerea* (XP_001548518, XP_001558317, XP_001558914), *A. nidulans* (XP_662365, XP_662709, XP_659063), *B. bassiana* (EJP63368, EJP63582, EJP70423), *Metarhizium anisopliae* (EFY94173, EFZ02257, EFZ00337), *Aspergillus niger* (XP_001394947, XP_001392110, XP_001398147), *A. fumigates* (EAL92923, XP_754961, XP_747257), *Penicillium mameffei* (EEA19578, EEA22196), *Neurospora crassa* (XM_960450, XM_951177, XM_958833), *P. digitatum* (KC757712, KC757713, KC757714), and *Penicillium crysogenum* (AM920435, AM920427, AM920436).

Figure S2 | The relative expression, targeted gene replacement and complementation of *MoPmt2*. (A) *MoPmt2* expression at different developmental stage. Significant differences are presented in the figure ($P < 0.01$), and the error bar represents the standard deviation. **(B)** Targeted gene replacement strategies. The DNA fragment deleted from the *MoPmt2* region was used as the probe to validate the deletion of *MoPmt2* by Southern blot (Scale bar = 1 kb). **(C)** Validation of the transformants by PCR amplification. Primer pairs (p1 to p4) showed in this figure were used to validate the transformants by PCR amplification. **(D,E)**. Southern blot analysis. To confirm the copy number of *MoPmt2* gene in Guy11 and the deletion of *MoPmt2* gene in the mutants, both the genomic DNA of Guy11 and the mutants, which were digested with *Sal*I, respectively, were hybridized with probe of *MoPmt2* left flank. To validate the integration of a single copy of *HPH* gene in the mutants, genomic DNA of Guy11 and *MoPmt2* mutants were digested with *Sal*I, and hybridized with *HPH* probe. **(F)** Semiquantitative RT-PCR. RNA samples from Guy11, *MoPmt2* mutants and *MoPmt2c* were reversely transcripted and used to confirm the deletion and reintroduction of the *MoPmt2* gene by PCR amplification.

Figure S3 | Mycelial growth of the *MoPmt2* mutants on different media. The wild-type strain Guy11, *MoPmt2* mutants and complemented strain *MoPmt2c* was inoculated on CM, MM, OM, and RDC, and cultured at 28°C for 5 days.

Figure S4 | Conidia bipolar germination in *MoPmt2* mutants. (A) Polarity growth defects of *MoPmt2* mutants. CFW staining of mycelia show polarity growth defects and swollen of mycelia of *MoPmt2* mutants. **(B)** Conidial suspension (1×10^5 ml^{-1}) of Guy11, *MoPmt2-6* mutant and *MoPmt2c*, harvested from 14-day-old cultures, were inoculated on the hydrophobic surface of the coverslips for 24 h, and then observed under light microscope. **(C)** Statistical analysis of conidia with bipolar germination. The percentage of conidia with unipolar and bipolar germination was calculated and statistically analyzed, respectively.

Figure S5 | Conidial morphology of *MoPmt2* mutants on conidiophores. The development of conidia on conidiophores was examined by light microscope using strains grown on RDC medium for 7 days. Scale bar = 30 μm.

Figure S6 | The staining of appressorium with FITC-ConA or CFW. (A) Mucilage secreted from the appressorium of Guy11 and *MoPmt2* mutants were stained with FITC-ConA. The fluorescence signal from mature appressoria were visualized by a Nikon inverted T*i*-S epifluorescence microscope. **(B)** The CFW staining of appressorium of Guy11, *MoPmt2* mutant and *MoPmt2c*. The fluorescence signal from mature appressoria were captured by a Nikon inverted T*i*-S epifluorescence microscope.

Figure S7 | Decreased extracellular laccase and peroxidase activities in the *MoPmt2* mutants. Guy11, *MoPmt2* mutants and *MoPmt2c* were inoculated in CM liquid medium and the peroxidase activity **(A)** and laccase activity **(B)** were measured in the filtrate cultures through ABTS oxidization test with or without H_2O_2. Error bars represent the standard deviations and asterisks represent significant differences among the strains tested ($p < 0.01$).

Table S1 | Bioinformatics of putative *M. oryzae* PMT proteins.

Table S2 | Primers used in this paper.

REFERENCES

Chi, M. H., Park, S. Y., Kim, S., and Lee, Y. H. (2009). A novel pathogenicity gene is required in the rice blast fungus to suppress the basal defenses of the host. *PLoS Pathog.* 5:e1000401. doi: 10.1371/journal.ppat.1000401

Chen, X. L., Shi, T., Yang, J., Shi, W., Gao, X., Chen, D., et al. (2014). N-glycosylation of effector proteins by an alpha-1,3-mannosyltransferase is required for the rice blast fungus to evade host innate immunity. *Plant Cell* 26, 1360–1376. doi: 10.1105/tpc.114.123588

Dean, R., Van Kan, J. A., Pretorius, Z. A., Hammond-Kosack, K. E., Di Pietro, A., Spanu, P. D., et al. (2012). The Top 10 fungal pathogens in molecular plant pathology. *Mol. Plant Pathol.* 13, 414–430. doi: 10.1111/j.1364-3703.2011.00783.x

Dean, R. A., Talbot, N. J., Ebbole, D. J., Farman, M. L., Mitchell, T. K., Orbach, M. J., et al. (2005). The genome sequence of the rice blast fungus *Magnaporthe grisea*. *Nature* 434, 980–986. doi: 10.1038/nature03449

Fang, W., Ding, W., Wang, B., Zhou, H., Ouyang, H., Ming, J., et al. (2010). Reduced expression of the O-mannosyltransferase 2 (AfPmt2) leads to deficient cell wall and abnormal polarity in *Aspergillus fumigatus*. *Glycobiology* 20, 542–552. doi: 10.1093/glycob/cwp206

Fernández-Álvarez, A., Elias-Villalobos, A., and Ibeas, J. I. (2009). The O-mannosyltransferase PMT4 is essential for normal appressorium formation and penetration in *Ustilago maydis*. *Plant Cell* 21, 3397–3412. doi: 10.1105/tpc.109.065839

Fernández-Álvarez, A., Marin-Menguiano, M., Lanver, D., Jimenez-Martin, A., Elias-Villalobos, A., Perez-Pulido, A. J., et al. (2012). Identification of O-mannosylated virulence factors in *Ustilago maydis*. *PLoS Pathog.* 8:e1002563. doi: 10.1371/journal.ppat.1002563

Frieman, M. B., McCaffery, J. M., and Cormack, B. P. (2002). Modular domain structure in the *Candida glabrata* adhesin Epa1p, a beta1,6 glucan-cross-linked cell wall protein. *Mol. Microbiol.* 46, 479–492. doi: 10.1046/j.1365-2958.2002.03166.x

Gandia, M., Harries, E., and Marcos, J. F. (2014). Identification and characterization of chitin synthase genes in the postharvest citrus fruit pathogen *Penicillium digitatum*. *Fungal Biol.* 116, 654–664. doi: 10.1016/j.funbio.2012.03.005

Gaur, N. K., and Klotz, S. A. (1997). Expression, cloning, and characterization of a Candida albicans gene, ALA1, that confers adherence properties upon *Saccharomyces cerevisiae* for extracellular matrix proteins. *Infect. Immun.* 65, 5289–5294.

Gentzsch, M., Immervoll, T., and Tanner, W. (1995). Protein O-glycosylation in *Saccharomyces cerevisiae*: the protein O-mannosyltransferases Pmt1p and Pmt2p function as heterodimer. *FEBS Lett.* 377, 128–130. doi: 10.1016/0014-5793(95)01324-5

Gentzsch, M., and Tanner, W. (1996). The PMT gene family: protein O-glycosylation in *Saccharomyces cerevisiae* is vital. *EMBO J.* 15, 5752–5759.

Girrbach, V., and Strahl, S. (2003). Members of the evolutionarily conserved PMT family of protein O-mannosyltransferases form distinct protein complexes among themselves. *J. Biol. Chem.* 278, 12554–12562. doi: 10.1074/jbc.M212582200

Girrbach, V., Zeller, T., Priesmeier, M., and Strahl-Bolsinger, S. (2000). Structure-function analysis of the dolichyl phosphate-mannose: protein O-mannosyltransferase ScPmt1p. *J. Biol. Chem.* 275, 19288–19296. doi: 10.1074/jbc.M001771200

Gonzalez, M., Brito, N., and Gonzalez, C. (2012). High abundance of Serine/Threonine-rich regions predicted to be hyper-O-glycosylated in the secretory proteins coded by eight fungal genomes. *BMC Microbiol.* 12:213. doi: 10.1186/1471-2180-12-213

Gonzalez, M., Brito, N., Frias, M., and Gonzalez, C. (2013). *Botrytis cinerea* protein O-mannosyltransferases play critical roles in morphogenesis, growth, and virulence. *PLoS ONE* 8, e65924. doi: 10.1371/journal.pone.0065924

Goto, M., Harada, Y., Oka, T., Matsumoto, S., Takegawa, K., and Furukawa, K. (2009). Protein O-mannosyltransferases B and C support hyphal development

and differentiation in *Aspergillus nidulans*. *Eukaryotic Cell* 8, 1465–1474. doi: 10.1128/EC.00371-08

Guo, M., Chen, Y., Du, Y., Dong, Y., Guo, W., Zhai, S., et al. (2011). The bZIP transcription factor MoAP1 mediates the oxidative stress response and is critical for pathogenicity of the rice blast fungus *Magnaporthe oryzae*. *PLoS Pathog.* 7:e1001302. doi: 10.1371/journal.ppat.1001302

Guo, M., Gao, F., Zhu, X., Nie, X., Pan, Y., and Gao, Z. (2015). MoGrr1, a novel F-box protein, is involved in conidiogenesis and cell wall integrity and is critical for the full virulence of *Magnaporthe oryzae*. *Appl. Microbiol. Biotechnol.* 99, 8075–8088. doi: 10.1007/s00253-015-6820-x

Guo, M., Guo, W., Chen, Y., Dong, S., Zhang, X., Zhang, H., et al. (2010). The basic leucine zipper transcription factor Moatf1 mediates oxidative stress responses and is necessary for full virulence of the rice blast fungus *Magnaporthe oryzae*. *Mol. Plant Microbe Interact.* 23, 1053–1068. doi: 10.1094/MPMI-23-8-1053

Hamer, J. E., Howard, R. J., Chumley, F. G., and Valent, B. (1988). A mechanism for surface attachment in spores of a plant pathogenic fungus. *Science* 239, 288–290. doi: 10.1126/science.239.4837.288

Han, J. H., Lee, H. M., Shin, J. H., Lee, Y. H., and Kim, K. S. (2015). Role of the MoYAK1 protein kinase gene in Magnaporthe oryzae development and pathogenicity. *Environ Microbiol.* 17, 4672–4689. doi: 10.1111/1462-2920.13010

Harries, E., Carmona, L., Munoz, A., Ibeas, J. I., Read, N. D., Gandia, M., et al. (2013). Genes involved in protein glycosylation determine the activity and cell internalization of the antifungal peptide PAF26 in *Saccharomyces cerevisiae*. *Fungal Genet. Biol.* 58–59, 105–115. doi: 10.1016/j.fgb.2013.08.004

Harries, E., Gandia, M., Carmona, L., and Marcos, J. F. (2015). The *Penicillium digitatum* protein O-mannosyltransferase Pmt2 is required for cell wall integrity, conidiogenesis, virulence and sensitivity to the antifungal peptide PAF26. *Mol. Plant Pathol.* 16, 748–761. doi: 10.1111/mpp.12232

Howard, R. J., Ferrari, M. A., Roach, D. H., and Money, N. P. (1991). Penetration of hard substrates by a fungus employing enormous turgor pressures. *Proc. Natl. Acad. Sci. U.S.A.* 88, 11281–11284. doi: 10.1073/pnas.88.24.11281

Howard, R. J., and Valent, B. (1996). Breaking and entering: host penetration by the fungal rice blast pathogen *Magnaporthe grisea*. *Annu. Rev. Microbiol.* 50, 491–512. doi: 10.1146/annurev.micro.50.1.491

Jelitto, T., Page, H., and Read, N. (1994). Role of external signals in regulating the pre-penetration phase of infection by the rice blast fungus, *Magnaporthe grisea*. *Planta* 194, 471–477. doi: 10.1007/BF00714458

Jeon, J., Goh, J., Yoo, S., Chi, M. H., Choi, J., Rho, H. S., et al. (2008). A putative MAP kinase kinase kinase, MCK1, is required for cell wall integrity and pathogenicity of the rice blast fungus, *Magnaporthe oryzae*. *Mol. Plant Microbe Interact.* 21, 525–534. doi: 10.1094/MPMI-21-5-0525

Kankanala, P., Czymmek, K., and Valent, B. (2007). Roles for rice membrane dynamics and plasmodesmata during biotrophic invasion by the blast fungus. *Plant Cell* 19, 706–724. doi: 10.1105/tpc.106.046300

Kriangkripipat, T., and Momany, M. (2009). *Aspergillus nidulans* protein O-mannosyltransferases play roles in cell wall integrity and developmental patterning. *Eukaryotic Cell* 8, 1475–1485. doi: 10.1128/EC.00040-09

Krogh, A., Larsson, B., von Heijne, G., and Sonnhammer, E. L. (2001). Predicting transmembrane protein topology with a hidden Markov model: application to complete genomes. *J. Mol. Biol.* 305, 567–580. doi: 10.1006/jmbi.2000.4315

Lee, K., Singh, P., Chung, W. C., Ash, J., Kim, T. S., Hang, L., et al. (2006). Light regulation of asexual development in the rice blast fungus, *Magnaporthe oryzae*. *Fungal Genet. Biol.* 43, 694–706. doi: 10.1016/j.fgb.2006.04.005

Lehle, L., Strahl, S., and Tanner, W. (2006). Protein glycosylation, conserved from yeast to man: a model organism helps elucidate congenital human diseases. *Angew. Chem. Int. Ed Engl.* 45, 6802–6818. doi: 10.1002/anie.200601645

Letunic, I., Doerks, T., and Bork, P. (2012). SMART 7: recent updates to the protein domain annotation resource. *Nucleic Acids Res.* 40, D302–D305. doi: 10.1093/nar/gkr931

Livak, K. J., and Schmittgen, T. D. (2001). Analysis of relative gene expression data using real-time quantitative PCR and the $2^{-\Delta\Delta CT}$ method. *Methods* 25, 402–408. doi: 10.1006/meth.2001.1262

Liu, W., Xie, S., Zhao, X., Chen, X., Zheng, W., Lu, G., et al. (2010). A homeobox gene is essential for conidiogenesis of the rice blast fungus *Magnaporthe oryzae*. *Mol. Plant Microbe Interact.* 23, 366–375. doi: 10.1094/MPMI-23-4-0366

Loibl, M., and Strahl, S. (2013). Protein O-mannosylation: what we have learned from baker's yeast. *Biochim. Biophys. Acta* 1833, 2438–2446. doi: 10.1016/j.bbamcr.2013.02.008

Lommel, M., and Strahl, S. (2009). Protein O-mannosylation: conserved from bacteria to humans. *Glycobiology* 19, 816–828. doi: 10.1093/glycob/cwp066

Lussier, M., Gentzsch, M., Sdicu, A. M., Bussey, H., and Tanner, W. (1995). Protein O-glycosylation in yeast. The PMT2 gene specifies a second protein O-mannosyltransferase that functions in addition to the PMT1-encoded activity. *J. Biol. Chem.* 270, 2770–2775. doi: 10.1074/jbc.270.6.2770

McGinnis, S., and Madden, T. L. (2004). BLAST: at the core of a powerful and diverse set of sequence analysis tools. *Nucleic Acids Res.* 32, W20–W25. doi: 10.1093/nar/gkh435

Mouyna, I., Kniemeyer, O., Jank, T., Loussert, C., Mellado, E., Aimanianda, V., et al. (2010). Members of protein O-mannosyltransferase family in *Aspergillus fumigatus* differentially affect growth, morphogenesis and viability. *Mol. Microbiol.* 76, 1205–1221. doi: 10.1111/j.1365-2958.2010.07164.x

Olson, G. M., Fox, D. S., Wang, P., Alspaugh, J. A., and Buchanan, K. L. (2007). Role of protein O-mannosyltransferase Pmt4 in the morphogenesis and virulence of *Cryptococcus neoformans*. *Eukaryotic Cell* 6, 222–234. doi: 10.1128/EC.00182-06

Park, G., Bruno, K. S., Staiger, C. J., Talbot, N. J., and Xu, J. R. (2004). Independent genetic mechanisms mediate turgor generation and penetration peg formation during plant infection in the rice blast fungus. *Mol. Microbiol.* 53, 1695–1707. doi: 10.1111/j.1365-2958.2004.04220.x

Prill, S. K., Klinkert, B., Timpel, C., Gale, C. A., Schroppel, K., and Ernst, J. F. (2005). PMT family of *Candida albicans*: five protein mannosyltransferase isoforms affect growth, morphogenesis and antifungal resistance. *Mol. Microbiol.* 55, 546–560. doi: 10.1111/j.1365-2958.2004.04401.x

Sambrook, J., Fritsch, E. F., and Maniatis, T. (1989). *Molecular Cloning: A Laboratory Manual*. Cold Spring Harbor, NY: Cold Spring Harbor Laboratory Press.

Shaw, B. D., and Momany, M. (2002). *Aspergillus nidulans* polarity mutant swoA is complemented by protein O-mannosyltransferase pmtA. *Fungal Genet. Biol.* 37, 263–270. doi: 10.1016/S1087-1845(02)00531-5

Shimizu, K., Imanishi, Y., Toh-e, A., Uno, J., Chibana, H., Hull, C. M., et al. (2014). Functional characterization of PMT2, encoding a protein-O-mannosyltransferase, in the human pathogen *Cryptococcus neoformans*. *Fungal Genet. Biol.* 69, 13–22. doi: 10.1016/j.fgb.2014.05.007

Strahl-Bolsinger, S., Gentzsch, M., and Tanner, W. (1999). Protein O-mannosylation. *Biochim. Biophys. Acta* 1426, 297–307. doi: 10.1016/S0304-4165(98)00131-7

Strahl-Bolsinger, S., and Scheinost, A. (1999). Transmembrane topology of pmt1p, a member of an evolutionarily conserved family of protein O-mannosyltransferases. *J. Biol. Chem.* 274, 9068–9075. doi: 10.1074/jbc.274.13.9068

Talbot, N. J. (2003). On the trail of a cereal killer: Exploring the biology of *Magnaporthe grisea*. *Annu. Rev. Microbiol.* 57, 177–202. doi: 10.1146/annurev.micro.57.030502.090957

Tamura, K., Dudley, J., Nei, M., and Kumar, S. (2007). MEGA4: molecular evolutionary genetics analysis (MEGA) software version 4.0. *Mol. Biol. Evol.* 24, 1596–1599. doi: 10.1093/molbev/msm092

Tanner, G. A., Gretz, N., Connors, B. A., Evan, A. P., and Steinhausen, M. (1996). Role of obstruction in autosomal dominant polycystic kidney disease in rats. *Kidney Int.* 50, 873–886. doi: 10.1038/ki.1996.387

Thines, E., Weber, R. W., and Talbot, N. J. (2000). MAP kinase and protein kinase A-dependent mobilization of triacylglycerol and glycogen during appressorium turgor generation by *Magnaporthe grisea*. *Plant Cell* 12, 1703–1718. doi: 10.1105/tpc.12.9.1703

Thompson, J. D., Higgins, D. G., and Gibson, T. J. (1994). CLUSTAL W: improving the sensitivity of progressive multiple sequence alignment through sequence

weighting, position-specific gap penalties and weight matrix choice. *Nucleic Acids Res.* 22, 4673–4680. doi: 10.1093/nar/22.22.4673

Wang, J. J., Qiu, L., Chu, Z. J., Ying, S. H., and Feng, M. G. (2014). The connection of protein O-mannosyltransferase family to the biocontrol potential of *Beauveria bassiana*, a fungal entomopathogen. *Glycobiology* 24, 638–648. doi: 10.1093/glycob/cwu028

Willer, T., Brandl, M., Sipiczki, M., and Strahl, S. (2005). Protein O-mannosylation is crucial for cell wall integrity, septation and viability in fission yeast. *Mol. Microbiol.* 57, 156–170. doi: 10.1111/j.1365-2958.2005.04692.x

Willer, T., Valero, M. C., Tanner, W., Cruces, J., and Strahl, S. (2003). O-mannosyl glycans: from yeast to novel associations with human disease. *Curr. Opin. Struct. Biol.* 13, 621–630. doi: 10.1016/j.sbi.2003.09.003

Xu, J. R., Zhao, X., and Dean, R. A. (2007). From genes to genomes: a new paradigm for studying fungal pathogenesis in *Magnaporthe oryzae*. *Adv. Genet.* 57, 175–218. doi: 10.1016/S0065-2660(06)57005-1

Xu, Y., Li, H., Zhang, J., Song, B., Chen, F., Duan, X., et al. (2010). Disruption of the chitin synthase gene *CHS1* from *Fusarium asiaticum* results in an altered structure of cell walls and reduced virulence. *Fungal Genet. Biol.* 47, 205–215. doi: 10.1016/j.fgb.2009.11.003

Zhou, H., Hu, H., Zhang, L., Li, R., Ouyang, H., Ming, J., et al. (2007). O-Mannosyltransferase 1 in Aspergillus fumigatus (AfPmt1p) is crucial for cell wall integrity and conidium morphology, especially at an elevated temperature. *Eukaryot. Cell* 6, 2260–2268. doi: 10.1128/EC.00261-07

Zhang, H., Zhao, Q., Liu, K., Zhang, Z., Wang, Y., and Zheng, X. (2009). MgCRZ1, a transcription factor of *Magnaporthe grisea*, controls growth, development and is involved in full virulence. *FEMS Microbiol. Lett.* 293, 160–169. doi: 10.1111/j.1574-6968.2009.01524.x

Conflict of Interest Statement: The authors declare that the research was conducted in the absence of any commercial or financial relationships that could be construed as a potential conflict of interest.

frontiers in Plant Science

ORIGINAL RESEARCH
published: 06 July 2016
doi: 10.3389/fpls.2016.00982

Transient Expression of *Candidatus* Liberibacter Asiaticus Effector Induces Cell Death in *Nicotiana benthamiana*

Marco Pitino[1], *Cheryl M. Armstrong*[1], *Liliana M. Cano*[2] *and Yongping Duan*[1]*

[1] U.S. Horticultural Research Laboratory, Agricultural Research Service, United States Department of Agriculture, Fort Pierce, FL, USA, [2] Institute of Food and Agricultural Sciences, Department of Plant Pathology, Indian River Research and Education Center, University of Florida, Fort Pierce, FL, USA

Candidatus Liberibacter asiaticus "Las" is a phloem-limited bacterial plant pathogen, and the most prevalent species of Liberibacter associated with citrus huanglongbing (HLB), a devastating disease of citrus worldwide. Although, the complete sequence of the Las genome provides the basis for studying functional genomics of Las and molecular mechanisms of Las-plant interactions, the functional characterization of Las effectors remains a slow process since remains to be cultured. Like other plant pathogens, Las may deliver effector proteins into host cells and modulate a variety of host cellular functions for their infection progression. In this study, we identified 16 putative Las effectors via bioinformatics, and transiently expressed them in *Nicotiana benthamiana*. Diverse subcellular localization with different shapes and aggregation patterns of the effector candidates were revealed by UV- microscopy after transient expression in leaf tissue. Intriguingly, one of the 16 candidates, Las5315mp (mature protein), was localized in the chloroplast and induced cell death at 3 days post inoculation (dpi) in *N. benthamiana.* Moreover, Las5315mp induced strong callose deposition in plant cells. This study provides new insights into the localizations and potential roles of these Las effectors *in planta.*

Keywords: huanglongbing, *Candidatus* Liberibacter asiaticus, bacterial effectors, cell death, *Nicotiana benthamiana*, callose deposition, chloroplast localization

OPEN ACCESS

Edited by:
Pietro Daniele Spanu, Imperial College London, UK

Reviewed by:
William Underwood, Agricultural Research Service, United States Department of Agriculture, USA
Daolong Dou, Nanjing Agricultural University, China

***Correspondence:**
Yongping Duan
yongping.duan@aus.usda.gov

Specialty section:
This article was submitted to Plant Biotic Interactions, a section of the journal Frontiers in Plant Science

Received: *14 April 2016*
Accepted: *21 June 2016*
Published: *06 July 2016*

Citation:
Pitino M, Armstrong CM, Cano LM and Duan Y (2016) Transient Expression of Candidatus Liberibacter Asiaticus Effector Induces Cell Death in Nicotiana benthamiana. Front. Plant Sci. 7:982. doi: 10.3389/fpls.2016.00982

INTRODUCTION

Citrus huanglongbing (HLB), also known as citrus greening, is a devastating disease with high economical costs to the worldwide citrus industry (Hodges and Spreen, 2012). The disease is caused by three species of alpha-proteobacterium, "*Candidatus* Liberibacter asiaticus (Las)," "*Ca.* L. africanus," and "*Ca.* L. americanus." Las, the most widespread pathogen, is vectored by the Asian citrus psyllid (ACP) *Diaphorina citri Kuwayama* (Hemiptera: Psyllidae) (Jagoueix et al., 1996; Garnier et al., 2000; Bove, 2006; Hall et al., 2013). Las attacks all species and hybrids in the *Citrus* genus, and upon infection, Las resides in the phloem of the host, which causes a systemic disease and can eventually result in the death of the tree (Halbert and Manjunath, 2004; Bove, 2006; Gottwald, 2010). Once a tree is infected, it is extremely difficult to cure, and currently there is no adequate strategy for HLB management.

Host-pathogen relationships encompass a myriad of protein-protein interactions that include not only pathogen detection and removal by the host but also mechanisms to avoid such processes by the pathogen. Understanding this interplay would open the door to more successful HLB control methods, however, the corresponding mechanisms are currently largely unknown. Plants, including citrus, are able to detect conserved microbial molecular signatures termed pathogen-associated molecular patterns (PAMP), and initiate a process known as PAMP-triggered immunity (PTI) (Boller and Felix, 2009; Segonzac and Zipfel, 2011). Pathogens, in turn, can suppress the PTI response by deploying diverse effector proteins that modulate various host cellular functions in order to promote bacterial colonization and replication (Chisholm et al., 2006; Hogenhout et al., 2009; Dodds and Rathjen, 2010). Effectors that are deployed to suppress host defenses may be recognized by plant disease resistance (R) proteins in particular host genotypes, resulting in effector-triggered immunity (ETI) (Jones and Dangl, 2006; Boller and Felix, 2009). A common strategy for plant pathogens to avoid the immune responses is to either lose their effectors or mutate by developing new effectors that are once again able to suppress ETI (Stergiopoulos and De Wit, 2009). This is important because together PTI and/or ETI limit microbial entry, restrict pathogen propagation, or kill pathogens inside plant tissues (Dou and Zhou, 2012). Overall, an in-depth investigation into the roles of putative Las candidate effectors is key not only to understanding how Las manipulates host defense responses and results in HLB disease but to identifying pathogenicity mechanisms that can ultimately lead to the development of novel control methods.

In 2009, the complete genome sequence of Las was obtained (Duan et al., 2009), enabling heterologous expression of Las proteins to be performed. Expression studies have demonstrated that the Las bacterium can act as an "energy parasite" through its encoded ATP translocase, which allows for direct ATP/ADP importation from its host cells (Vahling et al., 2010), and that two novel autotransporter proteins encoded in the Las prophages target the mitochondria of plants (Hao et al., 2013). In addition, using *Liberibacter crescens* strain BT-1 as model system, a peroxidase of Las was confirmed to be involved in suppressing the plant innate immunity via detoxification of H_2O_2 (Jain et al., 2015). From the host plant aspect, Las infection is correlated with significant changes in protein regulation in *Citrus paradisi*, indicating that Las actively alters molecular processes in citrus (Nwugo et al., 2013).

Unfortunately, even with the examination of citrus transcriptomes in response to Las infection and comparative transcriptome analyses (Albrecht and Bowman, 2008, 2012; Kim et al., 2008; Rawat et al., 2015; Zhong et al., 2015), Las genes involved in psyllid or citrus colonization remain largely unknown. This lack of accomplishment is due in part to the limited success in culturing the bacterium (Sechler et al., 2009) and the large number of hypothetical proteins in the Las genome (Duan et al., 2009). Alternative tactics involving heterologous systems are necessary in order to overcome these hurdles and speed the process of identification and functional characterization of candidate Las effector proteins (Boller and Felix, 2009; Segonzac and Zipfel, 2011; Dou and Zhou, 2012). Genome sequencing together with computational methods have revealed a wide catalog of candidate effectors genes in filamentous plant pathogenic: fungi (Chaudhari et al., 2014; Petre and Kamoun, 2014), oomycetes (Ellis et al., 2009), nematodes (Davis et al., 2008), bacteria (Block et al., 2008; Zhou and Chai, 2008; Hogenhout et al., 2009), and insects such as aphids (Bos et al., 2010; Pitino and Hogenhout, 2013). To functionally characterize pathogen effectors and how these proteins manipulate host cells, it is crucial to identify the host compartments where the effectors localize (Alfano, 2009). Thus, subcellular localization is one of the first aspects to consider when assessing effector function.

Utilizing a pathogen secretome analysis we uncovered 16 putative effectors in the Las genome. Similar to other studies, in an attempt to characterize these candidate effector proteins, they were transiently expressed in *N. benthamiana* leaves to allow both the localization pattern as well as any overt phenotype to be observed (Vleeshouwers et al., 2008; Wang et al., 2011; Du et al., 2014; Petre et al., 2015). These findings not only help establish *N. benthamiana* as a valuable heterologous system for fast-forward effectoromic analysis of plant pathogens regardless of their host plant (Petre et al., 2016) but also represent the first attempt to characterize and locate putative Las effectors by combining a pathogen secretome analysis with an *in planta* transient expression assay. Knowledge obtained from this Las effector screen enhances our understanding of HLB and may aid in the development of new and more efficient management strategies.

MATERIALS AND METHODS

Genomic DNA Extraction of Las Bacterial Pathogen

In addition to transmission by insects, Las can be experimentally transferred to non-rutaceous hosts such as periwinkle (*Catharanthus roseus*), which acts as a model organism for HLB because when infected via parasitic dodder (*Cuscuta campestri*) it allows Las to replicate to high titers (Garnier and Bové, 1983). Total genomic DNA was extracted from Las infected periwinkle leaves using the following protocol. Collected leaf tissue was chopped via razorblade and transferred to an autoclaved 2 ml screw-capped tube containing two 4 mm silicone-carbide sharp particles and four 2.3 mm chrome-steel beads in 800 μL of extraction buffer (100 mM HCl, 30 mM EDTA, 500 mM NaCl, 5% polyvinylpyrrolidone and 3% CTAB). Tissue was homogenized using a Fast Prep®-24 homogenizer at speed 6.0 m/s for 60 s and incubated at 65°C for 30 min after the addition of 80 μl 20% SDS. After adding one-third volume of 5 M potassium acetate, the tubes were incubated on ice for 5 min and centrifuged at 18,000 rpm (Eppendorf 5424, Sunnyvale, CA, USA) for 5 min to remove plant debris. The supernatants were removed and placed into a new tube and centrifuged for an additional 10 min at the same speed and then 800 μL of supernatant was transferred to a new 1.5 ml tube containing two-third volume of cold isopropanol. The sample was then placed in a Genesee filter column (Genesee Scientific, San Diego,

CA), centrifuged 1 min at 10000 rpm and washed twice with 70% ethanol. Samples were then eluted with 100 µl nuclease-free water and analyzed using the Nanodrop 1000 spectrophotometer (Thermo Scientific, Wilmington, DE) with the concentrations being adjusted to 50 ng/µl DNA prior to PCR.

Expression of *Las5315* Effector Gene from Infected and Uninfected Citrus by RT-PCR

Total RNA was extracted from Las infected and uninfected *Citrus paradise* (Grapefruit cultivar Duncan) and *Citrus sinensis* (Sweet orange cultivar Valencia) leaves using TRIzol reagent according to the manufacturer's protocol. DNA contaminations were removed by treating RNA extraction with RNase-free DNase (QIAGEN, West Sussex, UK) and subsequently purified with QIAamp columns (QIAGEN). First-strand cDNA was synthesized at 42°C from total RNA using M-MLV (Invitrogen) reverse transcriptase according to the manufacturer's instructions with the individual PCR reactions containing 1 µl of cDNA, 0.5 µl of each specific primer (10 pmol/µl) (**Table S1**), 10 µl of 2X Green GoTaq® Reaction Buffer (Promega) in a final volume of 20 µl. The following standard thermal profile was used for all amplifications: 95°C for 3 min followed by 30 cycles of 95°C for 30 s, 58°C for 30 s, and 70°C for 30 s.

Bioinformatic Identification of Las Secreted Effector Candidates

We used as input the genome version v1 from Las isolate psy62 (Duan et al., 2009) (genbank accession NC_012985.3), which is also deposited under accession 537021.9 at Pathosystems Resource Integration Center (PATRIC) (https://www.patricbrc.org/portal/) (Wattam et al., 2014). A protein was predicted to be secreted when a signal peptide was present using SignalP v2.0 and (Nielsen et al., 1997), signalP4.0 and no transmembrane domains were present using TMHMM v2 (Petersen et al., 2011). Then, putative Las secreted candidate effectors were screened for: (1) secreted proteins that were ≤250 amino acids and (2) secreted proteins with a previously uncharacterized function according to the NCBI BLAST database. The genbank "GI" accessions for all 16 secreted candidate effectors are shown in **Table 1**.

Amplification and Cloning of Las Secreted Effector Candidates

The mature form of each effector protein without its corresponding signal peptide was cloned to create a C-terminal translation fusion with green fluorescent protein (GFP) under the control of 35S promoter in the binary vector ImpGW405 (Nakagawa et al., 2007). Primers were designed to amplify the corresponding ORFs and contained the complete ATTB sites (**Table S1**). The sequences were amplified using Las infected periwinkle DNA and HIFI PCR mastermix (Clontech, Mountain View, CA, USA). The PCR fragments were first cloned into pDONRzeo by Gateway® BP Clonase® II (Invitrogen, Carlsbad, CA, USA) and then subcloned into the Gateway destination vectors ImpGWB405 (Nakagawa et al., 2007).

Transient Expression of Las Secreted Effectors in *Nicotiana Benthamiana*

Sequences encoding for mature protein form (lacking signal peptide) of a total of 16 effector candidates were cloned into the binary vector ImpGWB405 and transformed into *Agrobacterium tumefaciens* strain GV3101. Agrobacterium transformant cells were cultured overnight in LB medium with 50 µg ml^{-1} of rifampicin and 100 µg ml^{-1} spectinomycin and resuspended in 10 mM $MgCl_2$. The culture was diluted to an optical density at 600 nm (OD_{600}) of 0.5 and acetosyringone (final concentration of 100 µM) was added. For each construct, we infiltrated three leaves of young *N. benthamiana* plants with the *A. tumefaciens* suspension. Agroinfiltrated plants were kept in a greenhouse for the duration of the experiment. The agrobacteria-infiltrated leaves were observed for phenotypic changes and then detached from plants and analyzed under microscope (Olympus BX51-P, Center Valley, PA, USA) equipped with a UV light source at 3 dpi for protein localization.

Staining of Callose Deposition and Relative Callose Intensity Measurement

Aniline blue staining allowed visualization of callose through fluorescence microscopy. An aniline blue signal indicates deposited callose. Four *N. benthamiana* leaves were used after 1, 2, 3, and 4 dpi for Las5315mp and the GFP control. To distain the chlorophyll, ethanol (90% v/v) was added for 6 h at 37°C, followed by ethanol (50% v/v) for 1 h, ethanol (30% v/v) for 1 h, and finally dH_2O for 2 h. The distained leaves were incubated for 2 h in 150 mM K_2HPO_4 and 0.01% aniline blue, samples were embedded in 50% glycerol before microscope analysis. Three leaves from 3 different plants were used in the analysis.

Callose was quantified from digital photographs by the number of white pixels (callose intensity) relative to the total number of pixels covering plant material, using Photoshop CS5 software (Adobe System, San Jose, CA, USA). Callose was selected automatically, using the "Color Range" tool. Data sets were analyzed for statistical differences by Student's *t*-tests ($^*P < 0.01$).

H_2O_2 Production and Electrolyte Leakage Measurement

H_2O_2 detection was conducted as described in previous studies with minor modification (Zhang et al., 2001; Liao et al., 2013). Briefly, *N. benthamiana* leaf discs expressing Las5315mp were collected using a circular 4 mm diameter cork borer at 4 dpi. 6 leaf discs from three leaves were placed into a loading buffer with 50 mM Tris-KCl (pH 7.2) containing 100 µM of H2DCF-DA for 10 min. Fluorescence emission was measured by the LUMIstar microplate luminometer (excitation wavelength, 484 nm; emission wavelength, 525 nm). To quantify cell death, electrolyte leakage was performed according to (Huang et al., 2013). Five leaf discs (∼5 mm in diameter) were collected from the Las5315mp and control *Agrobacterium*-infiltrated areas and immersed in 10 mL of non-ionic, double-distilled water. After incubation at room temperature for 1 h with shaking at 160 rpm,

TABLE 1 | Features of 16 Las candidate secreted effectors proteins.

Gene ID v1 (genbank accession)	Sequence length (aa)	Number of cysteines	Chloroplast target domain	Subcellular localization in *Nicotiana benthamiana*
CLIBASIA_00460 (ACT56680.1; GI:254039884)	98	2	NO	Long shape aggregates in the cytoplasm
CLIBASIA_00525 (ACT56693.1; GI:254039897)	97	1	NO	Uninformative and unspecific
CLIBASIA_00530 (ACT56694.1: GI:254039898)	97	1	NO	Round big vesicles in the cytoplasm
CLIBASIA_02215 (ACT57029.1; GI:254040233)	120	1	NO	Aggregates in the cytoplasm
CLIBASIA_02470 (ACT57080.1; GI:254040284)	131	7	NO	Small vesicles in the cytoplasm
CLIBASIA_03230 (ACT57232.1; GI:254040436)	162	7	NO	Aggregates in the cytoplasm
CLIBASIA_03695 (ACT57317.1; GI:254040521)	113	5	NO	Vesicles in the cytoplasm
CLIBASIA_04025 (ACT57379.1; GI:254040583)	96	1	NO	Vesicles in the cytoplasm
CLIBASIA_04040 (ACT57382.1; GI:254040586)	159	1	NO	Small vesicles in the cytoplasm
CLIBASIA_04320 (ACT57436.1; GI:254040640)	215	2	NO	Aggregates and dots in the cytoplasm
CLIBASIA_04330 (ACT57438.1; GI:254040642)	229	4	NO	Cytosolic bodies in the cytoplasm
CLIBASIA_04425 (ACT57457.1; GI:254040661)	125	2	NO	Strong signal with variable shape in the cytoplasm
CLIBASIA_04560 (ACT57483.1; GI:254040687)	195	3	NO	Vesicles in the cytoplasm and nucleus distribution
CLIBASIA_05115 (ACT57594.1; GI:254040798)	185	2	NO	Aggregates in the cytoplasm
CLIBASIA_05320 (ACT57630.1; GI:254040834)	85	1	NO	Punctuated distribution within vesicles in the cytoplasm
CLIBASIA_05315 (ACT57629.1; GI:254040833)	154	2	YES	Chloroplast within the cytoplasm

conductivity of the solution was measured using a conductivity meter (Horiba scientific, Edison, NJ, USA).

RESULTS

Sixteen Putative Las Effectors were Selected

We analyzed 1,136 protein-encoding genes of Las Psy62 genome version 1 (genbank accession NC_012985.3) (Duan et al., 2009) for the presence of signal peptide and lack of transmembrane domain. To identify candidate effectors, we filtered the secretome for (1) proteins $\leq$250 amino acids in length and (2) previously uncharacterized proteins (**Figure 1A**). These 16 secreted effector proteins exhibit sequence lengths that varied from 85 to 229 amino acids. The mature proteins (**Figure 1B**), without their putative signal peptides, were transiently expressed in *N. benthamiana* in order to characterize the location of the putative effectors and analyze phenotypic changes produced by the proteins (**Figure 1C**).

Las Candidate Effectors Exhibited Diverse Subcellular Localization Patterns in *N. benthamiana*

In order to determine the location of the 16 putative effectors in the plant cells, C-terminal translational fusions were produced using the mature form of each protein and the green-fluorescent protein (GFP) expressed from the 35S promoter in a gateway binary vector (**Figure 1B**). The leaf epidermal layer of the infiltrated zones for each of the 16 candidate effectors showed different localization and accumulation patterns in the plant cells (**Figure 2**, **Figure S1**) compared to the control GFP only (**Figure 2S**). In particular, Las460mp was distributed in the cytosol and accumulated in small vesicles and in elongated shapes. Las525mp was dispersed throughout the cytosol and the nucleus. Las530mp accumulated heavily in vesicle structures while Las2215mp accumulated in aggregated structures. Las2470mp had an intense signal with dot shape bodies covering the total cell area. Las3230mp formed small crystal shape aggregates, while Las3695mp showed an increased signal intensity and was localized in big vesicles, and Las4025mp accumulated in small vesicles and cytosol bodies. Las4040mp was similar to Las4025mp with small vesicles and punctate spots, Las4320mp was expressed evenly in the cell taking the shape of dots, Las4330mp small cytosolic bodies, Las4425mp accumulate in large cytosolic aggregates, Las4560mp was localized in large and small bodies and in the nucleus, Las5115mp accumulated mostly on the edge of the cell with large aggregates, and Las5320mp fluoresced strongly and accumulated in dots inside vesicles. The Las5315mp effector protein was localized in vesicles surrounding chloroplast (**Figures 2P,Q**), while the effector Las5315 that contained the signal peptide sequence was not present in chloroplast, but accumulated as crystal shape aggregates (**Figure 2R**).

Las5315mp Induced Cell Death and is Associated with H_2O_2 Accumulation, Electrolyte Leakage, and Callose Deposition in *N. benthamiana*

In an effort to further characterize these effectors and define a potential role regarding Las virulence, putative effector genes were transiently expressed in *N. benthamiana* and their phenotypes were observed. Of the 16 putative effectors only Las5315mp appeared to induce necrosis or cell death (**Figure 3A** and **Figures S2A–C**). Compared to the negative control *at 3 dpi*, cell death appeared in the *N. benthamiana* leaf infiltrated with the mature form of effector Las5315mp at three different concentrations: OD_{600} =0.1, 0.3 and 0.5 (**Figure S2A**). The cell death phenotype was not observed in

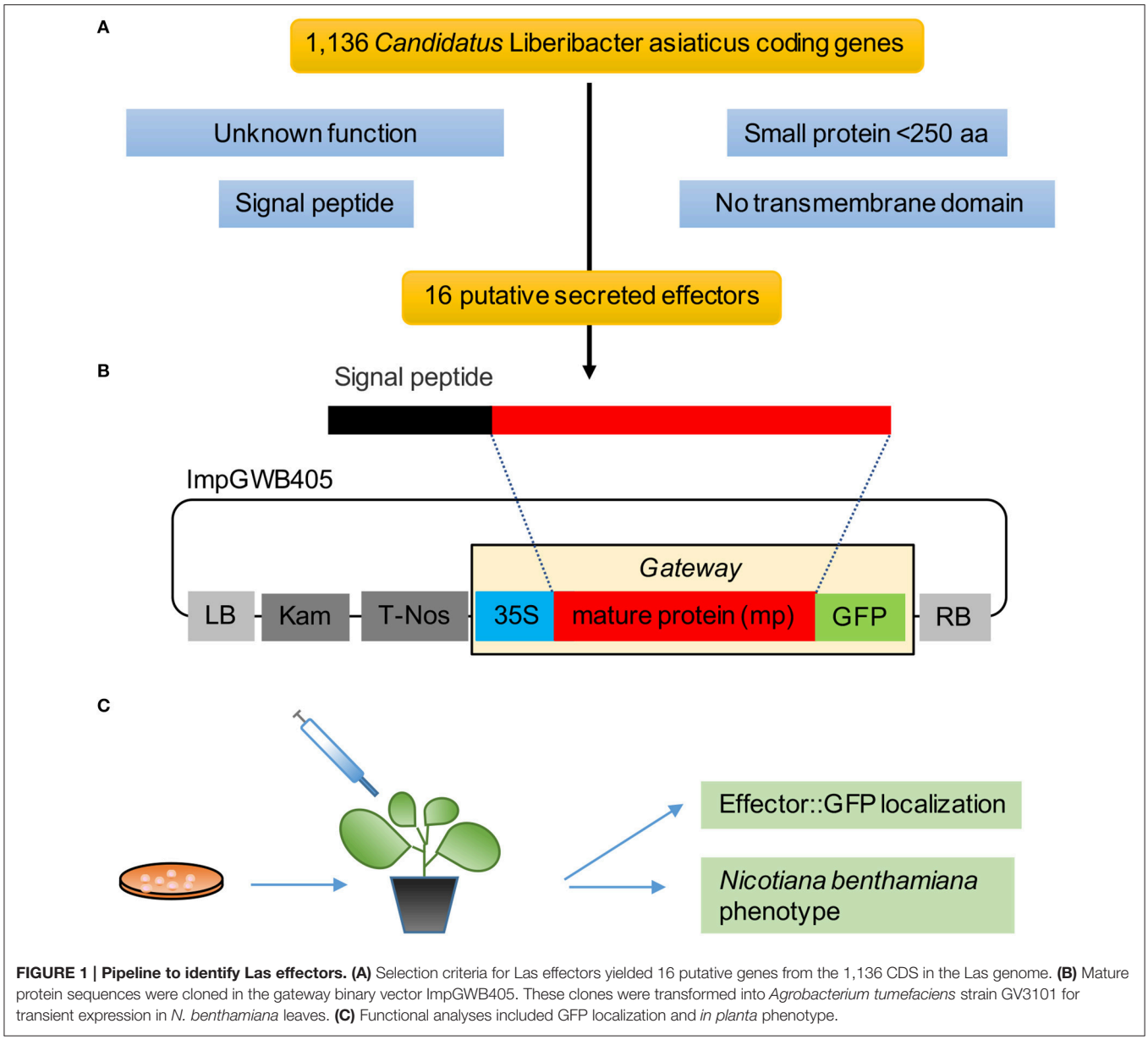

FIGURE 1 | Pipeline to identify Las effectors. (A) Selection criteria for Las effectors yielded 16 putative genes from the 1,136 CDS in the Las genome. **(B)** Mature protein sequences were cloned in the gateway binary vector ImpGWB405. These clones were transformed into *Agrobacterium tumefaciens* strain GV3101 for transient expression in *N. benthamiana* leaves. **(C)** Functional analyses included GFP localization and *in planta* phenotype.

the premature form containing the signal peptide, Las5315, at the same three concentrations (**Figure S2B**). A side-by-side comparison on the same leaf demonstrated that chlorosis and increasing levels of cell death could be observed at 7 dpi in the infiltration zone expressing Las5315mp, while visually Las5315 remained unchanged (**Figure S2C**). Cell death is often associated with electrolyte leakage resulting from membrane damage (Bai et al., 2012). Ion leakage assays were performed to quantify the cell death induced by Las5315mp. As shown in (**Figure 3B**) significant amounts of ion leakage were detected 2, 3, and 4 days dpi after infiltration with the *Agrobacterium* harboring the *Las5315mp*. The cell death produced upon expression of Las5315mp is associated with H_2O_2 accumulation in the leaves (**Figure 4**) and electrolyte leakage (**Figure 3B**). Ion leakage was not induced by agroinfiltration of the control. These data confirm the cell death activity of Las5315mp.

In addition to ion leakage and H_2O_2 accumulation, fluorescence microscopy with aniline blue staining revealed a strong callose deposition induced by Las5315mp from 1 dpi (**Figure 5**). This accumulation continued to increases both within the plant cells and inside the vascular tissue for the entire 4 day observation period.

Las5315 Contained a Signal Peptide and a Chloroplast Targeting Domain

Sequence analysis of the Las5315mp revealed a 154 aa protein with a signal peptide predicted using SignalP v2.0 (Nielsen et al., 1997) and SignalP v4.0 (Petersen et al., 2011), a cleavage site between position 24 and 25 and no transmembrane domains

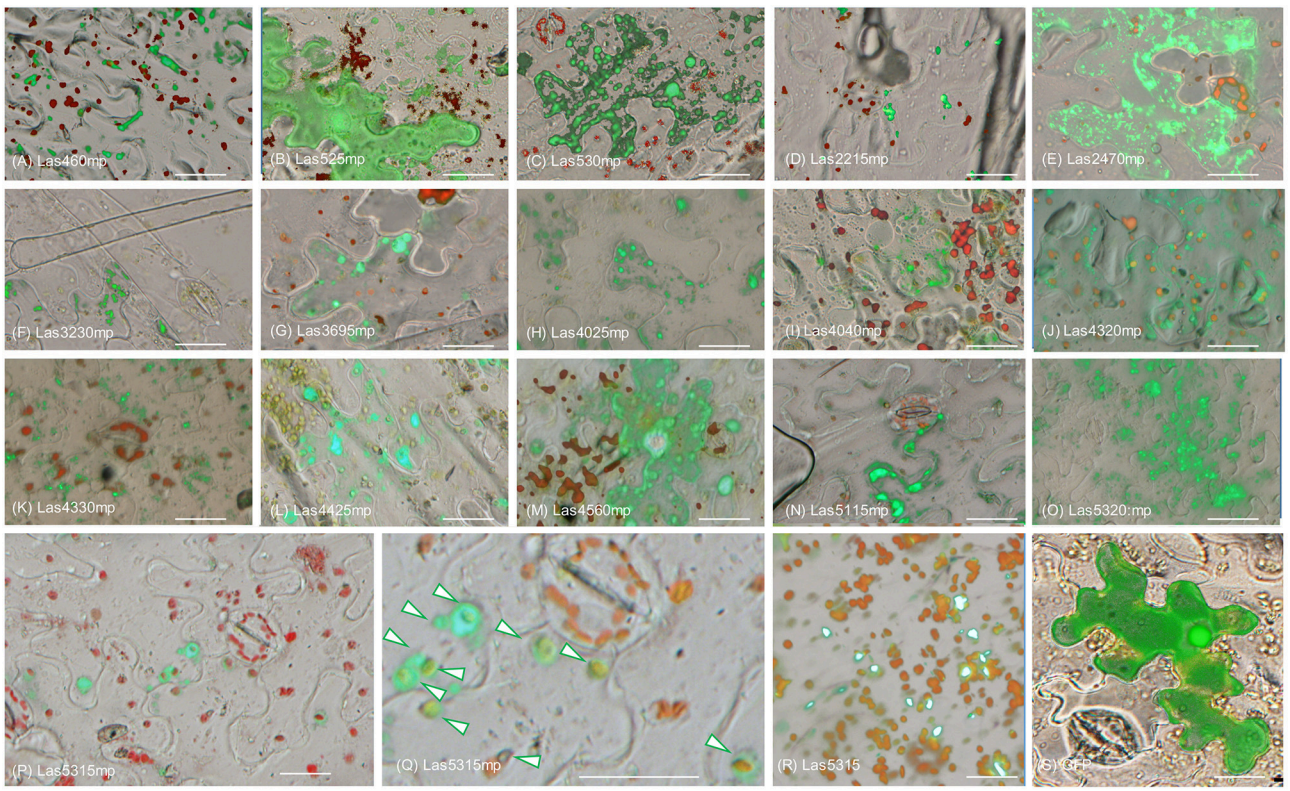

FIGURE 2 | Subcellular localization of putative Las effector proteins in *Nicotiana benthamiana*. Epi-fluorescence micrograph overlaid with bright field micrograph of each of the 16 effector translation fusions expressed in *N. benthamiana*. Images depict protein effector**:** GFP (green) and chlorophyll autoflourescence (red). **(A–Q)** Micrograph of the localization of the 15 candidate effectors that did not elicit a phenotype in *N. benthamiana*. **(P)** Image shows localization of Las5315mp:GFP (green) surrounding chloroplasts (red). **(Q)** Enlarged image of panel **(R)** with arrows indicating Las5315mp localization surrounding chloroplasts. **(R)** Las5315::GFP accumulated in aggregate structures **(S)** GFP only. Scale bars are 20 μm.

using TMHMM v2 (Krogh et al., 2001) (**Figure 6**). Downstream of the N-terminal signal peptide sequence of Las5315 effector protein we found a chloroplast targeting peptide domain of 56 aa length (**Figure 6**) using ChloroP 1.1 (Emanuelsson et al., 1999) with a score of 0.562 and CS-score of 3.203.

Las5315 Gene is Expressed in Las-Infected Citrus

In order to determine if *Las5315* is indeed expressed in citrus infected with Las, reverse transcription PCR was used to identify the level of expression of *Las5315* in both Las infected and uninfected grapefruit and sweet orange. Amplicons produced via reverse transcription PCR demonstrate the expression of *Las5315* both grapefruit and sweet orange but only when infected with Las.

DISCUSSION

"*Ca.* Liberibacter asiaticus" is an insect-vectored obligate intracellular bacterium with a significantly reduced genome associated with HLB disease in citrus. Powerful functional genomic and genetic approaches integrated with comparative studies have contributed a great deal to the knowledge and identification of global gene expression changes during HLB disease development (Albrecht and Bowman, 2008, 2012; Fan et al., 2011; Martinelli et al., 2012, 2013; Aritua et al., 2013; Mafra et al., 2013; Rawat et al., 2015). Other studies have revealed the disruption in carbohydrate source and phloem plugging as main causes of HLB symptoms (Liao and Burns, 2012; Martinelli et al., 2013). However, knowing how effector proteins function in host plant cells is key to fully understanding the molecular basis behind the pathogen-plant interactions and for the development of sustainable management strategies.

Las, like spiroplasmas and phytoplasmas, is injected directly into the cytoplasm of phloem cells by its insect vector. It is the intracellular nature of these organisms that allows them to secrete proteins into the host cell cytoplasm despite their lack of type III secretion systems, permitting movement of these proteins to other plant cells via plasmodesmata (Hogenhout and Loria, 2008). Several examples of his include the plant gene-regulating effector, SAP11, which contains a nuclear localization signal that is functional in plant cells (Hogenhout et al., 2008) and SAP54, which manipulates its host to produce leaf-like flowers, making it more attractive for colonization by phytoplasma leafhopper vectors (Maclean et al., 2014). Las appears to contain all type I secretion system genes necessary for both multidrug efflux and toxin effector secretion. Moreover, all proteins required for the first step of the type II secretion system, the general secretory

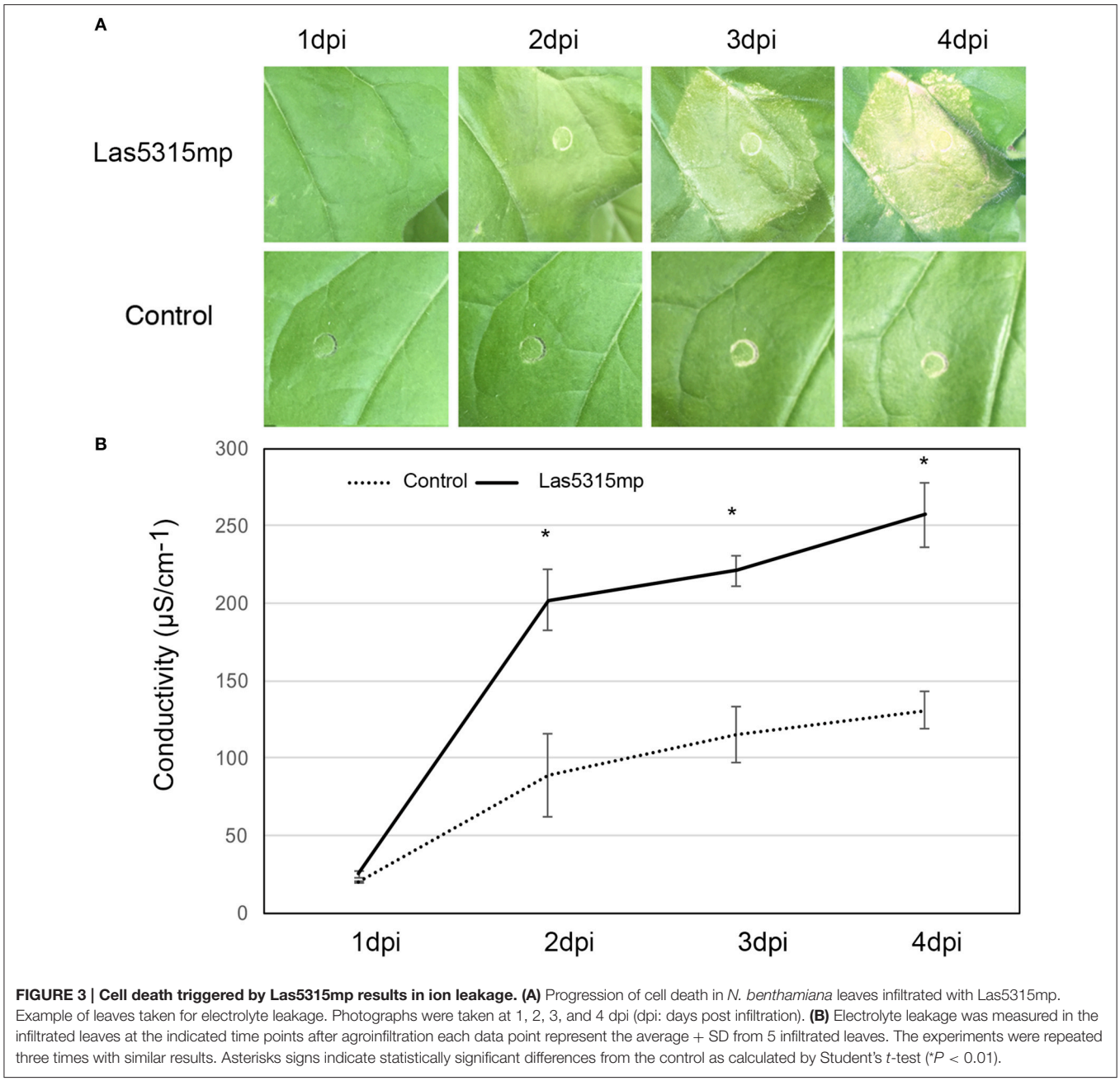

FIGURE 3 | Cell death triggered by Las5315mp results in ion leakage. (A) Progression of cell death in *N. benthamiana* leaves infiltrated with Las5315mp. Example of leaves taken for electrolyte leakage. Photographs were taken at 1, 2, 3, and 4 dpi (dpi: days post infiltration). **(B)** Electrolyte leakage was measured in the infiltrated leaves at the indicated time points after agroinfiltration each data point represent the average + SD from 5 infiltrated leaves. The experiments were repeated three times with similar results. Asterisks signs indicate statistically significant differences from the control as calculated by Student's *t*-test (*$P < 0.01$).

pathway (TC 3.A.5.) responsible for the export of proteins to the periplasm (Pugsley, 1993), were found in the "*Ca.* L. asiaticus" Psy62 genome (Duan et al., 2009). In addition, 10 putative proteins required for pilin secretion and assembly as part of the main terminal branch MTB (TC 3.A.15) were found, indicating the potential for a type IV pilus secretion assembly (Duan et al., 2009).

Therefore, in an attempt to identify novel proteins that function in the pathogenesis of HLB, we analyzed and selected the most promising candidate effector proteins from the current reference Las genome Psy62 (Duan et al., 2009). Based on the assumption that Las secretes proteins into the plant to manipulate host processes and facilitate colonization, proteins with a predicted signal peptide that did not contain transmembrane domains and had no predicted function were selected for further study. We obtained 16 candidates using this criteria and created C-terminal translation fusions for localization studies in plants by cloning the mature form of each candidate (sequence without the signal peptide regions) into the GFP vector ImPgwb405 (**Figures 1A,B**).

Pathogen effectors are known to target different parts of the host cell including nuclear components, membranes, and subcellular compartments such as the mitochondria or chloroplasts. This targeting of cellular components is a broadly

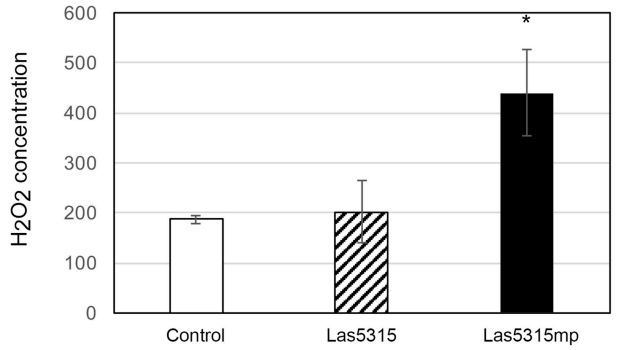

FIGURE 4 | Cell death triggered by Las5315mp results in the accumulation of H_2O_2. The concentration of H_2O_2 was determined in leaves agro-infiltrated with the Las5315mp effector or the empty vector (EV) using H_2DCFDA as an indicator at 4 dpi. Leaves were used as a control. Error bars represent the standard deviation ($n = 8$). Asterisks signs indicate statistically significant differences from the control as calculated by Student's *t*-test (*$P < 0.01$).

conserved pathogenic strategy that controls the fate of cell organelles and regulates cellular activities (Deslandes and Rivas, 2012; Lindeberg et al., 2012). Mitochondria for instance play important roles in biological processes such as energy conversion for ATP synthesis, ion homeostasis, and calcium storage as well as in plant innate immunity signaling (Maxwell et al., 2002). Effector proteins produced by pathogens, such as HopG1 from *Pseudomonas syringe*, suppress the host's innate immunity by disrupting mitochondrial function (Block et al., 2010). The mitochondria is not the only system targeted by *P. syringae*, which produces the effectors HopI1, HopN1, HopK1, and AvrRps4 that localize to chloroplasts instead. Hopl1 and HopN1 are known to inhibit photosystem II (PSII) activity in chloroplast preparations by degrading PbsQ (Rodríguez-Herva et al., 2012) while HopK1 and AvrRps4 suppress plant immunity (Li et al., 2014).

Although only one effector displayed a clear cell death phenotype in *N. benthamiana*, all of the putative effectors tested showed unique subcellular accumulation patterns with the exception of Las525mp, which was diffused throughout the cytosol and the nucleus (**Figures 2A–Q**). The different accumulation and localization patterns may be indicative of a specific interaction between the Las protein and plant cell organelles and warrants further investigation in the future. It is important to point out that the Las5315mp effector protein (the mature protein) was localized in vesicles surrounding chloroplast (**Figures 2P,Q**), while the premature protein did not accumulate in the chloroplast (**Figure 2R**). These results are rationalized by the fact that the full length protein, Las5315, contains a signal peptide and a chloroplast targeting signal in succession (**Figure 6**). In an obligate intracellular bacterium such as Las, the signal peptide is assumed to be cleaved by the bacterium upon translocation; leaving only the mature Las5315mp effector protein in the host cell's cytosol. Here, the protein is no longer subjected to this cleavage reaction since it is being produced by the transformed plant not the bacterium and, thus, only the protein without the signal sequence is active.

Plant pathogens secrete effector proteins that are subsequently delivered to the inside of host cells and interfere with their molecular pathways, thereby promoting infection (Dangl and Jones, 2001; Nomura et al., 2005; Hann et al., 2010). These effectors often affect host immunity and cause phenotypes ranging from chlorosis to necrosis (Cunnac et al., 2009). The ability of protein Las5315mp to induce chlorosis and cell death at 3 dpi in *N. benthamiana* in the infiltration zone (**Figure 3A**) suggests that it may be affecting host immunity, an observation further supported by ion leakage assays (**Figure 3B**). Plant cell death is a common defense mechanism used by plants against invading pathogens to prevent the spread of the microbial pathogens and can occur in both resistant and susceptible plant–pathogen interactions. Cell death results when the host plant's receptors perceive the pathogen and trigger plant immunity reactions (Zipfel and Felix, 2005; Jones and Dangl, 2006; Takahashi et al., 2007; Coll et al., 2011). Interestingly, cell death has not been detected in citrus in response to Las infection comparable to that seen with *N. benthamiana* infiltrated with Las5315mp, suggesting that although *N. benthamiana* may possess resistance (R) genes, intracellular nucleotide-binding domains, or leucine-rich repeat containing (NB-LRR) immune receptors that specifically recognize Las5315mp effector protein, these NB-LRRs might not be conserved in citrus. Thus, only *N. benthamiana* can generate an effector triggered immunity response and induce cell death upon recognition of the pathogen effector Las5315mp. Indirect support of this is also demonstrated by the fact that previous attempts to infect *Nicotiana tabacum* with Las were unsuccessful (Duan, unpublished data), however *Ca.* L. americanus, which does not have a Las5315mp homolog, was able to infect *N. tabacum* L. cv Xanthi through *Cuscuta* spp (dodder) (Francischini et al., 2007).

Previously, NB-LRR genes have been identified and used to confer broad-spectrum resistance in different crops. Examples include the *WRR4* gene from Arabidopsis that confers white rust resistance in transgenic oilseed brassica crops (Borhan et al., 2010); two other Arabidopsis genes (*RFO1* and *RPW8)* that confer resistance against a diverse collection of Fusarium or powdery mildew fungi (Xiao et al., 2001; Diener and Ausubel, 2005); RCT1 from *Medicago truncatula* that confers resistance to races of the anthracnose fungi *Colletotrichum trifolii* and *C. destructivum* (Yang et al., 2008); the Mi-1.2 gene in tomato *Solanum lycopersicum* that confers resistance to the root-knot nematode *Meloidogyne javanica* in *Solanum melongena* (Goggin et al., 2006); and the *RPS4/RRS1* genes from Arabidopsis that confer resistance to the fungal pathogen *C. higginsianum* to other *brassicaceae* plants including *B. rapa* and *B. napus* as well as in *N. benthamiana* and *Solanum lycopersicum* (Narusaka et al., 2013). In addition, *RGA4 and RGA5* genes from rice mediate resistance to the fungal pathogen *Magnaporthe oryzae* in both rice protoplasts and *N. benthamiana* (Cesari et al., 2014*).* Therefore, it is quite plausible that identification of the *N. benthamiana* receptor of Las5315mp and its heterologous expression in citrus plants may trigger an innate immune

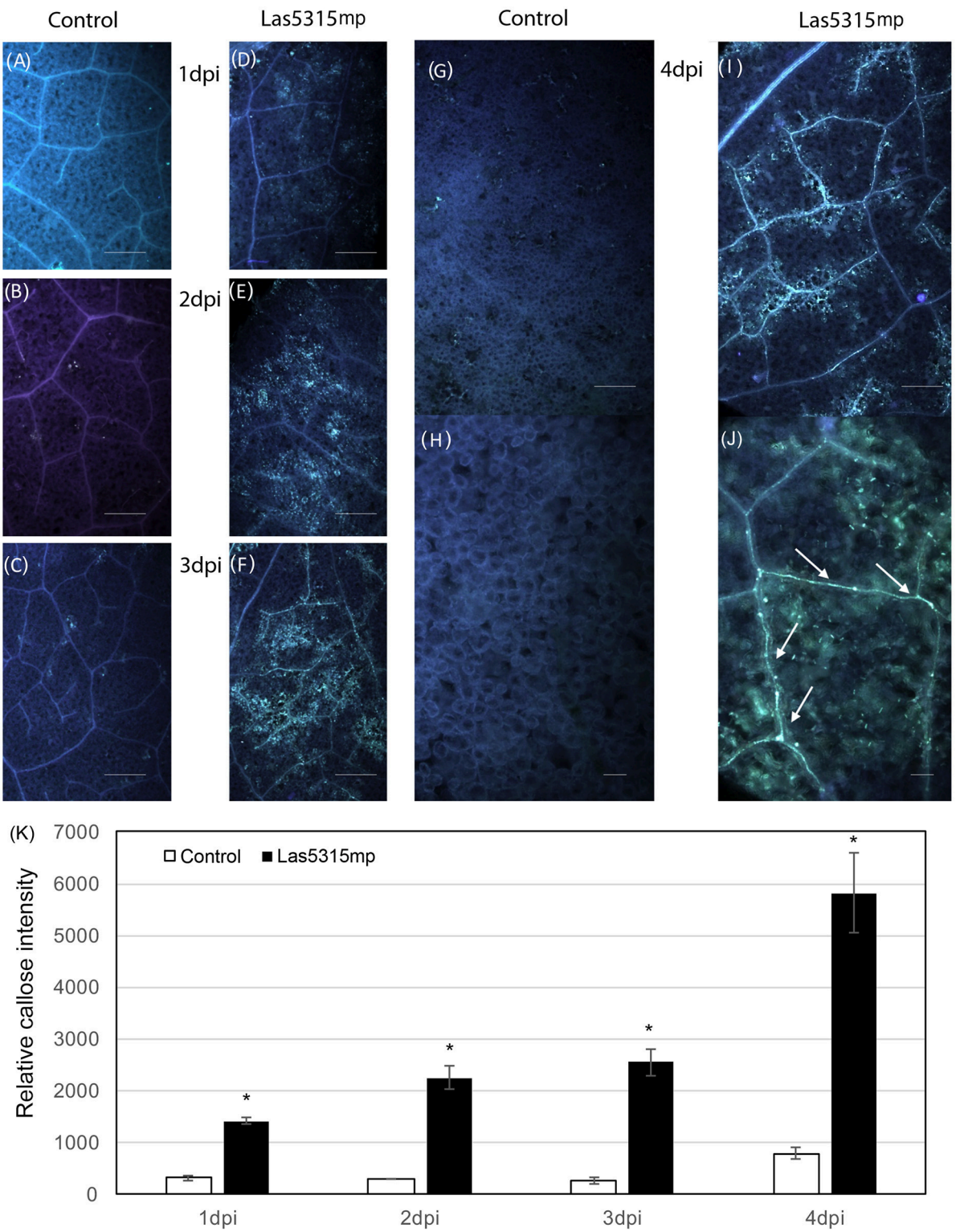

FIGURE 5 | Callose deposition after Las5315mp agroinfiltration. *N. benthamiana* leaves agroinfiltrated with either the GFP control **(A–C,G)** or with Las5315mp **(D–F,I)** corresponding to 1, 2, 3, and 4 dpi respectively. Enlarged image of the leaf at 4 dpi infiltrated with either GFP **(H)** or Las5315mp **(J)** showing accumulation of callose in the vascular tissue (arrows). Leaves were stained with aniline blue and callose deposition was observed under a UV epifluorescence microscope. **(K)** Relative callose deposition was measured in the infiltrated leaves at the indicated time points after agroinfiltration (dpi: days post infiltration). Asterisks signs indicate statistically significant differences from the control as calculated by Student's *t*-test (*$P < 0.01$).

MRKNLLTSTSSLMFFFLSSGYALSGSSFGCCGEFKKKASSPRIHMRPFTKSS
PYNNSVSNTVNNTPRVPDVSEMNSSRGSAPQSHVNVSSPHYKHEYSSSSA
SSSTHASPPPHFEQKHISRTRIDSSPPPGHIDPHPDHIRNTLALHRKMLEQS

FIGURE 6 | Las5315mp secreted effector sequence and its predicted C-terminal chloroplast targeting domain. Amino acid sequence of Las5315mp with N-terminal signal peptide (highlighted in yellow) predicted using SignalP v4 (Petersen et al., 2011), the cleavage site between 24 and 25 amino acid positions (ALS-GS), and the chloroplast targeting (highlighted in green) predicted using ChloroP v1.1 (Emanuelsson et al., 1999).

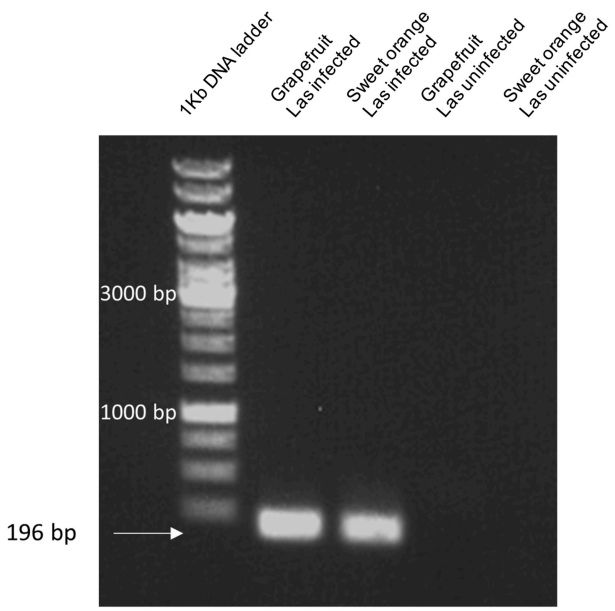

FIGURE 7 | *Las5315* expression in citrus using reverse transcription PCR. Amplicons corresponding to the expression levels of *Las5315* in both Las infected and uninfected grapefruit and sweet orange were produced via reverse transcription PCR. Amplification products were subsequently run on a 1% agarose gel and visualized with ethidium bromide.

response to the Las pathogen and confer resistance to HLB disease in citrus plants.

The inhibition of photoassimilate export and the subsequent starch accumulation in the Las infected leaves indicates that Las infection perturbs normal carbon partitioning (Koh et al., 2012). Previous studies have demonstrated that Liberibacter infection is accompanied by callose deposition in sieve pores of the sieve tubes and it has been suggested this callose deposition is the main reason for the phloem plugging associated with starch accumulation and ultimately chlorosis of the leaf in infected plants (Masaoka et al., 2011). In addition, genes involved in callose deposition have been shown to be up-regulated in HLB-infected citrus (Koh et al., 2012; Zhong et al., 2015). In this work, we found that Las5315mp induces excessive callose in the infiltration zone starting at 1 dpi (**Figure 5**) and increases the accumulation of callose in the cells and inside the vascular tissue in a fashion similar to that seen in citrus plants infected by Las (Koh et al., 2012). Since *Las5315* is also expressed in HLB infected citrus (**Figure 7**), it stands to reason that Las5315mp may be the protein associated with callose deposition in HLB affected citrus. Further functional characterization and identification of Las effectors associated with pathogenicity and virulence should lead to identification of potential targets for controlling Las infection and HLB disease progression.

AUTHOR CONTRIBUTIONS

Conceived and designed the experiments: MP, YD. Performed the experiments: MP. Analyzed the data: MP, CA, LC. Contributed reagents/materials/analysis tools: MP, CA, YD. Wrote the paper: MP, CA, YD.

ACKNOWLEDGMENTS

We would like to thank Melissa Doud for her critical review, Carrie Vanderspool for the plants used in this study and Christina Latza for her excellent technical assistance. Funding was provided by the U. S. Department of Agriculture and Citrus Research and Development Foundation. Mention of trade names or commercial products in this article is solely for the purpose of providing specific information and does not imply recommendation or endorsement by the U.S. Department of Agriculture.

SUPPLEMENTARY MATERIAL

The Supplementary Material for this article can be found online at: http://journal.frontiersin.org/article/10.3389/fpls.2016.00982

Figure S1 | Subcellular localization of putative Las effector proteins in *Nicotiana benthamiana*. Sixteen putative effector proteins expressed in leaves of *N. benthamiana*, visualized by epifluorescence microscopy 3 days post infiltration. **(A–O)** Micrograph of the localization of the 15 candidate effectors that did not elicit a phenotype in *N. benthamiana*. **(P)** Image shows localization of Las5315mp:GFP (green) surrounding chloroplasts (red). **(Q)** Enlarged image of panel **(P)** with arrows indicating Las5315mp localization surrounding chloroplasts. **(R)** Las5315::GFP accumulated in aggregate structures **(S)** GFP only. Scale bars are 20 µm.

Figure S2 | Effector Las5315mp induces cell death in *N. benthamiana*. Phenotype of *N. benthamiana* leaves expressing **(A)** Las5315mp or **(B)** Las5315 at several different concentrations (OD_{600} = 0.1, 0.3, 0.5) compared to the empty vector control. **(C)** Overexpression of Las5315mp and Las5315 in the same leaf 7 days post infiltration (dpi) at an OD_{600} = 0.5.

Table S1 | Primers used in this study.

REFERENCES

Albrecht, U., and Bowman, K. D. (2008). Gene expression in *Citrus sinensis* (L.) Osbeck following infection with the bacterial pathogen Candidatus Liberibacter asiaticus causing Huanglongbing in Florida. *Plant Sci.* 175, 291–306. doi: 10.1016/j.plantsci.2008.05.001

Albrecht, U., and Bowman, K. D. (2012). Transcriptional response of susceptible and tolerant citrus to infection with Candidatus Liberibacter asiaticus. *Plant Sci.* 185, 118–130. doi: 10.1016/j.plantsci.2011.09.008

Alfano, J. R. (2009). Roadmap for future research on plant pathogen effectors. *Mol. Plant Pathol.* 10, 805–813. doi: 10.1111/j.1364-3703.2009.00588.x

Aritua, V., Achor, D., Gmitter, F. G., Albrigo, G., and Wang, N. (2013). Transcriptional and microscopic analyses of citrus stem and root responses to Candidatus Liberibacter asiaticus Infection. *PLoS ONE* 8:e73742. doi: 10.1371/journal.pone.0073742

Bai, S. W., Liu, J., Chang, C., Zhang, L., Maekawa, T., Wang, Q. Y., et al. (2012). Structure-function analysis of barley NLR immune receptor MLA10 reveals its cell compartment specific activity in cell death and disease resistance. *PLoS Pathog* 8:e1002752. doi: 10.1371/journal.ppat.1002752

Block, A., Guo, M., Li, G. Y., Elowsky, C., Clemente, T. E., and Alfano, J. R. (2010). The *Pseudomonas syringae* type III effector HopG1 targets mitochondria, alters plant development and suppresses plant innate immunity. *Cell. Microbiol.* 12, 318–330. doi: 10.1111/j.1462-5822.2009.01396.x

Block, A., Li, G. Y., Fu, Z. Q., and Alfano, J. R. (2008). Phytopathogen type III effector weaponry and their plant targets. *Curr. Opin. Plant Biol.* 11, 396–403. doi: 10.1016/j.pbi.2008.06.007

Boller, T., and Felix, G. (2009). A renaissance of elicitors: perception of microbe-associated molecular patterns and danger signals by pattern-recognition receptors. *Annu. Rev. Plant Biol.* 60, 379–406. doi: 10.1146/annurev.arplant.57.032905.105346

Borhan, M. H., Holub, E. B., Kindrachuk, C., Omidi, M., Bozorgmanesh-Frad, G., and Rimmer, S. R. (2010). WRR4, a broad-spectrum TIR-NB-LRR gene from Arabidopsis thaliana that confers white rust resistance in transgenic oilseed brassica crops. *Mol. Plant Pathol.* 11, 283–291. doi: 10.1111/j.1364-3703.2009.00599.x

Bos, J. I. B., Prince, D., Pitino, M., Maffei, M. E., Win, J., and Hogenhout, S. A. (2010). A functional genomics approach identifies candidate effectors from the aphid species *Myzus persicae* (green peach aphid). *PLoS Genet* 6:e1001216. doi: 10.1371/journal.pgen.1001216

Bove, J. M. (2006). Huanglongbing: a destructive, newly-emerging, century-old disease of citrus. *J. Plant Pathog.* 88, 7–37. doi: 10.4454/jpp.v88i1.828

Cesari, S., Kanzaki, H., Fujiwara, T., Bernoux, M., Chalvon, V., Kawano, Y., et al. (2014). The NB-LRR proteins RGA4 and RGA5 interact functionally and physically to confer disease resistance. *EMBO J.* 33, 1941–1959. doi: 10.15252/embj.201487923

Chaudhari, P., Ahmed, B., Joly, D. L., and Germain, H. (2014). Effector biology during biotrophic invasion of plant cells. *Virulence* 5, 703–709. doi: 10.4161/viru.29652

Chisholm, S. T., Coaker, G., Day, B., and Staskawicz, B. J. (2006). Host-microbe interactions: shaping the evolution of the plant immune response. *Cell* 124, 803–814. doi: 10.1016/j.cell.2006.02.008

Coll, N. S., Epple, P., and Dangl, J. L. (2011). Programmed cell death in the plant immune system. *Cell Death Differ.* 18, 1247–1256. doi: 10.1038/cdd.2011.37

Cunnac, S., Lindeberg, M., and Collmer, A. (2009). *Pseudomonas syringae* type III secretion system effectors: repertoires in search of functions. *Curr. Opin. Microbiol.* 12, 53–60. doi: 10.1016/j.mib.2008.12.003

Dangl, J. L., and Jones, J. D. G. (2001). Plant pathogens and integrated defence responses to infection. *Nature* 411, 826–833. doi: 10.1038/35081161

Davis, E. L., Hussey, R. S., Mitchum, M. G., and Baum, T. J. (2008). Parasitism proteins in nematode-plant interactions. *Curr. Opin. Plant Biol.* 11, 360–366. doi: 10.1016/j.pbi.2008.04.003

Deslandes, L., and Rivas, S. (2012). Catch me if you can: bacterial effectors and plant targets. *Trends Plant Sci.* 17, 644–655. doi: 10.1016/j.tplants.2012.06.011

Diener, A. C., and Ausubel, F. M. (2005). Resistance to *Fusarium oxysporum* 1, a dominant Arabidopsis disease-resistance gene, is not race specific. *Genetics* 171, 305–321. doi: 10.1534/genetics.105.042218

Dodds, P. N., and Rathjen, J. P. (2010). Plant immunity: towards an integrated view of plant-pathogen interactions. *Nat. Rev. Genet.* 11, 539–548. doi: 10.1038/nrg2812

Dou, D. L., and Zhou, J. M. (2012). Phytopathogen effectors subverting host immunity: different foes, similar battleground. *Cell Host Microbe* 12, 484–495. doi: 10.1016/j.chom.2012.09.003

Du, J., Rietman, H., and Vleeshouwers, V. G. (2014). Agroinfiltration and PVX agroinfection in potato and *Nicotiana benthamiana*. *J. Vis. Exp.* 83:e50971. doi: 10.3791/50971

Duan, Y. P., Zhou, L. J., Hall, D. G., Li, W. B., Doddapaneni, H., Lin, H., et al. (2009). Complete genome sequence of Citrus Huanglongbing bacterium, 'candidatus liberibacter asiaticus' obtained through metagenomics. *Mol. Plant Microbe Interact.* 22, 1011–1020. doi: 10.1094/MPMI-22-8-1011

Ellis, J. G., Rafiqi, M., Gan, P., Chakrabarti, A., and Dodds, P. N. (2009). Recent progress in discovery and functional analysis of effector proteins of fungal and oomycete plant pathogens. *Curr. Opin. Plant Biol.* 12, 399–405. doi: 10.1016/j.pbi.2009.05.004

Emanuelsson, O., Nielsen, H., and Von Heijne, G. (1999). ChloroP, a neural network-based method for predicting chloroplast transit peptides and their cleavage sites. *Protein Sci.* 8, 978–984. doi: 10.1110/ps.8.5.978

Fan, J., Chen, C. X., Yu, Q. B., Brlansky, R. H., Li, Z. G., and Gmitter, F. G. (2011). Comparative iTRAQ proteome and transcriptome analyses of sweet orange infected by "Candidatus Liberibacter asiaticus". *Physiol. Plant.* 143, 235–245. doi: 10.1111/j.1399-3054.2011.01502.x

Francischini, F. J. B., Oliveira, K. D. S., Astua-Monge, G., Novelli, A., Lorenzino, R., Matiolli, C., et al. (2007). First report on the transmission of 'Candidatus liberibacter americanus' from citrus to Nicotiana tabacum cv. *Xanthi*. *Plant Dis.* 91, 631–631. doi: 10.1094/PDIS-91-5-0631B

Garnier, M., and Bové, J. (1983). Transmission of the organism associated with citrus greening disease from sweet orange to periwinkle by dodder. *Phytopathology* 73, 1358–1363. doi: 10.1094/Phyto-73-1358

Garnier, M., Jagoueix-Eveillard, S., Cronje, P. R., Le Roux, H. F., and Bove, J. M. (2000). Genomic characterization of a liberibacter present in an ornamental rutaceous tree, Calodendrum capense, in the Western Cape province of South Africa. *Proposal of 'Candidatus Liberibacter africanus subsp capensis'*. *Int. J. Syst. Evol. Microbiol.* 50, 2119–2125. doi: 10.1099/00207713-50-6-2119

Goggin, F. L., Jia, L. L., Shah, G., Hebert, S., Williamson, V. M., and Ullman, D. E. (2006). Heterologous expression of the Mi-1.2 gene from tomato confers resistance against nematodes but not aphids in eggplant. *Mol. Plant Microbe Interact.* 19, 383–388. doi: 10.1094/MPMI-19-0383

Gottwald, T. R. (2010). Current epidemiological understanding of citrus huanglongbing. *Annu. Rev. Phytopathol.* 48, 119–139. doi: 10.1146/annurev-phyto-073009-114418

Halbert, S. E., and Manjunath, K. L. (2004). Asian citrus psyllids (Sternorrhyncha: Psyllidae) and greening disease of citrus: a literature review and assment of risk in Florida. *Florida Entomol.* 87, 330–353. doi: 10.1653/0015-4040(2004)087[0330:ACPSPA]2.0.CO;2

Hall, D. G., Richardson, M. L., Ammar, E. D., and Halbert, S. E. (2013). Asian citrus psyllid, Diaphorina citri, vector of citrus huanglongbing disease. *Entomol. Exp. Appl.* 146, 207–223. doi: 10.1111/eea.12025

Hann, D. R., Gimenez-Ibanez, S., and Rathjen, J. P. (2010). Bacterial virulence effectors and their activities. *Curr. Opin. Plant Biol.* 13, 388–393. doi: 10.1016/j.pbi.2010.04.003

Hao, G. X., Boyle, M., Zhou, L. J., and Duan, Y. P. (2013). The Intracellular Citrus Huanglongbing Bacterium, 'Candidatus Liberibacter asiaticus' encodes two novel autotransporters. *PLoS ONE* 8:e68921. doi: 10.1371/journal.pone.0068921

Hodges, A. W., and Spreen, T. H. (2012). *"Economic impacts of citrus greening (HLB) in Florida, 2006/07-2010/11,"* in *Electronic Data Information Source (EDIS) FE903* (Gainseville, FL: University of Florida).

Hogenhout, S. A., and Loria, R. (2008). Virulence mechanisms of Gram-positive plant pathogenic bacteria. *Curr. Opin. Plant Biol.* 11, 449–456. doi: 10.1016/j.pbi.2008.05.007

Hogenhout, S. A., Oshima, K., Ammar El, D., Kakizawa, S., Kingdom, H. N., and Namba, S. (2008). Phytoplasmas: bacteria that manipulate plants and insects. *Mol. Plant Pathol.* 9, 403–423. doi: 10.1111/j.1364-3703.2008.00472.x

Hogenhout, S. A., Van Der Hoorn, R. A., Terauchi, R., and Kamoun, S. (2009). Emerging concepts in effector biology of plant-associated organisms. *Mol. Plant Microbe Interact.* 22, 115–122. doi: 10.1094/MPMI-22-2-0115

Huang, X. E., Liu, X. Y., Chen, X. H., Snyder, A., and Song, W. Y. (2013). Members of the XB3 family from diverse plant species induce programmed cell death in *Nicotiana benthamiana*. *PLoS ONE* 8:e63868. doi: 10.1371/journal.pone.0063868

Jagoueix, S., Bove, J. M., and Garnier, M. (1996). PCR detection of the two 'Candidatus' liberobacter species associated with greening disease of citrus. *Mol. Cell. Probes* 10, 43–50. doi: 10.1006/mcpr.1996.0006

Jain, M., Fleites, L. A., and Gabriel, D. W. (2015). Prophage-encoded peroxidase in '*Candidatus* Liberibacter asiaticus' is a secreted effector that suppresses plant defenses. *Mol. Plant Microbe Interact.* 28, 1330–1337. doi: 10.1094/MPMI-07-15-0145-R

Jones, J. D. G., and Dangl, J. L. (2006). The plant immune system. *Nature* 444, 323–329. doi: 10.1038/nature05286

Kim, J., Sagaram, U. S., Burns, J. K., and Wang, N. (2008). Microscopy and microarray analyses of host response of sweet orange (*Citrus sinensis*) to Candidatus Liberibacter asiaticus infection. *Phytopathology* 98, S81–S81. doi: 10.1094/PHYTO-99-1-0050

Koh, E. J., Zhou, L. J., Williams, D. S., Park, J., Ding, N. Y., Duan, Y. P., et al. (2012). Callose deposition in the phloem plasmodesmata and inhibition of phloem transport in citrus leaves infected with "Candidatus Liberibacter asiaticus." *Protoplasma* 249, 687–697. doi: 10.1007/s00709-011-0312-3

Krogh, A., Larsson, B., Von Heijne, G., and Sonnhammer, E. (2001). Predicting transmembrane protein topology with a hidden markov model: application to complete genomes. *J. Mol. Biol.* 305, 567–580. doi: 10.1006/jmbi.2000.4315

Li, G. Y., Froehlich, J. E., Elowsky, C., Msanne, J., Ostosh, A. C., Zhang, C., et al. (2014). Distinct Pseudomonas type-III effectors use a cleavable transit peptide to target chloroplasts. *Plant J.* 77, 310–321. doi: 10.1111/tpj.12396

Liao, H. L., and Burns, J. K. (2012). Gene expression in *Citrus sinensis* fruit tissues harvested from huanglongbing-infected trees: comparison with girdled fruit. *J. Exp. Bot.* 63, 3307–3319. doi: 10.1093/jxb/ers070

Liao, Y. W., Sun, Z. H., Zhou, Y. H., Shi, K., Li, X., Zhang, G. Q., et al. (2013). The role of hydrogen peroxide and nitric oxide in the induction of plant-encoded RNA-dependent RNA polymerase 1 in the basal defense against Tobacco mosaic virus. *PLoS ONE* 8:e76090. doi: 10.1371/journal.pone.0076090

Lindeberg, M., Cunnac, S., and Collmer, A. (2012). *Pseudomonas syringae* type III effector repertoires: last words in endless arguments. *Trends Microbiol.* 20, 199–208. doi: 10.1016/j.tim.2012.01.003

Maclean, A. M., Orlovskis, Z., Kowitwanich, K., Zdziarska, A. M., Angenent, G. C., Immink, R. G. H., et al. (2014). phytoplasma effector SAP54 hijacks plant reproduction by degrading MADS-box proteins and promotes insect colonization in a RAD23-dependent manner. *PLoS Biol.* 12:e1001835. doi: 10.1371/journal.pbio.1001835

Mafra, V., Martins, P. K., Francisco, C. S., Ribeiro-Alves, M., Freitas-Astua, J., and Machado, M. A. (2013). Candidatus Liberibacter americanus induces significant reprogramming of the transcriptome of the susceptible citrus genotype. *BMC Genomics* 14:247. doi: 10.1186/1471-2164-14-247

Martinelli, F., Reagan, R. L., Uratsu, S. L., Phu, M. L., Albrecht, U., Zhao, W. X., et al. (2013). Gene regulatory networks elucidating huanglongbing disease mechanisms. *PLoS ONE* 8:e74256. doi: 10.1371/journal.pone.0074256

Martinelli, F., Uratsu, S. L., Albrecht, U., Reagan, R. L., Phu, M. L., Britton, M., et al. (2012). Transcriptome profiling of citrus fruit response to huanglongbing disease. *PLoS ONE* 7:e38039. doi: 10.1371/journal.pone.0038039

Masaoka, Y., Pustika, A., Subandiyah, S., Okada, A., Hanundin, E., Purwanto, B., et al. (2011). Lower concentrations of microelements in leaves of citrus infected with 'candidatus Liberibacter asiaticus'. *Jpn. Agric. Res. Q.* 45, 269–275. doi: 10.6090/jarq.45.269

Maxwell, D. P., Nickels, R., and Mcintosh, L. (2002). Evidence of mitochondrial involvement in the transduction of signals required for the induction of genes associated with pathogen attack and senescence. *Plant J.* 29, 269–279. doi: 10.1046/j.1365-313X.2002.01216.x

Nakagawa, T., Suzuki, T., Murata, S., Nakamura, S., Hino, T., Maeo, K., et al. (2007). Improved gateway binary vectors: high-performance vectors for creation of fusion constructs in Transgenic analysis of plants. *Biosci. Biotechnol. Biochem.* 71, 2095–2100. doi: 10.1271/bbb.70216

Narusaka, M., Kubo, Y., Hatakeyama, K., Imamura, J., Ezura, H., Nanasato, Y., et al. (2013). Interfamily transfer of dual NB-LRR genes confers resistance to multiple pathogens. *PLoS ONE* 8:e55954 doi: 10.1371/journal.pone.0055954

Nielsen, H., Engelbrecht, J., Brunak, S., and Von Heijne, G. (1997). A neural network method for identification of prokaryotic and eukaryotic signal peptides and prediction of their cleavage sites. *Int. J. Neural Syst.* 8, 581–599. doi: 10.1142/S0129065797000537

Nomura, K., Melotto, M., and He, S. Y. (2005). Suppression of host defense in compatible plant- *Pseudomonas syringae* interactions. *Curr. Opin. Plant Biol.* 8, 361–368. doi: 10.1016/j.pbi.2005.05.005

Nwugo, C. C., Lin, H., Duan, Y. P., and Civerolo, E. L. (2013). The effect of 'Candidatus Liberibacter asiaticus' infection on the proteomic profiles and nutritional status of pre-symptomatic and symptomatic grapefruit (Citrus paradisi) plants. *BMC Plant Biol.* 13:59 doi: 10.1186/1471-2229-13-59

Petersen, T. N., Brunak, S., Von Heijne, G., and Nielsen, H. (2011). SignalP 4.0: discriminating signal peptides from transmembrane regions. *Nat. Methods* 8, 785–786. doi: 10.1038/nmeth.1701

Petre, B., and Kamoun, S. (2014). How do filamentous pathogens deliver effector proteins into plant cells? *PLoS Biol.* 12:e1001801. doi: 10.1371/journal.pbio.1001801

Petre, B., Saunders, D. G. O., Sklenar, J., Lorrain, C., Krasileva, K. V., Win, J., et al. (2016). Heterologous expression screens in *Nicotiana benthamiana* identify a candidate effector of the wheat yellow rust pathogen that associates with processing bodies. *PLoS ONE* 11:e0149035. doi: 10.1371/journal.pone.0149035

Petre, B., Saunders, D. G. O., Sklenar, J., Lorrain, C., Win, J., Duplessis, S., et al. (2015). Candidate effector proteins of the rust pathogen Melampsora larici-populina target diverse plant cell compartments. *Mol. Plant Microbe Interact.* 28, 689–700. doi: 10.1094/MPMI-01-15-0003-R

Pitino, M., and Hogenhout, S. A. (2013). Aphid protein effectors promote aphid colonization in a plant species-specific manner. *Mol. Plant Microbe Interact.* 26, 130–139. doi: 10.1094/MPMI-07-12-0172-FI

Pugsley, A. P. (1993). The complete general secretory pathway in gram-negative bacteria. *Microbiol. Rev.* 57, 50–108.

Rawat, N., Kiran, S. P., Du, D. L., Gmitter, F. G., and Deng, Z. A. (2015). Comprehensive meta-analysis, co-expression, and miRNA nested network analysis identifies gene candidates in citrus against Huanglongbing disease. *BMC Plant Biol.* 15:184. doi: 10.1186/s12870-015-0568-4

Rodríguez-Herva, J. J., González-Melendi, P., Cuartas-Lanza, R., Antúnez-Lamas, M., Río-Alvarez, I., Li, Z., et al. (2012). A bacterial cysteine protease effector protein interferes with photosynthesis to suppress plant innate immune responses. *Cell. Microbiol.* 14, 669–681. doi: 10.1111/j.1462-5822.2012.01749.x

Sechler, A., Schuenzel, E. L., Cooke, P., Donnua, S., Thaveechai, N., Postnikova, E., et al. (2009). Cultivation of 'Candidatus Liberibacter asiaticus', *'Ca. L. africanus', and 'Ca. L. americanus' associated with Huanglongbing. Phytopathology* 99, 480–486. doi: 10.1094/PHYTO-99-5-0480

Segonzac, C., and Zipfel, C. (2011). Activation of plant pattern-recognition receptors by bacteria. *Curr. Opin. Microbiol.* 14, 54–61. doi: 10.1016/j.mib.2010.12.005

Stergiopoulos, I., and De Wit, P. J. G. M. (2009). Fungal effector proteins. *Annu. Rev. Phytopathol.* 47, 233–263. doi: 10.1146/annurev.phyto.112408.132637

Takahashi, Y., Bin Nasir, K. H., Ito, A., Kanzaki, H., Matsumura, H., Saitoh, H., et al. (2007). A high-throughput screen of cell-death-inducing factors in *Nicotiana benthamiana* identifies a novel MAPKK that mediates INF1-induced cell death signaling and non-host resistance to *Pseudomonas cichorii*. *Plant J.* 49, 1030–1040. doi: 10.1111/j.1365-313X.2006.03022.x

Vahling, C. M., Duan, Y. P., and Lin, H. (2010). Characterization of an ATP translocase identified in the destructive plant pathogen "Candidatus Liberibacter asiaticus". *J. Bacteriol.* 192, 834–840. doi: 10.1128/JB.01279-09

Vleeshouwers, V. G., Rietman, H., Krenek, P., Champouret, N., Young, C., Oh, S. K., et al. (2008). Effector genomics accelerates discovery and functional profiling of potato disease resistance and phytophthora infestans avirulence genes. *PLoS ONE* 3:e2875. doi: 10.1371/journal.pone.0002875

Wang, Q. Q., Han, C. Z., Ferreira, A. O., Yu, X. L., Ye, W. W., Tripathy, S., et al. (2011). Transcriptional programming and functional interactions within the Phytophthora sojae RXLR Effector Repertoire. *Plant Cell* 23, 2064–2086. doi: 10.1105/tpc.111.086082

Wattam, A. R., Abraham, D., Dalay, O., Disz, T. L., Driscoll, T., Gabbard, J. L., et al. (2014). PATRIC, the bacterial bioinformatics database and analysis resource. *Nucleic Acids Res.* 42, D581–D591. doi: 10.1093/nar/gkt1099

Xiao, S. Y., Ellwood, S., Calis, O., Patrick, E., Li, T. X., Coleman, M., et al. (2001). Broad-spectrum mildew resistance in Arabidopsis thaliana mediated by RPW8. *Science* 291, 118–120. doi: 10.1126/science.291.5501.118

Yang, S. M., Gao, M. Q., Xu, C. W., Gao, J. C., Deshpande, S., Lin, S. P., et al. (2008). Alfalfa benefits from Medicago truncatula: the RCT1 gene from M-truncatula confers broad-spectrum resistance to anthracnose in alfalfa. *Proc. Natl. Acad. Sci. U.S.A.* 105, 12164–12169. doi: 10.1073/pnas.0802518105

Zhang, X., Zhang, L., Dong, F. C., Gao, J. F., Galbraith, D. W., and Song, C. P. (2001). Hydrogen peroxide is involved in abscisic acid-induced stomatal closure in Vicia faba. *Plant Physiol.* 126, 1438–1448. doi: 10.1104/pp.126.4.1438

Zhong, Y., Cheng, C. Z., Jiang, N. H., Jiang, B., Zhang, Y. Y., Wu, B., et al. (2015). Comparative transcriptome and iTRAQ proteome analyses of citrus root responses to Candidatus Liberibacter asiaticus Infection. *PLoS ONE* 10:e0126973. doi: 10.1371/journal.pone.0126973

Zhou, J. M., and Chai, J. (2008). Plant pathogenic bacterial type III effectors subdue host responses. *Curr. Opin. Microbiol.* 11, 179–185. doi: 10.1016/j.mib.2008.02.004

Zipfel, C., and Felix, G. (2005). Plants and animals: a different taste for microbes? *Curr. Opin. Plant Biol.* 8, 353–360. doi: 10.1016/j.pbi.2005.05.004

Conflict of Interest Statement: The authors declare that the research was conducted in the absence of any commercial or financial relationships that could be construed as a potential conflict of interest.

The reviewer WU declared a shared affiliation, though no other collaboration, with several of the authors MP, CA, YD to the handling Editor, who ensured that the process nevertheless met the standards of a fair and objective review.

Advantages of publishing in Frontiers

OPEN ACCESS
Articles are free to read, for greatest visibility

COLLABORATIVE PEER-REVIEW
Designed to be rigorous – yet also collaborative, fair and constructive

FAST PUBLICATION
Average 85 days from submission to publication (across all journals)

COPYRIGHT TO AUTHORS
No limit to article distribution and re-use

TRANSPARENT
Editors and reviewers acknowledged by name on published articles

SUPPORT
By our Swiss-based editorial team

IMPACT METRICS
Advanced metrics track your article's impact

GLOBAL SPREAD
5'100'000+ monthly article views and downloads

LOOP RESEARCH NETWORK
Our network increases readership for your article

Frontiers
EPFL Innovation Park, Building I • 1015 Lausanne • Switzerland
Tel +41 21 510 17 00 • Fax +41 21 510 17 01 • info@frontiersin.org
www.frontiersin.org

Find us on